

Sunday Afternoon, November 9, 2014

Biomaterials Plenary Session

Room: 317 - Session BP+BI+AS-SuA

Biomaterials Plenary Session

Moderator: Morgan Alexander, The University of Nottingham, UK, Ian Gilmore, National Physical Laboratory

3:00pm **BP+BI+AS-SuA1 Imaging Mass Spectrometry: Molecular Mapping Beyond the Microscope**, *Richard Caprioli*, Vanderbilt University School of Medicine **INVITED**

MALDI Imaging MS produces molecular maps of peptides, proteins, lipids and metabolites present in intact tissue sections. It employs desorption of molecules by direct laser irradiation to map the location of specific molecules from fresh frozen and formalin fixed tissue sections without the need of target specific reagents such as antibodies. Molecular images of this nature are produced in specific m/z (mass-to-charge) values, or ranges of values, typically covering the MW range 200-100,000. We have also developed a similar approach for the analysis of targeted areas of tissues by integrating mass spectrometry and microscopy, termed histology-directed molecular analysis, whereby only selected areas of cells in the tissue are ablated and analyzed.

We have employed Imaging MS in studies of a variety of biologically and medically relevant research projects. One area of special interest is the molecular mapping of changes observed in diabetes in both a mouse model and in the human disease. Major molecular alterations have been recorded in advanced diabetic nephropathy. Other applications include developmental studies of embryo implantation in mouse, renal cancers as well as that in other organs, and neurodegenerative disease. Molecular signatures have been identified that are differentially expressed in diseased tissue compared to normal tissue and also in differentiating different stages of disease. These signatures typically consist of 10-20 or more different proteins and peptides, each identified using classical proteomics methods. In addition, Imaging MS has been applied to drug targeting and metabolic studies both in specific organs and also in intact whole animal sections following drug administration.

This presentation will focus on recent technological advances both in sample preparation and instrumental performance to achieve images at high spatial resolution (1-10 microns) and at high speeds so that a typical sample tissue once prepared can be imaged in just a few minutes. Finally, new biocomputational approaches will be discussed that deals with the high data dimensionality of Imaging MS and our implementation of 'image fusion' in terms of predictive integration of MS images with microscopy and other imaging modalities.

3:40pm **BP+BI+AS-SuA3 Nanotechnology Platforms for Triple Negative Breast Cancer**, *Mauro Ferrari*, Houston Methodist Research Institute **INVITED**

The advent of novel engineering technologies affords unprecedented advances toward long-elusive objectives of medical research. Individualized medicine responds to the basic but generally unattainable questions of diagnosing a pathology at its earliest stage, when therapy is most effective, identifying the right therapy, reaching the right therapeutic target in the body at the right time, and securing immediate feedback as for its efficacy and undesired collateral effect. Individualized medicine appears to be a credible general objective in cancer and other fields of medicine, owing to the integration of classical disciplines of clinical medicine, methods of molecular biology, and novel technology platforms.

Nanotechnologies are of great interest in the context of the drive toward individualized medicine, and may prove to be the necessary catalyst for its large-scale implementation. In this talk I will present several nanoporous-silicon-based approaches for triple-negative breast cancer (TNBC). First, nano-textured chips for proteomic and peptidomic content profiling of biological fluid samples will be demonstrated for the identification of new biomarkers of TNBC. Second, employing methods of Transport Oncophysics, multistage vectors (MSV) will be shown to afford unprecedented therapeutic results in animal models of TNBC with pulmonary metastases, and to allow the in-vivo verification of novel hypotheses about the fundamental driver mechanisms for TNBC. Methods will also be shown to deliver combination therapeutics in exactly the same optimal proportions in vivo as their preparation in the laboratory. Thirdly, a nanochannel implant will be demonstrated, for the long-term release of agents for the prevention of local recurrences of TNBC, with a reduction of the concurrent loss of bone density.

It is hoped that these innovations will contribute to the fight against TNBC, which encompass multiple varieties of breast cancer, including those that arise from BRCA mutations, and which share the unfortunate reality of being associated with much poorer prognosis than the breast cancers that are responsive to estrogen therapy or Herceptin.

4:20pm **BP+BI+AS-SuA5 Nanotechnology in the Pharmaceutical Sciences: From Lab to Industry**, *Martyn Davies*, The University of Nottingham and Molecular Profiles Ltd., UK **INVITED**

Surface and Interfacial phenomena influence the function and performance of many pharmaceutical and biomedical systems. This presentation will provide an insight into how the surface chemistry, morphology and bioactivity of novel drug delivery systems and biomedical materials may be probed at the nanoscale using a suite of complimentary advanced biophysical analytical techniques. The potential of such techniques for high-resolution imaging, the measurement of molecular and inter-particulate forces, biorecognition events and determining interfacial chemical structure will be explored for systems for gene delivery, inhalation therapy and tissue engineering scaffolds. The talk will encourage a comprehensive approach for the characterisation of complex pharmaceutical systems and will highlight the recent developments in high throughput surface analysis that provide a rapid screening strategy that has been shown to be valuable in understanding biological interactions at tissue engineering scaffold interfaces for stem cell applications. The successful translation of these methodologies and technologies into the commercial field through the spin-out Molecular Profiles Ltd will be discussed. The company has exploited surface and interfacial techniques in pharmaceutical research and development to help identify and resolve problems, in assisting in the design of novel delivery systems and in helping to understand the in-life performance of materials within complex pharmaceutical systems.

5:00pm **BP+BI+AS-SuA7 Shape Control in DNA-Polymer Nanoparticle Assembly and Gene Delivery**, *Hai-Quan Mao*, Whiting School of Engineering **INVITED**

One of the critical challenges for efficient non-viral gene delivery in vivo is the ability to control the transport properties in biological milieu of DNA-containing nanoparticles. Recently, nanoparticle shape has been identified as an important factor determining these properties. However, until now it has not been possible to control the shape of nanoparticles containing packaged plasmid DNA. We have developed a new approach to achieve effective shape control of nanocomplexes of plasmid DNA and polyethylene glycol (PEG)-polycation copolymers. Specifically, we have developed the experimental strategies to realize shape tunability from spherical and rod-like to worm-like DNA/polymer nanoparticles through variation of polymer structure and solvent polarity, and molecular dynamics simulations aiming at identifying the key parameters modulating shape control in DNA/polymer nanoparticle assembly. In addition, we have also developed methods to characterize the composition and its distribution of these complex nanoparticles. More importantly, we have demonstrated the shape-dependent cellular uptake, transfection efficiency in vitro and in vivo. These findings open up a new avenue for controlling the shape of DNA-compacting nanoparticles and enhancing gene delivery efficiency. These micelles may serve as virus-mimetic nanoparticles for elucidating the role of shape in determining particle transport properties and bioactivities.

Monday Morning, November 10, 2014

2D Materials Focus Topic

Room: 310 - Session 2D+EM+NS+PS+SS+TF-MoM

2D Materials Growth and Processing

Moderator: Thomas Greber, University of Zurich

8:20am **2D+EM+NS+PS+SS+TF-MoM1 Exploring the Flatlands: Synthesis, Characterization and Engineering of Two-Dimensional Materials, Jun Lou**, Rice University **INVITED**

In this talk, we report the controlled vapor phase synthesis of MoS₂ atomic layers and elucidate a fundamental mechanism for the nucleation, growth, and grain boundary formation in its crystalline monolayers. The atomic structure and morphology of the grains and their boundaries in the polycrystalline molybdenum disulfide atomic layers are examined and first-principles calculations are applied to investigate their energy landscape. The electrical properties of the atomic layers are examined and the role of grain boundaries is evaluated. More importantly, if precise two-dimensional domains of graphene, h-BN and MoS₂ atomic layers can be seamlessly stitched together, in-plane heterostructures with interesting electronic applications could potentially be created. Here, we show that planar graphene/h-BN heterostructures can be formed by growing graphene in lithographically-patterned h-BN atomic layers. Our approach can create periodic arrangements of domains with size that ranging from tens of nanometers to millimeters. The resulting graphene/h-BN atomic layers can be peeled off from their growth substrate and transferred to various platforms including flexible substrate. Finally, we demonstrate how self-assembled monolayers with a variety of end termination chemistries can be utilized to tailor the physical properties of single-crystalline MoS₂ atomic-layers. Our data suggests that combined interface-related effects of charge transfer, built-in molecular polarities, varied densities of defects, and remote interfacial phonons strongly modify the electrical and optical properties of MoS₂, illustrating an engineering approach for local and universal property modulations in two-dimensional atomic-layers.

9:00am **2D+EM+NS+PS+SS+TF-MoM3 Influence of Substrate Orientation on the Growth of Graphene on Cu Single Crystals, Tyler Mowll**, University at Albany-SUNY, Z.R. Robinson, U.S. Naval Research Laboratory, P. Tyagi, E.W. Ong, C.A. Ventrice, Jr., University at Albany-SUNY

A systematic study of graphene growth on on-axis Cu(100) and Cu(111) single crystals oriented within 0.1° from the surface normal and a vicinal Cu(111) crystal oriented 5° off-axis has been performed. Initial attempts to grow graphene by heating each crystal to 900°C in UHV, followed by backfilling the chamber with C₂H₄ at pressures up to 5x10⁻³ Torr did not result in graphene formation on either the on-axis Cu(100) or on-axis Cu(111) surfaces. For the vicinal Cu(111) surface, epitaxial graphene was formed under the same growth conditions. By backfilling the chamber with C₂H₄ before heating to the growth temperature, epitaxial graphene was formed on both the on-axis Cu(100) and off-axis Cu(111) surfaces, but not the on-axis Cu(111) surface. By using an argon overpressure, epitaxial overlayers could be achieved on all three Cu substrates. These results indicate that the most catalytically active sites for the dissociation of ethylene are the step edges, followed by the Cu(100) terraces sites and the Cu(111) terrace sites. The need for an argon overpressure to form graphene the on-axis Cu(111) surface indicates that the Cu sublimation rate is higher than the graphene growth rate for this surface. This research was supported in part by the NSF (DMR-1006411).

9:20am **2D+EM+NS+PS+SS+TF-MoM4 Synthesis of Large Scale MoS₂-Graphene Heterostructures, Kathleen McCreary, A.T. Hanbicki, J. Robinson, B.T. Jonker**, Naval Research Laboratory

A rapidly progressing field involves the stacking of multiple two-dimensional materials to form heterostructures. These heterostructures have exhibited unique and interesting properties. For the most part, heterostructure devices are produced via mechanical exfoliation requiring the careful aligning and stacking of the individual 2D layered components. This tedious and time consuming process typically limits lateral dimensions to micron-scale devices. Chemical vapor deposition (CVD) has proven to be a useful tool in the production of graphene and has very recently been investigated as a means for the growth of other 2D materials such as MoS₂, MoSe₂, WS₂, WSe₂, and hexagonal boron nitride. Using a two-step CVD process we are able to synthesize MoS₂ on CVD grown graphene. AFM, Raman spectroscopy, and Photoluminescence spectroscopy of the MoS₂-graphene heterostructure show a uniform and continuous film on the cm scale.

9:40am **2D+EM+NS+PS+SS+TF-MoM5 Growth of 2D MoS₂ Films by Magnetron Sputtering, Andrey Voevodin**, Air Force Research Laboratory, C. Muratore, University of Dayton, J.J. Hu, Air Force Research Laboratory/UDRI, B. Wang, M.A. Haque, Pennsylvania State University, J.E. Bultman, M.L. Jespersion, Air Force Research Laboratory/UDRI, P.J. Shamberger, Texas A&M University, R. Stevenson, Air Force Research Laboratory, A. Waite, Air Force Research Laboratory/UTC, M.E. McConney, R. Smith, Air Force Research Laboratory

Growth of two dimensional (2D) MoS₂ and similar materials over large areas is a critical pre-requisite for seamless integration of next-generation van der Waals heterostructures into novel devices. Typical preparation approaches with chemical or mechanical exfoliation lack scalability and uniformity over appreciable areas (>1 mm) and chemical vapor deposition processes require high substrate temperatures. We developed few-layer MoS₂ growth under non-equilibrium magnetron sputtering conditions selected to minimize the MoS₂ nucleation density and maximize 2D growth of individual crystals [1]. In this process, the thermodynamically driven tendency to form islands is accomplished by maximizing atomic mobility through the control of incident flux kinetic energies, densities, and arriving angle to the substrate while avoiding defect formation (i.e., vacancy creation by sputtering of S atoms). Amorphous SiO₂, crystalline (0001) oriented Al₂O₃, and (002) oriented graphite substrates were used to grow few monolayer thick MoS₂ films. Continuous 2D MoS₂ films were produced over 4 cm² areas. They were composed of nano-scale domains with strong chemical binding between domain boundaries, allowing lift-off from the substrate and electronic transport measurements with contact separation on the order of centimeters. Their characteristics were similar to few-layer MoS₂ films produced by exfoliation with a direct band gap in thin samples of approximately 1.9 eV from photoluminescence spectra. The electron mobility measured for as-grown MoS₂ films was very strongly dependent on film thickness and substrate choice.

[1] "Continuous ultra-thin MoS₂ films grown by low-temperature physical vapor deposition", C. Muratore, J.J. Hu, B. Wang, M.A. Haque, J.E. Bultman, M. L. Jespersion, P.J. Shamberger, A.A. Voevodin, Applied Physics Letters (2014) in press.

10:00am **2D+EM+NS+PS+SS+TF-MoM6 Formation of Graphene on the C-face of SiC{0001}: Experiment and Theory, Jun Li, G. He, M. Widom, R.M. Feenstra**, Carnegie Mellon University

There are two {0001} surfaces of SiC, the (0001) surface known as the "Si-face", and the (000-1) surface or "C-face". The formation of graphene (by heating the SiC to 1100 – 1600 °C in various gaseous environments) has been studied for both surfaces, although it is much better understood on the Si-face. In that case, an intermediate C-rich layer, or "buffer layer" forms between the graphene and the SiC crystal. This buffer layer has 6√3x6√3-R30° symmetry; its structure is well established,¹ and it acts as a template for the formation of subsequent graphene layers. In contrast, graphene formation on the C-face is much less well understood. More than one interface structure between the graphene and the SiC has been observed,^{2,3} and, with one notable exception,⁴ the quality of the graphene formed on the C-face is generally lower than that for the Si-face.

In this work we provide new experimental and theoretical results that allow us to understand graphene formation on the C-face of SiC. Experimentally, by heating the SiC in a disilane environment, we map out the phase diagram of different surface and interface structures that form on the SiC as a function of disilane pressure and sample temperature. New surface structures that develop just prior to the graphene formation are observed. With additional heating, graphene forms on the surface, but some remnant of the surface structure prior to the graphene formation is believed to persist at the graphene/SiC interface. From first-principles theory, we find that the hydrogen in the disilane environment plays a critical role in the surface/interface structures that form. Experimentally, for disilane pressures below 5x10⁻⁵ Torr, we find a 2x2 surface structure forming prior to graphene formation. From theory we identify this structure as consisting of a silicon adatom together with a carbon restatom on the surface, with H-termination of those atoms being possible but not necessary. At higher disilane pressures we observe a 4x4 structure, and we identify that as consisting of a lower density of Si adatoms than the 2x2, now with at least some of the adatoms and restatoms being H-terminated. With graphene formation, this structure converts to the observed √43x√43-R± 7.6° interface structure. At higher disilane pressures we theoretically predict the formation of a surface consisting simply of H-terminated carbon restatoms. Experiments are underway to observe that surface, along with subsequent graphene formation on the surface.

(1) Y. Qi et al., PRL **105**, 085502 (2010).

- (2) F. Hiebel et al., PRB **78**, 153412 (2008).
 (3) N. Srivastava et al., PRB **85**, 041404 (2012).
 (4) W. A. de Heer et al., PNAS **108**, 16900 (2011).

10:40am **2D+EM+NS+PS+SS+TF-MoM8 Graphene on Hexagonal Boron Nitride Heterostacks Grown by UHV-CVD on Metal Surfaces**, *Juerg Osterwalder, S. Roth, A. Hemmi*, University of Zurich, Switzerland, *F. Matsui*, Nara Institute of Science and Technology, Japan, *T. Greber*, University of Zurich, Switzerland **INVITED**

Chemical vapor deposition (CVD) performed under ultra-high vacuum conditions on single-crystal metal surfaces enables the growth of large-area and high-quality graphene and hexagonal boron nitride (h-BN) single layers. We explore the CVD parameter space of precursor pressure and temperature in order to go beyond the self-saturating single-layer growth, or to grow heterostacks of the two materials. Formed layers are characterized structurally by LEED, STM and x-ray photoelectron diffraction. On Cu(111) a graphene layer could be grown on a pre-deposited single layer of h-BN when using 3-pentanone as a precursor at a pressure of 2.2 mbar and a substrate temperature of 1100 K [1]. On Rh(111) the same procedure leads to incorporation of carbon into the metal surface layers, while a graphene layer is formed only upon a second high-pressure dose [2]. In both cases the heterostructures show clearly the stacking sequence and structural and ARPES signatures of graphene on h-BN but are far from defect-free.

[1] S. Roth et al., Nano Lett. **13**, 2668 (2013).

[2] S. Roth, PhD Thesis, Department of Physics, University of Zurich (2013).

11:20am **2D+EM+NS+PS+SS+TF-MoM10 Kinetics of Monolayer Graphene Growth by Carbon Segregation on Pd(111)**, *Abbas Ebnoussair, H.S. Mok, Y. Murata*, University of California at Los Angeles, *S. Nie, K.F. McCarty*, Sandia National Laboratories, *C.V. Ciobanu*, Colorado School of Mines, *S. Kodambaka*, University of California at Los Angeles

In this research, using in situ low-energy electron microscopy and density functional theory calculations, we elucidate the growth kinetics of monolayer graphene on single-crystalline Pd(111). In our experiments, carbon saturated Pd(111) samples were cooled down from 900 °C to segregate carbon on the surface in the form of graphene. Upon cooling the substrate, graphene nucleation begins on bare Pd surface and continues to occur during graphene growth. Measurements of graphene growth rates and Pd surface work functions along with DFT calculations establish that this continued nucleation is due to increasing C adatom concentration on the Pd surface with time. We attribute this anomalous phenomenon to a large barrier for attachment of C adatoms to graphene coupled with a strong binding of the non-graphitic C to the Pd surface.

Actinides and Rare Earths Focus Topic

Room: 301 - Session AC+AS+MI+SA+SS-MoM

Spectroscopy, Microscopy and Dichroism of Actinides and Rare Earths

Moderator: David Shuh, Lawrence Berkeley National Laboratory

8:20am **AC+AS+MI+SA+SS-MoM1 Novel Synthetic and Spectroscopic Techniques in Actinide Materials Chemistry**, *Stefan Minasian*, Lawrence Berkeley National Laboratory, *E. Batista*, Los Alamos National Laboratory, *C.H. Booth*, Lawrence Berkeley National Laboratory, *D. Clark*, Los Alamos National Laboratory, *J. Keith*, Colgate University, *W. Lukens*, Lawrence Berkeley National Laboratory, *S. Kozimor, R.L. Martin*, Los Alamos National Laboratory, *D. Nordlund*, SLAC National Accelerator Laboratory, *D. Shuh, T. Tyliczszak*, Lawrence Berkeley National Laboratory, *D. Sokaras*, SLAC National Accelerator Laboratory, *X.-D. Weng*, Los Alamos National Laboratory, *T.-C. Weng*, SLAC National Accelerator Laboratory **INVITED**

The development of a detailed, quantitative understanding of electronic structure and bonding for a broad range actinide materials remains a significant scientific challenge. Recent advances have shown that the 1s to np transition intensities measured by Cl and S K-edge X-ray absorption spectroscopy (XAS) directly relate to coefficients of covalent orbital mixing in M–Cl and M–S bonds. The scientific progress associated with these Cl and S XAS studies suggests that using synchrotron-generated radiation to quantify covalency for ligands beyond Cl and S would have a wide impact. The nature of chemical bonds between actinides and light atoms such as oxygen, nitrogen, and carbon is of particular interest because these

interactions control the physics and chemistry of many technologically important processes in nuclear science. However, obtaining accurate light atom K-edge XAS spectra on non-conducting compounds is notoriously difficult, because the measurement is highly sensitive to surface contamination, self-absorption, and saturation effects. Fortunately, recent upgrades at synchrotron facilities, advancements in beamline instrumentation, and sample preparation methods suggest that these insights are now within reach. Specifically, comparing XAS spectra measured in transmission with a scanning transmission X-ray microscope (STXM) with those from non-resonant inelastic X-ray scattering (NIXS) and time-dependent density functional theory provides a sound basis for validation of bulk-like excitation spectra.

Herein, a new effort is discussed that employs these techniques to understand bonding interactions in two well defined series of f-element materials. The actinide sandwich complexes, “actinocenes,” $(C_8H_8)_2An$ ($An = Th, Pa, U, Np, Pu$) have played a central role in the development of organoactinide chemistry. Results showed two contrasting trends in actinide–carbon orbital mixing, and evidence that covalency does not increase uniformly as the actinide series is traversed. Additionally, the C K-edge XAS spectrum of thorocene represents the first experimental evidence of a ϕ -type orbital interaction. Oxygen K-edge XAS measurements and DFT studies began the lanthanide dioxides LnO_2 ($Ln = Ce, Pr, Tb$), because their electronic structures are well-established from hard X-ray spectroscopies. Preliminary efforts to use lanthanide oxides and lanthanide organometallics as experimental benchmarks for quantitative determinations of covalency in d-block and f-block materials will also be discussed.

9:00am **AC+AS+MI+SA+SS-MoM3 X-ray Magnetic Circular Dichroism of Actinides**, *Andrei Rogalev, F. Wilhelm*, European Synchrotron Radiation Facility (ESRF), France **INVITED**

Actinides compounds, which are straddling the magnetic properties of rare-earths and transition metals, have been the subject of increasing interest due to their very different properties, such as Pauli paramagnets, localized and itinerant ferromagnets, and heavy fermion superconductors. The key parameter responsible for the large variety of magnetic properties is obviously degree of localization of the 5f states which are indeed involved in both the chemical bonding and the magnetism. To unravel the details of the electronic structure and magnetic properties of these 5f states, polarization dependent X-ray spectroscopy at the $M_{4,5}$ edges appears as the most suitable experimental tools. At the third generation synchrotron radiation facilities, small x-ray beam with flexible polarization sized down to few microns can be routinely achieved. This technique is thus perfectly suited for studying minute samples (a few micrograms) of transuranium materials. This talk reviews recent advances in use of polarized x-rays to study local magnetic properties and electronic structure of actinides compounds.

The magnetic properties are mostly studied with X-ray Magnetic Circular Dichroism (XMCD). The great advantage of this technique is its capability to probe the orbital and spin magnetization of 5f states separately. XMCD experiments have been reported for a great number of uranium compounds and have permitted to understand, at least qualitatively, which is the ground state despite the difficulty over assigning a valency. It has also revealed differences between localized and itinerant systems that are not yet fully understood. To our knowledge there are very few reports on XMCD measurements on other trans-uranium materials. This is unfortunate, as the questions of localization of 5f states become more interesting as the 5f count increases. In order to improve our understanding of the magnetism of actinides, which is based up to now solely on uranium compounds, and thus better to describe the differences between localized and itinerant 5f systems, we report a thorough XMCD study of a series of ferromagnetic $AnFe_2$ Laves-phase compounds. Moreover, we show that additional information regarding exchange interaction between neighboring actinides atoms can be extracted from the XMCD measurements performed at absorption edges of other “nonmagnetic” atoms in the compounds.

Finally, we demonstrate that the study of the branching ratio in $M_{4,5}$ absorption spectra can bring valuable information regarding the coupling scheme, within which to discuss the electronic and magnetic properties of actinides atoms.

9:40am **AC+AS+MI+SA+SS-MoM5 Magnetic Circular Dichroism Measured with Transmission Electron Microscope**, *Jan Rusz*, Uppsala University, Sweden **INVITED**

X-ray magnetic circular dichroism (XMCD; [1]) is an established experimental probe of atom-specific magnetic properties of lanthanides and actinides. In XMCD, a photon of well-defined energy and polarization is absorbed by an atom in the sample with a probability that is proportional to the number available unoccupied states with an energy that allows fulfilling the energy conservation and selection rules. An essential element of XMCD

are so called sum rules [2,3], which relate the XMCD spectra to the spin and orbital angular momenta, respectively.

Recently, a new experimental method has been developed that is closely related to XMCD. It was named electron magnetic circular (or chiral) dichroism (EMCD) and it is measured with a transmission electron microscope (TEM) instead of a synchrotron beam-line. We will review the short history of this method starting from its proposal in 2003 [4], first experimental proof-of-the-concept in 2006 [5], formulation of the theory [6] and sum rules [7,8] in 2007 to the present state-of-the-art and early applications, for example [9-12]. Yet, despite intense efforts, EMCD is still in its development phase, particularly from the point of view of quantitative studies. On the other hand, qualitative EMCD experiments have reached resolutions below 2nm [13].

The primary advantages of the EMCD, when compared to XMCD, are costs, availability and lateral resolution. Even a state-of-the-art TEM is a device considerably cheaper than a synchrotron beam-line and as such it can be available locally to a research group. TEM is also a very versatile instrument that combines diffraction experiments, elemental analysis, local electronic structure studies via electron energy loss spectroscopy [14] and now also magnetism via EMCD.

- [1] J. L. Erskine, E. A. Stern, Phys. Rev. B **12**, 5016 (1975).
- [2] B. T. Thole et al., Phys. Rev. Lett. **68**, 1943 (1992).
- [3] P. Carra et al., Phys. Rev. Lett. **70**, 694 (1993).
- [4] C. Hebert, P. Schattschneider, Ultramicroscopy **96**, 463 (2003).
- [5] P. Schattschneider et al., Nature **441**, 486 (2006).
- [6] J. Ruzs, S. Rubino, and P. Schattschneider, Phys. Rev. B **75**, 214425 (2007).
- [7] J. Ruzs et al., Phys. Rev. B **76**, 060408(R) (2007).
- [8] L. Calmels et al., Phys. Rev. B **76**, 060409(R) (2007).
- [9] S. Muto et al., Nature Comm. **5**, 3138 (2013).
- [10] Z. H. Zhang et al., Nature Nanotech. **4**, 523 (2009).
- [11] Z.Q. Wang et al., Nature Comm. **4**, 1395 (2013).
- [12] J. Verbeeck et al., Nature **467**, 301 (2010).
- [13] P. Schattschneider et al., Phys. Rev. B **78**, 104413 (2008).
- [14] K. T. Moore and G. v.d. Laan, Rev. Mod. Phys. **81**, 235 (2009).

10:40am **AC+AS+MI+SA+SS-MoM8 The Microstructure of Plutonium Hydride Growth Sites**, *Martin Brierley, J.P. Knowles, AWE, UK, M. Preuss, A.H. Sherry*, University of Manchester, UK

Under certain conditions plutonium is able to form plutonium hydride during long term storage [1]. Plutonium is radioactive, decaying via release of an alpha particle. Alpha particles are particularly damaging within the body and every attempt should be made to limit the distribution of loose material. Plutonium hydrides have been shown to be pyrophoric when exposed to oxygen; a reaction that could potentially liberate loose particulate outside of suitable containment.

Previous work into the hydriding rate of plutonium has investigated the reaction rate of various hydrides on the surface of these materials; specifically the nucleation rate, the lateral growth rate and the specific hydriding rate [2, 3]. Plutonium is a reactive metal and quickly forms a semi-protective oxide layer in air. Upon exposure of an oxide-covered sample to hydrogen, hydride is formed at discrete sites on the surface, which then grow radially across the surface [1]. Recent work has suggested a grain boundary enhanced growth rate [4].

In the present study, the microstructure associated with selected plutonium hydride growth sites was studied to provide information regarding the nucleation and growth mechanisms that govern the formation of plutonium-hydride. The samples were ground to 600 grit and evacuated before being exposed to ultra-pure hydrogen at pressures between 10 mbar and 1000 mbar for sufficient time to have nucleated a number of hydride sites.

Post-test analysis was performed using Scanning Electron Microscopy (SEM) and Optical Microscopy (OM) to determine the microstructure of the hydride growth sites. The morphology of individual hydride growth sites indicates that the hydride-metal interface has a highly discontinuous boundary, resulting from enhanced grain boundary diffusion and spears of transformed material; the microstructure within the plutonium hydride growth sites indicates that a preferred growth habit was adopted by the hydride product.

References

- [1] J.M. Haschke and J.C. Martz, Los Alamos Science, 26 (2000) 266-267
- [2] G. W. McGillivray, J. P. Knowles, I. M. Findlay, M. J. Dawes, J. Nucl. Mater. 385 (2009) 212-215.

[3] C. Kenney, R. Harker "Specific Hydriding Rates of δ -Plutonium", Presentation at Pu Futures, Keystone Colorado (2010)

[4] C.K. Saw, J.M. Haschke, P.G. Allen, W. Mclean II, L.N. Dinh, J. Nucl. Mater. 429 (2012) 128-135

11:00am **AC+AS+MI+SA+SS-MoM9 Hydrides of U-Mo and U-Zr Alloys: Structure and Electronic Properties**, *Ladislav Havela, M. Pavlov, I. Tkach, D. Drozdenko, M. Cieslar, Z. Matej*, Charles University, Czech Republic

When U metal (α -U) is exposed to H gas, it forms a stable hydride β -UH₃. The lattice expansion stabilizes the ferromagnetic order with the Curie temperature around 170 K. The metastable form, α -UH₃, could not be synthesized as a pure phase, and the admixture of β -UH₃ did not allow to determine reliably its intrinsic magnetic properties. We have been testing the reaction to H exposure of γ -U (bcc), which was synthesized as a single phase by combination of Mo or Zr doping into U and ultrafast cooling. We found that such alloys need high H₂ pressure and long exposure to absorb hydrogen. The products can be characterized by the formula UH₃Mo(Zr)_x. The hydrides with Mo have a structure corresponding to β -UH₃ with grain size around 1 nm, i.e. almost amorphous. Its ordering temperatures increase to 200 K for UH₃Mo_{0.18} and then decrease for higher Mo concentrations. The hydrides UH₃Zr_x exhibit the UH₃ structure (bcc U lattice filled with H atoms). Their Curie temperature weakly decreases with increasing Zr concentration and the extrapolation to Zr-free state indicates $T_C = 170$ K, i.e. identical to β -UH₃. The results can be compared with numerous hydrides obtained by hydrogenation of U₆X compounds (X = Mn, Fe, Co, Ni), all probably having similar magnetic properties. We present a detailed study of magnetic properties, electrical resistivity and specific heat. The structure characterization of initial alloys and the hydrides has been done by means of XRD, SEM with EBSD and TEM. The hydrides represent and new class of U materials, which exhibit, irrespective of details of composition or crystal structure, strong ferromagnetism with relatively very high ordering temperatures, quite surprising at materials at which the inter-U spacing does not exceed appreciably the Hill limit 340-360 pm. At last, the variations using double doping (both Mo and Zr) will be presented.

11:20am **AC+AS+MI+SA+SS-MoM10 Unraveling the Mystery of Reactively-Sputtered UO(4+x)**, *David Allred, R.S. Turley, B.S. McKeon, A. Divan, E.A. Scott, R.R. Vanfleet*, Brigham Young University

We recently found EDX and XPS evidence in reactive sputtered uranium oxide thin films of higher oxygen-to-uranium ratios than the 3-to-1 allowed by stoichiometry. We used reactive, DC-magnetron sputtering in 100% oxygen to prepare uranium-oxide thin films on silicon wafer with the highest possible oxygen content to investigate this. Both EDX & XPS showed that the ratio of oxygen-to-uranium in freshly samples was at least 4-to-1, with compositions approached 5 to 1. The potential explanations are uranates or peroxides. Detecting hydrogen- and an element difficult to detect in thin films-is crucial in understanding what is happening chemically. Uranates require cations. The only one possible in our films would be hydrogen. Similarly, bulk uranium peroxides without water/hydrogen peroxide of hydration are not known. (We have found evidence of uranium trioxide being weekly hygroscopic and stored samples in a dry environment, nonetheless these samples show high oxygen contents as prepared.) We report our chemistry and structural (TEM and XRD) attempts to solve this mystery. We also report a measurement of extreme ultraviolet reflectance of this material. (ALS-beamline 6.3.2)

11:40am **AC+AS+MI+SA+SS-MoM11 Cathodoluminescence and Band Gap Studies of Single Crystal U_xTh_{1-x}O₂ (x = 0.00, 0.01, 0.22)**, *David Turner, Oak Ridge Institute for Science and Education, J. Reding, R. Hengehold, T. Kelly*, Air Force Institute of Technology, *J.M. Mann*, Air Force Research Laboratory, *J. Kolis*, Clemson University, *J. Petrosky*, Air Force Institute of Technology

Analyses of depth- and temperature-resolved cathodoluminescence experimental techniques have identified many previously unobserved spectral characteristics in U_xTh_{1-x}O₂ compounds grown using a slow growth hydrothermal method. Three U_xTh_{1-x}O₂ (x = 0.00, 0.01, 0.22) hydrothermally grown, single crystals were examined using cathodoluminescence. Unique luminescence features were identified as a function of uranium concentration. In the undoped and x = 0.01 U_xTh_{1-x}O₂, an electronic phase transition is observed as a 20 nm (0.21 eV) red-shift in the wavelength of maximum emission. This red-shift appears when the crystals are heated during both 5 and 10 keV electron beam irradiation. Conversely, a similar phase transition is not observed in the U_xTh_{1-x}O₂ alloy (x = 0.22). Instead, the wavelength of maximum emission remains constant at 305 nm (4.07 eV). Ultimately, the addition of uranium to the ThO₂ lattice increases the band gap of the material which is identified as a 10 nm (0.13 eV) blue shift if the luminescence. Finally, a quadrupole transition is

observed in the uranium-containing crystals (O 2p to U 5f) at approximately 600 nm (2.07 eV).

Applied Surface Science

Room: 316 - Session AS+MC-MoM

Quantitative Surface Analysis

Moderator: James A. (Tony) Ohlhausen, Sandia National Laboratories, William Stickle, Hewlett Packard

8:20am **AS+MC-MoM1 Automating Multi-Technique Surface Analyses for Materials Characterisation**, *Andrew Wright, P. Mack, T.S. Nunney, A. Bushell, A. Yeadon*, Thermo Fisher Scientific, UK

X-ray photoelectron spectroscopy (XPS) is a well-established technique that has become a cornerstone of surface analysis due to the wealth of chemical bonding information that it provides. Many other surface sensitive techniques exist, of course, and often can be found on the same instrumentation. Ultraviolet photoelectron spectroscopy (UPS) provides detailed valence electronic structure information. Reflection electron energy loss spectroscopy (REELS) can yield hydrogen quantification, shake-up transition and band gap information. Ion scattering spectroscopy (ISS) offers the most surface-sensitive probe of composition. Auger electron spectroscopy (AES) offers chemical information with high spatial resolution. In addition, monatomic and cluster ion beams can be used in concert with these methods for cleaning or depth profiling.

The various techniques can each provide important information in isolation, but the real power of surface analysis comes from combining these analyses of a sample and correlating the information to provide a more thorough characterisation of the material. Traditionally, however, switching between techniques has been difficult or laborious, and this has tended to deter analysts from performing multitechnique studies. Improvements to automation and usability are vital for bringing the less-used methods into common practice.

This paper presents several multitechnique surface analyses of samples in a single instrument (the Thermo Scientific Escalab250Xi), showing how automated, sequential applications of these complementary chemical, electronic and structural characterisation methods can be applied to polymeric, catalyst, photovoltaic and semiconductor materials, yielding valuable results with minimal effort.

8:40am **AS+MC-MoM2 The S' component in the Si 2p X-ray Photoemission Spectrum of Si [001]**, *Alberto Herrera-Gomez*, CINVESTAV-Querretaro, Mexico, *M.O. Vazquez-Lepe*, Universidad de Guadalajara, Mexico, *P.G. Mani-Gonzalez*, Universidad Autónoma de Ciudad Juárez, Mexico, *O. Ceballos-Sanchez*, CINVESTAV-Querretaro, Mexico

Because of the technological relevance of the Si [001] surface, the Si 2p is one of the most studied core levels with laboratory X-Ray Photoelectron Spectroscopy (XPS). An important application is the quantification of the thickness of oxide layer, which is done by comparing the intensity of the substrate and Si⁴⁺ components. Peak-fitting is usually done by employing one doublet for the substrate and another for the Si⁴⁺ shifted around 3.5 or 4 eV to higher binding energy (from the substrate). In detailed studies, the quantification of the suboxides is usually done employing components, originally proposed by Himpsel *et al.*,¹ with the following shifts: 2.5 eV for Si³⁺, 1.75 eV for Si²⁺, and 0.95 eV for Si¹⁺. A proper fit, besides those five components, actually requires a six component shifted by approximately 0.3 eV. This peak has been clearly identified in various synchrotron studies such as that by Landemark *et al.*,² where it is referred as S'. In that study, and in others, it is assigned to one monolayer (the second) of the substrate. Although clearly present in Si 2p spectra obtained with laboratory XPS equipped with monochromatized Al K α radiation, this component is largely unspoken in the literature. In one of the few studies that mention its existence it is assigned to an asymmetry of the bulk peak.³ In this presentation it is going to be shown that this interpretation is inconsistent with the angular dependence observed by S'. The physical origin of S', which is going to be discussed in detail, goes in a direction compatible with that proposed by Landemark *et al.*: although it represents one monolayer for the clean Si [001] surface, for oxide-covered surfaces it corresponds to a few monolayers of the substrate.

[1] F. J. Himpsel, F. R. McFeely, A. Taleb-Ibrahimi, and J. A. Yarmoff, *Phys. Rev. B* 38, 6084 (1998).

[2] E. Landemark, C. J. Karlsson, Y.-C. Chao, and R. I. G. Uhrberg, *Phys. Rev. Lett.* 60, 1588 (1992).

[3] D. F. Mitchell, K. B. Clark, J. A. Bardwell, W. N. Lennard, G. R. Massoumi and I. V. Mitchell. *Surf. Inter. Anal.* 21. 44-50 (1994).

9:00am **AS+MC-MoM3 Quantitative Analysis of Nanostructured Surfaces by means of X-ray Photoelectron Spectroscopy: Theory and Applications**, *Wolfgang Werner*, Vienna University of Technology, Austria **INVITED**

The theory of signal emission in electron spectroscopy is discussed on the basis of the so-called Landau-Goudsmit-Saunderson (LGS) loss function, which leads in a natural way to rigorous spectrum analysis techniques, the so-called partial intensity analysis (PIA). Examples of applications include theoretical calculation of model spectra as well as analysis of experimental spectra using of X-ray Photoelectron Spectroscopy (XPS) and Reflection Electron Energy Loss Spectroscopy on nanostructured surfaces [1], the contribution of in-vacuo electron scattering to electron spectra [2] and secondary electron-electron energy loss coincidence spectroscopy (SE2ELCS) [3]. In the latter technique correlated electron pairs are analysed and detected, thereby giving unique insight into the dielectric properties of a solid.

A layered electron gas system will be considered as an important case study for quantitative surface analysis: it is shown how single layer graphene data can be extracted from measurements on macroscopic three dimensional highly oriented pyrolytic graphite (HOPG) samples. After appropriate analysis, a feature in the spectrum can be identified which quantitatively correlates with the sp²-content in arbitrary carbon samples, as follows from comparison with Raman measurements.

[1] W S M Werner, *Surf. Interf. Anal.* 31(2001)141

[2] Werner, Wolfgang S. M., Novak, Mihaly, Salvat-Pujol, Francesc, Jiricek, Petr, Zemek, Josef, *PRL* 110(2013)086110

[3] W. S. M. Werner, F. Salvat-Pujol, A. Bellissimo, R. Khalid, W. Smekal, M. Novak A. Ruocco and G. Stefani, *Phys. Rev. B* 88(2013)201407

9:40am **AS+MC-MoM5 Effective Attenuation Lengths for Hard X-ray Photoelectron Spectroscopy (HAXPES)**, *A. Jablonski*, Polish Academy of Sciences, Poland, *Cedric Powell*, National Institute of Standards and Technology (NIST), *S. Tanuma*, National Institute for Materials Science (NIMS), Japan

HAXPES is now being used to characterize thicker overlayer films than is possible with conventional XPS using Al and Mg K α x-ray sources. As a result, there is a need for effective attenuation lengths (EALs) to determine film thicknesses at electron energies larger than about 1.5 keV. Jablonski and Powell [1] published a simple practical EAL expression from fits to EALs calculated from solution of the kinetic Boltzmann equation within the transport approximation for electron energies between 61 eV and 2 keV and photoelectron emission angles between 0° and 50°. This approach has now been extended to electron energies up to 5 keV with account also taken of non-dipole terms in the photoionization cross section. EALs have been calculated for Si 1s, Cu 2p_{3/2}, Ag 3d_{5/2}, and Au 4f_{7/2} photoelectrons excited by Mg K α , Al K α , Zr L α , and Ti K α x rays using the inelastic mean free paths of Tanuma *et al.* [2] for each solid. EALs from the non-dipole approximation were up to about 2% larger than those from the dipole approximation. Good agreement has been found between the new EALs and EALs determined from Monte Carlo simulations and from the NIST SESSA database [3]; with the latter database, simulations can be made for photoelectron energies up to 20 keV. We found that the new EALs were also consistent with the previous expression [1]. Finally, the new EALs are reasonably consistent with the EALs measured by Sacchi *et al.* [4] for Co, Cu, and Ge but there was poorer agreement with the EALs measured by Rubio-Zuazo and Castro [5] for Au. Disagreements between the calculated and measured EALs for Au at energies less than 5 keV were attributed to non-ideal morphologies of the thinner Au films.

[1] A. Jablonski and C. J. Powell, *J. Vac. Sci. Technol. A* 27, 253 (2009).

[2] S. Tanuma, C. J. Powell, and D. R. Penn, *Surf. Interface Anal.* 43, 689 (2011).

[3] <http://www.nist.gov/srd/nist100.cfm>.

[4] M. Sacchi *et al.*, *Phys. Rev. B* 71, 155117 (2005).

[5] J. Rubio-Zuazo and G. R. Castro, *J. Electron Spectrosc. Relat. Phenom.* 184, 384 (2011).

10:00am **AS+MC-MoM6 Angle-Resolved XPS Test Structures Fabricated In Situ by Argon Ion and Argon Cluster Ion Treatment**, *Peter Cumpson*, *A.J. Barlow*, *J.F. Portoles*, *N. Sano*, Newcastle University, UK

Nondestructive depth-profiling by inversion of Angle Resolved XPS spectra [1] has been a desire in the XPS community for a long time. The lack of reference specimens with known structures has been a severe handicap in the development of the technique. Until now, reference materials with

known depth-profiles have largely been confined to thin oxide layers on aluminium or silicon, and even these have uncertain carbon contamination layers. Progress has been made, though, with depth-profiling numerical methods[2] that need comparison with real known structures. It is difficult to fabricate structures with nanometre-scale variation in concentration with depth, and even more difficult to transport them without contamination (and the potentially damaging removal of such contamination).

We have developed protocols for the fabrication of two different samples, one organic and the other inorganic, with known depth-profiles *in situ* in XPS instruments;

Glancing-angle monatomic argon sputtered PEDOT:PSS, a common conducting polymer blend, and

Argon cluster-ion sputtered indium arsenide (InAs), a compound semiconductor

Indium arsenide and PEDOT:PSS are both widely-available, almost atomically flat and sufficiently electrically conductive to ensure no sample charging occurs. Glancing angle monatomic sputtering of PEDOT:PSS leaves a PEDOT enhanced region at the surface, the spatial parameters of which depend only on sputter ion conditions under direct experimental control. Recently we have demonstrated the unexpected result that argon gas-cluster sputtering of InAs results in a thin, coherent metallic indium layer at the surface[3], the basis for InAs reference material structure.

The ill-posed nature of the inversion of ARXPS data means it is sensitive to small experimental uncertainties. We apply three different ARXPS algorithms, including regularization, to the data from these *in situ* reference structures. This gives a set of reference data that will allow comparison with results from any XPS work following the same preparation protocol. This should greatly improve confidence in the results of ARXPS depth-profiling.

[1] P J Cumpson, Angle-resolved XPS and AES: depth-resolution limits and a general comparison of properties of depth-profile reconstruction methods, *J Electron Spectrosc. and Rel. Phenom.* 73 (1995) 25-52.

[2] R W Paynter, Regularization methods for the extraction of depth profiles from simulated ARXPS data derived from overlayer/substrate models, *J Electron Spectrosc. and Rel. Phenom.* 184 (2012) 569-582.

[3] A J Barlow and P J Cumpson, Observed damage during Argon gas cluster depth profiles of compound semiconductors, submitted to *J Appl. Phys.*

10:40am **AS+MC-MoM8 Metrology for Surface Chemical Analysis: Active Parties, Status and Challenges**, *Wolfgang Unger*, BAM Federal Institute for Materials Research and Testing, Germany

The International Bureau of Weights and Measures (BIPM) defines metrology, i.e. the *Art of Measurement*, as "the science of measurement, embracing both experimental and theoretical determinations at any level of uncertainty in any field of science and technology." Besides the establishment of full uncertainty budgets traceability is another aspect of metrology.

Surface chemical analysis is a much younger discipline in comparison to other branches in analytical chemistry as, e.g., electro-chemistry, inorganic and gas analysis and lots of work has to be done to make XPS, AES and SIMS based quantitative analysis a metrological one. Looking to the analytical methods established in surface chemical analysis we may differentiate classes:

1. Primary methods measuring amount of substance as [atoms/cm², ...]
2. Empirical methods measuring amount of substance after calibration as fractions of a nano scaled surface layer
3. Primary and empirical methods measuring amount of substance expressed as the thickness of a thin film [nm]

In most cases we are using empirical methods when XPS, AES and SIMS are applied to deliver quantitative data. It follows also from that list that, principally, traceability to the mol or the meter can be established.

Relevant initiatives to metrologically underpin surface chemical analysis have been launched under the umbrella of the Surface Analysis Working Group at CCQM/BIPM where the National Metrology Institutes are running world-wide inter-laboratory comparisons. In Europe we have the European Metrology Research Program (EMRP) where a number of projects directly address issues of surface chemical analysis and most often also by individual websites. Another aspect is that there is a strong impact of metrology in surface chemical analysis on standardization in ISO TC 201 and 202. For example, ISO 14701 has been prepared using outcome of a huge key comparison organized under CCQM/BIPM.

The talk will present some basics of metrology in surface chemical analysis, results of successful key comparisons organized under CCQM/BIPM and a survey on the main scientific challenges to be addressed in quantitative surface chemical analysis in the next future.

11:00am **AS+MC-MoM9 Local Crystallography: Phases, Symmetries, and Defects from Bottom Up**, *A. Belianinov, Q. He, A. Borisevich, S. Jesse, Sergei Kalinin*, Oak Ridge National Laboratory

Progress in high-resolution real space imaging techniques such as (Scanning) Transmission Electron Microscopy (STEM) and Scanning Tunneling Microscopy (STM) has allowed high veracity, direct imaging of atomic columns (STEM) and surface atomic structures. While the data acquisition platforms are continuously evolving, the basic data processing principle - analysis of structure factor, or equivalently two point correlation function averaged over probing volume - remained invariant since the early days of Braggs. We propose an approach based on the multivariate statistical analysis of the coordination spheres of individual atoms to reveal preferential structures and symmetries. The underlying mechanism is that for each atom, *i*, laying on the lattice site with indices (*l, m*), we construct a near coordination sphere as a vector $\mathbf{N}_i = (x_1, \dots, x_8)$, where (*x_j, y_j*) is the radius-vector to *j*/2-th nearest neighbor. Once the set of \mathbf{N}_i vectors is assembled, its statistical properties are analyzed through cluster analysis and various multivariate methods to reveal and extract regions of symmetry, distortions, different phases, boundaries, defects, etc. Results are presented on various model and real material systems including La_{0.7}Sr_{0.3}MnO₃, BiFeO₃, LaCoO₃ and discussed in light of physical parameter extraction.

Acknowledgement:

Research for (AB, QH, AB, SJ, SVK) was supported by the US Department of Energy, Basic Energy Sciences, Materials Sciences and Engineering Division. Research was conducted at the Center for Nanophase Materials Sciences, which is sponsored at Oak Ridge National Laboratory by the Scientific User Facilities Division, Office of Basic Energy Sciences, US Department of Energy.

11:20am **AS+MC-MoM10 Chemical Warfare Agent Surface Adsorption: Hydrogen Bonding of Sarin and Soman to Amorphous Silica**, *Erin Durke, W.O. Gordon*, Edgewood Chemical Biological Center, *A.R. Wilmsmeyer*, Augustana College, *D. Troya, J.R. Morris*, Virginia Tech

Sarin and soman are warfare nerve agents that represent some of the most toxic compounds ever synthesized. The extreme risk in handling such molecules has, until now, precluded detailed research into the surface chemistry of agents. We have developed a surface science approach to explore the fundamental nature of hydrogen bonding forces between these agents and a hydroxylated surface. Sarin and soman are deposited via a directional doser onto an amorphous silica surface and characterized by reflection-absorption infrared spectroscopy (RAIRS) in an ultra-high vacuum (UHV) chamber. Once the chemical agent coverage reached monolayer values, temperature programmed desorption is performed to determine the binding energy. Changes in the OH region of the IR spectra are monitored in real time with RAIRS, and the degree of shift in the H-bonded OH peak shows a linear relationship with the strength of the interaction between agent and silica surface. Infrared spectroscopy revealed that both agents adsorb to amorphous silica through the formation of surprisingly strong hydrogen-bonding interactions with primarily isolated silanol groups (SiOH). Comparisons with previous theoretical results reveal that this bonding occurs almost exclusively through the phosphoryl oxygen (P=O) of the agent. Temperature-programmed desorption experiments determined that the activation energy for hydrogen bond rupture and desorption of sarin and soman was 50 ± 2 kJ/mol and 52 ± 2 kJ/mol, respectively. X-ray photoelectron spectroscopy (XPS) is also used to confirm molecular desorption of the agents from the silica substrate. Together with results from previous studies involving other phosphoryl-containing molecules, we have constructed a detailed understanding of the structure-function relationship for nerve agent hydrogen bonding at the gas-surface interface.

11:40am **AS+MC-MoM11 The Shake-up Satellites in the Fe 2p Core Level X-ray Photoelectron Spectra Analyzed with the Double Lorentzian Line Shape**, *M. Bravo-Sanchez*, CINVESTAV-Queretaro, Mexico, *J.A. Huerta-Ruelas*, Centro de Investigación en Ciencia Aplicada y Tecnología Avanzada, Mexico, *A. Herrera-Gomez*, CINVESTAV-Queretaro, Mexico, *M.O. Vazquez-Lepe*, Universidad de Guadalajara, Mexico, *F. Espinosa-Magaña*, CIMAV-Unidad Chihuahua, Mexico

Within the transition metal oxides, Fe oxides are among the most technologically relevant. Surfaces analysis through techniques such as X-ray photoelectron spectroscopy (XPS) plays a crucial role in the development of new applications. Despite that a considerable effort has been made on Fe oxides with XPS, many questions are still unanswered mainly due to the lack of a simple and standardized method to adequately model the spectrum of the Fe 2p core level. Complex characteristics such as a steeply background, shake-up satellites, and an asymmetrical line-shape, have been the principal obstacle to obtain accurate areas for proper quantification. In this work, this problem has been confronted by employing the SVSC background [1] and the double Lorentzian line shape [2]. The

latter has many advantages over the traditionally employed Doniach-Sunjic line shape, since it is integrable and, then, suitable for quantitative studies.

With this combination of methods it has been possible to closely model the entire Fe 2p spectra (including both the 3/2 and 1/2 branches), which implied accounting for the shake-up satellite already known and the inclusion of a second satellite rarely reported in the literature. A proper determination of areas for accurate quantification of composition and thickness has been achieved taking into account this second satellite located around 725 eV (binding energy), hidden under the 1/2 branch of the main oxide peak. The inclusion of this second signal, together with the already known satellite, improves notably the quantitative analysis of the Fe oxides spectra. The position of the satellites shows a clear dependence on the oxide thickness. Thickness assessment has been confirmed with high-resolution transmission electron microscopy.

[1] A. Herrera-Gomez, M. Bravo-Sanchez, O. Ceballos-Sanchez, and M.O. Vazquez-Lepe. *Journal of Electron Spectroscopy and Related Phenomena* (in press) DOI 10.1002/sia.5453.

[2] A. Herrera-Gomez. "A double Lorentzian shape for asymmetric photoelectron peaks." Internal Report. Cinvestav-Querétaro.(2011). <http://www.qro.cinvestav.mx/~aherrera/reportesInternos/doubleLorentzian.pdf>

Biomaterial Interfaces

Room: 317 - Session BI+AS-MoM

Biomolecules & Biomaterials Interfaces

Moderator: Ilya Reviakine, CIC biomaGUNE

8:40am **BI+AS-MoM2 Deposition of Porous Polyparylene Layers with Even Thickness in Narrow Tubes**, *Gerhard Franz, H. Heidari*, Munich University of Applied Sciences, Germany

To coat a thin hollow tube with an equally thick layer along the whole length, is one of the most challenging issues of surface refinement. Even for long mean free paths and large diffusion lengths, a drop in thickness is common, which is simply caused by the abstraction of deposited molecules, which cannot walk randomly any longer. To overcome these inherent spatial inhomogeneities, we made use of the mechanism of the temperature-dependent surface polymerization, which is manifested in the occurrence of a "ceiling temperature". Negatively turned, no deposition is possible beyond this temperature. Positively spoken, the spatially inhomogeneous deposition rate along a tube can be equalized with a counteracting temperature gradient. Experimentally, a configuration with four furnaces in line has been constructed which allows the inner wall of a tube 12" in length and 1/8" in inner diameter to be coated with a layer of even thickness. The most prominent application is the partial protection of thin silver layers which are deposited on the inner walls of catheters of polyurethane or polysilicone not as a contiguous film but with a zebra-stripe design applying a patent-pending procedure [1]. These silver rings act as antibacterial means to combat infections and induced incrustations in the urological area. To prolong the lifetime of the silver depot, it has to be protected with a porous human compatible top layer. We chose FDA approved polyparylene with thicknesses between 100 and 400 nm to ensure a long-term antibacterial activity, which should be kept above threshold level by a safety factor of 2 [2,3]. First results for the CVD of polyparylene are presented and are discussed and modeled with COMSOL in terms of diffusion laws with an abstraction reaction of 1st order. After having shown the antibacterial effect for a static case [4], here a dynamic trial is presented to simulate the antibacterial activity during flow of bacteria-containing urine in the ureters. [1] G. Franz, F. Schamberger, A. Kutschera, S. Seyedi, D. Jocham, German patent disclosure DE 102012023349.3, Nov. 29, 2012, [2] F. Schamberger, A. Ziegler, and G. Franz, *J. Vac. Sci. Technol. B30*, 01801 (2012) [3] G. Franz, F. Schamberger, *J. Vac. Sci. Technol. A31*, 061602 (2013) [4] H. Heidari, St. Sudhop, F. Schamberger, G. Franz, *Biointerphases*, accepted May 05, 2014

9:00am **BI+AS-MoM3 Deciphering the Scaling of Single Molecule Acid-Amine Interactions using Jarzynski's Equality**, *S. Raman, T. Utzig, T. Baimpos, B.R. Shrestha, Markus Valtiner*, Max Planck Institut für Eisenforschung GmbH, Germany

Unraveling the complexities of the macroscopic world based on molecular level details relies on understanding the scaling of single molecular interactions towards integral interactions, which are mediated through a large number of simultaneously interacting molecular bonds. Here we demonstrate how to decipher the scaling of acid-amine interactions from the single molecular level towards the macroscopic level through a synergistic experimental approach combining equilibrium Surface Forces Apparatus

(SFA) experiments and non-equilibrium single molecule force spectroscopy (SM-AFM). Combining these two techniques is ideally suited for testing the largely praised Jarzynski's equality (JE), which relates the work performed under non-equilibrium conditions with the equilibrium free energy. Large-scale equilibrium force measurements using SFA scale linearly with the number density of acid-base bonds at an interface and we measure molecular acid-amine interaction energies of 10.9 ± 0.2 kT. AFM single molecule experiments reveal two distinct regimes. As expected, far from equilibrium the measured single molecule unbinding forces increase exponentially with the loading rate. A second quasi-equilibrium regime at loading rates close to and below the natural binding/unbinding rate of the acid-amine bond shows little loading rate dependence. Irrespective of how far from equilibrium AFM experiments are performed, the energy calculated using JE converges rapidly to 10.7 ± 1.1 kT. This is essentially equivalent to the value measured by the equilibrium measurements using SFA. Our results suggest that using Jarzynski's equality allows direct scaling of non-equilibrium single molecule interaction force measurements to scenarios where a large number of molecules are simultaneously interacting, giving rise to macroscopic equilibrated interaction energies. Taken together, the developed approach provides a strategy for molecular design of novel functional materials through predicting of large-scale properties such as adhesion or cell-substrate interactions based on single molecule or simulation experiments.

9:20am **BI+AS-MoM4 Fabrication of ssDNA Monolayers, Custom Designed ssDNA Arrays and Brush Patterns in Biorepulsive Templates by Promoted Exchange Reaction**, *M.N. Khan*, University of Heidelberg, Germany, *V. Tjong, A. Chilkoti*, Duke University, *Michael Zharnikov*, University of Heidelberg, Germany

We present here a versatile approach to prepare mixed monolayers of thiolate-bound single stranded DNA (ssDNA) and oligo(ethylene glycol) substituted alkanethiols (OEG-AT) in a broad range of compositions as well as ssDNA/OEG-AT patterns of desired shape embedded into a biorepulsive background. The procedure involves two steps. First, a OEG-AT monolayer on a solid support is exposed to electrons or UV light in either homogeneous or lithographic fashion. Second, the promoted (by the irradiation in the first step) exchange reaction between the damaged OEG-AT species in the film and ssDNA substituents in solution occurs, resulting in formation of a ssDNA/OEG-AT monolayer or pattern. The composition of the mixed films or ssDNA/OEG-AT spots (lithography) can be precisely adjusted by electron or UV dose in almost entire composition range. The above procedure relies on commercially available compounds and is applicable to both thiol-terminated and symmetric and asymmetric disulfide-terminated ssDNA. The fabricated OEG-AT/ssDNA templates and patterns can be extended into the z-dimension by surface-initiated enzymatic polymerization of ssDNA, which results in the formation of highly ordered ssDNA brushes and allows topographically complex ssDNA brush patterns to be sculpted on the surface.

9:40am **BI+AS-MoM5 High Throughput BioMaterials Screening using Microarrays and High Information Content Imaging Methods**, *S. Boudjabi, D. Covelli, M. Keramane, E. Luckham, John Brennan*, McMaster University, Canada

INVITED

This presentation will highlight recent work in the area of high throughput screening of biologically modified surfaces for production of biosensors, protein and cell microarrays, and non-fouling surfaces. Using robotic material synthesis and assay systems and a combination of contact and noncontact microarray printing, we have produced several libraries of biomaterials with a wide range of chemical compositions based on acrylate, silicone and silica-based polymers. Using silica-based materials as an example, the presentation will show the workflow utilized to develop new bioactive polymer materials for generation of bioactive and stealth materials and coatings. This includes methods to produce several thousand materials very rapidly via printing, rapid imaging tools and assays for screening to identify "hits" that show a desired property (i.e., high bioactivity, low non-specific binding), and methods for detailed material analysis using a range of imaging methods based on fluorescence, XPS, MALDI-MS/MS, FTIR and SPR to fully characterize the properties of biologically active materials. Methods for mining and analyzing the large datasets produced using our in-house developed Biointerphases Research Gateway will be described.

10:40am **BI+AS-MoM8 Osteocalcin Adsorption onto Calcium Phosphate and Silica Surfaces**, *L.A. Scudeller, David Castner*, University of Washington

Osteocalcin (OC) is the most abundant, non-collagenous protein in bone and accounts for almost 2% of total protein in the human body. OC plays a role in the body's metabolic regulation and bone building, as well as being used as a biochemical marker for bone formation. However, its precise function is not known. OC is known to bind strongly to hydroxyapatite (HAP). This strong binding is likely the result of the γ -carboxylated

glutamic acid residues (Gla) in OC interacting with Ca^{2+} ions on the HAP surface. OC has three helical units (α -1, α -2 and α -3) and the spacing of the 3 Gla residues in the α -1 unit match well the lattice spacing of the (001) HAP surface.

This study uses x-ray photoelectron spectroscopy (XPS) and time-of-flight secondary ion mass spectrometry (ToF-SIMS) to investigate the adsorption of OC and decarboxylated (i.e., Gla converted back to Glu) OC (dOC) onto various calcium phosphate surfaces as well as silica surfaces. The XPS nitrogen signal is used to track the amount of adsorbed OC and dOC. The intensities of key ToF-SIMS amino acid fragments are used to assess changes in the structure of adsorbed OC and dOC.

The largest differences were observed between OC and dOC adsorbed onto the silica and HAP surfaces. Similar amounts (3-4 atomic % N) of OC and dOC were adsorbed onto the silica surface. Higher amounts adsorbed on the HAP surface (~5 atomic % N for dOC and ~8 atomic % N for OC). The ToF-SIMS data showed the intensity of the Cys amino acid fragment, normalized to intensity of all amino acid fragments, was significantly higher (~x10) when the proteins were adsorbed onto silica. Since in the native OC structure the cysteines are buried in the center of the 3 α -helices, this indicates both OC and dOC are more denatured on the silica surface. As OC and dOC denature upon adsorption to the silica surface the cysteines become more exposed and are more readily detected by ToF-SIMS. No significant differences were detected between OC and dOC adsorbed onto the silica surface, but small differences were observed between OC and dOC adsorbed onto the HAP surface. In the OC structure the α -3 helix is located above the α -1 and α -2 helices. Small differences in the ToF-SIMS intensities from amino acid fragments characteristic of each helical unit (Asn for α -1; His for α -2; and Phe for α -3) suggests either slight changes in the orientation or a slight uncovering of the α -1 and α -2 for adsorbed dOC.

XPS showed similar amounts of OC and dOC were absorbed onto amorphous HAP, crystalline HAP and octacalcium phosphate, but ToF-SIMS detected some small differences in the amino acid fragment intensities between adsorbed OC and dOC.

11:00am **BI+AS-MoM9 Reversible Activation of a pH-sensitive Cell Penetrating Peptides Attached to Gold Surfaces**, *Joe Baio*, Oregon State University, *D. Schach*, University of Chicago, *M. Bonn*, *T. Weidner*, Max Planck Institute for Polymer Research, Germany

GALA peptides (WEAALAEALAEALAEHLAEALAEALAEALAA) mimic pH-sensitive viral fusion proteins and are widely touted as a promising route to achieve site-specific delivery of therapeutic compounds. At basic pH, GALA assumes a random coil structure but when lowering the pH to acidic conditions the peptide transitions into an alpha helical structure. In this state, GALA has the ability to penetrate cell membranes and form pores. This mechanism is mainly driven by the change in overall charge of the glutamic acid side chains. One development of GALA mediated drug delivery is the immobilization of these peptides onto Au nanoparticles. Here we demonstrate, using a variety of spectroscopic techniques, that GALA can self-assemble into a protein monolayer on a gold film, linked to the surface via a single cysteine synthesized to the carbonyl terminus. Transmission IR vibrational spectroscopy demonstrates that the addition of this cysteine does not impede the pH transition between a helix and random coil structure in solution. Detailed characterization of the thiol-Au immobilization scheme by X-ray photoelectron spectroscopy illustrates that this single cysteine induced the formation of a well-ordered protein monolayer. To directly observe any pH triggered transition of this protein monolayer, sum frequency generation (SFG) vibrational spectra, at the amide I vibrational band, were collected at four different pH environments. A vibration mode at 1655 cm^{-1} , related to a helical structure, appears when this monolayer is immersed in a buffer at acidic conditions (pH 3 and 5) and then disappears under basic conditions (pH 9 and 12). While the surface immobilization clearly reduces the effective glutamic acid pK_a from a bulk solution value of 6 to 5.5, the covalently bound GALA-cysteine monolayer reliably retained the reversible, pH-driven helix-coil transition mechanism. Our findings establish that covalent attachment of GALA via cysteine linkers is a promising route for drug delivery applications and the design of 'smart' biological coatings.

11:20am **BI+AS-MoM10 Polydopamine Modification Using Small Molecule Thiols and Dithiols: Problems and Solutions for Creating Protein Resistant Coatings**, *Marlon Walker*, *A. Vaish*, *D. Vanderah*, National Institute of Standards and Technology (NIST)

Polydopamine (PDA) is emerging as an increasingly useful bio-inspired coating for surface modification. Generated by a condensation reaction of dopamine in aqueous media under alkaline conditions, it can be readily deposited on almost any surface, forming thin films of controllable thicknesses. One useful attribute of a PDA coating is that it can be placed on and further modified to exhibit desired properties not possible with the underlying substrate. We present results of functionalizing PDA-coated

surfaces on substrates such as silicon with oligo (ethylene oxide) thiols and dithiols for non-specific protein adsorption resistance.

11:40am **BI+AS-MoM11 A Process to Functionalize Polyaniline for Biotin-Avidin Biosensing**, *Tiana Shaw*, *M.D. Williams*, Clark Atlanta University

Biotin-avidin technology is a widely explored interaction in bioscience. Biotin's affinity for the protein avidin, makes it ideal for protein and nucleic acid detection or purification methods. This strong interaction is often used in pretargeting strategies for cancer treatment. In most cases a probe molecule (antibody) is connected to a marker molecule (fluorophore or nanoparticle) through the biotin-avidin bridge. Biotinylated nanoparticles can play a role in improving this interaction and creating an electronic or optical detection method. Polyaniline is a polymer which can be easily functionalized to be specific for various biomolecules and has ideal sensor characteristics. In this study we will design a process to functionalize polyaniline with biotin to create a biotin-avidin biosensor. We began with 2-acetamidophenol which is a hydroxyl substituted aniline monomer. This monomer undergoes polymerization to yield 2-hydroxy polyaniline. The polymer's hydroxyl group was functionalized by Steglich esterification which refluxes a carboxylic acid with an alcohol. This esterification drives the reaction and dehydrates the products shifting the equilibrium towards the product. In this reaction DCC (dicyclohexylcarbodiimide) activates the carboxylic acid of biotin to further reaction and DMAP (4-dimethylaminopyridine) acts as the acyl transfer catalyst. The biotinylated polyaniline derivative was characterized using FT-IR spectroscopy, ^1H NMR spectroscopy, UV-VIS spectroscopy, and Scanning Electron Microscopy. Fluorescence emission studies were also carried out with the avidin protein.

Electronic Materials and Processing

Room: 314 - Session EM+MI+NS-MoM

Complex Oxides and Their Interfaces

Moderator: Jessica Hilton, Mantis Deposition, Lisa M. Porter, Carnegie Mellon University

8:20am **EM+MI+NS-MoM1 Emergent Phenomena at Complex Oxide Interfaces**, *Susanne Stemmer*, University of California at Santa Barbara
INVITED

Two-dimensional electron gases (2DEGs) at interfaces between two insulating oxides have attracted significant attention because they can exhibit unique properties, such as strong electron correlations, superconductivity, and magnetism. In this presentation, we will discuss properties arising from strong electron correlations in narrow quantum wells of the band insulator SrTiO_3 , sandwiched between Mott insulating rare earth titanates, SmTiO_3 and GdTiO_3 , respectively. These quantum wells exhibit very high sheet electron high-densities, of approximately 1 electron per planar unit cell of the quantum well. We demonstrate electron correlation effects due to short-range Coulomb interactions, including mass enhancement, interface-induced magnetism in the electron gas, and a transition to a correlated insulator at the lowest thickness in quantum wells bound by ferrimagnetic GdTiO_3 . We show that the metal-insulator transition is coupled with the sudden onset of structural distortions in the quantum well. In contrast, quantum wells bound by antiferromagnetic SmTiO_3 exhibit almost no structural distortions, incipient antiferromagnetism, no metal-insulator transition, and non-Fermi liquid behavior. We will discuss the implications of the results in the context of two-dimensional electron correlation physics.

This work was performed in collaboration with Clayton Jackson, Pouya Moetakef, Jack Zhang, Jinwoo Hwang, Leon Balents, and Jim Allen.

9:00am **EM+MI+NS-MoM3 Atomic and Electronic Structure of the Ferroelectric BaTiO_3 -Ge (001) Interface**, *Kurt Fredrickson*, The University of Texas at Austin, *P. Ponath*, *A.B. Posadas*, University of Texas at Austin, *M.R. McCartney*, *T. Aoki*, *D.J. Smith*, Arizona State University, *A.A. Demkov*, University of Texas at Austin

In this study, we demonstrate the epitaxial growth of BaTiO_3 on Ge(001) by molecular beam epitaxy using a thin Zintl template buffer layer. A combination of density functional theory, atomic-resolution electron microscopy and *in situ* photoemission spectroscopy is used to investigate the electronic properties and atomic structure of the BaTiO_3 /Ge interface. Aberration-corrected scanning transmission electron micrographs reveal that the Ge(001) 2×1 surface reconstruction remains intact during the subsequent BaTiO_3 growth, thereby enabling a choice to be made between several theoretically predicted interface structures. The measured valence

band offset of 2.7 eV matches well with the theoretical value of 2.5 eV based on the model structure for an in-plane-polarized interface. The agreement between the calculated and measured band offsets, which is highly sensitive to the detailed atomic arrangement, indicates that the most likely BaTiO₃/Ge(001) interface structure has been identified.

9:20am **EM+MI+NS-MoM4 Strain-Controlled Stoichiometry Variations in CaMnO₃ Epitaxial Thin Films**, *Rajeswari Kolagani, G. Yong, Z. Warecki, C. Stumpf, D. Schaefer, P. Sharma, C. Hart, A. Burger*, *Towson University*

CaMnO₃ is a material of interest for application in novel energy technologies such as thermoelectric power generation, and as a photo catalyst for hydrogen energy storage. We are currently investigating the properties of epitaxial thin films of CaMnO₃ (CMO) and its electron doped derivatives towards tuning material properties that enable these applications. Oxygen stoichiometry and its effect on structural and electronic properties are key variables in optimizing thin films of these materials. We will present our studies of CMO thin films grown epitaxially by Pulsed Laser Deposition on several compatible oxide substrates with varying degrees of tensile and compressive lattice mismatch. Lattice mismatch results in the distortion of the unit cell symmetry from cubic to tetragonal. In hole-doped rare earth manganites such as La_{0.7}CaMnO₃, tensile as well as compressive lattice mismatch strain is known to cause a suppression of the insulator-metal transition, leading to an increase in electrical resistivity. In contrast, our studies of the structural and electrical properties of CMO thin films indicate that tensile strain causes a pronounced decrease in the electrical resistivity. The strained films have an expanded out of plane lattice parameter which is consistent with reduced oxygen stoichiometry. These results indicate that the tensile strain causes CMO thin films to be more susceptible to the formation of oxygen vacancies, thus reducing electrical resistivity. This is in agreement with recent theoretical predictions correlating strain and oxygen vacancies, where tensile strain induced in-plane expansion of the unit cell is shown to favor oxygen deficiency. The potential for employing lattice mismatch strain for tuning film composition has important implications for technological applications. We will present our detailed investigations of the correlation of strain and oxygen stoichiometry in CaMnO₃ and related manganese compositions, employing high resolution X-ray diffraction, temperature dependent resistivity measurements, and characterization of the film surface morphology using atomic force microscopy.

9:40am **EM+MI+NS-MoM5 Controlling Complex Oxide Chemistry to Enable Advanced Dielectric, Ferroelectric, and Electronic Applications**, *Lane Martin*, *University of California, Berkeley* **INVITED**

Current and next-generation advanced functional materials are testing our ability to produce high-quality, complex materials with ever increasing precision. Particular interest has been given to candidate complex oxide materials which present a diverse range of material properties and functionality not easily produced in other classes of materials. The ultimate integration and utilization of these materials, however, will require that we can carefully and deterministically balance the intrinsic phenomena of interest in these materials with a knowledge of the potential extrinsic effects that can arise from defects which result from our inability to produce these complex materials with the precision we desire. This is made more challenging by the fact that these complex oxide systems are prone to and can accommodate large densities of point defects through a range of internal compensation mechanisms. In this presentation, we will explore the interrelationship between the complex oxide growth process, the chemical nature of these complex materials, the resulting structure and strain evolution, and the ultimate effect on properties in a range of prototypical complex oxide materials. We will explore these interrelationships in model systems including the classic dielectric materials SrTiO₃ and LaAlO₃, highly-controlled heterointerfaces that exhibit exotic physics including the LaAlO₃/SrTiO₃ system, and ferroic systems such as BaTiO₃ and others. In this context, we will demonstrate routes by which we can deterministically utilize the tendency for these materials to form point defects to enhance epitaxial thin film strain, developing new modalities of strain control of thin-film materials that go beyond traditional lattice mismatch effects, and how the combination of epitaxial strain and defects in materials can be used to enhance performance, independently tune susceptibilities, and provide new insights into the nature of these complex materials. For instance, in BaTiO₃ we will illustrate how one can couple epitaxial strain to defect structures to provide an additional out-of-plane strain component that can dramatically enhance ordering temperatures and will explore the use of compositionally-graded heterostructures to further extend what can be done with epitaxial strain to manipulate dielectric, ferroelectric, and electronic properties of materials.

10:40am **EM+MI+NS-MoM8 Monolithic Integration of Epitaxial BaTiO₃ on Si and SiGe for Ferroelectric Devices**, *L. Mazet, R. Bachelet, G. Saint-Girons*, *Institut des Nanotechnologies de Lyon (INL) - CNRS - ECL, France*, *D. Albertini, B. Gautier*, *Institut des Nanotechnologies de Lyon (INL) - CNRS - INSA de Lyon, France*, *M.M. Frank, J. Jordan-Sweet, I. Lauer, V. Narayanan*, *IBM T.J. Watson Research Center*, *M. Hytch, S. Schamm-Chardon*, *CEMES - CNRS - Université de Toulouse, France*, *Catherine Dubourdieu*, *Institut des Nanotechnologies de Lyon (INL) - CNRS - ECL, France* **INVITED**

Ferroelectric oxides integrated on a semiconductor substrate are of particular interest for various applications such as memory or logic devices, electro-optic devices or as piezoelectric materials for sensors and actuators. Among the ferroelectric compounds, BaTiO₃ is an attractive candidate for large-scale applications compared to Pb- or Bi-based oxides. It is a well-known perovskite largely studied for its dielectric, piezoelectric and ferroelectric properties.

In this talk, I will briefly review the challenges associated with the monolithic integration of crystalline complex oxides on a semiconductor and more particularly with the integration of ferroelectrics. Molecular Beam Epitaxy (MBE) provides unique advantages to precisely construct, almost atom by atom, the oxide/semiconductor interface.

I will then present an experimental work on the epitaxy of BaTiO₃ thin films (1.2 - 20 nm) on silicon and Si_{1-x}Ge_x substrates. Films are grown by MBE, in the thickness range of 1.2-20 nm. Different growth conditions such as temperature and oxygen pressure are explored to optimize the BaTiO₃ film quality and to minimize the SiO₂ interfacial layer regrowth between Si and the SrTiO₃ buffer layer. The surface quality is monitored *in-situ* by reflection high-energy electron diffraction (RHEED) and *ex-situ* by X-ray reflectometry (XRR) and atomic force microscopy (AFM). The crystalline structure is studied by conventional and synchrotron X-ray diffraction. It is also investigated at the nanoscale using advanced transmission electron microscopy techniques. Strain maps determined with high precision (0.05%), 5 nm spatial resolution and with a large field of view (1 μm) using dark field electron holography will be discussed for selected samples. The crystalline domain orientations (*c*- versus *a*-domains) will be discussed with respect to the growth conditions and thickness. The ferroelectric properties are investigated by piezoresponse force microscopy (PFM). Ferroelectric films are obtained in optimized conditions that will be discussed. Ultrathin films of few monolayers are investigated to determine the onset of ferroelectricity.

I will conclude with ongoing perspectives on the integration of such heterostructures in new field-effect devices for low power logic applications.

11:20am **EM+MI+NS-MoM10 The Surface Study of Hexagonal LuFeO₃ Multiferroic Thin Films**, *Shi Cao, X.S. Xu, T. Paudel, E.Y. Tsymlal, P.A. Dowben*, *University of Nebraska-Lincoln*

The surface properties of hexagonal LuFeO₃ thin film have been studied by ultra-high vacuum based characterization technologies such as X-ray/ultra-violet photoemission spectroscopy (XPS/UPS), inverse photoemission spectroscopy (IPES) and XMCD-PEEM. Hexagonal LuFeO₃ is a stable multiferroic at room temperature with potential magneto-electric properties. The application of this material in voltage controlled magnetic devices depends very significantly on the interface composition and interface magnetism. The angle resolved XPS shows the possible iron-rich termination and the oxygen deficiency due to the sensitivity of the surface to the of sample preparation methods. The combined UPS and IPES allow us to infer that this multiferroic oxide, LuFeO₃, has a band gap about 2.35eV. All these characterizations are consistent with the density function theory calculations of the surface and bulk band structure.

11:40am **EM+MI+NS-MoM11 Integration of Ferroelectric Perovskites on Ge(001) by ALD: A Case Study of BaTiO₃**, *Thong Ngo, M.D. McDaniel, S.N. Chopra, J.G. Ekerdt, A.B. Posadas, A.A. Demkov*, *The University of Texas at Austin*

Gemanium, which exhibits higher hole and electron mobilities than silicon, might become a candidate to replace silicon as a channel material in a field effect transistor (FET) beyond the 3D FET generation. Unlike Si, when the high-κ dielectrics are integrated on Ge, the chemical instability of GeO₂ is an advantage. Moreover, the instability of GeO₂ also enables epitaxial functional oxides on Ge. Crystalline perovskites can be high-κ insulating, with many also being ferromagnetic, ferroelectric, multiferroic, or superconducting. This wide range of properties, combined with possibilities for lattice match to Ge(001), allows for multi-functional oxides to be engineered on Ge(001).

Epitaxial integration of ferroelectric barium titanate, BaTiO₃ (BTO), on Ge has attracted much attention due to the low lattice mismatch between Ge(001) and BTO (0.25% above Curie temperature, T_c = 120 °C). The efforts to epitaxially integrate ferroelectric BTO on Ge(001) have been

demonstrated using molecular beam epitaxy (MBE) by several groups. However, for device manufacturing applications, atomic layer deposition (ALD) has advantages over MBE due to its high step coverage, significantly low thermal budget, scalability, and low cost.

We demonstrate an all-chemical route to epitaxially integrate BTO directly on Ge(001). Amorphous BTO films were grown on the 2×1 reconstructed, clean Ge(001) surface at 225 °C using ALD. Barium bis(triisopropylcyclopentadienyl), titanium tetraisopropoxide, and water were employed as co-reactants. The films become highly crystalline after a vacuum anneal at 600–700 °C. In-situ x-ray photoelectron spectroscopy confirms the stoichiometry of the BTO films with no detectable GeOx formation or carbon incorporation. In-situ reflection high energy electron diffraction (RHEED) shows high order of BTO film crystallinity after vacuum annealing. X-ray diffraction (XRD) is used to determine the crystallinity and the orientation of BTO films. Electrical characterization, including capacitance-voltage, leakage current, interface trap density, and piezoresponse force microscopy measurements will also be performed to explore the high-κ insulating and ferroelectric properties of BTO films on Ge(001). The integration of BTO films on Ge(001) by ALD is a promising method for fabricating a ferroelectric FET at production scale.

Materials Characterization in the Semiconductor Industry Focus Topic

Room: 313 - Session MC+AP+AS-MoM

Characterization of 3D Structures, 2D films and Interconnects

Moderator: Paul Ronsheim, CTO, PAR Technical Consulting, previously with IBM, Paul van der Heide, GLOBALFOUNDRIES, NY, USA

8:20am MC+AP+AS-MoM1 **Dopant/Carrier and Compositional Profiling for 3D-Structures and Confined Volumes.**, *Wilfried Vandervorst, A. Kumar, J. Demeulemeester, A. Franquet, P. Eyben, J. Bogdanowicz, M. Mannarino, A. Kambham, U. Celano*, IMEC, KU Leuven Belgium **INVITED**

The introduction of three-dimensional devices (FinFets, TFETs and nanowires), has created a new metrology challenges the characterization of dopant /carrier and impurity distributions in 3D-devices and confined volumes. Beyond these dimensional challenges, the use of alternative materials such SiGe, Ge, GeSn alloys as well as III-V materials, adds to the metrology requirements. Recent evolution towards growth (and strain relaxation) mediated by the confined volume (for instance relying on aspect ratio trapping) calls for metrology suited for very small volumes and more atomic scale observations. Metrology in 3D-structures and confined volumes has demonstrated that the changing surface/volume ratios in confined devices versus blanket films lead to phenomena (dopant deactivation, enhanced diffusion,...) which cannot be observed in blanket experiments. Hence more emphasis should be placed on the analysis of device and structures with relevant dimensions relative to the exploration of blanket experiments.

Atomprobe tomography is able to provide composition analysis within very small volumes (a few nm³) with high sensitivity and accuracy and excellent spatial resolution. Hence this enables to observe dopant atom migration in 3D-devices, and through some data mining analysis, even cluster formation as precursor to strain relaxation such as seen in metastable alloys like GeSn. Field Ion Microscopy, a complement to APT, can be used to image impurity atoms clustered around defects within the crystal. Routine application of APT is still hampered by localization problems, reconstruction artifacts due to inhomogeneous evaporation, local magnification effects, sensitivity due to the limited statistics, laser-tip interaction phenomena, etc.

Although scanning spreading resistance microscopy is inherently 2D, analysis of 3D-devices (FinFet, ReRam, Sonos...) is possible by novel approaches such as SPM scalping. The introduction of novel modes such as soft retrace, FFT-SSRM has led to improved resolution and eliminates series resistances resulting from the current confinement in these narrow devices, decoupling the actual “spreading resistance” from the total resistance. Finally SSRM-carrier distribution have been coupled to device simulators leading to an accurate prediction of device performance.

In addition to APT we also present here the concept of “self focusing SIMS” whereby we demonstrate that it is possible to determine, for instance, the SiGe(III-V) composition in trenches as small as 20 nm without having an ion beam with nm-resolution. This represents a significant step forward in terms of production control and statistical relevance.

9:00am MC+AP+AS-MoM3 **Characterization of the Periodicity (Pitch) and Stress of Transistor Fin Structures using X-Ray Diffraction Reciprocal Space Mapping.** *Alain Diebold, M. Medikonda*, SUNY College of Nanoscale Science and Engineering, *M. Wormington*, Jordan Valley Semiconductors Inc

Cleanroom compatible, high resolution X-Ray diffraction systems are now capable of measuring the average pitch and critical dimensions of ordered arrays of fins and the stress state of high mobility layers at the top of the fins. Reciprocal Space Mapping (RSM) characterizes both the main Bragg diffraction peak and the satellite peaks associated with the fin periodicity. The periodicity of the fin arrays has decreased to the point where the fin array adds satellite diffraction peaks to the main Bragg diffraction peak from the semiconductor. The pitch can be calculated from the angular spacing of the satellite peaks. State of the art lithographic processing using the spacer patterning process often results in a different spacing between every other fin. This is known as pitch walking. Pitch walking is very difficult to observed, even using TEM cross-sectional images. The stress state of the high mobility epilayers such as Si_{1-x}Ge_x on Si fins can also be characterized using RSMs. In addition, some of the higher order satellite peaks will split when the fins have a near rectangular shape. This presentation compares the capability of cleanroom and synchrotron based XRD systems for reciprocal space mapping of Si and Si_{1-x}Ge_x / Si transistor fins arrays.¹

¹ Measurement of Periodicity and Strain in Arrays of Single Crystal Silicon and Pseudomorphic Si_{1-x}Ge_x/Si Fin Structures using X-ray Reciprocal Space Maps, M. Medikonda, G. Muthinti, J. Fronheiser, V. Kamineni, M. Wormington, K. Matney, T. Adam, E. Karapetrova and A.C. Diebold, J. Vac. Sci. Technol. **B32**, (2014), 021804.

9:20am MC+AP+AS-MoM4 **MBE Grading Techniques for the Growth of InAsSb Films with Inherent Properties Unaffected by Strain.** *Wendy Sarney, S.P. Svensson*, US Army Research Laboratory, *Y. Lin, D. Wang, L. Shterengas, D. Donetsky, G. Belenky*, Stony Brook University

By using compositionally graded buffer layers, InAsSb can be grown by molecular beam epitaxy with its inherent lattice properties across the entire composition range. This direct bandgap, III-V alloy is of great interest for infrared detector applications, as it can cover both the mid (3-5 μm) and long wavelength (8-12 μm) bands. The direct bandgap provides the high quantum efficiency that allows it to directly compete with HgCdTe but at potentially much reduced fabrication costs. InAsSb was sidelined for decades, because conventional wisdom indicated its bandgap bowing parameter would not allow it to reach the needed 10-12 μm benchmark. The material was further maligned because it was thought to exhibit CuPt ordering, which affects the bandgap. By revisiting the growth techniques we have determined that the bandgap bowing parameter of InAsSb is more than sufficient for LWIR applications and it can be grown free of ordering, provided that the material is grown with its inherent, undistorted lattice constant.

As there is no perfect substrate available for the InAsSb compositions of interest (typically containing ~40-50% Sb), we grow the films on compositionally graded buffer layers on GaSb substrates. The buffer layers consist of AlGaInSb, GaInSb, or InAsSb grades based on the theories described by J. Tersoff.¹ In this paper we provide experimental verification of Tersoff's theories applied to ternary and quaternary grades, and for both tensile and compressive grades. Furthermore, the specific parameters calculated by Tersoff, such as the boundary for the dislocation-free region (Zc) is exactly verified by transmission electron microscopy (TEM).

Reciprocal space maps show that the InAsSb layers grown on compositional graded buffer layers have their native lattice constant. The films are free from strain-relieving dislocations within the field of view allowed by TEM. Furthermore, we see no evidence of group V ordering for films grown in this manner. Although ordering is known to further reduce the bandgap, it is a difficult property to control, and it would be very undesirable to rely on it to induce the needed longer wavelengths. We have observed that a finite amount of residual strain that is small enough not to cause dislocation formation can induce CuPt ordering, but this can be completely avoided by using appropriate grading techniques. We also see no evidence of phase segregation or miscibility gaps.

Photoluminescence wavelengths have been measured for numerous InAsSb films, with a maximum wavelength to date of 12.4 μm. This may be the ideal material for direct bandgap infrared device applications.

J. Tersoff, Appl. Phys. Lett. 62, 693 (1993);

9:40am **MC+AP+AS-MoM5 Quantitative 3-D Imaging of Filaments in Hybrid Resistive Memory Devices by Combined XPS and ToF-SIMS Spectroscopies**, *Y. Busby, Jean-Jacques Pireaux*, University of Namur, Belgium

Resistive switching has been observed in a multitude of inorganic (oxides, chalcogenides...) and hybrid (organic or polymers plus metal nanoparticles) thin films simply sandwiched between two metal electrodes. Organic memory devices are particularly promising candidates for developing large scale, high density, cost efficient, non-volatile resistive memories. Their switching mechanism has been for a long time suggested to depend on the formation/rupture of localized conducting paths (filaments). Using electrical characterization by impedance spectroscopy, filament formation has been experimentally demonstrated to be the dominant switching mechanism in many organic memories, only very recently (2014). Otherwise, despite of very dedicated efforts, few experimental techniques have so far succeeded in characterizing and providing information on filament(s).

The present work combines for the first time High Resolution X-Ray induced Photoelectron Spectroscopy (for its quantitative information capability) and Time-of-Flight Secondary Ion Mass Spectrometry (for its very high atomic sensitivity and 3D imaging capabilities) to quantitatively study both lateral and in depth elements distribution in a complete and operative organic memory device: what happens to be top electrode metal diffusion and filament formation is evidenced and quantitatively evaluated in memory devices which are based on a highly insulating and *cross-linked polystyrene layer*, processed by plasma polymerization, sandwiched between silver and indium tin oxide electrodes. Depth profiles evidence the metal diffusion in pristine and electrically addressed memory elements through the whole organic layer where the silver concentration can reach value as high as $5 \cdot 10^{19}$ at/cm³. Filament formation is shown to be initiated during the top electrode evaporation, and is then successively enhanced by field induced diffusion during the electrical addressing. The 3-D ToF-SIMS images evidenced the formation of metallic paths extending through the entire device depth, electrically bridging the two electrodes when the element is in its low resistance state. Filaments with different characteristics have also been studied in organic memories based on a semiconducting polymer (Polyera N1400 ActiveInk) or on semiconducting small molecules (Tris-(8-hydroxyquinoline)aluminum, AlQ₃). It appears therefore that metallic filaments are indeed at the origin of switching in organic memory devices.

10:00am **MC+AP+AS-MoM6 High Throughput Electron Diffraction-Based Metrology of Nanocrystalline Materials**, *X. Liu*, Carnegie Mellon University, *D. Choi*, Korea Railroad Research Institute, Republic of Korea, *N.T. Nuhfer*, Carnegie Mellon University, *D.L. Yates, T. Sun*, University of Central Florida, *G.S. Rohrer*, Carnegie Mellon University, *K.R. Coffey*, University of Central Florida, *Katayun Barmak*, Columbia University

The resistivity of Cu, the current interconnect material of choice, increases dramatically as the conductor's dimensions decrease towards and below the mean free path of electrons (39 nm at the room temperature). Two scattering mechanisms that contribute to this resistivity size effect are surface scattering, evidenced by thickness dependence of resistivity, and grain boundary scattering, evidenced by grain size dependence of resistivity. Quantification of microstructural parameters, such as grain size, at the scale of the resistivity size effect necessitates the use of transmission electron microscopy (TEM). In this work, an electron diffraction-based orientation mapping system installed on the TEM is used to characterize not only nanometric Cu films, but also new materials, W, Ni, Ru and Co, that are potential candidates to replace Cu as the next-generation interconnect material. In this characterization technique, spot diffraction patterns are collected as the nano-sized beam scans the area of interest. The crystallographic orientation of each scanned pixel is determined by cross-correlation with pre-calculated diffraction patterns (termed, templates). Precision is used to reduce the dynamical scattering effects, increasing the reliability of the orientation mapping. The raw orientation data is then processed to yield the microstructural data via a well-defined procedure developed to parallel that used to process electron backscatter orientation data taken in scanning electron microscopes. This characterization yields full range of microstructural parameters including grain size, grain size distribution, orientation distribution, misorientation distribution, grain boundary and interface character and plane distribution that are extracted from the crystal orientation maps in a nearly fully-automated manner. These microstructural parameters, along with sample thicknesses, are used to evaluate the validity of the semiclassical resistivity size models for Cu and the new materials, and, where applicable, to determine the relative contributions of surface and grain boundary scattering to the resistivity increase.

10:40am **MC+AP+AS-MoM8 LEIS Characterization of the Outer Surface, Ultra-Thin Layers and Contacts**, *Hidde Brongersma*, ION-TOF / Tascon / Calipso, Netherlands, *P. Bruener, T. Grehl*, ION-TOF GmbH, Germany, *H.R.J. ter Veen*, Tascon GmbH, Germany **INVITED**

Modern day technologies are increasingly based on high performance nanomaterials and novel preparation techniques for such materials are developed at a rapid pace. Advances in nanoscience and nanotechnology heavily rely on the availability of analytic techniques that can validate and support new nanomaterials synthesis procedures. With the introducing of the Qtac¹⁰⁰, a new high-sensitivity Low Energy Ion Scattering (HS-LEIS) instrument, one can quantitatively analyze the atomic composition of the surface of a wide range of materials with an unparalleled surface sensitivity.

The outermost atoms of a surface largely control processes such as growth, nucleation, poisoning, adhesion and electron emission. While analytic tools (such as XPS) probe an average of many atomic layers, LEIS can selectively analyze the outer atoms. In addition, non-destructive in-depth information, with high depth resolution, is obtained for the heavier elements (0 - 10 nm). HS-LEIS is just as well suited for the *quantitative analysis* of amorphous, insulating and extremely rough surfaces as for flat single crystals. Since HS-LEIS is a fast analysis technique, it can be used to follow diffusion processes in-situ.

The focus will be on applications where valuable information has been obtained that is impossible (or very difficult) to obtain with other analytical techniques. The unique possibilities will be illustrated with state-of-the-art applications for: ALD growth of ultra-thin layers, surface modification, interface diffusion, core/shell nanoparticles, graphene, self-assembled monolayers for sensors.

The findings will be compared and contrasted to those obtained by other analytic techniques such as XPS, Auger, SIMS, RBS and conventional LEIS.

11:20am **MC+AP+AS-MoM10 Backside versus Frontside Characterization of High-k/Metal Gate Stacks for CMOS sub-14 nm Technological Nodes**, *Eugenie Martinez*, CEA, LETI, MINATEC Campus, France, *B. Saidi, P. Caubet, F. Pierrat*, STMicroelectronics, France, *H. Kim*, CEA, LETI, MINATEC Campus, France, *S. Schamm-Chardon*, CEMES-CNRS, France, *R. Gassilloud*, CEA, LETI, MINATEC Campus, France

Down-scaling of CMOS transistors beyond the 14 nm technological node requires the implementation of new architectures and materials. The gate last integration scheme is a promising solution to better control the threshold voltage of future MOSFETs, because of its low thermal budget [1]. Advanced characterization methods are needed to gain information about the chemical composition of such structures. The analysis of thin layers and interfaces buried under a thick metal electrode is particularly challenging. An effective approach based on backside sample preparation is proposed here.

To tune the work-function toward nMOS values, the technology currently investigated is based on HfO₂ for the dielectric and a thin TiN layer capped by a TiAl alloy for the gate [2]. For a better understanding of aluminium and other elements redistributions after a 400°C annealing, a specific methodology has been developed based on the removal of the Si substrate. It allows to achieve XPS and Auger analyses from the backside of the sample [3].

In particular, Auger depth profiling performed on HfO₂/TiN/TiAl/TiN/W gate stacks at low energy (500 eV Ar⁺) brought the following main conclusions: a) no Al diffusion toward the HfO₂/TiN interface, b) nitrogen out diffusion in the upper TiAl film, c) significant oxygen scavenging. By comparison, these results evidenced that Auger frontside analyses suffer from sputter-induced artifacts.

In a further study, to understand the behavior of nitrogen out diffusion in the TiAl layer, we deposited TiAlN_x thin films with various nitrogen flows by reactive sputtering deposition and performed backside XPS analyses. At low/medium nitrogen flows, which correspond to the TiAlN_x film after TiN/TiAl bilayer anneal, the N1s core level spectra obviously shows that N is mainly bonded to Al rather than Ti. Results are compared with frontside XPS performed with a thinner TiN upper layer. The backside approach is shown to be more representative of the technological stack, in particular with respect to the TiN oxidation.

Measurements were carried out at the NanoCharacterization Platform (PFNC) of MINATEC.

[1] C. L. Hinkle et al., Appl. Phys. Lett. 100, 153501 (2012).

[2] A. Veloso et al., Symposium on VLSI Technology, Digest of Technical Papers (2011).

[3] M. Py et al., AIP conference proceedings 1395, 171 (2011).

11:40am **MC+AP+AS-MoM11 Charge Storage Properties of Al(1-x)BaTiO_{3-x}Ba(Cu_{1/3}Nb_{2/3})O₃ (x = 0.025) (BTBCN)/HfO₂/p-Si Metal/Ferroelectric/Insulator/Semiconductor Devices**, *Souvik Kundu, M. Clavel, D. Maurya, M. Hudait, S. Priya*, Virginia Tech

Metal-ferroelectric-insulator-semiconductor (MFIS) devices with pulsed laser deposited 300 nm (1-x)BaTiO_{3-x}Ba(Cu_{1/3}Nb_{2/3})O₃ (x = 0.025) (BTBCN) ferroelectric film and atomic layer deposited 10 nm HfO₂ insulating layer on silicon semiconductor substrate were developed for next generation ferroelectric non-volatile memory applications. For the first time, the structural, interfacial, and electrical properties of these Al/BTBCN/HfO₂/p-Si MFIS devices were studied, and the role of BTBCN as charge storing elements was also established. The X-ray diffraction and transmission electron micrograph with selected area diffraction pattern clearly demonstrate the single crystallization of BTBCN ferroelectric films. It was found that insertion of 10 nm HfO₂ in-between BTBCN and Si improves the interfacial properties and also prevents the interdiffusion of semiconductor into the ferroelectric layer. The optical bandgap of BTBCN was found to be 4.38 eV using transmission spectrum analysis. The MFIS structure showed capacitance-voltage hysteresis loops due to the ferroelectric polarization of BTBCN and the maximum memory window was found to be 1.65 V when the sweeping voltage was ±10 V. However, no memory window was found in metal-insulator-semiconductor devices, i.e., when there is no BTBCN layer in between metal and insulating layer. The leakage current of these devices was found to be 7×10⁻⁹ A/cm² at an applied voltage of -1 V. The wide memory window and superior retention properties were achieved due to the presence of BTBCN. The electronic band diagrams of these MFIS devices during program and erase operations were proposed.

Keywords: BTBCN; MFIS; Memory window; Leakage current; Band-diagram

Magnetic Interfaces and Nanostructures

Room: 311 - Session MI+EM-MoM

Interfacial Effects in Oxide Heterostructures

Moderator: Greg Szulczewski, The University of Alabama

8:40am **MI+EM-MoM2 Linear Dichroism of La_{0.7}Sr_{0.3}MnO₃ Magnetic Dead Layers**, *Robbyn Trappen, M.B. Holcomb, J. Zhou, C.-Y. Huang*, West Virginia University, *Y.-H. Chu, V. Tra*, National Chiao Tung University, Taiwan, Republic of China

Magnetic dead layers are a phenomenon in which a normally ferromagnetic material loses its magnetization below a critical thickness, which poses a problem for thin film applications. Density functional calculations predict the behavior of the dead layer in complex oxide films to be antiferromagnetic, which is attributed to interdiffusion of the magnetic film into the neighboring layers. Here, we investigate the transition from ferromagnetic to antiferromagnetic behavior in the complex oxide La_{0.7}Sr_{0.3}MnO₃ using x ray magnetic linear and circular dichroism on the Mn L-edge (2p to 3d transition). These measurements were taken at the Advanced Light Source at Lawrence Berkeley National Labs. If the mechanism of the formation of the dead layers is understood, it can potentially be reversed and the same physics may be able to even enhance the magnetization beyond its bulk parameter.

9:00am **MI+EM-MoM3 Magnetotransport at the Superconducting LaAlO₃/SrTiO₃ Interface**, *Stefano Gariglio, D. Li, A. Fête, W. Liu, J.-M. Triscone*, University of Geneva, Switzerland **INVITED**

The conducting interface between the two band insulators LaAlO₃ and SrTiO₃ has drawn a large share of attention, as it presents a variety of exciting electronic properties that are tunable by an electric field [1].

At low temperatures, magnetotransport analysis has revealed a strong Rashba spin-orbit interaction originating from the breaking of inversion symmetry [2] and, in field effect devices, the ground state has been tuned from an insulating to a superconducting state. I will discuss these results in light of recent magnetotransport experiments in field-effect devices to probe the evolution across the phase diagram of the weak localization/weak anti-localization transport regime, its relation to the strength and anisotropy of the superconducting state.

Moreover, this interface naturally provides a versatile system to artificially build stacks of multiple 2D superconductors that would allow coupled 2D superconducting layers to be studied. I will show that we can prepare metallic and superconducting interfaces with LaAlO₃ layers grown on an artificial SrTiO₃ film [3].

[1] A. D. Caviglia *et al.*, *Nature* **456**, 624 (2008). [2] A. D. Caviglia *et al.*, *Phys. Rev. Lett.* **104**, 126803 (2010); A. Fête *et al.*, *Phys. Rev. B* **86**, 201105 (2012). [3] D. Li *et al.* *Appl. Phys. Lett. Mat.* **2**, 012102 (2014).

9:40am **MI+EM-MoM5 Symmetry Breaking in Strained Vanadium Dioxide Films**, *Mengkun Liu*, UC San Diego **INVITED**

We report on nanoscopic aspects of the insulator-to-metal transition (IMT) in a canonical correlated electron material, vanadium dioxide (VO₂). Using scattering-type scanning near-field optical microscopy (s-SNOM) and spectroscopy (nano-FTIR), we revealed unique phase separation in strained VO₂ films at sub-micrometer scale over a wide temperature range (320K-380K). Investigating the three dimensional formation of this microscopic stripe state, we resolved the enigma of the macroscopic electronic anisotropy and disentangled distinct stages of the VO₂ phase transition with spontaneous symmetry breaking [Phys. Rev. Lett. **111** (9), 096602 (2013), Appl. Phys. Lett. **104** (12), 121905 (2014) and follow-up studies]. With these results we demonstrated that the novel spectroscopic techniques of near-field optics provide powerful and universal methodologies for studying mesoscopic and interfacial physics for many classes of transition metal oxides and phase transition materials.

10:40am **MI+EM-MoM8 Interface Assisted Molecular Spintronics**, *Karthik Raman*, Indian Institute of Science, India **INVITED**

The adsorption of molecules on magnetic surfaces offers a new directionality to the study of molecular spintronics. The creation of new interface states formed by the hybridization of molecular orbitals with the spin-polarized bands of the surface leads to the development of a unique electronic and magnetic character. Such a richness of the interface spin-chemistry allows developing new handles to functionalize the properties of the adsorbed molecules, opening up a molecular-genome initiative to develop spin-functional tailor-made devices. Along with the exploration of single molecular magnets, the use of carbon based aromatic molecules, both non-magnetic and open shell magnetic systems, have presented many interesting interface phenomena. In addition to the experimental demonstrations, these studies share a strong theoretical support from computational *ab initio* interface modeling. The mechanism of inducing molecular magnetism with stability up to room temperature, inducing interface magnetic exchange coupling with strengthens of the order of thermal energy at and above room temperature, enhancement in the magnetic anisotropy of the surface and the spin-filtering property demonstrating interfacial magnetoresistance opens up a new channel to develop molecular designs for applications in sensor, memory and computing applications. This talk shall drive interest in the emergent subfield of interface assisted molecular spintronics, by presenting a strong foundation of the interface spin-physics and spin-chemistry and propose novel schemes promoting the use of advanced spectroscopy tools for the investigation of molecular spin responses. Efforts to template molecules on surfaces offer a way forward towards molecular scaling-up, providing a future outlook to the field.

References:

1. N. Atodiresei & K. V. Raman, "Interface assisted spintronics: tailoring at the molecular scale", *MRS Bulletin* (**July** 2014).
2. K. V. Raman, "Focusing on the molecular scale", *Nature Nanotechnology* **8**, 886 (2013).
3. K. V. Raman *et al.*, "Interface engineered templates for molecular spin memory devices", *Nature* **493**, 509 (2013).
4. K. V. Raman, J. Chang, J. S. Moodera, "New method of spin injection into organic semiconductors using spin filtering tunnel barriers", *Org. Electronics* **12**, 1275 (2011).
5. K. V. Raman, S. M. Watson, J. H. Shim, J. A. Borchers, J. Chang, J. S. Moodera, "Effect of molecular ordering on spin and charge injection in rubrene", *Phys. Rev. B* **80**, 195212 (2009).

11:20am **MI+EM-MoM10 Coverage-Dependent Surface Magnetism of Iron Phthalocyanine on an O-Fe(110) Surface**, *Jack Rowe, D.B. Dougherty*, North Carolina State University, *E. Vescovo*, National Synchrotron Light Source

Iron phthalocyanine adsorbed on an oxygen covered Fe(110) surface shows a complex coverage-dependent spin polarization during growth of the first molecular monolayer. Spin polarization is modified at low submonolayer coverages, absent at intermediate submonolayer coverages, and re-appears in modified form for a complete monolayer. This is attributed to coverage-dependent adsorption configurations from a random adsorption system to a packed monolayer with a well-defined interfacial spin polarization. In addition, we report on the observation of a rotation of the spin direction of photoelectrons in the presence of molecules, which is attributed to molecular modifications of surface magnetic anisotropy.

11:40am **MI+EM-MoM11 Time Resolved Imaging At 10Ghz And Beyond Using The Ssrl Scanning Transmission X-Ray Microscope**, *Hendrik Ohldag*, SLAC National Accelerator Laboratory, *S. Bonetti, R. Kukreja*, Stanford University, *J. Frisch, H. Duerr, J. Stoehr*, SLAC National Accelerator Laboratory

Understanding magnetic properties at ultrafast timescales is crucial for the development of new generations of magnetic devices. Such devices will employ the spin torque or spin Hall effect, whose manifestation at the nanoscale is not yet sufficiently understood, which is why studies addressing these effects are of great fundamental significance as well. The samples of interest are often thin film magnetic multilayers with thicknesses in the range of a atomic layers. This fact alone presents a sensitivity challenge in STXM microscopy, which is more suited toward studying thicker samples. In addition the relevant time scale is of the order of 10 ps, which is well below the typical x-ray pulse length of 50 – 100 ps. Altogether this means that pushing the time resolution of a synchrotron x-ray microscopy experiment is synonymous with improving the signal to noise ratio on the detector and providing stable, low jitter excitation to not further dilute the already small magnetic signals.

The SSRL STXM is equipped with a single photon counting electronics that effectively allows us to use a double lock-in detection at 476MHz (the x-ray pulse frequency) and 1.28MHz (the synchrotron revelation frequency). The pulsed or continuous sample excitation source is synchronized with the synchrotron source with a few picosecond drift over 24 hours. This setup currently allows us to achieve a signal to noise ratio of better than 10000, enabling us to detect miniscule variations of the x-ray absorption cross section.

In this talk I will describe the time resolved STXM setup developed at SSRL and present firsts results that have been obtained using the instrument in collaboration with an outstanding group of external users. The instrument operates in ultra high vacuum ($\sim 10^{-8}$ torr) and allows us to apply electrical pulses to our samples that can be placed in out of plane magnetic fields up to 0.8 Tesla or in plane magnetic fields up to 0.3 Tesla. We have used the instrument to successfully image spin waves excited in spin-torque and spin Hall oscillators with nano contacts of the size of ~ 100 nm. We also succeeded in imaging different excitation modes of magnetic samples in ferromagnetic resonance at 9.6GHz excitation frequency, where the opening angle of the precession cone is of the order of 10mrad.

The facility that is dedicated to ultrafast studies of materials under electric and magnetic fields is open to general users who are interested in this field.

Nanometer-scale Science and Technology

Room: 304 - Session NS+SE-MoM

Delivering Energy and Mass at the Nanoscale

Moderator: Paul Sheehan, Naval Research Laboratory

8:20am **NS+SE-MoM1 Mechanical Properties of Polymer Systems Using Atomic Force Microscopy**, *Gregory Meyers*, The Dow Chemical Company **INVITED**

Scanned probe microscopy (SPM) has had a long history at The Dow Chemical Company, beginning in the late 1980s when commercial scanning tunneling microscopes were just hitting the market. Since that time Dow has invested in internal and external collaborative efforts to drive and develop atomic force based technologies for property measurements of polymeric materials at nanometer length scales.

Our most cited early work described a unique phenomenon of surface wear of polystyrene thin films where the interaction of a sliding AFM tip lead to characteristic patterns that depended on the polymer molecular weight. Since that time work such as this has been studied in order to understand elastic, adhesive, and thermal properties of polymer coatings and films near rigid interfaces. Collaborations with NIST in the late 1990s provided our first attempts at quantifying mechanical properties at the nanoscale, combining knowledge gained from classical nanoindentation to the calibration of AFM systems for quantitative AFM based indentation. This work set the stage for a large scale effort in the latter 2000 time frame, funded by the NIST-ATP program in collaboration with Veeco Instruments (now Bruker-Nano). The objective of this program was to develop an AFM based platform for quantitative modulus measurements of polymers at sub 100 nm length scales, to provide better than 10% precision for polymer materials with bulk properties in the 10 MPa to 10 GPa range. As a result of this program, we now have quasistatic AFM based indentation capability that provides the most comprehensive suite of analytical models (elastic, elastic-plastic, and adhesive) to interpret material properties at these scales. Within the last few years the ability to map properties at high spatial resolution via high speed AFM indenting has been realized. A key

consideration in all of the mechanical probing is the time scale over which the tip-surface interaction occurs and so we have looked to computational simulations with Purdue University to study the role of dissipative factors – viscoelasticity and surface adhesion hysteresis – to help interpret our measurements.

9:00am **NS+SE-MoM3 Extension of Loss-Tangent Mode to Characterization of Materials' Stiffness and Damping**, *X. Yu, M. Tao, Nancy Burnham*, Worcester Polytechnic Institute

Viscoelastic materials are engineered and used in a variety of applications; however, it has been a great challenge to characterize their viscoelasticity at the nanoscale, at which the degradation and failure mechanisms often initiate. For linear viscoelastic materials, an atomic force microscopic (AFM) technique, loss-tangent mode, has been recently developed to fulfill this need [1]. The loss tangent of a material is expressed as the ratio of the lost energy (damping) over the stored energy (stiffness) and is claimed to be independent of the tip-sample contact area. Since this new mode was invented, only a few example materials have been studied. In this project, viscoelasticity of several different materials (i.e., asphalt binders [2], epoxy, silica tire, and graphite) were investigated using loss-tangent mode; the damping and stiffness terms were derived with easily measurable terms for a more detailed understanding of materials' viscoelasticity.

Results show that both free amplitude and set-point ratio affect the loss-tangent measurement. For all the examined materials, the loss tangent and damping decreased (power laws of -2.4 ± 1.1 and -2.1 ± 1.0 , respectively) with increasing free amplitude at constant set-point ratio, while stiffness increased (power law 0.32 ± 0.18). The loss tangent increased (power law 0.8 ± 0.5) with increasing set-point ratio at constant free amplitude; stiffness decreased more rapidly than damping (power laws of -1.75 ± 0.06 and -1.0 ± 0.4 , respectively). These trends might indicate that the loss tangent, as measured by AFM, is not independent of the tip-sample contact area. Computer simulation of loss-tangent mode is ongoing for explanation of these observations, in order to advance understanding of nanoscale viscoelastic measurements.

1. R. Proksch and D.G. Yablon, *Appl. Phys. Lett.* **100**, 073106 (2012)

2. X. Yu, N.A. Burnham, R.B. Mallick, M. Tao, *Fuel* **113**, 443 (2013)

9:40am **NS+SE-MoM5 Direct Mechanical Measurements of Viscoelasticity in Simple Liquids Using Vibrating Nanostructures**, *Matthew Pelton*, University of Maryland, Baltimore County, *D. Chakraborty*, University of Melbourne, Australia, *E. Malachosky, P. Guyot-Sionnest*, University of Chicago, *J.E. Sader*, University of Melbourne, Australia

Studies of acoustic vibrations in nanometer-scale particles can provide fundamental insights into the nanomechanical properties of nanoscale materials, and into the mechanical coupling between the nanoparticles and their environment. Metal nanoparticles allow for all-optical, non-contact measurements, using ultrafast laser pulses to generate and probe high-frequency acoustic vibrations. In early studies, the decay of the signal due to nanoparticle vibrations was dominated due to vibrations in nanoparticle size. By using highly uniform bipyrnyl gold nanoparticles, we were able to overcome the effects of inhomogeneous damping and measure the rate at which the acoustic oscillations dissipate energy. Measurements in low-viscosity liquids such as water showed a strong “intrinsic” damping occurring within the nanoparticles themselves, and an environmental damping due to viscous coupling to the surrounding liquid. This fluid damping was described quantitatively using a parameter-free model.

In higher-viscosity liquids, however, the measured oscillation frequencies and damping rates deviate strongly and qualitatively from the predictions of this model. The deviations are explained quantitatively as arising from non-Newtonian effects in the liquid. The nanoparticles vibrate at very high frequencies (20 GHz), so that their vibration periods are comparable to the intrinsic relaxation times of the liquid. The structure-fluid interaction is thus dominated by viscoelastic effects. The observed viscoelasticity is not due to molecular confinement, but is a bulk continuum effect arising from the short time scale of vibration. This represents the first direct mechanical measurement of the intrinsic viscoelastic properties of simple bulk liquids, and opens a new paradigm for understanding extremely high frequency fluid mechanics, nanoscale sensing technologies, and biophysical processes.

10:00am **NS+SE-MoM6 Electronic and Optical Properties of Nanometer Sized Structures formed via Local Intercalated of Carbon in Layered Materials**, *Andrew Stollenwerk*, University of Northern Iowa

Electron beam radiation is often used to synthesize nanometer scale structures through lithographic techniques, direct altering of chemical bonds, or milling away material. We have recently demonstrated a new method to locally intercalate carbon with nanometer precision using the electron beam of a scanning electron microscope to break apart residual

organics. This process was found to work only on layered materials such as topological insulators, novel superconductors, charge density wave materials, and graphite. Structurally, the incorporation of carbon raises the height of the substrate from a few nanometers up to several hundred nanometers depending on the exposure time. While easily observable using atomic force microscopy, these features are effectively invisible to the scanning tunneling microscope at tunneling biases below approximately 0.75 V. Tunneling spectrum of these structures exhibit semiconducting properties with band gaps varying between 0.5 eV – 2.5 eV. This is in agreement with the broad-wavelength photoluminescence observed in the corresponding optical spectrum. Both of these results suggest that the carbon intercalates form nano-clusters with a wide distribution in the size and density.

10:40am **NS+SE-MoM8 Effects of Chemical Bonding on Heat Transfer Across Interfaces**, *Paul Braun, M. Losego, M. Grady, N. Sottos, D.G. Cahill*, University of Illinois at Urbana-Champaign **INVITED**

Interfaces often dictate heat flow in micro- and nanostructured systems. However, despite the growing importance of thermal management in micro- and nanoscale devices, a unified understanding of the atomic-scale structural features contributing to interfacial heat transport does not exist. Herein, we experimentally demonstrate a link between interfacial bonding character and thermal conductance at the atomic level. Our experimental system consists of a gold film transfer-printed to a self-assembled monolayer (SAM) with systematically varied termination chemistries. Using a combination of ultrafast pump-probe techniques (time-domain thermoreflectance, TDTR, and picosecond acoustics) and laser spallation experiments, we independently measure and correlate changes in bonding strength and heat flow at the gold-SAM interface. For example, we experimentally demonstrate that varying the density of covalent bonds within this single bonding layer modulates both interfacial stiffness and interfacial thermal conductance. We believe that this experimental system will enable future quantification of other interfacial phenomena and will be a critical tool to stimulate and validate new theories describing the mechanisms of interfacial heat transport. Ultimately, these findings will impact applications, including thermoelectric energy harvesting, microelectronics cooling, and spatial targeting for hyperthermal therapeutics.

11:20am **NS+SE-MoM10 Enhanced Thermal Transport at Covalently Functionalized Carbon Nanotube Array Interfaces to Oxide-forming and Noble Metals**, *S. Kaur*, Lawrence Berkeley National Laboratory, *N. Ravivikar*, Intel Corporation, *B.A. Helms*, Lawrence Berkeley National Laboratory, *R. Prasher*, Sheetak, Inc., *D.Frank Ogletree*, Lawrence Berkeley National Laboratory

It has been more than a decade since the experimental demonstration that the thermal conductivity of carbon nanotubes can exceed that of diamond, which has the highest thermal conductivity among naturally existing materials. In spite of tremendous promise as a thermal material, results have been disappointing for practical thermal systems and applications based on nanotubes. The main culprit for the dramatic shortfall in the performance of nanotubes in practical systems is high thermal interface resistance between them and other components due to weak adhesion at the interface. We demonstrated a six-fold reduction in the thermal interface resistance between both oxide-forming and noble metal surfaces and vertically aligned multi-wall carbon nanotube arrays after bridging the interface with short, covalently-bonded organic molecules. Increased thermal transport was associated with a significant increase in interface mechanical adhesion [1]. Functionalized CNT thermal interfaces were shown to be stable in air for many months and resistant to thermal stress up to 180° C. We were also able to independently determine the intrinsic CNT interface resistance and the fraction of the CNT array contributing to thermal transport by preforming multi-frequency time-domain thermo-reflectance (TDTR) measurements. Since our interface-functionalization method avoids destructive solution-phase processing, this development may lead to the practical integration of CNT arrays for thermal management in microelectronic devices

[1] "Enhanced thermal transport at covalently functionalized carbon nanotube array interfaces", Sumanjeet Kaur, Nachiket Ravivikar, Brett A. Helms, Ravi Prasher & D. Frank Ogletree, *Nature Communications* 5 3082 (2014) doi: 10.1038/ncomms4082

11:40am **NS+SE-MoM11 Desktop Nanofabrication with Cantilever-Free Scanning Probes**, *Keith A. Brown, D.J. Eichelsdoerfer, X. Liao, C.A. Mirkin*, Northwestern University

The availability of reliable nanofabrication methods has dictated the pace of progress in many areas of physics, materials science, electronics, and biotechnology. A major deficiency in these fields is our inability to simultaneously control the architecture of soft materials from macroscopic

to nanoscopic length scales. Scanning probe instruments, such as the atomic force microscope, are promising platforms for nanofabrication because they provide direct access to the nanoscale. However, the central barrier to their widespread use as lithographic instruments is throughput, as it is prohibitively slow to pattern large areas with a single nanoscale probe. To address this challenge, we explored a new architecture that utilizes a thin elastomeric film on a glass slide in lieu of cantilevers to enable the use of a massive array of probes in a simple format. Unfortunately, these cantilever-free probe arrays are passive duplication tools where each probe writes a copy of the same pattern. Here, we report on our recent advances in developing techniques for actuating individual probes in cantilever-free arrays and discuss the new scientific directions that these advances enable. Specifically, we present methods for both physically actuating cantilever-free probes using local heating and optically addressing probes that function as light valves for near-field photolithography, and find both to be capable of stitching together high resolution patterns that span multiple probes. These advances in nanofabrication have enabled new types of experiments, and in particular, we present recent progress in the combinatorial study of biochemical interactions and the high throughput fabrication of functional metamaterials using cantilever-free techniques. Taken together, these observations indicate that versatile desktop nanofabrication is possible using scanning probes and that these techniques can address the emerging challenges related to patterning soft materials.

Plasma Science and Technology
Room: 308 - Session PS-MoM

Current Challenges of Plasma Etching Technologies

Moderator: Saravanapriyan Sriraman, Lam Research Corp

8:20am **PS-MoM1 Dielectric Etch Challenges and Evolutions**, *Masanobu Honda*, Tokyo Electron Miyagi Limited, Japan **INVITED**

For 7nm and beyond VLSI nano fabrication, fine process control in the order of nm or less is required, current incremental techniques may not address the challenges for future nano fabrication. In the High Aspect ratio processing such as 3DNAND and DRAM capacitor, miniaturization of the feature dimensions adds challenges to ion-radical transportation to the bottom of the feature, further aggravating etch yield and etch linearity. Further, in Logic MOL SAC, trade-off between the etch linearity and substrate recesses reduction are increasingly being focused. On the other hand, for BEOL interconnects, achievement of within-wafer uniformity of nm or less, and defect reduction at fine-node are added challenges. We have continued to challenge a variety of these dielectric etch issues, in order to provide technical solutions to enable future devices.

With further lithography related challenges and delays, complexity in patterning increases etch related challenges, continuous processing of the multilayer film with high accuracy corresponding to the multi-pattern is required. ARDE, reducing line roughness (LER/LWR), Trim, Hole Shrink and countermeasures in accordance with the thinning of the EUV resist are important challenges that etch has to overcome. We have effectively overcome these problems using unique resist treatment technologies based on high-speed electron beam and a sidewall protection film using DC super-imposed RF plasma system [1,2]. However, we still encounter trade-off when solving these challenges, it is necessary to overcome the trade-off by introducing a new concept to enable further miniaturization.

As noted above, there are many challenges and potential tradeoffs to arrive at an optimal solution; we need a breakthrough to overcome these challenges. We have continued to explore and innovate solutions, as a result we are honing on a possible solution integrating etch and ALD techniques. Establishing this Etch-ALD concept and developing a robust flow will be a major breakthrough in overcoming patterning and other critical level issues related to nano-feature processing dielectrics and to sustain the Moore's Law.

Reference

[1] M. Honda et al., AVS 60th Int. Symp. & Exhibit. (2013)

[2] M. Honda et al., Proc. of SPIE 8328-09 (2012)

9:00am **PS-MoM3 Improving Selectivity for 10nm BEOL Etch Using CSHF7 Gas**, *Robert Bruce*, IBM T.J. Watson Research Center, *T. Suzuki, M. Nakamura*, ZEON Chemicals L.P., *A. Itou, G. Matsuura*, Zeon Corporation, *S.U. Engelmann, N.P. Marchack, E.M. Sikorski*, IBM T.J. Watson Research Center, *J. Lee*, IBM Albany Nanotech Center, *E.A. Joseph*, IBM T.J. Watson Research Center

As the industry moves to the 10nm technology node and beyond, new plasma etch challenges arise in the fabrication of back-end-of-line (BEOL) interconnects that need to be overcome. New materials and ever smaller

critical dimensions require superior performance in etch, especially in minimizing line-edge roughness and low-k dielectric damage and improving hard mask selectivity. During dual damascene trench etch, low-k plasma damage leads to an increase in dielectric constant and pattern collapse. Also, during the self-aligned via (SAV) etch, vias short between one another due to poor metal hard mask selectivity and merging from via to via. Incorporating C5HF7 gas in these etch processes has shown significant improvements overall, because of its selective deposition properties. However, the C5HF7-based etch process needs to be tuned for the specific application, such as superior TiN selectivity for SAV or SiN selectivity for contact etch. In this talk, the optimized C5HF7-based processes for trench, SAV and contact are reviewed and compared. Furthermore, fundamental learning is accomplished using optical emission spectroscopy and x-ray photoelectron spectroscopy to understand the differences in mechanism between the various process regimes.

9:20am PS-MoM4 Effect of 147nm Photons on Porous Organo-Silicon Glass Materials and Damage Improvement by Optimized Cu/Low-k Integration Approaches, L. Zhang, IMEC, KU Leuven, Belgium, Jean-Francois de Marneffe, IMEC, Belgium, M. Lukaszewicz, Wroclaw University of Technology, Poland, S. Barry-Porter, F. Vajda, Trinity College Dublin, Ireland, Y. Sun, IMEC, Belgium, M.H. Heyne, IMEC, KU Leuven, Belgium, M. Baklanov, IMEC, Belgium

Porous organo-silicon glass thin films, with porosities ranging from 8 to 48% and k-values from 2.7 to 1.9 were exposed to 147nm photons and ions emitted in a CCP discharge of Xe. The material changes have been measured by means of various surface and bulk analytical techniques. For high-porosity/low k-value, a strong Si-CH₃ depletion is observed, concomitant with moisture and increase of silanol group density. Surface densification occurs, as well as reduction of porosity. TOF-SIMS elemental profile indicate however that C and O profiles stay rather constant through the film thickness, only slightly changing in absolute value. Change of material properties are reflected in a rapid increase of the bulk dielectric constant. It is observed that 147nm VUV photons dissociate Si-C bonds, releasing -CH₃ and other H-based radicals in the porous matrix, reacting with dangling Si* and forming Si-H. It is shown that Si-H bonds are also dissociated by VUV but their loss is compensated until -CH₃ are completely dissociated. In absence of reactant to form volatile compound with, a major part of those radicals form complex polymers that condensate into the pores, while, upon ambient exposure, moisture react with remaining Si-dangling bonds forming highly polarizable silanol groups. The impact of VUV exposure on low-k dielectrics with varying porosities indicate a direct correlation between absolute Si-CH₃ loss and VUV dose, independent of initial methyl bond density. Change in dielectric properties (k-value) follows the same trend, showing, at fixed VUV dose, a dielectric shift $\Delta k = 1.0$ independent of the pristine k-value.

The observed trend suggest that, besides reactive radical diffusion, photons emitted during plasma processing do severely impede dielectric properties, and therefore need to be tackled appropriately during patterning and integration.

In order to reduce the impact of VUV, hardmasks with high photon absorption and the effect of polymer filling by the P4 or 'pore stuffing' approach were evaluated. Several mask materials were deposited on top of blanket OSG 2.0 low-k films and exposed to 147nm photons. Various polymers with different UV absorption properties were stuffed into porous OSG 2.0 low-k films and then exposed to 147nm photons. For both cases, low-k damage was evaluated and showed reduced VUV damage.

9:40am PS-MoM5 Non-PFC Plasma Chemistries for Patterning Low-k Dielectric Materials, Jack Kun-Chieh Chen, N. Altieri, M. Paine, T. Kim, J.P. Chang, UCLA

Low-k materials, such as fluorine-doped and carbon-doped silicon dioxide, exhibit reduced dielectric constants necessary to curtail parasitic capacitance and avoid crosstalk in devices, keeping pace with the trend of increasing device densities. SF₆ and perfluorocarbons (PFC) gases, which are primarily used in plasma etch of interlayer dielectric materials, generally have high global warming potentials (GWP), making their increased usage undesirable. This work focuses on evaluating etch chemistries from a thermodynamic standpoint for back end of line (BEOL) applications in patterning of proposed low-k carbon-doped silica compounds with varying carbon content. Group and bond additivity methods were used to estimate the Gibbs free energies of formation for these carbon-doped compounds. PFC and non-PFC etchants with H₂/NH₃ were assessed through the use of volatility diagrams comparing partial pressures of volatile etch products as a function of etchant partial pressure at 300K. Minimization of Gibbs free energy was employed to calculate the equilibrium distribution of species in the etch system across a range of temperatures. NF₃ and CF₃I were identified as potentially viable for etching carbon-doped silica. NF₃, a non-PFC gas with an atmospheric presence of 1ppt, GWP of 16,800, and much greater abatement efficacy, is the most effective etchant in pure form,

producing volatile etch product pressures between six and eight times that produced by CF₄. CF₃I, despite being an iodofluorocarbon gas, exhibited a GWP of unity and displays reduced damage to doped carbon, making it preferable in etching carbon-doped silica. Pure CF₃I shows reduced product pressure with increasing carbon content; however, addition of H₂ and NH₃ improves its performance for the three most highly doped silica compounds. Given the higher cost associated with using NF₃ and CF₃I, the introduction of an additive (H₂ or NH₃) was assessed. Addition of H₂ and NH₃ generally showed an increase in partial pressures predicted by the volatility diagrams, with H₂ producing a much more significant increase than the pure etchant or the addition of NH₃. Preliminary experimental results comparing etch rates for moderately to highly carbon-doped silica samples with 20 sccm CF₄ and hydrogen addition generally agree with theorized predictions. Varying the feed composition between 0%, 20%, and 50% H₂, etch rates of 38.2, 44.8 and 48.86 nm/min were recorded for lightly doped silica, and 49.2, 73.0 and 128.2 nm/min were recorded for heavily carbon-doped silica.

10:00am PS-MoM6 Optimization of the Optical Transmission of Submicron Silicon-on-Insulator Rib Waveguides, Marc Fouchier, E. Pargon, CNRS/UJF/CEA-LTM, France, B. Ben Bakir, P. Brianceau, J. Harduin, S. Barnola, P. Grosse, CEA-LETI, France

Optical interconnects have largely replaced copper for long distance data transmission and are gaining interest on shorter distances. At the intra-chip level, silicon waveguides are foreseen to relieve copper wire bottlenecks in the BEOL layers. The strong light confinement allowed by the large refractive index difference between Si and SiO₂ permits the building of submicron silicon on insulator (SOI) waveguides with small bending radii and thus of compact photonic circuits. However, the strong light confinement also results in large propagation losses due to the scattering of the guided light on the rough etched sidewalls of the silicon core. Modeling shows that the transmission loss mostly depends on the line edge roughness (LER) of the guide and on its correlation length.

In the present work, we apply our silicon processing and sidewall roughness metrology know-how developed for transistor gates to optimize the fabrication process of submicron rib waveguides on 200 mm SOI wafer in order to reduce their optical loss. First SiO₂ and photoresist etch masks are evaluated. In both cases, the eventual benefit of an HBr plasma cure treatment, originally developed for FEOL processing, on the photoresist is also assessed. Second, we investigate the impact of several silicon smoothing strategies on the patterned waveguides: thermal oxidation and hydrogen annealing. Oxidations are performed in pure O₂ at 1000°C, above the SiO₂ viscous transition. The following thicknesses are tested: 5, 10, 30 and 3 × 10 nm. Oxidizing in three steps compared to a single longer step is believed to increase LER reduction because smoothing is faster in the initial reaction limited regime than in the subsequent diffusion limited regime. Hydrogen annealing is performed in pure H₂ for 2 min at several temperatures between 850 and 1000°C. After each process step the LER is measured by CD-SEM. In order to obtain LER values freed from instrumental noise and their correlation length, CD-SEM data are treated by spectral analysis. At the end of the process, the sidewall roughness of the rib waveguides is also characterized by AFM on a tilted sample. In addition, their profile is measured by cross-sectional SEM and their transmission loss on an optical test bench.

Measurements show that a resist mask is better than the SiO₂ mask for minimizing optical attenuation at the price of a degraded profile while the photoresist cure treatment does not have much influence. Further experiments are ongoing to evaluate the impact of the silicon smoothing processes (hydrogen annealing or thermal oxidation) on the roughness and to correlate it with optical loss measurements.

10:40am PS-MoM8 Using Post Etch Treatment (PET) to Resolve Poly Residue Defect Issue of Dummy Poly Removal (DPR) in hi-K Metal Gate Processing, Chih-Chien Wang, F.Y. Chang, C. Li-Chiang, S.-Y. Lu, United Microelectronics Co., Taiwan, Republic of China, P.-W. Huang, Y.-C. Kao, S.-Y. Cheng, T.-T. Su, Lam Research Corporation

Dummy Poly Removal (DPR) is one of the critical processes of hi-K metal gate formation of gate last integration scheme of semiconductor wafer fabrication. A typical DPR process flow includes plasma etching a wafer to open hardmask and to remove dummy poly, then wet etch the wafer with Tetra-Methyl Ammonium Hydroxide (TMAH) to remove any residue that is remained inside the dummy gate trench.

Amorphous silicon is commonly used as the dummy poly materials. A plasma composed of Cl₂, HBr, NF₃, or combination of above is used to dry etch the dummy poly; however, poly residue defect is observed after DPR process flow. Experimental data indicates that after plasma etch, a Si-O layer is formed on the surface of amorphous silicon which suppress the dummy poly removal capability of the subsequent wet etch. Therefore, dummy poly material is left behind and forms the poly residue defects.

If extended plasma is used to remove the poly residue, the barrier layer (TiN) will be etched and thus damage the hi-K.

To resolve the poly residue defect issue, a post etch treatment (PET) is added after dummy poly is etched by plasma. The purpose of PET is three-folded: it converts the Si-O layer to a layer of which wet etch rate is significantly improved; PET activates the residual F, Cl or Br inside the gate trench and enhance the poly removal; PET has high selectivity to the barrier layer (TiN) and thus TiN film is preserved. The result is no poly residue defects and no hi-K damage.

11:00am **PS-MoM9 Sidewall Roughness Characterization of an Advanced Spacer Patterning Process**, *Emmanuel Dupuy, M. Fouchier, E. Pargon, CNRS-LTM, France, J. Pradelles, CEA-Léti, France, H. Grampeix, CEA-LETI, France, P. Pimenta-Barros, S. Barnola, CEA, LETI, France, O. Joubert, LTM - CEA/LETI, France*

Line width roughness (LWR) or line edge roughness (LER) is considered today by the microelectronic industry as a critical factor limiting CMOS transistors downscaling. According to the international technology roadmap for semiconductors, LWR and LER values must be controlled below 2 nm for the next sub-20 nm nodes, which remain a technological challenge for all nanopatterning options and metrology tools. Understanding and minimizing LER at this nanometer scale thus requires an accurate and insightful characterization of the sidewall roughness.

Among advanced nanopatterning solutions, spacer patterning has emerged as a reliable and competitive technique to fabricate fine patterns down to 10 nm. This technique consists in depositing a spacer material on each side of a core (mandrel) defined by lithography and then removing the core to halve the pitch. One critical aspect of this approach is the control of the LER since the spacer patterns are asymmetric from their formation. The right and left sides of the spacer are not obtained by the same technological step and could lead to different LER values on the left and right sidewalls. This behaviour could be problematic if this asymmetry is transferred to the final pattern.

In this work, we propose to characterize and evaluate finely the LWR/LER evolution after each technological step involved in a resist-core spacer patterning process targeting a half-pitch of 20 nm and 10 nm. In this particular case, spacers are directly deposited on the side of the resist. Advantages are less processing steps, a simplified stack and a reduced production cost. A method based on a power spectral density (PSD) analysis is used take into account the noise level of CDSEM images in the LWR/LER estimation of these fine patterns. A full description of the sidewall roughness including its spatial frequency distribution is obtained at each step with an estimation of noise-free parameters such as roughness amplitude (3σ), correlation length (ξ), and roughness exponent (α). For the 20 nm node, LWR and LER values are drastically reduced to 2.5nm and 2.2nm respectively. The correlation length is found to range from 8 to 22 nm and the roughness exponent from 0.4 to 0.9 for the final silicon lines. Results for the 10 nm node will be discussed in view of evaluating and optimizing process performances.

11:20am **PS-MoM10 Improving Pattern Fidelity for Selective Etch Processes**, *Nathan Marchack, S.U. Engelmann, E.A. Joseph, R.L. Bruce, H. Miyazoe, E.M. Sikorski, IBM T.J. Watson Research Center, T. Suzuki, M. Nakamura, ZEON Chemicals L.P., A. Itou, H. Matsumoto, Zeon Corporation*

As critical dimensions and pitch sizes of integrated circuit technologies continue to decrease, the challenges associated with maintaining pattern transfer fidelity become especially difficult to surmount. LER/LWR, CD variation, iso/dense feature loading and deformation of the organic soft masks are commonly observed phenomena. Other issues include extensive plasma damage or mask retention for post-lithography solutions.¹

Our team recently introduced a new etch gas which is able to etch nitride by selective deposition of a fluorocarbon layer², analogous to the well established oxide etch mechanism commonly used in manufacturing.³ Selective deposition was achieved by redesigning the FC etch gas, where reaction with a nitride substrate layer reduces the FC film thickness compared to silicon or oxide substrates. Owing to the complex, distinct nature of the reaction pathways offered by this new plasma chemistry, optimizing the etch performance involves tuning plasma parameters that have not been traditionally investigated. We have evaluated the influence of substrate and showerhead temperatures, gas admixture chemistry and plasma pulsing on the performance of this etch gas for hard mask patterning applications.

By tuning the chemical admixture of the plasma, 50nm pitch patterning of an 80nm thick nitride hard mask layer using a 65nm carbon mask was achieved with greatly reduced LER/LWR (~2.3/2/7) and minimal iso/dense feature loading compared to a traditional CF₄/CHF₃ mixture (LER/LWR ~5/8). The use of plasma pulsing, as well as lowering the lid temperature, was found to increase the carbon mask retention while maintaining reduced

LER/LWR. The effect of lid temperature was shown to be related to gas dissociation, which was observed through full spectrum OES spectra collected. The improved mask retention under these conditions allowed for LER/LWR to be reduced even further by reducing the aspect ratio of the structures.

1. S. Engelmann et al., Proc. SPIE 8328-9
2. S. Engelmann et al., AVS 58th Int. Symp. & Exhibit. (2011)
3. M. Schaeckens et al., J. Vac. Sci. Technol. A 17, 26 (1999)

Novel Trends in Synchrotron and FEL-Based Analysis Focus Topic

Room: 312 - Session SA-MoM

Synchrotron Studies of Processes in Energy Conversion, Electronic Devices and Other Materials I

Moderator: Franz Himpsel, University of Wisconsin-Madison

8:20am **SA-MoM1 Looking Into Buried Interfaces with Soft/hard X-Ray Photoemission and Standing-Wave Excitation**, *Charles Fadley, University of California, Davis* **INVITED**

I will present some new directions in synchrotron radiation soft x-ray photoemission (XPS, SXPS) and hard x-ray photoemission (HXPES, HAXPES, HIKE) [1-6], with illustrative examples of applications to a range of sample types. These involve combined SXPS and HXPES studies of buried layers and interfaces in magnetic and transition-metal oxide multilayers [1,2], as well as in semiconductor junctions [3]; solid-gas or solid-liquid interfaces with high ambient pressures [5]; band-offset measurements in multilayer structures [6]; and the use of standing waves from multilayer mirrors to enhance depth contrast in spectroscopy [1-5].

References

This work was supported by the U.S. Department of Energy under Contract No. DE-AC02-05CH11231, the Army Research Office, under MURI Grant W911-NF-09-1-0398, the Forschungszentrum Julich, Peter Grunberg Institute, and the APTCOM project of Le Triangle de Physique, Paris.

1 "Determination of layer-resolved magnetic and electronic structure of Fe/MgO by standing-wave core- and valence- photoemission", See-Hun Yang, Benjamin Balke, Christian Papp, Sven Döring, Ulf Berges, L. Plucinski, Carsten Westphal, Claus Schneider, Stuart S. P. Parkin, and Charles S. Fadley, Phys. Rev. B 84, 184410 (2011).

2 "Interface properties of magnetic tunnel junction La_{0.7}Sr_{0.3}MnO₃/SrTiO₃ superlattices studied by standing-wave excited photoemission spectroscopy", A. X. Gray et al., Phys. Rev. B 82, 205116 (2010); and A.X. Gray et al., Europhysics Letters 104, 17004 (2013).

3 "Nondestructive characterization of a TiN metal gate: chemical and structural properties by means of standing-wave hard x-ray photoemission spectroscopy", C. Papp, G. Conti, et al. J. Appl. Phys. 112, 114501 (2012).

4 "Hard X-ray Photoemission with Angular Resolution and Standing-Wave Excitation", C. S. Fadley, invited review, J. Electron Spectrosc. 190, 165-179 (2013)

5 "Chemical-state resolved concentration profiles with sub-nm accuracy at solid/gas and solid/liquid interfaces using standing-wave ambient-pressure photoemission (SWAPPS)", S. Nemsak et al., in preparation

6 "Band Offsets in Complex-Oxide Thin Films and Heterostructures of SrTiO₃/LaNiO₃ and SrTiO₃/GdTiO₃ by Soft and Hard X-ray Photoelectron Spectroscopy", G. Conti, A. M. Kaiser, A. X. Gray, S. Nemsák, G. K. Pálsson, J. Son, P. Moetakef, A. Janotti, L. Bjaalie, C.S. Conlon D. Eiteneer, A.A. Greer, A. Keqi, A. Rattanachata, A.Y. Saw, A. Bostwick, W.C. Stolte, A. Gloskovskii, W. Drube, S. Ueda, M. Kobata, K. Kobayashi, C. G. Van de Walle, S. Stemmer, C. M. Schneider and C. S. Fadley, J. Appl. Phys. 113 143704 (2013).

9:00am **SA-MoM3 Hard X-ray Photoelectron Spectra (HXPES) of Bulk Non-Conducting Silicate Glasses**, *Yongfeng Hu, Q.F. Xiao, X.Y. Cui, D. Wang, Canadian Light Source, Canada, G.M. Bancroft, H.W. Nesbitt, M. Biesinger, University of Western Ontario, Canada*

Bulk studies of non-conducting oxides and silicates, such as silicate glasses containing cations such as Na, K, Mg and Ca are important to obtain quantitative *bulk* information of bridging oxygen (Si-O-Si, so-called BO), non-bridging oxygen (Si-O-M, so-called NBO), and "free oxygen (M-O-M). These studies have been so far limited to the XPS studies using spectrometers equipped with modern charge compensation systems, such as Kratos or ESCALAB 250Xi.^{1,2} Such measurements are very important for

determining the chemical and physical properties of a wide variety of silicate minerals and glasses². Synchrotron-based hard X-ray photoelectron spectroscopy (HXPES) has recently been applied to the characterization of surfaces and interfaces of advanced materials. In this work, we will demonstrate that the HXPES, without any charge compensation system, can avoid the large differential charging problems usually seen with bulk non-conductors using conventional XPS instruments. These problems are overcome by depositing a thin metal coating on the glass surface and by taking advantage of the large and variable probing depth offered by HXPES. We show that the optimal O 1s linewidth, matching to that of the Krotos' results, can be obtained for the non-conducting silicate glasses using HXPES. Together with the high resolution Si 1s results, these HXPES data are critical for accurate analysis of the BO, NBO and free oxide content of these silicate glasses.

[1] H. W. Nesbitt, G.M. Bancroft, G.S. Henderson, R.Ho, K.N. Dalby, Y. Huang, Z. Yan, *J. Non-Cryst. Solids* 357 (2011) 170.

[2] H.W.Nesbitt, G.M. Bancroft, *Rev. Min. Geochem.* 78 (2014) 271.

9:20am **SA-MoM4 In Situ Study of Plasma Assisted Atomic Layer Epitaxy of III-N Semiconductors Using Synchrotron X-ray Methods**, N. Nepal, Naval Research Laboratory, M.G. Erdem, Boston University, S.D. Johnson, V.R. Anderson, Naval Research Laboratory, A. DeMasi, K.F. Ludwig, Boston University, **Charles Eddy, Jr.**, Naval Research Laboratory Atomic layer epitaxy (ALE) is a relatively new method to grow crystalline materials in a layer-by-layer fashion by separating the growth reaction into two surface-mediated, self-limiting half reactions at relatively low temperatures. Recently, plasma assisted ALE (PA-ALE) has been used to grow epitaxial III-nitride films at temperatures from 180-500°C [1-2]. At these growth temperatures, the ad-atom mobility is low and the growth process is highly dependent on the quality of the growth surface. Thus, understanding the mechanism of nucleation and growth kinetics is very important to improving material quality. A promising method for *in situ* monitoring involves the use of high intensity coherent x-rays, such as from a synchrotron light source, and includes small angle reflectance/scattering, diffraction, and fluorescence.

We present initial *in situ* studies of the PA-ALE process using synchrotron x-ray radiation, and grazing incidence small angle x-ray scattering (GISAXS), x-ray reflectivity (XRR), and in-plane x-ray diffraction (XRD) measurements. Investigations focus on the *in situ* surface preparation process and initial stages of epitaxial growth of AlN and InN on GaN template layers. Experiments were conducted in a custom PA-ALE growth facility installed at beamline X21 of the National Synchrotron Light Source. Surface evolution during the *in situ* surface preparation process was monitored by GISAXS and the nucleation and growth processes for AlN and InN were monitored using GISAXS, XRR, and in-plane XRD. Atomic force microscopy (AFM), x-ray photoelectron spectroscopy and out-of-plane XRD were employed as post growth characterizations.

In situ XRR measurements of an optimized growth process for AlN on a 450°C substrate revealed a 0.08 nm/cycle growth rate and clearly shows each half-cycle of the AlN growth process. *Ex situ* AFM measurements confirm that the surface roughness after growth was similar (RMS roughness = 0.74 nm) to that of the GaN substrate. We compare the *in situ* in-plane synchrotron XRD study with previous reports[2] of AlN/GaN grown in a Cambridge Nanotech Fiji reactor to assess the material quality grown in the *in situ* chamber. The in-plane XRD measurement on pre-grown ALE AlN confirms the epitaxial nature and wurtzite structure with 60 degree symmetry in Φ -scan. These early results demonstrate that *in situ* synchrotron x-ray characterization methods are a powerful tool for exploring the epitaxial nucleation and growth mechanisms of III-nitride layers by PA-ALE.

1. N. Nepal, et al., *J. Cryst. Growth and Des.* **13**, 1485 (2013).

2. N. Nepal, et al., *Appl. Phys. Lett.* **103**, 082110 (2013).

9:40am **SA-MoM5 Application of Synchrotron Radiation Based Hard X-ray Photoelectron Spectroscopy (HXPES) to Characterise Semiconductor Device Structures**, **Greg Hughes, L. Walsh**, Dublin City University, Ireland, J.C. Woicik, National Institute of Standards and Technology (NIST), P.K. Hurley, Tyndall National Institute, Ireland

INVITED

Hard x-ray photoelectron spectroscopy (HXPES) is emerging as a technique which has the capability to provide chemical and electronic information on much larger depth scales than conventional XPS. This has potential applications in the study of oxide/semiconductor and metal/semiconductor buried interfaces found in device structures, particularly after annealing cycles. In this presentation results of combined hard x-ray photoelectron spectroscopy (HXPES) and electrical characterisation measurements on identical Si and III-V based metal-oxide-semiconductor (MOS) structures will be presented. The experimental

findings obtained indicate that surface potential changes at the semiconductor/dielectric interface due to the presence of a thin metal gate layer can be detected with HAXPES. Changes in the semiconductor band bending at zero gate voltage and the flat band voltage for the case of metal gate layers derived from the semiconductor core level shifts observed in the HAXPES spectra are in agreement with values derived from C-V measurements.

The III-V material InGaAs, shows promise as the channel material in high speed n-MOSFETs however, the issue of low resistance source/drain (S/D) contacts to InGaAs remains. A possible solution is to find a self-aligned silicide like material (salicide) to act as the S/D contacts. The search for this material has recently focussed on Ni-InGaAs, due to its promisingly low R_s and its apparent abrupt interface with InGaAs. Results of a HAXPES study of the Ni-InGaAs alloy system has been undertaken in order to determine the nature of the Ni-InGaAs interface and its evolution as a function of annealing temperature. The results show that Ni readily interacts with InGaAs upon deposition at room temperature resulting in significant inter-diffusion and the formation of NiIn, NiGa, and NiAs alloys. This information when combined with x-ray absorption spectroscopy (XAS) measurements can be used to develop a structural and chemical compositional model of the Ni-InGaAs system as it evolves over a thermal annealing range of 250-500 °C.

10:40am **SA-MoM8 Correlative Probing of the Surface Chemistry and Electron Transport of Nanodevices in Operando Mode using Scanning Photoelectron Emission Microscopy**, **Andrei Kolmakov**, National Institute of Standards and Technology (NIST)

INVITED

The surface as well as interfacial properties of nanoscopic devices are intimately linked to their electronic transport properties. In addition, they have a strong dependence on their dimensions, faceting and stoichiometry. As a result, the traditional measurements on the ensembles of nanostructures would suffer from significant averaging effects and need to be replaced with testing of individual well characterized nanostructure. In this report, we demonstrate few examples of correlative imaging, spectroscopy and transport measurements on individual working nanodevices using capabilities of modern synchrotron radiation based photoelectron microscopy. In particular, the surface analysis of the operating MEMS nanowire sensor model device being coupled with scanning x-ray beam induced current microscopy correlates real time changes in conductance of the nanowire with formation of the specific surface groups upon redox reaction. The effect of the electrodes and electroactive defects in the devices on their performance will be discussed. The perspectives of the in operando device characterization at real world pressures and temperatures will be outlined.

11:20am **SA-MoM10 A NEXAFS Spectromicroscope for Structural and Chemical Imaging Analysis**, **Conan Weiland**, Synchrotron Research, Inc., Z. Fu, C. Jaye, D.A. Fischer, National Institute of Standards and Technology, K. Scammon, University of Central Florida, P.E. Sobol, E.L. Principe, Synchrotron Research, Inc.

INVITED

We present the development of a Large Area Rapid Imaging Analytical Tool (LARIAT MKII) for near edge x-ray absorption fine structure (NEXAFS) surface chemical and structural analysis. This analyzer utilizes magnetostatic and grid-less electrostatic lenses to maintain the lateral distribution of electrons into a 16 mega channel detector, allowing for a 180° collection angle for high collection efficiency enabling rapid parallel imaging. The system is in development for installation at the NIST SST beamline at NSLS II. Initial images from LARIAT MKII, currently installed at NSLS, will also be presented. The images demonstrate the system's imaging capabilities, with resolution approaching 5 μm for C K-edge images.

Advanced Surface Engineering

Room: 302 - Session SE+EM+EN+PS+TF-MoM

New Developments in Atmospheric Pressure Plasma Deposition and Thin Films for Energy Applications

Moderator: Hana Barankova, Uppsala University, Sweden, Michael Stueber, Karlsruhe Institute of Technology

8:40am **SE+EM+EN+PS+TF-MoM2 Real Time Characterization of Polymer Surface Modification by an Atmospheric Pressure Plasma Jet**, Andrew Knoll, P. Luan, E.A.J. Bartis, C. Hart, University of Maryland, College Park, Y. Raitses, Princeton Plasma Physics Laboratory, G.S. Oehrlein, University of Maryland, College Park

Atmospheric pressure plasma jets (APPJ) have been shown to modify surfaces, leading to a variety of potential industrial and medical applications. APPJ treated surfaces are typically evaluated post treatment, but few studies exist showing surface changes in real time. In this study, we characterized both closely-coupled and remote APPJ treatments of a PMMA-based 193 nm photoresist polymer (PR193) using *in situ* ellipsometry to monitor film thickness and refractive index in real time. The kilohertz-driven, two-ring electrode APPJ was fed with low admixtures of O₂ and N₂ to Ar. Voltage and current waveforms were collected to electrically characterize the APPJ and measure power dissipation. In addition, high speed photography of the APPJ was conducted in order to characterize plasma interaction with various controlled environments and with PR193. Ellipsometry shows that PR193 etch rates depend on the feed gas chemistry and treatment time. Etch rates are reduced for Ar/O₂ compared with pure Ar and Ar/N₂. This reduction is correlated to a decrease in plasma density with O₂ addition. It is also shown that the etch rate changes over time initially during APPJ heating and reaches steady state as the temperature stabilizes. When the plasma is brought close enough to the sample, the discharge couples with the surface and arcing to the film occurs. This interaction greatly increases the etch rate and introduces major damage to the polymer, which can be observed by the naked eye. From electrical data and high speed photography we see that the pure Ar discharge exhibits filamentary behavior that is enhanced by O₂ addition and rendered more diffuse by N₂ addition. High speed photography shows that the coupling of the plasma and the environment increases when the environment matches the feed gas chemistry, which causes the plume to extend farther than in open air. While the Ar plume is confined to a single plasma channel, N₂ admixture to Ar branches out into many smaller discharges, similar to a Lichtenberg figure. We also correlate damage seen on the polymer surface with observed arcing. The authors gratefully acknowledge financial support by US Department of Energy (DE-SC0001939).

9:00am **SE+EM+EN+PS+TF-MoM3 Gas-Liquid Mixed Phase Plasma at Atmospheric Pressure**, Akira Ando, G. Tang, R. Ohno, A. Komuro, K. Takahashi, Tohoku University, Japan **INVITED**

A gas-liquid mixed phase plasma discharge is investigated using nanosecond high-voltage pulse generator. Non-thermal atmospheric pressure plasmas have recently attracted significant attention due to their good energy efficiency in production of reactive species. Plasma in water can generate many reactive species, such as ozone, hydroxyl radicals and oxygen radicals. These products have strong oxidizing power and is applicable for many applications without any thermal stress.

We have utilized a nanosecond high-voltage pulse to produce a discharge within bubbles introduced into water, where semiconductor opening switching (SOS) diodes are used in the pulse generator.

The reactor for the gas-liquid hybrid plasma consists of two regions, gas and liquid regions, separated by a thin plate with a small holes (1mm in diameter). Several working gases are fed into the reactor from the gas region and bubbles are formed via the separator holes in the water. High-voltage pulse with 10-15kV are applied to a wire electrode situated in the gas phase. A grounded electrode is set into the water. When the high voltage pulse with the duration of 40ns is applied, a streamer-like discharge occurs within the bubbles and the streamer extends along the surface of gas-liquid interface.

The formation process of discharge bubbles were observed with a high-speed CCD images of the discharge. The area of discharge extension depends on the gas species and conductivity. Production rate of reactive species, ozone and hydroxyl radicals in a discharge reactor was also depends on the parameters. As the life time of hydroxyl radicals is very short, the amount is estimated from concentration of hydrogen peroxide produced in treated water, which is produced by the recombination process of hydroxyl radicals.

In order to evaluate the oxidation power in the gas-liquid mixed plasma, we applied it to water purification, such as decolorization, sterilization and

decomposition of persistent organic pollutants (POPs). The sterilization effect in the water is estimated from the survival ratio of bacillus subtilis and it reaches more than 99.5% after 15min treatment. The survival ratio is large in air discharge and the value of pH in water as well as ultraviolet (UV) ray generated by plasma discharge affects the sterilization. SEM images shows the surface of the bacteria were damaged by the treatment.

9:40am **SE+EM+EN+PS+TF-MoM5 Atmospheric Pressure High Power Impulse Plasma Source (AP-HiPIPS) for Plasma Enhanced Chemical Vapor Deposition of Thin Films**, Vasiliki Poenitzsch, R. Wei, M.A. Miller, K. Coulter, Southwest Research Institute

Southwest Research Institute is currently developing a High Power Impulse Plasma Source (HiPIPS) that supplies a high flux of energetic reactants to a surface while maintaining a low processing temperature. HiPIPS is a new plasma enhanced chemical vapor deposition technology that combines variable pressure plasma jets with advanced pulsed power technology. Several complementary techniques, including mass spectroscopy, optical emission spectroscopy (OES) and electrical and thermal probes were employed, for measuring and calculating the plasma characteristics in a wide range of the HiPIPS process parameters and conditions. The preliminary HiPIPS experiments have revealed that high peak power (~40 kW) in the pulses can be achieved resulting in a high peak current (~200 A) and increased plasma density (i.e. $n = \text{Ar}: 10^{20} \text{ cm}^{-3} \text{ s}^{-1}$) while maintaining a low average power (35W) and a low substrate processing temperature (50-150 °C). A prototype atmospheric-pressure HiPIPS (AP-HiPIPS) was successfully developed and proof-of-concept AP-HiPIPS diamond-like carbon (DLC) film deposition was demonstrated. Beyond DLC films, HiPIPS plasmas could be applicable to deposition of many classes of films and many types of surface treatments. In contrast to conventional state-of-the-art non-thermal atmospheric pressure plasma jets, typically driven by RF or AC, the power densities and currents during pulse on-time are 2-3 orders of magnitude higher in HiPIPS. Since plasma is created through inelastic electron collision with precursor gas molecules, the increased power and current directly equates to significantly improved ionization and dissociation of precursor gases in HiPIPS. Thus, distinguishing features of HiPIPS as compared to RF or AC APPJs are increased ionization, enhanced molecular gas dissociation, and higher flux of reactive species while maintaining the same low deposition temperatures. In this presentation, an overview of HiPIPS and AP-HiPIPS will be given with a specific focus on plasma characteristics and areas for further development.

10:00am **SE+EM+EN+PS+TF-MoM6 Importance of Argon's Spectral Emission for Plasma Diagnostics at an Atmospheric Open Air Plasma Discharge**, Vladimir Milosavljevic, J. Lalor, P. Bourke, P.J. Cullen, Dublin Institute of Technology, Ireland

In recent years, plasma on atmospheric pressure attracts a lot of attention due to their numerous applications in plasma biology, health care, and medicine, as well as surface and materials processing and nanotechnology. Among several atmospheric pressure plasma devices, a dielectric barrier discharge plasma jet (DBDPJ) is the most used, because of its simplicity and a fact that the generated plasma is in surrounding air and not in a confined space. The dynamics of DBDPJ in noble gases reveal that the plasma plumes propagate at a speed several orders of magnitude higher than the gas flow velocity. This is why it is generally accepted that the propagation of the plasma plumes is driven electrically rather than by the gas flow, which imposes in the first place the importance of the plasma diagnostics. Because of the frequent collisions between electrons and neutrals at high pressure, the electrical probe methods are generally less useful for plasmas produced at atmospheric pressure. Therefore, other diagnostic methods are needed and optical emission spectroscopy (OES) has been used as one of the alternative diagnostics because of its simplicity and non-intrusive nature.

Nitrogen dominates the ionic composition of atmospheric discharge and has an impact on the breakdown voltage. Nitrogen acts as a 'sensor gas' and OES diagnostics are applied in assumption that most nitrogen molecular emissions are excited during electron impact of ground state N₂(X). When nitrogen is added/mixed with argon plasma discharges, the argon emission lines are significantly quenched and the resulting plasma spectral emission is changed. Measurements and analysis of neutral argon spectral emission lines give very important information about the plasma properties. In this work the absolute spectral emissions of the atomic and molecular lines associated with argon, oxygen, nitrogen and hydrogen are presented. Wavelength resolved optical emission profiles of argon's spectral lines shows that the change in electron energy distribution functions (EEDF) has taken place for a low gas flow rate only. After the gas flow rate goes above a certain limit, the EEDF remains constant. At the same time the density of argon metastable atoms are changed with the gas flow rate. Overall, analysis of the spectral intensities assist in the development of optimised plasma processing parameters for treatments such as surface activation or removal of contaminants.

The research leading to these results has received funding from the European Union's Seventh Framework Programme managed by REA Research Executive Agency (FP7/2007-2013) under Grant Agreement number 605125

10:40am **SE+EM+EN+PS+TF-MoM8 Hot 'n Flaky: Thermal Properties of Layered Atomic Structures, Christopher Muratore, University of Dayton, V. Varshney, Air Force Research Laboratory/UTC, J.J. Hu, Air Force Research Laboratory/UDRI, A.A. Voevodin, Air Force Research Laboratory** **INVITED**

Synthesis capability for uniform growth of 2D materials over large areas at lower temperatures without sacrificing their unique properties is a critical pre-requisite for seamless integration of next-generation van der Waals heterostructures into novel devices. We have demonstrated, for the first time, vapor phase growth techniques for precisely controlled synthesis of continuous, uniform molecular layers of all MoX₂ and WX₂ transition metal dichalcogenide (TMD) compounds on diverse substrates, including graphene, hexagonal boron nitride, highly oriented pyrolytic graphite (HOPG), SiO₂, and metal substrates over several square centimeters. Preliminary results show MoX₂ and WX₂ transition metal dichalcogenide materials grown in a novel ultra-high vacuum (UHV) physical vapor deposition (PVD) process demonstrate properties identical or even superior (e.g., electron mobilities >500 cm² V⁻¹ s⁻¹) to exfoliated layers. Growth of bi-layer MoS₂ on few-layer graphene with a 30% lattice mismatch and TMD/TMD heterostructures are shown to demonstrate how natural accommodation of stresses at 2D van der Waals interfaces has the remarkable potential to transform the way materials selection is considered for synthetic heterostructures, as concerns regarding lattice constant matching can be abandoned with preference given to desired properties and performance. Investigations relating to application of these materials in thermoelectric device applications are presented. Thermal conductivity values of TMD thin films were compared to bulk crystals, revealing expected trends with mass, but a >10 fold reduction in thin film thermal conductivity. Phonon scattering lengths at domain boundaries based on computationally derived group velocities were consistent with the observed film microstructure, accounting for the reduction. We also explore thermal anisotropy in MoS₂ films. Measurement results are correlated with MD simulations of thermal transport for perfect and defective MoS₂ crystals, demonstrating the importance of thermal boundary scattering.

Surface Science

Room: 309 - Session SS+AS+EN-MoM

Mechanistic Insights into Surface Reactions: Catalysis, ALD, etc.

Moderator: Falko Netzer, University of Graz, Junseok Lee, National Energy Technology Laboratory

8:20am **SS+AS+EN-MoM1 Electron Trap or Atomic Hydrogen Recombination Catalyst? The Role of Metals in Photocatalysis Revisited, J.-B. Joo, R.J. Dillon, I. Lee, C.J. Bardeen, Francisco Zaera, University of California - Riverside** **INVITED**

The production of hydrogen from water with semiconductor photocatalysts is often promoted by the addition of a small amount of a metal to their surfaces. It is commonly believed that the resulting enhancement in catalytic activity is due to a fast transfer of the excited electrons generated by photon absorption from the semiconductor to the metal, a step that prevents de-excitation back to the ground electronic state. Here we provide several pieces of evidence to argue against this mechanism. An alternative explanation is advanced where the metal acts as a catalyst for the recombination of the hydrogen atoms made via the reduction of protons on the surface of the semiconductor instead. New metal@TiO₂ yolk-shell nanomaterials were conceived to test our hypothesis, and the preparation and characterization of those will be discussed in this presentation as well.

9:00am **SS+AS+EN-MoM3 Atomically Resolved Observation of Defects Catalysing Phase Transitions in an Adsorbate System, M. Cordin, B.A.J. Lechner, S. Duerrbeck, A. Menzel, Erminald Bertel, University of Innsbruck, Austria, J. Redinger, Vienna University of Technology, Austria, C. Franchini, University of Vienna, Austria**

First order phase transitions exhibit a nucleation barrier. Normally, the barrier is lowered by heterogeneous nucleation at interfaces or extrinsic defects. Homogeneous nucleation, in contrast, is strongly activated and results in a significant hysteresis. Molecular dynamics calculations have suggested that an important step in homogeneous nucleation involves the formation and subsequent separation of defect pairs¹⁻².

Here we report a (2x1)→c(2x2) order-order phase transition in a two-dimensional (2D) adsorbate system (Br/Pt(110) at 0.5 monolayer coverage) as a function of temperature³. Although an order-order phase transition is first-order according to Landau rules, the present system exhibits strong fluctuations within a wide temperature range (50K-250K). At 50 K the fluctuations are sluggish enough to allow atomically resolved observation of the phase conversion mechanism by temperature-variable Scanning Tunneling Microscopy. The transition is heralded by local density fluctuations in the adsorbate. The density variation consists of a compression (soliton) and a dilution (anti-soliton). At the transition temperature the two defect moieties are able to separate and travel independently through the system, thereby converting one phase into the other. Away from the transition temperature, separation of the defect pair would create the "wrong" phase, thus increasing the free energy of the system. This is equivalent to an effective attractive interaction between soliton and anti-soliton, in close analogy to the string interaction in spin systems⁴. The one-to-one correspondence can be made transparent by introducing a pseudo-spin variable, i.e. an occupation number +/-1 assigned to every bonding site. The defect-pair separation mechanism partially circumvents the nucleation barrier and thus promotes fluctuations, particularly in low-dimensional systems.

Defect-pair separation as a key step in phase transitions is a concept which arose from the analysis of molecular dynamics calculations. To our knowledge, the present study represents the first direct experimental observation with atomic resolution of such a mechanism. Furthermore, it illustrates the important role of the string interaction in suppressing fluctuations, which is very efficient in 3D systems, weaker in 2D systems and totally absent in 1D.

¹ K. Mochizuki, M. Matsumoto, and I. Ohmine, *Nature* **498**, 350 (2013).

² M. Forsblom and G. Grimvall, *Nat Mater* **4**, 388 (2005).

³ M. Cordin, B. A. J. Lechner, S. Duerrbeck, et al., *Sci. Rep.* **4** (2014).

⁴ T. Giamarchi, *Quantum Physics in One Dimension* (Oxford University Press, New York, 2004).

9:20am **SS+AS+EN-MoM4 The Co-adsorption of Water and ammonia on Pt(111), B.A.J. Lechner, Lawrence Berkeley National Laboratory, Y. Kim, H. Kang, Seoul National University, Korea, Miquel Salmeron, Lawrence Berkeley National Laboratory**

Water (H₂O) and ammonia (NH₃) are arguably the most important inorganic molecules in the chemical industry. Both have the ability to form hydrogen bonds and mix readily in the liquid form. However, upon adsorption onto a metal surface, the molecules can form fewer yet more directional hydrogen bonds. To investigate the interaction between these two species at the molecular level we present a scanning tunneling microscopy (STM) study of the co-adsorption of water and ammonia on Pt(111), a substrate which bonds both molecules strongly but does not promote their decomposition.

Prior investigations have suggested the formation of the ammonium ion, NH₄⁺, upon adsorption of ammonia onto a water monolayer on Ru(0001) [1], implying that the two molecules react readily when adsorbed on transition metal surfaces. Furthermore, a theoretical study of the co-adsorption of ammonia and water on Cu(110) proposed an intimately mixed layer of ammonia and water as the energetically most favorable structure [2].

Here, we present the first microscopic investigation of co-adsorbed water and ammonia species. Upon adsorption at 4 K, ammonia and water form disordered structures, yet as the temperature is increased the two species segregate on the substrate. Indeed, at temperatures above 77 K, ammonia invariably prefers to bond to the Pt surface and only adsorbs on a water film once the monolayer is complete and no active sites remain on the substrate. When adsorbed on the water layer, we find that ammonia bonds to the water molecules that are lifted off the substrate due to a lattice mismatch of the water monolayer and the Pt(111) geometry, which we believe is due to their ability to provide a hydrogen atom for the hydrogen bond more readily than the molecules bonded more strongly to the substrate.

[1] Y. Kim, E. Moon, S. Shin, H. Kang, *Angew. Chem. Int. Ed.* **51**, 12806 (2012).

[2] G. Jones, S. J. Jenkins, *Phys. Chem. Chem. Phys.* **15**, 4785 (2013).

9:40am **SS+AS+EN-MoM5 Thermal Decomposition of Ethylene on Ru(001), Yuan Ren, I. Waluyo, M. Trenary, University of Illinois at Chicago**

Ruthenium is an important catalyst in the Fischer-Tropsch process which deals with the conversion of syngas (CO and H₂) into hydrocarbons. One of the most important aspects in the Fischer-Tropsch reaction is the chain growth from a C₁ species to longer chain hydrocarbons. It is, therefore, important to study the chemistry of various C_xH_y hydrocarbon fragments on transition metal surfaces as building blocks in the chain growth mechanism.

Ethylidyne (CCH₃) is an interesting hydrocarbon fragment that has been studied on many surfaces as the decomposition product of ethylene. Although the formation of ethylidyne on Ru(001) from the dehydrogenation of ethylene has been studied using high resolution electron energy loss spectroscopy (HREELS) and reflection absorption infrared spectroscopy (RAIRS) in the past, there is a lack of agreement in the literature about the mechanism of ethylene decomposition.

In this study, reflection absorption infrared spectroscopy (RAIRS) and temperature programmed desorption (TPD) were used to characterize and identify the surface intermediates formed in the thermal decomposition of ethylene (C₂H₄) on Ru(001). Ethylene is found to adsorb to the surface in a di-σ bonded complex at 95 K and dehydrogenates to form ethylidyne (CCH₃) above 150 K. Upon further annealing the crystal to above 300 K, ethylidyne dehydrogenates to ethynyl (CCH). Annealing to higher than 450 K causes ethynyl to decompose to methylidyne (CH). The characterization of surface intermediates provides us with more insights into the thermal decomposition of ethylene on Ru(001), which is essential to reveal the reaction mechanism.

10:00am **SS+AS+EN-MoM6 Kinetics of Alkyl Species on Pt(111)**, *Yifeng Song, I.A. Harrison*, University of Virginia

Kinetics of Alkyl Species on Pt(111)

Yifeng Song and Ian Harrison

University of Virginia

Charlottesville, VA 22904

A heated effusive molecular beam was used to dose hot alkanes on to a relatively cold Pt(111) surface to overcome the initial activation barrier for dissociative chemisorption and to trap reactive intermediate species on the surface for subsequent spectroscopic and kinetic studies. Both reflection absorption infrared spectroscopy (RAIRS) and temperature programmed reaction (TPR) techniques were employed, in a complimentary way, to investigate the kinetics of alkyl fragments. Particular attention was paid to methylidyne (-CH) decomposition kinetics, which have been proposed to be potentially rate-limiting in catalytic steam reforming of methane according to recent DFT calculations. Comparison between reforming kinetics of single crystal surfaces and nanocatalysts are made. Elementary steps including the cleavage and formation of C-H and C-C bonds within other C1, C2 and C3 reactive intermediates were also studied. The experimental findings, together with some theoretical work, provide molecularly resolved information relevant to catalytic reforming of light alkanes.

10:40am **SS+AS+EN-MoM8 C₂ Hydrogenation at Ambient Pressure on Pt(111)**, *Joel Krooswyk, M. Trenary*, University of Illinois at Chicago

Carbon has been shown to be the decomposition product from catalytic reactions involving hydrocarbons adsorbed on metal catalysts. Its presence reduces the amount of active surface sites available during a reaction. The decomposition products from adsorbed acetylene and ethylene on Pt(111) are C₂ and C₁ species, respectively. A previous UHV study showed that C₂H₂ adsorbed on Pt(111) at 750 K immediately decomposes to mostly C₂ species. H₂ was then coadsorbed with C₂ at 85 K and annealed to 400 K, which produced ethylidyne (CCH₃), ethynyl (CCH), and methylidyne (CH) species. None of the species were hydrogenated to ethylene or ethane, and after annealing to 750 K, a percentage of the carbon on the surface could be rehydrogenated after cooling the crystal to 300 K and coadsorbing H₂.

In this study, the hydrogenation of C₂ species in 1×10⁻² to 1 Torr of H₂ was monitored with RAIRS. The species was created on Pt(111) with C₂H₂ adsorption at 750 K as done previously and the crystal was cooled to 300 K. The crystal was then annealed in an ambient pressure of H₂. The C₂ species are hydrogenated to ethylidyne at 400 K and then to ethane at approximately 450-500 K. This reaction is shown to be dependent on the pressure of H₂. The results show that ethylidyne will be hydrogenated at 450 and 500 K at 1.0 and 1×10⁻² Torr H₂, respectively. To show that the C₂ species are fully hydrogenated and desorbed as ethane, which indicates that the surface is clean, CO was leaked into the cell with H₂. We observe after the 500 K anneal that the peak assigned to the CO species is similar in intensity to one from CO adsorbed on a clean surface. This indicates that there are no C₂ species remaining on the surface. Also, the peak positions of the terminal and bridge sites are shifted, which indicates that there is a high coverage of H atoms adsorbed on the surface.

11:00am **SS+AS+EN-MoM9 Reaction Kinetics and Mechanism between Nitrate Radicals and Functionalized Organic Surfaces**, *Yafen Zhang, J.R. Morris*, Virginia Tech

Interfacial reactions of nitrate radicals (NO₃) with organic surfaces play an important role in atmospheric chemistry. To gain insight into the kinetic and mechanistic details, reactions between gas-phase nitrate radicals and model organic surfaces have been investigated. The experimental approach employs *in situ* reflection-absorption infrared spectroscopy (RAIRS) to

monitor bond rupture and formation while a well-characterized effusive flux of NO₃ impinges on the organic surface. Model surfaces are created by the spontaneous adsorption of either vinyl-terminated alkanethiols (HS(CH₂)₁₆CHCH₂) or hydroxyl-terminated alkanthiols (HS(CH₂)₁₆OH) onto a polycrystalline gold substrate. The H₂C=CH-terminated self-assembled monolayers (SAMs) provide a well-defined surface with the double bond positioned precisely at the gas-surface interface. The surface reaction kinetics obtained from RAIRS revealed that the consumption rate of the terminal vinyl groups is nearly identical to the formation rate of a surface-bound nitrate species and implies that the mechanism is one of direct addition to the vinyl group rather than hydrogen abstraction. Upon nitrate radical collisions with the surface, the initial reaction probability for consumption of carbon-carbon double bonds was determined to be (2.3 ± 0.5) × 10⁻³. This rate is approximately two orders of magnitude greater than the rate of ozone reactions on the same surface, which suggests that oxidation of surface-bound vinyl groups by nighttime nitrate radicals may play an important role in atmospheric chemistry despite their relatively low concentration. In addition to studies involving the H₂C=CH-terminated SAMs, we have probed the reaction dynamics of NO₃ on HO-terminated SAMs. These experiments have revealed that the polarity of the terminal group has a large effect on the interfacial reaction rates. For the HO-terminated SAMs, the initial reaction probability was determined to be (5.5 ± 0.6) × 10⁻³ and the reaction mechanism appears to involve efficient hydrogen abstraction at the methylene group adjacent to hydroxyl terminus.

11:20am **SS+AS+EN-MoM10 Oxide Growth Kinetics at SiO₂/Si(001) Interfaces Induced by Rapid Temperature Raising**, *Shuichi Ogawa, J. Tang*, Tohoku University, Japan, *A. Yoshigoe*, JAEA, Japan, *K. Nishimoto*, Tohoku University, Japan, *S. Ishidzuka*, Akita Nat. Col. Technol., Japan, *Y. Teraoka*, JAEA, Japan, *Y. Takakuwa*, Tohoku University, Japan

Thermal oxidation of Si is widely used in the fabrication of electric devices and MEMS. In the recent process, rapid thermal annealing (RTA) is used in a thermal oxidation process. In the RTA process, the temperature changes during the oxidation, but the temperature changing effects in the oxidation rate have not been cleared yet. In this study, the dependence of interface oxidation kinetics on the temperature was investigated by real-time RHEED combined with AES to measure the oxide growth rate. Based on the activation energy and pre-exponential factor of the interface oxidation at SiO₂/Si(001) interface, the rate-limiting reaction of the interface oxidation is discussed.

The oxidation experiments were performed with an apparatus equipped with facilities of RHEED combined with AES (Tohoku Univ.), and chemical bonding states including not only suboxide components but also strained Si atoms were investigated XPS at BL23SU, SPring-8. The clean Si(001) surfaces were oxidized by dry O₂ gas at initial temperature T₁. When the clean surfaces were completely oxidized, the temperature was raised from T₁ to T₂. T₁ was changed between room temperature (RT) and 561 °C.

When temperature was raised from T₁ to T₂, the interface oxidation is enhanced. The initial oxidation rate after rising temperature k₂ is discussed in this study. The k₂ strongly correlates to the difference of T₁ and T₂. The Arrhenius equations between k₂ and T₂ are obtained in various T₁. As the result, activation energy is obtained as 0.27 eV in good agreement with the previous experimental result[1] and theoretical study[2]. In addition, it is found that activation energy is independent from T₁. On the other hand, pre-exponential factor decreases with increasing T₁, decreasing by about one order when T₁ increases from RT to 561 °C. In the XPS results, the Si⁴⁺ component increases and suboxide components and strained Si components (Si^α and Si^β)[3] decrease with temperature elevation from 300 to 600 °C.

Based on these results, we propose the reaction between point defects (emitted Si atoms and its vacancies) generated by the oxidation-induced strain and O₂ molecules as the rate-limiting reaction of the interface oxidation.

[1] H. Watanabe et al., Phys. Rev. Lett. **80** (1998) 345.

[2] H. Kageshima et al, Jpn. J. Appl. Phys. **45** (2006) 7672.

[3] S. Ogawa et al., Jpn. J. Appl. Phys. **52** (2013) 110128.

11:40am **SS+AS+EN-MoM11 Electron Beam Induced Surface Reactions of Adsorbed π-allyl Ruthenium Tricarbonyl Bromide: Towards the Design of Precursors Specifically for Electron Beam Induced Deposition**, *Julie Spencer*, Johns Hopkins University, *R.G. Thorman*, University of Iceland, *M.S. Barclay*, Johns Hopkins University, *J.A. Brannaka*, University of Florida, *O. Ingólfsson*, University of Iceland, *L. McElwee-White*, University of Florida, *D.H. Fairbrother*, Johns Hopkins University

This surface science study focuses on elucidating the electron stimulated elementary reactions involved in Electron Beam Induced Deposition (EBID) of π-allyl ruthenium tricarbonyl bromide (π-C₃H₅Ru(CO)₃Br), an organometallic precursor synthesized specifically to test its suitability as an

EBID precursor. EBID is a minimally invasive, resistless lithographic process which uses the electron stimulated decomposition of volatile organometallics under low vacuum conditions to fabricate and prototype three-dimensional metallic nanostructures. To date, EBID of nanostructures has used precursors designed for thermal processes, such as chemical vapor deposition (CVD). However, precursors that yield pure metal deposits in CVD often create EBID deposits with high levels of organic contamination which severely limits the range of potential applications for EBID nanostructures, highlighting the need to better understand how the structure of organometallics influences their electron stimulated reactions. To address this knowledge gap we have conducted ultra-high vacuum (UHV) surface science studies to probe the effects of 500eV electrons on nanometer scale films of organometallics adsorbed on inert substrates at low temperatures using X-ray Photoelectron Spectrometry and Mass spectrometry. Recently, we have collaborated with synthetic organometallic chemists to study organometallic complexes not designed for CVD to test specific hypotheses about how the EBID process occurs; the first example of this new collaboration is π -allyl ruthenium tricarbonyl bromide (π -C₃H₅Ru(CO)₃Br). Experimental results indicate that electron stimulated decomposition of π -C₃H₅Ru(CO)₃Br causes the central Ru atom to become reduced and in the process causes the vast majority of the carbonyl ligands to be ejected into the gas phase, with no loss of Br or the carbon atoms in the π -allyl ligand. A parallel study of π -C₃H₅Ru(CO)₃Cl indicated that the identity of the halogen does not affect the decomposition process. However, although halogen atoms are not labile in the initial decomposition step, they can be removed by a slower electron stimulated desorption process at higher electron fluxes more representative of those encountered in typical EBID experiments which are conducted in electron microscopes. Collectively, these results suggest that organometallic precursors whose ligand architecture contains a combination of carbonyl and halogen ligands could be used to create EBID deposits with higher metal contents than are currently possible. To test this hypothesis we will also present results on the behavior of cis-dicarbonyldichloro platinum(II), *cis*-PtCl₂(CO)₂.

Surface Science

Room: 315 - Session SS+EN-MoM

Photocatalysis and Photochemistry at Surfaces

Moderator: Andrew Gellman, Carnegie Mellon University, Bruce Koel, Princeton University

8:20am **SS+EN-MoM1 Reaction Chemistry at Surfaces of Hematite-Based Photoelectrocatalysts**, *P. Zhao, C. Kronawitter, Bruce Koel*, Princeton University

Hematite (α -Fe₂O₃)-based photoanodes are promising materials for photoelectrochemical hydrogen generation. We report on fundamental studies of surface structure and reaction chemistry associated with the heterogeneous oxidation of water on such materials by applying a classical surface science approach. We have characterized the structure and properties of Ni-doped and mixed-oxide hematite surfaces formed by vapor deposition under controlled conditions utilizing a range of techniques for surface analysis. The structure of Ni-modified thin films of α -Fe₂O₃ model catalysts with different morphology and geometry was characterized by LEED and STM. Then, water adsorption and reaction were studied by TPD, XPS, UPS, and vibrational spectroscopy by HREELS, characterizing the influence of Ni-modification on thermal and photochemical reaction mechanisms. Ni doping is found to be associated with a new termination for the α -Fe₂O₃(0001) film. Water TPD shows that Ni doping induces new surface chemistry, as revealed by a new, higher temperature OH recombination desorption peak, which is due to more stable surface-bound OH groups as identified by UPS. These surface-science type experiments were combined with photoelectrochemical water oxidation measurements on photoanodes prepared by thin-film and nano-materials synthesis to elucidate new information on the surface phases of hematite-based photoanodes and about their specific stability and reactivity toward photoelectrochemical water splitting.

This work was supported by the Addy/ISN North American Low Carbon Emission Energy Self-Sufficiency Fund of the Andlinger Center for Energy and the Environment (ACEE) and by the Grand Challenges Program at Princeton University.

8:40am **SS+EN-MoM2 Infrared Reflection-Absorption Spectroscopy Study of Adsorption and Photo-Decomposition of Formic Acid on Reduced and Defective Rutile TiO₂ (110) Surfaces**, *Andreas Mattsson, L. Österlund*, Uppsala University, Sweden

Adsorption and photo-decomposition of formic acid on rutile TiO₂(110) have been investigated with infrared reflection-absorption spectroscopy

(IRRAS) employing p- and s-polarized light along the [001] and [1-10] crystal directions. The single crystal surfaces were prepared either by sputtering and annealing in ultra-high vacuum (UHV) to obtain a reduced surface (r-TiO₂), or by sputtering alone to create a rough, highly defective surface (sp-TiO₂). Results are compared with corresponding measurements in synthetic air on rutile nanocrystals performed. IRRAS spectra obtained on r-TiO₂ and rutile nanocrystals are very similar (Fig. S1), and show that in both cases formic acid dissociates and is predominately adsorbed as a bridging bidentate formate species,¹ demonstrating that the adsorption structure on the nanocrystals is determined by interactions with majority (110) surfaces. In contrast, the IRRAS spectra on sp-TiO₂ are different (Fig. S1), with only minor spectral features associated with (110) surfaces, which can be explained by changed adsorption geometry due to bonding to low-coordinated Ti³⁺ atoms. IRRAS measurements in UHV on thin nanoporous rutile films, made by reactive DC sputtering, were performed to compare the adsorption geometry of formate with that for single crystal surfaces and nanoparticles. The UV-induced rate of formate photo-decomposition is about 30 times higher on rutile nanocrystals in synthetic air compared with sp-TiO₂ under UHV conditions, and even larger than on r-TiO₂.² These differences are explained by the lack of oxygen and limited hydroxyl coverage under UHV conditions (thus quenching electron scavenging by adsorbed O₂ and lowering OH radical formation), and by strong bonding of formate on (110) surfaces which lowers the reactivity on r-TiO₂ further. Our results suggest that surface reaction studies of formic acid conducted at elevated pressures on rutile nanocrystals can be accurately modelled with single crystal studies conducted in UHV.

¹ A. Mattsson, S-L. Hu, K. Hermansson, L. Österlund, Journal of Chemical Physics 140 (2014) 034705

² L. Österlund, Solid State Phenomena 162 (2010) 203-219

9:00am **SS+EN-MoM3 Molecular Beam Epitaxy of Highly Mismatched GaN Alloys with GaAs, GaSb and GaBi for Potential Water Splitting and Other Solar Energy Conversion Applications**, *Sergei Novikov*, University of Nottingham, UK, *K.M. Yu*, Lawrence Berkeley National Laboratory, *W.L. Sarney*, US Army Research Laboratory, *Z. Liliental-Weber*, Lawrence Berkeley National Laboratory, *R.W. Martin*, University of Strathclyde, UK, *S.P. Svensson*, US Army Research Laboratory, *W. Walukiewicz*, Lawrence Berkeley National Laboratory, *C.T. Foxon*, University of Nottingham, UK **INVITED**

We have grown GaN layers alloyed with GaAs, GaSb and GaBi compounds using plasma-assisted molecular beam epitaxy (PA-MBE) and extensively characterized their structural, optical and electrical properties.

Electronic band structures of these so-called highly mismatched alloys (HMAs) are described by the band anticrossing (BAC) model which predicts that the alloys should exhibit a wide range of direct energy gaps. We have shown previously that the energy gap of GaN_{1-x}As_x alloys varies from 0.7eV to 3.4eV. An even larger modification of the band structures is anticipated for more extremely mismatched GaN_{1-x}Sb_x and GaN_{1-x}Bi_x alloys. The large band gap range and controllable conduction and valence band edge positions makes the HMAs promising materials for efficient solar energy conversion devices. For example, these HMAs may be suitable for solar water splitting applications for hydrogen production. As efficient photoelectrodes, the bandgap of the semiconductor must be >2 eV to induce electrochemical decomposition of water but still small enough to absorb a significant portion of the solar spectrum. In addition the band edges must also straddle the H₂O redox potentials.

At dilute doping levels, substitutions of As, Sb and Bi into the N sublattice results in formation of localized energy levels above the valence band in GaN. Our measurements on GaN doped with As and Sb have demonstrated that the As and the Sb impurity levels lie at about 0.7eV and 1.2eV above the valence band edge of GaN, respectively.

The BAC model predicts that at a higher concentration of the group V elements the interaction of the impurity levels with the extended states of the valence band leads to formation of an impurity-derived, fully occupied narrow band that plays a role of the new valence band edge. This results in an abrupt upward shift of the valence band edge and a reduction of the optical gap of the HMAs. We have achieved the enhanced incorporation of As, Sb and Bi by growing the layers at extremely low temperatures (down to about 100°C). Although the layers become amorphous for high As, Sb and Bi content, the measured composition dependence of the optical absorption edge are consistent with the predictions of the BAC model, indicating that the amorphous HMAs samples have a short-range order resembling random crystalline alloys. The large band gap range and controllable positions of the conduction and valence bands make these HMAs promising materials for efficient solar energy conversion devices.

9:40am **SS+EN-MoM5 Photochemistry of Acetone on Reduced Rutile TiO₂(110)**, *Nikolay Petrik, M.A. Henderson, G.A. Kimmel*, Pacific Northwest National Laboratory

TiO₂ is an important photocatalyst with many practical applications. However, fundamental understanding of thermal and non-thermal reactions on TiO₂ surfaces is still lacking. We have investigated the ultraviolet (UV) photon-stimulated reactions acetone and oxygen adsorbed on reduced rutile TiO₂(110). Previous research suggests that a thermal reaction between acetone and chemisorbed oxygen forms acetone diolate – a photochemically active product.¹ During UV irradiation, a methyl radical is ejected leaving acetate on the surface. Using infrared reflection absorption spectroscopy, we have identified the acetone diolate, which degrades during UV irradiation forming a new product. We have also measured the angular distribution of the photodesorbing methyl radicals, which is consistent with their ejection from the acetone diolate. Specifically, a peak in the distribution near ~60° to the surface normal is detected in the plane perpendicular to the BBO rows. However, we have also observed a second channel for photo-ejection of methyl radical for larger acetone:O₂ ratios. It manifests itself with a photodesorption peak normal to the surface and slower signal decay kinetics. These studies provide new insights into mechanisms responsible for the photochemistry of small molecules on TiO₂ and other oxide surfaces. This work was supported by the US Department of Energy, Office of Basic Energy Sciences, Division of Chemical Sciences, Geosciences & Biosciences. The work was performed using EMSL, a national scientific user facility sponsored by the Department of Energy's Office of Biological and Environmental Research and located at Pacific Northwest National Laboratory (PNNL). PNNL is a multiprogram national laboratory operated for DOE by Battelle under Contract DE-AC05-76RL01830.

(1) Henderson, M. A. Relationship of O₂ Photodesorption in Photooxidation of Acetone on TiO₂. *J. Phys. Chem. C*, 2008, 112, 11433-11440.

10:00am **SS+EN-MoM6 STM Spectroscopic Studies of TMAA Photocatalysis on TiO₂**, *Denis Potapenko, Z. Li, R.M. Osgood*, Columbia University

Titanium oxide is a versatile photocatalytic material and it has been the subject of much research throughout the last two decades. Scanning Tunneling Microscopy (STM) allows explorations on the single molecule basis thus providing important insight into the physical phenomena involved in photocatalysis. Our experiments examine the tip-induced chemistry of tri-methyl acetic acid (TMAA) molecules adsorbed on TiO₂ rutile(110) surface; this system was chosen as a model for light-driven catalysis since it is easily imaged with STM and since this system has been the subject of many earlier studies of photo and thermal chemistry. In the present work we combine three methods of initiation of surface chemistry: a) excitation of charge carriers in bulk TiO₂ with monochromated light from a UV-vis lamp, b) injection of the charge carriers from the STM tip directly into an adsorbed molecule, and c) injection of hot carriers into the substrate from the STM tip. In the latter case the surface reactions are initiated in the vicinity of the injection point by the electrical charges diffusing in the bulk of TiO₂, thus giving a unique insight into the charge dynamics. We show that there is a threshold energy for a hot hole below the edge of the TiO₂ valence band that is required for TMAA photo-decomposition.

11:00am **SS+EN-MoM9 Photoluminescence Response of p-GaInP₂ Photocathodes to Vapor and Solution Ambients**, *James Young*, University of Colorado, Boulder, *H. Doscher, T.G. Deutsch, J.A. Turner*, National Renewable Energy Laboratory, *S.M. George*, University of Colorado, Boulder

III-V photoelectrochemical (PEC) devices have achieved high solar-to-hydrogen water splitting efficiencies but corrosion greatly limits their operating lifetime. A dynamic three-phase semiconductor-electrolyte-hydrogen (oxygen) system exists at a photocathode (photoanode) surface during operation. Understanding the interaction of water, hydrogen, and oxygen with III-V surfaces is critical to optimizing device performance and applying corrosion-resistant surface modifications. In this work, we use photoluminescence (PL) to probe the surface response of p-type GaInP₂ to several gas and solution ambients *in-situ*. X-ray photoelectron spectroscopy and photoelectrochemical techniques are used to characterize surface changes *ex-situ*. Pretreating p-GaInP₂ with sulfuric acid removes surface oxide and doubles p-GaInP₂ band-to-band PL yield when measured in air. Measurements in vacuum show that PL of pretreated samples increases reversibly with adsorption isotherm dependence on water vapor at partial pressures below 2 Torr while samples without the pretreatment show no PL response to water vapor. A comparison of water to other vapor phase ambients suggests that PL response increases with the dipole strength and involves dissociative adsorption. In oxygen ambient, the PL decays irreversibly which we attribute to photo-oxidation of the p-GaInP₂ surface. We will also present results from measurements in hydrogen ambient and PL measurements and monitoring in electrolyte solutions with a discussion

of their relevance to PEC device performance and usefulness in characterizing corrosion resistant surface modifications.

Thin Film

Room: 305 - Session TF+PS+SE-MoM

Advanced PVD Methods

Moderator: Subhadra Gupta, University of Alabama

9:00am **TF+PS+SE-MoM3 Ternary and Quaternary Thin Layers Deposited by Magnetron Sputtering**, *Marie-Paule Besland, J. Tranchant, E. Janod, C. Benoit, L. Cario, P.Y. Jouan, M. Carette, A. Lafond*, Institut des Matériaux Jean Rouxel – Université de Nantes, France, *R. Meunier, S. Fabert*, Institut des Matériaux Jean Rouxel – Université de Nantes and Crosslux, France, *P.Y. Thoulon, M. Ricci*, Crosslux Company, France

Developing new functionalities mainly depend on the use of new functional material. Nevertheless, prior to envision any development of functional materials towards devices, two major challenges have to be tackled. The former one is to obtain thin layers of active and functional materials. The second challenge is to recover the functional properties on thin layers. For several decades, magnetron sputtering is a widely used deposition technique in microelectronics. Moreover, magnetron sputtering enables to deposit well-crystallized film of insulating or conducting materials, at low temperatures, over large areas, while controlling the film composition and microstructure, even for complex and multi-component materials. Thus, on the basis of well established know-how in deposition process and multi-layered functional structures [1], the deposition of GaV₄S₈ material in the form of thin layers has been investigated by both non-reactive RF magnetron sputtering and reactive process in Ar/H₂S mixture [2]. While the functionality (Resistive switching =RS) was first evidenced on single crystals, our studies demonstrated that metal-insulator-metal (MIM) structures based on GaV₄S₈ thin layers, deposited by magnetron sputtering, exhibit as well a similar RS [3]. More recently, we focus on the historical chalcogenide absorber for solar cells: CIGSe. We developed a dedicated and home-designed vacuum chamber for CIGSe thin films deposition using “one step sputtering”. In that study, CIGSe thin films were deposited on SLG/Mo substrates by RF magnetron sputtering and then ex-situ annealed under controlled atmosphere. Deposition and annealing parameters can modify both chemical composition and structural properties. In particular, different preferential crystalline orientation may be induced and can modify functional properties in a large extend. Finally, the performances of CIGSe solar cell completely realized by magnetron sputtering technique will be compared to published efficiency values in the 8.9- 10.5 % range [5].

1- C. Duquenne et al. *J. Appl. Phys.* 104 (2008) 063301; M.P. Besland et al. *Thin Solid Films* 495 (2006) 86.

2- E. Souchier et al. *Thin Solid Films* 533 (2013) 54 ; J. Tranchant et al. *J. Phys. D: Appl. Phys.* 47 (2014) 065309.

3- J. Tranchant et al. *Thin Solid Films* 533 (2013) 61.

4- J. A. Frantz et al. *Thin Solid Films* 519 (2011) 776; A.J. Zhou et al. *Thin Solid Films* 520 (2012) 6068.

5- C. Chen et al. *Solar Energy Materials & Solar Cells* 103 (2012) 25; *Thin Solid Films* 535, (2013) 122.

9:20am **TF+PS+SE-MoM4 Molecular Dynamics Simulations of TiN/TiN(001) Growth**, *Daniel Edström, D.G. Sangiovanni, V. Chirita, L. Hultman*, Linköping University, Sweden, *I.G. Petrov, J.E. Greene*, University of Illinois at Urbana Champaign

The Modified Embedded Atom Method (MEAM) interatomic potential within the classical Molecular Dynamics (MD) framework enables realistic, large-scale simulations of important model materials such as TiN. As a step toward understanding atomistic processes controlling the growth of TiN on a fundamental level, we perform large-scale simulations of TiN/TiN(001) deposition using a TiN MEAM parameterization which reproduces experimentally-observed surface diffusion trends, correctly accounts for Ehrlich barriers at island step edges [1], [2], and has been shown to give results in excellent qualitative and good quantitative agreement with Ab Initio MD based on Density Functional Theory (DFT) [3], [4]. Half a monolayer of TiN is deposited on 100x100 atom TiN(001) substrates at a rate of 1 Ti atom per 50 ps, resulting in simulation times of 125 ns. The TiN substrate is maintained at a typical epitaxial growth temperature, 1200 K during deposition using Ti:N flux ratios of 1:1 and 1:4 with incident atom energies of 2 and 20 eV to probe the effects of N₂ partial pressure and substrate bias on TiN(001) growth modes. We observe nucleation of Ti_xN_y molecules; N₂ desorption; the formation, growth and coalescence of mixed <100>, <110>, and <111> faceted islands; as well as intra- and interlayer mass transport mechanisms. For equal flux ratios at 2

eV incidence energy, islands begin to form atop existing islands at coverages ≥ 0.25 ML, leading to 2D multilayer growth. At 20 eV, the film growth mode shifts toward layer-by-layer growth. We discuss the implications of these results on thin film growth and process tailoring. Our classical MD predictions are supported and complemented by DFT-MD simulations.

[1] D. G. Sangiovanni, D. Edström, L. Hultman, V. Chirita, I. Petrov, and J. E. Greene, "Dynamics of Ti, N, and TiN_x (x=1–3) adatom transport on TiN(001) surfaces," *Phys. Rev. B*, vol. 86, no. 15, p. 155443, Oct. 2012.

[2] D. Edström, D. G. Sangiovanni, L. Hultman, V. Chirita, I. Petrov, and J. E. Greene, "Ti and N adatom descent pathways to the terrace from atop two-dimensional TiN/TiN(001) islands," *Thin Solid Films*, vol. 558, pp. 37–46, May 2014.

[3] D. G. Sangiovanni, D. Edström, L. Hultman, I. Petrov, J. E. Greene, and V. Chirita, "Ab initio and classical molecular dynamics simulations of N₂ desorption from TiN(001) surfaces," *Surf. Sci.*, vol. 624, pp. 25–31, Jun. 2014.

[4] D. G. Sangiovanni, D. Edström, L. Hultman, I. Petrov, J. E. Greene, and V. Chirita, "Ti adatom diffusion on TiN(001): Ab initio and classical molecular dynamics simulations," *Surf. Sci. (In Press)*. doi: 10.1016/j.susc.2014.04.007

9:40am **TF+PS+SE-MoM5 Surface Chemistry of Pd and Ag Interaction with 3C-SiC Thin Films Deposited on Si(111) by Pulsed Laser Deposition**, *Rachel Seibert, D. Velazquez, J. Terry*, Illinois Institute of Technology, *K.A. Terrani, C. Baldwin, F. Montgomery, K. Leonard, J. Hunn, P. Schuck, R. Stoller*, Oak Ridge National Laboratory, *S. Sadow*, University of South Florida

The surface interactions of nuclear fission products with the barrier SiC layer of Tri-Structural Isotropic (TRISO) coated fuel particles limit fuel cell performance. In particular, Pd and Ag reduce the structural integrity of SiC. An understanding of the reaction mechanisms and kinetics of these interactions under normal operation as well as accident conditions is critical for the development of advanced nuclear reactors, but currently is not well understood. This surface chemistry is examined both in spent TRISO fuel on SiC/Si(111) thin films and compared to theoretical calculations done by Schuck and Stoller at Oak Ridge National Laboratory [1]. Synchrotron extended X-ray absorption fine structure (EXAFS) spectroscopy measurements were conducted on the irradiated TRISO fuel pellet to characterize atomic interactions at the Pd K-edge (24350 eV). The thin films were grown epitaxially via pulsed laser deposition (PLD), as evidenced by reflection high energy electron diffraction (RHEED) patterns. Pd and Ag were deposited on separate SiC/Si(111) films in thickness increments from 0.5-5 monolayers. The chemical structure of the thin films is analyzed using X-ray photoelectron spectroscopy (XPS).

[1] Schuck, P.C. and R.E. Stoller, *Ab initio study of the adsorption, migration, clustering, and reaction of palladium on the surface of silicon carbide*. *Phys. Rev. B* **83**, (2011)

10:00am **TF+PS+SE-MoM6 High Thermal Stability Nanocrystalline Gold, Part I**, *Ronald Goeke, N. Argibay, J.E. Mogyony, K.M. Hattar, S.V. Prasad*, Sandia National Laboratories

Gold coatings that are ideally suited for low electrical contact resistance (ECR) applications are mechanically soft and exhibit unacceptable amounts of adhesion and friction. To mitigate these problems gold for ECR applications is typically alloyed with Ni, Co or Fe which increases the film hardness and wear resistance. A key limitation of hard gold coatings is the propensity for the non-noble alloying metal species to diffuse to the surface and form non-conductive oxide films that can severely impact the electrical contact behavior. These traditional hard gold films, which are fabricated via electro-deposition, have been limited to electrochemical compatible materials. Using co-deposition of Au-ZnO by electron beam evaporation we have eliminated the electrochemical material limitations and synthesized a new class of hard gold thin films. The ceramic phase is used to strengthen the composite via grain refinement. The resulting nanocrystalline gold thin film can replace typical hard gold films and exhibits enhanced thermal stability as the refractory ceramic phase is kinetically limited and has no oxidative potential for migration to the surface. The synthesis, characterization, and thermal stability against grain sintering will be discussed.

Sandia National Laboratories is a multi-program laboratory managed and operated by Sandia Corporation, a wholly owned subsidiary of Lockheed Martin Corporation, for the U.S. Department of Energy's National Nuclear Security Administration under contract DE-AC04-94AL85000.

10:40am **TF+PS+SE-MoM8 High Thermal Stability Nanocrystalline Gold Thin Films, Part II**, *Nicolas Argibay, J.E. Mogyony, R.S. Goeke, K.M. Hattar, M.T. Dugger, S.V. Prasad*, Sandia National Laboratories

In the second part we present the result of investigations of the bulk transport properties, thermal and mechanical stability, and mechanical properties of electron beam codeposited Au-ZnO as a function of composition and temperature (up to a homologous temperature of 0.5). A high throughput method for determining the average grain size in electrically conductive metal-ceramic thin films will be presented, founded on a correlation between grain boundary density and electrical resistivity (Mayadas-Shatzkes and Sondheimer-Fuchs models), and compared to microstructural characterization using backscatter and transmission electron diffraction, SEM, and XPS.

Sandia National Laboratories is a multi-program laboratory managed and operated by Sandia Corporation, a wholly owned subsidiary of Lockheed Martin Corporation, for the U.S. Department of Energy's National Nuclear Security Administration under contract DE-AC04-94AL85000.

11:00am **TF+PS+SE-MoM9 Growth and Phase Stability of Zirconium Diboride Thin Films**, *David Stewart, D.J. Frankel, R.J. Lad*, University of Maine

Zirconium diboride (ZrB₂) has metallic-like electrical and thermal conductivities up to its melting point of 3246°C and is also thermal shock resistant, making it an excellent material for use in harsh, high temperature environments. Presently, much of the literature on boride materials concerns bulk, sintered materials, and less is known about ZrB₂ thin films. Here we demonstrate the growth of ZrB₂ thin films by e-beam co-evaporation of elemental Zr and B sources on sapphire, silicon, and silica substrates. Films were deposited over a range of Zr:B compositions and were characterized before and after annealing up to 1000°C in air or under vacuum (10⁻⁸ Torr). Scanning electron microscopy and X-ray photoelectron spectroscopy (XPS) indicated that as-deposited films are homogeneous, with a smooth morphology and covalent bonding character. X-ray diffraction (XRD) revealed that films deposited at temperatures from ambient to 600°C are typically amorphous, and annealing in vacuum up to 1000°C can cause the formation of a ZrB₂ crystalline phase that coexists with an amorphous matrix, depending on the Zr:B ratio. Films annealed in air as low as 800°C become heavily oxidized and boron-depleted, leaving behind a monoclinic ZrO₂ polycrystalline film. XPS depth profiles suggest the formation of a boron oxide phase in air that evaporates from the surface at high temperatures, consistent with surface oxidation behavior reported for bulk ZrB₂ materials. Electrical conductivities of as-deposited films, measured with a 4-point probe, range from 0.3 – 8.3 x 10⁶ S/m depending on the Zr:B ratio, and the films retain their conductive nature after vacuum annealing. The ZrB₂ crystalline phases exhibit a preferred (100) crystallographic texture, and valence band XPS measurements confirm the existence of hybridized B2p-Zr4d bonding states. Understanding the high temperature stability of ZrB₂ films is important for developing it as a potentially stable conducting film for electronic device applications in harsh environments.

11:20am **TF+PS+SE-MoM10 Thickness Dependence of High Frequency Magnetic Properties for Thin Films of Iron-Gallium-Boron**, *Colin Rementer, Y. Kim, J.P. Chang*, University of California at Los Angeles

Iron gallium boron, i.e. (Fe₈₀Ga₂₀)_xB_{1-x} or FeGaB, is a material of considerable interest for high frequency, multiferroic applications. Lou *et al.* discovered that the addition of boron to the magnetostrictive material Galfenol (Fe₈₀Ga₂₀ or FeGa) led to a decrease in coercivity (~1 Oe), decrease in ferromagnetic resonance (FMR) linewidth (~20 Oe) at *X* band, and an increase in piezomagnetic coefficient (~7 ppm/Oe). The physical properties were optimized in (Fe₈₀Ga₂₀)₈₈B₁₂ with ~100 nm thickness (Lou, J. et al. 2007). The material has been incorporated into several multiferroic systems with great success (Lou, J. et al. 2009). It is a material of great interest for integration into various multiferroic antenna systems. To have a better understanding of the material, a more thorough study on the fundamental properties of the material at different thicknesses is needed, as well as how that thickness can affect the tunability of resonant frequency and magnetoelectric coupling in multiferroic heterostructures when incorporated with ferroelectric single crystals.

FeGaB was grown via co-sputtering of Fe₈₀Ga₂₀ and boron targets via DC magnetron and RF magnetron sputtering, respectively. The FeGa target was held at 60 W and the boron power was adjusted to tune the boron concentration, from 9 - 18%. FeGaB films were grown with thicknesses ranging from 30 nm – 500 nm, and a growth rate of 7 nm/min was achieved. The coercivity and saturation magnetization of the FeGaB films decreased (~10 Oe), and increased (1200 emu/cc), respectively, with decreasing thickness (30 nm). Ferromagnetic resonance (FMR) linewidth was measured at *X* band (9.6 GHz), and it was found that it narrowed to 140 Oe with decreasing thickness at 30 nm. Both Fe₇₅Ga₂₅ and Fe₆₀Ga₂₂B₁₈ were

shown to be magnetoelastic, having magnetostriction constants of around 30 ppm and 60 ppm, respectively. The magnetic properties of FeGaB are being optimized to the properties measure by Lou et al. to ensure the rigor of the thickness dependence study (Lou, J. et al. 2007). The effect of inducing stronger in-plane anisotropy in the FeGaB films was investigated via an *in situ* magnetic field applied during deposition, and post-deposited magnetic annealing is being explored as a function of thickness.

11:40am **TF+PS+SE-MoM11 Optimizing Magnetic Confinement for High Productivity PVD System Linear Scanning Magnetron**, *V. Kudriavtsev, Robert Norris, T. Bluck, I. Latchford*, Intevac, Inc.

High productivity vacuum PVD system cost of ownership is very sensitive to sputtering target utilization. In this paper we discuss magnetic array design methodology that is required to achieve excellent plasma confinement that can lead to most uniform target erosion both magnetic and nonmagnetic targets. Design trade-offs are more challenging when using highly magnetic target materials, such as Nickel. These materials have lower PTF (pass through flux) and also affect magnetic field in all directions. Stronger magnets allow the fields to penetrate magnetic target material and judicious design process allows minimizing negative effects of field shunting.

First we develop static magnetic simulations model; magnetic properties are assigned to magnets, magnetic materials and also properties to nonmagnetic elements. Resulting computations are presented in a form of magnetic field component and Bz component on the surface of the target or in the vicinity of that surface. The magnetic track is determined by searching for locations where perpendicular component of magnetic field Bz=0 and we review variations in Bx and By along this track. Magnetic field characteristics are studied at various distances from magnets, sizing the magnetic array configuration, magnet dimensions, and their polarity for a selected objective. Usually this objective is to provide certain field strength at certain distance away from magnets. One can increase the strength of N or S polarity in the array, creating balanced or unbalanced magnetron configuration, that affect maximum field strength, erosion profile and erosion in the middle of the target where the absolute value of magnetic field reaches a maximum. Magnetic field characteristics are extracted from the erosion track profile and theoretical erosion profile is calculated resulting from the current array design. These profiles allow estimation of the "static" target utilization and if necessary to create optimization cycle where magnetic characteristics of the design (parameters) are computationally changed to reach desired erosion profile. Once the final computer design is selected, engineers build the first prototype of magnetic array and evaluate its magnetic properties using a 2d magnetic scanner that provide B, Bx, By, Bz components of magnetic field in plane on a distance from magpack. The next step of the analysis utilizes experimentally extracted magnetic field (or previously computed theoretical magnetic field) to estimate resulting 2D erosion profile that is due to the magnet non-uniform and non-linear motion. Finally, using the ray tracing method we perform film uniformity analysis for a substrate of given size which is located on a defined distance away from the sputtering target. That analysis is transient and factors in substrate nonlinear motion. Resulting film uniformity is estimated as a superposition of multiple substrate positions as it moves under the target.

Thin Film

Room: 307 - Session TF+PS-MoM

Atmospheric, Roll-to-Roll and other Manufacturing Advances in ALD

Moderator: Paul Poodt, Holst Centre / TNO

8:20am **TF+PS-MoM1 Barrier Properties of Plastic Films Coated with Al₂O₃ by Roll-to-Roll ALD**, *Charles Dezelah*, Picosun USA, LLC, *T. Hirvikorpi, R. Laine, W.-M. Li*, Picosun Oy, Finland, *M. Vähä-Nissi, E. Salo*, VTT Technical Research Centre of Finland, *V. Kilpi, S. Lindfors*, Picosun Oy, Finland, *J. Vartiainen, E. Kenttä, J. Nikkola, A. Harlin*, VTT Technical Research Centre of Finland, *J. Kostamo*, Picosun Oy, Finland
INVITED

Atomic layer deposited (ALD) Al₂O₃ has proven to be effective in enhancing the moisture and gas barrier properties of various plastic films and coatings [1-3]. The key challenge in several applications is to find a flexible, reliable, and cost efficient means to protect sensitive goods from ambient atmosphere. In this presentation we describe the first deposition trials on plastic films with a new PICOSUN™ roll-to-roll (R2R) chamber. This study demonstrated that a thin Al₂O₃ layer deposited with this continuous process enhances the barrier performance of these materials with results similar to those obtained in a non-R2R batch processing module.

Silicon wafers, cellophane, polylactic acid, and polyimide film substrates were coated with Al₂O₃ at 100 °C using both a batch PICOSUN™ reactor and a test setup for a R2R ALD fit to the same reactor. The precursors were trimethyl aluminum and H₂O, and 500 deposition cycles were used. The Al₂O₃ deposited samples were characterized for their barrier and surface characteristics. The deposition rate of Al₂O₃ on silicon wafer was similar for the batch and the R2R ALD processes. The results from the oxygen transmission rate (OTR) and water vapor transmission rate (WVTR) measurements in 50 % relative humidity and 23 °C were compared between samples across substrate types and deposition modes. It was found that the R2R chamber provided barrier performance was comparable to traditional batch deposition in several cases, and considerably enhanced relative to uncoated substrates.

The initial mechanical properties of the polymeric substrate were found to be crucial for the barrier properties. For example, an Al₂O₃ coating fabricated on cellophane film was less sensitive to mechanical stresses, and the barrier values obtained were similar to those obtained with batch process for the same substrate. FTIR analyses detected Al₂O₃ covered surfaces after the R2R ALD. AFM images for the batch and R2R produced samples that were quite similar. The relative polarities of surface energy for Al₂O₃ deposited with R2R ALD on all three films were lower than for the batch samples. This indicates some differences in the thin film growth. Implications for manufacturability and scalability will also be discussed.

References:

1. P.F. Carcia, R.S. McLean, M.H. Reilly, M.D. Groner, et al., Appl. Phys. Lett. 89 (2006) 031915.
2. T. Hirvikorpi, M. Vähä-Nissi, T. Mustonen, E. Iiskola, et al., Thin Solid Films 518 (2010) 2654.
3. T. Hirvikorpi, M. Vähä-Nissi, A. Harlin, M. Karppinen, Thin Solid Films 518 (2010) 5463.

9:00am **TF+PS-MoM3 An Industrial Approach to Roll-to-Roll Atomic Layer Deposition**, *M.J. Söderlund, P.T. Soininen, Ville Malinin*, Beneq, Finland

Spatial ALD method has attracted considerable attention lately as means to increase the throughput and coating area of ALD processes to meet industrial requirements. This interest is driven largely by the superior film quality of ALD thin-films, but also by the other foreseen benefits associated with spatial ALD process (in addition to high process) such as high material utilization efficiency and low maintenance requirement. These benefits, enable by the spatial ALD concept, are coming together today specifically for flexible moisture barrier application, driven by need to improve the quality and reduce the costs of ultra barrier films for moisture sensitive devices (e.g. OLEDs). However, for ALD to break into mainstream in roll-to-roll manufacturing of e.g. various different moisture barrier films, the spatial ALD technological approach should be applicable to a wide range of substrates materials (e.g. polymer, metal, paper), as well as meters wide webs and web thicknesses ranging from tens up to hundreds of micrometers.

This paper describes a scalable roll-to-roll ALD system approach, and presents recent results using a commercial WCS 600 R2R ALD system. The approach is based on relative movement between a web, tensioned on a processing drum, and the spatial ALD coating head, which is in oscillating motion around the central process drum. Process for Al₂O₃ based on TMA and H₂O precursors at 100 C demonstrates growth rates between 0.7 - 1.0 Å/cycle with refractive index higher equal or higher than 1.61. Low non-uniformity of less than 10 % is measured across 480 mm effective coating area. Ultra barrier performance of <5*10⁻⁴ g/(m² day) at 38 C/90 % conditions is demonstrated with only 20 nm thick Al₂O₃ films, made on roll-to-roll basis on 500 mm wide PEN film substrate. Prospects for scaling the technology further in web width and speed are discussed.

9:20am **TF+PS-MoM4 Modular Rotating Cylinder Design for Spatial ALD on Porous Flexible Substrates**, *Kashish Sharma, R.B. Hall, S.M. George*, University of Colorado at Boulder

Li-ion batteries (LIBs) have a capacity that typically decays versus number of charge-discharge cycles. Surface coatings on LIB electrodes fabricated using atomic layer deposition (ALD) can dramatically improve the capacity stability. The commercialization of these ALD coatings requires the ability to perform ALD on porous battery electrodes on flexible metal webs. In this work, a new spatial ALD (S-ALD) reactor is developed that is based on a modular rotating cylinder design. The outer cylinder remains fixed and contains a series of slits. The slits can accept a wide range of modules that attach from the outside and accommodate precursor dosing, purging or pumping. The inner cylinder rotates (0-200 RPM) and passes underneath the various slits that are spatially separated. This new S-ALD reactor has been characterized using trimethyl aluminum (TMA) and ozone to grow Al₂O₃ ALD films at 40°C on metallized PET substrates. Spectroscopic

ellipsometry measurements obtained Al₂O₃ ALD growth rates of 0.6 -1.1 Å/cycle depending on the O₂ pressure used to prepare the ozone. The Al₂O₃ ALD growth rate was also constant with changing rotation speeds from 60 to 150 RPM. Future experiments will deposit Al₂O₃ ALD films on porous electrodes on flexible metal webs. For these depositions, a “push-pull” design will be utilized where the pressure of the precursor dose will “push” the precursor and carrier gas into the evacuated porous electrode. The reaction products and carrier gas will then be “pulled” from the porous electrode by vacuum pumping. This new spatial ALD reactor has the potential to deposit uniform and conformal thin films on large area and flexible porous substrates at high deposition rates.

9:40am TF+PS-MoM5 Spatial Atmospheric Atomic Layer Deposition of Oxide and Oxsulfide Semiconductors, *Andrea Illiberi, TNO, Netherlands**

INVITED

Oxide and oxsulfide semiconductors are key components in a wide variety of devices including displays and solar cells. Spatial ALD is emerging as a disruptive deposition technique for the electronic industry because it combines the advantages of temporal ALD, i.e. excellent control of film composition and uniformity on large-area substrates, with high growth rates (up to nm/s) at atmospheric pressure. In this paper we present *spatial atmospheric ALD* of Zn-based multi-component oxides for use as front window in CuInGaSe₂ (CIGS) solar cells (i.e. i-ZnO, Zn(O,S), Al:ZnO) and as active channel (i.e. InGaZnO) in TFT-displays. Films are grown by sequentially exposing the substrate to oxygen and/or sulfur precursors (H₂O, H₂S) and the metal precursor vapors (i.e. DEZ, TMIn, TEGa, or TMAI). By controlling the kinetics of surface reactions between vaporized precursors and reactive sites at the film surface, the composition of the films can be precisely tuned, achieving a constant concentration-depth profiles of the elements along the growth direction, as measured by EDX and XPS analysis.

CIGS solar cells: The front window of CIGS solar cells consists of a stack of CdS/i-ZnO/Al:ZnO layers. Zn(O,S) is emerging as a successful replacement for the CdS buffer layer, being free of toxic elements and having a wider band gap (> 2.4 eV). Both the [S] and [Al] content in ZnO are accurately controlled in the range from 0 < [S]/[O] < 1 and 0 < [Al]/[Zn] < 1, enabling the deposition of the entire front window stack by spatial-ALD. The degradation of the electrical properties of Al:ZnO during damp heat test is prevented by a spatial-ALD Al₂O₃ moisture barrier. The use of spatial ALD Zn(O,S)/i-ZnO/Al:ZnO/Al₂O₃ stack as front windows in CIGS cells is being tested.

TFT-displays: InGaZnO (IGZO) has drawn great attention in the display industry over the last few years, because of its high electron mobility (> 10 cm²/Vs), as compared to the commonly used amorphous silicon. The growth of IGZO has been investigated by Spectroscopic Ellipsometry, while the surface and bulk composition of the films has been measured by Low Energy Ion Scattering and XPS. An initial In-rich phase induces a nucleation phase of about 250 ALD-cycles, followed by film closure. IGZO films have an amorphous structure, as indicated by X-ray diffraction analysis. Spatial ALD IGZO films have been tested as active channel in TFT, achieving a maximum device mobility of 10 cm²/Vs.

Upscaling: Large area (30 cm wide) spatial ALD of Zn(O,S), Al:ZnO and IGZO will be developed by the roll to roll and sheet-to-sheet technology, respectively, as a new nanomanufacturing platform for the solar and display industry.

10:40am TF+PS-MoM8 Large Area Atmospheric Spatial Atomic Layer Deposition of Zn(O,S) Buffer Layers for CIGS Solar Cells on Glass Substrates, *M.D. Bijker, R.S.R. Archer, Smit Ovens B.V., Netherlands, P. Poodt, Holst Centre / TNO, Netherlands, A. Illiberi, Solliance / TNO, Netherlands, Karel Spee, Smit Ovens B.V., Netherlands*

Spatial ALD (S-ALD) is emerging as a disruptive deposition technique for the electronics and photovoltaics industry because it combines the advantages of ALD, i.e. excellent control of film composition and uniformity, with high deposition rates (up to nm/s) at atmospheric pressure. This allows for a reduction of the Cost of Ownership (CoO) to a level where, for a range of high-volume and low-cost application areas, commercial exploitation is within reach.

S-ALD as developed by the authors makes use of an injector in close proximity (typically less than 100 μm) of a substrate which moves with high speed underneath the injector. This process has been proven to work very well for very flat substrates. Large area glass panels, however, provide quite a challenge as there are large thickness variations over the sheet due to glass thickness variations, surface roughness, bow and warp of the glass. We will present the design and operation of an atmospheric pressure S-ALD sheet-to-sheet tool which can handle 30x40 cm² glass panels. The glass

panels enter the system through a load lock, pass two heating zones to fast heat-up the substrates and enter a deposition zone. The glass plates are placed on a super flat susceptor and straightened using a vacuum clamp. Sensors detect the remaining thickness variations of each individual glass plate and adjust the injector head proximity for each glass plate. In high speed the glass plate is moved back and forth underneath the injector. Maximum deposition temperatures are 350°C. The injector is equipped with 7 slots, equipped with injectors for trimethylaluminum (TMA), diethylzinc (DEZ), H₂O and H₂S. Each precursor can be entered independently, but also TMA-DEZ premixing and H₂O-H₂S premixing is possible.

The tool will be used for the deposition of Zn(O,S) buffer layers in CuInGaSe₂ (CIGS) solar cells as an alternative for Chemical Bath Deposition (CBD) of CdS. This replaces an environmentally polluting process with a Cd-free solution. Several authors have reported CIGS solar cells utilizing Zn(O,S) buffer layers with properties very comparable or even somewhat better (+0,5%) to existing CIGS cells using CdS. Cost of ownership (CoO) calculations show that the production cost using S-ALD are also comparable (~\$0,02/Wp).

First Zn(O,S) layers have been prepared using a S-ALD lab-reactor, using DEZ and a mixture of H₂O and H₂S. The composition, optical- and electrical properties of the films can be continuously controlled by different H₂O/H₂S mixing ratios from ZnO. Further experiments are ongoing, including the deposition of Zn(O,S) buffer layer in full CIGS solar cells and its effect of solar cell performance.

11:00am TF+PS-MoM9 Growth Rates and Mechanisms for Al₂O₃ ALD using TMA/ O₃ at Atmospheric Pressure, *MoatazBellah Mousa, C.J. Oldham, G.N. Parsons, North Carolina State University*

Under typical low pressure ALD conditions, ozone (O₃) is reported to speed up ALD processes compared to water-based reactions because shorter purge times are needed to fully desorb ozone O₃. Many high-throughput ALD processes are designed to operate at atmospheric pressure where viscous fluid transport can have significant effects. We developed an ALD process using trimethyl aluminum (TMA) and O₃ in a variable-pressure flow tube reactor and measured growth rates, film composition and film uniformity in the growth zone for pressures between ~2 Torr and 760 Torr and temperature ranging from 70°C to ~250°C. We also adjusted overall gas flow rate to study the role of gas residence time. Film thickness was determined by ellipsometry and growth was monitored using an in-situ Quartz Crystal Microbalance (QCM). We observe self-limiting growth between ~150 °C and 250 °C at both ~2 Torr and 760 Torr, and larger growth rate at lower temperature. At high pressure the growth rate is ~20% larger than at low pressure, which is ascribed to slower transport of desorbing product species through the boundary layer at high pressure. We also find that longer O₃ exposure times are needed compared to low pressure growth. This is consistent with a model for the ozone dissociation kinetics showing that higher pressure enhances the rate of ozone loss. The ozone depletion also predicts an observed gradient in film growth rate under sub-saturation conditions along the length of the reactor. During TMA/O₃, O insertion leads to surface methoxy and formate groups at low temperature, whereas surface hydroxyls form at higher temperature. In our reactor, QCM analysis shows evidence for this temperature-dependent surface reaction mechanism at 2 Torr, and it persists at 760 Torr under saturated conditions. Under saturated growth conditions, TOF-SIMS analysis shows films deposited at 2 Torr and 760 Torr have similar composition, with some extra carbon contamination at higher pressure. Overall, similar ALD growth can be achieved for TMA/O₃ at 760 Torr and ~2 Torr, where care must be taken to take into account the faster rate of O₃ dissociation at higher pressures, especially at higher temperature.

11:20am TF+PS-MoM10 Integration of Feature and Reactor Scales during the Simulation of ALD Scale Up, *Angel Yanguas-Gil, J.A. Libera, J.W. Elam, Argonne National Laboratory*

As the number of ALD processes, materials and applications increase, it is becoming increasingly important to develop the ability to screen and identify the most prominent candidates for scale up. Precursor pressure, reaction probability, ideality of the surface chemistry, but also other considerations like throughput, surface area, and materials utilization, are critical factors that will determine the feasibility of a particular process. In particular, there are three questions that need to be answered in the transition from lab-scale to manufacturing: 1) what is the impact of a particular precursor chemistry, 2) what are the best processing conditions for a given precursor and substrate, 3) what is the optimal reactor design?

In this talk we will focus on the issue of predicting the scalability and fundamental economics (throughput, precursor utilization) of lab-scale ALD processes. Our approach, developed as part of our work on process development and scale up, combines the experimental characterization of ALD processes in bench-scale reactors, the use of simple analytic models, and the development of new 3D multiscale simulation tools that are

* Paul Holloway Award Winner

optimized to the conditions typically found under ALD conditions, including providing simulated quartz crystal microbalance and mass spectrometry data at any point of the reactor.

Our code, based on open-source libraries, is able to incorporate high-surface area substrates on reactor scale simulations for both cross-flow and roll-to-roll processes, and it takes advantage of the ALD surface chemistry to achieve an extremely efficient two-way coupling between reactor and feature length scales. This method is based on a new approach to simulate feature scale coating that essentially provides the infinite trajectory-limit of the Monte Carlo simulations typically used in the literature.

Besides the description of the model and its implementation, we will exemplify our methodology by presenting results of different metal oxides by ALD, including the validation of the code in a large area reactor. We will also show the results of a parametric study on the impact of non-ideal surface chemistry as well as the presence of high surface area materials / nanostructured features on the substrate. According to the results obtained, the presence of high surface area materials makes continuum ALD processes like R2R more efficient. This is a consequence of a more general result of our parametric study, which shows that high reaction probabilities play an important role in ALD scale up.

Vacuum Technology

Room: 303 - Session VT-MoM

Vacuum Measurement, Calibration, and Primary Standards

Moderator: Steve Borichevsky, Applied Materials, Varian Semiconductor Equipment, Yulin Li, Cornell University

8:20am **VT-MoM1 Miniature Fiber Optic Pressure Sensors: Technologies and Applications**, *Miao Yu*, University of Maryland, College Park **INVITED**

Compared with their electrical counterparts, fiber optical sensors offer many advantages including small size, immunity to electromagnetic interference, convenient light guiding through optical fibers, high sensitivity, high resolution, large bandwidth, and low noise. Recently, miniature fiber optic pressure sensors have attracted much attention for many applications including biomedical, surveillance, and industrial applications. Most of these sensors are based on a Fabry-Perot interferometer fabricated directly on an optical fiber end face with a silica/silicon (Si) diaphragm serving as a pressure transducer. Although these sensors have a small size (~100s microns in diameter), they suffer from important issues including low sensitivity due to the high elastic moduli of silica/Si (130-185 GPa), and high brittleness and easy breakage of the sensor elements.

In this paper, the research program at the Sensors and Actuators Laboratory (SAL) of the University of Maryland on miniature fiber optic pressure sensors based on polymer or graphene diaphragms will be introduced. First, our work on polymer based miniature optical pressure sensors will be discussed. The polymer materials have superior elasticity and high fracture strength, which enables polymer based sensors to have superior sensitivity even at a small size and helps prevent cracking or breaking of the sensors. Furthermore, these sensors can be fabricated by using relatively simple and inexpensive processes. We have developed several unique low-cost micro-fabrication processes for these sensors, including self-aligned photolithography and UV molding process. By using simple and safe procedures, a polymer based Fabry-Perot cavity can be directly fabricated at the end of optical fiber, thus eliminating the necessity for complicated assembly of the sensing element and the optical fiber. Further, since polymer based sensors inherently suffer from temperature drift due to the large thermal expansion coefficient of polymer materials, novel temperature compensation methods for the polymer based fiber optic pressure sensors will also be discussed. Second, miniature fiber optic pressure sensors utilizing a graphene diaphragm will be presented. Graphene is believed to be one of the strongest materials and the thinnest film in the universe, and it can be stretched by as much as 20%. These unique mechanical properties render graphene an excellent choice for miniature acoustic sensors with unprecedentedly high sensitivity, large bandwidth, and large dynamic range. Finally, the potential applications of these different sensors will be discussed.

9:00am **VT-MoM3 Quantum Based Vacuum Standard**, *Jay Hendricks, J.A. Stone, J.E. Ricker, P.F. Egan, G.E. Scace, D.A. Olson*, National Institute of Standards and Technology, *D.R. Gerty*, Sandia National Laboratories, *G.F. Strouse*, National Institute of Standards and Technology. The future of pressure and vacuum measurement will employ lasers, Fabry-Perot optical cavities, and quantum physics. Photons interact at the quantum

level with matter such that light travels at a slower speed in gas than it does in vacuum. NIST is developing a fixed length optical cavity (FLOC) and variable length optical cavity (VLOC) that will make simultaneous ultra-precise measurements of vacuum and gas cavity photon-path-lengths. While pressure is a widely measured unit in every day processes, the standard on which it is based, the mercury manometer is quite old and traces its early beginnings to 1643. In the future, the mercury barometer will be replaced with a new standard based on quantum chemistry calculations of helium's refractive index. This will enable the replacement of all artifact-based mercury standards. Measuring pressure optically represents a paradigm shift in the way the unit is realized and will move us from a primary standard based on an artifact to a primary standard based on quantum-chemistry calculations of helium's refractive index. This talk will cover current status and early prototype results of NIST's Innovations Measurement Science (IMS) project (the second year of five) that will have profound impacts on how pressure, temperature and length in air measurements are made in the future. While the primary aim of the project is to create new measurement infrastructure for NIST, it will also create exciting spin-off technology that will have large impacts for US manufacturing and world metrology.

9:20am **VT-MoM4 New PTB Standard to Provide Traceability for Partial Pressure Measurement**, *Karl Jousten*, Physikalisch-Technische Bundesanstalt (PTB), Germany

Partial pressure measurement in vacuum by quadrupole mass spectrometer (QMS) is an important tool to control and monitor processes in industry and to measure outgassing rates. It is, however, difficult to obtain reliable results with quadrupole mass spectrometers, since its calibration is ill-defined and at present there is no traceability to any national primary standard.

PTB has recently established a new calibration system to calibrate QMS. It is based on the continuous expansion method and allows generating three partial pressures at the same time in the calibration chamber with pressure ratios between them of a factor of up to 10^8 with the uncertainty of each partial pressure depending on the value and the gas species. In the minimum the uncertainty of partial pressure is close to 1%. With less accuracy more gas species than three can be mixed.

The flow of desired gas into the calibration chamber is generated by nano-holes, glass capillaries or sintered elements characterized in terms of conductances for some gas species. Since the flow through these conductance elements is of molecular type up to about 10 kPa, the flow can be predicted for any gas species.

Four QMS were characterized with the new system and some results will be given. The first goal with this standard is to test and establish calibration procedures for written standards for several parameters of QMS like sensitivity, minimum partial pressure and minimum concentration.

Support through the EMRP IND12 project is gratefully acknowledged. The EMRP is jointly funded by the EMRP participating countries within EURAMET and the European Union.

9:40am **VT-MoM5 Study of Long Term Stability of Quadrupole Mass Spectrometers**, *Janez Setina*, Institute of Metals and Technology (IMT), Slovenia, *A. Elkatmis, R. Kangi*, Ulusal Metroloji Enstitüsü (TUBITAK UME), Turkey, *K. Jousten*, Physikalisch-Technische Bundesanstalt (PTB), Germany, *M. Bergoglio*, Istituto Nazionale di Ricerca Metrologica (INRIM), Italy, *F. Boineau*, Laboratoire National de métrologie et d'Essais (LNE), France, *S. Ruiz*, Centro Español de Metrología (CEM), Spain, *M. Vicar*, Czech Metrology Institute (CMI), Czech Republic

Quadrupole mass spectrometers (QMS) are widely used in industry for leak detection, residual gas analysis and measurements and control of gas composition in vacuum processes, which require well defined partial pressures of different gases in low pressure environment. Consistent measurements and process stability are possible solely if measurement instrumentation is sufficiently stable with time. Only few studies about the time stability of QMS have been reported in the literature. They mainly indicate that QMS instruments are less stable than typical Bayard-Alpert ionization gauges, so frequent recalibrations may be required.

To get information about typical quality of commercial instruments, a group of European national metrology institutes performed a joint study of time stability of some metrological characteristics of seven different QMS. Parameters under study included: sensitivity for gases He and N₂, mass resolution, mass scale stability, secondary electron multiplier (SEM) gain, and minimum detectable partial pressure. Typical check intervals were 3 months. Study started in the middle of 2012 and the overall duration was two years.

In 3 months periods the typical changes of sensitivity between 10% and 30% were observed. The peak positions were stable within 0.05 amu and 0.2 amu and mass resolution was stable within 0.02 and 0.05 amu. For most of instruments a gradual decrease of the SEM gain as a result of aging of the

multiplier was observed. For some instruments the SEM gain dropped by more than 40 % in 2 years period.

Support through the EMRP IND12 project is gratefully acknowledged. The EMRP is jointly funded by the EMRP participating countries within EURAMET and the European Union.

10:00am **VT-MoM6 The Stability of Spinning Rotor Gauges as Transfer Standards, James Fedchak**, National Institute of Standards and Technology (NIST)

The spinning rotor gauge (SRG) has long been used as a transfer standard for high vacuum calibrations and in national and international intercomparisons of high-vacuum standards. It is typically used over a pressure range of 1×10^{-4} Pa to 1.0 Pa (10^{-6} Torr to 10 mTorr) and tends to be favored by metrology and calibration laboratories because of its reputation as being a very stable standard. Here we will review the stability data for SRGs used in international key comparisons. Different rotor materials and various transfer techniques have been employed in these comparisons. These will be discussed in context of the best practices and techniques that have produced the best rotor stability. Various factors which may affect rotor stability will also be discussed, and data taken at NIST as well as that found in the literature will be presented. The goal of this study is to establish the best practices for the use of a spinning rotor gauge as a transfer standard, as well as establishing the best stability that can be reasonably achieved.

10:40am **VT-MoM8 Pilot Study for International Comparison of Absolute Pressure Measurement from 3×10^{-9} Pa to 9×10^{-4} Pa, Hajime Yoshida, K. Arai, E. Komatsu, K. Fujii**, National Institute of Advanced Industrial Science and Technology (AIST), Japan, *K. Jousten, T. Bock*, Physikalisch-Technische Bundesanstalt (PTB), Germany

International comparison of absolute pressure measurements in gas from 3×10^{-6} Pa to 9×10^{-4} Pa, identified as CCM.P-K3, was performed from 1998 to 2002 to determine the degree of equivalence of national metrology institutes (NMIs). A new international comparison, where the pressure range is expanded down to 3×10^{-9} Pa, is planned as CCM.P-K3 follower. A pilot study was performed in advance because two challenging issues are including the CCM.P-K3 follower. One is the stability of extreme high vacuum (XHV) gauge as a transfer standard. XHV gauges are kinds of hot cathode ionization gauges with a structure to reduce disturbances such as X-ray, electron stimulated desorption (ESD) ion, and so on. Few experiments are reported about the stability of XHV gauges from the viewpoint of metrology. The other is the stability of transfer gauges against to repeating bake-out because baking the calibration chamber including transfer gauges is inevitable to achieve XHV.

At first, three types of XHV gauges; Axial-symmetric transmission gauge (ATG), extractor gauge (EXG), and bent belt-beam gauge (3BG) were tested in NMIJ. Stabilities against air exposure and following bake-out were also tested for both XHV gauges and spinning rotor gauges (SRGs). A protocol for pilot study from 3×10^{-9} Pa to 9×10^{-4} Pa was prepared based on the results of both these tests and previous CCM.P-K3. ATG and EXG were adopted as transfer gauges because of achievements so far, although the stabilities of tested XHV gauges were comparable. In addition, two SRGs (SRG-1 and SRG-2) were also adopted as transfer gauges to calibrate at 9×10^{-4} Pa because stabilities of SRGs were expected to be better than those of XHV gauges. Measurement results of XHV gauges are normalized by those of SRGs. No significant differences of stabilities were observed whether the calibration gas was N_2 or Ar. N_2 was selected as the calibration gas because N_2 is typical calibration gas for ionization gauges.

A bilateral comparison between NMIJ and PTB was performed from May 2013 to Jan 2014 to confirm the effectiveness and to test the transport stability of the transfer standards. Shift of sensitivities of ATG, EXG, SRG-1, and SRG-2 were less than 0.58 %, 0.67 %, 3.5 %, and 0.28 %, respectively. The results of comparison were summarized except for data of SRG-1 because it clearly shows the drift of the sensitivity (effective accommodation coefficient). Results of the comparison show good agreement within the claimed uncertainty. Details will be presented at the conference.

11:00am **VT-MoM9 Stability of the Cold Cathode Ionization Gauge, Paul Arnold, G.A. Brucker**, Granville-Phillips Vacuum Products

A study of the stability of cold cathode ionization gauges (CCIG) using an evaluation of physics principles affecting the ionization properties of the CCIG has been performed. The variation of the response to pressure of the CCIG is significantly dependent upon the interaction of the plasma discharge with the interior surfaces of the CCIG occurring during operation of the CCIG. New investigations will demonstrate these effects. The concept of measured pressure dose provides an index of likely drift in CCIG performance resultant from the magnitude of the plasma interaction, including the concept of remaining gauge useful life. The nature of the

above plasma interaction changes the magnetic field internal to the CCIG as well as electron production from the cathode electrode, resulting in drift in CCIG performance. Both simulation and test data of these phenomena will be presented, showing relation of pressure dose to pressure performance with explanation of mechanisms.

11:20am **VT-MoM10 Cold Cathode Ionization Gauge Design Mitigates Well-known Performance Issues, Brandon Kelly, G.A. Brucker**, Granville-Phillips Vacuum Products

Cold Cathode Ionization Gauges (CCIGs) are a well established indirect pressure measurement tool that has well documented advantages and shortcomings. In an attempt to overcome these design challenges a series of experiments have been conducted exploring different electrode geometries and configurations. Included in these experiments are high power magnet assemblies with unique discharge chamber geometries aimed at increasing device sensitivity at UHV pressures. Various modifications and methods have been tested to control the plasma discharge interaction with the interior of the CCIG for which increased lifetime will be shown. In addition to gauge sensitivity, other common shortcomings are addressed such as high vacuum starting time statistics and the separation of leakage current from plasma (i.e. discharge) current. A novel ionization chamber design prevents the escape of material from the internal surfaces of the gauge while preserving adequate conductance to the vacuum chamber and providing the ability to replace parts in the field. The theory and details of these new sensor design modifications will be discussed offering an insight into the next generation of cold cathode ionization gauges.

11:40am **VT-MoM11 A Systematic Study of Long-Term Vacuum Gauge Performance, Gerardo Brucker, S. Heinbuch, T.C. Swinney**, Granville-Phillips Vacuum Products

Cold Cathode Ionization Gauges (CCIGs) have been the subject of numerous investigations throughout several decades. The free-running characteristics of their pure electron plasma, combined with the in-depth investigation of this phenomenon interacting with the interior of these devices, have led to numerous theories and speculation regarding the factors that regulate the long term performance of the gauges. Our laboratory has become increasingly interested in extending gauge lifetime through improved design and in the development of innovative dose calculation methodologies that can provide an adequate estimation of gauge remaining lifetime. We are particularly interested in understanding the phenomena that lead to drifts in gauge sensitivity with dose and specific gas chemistry. During our long term studies, gauge sensitivity is tracked over time against dose and the most modern surface and chemical analysis methodologies are employed to detect and understand the physico-chemical changes that take place at the internal electrodes. In this presentation we will demonstrate that while attempting to understand changes in gauge sensitivity it is equally important to consider changes in the magnetic as well as the internal electric characteristics of cold cathode gauges. Prior work by other groups has focused heavily on the influence of surface chemistry modifications. Our recent work will demonstrate that equal attention must be paid to the internal magnetic properties to fully account for long term changes in sensitivity.

Monday Afternoon, November 10, 2014

2D Materials Focus Topic

Room: 310 - Session 2D+AS+EM+NS+SS-MoA

Dopants, Defects, and Interfaces in 2D Materials

Moderator: Jun Lou, Rice University

2:00pm **2D+AS+EM+NS+SS-MoA1 Cutting and Assembling 2 Nanometer Voids in Single Layer Hexagonal Boron Nitride**, *Thomas Greber, H.Y. Cun, M. Iannuzzi, A. Hemmi, J. Osterwalder*, University of Zurich, Switzerland **INVITED**

Argon implantation beneath hexagonal boron nitride nanomesh on Rh(111) [1] leads to the formation of vacancy and interstitial defects [2]. The nanomesh is a single layer of hexagonal boron nitride on Rh(111), where 13x13 h-BN units accommodate on 12x12 Rh unit cells. The resulting super-honeycomb has a lattice constant of 3.2 nm and consists in regions where the h-BN “wets” the Rh substrate (pores), and regions where h-BN is quasi freestanding (wires) [3].

The interstitial defects are called “nanotents”, where atoms are trapped beneath the ultimately thin “rainfly” made of a single layer of h-BN [2,4]. They are stable at room temperature and survive exposure to air.

The vacancy defects are sites where a boron or a nitrogen atom was kicked out by the Ar ion impact. If the implanted structures are annealed to 900 K the can-opener effect occurs: 2 nm h-BN-flakes or “lids” are cut out of the h-BN nanomesh and 2 nm voids form [2]. At higher temperatures the resulting voids may diffuse and assemble, due to their repulsive interaction, in a super-structure with some order, i.e., a nearest neighbor distance of about 15 nm. Near the disintegration temperature of the h-BN nanomesh we finally observe self-healing of the voids in the nanomesh, which we assign to their annihilation in larger holes in the structure.

The report bases on scanning tunneling microscopy, x-ray photoelectron spectroscopy, molecular dynamics and density functional theory calculations.

Financial support by the Swiss National Science Foundation and support by the EC under the Graphene Flagship (contract no. CNECT-ICT-604391) is gratefully acknowledged. We thank the Swiss National Supercomputer Centre (CSCS) for allocation of computer time.

[1] M. Corso et al. *Science*, 303 (2004) 217.

[2] H. Y. Cun et al. *Nano Letters* 13 (2013) 2098.

[3] S. Berner et al. *Angew. Chem. Int. Ed.* 46 (2007) 5115.

[4] H.Y. Cun et al. *ACS Nano* 8 (2014) 1014.

2:40pm **2D+AS+EM+NS+SS-MoA3 Engineering Structural Defects in Graphene Materials**, *Jeremy Robinson, M. Zhaludinov, J. Culbertson, C. Junkermier, P.E. Sheehan, T. Reinecke, A. Friedman*, Naval Research Laboratory

Graphene's atomic thinness makes it highly sensitive to surface adsorbates or defects within its carbon backbone. Aside from the known effects and impact on electronic properties, here we demonstrate the impact of defects on the mechanical properties and the response of mechanical resonators. In particular, once defects are formed in atomically-thin materials they can be quite mobile and form more complicated defect structures such as bi- or tetra-vacancy clusters. We execute experiments using mechanical drum resonators made from single- to multi- to many-layer graphene systems. We use both CVD grown graphene and reduced graphene oxide (rGO) films to capture a wide range of defect structures. By measuring the fundamental frequency response of the resonators (in the MHz range) we extract properties such as tension, quality factor, and modulus as a function of external manipulation [1]. For highly defective rGO films measuring 10-40nm thick, we can tune the frequency response by 500% and quality factor by 20x through laser annealing, which effectively rearranges defects throughout the film [1]. Alternatively, using graphene 1-4 layers thick, we find the resonator response is significantly more sensitive to the formation and annihilation of meta-stable defects, such as the tetra-vacancy structure. We will show how the defect mobility and resonator response changes with different energy photons and come to understand these differences based on calculated defect migration energies of different defects types in graphene.

[1] *Nano Letters* 12, 4212 (2012)

3:00pm **2D+AS+EM+NS+SS-MoA4 Graphene Cleaning using a Low Energy Ar Ion Beam**, *KiSeok Kim, G. Yeom*, Sungkyunkwan University, Republic of Korea

Recently, graphene has been widely investigated due to the superior electrical, mechanical, thermal, and chemical properties. Especially, CVD graphene which was grown on Cu foil and transferred to various substrates using PMMA has been used most widely due to the possible large area applications such as electronic devices for displays, semiconductors, etc. However, in order to apply the transferred CVD graphene to the various electronic device fabrication, PMMA residue on the graphene surface formed during the transfer process and lithography process needs to be completely removed without damage. Various methods have been investigated to remove the residue on the graphene surface such as current cleaning, heat treatment, chemical cleaning, etc. However, it is reported that these methods are not effective in removing the residue on graphene or not applicable to industry.

In this study, a controlled Ar ion beam has been used to effectively remove the PMMA residue on graphene surface. By controlling the Ar ion beam condition, the residue on graphene surface could be removed while minimizing the damage on the graphene surface. Especially, by lowering the Ar beam energy less than 10 eV, it was possible to effectively remove the PMMA residue without damaging the graphene. The removal of PMMA residue on the graphene surface could be identified using Raman Spectroscopy showing the red shift of 2D peak (2670 cm^{-1}) and blue shift of G peak (1580 cm^{-1}) in addition to the decrease of RMS roughness from 1.3nm to 0.3 nm using an AFM (Atomic Force Microscopy). The effectiveness of graphene cleaning was also confirmed by XPS (X-ray Photoelectron Spectroscopy), by the uniform deposition of ALD HfO_2 layer on the cleaned graphene surface, by measuring the electrical properties of deposited ALD HfO_2 , etc.

3:40pm **2D+AS+EM+NS+SS-MoA6 Electronic Structure Modification in van der Waals Heterostructures: Interlayer Hybridization in the Case of Graphene/MoS₂**, *Matthias Batzill, H. Coy-Diaz*, University of South Florida, *M.C. Asensio*, Synchrotron Soleil, France, *J. Avila*, Synchrotron Soleil

Artificial van der Waals heterostructures promise to combine materials with diverse properties. Simple mechanical stacking or conventional growth of molecular hetero-layers would enable fabrication of novel materials or device-structures with atomically precise interfaces. Because covalent bonding in these layered materials is limited to molecular-planes, interface interactions between dissimilar materials are expected to modify the properties of the individual layers only weakly. Here we prepare graphene/MoS₂ heterostructures by transferring CVD-grown graphene onto a MoS₂ substrate. It is shown that high quality interfaces between graphene and MoS₂ can be obtained by UHV annealing. The quality of the graphene is demonstrated by atomic resolution scanning tunneling microscopy of ultraflat graphene. The electronic structure of the interface between the polycrystalline graphene and a MoS₂ substrate is measured by angle resolved photoemission spectroscopy (ARPES) and nano-ARPES utilizing a focused photon beam at the SOLEIL synchrotron. We show that at the Fermi-level graphene exhibits a perfect, gapless and undoped Dirac-cone. However, in regions where the π -band of graphene overlaps with states of the MoS₂ substrate, opening of several band-gaps are observed. This demonstrates that the electronic properties in van der Waals heterostructures can be significantly modified by interlayer interaction and thus exemplifying opportunities for tuning materials properties of graphene and other 2D-materials by interfacing them with dissimilar van-der Waals materials.

4:00pm **2D+AS+EM+NS+SS-MoA7 Edge States and Exposure to Hydrogen of Silicon at the 2D Limit on Ag(111)**, *A.J. Mannix, B.T. Kiraly*, Argonne National Laboratory, *M.C. Hersam*, Northwestern University, *Nathan Guisinger*, Argonne National Laboratory

Chemical functionalization of atomically thin materials results in significant modifications to their electronic properties, which can be exploited in device applications. Compared to the chemical inertness of graphene, 2D silicon is expected to exhibit greater reactivity, and thus a greater amenability to chemical functionalization. Among potential functionalization chemistries, hydrogen termination is favored for its relative simplicity and proven efficacy with graphene and bulk Si surfaces. Using ultra-high vacuum (UHV) scanning tunneling microscopy (STM), we have studied the temperature-dependent effects of exposing 2D silicon platelets grown on Ag(111) to molecular and atomic hydrogen. At low doses, atomic hydrogen results in limited adsorption and temperature dependent etching. In the bulk, the formation of vacancies and extended

etch pits is observed. In addition, edge states can play a critical role in the electronic properties of 2D materials. We have also examined at the atomic-scale the edges of 2D silicon platelets.

4:20pm **2D+AS+EM+NS+SS-MoA8 Chlorine Trap-Doping for Transparent, Conductive, Thermally Stable and Damage-Free Graphene.** *Pham Viet Phuong, K.N. Kim, M.H. Jeon, K.S. Kim, G. Yeom*, Sungkyunkwan University, Republic of Korea

We propose a novel doping method of graphene by cyclic trap-doping with low energy chlorine adsorption. Low energy chlorine adsorption for graphene chlorination avoided defect (D-band) formation during doping by maintaining the π -bonding of the graphene, which affects conductivity. In addition, by trapping chlorine dopants between the graphene layers, the proposed doping method dramatically decreased the sheet resistance by ~88% at an optimized condition. Among the reported doping methods including chemical, plasma, photochemical methods etc., the proposed doping method is believed to be the most promising for producing graphene of extremely high transmittance, low sheet resistance, high thermal stability, and high flexibility for use in various flexible electronic devices. Results of angle resolved X-ray photoelectron spectroscopy (XPS), high-resolution transmission electron spectroscopy (HR-TEM), Raman spectroscopy, ultraviolet-Visible spectroscopy (UV-Vis) and sheet resistance, showed that this method is also non-destructive and controllable. The sheet resistance of the doped tri-layer graphene was 70 Ω /sq at 94% transmittance, which was maintained for more than 6.5 h at 230°C. Moreover, the defect intensity of graphene was not increased during the cyclic trap-doping.

4:40pm **2D+AS+EM+NS+SS-MoA9 Modification of Graphene by Neutral Beam Irradiation and Edge Structure Analysis.** *Takeru Okada, S. Samukawa*, Tohoku University, Japan

Since the discovery of single layer of Graphite, Graphene, a single layer of hexagonal carbon atoms, has attracted much attention and shown exciting specific properties. Graphene is a zero band gap semiconductor. Therefore band gap control is one of most important issue to apply for electronic device applications. In order to construct electronic devices with logic operation, both p- and n-type conduction and the control of the carrier density in an active channel are required. Doping with foreign atoms, such as N and B, has proven to be an effective way to modify the electronic properties of carbon related materials and extend their applications. In particular, nitrogen doping brings a carrier which could turn carbon nanotube into n-type semiconductors. It is also feasible to modify the electronic properties of Graphene. Although several doping methods have reported so far, process damages (defect generation) cause degradation of electronic properties.

In this paper, we introduce ultra-low damage neutral beam system which consists of a plasma and process chambers that are separated by a carbon aperture. Charged species and ultra-violet photon from the plasma can be effectively eliminated by the aperture. As a result, only the neutral beam arrives the surface of the sample at the substrate in the process chamber.

We used nitrogen gas for plasma generation and adopted multi-layer Graphene to investigate nitridation mechanism. Graphene multi-layer was irradiated by nitrogen neutral beam with controlled energy of 10 eV at room temperature. The surface modification was analyzed by x-ray photoelectron spectroscopy (XPS). XPS analysis indicated that the carbon atoms were substituted to nitrogen atom and atomic concentration of nitrogen reaches 15 %. Additionally, bonding state of C and N was found to depend on neutral beam irradiation time. Thus beam energy controlled neutral beam can selective nitridation of Graphene. Furthermore the doping density is estimated by Raman spectroscopy and result in 10^{12} [cm⁻²], which is enough to n-type doping of Graphene.

5:00pm **2D+AS+EM+NS+SS-MoA10 Growth Mechanism of Metal Clusters on a Graphene/Ru(0001) Template.** *Shixuan Du, L.Z. Zhang*, Chinese Academy of Sciences, *W. Hofer*, University of Liverpool, UK, *H.-J. Gao*, Chinese Academy of Sciences

Metal nano-clusters have attracted considerable interest because of the potential applications in catalysis and information storage. Due to the soft nature of epitaxial graphene and the lattice mismatch between graphene and metal substrates periodic moiré patterns can be formed. A graphene/metal template, moiré template, can be used to grow dispersed metal nano-clusters with controllable size and shape, or metal clusters with large size and metal layers. However, how intrinsic properties of metal atoms and the moiré template influence the selective adsorption and the growth mode of metal clusters is still open to debate. A general rule, predicting the morphology of metal nano-clusters on a G/metal surface, important to guide experimenters, is still missing. Using first-principles calculations combined with scanning tunneling microscopy experiments, we investigated the adsorption configurations, electronic structures and the corresponding growth mechanism of several transition metal (TM) atoms (Pt, Ru, Ir, Ti, Pd, Au,

Ag, and Cu) on a graphene/Ru(0001) moiré template (G/Ru(0001)) at low coverage. We find that Pt, Ru, Ir, and Ti selectively adsorb on the fcc region of G/Ru(0001) and form ordered dispersed metal nano-clusters. This behavior is due to the unoccupied *d* orbital of the TM atoms and the strong *sp*³ hybridization of carbon atoms in the fcc region of G/Ru(0001). Pd, Au, Ag, and Cu form nonselective structures because of the fully occupied *d* orbital. This mechanism can be extended to metals on a graphene/Rh(111) template. By using Pt as an example, we provide a layer by layer growth path for Pt nano-clusters in the fcc region of the G/Ru(0001). The simulations agree well with the experimental observations. Moreover, they also provide guidance for the selection of suitable metal atoms to form ordered dispersed metal nano-clusters on similar templates.

References:

1. L.Z. Zhang *et al.* Advanced Materials Interfaces, accepted.
2. Y. Pan *et al.* Applied Physics Letter, 95, 093106 (2009)

Actinides and Rare Earths Focus Topic
Room: 301 - Session AC+AS+MI+SA+SS-MoA

Theoretical Modeling of f Electron Systems

Moderator: Ladislav Havela, Charles University, Czech Republic

2:00pm **AC+AS+MI+SA+SS-MoA1 Nonmagnetic Ground State of PuO₂.** *Jindrich Kolorenc*, Academy of Sciences of the Czech Republic
INVITED

The correlated band theory implemented as a combination of the local density approximation with the dynamical mean-field theory is applied to PuO₂. We obtain an insulating electronic structure consistent with the experimental photoemission spectra, and a nonmagnetic ground state that is characterized by a noninteger filling of the plutonium *f* shell ($n_f \approx 4.4$). Due to a sizable hybridization of the *f* shell with the *p* states of oxygen, the ground state is more complex than the four-electron Russell-Saunders ³L₄ manifold split by the crystal field. The dynamical mean-field theory, which in the present case can be schematically viewed as an extension of the crystal-field model with hybridization terms, improves the agreement between the theory and experiment for the magnetic susceptibility [1]. Encouraged by the good accuracy achieved for PuO₂, we apply the theory to several other tetravalent actinide oxides.

[1] A. B. Shick, J. Kolorenc, L. Havela, T. Gouder, and R. Caciuffo, Phys. Rev. B **89**, 041109 (2014).

2:40pm **AC+AS+MI+SA+SS-MoA3 DMFT Modeling of Local Spectral Properties in Pu-based Actinides.** *Jian-Xin Zhu*, Los Alamos National Laboratory
INVITED

Plutonium-based materials have been studied for many years due to their importance in nuclear energy applications. Scientifically, these materials exhibit highly complex properties. Pu metal shows a significant volume expansion and anomalous magnetic properties; while Pu-115 (like PuCoGa₅) are found to be superconductors. These intriguing phenomena originate from the special location of Pu in the Periodic Table, which is at the boundary between the light actinides that have itinerant 5*f* electrons and the heavy actinides with localized 5*f* electrons. They call out the notion of strong correlation of 5*f* electrons. In this talk, I will present a study of the electronic structure of Pu metals and its 115 compounds in the framework of the combination of local density functional approximation and dynamical mean-field theory. In particular, the results on momentum-resolved spectral functions will be presented and be compared with those based on the LDA only. In addition, the effect of Pu 5*f* electron occupancy on the electronic structure of these systems will also be discussed. The test of these results by future angle-resolved photoemission spectroscopy measurements will give a stringent constraint on the theoretical approach.

3:40pm **AC+AS+MI+SA+SS-MoA6 The Evolution in Pu Nanocluster Electronic Structure: From Atomicity to Three-Dimensionality.** *James Tobin, S.W. Yu, B.W. Chung*, Lawrence Livermore National Laboratory, *M.V. Ryzhkov*, Russian Academy of Science-Urals, *A. Mirmelstein*, Russian Federation Nuclear Lab (VNIITF)

The development of electronic structure in solid systems as a function of size has long been a subject of great interest and extensive scientific investigation. Experimentally, the transition, from nanoscale or mesoscopic to bulk behavior in metal clusters, was reported in 1981 by Mason and co-workers. Similarly, the evolution from two-dimensional to three-dimensional band structure in metal overlayers and the manifestation of nanoscale effects in compound semiconductor have also observed. In the

area of actinide materials, the progress has been slowed by the limitations imposed by the highly radioactive, chemically toxic and pyrolytic nature of these materials. Havela and Gouder and colleagues performed investigations upon Plutonium (Pu) ultra-thin films, deposited in situ by means of a discharge-plasma, and Trelenberg and co-workers developed an approach using laser ablation of Uranium (U). Gas phase studies of actinides have also been pursued including atoms, molecules and reactions. Recent theoretical studies include UO_2 molecules, solid actinide oxides, and actinide carbide clusters. A new approach to cluster calculations has been taken in this study. Past cluster calculations were arranged in such a way that the central atom would exist in a bulk like environment. In calculations herein, it is expected that the central atom will be in the most bulk-like environment as well. However, just as in any finite size object, there will be variation of potential at the positions of symmetry non-equivalent atoms within the simulated cluster. Hence, averaging over all of the atoms in the cluster will give a measure of the effect of size. We will use this aspect of cluster calculations to investigate size related effects. Here, we report the result of the calculation of the electronic structure of clusters of Pu and their comparison to bulk spectroscopic results. Lawrence Livermore National Laboratory is operated by Lawrence Livermore National Security, LLC, for the U.S. Department of Energy, National Nuclear Security Administration under Contract No. DE-AC52-07NA27344. Work at the RAS and VNIITF was supported in part by Contract B590089 between LLNL and VNIITF. The Advanced Light Source (ALS) in Berkeley and the Stanford Synchrotron Radiation Laboratory are supported

by the DOE Office of Science, Office of Basic Energy Science. For more detail see: M.V. Ryzhkov, A. Mirmelstein, S.-W. Yu, B.W. Chung and J.G. Tobin, "Probing Actinide Electronic Structure through Pu Cluster Calculations," *Intl. J. Quantum Chem.* **113**, 1957 (2013); COVER ARTICLE .

4:00pm **AC+AS+MI+SA+SS-MoA7 First-Principles Density Functional Theory Simulation on Rare-Earth-Based Oxides as Fast Oxygen Ion Conductors, Mamoru Sakaue, M. Alaydrus, H. Kasai, Osaka University, Japan, T. Ishihara, Kyushu University, Japan**

Development of novel fast ion conductors is a crucial issue for realizing solid oxide fuel cells (SOFCs) which can operate in low temperatures. While yttria-stabilized zirconia (YSZ) had been well-studied both by experiments and theories, exploration of other types of materials retaining high ionic conductivities in lower temperatures is still desired. Experimental studies in the recent twenty years have found some rare-earth-based oxides having higher ionic conductivities to be promising for operation below 600°C , and first-principles simulation studies on the materials have begun.

We studied atomic and electronic properties on oxygen-ionic conduction of LaGaO_3 -, La_2GeO_5 -, Pr_2NiO_4 - and CeO_2 -based materials by first-principles calculations based on density functional theory (DFT). We analyzed stable structures, electronic densities of states, oxygen migration paths and activation energies in the paths of pure and doped materials in order to evaluate their capabilities in application to electrolytes or electrodes. The obtained results of the activation energies showed good agreements with experiments in several aspects. However, for Pr_2NiO_4 - and CeO_2 -based materials that contain lanthanoid elements, there remains an open question about theoretical treatment of $4f$ electron states. The strong localization was found to affect oxygen ion motions fundamentally as well as electronic/magnetic properties. Then the strong electron-electron correlation modifies simple trends in activation energies found for the lanthanoid series within an approximation in which the correlation effects were neglected [1].

While fundamental reproduction of the strong electron-electron correlation in localized states by DFT is extremely difficult, empirical corrections by Hubbard U terms enable a practical solution to this problem. Here, the U value can be determined only by comparison with experiments in most cases because the value is affected by environment of the lanthanoid atoms. However, a theoretical study based on an empirical model demonstrated that the environment effects on $4f$ orbitals can be small if its strong localization is maintained [2]. In the presentation, we confirm this rule based on the results by the DFT first-principles calculations with Hubbard U corrections and discuss possibilities of computational materials design of lanthanoid-doped ceria ($\text{Ce}_{1-x}\text{Ln}_x\text{O}_{2-x/2}$) as electrolyte materials.

[1] M. Alaydrus, M. Sakaue, S. M. Aspera, T. D. K. Wungu, T. P. T. Linh, H. Kasai, T. Ishihara and T. Mohri, *J. Phys. Condens. Matter* **25**, 225401 (2013).

[2] E. Rogers, P. Dorenbos and E. van der Kolk, *New J. Phys.* **13**, 093038 (2011).

4:20pm **AC+AS+MI+SA+SS-MoA8 Electronic Structure, Magnetic Properties, and Magneto-Structural Transformations of Rare Earth Magneto-Caloric Materials, Durga Paudyal, Ames Laboratory, V.K. Pecharsky, K.A. Gschneidner, Jr., Ames Laboratory and Iowa State University** **INVITED**

We present first principles modeling of structural and magnetic properties of Gd_5Ge_4 based magneto-caloric materials. The total energy as a function of the shear displacement of slabs confirms stability of experimentally observed crystal and magnetic structures. Small substitutions of the Gd by Y and Lu lead to a catastrophic loss of ferromagnetism, but the substitutions by La have no effect on the magnetism. Furthermore, substitutions of the Ge by Si exert chemical pressure and transform the antiferromagnetic O(II) to the ferromagnetic O(I) ground state. In addition, we present a pathway for estimating the magnetic entropy change in the room temperature giant magnetocaloric compounds, i.e. $\text{Gd}_5\text{Si}_2\text{Ge}_2$, by coupling first principles outputs with the established magneto-thermodynamic models. The theoretical values of the magnetic entropy change compare well with experimental results.

This work was supported by the U.S. Department of Energy (DOE), Office of Science, Basic Energy Sciences, Materials Science and Engineering Division. The research was performed at the Ames Laboratory, which is operated for the U.S. DOE by Iowa State University under contract # DE-AC02-07CH11358.

Applied Surface Science

Room: 316 - Session AS+BI+MC+SS-MoA

The Liquid Interface & Depth Profiling and Sputtering with Cluster Ion Beams

Moderator: Ian Gilmore, National Physical Laboratory, Michaelaelen Pacholski, The Dow Chemical Company

2:00pm **AS+BI+MC+SS-MoA1 Quantifying the Impact of Curvature, Convection and Complexity on Dynamic Interfacial Tension of Fluid-fluid Interfaces, Lynn Walker, Carnegie Mellon University** **INVITED**

The ability to control and predict the adsorption of species at fluid-fluid interfaces is a central issue in many materials processing problems. In most processing steps, this adsorption is dynamic and part of a larger transport problem that requires understanding of local fluid flow, bulk diffusion, interfacial curvature and the details of the adsorption and desorption kinetics. We have been developing tools and a protocol to allow the details of transport of surface active species to interfaces to be quantified. Several examples of the characterization of complex fluid-fluid interfaces will be discussed. The dynamics of adsorption of single and multicomponent surfactant mixtures at oil-water and air-water interfaces has been characterized using a microtensiometer. The use of microscale interfaces allows the transport processes involved in adsorption to be analyzed and both diffusion and kinetic parameters characterized. Microscale interfaces with high curvature allow the impact of curvature to be characterized on the dynamic interfacial tension (IFT) and mechanics of the interface. The scale of the device allows the bulk solution in contact with the interface to be changed rapidly. We are able to remove the bulk surfactant at different points in during the dynamics of adsorption by rinsing the interface and continuously replacing the bulk fluid with surfactant-free aqueous phase to investigate the reversibility of adsorption. For a bulky nonionic surfactant, a critical interfacial tension arises that links the transport dynamics to the onset of partial reversibility in the system. By measuring the mechanical properties of pre-rinsed and rinsed interfaces, we also find a critical interfacial tension that leads changes in the elasticity of the interfaces. The impact of changes in interfacial coverage on coalescence and competitive adsorption are characterized to demonstrate the connection between structure of complex interfaces and interfacial behavior.

2:40pm **AS+BI+MC+SS-MoA3 In Situ Probing of Liquid Surfaces and Interfaces by Time-of-Flight Secondary Ion Mass Spectrometry, Xiao-Ying Yu, Pacific Northwest National Laboratory**

The surfaces of aqueous phases and films can have unique kinetics and thermodynamics, distinct from the bulk. However, major surface analytical techniques are mostly vacuum-based and direct applications for volatile liquid studies are difficult. We developed a vacuum compatible microfluidic interface to enable direct observation of liquid surfaces and liquid-solid interactions. The unique aspect of our approach is that 1) the detection window is an aperture of 2-3 micrometers in diameter, which allows direct imaging of the liquid surface, and 2) surface tension is used to hold the liquid within the aperture. The microfluidic reactor is composed of a silicon nitride (SiN) membrane and polydimethylsiloxane (PDMS). Its application

in time-of-flight secondary ion mass spectrometry (ToF-SIMS) as an analytical tool was evaluated using a variety of aqueous solutions and complex liquid mixtures, some of which contain nanoparticles. Most recently, we demonstrated *in situ* probing of the electrode-electrolyte solution interface (or solid-electrolyte interface, SEI) using a new electrochemical probe based on our original invention. It provides the first direct observation of the surface and diffused layer of SEI in a liquid with chemical speciation using ToF-SIMS. Moreover, we extended the microfluidic reactor for biofilm growth and mammalian cell cultures and real-time correlative characterization by more than one spectroscopy and microscopy technique. Results from our latest development will also be presented in additional to published ones, showcasing new directions and applications using this novel approach based on microfluidics and combined vacuum and ambient spectroscopy and microscopy multimodal imaging.

3:00pm AS+BI+MC+SS-MoA4 Mass Spectrometric Characterization of Droplet Surfaces at Ambient Pressure, Kaveh Jorabchi, Georgetown University

Mass spectrometric methods provide excellent selectivity and sensitivity for chemical characterization of samples. For these methods, ionization constitutes a key step where chemical information from the sample is encoded into populations of gas-phase ions. Investigations on electrospray ionization have shown that the ionization efficiency has a positive bias with respect to surface affinity of analytes in droplets, opening a new avenue for liquid surface analysis. This ionization bias stems from higher ion production rates for surface active analytes. To this end, we have developed a new method to monitor gas-phase ion formation rates from charged nano-droplets. A pulsed nano-spray is used to emit a cloud of charged nano-droplets within an atmospheric-pressure mobility cell. The droplets are guided by a pulsed electric field through the mobility cell, undergoing desolvation and ion production prior to detection by a time-of-flight mass spectrometer. Each chemical species within the droplets creates an ion cloud. The arrival times of the ions at the mass spectrometer are recorded by varying the on-time of the pulsed electric field within the mobility cell, enabling ion cloud size measurements. We demonstrate that the ion cloud sizes are correlated with ion production rates, reflecting interfacial propensity of the analytes. These measurements are consistent with the ion evaporation mechanism from charged nano-droplets, providing a method for liquid surface analysis based on gas-phase ion formation rates.

3:40pm AS+BI+MC+SS-MoA6 Organic Depth Profiling Alchemy: Can We Transmute Data into Meaning?, Alexander Shard, National Physical Laboratory, UK

INVITED

Argon cluster sources suitable for depth profiling organic materials have developed rapidly and are now widely available and routinely used to analyse materials ranging from organic electronic devices to biological samples. This fantastic progress allows detailed insight into the chemistry and structure of organic materials with depth resolutions below 10 nm over many micrometres. When combined with 2D surface chemical imaging, detailed 3D reconstructions can be obtained allowing the label-free visualisation of chemical distributions which were previously impossible to obtain. However, because detailed understanding of the processes involved is still developing, it is necessary to view such data with scepticism when a quantitative answer is required. Conversely, the ability to perform nearly damage-free profiles of organic materials allows us to answer fundamental questions about surface analytical methods provided that the sample analysed has a known structure and composition.

The recurring questions in organic depth profiling and 3D imaging relate to the depth scale and the translation of a signal into a concentration, or amount of material. At NPL, we have developed reference materials which are designed to address these questions and in this talk an overview of developments in quantitative organic depth profiling will be provided. The use of XPS is shown to provide accurate compositions, as expected. However, there are some practical issues to be understood involving X-ray and electron damage and sample heating. Additionally, XPS suffers from low sensitivity, specificity and lateral resolution compared to SIMS. Whilst SIMS is fast, specific, sensitive and has high lateral resolution it suffers from the lack of an adequate means of converting data into compositions. Here, reference materials have been constructed which enable the most important effects of the sample on SIMS data to be described. These effects are outlined and include an apparent depth of origin difference for secondary ions, surface transient behaviour and the matrix effect. It is also shown how it is possible to use the matrix effect to assess the nanoscale phase separation of materials.

4:20pm AS+BI+MC+SS-MoA8 Argon Clusters - A Novel Solution for the Depth Profiling of Metal Alloys and Inorganic Materials, Jonathan Counsell, H.L. Brannon, S.J. Coultas, S.J. Hutton, A.J. Roberts, C.J. Blomfield, Kratos Analytical Limited, UK

Depth profiles are routinely used to gain information regarding elemental concentration and chemical composition of complex heterogeneous materials. Ion bombardment removes successive layers, exposing bulk material. The difference in the chemical composition of the surface relative to the sub-surface or bulk is often significant to the mechanical or electrical performance of the material.

Here we will discuss the use of Argon clusters for depth profiling a range of inorganic and alloyed materials. Traditionally, depth profiling inorganic materials employed Ar^+ as the bombardment ion. Unfortunately, monatomic Ar^+ can cause significant damage to the bulk structure of the material and can preferentially remove lighter and less well bound elements leading to misleading results. Recent studies show Argon cluster ions greatly diminish the effects of preferential sputtering with simple metal oxides such as titania.¹ Here we wish to broaden this application to a wider variety of materials including precious metal/non-precious metal binary alloys for novel electrode surfaces and ternary and quaternary chalcogenides. We show that with gentler ions, where the energy per atom can be as low as 5-40 eV, it is possible to greatly reduce bulk damage and the preferential removal of weakly bound elements in complex materials.²

References:

[1] J. D. P. Counsell, A. J. Roberts, W. Boxford, C. Moffitt and K. Takahashi, *J. Surf. Anal.*, **20** [3], 2014, 211–215

[2] A. Etin, G. E. Shter, R. Brenner, S. Baltianski and G. S. Grader., *J. Am. Ceram. Soc.*, **90** [12], 2007, 3800–3803.

4:40pm AS+BI+MC+SS-MoA9 Low Temperature Plasma for Crater Edge Depth Profiling of Crosslinking Organic Multilayers: Comparison with C_{60} and Argon Cluster Sputter Sources, Shin Muramoto, National Institute of Standards and Technology (NIST), D. Rading, ION-TOF GmbH, Germany, B. Bush, G. Gillen, National Institute of Standards and Technology (NIST), D.G. Castner, University of Washington

A model organic layer system consisting of three 1 nm delta layers of 2,9-dimethyl-4,7-diphenyl-1,10-phenanthroline (BCP) separated by three 30 nm layers of tris(8-hydroxyquinolinato)aluminum (Alq_3) was used to evaluate the effectiveness of helium low temperature plasma (LTP) etching for the preparation of crater edge surfaces for subsequent compositional depth profile analysis. The quality of the depth profile was determined by comparing the depth resolutions of the BCP delta layers obtained from the plasma-etched craters with those obtained using ToF-SIMS dual-beam depth profiling equipped with C_{60}^{2+} and argon cluster ($\text{Ar}_{1000 \text{ to } 2500}$) sputter sources. Using the full width at half maximum (FWHM) of each delta peak, the depth resolutions of the second and third delta layers were measured to be 6.9 nm and 6.0 nm for the plasma-etched crater, respectively, which were very close to the depth resolutions of 6.2 nm and 5.8 nm obtained from the argon cluster depth profile. In comparison, the use of a $1/e$ decay length to approximate the depth resolution gave results that identified the artifacts caused by ion bombardment in SIMS depth profiling. The $1/e$ decay length for the trailing edge of each delta were 2.0 nm and 1.8 nm for the plasma-etched crater, respectively, while the argon cluster depth profile gave decay lengths of 3.5 nm and 3.4 nm, owing to the longer tails produced by artifacts and possibly by slower sputter rate through the delta layers. For the C_{60}^{2+} depth profile, the need to rescale the axis as a result of a strong nonlinear sputter rate gave artificially improved depth resolutions, where FWHM of the delta peaks were 5.6 nm and 7.3 nm, respectively, and $1/e$ decay lengths were 1.7 nm and 2.3 nm, respectively. Although some artifacts such as contaminant deposition remain, low temperature plasma was shown to be a viable option for creating crater edges for compositional depth profiling without artifacts seen in ToF-SIMS depth profiling.

5:00pm AS+BI+MC+SS-MoA10 Desorption/Ionization induced by Neutral Cluster Impact as a Versatile Tool for the Investigation of Sensitive and Complex Biosamples, A. Portz, Justus Liebig University, Germany, M. Baur, University of Applied Sciences, Germany, C.R. Gebhardt, Bruker Daltonik GmbH, Germany, Michael Durr, Justus Liebig University, Germany

Desorption and ionization induced by neutral clusters (DINeC) can be employed as a soft and matrix-free method for transferring surface-adsorbed biomolecules into the gas phase. Using neutral clusters with polar constituents such as SO_2 , the impacting clusters do not only provide the energy necessary for desorption but also serve as a transient matrix in which the desorbing molecule is dissolved during the desorption process. As a consequence, desorption and ionization of oligopeptides and smaller proteins can proceed at comparably low energies of the impacting clusters and without any fragmentation [1]. Using a combination of DINeC and ion

trap mass spectrometry, femtomol sensitivity was achieved for standard oligopeptides such as angiotensin II or bradykinin [2]; good ion-to-neutral ratio was observed [3].

In this contribution, we show that the signal of the intact molecules (M+H)⁺ is predominant even in the case of phospho- and glycopeptides, and typical fragments were observed only in low abundance. The origin of these fragments was investigated by comparison with ESI measurements of the original solution as well as of samples which have undergone a similar treatment as for the preparation of the DIneC samples. In that way, we could show that fragmentation takes place already during sample preparation and DIneC is suitable to directly measure such changes of the samples.

Samples with a multitude of components as obtained from realistic biotechnological processes such as tryptic digest of proteins were also successfully analyzed. Peptide mass fingerprint analysis was applied for the evaluation of the respective spectra with very good sequence coverage and protein score. When compared to ESI or MALDI, a substantial number of the unique peptides which were identified with DIneC were not detected with the other methods. Notably, even in the presence of a large excess of salt in the original solution clear spectra of the intact biomolecules were detected. The results are correlated to the very properties of the DIneC process. The method was furthermore successfully applied to a variety of different classes of molecules such as lipids, dye molecules, and pesticides.

References:

- [1] C. R. Gebhardt, et. al., *Angew. Chem. Int. Ed.* **48**, 4162 (2009).
- [2] M. Baur, et al., *Rapid Commun. Mass Spectrom.* **28**, 290 (2014).
- [3] B.-J. Lee, et al., *Rapid Commun. Mass Spectrom.* **27**, 1090 (2013).

5:20pm **AS+BI+MC+SS-MoA11 C₆₀ and Argon Gas Cluster Ion Sputter Depth Profiling for Quantitative Inorganic Thin Film Analysis**, *Saad Alnabulsi, G.L. Fisher, S.R. Bryan, J.S. Hammond, J.F. Maulder*, Physical Electronics Inc.

A successful sputter depth profile accurately identifies layer thickness and composition of materials as a function of depth within film structures. In the case of inorganic thin films, monoatomic argon ion beam depth profiling continues to be the preferred choice despite issues with preferential sputtering, material migration, and chemical reduction that may occur during the sputter process to alter the apparent profile of the analyzed material^{[1][2]}.

The introduction of C₆₀ cluster ion beam and argon gas cluster ion beam (GCIB) sputtering in recent years provided the capability of successful depth profiling of polymer and organic materials while preserving the stoichiometry and chemical structure below the surface^{[3][4]}.

Currently, there is great interest in establishing the viability of these cluster ion sources as an alternative to monoatomic argon ion beam sources for analyzing inorganic semiconductor and glass films, with anticipated improvement in the quantitative accuracy of inorganic depth profile results^{[5][6]}.

The purpose of this study is to present a comparative evaluation of quantitative XPS analysis to demonstrate the benefits and limitations of monoatomic argon, C₆₀, and argon gas cluster ion beam sputtering for compositional inorganic depth profiling.

- [1] R. K. Brow. *J. of Vac. Sci. Technol. A* **7**, 1673 (1989).
- [2] V. Smentkowski. *Prog. in Sur. Sci.* **64**, 1 (2000).
- [3] T. Nobuta, T. Ogawa. *J. of Mater. Sci.* **44**, 1800 (2009).
- [4] C. M. Mahoney. *Mass Spec. Rev.* **29**, 247 (2010).
- [5] Y. Yamamoto, K. Yamamoto. *Mater. Sci. Eng.* **18** (2011).
- [6] D. Kobayashi, Y. Yamamoto, T. Isemura. *Sur. and Inter. Anal.* **45** 113 (2013).

Biomaterial Interfaces

Room: 317 - Session BI+AS+NS-MoA

Bio/Nano Interfaces

Moderator: Patrick Koelsch, University of Washington

2:00pm **BI+AS+NS-MoA1 Controlling Bio/Nano Interface Response using Metal Oxide Atomic Layer Deposition: Zinc Oxide ALD Modifies how Human Lung Fibroblasts respond *In Vitro* to Multiwall Carbon Nanotubes**, *Erinn Dandley, A. Taylor, G.N. Parsons, J. Bonner*, North Carolina State University

Carbon nanotubes have been reported to cause pulmonary fibrosis in mice after inhalation exposure. When inhaled, multiwall carbon nanotubes (MWCNTs) activate macrophage inflammasomes and interleukin (IL)-1 β release, key cellular components of the innate immune response. Macrophages are the first line of defense that engulf and remove inhaled MWCNTs from the lungs. Macrophages are also a source of secreted osteopontin (OPN), which promotes tissue matrix remodeling and fibrosis. These responses may be triggered by the unique aspect ratio, aggregation or surface chemistry of MWCNTs. In previous studies, we explored atomic layer deposition (ALD) as a means to modify the surface functionality of MWCNTs and studied how the surface coating affected the toxic response of THP-1 cells, a widely used human monocyte/macrophage cell line, and primary peripheral blood monocytes (PBMCs) obtained from normal human donors. Compared to uncoated MWCNTs, we found that nanotubes with Al₂O₃ nanocoatings showed enhanced IL-1 β secretion and decreased OPN production in THP-1 cells and PBMCs, indicating that the coating enhances the innate immune response and decreases pro-fibrotic activity.

In this study we examined the effect of ALD ZnO coatings on the fibrogenic response in human lung fibroblast (HLFs) using mRNA expression and secretion of transforming growth factor (TGF)- β 1 and CXCL10, mediators that promote and deter fibrosis respectively. We find that the ALD ZnO layer thickness can be controlled down to ~5nm, and the thickness scaled directly with the number of ALD cycles, as observed by TEM. Thicker coatings inhibited MWCNT aggregation, and sonication allowed us to induce fiber fragmentation. In this way the ALD coating allowed us to independently adjust surface termination, fiber aggregation, and fiber aspect ratio, providing us a unique tool to examine how each of these factors influences cellular response. Initial results show that the ZnO coating significantly increased TGF- β 1 mRNA expression and stimulated a larger pro-fibrogenic response in HLFs compared to uncoated MWCNTs. Control experiments using ZnO nanoparticles also showed potent induction of TGF- β 1 mRNA in HLFs. Also, the response tends to correlate with extent of dispersion, and is nearly independent of MWCNT aspect ratio. These experiments show that nanoscale surface functionalization of nanoscale materials may help us gain better understanding of the mechanisms associated with toxicology of nanomaterials, and expand knowledge of biological response at nano/bio interfaces.

2:20pm **BI+AS+NS-MoA2 Mechanically Optimized Fe (III) Doped Silica Nanoshells as a Contrast Agent for Ultrasound Imaging and HIFU Therapy**, *James Wang, A. Liberman, R. Viveros, C. Barback, S.L. Blair, Z. Wu, R. Mattrey, W. Trogler, A.C. Kummel*, University of California at San Diego

Ultrasound (US) is a common medical imaging modality due to its flexibility, low-cost and therapeutic potential. 500 nm silica nanoshells were synthesized as a contrast agent to improve US imaging signal for better diagnostic performance. Iron (III) was included into the silica network to enhance the biodegradability of the silica nanoshells. Previously, ferric iron was shown to facilitate silica nanoshell biodegradation due to its strong binding affinity with serum transferrin proteins. The removal of iron from the silica network by serum proteins fragments the nanoshells enabling effective biodegradation for *in vivo* applications. The silica nanoshells are filled with perfluorocarbon (PFC) vapor which expands and shatters the nanoshells during US irradiation. A mechanically weaker silica nanoshell increases US signal at lower power. A range of alkoxyxilanes with selected R-groups such as long chain hydrocarbons, fluorinated carbon chains, fluorinated phenyl groups and vinyl groups were employed along with tetramethyl orthosilicate and iron (III) ethoxide in a modified sol-gel synthesis to create structural defects that alter the mechanical properties of the nanoshells. Monodispersed 500 nm polystyrene beads were used as a soft template during the reaction. The silica nanoparticles were calcined at 550 C to remove the polystyrene core and form hollow nanoshells. SEM and TEM showed that 500 nm silica nanoshells with different microstructures were synthesized incorporating alkoxyxilanes with different R-groups. Formulations with higher concentrations of alkoxyxilanes with large R-groups such as long chain hydrocarbons resulted in stronger *in vitro* contrast enhanced ultrasound (CEUS) signals due to the increase of

structural voids that resulted in weaker shell strength. CEUS experiments demonstrated that mechanically weaker silica nanoshells exhibited longer signal life time and required a lower mechanical index (MI) for imaging. The high intensity focused ultrasound (HIFU) properties of the modified silica nanoshells were tested for potential therapeutic applications. Mechanically weaker silica nanoshells were shown *in vitro* to require a lower HIFU power to fracture which is consistent with safer HIFU therapy. By synthesizing strength tunable silica nanoshells as US contrast agents, it is possible to improve diagnostic US imaging performance in order to detect smaller tissue structures or early stage tumors. Additionally, mechanically weaker silica nanoshells may also increase the efficiency of HIFU enabling HIFU at lower US power and/or higher speed.

2:40pm BI+AS+NS-MoA3 Synthesis, Functionalization, and Biological Imaging with Quantum Dots. *Preston Snee*, University of Illinois at Chicago **INVITED**

Semiconductor quantum dots (QDs, or nanocrystals), are very bright chromophores that possess unlimited potentials in alternative energy generation and for biological sensing and imaging applications. Our group has made advances in the synthesis QDs to produce 100% efficient emitters; furthermore, we can dope the semiconductor with guest ions to alter the bandgap. We recently invented a method to dope each quantum dot with an exact number of guest ions, a feat that was previously considered impossible. As very bright fluorophores, quantum dots are ideal for biological imaging and sensing. Our first contribution in this regard was to develop methods of chemical and biological functionalization of water-soluble quantum dots as many existing methods either quenched the QDs or had very low reaction yields. We have circumvented these problems by synthesizing polymers which serve as QD functionalization reagents; the polymer – QD activated intermediate has increased stability and allows us to conjugate chemical and biological vectors to the nanocrystals with ~100% reaction yields. We use these methods to functionalize QDs with organic fluorophores that can report on the local chemical and biological environment. We have synthesized several ratiometric, or “self-calibrating” sensors, for pH, toxic metals, DNA, and proteins. In our recent work on protein sensing, we have developed an all optical method for sensing unlabeled proteins with a better detection limit than any currently existing technology. We have also circumvented the well-known problem of cytoplasmic delivery of quantum dots into live, adherent cells.

3:40pm BI+AS+NS-MoA6 Easynanofab: Fast, Simple, Combinatorial Routes to Reusable Plasmonically Active Gold Nanostructures Over Macroscopic Areas. *A. Tsargorodskaya, O. El Zubir, Graham Leggett*, University of Sheffield, UK

Plasmonic effects associated with gold nanocrystals have attracted widespread interest for the interrogation of biological molecules. Existing approaches to fabrication of plasmonic nanostructures fall into two categories: high precision methods such as electron beam lithography that rely on complex, specialised infrastructure; and simple, low-cost methods such as colloidal lithography that offer limited capacity. Here, we describe a fast, simple method for the fabrication of re-usable, robust gold nanostructures over macroscopic (cm²) areas that provides enormous scope to control nanostructure morphology and dimensions, and which also uses only simple apparatus and requires no access to a clean-room. We have assembled a combinatorial library of over 200 different samples consisting of highly crystalline gold nanostructures that exhibit varying morphologies, dimensions and periodicities but yield intense plasmon bands. These structures enable the rapid identification of optimum substrates for the detection and analysis of biological targets, and provide a platform for exploring the relationship between particle morphology and optical properties. Self-assembled monolayers (SAMs) of alkythioliates on chromium-primed polycrystalline gold films are patterned using a Lloyd's mirror interferometer and etched using mercaptoethylamine in ethanol in a rapid process. The use of a Cr adhesion layer facilitates the cleaning of specimens by immersion in piranha solution, enabling their repeated re-use without significant change in their absorbance spectra over two years. Annealing yields structures with a uniformly high degree of crystallinity that exhibit strong plasmon bands. Because of the ease with which nanoparticle morphology may be controlled using interferometric lithography (IL), it provides a convenient means to investigate the correlation between structural parameters (particle dimensions, spacing) and optical responses. The shift in the position of the plasmon band after site-specific attachment of histidine-tagged green fluorescent protein (His-GFP) and after adsorption of chlorophyll and bacteriochlorophyll was measured for a range of nanostructured films, enabling the rapid identification of structures that yielded the largest shifts. Strong resonant coupling was observed when light-harvesting membrane protein complexes from plants and bacteria were coupled to gold nanostructure arrays, yielding absorbance spectra that were very different from those of the clean gold nanostructures. This approach offers a simple route to the production of durable, reusable,

macroscopic arrays of gold nanostructures with precisely controllable morphologies.

4:00pm BI+AS+NS-MoA7 Impacts of Nanoparticle Synthesis Route, Structure and Serum Proteins on the Dispersion and Dissolution of Ag Nanoparticles in Biological Media. *P. Munusamy, J.N. Smith, C. Liu, C.-M. Wang*, Pacific Northwest National Laboratory, *S. Chen*, Imperial College London, UK, *M.H. Engelhard*, Pacific Northwest National Laboratory, *A.E. Porter, M.P. Ryan*, Imperial College London, UK, *Donald Baer*, Pacific Northwest National Laboratory

The wide-spread use of silver nanoparticles in consumer products raises questions of environmental impact and toxicity. Because both silver particles, and silver ions formed by particle dissolution, may impact biological systems, it is important to understand the characteristics of silver nanoparticles as they are made and their stability and dissolution in the medium relevant to environmental and toxicological studies. Silver nanoparticles produced by different synthesis routes can have significantly varying physical and chemical characteristics. In this talk we will summarize the characterization and dissolution stability of three types of silver nanoparticles (20 nm particles synthesized with and without gold core (~7 nm) and 110 nm particles with gold core) in cell culture media with serum proteins: FBS10%/RPMI, the culture media used at Pacific Northwest National Laboratory for *in-vitro* toxicity studies. These nanoparticles were synthesized and prepared for biological study in aqueous solution. They were examined *in situ* using dynamic light scattering, zeta potential measurements and optical adsorption and *ex situ* with x-ray photoelectron spectroscopy and transmission electron microscopy. For the dissolution studies, concentrations of particles examined were varied from 1 µg/ml to 50 µg/ml, consistent with the range of concentrations typically used during *in-vitro* studies. Silver particles with gold cores had smaller crystallite size and higher apparent solubility than three different batches of pure ~ 20 nm silver particles. A simple dissolution model was found to describe the time variation of particle size and amount of dissolved silver for particle loadings above 9 µg/ml. The effective solubility product obtained from fitting the data was higher for the 20 nm particles with the gold core in comparison to the pure silver or 110 nm particles. The dissolution of silver nanoparticles was also found to be enhanced by presence of serum proteins contained in fetal bovine serum (FBS). In addition, the protocol of dispersion in cell culture medium was found to influence particle agglomeration and the rate of dissolution. In these measurements focusing on a 24 hour time point, we found that the structure of the silver nanoparticles can have a significant impact on the concentration of dissolved silver in media and thus the dosimetry to which cells would be exposed during *in vitro* studies.

This work has been supported by the NIEHS under Center grant U19 ES019544. Portions of this work were performed using EMSL, a national scientific user facility sponsored by the US Department of Energy, Biological and Environmental Research and located at PNNL.

4:20pm BI+AS+NS-MoA8 Analysis of Protein Coated Nanoparticles by X-ray Photoelectron Spectroscopy and Solution-Based Particle Size Techniques. *C. Minelli, Natalie Belsey, A.G. Shard*, National Physical Laboratory, UK

The attachment of proteins to nanoparticles' surface is of increasing interest in medicine for applications such as drug delivery and diagnostics. The unintentional acquisition of a protein corona from biological media is also important in determining the performance and potential toxicity of such particles. Understanding and refinement of the performance of nanoparticles of use in medical applications require accurate and quantitative characterisation of their protein interface. Our efforts are focussed upon developing measurement techniques to enable useful characterisation of this interface. In this study, three biomolecules of a range of sizes, shapes and mechanism of interaction with gold surfaces, i.e. 16 AA peptide, BSA and IgG, were adsorbed to gold nanoparticles (10, 20, 40, 60 and 80 nm) and the shell thickness was measured in solution using dynamic light scattering (DLS) and differential centrifuge sedimentation (DCS). UV-visible spectrophotometry was used to monitor localised surface plasmon resonance (LSPR) shifts of the nanoparticles due to the acquisition of the protein shell. Combination of this information with thickness measurements allowed for an estimation of the protein shell refractive index and average number of biomolecules at the nanoparticle surface. X-ray photoelectron spectroscopy (XPS) analysis of the same nanoparticles deposited on a PTFE substrate enabled determination of the nanoparticle shell chemical composition and dehydrated thickness, from which the number of molecules at the nanoparticle surface was also estimated. Parallel characterisation of the nanoparticles in their colloidal form and *in vacuo* provided consistent results and the combination of the techniques revealed further insight into molecular adsorption at nanoparticles' interfaces. The complementarity of the approaches also allowed for validation of the methods, which is important for their application to a wide range of

nanoparticle types. For example, DLS and LSPR analysis are not suitable for dealing with aggregated samples, but XPS is, while XPS measurements of organic nanoparticles are challenging and liquid based techniques may be preferred.

4:40pm **BI+AS+NS-MoA9 Development of Nanofibrous Meshes as Smart Dressings for Chronic Wound Care**, *Martina Abrigo, P. Kingshott, S.L. McArthur*, Swinburne University of Technology, Australia
Diabetic, pressure, venous and arterial ulcers are a large social, economic and healthcare burden. These chronic non-healing wounds show delayed and incomplete healing processes exposing patients to high risk of infection. The design of wound dressings that combine the necessary morphological and physical requirements for wound healing with the value-added capability to address optimal cell responses and impair bacterial proliferation represents a major challenge in chronic wound care. Polymeric nanofibrous meshes fabricated through the electrospinning process are promising candidates as wound dressings due to their high surface area, micro-porosity and non-woven structure. In this study, the parameters of the electrospinning process (such as spinning rate and electric field intensity) were optimized to fabricate nanofibrous membrane in Polystyrene (M.W. 250,000). The morphological properties of the electrospun meshes were analysed by bright microscopy, three-dimensional optical profiler, Scanning Electron Microscopy (SEM) and Atomic Force Microscopy (AFM). Electrospun materials have been used as scaffolds for tissue engineering for a number of years, but there is surprisingly little literature on the interactions of fibres with bacteria. In order to understand microbial infiltration and control in wound dressings, a number of microbiological assays (MTT, MTS and live/dead) were completed using *E. Coli*, *P. Aeruginosa*, *S. Aureus* in an effort to understand how the morphological and structural properties of the electrospun meshes influence bacterial attachment, proliferation and growth.

5:00pm **BI+AS+NS-MoA10 Electrophoretic Stretching of Tethered DNA in Nanoslits**, *Jia-Wei Yeh, K. Szeto, H.G. Craighead*, Cornell University

We have investigated the field-extension of tethered DNA in nanoslits with slit heights ranging from 30 to 130 nm, and performed an analysis from an approximated modified worm-like chain (mWLC) field-extension relation. DNA molecules attached to microspheres were anchored at a micro-nanofluidic interface and the molecules electrophoretically extended. We demonstrated that both the DNA segmental correlation and equilibrium lengths increased as the slit height decreased. Furthermore, for extremely confined DNA where $h \leq 30$ nm, we observed reptation of the DNAs' contours within the nanoslit, a phenomena that may be induced by inhomogeneous surface charge distributions. This nano-confined system may have implications for single-molecule sensors on detecting and analyzing genetic, epigenetic markers, and related nanobiotechnological applications.

5:20pm **BI+AS+NS-MoA11 Measuring DNA Looping Pathways using Nanofluidic Manipulation**, *M. Roushan, Z. Azad, H. Wang, Robert Riehn*, NC State University

DNA performs a carefully choreographed ballet during the cell cycle. The organization is driven by the specific binding of proteins to form tertiary DNA-protein-DNA complexes. The search process that precedes the formation must overcome the challenge of very low effective mobility of genomic-sized DNA pieces in the dense cellular environment.

In this paper we will discuss a group of nanofluidic device that force two DNA molecules to either slide past each other in parallel, or cross over each other at a steep angle. Nanochannel cross-sections are 100×100 nm², and are hundreds of microns long. Because DNA is elongated through confinement, loop with a length down to 2 kb can be directly observed in real time. Channels are made of fused silica, enabling single-molecule observation of both DNA and proteins. Because the effective concentration of DNA inside channels exceeds 1 mg/ml with the channel at the point of DNA-DNA contact, protein-mediated capture cross-sections are very high.

We will present analyses of different DNA-binding proteins that demonstrate that we can distinguish dense and sparse binding modes and the compensation of electrostatic DNA-DNA repulsion through protein binding. We further report the detection of long-lived tertiary complexes acting as a lock for looped DNA configurations, and the presence of very short-lived transient links. We further demonstrate a pathway for loop formation that is enhanced in nanochannel devices, and that may be important in a cellular context. By using precision hydrodynamic flows, we are able to measure free energies of the search process.

Electronic Materials and Processing Room: 314 - Session EM-MoA

Nanoparticles for Electronic Materials

Moderator: Jessica Hilton, Mantis Deposition, Joseph G. Tischler, Naval Research Laboratory

2:00pm **EM-MoA1 Synthesis of Nanoparticles Via Gas-Aggregated Sputtering**, *Cathal Cassidy*, Okinawa Institute of Science and Technology, Japan **INVITED**

Synthesis of nanoparticles via gas-aggregated sputtering allows direct integration with electronic devices and their manufacturing processes. In this talk, I will discuss the fundamentals of gas-aggregated sputtering, and the diverse capabilities it offers for synthesis of novel nanoparticle materials. Analytical models will be introduced, as well as molecular dynamics modeling insights into growth and substrate landing of nanoparticles. Example results, with a focus on transmission electron microscopy studies, will be presented. Finally, the strengths and weaknesses of sputtered nanoparticles for various device applications, such as sensor layers, data storage and backend interconnects, will be discussed.

2:40pm **EM-MoA3 Soft Landing of Size-Selected Nanoparticles: Novel Materials for Electrocatalysis**, *Grant Johnson, R.J. Colby, M.H. Engelhard, D. Du, Y. Lin, J. Laskin*, Pacific Northwest National Laboratory

Soft landing of mass-selected ions onto surfaces is a powerful approach for the highly controlled preparation of materials that are often unobtainable using conventional synthesis techniques. A non-thermal physical synthesis method, DC magnetron sputtering combined with inert gas-aggregation, has been employed to produce anionic metal nanoparticles in the gas-phase across a range of sizes, shapes and elemental compositions for controlled deposition onto conductive electrode surfaces. Simultaneous sputtering of multiple metal targets employing up to three independent DC magnetrons in the same gas aggregation region is demonstrated to produce complex binary alloy nanoparticles with well-defined elemental composition and morphology. Size-selection of the anionic nanoparticles employing a quadrupole mass-filter prior to soft landing is shown to provide effective control over the size of nanoparticles delivered to surfaces. A suite of cutting edge analytical techniques including atomic force microscopy, scanning and transmission electron microscopy, x-ray photoelectron spectroscopy and medium energy ion scattering is utilized to demonstrate how the size, shape, elemental composition and surface density of soft landed nanoparticles may be tuned to promote the efficient electrocatalytic reduction of oxygen.

3:00pm **EM-MoA4 Aerosol Spray Pyrolysis Synthesis and Characterization of CZTS Nanoparticles**, *Stephen Exarhos, L. Mangolini*, University of California - Riverside

A novel synthesis technique for the production of copper zinc tin sulfide (CZTS) nanocrystals has been developed using aerosol spray pyrolysis. CZTS is a quaternary semiconducting material that shows promise as a replacement to common semiconductors such as CdTe and CIGS for use in photovoltaic devices. CIGS is currently being commercialized in the photovoltaic industry, but rare and expensive indium and gallium components threaten its long term viability. CZTS looks to be one of the best alternatives to CIGS with all earth abundant and non-toxic materials and a band gap of 1.5 eV [1]. A number of synthesis techniques have been thoroughly studied and detailed previously. In our novel approach, we synthesize single-phase 15 nm nanocrystals starting with zinc, copper, and tin diethyldithiocarbamate precursors in a toluene solvent. The precursor solution is aerosolized using a Collison type nebulizer wherein the droplets are pushed through a tube furnace and nucleation occurs at atmospheric pressure. The powder is then collected in a series of methanol-filled bubblers. We reproducibly synthesize kesterite, $\text{Cu}_2\text{ZnSnS}_4$, nanocrystals. This technique continuously converts the chemical precursor into high-purity nano powder with a production rate of ~50mg/hour from ~100mL of precursor solution with ~500mg total of the three diethyldithiocarbamate precursors for an un-optimized lab-scale reactor. The motivation to use this synthesis process as an inexpensive, quick, and simple method of nanocrystal formation will be outlined. Further, a discussion of process parameters on the stoichiometry of the nanoparticles will be presented as well as results from extensive material characterization via Raman spectroscopy, EDS, XRD, and TEM. We are currently in the process of producing a printable ink technique with which to coat CZTS as the absorbing layer for use in photovoltaic devices.

[1] H. Wang. "Progress in Thin Film Solar Cells Based on $\text{Cu}_2\text{ZnSnS}_4$," International Journal of Photoenergy, 2011.

3:40pm **EM-MoA6 Peter Mark Memorial Award Lecture - Novel Semiconductor and Epitaxial Nanocomposite Materials for Electronic and Photonic Applications, Joshua Zide***, University of Delaware

INVITED

Advances in electronic materials (specifically, semiconductors and nanocomposites) enable new device technologies and improve the properties of existing technologies. In this talk, I will present efforts within my group on the growth of new materials by molecular beam epitaxy and the resulting advances in solar cells, thermoelectrics, and optoelectronics.

Specifically, I will discuss two material systems: (1) nanocomposites consisting of metallic nanoparticles (such as ErAs and TbAs) within III-V semiconductors (such as InGaAs and GaAs), and (2) dilute bismuthide semiconductors in which bismuth is incorporated into III-V materials to reduce the bandgap significantly, with unique band alignments that cannot be easily achieved in other materials. In the former, the nanoparticles serve as buried Schottky junctions, pinning the Fermi level and significantly altering carrier dynamics. In the latter, we focus on In(Ga/Al)BiAs, where compositional variations permits independent tuning of valence and conduction bands.

Although these materials are built upon relatively-mature III-V systems, electronic, thermal, and optical properties can be quite different from those of conventional materials, with significant promise for applications in a variety of technologies. Understanding the properties of these materials enables the creation of designer semiconductors for particular applications of interest.

4:20pm **EM-MoA8 Assembly of Functional Nanocrystal Films at Fluid Interfaces, Kevin Whitham, T. Hanrath**, Cornell University

Opportunities to create materials with properties by design continue to emerge from our ability to control the structure and composition of nanomaterials through wet-chemistry synthesis methodologies. Access to these materials has provided critical insights into basic structure-property relationships. Concurrent advances in prototype nanomaterial-based devices underscored their immense technological potential in a broad range of energy applications including photovoltaics, catalysis, energy storage, and thermoelectrics. Along with rising expectations, there is growing recognition that sustained progress towards the acclaimed promise of nanomaterial-enabled energy technologies depends critically on solving outstanding processing challenges - in particular the directed assembly of nanoparticles (NPs) into functional superstructures. We embrace this challenge as an opportunity to establish the scientific and engineering foundation for the processing of ordered and multifunctional NP thin films via advanced liquid coating methods.

Our group recently demonstrated a significant advance to resolve this challenge by creating NP assemblies that combine high spatial coherence and strong interparticle electronic coupling. In brief, we discovered that spreading a NP suspension across the surface of a non-polar antisolvent subphase results in the formation of two-dimensional (2D) superlattice of epitaxially connected NPs. Our approach to 'connect the dots' was inspired by analogies to polymerize or crosslink NPs as monomers into highly connected superstructures. The ability to form 'confined-but-connected' 2D NP assemblies with predefined symmetries introduces exciting opportunities to create materials with properties by design. By analogy to atomic 2D systems (e.g. graphene), we see 2D NP assemblies as a fertile ground for scientific discovery with a clear path towards practical applications.

4:40pm **EM-MoA9 Characterization of Cu_{2-x}S Nanoparticles in Organic Matrices, Michael Majeski, I. Bolotin, L. Hanley**, University of Illinois at Chicago

Transition-metal chalcogenide nanomaterials show promise for applications in photovoltaics and plasmonic devices. Of these class of materials, Cu₂S encompasses the environmentally friendly and earth abundant qualities not afforded to many other heavy metal semiconductors. Copper sulfide nanoparticles are prepared by physical vapor deposition without the surface ligand capping effects known to inhibit and otherwise complicate charge transfer. Another obstacle to the use of copper sulfide for photovoltaics is the self-doping that occurs upon oxidation, which is compensated for here by all-gaseous preparation of Cu_{2-x}S nanoparticles into organic matrices. These films are characterized by X-ray photoelectron spectroscopy, transmission electron microscopy, high-angle annular dark-field scanning transmission electron microscopy, X-ray absorption experiments, and other methods. 2.3± 0.4 nm Cu_{2-x}S nanoparticles with copper in the +1 oxidation state were deposited into pentacene films and additional structural information will be presented.

5:00pm **EM-MoA10 Optical Properties of PbSe Nanorods with Controlled Diameter and Length, Diogenes Placencia, J.E. Boercker, E.E. Foos, J.G. Tischler**, Naval Research Laboratory

PbSe nanorods are attractive for use in next-generation optoelectronic devices due to their exceptional physical properties such as larger Stokes shifts and more efficient multiple exciton generation (MEG), relative to spherical nanocrystals.¹⁻³ However, further development of PbSe nanorods for viable technological components requires precise control of the nanorod diameter and length as well as an understanding of how the nanorod dimensions affect their optoelectronic properties. We have investigated the nature of the PbSe nanorod synthesis, yielding an understanding of how to independently control the nanorod diameter and length. Additionally we have developed an elementary comprehension of how the nanorod dimensions affect their optical properties.

Recently, single-crystal, homogeneous, PbSe nanorods were synthesized using a solution synthesis.⁴ In our work, we show that water present in this synthesis has a dramatic effect on the nanorod aspect ratio and yield. By varying the water concentration from 0 to 204 mM, the nanorod aspect ratio and yield can be controlled from 1.1 to 10 and 1 to 14%, respectively. Water indirectly affects the nanorod morphology and yield by reacting with the tris(diethylamino)phosphine used in the reaction to form bis(diethylamido)phosphorus acid. The latter is responsible for both the nanorod aspect ratio and yield variations. Furthermore, the excess oleic acid in the reaction can also create bis(diethylamido)phosphorus acid from tris(diethylamino)phosphine. When both excess oleic acid and water are removed, the reaction slows and highly uniform, non-branching, nanorods are formed.⁵

Exploration of various synthetic parameters (e.g., temperature, reaction time) within the nanorod reaction free of water and excess oleic acid resulted in our ability to independently control the nanorod diameter and length. Aspect ratios ranging from 1 to 14 have been synthesized, showing no branching, varying levels of quantum yields, and a wide absorption energy range (~1200 nm – 2000 nm).

References

- [1] Tischler J G, Kennedy T A, Glaser E R, Efros A L, Foos E E, Boercker J E, Zega T J, Stroud R M and Erwin S C 2010 *Phys. Rev. B* **82** 245303
- [2] Cunningham P D, Boercker J E, Foos E E, Lumb M P, Smith A R, Tischler J G and Melinger J S 2011 *Nano Lett.* **11** 3476
- [3] Sandberg R L, Padilha L A, Qazilbash M M, Bae W K, Schaller R D, Pietryga J M, Stevens M J, Baek B, Nam S W and Klimov V I 2012 *ACS Nano* **6** 9532
- [4] Koh W-K, Bartnik A C, Wise F W and Murray C B 2010 *JACS* **132** 3909
- [5] Boercker J E, Foos E E, Placencia D and Tischler J G 2013 *JACS* **135** 15071

5:20pm **EM-MoA11 Plasmonic Behavior of Copper Iron Sulfide Nanoparticles, Katherine Plass, N.J. Freymeyer, C. Kim, C.J. Wisdo**, Franklin & Marshall College

Copper vacancies in copper chalcogenide result in sufficiently high levels of p-type doping to generate plasmon resonances. The natural tendency towards increased copper vacancies with time and air exposure is exacerbated in nanoparticles.¹ We present here investigations into the stabilization of plasmonic copper sulfide-based semiconductors. Incorporation of iron slows the transition to copper deficiency² Here we will discuss the affect of iron incorporation into copper sulfide nanoparticles on the plasmonic behavior. Various phases were produced, ranging from different polymorphs of Cu₂S to CuFeS₂, including solid solutions. The solid-state structure, band gaps and edges, and plasmon band absorption of these copper iron sulfide nanoparticles were responsive to the extent of iron incorporation, as investigated by powder X-ray diffraction, cyclic voltammetry, and visible/near-IR light absorption spectroscopy. The surface chemistry influences the plasmonic behavior of these copper iron sulfide nanoparticles and will be examined.³

- (1) Lotfipour, M.; Machani, T.; Rossi, D. P.; Plass, K. E. *Chem. Mater.* **2011**, *23*, 3032–3038.
- (2) Machani, T.; Rossi, D. P.; Golden, B. J.; Jones, E. C.; Lotfipour, M.; Plass, K. E. *Chem. Mater.* **2011**, *23*, 5491–5495.
- (3) Freymeyer, N. J.; Cunningham, P. D.; Jones, E. C.; Golden, B. J.; Wiltrott, A. M.; Plass, K. E. *Cryst. Growth Des.* **2013**, *13*, 4059–4065.

* Peter Mark Memorial Award Winner

Energy Harvesting with Nanostructures**Moderator:** Phillip Christopher, University of California - Riverside**2:00pm EN+EM+MN+NS+TR-MoA1 Optical Engineering for Colloidal Quantum Dot Photovoltaics, Susanna Thon, Johns Hopkins University** **INVITED**

The next generation of photovoltaics seeks to improve both efficiency and cost through the use of flexible platforms and new materials. Colloidal quantum dots (CQDs), semiconductor nanoparticles synthesized from solution, are a particularly attractive material for solar energy. The bandgap of films composed of arrays of CQDs can be tuned via the quantum confinement effect for tailored spectral utilization. The performance of CQD solar cells is currently limited by an absorption-extraction compromise, whereby photon absorption lengths in the near infrared regime exceed minority carrier diffusion lengths. I will review several photonic and optical engineering schemes aimed at overcoming this compromise. These include nanophotonic and geometric light trapping techniques, as well as jointly-tuned plasmonic-excitonic photovoltaics. Additionally, I will discuss how nanoscale engineering of CQDs and related materials can lead to emergent optical properties for building color-tuned optoelectronic films.

2:40pm EN+EM+MN+NS+TR-MoA3 Energy Transfer from Nanocrystal Quantum Dots to Si Nanomembranes Monitored via Wavelength Dependent Photocurrent Response, Weina Peng, S. Sampat, S. Rupich, B. Anand, H. Nguyen, D. Taylor, Y. Gartstein, Y.J. Chabal, A. Malko, University of Texas at Dallas

We report the observation of wavelength dependent photocurrent in thin silicon nanomembranes (75 nm) coupled to colloidal CdSe/ZnS nanocrystal quantum dots (NQDs). The measurement was performed on back-gated, FET-type thin Si structures, which are functionalized with self-assembled monolayer (SAM) of ester termination groups to prevent surface oxidation and the formation of surface defect states. A thin film of nanocrystals is drop casted on the surface and an increase of photocurrent, up to several hundred nA, are recorded as a function of excitation wavelength on NQD/SAM/Si devices vs. plain SAM/Si structures. Quantitative analysis of photocurrent vs. NQD absorption spectrum allows us to ascribe the observed photocurrents to the photoexcited NQD excitons transferred to the underlying Si substrate via non-radiative and radiative energy-transfer mechanisms¹.

¹H. M. Nguyen, O. Seitz, W. N. Peng, Y. N. Gartstein, Y. J. Chabal, and A. V. Malko, *ACS Nano* **6**, 5574 (2012).

3:40pm EN+EM+MN+NS+TR-MoA6 Triboelectric Nanogenerator - A New Energy Technology, ZhongLin Wang, Georgia Institute of Technology **INVITED**

Triboelectrification is an effect that is known to each and every one probably ever since the ancient Greek time, but it is usually taken as a negative effect and is avoided in many technologies. We have recently invented a triboelectric nanogenerator (TENG) that is used to convert mechanical energy into electricity by a conjunction of triboelectrification and electrostatic induction. As for this power generation unit, in the inner circuit, a potential is created by the triboelectric effect due to the charge transfer between two thin organic/inorganic films that exhibit opposite tribo-polarity; in the outer circuit, electrons are driven to flow between two electrodes attached on the back sides of the films in order to balance the potential. Ever since the first report of the TENG in January 2012, the output power density of TENG has been improved for five orders of magnitude within 12 months. The area power density reaches 500 W/m², volume density reaches 490 kW/m³, and a conversion efficiency of ~50% has been demonstrated. The TENG can be applied to harvest all kind mechanical energy that is available but wasted in our daily life, such as human motion, walking, vibration, mechanical triggering, rotating tire, wind, flowing water and more. Alternatively, TENG can also be used as a self-powered sensor for actively detecting the static and dynamic processes arising from mechanical agitation using the voltage and current output signals of the TENG, respectively, with potential applications for touch pad and smart skin technologies. The TENG is possible not only for self-powered portable electronics, but also as a new energy technology with a potential of contributing to the world energy in the near future.

[1] Z.L. Wang "Triboelectric Nanogenerators as New Energy Technology for Self-Powered Systems and as Active Mechanical and Chemical Sensors", *ACS Nano* **7** (2013) 9533-9557.

[2] G. Zhu, J. Chen, T. Zhang, Q. Jing, Z. L. Wang* "Radial-arrayed rotary electrification for high-performance triboelectric generator", *Nature Communication*, **5** (2014) 3456.

4:20pm EN+EM+MN+NS+TR-MoA8 Conflicting Roles of Charge Traps in ETA Solar Cells: The CREM Point of View, Hagai Cohen, Weizmann Institute of Science, Israel

The characterization of multi-interfacial devices commonly encounters critical difficulties due to the limited access of standard electrical probes to selected inner domains. In this respect, the XPS (x-ray photoelectron spectroscopy) based CREM (chemically resolved electrical measurements) [1] is a technique proposing particularly useful capabilities. Demonstration of internal junction fields evaluation has already been provided, as well as the direct measurement of layer-specific photovoltages in ETA (extremely thin absorber) solar cells.[2] However, the complex dynamics realized during charge separation in such cells has not yet been investigated thoroughly by CREM.

The present work focuses on this issue, showing conflicting roles of charge trap states and, specifically, their different expression under controllably varied conditions. Comparison with complementary characterization techniques is further discussed, demonstrating the unique insight provided by CREM for their interpretation.

References

1. H. Cohen, *Appl. Phys. Lett.* **85**, 1271 (2004).
2. Y. Itzhaik, G. Hodes, H. Cohen, *J. Phys. Chem. Lett.* **2**, 2872 (2011).

4:40pm EN+EM+MN+NS+TR-MoA9 Understanding Morphological and Structural Effect on Organic Photovoltaic Devices from Plasmonic Particles using Advanced Characterization Techniques, Nuradhika Herath, V. Lauter, J. Browning, Oak Ridge National Laboratory

Organic electronics have been under intense scientific interest in recent years because of their attractive properties such as low cost fabrication processes, ability to performance under low light, and flexibility. Major achievements are based on use of new conjugated polymer and small molecules in bulk heterojunction (BHJ) devices to increase the inner donor acceptor interfaces of fully functional devices such as organic photovoltaics (OPVs) and organic light emitting devices (OLEDs). Many strategies have been introduced to enhance the power conversion efficiency (PCE) of organic electronics. Among them, one of the most promising solutions to enhance the absorption and device efficiencies of OPVs is incorporation of various metal nanoparticles (NPs). Metallic NPs enhanced the efficiency of the devices through local surface plasmonic responses (LSPR). This phenomenon reduced the recombination level of geminate excitons and increases the exciton dissociations, which enhanced the photocurrent and fill factors of devices. However, metallic NPs blended within the active layer can act as polaron traps detracting the device performances. In this study, we investigate layer and interfacial structure of small molecule (SM), *p*-DTS(FBTTh₂) and fullerene, PC₇₀BM system incorporated with silver (Ag) NPs, using neutron reflectometry (NR), X-ray reflectometry and Atomic Force Microscopy (AFM). We present detailed composition changes with Ag NPs concentrations along the film depth to understand morphological and dynamical effects of BHJ devices incorporated with plasmonic particles. To complement and enhance the findings from NR, we report optical properties of the samples using UV-Visible absorption and Photoluminescence spectroscopy. Our findings provide unique information and clear insights into dynamics of plasmonic organic solar cells and their future applications for further enhancement of PCE.

This research was conducted at Spallation Neutron Source and at the Center for Nanophase Materials Sciences, which is sponsored at ORNL by the Scientific User Facilities Division, Office of Basic Energy Sciences, U.S. Department of Energy.

5:00pm EN+EM+MN+NS+TR-MoA10 Doped TiO₂ Based Core-Shell Structures for High Efficiency Hybrid Solar Cells, Jonas Weickert, J. Dorman, M. Noebels, M. Putnik, T. Pfadler, University of Konstanz, Germany, A. Wisnet, C. Scheu, LMU Munich, Germany, L. Schmidt-Mende, University of Konstanz, Germany

Hybrid solar cells, with an inorganic/organic interface for charge separation, have been extensively investigated in the past decade in order to replace the expensive Si based technology with an inexpensive alternative. Typically, these devices incorporate a mesoporous TiO₂ film which is decorated with dye molecules and filled with a hole transport polymer, for example P3HT, to conduct the electrons and holes, respectively. Recently, we have shown that the efficiency of nanowire based hybrid solar cells can be increased from ~1.8 % to 2.5 % through the formation of a Sn-doped TiO₂|TiO₂ core-shell device created via a hydrothermal growth and subsequent TiCl₄ treatment. However, this surface treatment presents difficulties in creating a crystalline conformal coating, limiting the control over the extent of coating

and the crystallinity, directly affecting the charge injection from the polymer into the TiO₂ array. In this work, we directly deposit a controllable TiO₂ film through atomic layer deposition to conformally coat the nanowire arrays with various thicknesses. By changing the thickness and TiO₂ crystallinity, we are able to engineer the energy levels at the TiO₂-dye-P3HT interface due to the magnitude and position of the Fermi levels of the core and shell material, influencing the rate of charge injection and recombination. Furthermore, the crystallinity of the shell layer directly affects the amount of dye that can be absorbed on the surface of the nanostructures with a reduction in light absorption by roughly 30% from anatase to rutile TiO₂. Finally, a detailed mechanism will be proposed for the device performances based on the energy level alignment between the pinned Fermi-level TiO₂ structure and the HOMO of the P3HT resulting in a shifting open circuit voltage based on the crystal phases. Additionally, the core-shell structures are characterized with photovoltage decay and impedance spectroscopy measurements to study the charge transport and recombination across these various interfaces.

5:20pm EN+EM+MN+NS+TR-MoA11 Stack Numbers Dependence of the Activation Energies for Carrier Escape from and Recombination in Strain-Balanced InGaAs/GaAsP MQW, Atsuhiko Fukuyama, T. Ikari, K. Nishioka, T. Aihara, H. Suzuki, University of Miyazaki, Japan, H. Fujii, M. Sugiyama, Y. Nakano, The University of Tokyo, Japan

Fabrication of multiple quantum well (MQWs) in an absorption layer can extend the absorption region toward a longer wavelength and enhance the short-circuit current in the solar cells. However, MQWs function as recombination centers, leading to degradation in both open-circuit voltage and fill factor. We have already reported that the increase in stack number of QW causes the degradation of carrier collection efficiency [1]. In this study, we investigate the effects of stacks number on temperature dependences of the photoluminescence (PL), photothermal (PPT) and the surface photovoltage (SPV) signals. Although the photoexcited carriers in the barrier should relax by the radiative recombination (PL), carriers can thermally escape (SPV) or non-radiatively recombine (PPT) at the same time. Therefore, the latter two methodologies give us new insights for the carrier recombination and drift through the QW.

The present strain-balanced InGaAs/GaAsP MQWs absorption layer was composed of a 7.0-nm-thick In_{0.25}Ga_{0.75}As well and a 10.8-nm-thick GaAs_{0.66}P_{0.34} barrier. All layers were grown on an *n*-type GaAs substrate using metal-organic vapor phase epitaxy. We prepared different samples with MQW stack numbers of 10, 20, 30, and 40 in the *i*-region.

All PPT and SPV spectra showed three distinctive peaks followed by a step like function. They were decomposed into inter-subband transitions expressed by the two dimensional density of states for the QW and exciton peaks [2]. Although the PL intensity decreases with increasing the temperature, signals for PPT and SPV increases. We suppose two activation energies for the process: one is that for the carrier escape from the QW and another is for the non-radiative recombination in the QW. The three rate equations were built for PL, PPT and SPV and the temperature dependences are numerically fitted to estimate the two activation energies. As a result, we have estimated the activation energy for carrier escaping from the QW is constant as 70 meV for all samples with different stacks number. This is the same as the calculated barrier height. However, the activation energy for the non-radiative recombination increases from 6 to 49 meV for the sample with 10 and 40 stacks. This means that radiative recombination increases with increasing the stack number. The carriers thermally escape from the QW again relax into next well and may contribute to increase the radiative recombination.

[1] H. Fujii et al., *Jpn. J. Appl. Phys.* **51**, 10ND04 (2012).

[2] M. Kondow, A. Fukuyama, and T. Ikari et al., *Appl. Phys. Express* **2**, 041003 (2009).

Materials Characterization in the Semiconductor Industry Focus Topic

Room: 313 - Session MC+2D+AP+AS-MoA

Characterization of III-Vs (2:00-3:20 pm)/Photovoltaics, EUV masks, etc. (3:40-4:40 pm)

Moderator: Alain Diebold, SUNY College of Nanoscale Science and Engineering, Paul van der Heide, GLOBALFOUNDRIES, NY, USA

2:00pm MC+2D+AP+AS-MoA1 High Resolution SIMS Depth Profiling in III-V Compound Semiconductors, Marinus Hopstaken, M.S. Schamis, Y. Sun, A. Majumdar, C.-W. Cheng, B.A. Wacaser, G. Cohen, K.K. Chan, D.K. Sadana, D.-G. Park, E. Leobandung, IBM T.J. Watson Research Center

Recently, there has been renewed technological interest for application of InGaAs and related III-V high-mobility materials as a potential replacement for the MOSFET Si-channel [1]. Successful integration of novel materials and processes requires accurate physical characterization of in-depth chemical distribution with nm-scale resolution. We will address some of the challenges regarding SIMS depth profiling of III-V materials and propose analytical solutions for the characterization of more complex multilayer substrates, impurities therein, and Ultra-Shallow Junction (USJ) doping profiles.

Ion beam based sputtering of III-V compounds is intrinsically more complex than in conventional Si substrates. One of the major issues with depth profiling of III-V materials is their higher sensitivity to formation of ion-beam induced topography, which has a detrimental impact on depth resolution [2]. We have previously reported anomalous sputtering behavior of (In)GaAs under low energy O₂⁺ sputtering, causing severe degradation of depth resolution [3].

In case of low energy Cs⁺ sputtering at oblique incidence, we have achieved uniform sputtering conditions on different III-V compounds with no significant topography formation. We have demonstrated constant depth resolution in III-V multilayer structures with decay lengths as low as 2 nm/decade at low Cs⁺ impact energy (down to 250 eV).

We will address some of the analytical challenges regarding the quantification of depth and concentration scales in III-V multilayer structures, grown by hetero-epitaxy. We employ explicit corrections for yield variations using appropriate standards in their respective matrices. A special case occurs for the group IV *n*-type dopants (*i.e.* Si, Ge), which are typically monitored as negative cluster ion attached to the group V element for reasons of sensitivity. We have developed a quantification scheme to determine [Si] doping profiles in hetero-epitaxial structures, composed from the negative cluster ions (e.g. SiAs⁻, SiP⁻) in the respective matrices.

In summary, this work has improved our fundamental understanding of low-energy ion beam interactions in III-V materials, which is essential for achieving sub-nm depth resolution in thin-film structures. In addition, this work has provided with an optimum window of analytical conditions for quantitative analysis of a wide variety of impurities and dopants with high sensitivity in different III-V materials.

1. Y. Sun et al., *IEDM 2013 Conf. Proc.*, p. 48-51.

2. E.-H. Cirilin, J. J. Vajo, R. E. Doty, and T. C. Hasenberg, *J. Vac. Sci. Technol.* **A9**, 1395 (1991).

3. M. J. P. Hopstaken et al., *J. Vac. Sci. Technol.* **B28**, 1287, (2012).

2:20pm MC+2D+AP+AS-MoA2 Nitrogen Incorporation in Dilute Nitride III-V Semiconductors Measured by Resonant Nuclear Reaction Analysis and Ion Beam Channeling, John Demaree, S.P. Svensson, W.L. Sarney, US Army Research Laboratory

The behavior of dilute nitride III-V semiconductors depends critically on the number of nitrogen atoms residing substitutionally on Group V sites, and this small nitrogen incorporation may be used to tailor the optical bandgap for detection of electromagnetic radiation in future low-cost near-infrared imaging systems. In this study, films of GaAsN and GaSbN were synthesized using molecular beam epitaxy at various temperatures and growth rates, with the assistance of a nitrogen plasma source isotopically enriched with ¹⁵N. The films were examined using x-ray diffraction, secondary ion mass spectroscopy, x-ray photoelectron spectroscopy, and resonant nuclear reaction analysis (RNRA) to assess the amount of nitrogen incorporation. Furthermore, RNRA measurements were combined with ion beam channeling methods to ascertain the fraction of incorporated nitrogen atoms residing on substitutional and interstitial lattice sites. The narrow energy resonance and corresponding high depth resolution of the nuclear reaction used (the 897 keV p,γ reaction with ¹⁵N) also enabled an

assessment of the substitutional incorporation of the nitrogen throughout the thickness of the 100-400 nm thick films.

2:40pm MC+2D+AP+AS-MoA3 Determination of Growth Conditions for Highly Mismatched Alloys, Using In Situ Auger Electron Spectroscopy and Flux grading, Stefan Svensson, W.L. Sarney, US Army Research Laboratory, M. Ting, K.M. Yu, Lawrence Berkeley National Laboratory, L.W. Calley, Staib Instruments, Inc.

The electronic band structures of GaN can be effectively modified by the incorporation of Sb. Because of the high electronegativity mismatch between Sb and N growth of GaNSb by molecular beam epitaxy (MBE) must be done at relatively low temperatures and under N-rich condition in order to control the bandgap of the material. The Sb-flux must also be chosen carefully in relation to the growth rate and N-overpressure to control composition and crystallinity. These growth conditions represent a vast parameter space, which is extremely time-consuming to explore in a systematic fashion.

The typical approach for attacking such a problem is to judiciously select a limited set of parameter combinations based on experience and literature data. However, if growth windows are narrow there is no guarantee for success. To more quickly cover a larger parameter range we have grown a very limited number of samples but continuously varied one parameter at a time while employing a combination of in situ and ex situ probes that can reveal critical parameter points. The most novel piece of equipment is the in situ *STAIB Auger Probe*, which allows uninterrupted chemical analysis during crystal growth. In all of the following experiments the substrate temperature was fixed at 325 °C.

In one experiment we determined the transition between Ga- and N-rich MBE growth conditions of GaN by setting a fixed N-flow that generated a steady-state background chamber pressure of 1.5×10^{-5} Torr, while the Ga-source was set up to generate a linear flux ramp from 9.8×10^{16} to 3.9×10^{18} at/m²/s over two hours. During this ramp, the Auger electron signals for N (375 eV), and Ga (1050 eV) were continuously monitored. As expected, both the Ga and N signals increased as a GaN film was starting to form under N-rich conditions and subsequently stabilized. At about 80 min the N-signal started decreasing, which we define as the boundary between N- and Ga-rich conditions and could thus determine the critical Ga-flux relative to the N gas-flow.

In a second experiment the previous information was used to set Ga- and N-fluxes to slight N-rich conditions, while the Sb-valve was slowly opened. In this case both the Auger signals and the reflection high-energy electron diffraction pattern were observed to find the transition between crystalline and amorphous growth conditions. The sample was subsequently analyzed with Rutherford backscattering, which verified the varying Sb-composition. With the data from these two test samples subsequent films were grown with the desired bandgap of 2.2 eV suitable as photoelectrodes for photoelectrochemical water splitting application.

3:00pm MC+2D+AP+AS-MoA4 Electron Channeling Contrast Imaging: Examining Dislocation Effects in III-Ns, J.K. Hite, U.S. Naval Research Laboratory, P. Gaddipati, American Society for Engineering Education, Michael Mastro, C.R. Eddy, D.J. Meyer, U.S. Naval Research Laboratory

III-N materials continue to play a significant role in a range of technologies from rf electronics to visible and UV emitters and detectors. This is true despite a heavy population of extended defects in the active regions of these devices, which degrade the operation, potential performance, and reliability of such devices. With such high dislocation densities when grown heteroepitaxially on sapphire or SiC (10^8 - 10^{10} cm⁻²), techniques to reliably, rapidly, and non-destructively determine spatially defect density are necessary to determine the effects of these defects on device performance.

The most precise characterization tool for defect density has been transmission electron microscopy, but this is a destructive technique, as are other methods such as molten KOH or photo-electrochemical etching of the surface to reveal dislocation sites. Cathodoluminescence imaging only detects dislocations which change the optical emission of the material. X-ray diffraction can be used to extrapolate dislocation density, but not identify individual defects.

Electron channeling contrast imaging (ECCI), a non-destructive technique that has been used to examine defects in metals and ceramics, has recently seen use in III-nitride semiconductors. This technique allows for direct imaging of dislocations, grain boundaries, and topological information all at once. We will present an overview of the uses of ECCI in characterizing III-N materials, culminating in recent work applying the technique to AlGaIn/GaN HEMT structures. By imaging the active areas of van der Pauw structures on a single sample with varying mobility, we find a direct negative correlation between screw dislocation and electron mobility.

3:40pm MC+2D+AP+AS-MoA6 EUV Lithography Mask Cleaning Applications of TOF SIMS Analysis, Thomas Laursen, S.W. Novak, SUNY College of Nanoscale Science and Engineering, A. Rastegar, SEMATECH, T. Nakayama, SUNY College of Nanoscale Science and Engineering

Extreme-UV Lithography (EUVL) is the current R&D frontier for the semiconductor industry. Developing this new technology is generating new studies into a range of new materials issues. EUVL photomask is one important branch of this technology and serious issues have been identified related to the mask surfaces. Photomask performance is usually characterized in terms of EUV ($\lambda = 13.5$ nm) Reflectivity (EUVR) and absorption. But when it comes to surface degradation by radiation exposure and mask cleaning of defects, it is valuable to complement EUVR with a surface analytical technique in order to elucidate the material changes taking place. TOF SIMS has proven to be a versatile analytical technique in this regard. While it may not be the optimal technique in each and every case, it does provide high sensitivity to compositional changes and high-resolution depth profiles. Furthermore, TOF-SIMS analysis on the IonToF V-300 can be done using full-size photomasks which allow analysis at the various stages of processing.

The surface structures on the EUV mask surface consist of a stack of thin films having thicknesses ranging from 1 to 50 nm. The reflective layer contains 40 bilayers of Mo-Si consisting of 2.7 nm Mo and 4.1 nm Si—ending with a Si layer. This multilayer is usually capped with either a 2.5 nm Ru or in some cases a 2 nm TiO₂ surface film. Metallic films with high extinction coefficient with thicknesses in the range from 35 to 75 nm are deposited as an absorber layer and patterned on Ru-capped multilayer blanks.

The combination of EUVR and TOF-SIMS analysis of the Ru capped multilayer EUV masks and blanks provided detailed information on the effects of cleaning on contamination, materials degradation and oxidation. Whereas the EUVR measurements could be directly related to mask specifications, the TOF-SIMS analysis provided more detailed information on surface contamination and oxidation levels, as well as surface-film integrity.

The interactions of the various segments constituting a cleaning process have been characterized in terms of their effect on film etching and removals as well as film oxidation. In general sulfuric acid - H₂O₂ -based treatments caused a severe deterioration of the film structures, whereas NH₄OH - H₂O₂ -based treatments (SC1) caused a more manageable deterioration. Current mask cleaning processes are therefore primarily based on SC1 cleaning. Another concern for mask defectivity is progressive defects generated by sulfate and ammonium compounds. TOF-SIMS was also used to study the aggregation of these compounds during electron irradiation (simulating EUV-irradiation conditions), which was visualized by stage-scan imaging.

4:00pm MC+2D+AP+AS-MoA7 Characterization of Ag/CuInSe₂ Thin-Film Photovoltaics by Photoelectron Spectroscopy, Pinar Aydoğan, Bilkent University, Turkey, N. Johnson, A. Rockett, University of Illinois at Urbana-Champaign, S. Suzer, Bilkent University, Turkey

Photovoltaic power source technology is one of the most desirable ways to provide energy for the world of tomorrow. Hence, it is important to understand the surface, electrical and photo-induced properties of these materials in order to enhance their efficiencies. Currently used materials in photovoltaic manufacturing technology are mainly crystalline silicon, CdTe (cadmium telluride), amorphous and nanocrystalline silicon, CIS (copper indium diselenide) and CIGS (copper indium gallium selenide). In this study, we focused only on the silver/copper indium diselenide cells, which contain a CdS layer on top. X-ray photoelectron spectroscopy (XPS) that we used for analysis was modified to apply both an external photo illumination and voltage bias during data acquisition. The first part of the research focuses on the result of photo induced variations in binding energies of elements and the main objective is to understand the different binding energy shifts of each element in the Ag/CuInSe₂ films in both wavelength- and intensity-sensitive fashion under illumination with three different continuous wave lasers. Furthermore, electrical charging properties of CIS/CdS thin film are studied with externally applied electrical square-wave pulses (SQW), so-called Dynamic XPS. Results will be presented with an ultimate aim of better understanding of the roles of defects affecting the performance of CIS devices. This work was supported by a joint NSF-TUBITAK collaborative research project (NSF Grant No: 1312539 TUBITAK Grant No: 212M051).

4:40pm **MC+2D+AP+AS-MoA9 Facile Synthesis of Composition Tuned $\text{Cu}_{1-x}\text{Zn}_x\text{O}$ Nanoarchitecture on Alpha-Brass.** *Y. Myung, Sriya Banerjee*, Washington University, St. Louis, *H. Im, J. Park*, Korea University, *S. Raman*, Physical Electronics Inc., *P. Banerjee*, Washington University, St. Louis

Composition controlled $\text{Cu}_{1-x}\text{Zn}_x\text{O}$ layers have been synthesized on pretreated α -brass followed by ambient oxidation. The pretreatment consists of a vacuum anneal step which effectively depletes the surface of Zn. The depleted Zn specimens were then oxidized at various temperatures ranging from 300°C – 600°C. SEM and XRD result shows the oxide consists of CuO/ZnO film/nanowire composite architecture. The analysis of electronic structure (XPS) and optical properties (PL) shows the formation of Zn containing alloy in the surface region of CuO films. The composition ratio of Cu and Zn were calculated based on XPS survey spectra. In particular, XPS fine spectra revealed that as the oxidation temperature increases, the binding energy of Zn $2p_{3/2}$ shifts to higher energy, suggesting the possibility of hybridization between the Zn ions and Cu ions.

Photoelectrochemical properties of $\text{Cu}_{1-x}\text{Zn}_x\text{O}$ cathodes exhibit robust photocurrent densities (~ 3 mA/cm²). We suggest the dezincification followed by thermal oxidation provides a better approach for composition tuned nanostructure design and fabrication. These semiconductor nanoarchitectures are excellent candidate materials for fabricating solar energy harvesting photoelectrodes as well as optoelectronic devices.

5:00pm **MC+2D+AP+AS-MoA10 In-line Dimensional Measurement via Simultaneous Small Spot XPS and XRF for Cu CMP Process Control.** *B. Lherron*, ST Microelectronics, *Wei Ti Lee*, Revera, *Motoyama, Chao, Deprosio, Kim*, IBM

As Cu lines used for CMOS devices interconnections become thinner and smaller, current metrology solutions reach their limits. XRay Photoelectron Spectroscopy (XPS) and XRay Fluorescence (XRF) are commonly used as Semiconductor manufacturing process control techniques to measure composition and/or film thickness. In this paper we are exploring the use of a combination of XPS and XRF collected simultaneously to measure the dimensions (line top CD, area and thickness) of Cu lines post Cu CMP on patterned structures. A set of structures with different Cu line width and pitch were used to demonstrate the capability of XPS/XRF on this new application. Results obtained showed good correlation with predicted CD measured by XPS and line section measured by XRF. The paper will also present the comparison with cross section as well as the performance in precision, sensitivity and accuracy of the newly developed technique.

This work was performed by the Research and Development Alliance Teams at various IBM Research and Development Facilities

5:20pm **MC+2D+AP+AS-MoA11 Imaging of the Native Inversion Layer on Silicon-on-Insulator via Scanning Surface Photovoltage; Implications for RF harmonic generation.** *Daminda Dahanayaka*, IBM, *A. Wong*, Dartmouth College, *P. Kaszuba*, *L. Moszkowicz*, *R. Wells*, *F. Alwine*, IBM, *L.A. Bumm*, University of Oklahoma, *R. Phelps*, *J. Slinkman*, IBM

Imaging of the native inversion layer on Silicon-on-Insulator via Scanning Surface Photovoltage;

Implications for RF harmonic generation

*Daminda Dahanayaka*¹, *Andrew Wong*², *Phil Kaszuba*¹, *Leon Moszkowicz*¹, *Randall Wells*¹, *Frank Alwine*¹, *Lloyd A. Bumm*³, *Richard Phelps*¹ and *James Slinkman*¹

¹IBM Microelectronics, 1000 River Street, Essex Junction, Vermont 05452

²Thayer School of Engineering, Dartmouth College, 14 Engineering Drive, Hanover, NH 03755

³Homer L Dodge Department of Physics and Astronomy, University of Oklahoma, 440 W. Brooks Street, Norman, OK 73019

Email: damindahd@us.ibm.com

One of the major challenges encountered during the development of IBM's state-of-the-art RF CMOS Technology on Silicon-on-Insulator (SOI) was to overcome the adverse effects on the harmonic performance of stacked switch devices and transmission lines due to the presence of trapped positive charge, Q^+ , at the interface of the buried oxide (BOX) and the underlying high-resistivity substrate (SX). Most commercially available standard SOI substrates for RF applications have specifications to maintain Q^+ less than 10^{11} cm⁻². The substrate resistivity for IBMs technology is specified to be greater than 1000 ohm-cm, (p-type), i.e. $\rho_0 \approx 5 \times 10^{13}$ cm⁻³. This combination induces a "built-in" n-type inversion layer just under the BOX/SX interface. Using "Scanning Surface Photovoltage" (SSPV) microscopy, we present the first data to show quantitatively the extent of this inversion layer into the substrate. The technique disclosed here quantifies the inversion layer, the degree to which it can be suppressed, and

has led to further enhancements to the RF technology on SOI, such as substantial NFET off-state leakage reduction.

References

- [1] A. Botula et al., IEEE Topical Meeting on Silicon Monolithic Integrated Circuits in RF Systems, 2009. SiRF '09, 1-4 (2009).
- [2] L.A. Bumm et al., US Patent No. 7,944,550.
- [3] T. Ohno, IEDM Tech. Digest, 627-630 (1995).
- [4] J. Greco et al., US Patent No. 8299537 B2.

Magnetic Interfaces and Nanostructures

Room: 311 - Session MI-MoA

Topological Insulators/Rashba Effect

Moderator: Rosa Alejandra Lukaszew, The College of William and Mary

2:00pm **MI-MoA1 Spin-Polarized Electronic Structure at Strongly Spin-Orbit Coupled Surface.** *Koji Miyamoto*, Hiroshima Synchrotron Radiation Center, Japan **INVITED**

Topological insulators and Rashba systems possess peculiar spin dependent electronic structure arising from a combination between a broken space inversion symmetry and strong spin-orbit interaction and are expected as key materials to revolutionize spin current devices without external magnetic field. However, the spin-orbit interaction cause the spin diffuse scattering and spin relaxation time shortens. For promoting practical use, it is necessary to enhance the short spin relaxation time. Topological insulators and Rashba systems possess peculiar spin dependent electronic structure arising from a combination between a broken space inversion symmetry and strong spin-orbit interaction and are expected as key materials to revolutionize spin current devices without external magnetic field. However, the spin-orbit interaction cause the spin diffuse scattering and spin relaxation time shortens.

For promoting practical use, it is necessary to enhance the short spin relaxation time. The spin relaxation time is also dependent on the spin texture caused by spin-orbit interaction, therefore, it enhance demand to directly observe the spin dependent electronic structure. The spin- and angle-resolved photoemission spectroscopy (spin-ARPES) is a most powerful tool to do it. However, it is not enough energy- and angle-resolution ($\Delta E \sim 100$ meV, $\Delta \theta \sim 2^\circ$) of common spin-ARPES systems to clarify the detail spin texture due to the low efficiency ($\epsilon \sim 10^{-4}$) of the conventional Mott-type spin detector. Recently, our group have developed novel high-efficient spin-ARPES system[1]. The system consists of a high performance hemispherical analyzer (VG-Scienta R-4000) and high efficient spin detector based on very low energy electron diffraction of $\text{Fe}(001)p(1 \times 1)-\text{O}$, which has 100 times higher efficiency. Finally, the highest ΔE and $\Delta \theta$ have been improved to 8meV and 0.37°.

In this symposium, I present the researches on spin texture for several strongly spin-orbit coupled system such as Rashba systems [2] and topological insulators [3] studied by our developed high efficient spin-ARPES system.

Reference

- [1] T. Okuda, K. Miyamoto et al., Rev. Sci. Instrum. **82**, 103302 (2011).
- [2] K. Miyamoto et al., New. J. Phys. accepted.
- [3] K. Miyamoto et al., Phys. Rev. Lett. **109**, 166802(2012).

2:40pm **MI-MoA3 Spin Chirality in Momentum Space for Surface States on $\text{Ti}/\text{Si}(111)$ and $\text{Ti}/\text{Ge}(111)$.** *Markus Donath*, *S.D. Stolwijk*, *P. Eickholt*, *A.B. Schmidt*, Muenster University, Germany, *K. Sakamoto*, Chiba University, Japan, *P. Krueger*, Muenster University, Germany

The $\text{Ti}/\text{Si}(111)-(1 \times 1)$ surface is known for its outstanding properties due to spin-orbit interaction: a rotating spin pattern in momentum space and an unoccupied surface state with giant spin splitting at the K point [1,2]. In this contribution, we focus on the unoccupied surface electronic structure along the ΓM and MK high-symmetry directions. Spin- and angle-resolved inverse-photoemission experiments with sensitivity to the in-plane and the out-of-plane components of the spin-polarization vector were performed with our recently developed rotatable spin-polarized electron source [3]. Along both high-symmetry directions, our experiments reveal a surface-derived state with giant spin-orbit-induced splitting, in agreement with our theoretical findings. The state is purely in-plane polarized along ΓM , whereas the out-of-plane component is dominant along KM . As a

consequence, spin chirality is found in momentum space around the M point.

We will compare our results for Ti/Si(111) with data for the isoelectronic Ti/Ge(111) surface. Differences in the surface electronic structure between the two surfaces appear along ΓM , where the Rashba-type spin-split surface state on Ti/Ge(111) lies within a band gap, while it is degenerate with bulk bands on the Si substrate. Consequences for the spin texture will be discussed.

- [1] K. Sakamoto *et al.*, Nature Commun. **4**, 2073 (2013).
- [2] S.D. Stolwijk *et al.*, Phys. Rev. Lett. **111**, 176402 (2013).
- [3] S.D. Stolwijk *et al.*, Rev. Sci. Instrum. **85**, 013306 (2014).

3:00pm MI-MoA4 Spin-Orbit-Induced Spin Polarization in the Unoccupied Electronic Structure of W(110), Henry Wortelen*, Westfälische Wilhelms-Universität Münster, Germany, H. Mirhosseini, Johannes Gutenberg-Universität, Germany, J. Henk, Martin-Luther-Universität Halle-Wittenberg, Germany, A.B. Schmidt, M. Donath, Westfälische Wilhelms-Universität Münster, Germany

The spin texture in the electronic structure of heavy elements and topological insulators, which is caused by spin-orbit interaction, is a hot topic of today's research in condensed matter physics. On W(110) , a spin-polarized Dirac-cone-like surface state has been found recently, which is reminiscent of topological surface states [1, 2]. While the occupied bands including this surface state are well investigated by spin- and angle-resolved photoemission, there is basically a blank area on the $E(k_{\parallel})$ -map above the Fermi level.

We present a combined experimental and theoretical study on the unoccupied electronic structure of W(110) . We interpret our spin- and angle-resolved inverse photoemission experiments on the basis of band structure and one-step-model calculations. We compare results for $\Gamma\text{-N}$ and $\Gamma\text{-H}$, which are nonequivalent due to the two-fold symmetry of the W(110) surface.

A complex spin structure is observed for the surface-state emissions, in which the symmetry of the respective states plays a crucial role. Using several photon detectors and therefore being sensitive to different photon takeoff angles result in different spin-polarization signals of the same electronic state even for normal electron incidence. This shows that the measured spin polarization is highly dependent on the geometry of the experimental setup and does not necessarily resemble the spin structure of the state under investigation. To derive the spin texture of the electronic states experimentally, the photon-emission process has to be taken into account. In this context, we will address how the symmetry of the states influences the observed spin polarization.

- [1] K. Miyamoto *et al.*, Phys. Rev. Lett. **108**, 066808 (2012)
- [2] H. Mirhosseini *et al.*, New J. Phys. **15**, 033019 (2013)

3:40pm MI-MoA6 Reorganization and Annihilation of Topologically Nontrivial Surface and Interface States, Jürgen Henk, Martin Luther University Halle-Wittenberg, Germany **INVITED**

Topological insulators are characterized by an insulating bulk and topologically protected surface states. The latter bridge the fundamental band gap and often show linear dispersion, i.e., a Dirac cone. In this presentation, I am going to answer two questions: how is the Dirac surface state of Bi_2Te_3 modified upon deposition of noble metal atoms? And second, is it possible to confine nontrivial interface states between two topological insulators? The findings have impact for spin-dependent transport.

The electronic structure of Au-covered Bi_2Te_3 is investigated by first-principles calculations [1]. The Dirac surface state of Bi_2Te_3 hybridizes with the Au sp states, which gives rise to strong reorganization of the surface electronic structure. Striking features of the modified Dirac surface state are (i) the introduction of new Dirac points within the fundamental band gap of Bi_2Te_3 , (ii) an extremely weak dispersion, and (iii) an anisotropic number of conducting channels in the fundamental band gap of Bi_2Te_3 which leads to a complicated Fermi surface.

I shall also show that nontrivial electronic states exist at an interface of a Z_2 topological insulator and a topological crystalline insulator [2]. At the exemplary (111) interface between Bi_2Te_3 and SnTe , the two Dirac surface states at the Brillouin zone center annihilate upon approaching the semi-infinite subsystems but one topologically protected Dirac surface state remains at each time-reversal invariant momentum M . This leads to a highly conducting spin-momentum-locked channel at the interface but insulating bulk regions. For the $\text{Sb}_2\text{Te}_3/\text{Bi}_2\text{Te}_3$ interface, there is complete

annihilation of Dirac states because both subsystems belong to the same topology class.

This work is supported by the Priority Program 1666 of DFG.

- [1] Francisco Muñoz, Jürgen Henk, and Ingrid Mertig, submitted (2014).
- [2] Tomáš Rauch, Markus Flieger, Jürgen Henk, and Ingrid Mertig, Phys. Rev. B **88** (2013) 245120.

4:20pm MI-MoA8 Unconventional Relativistic Electron Structure on Polar Bi Chalcogenide Surfaces, Andrew Weber*, University of Missouri-Kansas City, I. Pletikoscic, Q.D. Gibson, H. Ji, Princeton University, T. Yilmaz, University of Connecticut, J.T. Sadowski, E. Vescovo, Brookhaven National Laboratory, A.V. Fedorov, Lawrence Berkeley National Laboratory, A.N. Caruso, University of Missouri-Kansas City, G. Gu, Brookhaven National Laboratory, B. Sinkovic, University of Connecticut, R.J. Cava, Princeton University, T. Valla, Brookhaven National Laboratory Spin-polarized surface electronic structures arising from broken inversion symmetry and a topologically non-trivial excitation gap in the underlying bulk show promise as platforms for realizing of exotic quantum phases (e.g. Majorana fermion modes) and spin-filter transport applications, however, the opportunities presented by these systems for exploring fundamental aspects of the spin-orbit interaction (SOI) in 2D have been underemphasized. The effect of SOI in solids can deviate from conventional models because it is sensitive to the full quantum description of the system, including atomic quantum numbers, the effective electric field, and spatial orbital and crystal symmetries. Together, these conditions shape the band structure and spin- and orbital-texture, and dictate the strength and anisotropy of interband hybridizations. Through spin- and angle-resolved photoemission spectroscopy of semi-ionic topological $(\text{Bi}_2)_m(\text{Bi}_2\text{X}_3)_n$ ($X = \text{Se}, \text{Te}$) superlattice materials, we have identified a variety of unconventional SOI effects acting on topological surface states. We will discuss how tuning the surface charge dipole and termination chemistry controls: (1) the electron band dispersion, (2) interband hybridizations, (3) the size, shape, and spin-topology of the Fermi surface and (4) the sign and magnitude of the Fermi velocity.

4:40pm MI-MoA9 Identifying the Intrinsic Atomic Defects in Bi_2Se_3 with Scanning Tunneling Microscopy, Jixia Dai, Rutgers University, D. West, Rensselaer Polytechnic Institute, X.-Y. Wang, Y.-Z. Wang, D. Kwok, Rutgers University, S.B. Zhang, Rensselaer Polytechnic Institute, S.-W. Cheong, W. Wu, Rutgers University

In topological insulators the helical Dirac fermions are immune to backscattering as long as the time reversal symmetry is preserved. However, the existence of intrinsic atomic defects in materials such as Bi_2Se_3 and Bi_2Te_3 still represents one of the major issues for applications. Intrinsic atomic defects such as vacancies or antisites not only could dope charges, make the insulators conductive and shift the Dirac electrons away from the fermi energy but also affect the mobility of the materials by introducing disorder. By studying a series of Bi_2Se_3 samples that were grown with different conditions with atomic resolving scanning tunneling microscopy, we have successfully identified several types of intrinsic defects, including Se vacancies and Bi-Se antisites. The densities of these different types of defects could be correlated with growth conditions and the total density is related to the band shift measured by tunneling spectroscopy. Our study demonstrates the capability of scanning tunneling microscopy in diagnosing materials like Bi_2Se_3 and similar ones at the atomic level.

5:00pm MI-MoA10 Probing Topological Crystalline Insulator SnTe (001) Surface States via Energy Resolved Quasiparticle Interference, Duming Zhang, NIST and University of Maryland, H. Baek, NIST and Seoul National University, Korea, J. Ha, T. Zhang, NIST and University of Maryland, J.E. Wyrick, A.V. Davydov, National Institute of Standards and Technology, Y. Kuk, Seoul National University, Korea, J.A. Stroscio, National Institute of Standards and Technology

Recently, the topological classification of electronic states has been extended to a new class of matter known as topological crystalline insulators. Similar to topological insulators, topological crystalline insulators also have spin-momentum locked surface states; but they only exist on specific crystal planes that are protected by crystal reflection symmetry. Here, we report an ultra-low temperature scanning tunneling microscopy and spectroscopy study on topological crystalline insulator SnTe nanoplates grown by molecular beam epitaxy. We observed quasiparticle interference patterns on the SnTe (001) surface that can be interpreted in terms of electron scattering from the four Fermi pockets of the topological crystalline insulator surface states in the first surface Brillouin zone. A quantitative analysis of the energy dispersion of the quasiparticle interference intensity shows two high energy features related to the crossing point beyond the Lifshitz transition when the two neighboring low energy surface bands near the X point merge. We present

* **Falicov Student Award Finalist**

two possible interpretations for the two high energy features due to different scattering vectors along the ΓX and XM line cuts. A comparison between the experimental and computed quasiparticle interference patterns reveals possible spin texture of the surface states.

5:20pm **MI-MoA11 Control of Graphene Nucleation on Magnetic Oxides: Spintronics without Spin Injection**, *Yuan Cao*, University of North Texas, *P. Kumar*, Indian Institute of Technology-Mandi, India, *I. Tanabe*, University of Nebraska-Lincoln, *J. Beatty*, *M. Driver*, University of North Texas, *A. Kashyap*, Indian Institute of Technology-Mandi, India, *P.A. Dowben*, University of Nebraska-Lincoln, *J.A. Kelber*, University of North Texas

Graphene direct growth by molecular beam epitaxy (MBE) occurs on a p-type but not n-type oxide, with resulting charge transfer and substrate-induced graphene spin polarization to > 400 K. C MBE on 10 \AA p-type $\text{Co}_3\text{O}_4(111)/\text{Co}(0001)$ at ~ 800 K yields layer-by-layer growth of graphene sheets in azimuthal registry. Significant charge transfer $\sim 0.04 e/C$ atom - confined to the first 1-2 graphene layers, results in oxide reduction at the oxide/Co(0001) interface. In contrast, MBE on 10 \AA n-type $\text{Cr}_2\text{O}_3(0001)/\text{Co}(0001)$ under similar conditions yields only the desorption of C and lattice O, despite similar oxide lattice constants and a stronger Cr-O vs. Co-O bond strength. These results demonstrate that downward band bending at the $\text{Co}_3\text{O}_4/\text{Co}$ interface enhances charge transfer and graphene formation. Upward band bending at the $\text{Cr}_2\text{O}_3/\text{Co}$ interface inhibits such charge transfer. DFT electronic structure calculations show that such charge transfer leads to strong Co(II)/graphene carrier exchange interactions, yielding an enhanced magnetic moment and spin ordering temperature, in excellent agreement with experiment. Such substrate-induced graphene spin polarization makes possible a variety of spintronic devices operating at $>> 300$ K, without the bottleneck of spin injection, and with predicted magnetoresistance values of $\sim 500\%$ or more. The model further predicts such results for other p-type magnetic oxides, making possible high magneto-resistance voltage-switchable devices.

Nanometer-scale Science and Technology

Room: 304 - Session NS+EN-MoA

Nanophotonics and Plasmonics

Moderator: WeiDavid Wei, University of Florida

2:00pm **NS+EN-MoA1 Sculpting the Flow of Light at the Nanoscale**, *Harry Atwater*, California Institute of Technology **INVITED**

Understanding the fundamental properties of plasmonic and dielectric materials in resonant subwavelength structures has fueled an explosion of interest in metamaterials and nanophotonic devices. In this seminar, we explore new directions for plasmonics by examining the relationship between plasmons and the electrochemical potential of the electron gas, and we discuss opportunities to observe quantum coherent states in plasmonic structures. Usually plasmons are described in a classical electromagnetic theory context, yet plasmons are fundamentally quantum excitations. Moreover, the carrier density and optical properties of plasmonic materials are typically fixed at the time of fabrication. Field effect tuning of the electrochemical potential in graphene nanoresonators enables the plasmon and phonon dispersion to be measured. Electrochemical and carrier density modulation in metals yields tunable resonances in metal nanostructures and reveals the plasmoelectric effect, a newly-discovered photoelectrochemical potential. By tuning the permittivity and index to near-zero values, expands the length scale over which coherent quantum emitter phenomena (e.g., concurrence, superradiance) can be observed in epsilon-near-zero media. Finally, we demonstrate entanglement or coherent superposition states of single plasmons using two plasmon-quantum interference in chip-based plasmon waveguide directional couplers.

Web resources:

<http://www.lmi.caltech.edu/>

<http://daedalus.caltech.edu/>

2:40pm **NS+EN-MoA3 Patterning of Plasmonic Structures for Chiroptical Spectroscopy**, *Oded Rabin*, *A.P. Lawson*, *P.C. McAvoy*, *I.D. Mayergoyz*, University of Maryland, College Park

Fabrication of truly chiral nanostructures is a challenging process, often requiring multiple cycles of patterning, deposition and planarization. Planar and three dimensional plasmonic nanostructures were fabricated through focused ion beam (FIB) milling, electron beam lithography (EBL) patterning, and a combination thereof, achieving truly chiral nanoscale patterns in a single deposition step. Using computational modeling tools, the plasmon resonance spectra of the structures were predicted. We have

combined our computational results and novel fabrication methods to achieve chiral plasmonic nanostructures with useful resonances in the visible and near infrared ranges of the EM spectrum. These substrates are promising for the selective manipulation of circularly polarized radiation at nanometer length scales.

3:00pm **NS+EN-MoA4 Hot Electron Generation Enhanced by Carrier Multiplication Probed with a Graphene/TiO₂ Nanodiode**, *YoungKeun Lee*, KAIST, Republic of Korea, *H.K. Choi*, ETRI, Republic of Korea, *H. Lee*, KAIST, Republic of Korea, *J.S. Choi*, ETRI, Republic of Korea, *E. Hwang*, Sungkyunkwan University, Republic of Korea, *J.Y. Park*, KAIST, Republic of Korea

Graphene has attracted intensive attention for viable applications such as energy conversion and optoelectronic devices. When photons hit the graphene, the photon energy can be transferred to hot carriers above the Fermi level from the valence band of the graphene before the photon energy is lost as heat. The efficiency of the conversion depends on the interaction of photons with electrons/holes in the system. In graphene without a bandgap, the process of energy relaxation consists of the Auger process (impact ionization), which leads to carrier multiplication. Here, we fabricated a graphene/TiO₂ nanodiode to investigate carrier multiplication by experimental detection and theoretical confirmation of hot electron amplification. Our findings indicate that carrier multiplication of the graphene based on the strong electron-electron interaction is highly efficient, compared with Au/TiO₂ at a given photon energy. Multiple generations of hot electrons can induce photocurrent, which suggests the possibility of feasible applications such as photovoltaics and photodetectors.

3:40pm **NS+EN-MoA6 Doping Induced 1D Plasmons in Ag Monolayer Stripes on Si(557)**, *Timo Lichtenstein*, *U. Krieg*, *C. Tegenkamp*, *H. Pfnür*, Leibniz Universität Hannover, Germany

An efficient way to transfer energy, e.g. light, into an electronic system is by excitation of plasmons. Due to their flat and almost linear dispersion, allowing extreme confinement in a broad frequency range, and their natural function as wave guides 1D plasmons are particularly interesting.

As we show here for the system Ag adsorbed on Si(557), the interaction between adsorbate layers of transition metal atoms and strongly anisotropic surfaces can lead to various quasi-one-dimensional (1D) signatures, which, however, are not all necessarily metallic. Using low energy electron diffraction in combination with scanning tunneling microscopy and electron energy loss spectroscopy, we correlate the structure, determined by SPALEED and STM, with the properties of low dimensional collective excitations, as measured with momentum and energy resolving electron loss spectroscopy. Semiconducting structures with double periodicity along the chains are formed Ag coverages below 0.3 monolayers (ML). At higher coverages, the formation of wires with $(\sqrt{3}\times\sqrt{3})$ order sets in. Only these wires turn out to be metallic, as is evident from the appearance of plasmonic losses, which show 1D dispersion only along the wires. This 1D property even persists up to one monolayer, where a densely packed array of metallic $(\sqrt{3}\times\sqrt{3})$ stripes is formed. We show evidence that the metallic property is induced by an extrinsic doping process of excess Ag (or other) atoms localized at the step edges, which can be reversibly removed and added. With this system we were able to explicitly show that the 1D plasmon frequency depends on the electron density proportional to $\sqrt{n_c}$ also in the 1D case, and that the confinement of the electrons on the wires is also dependent on doping concentration.

4:00pm **NS+EN-MoA7 Surface Plasmon-Mediated Gold Nanoparticle Deposition via Two Different Mechanisms**, *Jingjing Qiu**, *W.D. Wei*, University of Florida

Utilizing intrinsic surface properties to direct and control nanostructure growth on a large-scale surface is fundamentally interesting and holds great technological promise. We have developed a novel "bottom-up" approach to fabricating sub-15 nm Au nanoparticles on a nanostructured Ag surface via a chemical solution deposition by using localized surface plasmon resonance (SPR) excitation. Nanoparticle sizes were tunable between 3 to 10 nm by adjusting the deposition time utilizing the photothermal effects on a nanostructured Ag film surface. In addition, Au nanoparticles can be selectively deposited at the tip of a Ag bowtie nanostructure with the enhanced electric field.

4:20pm **NS+EN-MoA8 Enhanced Light-Matter Interactions in Nanoparticle Arrays**, *Teri Odom*, Northwestern University **INVITED**

Metal nanostructures concentrate optical fields into highly confined, nanoscale volumes that can be exploited in a wide range of applications. This talk will describe new ways to design arrays of strongly coupled

* NSTD Student Award Finalist

nanoparticles and plasmonic hetero-oligomers that can exhibit extraordinary properties such as plasmon lasing and enhanced gas sensing. First, we will describe a new type of nanocavity based on arrays of metal nanoparticles. These structures support lattice plasmon modes that can be amplified and that can result in room-temperature lasing with directional beam emission. Second, we will focus on nanoparticle assemblies composed of more than one type of material. Hetero-oligomers composed of strong and weak plasmonic materials (Au-Pd dimers and trimers) showed unusual wavelength shifts when subjected to hydrogen gas. We performed detailed modeling to understand the near-field coupling responsible for these amplified light-matter interactions.

5:00pm **NS+EN-MoA10 Plasmon-induced Current Enhancement at Nano-sized Metal-Oxide Interfaces, Jiechang Hou***, D.A. Bonnell, University of Pennsylvania

Nano-sized metal-oxide interfaces possess unique physical properties and offers new access to novel functionalities. We have shown that at the nanoscale the electronic properties of Au/ SrTiO₃ interfaces are size and atomic structure dependent [1]. This size dependence of interface properties has consequences to related behavior, such as resistive switching [2]. Earlier we have shown that plasmon induced hot electrons can be extracted from Au nanoparticles into molecular devices [3]. Here we use Au nano-antennas/SrTiO₃ interfaces as a facile model system to study this phenomenon. The study combines nanofabrication, optical spectroscopies, field simulation and advanced scanning probe microscopy. The dependences of photocurrent on power density and temperature are quantified, and the mechanism of photocurrent enhancement is discussed. We believe that this study can improve the understanding of the mechanism of plasmon-induced current enhancement and facilitate the modern device design.

References:

- [1] J. Hou, S. S. Nonnenmann, W. Qin, D. A. Bonnell, *Appl. Phys. Lett.* **103**, 252106, 2013.
- [2] J. Hou, S. S. Nonnenmann, W. Qin, D. A. Bonnell, *Adv. Funct. Mater.* (2014). doi: 10.1002/adfm.201304121.
- [3] D. Conklin, S. Nanayakkara, T. Park, M. F. Lagadec, J. T. Stecher, X. Chen, M. J. Therien, D. A. Bonnell, *ACS Nano* **7**, 4479 (2013).

5:20pm **NS+EN-MoA11 Extreme Tunability of Metal-Dielectric Multilayered Structures using Al-doped ZnO Grown by Atomic Layer Deposition, Jonathan Skuza, R.M. Mundle, K.C. Santiago**, Norfolk State University, D.L. Lepkowski, Louisiana State University, A.K. Pradhan, Norfolk State University

Plasmonic metamaterials have been a burgeoning area of research in recent years, where surface plasmon polaritons (SPPs) can manipulate light on the nanoscale. Typically, noble metals (e.g. Ag, Au) have been the key materials in this field of research, but suffer drawbacks (e.g. high loss) especially in the mid- and near-infrared (NIR) spectral ranges. Recently, wide bandgap semiconductors, such as Al-doped ZnO (AZO), have been shown to hold great potential in surpassing the tunability and flexibility of traditional noble metals in nanoplasmonic applications. Generally, these transparent conducting oxides have been extremely important for various optoelectronic applications due to the coexistence of high conductivity and high transparency, which can be tuned through doping. Recent studies have shown that these wide bandgap semiconductors, in particular AZO, are also efficient nanoplasmonic materials in the NIR due to their metallic behavior, strong confinement of SPPs, and low loss. AZO has been studied extensively using a multitude of deposition techniques, especially atomic layer deposition (ALD), which is particularly useful to grow uniform and conformal films with a high degree of thickness control on complex three-dimensional topographies because it is based on a binary sequence of self-limiting surface chemical reactions. Furthermore, the doping concentration can be precisely controlled by adjusting the ALD cycle ratios of the host and dopant materials, thus making ALD a unique and powerful method to deposit AZO into high aspect ratio structures for nanoplasmonic applications. Recently, it has been shown that ALD-grown AZO offers extreme tunability that can be utilized for many applications, including plasmonic components for epsilon-near-zero metamaterials. This extreme tunability is exploited here in metal-dielectric multilayered structures in order to manipulate and control light in subwavelength volumes for various optical applications.

* NSTD Student Award Finalist

Plasma Science and Technology Room: 308 - Session PS-MoA

Advanced FEOL/Gate Etching

Moderator: Eric A. Joseph, IBM Research Division, T.J. Watson Research Center

2:00pm **PS-MoA1 Breaking Through Limits in Semiconductor Technology, Chang-Jin Kang**, Samsung Electronics, Republic of Korea
INVITED

[Abstract]

Our current IT industry, which possesses a strong demand of personal mobile devices, is accelerating towards smart devices with the convergence of new technologies.

Under these circumstances, the development of semiconductors with high speed, high density, low power and high reliability are crucial. Scaling down of devices and to ensuring cost-effective technologies are the two most important tasks the semiconductor industry is facing.

To find proper solutions for the development of future devices and to overcome the limitations of current technologies, mid and long-term projections of future silicon technology as well as DRAM, NAND and Logic technology trends will be covered.

2:40pm **PS-MoA3 Mechanism of Silicon Damage during N₂/H₂ Block Etching for FinFET CMOS, Tamotsu Morimoto**, Tokyo Electron Limited, Japan, H. Ohtake, Tokyo Electron America, Inc., T. Wanifuchi, Tokyo Electron Miyagi Limited, Japan

In this study, we found that the degradation of a silicon active area during N₂/H₂ block etching strongly depends on ion energy and flux because ions generate significant damage on the silicon surface as compared with the damage to the active area due to hydrogen radicals.

Plasma-induced damage on Si substrates has become a serious concern in CMOS fabrication processes. In addition, the appearance of Fin-FETs have made it necessary for plasma etching processes to use masks made by the organic film opening process and block etching in order to implant the P- or N-type regions. In this study, part of the fin structure was exposed to plasma during organic block etching. It was found that the source and drain regions of the fin area were damaged. However, the impact of the generated damaged layer on the electrical properties has not been clarified, especially junction leakage of the source and drain. In this paper, effect of etching using N₂/H₂ gas combination on p-n junction leakage current at reverse bias was investigated. Parameters of the N₂/H₂ plasma like flow rate, etching time, peak-to-peak voltage of the RF bias (V_{pp}), and the micro wave power (MW) were varied. Si substrate with a p-n junction was exposed to the N₂/H₂ plasma, followed by nickel silicidation to enable electrical characterization.

Junction leakage current increased by increasing V_{pp} and reducing MW for fixed etching times and was independent of the hydrogen ratio in the N₂/H₂ gas. This indicates that ion has a stronger influence on Si damage than H₂ radicals. With etching depth kept fixed, a high hydrogen ratio showed less damage because etching rate was higher. In addition, we obtained smaller damage for higher V_{pp} at constant MW because etching time was shorter owing to the high etching rate. Accordingly, we can infer that ion energy and cumulative ion flux have a significant impact on the degradation of the p-n junction. From the transmission electron microscopy analysis, the damaged layer, which degraded Si crystallinity, became thicker by increasing the exposure time of the Si substrate to the N₂/H₂ plasma. Most probably, the damaged layer has a lot of defect sites which act as trap sites beside the junction, which in turn causes the p-n junction leakage current to increase.

We found that the ratio of ion/radical in the plasma should be lower to reduce the damage of silicon active area by N₂/H₂ block etching. High etching rate and low V_{pp}, which correspond to high hydrogen ratio and low RF bias, is the best combination for low-damage organic block etching.

3:40pm **PS-MoA6 Plasma Etch in the Era of Atomic Scale Fidelity, Vahid Vahedi, J. Marks**, Lam Research Corp
INVITED

The ultimate goal of IC manufacturing is to produce the structures that are conceived and modeled by design engineers in the real world with high fidelity. We choose the term "fidelity" deliberately to express that what is needed in the end is the highest possible degree to which a material structure matches the design intent. It includes but is not limited to statistical criteria such as accuracy and precision.

Plasma etch plays a key role in obtaining structural fidelity in all three dimensions. Precision is obtained by means of wafer-to-wafer, chamber-

to-chamber and tool-to-tool matching. Accuracy on the other hand requires control of proximity and 3D effects such as critical dimension (CD) loading, profile loading, aspect ratio dependent etching (ARDE), and selectivity.

As we approach devices with a half pitch of 10 nm and below, atomic scale fidelity is required because the device dimensions and their allowed tolerances are of the same order of magnitude as the inter-atomic distances in the crystal lattice. This type of performance can be obtained when the material is removed layer by layer. The etch process is comprised of single unit steps which repeat in cycles. Each step uses the simplest possible chemistry to surgically target specific reactions at the wafer surface such as activation, removal, and passivation. We call this layer-by-layer etch with atomic fidelity Atomic Layer Etch/atomic layer etch1.

In this presentation, we introduce the framework of high productivity, production-worthy ALE atomic layer etch and the implications for hardware and process development. Results for both dielectric and conductor etch obtained with Lam's Research' latest etch products will be presented.

References:

1. Kanarik, et al., Solid State Technology, (2013) 14-17.

4:20pm **PS-MoA8 Challenges of 3D NAND Staircase Patterning Process**, *Hui Zhou, S. Srinivasan, J. Choi, A. Khan, L. Yu, Z. Yao, A. Agarwal, S. Rauf*, Applied Materials Inc.

NAND memory microfabrication is at the transition point to vertical structures. A variety of 3D NAND device designs have been reported, such as bit cost scalable (BiCS) and terabit cell array transistor (TCAT). Despite the difference in the structures and operational mechanisms of 3D NAND devices, the microfabrication processes share a common first step, the formation of the landing pads for the control gate via contacts. The "staircase" of pad landings is realized by alternating film etching and resist trimming. To ensure high yield, the registration for the vias must be ensured by the insitu staircase patterning process with CD uniformity being the most critical figure of merit for desired yield. CD uniformity is most sensitive to the resist trimming process and is controlled by plasma distribution and electrostatic chuck temperatures. Local CD non-uniformity may originate from microloading effect or asymmetry impact, and the approaches to improve the local CD uniformity focus on mitigating loading and reducing the asymmetry with process and hardware development, that are also supported by quantitative modeling results. Early versions of the staircase patterning process resulted in low throughput due to multiple resist trimming steps. High throughput is required to reduce the cost of fabrication. Power, flow, and pressure are effective knobs in improving the resist trimming rate. Reducing the gas transition time and using continuous plasma between different gas has also proven effective for further improving throughput. Challenges and progress for 3D NAND staircase patterning process will be discussed, and innovative hardware and process solutions will also be presented.

4:40pm **PS-MoA9 Impact of the Addition of SiCl₄ in a CH₃F/O₂/He Chemistry for the Nitride Spacer Etching of FDSOI 14 nm Technology**, *C. Arvet, S. Lagrasta, Maxime Garcia Barros*, STMicroelectronics, France, *S. Barnola, N. Posseme*, CEA, LETI, MINATEC Campus, France, *F. Leverd*, STMicroelectronics, France

Today, the choice of chemistry for nitride spacer etching is a CH₃F/O₂/He based chemistry. But such chemistry leads to 10A and 15A silicon and silicon germanium consumption, respectively. Furthermore the remaining carbon at the silicon or silicon germanium surface can lead to a poor silicon surface quality which does not allow the film regrowth. The optimization of this process is not enough reliable in order to be used in production for the FDSOI 14 nm technologies.

In this context, we investigated the impact of SiCl₄ addition to CH₃F/O₂/He/CH₄ chemistry.

Ellipsometry measurements performed on blanket silicon nitride and silicon germanium film allow us to investigate two essential points for the FDSOI 14 nm technologies:

-The resist consumption

-The opportunity to obtain an infinite selectivity of silicon nitride to silicon germanium.

Complementary XPS and FTIR analyses have been performed for a better understanding of the etch mechanisms and will be presented.

These results have been confirmed on patterned structures. TEM analyses have shown no silicon germanium recess with no foot formation after silicon nitride spacer etching and wet cleaning. Finally, the compatibility of this new etch chemistry on epitaxial growth quality will also be presented.

5:00pm **PS-MoA10 Hydrofluorocarbon Gases for Selective, Low-Damage, Silicon Nitride Etching**, *James Royer, R. Gupta, V. Pallem*, American Air Liquide

Maintaining Moore's law has introduced increasingly stringent process requirements for front-end device technologies. These requirements create considerable technical challenges for silicon nitride gate spacer etching. Etch processes must remove thin silicon nitride layers while maintaining stringent physical constraints and chemical integrity of the underlying substrate. Therefore, the etch gases must be tailored with appropriate functionality for selective silicon nitride etching. This study presents hydrofluorocarbon (HFC) etch gases which demonstrate selective etching of silicon nitride with respect to silicon oxide, and poly-silicon. Using a RIE plasma etch tool, the performance of each molecule is studied on blanket wafers and analyzed using spectroscopic ellipsometry, x-ray photoelectron spectroscopy (XPS), and scanning electron microscopy (SEM). Etch rates and selectivities for each HFC are evaluated over a range of O₂ flow to determine the desirable process windows. Select HFCs have large process windows with infinite silicon nitride to poly-silicon selectivity due to fluorocarbon deposition on the poly-silicon. The fluorocarbon deposition layer on poly-silicon inhibits undesired silicon-carbide or silicon-oxide formation. XPS surface analysis and depth profiling shows a reduction in carbon and oxygen incorporation in poly-silicon compared to similar processes using the industry standard molecule, fluoromethane.

5:20pm **PS-MoA11 Alternative Process for Thin Layer Etching: Application to Nitride Spacer Stopping on Silicon Germanium**, *Nicolas Posseme, G. Santini, O. Pollet, C. Arvet, S. Barnola*, CEA-LETI, France

Today, minimizing the so-called silicon germanium (or silicon) recess during nitride spacer etching is extremely difficult to achieve but mandatory since it directly impacts the device performances. Despite of etch chemistry or tool improvement, this silicon germanium recess is only limited.

In this context, we proposed an alternative etching process to overcome these issues and meet the highly complex requirements imposed by device fabrication processes. This new etching process is based on two steps. In a first step, the film is modified in volume by a H₂ plasma performed in a conventional etch tool (ICP or RIE) followed in a second step by a selective removal of the modified layer with respect to the non-modified material.

In this study, we will present this alternative process for nitride spacer etching stopping on silicon germanium for FDSOI devices. It will be demonstrated that the silicon nitride film modification can be adjusted by playing on plasma parameters. XPS and infrared spectroscopy analyses have been performed on blanket silicon nitride film to understand the silicon nitride film modification induced by H₂ plasma. These mechanisms of the silicon nitride film damage will be discussed.

In the meantime, different approaches (dry or wet) to remove the modified silicon nitride film without non-modified nitride or silicon germanium films consumption have also been investigated. The advantages and the drawbacks of these approaches will be presented.

Starting from the best process conditions (modification and removal steps), TEM analyses performed on patterned structures have revealed that the silicon germanium recess is less than 5A for a wide range of nitride film over etch (from 30 to 120%) with no foot formation compared to more than 15A recess and 20 A foot formation using the best current etching processes (CH₃F/O₂/He chemistries targeting 50% over etch).

Finally, the compatibility of this new nitride spacer etching process on SiGe epitaxial growth quality will also be presented. It will be shown, that the clean surface obtained after the modified nitride film removal leads to a perfect epitaxial growth for different silicon nitride over etch from 30 to 120%.

Novel Trends in Synchrotron and FEL-Based Analysis Focus Topic

Room: 312 - Session SA-MoA

Synchrotron Studies of Processes in Energy Conversion, Electronic Devices and Other Materials II

Moderator: Charles Fadley, University of California, Davis

2:00pm **SA-MoA1 Synchrotron-based In Situ Study of PEMFC, SOFC, Battery and Supercapacitor Components**, *Benedetto Bozzini*, Universita' del Salento - Italy **INVITED**

Fuel cells and supercapacitors are electrochemical devices providing efficient and pollution-free production and transformation of electricity. Notwithstanding their environmental appeal, a host of materials-science problems – chiefly related to the limited durability of crucial functional

components – are hindering the widespread application of these otherwise promising devices. Nanotechnology is foreseen to play a key role in the elimination of such drawbacks. Some nanotechnology solutions have already led to sensitive improvements of properties, functionality and performance of some components. However, the present knowledge is mostly at the macroscopic and empirical trial-and-error level and the answers to many questions require much deeper scientific understanding of the origin of degradation processes. In this regard, the development and implementation of appropriate methods for in-situ characterization of cell components at the functionally relevant length scales is highly required. Soft X-ray spectroscopies, namely X-ray absorption spectroscopy, X-ray emission (fluorescence) spectroscopy, resonant inelastic X-ray spectroscopy and X-ray photoelectron spectroscopy have been extensively employed for ex-situ characterization of materials used in electrochemical systems. Furthermore, adding spatial resolution capabilities by implementing proper optical solutions has opened unique opportunities for monitoring material changes and mass transport events occurring at submicron length scales. The input from these methods is providing correlative information about the status of the electrode surface and of the electrode/electrolyte interface and also of the processes occurring under operation conditions at the three phase boundary, namely the electrode-electrolyte-reactant interface¹⁻⁴.

REFERENCES [1] B. Bozzini, A. Gianoncelli, P. Bocchetta, S. Dal Zilio, G. Kourousias, *Anal. Chem.* **86**, 664 (2014)

[2] B. Bozzini, M. Amati, L. Gregoratti, M. Kiskinova, *Sci. Rep.* **3**, 2848 (2013)

[3] B. Bozzini, A. Gianoncelli, C. Mele, M. Kiskinova, *Electrochim. Acta* **114**, 889 (2013)

[4] B. Bozzini, M. Kazemian Abyaneh, M. Amati, A. Gianoncelli, L. Gregoratti, B. Kaulich, Maya Kiskinova, *Chemistry – A European Journal* **18**, 10196 (2012)

2:40pm **SA-MoA3 Structure/Selectivity Studies of Promoted Rh/TiO₂ Catalysts under CO Hydrogenation Reaction Conditions**, *Robert Palomino*, *J. Magee*, *P. Carrillo Sanchez*, Stony Brook University, *M. White*, Brookhaven National Laboratory and SUNY Stony Brook

Rh-based catalysts are sought after for the conversion of syn gas (CO +H₂) to higher oxygenates due to their C-C coupling capabilities, but are highly selective to hydrocarbons. Through the addition of promoters (Fe, Mn, Mo), the selectivity can be altered to oxygenates by varying mechanisms.[1] Fe and Mo in particular have been known to enhance ethanol and other C₂-oxygenates through the suppression of methane. Unfortunately, little is known of the structure of these promoted catalysts under reaction conditions. This work focuses on the atomic structure determination of Fe- and Mo-promoted Rh/TiO₂ catalysts with varying promoter concentration. The atomic structure was monitored as a function of promoter concentration under reduced and CO hydrogenation conditions with synchrotron radiation at beamline X7B of the NSLS. X-ray diffraction (XRD) was utilized to elucidate the phase components in the catalysts, while Pair Distribution Function (PDF) analysis was used to determine the local atomic structure of the active components contained in the catalyst. By monitoring the evolution of phase and local atomic structure, we correlate the structure-selectivity relationship by direct comparison with selectivity measurements performed on the same catalysts.

1. Spivey, J.J. and A. Egbeki, *Heterogeneous catalytic synthesis of ethanol from biomass-derived syngas*. *Chemical Society Reviews*, 2007. **36**(9): p. 1514-1528.

3:00pm **SA-MoA4 Synchrotron Infrared Nano-spectroscopy**, *Hans Bechtel*, Lawrence Berkeley National Laboratory, *E.A. Muller*, *R.L. Olmon*, University of Colorado at Boulder, *M.C. Martin*, Lawrence Berkeley National Laboratory, *M.B. Raschke*, University of Colorado at Boulder

By combining scattering-scanning near-field optical microscopy (s-SNOM) with mid-infrared synchrotron radiation, synchrotron infrared nano-spectroscopy (SINS) enables molecular and phonon vibrational spectroscopic imaging, with rapid spectral acquisition, spanning the full mid-infrared (500-5000 cm⁻¹) region with nanoscale spatial resolution. This highly powerful combination provides access to a qualitatively new form of nano-chemometric analysis with the investigation of nanoscale, mesoscale, and surface phenomena that were previously impossible to study with IR techniques. We have installed a SINS end-station at Beamline 5.4 at the Advanced Light Source (ALS) at Lawrence Berkeley National Laboratory, making the s-SNOM technique widely available to non-experts, such that it can be broadly applied to biological, surface chemistry, materials, or environmental science problems. We demonstrate the performance of synchrotron infrared nano-spectroscopy (SINS) on semiconductor, biomineral and protein nanostructures, providing vibrational chemical imaging with sub-zeptomole sensitivity.

3:40pm **SA-MoA6 Synchrotron-Based Spectroscopy Shedding Light on Solar Cells**, *Franz Himpfel*, University of Wisconsin-Madison
INVITED

After briefly discussing the role of photovoltaics in the current energy picture, this talk illustrates how spectroscopy with soft X-rays can assist the development of new types of solar cells with improved price/performance ratio. The starting point is the most general layout of a solar cell, which involves of a light absorber sandwiched between an electron donor and an electron acceptor. In contrast to the widely-used silicon solar cells, one can choose three different materials to optimize the four energy levels that are crucial for the performance of a solar cell. These are measured by a combination of X-ray absorption spectroscopy and photoelectron spectroscopy. Close coupling with first principles calculations makes it possible to discover and exploit systematic trends. Examples will be given, such as the combination of all three components in one molecule (donor- π -acceptor complexes [1],[2]). In addition to the energy levels one has to consider the lifetime of the photo-generated carriers. A future dream experiment will be discussed where the carriers are followed in real time on their way from the absorber to the contact electrodes, using pump-probe techniques at the latest generation of soft X-ray light sources. Such experiments have been performed in the UV/visible [3], but they would greatly benefit from the element- and bond-specific capabilities of X-ray absorption spectroscopy.

[1] A. Yella, H.-W. Lee, H. N. Tsao, C. Yi, A. K. Chandiran, Md. K. Nazeeruddin, E. W.-G. Diau, C.-Y. Yeh, S. M. Zakeeruddin, M. Grätzel, *Science* **334**, 629 (2011).

[2] I. Zegkinoglou, M.-E. Ragoussi, C. D. Pemmaraju, P. S. Johnson, D. F. Pickup, J. E. Ortega, D. Prendergast, G. de la Torre, and F. J. Himpfel, *J. Phys. Chem. C* **117**, 13357 (2013).

[3] G. Duvanel, J. Grilj, and E. Vauthey, *J. Phys. Chem. A* **117**, 918 (2013).

4:20pm **SA-MoA8 In Situ Soft X-Ray Absorption Spectroscopy for Investigation of Charge Storage and Actuation in Nanostructured Carbon Aerogels**, *J.R.I. Lee*, *M. Bagge-Hansen*, *B. Wood*, *T. Ogitsu*, *A. Wittstock*, *M. Worsley*, *Trevor Willey*, *M. Merrill*, Lawrence Livermore National Laboratory, *D. Prendergast*, Lawrence Berkeley National Laboratory, *I.C. Tran*, *M. Biener*, *T. Baumann*, *J. Biener*, Lawrence Livermore National Laboratory, *J.-H. Guo*, Lawrence Berkeley National Laboratory, *T.W. van Buuren*, Lawrence Livermore National Laboratory

Carbon aerogels (CAs) are a class of nanostructured, porous materials that have demonstrated applications in electrical energy storage (EES) due to their very high surface area, chemical and electrochemical stability, and relatively low cost. Tailoring these materials towards improved ESS performance can be significantly enhanced by a better understanding of nanostructured materials in aqueous environments under various potential gradients; therefore, we have pursued advanced in situ characterization techniques capable of probing the electronic structure and bonding of these electrode materials during charge-discharge cycling. We report the successful development of a cell for in situ soft x-ray absorption spectroscopy (XAS) studies of EES materials and the application of this cell to the investigation of CA supercapacitors. Our XAS measurements, combined with complementary ab initio modeling, reveal profound changes in the structure and bonding of the CAs in operando, which will be discussed in terms of their macroscopic physical properties. This work performed under the auspices of the U.S. Department of Energy by Lawrence Livermore National Laboratory under Contract DE-AC52-07NA27344.

4:40pm **SA-MoA9 First-Principles Modeling of Near-Edge X-ray Spectroscopy for Lithium Compounds**, *John Vinson*, National Institute of Standards and Technology (NIST)

X-ray spectroscopy is a widely-used tool for probing local structural and chemical properties of materials. For devices such as batteries *operando* measurements are vital for understanding the structural changes that take place during the device's lifecycle. Computational modeling can assist experimental investigation by providing complementary data: pointing from proposed structure to observed spectra. The OCEAN spectroscopy package is capable of calculating K- and L-edge spectra of periodic or semi-disordered extended systems using a Bethe-Salpeter equation formalism. Here we present the OCEAN package and near-edge x-ray absorption calculations of lithium compounds. We showcase the effects of accounting for vibrational disorder as well as how a computational approach can be used to decouple the structural and charge-transfer effects on the x-ray spectra observed during (de)lithiation.

5:00pm **SA-MoA10 Soft X-ray Spectroscopy for Fundamental Understanding and Practical Optimization of Battery Materials, Wanli Yang**, Lawrence Berkeley National Laboratory **INVITED**

Improving the energy-density and safety of batteries remains a formidable and critical challenge for sustainable energy applications, especially for electric vehicles. The pressing demand calls for novel approaches based on modern material synthesis and advanced characterization tools. Synchrotron based soft x-ray spectroscopy is one of such incisive tools that probe the electronic states in the vicinity of the Fermi Level, which are directly related to battery operations.

This presentation will focus on the concepts of how the electronic structure revealed by soft x-ray spectroscopy could help the battery material research. The link between fundamental electron states and battery performance will first be explained in general^[1]. Several recent spectroscopic results will be discussed from both chemical and physical point of view: The chemical information delivered by soft x-ray indicates the complicated formation process of solid-electrolyte-interphases^[2]. The evolution of the transition-metal 3d states provides in-depth information of the phase transformation in positive electrodes^[3]. Key electronic states that could be directly detected by soft x-ray experiments provide clear guidelines for optimizing battery binder materials in negative electrodes^[4]. Additionally, *in-situ/operando* soft x-ray experiments reveal distinct charge dynamics in operating battery electrodes^[5]. Perspectives will be provided at the end on how to advance the battery material studies through novel instrumentation and methodology.

[1] Yang et al., JESRP 190, 64 (2013); [2] Qiao et al., Adv. Mater. Interf. 10.1002/admi.201300115 (2014); [3] Liu et al., JACS 134, 13708 (2012); [4] Liu et al., Adv. Mater. 23, 4679 (2011); [5] Liu et al., Nat. Commun. 4, 2568 (2013)

Advanced Surface Engineering

Room: 302 - Session SE+PS+TF-MoA

Pulsed Plasmas in Surface Engineering

Moderator: Jolanta Klemberg-Sapieha, Ecole

Polytechnique de Montreal, Canada, Michael Stueber, Karlsruhe Institute of Technology

2:00pm **SE+PS+TF-MoA1 Complex Magnetic Systems for High Power Pulsed Magnetron Sputtering, Priya Raman***, I.A. Shchelkanov, J. McLain, University of Illinois at Urbana Champaign, S. Armstrong, Kurt J. Lesker Company, B. Zhang, M. Schilling, DEXTER Magnetic Technologies, D.N. Ruzic, University of Illinois at Urbana Champaign

High Power Pulsed Magnetron Sputtering (HPPMS) is a type of magnetron sputtering technique where high peak power pulses reaching tens of kilowatts are applied to the sputter magnetron target keeping the average power equal to that of direct current magnetron discharges by using low duty cycles. Due to very high power densities, HPPMS discharge leads to high degree of ionization of the sputtered material. These ionized sputtered materials assist in film growth leading to more adhesive, dense, and smoother films. Therefore, HPPMS is considered an ideal candidate for the next generation magnetron sputtering systems, however these techniques suffer from low deposition rate due to "return effect" of the ionized sputter material [1]. One way to solve this problem is to have a magnetic field configuration that is optimized for HPPMS discharges. Magnetic pack design is critical as it helps in achieving full-face target erosion and higher deposition rate in HPPMS. Magnet pack design is generally selected by experimental observation. It has been confirmed from our previous work on HPPMS that a spiral-shaped magnetic field design on 14 inch (36 cm) diameter copper target was able to produce superior plasma uniformity on the substrate in addition to improved target utilization without the need for magnet rotation [2]. Commercial 4 inch (10cm) magnetron sputter guns function with a variety of power supplies like DC, Pulsed-DC, Modulated Pulsed Power Magnetron sputtering (MPP) and HPPMS. These 4 inch magnetron sputter guns typically have a conventional circular magnetic field configuration and suffer from low deposition rate in HPPMS discharges. To optimize the magnet field configuration in HPPMS for the 4 inch magnetron sputter gun, the spiral design from the 14 inch target was scaled down and modified to fit into 4 inch magnetron sputter gun. A new "ε" design magnet pack with enhanced discharge parameters was developed by modifying the spiral magnet pack in COMSOL Multiphysics, which leads to higher deposition rate and better target utilization in HPPMS compared to the conventional magnet pack. The influence of "ε" design magnet pack configuration on deposition rate, plasma parameters, and

discharge stability with HPPMS (Huettinger's HiPIMS), MPP(zPulser), DC and pulsed DC power supplies were investigated. The deposition rate for "ε" pack is 2.1±0.2 times the conventional pack for an average discharge power of 500W with zPulser power supply.

1. Papa F et al 2011 *Thin Solid Films* 520.5 1559-1563.
2. He Yu et al 2013 *Plasma Sources Sci. Technol.* 22 045012.

2:20pm **SE+PS+TF-MoA2 Triple Langmuir Probe and Ion Fraction Measurements in an Industrial PVD Deposition System, YuiLun Wu, S.S. Ma, I.A. Shchelkanov, D.N. Ruzic**, University of Illinois at Urbana-Champaign

High Power Pulsed Magnetron Sputtering (HPPMS) discharges are an ideal candidate for the next generation PVD magnetron sputtering systems. Compared with traditional DC sputtering, HPPMS discharges offer high degree of ionization of the sputtered material with very high peak power on the target. An industrial size chamber will be used to investigate the HPPMS discharge operation in full scale production environments utilizing different power supplies. Plasma was observed to be originated from the race track region then expanded downward afterwards. Plasma density was very high ($\sim 10^{19}$ - 10^{20} m⁻³) when generated then decreases as it expanded [1] In order to understand the temporal evolution of the plasma between the target and the wafer plane, a time resolved triple Langmuir probe was employed to measure the plasma parameters such as electron temperature and density and scanning in a three dimensional map. Plasma parameters between traditional DC discharge and HPPMS discharge will be compared. Quartz crystal microbalance and 2 inch gridded energy analyzer will be designed to determine fluxes of metal ions, metal atoms and argon ions. The setup will be able to tilt around 10 degrees about the wafer plane in 1 degree intervals and measure the angular distribution of the ion and neutral fluxes generated by the HPPMS discharge.

Reference:

- [1] H.Yu, L. Meng, M. Szott, J. McLain, T.S. Cho, D.N. Ruzic, Investigation and optimization of the magnetic field configuration in high-power impulse magnetron sputtering, *Plasma Sources Sci. Technol.* 22 045012, 2013

2:40pm **SE+PS+TF-MoA3 Understanding the Physics of Magnetron Discharges: Ionization Zones and Their Role in Transport of Charged Particles, Matjaž Panjan, R. Franz, A. Anders**, Lawrence Berkeley National Laboratory **INVITED**

Magnetron sputtering is one of most commonly used techniques for the deposition of thin films. The physics of magnetron discharges has been intensively studied, however, recent investigations revealed that our understanding is rather incomplete. To the naked eye the ionization process appears to be homogeneously distributed along the racetrack – i.e. the region of strongest target erosion caused by sputtering. Imaging of the magnetron discharges with intensified CCD cameras using short exposure times revealed differently, namely, the plasma is concentrated in several zones along the racetrack [1-3]. These so-called ionization zones or spokes are organized in periodic or quasi-periodic patterns that move in the $\mathbf{E} \times \mathbf{B}$ direction with approximately 1/10 of the electron drift speed (where \mathbf{E} and \mathbf{B} are the electric field and magnetic field vectors). Recent experiments further revealed that ionization zones are a fundamental feature of magnetron discharges run in pulsed and continuous mode [4]. In this talk, recent advances in understanding the ionization zone phenomenon will be reviewed. The interpretation of the formation, drift, self-sustainability, and self-organization of ionization zones will be presented with emphasis on potential, electric field and ionization rate distributions. It will be shown that ionization zones play a critical role in the transport of both electrons and ions [4-6].

- [1] A. Kozyrev et al., *Plasma Physics Reports* 37 (2011) 621
- [2] A. Anders et al., *J. Appl. Phys.*, 111 (2012) 053304
- [3] A.P. Ehasarian et al., *Appl. Phys. Lett.* 100 (2012) 114101
- [4] M. Panjan et al., *Plasma Sources Sci. Technol.*, 23 (2014) 025007
- [5] A. Anders et al., *Appl. Phys. Lett.*, 103 (2013) 144103
- [6] P.A. Ni et al., *Appl. Phys. Lett.*, 101 (2012) 224102

3:40pm **SE+PS+TF-MoA6 Properties of Ionization Zones in Magnetron Sputtering Observed in the Transition Region between dc and HiPIMS, André Anders, Y. Yang, J. Liu, Y. Qiu**, Lawrence Berkeley National Laboratory

Research in the last years revealed that the plasma in high power impulse magnetron sputtering (HiPIMS) is rich in structure, featuring self-organized patterns [1], plasma flares [2], and azimuthally asymmetric particle jets [3]. Most prominent are drifting regions of enhanced excitation and ionization, which are called ionization zones but sometimes also labeled spokes in

* Coburn & Winters Student Award Finalist

analogy to similar phenomena seen in other $\mathbf{E} \times \mathbf{B}$ devices such as Hall thrusters. Fast imaging of ionization zones in HiPIMS revealed the presence of several distinct ionization zones, for example 3-5 zones in the case of sputtering with a 3-inch magnetron at peak currents of the order 100 A. The zone drift velocity is several 1000 m/s, up to 10^4 m/s, yet much slower than the $\mathbf{E} \times \mathbf{B}$ drift of electrons, which is of the order of 10^5 m/s. In contrast, when sputtering continuously (dc) at very low current (less than 1 A), and at low pressure (less than 1 Pa), we find only one ionization zone moving at low velocity in the reverse, i.e. the $-\mathbf{E} \times \mathbf{B}$ direction. Increasing the current and pressure tends to split the zone into two and occasionally three zones. The appearance of each zone depends on current and other factors such as the pressure of the process gas. In this contribution, we explore the transition regime between dc operation at low current and HiPIMS operation with high peak currents. Using fast streak and frame imaging cameras we detect even more structures and structure changes than anticipated. We conclude that the discharge and its particle transport is governed by zone-related instabilities and turbulence.

- [1] A. Anders, et al., J. Appl. Phys. 111 (2012) 053304.
 [2] P.A. Ni, et al., Appl. Phys. Lett. 101 (2012) 224102.
 [3] M. Panjan, et al., Plasma Sources Sci. Technol. 23 (2014) 025007.

4:00pm SE+PS+TF-MoA7 Observation of Multiple Charge States and High Ion Energies in High-Power Impulse Magnetron Sputtering (HiPIMS) and Burst HiPIMS using a LaB₆ Target, Robert Franz, Montanuniversität Leoben, Austria, C. Clavero, Lawrence Berkeley National Laboratory, R. Bolat, Nazarbayev University, Kazakhstan, R. Mendelsberg, A. Anders, Lawrence Berkeley National Laboratory

In high-power impulse magnetron sputtering (HiPIMS), a variation of pulsed magnetron sputtering, short high-voltage pulses are utilized to create discharges with high current densities and a high degree of ionization of the target atoms. In recent years, more complex pulse patterns than the single pulses used in the original or conventional HiPIMS have been developed, e.g. burst-HiPIMS where a series of very short (few μ s) pulses are bunched to form bursts.

In the present work, the charge-state-resolved ion energies of HiPIMS discharges were measured, using a LaB₆ target, as a function of charging voltage, pulse length, pulse frequency and on/off time ratio within applied HiPIMS bursts [1]. The highest charge states can reach +2 and +3 for boron and lanthanum ions, respectively. At high discharge powers, the B/La ion ratio can exceed the respective atom ratio in the target producing B-rich plasma with up to 98% boron ions. In the case of two-segmented bursts with high on/off time ratios, La³⁺ is the dominating lanthanum ion species and the ion energy distribution of B⁺ shows a pronounced high-energy tail extending up to 750 eV. The measured plasma compositions, ion charge states and ion energies are discussed within the established framework of HiPIMS discharges and the recent postulation that potential humps are associated with drifting ionization zones. The recorded high B/La ion ratios are a result of complex effects related to particle fluxes in the HiPIMS plasma of compound targets, as explained with the help of an expanded schematic representation of self-sputtering and gas atom recycling. The high energies of the B⁺ ions are based on a combination of the self-sputtering of boron, backscattering of incident boron ions on lanthanum atoms in the target and acceleration by localized potential humps [2]. Further evidence for potential humps is provided by the observed charge-state dependence of ion energies and features between the thermal peak and high-energy tail of the ion energy distribution functions.

- [1] R. Franz, C. Clavero, R. Bolat, R. Mendelsberg, A. Anders, Plasma Sources Sci. Technol. 23 (2014) 035001.
 [2] A. Anders, M. Panjan, R. Franz, J. Andersson, P. Ni, Appl. Phys. Lett. 103 (2013) 144103.

4:20pm SE+PS+TF-MoA8 Pulsed Magnetron Sputtering of Novel Multifunctional Films, Jaroslav Vlcek, J. Rezek, J. Kohout, University of West Bohemia, Czech Republic

High-power impulse magnetron sputtering with a pulsed reactive gas flow control was used for the reactive deposition of Ta-O-N films with tunable composition and properties [1]. The depositions were performed using a strongly unbalanced magnetron with a planar directly water-cooled Ta target in Ar-O₂-N₂ gas mixtures at an average target power density of up to 2.4 kWcm⁻² in a pulse. The repetition frequency of pulses was 500 Hz at a fixed 50 μ s voltage pulse length and the total pressure close to 2 Pa. An effective reactive gas flow control made it possible to adjust the film composition from Ta₂O₅ to a mixture of Ta₃N₅ and TaN. We prepared Ta-O-N films possessing appropriate band-edge levels for water splitting and a narrow optical band gap of 2.5 eV that permits a visible light absorption up to 500 nm.

Pulsed dc magnetron co-sputtering of a single target (B₄C-Si, B₄C-Zr or B₄C-Hf-Si) in Ar-N₂ gas mixtures was used for deposition of different

multifunctional films. The repetition frequency of pulses was 10 kHz at a fixed 85 μ s voltage pulse length and the total pressure of 0.5 Pa. We present the results obtained for amorphous Si-B-C-N films with an exceptionally high thermal stability (above 1500°C) and very high optical transparency [2], for nanostructured Zr-B-C-N films with a high hardness (37 GPa) and high electrical conductivity [3], and for nanostructured Hf-B-Si-C films with a high hardness (34-37 GPa), high electrical conductivity and significantly improved oxidation resistance in air up to 800°C [4].

- [1] J.Rezek, J.Vlcek, J.Houska, R.Cerstvy, Thin Solid Films (submitted).
 [2] J.Vlcek, P.Calta, P.Steidl, P.Zeman, R.Cerstvy, J.Houska, J.Kohout, Surf. Coat. Technol. 226 (2013) 34.
 [3] J.Vlcek, P.Steidl, J.Kohout, R.Cerstvy, P.Zeman, S.Proksova, V.Perina, Surf. Coat. Technol. 215 (2013) 186.
 [4] J.Kohout, J.Vlcek, J.Houska, P.Mares, R.Cerstvy, P.Zeman, M. Zhang, J.Jiang, E.I. Meletis, S. Zuzjakova, Surf. Coat. Technol. (submitted).

4:40pm SE+PS+TF-MoA9 Surface Engineering of Magnesium and Magnesium Alloys for Improved Corrosion Resistance, Michael Melia, J.R. Scully, J.M. Fitz-Gerald, University of Virginia

Due to the need for significant weight reduction of structural components, the development of Mg alloys has been ongoing over the last 100 years. One long-standing obstacle regarding the use of Mg alloys for widespread field application is their intrinsically poor corrosion resistance and lack of surface films or oxides that enable "self-healing" or active scratch protection. Micro-galvanic induced "self-corrosion" due to alloy heterogeneity is a key concern. The effects of Excimer laser surface modification and electric arc surface processing on the corrosion resistance of commercially pure Mg (99.8 wt% Mg) and Mg alloy (AZ31B) is investigated. Non-equilibrium processing is being investigated to control surface chemistry, microstructure, and phase formation in order to mitigate the micro-galvanic corrosion with the initial goal of microstructural and composition homogenization. In an attempt to achieve surface homogenization and control Mg evaporation, a range of operating parameters (energy density, dwell time, and processing atmosphere) were explored.

Surface morphology, composition, and local phase imaging were performed with scanning electron microscopy in secondary and backscattered electron imaging modes. X-ray diffraction was used to examine phase and surface regions in grazing incidence mode. Corrosion characterization was performed in a standard three electrode corrosion cell with an aerated 0.6 M NaCl solution. Electrochemical Impedance Spectroscopy (EIS) (10,000 to 0.001Hz) and potentiodynamic polarization scans (0.1 mV/s) were used to determine corrosion resistance, anodic/cathodic behavior, pitting potential and open circuit potential (OCP).

Preliminary results confirm that a measured level of surface homogenization was achieved irrespective of process gasses used (Ar, N₂, He). Moreover, in the case of N₂ processed 99.8% purity Mg samples, the formation of Mg₃N₂ was found to have a significant impact on the corrosion resistance. The AZ31B samples processed in Ar exhibited a similar corrosion response to the N₂ processed surfaces, suggesting homogenization was a larger factor than nitriding. The cathodic behavior consistently exhibited a significant reduction in the rate of the H₂ evolution reaction, more apparent in 99.8% purity Mg. Furthermore, the OCP was reduced by 100-350 mV. Impedance results support these findings with a significant improvement in polarization resistance after treatment. However, processed samples exhibited a minimal change in anodic behavior besides minor fluctuations in pitting potential. Possible mechanisms for the inhibition of the cathodic reaction rate will be presented and discussed.

5:00pm SE+PS+TF-MoA10 Designing a Precious Metal-Free Catalyst for Purification of Automotive Exhausts: NO Reduction and CO Oxidation on CuO(110) Surface, H. Kasai, J. Moreno, A.A. Padama, Osaka University, Japan, C. Matsuda, K. Naito, M. Uenishi, H. Tanaka, Daihatsu Motor Co., Ltd, Japan, Y. Nishihata, Japan Atomic Energy Agency, Japan, Mamoru Sakaue, Osaka University, Japan

Nitrogen oxide (NO_x) and carbon monoxide (CO) are known by-products of fossil fuel combustion, which greatly contribute to atmospheric pollution. Thus, understanding the conversion process of NO_x and CO into less hazardous gases is of utmost importance. It is well known that precious metals (such as Rh, Pd and Pt) work well to reduce these pollutant gases, but their high cost is a road block to a more prevalent use. Therefore, a more readily available and inexpensive material with comparable, if not better, catalytic performance is needed. Our group has investigated the role of surfaces as a foundation to realizing designer materials, in this case for exhaust purification [1]. In particular, we have previously studied the dissociation of nitric oxide (NO) on Cu₂O(111) surface [2-4]. In this work, we look at the possibility of using a CuO catalyst for NO reduction and CO

oxidation. Using density functional theory, we first investigated the dissociation process of NO on CuO(110) surface [5]. We found that NO is molecularly adsorbed perpendicular to the surface on the active hollow site between the surface Cu-atoms with an N-end configuration. An energy barrier of 1.1 eV was obtained for NO dissociation. The dissociated state was found to be most stable when the coadsorbed N and O atoms are on adjacent hollow sites. In comparison with the Rh(111) surface, the CuO(110) provides lower activation barrier for NO dissociation and lower adsorption energies for coadsorbed N and O atoms. To further investigate the oxidation of CO after the NO dissociation process, CO was adsorbed on the CuO(110) surface with coadsorbed N and O atoms. In this case, CO was molecularly adsorbed on top of a surface Cu atom while attracting the adsorbed O atom. An energy barrier of 0.9 eV was obtained for the CO oxidation process. This barrier was lower than the case of CO oxidation on Rh(111) surface with adsorbed oxygen atoms. The resulting CO₂ molecule was stably adsorbed with its center on top of a surface Cu atom. The results obtained in this study are in agreement with our experimental findings. In conclusion, we believe that CuO is a very promising catalyst for the purification of automotive exhausts.

Surface Science

Room: 309 - Session SS+EN-MoA

Metals, Alloys and Oxides: Structure, Reactivity & Catalysis

Moderator: Jason Weaver, University of Florida

2:00pm **SS+EN-MoA1 High Throughput Discovery and Optimisation of Metal Alloy Electrocatalysts**, *Brian Hayden*, University of Southampton **INVITED**

High-throughput synthesis and screening methodologies provide a powerful tool for the optimisation of alloy electrocatalysts. Libraries of thin film metal alloys have been synthesised using MBE sources to produce compositional gradient thin films in masked fields on micro-fabricated electrochemical screening chips. Examples will be given of ternary metal alloy catalysts designed as alternatives to platinum for the oxygen reduction reaction at the cathode in PEM Fuel Cells. The combination of ab-initio theory and high throughput synthesis and electrocatalyst screening is also shown to provide a powerful combination in the search for alternative catalysts to platinum for hydrogen oxidation at the anode. The approach has also been extended to the development of PdCu and PdSn alloys for the electro-reduction of nitrate, alloys which exhibit strong compositional dependencies which can be related to the redox behaviour of the surfaces. A full structural characterisation allows a direct comparison of catalytic activity to not only composition but also to the structure and phase of the alloy. In addition to measuring the total activity of the electrocatalysts, a secondary screen has been developed adapting the Differential Electrochemical Mass Spectroscopy (DEMS) method to assess the specificity of the reaction to produce the desired gas phase product.

2:40pm **SS+EN-MoA3 Methanol Oxidation on Pt-Re Surfaces: Ambient Pressure XPS and Reactor Studies**, *A.S. Duke, R.P. Galhenage, K. Xie*, University of South Carolina, *S.A. Tenney, P. Sutter*, Brookhaven National Laboratory, *Donna Chen*, University of South Carolina

Methanol oxidation has been investigated on Pt-Re bimetallic surfaces in order to understand how the addition of Re promotes activity on Pt in alcohol reforming and other oxidation reactions. Pt-Re alloy surfaces were prepared by depositing Re on Pt(111) or polycrystalline Pt foils and annealing to 1000 K. Scanning tunneling microscopy studies demonstrate that the deposited Re islands diffuse into the Pt(111) surface upon annealing, and low energy ion scattering studies indicate that the top monolayer consists mainly of Pt. XPS investigations were carried out at the X1A1 beamline at the National Synchrotron Light Source under methanol oxidation conditions of 200 mtorr O₂/100 mtorr methanol between 300 and 550 K, and gaseous products were monitored using a mass spectrometer. Methanol oxidation was studied on clean Pt(111), the Pt-Re alloy and Re films grown on Pt before and after surface oxidation at 450 K. The main products on all surfaces were CO₂ and H₂O with formaldehyde, CO and H₂ as minor products. On the unoxidized surfaces, the selectivity toward H₂ and CO production increased above 500 K. Deposition of atomic carbon during reaction was suppressed on the Pt-Re alloy surfaces as compared to pure Pt, and the oxidized Pt-Re alloy was found to reach maximum activity at the lowest temperatures. The Re films were unstable under methanol oxidation conditions at temperatures above 450 K due to the sublimation of Re oxides, but the Re in the Pt-Re alloy remained on the surface under the same conditions. Activity studies in a flow reactor coupled to the ultrahigh vacuum chamber showed that methanol oxidation activity increases with

surface oxidation; unoxidized Pt and Pt-Re surfaces initially exhibit minimal activity until the surface becomes oxidized under reaction conditions.

3:00pm **SS+EN-MoA4 Ångstrom-resolved Real-Time Dissection of Electrochemically Active Noble-Metal Interfaces during Oxidation and Reduction**, *B.R. Shrestha, T. Baimpos, S. Raman, Markus Valtiner*, Max Planck Institut für Eisenforschung GmbH, Germany

Electrochemical metal-oxide|liquid interfaces are critically important for a variety of technological applications and materials for energy storage, harvesting and conversion. Yet, a real-time Ångstrom-resolved visualization of dynamic processes at electrified metal-oxide|liquid interfaces has not been feasible. Here we present a unique direct and real-time atomistic experimental view into dynamic processes at electrochemically active metal interfaces using white light interferometry in an electrochemical surface forces apparatus. This method allows to simultaneously decipher both sides of an electrochemical interface - the solution side and the metal side - in real-time under dynamically evolving reactive conditions, which are typically found in technological systems *in operando*. Quantitative *in situ* analysis of the electrochemical oxidation and reduction of noble metal surfaces shows that the Å-thick oxide films formed on Au and Pt are reflecting high-*ik* materials, *i.e.* they are metallic or highly doped semiconductors, while Pd forms a transparent low-*ik* oxide during dynamic change of applied electrochemical potentials. In contrast, under potentiostatic growth conditions all electrochemically grown noble metal oxides are transparent, with thicknesses ranging from 2-10 Å. On the solution side the data simultaneously reveals hitherto unknown strong electrochemical depletion forces, which are due to a temporary charge imbalance in the electric double layer caused by the consumption or generation of charged species. The real time capability of our approach shows significant time lags between electron transfer, oxide reduction/oxidation and solution side equilibration during a progressing electrode process. Comparing the kinetics of solution side and metal side reactions provide detailed experimental evidence that noble metal oxide reduction initiates via hydrogen loading and subsequently proceeds via a dissolution/re-deposition mechanism. The presented approach may have important implications for designing emerging materials utilizing electrified interfaces such as fuel cells, batteries or super-capacitors.

3:40pm **SS+EN-MoA6 Catalytic Dehydration of 2-propanol on Size Selected (WO₃)_n and (MoO₃)_n Metal Oxide Clusters**, *Xin Tang*, Johns Hopkins University, *D. Bumüller, G. Gantefoer*, Universität Konstanz, Germany, *D.H. Fairbrother, K.H. Bowen*, Johns Hopkins University

Metal oxide nanoparticles and clusters are widely used as redox and acid/base catalysts in heterogeneous catalysis. The catalytic activity of the size selected metal oxide clusters (WO₃)_n and (MoO₃)_n (n = 1, 2, 3, 5, 30) were studied as a function of their size. The 2-propanol dehydration reaction was conducted on both two cluster catalysts. Temperature programmed reaction (TPR) was utilized to characterize the catalytic activity of the deposited cluster catalysts. The cluster size, supporting substrates, and the chemical compositions of the clusters were found to play an important role in determining the catalytic activity of the metal oxide clusters. For tungsten oxide clusters on the annealed oxide films, the catalytic activity of the clusters was found to be linear correlated to the size of the cluster. In addition, lower catalytic activity was observed for (WO₃)₁ monomer supported on the HOPG surface compared to the annealed oxide support. Meanwhile, molybdenum oxide clusters exhibited low catalytic activity toward 2-propanol dehydration reactions.

4:00pm **SS+EN-MoA7 Growth and Characterization of Ultrathin ZnO Layers on Au(111) – STM Study of Growth Mode and Adsorption of Water**, *Junseok Lee, X. Deng, D.C. Sorescu*, National Energy Technology Laboratory

Zinc oxide is an important material in the low-temperature synthesis of methanol. In this study, the growth mode of ZnO ultrathin films has been studied on the Au(111) surface using scanning tunneling microscopy (STM). The ultrathin ZnO layers have been found to grow by forming islands on Au(111). Different growth conditions during reactive deposition resulted in ZnO islands whose thickness ranging from one to four layers. The STM results and the density functional theory (DFT) calculation have been used to model the observed phenomena. STM results indicate that the brightness of the Moiré pattern of the ZnO layer on Au(111) surface is significantly modulated by the adsorption of water molecule at the positive tip bias. Various water adsorption sites have been identified in the STM results after annealing the sample to various temperatures that correspond to temperature programmed desorption (TPD) peaks. The DFT calculation results provide the most stable configurations of water molecules at each adsorption site.

4:20pm **SS+EN-MoA8 In Situ Imaging of the Dynamic Interaction of the Oxide with the Atomic Steps During the Oxide Growth on NiAl(100)**, *Hailiang Qin*, SUNY Binghamton, *X. Chen*, Biola University, *P. Sutter*, Brookhaven National Laboratory, *G.W. Zhou*, SUNY Binghamton

Ultrathin oxide films on metal supports represent a unique combination of materials systems with potential applications ranging from heterogeneous catalysis to electronic devices. In particular, the oxidation of NiAl alloys has received extensive interest for its ability to form a well-ordered Al_2O_3 film. Here we study the dynamic interaction of the atomic steps with the oxide stripes during their growth on single-crystal NiAl(100) at high temperature. With in-situ low-energy electron microscopy (LEEM) imaging and theoretical modeling, it is shown that the oxygen surface diffusion is the main mechanism controlling the oxide growth kinetics while the migration and shape evolution of the substrate steps follows the fluid-like Hele-Shaw flow governed by the attachment/detachment of Al atoms at step edges. When the oxide stripe encounters a series of step edges, the step edges are "pushed" along with the oxide stripe growth and bent towards the growth direction of the stripe. However, the growing oxide stripes do not cross over the substrate steps; instead, they stay on the same terrace even after encountering a number of step edges. Such a process is reversible during the oxide decomposition. The scanning tunneling microscopy (STM) images of the oxide stripes and the atomic steps after the interaction further confirm that the oxide stripes stay on the same terrace after encountering multiple substrate steps, instead of crossing the step edges.

4:40pm **SS+EN-MoA9 Subsurface Oxygen on Ni(111) and Ag(111)**, *Daniel Killelea*, *J. Derouin*, *R. Farber*, Loyola University Chicago

Subsurface oxygen atoms are enigmatic sources of energetic reagents in the heterogeneously catalyzed partial oxidation of small hydrocarbons on metal surfaces. Subsurface oxygen atoms are absorbed in the selvage of a metal, and may emerge to the surface at elevated temperatures to react with adsorbed molecules. Furthermore, when subsurface atoms emerge from beneath adsorbed molecules new reaction geometries are enabled that are otherwise inaccessible between reactants co-adsorbed to a surface. Although believed to be important reactive intermediaries, a systematic study of their fundamental chemistry has yet to be undertaken. To address this, we have selected two model systems for study; oxygen on Ni(111) and Ag(111). These are two systems that will provide basic details of subsurface absorption and reactivity, and further provide guidance for utilization of these species to selectively control chemistry. Subsurface atoms are key components of catalytic processes, but it remains unclear how they enhance reactions. The surface-subsurface dynamics will be elucidated using scanning tunneling microscopy (STM) to image the surfaces with and without subsurface O atoms. We will use the images to determine the presence of a bias for particular surfaces sites for the absorption / emergence processes and further study any structural or electronic effects of the subsurface O atoms on the host metal surface. To complement STM images, temperature programmed desorption and Auger electron spectroscopy will identify adsorbates and provide thermodynamic information. Our results will show mechanisms for subsurface migration and we will also probe the energetics of subsurface incorporation. Taken together, this new information seeks to narrow the gap our understanding between model and actual catalytic systems and enable chemists to accurately gauge the role of subsurface species in the transformation of plentiful feedstock into energy-rich chemicals over metal catalysts.

5:00pm **SS+EN-MoA10 Direct Imaging of the Amphoteric Nature of Rutile (110) Surfaces in Solution**, *Dapeng Jing*, *A. Song*, *M.A. Hines*, Cornell University

High-profile applications of nanocrystalline TiO_2 , such as next-generation solar cells and self-cleaning surfaces, have triggered extensive studies on the structure and chemical reactivity of rutile surfaces. But are UHV-prepared clean surfaces a good representation of technologically relevant surfaces? In this study, we show that a simple aqueous procedure produces near-ideal hydrocarbon-free rutile (110) surfaces characterized by well-defined terraces and nearly straight, single-layer-high steps without high-temperature annealing. The structure of rutile surfaces after water exposure is very different from that observed on UHV-prepared clean surfaces. In particular, the O vacancies that dominate the reactivity of surfaces in UHV are not present, as evidenced by both XPS spectra and STM images. This water-induced "healing" of O vacancies is consistent with chemical intuition. The step structures, too, are quite different. In addition, the amphoteric nature of the surface is directly observed in STM. Depending on the pH of the solution, a low density of protrusions decorate either the Ti rows or the bridging oxygen atoms, consistent with pH dependent protonation/deprotonation of the basic/acidic sites on the surface. No evidence of the corresponding counterions is observed.

5:20pm **SS+EN-MoA11 Water Splitting Kinetics at MgO(100) Terrace Sites**, *John Newberg*, University of Delaware

Understanding the surface chemistry of water with metal oxide interfaces has important implications in energy and environmental research. In order to understand surface kinetics and thermodynamics under environmental conditions, in situ molecular level studies are needed to assess adsorbate chemistry and coverage under conditions where adsorption and desorption occur concomitantly. In this talk we will outline a proposed precursor kinetic model to describe recently published ambient pressure XPS (APXPS) results for MgO(100) terrace hydroxylation observed under adsorption-desorption conditions. By combining APXPS with computational studies, mechanistic details for water dissociation on MgO(100) terrace sites are put forth.

Thin Film

Room: 307 - Session TF+PS-MoA

ALD Surface Reactions and Precursors

Moderator: Andrew Cavanagh, University of Colorado, Boulder

2:00pm **TF+PS-MoA1 Broadband Sum-frequency Generation: Studying the Initial Growth of ALD Al_2O_3 by Nonlinear Surface Vibrational Spectroscopy**, *Vincent Vandalon*, *R.H.E.C. Bosch*, *W.M.M. Kessels*, Eindhoven University of Technology, Netherlands

The understanding of the atomic layer deposition (ALD) processes has advanced significantly through the insight obtained with in situ linear vibrational surface spectroscopy, in particular by Fourier transform infrared (FTIR) spectroscopy. In this work we apply a nonlinear vibrational spectroscopy technique, the so-called broadband sum-frequency generation (BB-SFG) method, to study the ALD surface chemistry in situ. BB-SFG is a laser based technique, new to the field of ALD, in which a short visible spectrally-narrow laser pulse (~1 ps) is combined with an ultrashort broadband IR pulse (~90 fs) impinging simultaneously on the sample. The generated sum-frequency spectrum, detected in the visible, contains a part of the vibrational fingerprint of the IR region (bandwidth ~100 cm^{-1}) which can be detected "background-free" with a high sensitivity even at short integration times (1-100 s). Moreover, the surface selective nature of BB-SFG is uniquely suited for the study of the ALD surface chemistry in which the surface groups can be monitored accurately. In this presentation, first the BB-SFG method developed in our group in the last few years will be explained. Subsequently, the application of the method during ALD Al_2O_3 (from $\text{Al}(\text{CH}_3)_3$ and H_2O) will be addressed. In particular the initial film growth of Al_2O_3 on H-terminated Si(111) will be followed by probing the Si-H stretch mode (2084 cm^{-1}) with BB-SFG. The decrease in Si-H signal due to $\text{Al}(\text{CH}_3)_3$ and H_2O exposure will be correlated with the increase of the second-harmonic signal [1], revealing insight into the kinetics of initial film growth as well as the surface chemistry during steady-state growth. The results will be combined with observations by FTIR studies from our own work and from literature [2]. The surface reactions during the initial growth of Al_2O_3 by ALD will be addressed.

References:

[1] Höfler, APPL PHYS A-MATER 63, 533-547, 1996

[2] Frank, Chabal, Wilk, APL 82, 4758, 2003

2:20pm **TF+PS-MoA2 In Situ FTIR Analysis of Reaction Mechanisms between Trimethylaluminum and Carbonyl-Containing Polymers During ALD**, *Philip Williams*, *E.C. Dandley*, *A. Brozena*, *C. Needham*, *C.J. Oldham*, *G.N. Parsons*, North Carolina State University

New methods to modify polymers are of interest for numerous applications. The chemical mechanisms during trimethylaluminum (TMA) and water exposure during Al_2O_3 ALD onto polymers depends strongly on the polymer substrate and ALD conditions. Under some conditions, a solid oxide film can form with a relatively abrupt polymer/oxide interface. Typically however, TMA can diffuse sub-surface and react with the polymer in the substrate near-surface or bulk. Recently, we studied mechanisms during TMA vapor infiltration into various polymers using *in situ* infrared spectroscopy. In many polymers, the TMA coordinates with a polymer functional group, either on the backbone or on a side-chain, to form a Lewis acid/base adduct. For example, in poly(vinylpyrrolidone) (PVP), the carbonyl of the amide moiety (~1780 cm^{-1}) is observed to coordinate strongly with trimethylaluminum and shift to ~1725 cm^{-1} , and the adduct remains stable until water exposure. After water treatment, the adduct mode decreases and the original amide carbonyl signal appears to return. This could indicate release of TMA, but aluminum oxide formation in the polymer shows clearly that the TMA reacts within the polymer. Ab

initio calculations (B3LYP) were performed to support mechanistic analyses of TMA within the polymer. A similar TMA/carbonyl adduct formation/release mechanism is observed during TMA/water exposure to poly(methyl methacrylate). On the other hand, when poly(acrylic acid) is exposed to TMA, the carbonyl mode disappears then does not reappear after water exposure. This suggests that in PAA, the TMA reacts with the carbonyl to form a stronger covalent bond that does not change upon water exposure. This difference in reactivity for TMA in the polyacid is likely associated with the presence of acidic hydrogens aiding in the formation of the methane byproduct and more stable covalent aluminum-oxygen bonds. These results help expand understanding of ALD onto polymers and can enable better control of coating and infiltration processes.

2:40pm TF+PS-MoA3 Time-resolved FT-IR Spectroscopy during ALD using La(PrCp)₃ and H₂O, Brent Sperling, J.E. Maslar, W.A. Kimes, NIST

In situ Fourier transform infrared (FT-IR) spectroscopy has provided many valuable insights into various chemistries used for atomic layer deposition (ALD). Frequently, it is used to observe the molecular fragments remaining on a surface after exposure to each precursor or the phonon modes of films as they are deposited layer-by-layer. The limitations of FT-IR spectroscopy, however, have restricted it to quasi-static conditions that differ dramatically from most growth studies. Spectra cannot easily be obtained with the temporal resolution needed to keep pace with typical ALD cycle times. We have developed a method that signal averages time-resolved spectra over multiple ALD cycles to improve the rate of data acquisition to around 150 ms. Additionally, by using external reflection from a metal surface, absorption by surface species is enhanced; alternating polarization states allows the surface to be differentiated from gas-phase species and deposition on the windows. We apply this method to La(PrCp)₃/H₂O chemistry (PrCp = isopropyl-cyclopentadienyl), which has proved to be difficult to understand from growth studies. We present our attempts to recreate literature conditions in our laminar flow reactor with *in situ* FT-IR spectroscopy to observe surface and gas-phase species.

3:00pm TF+PS-MoA4 Surface Reactions and Interface Evolution during the ALD of HfO₂ on GaAs Surfaces Studied by *In Situ* ATR-FTIR, Liwang Ye, T. Gougousi, University of Maryland, Baltimore County

In situ attenuated total reflectance Fourier transform infrared (ATR-FTIR) spectroscopy was utilized to study the surface reactions and interface evolution during the Atomic Layer Deposition (ALD) of HfO₂ on GaAs(100) surfaces. The chemistry studied involves the use of tetrakis(dimethylamino) hafnium (TDMAH) and H₂O. The experiments were performed on chemical oxide and HF etched GaAs(100) starting surfaces. For the deposition of HfO₂ on chemical oxide GaAs surface at 275°C, which corresponds to the optimal ALD process temperature, considerable arsenic oxide consumption was observed at the 1st TDMAH exposure. The arsenic oxide removal continued during subsequent ALD cycles albeit at a reduced rate. For similar experiments performed at 200°C, the arsenic oxide consumption was significantly lower than that at 275°C in agreement with the observations of Suri et al.¹ A clear ligand exchange process is identified through the alternate appearance of the CH and OH terminated surfaces. However, additional byproducts that contain -C=N- bonds are produced during the water pulse and accumulate in the film. Isotope exchange experiments indicate that these species are compatible with the formation of methylmethyleimine (MMI) that may be produced through a beta hydride elimination pathway.^{2,3}

[1] R. Suri, D. J. Lichtenwalner, and V. Misra, *Appl. Phys. Lett.* **96**, 112905 (2010).

[2] C. M. Truong, P. J. Chen, J. S. Corneille, W. S. Oh, and D. W. Goodman, *J. Phys. Chem.* **99**, 8831 (1995).

[3] M. Bouman and F. Zaera, *J. Electrochem. Soc.* **158**, D524 (2011).

3:40pm TF+PS-MoA6 Precursor Design: Controlling Melting Point, Volatility, Reactivity and Other Important Characteristics of CVD and ALD Precursors, Seán Barry, Carleton University, Canada INVITED

Chemical vapour deposition methods (CVD) including atomic layer deposition (ALD) are relatively forgiving processes in many respects: the pressure does not have to be very low or strictly controlled, and to some extent the temperature of deposition likewise can have a certain amount of error. These forgiving conditions are largely due to the fact that growth of a film by CVD and ALD is controlled by the surface chemistry of the precursor used, as well as the behaviour of the precursor under thermal stress and in the gas phase. It is often said that precursor "design" is important in these fields: this refers to the control over several key characteristics of the precursor with respect to thermal and chemical behaviour.

My research hinges on the design of precursors with respect to four key characteristics, and each will be discussed using examples. Control of melting point is important to allow better kinetics of evaporation, and this can be tuned by ligand design and asymmetry in the precursor compound. Volatility is a key factor for a precursor, and this can be controlled many ways, including the coordinative saturation of the central (typically metal) atom of the precursor. Thermal stability and chemical reactivity are intimately related, and here choice of ligand, and knowledge of gas phase and surface chemistry is critical for fine control over the difference between a CVD precursor (which undergoes continual deposition) and an ALD precursor (which requires at least a measure of surface stability to allow for self-limiting behaviour).

4:20pm TF+PS-MoA8 Characterizing Vapor Delivery of $\mu^2-\eta^2$ -(Bu-Acetylene)Dicobalthexacarbonyl (CCTBA) for Deposition Processes, James Maslar, W.A. Kimes, B.A. Sperling, National Institute of Standards and Technology (NIST), R. Kanjolia, SAFC Hitech

Cobalt metal is a promising material for the formation of enhanced copper barrier and/or seed layers for copper interconnects in integrated circuits. For these applications, atomic layer deposition of cobalt using a gas-phase precursor can provide advantages in the device fabrication process. $\mu^2-\eta^2$ -(Bu-acetylene)dicobalthexacarbonyl (CCTBA) is a cobalt precursor that can be delivered as a vapor in a carrier gas. However, CCTBA exhibits a relatively low vapor pressure at ambient conditions and typically must be delivered at elevated temperatures to increase the amount of material delivered to the growth surface. As is typically the case for deposition precursors, prolonged heating can lead to decomposition of CCTBA. Therefore, this work was undertaken to help identify optical delivery conditions for CCTBA by investigating 1) the decomposition of CCTBA in an ampoule at various ampoule temperatures and 2) the delivery of CCTBA from an ampoule as a function of carrier gas flow rate, system pressure, and ampoule temperature. CCTBA decomposition in an ampoule was investigated by using Fourier transform infrared (FT-IR) spectroscopy to identify the species present in the headspace of a CCTBA-containing ampoule as a function of time and ampoule temperature. CCTBA delivery was investigated using two optical techniques installed onto a delivery line from the ampoule. Optical access to the delivery line was achieved using two custom-built in-line optical flow cells that were designed to minimize perturbations to the gas flow. One flow cell was utilized for time-resolved FT-IR spectroscopy. This technique was used to identify the species entrained in the carrier gas. However, time response was limited to ~150 ms which is insufficient to resolve many thermal processes impacting CCTBA entrainment. In order to improve time resolution, a CCTBA-specific region of the mid-IR spectrum was identified and a direct optical absorption technique designed for CCTBA. This technique employed a broadband infrared source with a mid-IR bandpass filter for isolating CCTBA-specific absorption features. This technique was installed on the second optical flow cell and used to measure the time-dependent CCTBA partial pressure as a function of gas flow rate, system pressure, and ampoule temperature for each CCTBA pulse with a time resolution of ~5 ms. In this manner, the dependence of CCTBA partial pressure on delivery conditions was identified. From these data and the time-dependent partial pressure data obtained with this optical measurement, the dependence of the actual amount of CCTBA delivered on delivery conditions was calculated.

4:40pm TF+PS-MoA9 Effect of Precursor on Coating Uniformity in Mesoporous Metal Oxide Films during Steady and Hold-Step ALD Processes, Berç Kalanyan, M.D. Losego, G.N. Parsons, North Carolina State University

Mesoporous film substrates with surface areas greater than 100 m²/g see use in a variety of applications, most notably in photovoltaic and photoelectrochemical energy conversion. Pastes composed of 10-20 nm diameter metal oxide particles (ITO, FTO, ATO, TiO₂) are cast as a thick film and sintered to form conductive substrates. Atomic layer deposition (ALD) is uniquely suited to apply conformal coatings into these types of mesostructured films. To date, ALD coatings have been used in this fashion for dye sensitized solar cells, photoelectrochemical cells, and thermal photovoltaic devices. Beyond common "steady" or "continuous-flow" ALD processes, several research groups have explored the use of "gas hold steps", where the reactor is isolated from the pump for some period of time during the precursor exposure, for example, to enhance precursor infusion into high surface area or porous substrates.

In this study we examine ALD processing under steady and hold-step sequences for applying TiO₂ coatings into mesoporous Sn-doped indium oxide (ITO). Typical mesoporous films are up to 10 μ m thick, which represents the minimum distance (without tortuosity) that precursor vapors need to travel in order to reach the bottom of the mesostructure. We choose two Ti-containing precursors, titanium tetrachloride (TiCl₄) and titanium tetrakisopropoxide (TTIP), to understand the influence of bulky functional groups on precursor diffusion. The TTIP diffusivity will be smaller than

TiCl₄, but it is also sterically hindered by its larger molecular size. We characterize film uniformity in mesoporous substrates by dynamic time-of-flight secondary ion mass spectrometry (TOF-SIMS), in-situ quartz crystal microbalance (QCM), and Krypton gas adsorption experiments.

We show that the TiCl₄/H₂O process can readily infiltrate into nanoporous ITO films as thick as 15 μm using a typical ALD process sequence, without gas “hold” steps. On the other hand, SIMS analysis shows that TiO₂ films deposited using TTIP and H₂O under the same exposure condition reach a depth of only 6 μm before exhibiting a large decay in TiO₂ secondary ion intensity. While the TiCl₄ shows much better coverage, the process suffers from potential contamination, for example, from Cl which is observed in SIMS analysis. Therefore the use of bulky precursors such as TTIP is critical for ALD infiltration into mesoporous substrates, especially under conditions where coating impurity content is an important concern.

5:00pm TF+PS-MoA10 Study of the Growth of Zinc Tin Oxide As Model System for Ternary Metal Oxide Atomic Layer Deposition, Adriaan Mackus, R.W. Johnson, W.-H. Kim, S.F. Bent, Stanford University
In recent years there is increasing interest in atomic layer deposition (ALD) processes that go beyond traditional AB cycles to enable the deposition of alloyed, doped, or ternary materials. The composition of a ternary material can be tuned by mixing the cycles of two different AB processes in a certain ratio ((AB)_n(CD)_m). However, in practice, the composition and the growth rate tend to deviate from what is expected based on the cycle ratio n/m, whereas the formation of a certain crystallographic phase strongly depends on the mixing of ALD cycles and post-deposition anneal conditions. A detailed understanding of how to deposit ternary metal oxides with control of composition and crystallographic phase is currently lacking.

In this work, the material zinc tin oxide (ZTO) has been selected as a model system for studying ternary metal oxide ALD, motivated by its applications as transparent conducting oxide (TCO)¹ or buffer layer² in solar cells. For these applications it is important that ZTO consists of earth-abundant non-toxic elements, and therefore has the potential to replace indium-based TCOs or Cd-based buffer layers. ZTO films were deposited by combining the ALD processes of ZnO from diethylzinc (DEZn) and water, and SnO₂ from tetrakis(dimethylamido)titanium (TDMASn) and water.^{1,3} Synchrotron-radiation X-ray diffraction (SR-XRD) has been performed at the Stanford Synchrotron Radiation Lightsource (SSRL) to investigate the crystallographic phase of the films as a function of composition, cycle ratio, and anneal conditions. It was found that the zinc orthostannate (Zn₂SnO₄) phase forms upon high-temperature annealing, thereby confirming the deposition of ZTO. In addition, Fourier transform infrared spectroscopy (FTIR) was employed to elucidate the surface chemistry of the ZTO ALD process.

1. Mullings *et al.*, *Thin Solid Films* **556**, 186 (2014)
2. Lindahl *et al.*, *Prog. Photovolt: Res. Appl.* **21**, 1588 (2013)
3. Mullings *et al.*, *J. Vac. Sci. Technol. A* **31**, 061503 (2013)

Thin Film

Room: 305 - Session TF-MoA

Self-Assembled Monolayers, Layer-by-Layer Assemblies, and Hydrophobic/Amphiphobic Thin Films

Moderator: Subhadra Gupta, University of Alabama

2:40pm TF-MoA3 Embedded Dipole in Alkanethiolate Self-Assembled Monolayers: Electronic Structure and Work Function Effects, Swen Schuster, Heidelberg University, Germany, N. Sullivan, O. Cabarcos, Pennsylvania State University, I. Hehn, Graz University of Technology, Austria, J.-F. Morin, Université Laval, Canada, E. Zojer, Graz University of Technology, Austria, M. Zharnikov, Heidelberg University, Germany, D.L. Allara, Pennsylvania State University

Self-assembled monolayers (SAMs) bonded to metal-electrodes are frequently used to modify charge-carrier injection and also serve as prototypical systems for studying charge transport processes through molecular assemblies. Usually, control over charge-carrier injection is achieved by use of the terminal dipolar groups (terminal dipole) comprising the SAM-ambient interface. But this architecture affects the growth mode of an organic semiconductor (in the standard device configuration) entangling it with the dipole control. In contrast, for the molecules with an embedded dipolar element, the dipole control and the chemistry at the SAM-ambient interface are decoupled. In this context, we studied a series of SAMs on Au{111} prepared from the mid-chain ester functionalized thiols, HS(CH₂)_mCO₂(CH₂)_n-CH₃ (C_mEC_n) with different combinations of *m* and *n*, different dipolar group orientations, and partial deuteration for

some of these films. Electronic properties were analyzed by high resolution x-ray photoelectron spectroscopy (HRXPS), near edge x-ray absorption fine structure spectroscopy, work function measurements, and theoretical simulations with supporting characterization by infrared spectroscopy and AFM. The presence of the ester moiety leads to the formation of a strong electric dipole layer with a component of ~1.05 Debye normal to the surface for most of the C_mEC_n SAMs and results in a strong electrostatic effect on the HRXPS spectra in which the C 1s photoelectron kinetic energies are consistently shifted by 0.7-1.0 eV between the alkyl segments below and above the embedded ester group. In addition, this group affects the work function of the entire assembly, with the direction of the change following the direction of the embedded dipole. There is however no perfect correlation between the behavior of the HRXPS spectra and the work function, which has to be understood with the help of theoretical simulations.

3:00pm TF-MoA4 Formation of Highly Ordered Self-Assembled Monolayers of Alkynes on Au (111) Substrates, T. Zaba, A. Noworolska, Jagiellonian University, Poland, C.M. Bowers, B. Breiten, G.M. Whitesides, Harvard University, Piotr Cyganik, Jagiellonian University, Poland

Self-assembled monolayers (SAMs) based on C-Au bonding and prepared by reaction of terminal *n*-alkynes (HC≡C(CH₂)_nCH₃, *n* = 5, 7, 9, and 11) with Au(111) at elevated temperatures (60 °C), were characterized using scanning tunneling microscopy (STM), infra-red reflection absorption spectroscopy (IRRAS), X-ray photoelectron spectroscopy (XPS) and contact angle of water.¹ In contrast to previous spectroscopic studies²⁻⁴ of this type of SAM, these combined microscopic and spectroscopic experiments confirm the formation of highly-ordered SAMs having packing densities and molecular chain orientations very similar to those of alkanethiols on Au(111). Physical properties—hydrophobicity, high surface order, and packing density—also suggest that SAMs of alkynes are similar to SAMs of alkanethiols. The preparation of high-quality SAMs from alkynes requires careful preparation and manipulation of the reactants in a rigorously oxygen-free environment: trace quantities of oxygen lead to oxidized contaminants and disordered surface films. The influence of oxygen on the quality of the SAM is apparently not related to reaction of the Au–C bonds in a SAM with oxygen as suggested earlier,³ but instead, suggests gold-catalyzed oxidation of the terminal acetylene in solution before incorporation into the SAM. Importantly, once clean alkyne based SAM is formed it becomes resistant to further oxidation in ambient conditions. This stability, together with high structural order, provides the basis for potential applications of this new type of SAM.

References

- (1) Zaba, T.; Noworolska, A.; Bowers, C. M.; Breiten, B.; Whitesides, G. M.; Cyganik, P. *submitted*, **2014**
- (2) Zhang, S.; Chandra, K. L.; Gorman, C. B. *J. Am. Chem. Soc.* **2007**, *129*, 4876.
- (3) McDonagh, A. M.; Zareie, H. M.; Ford, M. J.; Barton, C. S.; Ginic-Markovic, M.; Matisons, J. G. *J. Am. Chem. Soc.* **2007**, *129*, 3533.
- (4) Scholz, F.; Kaletova, E.; Stensrud, E. S.; Ford, W. E.; Kohutova, A.; Mucha, M.; Stibor, I.; Michl, J.; Wrochem, F., *J. Phys. Chem. Lett.* **2013**, *4*, 2624.

3:40pm TF-MoA6 Dynamic and Angle-Resolved XPS Analysis of Ultra Thin Polyelectrolyte Films Containing Metal Nanoparticles, Merve Taner-Camci*, S. Suzer, Bilkent University, Turkey

Ultra thin polyelectrolyte layers have been constructed by sequential adsorption of PAH (polyallylamine hydrochloride) as cationic polyelectrolyte and PSS (polystyrene sulfonate) as anionic polyelectrolyte on silicon substrates using layer-by-layer assembly. Negatively capped AgCu nano-sized particles are incorporated as the outermost layer on the ultra thin film. The sequential order of adsorbed layers and nanoparticles are monitored by relative depth profile of the sample with respect to the intensity changes of corresponding photoelectron peaks, via Angle Resolved XPS analysis at different take off angles. Dynamic XPS analysis is performed under the application of external voltage bias with a known amplitude and frequency to control and probe the charging shifts, as well as polarity dependent intensity changes. The shifts in the binding energy position and the intensity fluctuations of photoelectron peaks reveal information about the relative position of the adsorbed polyelectrolyte layers, as well as proximity of atomic constituents of the nanoparticles.

* TFD James Harper Award Finalist

4:00pm **TF-MoA7 Growth Ambient Dependent and Photoinduced Reversible Wetting Property of Indium Oxide Nanowires**, *Kavita Yadav, B.R. Mehta, J.P. Singh*, Indian Institute of Technology Delhi, India

In recent years, production of materials with tunable wetting properties is of immense interest. The extreme water repellent property of superhydrophobic surfaces and complete water spreading on superhydrophilic surface allow them to have considerable technical potential for various applications. The wetting properties of the materials can be explained by their surface chemistry and topographical structures.

In this report, we demonstrate that the growth ambient induced drastic change in wetting properties of indium oxide (IO) nanowires. The IO nanowires were synthesized by using chemical vapor deposition method where Ar gas (200 sccm) was used as carrier gas. The deposition parameters were calibrated in such a way to obtain nanowire morphology. Three different ambient conditions were used for growth of IO nanowires; (a) Ar gas mixed with water vapors, (b) only Ar gas and (c) Ar gas mixed with hydrogen gas (50 sccm) and keeping other deposition parameters constant. The Scanning electron microscope (SEM) images confirm that all the three samples have nanowires like morphology. The diameter and length of nanowires ranges from 50 - 120 nm and 6 - 15 μm . The contact angle measurements were done on all the three samples. It is found that the nanowires prepared in presence of Ar gas mixed with water vapors (oxidising ambient) are superhydrophilic in nature with contact angle of $8^\circ \pm 5^\circ$. The IO nanowires synthesized in presence of only Ar gas are hydrophobic in nature with contact angle of $144^\circ \pm 4^\circ$ whereas the IO nanowires synthesized in presence of Ar gas mixed with H_2 gas (reducing ambient) are superhydrophobic in nature with contact angle of $168^\circ \pm 2^\circ$ and water droplet rolling downward with a roll-off angle of 3° over the superhydrophobic surface. The mechanism behind the drastic change in contact angle on IO nanowires prepared in different growth ambient is examined by using photoluminescence (PL) and electron paramagnetic resonance (EPR) measurements. The mechanism of change in wetting properties of IO nanowires has been proposed and can be attributed as on the reduced surface where oxygen vacancy are more, only molecular water is stable and absorb weakly. This is most likely because of the lack of surface oxygen that could accept hydrogen from dissociated water or decrease water dissociation probability and hence the surface is superhydrophobic. Whereas the sample prepared in oxidizing ambient have more surface oxygen and hence both molecular and dissociative adsorption of water is possible results in superhydrophilic surface. The photoinduced reversible wetting properties of IO nanowires (sample b) are also studied.

4:20pm **TF-MoA8 Ultralow Friction and Adhesion on Fluorinated Covalently Surface-Bound Polymer Brushes**, *S. Pujari, N. Bhairamadgi, Han Zuilhof*, Wageningen University, Netherlands

For an ever increasing range of applications, such as in MEMS and NEMS, highly stable surfaces with minimal adhesion and friction are desired. In the current paper we present a method to achieve such polymer surfaces via a combination of high-density attachment of surface-bound initiators on the Si(111) surface followed by a surface-initiated ATRP reaction with a series of fluorine-rich methacrylate monomer. Subsequently, the adhesion and friction forces were determined using colloidal probe scanning force microscopy. The resulting surfaces display the lowest adhesion force and friction coefficient in air currently reported for any flat surface, which is for example about 1 order of magnitude less than teflon, yet with an appreciably higher chemical and mechanical stability. The presentation will focus on preparation and characterization (both structural and tribological) of these surface-bound polymer brushes, and outline the potential of such minimally interacting surfaces.

4:40pm **TF-MoA9 Proton Conductive Crystalline Coatings by Initiated Chemical Vapor Deposition**, *Anna Maria Coclite, C. Ranacher*, Graz University of Technology, Austria

Proton conductive copolymers of perfluorodecylacrylate (PFDA) and methacrylic acid (MAA) are synthesized by initiated Chemical Vapor Deposition (iCVD). The MAA provides the $-\text{COOH}$ groups useful to conduct protons, while the PFDA is responsible for creating the hydrophobic backbone to stabilize the structure during tests in water. The ultimate goal is to use these copolymers as proton exchange membranes in fuel cells. Preliminary experiments have shown that proton conductivities in the range of 70 mS/cm can be reached with these copolymers.¹ The aim of the new research is to study the effect of preferred crystallographic orientation on the proton conductivity and water / temperature stability of the copolymers. Preferred crystallographic orientation (texture) in thin films frequently has a strong effect on the properties of the materials and it is important for stable surface properties. Poly-PFDA has a high tendency to give organized molecular films. Crystalline poly-PFDA have been fully obtained also by iCVD.² The degree of crystallinity and the preferred orientation of the perfluoro side chains, either parallel or perpendicular to the surface, can be controlled by tuning the CVD process parameters (i.e.

initiator to monomer flow rate ratio, filament temperature, and substrate temperature). Super-hydrophobicity (advancing water contact angle, WCA, of 160° , low hysteresis of 5°), and oleophobicity (advancing CA with mineral oil of 120°) were achieved.³ Low water contact angle hysteresis was obtained with high crystallinity, particularly when the orientation of the crystallites resulted in the perfluoro side groups being oriented parallel to the surface. The latter texture resulted in smoother film (RMS roughness < 30 nm) than the texture with the chains oriented perpendicularly to the surface. This can be very advantageous for our application that require smooth but still crystalline films. When the PFDA is copolymerized with MAA, the degree of crystallinity decreases and therefore also the stability in water, but the proton conductivity increases due to the higher number of acid groups embedded in the structure. A good trade-off has been obtained when using 20% of MAA in the gas feed.

¹ A.M. Coclite et al., *Polymer*, 2013, 54, 24-30

² A. M. Coclite et al., *Adv. Funct. Mater.* 2012, 22, 2167–2176

³ A. M. Coclite et al., *Adv. Mater.* 2012, 24, 4534–4539

5:00pm **TF-MoA10 Tailoring Polymeric Structures on Surfaces for Lubrication**, *Nicholas Spencer*, ETH Zürich, Switzerland **INVITED**

Nature generally lubricates its tribosystems in water, using sugar chains for lubricity, immobilized on a protein backbone that links them to the surface. These glycoproteins function by being able to immobilize water near the sliding surfaces. Man's attempts to mimic this behavior have involved end-grafted, hydrophilic polymers, and much has been published on the use of poly(ethylene glycol) (PEG) to this end. Man-made machines are more challenging to lubricate than those in nature, since they generally involve hard-hard contact, which nature usually avoids. PEG has been useful as a model system for aqueous lubrication, but has certain inherent problems, including a lack of stability. This presentation will therefore focus on "life after PEG", covering alternative water-compatible, polymer-brush systems, those created by grafting-from methods, and finally the extension of these approaches into a non-aqueous environment: oil.

Vacuum Technology

Room: 303 - Session VT-MoA

Vacuum Measurement, Applications of UHV and Ultraclean Processes

Moderator: Joe Becker, Kurt J. Lesker Company, Bob Garcia, SAES Getters

2:00pm **VT-MoA1 A Capacitance Diaphragm Gauge with 10 mTorr Full Scale**, *Martin Wüest*, INFICON Ltd., Liechtenstein, *P. Björkman, J. Bäckman*, INFICON Ab, Finland

Etching of semiconductor chips is a complex process and there are critical process steps that tend to go to lower pressures. At lower pressures scattering at the residual gas is reduced which allows obtaining narrower and deeper vias, important for three-dimensional chip structures. Many etch process pressures today are around 1 Pa and use a 13.3 Pa full scale CDG in the second measurement decade where accuracy is already lower. We use ceramic technology to build pressure sensors that measure an elastic deformation of a diaphragm under the feeble pressure forces while being highly resistant to etch chemistries. Improvements to the manufacturing process now allow us to manufacture thinner, highly elastic, leak tight membranes. We now have developed a heated capacitance diaphragm gauge with 1.33 Pa (10 mTorr) full scale. The low full scale is achieved by the deflection of a thinner membrane and focus on noise reduction and not by electronic amplification. We will present pertinent performance parameters.

2:20pm **VT-MoA2 What if Saving Energy become Important on Bayard Alpert Hot Ionization Gauges?**, *Simon Naef*, INFICON Ltd., Liechtenstein

Hot ionization gauge have been on the market for decades and many refinements have been made over the time. A lot of common knowledge how to build a stable, sensitive, and accurate BA-gauge is recorded. How about overall power consumption and the energy efficiency of hot ion gauges? The topic of energy conservation has been neglected so far.

The saved energy per gauge is not essential, but on the global view the power consumption can be reduced significantly. Even the high energy consuming semiconductor industry tries to reduce their footprint, since 80% of energy used in this industry is manufacturing and transportation.

How can that are achieved? Integration and miniaturization is way used in the past. So there are many compact hot ion gauge designs available on the market today, which use obviously less energy than larger full-size hot

ionization systems. But what is drawback of going small and is worth going small?

On one hand the heated cathode defines mainly the power consumption, which is based on the electron emissivity of the surface material used and the resistance of the used wire material. On the other hand the sensitivity of BA-gauge is based on the geometry of the electrodes, which can be correlated to the efficiency of the gauge. Is there any option with any optimal compromise size?

3:40pm VT-MoA6 How to Create as Less as Possible to Make the Best as Possible, Norbert Koster, TNO Technical Sciences, Netherlands INVITED

The field of vacuum technology is rapidly becoming a full blown industry, with parts and component suppliers, OEM manufacturers and end users (IDM). The generation of vacuum is not the goal, but the means to realize products and devices. Especially the semiconductor industry is one of the driving forces in this development, but also large scientific projects like ITER, Cern and others require a supply chain that can deliver parts that meet the requirements and certification. The upcoming introduction of EUV lithography required a change in the supply chain for manufacturers like ASML with suppliers that had to deliver vacuum qualified assemblies without any knowledge of vacuum technology.

The introduction of EUV also meant very complex vacuum systems that could not be baked anymore but with cleanliness demands that superseded the cleanliness that can be achieved with baked UHV systems. This was achieved by a rigorous cleaning and qualification process, standardized outgassing measurements and budgeting of all the parts and assemblies. To make a distinction between ordinary type of vacuum system building and this new way of making vacuum systems the phrase Ultra Clean Vacuum (UCV) was introduced. This presentation will describe how we solved a number of problems that occurred during this type of manufacturing, this includes supply chain engineering, cleaning procedures and solutions in the tool itself. This way of creating vacuum systems is now also being used by other OEM's like AMAT, KLA-Tencor who are building highly complicated metrology tools and processing equipment, while vacuum generation is not their core business.

4:20pm VT-MoA8 Study of Potential Particle Generation by Ion Sources During EUV Mask Blank Deposition, Ivan Shchelkanov, A.M. Lietz, J. Pachicano, University of Illinois at Urbana-Champaign, A. Antohe, P. Kearney, SEMATECH, D.N. Ruzic, University of Illinois at Urbana-Champaign

We summarise the research accomplishments of the CPMI-SEMATECH research project "Identification of possible defect sources and particle characterisation from sources used in EUVL chambers for mask blank manufacturing". The main goal of the project is the determination of nanoparticle production (100-350 nm in size) from the ion source currently used for mask blank manufacturing in EUV lithography chambers at SEMATECH. Combination of Volumetric Laser Scattering and Surface Laser Scattering system, and Scanning Electron Microscopy (SEM) was used to develop time resolved phenomenological model of nano-particle generation inside vacuum chamber during ion beam source operation. In this project a Veeco 3cm RF ion beam source with two molybdenum grids and RF neutralizer was investigated. Stiletto Volumetric Laser Scattering system developed by INFICON together with Surface Laser Scattering system, developed at CPMI were used to detect nano-particles. This combination of laser systems was able to detect particles with the size of 100 nm and bigger. Scanning Electron Microscopy was used to track evolution of the ion source grids surface. SEM photos of the grids and polished silicon wafers on the ion beam path were used to identify and characterize nano-particles via size, shape and material. Nano-particle generation rate by the ion beam source was measured and recommendations for the source operation are made.

4:40pm VT-MoA9 Particle Defect Reduction in EUV Mask Blank Production Devices, Amanda Lietz, I.A. Shchelkanov, University of Illinois at Urbana-Champaign, A. Hayes, Veeco Instruments, Inc., J. Pachicano, S. Keniley, D.N. Ruzic, University of Illinois at Urbana-Champaign

Extreme UltraViolet Lithography (EUVL) requires reflective mask blanks, manufactured by ion beam sputtering a multilayer stack of thin films, primarily Mo and Si, onto a mask substrate. At least 40 bilayers of Mo and Si are necessary to produce a surface which has sufficient EUV light reflectivity for use in high volume manufacturing exposure tools. When contaminant particles deposit between these layers, the EUV light is absorbed or scatters irregularly, rendering the mask blank unusable. One possible source of such particles is bombardment of shields in the deposition chamber by energetic particles scattered from the ion beam and target and "overspill" of the tails of the ion beam off the edge of the target.

Stainless steel shields are used to cover targets that are not in use and prevent deposition or sputtering nearby surfaces and equipment. These shields must be able to accept many successive layers of deposition without flaking and forming particles of deposited material. They also must be able to withstand ion beam overspill bombardment, while forming a minimal amount of particles.

In order to evaluate improved shield materials and surface finishes, shield samples of various treatments were placed under a broad angle ion beam and particles were collected on a witness plate. The total number of particles on the witness plates was quantified using laser scattering particle detection which was capable of detecting particles greater than 125nm in size. Etching treatments of the shields show an improvement from 13.0 ± 7 particles/mm² (for untreated steel) to $.022 \pm .016$ particles/mm² (for etched steel). Shields of various materials and surface finishes were compared to determine the lowest level of particle formation

5:00pm VT-MoA10 VTD Early Career Award: Novel Vacuum Processing of Thin-Film Photovoltaic Materials, Jason D. Myers*, J.A. Frantz, R.Y. Bekele, V.Q. Nguyen, C.C. Baker, S.C. Erwin, N.D. Bassim, U.S. Naval Research Laboratory, A. Bruce, S.V. Frolov, Sunlight Photonics, J.S. Sanghera, U.S. Naval Research Laboratory INVITED

In this presentation, two different avenues of research into thin film photovoltaics will be discussed. The first part of the talk will be focused on quaternary-sputtered Cu(In,Ga)Se₂ (CIGS) thin film photovoltaic devices. Current state-of-the-art CIGS devices are produced using a multistage thermal coevaporation process that has resulted in laboratory efficiencies in excess of 20%, but this process is difficult to implement at a commercial scale. Our work has instead focused on developing a scalable deposition technique using RF magnetron sputtering of quaternary CIGS. The resulting films do not require post-selenization, reducing processing time and cost. We have fabricated devices above 10% efficiency using this approach, showing its promise as a production method for high-performance CIGS.

The second part of the talk will be focused on an emerging thin film photovoltaic system, FeS₂. Based on its favorable bandgap, high absorption coefficient, and immense earth abundance, FeS₂ is a highly promising material for grid-scale energy production. However, no successful thin-film photovoltaic devices have been realized due to surface defect states that arise due to the cubic pyrite structure, where sulfur atoms are differentially bonded at the surface compared to the bulk; this leads to extremely low open circuit voltages and poor diode characteristics. To solve this issue, we are developing vacuum-deposited inorganic capping films to heal these defects by providing bulk-like coordination at the FeS₂ surface. FeS₂ films with ZnS capping layers show a significant decrease in surface state character, an important step towards efficient FeS₂ photovoltaics.

*** VTD Early Career Award**

2D Materials Focus Topic

Room: 310 - Session 2D+AS+BI+PS+SS-TuM

2D Materials: Surface Chemistry, Functionalization, Bio and Sensor Applications

Moderator: Richard Osgood, Columbia University

8:00am 2D+AS+BI+PS+SS-TuM1 Phase Engineering in 2D Transition Metal Dichalcogenides, *Manish Chhowalla*, Rutgers University INVITED

Two-dimensional transition metal dichalcogenides (2D TMDs) — whose generalized formula is MX_2 , where M is a transition metal of groups 4–7 and X is a chalcogen — exhibit versatile chemistry and consist of a family of over 40 compounds that range from complex metals to semiconductors to insulator. Complex metal TMDs assume the 1T phase where the transition metal atom coordination is octahedral. The 2H phase is stable in semiconducting TMDs where the coordination of metal atoms is trigonal prismatic. Unlike mechanical exfoliation and chemical vapor deposition, chemical exfoliation of semiconducting layered TMDs yields monolayered nanosheets with heterogeneous atomic structure consisting of metallic (1T) and semiconducting (2H) phases. Metal (1T phase) to semiconductor (2H phase) transition can be achieved via mild annealing of exfoliated materials. Semiconductor to metal transitions can be achieved via chemistry. The 1T phase in semiconducting TMDs has scarcely been studied but it deserves urgent attention as it exhibits promise as a hydrogen evolution catalyst and as contact electrode in electronic devices. We will describe these phase transitions in semiconducting TMDs and provide examples of how we have learned to exploit them for covalent functionalization, enhanced catalytic and electronic performance.

8:40am 2D+AS+BI+PS+SS-TuM3 Transition Metal Nanoparticles on Single-Layer MoS_2 : Structural, Electronic and Catalytic Properties, *Takat B. Rawal, D.T. Le, T.S. Rahman*, University of Central Florida

We will present results of density functional theory based calculations of the geometric and electronic structure of several types of sub-nanometer sized transition metal nanoparticles (TMNPs) on pristine and defect-laden single-layer MoS_2 . We will show that among the investigated TMNPs (Cu, Ag, Au), Cu nanoparticles bind strongest to pristine MoS_2 while Au and Ag nanoparticles bind with similar, weaker strengths. The presence of the vacancy defect on MoS_2 enhances significantly the binding strength of Cu nanoparticles, while it has very little effect on the binding strength of Au NPs. More interestingly, the amounts of charge transfer from TMNPs to MoS_2 vary following the order of the binding energies of TMNPs on MoS_2 . Additionally, the shape of the nanoparticles also has an impact on the binding characteristics. Of particular interest is the role of the substrate on the catalytic properties of the TMNP and conversely that of the TMNP on the defect-laden MoS_2 single layer. In this regard we will examine in detail the reactivity of the atoms at the TMNP/ MoS_2 interface in reactions such as CO oxidation and methanol decomposition and compare them to that of similar nanoparticles when supported on titania.

Work supported in part by DOE Grant No. DE-FG02-07ER15842

9:00am 2D+AS+BI+PS+SS-TuM4 How Fluorination Enhances Friction Forces for Graphene, *Xin Liu, Q. Li*, University of Pennsylvania, *S.P. Kim*, Brown University, *V.B. Shenoy*, University of Pennsylvania, *P.E. Sheehan, J. Robinson*, Naval Research Laboratory, *R.W. Carpick*, University of Pennsylvania

The chemical functionalization of graphene can alter its electronic, chemical, mechanical, and tribological properties. Here we employ atomic force microscopy (AFM), Raman microscopy, and molecular dynamics (MD) simulations to show that friction can be fine-tuned by chemically modifying graphene. Although bulk fluorinated graphite has a very low surface energy, our experiments and simulations both show that friction between nanoscale tips and FG is up to 9 times higher than that for pristine graphene. The ability to resolve an ordered lattice in atomic stick-slip friction measurements also diminishes with greater fluorination, indicating that the fluorinated graphene is disordered. Our observation suggests that AFM friction measurements provide a sensitive local probe of the degree of fluorination of graphene. Motivated by MD simulations, we propose that the dramatic enhancement of friction results from increased corrugation of the interfacial potential due to the strong local charge concentrated at fluorine sites, consistent with the Prandtl-Tomlinson model.

9:20am 2D+AS+BI+PS+SS-TuM5 Chemical, Structural and Electrical Modification of Graphene, *Sandra Hernández, E.H. Lock, M. osofsky, S. Tsoi*, Naval Research Laboratory, *C. Junkermeier*, Penn State University, *R. Stine*, Nova Research, *J. Robinson*, Naval Research Laboratory, *A. Nath*, George Mason University, *V.D. Wheeler, R.L. Myers-Ward, J. Caldwell, C.R. Tamana, T. Reinecke, P.E. Sheehan, D.K. Gaskill, S.G. Walton*, Naval Research Laboratory

2D nanomaterials have been vigorously investigated due to their superlative mechanical, thermal, and electronic properties. Being composed entirely of surface atoms, they are incredibly amenable to surface modification thus providing the opportunity towards excellent control over their properties. Surface engineering of 2D materials composed of carbon materials, such as graphene, can be achieved by plasma modification. We will discuss our efforts in understanding the chemical, structural, and electrical properties of plasma functionalized graphene by introducing -oxygen, -fluorine, and -nitrogen chemical moieties, and discuss their impact on chemical reactivity, electrical transport, and enhanced sensing behavior. Demonstrating how precise nano-engineering of surface chemistry impacts contact engineering, biosensing and device based applications.

This work is supported by the Naval Research Laboratory Base Program.

9:40am 2D+AS+BI+PS+SS-TuM6 The Mechanochemistry of Chemically Modified Graphene, *Jonathan Felts, S.C. Hernandez, A.J. Oyer, J. Robinson, S.G. Walton, P.E. Sheehan*, Naval Research Laboratory

Defining the optoelectronic properties of graphene through controlled chemical functionalization provides a route to fabricating a wide range of graphene based devices. In prior work, we showed that heat supplied by a scanning probe removed functional groups from chemically modified graphene (CMG) thereby restoring it to graphene [1]. Here we show that mechanical stress alone effectively removes functional groups. We measured the degree of surface functionalization by monitoring both normal load and friction between the sliding tip and a plasma processed CMG sheet. For oxygenated graphene, friction decayed exponentially with sliding distance, dropping to ~15% of the starting value. These measurements revealed an initial drop in friction that was independent of applied stress, suggesting the presence of an adsorbed water layer on the surface. More importantly, they reveal an Arrhenius-like relationship between contact stress and degree of surface reduction. The reduction in friction persisted, precluding the presence of the adsorbed contaminants as the source of the friction change. Conductive AFM and Raman measurements provide further evidence for chemical reduction. Conductive diamond AFM tips measure the current through the surface during the reduction process, revealing a 5x increase in conductivity corresponding to the friction force reduction. Additionally, Raman measurements on a 5 mm² reduced area showed a relative increase in both the G and 2D peaks, consistent with a reduction in functionalization. These experiments enabled detailed comparison of tribochemical reactions without the complications of transfer films or the initial run-in of the film. They also enable experiments difficult by other means. For instance we could directly compare the mechanical barrier to functional group removal by monitoring friction while slowly ramping the applied stress between the tip and a graphene surface functionalized with either oxygen or fluorine groups. For oxygenated graphene, the contact stress at the maximum reduction rate was $\sim 0.47 \pm 0.14$ GPa; for fluorinated graphene it was $\sim 0.85 \pm 0.27$ GPa. Thus, by using the same tip and same supporting substrate we could directly compare the bond strengths between different functional groups and the graphene lattice. This work demonstrates the ability to measure and control the chemistry of single-layer functionalized surfaces at the nanometer scale, and has wide application in tribochemical wear, mechanochemistry, and nanoelectronic device fabrication with chemically tuned optoelectronic properties.

[1] Z. Wei, et al, *Science* **328**, 1373-1376 (2010)

11:00am 2D+AS+BI+PS+SS-TuM10 Fe-catalyzed Etching of Graphene, Few-Layer Graphene, and Graphite, *Guangjun Cheng, A.R. Hight Walker*, National Institute of Standards and Technology

Mechanically exfoliating graphite onto a substrate provides a family of layered materials with adjustable thickness, including monolayer graphene, few-layer graphene (FLG), and graphite. In this work, we investigated the Fe-catalyzed etching of graphene, FLG, and graphite in forming gas (10% H_2 /90% N_2) or N_2 using low-voltage scanning electron microscopy and Raman spectroscopy. Fe thin films were deposited by sputtering onto mechanically exfoliated graphene, FLG, and graphite flakes on a Si/SiO₂ substrate. When the sample is rapidly annealed in either gas environment, particles are produced due to the dewetting of the Fe thin film and expected to catalyze the etching of graphene, FLG, and graphite. The combined microscopic and spectroscopic evidence reveals a thickness-dependent,

catalytic etching behavior in these two gas environments and provides insights into the catalytic mechanisms involving carbon hydrogenation and carbon dissolution.

11:20am **2D+AS+BI+PS+SS-TuM11 Tunable Graphene/Si Schottky Diode Sensor: Before and After Functionalization for Wide Range of Molecular Sensing.** *MdAhsan Uddin, A. Singh, T. Sudarshan, M.V.S. Chandrashekar, G. Koley*, University of South Carolina

Graphene/Semiconductor Schottky devices attracted significant research attention due to wide range of applications from transistor to IR detector [1-2]. Such heterojunctions are also promising for sensing applications due to the molecular adsorption induced Schottky barrier height (SBH) change at the interface, affecting the junction current exponentially in reverse bias, which leads to ultrahigh sensitivity. Graphene/p-Si diode sensor [Device image, Raman spectra and I-V characteristics shown in fig. 1(a), (b) and (c)] has been developed with high bias-dependent sensitivity and low operating power.

Performance enhancement has been demonstrated by fabricating graphene chemiresistor and diode sensor on the same chip. The diode sensor exhibited 13 times higher sensitivity for NO₂ [Fig. 2(a)] and 3 times higher for NH₃ [Fig. 2(b)] in ambient condition, while consuming ~500 times less power for same applied voltage. Sensing tunability is achieved by operating the device in reverse bias, tuning the graphene work function and hence the SBH by the applied bias. The sensitivity varied from 268 to 574% for NO₂ as the bias magnitude varied from -1 to -8V [Fig. 3(a)]. Optimized sensor design to detect particular analyte is also possible by careful selection of graphene/Si heterojunction SBH. For example, graphene/p-Si with larger SBH is better NO₂ sensor while smaller SBH device has better NH₃ sensitivity. The sensing mechanism based on SBH change has been confirmed by capacitance-voltage measurements [Fig. 3(b)]. The SBH decreased by 0.23eV for NO₂ exposure while increased by 0.16eV for NH₃. Variation in sensitivity with NO₂ and NH₃ concentration has also been demonstrated (Fig. 4).

Pd and Pt functionalization has been carried out to make the graphene/Si diode [Fig 5] sensitive to H₂. Extrapolated SBH from the I-V characteristics, before and after few nm metal decoration, and H₂ exposure showed initial SBH decrease after functionalization and subsequent increase in presence of H₂, respectively [Fig. 6(a) and (b)]. Compared to graphene chemiresistor, the chemi-diode sensor offers more than one order of magnitude higher H₂ sensitivity for both types of functionalization. Similarly, the reverse bias operation also enables low power consumption, tunable sensitivity and detection of H₂ down to 1 ppm [Fig. 7(a)] in air which is close to the atmospheric background of 0.6 ppm [3]. Among the two metals, Pd-functionalization always exhibited better sensing response irrespective of the bias voltage [Fig. 7(b)]. Remarkably, for Pd-functionalization, the sensor response showed absolute exponential change with varying H₂ concentration ranging from 2 to 1000 ppm [Fig. 7(c)].

12:00pm **2D+AS+BI+PS+SS-TuM13 Dielectrics Layer Deposition on Graphene Surface by Functionalization with Polar Titanyl Phthalocyanine.** *Jun Hong Park, I.J. Kwak, K. Sardashti, A.C. Kummel*, University of California at San Diego

Several novel designs for beyond CMOS devices have emerged using two-dimensional semiconductors. These devices require deposition of thin insulators on 2D semiconductors or between two sheets of 2D semiconductors. However, 2D semiconductors are nearly inert surfaces thereby making uniform nucleation of oxide growth challenging preventing scaling of the insulator thickness. A new technique has been developed to employ a monolayer of ordered metal phthalocyanines (MPc) on 2D semiconductors directly as a monolayer low-k dielectric or as a nucleation layer for growth of high-k insulators. This study demonstrates the molecular scale observation of formation of O-TiPc mono and bilayers on graphene with UHV scanning tunneling microscopy (STM). O-TiPc monolayers were deposited on HOPG surfaces by organic molecular beam epitaxy. After deposition, O-TiPc forms a monolayer with only few defects, and the crystal structure of monolayer has four-fold symmetry in a 1.4 x 1.4 nm grid. Observation of bright protrusions on each O-TiPc indicates that each O-TiPc in the monolayer is directed outward to vacuum. STS shows the band gap of the monolayer is 1.7 eV and the band gap of the bilayer is 2.3 eV. The monolayer or bilayer can directly be employed for sub-nanometer insulators on 2D semiconductors at low bias. Multiple cycles of TMA and water were dosed onto O-TiPc/HOPG to investigate nucleation of Al₂O₃ on the O-TiPc layers. The first cycle of TMA was observed to chemisorb on a 1.4 x 1.4 nm grid on the TiOPc monolayer. After exposure O-TiPc monolayer to 5 cycles ALD pulse (tri-methyl-aluminum (TMA)+H₂O), insulating aluminum oxide was deposited uniformly on O-TiPc/HOPG. After formation of Al₂O₃ on O-TiPc/HOPG, the band gap of surface increases from 1.7 eV to 2.7 eV, while the conductance decreased. As shown in XPS spectra, the quality of Al₂O₃ can be improved by post annealing, consisting with transition of chemical states in O 1s peak and Al

2p. The chemical shifts of O and Al indicate that post annealing converts remained the Al-OH to Al₂O₃. Consequently, O-TiPc can not only act as a low-K dielectric but also induce high density ordered nucleation of ALD on central ion of O-TiPc for high-k dielectric growth.

Actinides and Rare Earths Focus Topic
Room: 301 - Session AC+AS+MI+SA+SS-TuM

Synchrotron Radiation and Laboratory Based Investigations of Actinides and Rare Earths

Moderator: David Geeson, AWE

8:00am **AC+AS+MI+SA+SS-TuM1 The Role of the 5f Band and Partial Occupancy in Actinide L3-edge XANES and RXES Measurements.** *Corwin Booth, S.A. Medling, Y. Jiang*, Lawrence Berkeley National Laboratory, *J.G. Tobin*, Lawrence Livermore National Laboratory, *P.H. Tobash, J.N. Mitchell, D.K. Veirs*, Los Alamos National Laboratory, *M.A. Wall, P.G. Allen*, Lawrence Livermore National Laboratory, *J.J. Kas*, University of Washington, *D. Sokaras, D. Nordlund, T.-C. Weng*, SLAC National Accelerator Laboratory, *E.D. Bauer*, Los Alamos National Laboratory

INVITED

Although actinide (An) L3-edge x-ray absorption near-edge structure (XANES) spectroscopy has been very effective in determining An oxidation states in insulating, ionically-bonded materials, such as in certain coordination compounds and mineral systems, the technique fails in systems featuring more delocalized 5f orbitals, especially in metals. Recently, actinide L3-edge resonant x-ray emission spectroscopy (RXES) has been shown to be an effective alternative. This technique is further demonstrated here using a parametrized partial unoccupied density of states method to quantify both occupancy and delocalization of the 5f orbital in alpha-Pu, delta-Pu, PuCoGa5, PuCoIn5, and PuSb2. These new results, supported by FEF calculations, highlight the effects of strong correlations on RXES spectra and the technique's ability to differentiate between f-orbital occupation and delocalization. Potential temperature-dependent spectral changes in the hidden order compound URu2Si2 and the superconductor PuCoGa5 will be discussed.

8:40am **AC+AS+MI+SA+SS-TuM3 Actinide Research with Hard Synchrotron Radiation.** *Roberto Caciuffo*, European Commission, JRC-ITU, Germany

INVITED

Advanced x-ray synchrotron radiation techniques, addressing spatial and temporal fluctuations of structural and electronic degrees of freedom, hold outstanding scientific promises for the future of actinide research [1]. Indeed, by probing hidden order parameters and elementary electronic excitations with high sensitivity and resolution, element- and edge-specific (resonant and non-resonant) x-ray scattering experiments provide the bricks for building the novel conceptual frameworks necessary to unravel the complexity of actinides. Here, I will present selected results from these experiments and discuss what they tell us.

Whereas resonant x-ray diffraction (RXD) with photon energies tuned to the M_{4,5} absorption edges of actinide ions are used to study the order of electric quadrupole moments in oxides and intermetallics [2-4], resonant x-ray emission spectroscopy (RXES) and non-resonant inelastic X-ray scattering (NIXS) are applied to study the bulk electronic configuration in solids, liquids and gases [5,6]. In particular, the high penetration depth of hard X-rays employed in NIXS enables flexible containment concepts, facilitating investigations of radioactive materials in the liquid phase or under extreme conditions. Finally, inelastic x-ray scattering (IXS) can be used to map phonon dispersion branches with an energy resolution comparable to the one afforded by inelastic neutron scattering, but using crystal samples with sizes orders of magnitude smaller than those required by neutrons.

In the first example, I will show how a combination of diffraction, RXES, and absorption near-edge spectroscopy experiments at high-pressure can be used to study the correlation between polymorphism, mixing of different electronic configurations, and hybridization effects in elemental americium [7]. The potential of RXD in elucidating the nature of "hidden order" will be illustrated by the examples of the low-temperature phases in NpO₂ [8] and URu₂Si₂ [9]. Then, I will present NIXS results interrogating the O_{4,5} absorption edges of uranium and plutonium materials, and results of IXS studies of the vibrational dynamics in PuCoGa₅ and NpO₂.

[1] R. Caciuffo, E. C. Buck, D. L. Clark, G. van der Laan, MRS Bulletin **35**, 889 (2010)

[2] P. Santini et al., Rev. Mod. Phys. **81**, 807 (2009)

[3] H. C. Walker et al., Phys. Rev. Lett. **97**, 137203 (2011)

- [4] Z. Bao et al., Phys. Rev. B **88**, 134426 (2013)
 [5] T. Vitova et al., Phys. Rev. B **82**, 235118 (2010)
 [6] R. Caciuffo et al., Phys. Rev. B **81**, 195104 (2010)
 [7] S. Heathman et al., Phys. Rev. B **82**, 201103(R) (2010)
 [8] N. Magnani et al., Phys. Rev. B **78**, 104425 (2008)
 [9] H. C. Walker et al., Phys. Rev. B **83**, 193102 (2011)

9:20am **AC+AS+MI+SA+SS-TuM5 Lumps, Bumps and Pyrophoric Powders - Nuclear Waste Viewed in a New Light**, *Tom Scott*, University of Bristol, UK, *C.A. Stitt, M. Hart*, Diamond Light Source Ltd., UK, *J. MacFarlane, A. Banos, H. Paraskevoulakos, K. Hallam*, University of Bristol, UK

INVITED

How do you look inside a nuclear waste package without breaking it open? This question is important when the contained corrosion products are potentially flammable and radioactive. Synchrotron x-rays have been used to perform micro-scale in situ observation and characterisation of uranium entrapped in grout; a simulation for some intermediate level waste. Using specially designed analysis cells X-ray tomography and x-ray diffraction have been used to generate both qualitative and quantitative data from a grout encapsulated uranium sample before, and after, deliberately constrained H₂ corrosion. Tomographic reconstructions determined the extent, rates and mechanisms of the oxidation reaction by assessing the relative densities between the materials and the volume of corrosion products. The oxidation of uranium in grout was shown to follow the anoxic U + H₂O oxidation regime, and the pore network within the grout was observed to influence the induction period for the initiation of uranium hydride formation across the surface of the metal. Powder diffraction analysis identified the corrosion products UO₂ and UH₃, and permitted measurement of corrosion induced stress. Together, x-ray tomography and diffraction provide a means of accurately determining the types and degree of uranium corrosion occurring, thereby offering a future means for studying the reactions occurring in real full-scale waste package systems.

11:00am **AC+AS+MI+SA+SS-TuM10 Isotopic Measurements of Uranium in Particles by SIMS**, *David Simons*, National Institute of Standards and Technology (NIST)

INVITED

Secondary ion mass spectrometry (SIMS) has become a primary tool for the International Atomic Energy Agency (IAEA) and its Network of Analytical Laboratories (NWAL) to monitor activities at uranium enrichment sites. IAEA inspectors collect samples by wiping surfaces within facilities with cloth wipes that are later distributed to the NWAL for analysis. At the laboratories particles are extracted from the wipes and searched by various means to find those that contain uranium. The uranium-bearing particles are analyzed by mass spectrometry for their isotopic composition that is the key signature to be compared with the declared use of the facility. Large-geometry (LG) SIMS instruments based on magnetic sector mass spectrometers with multicollector array detectors are used by five members of the NWAL to both search for the uranium particles and analyze those that are found. We have characterized the performance of this type of instrument and found that it can be set up with a mass resolving power that excludes nearly all mass spectral interferences from uranium isotopes while maintaining high instrument transmission and high abundance sensitivity. The total efficiency for uranium detection has been measured with monodisperse microspheres and found to exceed 1 %. Detection of U236 presents a special case because of interference from the U235 hydride ion that is removed by peak-stripping. The effect of the hydride on the uncertainty in the U236 abundance determination has been modeled for different uranium enrichments and hydride-to-parent ratios, and the effect of the particle substrate on hydride production has been investigated. The performance of LG-SIMS instruments for isotopic measurements of uranium in particles was recently demonstrated in the NUSIMEP-7 study organized by the Institute of Reference Materials and Measurements in which these instruments were able to detect and measure all uranium isotopes in particles smaller than 400 nm, including U236 at an isotopic abundance of 8x10⁻⁶.

11:40am **AC+AS+MI+SA+SS-TuM12 X-ray Excited Auger Transitions of Pu Compounds**, *Art Nelson, W.K. Grant, J.A. Stanford, W.J. Siekhaus, W. McLean*, Lawrence Livermore National Laboratory

X-ray excited Pu NOO Auger line-shapes were used to characterize differences in the oxidation state of Pu compounds. The Auger line-shapes were combined with the associated chemical shift of the Pu 4f_{7/2} photoelectron line, which defines the Auger parameter and results in a reliable method for definitively determining oxidation states independent of binding energy calibration. Results show that PuO₂, Pu₂O₃, PuH_{2.7} and Pu have definitive Auger line-shapes. These data were used to produce a chemical state (Wagner) plot for select plutonium oxides. This Wagner plot

allowed us to distinguish between the trivalent hydride and the trivalent oxide, which cannot be differentiated by the Pu 4f_{7/2} binding energy alone.

Applied Surface Science

Room: 316 - Session AS+BI+VT-TuM

Ambient Ionization Mass Spectrometry

Moderator: Gerardo Brucker, Granville-Phillips Vacuum Products, Steven Pachuta, 3M Company

8:00am **AS+BI+VT-TuM1 Laser Ablation Electrospray Ionization Mass Spectrometry with Ion Mobility Separation for Cell and Tissue Analysis**, *Akos Vertes, B. Shrestha, H. Li, S.A. Stopka, L. Zhang*, George Washington University

INVITED

Laser ablation electrospray ionization (LAESI) is a novel ion source that enables the direct analysis of biological samples, including tissues and individual cells. In this ionization method, mid-IR laser ablation is followed by electrospray ionization of the ablated material in the expanding plume. Molecular coverage in complex biological samples is limited, in part, by the large number of components and the absence of a separation step prior to ionization. In addition, isobars, such as structural isomers and conformers, are not distinguished by mass analysis alone. To overcome these limitations, LAESI is combined with ion mobility separation (IMS) before mass spectrometry (MS). In this contribution, we describe the first results with such a LAESI-IMS-MS system for metabolite, lipid and protein analysis, including its application to plant and animal tissues, MS imaging and single cell analysis. The studied systems, among others, comprise mouse brain sections, *Arabidopsis thaliana* leaves and green algae (*Chlamydomonas reinhardtii*) cell pellets. The introduction of IMS resulted in enhanced molecular coverage, reduced interferences, distinction of structural isomers, observation of larger multiply charged ions typically suppressed by singly charged abundant metabolites and phospholipids, and in extended dynamic range.

8:40am **AS+BI+VT-TuM3 Miniature Mass Spectrometry Systems with Ambient Ionization and MS/MS Capabilities**, *Zheng Ouyang, L. Li, Y. Ren, X. Wang, X. Ma, R. Zou, R.G. Cooks, Y. Xia*, Purdue University

INVITED

As a technique for chemical analysis, mass spectrometry is versatile and provides very specific information. High sensitivity can be achieved when sample matrix effect is properly suppressed. Miniaturization of the mass spectrometry instrument system and simplification of the operation procedure enable the chemical analysis outside the analytical laboratories and/or by personnel without special trainings. The development of these systems goes beyond the miniaturization of the mass analyzers and mass spectrometers. At Purdue, we have taken an approach of combining the ambient ionization for direct sampling and the miniature ion trap mass spectrometer with MS/MS capability. The miniature systems use linear ion traps (LIT) for mass analysis and can perform multi-stage MS/MS, which help to improve the specificity of the analysis using the fragmentation pattern of the target analyte and to eliminate the chemical noise from the complex mixtures. A discontinuous atmospheric pressure interface (DAPI) has been developed to allow coupling of ionization sources at atmospheric pressure with the instruments using miniature pumping systems to support the vacuum. The DAPI opens for about 20 ms for ion introduction and requires a 200 ms delay for pressure drop prior to mass analysis. The complex gas dynamics has been characterized using direct simulation Monte Carlo method and an electro-hydrodynamic simulation method has been developed for predicting the ion trajectory for DAPI instrument design. While mass spectrometers as light as 4 kg have been previously developed with capability of analyzing non-volatile compounds, two complete MS analytical systems have recently developed as the backpack MS for in-field analysis and the Mini 12 desktop system for point-of-care analysis by nurses and physicians. These two systems use ambient ionization for direct sampling analysis. The low temperature plasma (LTP) probe was modified with an in-line configuration for point-and-shoot operation with the backpack MS. New ambient ionization methods have been explored for development consumable sample cartridges for the Mini 12 system, which include the paper spray, extraction spray and the most recent slug flow microextraction nanoESI. IS-coated capillary samplers have been developed for highly quantitative analysis using several microliters of biofluid samples and extremely operation procedures. On-cartridge chemical derivatization has been developed to significantly improve the sensitivity of the target analytes in complex biological samples and on-cartridge assays have also been studied for direct monitoring the enzymatic functions. Direct analysis of the biological tissues have also been explored using Mini 12 and on-line Patenò-Büchi (P-B) reactions facilitated

by UV irradiation has also been implemented to identify the locations of C=C bonds in the lipids, which is highly relevant to the biosynthetic pathways and the function of the lipids. The relative ratios of the unsaturated isomers can now be quantified, as the potential biomarkers for diagnosis of diseased tissues.

9:20am **AS+BI+VT-TuM5 The Importance of Sample Form and Surface Temperature for Analysis by Ambient Plasma Mass Spectrometry (PADI)**, *Ian Gilmore, T.L. Salter, J. Bunch*, National Physical Laboratory, UK

Plasma sources for ambient mass spectrometry are of increasing importance owing to their ability to analyse a wide range of organics including polymers. Some industrially important molecules are not successfully analysed by electrospray based methods and here plasma methods are making an important contribution. For analysis in industry, it is essential to understand the fundamental mechanisms so that predictions can be made of which types of materials can and cannot be detected. In this study, we develop a metrology framework to understand the sensitivity of PADI to different substances and material form. We study in detail, the effect of sample temperature on the signal intensity and show that the intensity is proportional to the vapour pressure. Importantly, we also show the sample form, as a film or powder, has a strong effect of sensitivity. For the analysis of thin films at room temperature and using a low plasma power, a vapour pressure of greater than 10^{-4} Pa is required to achieve a sufficiently good quality spectrum. Using thermal desorption we are able to increase the signal intensity of materials with vapour pressures less than 10^{-4} Pa, in thin film form, by between 4 and 7 orders of magnitude. This is achieved by increasing the temperature of the sample up to a maximum of 200 °C. Thermal desorption can also increase the signal intensity for the analysis of powders. Prospects for imaging PADI and sub-micron imaging ambient mass spectrometry imaging will also be discussed.

9:40am **AS+BI+VT-TuM6 A VAMAS Interlaboratory Study for Desorption Electrospray Ionisation Mass Spectrometry (DESI MS) - Survey of the Measurement Issues**, *Paulina Rakowska, E. Gurdak, F.M. Green, M.P. Seah, T.L. Salter, I.S. Gilmore*, National Physical Laboratory, UK

The DESI technique is celebrating a decade of application since its innovation in 2004. There has been significant progress in understanding its fundamentals and a rapid expansion in the applications, covering a diverse range of science and technologies. For wider uptake in industry, measurements need to be repeatable and constant. It is especially important to test that methods are transferable between different instrument designs and that analytical procedures are clear. This requires the development of a metrological infrastructure. Interlaboratory studies are an effective route to do this. VAMAS provides an excellent mechanism for such evaluation. Under this framework, the National Physical Laboratory (UK) has conducted a DESI interlaboratory comparison. The objectives of this study were to determine the current achievable repeatability and constancy of instruments. The comparison was conducted with the involvement of 20 laboratories from 10 different countries. The instruments used included 7 commercially made DESI sources with the remainder home-built. A variety of mass spectrometers were used including 13 Ion Traps, 4 Orbitraps and 4 Time-of-Flight. Participants were provided with an analytical protocol and two reference samples: a thin layer of Rhodamine B and a double-sided adhesive tape. The studies comprised acquisition of positive ion mass spectra in pre-determined m/z ranges. No sample preparation was required. Results for Rhodamine B show that intensity repeatabilities below 20 % may be achieved. However, inadequacies of the spray and sample stage designs lead to repeatabilities that average 50 % with some worse than 80 %. Rhodamine B is an excellent reference sample to check the sample erosion, the sample stage movement and memory effects. The adhesive tape samples show that the absolute intensity repeatability is 31 % with several achieving below 20%. Importantly, the spectral response, given by the relative repeatability, not measurable with Rhodamine B, was reduced to 9 % with a significant number achieving the 5 % expected of more mature analytical methods. The constancy of these spectra from relative intensities gives day-to-day averages of 31 %, over three times worse than the short term repeatability. Significant differences in the spectra from different laboratories arise from different factors. This first interlaboratory study has provided an effective survey of the measurement issues and some important conclusions can be drawn about the possibilities for DESI MS concerning overall practice, reference samples and recommendations for the future. These will be discussed.

11:00am **AS+BI+VT-TuM10 Mass spectrometry surface analysis outside the vacuum**, *Justin Wiseman, M.E. ElNaggar, J.K. Kennedy, B.L. Laughlin*, Prosolia Inc. **INVITED**

Advances in mass spectrometry in the last 20 years has produced instruments with higher resolving power, smaller footprints, even portable,

and the capability of measuring surfaces for molecules in the ambient air; the former truly enabling the latter. Ambient mass spectrometry involves the characterization of samples in their native state in the open air and is exemplified by the development of Desorption Electrospray Ionization (DESI) and Direct Analysis in Real Time (DART). DESI uses high velocity charged droplets produced by a pneumatically-assisted electrospray to effect desorption and ionization of surface-bearing analytes. The applications of the technique are broad and span from the detection of leachables to thin-layer chromatography to imaging of drugs, metabolites and lipids in histological tissue sections, where the lateral spatial resolution has been reported to be as high as 50µm. The flowprobe, also an ambient technique, uses a liquid-microjunction formed at the surface to extract and deliver analytes to the mass spectrometer via an electrospray source. The applications of the flowprobe are also broad and have included microarray sampling, thin-layer chromatography plate analysis, and biological tissue analysis. This presentation will discuss the merits and applications of each of the DESI and flowprobe devices, with emphasis on their application to imaging biological tissue.

11:40am **AS+BI+VT-TuM12 Transporting Ions from Ambient Pressure into Vacuum for Lab-based and Mobile Mass Spectrometers**, *Mitch Wells*, FLIR Mass Spectrometry **INVITED**

The proliferation of Atmospheric Pressure Ionization (API) sources for mass spectrometry (MS) has expanded the applicability of the MS analysis technique to a wide range of chemical and biological challenges, to the extent that the 2002 Nobel Prize in Chemistry was awarded to John Fenn and Koichi Tanaka for their development of Electrospray Ionization (ESI) and Matrix-assisted Laser Desorption Ionization (MALDI), respectively. Furthermore, recent developments in a specific category of API, referred to as Ambient Ionization (AI), have simplified the applicability of API techniques by removing some or all of the need for sample preparation prior to analysis. AI techniques, such as Desorption Electrospray Ionization (DESI), Direct Analysis in Real Time (DART), and an ever increasing list of additional techniques and variations, allow for direct analysis of an enormous range of sample and matrix types; whole blood, illicit drugs in fingerprints, tissue cross-sections, pharmaceuticals, and forensic samples have all been examined with AI, to name just a relatively few examples.

All API techniques have in common the need to transport ions from atmospheric pressure into the high vacuum of the mass spectrometer - typically $<10^{-5}$ Torr (<1 mPa). Various ion sampling and transport mechanisms are used to transfer ions through differentially-pumped vacuum stages to the mass analyzer. In all cases, significant losses at each stage mean that only a very small fraction ($<<1\%$) of the ions generated from a sample are actually analyzed. The situation is even worse for systems that are intended to be used in mobile or field labs, where space and power are at a premium and large pumping systems are therefore not acceptable.

This talk will briefly review AI techniques to illustrate their value in analytical chemistry (including biological, clinical, and forensic analysis), and will then describe means by which ions are transported from atmosphere into vacuum, with the hope of stimulating dialog with the vacuum community about ways and means that this process could be improved, especially for small, rugged instruments designed for outside-the-lab use.

Biomaterial Interfaces

Room: 317 - Session BI+AS+MN+NS-TuM

Biosensors

Moderator: Graham Leggett, University of Sheffield

8:20am **BI+AS+MN+NS-TuM2 An Inductive-Capacitive Sensor for Real-time Biofilm Growth Monitoring**, *Ekaterina Tolstaya, Y.W. Kim, S. Chu, K.D. Gerasopoulos, W.E. Bentley, R. Ghodssi*, University of Maryland, College Park

We present a real-time biofilm monitoring device based on inductive-capacitive (LC) sensing principles. Bacterial biofilms cause severe infectious diseases and environmental contamination. The bacterial biofilm's complex structure and composition, as well as its ability to exchange genetic information, result in a high tolerance for antimicrobial agents. As a result, established biofilms on implanted or external biomedical devices, such as catheters, are difficult to treat. Traditional antibiotic therapies for biofilm infections often require doses 500-5000 times larger than for non-biofilm infections [1]. Moreover, biofilm growth in environmental and industrial facilities causes contamination and corrosion of equipment due to the toxins generated by biofilms. Therefore, early detection of biofilm growth is critical to facilitate treatment of severe infections and prevent equipment contamination.

In this work, an LC sensor was fabricated using conventional lithography and metal deposition via E-beam evaporation (Cr/Au, 15 nm/200 nm) (Figure 1). The resonant frequency of the sensor was approximately 16 MHz in air at room temperature. A device sensitivity of 1140 Hz/dielectric was demonstrated using a known dielectric material (deionized water) (Figure 2). *Escherichia coli* W3110 biofilms were grown for 48 hours over the LC sensor and the resonant frequency of the sensor was measured every 80 seconds using a spectrum analyzer (Figure 3). As the biofilm grew over the device, an increase in the resonant frequency of the LC sensor was observed. This is due to the lower dielectric permittivity of the biofilm compared to that of the growth media (Luria Broth, $\epsilon \sim 80$), which results in decrease in the capacitance of the sensor. In control experiments with water and air as the media, a slight decrease in the resonant frequency was observed. The resonant frequency shift over time is in good agreement with the natural trend of biofilm growth (Figure 4) [2, 3]. The results validate the use of LC sensing for continuous monitoring of biofilm growth. This sensitive and reliable detection scheme, as well as the capability for flexible substrate integration and wireless interfacing, can serve as a foundation for the development of microsystems for real-time biofilm monitoring for both clinical and environmental applications.

8:40am BI+AS+MN+NS-TuM3 The Interplay of Electrode Materials and Biomaterials in a Catechol-Modified Chitosan-Based Sensor for Clozapine Detection, Robert Dietrich, T.E. Winkler, H. Ben-Yoav, S.E. Chocron, E. Kim, University of Maryland, College Park, D.L. Kelly, University of Maryland School of Medicine, G.F. Payne, R. Ghodssi, University of Maryland, College Park

We present a study of atomic layer-deposited TiN and electroplated Pt black (PtB) as candidate electrode materials to replace Au in a catechol-modified chitosan redox cycling system (Fig. 1) for the electrochemical detection of the antipsychotic clozapine (CLZ). In complex biological fluids like blood, interference from other electrochemically active species is a major challenge. The choice of electrode material is critical in addressing this challenge, as surface morphology and composition may produce a stronger and more reproducible CLZ signal, while shifting that signal away from potential interferents and improving the signal-to-noise ratio. Our electrochemical characterization results indicate that TiN is superior to Au as a sensor material, with a 2.6 times higher CLZ signal and a 3.2-fold lower variability.

Identifying electrode materials with high CLZ signal-to-noise ratio will greatly aid in translating our detection approach into a point-of-care monitoring system. Such a device will reduce the burden currently associated with CLZ due to safety and efficacy monitoring requirements [1], thereby improving the quality of life for people affected by schizophrenia. Our previous work [2] has relied on gold electrodes as a substrate for our catechol-modified chitosan films. These 5x5 mm² micro-fabricated planar gold electrodes serve as controls, which we further modified here with: TiN for its inert properties; and PtB for its high surface area and potential electrocatalytic activity (Fig. 2).

The fabricated electrodes were characterized using cyclic voltammetry. Bare Au yields an oxidative CLZ peak signal of 1.06±0.20 μA, compared to 5.20±2.26 μA when coated with chitosan-catechol (Fig. 3). TiN electrodes produce a signal of 2.00±0.26 μA bare, and 13.7±0.7 μA when modified. The combination of higher signal and lower variability with the TiN is likely due to its inert chemical properties which also propagate more repeatable biomaterial modification. We observed a secondary peak with gold as well as bare TiN electrodes, likely due to interference related to chloride or oxygen. Modified TiN revealed only a single, CLZ-related peak. Results show that, as expected, signals from the bare PtB electrodes were 3370 times higher than from Au. However, they exhibited large variation between experiments, indicating the need for electroplating optimization. Testing the PtB electrodes with the chitosan-catechol film should increase both CLZ signal and resolution. Ongoing work is also focused on glassy carbon electrodes, which are expected to yield high repeatability by eliminating potential interfering oxygen signals in the redox cycling system.

9:00am BI+AS+MN+NS-TuM4 Characterization of an Amperometric Glucose Sensor on a Flexible Polyimide Substrate for Continuous Glucose Monitoring and Insulin Delivery through Single Device, X. Du, J.R. Motley, A.K. Herman, Liney Arndottir, G.S. Herman, X. Tan, J.F. Conley, Jr., Oregon State University, W.K. Ward, R.S. Cargill, J.R. Castle, P.G. Jacobs, Pacific Diabetes Technologies

Type 1 diabetes affects over one million people and every year more than 30,000 children and adults are diagnosed with type 1 diabetes in the United States alone. Patients with type 1 diabetes cannot produce their own insulin and depend upon glucose sensors to monitor their blood glucose and adjust insulin levels either by injection or an insulin pump. The continuous monitoring of glucose blood levels and automatic insulin release by an artificial pancreas is a promising alternative to current treatment options, and can significantly improve the comfort and quality of life for the patient.

Here we introduce a flexible catheter with an integrated glucose sensor capable of both continuously measuring glucose levels and deliver insulin through a single catheter. The amperometric glucose sensor includes multiple Pt indicating electrodes, Ag/AgCl reference electrode, electrohydrodynamic jet (e-jet) printed glucose oxidase enzyme layers, and permselective membrane for optimal glucose response from the interstitial tissue. The compact design is integrated on a flexible polyimide substrate and requires high durability for all the components due to the small radius of curvature of the catheter. The e-jet printing provides digital patterning flexibility and highly precise deposition of the enzyme layer, which allows improved uniformity and accuracy of the glucose sensor. Here we will discuss characterization and optimization of the indicating and reference electrodes using electrochemical methods, scanning electron microscopy, X-ray photoelectron spectroscopy (XPS), and time of flight secondary ion mass spectrometry. XPS was used to confirm full glucose oxidase coverage of the indicating electrode. Electrochemical testing indicates that e-jet printed glucose oxidase inks are still active towards glucose oxidation after printing and subsequent deposition of the permselective membrane. The operation and characterization of a fully functional glucose sensor integrated onto a catheter will also be discussed.

9:20am BI+AS+MN+NS-TuM5 Chemically Modifying Graphene for Biosensing and Interfacing with Biology, Paul Sheehan, Naval Research Laboratory, S.C. Hernandez, National Research Council, N. Long, Nova Research, S.P. Mulvaney, J. Robinson, Naval Research Laboratory, R. Stine, Nova Research, C.R. Tamana, S.G. Walton, Naval Research Laboratory
INVITED

Graphene has many properties that are highly suited for biological studies. For instance, its atomic thinness, high electrical conductivity, and simple production methods are ideal for biosensing. As another example, graphene can be attached to arbitrary substrates to lend them the chemical flexibility of carbon while adding only an ultrathin coating. For both biosensing and biofunctionalization, it is critical to produce high quality films that are precisely modified with the desired chemistry. For biosensing, the sensor must be functionalized for specific receptor-ligand recognition such as DNA-DNA or antibody-antigen binding. We will discuss our strategies for functionalization and the successful detection of specific DNA hybridization biologically-active field-effect transistors (BioFETs) based on chemically modified graphene. We will then discuss our use of graphene to interface biology with materials ranging from polymers to dielectrics to semiconductors. Graphene's incredible thinness enables its inclusion in more traditional sensing platforms as a non-intrusive functionalization layer, discreetly lending its chemical flexibility to other, more inert materials without otherwise impacting the sensing device.

11:00am BI+AS+MN+NS-TuM10 Bioresorbable Sensors and Electronics, John Rogers, University of Illinois at Urbana Champaign
INVITED

A remarkable feature of the modern integrated circuit is its ability to operate in a stable fashion, with almost perfect reliability. Recently developed classes of electronic materials create an opportunity to engineer the opposite outcome, in the form of devices that dissolve completely in water, with harmless end products. The enabled applications range from 'green' consumer electronics to bio-resorbable medical implants – none of which would be possible with technologies that exist today. This talk summarizes recent work on this physically 'transient' type of electronics and sensors, from basic advances in materials chemistry, to fundamental studies of dissolution reactions, to engineering development of complete sets of device components, sensors and integrated systems.

11:40am BI+AS+MN+NS-TuM12 Surface Chemistry Enhanced Microbial Bioelectrocatalysis, Kateryna Artyushkova, C. Santoro, S. Babanova, J. Cornejo, L. Ista, A. Schuler, P. Atanassov, University of New Mexico

Bioelectrochemical oxidation carried out by bacteria attached on a solid electrode is capturing the attention of scientists all over the world. Different species of bacteria have been shown as electroactive and being able to oxidize organic compounds releasing electrons that can be transferred to a conductive solid support. If the oxidation reaction is coupled with the oxygen reduction reaction (ORR), the degradation of organics could lead to a production of useful electricity and water. Those related aspects are currently utilized in the development of alternative and cost effective bioelectrochemical systems (e.g. microbial fuel cell (MFC)) for simultaneous organics removal and electricity production. Understanding the bioelectrocatalytic nature of organics dissimilation by bacteria and the subsequent internal and external electron transfer is of a high importance for the further development of these systems and a key moment in their future application.

In this work, an artificial approach for enhanced microbial bioelectrocatalysis was explored along with study of the parameters promoting bacteria external electron transfer. This approach consisted of artificial modification of electrode surfaces having, as a result, different surface chemistries. Mixed bacterial culture development, biofilm growth and electrochemical performance have been studied. Smooth gold surfaces were modified with organic thiols to form self assembled monolayers (SAMs) with various functional groups (-CH₃, -OH, -N(CH₃)₃ and -COOH).

Power curves and single electrode polarization curves have been taken to evaluate the performance of the MFC as a whole and of the electrodes separately. XPS analysis of electrodes was used to study the effect of chemistry on the performance. Confocal and SEM microscopy was used to study the bacteria biomass and biofilm development was tracked over time.

Electronic Materials and Processing

Room: 314 - Session EM-TuM

Advanced Interconnects and Materials

Moderator: Sean King, Intel Corporation, Andrew Antonelli, Lam Research

8:00am EM-TuM1 Cu/ULK ULSI On-Chip Wiring Technologies, and Related Devices, *Daniel Edelstein*, IBM **INVITED**

We are familiar with microelectronics "scaling" (reducing dimensions) of integrated circuits, so they get denser and cheaper (Moore's Law), and faster (Dennard's Law), in turn increasing the computational power of IC chips. Perhaps less appreciated is that scaling has always gone against the performance and reliability of the multilevel on-chip wiring, commonly termed "Back End of the (Manufacturing) Line", or BEOL, needed to connect these circuits. This invited talk focuses on forefront efforts in materials and nano-scale engineering to combat BEOL scaling and extendibility problems.

Our work has begun on the 7 nm CMOS node, with our 11th generation Cu BEOL. The smallest wires are ~17 nm wide, (< 1/10th the lithographic wavelength!), and represent ~1/25x scaling from the 1st Cu generation. As we migrate to these dimensions, significant innovations in patterning and metallization have been required to preserve defect-free fabrication and electromigration reliability. In order to reduce parasitic wiring capacitance, with its signal delay and power loading, our insulator dielectric constants have migrated from 4.1 to 2.4. But in turn, these materials get more fragile, both electrically and mechanically, requiring significant learning in interface and material mechanics, plus dielectric reliability physics.

Concurrently, system-level performance and cost scaling push more diverse functions onto the chip, and into the wiring levels. Recent innovations add new devices to the finer wiring levels, as well as "reverse-scaled" (larger) wiring levels allow us to collapse more diverse packaging functions onto the chip. Examples of what we fabricate will be presented, with some of their integration-specific issues and solutions. These include ultrathick Cu for data bandwidths, high-Q and magnetic inductors for RF and voltage converters, MEMs switches for antenna diversity, through-Si vias for 3D integration, and magnetic and phase-change non-volatile memory devices (MRAM and PCM).

8:40am EM-TuM3 Selectivity Characterization and Enhancement of Metal-Organic Chemical Vapor Deposited (MOCVD) Selective Cobalt Cap for Advanced Back End of Line, *Jeff Shu, Z. Sun, Y.B. Lee, J. Palazzo, Z. Bayindir, M. Hossain, S. Choi, J. Rullan, H. Liu*, GLOBALFOUNDRIES U.S. Inc.

The continuous shrink of Cu interconnect feature size leads to higher current densities, which lower electromigration lifetimes. The interface between post chemical mechanical polishing (CMP) Cu and dielectric cap has been identified as a key diffusion path for copper atoms, and the adhesion of the interface is critical to electromigration performance [1]. Alternate metallization schemes for copper interconnect using selective CVD Co capping are considered for 22nm technology and below from integration point of view, metal-organic deposition selectivity is the key for leakage and reliability. During the selective CVD Co deposition, both Cu and porous ultra low k dielectric surface are exposed to the metal-organic precursor, insufficient selectivity will increase metal line to line leakage, degrade metal shorts and time-dependent dielectric breakdown (TDDB) performance. In this paper, we focus on selectivity characterization and enhancement of MOCVD selective Co cap process. Selectivity of different precursors are thoroughly evaluated and compared. Lower reaction rate of the carbon based organic group of the Co precursor and the reducing agent was demonstrated to benefit selectivity. Different ultra low k films with various porosity also play a big role in selectivity. Key tuning knobs for the

process window have been defined as process pressure and temperature. The quantity of final Co deposition on porous ultra low k surface has been measured by both X-ray fluorescence (XRF) and Total Reflection X-ray Fluorescence (TXRF), which will subsequently be applied to the definition of selectivity, with comparison to the amount on polished Cu surface. XRF measurement shows some disadvantage due to weak signal to noise ratio while TXRF measurement results are more reliable. X-ray photoelectron spectroscopy (XPS) is used to profile the oxygen penetration into pristine film and the self-limited cobalt oxide thickness has been measured at 15A to 25A, which can be modulated by vacuum break between Co cap and dielectric cap, and by surface pre-clean process before dielectric cap deposition.

[1] J. R. Lloyd, M.W. Lane, E. G. Liniger, "Relationship between interfacial adhesion and electromigration in Cu metallization" 2002 IEEE International Integrated Reliability Workshop Final Report, p.32 - 35 (2002)

9:00am EM-TuM4 Precise Control of the Residual Stress Levels in Polycrystalline Thin Films for Advanced Interconnects and N/MEMS Applications, *Hang Yu, C.V. Thompson*, Massachusetts Institute of Technology

Precise control of residual stress in polycrystalline thin films, which remains a central but difficult task in advanced interconnects and N/MEMS applications, requires synergistic manipulation of multiple processing parameters. Our recent work has demonstrated that stress evolution during film growth is controlled by a series of kinetic processes that include adatom-edge interactions on the surfaces of individual grains, adatom interactions with grain boundaries, and grain growth during film thickening. By synergistically controlling the growth conditions and therefore controlling these kinetic processes, residual stress levels in polycrystalline films can be tailored for optimal performance for specific given applications. In particular, we find that the composition and partial pressure of residual gases in the deposition chamber have a profound effect on the stress evolution behavior. As a consequence, understanding and control of these effects allow tuning of the residual stress of a film. As an example, we demonstrate the use of low levels of oxygen impurities to produce zero stress Ni films.

9:20am EM-TuM5 CVD Mn-based Barrier for Advanced Copper Interconnect Technology: Integration Study, *Nicolas Jourdan*, IMEC, Belgium

To prevent copper diffusion in a circuit, commonly a PVD-TaN/Ta liner is formed on the dielectric surface as a diffusion barrier prior to Cu metallization. The integrity of the PVD-TaN/Ta barrier is expected to reach its limit at a trench dimension below 20nm width. As a result, alternatives must be found for further technology scaling. In recent years, Mn-based barriers have received great consideration as a thin self-formed MnSixOy diffusion barrier can be formed at the surface of the insulator without significant impact on the dielectric constant whilst preserving the total trench volume for Cu filling. Initially, such a "zero-thickness barrier" has been made using a PVD-CuMn seed layer, from which Mn atoms diffuse after a thermal anneal towards the surface of the insulator to form the diffusion barrier. However, because of the use of PVD, limited scalability of this option is expected. Therefore, CVD of Mn-based chemistries has been developed to enable the formation of a thin and conformal barrier [1, 2]. Such a layer has already been integrated in 2ML test vehicles (half pitch ranging from 40nm to 100nm) using a conventional scheme consisting of a PVD-Cu seed followed by Cu electroplating (ECD) and CMP. The authors reported significant RC reduction and comparable Time Dependent Dielectric Breakdown (TDDB) performance with respect to conventional PVD-TaN/Ta barrier [3]. However, integration of a thin Mn-based barrier faces a big challenge due to Mn dissolution taking place in the chemistries used in ECD and CMP operations. The impact of such a phenomenon is even more dramatic in narrow trenches used for advanced technology nodes due to the scaled PVD-Cu seed, which is no longer able to sufficiently protect Mn from dissolution.

In this work, we focus on the optimization of CVD Mn-based barrier in order to make it integration friendly. Furthermore, we will report on physical properties of such a barrier.

[1] N. Jourdan et al.: Electrochemical and Solid-State Letters 15 (5) (2012) H176-H178.

[2] Roy G. Gordon et al.: Proc. Advanced Metallization Conference, p. 1 (2008).

[3] Y. K. Siew et al., Proc. IEEE IITC 2013, p. 1.

9:40am **EM-TuM6 Cryogenic Etching vs P4 Approaches: Paths towards Ultra-low Damage Integration of Mesoporous Oxide Dielectric Materials**, *Jean-Francois de Marneffe*, IMEC, Belgium, *L. Zhang, M.H. Heyne, M. Krishtab*, IMEC, KU Leuven, Belgium, *A. Goodyear, M. Cooke*, Oxford Instruments Plasma Technologies, *N. Heylen, I. Ciofi, L.G. Wen, C.J. Wilson*, IMEC, Belgium, *V. Rutigliani*, University Bari, Italy, *S. Decoster*, IMEC, Belgium, *T. Savage*, SBA Materials, Inc., *K. Matsunaga, K. Nafus*, Tokyo Electron Kyushu Limited, Japan, *J. Boemmels, Z. Tokei, M. Baklanov*, IMEC, Belgium

In recent year, two innovative strategies have been proposed to decrease plasma-induced low-k damage: the P4 approach [Frot et al., 2011] and the cryogenic etch approach [Zhang et al., 2013]. The P4 or “pore stuffing” uses an extrinsic sacrificial pore filler, allowing protection during plasma etching and metallization steps. The cryogenic etch is based on in-situ pore filling by etch byproducts and/or SiO_x sidewall passivation.

In this work, a PMO spin-on material with pristine $k = 2.31$ from SBA has been integrated on 300mm wafers. The integration vehicle uses narrow-spacing structures, i.e. 30nm low-k lines at 180nm pitch.

For the cryogenic etch approach, after lithography, the SiC/SOC/SOG hardmask is trimmed and opened using standard etch. Low-k etching is performed by means of a SF₆-based plasma chemistry in an ICP chamber equipped with a liquid-N₂ cooled substrate holder set at a base temperature of -120°C. Careful optimization of etch conditions allows to considerably decrease the loss of Si-CH₃ bonds, keeping an acceptable etch rate, good hardmask selectivity, and reduced bottom roughness. After patterning and subsequent byproduct removal by annealing, a conventional Cu metallization is performed using TaNTa barrier, Cu seed and electroplating. After chemical-mechanical polishing (CMP) and SiC passivation, functional circuits gave integrated dielectric constant of $k_{int} = 2.38$, i.e. showing a $\Delta k = 0.07$ relative to pristine.

For the pore stuffing approach, PMMA was used as filling material and driven in after low-k deposition. Due to thermal instability of PMMA, a low-temperature Si₃N₄ hardmask was used, as well as low-temperature TaNTa barrier. PMMA was removed after CMP, by means of He-H₂ downstream plasma ashing or thermal decomposition. Functional circuits gave integrated dielectric constants $k_{int} = 2.73$ (thermal unstuffing) and $k_{int} = 3.14$ (He-H₂ ashing).

By comparison of both approaches, it is observed that pore stuffing increases interconnect flow complexity, by the addition of stuffing and unstuffing steps which can also damage the low-k material; however post-etch surfaces are smooth and barrier metal penetration is suppressed. The pore stuffing approach could be improved by using more thermally stable polymers and the search for damage-free unstuffing methods. The current cryogenic etch process requires only minor changes into the process flow, however currently it requires a base temperature of -120°C. The cryogenic etch process could be improved by the use of plasma additives enhancing by-products condensation and/or pre-condensation steps. We acknowledge support from the European Union under grant agreement No. 318804 (SNM).

11:00am **EM-TuM10 Reliability of Advanced Interconnects**, *Carl V. Thompson*, Massachusetts Institute of Technology **INVITED**

As interconnect dimensions have continued to shrink with each new CMOS generation, increased electrical resistivity has had a growing impact on overall circuit performance. This has driven the search for radical changes in interconnect technologies based, for example, on nanomaterials such as carbon nanotubes and graphene. However, with kilometers of interconnect per integrated circuit subject to stringent yield and reliability requirements, viable alternatives to metal-based interconnects have not yet been found. Therefore, for the foreseeable future, further improvements in IC performance and functionality will require evolutionary advances in interconnect materials systems. Recent work on performance enhancement has focused on reduced surface and grain boundary scattering in Cu, and the use of dielectric environments with low dielectric constants. These developments are constrained by the need to maintain high reliability, and sometimes come at the expense of reliability. Also, performance improvements can sometimes be enabled by reliability improvements and changes in design constraints imposed by reliability concerns. Design and layout strategies that lead to improved interconnect reliability and allow relaxation of constraints imposed by reliability concerns will be reviewed. The impact on evolving technologies on electromigration-limited reliability will also be discussed, as will needed changes in reliability assessment methodologies.

11:40am **EM-TuM12 Metal Resistivity Below 10 nm**, *Daniel Gall, P. Zheng, D. Guan*, Rensselaer Polytechnic Institute, *J.S. Chawla*, Intel Corporation, *T. Zhou*, Rensselaer Polytechnic Institute

Electron scattering at surfaces and grain boundaries causes the resistivity of metals to increase with decreasing wire width or film thickness. This effect

is quantified using (i) *in situ* transport measurements on single-crystal, atomically smooth Cu(001) layers, (ii) textured Cu(111) layers and patterned Cu wires with independently varying grain size, thickness and line width, (iii) *in situ* grown interfaces including Cu-Ni, Cu-Ta, Cu-MgO, Cu-Ti, Cu-SiO₂ and Cu-oxygen, and (iv) epitaxial layers of various other metals including Ag(001), W(001), Ta(001), Ni(001), and TiN(001). The layers are grown by ultra-high vacuum magnetron sputter deposition on MgO(001) substrates and are found to be atomically smooth single crystals by a combination of x-ray diffraction θ - 2θ scans, ω -rocking curves, pole figures, reciprocal space mapping, Rutherford backscattering, x-ray reflection, transmission electron microscopy, and *in-situ* scanning tunneling microscopy.

The measured resistivity is interpreted within the classical models by Fuchs and Sondheimer for surface scattering and Mayadas-Shatzkes for grain boundary scattering. The data is well described by these models. However, fitting of the resistivity vs thickness for metal layers with non-spherical Fermi surfaces provides values for the bulk electron mean free paths that deviates from the expected free-electron values by factors of 5-10, indicating the breakdown of these semiclassical models. In addition, the F-S model also does not correctly predict the temperature dependence, as the measured scattering specularly as well as the product of bulk resistivity times mean free path are temperature dependent.

First-principles density functional (DFT) calculations are employed to develop an understanding of electron transport in metals at reduced length scales: (i) The Fermi surface of the bulk metal is determined and the electronic-structure contribution to the conductivity calculated by integration over the Brillouin zone. This provides, in combination with the known bulk resistivity, values for the bulk electron mean free path of 40, 3.3, and 16 nm for Cu, Ta, and W, respectively. (ii) Application of the Boltzmann transport equation and simultaneous integration over real and reciprocal space of the thin film and Brillouin zone, shows considerable anisotropy effects. For example, electron scattering at a W(100) surface has a two times larger effect on the resistivity than scattering on W(110). (iii) Simulation of transport using the 2D Fermi surfaces of thin films, and (iv) non-equilibrium DFT simulations are used quantitatively determine electron scattering which will be directly mapped on a phenomenological model.

Energy Frontiers Focus Topic

Room: 315 - Session EN+AS+EM+SE-TuM

Fuel Formation and Thermal Transport

Moderator: Michael Filler, Georgia Institute of Technology

8:00am **EN+AS+EM+SE-TuM1 Unraveling Thermodynamic and Kinetic Factors in Solar-Thermochemical Fuel Production**, *Sossina Haile*, California Institute of Technology **INVITED**

Perhaps the greatest challenge facing our planet is sustainable energy. Given the vast solar energy resource base available to modern society, key to addressing this challenge is the conversion of solar energy into a storable form suitable for on-demand utilization. So emerges the concept of ‘Solar Fuels.’ Amongst many approaches currently pursued to generate solar fuels, thermochemical dissociation of water splitting is particularly attractive. It provides the benefits of full utilization of the solar spectrum and inherent temporal separation of hydrogen and oxygen gases. In recognition of these advantages, numerous multi-step cycles have been considered over the past several decades. Recently, two-step cycles making use of *non-stoichiometric* oxides have received attention because of the simplicity of their implementation. The approach relies on the large oxygen nonstoichiometry change that the material undergoes in response to variations in oxygen partial pressure (pO_2) and temperature (T). Specifically, upon exposure to high temperatures ceria undergoes reduction without change in crystalline phase to release oxygen. On cooling in the presence of H₂O (or CO₂), the oxide is reoxidized, releasing H₂ (or CO). The success of the method relies not only on favorable thermodynamics but also on facile kinetics, both in terms of surface reaction rates and bulk diffusion coefficient. Accordingly, we have undertaken a comprehensive study of ceria and its doped derivatives to assess both the equilibrium redox behavior by thermogravimetric methods and the kinetic response by conductivity relaxation methods. We find, for example, that introduction of Zr strongly increases the absolute non-stoichiometry of ceria, but at a penalty in terms of the sensitivity of the nonstoichiometry to changes in environmental conditions and in terms of bulk diffusivity. In another example, we find that the relaxation behavior of Sm-doped ceria is substantially more rapid than that of both undoped and Zr-doped ceria, a result that is tentatively assigned to differences in species mobilities. The implications of these fundamental differences in material properties for thermochemical fuel production are discussed.

8:40am **EN+AS+EM+SE-TuM3 Controlling Catalysis on Metal Nanoparticles by Direct Photoexcitation of Adsorbate-Metal Bonds**, *M.J. Kale, T. Avanesian*, University of California, Riverside, *H. Xin, J. Yan*, SLAC National Accelerator Laboratory, *Phillip Christopher*, University of California, Riverside **INVITED**

Heterogeneous photocatalysis is typically assumed to occur via photon absorption by a solid-state photocatalyst (only the photocatalyst electronic states are involved in photon absorption) followed by charge carrier diffusion through the photocatalyst bulk and subsequent transfer to adsorbates. This process of energetic charge carrier generation and transfer results in wavelength dependent quantum efficiencies that strictly follow the absorption spectrum of the solid-state photocatalysts, regardless of the chemical transformation. The substrate (photocatalyst) mediated photo-absorption process inhibits approaches to control reaction selectivity by matching photon excitation wavelengths to bond specific electronic transitions, as typically done in molecular systems.

Here, we show that strong chemisorption bonds formed between CO and Pt metal surfaces can be activated with visible photons to drive catalysis through direct, resonant photoexcitation of hybridized Pt-CO states. This is enabled as the dominant photoexcitation mechanism (over substrate mediated photoexcitation) driving catalysis by using sub-5-nanometer Pt nanoparticle catalysts, where high surface area to volume ratio force photon absorption onto surface metal atoms. The direct photoexcitation process is observed to be significantly more efficient for driving photocatalysis than the indirect photoexcitation process when the energy of exciting photons is resonant with adsorbate specific electronic transitions involving hybridized metal-adsorbate states. It is also demonstrated that resonant photoexcitation of Pt-CO bonds on sub-5-nanometer Pt nanoparticles by visible light significantly enhances selectivity towards CO₂, over H₂O production, in the selective oxidation of CO by O₂ in an H₂ rich stream (also known as preferential CO oxidation). These results open new avenues to control catalytic reaction selectivity on sub 5-nm catalytic particles by resonant photoexcitation of adsorbate-specific electronic transitions involving hybridized metal and adsorbate states. It is expected that the development of insights into resonant electronic transitions between hybridized metal-adsorbate states should allow rational control of catalytic selectivity that cannot be achieved exclusively with thermal energy input.

9:20am **EN+AS+EM+SE-TuM5 Atomistic Insights as the the pH Dependence of Onset Potential of the Oxygen Evolution Reaction on Hematite**, *Anders Hellman*, Chalmers University, Sweden

Hematite (α -Fe₂O₃) is an extensively investigated semiconductor for photoelectrochemical water oxidation, and recent research has shed light on many of the atomic processes involved. However, a controversy about the nature and role of surface states in the water oxidation reaction remains. Here first-principles calculations are used to investigate surface states present in hematite under photoelectrochemical conditions. Most specifically a model describing how the onset potential for oxygen evolution reaction on hematite depend on the pH of the electrolyte is put forth. The predictions of this model are confirmed to a high extent by measurements of the onset potential on hematite based model photoanodes. In particular, a linear dependence of the onset potential on the pH was observed, with a 49 mV / pH slope. Detailed photoelectrochemical characterization confirmed that the oxygen evolution reaction takes place via the same surface states irrespective of the pH. Moreover, the photovoltage and flat band potential of the hematite were also found to be pH independent. These results provide a framework for a deeper understanding of the OER when taking place on semiconductors (like hematite) via surface states

9:40am **EN+AS+EM+SE-TuM6 Rational Design of Pt₃Ni Alloy Surface Structures for Oxygen Reduction**, *Liang Cao, T. Mueller*, Johns Hopkins University

A cluster expansion approach based on ab-initio calculations has been used to investigate the relationship between surface structures of Pt₃Ni(111) alloy catalysts and their catalytic activity. With this approach, we build a direct bridge between the atomic structure and catalytic properties of Pt-Ni alloy system at a variety of compositions and chemical environments. The equilibrium near-surface structures are presented as a function of O₂ partial pressure and the chemical potential difference between Ni and Pt. We discuss the relative importance of strain, ligand, and ensemble effects in determining catalytic activity, and demonstrate how ensemble effects can be leveraged to rationally design alloy surfaces with optimal ORR activity by searching for surfaces with targeted oxygen binding energy.

11:00am **EN+AS+EM+SE-TuM10 Molecular and Mesoscale Design for Organic and Hybrid Thermoelectrics**, *Rachel Segalman*, University of California, Santa Barbara **INVITED**

Thermoelectric materials for energy generation have several advantages over conventional power cycles including lack of moving parts, silent operation, miniaturizability, and CO₂ free conversion of heat to electricity. Excellent thermoelectric efficiency requires a combination of high thermopower (S, V/K), high electrical conductivity (σ , S/cm), and low thermal conductivity (κ , W/mK). To date the best materials available have been inorganic compounds with relatively low earth abundance and highly complex, vacuum processing routes (and hence greater expense), such as Bi₂Te₃. Molecular materials and hybrid organic-inorganics bring the promise of solution processible, mechanically durable devices. While highly conductive polymers are now common place, they generally demonstrate low thermopower. Our work on molecular scale junctions that nanostructuring of organics allows them to act as thermionic filters between inorganic junctions which can lead to enhanced thermoelectric properties. We have taken inspiration from this fundamental understanding to design material systems in which we combine a high electrical conductivity, low thermal conductivity polymer with a nanoparticle that contributes high thermopower. Additionally, the work functions of the two materials are well-aligned which introduces the possibility of thermionic filtering at the interface and an additional boost to the power factor. The combination of these effects results in a new hybrid, solution processible material with a thermoelectric figure of merit within an order of magnitude of the Bi₂Te₃. In this talk, I will discuss both the use of thermoelectric measurements to gain insight to molecular junctions and how this insight translates to design principles for polymer and hybrid thermoelectrics.

11:40am **EN+AS+EM+SE-TuM12 Advances in Solid-State Energy Harvesting from Asymmetric Thermoelectric Devices**, *B. Cook, Jay Lewis*, RTI International

The amount of thermal energy rejected as waste heat from industrial processes in the United States has been estimated at 32 quadrillion BTU per year, with an associated emission of 1,680 million metric tons of carbon dioxide. The ability to cost-effectively convert a portion of this thermal energy into useful electrical energy could improve energy efficiency, reduce operating costs, and decrease CO₂ emissions. Waste heat is typically categorized by temperature as high-grade (650°C and above), medium-grade (232°C to 650°C, and low-grade (232°C and below). In order to improve the thermal-to-electrical conversion efficiency of medium-grade waste heat, RTI has combined two different materials to form a high figure-of-merit, hybrid thermoelectric (TE) device. Recently-developed enhanced "TAGS-85", or e-TAGS, was employed as the p-leg, while the n leg was comprised of improved half-Heusler (HH) material. This hybrid material pair provides a high ZT, lead-free TE material solution for waste heat recovery for use in vehicle or industrial platforms. The improved HH material employs two novel techniques to reduce thermal conductivity: (1) high-energy milling, and (2) addition of coherent inclusions. Single n-/p-couples were produced that achieved a 9.2% thermal to electric power conversion efficiency for T_{hot} = 559°C and ΔT = 523K. This is a significant efficiency improvement at a lower hot side temperature with the hybrid e-TAGS/HH single couple over the performance of a conventional, all HH couple. By optimizing the cross sectional areas of the pellets for equal heat flow, the resulting asymmetric couple achieved a conversion efficiency of 10.5% at T_{hot} = 537°C and ΔT = 497°C. A 49-couple hybrid module using HH materials paired with e-TAGS and operated with T_{hot} up to 600°C reached a maximum efficiency of 10%. The improved module efficiency is believed to be due to both improved materials and optimized cross-sectional area ratios between the n- and p- elements. We will also discuss additional advances in thermal to electric power conversion using multi-stage modules.

12:00pm **EN+AS+EM+SE-TuM13 The Effect of Particle Size and Surface Termination of n-Si on Thermal and Electrical Conductivity**, *Thomas Lopez, L. Mangolini*, University of California - Riverside, *S. Bux, J.P. Fleurial*, California Institute of Technology

A discussion of synthesis and characterization of bulk nanocrystalline silicon with grain sizes of around 20 nm and thermal conductivities as small as 100 mW/cmK at room temperature, will be presented. Nanostructured materials have great potential for thermoelectric applications because of the reduction in thermal conductivity due to phonon scattering at grain boundaries [1] and silicon is a well-understood, cheap, earth-abundant material. Other silicon nanostructures, such as nanowires [2], are being investigated as viable thermoelectric materials. We have used, for the first time, the combination of a non-thermal plasma process for the synthesis of silicon nanocrystals with hot pressing to produce bulk nanostructured silicon samples. The non-thermal plasma synthetic route has been proposed for the production of photo-luminescent silicon quantum dots with narrow size distribution (3 +/- 0.5 nm) [3]. The same reactor has been scaled up to

produce silicon nanocrystals at a rate of hundreds of milligrams per hour. Silicon powder with sizes between 5 nm and 15 nm has been produced using either silane (SiH₄) or silicon tetrachloride (SiCl₄), which are low-cost silicon precursors. Results have shown surface termination of the non-thermal plasma synthesized particle, i.e. H or Cl, play a role in densification kinetics. Hot pressing is a high pressure, high temperature process that allows for the production of samples with bulk like densities while limiting grain growth. In this study we have produced bulk (12 mm diameter, 2-4 mm in thickness) samples of nanocrystalline silicon with relative densities exceeding 95%. Characterization by XRD and TEM confirms that grain sizes are around 30 nm. The effects of surface termination of nano-silicon on grain growth and grain boundary conditions will be extensively discussed.

1. Dresselhaus, M.S., et al., *Advanced Materials*, 2007. 19(8): p. 1043-1053.
2. Hochbaum, A.I., et al., *Nature*, 2008. 451(7175): p. 163-U5.
3. Mangolini, L., et al., *Nano Letters*, 2005. 5(4): p. 655-659.

Exhibitor Technology Spotlight

Room: Hall ABC - Session EW-TuM

Exhibitor Technology Spotlight Session

Moderator: Chris Moffitt, Kratos Analytical Limited, UK

10:20am EW-TuM8 High Speed Water Vapor Cryopumps: Increasing Tool Throughput and Process Yield with Polycold PFC and MaxCool Products, *C. Rebecchi, Kevin Flynn*, Brooks Automation, Inc., Polycold

Water vapor is the primary reason for slow pumpdown from crossover to ultra high vacuum in most vacuum systems. At chamber pressures near crossover, water vapor easily accounts for the majority of a vacuum system's gas load. In addition, water vapor and dissociated oxygen are often unwanted contaminants that can physically or chemically reduce product quality and yield in vacuum deposition processes. Since water vapor is a polar molecule, it easily adheres to chamber surfaces and desorbs slowly. High speed water vapor pumping is especially critical in large-scale commercial vacuum processes, where maximum tool throughput, product quality, and process repeatability are most valued. When ambient chamber temperatures allow, the most effective method to increase the overall water vapor pumping speed in a vacuum system is to install a large cryosurface directly inside the vacuum process chamber. In this location, the cryosurface will add effective supplemental water vapor pumping that is not diminished by vacuum conductance limitations such as high vacuum ports or valves. Polycold PFC and MaxCool products feature extremely fast cryosurface cooldown and defrost capabilities, which allow cryosurface placement directly inside a vacuum process chamber for optimum high speed water vapor pumping. Polycold PFC and MaxCool products also feature both high cooling capacities and low-temperature performance able to cool very large cryosurfaces for very high speed water vapor pumping. The industry-leading Polycold MaxCool 2500L cryochiller features unbeaten low temperature performance for >100,000 l/s water vapor pumping down to 2E-9 torr water vapor partial pressure and >200,000 l/s of water vapor pumping down to 4E-8 torr water vapor partial pressure.

10:40am EW-TuM9 Stylus Profilometry – Bruker's DektakXTL delivers Innovation in Flexibility and Ease of Use, *Eric Rufe*, Bruker

Bruker will present DektakXTL large area stylus profilometry system and advantages of new automated scanning and alignment capabilities, as well as simplified quick acquisition tools for fastest time to data supporting applications in a range of industries including but not limited to flexible electronics, display and touch screen manufacture.

In-Situ Spectroscopy and Microscopy Focus Topic

Room: 313 - Session IS+AS+MC+SS-TuM

Ambient Pressure X-ray Photoelectron Spectroscopy (AP-XPS)

Moderator: Franklin (Feng) Tao, University of Notre Dame

8:00am **IS+AS+MC+SS-TuM1 The ISS Facility at BESSY II and Beyond: The Application of Near Ambient Pressure X-ray Electron Spectroscopy in the Surface Characterization of Technical Catalysts, *Michael Hävecker***, Helmholtz-Zentrum Berlin für Materialien und Energie/Elektronenspeicherring BESSY II, Germany, *Ch. Heine, M. Eichelbaum*, Fritz-Haber-Institut der Max-Planck-Gesellschaft, Germany, *F. Rosowski*, BasCat, UniCat-BASF JointLab, Germany, *A. Trunschke, R. Schlögl*, Fritz-Haber-Institut der Max-Planck-Gesellschaft, Germany
INVITED

The surface of functional materials like catalysts responds to the ambient conditions. Surface sensitive in-situ spectroscopy, i.e. in the presence of a reactive gas allows studying the formation of the gas/solid interface of a catalyst. The ISS facility operated by the FHI at the synchrotron radiation source BESSY II of the HZB is dedicated to this kind of in situ studies [1 - 3]. Online gas analytics allows correlating the electronic surface structure with the catalytic performance. Examples for the dynamic formation of the electronic surface structure by interaction with the ambient gas under equilibrium will be presented focusing on technical catalysts like multi-element mixed oxide powders. The direct catalytic oxidation of alkanes to olefins and oxygenates is becoming increasingly important for the chemical industry due to the up-coming shortage of crude oil resources. Vanadyl pyrophosphate is the industrially used catalyst in the selective oxidation of n-butane to maleic anhydride. We characterized the surface of this catalyst material with NAP-XPS in the mbar pressure range and with NAP-soft XAS in the electron yield mode at pressures up to 1000mbar at various gas mixtures. In addition to the determination of composition and vanadium oxidation state also semiconductor properties like work function changes and Fermi level pinning have been studied [4].

Finally, an outlook on future activities at HZB/BESSY to develop further synchrotron based ambient pressure characterization methodologies will be given. The Energy Materials In-Situ Laboratory Berlin (EMIL) is a research alliance of the HZB and FHI that will include a NAP-high kinetic energy XPS endstation capable to operate at kinetic energy of photoelectrons up to 7000eV that allows studying buried layers and liquid/solid interfaces.

References

- Salmeron, M., Schlögl, R., Ambient pressure photoelectron spectroscopy: A new tool for surface science and nanotechnology. *Surf. Sci. Rep.*, 32, 1022 (2008).
- Bluhm, H., Hävecker, M. et al., In situ x-ray photoelectron spectroscopy studies of gas-solid interfaces at near ambient conditions, *MRS BULLETIN.*, 63, 169 (2007).
- Bluhm, H. et al., Investigation of solid/vapor interfaces using ambient pressure X-ray photoelectron spectroscopy. *Chem. Soc. Rev.*, 42, 5833 (2013).
- Heine, Ch. et al., Work function, band bending, and microwave conductivity studies... *J. Phys. Chem. C*, 117, 26988 (2013).

8:40am **IS+AS+MC+SS-TuM3 Recent Trends and Instrument Development in Ambient Pressure Photoelectron Spectroscopy, *Henrik Bergersen, J. Åhlund***, VG Scienta AB, Sweden

The field of Ambient Pressure Photoelectron Spectroscopy (APPEs) has gone through rapid development in recent years. Although the field was pioneered in the 1970's, most instrument as well as application development has happened in the last decade. In this contribution we will discuss some recent trends in APPEs and present state-of-the-art work within the different applications areas.

Experiments done under normal surface science conditions (Ultra High Vacuum) are of limited use in some applications, e.g. catalysis, due to the pressure gap problem. This motivates the study of systems at ambient pressures. While the presence of a gas atmosphere surrounding the sample enables new types of studies, it also poses instrumentation difficulties. The most notable of these is signal decrease due to inelastic scattering of the photoelectrons in the surrounding gas. We will show state-of-the-art solutions to limit this scattering together with recent results.

Photoelectron spectroscopy went through a revolution in the 1990's, with the development of parallel angular detection using 2D detectors, a development that VG Scienta is proud to have contributed to. The possibility of simultaneous recording of Angular Resolved PES (ARPES) spectra enables not only band structure measurements, but also x-ray

photoelectron diffraction (XPD), depth profiling and standing wave spectroscopy. Recent examples within APPES will be given.

The use of 2D detectors to record parallel spatially resolved spectra is a related technique. Here we will show experimental results as well as very recent instrument development to obtain world leading spatial resolution at ambient conditions.

The combination of APPES and Hard X-ray Photoelectron Spectroscopy (HAXPES) has recently become an established technique. We will show results of the use of this combination to decrease inelastic scattering of the photoelectrons as well as to tailor the probing depth of advanced systems.

In APPES, more than in UHV PES, instrument usability and sample handling is a key to successful measurements. VG Scienta has developed several complete system offerings to maximize productivity in the lab. These will be discussed on a conceptual level, as well as in some detail.

9:00am IS+AS+MC+SS-TuM4 In Situ Studies of Exceptionally Active Catalyst of Earth Abundant Elements for Complete Combustion of Methane at a Relatively Low Temperature, F. Tao, J. Shan, L.T. Nguyen, S. Zhang, Weixin Huang, University of Notre Dame

It is critical to develop a catalyst made of earth-abundant elements highly active for a complete combustion of CH₄ at a relatively low temperature for catalytically transforming CH₄ to electrical energy in power plant. The currently available catalysts with high activity consist of precious metal nanoparticles supported on rare earth oxides. Their high cost limits the application of these catalysts at industrial scale. Here we report a new catalyst, early transition metal oxide-based mixed oxide only consisting of earth-abundant elements which can completely combust CH₄ at 350°C at a gas hourly space velocity of 240,000 ml 0.5% CH₄ on 1 gram in one hour. This comparable or even higher catalytic activity results from the integration of Ni cations and surface lattice oxygen atoms at the atomic scale. With such an integration, the carbon atom dissociated from CH₄ can bond with its neighboring surface oxygen atoms to form an intermediate of CO₂ and then desorb.

In-situ studies of catalyst surface using AP-XPS and monitoring of products formed from isotope-labeled catalysts show that (1) molecules O₂ dissociates on surface oxygen vacancies, (2) half of the dissociated oxygen atoms stay in oxygen vacancies, (3) the other half of dissociated oxygen atoms directly bond with hydrogen atoms dissociated from CH₄ to form OH and then H₂O molecules, (4) CH₄ progressively dissociates on Ni cations to form CH_n (n=3, 2, 1, 0), (5) carbon atoms bind to two surface lattice oxygen atoms nearby to form a carboxylate species, O-C-O intermediate, and then desorb. The mixed cations and surface lattice oxygen atoms in this mixed oxide at atomic level makes the formation of an -O-C-O- intermediate at a mild temperature since a spillover of dissociated species is not necessary.

9:20am IS+AS+MC+SS-TuM5 Ambient Pressure XPS Studies of Fuel Cell and Electrolysis Catalysis, Hirohito Ogasawara, SLAC National Accelerator Laboratory INVITED

Fuel cell and electrochemical reactions were studied by ambient pressure X-ray photoemission spectroscopy at Stanford Synchrotron Radiation Lightsource (SSRL) [1]. We will present our recent studies: platinum catalyst under different operating conditions of oxygen reduction fuel cell reaction, iridium oxide catalyst during the oxygen evolution reaction and molybdenum sulfides catalyst during the hydrogen evolution reaction. Surface changes under these electrochemical reactions, which are keys to understanding activity and durability will be shown [2,3].

[1] Ambient-pressure photoelectron spectroscopy for heterogeneous catalysis and electrochemistry, *CatalysisToday* 205 (2013) 101.

[2] Direct observation of the oxygenated species during oxygen reduction on a platinum fuel cell cathode, *Nature Communications* 4 (2014) 2817

[3] In situ observation of surface species on iridium oxide nanoparticles during the oxygen evolution reaction, submitted

11:00am IS+AS+MC+SS-TuM10 Environmental Cells with 2D Electron Transparent Windows for Ambient Pressure Photoelectron Imaging and Spectroscopy, Andrei Kolmakov, National Institute of Standards and Technology (NIST)

We have designed and characterized electron transparent windows for environmental cells dedicated for ambient pressure XPS spectroscopy and electron microscopy of liquid and gaseous samples. These windows made of single or multi-layered graphene have thicknesses comparable to the effective attenuation length of 200-1000 eV electrons what allow to conduct interfacial spectroscopy of fully hydrated samples without differential pumping setup. In addition, these membranes are thermally and chemically stable, gas impermeable and mechanically robust. Based on this unique combination of properties and on recent developments in graphene fabrication and transfer protocols we demonstrate the capability to perform

in situ XPS and electron microscopy studies of the electrochemical processes taking place at liquid electrolyte-solid interface.

11:20am IS+AS+MC+SS-TuM11 The Effect of Interfacial Ethanol on Ionic Distributions in Aqueous Solution, Marijke Van Spijk, K.A. Perrine, M.J. Makowski, University of California Irvine, H. Bluhm, Lawrence Berkeley National Laboratory, J.C. Hemminger, University of California Irvine

In this study, liquid microjet X-ray photoelectron spectroscopy (LJ-XPS), carried out at beam line 11.0.2 of the ALS synchrotron at LBNL, was used to probe the interfacial behavior of aqueous magnesium or sodium chloride solutions with the addition of organics including ethanol under one torr of water vapor. Our results address fundamental issues of solvation at the surface and in the bulk of ternary solutions. For these studies, aqueous ethanol solutions were generated, and salt was added to produce an ionic solution. The ternary solution is pumped continuously through a temperature-controlled quartz capillary to produce a micron-sized laminar jet within 0.5 mm of the PES analyzer aperture. Synchrotron radiation ionizes the solution, and ejected photoelectrons are detected using differentially pumped electron optics. Tunable photon energy, together with the inelastic scattering attenuation of photoelectrons in solution, provide a variable probe depth. Here, photoelectrons with low kinetic energies (200 eV) are detected from the surface of solution, and those with high kinetic energies (600 eV) are detected from deeper into solution, where chemistry is consistent with bulk solution. The high kinetic energy photoelectrons have sufficiently large inelastic mean free paths so that a percentage are not attenuated by inelastic scattering.

Carbon (C1s), oxygen (O1s), sodium (Na2s), magnesium (Mg2s), and chloride (Cl2p) photoelectron spectra were collected at two photoelectron kinetic energies to investigate the relative concentration of species at the surface and in the bulk for various ethanol concentrations. The C1s spectra were deconvoluted into two gas phase and two solution phase peaks corresponding to the carbon groups in ethanol. Surface adsorption was evident for aqueous ethanol without ions, and was diminished in the presence of ions. The relative ionic propensities at the surface change with ethanol concentration. In particular, the solvation of magnesium was impacted by dehydration. Understanding the interfacial solute distribution of these ternary solutions is important for predicting reactivity at aqueous surfaces.

11:40am IS+AS+MC+SS-TuM12 Studying Zeolites and Clays with the Tools of Surface Science from UHV to Near-Ambient Pressures, Jorge Boscoboinik, Brookhaven National Laboratory INVITED

While Surface Science provided useful insights into a variety of materials of interest for catalysis, its contribution to the understanding of zeolites and clays has been limited. This was mainly due to the lack of suitable well-defined surfaces that successfully mimic the properties of these important materials while allowing its analysis using the vast toolkit of surface science. This talk will describe an aluminosilicate ultra-thin (~ 0.5 nm) film that was recently synthesized, which provides a good model system for zeolites and clays. It consists of a bilayer structure, as shown in the figure, and it counts with bridging hydroxyl groups. The latter are the active sites in zeolite catalysts, of great importance for energy transformations such as the cracking of crude oil and the methanol to gasoline conversion. This model system allows then to study the interaction of molecules involved in these catalytic processes and potentially contribute to the understanding of these chemical transformations. I will provide first a description of the system itself as characterized in ultra-high vacuum (UHV) conditions and then move on to analyze the interaction of these aluminosilicate films with different molecules of interest from UHV to near-ambient pressures.

References

[1] J.A. Boscoboinik, X. Yu, B. Yang, F.D. Fischer, R. Wlodarczyk, M. Sierka, S. Shaikhutdinov, J. Sauer, H.-J. Freund, *Angew. Chem. Int. Ed.* 51 (2012) 24, 6005-6008. *Angew. Chem.* 124 (2012) 6107-6111.

[2] J.A. Boscoboinik, X. Yu, B. Yang, S. Shaikhutdinov, H.-J. Freund. *Micropor. Mesopor. Mater.* (2013) 165, 158-162.

[3] J.A. Boscoboinik, X. Yu, E. Emmez, B. Yang, S. Shaikhutdinov, F. Fischer, J. Sauer, H.-J. Freund. *J. Phys. Chem. C* (2013) 117, 13547-13556.

Magnetic Interfaces and Nanostructures

Room: 311 - Session MI+MG-TuM

Advanced Materials Discovery

Moderator: Markus Donath, Muenster University, Germany

8:00am MI+MG-TuM1 Combinatorial Approach to Novel Functional Materials, *Ichiro Takeuchi*, University of Maryland **INVITED**

Throughout the history of mankind, scientists and engineers have relied on the slow and serendipitous trial-and-error approach for materials discovery. In 1990s, the combinatorial approach was pioneered in the pharmaceutical industry in order to dramatically increase the rate at which new chemicals are identified. The high-throughput concept is now widely implemented in a variety of fields in materials science. We have developed combinatorial thin film synthesis and characterization techniques in order to perform rapid survey of previously unexplored materials phase space in search of new inorganic functional materials. Various thin film deposition schemes including pulsed laser deposition, electron-beam deposition, and co-sputtering are implemented for fabricating massive arrays of compositionally varying samples on individual combinatorial libraries. A suite of high-throughput characterization tools are employed to screen the combinatorial libraries and map different physical properties of materials as a function of sweeping composition changes. They include room-temperature scanning SQUID microscopy, microwave microscopy, and micromachined MEMS cantilever arrays. Advanced characterization techniques at synchrotron beam lines are used for rapid diffraction as well as x-ray magnetic circular dichroism measurements.

8:40am MI+MG-TuM3 Discovery and Design of Two-Dimensional Materials by Data-Mining and Genetic Algorithm Approaches, *Richard Hennig*, University of Florida, Gainesville **INVITED**

The rapid rise of novel single-layer materials, presents the exciting opportunity for materials science to explore an entirely new class of materials. This comes at the time when mature computational methods provide the predictive capability to enable the computational discovery, characterization, and design of single-layer materials and provide the needed input and guidance to experimental studies. I will present our data-mining and genetic algorithm approaches to identify novel 2D materials with low formation energies and show how unexpected structures emerge when a material is reduced to sub-nanometers in thickness. We discovered several 2D materials in the families of group III-V compounds and group-II oxides with promising properties for electronic devices and identify suitable metal substrates that can stabilize several of these as-yet hypothetical materials. In the families of group-III monochalcogenides and transition metal dichalcogenides we identify several 2D materials that are suitable for photocatalytic water splitting. We show that these 2D materials in contrast to their 3D counterparts have appropriate band gaps and alignments with the redox potentials of water, and exhibit high solvation energies, indicating their stability in aqueous environment. We show that strain can be used to tune the electronic and optical properties of these materials. Our results provide guidance for experimental synthesis efforts and future searches of materials suitable for applications in energy technologies.

9:20am MI+MG-TuM5 Complexities in the Molecular Spin Crossover Transition, *Xin Zhang**, *S. Mu*, University of Nebraska-Lincoln, *J. Chen*, Columbia University, *T. Palamarciuc*, *P. Rosa*, *J.-F. Létard*, Université de Bordeaux, France, *J. Liu*, *D. Arena*, Brookhaven National Laboratory, *B. Doudin*, Université de Strasbourg, France, *P.A. Dowben*, University of Nebraska-Lincoln

The electronic structures of three different spin crossover molecules have been obtained by temperature dependent X-ray absorption spectroscopy (XAS). We show compelling evidence that the electronic structure changes associated with the spin crossover transition occur at significantly lower temperature than observed for the change in the molecular spin state. The transition temperatures indicated by XAS is about 20~60 K lower than that given by the magnetic moment switching. The changes in electronic structure are in agreement with density function theory (DFT) results that shows that the molecular electronic structures are different for high spin (HS) and low spin (LS) states. The conclusion that the electronic structure changes occur at significantly lower temperature than observed for the change in the molecular spin state associated with the spin crossover transition are also supported by transport measurements and the temperature dependence of the dielectric properties of SCO molecular system: $[\text{Fe}(\text{PM-AzA})_2(\text{NCS})_2]$.

9:40am MI+MG-TuM6 Controlling and Imprinting Topological Spin Textures, *R. Streubel*, *L. Han*, IFW Dresden, Germany, *M.-Y. Im*, Lawrence Berkeley National Laboratory, *F. Kronast*, Helmholtz-Zentrum Berlin für Materialien und Energie/Elektronenspeicherung BESSY II, Germany, *U.K. Roessler*, Institute for Theoretical Solid State Physics, IFW Dresden, Germany, *F. Radu*, *R. Abrudan*, Ruhr-Universität Bochum, Germany, *G. Lin*, *O.G. Schmidt*, IFW Dresden, Germany, *Peter Fischer*, Lawrence Berkeley National Laboratory, *D. Makarov*, IFW Dresden, Germany

Topological states in magnetism, such as chiral skyrmions, with an integer topological charge are currently a topic of intensive fundamental research [1-3]. If one was able to control their properties in a digital manner, such as switching their topological charge deliberately in storage devices, a novel path in spintronics would be opened [4]. However, so far, most of these topological spin textures have been only observed in exotic materials with low symmetry and at low temperatures, making them rather impractical for applications. Here, we offer an alternative route by designing synthetic magnetic heterostructures where specific spin textures resembling swirls, vortices or skyrmions with distinct topological charge densities can be tailored at ambient temperatures. This is achieved by vertically stacking two magnetic nanopatterns with in-plane and out-of-plane magnetization and imprinting the in-plane non-collinear spin textures into the out-of-plane magnetized material. Key mechanisms of our concept are demonstrated both by micromagnetic simulations and experimental observations with element-specific magnetic soft x-ray microscopy [6] in a common ferromagnetic thin film element stack, e.g. Co/Pd multilayers coupled to Permalloy. Utilizing the interlayer coupling strength as tuning parameter, a gradual transition in the magnetic pattern of the out-of-plane layer from the decoupled magnetized state to a strongly coupled state with a vortex spin texture is achieved. At an intermediate coupling strength, magnetic spirals with tunable opening angle and in particular donut textures form which can be referred to as skyrmion system with D_n symmetry. Applying a small magnetic field, a controlled and reliable switching between two topologically distinct donut textures is realized.

Supported by the German Science Foundation (DFG) grant MA 5144/1-1, the European Research Council under European Union's Seventh Framework program (FP7/2007-2013)/ERC grant agreement n.306277. M.-Y.I. and P.F. acknowledge support by the Director, Office of Science, Office of Basic Energy Sciences, Materials Sciences and Engineering Division, of the U.S. Department of Energy under Contract No. DEAC02-05-CH11231 and by Leading Foreign Research Institute Recruitment Program through the National Research Foundation (NRF) of Korea funded by the Ministry of Education, Science and Technology (MEST)(2012K1A4A3053565).

- [1] X.Z. Yu et al, Nature **465** 901 (2010)
- [2] F. Jonietz et al, Science **330** 1648 (2010)
- [3] S. Heinze et al, Nat. Phys. **7** 713 (2011)
- [4] A. Fert et al, Nat. Nano **8** 152 (2013)
- [5] J. Sampaio et al, Nat. Nano **8** 839 (2013)
- [6] P. Fischer et al, JESRP **189** 196 (2013)

11:00am MI+MG-TuM10 Growth and Properties of Skyrmionic MnSi Nanowires and Thin Film on Silicon, *Jieyu Yi*, *S.W. Tang*, University of Tennessee, *I.I. Kravchenko*, *G.X. Cao*, Oak Ridge National Laboratory, *D.G. Mandrus*, University of Tennessee, *Z. Gai*, Oak Ridge National Laboratory

Magnetic skyrmion lattice, a vortex-like spin texture recently observed in chiral magnets, is of great interest to future spin-electronic data storage and other information technology applications. The origin of the magnetic skyrmion phase can be traced to the anti-symmetric Dzyaloshinski-Moriya (DM) interaction that is allowed in space groups lacking inversion symmetry. The combined effect of a large ferromagnetic exchange and a weak DM interaction is to twist the magnetization into a long-period spiral that can be tens to hundreds of nanometers in length. As these spirals are only weakly bound to the underlying lattice in cubic systems, they can be readily manipulated with modest applied fields. Prototypical materials with the skyrmion ordering are those compounds with B20 structure, like MnSi and FeGe. The skyrmion lattice in MnSi appears in a small region (known as the A phase) of the H-T phase diagram in bulk samples, but in 2D samples like thin films the skyrmion phase is much more robust. It is of great interest to determine the properties of the skyrmion phase in quasi-1D nanowires and 2D thin films. If skyrmion ordering can persist in one-dimensional MnSi nanowires and 2D films, then these systems may be very promising for spintronics applications as the magnetic domains and individual skyrmions could be manipulated with small currents. We have systematically explored the synthesis of single crystal MnSi nanowires via controlled oxide-assisted chemical vapor deposition and observed a characteristic signature of skyrmion magnetic ordering in MnSi nanowires.

* Falicov Student Award Finalist

The SiO₂ layer plays a key role for the high yield, correct stoichiometric and crystalline growth of the B20 MnSi nanowires. A growth phase diagram was constructed. For the thin films, an unique growth receipt was developed for the growth of high quality of thin films. The structure and magnetic properties of the films at different thickness were studied.

11:20am **MI+MG-TuM11 Depth Dependent Mapping of Valence and Other Factors in LaSrMnO₃/PrZrTiO₃ Magnetolectric Heterostructures**, *Mikel Holcomb, C.-Y. Huang, R. Trappen, J. Zhou*, West Virginia University, *Y.-H. Chu*, National Chiao Tung University, Taiwan, Republic of China

Our group focuses on the ability to study the unique properties occurring at material surfaces and interfaces. One of the most interesting types of interfaces are magnetolectric, because they offer the ability to electrically control magnetism or vice versa. This magnetolectric control offers potential advantages in computing, magnetic sensors, energy scavenging and more. Magnetolectric interfaces offer advantages over single layer magnetolectrics as the ordering temperatures can be above room temperature and the coupling can be significantly stronger. Despite these advantages, the mechanism responsible for magnetolectric coupling is currently unknown, which limits our ability to improve these systems to the parameters required for applications. In order to understand the mechanism for magnetolectric multilayers, we investigated LaSrMnO₃ on PbZrTiO₃. By varying the sample thickness and utilizing both surface and bulk sensitive synchrotron radiation techniques, we are able to map out the Mn valence throughout the LaSrMnO₃ layer. We have also studied how strain and magnetization change with layer thickness. I will discuss our how results enable us to understand the charge origin of magnetolectric interfaces.

11:40am **MI+MG-TuM12 Strain Measurements in LaSrMnO₃/PbZrTiO₃ Magnetolectric Heterostructures**, *Chih-Yeh Huang, J. Zhou*, West Virginia University, *Y.-H. Chu*, National Chiao Tung University, Taiwan, Republic of China, *M.B. Holcomb*, West Virginia University

LaSrMnO₃/PbZrTiO₃ (LSMO/PZT) magnetolectric heterostructures make them attractive not only for data storage applications but also for studying strain measurements. There are many reasons why LSMO/PZT magnetolectric heterostructures were selected for our studies such as the excellent lattice matching and high ordering temperatures. X-ray micro diffraction technique is used to observe local strain behavior at the interface of LaSrMnO₃/PbZrTiO₃ magnetolectric heterostructures. Due to high spatial resolution in X-ray spot size (~1 μm) laterally, the observation of strain measurements in thickness-dependent PbZrTiO₃ reveals shiftings of LSMO and PZT peaks, allowing an understanding of the behavior of strain at the interface which can be related to the mechanism of magnetolectric coupling.

12:00pm **MI+MG-TuM13 Bit-Patterned Media Using Block Copolymer Templating on FePt**, *S. Gupta, H. Su, Allen Owen, R. Douglas*, University of Alabama

Block copolymer (BCP) templating has been used to pattern perpendicular magnetic anisotropy media. Large-area arrays of magnetic dots with diameter of ~30nm have been obtained by BCP templating in FePt films. FePt was deposited by dc cosputtering of elemental targets and in situ annealing in the sputtering system at 550°C for 1hr. The polystyrene polyferrocenyldimethylsilane (PS-b-PFS) was spin-coated onto the film and annealed to cause phase separation, followed by oxygen plasma treatment to remove the polystyrene matrix and expose the PFS nanospheres[4]. The FePt films were subsequently etched using an ion mill. Then post-patterning annealing at 600°C was also performed to reverse the ion damage of the film. SEM and XRD were utilized to characterize the morphology and structural properties respectively, while magnetometry was carried out to show the magnetic properties. Response surface methodology was performed to optimize the power, etching time and etching angle of the block copolymer mask and magnetic film. The effects of these patterning parameters on structural and magnetic properties were discussed.

Nanometer-scale Science and Technology Room: 304 - Session NS+HI-TuM

Nanopatterning and Nanolithography

Moderator: Nancy Burnham, Worcester Polytechnic Institute, Leonidas Ocola, Argonne National Laboratory

8:00am **NS+HI-TuM1 Nanoetching and Characterization Towards sub-5 nm Patterning**, *Deirdre Olynick, D. Staaks, D. Tierno, S. Dallarto, S. Sassolini, B. Muddiman, Z. Lui, G. Calafiore*, Lawrence Berkeley National Laboratory, *X. Gu, T.P. Russell*, University of Massachusetts, Amherst, *M. Kocsis*, Inpria Corporation

INVITED

Plasma etching is the ubiquitous method for high-resolution pattern transfer in semiconductor and related technologies. As lithographic techniques advance towards 5 nm half-pitch for applications in storage media, nanoelectronics, and plasmonic based devices, plasma etching processes must follow suit. This brings enormous and arguably insurmountable challenges using typical plasma hardware. For instance, very high etching selectivity must be achieved to accommodate mask heights (~1-2 times the feature size) which must shrink to mitigate pattern collapse in the lithographic and etching steps. In addition, line edge roughness at down to sub 1 nm levels must be achieved. To meet these enormous challenges we are investigating etching processes with temperatures down to -140 °C. Low temperature etching was first introduced by Tachi.¹ Lower etching temperatures can bring benefits such as higher selectivity processes, larger process windows, and reduced plasma damage which will be important for achieving sub-5 nm features.

We will discuss nanoscale cryogenic etching work in silicon, chromium, and silicon dioxide. With careful micron and deep nanoscale etching we show that cryogenic temperature etching of silicon, previously studied in great detail at the micron scale,^{2,3} can provide extreme selectivity and anisotropy at the nanoscale even with soft masks derived from block copolymer lithography. Selectivity is enhanced while maintaining pattern verticality because resist etch rates decrease as temperature is lowered. Changing to a chromium hardmask increases selectivity towards deeper sub-10 nm features at 20:1 aspect ratios. Studies of chromium etching show a temperature dependent etch rate that can be used to enhance profile control and limit mask undercut, necessary when nanometer controlled is required. Finally, we will discuss investigations into reduced temperature silicon dioxide etching for applications in patterned media and vertical NAND.

References:

1. S. Tachi, K. Tsujimoto and S. Okudaira, Appl. Phys. Lett. (8), 616-618 (1988).
2. X. Mellhaoui, R. Dussart, T. Tillocher, P. Lefauchaux, P. Ranson, M. Boufnichel and L. J. Overzet, J. Appl. Phys. (10), 104901-104910 (2005).
3. J. Pereira, L. E. Pichon, R. Dussart, C. Cardinaud, C. Y. Dulaud, E. H. Oubensaid, P. Lefauchaux, M. Boufnichel and P. Ranson, Appl. Phys. Lett. , 071501-071501-071503 (2009).

Acknowledgements: This work was supported in part by the U.S. Department of Energy, Office of Basic Energy Sciences, under contract DE-FG02-96ER45612 (X. D. and T. R.) DE-AC02-05CH11231 (D.O. and S.C.). Z. Liu was supported by Oxford Instruments Plasma Science Division.

8:40am **NS+HI-TuM3 Cut Patterning Challenges for the 14nm-Node and Beyond**, *Ryan Jung, J.R. Sporre, F.L. Lie, S. Kanakasabapathy, S. Sieg*, IBM Albany Nanotech Center, *A. Ranjan, S. Voronin, A. Raley, V. Rastogi, A. Ko*, TEL Technology Center, America, LLC, *D. Lee*, Samsung Electronics

In order to satisfy certain device architecture, fabrication of certain levels such as channel and gate is typically done by first forming line and space arrays, followed by removing or cutting some lines or parts of lines to form the final pattern. For instance, the method of Sidewall Image Transfer (SIT) patterning generates pairs of lines that are structurally connected at the line ends. Accordingly, the line/space patterning must be supplemented with a companion cut mask pattern to remove these undesired features. The cut mask, in addition to removing undesired features, also facilitates orthogonal line end control and dense array tip-to-tip control, such as in memory device, that cannot be achieved solely from lithography side using mask optical proximity control (OPC) and negative tone developed resist. With channel and gate pitch being scaled down to below 80nm, the ability to precisely place the cut mask edge and to control the line end taper angle has a direct impact on defectivity and yield. The ability to control the critical dimension of the cut opening has a direct impact on the tip-to-tip CD and device density. This paper evaluates the advantages, technical challenges,

and extendibility of various cut schemes for 14nm node and beyond, focusing on line edge profile and tip-to-tip control. This work was performed by the Research and Development Alliance Teams at various IBM Research and Development Facilities

9:00am NS+HI-TuM4 Nanopore Memristors: Sub-10nm Devices Built on Membranes Milled with a Helium Ion Microscope, Douglas Ohlberg, J.P. Strachan, W. Thompson, Z.Y. Li, R.S. Williams, Hewlett Packard

A novel platform has been developed to fabricate and study the performance of memristive devices smaller than 10 nm. The platform consists of free-standing silicon nitride membranes into which holes or pores with diameters ranging in size from 7nm – 50 nm have been milled with a helium ion microscope. In addition to serving as a substrate, the membrane also acts as an interlayer dielectric, and devices are fabricated by sequential deposition of materials above and below the membrane to fill the nanopore. Since deposition of the layers does not require intervening exposures to resists, developer solutions, or plasma cleans, all interfaces are clean and free of contaminants that would otherwise degrade device operation. This approach enables the compositional engineering of ideal device stacks at the nanometer scale decoupled from the problems often introduced by conventional lithographies. Working memristors are demonstrated that have been successfully fabricated around nanopores with diameters as small as 7nm. In addition, we demonstrate, how the sidewall profiles of the nanopores can be engineered in a variety of shapes from conical to hour glass by the deposition, prior to helium ion milling, of materials on the membrane that influence the scattering dynamics of the ions during milling.

9:20am NS+HI-TuM5 Characterization of Cluster-Based High-Resolution Inorganic Resists, Rose Ruther, R.P. Oleksak, R. Frederick, B.T. Flynn, G.S. Herman, Oregon State University

Both near- and long- term challenges for nanomanufacturing require significant advances in lithography to obtain sub-ten nanometer half-pitch. One approach to meet these challenges is through inorganic resists based on clusters and nanoparticles. Inorganic resists are of considerable interest due to the potential for both high resolution and low line width roughness (LWR), but generally suffer from low sensitivity. Recently, incorporation of radiation sensitive ligands into inorganic resists has enabled significantly improved sensitivity. For example, we have demonstrated the use of H₂O₂ as a radiation sensitive ligand for resists based on inorganic nano-clusters with the general formula, Hf(OH)_{4-2x-2y}(O₂)_x(SO₄)_y·qH₂O (HafSOx). By including H₂O₂ the HafSOx has significantly improved sensitivity to extreme UV photons and electrons, while still displaying high-resolution and low LWR.

In this presentation we characterize key steps in the lithographic process to gain insight into the nanodimensional patterning of HafSOx. Dynamic light scattering (DLS) and transmission electron microscopy (TEM) confirm the presence of nanoscale particles in the precursor solutions. TEM is further used to characterize cross-sections of spin-coated HafSOx films before and after pattern exposure and development. Combined with energy dispersive X-ray spectroscopy (EDS) this allows for *in situ* investigations of the dynamic nature of both structural and compositional properties with electron exposure pertinent to the patterning process. In particular, oxygen species are found to be very mobile during TEM analysis and migrate to the Si interface with an associated densification of the HafSOx film. Cross-sectional TEM of patterned lines down to approximately 10 nm half-pitch provides unique information on pattern profiles and reveals the presence of inter-line residual material consisting of discrete structures consistent with solution species. Both temperature programmed desorption (TPD) and electron stimulated desorption (ESD) are used to characterize the key desorption species that occur during thermal and radiative processes during patterning. ESD indicates that the peroxy species have radiation sensitivity, where the primary desorption products are O₂ and H₂O. We find that the time evolution of the O₂ and H₂O desorption yields indicate much faster kinetics for O₂ desorption, suggesting that the formation of the insoluble oxide network is driven initially by desorption of peroxide groups as opposed to thermal dehydration. These data provide insight into the radiation-induced changes responsible for the contrast mechanism of this system.

9:40am NS+HI-TuM6 Development Characteristics of PMMA in Alternative Alcohol:Water Mixtures, Leonidas Ocola, Argonne National Laboratory

In the past decade there has been a shift from toxic solvents used in lithography processing towards more environmentally safer chemicals. The most widely used resist in electron beam lithography is polymethylmethacrylate (PMMA). The standard developer is a solution mixture of isopropanol (IPA) and methyl isobutyl ketone (MIBK) in a ratio of 3:1. The Globally Harmonized System (GHS) Classification for MIBK

includes the following entries: Flammable liquids (category 2), Acute toxicity, Oral (Category 5) and Inhalation (Category 4). The most popular environmentally friendly alternative is an IPA and water (H₂O) solution in a ratio of 7:3. Excellent results have been published using this developer. The mechanism of why this solution works, given the fact that pure IPA and pure H₂O do not develop exposed PMMA is not well understood. Furthermore, the IPA GHS Classification the following entry: Specific target organ toxicity - single exposure (Category 3), central nervous system. Our research is focusing on shedding light onto what would be the interaction of water with similar alcohols, such as methanol and ethanol, and environmentally safer alternatives to IPA. This turns out to be Ethanol. The only Ethanol GHS Classification entry is: Flammable liquids (Category 2). We find that ethanol water mixtures exhibit excellent contrast, sensitivity, and resolution, and should be considered as one of the most environmentally safe viable developer solution for PMMA. We will present results pertaining on our best lithography results using Ethanol:water solutions, and a possible explanation on the role of the water:alcohol interaction with the exposed PMMA resist. We do not believe it is just an issue of cosolvency but more of a localized molecular interaction. The goal of better understanding of this interaction is to help find safer developers for other resists that rely on solvent based development.

This work was supported by the Department of Energy under Contract No. DE-AC02-06CH11357. Use of the Center for Nanoscale Materials was supported by the U. S. Department of Energy, Office of Basic Energy Sciences, under Contract No. DE-AC02-06CH11357.

11:00am NS+HI-TuM10 Room Temperature Electron Beam Assisted Oxygen Purification of Electron Beam Induced Pt Deposits: Towards Pure and High-Fidelity Nanostructures, Brett Lewis, M.G. Stanford, University of Tennessee, H. Plank, Graz University of Technology, Austria, J.H. Noh, University of Tennessee, J. Fowlkes, Oak Ridge National Laboratory, P.D. Rack, University of Tennessee

Electron Beam Induced Deposition (EBID) is a direct write mode capable of fabricating highly precise nanoscale structures by employing a scanning electron beam to disassociate adsorbed precursor molecules which subsequently condense on a substrate. The major drawback of the EBID process is that high purity metallic deposition is rarely achieved due to residual impurities attributed to the inadequate disassociation of the precursor molecule remaining in the final structure. Thus, purification strategies for nanoscale EBID deposits has been a critically important research area as EBID is poised to impact many nanoscale science and technology applications. To this end, our recent work has been focused on the post-deposition purification of EBID structures. We demonstrate a room temperature purification method in which platinum-carbon nanostructures deposited from MeCpPtIVMe₃ are purified by the presence of oxygen gas during a post-electron exposure treatment. Deposit thickness, oxygen pressure and oxygen temperature studies suggest that the dominant mechanism is the electron stimulated reaction of oxygen molecules adsorbed at the defective deposit surface. In this presentation we will overview the electron-stimulated reaction regimes as a function of oxygen partial pressure and temperature, and electron beam current and energy. We will overview electron stimulated reaction and adsorption/diffusive transport models to demonstrate that, for our experimental regime, we believe the rate-limiting mechanism is oxygen adsorption/transport. In addition to purification, the post-deposition electron stimulated oxygen purification process enhances the resolution of the EBID process due to the carbon removal of the as-deposited materials. Notably, pure platinum deposits with low resistivity and retain the original deposit fidelity were accomplished at room temperature.

11:20am NS+HI-TuM11 Prospects for Nanofabrication using the Combination of STM-based Depassivation Lithography, Selective ALD, and Material Etch Processes, Joshua Ballard, Zyvex Labs, S. Anz, S. Sando, Systime, Inc., M. Bischof, University of North Texas, D. Dick, University of Texas at Dallas, J. Fu, National Institute of Standards and Technology (NIST), D. Jaeger, University of North Texas, R. Longo, University of Texas at Dallas, J. Owen, E. Fuchs, Zyvex Labs, S. McDonnell, University of Texas at Dallas, R. Reidy, University of North Texas, Y.J. Chabal, R.M. Wallace, University of Texas at Dallas, J. Randall, Zyvex Labs, A. Cherala, S. Singhal, S. Sreenivasan, University of Texas at Austin

Attaining the capability to produce top-down designed nanostructures at sizes and precisions at the nanometer and atomic scales will enable new classes of research into material and device behavior. First demonstrated in the mid-1990s, Scanning Tunneling Microscopy (STM) based hydrogen depassivation lithography has been shown to allow selective functionalization of surfaces with many types of molecules and materials with near absolute precision. Recently, selective Atomic Layer Deposition (ALD) of titania has also been demonstrated on such a functionalized surface, with the deposited material behaving as an etch mask in 3-D

nanostructure formation. This results in a process that combines the high precision of STM with standard processing techniques to produce 3-D structures.

Already, 3-D structures with arbitrary shapes with full-pitches down to 13 nm have been fabricated using this process. This work will describe this process as well as provide an overview of the problems that need to be addressed to further reduce the minimum feature size and improve precision. Given the current and near term limitations of the process, classes of devices that have been and are possible to be fabricated will be described, including designed quantum dots, photonic structures, and NEMS apparatuses. Finally, pathways for scalability will be discussed.

Plasma Science and Technology

Room: 308 - Session PS-TuM

Plasma Surface Interactions I

Moderator: Jane P. Chang, University of California at Los Angeles

8:00am **PS-TuM1 Directed Irradiation Synthesis: Manipulating Matter in Nanoscale Self-Organized Systems.** *Jean Paul Allain, Z. Koyun, B. Holybee, S. Arias*, University of Illinois at Urbana-Champaign **INVITED**
Deciphering self-organization mechanisms of nanostructures (e.g. nanodots, ripples) on compound semiconductors and silicon via low-energy ion-beam assisted plasma irradiation is critical to manipulate functionality in nanostructured systems. By operating at ultra-low energies near the damage threshold, irradiation-driven defect engineering can be optimized (e.g. 10-500 eV). Tunability of optical, electronic, magnetic and nuclear detection properties is realized by reaching metastable phases controlled by irradiation. This talk summarizes emerging research that exploits irradiation-driven materials modification with applications in: nanophotonics, nanoelectronics, biomaterials and nuclear detection. Furthermore advances of in-situ analysis conducted during modification to correlate tunable irradiation synthesis and device performance will be summarized.

8:40am **PS-TuM3 Contact Resistance Degradation Caused By Plasma Charging of Silicon on Insulator During Contact Etch.** *Todd Bauer, J.F. DiGregorio, R.L. Jarecki Jr.*, Sandia National Laboratories

Contact formation is of enduring importance to integrated circuit manufacturing. A typical contact etch process uses fluorocarbon plasmas to etch small diameter, high aspect ratio holes through deposited silicon dioxide, landing on silicide. Contact etch processes provide high etch rate selectivity due to fluorocarbon polymer deposition on non-oxide surfaces. This selectivity is necessary for bi-level contacts landed on gates and active Si but the interactions among etching, deposition, and the structures being formed are complex and given to non-obvious failure modes. In this presentation we report on the characterization of a failure mode in which contacts to device Si on silicon-on-insulator (SOI) wafers form voids between the interconnect plug and the underlying silicide after thermal stress. The initial parametric signature was an increase in contact resistance for Kelvin structures of a specific design. From a nominal resistance of 2.5Ω, resistance increases by a factor of 3 were common. Through destructive physical analysis we correlated the increase in Kelvin resistance to the formation of small voids at the base of the Kelvin contact. We developed the following model to describe the condition that leads to the voids. As the contact etch reaches the Si surface, the potential at the bottom of the hole shifts abruptly from equilibrium, balancing electron and ion currents, to a more positive potential. This positive potential suppresses ion bombardment at the base of the contact, reducing etch rate and allowing more fluorocarbon polymer to accumulate. Electron current to the bottom of the hole increases to equilibrate the disturbed potential, but is limited by electron shadowing and the available contact hole area. The duration of the excess positive potential is proportional to the specific capacitance of the revealed Si surface, which, for islands on SOI wafers with shallow trench isolation, may be thousands of times larger than an equivalent bulk wafer. Smaller contact area (i.e. fewer contact holes) in a single island exacerbates the transient potential duration and the resulting etch process disturbance. We developed test structures and executed experiments to explore the transient potential concept and the local Si capacitance relative to the open contact area. Without adequate mitigation, the accumulated polymer leads to a weakened interconnect interface that is vulnerable to voiding and delamination.

Sandia is a multiprogram laboratory managed and operated by Sandia Corporation, a Lockheed Martin Corporation, for the United States

Department of Energy's National Nuclear Security Administration under contract DE-AC04-94AL85000.

9:00am **PS-TuM4 3D Modeling of SiN Etching by Hydrofluorocarbon Plasma.** *Nobuyuki Kuboi, T. Tatsumi, T. Kinoshita, T. Shigetoshi, M. Fukasawa, J. Komachi, H. Ansai*, Sony Corporation, Japan

Silicon nitride (SiN) is as essential as silicon (Si) and silicon oxide (SiO₂) for fabricating complementary metal oxide semiconductor (CMOS) devices. Damage on Si substrates is caused during etching of the transistor side-wall and the contact through the drain region [1], and this can greatly affect transistor properties. Hence, for CMOS devices to achieve high performance, it is important to control the etching process quantitatively along with the mechanism of the SiN surface reaction.

We propose a surface reaction model for the SiN etching process by fluorocarbon (C₄F₈/O₂/Ar) and hydrofluorocarbon (CH₂F₂/O₂/Ar) plasma based on the Slab model of SiO₂ [2]. The surface layer is assumed to consist of two layers: a reactive layer divided by several thin slabs and a deposited C-F polymer layer on the reactive layer. We considered physical and chemical reactions in detail including reactivity of radicals (C, F, O, and H), dangling bonds ratio, outflux of N, and generation of by-products (HCN, C₂N₂, CH, CF₂, SiF₂, and SiF₄) as ion assist, which depend on process parameters. We confirmed that absolute values and trends of SiN etch rate, polymer thickness, damage thickness, and selectivity of SiN/SiO₂ and SiN/Si along with gas flow rates of C₄F₈ and CH₂F₂ were consistent with experimental data of conductively coupled plasma.

Furthermore, to analyze 3D damage distribution affected by the etched profile, we developed a new 3D simulation technique using an extended voxel model (called "smart voxel") also including the above Slab model. By using gas fluxes with local pattern effect, the Slab model is solved at each voxel. Then, the etch rate and thicknesses of polymer and damage are derived. Smart voxel has details of the history of the etching situation and gives them around existing voxels when etch front is evolved in the next calculation time step. By repeating these procedures, 3D damage distribution considering a time-dependent etched profile can be realized. In addition to this new concept, modeling of gas transportation in the pattern treated as fluid is adopted without interaction between voxels, which is different from a Monte Carlo (MC) method. Hereby, 3D damage for multi-layer (Si/SiN/SiO₂) can be predicted much faster and more accurately than the conventional MC model in spite of a large scale micro-meter. We will show a 3D etched profile and damage distribution for SiN side-wall etching and discuss how to control etching parameters to achieve low damage.

Acknowledgements: We thank Prof. S. Hamaguchi for stimulating discussion.

[1] K. Katahira *et al.* *J. Vac. Sci. Technol.* **A27**, (2009) 844.

[2] N. Kuboi *et al.* *Jpn. J. Appl.* **50**, (2011) 116501.

9:20am **PS-TuM5 Study of Plasma-Surface Interaction in HBr/Cl₂/O₂ ICP.** *Ashutosh Srivastava*, University of Houston, *T. Ohashi*, Hitachi High-Technologies, *V.M. Donnelly*, University of Houston

HBr plasmas are used to etch Si, as well as GaN, PZT, InP, Indium Zinc Oxide and other materials. In Si etching, HBr plasmas create better anisotropic profiles than Cl₂ plasmas, with better selectivity toward SiO₂. Selectivity can be further improved by adding oxygen to the plasma. The feed gas composition of HBr/Cl₂/O₂ plasmas is optimized to best meet the needs of the particular application. Keeping such a complex process stable over time requires tight control over all plasma parameters, including reactor wall conditions. Here, we have studied the interaction of HBr/Cl₂/O₂ inductively-coupled plasmas (ICP) with the etching products-coated reactor walls, using the "Spinning Wall" technique. Surface composition was determined by Auger electron spectroscopy, and species desorbing from the surface were detected by quadrupole mass spectrometry. It was observed that in a pure HBr ICP with no Si etching, an oxygen plasma-conditioned surface SiO_x layer remained unaltered, indicating the inability of Br-containing species to break the Si-O bond. When 5-50% oxygen was added to HBr ICPs, large fluxes of H₂O were found to desorb from the spinning wall surface, peaking at ~20% O₂. The H₂O signal dependence on spinning wall rotation frequency indicates that the reaction time, and/or water retention time on the surface is of the order of 10's of ms. After turning off the plasma, signal could be detected for several minutes. This is likely because of the highly disorder surface, leading to a stretched exponential decay of water desorption. Addition of Cl₂ to an HBr ICP (1:1 ratio) resulted in small amount (<3%) of Cl on the surface but no Br. This Cl was not removed by a pure HBr ICP, but was in an O₂ ICP. When a self-bias of -120Vdc was applied to the Si substrate in an HBr ICP, a Si:O:Br layer (32:7:60) was deposited on the spinning wall surface. As O₂ was added, the surface composition changed from a Br-rich layer at 6% O₂ to an O-rich layer at 20% O₂. Si etching in a Cl:HBr ICP (1:1) resulted in equal amounts of Cl and Br on the surface. Again, when O₂ is added the surface transitions

from Cl-rich at 6% O₂ to Cl/O-rich at 20% O₂ and finally to O-rich at 40% O₂.

9:40am **PS-TuM6 Experimental Evaluation of Ta Film Etching Characteristics by CO⁺ Ion Irradiation**, *Makoto Satake*, Hitachi, Japan, *H. Li, K. Karahashi, S. Hamaguchi*, Osaka University, Japan

Magnetic Random Access Memory (MRAM) is considered as a promising candidate for the next generation memory because of its non-volatility, fast reading or writing speed, and high write-cycle endurance. MRAM consists of magnetic tunnel junctions (MTJ) and CMOS devices. One of the issues concerning MRAM fabrication is the development of a nano-scale anisotropic etching technology for MTJ because an MTJ is used as the memory component of an MRAM device and high integration of MTJs is required for commercially competitive MRAM chips. One approach to MTJ etching is to use CO/NH₃ plasmas with Ta hard masks. With this process, vertical etching profiles with a taper angle of 80° have been achieved with high etching selectivity of magnetic materials over Ta [1].

In previous research [2], etching yields of Ta and Ni films were evaluated with a mass-selected ion beam system with incident ions of Ar⁺, N⁺, O⁺, and CO⁺. It has been found from X-ray photoelectron spectroscopy (XPS), for example, that the Ta film surface was oxidized while the Ni film surface was not oxidized by the same CO⁺ ion irradiation. Therefore, it was concluded that the oxidized layer of Ta, which was formed by CO⁺ irradiation, suppressed the Ta etching yield.

In this study, Ta etching yields by CO⁺ ions were compared with corresponding theoretical values of physical sputtering of Ta to understand why the Ta etching yield by CO⁺ ion irradiation was typically very low. The experimentally obtained sputtering yield is typically about 1 % of the theoretical yield of physical sputtering by non-reactive incident species of the same mass. Our XPS analysis of Ta after CO⁺ ion irradiation indicates that the Ta film is highly oxidized (i.e., to the equivalent degree of Ta₂O₅) by CO⁺ ion irradiation while Ar⁺ ion irradiation of a Ta oxide film reduces its oxidation degree. Therefore the low Ta etching yield by CO⁺ ion irradiation is caused by a larger amount of oxygen supply by incident CO⁺ ions with less oxygen sputtering. The dependence of the Ta sputtering yield by CO⁺ ions on the ion incident angle will be also discussed in terms of the angle dependence of the surface oxidation level.

[1] N. Matsui, et al., *Vacuum* **66**, 479-485 (2002).

[2] H. Li, et al., *AVS 60th Int. Symp* (2013).

11:00am **PS-TuM10 Study of Hydrofluorocarbon Precursor Parameters for Plasma Etching of ULK Dielectric**, *Chen Li, G.S. Oehrlein*, University of Maryland, College Park, *R. Gupta, V. Pallem*, Air Liquide

Plasma etching of ultra-low k (ULK) dielectrics requires gas precursors that enable very high etching selectivity of ULK over the mask and underlayer while minimizing ULK sidewall damage. We report a systematic study aimed at evaluating the impact of the nature of hydrofluorocarbon gas precursors on plasma etching performance of a representative ULK material, Black Diamond II (BDII) coated onto Si. The work was performed in a dual frequency capacitively coupled plasma (CCP) reactor with real-time characterization by ellipsometry, optical emission spectroscopy (OES), and electrical measurements. The chemical composition of deposited films and post plasma low-k surfaces was examined by X-ray photoelectron spectroscopy (XPS). Etching selectivity of BDII over amorphous carbon (aC), SiO₂ and Si₃N₄ masking materials was evaluated. The impact on the ULK material when exposed under sidewall-like plasma conditions was also studied for various precursor gases using the dilute HF etching method. The precursor gases studied included fluorocarbon (FC) and hydrofluorocarbon (HFC) precursors whose molecular weights and chemical structures were systematically varied i.e. fluorine/carbon ratio, presence/absence of carbon double bonds, and ring versus linear structure. The plasma process conditions were Ar with FC (or HFC) and O₂ admixture at a fixed total pressure with varying ion energies. The etch rate (ER) and deposition rate (DR) were measured by *in-situ* ellipsometry. We found that the DR was greater for precursors with a larger degree of unsaturation. Linearly shaped gases with higher F/C ratio showed the best etching performance, evaluated by the maximum value of product of BDII ER and BDII/aC selectivity value for each gas. By relating measured CF₂ optical emission for varying precursor concentrations to simultaneously determined FC (or HFC) film DR, we distinguished three deposition behaviors with qualitatively different etching performance based on the precursor structure. A gap structure, blocking direct ion bombardment, was used to simulate the sidewall plasma environment. With this approach, the evolution of the physical and chemical sidewall profile can be studied in real time using *in-situ* measurements. We found that gases exhibiting a particular deposition behavior differed systematically in formation/absence of a protective fluorocarbon film on the ULK sidewall. The dependence of improvements

in low-k etching performance on the FC chemical structures and the surface model for underlying mechanisms relating these properties will be reported.

11:20am **PS-TuM11 Characteristics of Reactive Ion Etching Processes for ITO and ZnO**, *Hu Li, K. Karahashi*, Osaka University, Japan, *M. Fukasawa, K. Nagahata, T. Tatsumi*, Sony Corporation, Japan, *S. Hamaguchi*, Osaka University, Japan

With the increasing demand for high-resolution optoelectronic devices and their applications, micro-pattern formation of transparent conducting oxides (TCOs), especially that of tin-doped indium oxide (ITO), has been required more frequently than before in the development of such devices. Since ITO contains indium, which is one of minor metals whose global production is typically small and are generally traded at high prices, less expensive alternative materials for TCOs are highly sought after. Zinc oxide (ZnO) is a possible candidate for such TCOs alternative to ITO.

Micro-pattern formation of thin film materials may be achieved by reactive ion etching (RIE), which uses chemically reactive plasmas that typically allow high selectivity of etching of specific materials over others and high controllability of micro/nano-scale structure formation. RIE has been widely used in fabrication processes of semiconductors. For high-resolution optoelectronic devices, there has been a considerable demand for RIE processes of ZnO with CH₄ based plasmas, which is a non-corrosive gas and expected to yield high etching rates for ZnO. The RIE process of ZnO with CH₄ based plasmas, however, has also various problems such as carbon deposition during the etching processes. To further develop RIE technologies of ZnO by CH₄ based plasmas, a better understanding of elemental processes of plasma-surface interactions of CH₄ based plasmas with ZnO.

In this study, sputtering yields and surface reaction characteristics of ITO and ZnO by energetic chemically reactive CH_x ions (CH⁺ and CH₃⁺) as well as inert-gas ions (Ar⁺, Ne⁺ and He⁺ ions) were examined with the use of a mass-selected ion beam system. It has been found that, for physical sputtering, sputtering yields of ZnO are much higher than those of ITO. For ZnO, etching by CH₃⁺ proceeds faster than Ar⁺ physical sputtering, which indicates that the etching rate is enhanced by chemical interactions of CH_x⁺ with ZnO. The chemical effect is more pronounced at a lower incident energy. With a fewer hydrogen atoms in the incident ion (i.e., in the case of CH⁺ ion incidence), however, carbon deposition tends to take place on the ZnO surface. Similar beam-surface interactions of ITO with CH_x ions as well as inert-gas ions were also examined and compared with those of ZnO. Mechanisms of chemical reactions of CH_x ions with ZnO and ITO will be discussed in the presentation.

11:40am **PS-TuM12 Selective Etch and Functionalization of Coblock Polymers**, *Evgeniya Lock, S.G. Walton*, Naval Research Laboratory

Coblock polymers have been applied as nanotemplates for production of nanocomposites and biomolecules nanoarrays due to their ability to spontaneously form dense periodic spherical, cylindrical, and lamellar domains. The final nanostructure is typically produced after chemical etch or dry plasma-based etch in fluorine containing gas environment. However, systematic studies of the effects of plasma etching of coblock polymers in different gas environments are limited. Furthermore, selective chemical functionalization of one of the blocks, while the other one is etched will enable more robust biomolecules/nanoparticles integration and is of critical importance. In order to achieve nanoscale high resolution etch, a precise control of the plasma/surface interactions is needed.

We have already shown that electron beam-generated plasmas can introduce large range of chemical functionalities in a polymer surfaces and etch polymers with low etch rates [1, 2]. In this work, we will show the ability of these plasmas to achieve nanoscale etch of PS-b-PMMA in different gas environments. In addition, the effect of ion energy (1 to 100 eV) on features definition and etch depth will be evaluated. This work was supported by the Naval Research Laboratory Base Program.

References:

1. E. H. Lock, D. Y. Petrovykh, P. Mack, T. Carney, R. G. White, S. G. Walton and R. F. Fernsler, "Surface composition, chemistry and structure of polystyrene modified by electron-beam-generated plasma", *Langmuir*, **26** (11), 8857 (2010).
2. E. H. Lock, S. G. Walton and R. F. Fernsler, "Physio-chemical modifications of polystyrene and polypropylene surfaces by electron beam-generated plasmas produced in argon", *Plasma Process. Polym.* **6** (4), 234 (2009).

12:00pm **PS-TuM13 Dry Etch Process Development for PMMA Removal Selectively to PS for sub-10nm Patterning.** *Aurelien Sarrazin, P. Pimenta-Barros, N. Posseme, S. Barnola, A. Gharbi, R. Tiron, CEA, LETI, MINATEC Campus, France, C. Cardinaud, CNRS-IMN, France*

For sub-10nm patterns, the semiconductor industry is facing the limits of conventional lithography to achieve narrow dimensions. Presently, extreme ultraviolet lithography (EUV) is under development but this technology is not mature. On another hand, multiple patterning, which benefits from a tremendous technological knowledge in conventional lithography, deposition and etching processes, could be an alternative technique but its major drawback is the complexity of integration generating wafer cost increases. These issues encourage the development of limitless resolution and low cost techniques such as Directed Self Assembly (DSA). Indeed, DSA is one of the promising solutions to reach sub-10nm patterns with a high selectivity.

One challenge of DSA integration is the PMMA removal selectively to PS. Using dry etch for this step is mandatory for line application since wet cleaning is prohibited with the risk of pattern collapse. In this work we propose to study PMMA block plasma etching with a high selectivity over PS using oxidizing and reducing chemistries. All experiments have been carried out in a CCP etching chamber.

First a screening of these chemistries has been performed on PS and PMMA films showing that CO based chemistry is the most interesting process providing infinite selectivity to PS. To achieve this result, studies have been performed with different gases to evaluate the evolution of etch rate with the process time. Complementary analyses using X-ray Photoelectron Spectroscopy (XPS), Fourier Transform Infrared Spectroscopy (FTIR) will also be presented for understanding volume and surface etch mechanisms.

These blanket results will be tested on lamellar block copolymers. The compatibility of these chemistries will be validated in term of etch rate, CD control using Scanning Electron Microscopy (SEM) and roughness using Atomic Force Microscopy (AFM). We will demonstrate that a trade-off is needed between high selectivity to PS and high etch rate to remove the PMMA.

Novel Trends in Synchrotron and FEL-Based Analysis

Focus Topic

Room: 312 - Session SA-TuM

Characterization of Nanostructured and LD Materials Using Synchrotron-Based Methods

Moderator: Maya Kiskinova, Elettra-Sincrotrone Trieste, Italy

8:00am **SA-TuM1 Analysis and Speciation of Nanoscaled Materials by Means of Grazing-Incidence and High-Resolution X-ray Spectrometry.** *Burkhard Beckhoff, M. Gerlach, I. Holfelder, P. Hoenicke, J. Lubeck, M. Mueller, A. Nutsch, B. Pollakowski, C. Streeck, R. Unterumsberger, J. Weser, Physikalisch-Technische Bundesanstalt (PTB), Germany INVITED*

The development of efficient nanoscaled materials requires the correlation of the materials' functionality with their chemical and physical properties. To probe these properties, analytical methods that are both sensitive and selective at the nanoscale are required. The reliability of most analytical methods relies on the availability of reference materials or calibration samples, the spatial elemental composition of which is as similar as possible to the matrix of the specimens of interest. However, there is a drastic lack of reference materials at the nanoscale. We address this challenge by means of a bottom-up X-ray analytical method where all instrumental and experimental parameters are determined with a known contribution to the uncertainty of the analytical results. This approach does not require any reference materials but a complete characterization of the analytical instruments' characteristics. X-ray spectrometric methods allow for the variation of the analytical sensitivity, selectivity, and information depth needed to effectively reveal the spatial, elemental, and chemical specimen parameters of interest. Examples of interfacial speciation, elemental depth profiling as well as layer composition and thickness characterizations in various nanoscaled materials will be given.

References

- [1] R. Unterumsberger, B. Pollakowski, M. Müller, and B. Beckhoff, *Anal. Chem.* 83 (2011) 8623
- [2] R. Unterumsberger, M. Müller, B. Beckhoff, P. Hönicke, B. Pollakowski, S. Bjeoumikhova, *Spectrochim. Acta B* 78 (2012) 37
- [3] F. Reinhardt, J. Osán, S. Török, A.E. Pap, M. Kolbe and B. Beckhoff, *J. Anal. At. Spectrom.* 27 (2012) 248

[4] A. Delabie, S. Sioncke, J. Rip, S. van Elshocht, G. Pourtois, M. Müller, B. Beckhoff, K. Pierloot,

J. Vac. Sci. Technol. A30 (2012), 01A127

[5] B. Pollakowski, P. Hoffmann, M. Kosinova, O. Baake, V. Trunova, R. Unterumsberger, W. Ensinger, and B. Beckhoff, *Anal. Chem.* 85 (2013) 193

[6] C. Becker, M. Pagels, C. Zachaus, B. Pollakowski, B. Beckhoff, B. Kanngießler, and B. Rech, *J. Appl. Phys.* 113 (2013) 044519

[7] C. Streeck, S. Brunken, M. Gerlach, C. Herzog, P. Hönicke, C.A. Kaufmann, J. Lubeck, B. Pollakowski, R. Unterumsberger, A. Weber, B. Beckhoff, B. Kanngießler, H.-W. Schock and R. Mainz, *Appl. Phys. Lett.* 103 (2013) 113904

[8] J. Lubeck, B. Beckhoff, R. Fliegau, I. Holfelder, M. Müller, B. Pollakowski, F. Reinhardt and J. Weser, *Rev. Sci. Instrum.* 84 (2013) 045106

[9] I. Holfelder, B. Beckhoff, R. Fliegau, P. Hönicke, A. Nutsch, P. Petrik, G. Roeder and J. Weser,

J. Anal. At. Spectrom. 28 (2013) 549

8:40am **SA-TuM3 X-Ray Photoemission Spectromicroscopy: Recent Achievements and Future Applications.** *Claus Schneider, Forschungszentrum Juelich GmbH, Germany INVITED*

Complex material systems play a pivotal role in many areas of modern technology, such as information storage and processing or energy conversion and storage. In particular, modern information technology exploits the full potential of very different material systems for the meticulous control of alternative state variables. These state variables are used to represent the individual information bits and may be electron charges in semiconductor nanoelectronics, electron spins in the case spintronics, or local redox configurations in resistive switching elements. Due to this broad range, the materials encompass intermetallic compounds, oxides or chalcogenides, elementary and compound semiconductors or even molecular components. In addition, the functional elements, for example, individual memory cells or transistor structures often involve nanometer dimensions and operate on nanosecond timescales or even below. This imposes considerable challenges on the characterization of electronic, chemical and magnetic states in the steady state or during operation.

Immersion lens microscopy with synchrotron radiation has matured into a versatile and powerful tool to investigate a broad range of issues in condensed matter physics and materials science. In its energy-filtered version photoemission microscopy combines high-resolution imaging with spectroscopic capabilities in a unique fashion, enabling access to valence and core electronic states. The excitation with photons ranging from the soft to the hard x-ray regime ensures element selectivity and variable information depth. Choosing the polarization state of the synchrotron radiation enables one to distinguish different states of magnetic order, such as ferro- and antiferromagnets. The intrinsic time structure of the synchrotron radiation permits the study of processes with picosecond time-resolution via pump-probe approaches.

This contribution will review the present status of x-ray photoemission spectromicroscopy with emphasis on applications in information technology. In particular, we will cover model systems in spintronics and in resistive switching [1,2]. The results address both static properties and dynamic processes. We will also discuss new developments, such as photoemission microscopy with hard x-rays and the implementation of imaging spin polarimetry.

Y. Aoki, et al., *Nat. Commun.* (2014) 3473.

C. Lenser et al., *Adv. Funct. Mater.* (2014) online publ.

9:20am **SA-TuM5 Growth and Characterization of Low Dimensional Materials for Applications in Energy and Sensor Devices.** *Andrea Goldoni, Elettra-Sincrotrone Trieste, Italy INVITED*

Nanostructured low dimensional systems, in particular carbon nanotubes and oxide nanopillars, have a number of aspects that make them suitable for applications in the fields of environmental gas sensors and energy devices. Here we present the growth and characterization of some nanostructures of interest [1-3] made by well-ordered tin oxide nanopillars on ITO and hybrid/functionalized carbon nanostructures, suitable both as electrodes for solar and electrochemical cells, as well as for extremely fast (and sensitive) gas sensors [4-6].

[1] S. Hofmann et al., "In-situ observations of catalyst dynamics during surface-bound carbon nanotube nucleation", *Nano Letters* 7, 602 (2007); C. Mattevi et al., "In-situ XPS study of catalyst-support interactions and growth of carbon nanotube forests", *J. Phys. Chem. C* 112, 12207 (2008).

[2] L. D'Arسيè et al., "Tubular Sn-Filled Carbon Nanostructures on Indium Tin Oxide: Nanocomposite material for multiple applications", *Carbon* 65, 13 (2013).

[3] P. Mbuyisa et al., "Controlled Synthesis of Carbon-Based Nanostructures Using Aligned ZnO Nanorods as Templates", *Carbon* 50, 5472 (2012).

[4] F.M. Toma et al., "Efficient Water Oxidation at Carbon Nanotube/Polyoxometalate Electrocatalytic Interfaces", *Nature Chemistry* 2, 826 (2010); S. Piccinin, et al., "Unifying Concepts in Water Oxidation Catalysis: Thermodynamic and kinetic pathways powered by a molecular, tetraruthenium-oxo complex as the blue-print of metal-oxide surfaces", *PNAS* 110, 4917 - 4922 (2013).

[5] F. Rigoni et al., "Enhancing the sensitivity of pristine carbon nanotubes to detect low-ppb ammonia concentrations in the environment", *Analyst* 138, 7392 (2013); F. Rigoni et al., "Water selective, high sensitivity gas sensors based on single-wall carbon nanotubes functionalized with indium tin oxide nanoparticles: towards low ppb detection of ammonia concentrations in the environment", submitted (2014).

[6] V. Alijani et al., "Extremely Sensitive and Fast Sensors Made of Vertical Nanostructures of SnOx on Indium Tin Oxide", submitted (2014).

11:00am **SA-TuM10 Novel 2D Electron Gases at the Surface of Transition-Metal Oxides: Role of Topology and Spin-Orbit Coupling**, **Andrés F. Santander-Syro**, Université Paris-Sud, France **INVITED**
Novel 2D electron gases at the surface of transition-metal oxides: role of topology and spin-orbit coupling

Andrés F. Santander-Syro
CSNSM – Université Paris-Sud (France)

Transition-metal oxides (TMOs) are correlated-electron systems with remarkable properties, such as high-temperature superconductivity or large magnetoresistance. The realization of two-dimensional electron gases (2DEGs) at surfaces or interfaces of TMOs, a field of current active research, is crucial for harnessing the functionalities of these materials for future applications. Additionally, these 2DEGs offer the possibility to explore new physics emerging from the combined effects of electron correlations and low-dimensional confinement.

Recently, we discovered that a 2DEG is simply realized at the vacuum-cleaved surface of SrTiO₃, a transparent, insulating TMO with a gap of 3.5 eV. We directly imaged its multiple heavy and light subbands using angle-resolved photoemission spectroscopy [1]. In this talk, I will show that one can also create and tailor 2DEGs in other TMO surfaces, opening vast possibilities for the study of correlations in low dimensions in materials showing diverse functionalities. I will first discuss the specific case of KTaO₃, a wide-gap insulator with a spin-orbit coupling 30 times larger than in SrTiO₃. I will show that quasi-2D confinement in this system results in comparable scales for the Fermi energy, the subband splitting, and the spin-orbit coupling, leading to a complete reconstruction of the orbital symmetries and band masses [2]. Then, I will show that by choosing various surface terminations of different symmetries one can modify the electronic structure of the 2DEGs at the surface of TMOs [3]. Additionally, I will discuss the experimentally observed effects of spin-orbit coupling in the 2DEG at the surface of SrTiO₃. All these results demonstrate that, in TMOs, the strong correlations, together with the electron confinement and the surface-lattice symmetry, can lead to novel states at the surface that are not simple extensions of the bulk bands.

- [1] A. F. Santander-Syro *et al.*, *Nature* **469**, 189 (2011).
[2] A. F. Santander-Syro *et al.*, *Phys. Rev. B* **86**, 121107(R) (2012).
[3] C. Bareille *et al.*, *Sci. Rep.* **4**, 3586 (2014).

11:40am **SA-TuM12 Effects of Interfacial Interaction: Electronic Structure of Graphene on Metallic and Insulating Surfaces**, **Petra Rudolf**, University of Groningen, The Netherlands **INVITED**

The interaction of graphene with substrates and its influence on the electronic properties is of paramount importance for designing novel electronic and optoelectronic devices. However, the capability of disentangling the surface contribution of the support from those of the graphene single layer is a challenging and unresolved problem. In this contribution I shall present results concerning the electronic states of a typical metallic interface, namely graphene/Cu, where the coupling is weak. These results will be compared to the electronic states of suspended graphene and graphene on an insulating substrate.

When the properties of the occupied electronic band structure were investigated by angle-resolved photoelectron spectromicroscopy, we demonstrated that a suspended CVD grown graphene membrane locally shows electronic properties comparable with those of samples prepared by micromechanical cleaving of graphite. CVD grown graphene on the Cu(111) surface was instead found to be slightly doped, while on an insulator surface it was demonstrated to fully preserve the intrinsic

properties, implying that the graphene monolayer is totally decoupled as if it were freestanding and not doped.

The unoccupied surface states at the weakly coupled graphene/Cu interface were studied by non-linear angle resolved photoemission spectroscopy. In particular, by comparing the band dispersion of the unoccupied image potential states and the occupied surface states of the interfaces graphene/Cu(111) and graphene/ polycrystalline copper foil, we were able to identify and characterise the Shockley surface state and the n=1 image state of the Cu(111) surface and the symmetric n=1 image state of the single layer of graphene.

Advanced Surface Engineering
Room: 302 - Session SE+NS+TR-TuM

Nanostructured Thin Films and Coatings
Moderator: Robert Franz, Montanuniversität Leoben,
Andrey Voevodin, Air Force Research Laboratory

8:00am **SE+NS+TR-TuM1 Electrostatic Coating with Ligandless Copper Nanoparticles**, **Lance Hubbard, A.J. Muscat**, University of Arizona

Physical vapor deposition is currently used to deposit copper seed layers in through Si vias, but this approach is already close to its limit and may not be an option for future scaling of high performance integrated circuits. An alternative is electroless deposition (ELD) since it produces conformal, selective coatings at low temperature. ELD occurs by chemical reduction of metal ions without an externally applied potential. In the conventional approach, a metal catalyst such as Pt, Pd, or Ni is used that can be both expensive and increase the resistance of interconnect lines. Previous work was done in an aqueous phase using a complexing agent or polymer to protect the particles. Good film continuity was demonstrated, but the sheet resistance was low.^{1,2} In this study, we report on a nonaqueous ELD process that uses a charge compensator, but not a ligand or complexing agent. The weak electrostatic attachment of the charge compensator to the ions and particles in solution and the high pH conditions improve the driving force for metal deposition. Si(100) coupons were hydroxylated using sulfuric acid-hydrogen peroxide mixture. The surface was terminated with an amine adhesion layer by immersion in a 4 mM solution of either (3-aminopropyl)-trimethoxysilane (APTMS) or (3-mercaptopropyl)-trimethoxysilane (MPTMS) in methanol followed by a 150°C anneal. Metal films were deposited by suspending samples in a bath made by dissolving Cu(II) chloride in ethylene glycol, which also served as the reducing agent, and adding 1-butyl-3-methylimidazolium tetrafluoroborate as a charge compensator. The surface plasmon resonance (SPR) peak of the Cu nanoparticles in the bath and film was at 585 nm. Light scattering measurements and transmission electron microscopy (TEM) images yielded a size distribution of 3.1±1.6 nm. The complex consisting of the Cu particle core and ion shell is attracted to the positively charged amine groups at high pH, and a thin metal film is deposited that is both continuous and cohesive. Annealing the coupons at 200°C in nitrogen promoted the formation of an electrically conductive film. Electron microscopy images of the coated substrates show a 20-50 nm thick film of 3 nm dia. particles; spectroscopic ellipsometry shows both bulk and nanophase properties. Four-point probe measurements of the films yielded electrical conductivities in the range 10⁵-10⁶ S/m (bulk Cu conductivity 4-6x10⁷ S/m).

References

- 1) 1) Armini and Caro, *J. Electrochem. Soc.* 2010, 157(1), D74-D80, doi: 10.1149/1.3258026.
2) 2) Inoue et al. *J. Electrochem. Soc.* 2012, 159(7), D437-D441, doi: 10.1149/2.070207jes.

8:20am **SE+NS+TR-TuM2 Electrically Stable Pt-ZrB₂ Nanocomposite Thin Films for High Temperature Applications**, **Julia Sell, D.M. Stewart, G.P. Bernhardt, D.J. Frankel, R.J. Lad**, University of Maine

Considerable cost savings could be achieved by incorporating high temperature sensors into high temperature machinery to optimize processes and monitor materials degradation. However, in order to achieve reliable sensor operation, the thin film electrodes, sensing elements, and packaging materials must remain stable over long times at high temperature. Metallic thin films, such as Pt, agglomerate and lose conductive pathways quickly when exposed to temperatures exceeding 700°C. In this work, we show that Pt-ZrB₂ nanocomposite films retain a continuous morphology and remain electrically conductive up to at least 1100°C in air. Nanolaminate Pt-ZrB₂ films comprised of ten alternating layers of Pt and ZrB₂ were deposited to a total thickness of 200nm at ambient temperature onto sapphire substrates using e-beam evaporation. Annealing the nanolaminate films above 800°C

in air causes intermixing, resulting in a nanocomposite Pt-ZrB₂ film architecture. Film electrical conductivities were measured using a 4-point probe as a function of time and temperature in air up to 1200°C. These results show that Pt-ZrB₂ nanocomposite films have conductivities in the 10⁶-10⁷ S/m range and remain stable above 1000°C, but that the overall conductivity and stability depends on the Pt-ZrB₂ layer thickness ratio. Analysis via x-ray photoelectron spectroscopy and x-ray diffraction indicates that both monoclinic and tetragonal ZrO₂ nanocrystallites are formed in the films during the annealing treatment, and they serve to hinder agglomeration of the Pt phase. Scanning electron microscopy shows highly conductive Pt-rich pathways in the films that coexist with the ZrO₂ phase. Some films were coated with an amorphous Al₂O₃ protective capping layer using atomic layer deposition (ALD), and this capping layer helped to limit oxygen diffusion into the films, thereby increasing the long term stability of film conductivity.

8:40am SE+NS+TR-TuM3 A Novel Reactive Plasma-Assisted Coating Technique (RePAC) for Thin BN/Crystalline-Si Structures and their Mechanical and Electrical Properties. *Koji Eriguchi*, Kyoto University, Japan, *M. Noma*, SHINKO SEIKI CO., LTD., Japan, *S. Hasegawa*, Osaka University, Japan, *M. Yamashita*, Hyogo Prefectural Institute of Tech., Japan, *K. Ono*, Kyoto University, Japan

Cubic boron nitride (c-BN) has attracted much attention as a hard coating film on cutting tools, owing to its high oxidation resistance and hardness—the second hardest material to diamond. Although various methods of forming c-BN films on various substrates have been proposed, the interface between c-BN and the substrate material was unstable against delamination and oxidation [1] after long-time machining and air exposure. In this study, we propose a novel reactive plasma-assisted coating technique (RePAC) for forming sub- μ m-thick BN film directly on crystalline Si substrates, where magnetically-confined high-density Ar/N₂ plasma was generated with a stable anodic current to promote the reaction between N radicals and B atoms evaporated onto a Si substrate placed on a sample stage [2]. Controlling substrate bias voltage V_{sub} in the RePAC, we fabricated various thin-BN/Si structures and identified a correlation among the properties such as mechanical hardness, friction coefficient, leakage current, and dielectric constants. TEM analyses revealed that nano-structures of the BN films were varied from bulk amorphous (a)-BN, layered hexagonal (h)-BN, to c-BN phase in turbostratic (t)-BN domain, in accordance with V_{sub} ($|V_{\text{sub}}|=10\text{--}120$ V). We speculate that bombardment of incident ions (Ar⁺ and/or N₂⁺) plays a key role in forming these characteristic features, in addition to stoichiometric N and B contents. Moreover, we clarified the high hardness (> 4000HK, by the Knoop indenter) and the dielectric constant higher than previously-reported values (10–20, by the electrical capacitance measurement) for the present thin c-BN/Si structure with anti-delamination feature after long-time air exposure. The obtained results suggest that the present BN film formed by the RePAC has wide applications not only as a hard coating film but also as a high dielectric-constant layer in electronic devices.

[1] For example, P. B. Mirkarimi *et al.*, Mater. Sci. Engin., **R21**, 47 (1997).

[2] M. Noma *et al.*, Jpn. J. Appl. Phys. **53**, 03DB02 (2014).

9:20am SE+NS+TR-TuM5 Multifunctional Protective Coatings for Aerospace Applications. *Etienne Bousser*, *L. Martinu*, *J. Klemberg-Sapieha*, Ecole Polytechnique de Montreal, Canada **INVITED**

Ever increasing technical, economic and environmental requirements give rise to situations where modern equipment and components are often pushed beyond the limits of their design capabilities. This frequently leads to tribological deficiencies, such as lubrication breakdown, excessive wear and tribo-corrosion, resulting in increased operational costs, decreased efficiency and premature failure. Therefore, appropriate material's selection for a given application must be guided by an accurate understanding of the intervening tribological processes while ensuring the maintained functionality of the surface for optimal application performance.

Solid Particle Erosion (SPE) occurs in situations where hard particles, present in the environment, are entrained in a fluid stream, and impact component surfaces such as in aircraft engines. It is well known that ductile materials erode predominantly by plastic cutting or ploughing of the surface, while brittle materials do so by dissipating the particle kinetic energy through crack nucleation and propagation. In the first part of this presentation, we examine the mechanisms by which surfaces dissipate the kinetic energy of impacting particles, and discuss the erosive response of hard protective coating systems. We investigate the means by which surface engineering can enhance erosion resistance, and correlate surface mechanical properties to the erosion behaviour. In addition, we will show that the architectural design of advanced coating systems is also well supported by finite element modelling of single particle impacts of the coated surfaces.

The second part of the talk will focus on the reparability of advanced coating systems. Indeed, because of the high fabrication costs of engine components, it is desirable to develop an effective and efficient industrially-viable technique to remove defective coatings with the aim of recycling the costly engine components. In particular, we will present our recent studies on the removal of TiN-based erosion resistant coatings using a non-line-of-sight reactive ion etching technique and a complementary laser ablation process.

11:00am SE+NS+TR-TuM10 Hard Coatings with Designed Thermal Conductivity. *P.H.M. Boettger*, Empa, ETH Zurich, Switzerland, *V. Shklover*, ETH Zurich, Switzerland, *M. Sobiech*, Oerlikon Balzers Coating AG, Liechtenstein, *Joerg Patscheider*, Empa, Switzerland

Hardness, thermal stability and oxidation resistance are often the main properties to optimize for most tool coatings developments for industrial applications. The thermal conductivity, however, has been regarded to a much lesser extent as property to improve tool life. So far, only little attention has been given to this fact and the explicit role of thermal conductivity in machining Ti and Ni-based alloys. These materials typically have low thermal conductivity, as well as modern tool coatings such as CrAlN and TiAlSiN. This unfavorable combination may lead to the formation of thermal hot spots during machining, which adds to the premature degradation of such coatings. For these reasons the thermal conductivity is an important process parameter.

This talk will discuss the relations between hardness, coatings architecture and thermal conductivity and how advanced coatings can be tuned to achieve significant anisotropy of the thermal conductivity. In arc-evaporated TiO_xN_{1-x} and CrO_xN_{1-x} thermal conductivity can be adjusted in a wide range between 2 and 35 W/m·K, while keeping hardness and oxidation resistance intact. The data for single phase oxynitrides as well as of multilayered coatings agree well with a newly developed model based on constant phonon scattering cross section of the introduced oxygen. It will be shown how temperature-mitigating multilayer coatings can be prepared using these materials by introducing highly anisotropic thermal conductivity.

11:20am SE+NS+TR-TuM11 Microstructure and Hardness Gradients in Sputtered CrN Films. *A. Riedl*, Materials Center Leoben, Austria, *R. Daniel*, Montanuniversität Leoben, Austria, *T. Schoeberl*, *M. Stefanelli*, Austrian Academy of Sciences, *B. Sartory*, Materials Center Leoben, Austria, *J. Keckes*, *Christian Mitterer*, Montanuniversität Leoben, Austria

Hardness and elastic modulus of a sputtered nanocrystalline CrN thin film, grown under varying ion bombardment conditions, were studied by nanoindentation using a depth-profiling technique and related to cross-sectional X-ray nanodiffraction data on the local microstructure. Changes in texture are shown to have almost no effect on the elastic modulus due to the isotropic response of the polycrystals. However, the locally varying growth conditions, which affect crystal size and number, determine the hardness values across the film thickness. Regions with highly distorted small crystals result in higher hardness in comparison to those with well-developed coarsened grains. This work confirms the notion of the existence of growth-related hardness gradients in single-phase nanocrystalline thin films.

11:40am SE+NS+TR-TuM12 Development of Low Friction Nanocomposite Coatings for Diesel Engine Piston Rings. *Jianliang Lin*, *R. Wei*, *K. Coulter*, *C. Bitsis*, *P.M. Lee*, Southwest Research Institute

Hard and thick (15-20 μ m) TiSiCN nanocomposite coatings have been developed to improve the wear resistance and reduce the overall average friction for diesel engine piston rings. The coatings were deposited by sputtering Ti metal targets in a reactive atmosphere using a plasma enhanced magnetron sputtering (PEMS) process. The reactive mixture contains argon, nitrogen, acetylene gases, and hexamethyldisilazane vapor which were introduced into the chamber using a liquid evaporation/delivery system. The substrates were AISI 304 stainless steel coupons and piston rings. The TiSiCN coatings with different elemental compositions and microstructures were prepared by varying the hexamethyldisilazane and acetylene gas/vapor concentrations and the target power. The microstructure of the coatings was characterized using scanning electron microscopy, energy dispersive spectroscopy, and X-ray diffraction. The adhesion strength and mechanical and tribological properties of the coatings were measured using HRC tests, nanoindentation and ball-on-disk wear tests. By optimizing the composition and microstructure of the coatings, thick TiSiCN nanocomposite coatings with excellent adhesion and a dry sliding friction less than 0.2 have been obtained. The optimized coating systems were applied on the piston rings, which were evaluated on a Plint TE77 reciprocating bench rig and in the real diesel engine test. The principle for the increased wear resistance and the potential applications will be discussed in the paper.

Surface Science

Room: 309 - Session SS+AS+EN-TuM

Synthesis, Structure and Characterization of Oxides

Moderator: Andrew Gellman, Carnegie Mellon University

8:00am **SS+AS+EN-TuM1 Coexisting Accessible Surface Phases on BaTiO₃ (001)**, *Erie Morales, J.M. Martinez*, University of Pennsylvania, *W.A. Saidi*, University of Pittsburgh, *A.M. Rappe, D.A. Bonnell*, University of Pennsylvania

Novel ferroelectric BaTiO₃ applications ranging from sensors to nanogenerators require a detailed understanding of atomic interactions at surfaces. Single crystals provides a platform that allows the exploitation of surface physical and chemical properties that can be readily transferred to other ABO₃ perovskite structures. The processes that result in the atomic and electronic structures of surfaces in tandem with details of surface reactivity are necessary steps towards an understanding of BaTiO₃. Here we demonstrate that two surface reconstruction phases can coexist on a surface and explain the stability of the surface with a quantitative comparison of thermodynamic and kinetic considerations. Specifically, scanning tunneling microscopy (STM) and scanning tunneling spectroscopy (STS) of atomically resolved c(2x2) and c(4x4) reconstructions on BaTiO₃ (100) are compared with density functional theory models to determine the structures of the phases. First principles calculations are also used to examine the thermodynamic stability of the phases and the reaction pathways to both the stable and meta stable structures. We also show the atomic structures of 1 D interfaces between the phases. The ferroelectric properties of BaTiO₃ lead to polarization dependent surface reactions and recent results based on poling at atomic level and will be discussed.

8:20am **SS+AS+EN-TuM2 Oxidation and Chemical Reactivity of TbO_x Thin Films on Pt(111)**, *W. Cartas, R. Rai, A. Sathe*, University of Florida, *A. Schaefer*, University of Bremen, Germany, *Jason Weaver*, University of Florida

Rare earth oxides (REOs) exhibit favorable catalytic performance for a diverse set of chemical transformations, including both partial and complete oxidation reactions. In this talk, I will discuss our recent investigations of the growth, oxidation and chemical reactivity of TbO_x(111) thin films on Pt(111), and make comparisons with results for Sm₂O₃(111) films grown on the same substrate. Bulk terbium and samaria represent examples of REOs that are reducible vs. effectively irreducible, respectively. From low energy electron diffraction and scanning tunneling microscopy, we find that samaria and terbium grow as high quality thin films on Pt(111) during deposition in ultrahigh vacuum. Both oxides develop in the Ln₂O₃ stoichiometry and adopt an oxygen-deficient fluorite structure wherein the metal cations form a hexagonal lattice in registry with the Pt(111) substrate, while oxygen vacancies are randomly distributed within the films. We find that plasma-generated O-atom beams are highly effective in transforming the Tb₂O₃(111) films to higher Tb oxides. Based on results of X-ray photoelectron spectroscopy and O₂ temperature programmed desorption (TPD), we show that exposure to O-atom beams completely oxidizes the Tb₂O₃(111) films to TbO₂ at 300 K, for film thicknesses up to at least seven layers. Heating to ~1000 K in UHV restores the films to the Tb₂O₃(111) stoichiometry, and produces O₂ desorption in two distinct TPD features centered at ~370 K and 660 K which we attribute to oxygen release from lattice sites located in the surface vs. bulk layers, respectively. We also find that O-atom adsorption at 90 K produces a weakly-bound state of oxygen on the TbO_x films which desorbs between ~100 and 270 K. This state of oxygen may correspond to a form of chemisorbed oxygen on the TbO_x film. Consistent with this interpretation, TPD experiments performed after oxidizing a Tb₂¹⁸O₃ film with ¹⁶O-atoms demonstrate that oxygen desorption below about 500 K originates only from the oxygen that is "added" to the Tb₂O₃ film, while all isotopic combinations of O₂ desorb from the bulk above 500 K. Lastly, I will present results which show that the oxidized TbO_x films exhibit high activity and selectivity for the dehydrogenation of methanol to formaldehyde, whereas the initial Tb₂O₃ films have limited reactivity toward methanol.

8:40am **SS+AS+EN-TuM3 Structure/Function Relationships on Cerium Oxide: Reactions on Single Crystal Films and Shape-Selected Nanocrystals**, *David Mullins*, Oak Ridge National Laboratory **INVITED** Cerium oxide is a principal component in many heterogeneous catalytic processes. One of its key characteristics is the ability to provide or remove oxygen in chemical reactions. Recent work has demonstrated how the reactivity and selectivity of various molecules are dramatically altered on different crystallographic faces of cerium oxide. The structure and composition of different faces determine the number of coordination vacancies (CV) surrounding surface atoms, the availability of adsorption

sites, the spacing between adsorption sites and the ability to remove O from the surface. The Ce cation sites are less accessible and have fewer coordination vacancies (CV) on CeO₂(111) than on CeO₂(100). Even though the Ce is in the second layer on CeO₂(100), molecules can adsorb in the open bridge sites between two Ce cations. While there has been numerous studies of the adsorption and reaction of various molecules on CeO₂(111) only recently have comparable experiments been conducted on CeO₂(100).

To investigate the role of surface orientation on reactivity, CeO₂ films with different orientations were grown by two different methods. CeO₂(100) films were grown ex situ by pulsed laser deposition on Nb-doped SrTiO₃(100). CeO₂(111) films were grown in situ by thermal deposition of Ce metal onto Ru(0001) in an oxygen atmosphere. The chemical reactivity was characterized by the adsorption and decomposition of various molecules such as CO₂, H₂O, alcohols, aldehydes and organic acids. In general the CeO₂(100) surface was found to be more active, i.e. molecules adsorbed more readily and reacted to form new products, especially on a fully oxidized substrate. However the CeO₂(100) surface was less selective with a greater propensity to produce CO, CO₂ and water as products. Experiments are underway to determine if CeO₂(110), where the Ce adsorption sites are in the top layer and have 2 CV but the O has only 1 CV, will produce an active yet more selective catalyst.

It is possible to synthesize high surface area shape-selected nanoparticles (octahedra and cubes), i.e. powders that expose a single, well-defined surface. Experiments have shown similarities between the single crystal surfaces and shape-selected nanoparticles, e.g. CeO₂(111)/octahedra are less active than CeO₂(100)/cubes. However there have also been significant differences in selectivity and the types of products formed. Possible explanations for the differences on the single crystal surfaces vs. the nanoshapes will be considered.

Research sponsored by the US Department of Energy, Office of Science, Basic Energy Sciences, Chemical Sciences, Geosciences, and Biosciences Division.

9:20am **SS+AS+EN-TuM5 Ceria on Cu(110): Formation of Nanostripe Strain Defects**, *L. Ma, N. Doudin, S. Surnev, Falko Netzer*, Karl-Franzens University, Austria

The growth morphology and atomic geometry of ceria nanostructures on Cu(110) have been investigated by STM, LEED and XPS. Ceria grows epitaxially in a two-dimensional (2-D) hexagonal layer, which is associated with a CeO₂(111)-type trilayer structure forming a (3x11) coincidence lattice. An important experimental parameter is the oxygen pressure during growth: it influences the stoichiometry of the ceria overlayer as well as the Cu surface oxide phase, which coexists with the ceria for coverages below the full monolayer. For oxygen pressures in excess of 10⁻⁷ mbar, stoichiometric CeO₂ and coexisting Cu-c(6x2) surface oxide are formed, whereas for lower oxygen pressures, in the 10⁻⁸ mbar range, slightly substoichiometric ceria (CeO_{-1.9}) and a Cu-(2x1) surface oxide are observed. The ceria overlayer grows essentially 2-D, but displays a peculiar nanostripe pattern, with varying periodicities ranging from 4-8 nm and a corrugation amplitude of 0.2-0.3 nm. This nanostripe pattern is due to a topographic modulation of the overlayer caused by the frustration of overlayer-substrate bonding as a result of the epitaxial mismatch at the ceria-Cu interface. Detailed STM investigation reveals a distortion of the ceria lattice in the transition region between dark (low) and bright (high) stripes, which gives rise to periodic regions of anisotropic lattice strain - so-called "lattice strain defects". It is speculated that these lattice strain defects may support particular chemical reactivity.

Work supported by the ERC Advanced Grant "SEPON" and by the COST Action CM1104

9:40am **SS+AS+EN-TuM6 Design Rules for Stabilizing Polar Metal Oxide Surfaces: Adsorption of O₂ on Zn-rich Polar ZnO(0001)**, *Ming Li, P. Gorai, E. Ertekin, E.G. Seebauer*, University of Illinois at Urbana-Champaign

For oxide semiconductors with appreciable ionic character, under-coordination of the surface atoms leads to thermodynamic instability that is typically restored by reconstruction, faceting, or extensive surface defect creation. Developing design rules for stabilizing polar metal oxide surfaces that avoid these phenomena could offer novel protocols for applications such as improved nanostructure growth and design of photocatalytic heterostructures. The present work describes calculations by density functional theory for Zn-rich polar ZnO(0001) which demonstrate that stabilization via chemisorbed O₂ together with vacancy formation is energetically as favorable as stabilization by vacancies alone. The stabilization mechanism including adsorption is so effective that it promotes O₂ adsorption to an extent that is not possible on non-polar ZnO. Experimental evidence for such stabilization behavior is presented based on measurements of O₂ adsorption on polar ZnO(0001) via the optical

modulation technique of photoreflectance. The measured isotherms yield a sizable adsorption enthalpy of adsorption near 1.8eV, confirming a strong interaction with the polar surface.

11:00am **SS+AS+EN-TuM10 The Growth of Catalytic Thin Films on a Polar Substrate: Cr₂O₃ on ZnO (0001) and ZnO (000-1), Xiaodong Zhu, Yale University**

Zinc oxide is a wurtzite-structured polar crystal with dramatic polarization direction-dependent surface chemistry. Meanwhile, chromium III oxide is a non-polar material catalytically active for a number of industrial chemical reactions, most notably dehydrogenation. Therefore, the Cr₂O₃/ZnO system has been chosen to demonstrate how the polarization direction of a substrate can be exploited to tailor the surface properties of catalytically active non-polar thin films. Photoelectron spectroscopy and electron diffraction have been performed to determine the growth mode as well as the film quality. The growth is 2D; however, the films appear initially disordered on both positive and negatively poled substrates. On both substrates the order was observed to improve with thickness. Small band offsets between Cr₂O₃ and oppositely poled substrates were observed that were consistent with charge compensation at the Cr₂O₃/ZnO interface. No obvious change in the oxidation state of the chromium was seen and so it is assumed that the charge compensation at the interface only involves Zn and/or O. The offset between the Cr peaks on positively and negatively poled substrates was obvious at the initial growth stages but then decayed with film thickness, suggesting that the compensating charges at the interface may migrate to the film surface. Valence band spectra were analyzed to characterize the bonding at the interface. The surface chemical behavior of Cr₂O₃ on the two zinc oxide surfaces is being characterized to determine how significantly the polar interface impacts the surface properties of thin supported layers.

11:40am **SS+AS+EN-TuM12 Chemical Characterization of Elements in Oxides using X-ray Satellite Lines, Terrence Jach, National Institute of Standards and Technology (NIST)**

X-ray satellite lines come about in x-ray fluorescence spectroscopy as a result of shake-off events in the excitation process. The ratio of their intensities has been shown to be a sensitive function of their oxidation states. We are able to observe the K satellite lines in the x-ray spectra of oxides and glasses, excited by the beam of an electron microscope and detected by a high resolution x-ray microcalorimeter detector. The results show surprising departures from the expected states of some metal elements that we expect to be fully oxidized. The satellite ratio is a way of determining the chemical environment of insulators without charging or ultra-high vacuum.

12:00pm **SS+AS+EN-TuM13 In Situ XPS and NRA Studies of Hydrogen Diffusion in TiO₂ Single Crystals, Vaithiyalingam Shutthanandan, M.I. Nandasiri, S.A. Thevuthasan, M.A. Henderson, S. Manandhar, Pacific Northwest National Laboratory**

The intrinsic point defects associated with oxygen vacancies and Ti³⁺ ions play a crucial role in the usage of titanium dioxide (TiO₂) in various technological applications including catalysis and photochemistry. It is well known that the interactions between H atoms and surface oxygen in TiO₂ lead to the formation of Ti³⁺ ions at elevated temperatures. However the Ti³⁺ ion formation and accumulation as a function of elevated temperatures in UHV conditions during hydrogen diffusion in TiO₂ is not well understood. In this study, we have used ion implantation method to incorporate hydrogen in single crystal TiO₂ (110) samples and investigated the behavior of point defects in both pure and hydrogen implanted TiO₂ as a function of elevated temperatures using Rutherford backscattering spectrometry (RBS), nuclear reaction analysis (NRA), x-ray photoelectron spectroscopy (XPS) and ultra violet photoemission spectroscopy (UPS). TiO₂ single crystals were implanted with 40 keV hydrogen ions at room temperature with ion fluences of 1x10¹⁵, 1x10¹⁶ and 1x10¹⁷ atoms/cm². Samples were isochronally annealed in vacuum for 30 minutes at each temperature up to 1100K and hydrogen and Ti³⁺ defects were quantified. Hydrogen depth profile measurements obtained from 1x10¹⁷ atoms/cm² implanted sample reveal that hydrogen diffused towards the surface at lower temperatures and it slowly diffuses out from the samples at higher temperatures. XPS and UPS measurements from the hydrogen implanted samples show significantly higher Ti³⁺ defects in comparison to pure TiO₂ at these temperatures under UHV conditions. These defects reach a maximum around 880 K in which almost all hydrogen was removed from the sample. When the implanted sample further annealed to high temperatures, the amount of Ti³⁺ in hydrogen implanted samples started to decrease and reaches the values from the pure TiO₂ samples around 1100K.

Thin Film

Room: 307 - Session TF+PS-TuM

ALD for Emerging Applications

Moderator: James Fitz-Gerald, University of Virginia

8:00am **TF+PS-TuM1 Atomic Layer Deposition: A New Strategy to Improve Metal Corrosion Resistance?, Lorenzo Fedrizzi, E. Marin, A. Lanzutti, University of Udine, Italy** **INVITED**

Interests on nanometric conformal coatings are nowadays growing in a wide range of applications, from electronic components to corrosion protection, chemical barriers or even wear resistance. Atomic Layer Deposition (ALD) is one of the most promising nanometric deposition technologies which offers the possibility to obtain conformal coatings even on very complex tridimensional substrates of different chemical nature, with a strict thickness tolerance and strong adhesion. During an ALD cycle, only one molecular layer is deposited on the substrate surface, enabling the theoretical possibility to tailor the composition of the deposit up to molecular resolution, thus obtaining almost unique properties.

Therefore this technology appears to be an interesting and innovative alternative to the existing ones aimed to metal corrosion protection, such as electrodeposition, painting or other chemical or physical vapor deposition technologies.

This work describes the use of ALD for the corrosion protection of different metal alloys of common industrial interest such as stainless steels, aluminum or magnesium alloys. Moreover, the possibility of combining this deposition technology with some traditional ones is also discussed to the aim of obtaining improved protection properties by multilayer coatings able to enhance a protective barrier action.

8:40am **TF+PS-TuM3 Atomic Layer Deposition of Thin VO₂ Films for Thermal Management Applications, Virginia Wheeler, M. Tadjer, N. Nepal, M. Currie, Z.R. Robinson, M.A. Mastro, K. Cheung, F. Kub, C.R. Eddy, Naval Research Laboratory**

Vanadium oxides are thermochromic materials which have significant changes in thermal emittance, optical transmittance and reflectance, and intrinsic electrical properties due to a metal-insulator phase transition (MIT). These materials offer great advantages in a variety of applications including electrochemical applications, energy storage, thermoelectric devices, Mott transistors, and smart windows. In this work, atomic layer deposition (ALD) was used to produce thin, highly uniform, amorphous VO₂ films which enabled the ability to investigate the impact structure (amorphous vs. crystalline) has on the rate of change of intrinsic properties due to the MIT.

Amorphous VO_x films (5-45nm) were deposited by ALD at 150°C using tetrakis(ethylmethyl)amido vanadium and ozone precursors. X-ray photoelectron spectroscopy (XPS) was used to verify the quality, stoichiometry, and depth uniformity of the films. All as-grown films exhibited carbon surface contamination due to atmospheric transfer from the ALD to XPS chambers. Moreover, the top ~1nm of the film exhibited V2p peaks at 517.7 and 516.3eV correlating to V₂O₅ and VO₂ components, respectively. At depths >1nm, XPS showed no residual carbon contamination and only a single VO₂ peak with a FWHM from 2-2.7 eV, which is similar to crystalline films and indicative of the high uniformity and quality of these films. XPS depth profiles near the VO_x/Si interface had a low binding energy shoulder at 513.5 eV, suggesting that initially the films are very oxygen deficient.

The influence of *ex situ* anneal temperature (200-550°C), time (0.17-2hr), and gas environment (forming gas, Ar, O₂, and ozone) on the ability to obtain single phase, crystalline VO₂ films was also examined. Initial results show that only O₂ anneals produce crystalline VO₂, but other factors such as gas flow, duration, and temperature require optimization to inhibit multiphase, polycrystalline films.

Electrical and optical performance of amorphous and crystalline ALD films was assessed from 77-500K and 300-380K, respectively. Unlike crystalline VO₂ films that exhibit an abrupt, up to five orders of magnitude change in resistance around the MIT at 60°C (333K), amorphous VO₂ films had an exponential change in resistance of ten orders of magnitude over the entire temperature range studied. Also, an average activation energy of -0.20eV and temperature coefficient of resistance of 2.39% at 310K was extracted. These results suggest that amorphous VO₂ films, with less structural order, have the potential to induce larger, more gradual electrical changes that could be useful for bolometers or passive thermal management on spacecraft.

9:00am **TF+PS-TuM4 Atomic Layer Deposition of Pb(Zr_xTi_{1-x})O₃ Thin Films to Engineer Nanoscale Multiferroic Composites, Diana Chien, T. Kim, J.P. Chang, UCLA**

As one of the best dielectric, piezoelectric, and ferroelectric materials, PZT is a promising material to engineer nanoscale multiferroic composites. The magnetoelectric (ME) effect occurs indirectly through strain at the interface. Using atomic layer deposition (ALD), a surface-reaction controlled process based on alternating self-limiting surface reactions, a thin film of PZT can be synthesized with precise control of the elemental composition (Zr/Ti = 52/48) and film thickness. ALD provides much superior uniformity and conformality over complex surface structures with high aspect ratios.

In this work, ALD PZT thin films were synthesized by depositing alternating layers of PbO, ZrO₂, and TiO₂ layers using Pb(TMHD)₂, Zr(TMHD)₄, and Ti(O-i-Pr)₂(TMHD)₂ as metal precursors and H₂O as the oxidant. The number of local cycles and global cycles were regulated to achieve the desired stoichiometry and thickness, respectively. ALD of PZT was studied to obtain (100) oriented Pb(Zr_{0.52}Ti_{0.48})O₃ on Pt (111) oriented platinumized silicon substrates. In order to attain a highly oriented PZT thin film, a (100) textured PbTiO₃ seed layer was required because PZT orientation is generally governed by nucleation. The stoichiometry and crystallinity of PZT films were confirmed by XPS and XRD measurements. The conformality was confirmed over hollow Si₃N₄ cylinders with aspect ratio of 2.2.

By controlling the composition, thickness, and conformality of ALD PZT thin films, the properties of PZT can be exploited to increase the ME coefficient. Specifically, PZT was coupled with MgO/CoFeB to fabricate magnetic tunnel junction for memory applications. With co-mediated effects from higher dielectric constant and strain transfer via the interface, the voltage-controlled magnetic anisotropy effect is expected to increase, thereby realizing magnetic anisotropy energy per area per electric field greater than 37 fJ/(V·m) (Zhu, J. et al., *Phys Rev Lett.*, 108, 2012). ALD PZT thin films were shown to uniformly coat the walls of nanoscale porous CFO template to form a 3-D composite and a larger ME coefficient is expected due to an increase in surface area to volume ratio.

9:20am **TF+PS-TuM5 Atomic Layer Deposition Enabled Synthesis of Nanoscale Multiferroics, Calvin Pham, Y. Kim, J.P. Chang, University of California at Los Angeles**

Complex metal oxides exhibit remarkable tunability in their ferromagnetic, ferroelectric, and multiferroic properties that enable future applications such as non-volatile memory, miniaturized antenna, sensors and actuators. Nanocomposites based on a magnetostrictive ferro/ferrimagnet paired with a piezoelectric have shown unique multiferroic behavior from effective strain-coupling at the interface. Motivated by the promise of high magnetoelectric coupling from nanostructured multiferroics, an atomic layer deposition (ALD) process was developed to synthesize CoFe₂O₄ (CFO) and BiFeO₃ (BFO), thereby enabling the formation of 2-D multilayered films with nanometer scale precision, as well as 3-D composites based on a mesoporous template. The highly conformal coating of ALD, due to self-limiting surface reactions, promises an intimate interface of the various ferroic phases to realize tunable magnetoelectric coupling by nano-texturing.

In this work, a radical enhanced ALD process was used to synthesize the complex oxide nano-structures, using metallorganic precursors Bi(tmhd)₃ (tmhd = 2,2,6,6-tetramethylheptane-3,5 dione), Co(tmhd)₂, and Fe(tmhd)₃ and oxygen atoms produced from a microwave power atomic beam source. The processing-structure-property relations were systematically studied. First, the nucleation delay for the initiation of the growth of one constituent oxide on another was quantified and a variety of process conditions were systematically examined to assess the effects of process temperature, precursor pulsing time, and precursor pulsing ratio on film composition, growth rate, and structure. The ALD BFO and CFO films were confirmed to be conformal and of the exact stoichiometry with a linear growth rate, and their individual ferroic responses are comparable to those reported in literature, as synthesized by other techniques. The 2D BFO/CFO multilayers were synthesized with each layer measuring between 2-50 nm each, while the 3D composites consisted of mesoporous templates with ~15 nm diameter pores that were filled with ALD films. The attainable magnetic, ferroelectric, and magnetoelectric properties, including magnetoelectric coupling, are shown to be sensitive to the composition, morphology and microstructure of the composites as they interrelate and affect the strain state at the interface.

9:40am **TF+PS-TuM6 Laser Assisted Electron Beam Induced Deposition: Towards a Nanoscale Atomic Layer Deposition Process, Michael Stanford, B.B. Lewis, J.H. Noh, University of Tennessee, H. Plank, Graz University of Technology, Austria, J. Fowlkes, Oak Ridge National Laboratory, N.A. Roberts, Utah State University, P.D. Rack, University of Tennessee**

Electron beam induced deposition (EBID) is a direct-write process which can be used to selectively deposit material with nanoscale resolution. EBID utilizes a scanning focused electron beam to dissociate adsorbed precursor molecules which subsequently condense onto the substrate. One of the major limitations of the EBID process is low material purity resulting from incomplete by-product removal of the typically organometallic precursor. Therefore, the development of EBID purification strategies for enhanced materials functionality is a grand challenge for wider application of this synthesis technique. While recently EBID deposits have been used as selective atomic layer deposition catalyst, here we demonstrate an in-situ ALD-like process driven by electron and laser-induced thermal half reactions. We have developed an O₂-assisted laser anneal process to enhance the purity of patterns deposited using MeCpPt^{IV}Me³ precursor gas. Additionally, we have demonstrated a laser assisted electron-beam-induced-deposition (LAEBID) process as an effective method to provide *in-situ* purification during deposition. The synchronized process is initiated by an approximately monolayer EBID cycle followed by a laser pulse which thermally desorbs by-products of the condensed phase. The process is repeated until the desired shape and size is achieved. The addition of a reactive O₂ gas and a synchronized electron and laser pulse begins to look a lot like a nanoscale atomic layer deposition process (ALD), however the half reactions are electron and thermally stimulated, respectively. We will demonstrate how factors such as laser pulse width, laser duty cycle, EBID beam current, and EBID dwell time have significant effects on the laser anneal and LAEBID processes. Importantly, the carbon reduction and apparent densification lead to higher resolution relative to standard EBID.

11:00am **TF+PS-TuM10 Effect of Film Stress on the Shape of Nanostructures Grown Using Atomic Layer Deposition, Jonas Gertsch, N.T. Eigenfeld, J.M. Gray, V.M. Bright, S.M. George, University of Colorado, Boulder**

Controlling the shape of nanostructures is crucial to the performance of nanodevices. Nanostructure shape can be tuned by varying stress in the various films that comprise the nanostructure. In this work, we explore the shape of Al₂O₃/W/Al₂O₃ trilayers fabricated using Al₂O₃ ALD and W ALD. Trilayer films were initially grown on polyimide molds that were formed into free standing "umbrella" nanostructures after processing and release. Depending on the stresses in the trilayer films and the thicknesses of the individual layers, the nanostructures can either remain flat or may curl up or down. The resulting shape can be controlled by varying the thicknesses of the individual Al₂O₃ ALD and W ALD layers in the trilayer. These "umbrella" nanostructures may be useful for microbolometer and other microelectromechanical systems (MEMS) applications. Additional studies will present stress measurements using atomic force microscope (AFM) investigations of ALD films in fixed-fixed and fixed-free cantilever structures.

11:20am **TF+PS-TuM11 Atomic Layer Deposition and Nucleation on Metallic Nanostructures for Plasmonic Devices, Jie Qi, X. Jiang, B.G. Willis, University of Connecticut**

Atomic layer deposition (ALD) has become an important technique for the deposition of nanometer thin dielectric and metallic thin films with applications in semiconductors, nanotechnology, catalysis, and energy. In particular, nanoscale metallic structures are gaining importance for fabrication of plasmonic antenna with applications in biochemical sensors, photocatalysis, and solar energy harvesting devices. A key feature of nanoscale plasmonic materials is a strong dependence of the plasmon resonance on size and shape of the nanostructure. ALD offers a unique means to control the size, composition, and particle-particle junctions of nanostructures with high precision. The latter is particularly important for creating hot spots where electric fields are strongly enhanced. A key challenge for ALD is the strict control of film composition and uniformity. Although a number of works have been published on the uniformity and layer by layer growth of amorphous dielectric thin films, the crystalline structures of metals present significantly increased complexity. Moreover, when seed layers, prefabricated nanostructures, or particles are involved, the sensitivity of film growth to surface structure has received relatively little attention so far.

In this work, we study the effects of surface preparation and seed layer properties on ALD Cu thin films relevant to plasmonic devices. Pd and Pt are used as seed layers for both planar thin films and two dimensional nanostructures. ALD growth was studied for different sized nanostructures and surface preparations including: e-beam deposition, high temperature annealing, solvent cleans, and UV/Ozone (UVO) pretreatment, as well as

different ALD growth conditions. Samples were analyzed by XPS, SEM, AFM, EDS, and other techniques to compare film uniformity and surface structures. A strong dependence of Cu ALD growth quality was found for different nanostructures and surface preparations. Nucleation of Cu was greatly enhanced when UVO pre-treatment was performed on e-beam evaporated seed layers, but AFM results showed surface roughness increased with UVO cleaning time, which indicates rough, non-uniform growth. Seed layer thickness also played a role and it was observed that smoother and more uniform Cu thin films are obtained with thinner seed layers. Overall, planar thin films are poor models for nanostructure growth. Nanostructures are significantly more sensitive to surface preparations and growth conditions because of the similar length scales of nuclei and nanostructure size.

11:40am **TF+PS-TuM12 Infrared and Thermoelectric Power Generation in Thin Atomic Layer Deposited Films**, *Harkirat Mann, B.N. Lang, Y. Schwab*, James Madison University, *J. Petteri-Niemelä, M. Karppinen*, Aalto University, Finland, *G.S. Scarel*, James Madison University

A mechanism for alternative energy, thermoelectric (TE) power generation, converts a temperature difference across two junctions into an electric potential. Although not as energy-efficient as solar panels or wind turbines, this mechanism is used in a wide variety of fields, e.g. to recapture waste heat. Recently it was discovered that a solid state TE power generators respond differently to heat or infrared (IR) radiation [1, 2]. To test the robustness of this finding, this research compares TE and IR power generation in the case of a nanometric TE device in which the active element is a thin TE film. The thin TE film is a 70 nm thick n-type Nb-doped titanium oxide film deposited by atomic layer deposition (ALD) onto a borosilicate glass substrate [3]. The interactions observed with heat show a linear relationship between temperature and voltage, whereas in IR radiation this linear relationship is broken down. The efficiency and the voltage stability obtained with the thin TE film is larger than that obtained by closing the electric circuit without the thin TE film. The possibility of using thin ALD films for IR power generation suggests that in the future the response to IR radiation can be tuned by exploiting the properties of the thin atomic layer deposited TE films.

[1] R. J. Parise and G. F. Jones, Collection of Technical papers – 2nd International Energy Conversion Engineering Conference, 1172–1181 (2004).

[2] Y. Schwab, H. S. Mann, B. N. Lang, J. L. Lancaster, R. J. Parise, A. J. Vincent-Johnson, and G. Scarel, *Complexity* **19**, 44-55 (2013).

[3] J. Niemelä, H. Yamauchi, and M. Karppinen, *Thin Solid Films* **551**, 19-22 (2014).

12:00pm **TF+PS-TuM13 Atomic Layer Deposition of Tin Doped Titanium Oxide on Type-V Titanium Implant Surface for Enhanced Photoactivated Antibacterial Property**, *S.K. Selvaraj, A. Butt, Christos Takoudis*, University of Illinois at Chicago

Atomic layer deposition (ALD) is used for the first time to modify type-V titanium (Ti-6Al-4V) surface, a commonly used dental and orthopedic implant material.¹ ALD of titanium oxide and tin doped titanium oxide thin films were deposited on Ti-6Al-4V disks to enhance photoactivated antibacterial property of its surface. Tetrakis(diethylamino)titanium (TDEAT) kept at 65 °C and tin(II)acetylacetonate (Sn(acac)₂) kept at 70 °C were used as titanium and tin sources, respectively. Custom built hot-wall flow-type ALD reactor was used to deposit antibacterial thin films at 200 °C substrate temperature and 0.5 Torr.^{2,3} Different composition of tin doping was achieved by changing the number of tin oxide ALD cycles. X-ray photoelectron spectroscopy was used to study the composition and purity of the thin films. Films were found to have titanium, tin, oxygen and trace amount of carbon. Excellent composition tunability of the ALD process was achieved. The resultant films were studied for photoactivated antibacterial property using a gram negative *Escherichia coli* bacterial strain ATCC 8739. The ALD coated Ti-6Al-4V disks were immersed in bacterial solution and illuminated with UV light for 3 min. Irradiated bacterial samples were plated on agar plate and incubated for 12 hours at 37 °C. Two fold increase in antibacterial property was achieved on ALD TiO₂ coated disks compared to uncoated (control) disks. Tin doping further increased the activity by about two fold. Any increase in tin composition beyond 15 atom % was found to have no effect on antibacterial activity.

References

1 Gallardo-Moreno, A. M., Pacha-Olivenza, M. A., Saldana, L., Perez-Giraldo, C., Bruque, J. M., Vilaboa, N., and Gonzalez-Martin, M. L., In vitro biocompatibility and bacterial adhesion of physico-chemically modified Ti6Al4V surface by means of UV irradiation, *Acta Biomaterialia* **2009**, 5 (1), 181.

2 Selvaraj, S. K., Jursich, G., and Takoudis, C. G., Design and implementation of a novel portable atomic layer deposition/chemical vapor deposition hybrid reactor, *Review of Scientific Instruments* **2013**, 84 (9), 095109.

3 Selvaraj, S. K., Feinerman, A., and Takoudis, C. G., Growth behavior and properties of atomic layer deposited tin oxide on silicon from novel tin(II)acetylacetonate precursor and ozone, *Journal of Vacuum Science & Technology A* **2014**, 32 (1), 01A112.

Thin Film

Room: 305 - Session TF+SE-TuM

Energetic Thin Films/Optical Characterization

Moderator: David Adams, Sandia National Laboratories, Christophe Vallee, LTM - CEA/LETI, France

8:00am **TF+SE-TuM1 Investigations on LiMn₂Ni₃O Thin Films Deposited by RF Sputtering using Powder Target for Thin Film Battery Applications**, *Kosuri Yellaeswara Rao*, Indian Institute of Science, India

Cathode materials in the form of thin films for all solid state Li ion batteries (thin film batteries) application have attracted wide attention among the scientific community because of the inherent benefit of studying pure phase of the active materials without any binders and conductive additives such as carbon black, NMP etc [1,2]. In the present work thin films of LiMn₂Ni₃O have been prepared in a cost effective approach using powder sputtering on nickel coated stainless steel (SS 304) substrates. Powder sputtering is more convenient with the advantages like less material consumption, slightly higher deposition rates and cost effective approach compared to pellet sputtering. The advantage of utilizing powder sputtering for the deposition and electrochemical performance of Li₂MnO₄ thin films has been reported [3]. Post deposition annealing at 500 °C for one hour was carried out in air ambient. XRD, XPS and electrochemical characterizations have been carried out to investigate the phase, surface atomic concentration and electrochemical performance. XPS analysis indicates the presence of manganese, nickel, oxygen, and lithium at the surface as shown in Figure. 1. Electrochemical investigations delivered a specific discharge capacity of 54 μAh. μm⁻¹.cm² in the potential window 2.0-4.4 V vs Li/Li⁺ in the first discharge cycle. Charge discharge profile up to 40 cycles have shown in the Figure.2. Discharge capacity values are in good agreement with the literature achieved using pellet sputtering.

References:

1. J.M. Tarascon, M. Armand. *Nature* **414**, 359 (2001)
2. J.B. Bates, N.J. Dudney, B. Neudecker, A. Ueda, C.D. Evans. *Solid State Ionics* **135**, 33– 45 (2000)
3. K.Yellaeswara Rao, D. Shanmugha sundaram, C.S. Nimisha, Tirupathi Rao Penki, N. Munichandraiah, G. Mohan Rao. *J. Electrochem. Soc* **161**, A28-A32 (2014)

8:20am **TF+SE-TuM2 The Dynamics of Reactive Foil Ignition after Pulsed Laser Irradiation**, *Ryan Murphy, R.V. Reeves*, Sandia National Laboratories, *J.P. McDonald*, Dow Corning Corporation, *D.P. Adams*, Sandia National Laboratories

It has been shown that forced mixing of reactive layers (foils) leads to an exothermic release of energy after initiation of mixing by forced impact or pulsed laser irradiation. In order to understand the ignition of foils initiated by laser irradiation, we study the interaction of laser pulses with Al/Pt multilayer reactive foils prepared by sputter deposition. It will be shown that the single-pulse ignition threshold and dynamics are dependent on the length of the laser pulse as the pulse length is varied from 100 fs to 100 ns. The dependence of the ignition threshold on pulse length is a combination of laser-material interactions such as the size of the heat affected zone, changes in reflectivity with pulse length, and the onset of ablation for ultrafast irradiation. The laser spot size is varied for each pulse length to explore the effects of heat confinement on the ignition threshold. The dynamics of foil ignition is further investigated by imaging ignition and the subsequent reaction with a high-speed camera. Varying the bilayer thickness and laser pulse length is shown to change properties such as mixing, ignition in the solid-state, and the onset time of reaction.

Sandia National Laboratories is a multi-program laboratory managed and operated by Sandia Corporation, a wholly owned subsidiary of Lockheed Martin Company, for the United States Department of Energy's National Nuclear Security Administration under Contract DE-AC04-94AL85000.

8:40am **TF+SE-TuM3 Probing Rapid Formation and Oxidation Reactions with Multilayer Films and Foils**, *Timothy Weihs*, Johns Hopkins University **INVITED**

Vapor-deposited multilayer films and foils provide model structures for studying exothermic formation and oxidation reactions. These reactions can proceed at slow to moderate rates (10^{-1} to 10^5 K/s) using controlled heating or at very rapid rates (10^6 to 10^8 K/s) by initiating self-propagating mixing within the films or foils. In this presentation we will probe the sequence of intermetallic phase formation and the kinetics of rapid oxidation as a function of heating rate, chemistry, and concentration gradients using novel characterization tools such as nanocalorimetry, bomb calorimetry, dynamic transmission electron microscopy and synchrotron X-ray diffraction. The experimental results will be compared with analytical predictions and molecular dynamic simulations and controlling factors will be identified.

9:20am **TF+SE-TuM5 Detonation in Vapor-deposited Explosive Films at the Micro-scale**, *Robert Knepper, M.P. Marquez, A.S. Tappan*, Sandia National Laboratories

Recent advances in physical vapor deposition of explosive materials have led to films that are capable of detonating at thicknesses smaller than 100 microns. The critical thickness needed to sustain detonation can be reduced even further (down to a few tens of microns) by confining the explosive with thin layers of a dense, inert material. The ability to sustain detonation at such small length scales opens the potential for such films to be integrated into micro-scale systems using standard micro/nanofabrication methods for use in actuation, gas generation, or similar functions. In this work, we present vapor-deposited hexanitroazobenzene (HNAB) and copper films as a model system to study the effects of confinement on the detonation properties of secondary explosives. Both the HNAB and copper confinement layers are vapor-deposited to promote intimate contact between the explosive and confinement and to provide precise control over both layer thicknesses and microstructure. Confinement thickness is varied to determine the minimum necessary to behave as though the confinement was effectively infinite, and the effects on detonation properties are quantified. In addition to the practical impact of these experiments, identification of the minimum effectively infinite confinement condition can provide insight into the kinetics of the detonation reaction.

Sandia National Laboratories is a multi-program laboratory managed and operated by Sandia Corporation, a wholly owned subsidiary of Lockheed Martin Corporation, for the U.S. Department of Energy's National Nuclear Security Administration under contract DE-AC04-94AL85000.

9:40am **TF+SE-TuM6 Investigating the Effect of Heating Rate on the Al/Ni Formation Reaction using *In Situ* Nanocalorimetry**, *Michael Grapes*, Johns Hopkins University, *M.K. Santala, T. LaGrange, G.H. Campbell*, Lawrence Livermore National Laboratory, *D.A. LaVan*, National Institute of Standards and Technology (NIST), *T.P. Weihs*, Johns Hopkins University

The Al/Ni formation reaction is highly exothermic and of both scientific and technological significance. In particular, Al/Ni thin-film multilayers have been used as a model system to understand how steep concentration gradients and large heating rates affect the identity and sequence of phases that form at the interface between two materials. We have developed an *in situ* nanocalorimetry system that enables us to simultaneously measure the heat generated by the Al/Ni reaction and observe the phases formed. The added ability to controllably vary the heating rate from 1000 K/s to 100,000 K/s makes possible a systematic assessment of the phase transformation sequence with heating rate that we hope will shed light onto the relative effects of kinetic and thermodynamic phase suppression in determining the first phase to form. In this talk I will describe the experimental system, present the baseline results that are obtained at low heating rates, and provide an update detailing recent results and potential conclusions of the systematic study.

11:00am **TF+SE-TuM10 The Role of Magnesium in Heat Generation from Al-Mg/Zr Laminate Foils**, *Kyle Overdeep*, Johns Hopkins University, *D.J. Allen, N.G. Glumac*, University of Illinois at Urbana-Champaign, *K.J.T. Livi, T.P. Weihs*, Johns Hopkins University

This study examines the ability of reactive multilayer foils to generate heat as a function of magnesium composition. This is accomplished by comparing the heat generated from the reactions of three chemistries: Al:Zr, Al-8Mg:Zr, and Al-38Mg:Zr, which correspond to foils with alternating aluminum and zirconium layers where the Al is either pure, an 8 at.% Mg alloy, or a 38 at.% Mg alloy, respectively. We have found that Al-8Mg:Zr releases 53% more heat than the Al:Zr foils when reacted in air (from 2.5 kJ/g for Al:Zr to 3.8 kJ/g for Al-8Mg:Zr), and 28% more heat than Al-38Mg:Zr (3.0 kJ/g), based on measurements performed in a specially designed bomb calorimeter. This may be a result of the expulsion of particles and vapor which is unique to the Mg-containing foils, because the

increase in surface area enhances combustion. In order to understand this mechanism more thoroughly, the ejected particles, ejected vapor, and remaining foils were all characterized to understand the amount and composition of all species being ejected, and how that influences the combustion of each foil.

11:20am **TF+SE-TuM11 Dynamics of the Inverse MAPLE Process for Deposition of Nanoparticles and Nanoporous Thin Films**, *Matthew Steiner, P.J. Steiner, J.M. Fitz-Gerald*, University of Virginia

Matrix assisted pulsed laser evaporation (MAPLE) was developed in the late 1990s at the U.S. Naval Research Laboratory as a non-destructive method of thin film deposition for polymers that could potentially be damaged by the ultraviolet radiation utilized for pulsed laser deposition. Conventionally MAPLE starts with a dilute organic compound dissolved in a volatile solvent that serves as a solid matrix when frozen at liquid nitrogen temperatures. By choosing a solvent with a significant UV absorption coefficient, the frozen matrix can be heated by preferential photothermal excitation during irradiation, leading to evaporation and desorption of the less volatile solute molecules onto a substrate in thin film form. Since its conception, use of MAPLE has expanded from the deposition of molecular polymers and proteins to more macroscopic species such as carbon nanotubes, living cells, and recently a number of inorganic nanoparticles.

Inspired by the laser decomposition of metal-acetate based sol-gels to form nanoparticle networks, it is also possible to simultaneously synthesize and deposit well-dispersed nanoparticles or nanoporous films through an inversion of the conventional MAPLE process, utilizing weakly absorbing solvents and photo-sensitive chemical precursor solutes. The chain of events following the laser pulse first entering the target and culminating with observation of nanoparticles on the substrate has been principally interpolated backwards from the nanoparticles produced; suggesting photothermal decomposition of the acetate precursors and formation of nanoparticles within the target prior to and eventually driving ejection. The research presented represents major developments in the understanding of the underlying sequence of multi-scale events controlling the inverse MAPLE deposition process. Modeling addresses optical absorption via Mie theory and the role of matrix conduction in solving nanoparticle heat balance within the target, which in turn is shown to play critical role in the deposition process. New supporting evidence is offered through direct observation of irradiated targets via cryo-stage scanning electron microscopy, as well as conventional scanning and transmission electron microscopy of deposited films and nanoparticles.

11:40am **TF+SE-TuM12 Structural, Optical and Electrical Properties of Fe-doped BiOCl**, *Yoon Myung, S. Banerjee, F. Wu, P. Banerjee*, Washington University, St. Louis

BiOCl is an attractive p-type semiconductor with a wide band-gap of 3.4 eV. It has a unique layered structure of alternating $[\text{Bi}_2\text{O}_2]^{2+}$ layers, interleaved by double slabs of Cl⁻ ions. The ionic layering guides the growth of BiOCl along the c-axis to form a 2D nanosheet morphology, favoring rapid and efficient electron/hole separation. Thus, BiOCl nanosheets can be naturally exploited as a photoactive material in applications such as solar harvesting, photocatalysis and sensing. However, given the large band-gap of BiOCl strategies to sensitize the BiOCl to the visible spectrum must be made. Substitutional doping of transition metal ions is an attractive approach given that many of the transition metal oxides are earth-abundant and have their band-gaps in the visible spectrum.

In this study, we demonstrate the effect of Fe doping on the structural, optical and electrical properties BiOCl nanosheets. Fe-doped BiOCl were synthesized by a facile hydrolysis process. Next, the samples are subjected to various annealing temperatures. We show that anneal temperatures >200 °C can initiate successful Fe incorporation in BiOCl crystal lattice. X-ray diffraction (XRD) shows a higher angle shift after thermal annealing, corresponding to decrease in the lattice constant as a result of Fe³⁺ substitution of the Bi³⁺ ions. Raman spectroscopy shows the E_g stretching mode of the Bi-Cl bond has lower frequency shift, which is consistent with the XRD analysis of Fe³⁺ substitution. Electrical property measurements including IV characteristics show a linear behavior with a resistance of (2.5x10¹¹, 9.8x10¹⁰ and 9.32 x 10¹⁰ Ω) for samples annealed at 200, 300 and 400°C respectively.

Finally, we demonstrate a highly sensitive O₂ sensor using Fe-doped BiOCl nanosheets, operating at room temperature. The interaction of vacancies and O₂ is explored in the context of the Fe-doping in BiOCl.

12:00pm **TF+SE-TuM13 Cathodoluminescent and Photoluminescent Properties of $\text{Sr}_2\text{SiO}_4:\text{Dy}^{3+}$ Thin Films Prepared by the Sol-gel Spin Coating Technique**, M.A. Tshabalala, H.C. Swart, O.M. Ntwaeaborwa, University of the Free State, South Africa, **Bakang Mthudi**, University of South Africa, South Africa

Phosphor thin films have been attracting attention because they play important roles in high resolution devices such as cathode ray tubes, thin film electro-luminescent panels and field emission displays¹. Displays based on thin film phosphors are characterized by high contrast and resolution, good thermal conductivity as well as high degree of uniformity and better adhesion to substrates². Efforts have been made in the past years to develop various types of luminescent thin films via the sol-gel method by using either dip-coating or spin-coating³. However spin-coating has emerged as the preferred technique because it is more versatile than the dip-coating technique. Thin film phosphors based on oxide hosts have received considerable attention for use in flat-panel displays due to their outstanding luminescent properties, high chemical stability in high vacuum and lack of emission of corrosive gases under electron bombardment⁴. In this study we investigated the structure, particle morphology, surface topography, chemical composition and luminescent (photoluminescent (PL) and cathodoluminescent (CL)) properties of dysprosium (Dy^{3+}) doped oxide based strontium silicate (Sr_2SiO_4) thin-film phosphor prepared by the sol-gel spin coating technique. Several parameters including number of sol drops, deposition times and post-deposition annealing temperatures were varied. Both the PL and CL intensities were dependent on the deposition conditions and post deposition annealing temperature. Data from scanning electron microscope and atomic force microscope show that the major influence of the deposition conditions on the CL/PL intensity was through changes in the morphology and topography of the films, which affects light scattering and out-coupling. The chemical states and composition, and the depth profiles of the films were examined using the x-ray photoelectron spectroscopy and Auger electron spectroscopy. The influence of the various deposition conditions on the luminescent intensities and the quality of the films will be discussed.

Vacuum Technology

Room: 303 - Session VT-TuM

Gas Dynamics, Modeling, and Pumping Systems

Moderator: Lily Wang, Los Alamos National Laboratory, Martin Wüest, INFICON Ltd., Liechtenstein

8:00am **VT-TuM1 A Fast Numerical Method for Determining the Pressure Distribution in Electrostatic Chucks**, **Jack McInerney**, Lam Research Corp

The excellent cooling capabilities of the electrostatic chuck enable high power plasma etching of modern semiconductor devices. In order to maintain a uniform temperature across the silicon wafer, a thin layer of helium is inserted between the wafer and chuck. Some of this gas leaks out at the wafer edge, and the resulting flow of helium can lead to pressure drops that compromise the heat transfer uniformity of the chuck. Fluid dynamics modeling of the helium distribution is often used in the design phase to ensure uniform pressure under various scenarios.

Because of the small gaps and low pressures, the gas behind the wafer is in the transitional or molecular flow regime. Modeling electrostatic chuck designs then requires using very computationally expensive methods such as Direct Simulation Monte Carlo (DSMC). In this paper, a simplified modeling approach is developed that allows the pressure distribution to be modeled as a two-dimensional conductance problem. This is done by extending the conductance calculations used in one-dimensional vacuum piping networks. The accuracy of the method is compared to molecular flow modeling. The method is then used to model some chuck configurations.

8:20am **VT-TuM2 Numerical Simulation of a Jet Disrupter in an Electrospray RF Ion Funnel**, **Eric Tridas**, R. Schlaf, University of South Florida, M. Anthony, Elion Systems

Electrospray ionization (ESI) is a versatile method for creating gas phase ions from solution while maintaining the native chemical functionality of the solute. Using this method, functional bio- and macromolecular thin films can be produced for use in biosensors, scaffolding for tissue generation, photovoltaics and other emerging fields of research. The Macromolecular Patterning System, designed and constructed at the University of South Florida (USF), utilizes ESI as a material source to create such films. The system is comprised of three differential pumping stages, each containing custom designed electrodes used to define the trajectory of the ions. The focus of this study is on the first of the three

stages which contains a radio frequency (RF) ion funnel. Computational fluid dynamics (CFD) simulations of the air flow into this chamber were performed and coupled with simulations calculating the generated electric field. Using the ion trajectory simulation software SIMION, the flight paths of ions within this first chamber were calculated. Experiments were then performed to test the results of the simulations. A "randomization parameter" based on the turbulence kinetic energy of the CFD simulations was used to model the time-varying component of the flow velocity yielding a result that closely matched the system. Variation of electrode voltages in the physical apparatus yielded similar results to those obtained from the simulations. Most significantly, the overall trend and peak values of ion transmission were accurately predicted from the simulations.

8:40am **VT-TuM3 Gas Dynamics Modelling Efforts at CERN**, **Roberto Kersevan**, CERN, Switzerland **INVITED**

The Vacuum Surfaces and Coatings (VSC) Group at CERN is involved in several large projects, either at CERN or in collaboration and/or support of other laboratories. The design of new vacuum chambers and components is taking a considerable amount of time of many physicist and engineers in the VSC. New accelerators are being designed, either for fabrication and installation in a short time or as part of the European strategy for future accelerators. Two extreme examples are: 1) The ELENA project (Extra-Low Energy Accelerator ring) a ~ 30 m circumference 100 keV anti-proton decelerator aimed at increasing the anti-proton production from the existing AD machine (Antiproton Decelerator ring). ELENA will require an average pressure better than 3E-12 Torr. ELENA is under design and construction now, with expected start of commissioning in 2016. On the other side of the spectrum are the TLEP and HE-LHC machines, which are part of the Future Circular Colliders lepton-lepton and hadron-hadron (FCC-ee, FCC-hh) versions of colliders aiming at greatly improving the production of Higgs and W/Z bosons, and top quarks (FCC-ee), and raising the center-of-mass energy in the 50+50 TeV range (FCC-hh). Such conceptual machines would require circumferences in an unprecedented 80~100+ km range. The FCC-ee versions would generate of the order of 50 MW of synchrotron radiation (SR) for 175+175 GeV electron-positron beams, and the FCC-hh would generate as well a considerable amount of SR in the 4~5 keV critical energy range, thanks to 16-20 tesla superconducting magnets. The already approved High-Luminosity upgrade of the LHC (HL-LHC) and this FCC program will require a thorough upgrade of the injector chain, composed of some accelerators which are today exceeding the 50 year mark. In parallel, there are accelerators like the HIE-ISOLDE upgrade of the ISOLDE machine, aimed at post-acceleration of radioactive ion-beams, and new-concept experiments like the AWAKE plasma-acceleration project. In order to tackle all these projects, the VSC group has decided to develop several numerical analysis tools, namely test-particle montecarlo (TPMC) codes and the electrical-network analogy (ENA) (implemented via the Ltspace freeware). This paper will briefly describe the various codes developed (Molflow+ for molecular flow, SYNRAD+ for SR, and McCRYO-T for radiative heat exchange) and the ENA approach. It will then show some examples of the application of these codes to CERN projects and also comparison and benchmarking with results published in the gas dynamics field and dedicated experiments carried out at CERN.

9:20am **VT-TuM5 Mixture Flow of Rarefied Gases through a Thin Orifice Over the Whole Range of Gas Rarefaction**, **Felix Sharipov**, Federal University of Parana, Brazil

Rarefied gas flow through a thin orifice is well studied on the basis of the direct simulation Monte Carlo (DSMC) method, see e.g. Ref.[1,2]. In spite of the fact that in practice one deals with gaseous mixtures more often than with a single gas, the information about such kind of flows is still poor. That is why it is attractive to treat gaseous mixtures as a single gas with the molecular mass equal to its average values of the corresponding mixture. However, such an approach not always provides reliable results. The aim of the present work is a numerical modeling of mixture flows of rarefied gases through a thin orifice on the basis of the direct simulation Monte Carlo (DSMC) method. The mass flow rate and flow field are calculated over the whole range of the rarefaction parameter for various values of the pressure ratio and for several values of the mole fraction. A comparison of the present numerical results with those obtained for a single gas is performed. A recommendation of the applicability of single gas results to gaseous mixture is given.

References

1. F. Sharipov, Numerical simulation of rarefied gas flow through a thin orifice. J. Fluid Mech. Vol.518, pp. 35-60 (2004).
2. F. Sharipov and J.L. Strapasson, Ab initio simulation of rarefied gas flow through a thin orifice. accepted in Vacuum.

9:40am **VT-TuM6 Numerical Modeling of Particle Transport in Rarefied Flow**, *Andreas Mack, Van der Donck, O. Kievit*, TNO Delft, the Netherlands

Within wafer handling devices, environments from ambient pressure to ultra-high vacuum are present. The wafers are moved by robots between the compartments which are separated by load locks. With closed load lock valves, the pressure is reduced by pumping-down such that the pressure level of the next compartment is roughly matched. Since the pumping speed is approximately constant, the pumping time to very low pressures would take long or require additional pumps such that usually the target pressure is only matched by two orders of magnitude. The final pressure is then achieved by opening the load lock valve such that the pressure in both compartments reach equilibrium. This process includes a strong expansion of the flow such that locally very high flow velocities can be reached up to supersonic speed. Since the flow is in the rarefied regime, the forces on surfaces such as the wafer are small but particles released during the wafer handling process can be dispersed downstream due to drag or gravitational forces. Since there is only sparse information available about the coupling between contaminating particles and the rarefied flow, the present paper focusses on the numerical modelling of particle transport in rarefied flow. A DSMC (Direct Simulation Monte Carlo) code is applied to typical domains of wafer handling such as load lock valves and coupled with a particle tracer. Both codes are available within the open source software package OpenFoam and have been validated in the relevant regimes by either generic numerical experiments or, where available, experimental or other numerical data. By this, particle contamination in low pressure environments can be investigated. On the one hand, possible particle contamination regions and active or passive measures to reduce particle contamination can be identified. On the other hand, the global dispersion behavior of different particle classes is investigated such that conclusions over the generic movement of particles within a low pressure environment can be drawn. By this, the dispersion of certain particles can be excluded due to geometrical or physical constraints which is valuable information for particle contamination measurement. Beside the modelling of particle transport for the generic valve opening between compartments the present paper includes also the venting-up of a representative load lock to ambient pressure whereas the results of pseudo-3d and a full 3D modelling are discussed with respect to flow topology and particle contamination.

Keywords: DSMC, rarefied flow, particle contamination, load lock

11:00am **VT-TuM10 Improving the Performances of Getter Pumps: Recent Developments in NEG Technology**, *Fabrizio Siviero, G. Bongiorno, L. Caruso, A. Gallitognotta, L. Viale, E. Maccallini, P. Manini*, SAES Getters, Italy **INVITED**

Non Evaporable Getter (NEG) pumps are commonly used when large pumping speeds for H₂ and active gases (i.e., H₂O, O₂, CO, CO₂) are required. The NEG pumps are very small, lightweight, with reduced magnetic interference, cause no vibration, and consume negligible power. Thanks to these qualities NEG pumps are widespread in many UHV applications.

Nevertheless, some factors still limit an even wider diffusion of NEG pump technology, mainly related to the topics of particle release and gas evolution during activation. Indeed, as a precaution, NEG pumps are generally not used in application requiring particle-free environment. Only recently, measurements performed at a large accelerator facility have shown the compatibility of St172[®] alloy sintered getters in particle free environments, i.e RF cavities, after suitable treatments. Also, it is well known during getter activation hydrogen as well as other physisorbed species are desorbed causing pressure increase up to the 1e-6 mbar range. In some applications this is seen as a problem due, for example to constraints in pumping efficiently hydrogen away from long and narrow chambers.

These topics will be discussed based on recent outcomes of research activities carried out in SAES R&D labs to address these issues. New alloys, belonging to the ZAO[®] family, and new production processes have been developed, showing interesting characteristics. Among them we highlight intrinsically reduced particle release, lower hydrogen equilibrium isotherms and more efficient management of the gas load during activation. These properties are combined with a new pump design, even more compact and simpler to install than before, with the aim of providing an enlarged community of users with smarter solutions to their vacuum needs.

11:40am **VT-TuM12 Advanced High Speed Water Vapor Cryopumps: Enabling Today's Vacuum Processes**, *Kevin Flynn, C. Rebecchi*, Brooks Automation, Inc., Polycold **INVITED**

Effective and efficient pumping of water vapor in vacuum systems via cryopumps or cryotraps is critical to achieving required vacuum system performance for many processes. A brief overview of general cryopumping methods is presented along with an in depth review of water vapor cryopumping. Water is of special importance due to its difficulty to be

pumped, its deleterious impact on coatings when it remains on the substrate, and its ability to form oxygen which reacts with and degrades thin film quality. In addition to the basic pumping function, the ability of a cryopump to rapidly cool and defrost or regenerate the cryosurface are important for enabling high chamber productivity. Required water vapor partial pressures vary widely among typical vacuum processes, ranging from 10⁻¹ torr to below 10⁻⁹ torr. Similarly required pumping speeds range from thousands of liters per second to over 200,000 liters per second. The combination of these varying requirements drive different demands for cryopump cooling capacity and temperatures. A variety of different vacuum applications covering medium, high and ultra high vacuum applications, and including batch and inline processes, are reviewed along with considerations of cryosurface location relative to the chamber and process.

Tuesday Lunch, November 11, 2014

Exhibitor Technology Spotlight

Room: Hall ABC - Session EW-TuL

Exhibitor Technology Spotlight Session

Moderator: Chris Moffitt, Kratos Analytical Limited, UK

12:40pm **EW-TuL2 New Developments in Surface Analysis from Thermo Fisher Scientific**, *Tim Nunnery, P. Mack, A.E. Wright, R.G. White, A. Bushell*, Thermo Fisher Scientific, UK

Thermo Scientific offers a broad range of analytical techniques for materials characterisation, including XPS, Raman spectroscopy, FTIR spectroscopy, EDS, WDS and EBSD. In this presentation we will discuss our latest developments in instrumentation and software to extend our surface analysis capabilities.

1:00pm **EW-TuL3 What's New from Physical Electronics**, *Scott Bryan, J.F. Moulder*, Physical Electronics Inc.

The latest innovations in our XPS, AES, and TOF-SIMS products will be presented.

1:20pm **EW-TuL4 Latest Developments and Applications of X-ray Photoelectron Spectroscopy**, *Chris Blomfield*, Kratos Analytical Limited, UK

X-ray Photoelectron Spectroscopy (XPS) is a mature surface analysis technique allowing quantitative surface chemical analysis on a wide range of materials. Recent developments in acquisition and data treatment methodologies have extended the capabilities of the technique. Nanoscale depth information can now routinely be obtained through angle resolved XPS and the data presented in classical depth versus concentration plots. XPS depth profiling techniques employing ion etching which have been used to investigate thin films of inorganic materials can now be extended to a range of organic materials through the introduction of giant gas cluster ion sources. XPS imaging can be used to observe the lateral distribution of different chemical species on the micron scale. New higher energy X-ray sources can increase the capability of laboratory XPS instruments with both extended photon energy range, exciting emission from deeper core levels and increased analysis depth capabilities which have previously only been available at synchrotron light sources. New generation data systems have made the operation and maintenance of XPS instruments routine with automated acquisition and processing workflows increasing the sample throughput and accuracy of measurements. The Axis Supra and ESCApe data system are the latest developments in XPS hardware and software which bring all of the above mentioned capabilities together in a new instrument and software platform, combining ease of use and high throughput with research grade performance and flexibility. The electron optics and underlying technology are an evolution of the well-established Axis spectrometers from Kratos Analytical. This presentation will illustrate the capabilities of the Axis Supra with a range of the latest applications from a diverse range of materials systems.

1:40pm **EW-TuL5 EW Bruker2 Abstract**, *Corporation Bruker*, Bruker Corporation

Tuesday Afternoon, November 11, 2014

2D Materials Focus Topic

Room: 310 - Session 2D+AS+HI+MC+NS+PS+SP+SS-TuA

2D Materials Characterization including Microscopy and Spectroscopy

Moderator: Manish Chhowalla, Rutgers University

2:20pm **2D+AS+HI+MC+NS+PS+SP+SS-TuA1 Layer-Dependent Electronic and Physical Structure of 2D van der Waals Crystals, Richard Osgood, Columbia University** **INVITED**

Because of their weak Van der Waals interlayer bonding transition-metal dichalcogenide (TMDC) semiconductors can be fabricated into atomically thin two-dimensional (2D) crystals with substantial ~1-2 eV bandgaps. As one example, monolayer MoS₂ consists of a single layer of Mo atoms sandwiched between two layers of S atoms in a trigonal prismatic structure. The TMDC 2D system has attracted great interest because of its distinctive electronic and optical properties, such as (i) a transition from indirect-to-direct band gap in going from the multilayer to monolayer crystal due to a missing interlayer interaction in monolayer form and (ii) strong spin-orbit-coupling-induced split valence bands, i.e. 100's of meV, due to broken inversion symmetry, which makes TMDCs interesting for spin-physics physics and devices. Both properties have been predicted with density functional theory (DFT) calculations and indirectly demonstrated using photoluminescence and Raman spectroscopy.

Recently we have made a series of direct observations of the thickness-dependent electronic-band and crystal structure of TMDCs of both exfoliated and CVD grown sample. Because of the relatively modest sample sizes we have used micrometer-scale, angle-resolved photo-emission spectroscopy (micro-ARPES) of both the exfoliated and chemical-vapor-deposition-grown crystals; these measurements provide direct evidence for the shifting of the valence band maximum from gamma bar (Brillouin zone center) to kappa bar (Brillouin zone corner), as the sample thickness decreases from bulk to monolayer. Our initial results were with MoS₂ and are described in a preliminary way in Refs 1 and 2. Our TMDC experimental results are compared with rigorous DFT calculations of both the bands and the UV transitions matrix elements. The results show an evolution in band structure, which is consistent with an indirect-to-direct bandgap transition in going from few-layer to monolayer TMDC and can be attributed to changes in quantum confinement as the number of layer decreases. Our microARPES and, subsequently, higher resolution nanospectroscopy data provide clear measurements of the hole effective mass, the strain present in the monolayer crystal films, and the valence-band spin-orbit splitting. Our results explain the low hole mobility of monolayer MoS₂ compared to thicker MoS₂ and show clearly the strong orbit split energies. Our results, using nanoLEED and LEEM also provide insight into the structure and defects in monolayer films. Experiments using K-doping of single-crystal samples and resulting level shifts are also described.

1. W. Jin, P.-C. Yeh, N. Zaki, D. Zhang, J. T. Sadowski, A. Al-Mahboob, A. M. van der Zande, D. J. A. Chenet, J. I. Dadap, I. P. Herman, P. Sutter, J. Hone, R. M. Osgood, Jr., "Direct Measurement of the Thickness-Dependent Electronic Band Structure of MoS₂ Using Angle-Resolved Photoemission Spectroscopy." *Phys. Rev. Lett.* **111**, 106801 (2013)

2. Po-Chun Yeh, Wencan Jin, Nader Zaki, Datong Zhang, Jerzy T. Sadowski, Abdullah Al-Mahboob, Arend M. van der Zande, Daniel A. Chenet, Jerry I. Dadap, Irving P. Herman, Peter Sutter, James Hone, and Richard M. Osgood, Jr., "Probing substrate-dependent long-range surface structure of single-layer and multilayer MoS₂ by low-energy electron microscopy and microprobe diffraction," *Phys. Rev. B* **89**, 155408 (2014)

3:00pm **2D+AS+HI+MC+NS+PS+SP+SS-TuA3 X-ray Photoemission and Electron Energy Loss Spectroscopy Investigation of the Band Gap and Band Alignment for h-BN and MoS₂ Materials and Interfaces, Benjamin French, J. Brockman, M. French, M. Kuhn, J.D. Bielefeld, S.W. King, Intel Corporation, E. Bersker, G. Bersuker, SEMATECH, J. DiStefano, Y.C. Lin, J.A. Robinson, Penn State University**

Hexagonal boron nitride (h-BN) and molybdenum disulfide (MoS₂) are two dimensional (2D) materials of significant interest for future nano-electronic devices. Due to a wide band gap (~6 eV), close lattice matching (<2%) and atomic planarity, hexagonal boron nitride (h-BN) is of primary interest as a potential substrate and gate dielectric in graphene channel transistor devices. In contrast, MoS₂ is a 2D semiconducting material with a band gap of ~1.8 eV that is attractive as a possible complement or alternative to

graphene for nano-electronic devices requiring a large band gap. A key property for the success of both h-BN and MoS₂ in such devices is the interfacial band alignment with graphene, the gate contact metallization and the surrounding insulating dielectric materials. In this regard, we have utilized x-ray photoelectron spectroscopy (XPS) to determine the Schottky barrier and valence band offsets present at the interfaces between plasma enhanced chemically vapor deposited amorphous h-BN:H and chemically vapor deposited MoS₂. In combination, we have utilized reflection electron energy loss spectroscopy (REELS) to investigate the band gap of both h-BN and MoS₂ materials to deduce the conduction band alignment. We show that in many instances the valence and conduction band offsets are significant and favorable for MoS₂/h-BN transistor devices.

3:20pm **2D+AS+HI+MC+NS+PS+SP+SS-TuA4 STM/STS Characterization of MoS₂ Monolayers and Nanostructures, A. Mills, C. Chen, Virginia Tech, Y. Yu, L. Cao, North Carolina State University, Chenggang Tao, Virginia Tech**

Atomically thin molybdenum disulfide (MoS₂) and nanostructures have been the subject of intense research efforts for their fascinating properties and potential applications in future electronic and optical devices. Especially, monolayer MoS₂, an atomically thin semiconductor with a direct band gap, as opposed to an indirect band gap in bulk MoS₂, has been demonstrated as field effect transistors, optoelectronic devices and chemical sensors. In our experimental study, Monolayer MoS₂ and MoS₂ triangular nanostructures are synthesized through a self-limiting chemical vapor deposition (CVD) approach. The precursor materials, MoCl₅ and sulfur, react at high temperatures to produce MoS₂ species and subsequently precipitate onto substrates to yield MoS₂ films and triangular nanostructures. Using scanning tunneling microscopy (STM), we have investigated the structural and electronic properties of monolayer MoS₂ grown on glassy carbon and triangular MoS₂ nanostructures on highly ordered pyrolytic graphite (HOPG). We will also discuss our scanning tunneling spectroscopy (STS) measurements on these structures.

4:40pm **2D+AS+HI+MC+NS+PS+SP+SS-TuA8 Surface Characterization of Metal Oxide Layers Grown on CVD Graphene and Spin Precession Measurements, Akitomo Matsubayashi, University at Albany-SUNY, W. Nolting, University of Albany-SUNY, D. Sinha, University at Albany-SUNY, A. Jayanthinarasimham, J.U. Lee, University of Albany-SUNY, V.P. LaBella, University at Albany-SUNY**

Ultra thin metal oxide films grown on graphene can be utilized as dielectric barriers between metals and graphene to help isolate a metal contact from the graphene channel for device applications. This is particularly important for graphene based spintronic devices as tunnel barriers between the ferromagnetic metal as a spin injector and graphene have been known to increase the spin relaxation time measured utilizing non-local detection technique of spin precession by avoiding the conductivity mismatch problem. However, simply depositing metal oxide layers such as aluminum oxide on graphene results in non-uniform film lowering the quality of the interface barrier. We will present a systematic study of aluminum oxide layers grown on CVD graphene under ultra-high vacuum conditions with and without titanium seed layers. The aluminum oxide layers with the 0.2 nm titanium seed layers showed reduced surface roughness. The chemical and structural composition determined by XPS will be also presented that shows full oxidation of the aluminum and partial oxidation of the titanium. The I-V characteristic study performed to electrically evaluate the metal oxide and the preliminary results of non-local spin precession measurements will be also addressed.

5:00pm **2D+AS+HI+MC+NS+PS+SP+SS-TuA9 Morphology of CVD-grown Hexagonal Boron Nitride on Cu Foils, Karthik Sridhara, W.G. Cullen, University of Maryland, College Park, J.K. Hite, Naval Research Laboratory, M.S. Fuhrer, Monash University, Australia, D.K. Gaskill, B.N. Feigelson, Naval Research Laboratory**

Hexagonal boron nitride (h-BN) has grown into prominence as a dielectric for graphene heterostructures. h-BN and graphene have been grown using chemical vapor deposition on various transition metal substrates. Compared to graphene, the morphology of CVD-grown h-BN on Cu has not been as widely studied. Here, we present a systematic study of the morphology of hexagonal boron nitride (h-BN) grown on polycrystalline Cu foils by chemical vapor deposition. The growth of h-BN is performed at ~1000°C in atmospheric pressure CVD with Ammonia Borane (H₃NBH₃) as the precursor. The copper foils, used as catalytic substrates, are thermally annealed at ~1030°C for >5 hours prior to growth and cooled slowly following growth termination. We utilized Ultra-high vacuum Scanning Tunneling Microscopy (STM), ambient AFM and SEM to assess the morphology of the CVD grown h-BN films. Highly symmetric single

crystallites of h-BN are observed for sub-monolayer growth, in agreement with recent reports. We consistently observe a corrugated topographic structure within the h-BN crystallites which is distinctly different from the surrounding copper surface, and this is consistently seen in STM, AFM, and high-resolution SEM. Our aim is to understand the nature of this difference and whether it might be due to effects of differential thermal contraction between h-BN and copper. However, complications arise due to possible changes in the copper substrate topography post-growth due to surface oxidation of the copper. Preliminary results with lateral force microscopy (LFM, frictional mode) show that these corrugations are unidirectional in a single Cu grain irrespective of the orientation of the h-BN crystal and generate frictional forces 200% greater than on the surrounding copper surface, reminiscent of earlier reports of unique frictional behavior in atomically-thin membranes [1]. STM and AFM are also used to study the twin crystal boundaries of h-BN. Preliminary STM observations indicate that merging h-BN crystals consistently have a gap of about 5 nm between them. The results of this study are independent of small variations of growth conditions.

References:

[1] C. Lee, Q. Li, W. Kalb, X.-Z. Liu, H. Berger, R. Carpick, and J. Hone, "Frictional characteristics of atomically thin sheets," *Science* (New York, N.Y.), vol. 328, no. 5974, pp. 76–80, 01-Apr-2010.

5:20pm **2D+AS+HI+MC+NS+PS+SP+SS-TuA10 Influence of Chemisorbed Oxygen on the Growth of Graphene on Cu(100) and Cu(111) by Chemical Vapor Deposition, EngWen Ong**, University at Albany-SUNY, Z.R. Robinson, U.S. Naval Research Laboratory, T.R. Mowll, P. Tyagi, University at Albany-SUNY, H. Geisler, SUNY College at Oneonta, C.A. Ventrice, Jr., University at Albany-SUNY

The influence of chemisorbed oxygen on the growth of graphene by catalytic decomposition of ethylene in an ultra-high vacuum (UHV) chamber on both the Cu(100) and Cu(111) surfaces has been studied. A custom UHV compatible heater stage was constructed that allows heating of a crystal to temperatures as high as 1000 °C at hydrocarbon pressures of up to 100 mTorr. System recovery to the low 10^{-10} Torr range is achieved within a few minutes of opening the gate valve to the turbo pump. The crystal structure of the graphene films was characterized with in-situ low energy electron diffraction (LEED), and the growth morphology was monitored by ex-situ scanning electron microscopy (SEM). For the clean Cu(100) substrate, heating from room temperature to the growth temperature while dosing with ethylene resulted in the formation of epitaxial graphene films. The crystal quality was found to depend strongly on the growth temperature. At 900 °C, well-ordered two-domain graphene films were formed. For the Cu(111) surface, heating from room temperature to the growth temperature while dosing with ethylene did not result in the formation of graphene. This is attributed to the lower catalytic activity of the (111) surface and the relatively high vapor pressure of the Cu surface. The use of an Ar overpressure to suppress Cu sublimation during the growth resulted in the formation of predominately single-domain epitaxial graphene films. Predosing either the Cu(100) or Cu(111) surface with a chemisorbed layer of oxygen before graphene growth was found to adversely affect the crystal quality of the graphene overlayers by inducing a much higher degree of rotational disorder of the graphene grains with respect to the substrate. The SEM analysis revealed that the nucleation rate of the graphene islands dropped by an order of magnitude after predosing either the Cu(100) or Cu(111) surface with a chemisorbed oxygen layer before growth. On the other hand, the average area of each graphene island was observed to increase by at least an order of magnitude. Therefore, the presence of oxygen during graphene growth affects both the relative orientation and average size of grains within the films grown on both substrates.

5:40pm **2D+AS+HI+MC+NS+PS+SP+SS-TuA11 Novel Materials Properties at Atomically Thin Limit, Zhi-Xun Shen**, Stanford University **INVITED**

In this talk, I will discuss recent progresses in uncovering novel materials properties at ultra-thin limit, with focus on mono-unit-cell superconductor FeSe and semiconductor MoSe₂ respectively.

The observation of a large superconducting-like energy gap which opens at temperatures up to 65 K in single unit cell (1UC) thick iron selenide films on SrTiO₃(FeSe/STO) has generated tremendous interest. A challenge is to understand the cause of enhanced Cooper pairing strength in this system, and possibly increase superconducting T_c. In this talk, we show angle-resolved photoemission spectroscopy, mutual inductance, and other measurements on 1UC and multi-UC thick FeSe films grown on Nb-doped SrTiO₃. Our data provide clear evidence for strong cross-interface electron-phonon coupling in single UC, raising the possibility that large pairing gap are caused by the strong coupling between the FeSe electrons and certain

collective modes of SrTiO₃. This suggests a pathway of "integrated functional components" approach to boost superconducting properties.

The intense interest of quantum systems in confined geometries is further amplified by the recent discovery of large enhancement in photoluminescence quantum efficiency and a potential route to "valleytronics" in atomically thin layered transition metal dichalcogenides (TMDs) MX₂ (M = Mo, W; X = S, Se, Te), which are closely related to the indirect to direct band gap transition in the single layer limit. Using angle-resolved photoemission spectroscopy (ARPES) on high quality thin film samples of MoSe₂ grown by molecular beam epitaxy (MBE), we have made a direct observation of a distinct transition from indirect to direct band gap as the thickness of the sample is reduced to a monolayer. The experimental band structure indicates a stronger tendency of monolayer MoSe₂ towards direct band gap with larger gap size than theoretical prediction. A comparison of directly measured ARPES band gap and optical data led to important new insights on semiconductor physics in 2D. Moreover, our finding of a significant spin-splitting of ~180meV at the valence band maximum (VBM) of a monolayer MoSe₂ film could greatly expand its possible application in spintronic devices.

If time permits, I will also discuss the superconductivity in CaC₆ and its implication on a possible pathway for superconducting graphene.

Applied Surface Science

Room: 316 - Session AS+MC+SS-TuA

Analysis of Modified Surfaces

Moderator: Xia Dong, Eli Lilly and Company, Carl Ventrice, Jr., University at Albany-SUNY

2:20pm **AS+MC+SS-TuA1 Analysis of Surface-oxidized Polypropylene Films, Mark Strobel, S.J. Pachuta, D. Poirier, H. Lechuga**, 3M Company **INVITED**

The most widely used industrial processes for modifying the surfaces of polymer films are flame and corona (dielectric barrier discharge) treatments. While both of these processes oxidize a thin surface region of the treated films, there are significant differences between the surfaces generated by the two surface-oxidation processes. A principal difference between corona and flame treatments is the likelihood to form water-soluble low-molecular-weight oxidized material (LMWOM). LMWOM is formed by the simultaneous oxidation and chain scission of a polymer material. LMWOM is an important surface characteristic that has a large effect on the wetting and adhesion properties of polymer surfaces.

LMWOM can be investigated by a number of surface analytical techniques, including x-ray photoelectron spectroscopy (XPS or ESCA), static secondary ion mass spectrometry (SIMS), atomic force microscopy (AFM), and contact angle measurements. This presentation will demonstrate how surface analysis enables the detection and detailed characterization of the LMWOM formed by the flame and corona treatment of polypropylene (PP) film surfaces. The mechanism of LMWOM formation can be then determined from these analytical results when coupled with an understanding of the bulk photo-and-thermal degradation of PP materials.

3:00pm **AS+MC+SS-TuA3 XPS Analysis for Modified Fabrics, Christopher Deeks**, Thermo Fisher Scientific, UK, M. Milošević, M. Radoičić, Z. Šaponjić, University of Belgrade, Serbia, T.S. Nunney, Thermo Fisher Scientific, UK, M. Radetić, University of Belgrade, Serbia

Modifications of fabrics are becoming more important for a wide variety of applications. For example, loading TiO₂ onto cotton can improve many of the material properties, such as anti-bacterial effects, UV protection, and stain resistance.

The conformity of these modifications across sample surfaces are an important part of the application process. By using XPS in addition to other techniques, surface concentration and conformity can be determined and deduced whether the samples have met certain criteria, and how the uniformity, of lack thereof, can affect the desired outcome of the modifications.

This presentation will look at the possibility of in situ photoreduction of Ag ions on the surface of TiO₂ nanoparticles to create "active fabrics", and will utilise XPS imaging to determine whether deposition on the surface of different fabrics has been successful.

3:20pm **AS+MC+SS-TuA4 Characterization of Corona Treated Polymers, Michaelen Pacholski**, The Dow Chemical Company

Corona treatment is often used to increase the surface energy and surface polarity of polyolefins and other polymers. In this study corona-treated,

formulated polyolefin was characterized over the course of one year by SIMS, XPS and surface energy. The changes in surface chemistry could be fit to simple models to predict long-term behavior. This system is more complex than many others discussed in literature, as the formulation ingredients change in surface concentration with time, in addition to the typical decrease in surface oxygen concentration over time. SIMS and XPS measurements were used to characterize the complex surface changes as the surface energy was monitored. Additional examples of corona treated PET will also be presented.

4:20pm AS+MC+SS-TuA7 Investigation of Atmospheric Pressure Plasma Jet as a Pre-Treatment for Adhesive Bonding of Structures Made of Carbon Fiber Reinforced Plastics (CFRP), Timo Hofmann, J. Holtmannspötter, Bundeswehr Research Institute for Material, Fuels and Lubricants, Germany, T. Meer, Airbus Group Innovations, Germany, J. Rehbein, G. Härtl, Bundeswehr Research Institute for Material, Fuels and Lubricants, Germany

Carbon fiber reinforced plastics (CFRPs) are increasingly employed in novel aircraft structures due to their high tensile strength, low weight, favorable fatigue behavior, and ruggedness against outer influences (corrosion). Joining of CFRP structures is currently performed using rivets and bolts. In order to exploit further weight-saving potential, the usage of adhesive bonding is intended.

An important key factor for the success of adhesive bonding is the surface pre-treatment of the adherents. Peel-plies are commonly used for the fabrication of CFRP structures and, in theory, are said to create a pristine and uncontaminated fractured surface upon removal. In reality, the presence of release agents leads to contaminated surfaces that may cause unforeseeable failures of structures in service.

In this contribution, CFRPs (Hexcel 8552 / IM7) were produced using various peel-plies and release foils currently employed in aerospace manufacturing processes. Atmospheric pressure plasma jet (APPJ) was investigated as a method to further improve adhesion and to clean the samples from release agents.

We present a detailed investigation of the surface morphology and composition of CFRPs before and after treatment with APPJ. The peel-plies and the CFRP surfaces were examined by a combination of Field-Emission Scanning Electron Microscopy (FE-SEM), X-Ray Photoelectron Spectroscopy (XPS), and Energy-Dispersive X-ray spectroscopy (EDX).

We studied the approach of surface functionalization and contaminant removal by variation of the type of peel ply, release agent, and plasma treatment parameters. In the experiments particular focus was placed on determining changes in the chemical composition of the surface and morphology. We demonstrate that APPJ-processes offer limited cleaning capabilities for CFRP surfaces. Furthermore, the ability to induce morphological changes is highly dependent on the initial level of surface roughness and chemistry. Finally, we show that overtreatment leads to degradation of the epoxy component and enrichment of the thermoplastic portion of the matrix on the surface.

4:40pm AS+MC+SS-TuA8 Thickness and Composition Determination of Thin Film Sn-Oxides Growth at Room Temperature using XPS Spectra, M. Bravo-Sanchez, CINVESTAV-Queretaro, Mexico, Jorge Huerta-Ruelas, Instituto Politecnico Nacional, Mexico, A. Herrera-Gomez, CINVESTAV-Queretaro, Mexico

The knowledge of the tin oxidation process is important for the development corrosion-free coatings and the engineering of alloys and compounds with specific functional properties. Tin, pure and well controlled oxidized samples were characterized by X-ray photoelectron spectroscopy (XPS). All samples were prepared on Si (100) substrates with RCA treatment before Sn deposition. The thickness of the Sn layer was approximately 100 Å as measured by a thickness monitor. The pure Sn sample was measured without ambient exposure. The oxidized samples were obtained by exposing pure Sn samples to pure oxygen at a pressure of 1×10^{-4} Torr. Three different exposure times were used: 10, 180 and 1200 seconds. To fit XPS spectra, traditional and novel method (using a double-Lorentzian) were employed to calculate thickness and composition of the oxide layer. High resolution transmission electron microscopy measurements were performed to validate calculations. Structural parameters obtained with different XPS data fitting approaches were compared, showing a clear advantage of the double-Lorentzian method in the understanding of the initial stages of tin oxidation.

5:00pm AS+MC+SS-TuA9 Understanding the Physiochemical and Ice-Nucleation Properties of Bare and Sulfuric Acid Coated Atmospheric Mineral Dust Aerosols, Manjula Nandasiri, N. Madaan, A. Devaraj, G.R. Kulkarni, T. Varga, V. Shutthanandan, S.A. Thevuthasan, Pacific Northwest National Laboratory

The relationship between atmospheric aerosols and the formation of clouds is among the most uncertain aspects in our current understanding of climate change. Especially, ice and mixed-phase clouds have been less studied even though they have extensive global coverage and dominate precipitation formation. As a result, the climatic impact of ice-containing clouds is not well-understood and there is urgent need to improve ice nucleation formulations in climate models. In order to understand this phenomenon, ice nucleation experiments and parameterization development need to be carried out. Specifically, heterogeneous ice nucleation processes are sensitive to surface properties of atmospheric aerosols, which can accumulate sulfates and organics during atmospheric transport. Thus, here we investigated the physical and chemical properties on the surface of a mixed mineral dust aerosol: Arizona test dust (ATD) and kaolinite mineral dust aerosol particles that trigger ice formation.

In this study, bare and sulfuric acid coated ATD and kaolinite particles were characterized using advanced spectroscopy and microscopy techniques. These particles were reacted with sulfuric acid with different strengths in a systematic way to obtain uniform coatings on the particle surface. Following the acid reaction, the surface composition, chemical state, and elemental mapping of ATD and kaolinite particles were studied using X-ray photoelectron spectroscopy (XPS) and XPS imaging techniques. XPS showed significant changes in composition, chemical state, and elemental distribution of Si and Al on the surface of ATD and kaolinite particles due to the acid reaction. These surface properties also depend on the strength and pH value of the sulfuric acid. The surface morphology, particle size and distribution, and composition of these samples were further studied using scanning electron microscopy (SEM) combined with energy dispersive X-ray spectroscopy (EDS). The high resolution SEM micrographs showed differences in surface morphology between bare and coated samples. X-ray diffraction was also carried out to study the changes in crystallinity of ATD and kaolinite particles due to the acid coating. The samples were further characterized using atom probe tomography and transmission electron microscopy to understand the 3-D chemical distribution and microstructure, respectively. Following the characterization of physiochemical properties, ice-nucleation experiments were also carried out on ATD and kaolinite samples, which will be discussed here.

5:20pm AS+MC+SS-TuA10 A Study of the Effect of Deep UV (172nm) Irradiation on Polyimide Surfaces, Lopamudra Das, M.J. Kelley, The College of William and Mary

Polyimides have a wide range of industrial and scientific applications where changes in surface structure due to UV radiation are of significant interest. Particularly in its use in spacecraft, the effect of deep UV is important to predict photo-degradation of the material. We investigated the response of commercial samples of PMDA-ODA (PI) films to 172nm UV from a xenon excimer lamp in the absence of oxygen, using XPS, ToF/SIMS, and AFM.

5:40pm AS+MC+SS-TuA11 Small-Angle/Wide-Angle X-ray Scattering Investigation of Functional Materials at Inorganic-Macromolecular Interfaces, Ich Tran, T.W. van Buuren, T.M. Willey, J.R.I. Lee, M. Bagge-Hansen, A. Noy, R. Tunuguntla, K. Kim, Lawrence Livermore National Laboratory

Development in nanoscale engineering has enabled bioelectronics that can mimic and/or interact with the biological systems. Lipid bilayer-functionalized Si nanowires are considered as a promising candidate for the construction of bio-nanoelectronic devices. These biomimetic lipid bilayers serve as a general host matrix for bio-functional components such as membrane proteins. Though meaningful technological advancements have been made, critical questions still remain, in particular on structural characteristics of lipid bilayers at the interface with inorganic nanomaterials. Small-angle and wide-angle x-ray scattering (SAXS/WAXS) techniques are used to investigate self-organizations of dioleoyl-phosphatidylcholine (DOPC) lipid bilayers on Si nanowires. Critical structural parameters of the lipid bilayers (lamellarity, bilayer thickness and packing order of lipid molecules) are obtained through analyzing SAXS-derived Electron Density Profile (EDP). A decrease in bilayer thickness and a packing disorder of the lipid head groups in adjacent to supported Si nanowires have been observed upon coating on Si nanowires. Furthermore, effects on the packing order of lipid hydrocarbon tails induced by the incorporations of proteins or carbon nanotubes into lipid bilayers (served as natural or artificial ion channels, respectively) have been identified and characterized. The results shed light on a number of unresolved questions that are crucial for the comprehensive understanding this class of materials.

Biomaterial Interfaces

Room: 317 - Session BI+AS-TuA

Characterization of Biointerfaces

Moderator: Joe Baio, Oregon State University

2:20pm **BI+AS-TuA1 Comparative Study of the Bonding and X-ray Induced Reactions of Thiolated and Unthiolated DNA Adsorbed on Gold**, *Richard Rosenberg*, Argonne National Laboratory, *J.M. Symonds*, Georgia Institute of Technology, *K. Vijayalakshmi*, Argonne National Laboratory, *D. Mishra*, Weizmann Institute of Science, Israel, *T.M. Orlando*, Georgia Institute of Technology, *R. Naaman*, Weizmann Institute of Science, Israel

High energy ionizing irradiation produces large amounts of low energy (<20 eV) secondary electrons (SEs). These electrons are produced via a cascade process following the ionization of a core (deeply bound) electron. Due to their low energy there is a high probability for the SEs to become trapped in antibonding orbitals, via resonant scattering, forming a temporary negative ion (TNI) resonance. If the lifetime of the TNI state is long enough, then bond rupture can occur by a process known as dissociative electron attachment (DEA). There is vast literature on the role of TNI states and DEA in DNA related radiation chemistry.[1,2] Due to its high flux density, synchrotron radiation (SR) has often been used to induce and study radiation chemistry in numerous systems,[3] including DNA and related molecules. SR has also been used to probe the electronic structure and bonding of such molecules, primarily by probing the occupied states with X-ray photoelectron spectroscopy (XPS) and the unoccupied states with X-ray absorption (XAS) measurements. Bond overlap and localization can be revealed by XPS while XAS can determine the density of unoccupied states and the orientation of the orbitals. In this presentation we examine X-ray induced reactions of DNA adsorbed on a gold substrate when the DNA is either thiolated (tDNA) or when it is unthiolated (uDNA). By performing polarization-dependent XAS at the N K edge we determined that tDNA protrudes from the surface at ~45 degrees, in agreement with previous studies. We also found that the unthiolated molecules have a similar orientation. However, due to differences in charge transfer between the gold and the DNA in the two systems there is a higher density of unoccupied states in the N-C=N derived π^* orbital for tDNA. We also found that the adsorbed tDNA has a significant higher cross section for radiation damage. The reason for this enhancement could arise from the greater probability of forming a TNI state for the tDNA due to the higher density of unoccupied π^* states.

1. E. Alizadeh and L. Sanche, Chem. Rev. **112**, 5578 (2012).
2. R. Naaman and L. Sanche, Chem. Rev. **107**, 1553 (2007).
3. R. A. Rosenberg and S. P. Frigo, in Chemical Applications of Synchrotron Radiation, Part II: X-ray Applications, edited by T.K. Sham (World Scientific Publishing Co., Singapore, 2002), Vol. 12A, p. 462.

2:40pm **BI+AS-TuA2 XPS Binding Energy Shifts for DNA Brushes on Gold**, *C.C.A. Ng*, *Dmitri Petrovykh*, International Iberian Nanotechnology Laboratory, Portugal

DNA biointerfaces are important in a wide range of existing and emerging applications, such as biosensors, functionalization of nanoparticles for biomedical applications, and self-assembly of complex and functional nanostructures. The complexity of many of the DNA biointerfaces created for such applications often limits the ability to unambiguously interpret the results obtained from spectroscopy measurements for such systems. A powerful and successful approach to improving the analytical capabilities has been based on creating robust and well-defined reference systems, which then provide the insight for data interpretation in more complex analyses. Brushes of oligo(dT) single-stranded DNA can be attached to gold either via terminal thiol linkers, or via terminal blocks of (dA) nucleotides. While the former method results in a brush of roughly upright oligo(dT) strands relatively weakly interacting with one another, the complementarity of (dA) and (dT) blocks within the same strand creates a possibility of intra-strand hairpin-like hybrids in the (dA)-anchored case. Varying the parameters of these DNA brushes and deposition solutions creates a series with expected variation of thickness, surface density, and intra-strand interactions. Gold substrate provides a convenient binding energy (BE) reference for accurate XPS measurements of the characteristic DNA peaks. Following this approach, we find an unexpected BE shift of a N 1s peak across the series of DNA brushes. Typical effects observed in organic films

do not appear to account for the full magnitude of the observed shift, so we will discuss the possible interpretations of this effect and its relation to the structure of DNA brushes.

3:00pm **BI+AS-TuA3 Simultaneous 3D Detection of Organics for Intact Samples with Infrared Spectromicrotomography**, *Carol Hirschmugl*, University of Wisconsin Milwaukee **INVITED**

The holy grail of chemical imaging is to provide spatially and temporally resolved information about heterogeneous samples on relevant scales. Synchrotron-based Fourier Transform infrared imaging combines rapid, non-destructive chemical detection with morphology at the micrometer scale, to provide value added results to standard analytical methods. Hyperspectral cubes of (x,y, z, Abs (λ)) are obtained employing spectromicrotomography², a label free approach, it inherently evaluates a broad array of wide organic materials, with minimal sample preparation and modification. Examples presented here (polymer composites, single cells and colonies of cells) demonstrate the broad applicability of this approach to detect complex chemical information of intact samples.

References

- 1 Nasse, M. J., Walsh, M. J., Mattson, E. C., Reininger, R., Kajdacsy-Balla, A., Macias, V., Bhargava, R., and Hirschmugl, C. J. (2011) Nat.Methods 8, 413-416
- 2 Martin, M. C., Dabat-Blondeau, C., Unger, M., Sedlmair, J., Parkinson, D. Y., Bechtel, H. A., Illman, B., Castro, J. M., Keilueit, M., Buschke, D., Ogle, B., Nasse, M. J., and Hirschmugl, C. J. (2013) Nat.Methods 10, 861-864

Acknowledgements

This work was supported by the US NSF under awards CHE-0832298, CHE-1112433, and DMR-0619759, the Research Growth Initiative of the University of Wisconsin-Milwaukee, and is based on research conducted at the Synchrotron Radiation Center, University of Wisconsin-Madison which is supported by the University of Wisconsin-Milwaukee and University of Wisconsin-Madison.

4:20pm **BI+AS-TuA7 Deep Thoughts: ToF-SIMS Profiling to New Depths**, *Daniel Graham*, *L.J. Gamble*, University of Washington

The development of argon cluster sources has opened up new opportunities for ToF-SIMS depth profiling. These sources have enabled depth profiling of a wide range of materials that previously could not be accurately depth profiled. In addition, due to the low damage accumulation and sputtering efficiency of these sources, it is now possible to depth profile through microns of material. This in turn has opened up new opportunities for exploring the 3D chemical environments of a wide range of samples including drug eluting polymers, thick multilayer polymer films and porous tissue scaffolds. However, the ability to dig deeper into samples also results in significant challenges in 3D image reconstruction. For example, due to the fixed geometry of the analysis beam (at 45 deg from the surface normal in our instrument), sputtering away 1 micron of the surface will shift the analysis position by 1 micron. This means that if one were to depth profile 50 microns into a surface, the final image would be shifted by 50 microns. Traditional image registrations methods can be used to accommodate for these shifts, however when digging to depths larger than 10 microns, this requires significantly increasing the initial image size in order to end up with a usable image stack after the image shifting and cropping.

In this presentation we will summarize methods we have been developing to reconstruct deep depth profiles including adjusting the sample height during data acquisition and post acquisition image shifting. We will also show results from a new 3D image overlay tool that enables localization of different chemical environments in 3D and that can show areas of overlap between selected peak area images. These methods and tools will be demonstrated on data from control samples made from polymer beads on silicon and from data taken from polymer tissue scaffolds.

4:40pm **BI+AS-TuA8 Development of Novel Pharmaceutical Systems Through Characterisation**, *David Scurr*, University of Nottingham, UK

The developments in pharmaceutical delivery systems such as injectable drug eluting microparticles [1], topically applied medicines [2] and wound dressings [3] can be utilised in areas such as the treatment of HIV, basal cell carcinoma and microbial infections respectively. In this study, the characterisation of such systems has been performed using time of flight secondary ion mass spectrometry (ToF-SIMS), x-ray photoelectron spectroscopy (XPS) and atomic force microscopy (AFM).

Injectable controlled release formulations were produced by spray drying two biocompatible polymers, poly(lactic-co-glycolic acid) (PLGA) and polyvinylpyrrolidone (PVP). The samples were analysed using a range of techniques including ToF-SIMS, XPS and AFM showing that the samples were hollow microparticles with a surface PLGA rich phase and an

underlying PVP phase [1]. Additionally, more complex ternary systems incorporating PLGA, PVP and a poorly soluble investigational drug compound were also analysed. These studies highlighted the influence of sample processing parameters and drug concentration upon factors such as surface composition which is influential in the drug release properties of the systems.

The permeation of an antibacterial drug, chlorhexidine, into skin tissue has been illustrated using ToF-SIMS chemical imaging of cross-sectioned treated skin samples [2]. This methodology has been further applied to investigate the topical delivery of imiquimod, a drug used in the treatment of basal cell carcinoma. This work demonstrates the ability of the ToF-SIMS technique to correlate chemical species specific to the drug with physiological features within tissue cross-sections. Further application of ToF-SIMS chemical mapping has also been used to successfully differentiate chemically dissimilar regions of anti-microbial films which could be developed as wound dressing materials. Observations made for these materials using a combination of ToF-SIMS and AFM analysis revealed the distribution of the active agents upon the surface which would be relevant to the anti-microbial performance.

[1] Meeus, Scurr, Amssoms, Davies, Roberts, and Van den Mooter (2014) *Molecular Pharmaceutics*, 10 (8)

[2] Judd, Scurr, Heylings, Wan, and Moss (2013) *Pharmaceutical Research*, 30 (7)

[3] Liakos, Rizzello, Scurr, Pompa, Bayer and Athanassiou (2014) *International Journal of Pharmacy*, 463 (2)

5:00pm BI+AS-TuA9 Analysis of Peptide Microarrays on Si Using ToF-SIMS, James A. (Tony) Ohlhausen, C. James, Sandia National Laboratories, D. Smith, HealthTell, S.A. Johnston, N. Woodbury, Arizona State University

A microarray containing over 1200 each 200 μ m diameter spots consisting of various length peptide chain monolayers was analysed using Time-of-flight Secondary Ion Mass Spectrometry (ToF-SIMS). This peptide microarray was created using lithographic processes where chains of peptides were built one amino acid at a time. A silane coupling agent was used to attach the peptides to the oxide surface creating a monolayer of peptides directly bonded to the Silicon oxide surface. By tracking ion fragments corresponding to specific amino acids, usually ammonium ions, we show that contrast consistent with the number of individual amino acid units in a given peptide dot is generally seen. While some ammonium ions are not specific enough to generate clear contrast patterns, most can be used to verify the presence expected amino acids in each peptide dot. Additionally, some amino acids were not found to generate a specific fragment for identification in the positive secondary ion mode.

**Sandia National Laboratories is a multi-program laboratory managed and operated by Sandia Corporation, a wholly owned subsidiary of Lockheed Martin Corporation, for the U.S. Department of Energy's National Nuclear Security Administration under contract DE-AC04-94AL85000.

5:20pm BI+AS-TuA10 Investigating Tumor Microenvironments with ToF-SIMS, Lara J. Gamble, B. Bluestein, D.J. Graham, University of Washington

Cancer is a heterogeneous malignancy that manifests itself in a variety of morphological types and clinical outcomes. Current evidence indicates that tumor metabolism plays a large role in cancer onset and progression, and its causes and effects are under intense scrutiny. Furthermore, it is of interest to know where changes in tumor metabolism occur within an affected tissue. However, there are few techniques that can specifically interrogate the tumor microenvironment. We use time-of-flight secondary ion mass spectrometry (ToF-SIMS) to determine differences in the chemical makeup of the tumor microenvironment of breast cancer tumor tissue samples. Human tissue biopsies from an ongoing trial have been subtyped using DASL genome assay and grouped into subtypes of Luminal B, Basal, and ERBB2. Images and spectra have been acquired on an IONTOF TOF-SIMS V using B_{15}^+ . The ToF-SIMS information, combined with gene expression array analysis is used to investigate the chemical differences between chemotherapeutic resistant tumors and elucidate the underlying mechanisms. Using imaging ToF-SIMS the cellular and stromal regions within the tissue can be separated out as regions of interest (ROI). Imaging principal component analysis (PCA) was successful in separating cellular regions of the tumor and stromal regions when compared with a hematoxylin and eosin (H&E) stained adjacent tissue slice. Using the ROIs identified from imaging PCA, we compare the chemical differences between cellular and stromal microenvironment chemistry. A comparison of spectral PCA using the entire analysis area vs spectral PCA of ROIs for cellular and stromal regions of the tissue is discussed. The chemistries of these subtypes are compared using ToF-SIMS image and spectral comparison from cellular and stromal regions. A spectral comparison of ROIs between tissue samples using PCA indicates that unique fatty acids

distributions may relate to a tumor phenotype and chemotherapeutic resistance.

5:40pm BI+AS-TuA11 Correlative Imaging of Mammalian Cells in Their Native Environments using a Microfluidic Reactor by ToF-SIMS and SIM, Xin Hua, C. Szymanski, Z.Y. Wang, B.W. Liu, Z. Zhu, J.E. Evans, G. Orr, Pacific Northwest National Laboratory, S.Q. Liu, Southeast University, China, X.Y. Yu, Pacific Northwest National Laboratory

Mammalian cell analysis is of significant importance in providing detailed insights into biological system activities. Due to the complexity and heterogeneity of mammalian cell behavior and the technical challenge of spatially mapping chemical components in a hydrated environment, correlated chemical imaging from multiplexed measurement platforms is needed. Fluorescence structured illumination microscope (SIM), with super high resolution and visualization of proteins and sub-cellular structures in 3-D, provides more detailed information in cell imaging. Time-of-flight secondary ion mass spectrometry (ToF-SIMS) is a unique surface-sensitive analytical tool that provides molecular information and chemical mapping with a sub-micron lateral resolution. However, the understanding of how the spatial heterogeneity and structural difference affect the mammalian cell activities in an unperturbed, hydrated state by ToF-SIMS is severely limited due to the challenge to detect liquids with high volatility under high vacuum environment using surface sensitive technique like ToF-SIMS.

We recently developed a novel microfluidic reactor for C10 mouse lung epithelial cell growth for SIM imaging and direct probing of hydrated cell in vacuum using ToF-SIMS. C10 cells were inoculated into the microchannel, incubated at 37 °C for 24 hr., fed with 5 nM quantum dots, and then fixed with 4% paraformaldehyde before SIM imaging. In subsequent ToF-SIMS analysis, an aperture of 2 μ m in diameter was drilled through SiN membrane to form the detection window to image biological surfaces directly; and surface tension is used for holding the liquid within the aperture.

SIM images show that C10 cells are successfully cultured on the SiN membrane, and quantum dots are uptaken by cells and dispersed in the cytoplasm. The ToF-SIMS m/z spectra showing characteristic fragments of dried cell sample, hydrated cells, and uninoculated medium in the microreactor will be presented. Moreover, 2D images of representative cell fragments and quantum dots ion mapping will be discussed. In addition, depth profiling will be used to provide time- and space-resolved imaging of the cells inside the microchannel. Furthermore, principal component analysis is conducted to evaluate the intrinsic similarities and discriminations among samples. Our results demonstrate feasibility for *in situ* imaging of cells in the hydrated state using ToF-SIMS for the first time. Correlative imaging using SIM and ToF-SIMS provides information across different space scales for investigating cell dynamics. This novel approach has great potential for studying intracellular processes in the future.

6:00pm BI+AS-TuA12 Mass Spectrometry using Femtosecond Lasers and Positionization to Characterize Biomaterials Interfaces, Y. Cui, Y.P. Yung, Luke Hanley, University of Illinois at Chicago

Secondary ion mass spectrometry (MS), matrix assisted laser desorption ionization MS, electrospray-based MS and other strategies are widely used for the analysis of intact bacterial biofilms, mammalian tissue, cell cultures, and their interfaces with biomaterials [Bhardwaj & Hanley, *Nat. Prod. Rev.* (2014) dx.doi.org/10.1039/C3NP70094A]. The combination of these desorption/ionization methods with high resolution MS and tandem MS capabilities permit metabolomic and proteomic imaging of such samples. Nevertheless, their use to detect many analyte classes within intact biological samples still often suffers from low sensitivity, selective ionization, and/or poor spatial or depth resolution. Laser desorption with ultrashort pulses can remove material from a solid with minimal damage to the remaining sample, potentially allowing both depth profiling and additionally, higher spatial resolution [Cui, *et al.*, *ACS Appl. Mater. Interf.* 5 (2013) 9269]. Furthermore, laser desorbed neutrals can undergo positionization by vacuum ultraviolet or ultrashort pulse radiation for subsequent detection by MS. Positionization has the additional advantage that proper selection of the delay time between the desorption and positionization laser can improve molecular analysis. Here, we demonstrate the small molecule imaging capability of these methods on intact, multispecies microbial biofilms and other complex organic/biological samples. Finally, comparisons are made to laser desorption MS under atmospheric pressure.

Electronic Materials and Processing

Room: 314 - Session EM+2D-TuA

High-k Dielectrics for Advance Semiconductor

Moderator: Andrew C. Kummel, University of California at San Diego

2:20pm **EM+2D-TuA1 Time-resolved XPS of ALD, Rainer Timm, Lund University, Sweden** **INVITED**

Atomic layer deposition (ALD) has been established as the main technique for creating MOS structures based on III-V semiconductors, but still device performance is limited by the quality of the interface towards the high-k oxide layer. X-ray photoemission spectroscopy (XPS) is a well-suited tool for analyzing the structure and chemical composition of such interfaces. However, conventional XPS studies under ultrahigh vacuum conditions can only compare the situation before and after individual half-cycles of the ALD process. Here I will show how ambient-pressure XPS can be used to study surface structure and chemistry live and *in-situ* during the ALD reaction. As an example, we have investigated the deposition of HfO₂ on InAs using TDMA-Hf and water as precursors, revealing several steps within the chemical reaction of InAs exposed to the Hf precursor material, which we interpret as a temperature-dependent adsorption of unreacted precursor molecules preceding the ligand exchange reaction.

3:00pm **EM+2D-TuA3 GaSb Oxide Thermal Stability Studied by Dynamic-XPS, Stephen McDonnell, B. Brennan, E. Bursa, University of Texas at Dallas, K. Winkler, P. Baumann, Omicron NanoTechnology, Germany, R.M. Wallace, University of Texas at Dallas**

GaSb is a III-V material with applications as a potential channel material for p-type metal-oxide-semiconductor field effect transistors,¹ optoelectronics in the infrared region,² quantum devices,³ and tunnel field effect transistors.⁴ Prior to application specific processing it is often necessary to remove the GaSb native oxide, which can be quite thick. Such oxides can inhibit subsequent epitaxy and also be a source of traps for devices as a result of defect levels in the energy gap.⁵ The thermal desorption of these oxides in ultra high vacuum has been examined in previous works, but is revisited in this study with dynamic-x-ray photoelectron spectroscopy (dynamic-XPS). Dynamic-XPS allows for the collection of core-level spectra in real time (i.e. data acquisition times are < 1 second). Combined with controlled heating, this allows for detailed chemical temperature-dependent chemical analysis to be carried out with temperature resolutions better than 1 Kelvin. The thermal decomposition of the native GaSb oxides is studied using dynamic-XPS. The expected transfer of oxygen from Sb-O to Ga-O before the eventual desorption of all oxides is observed. However an initial reaction resulting in the reduction of Sb₂O₃ along with the concurrent increase in both Ga₂O₃ and Sb₂O₄ is detected in the temperature range of 450-525 K. Using the relative changes in atomic concentrations of the chemical species observed, the initial reaction pathway is proposed.

A. Nainani, T. Irisawa, Z. Yuan, Y. Sun, T. Krishnamohan, M. Reason, B. R. Bennett, J. B. Boos, M. G. Ancona and Y. Nishi, presented at the Electron Devices Meeting (IEDM), 2010 IEEE International, 2010 (unpublished).

F. Chen, G. Liu, Z. Wei, R. Deng, X. Fang, S. Tian, Y. Zou, M. Li and X. Ma, presented at the Optoelectronics and Microelectronics (ICOM), 2012 International Conference on, 2012 (unpublished).

M. V. Lebedev, E. V. Kunitsyna, W. Calvet, T. Mayer and W. Jaegermann, The Journal of Physical Chemistry C **117**, 15996-16004 (2013).

A. W. Dey, B. M. Borg, B. Ganjipour, M. Ek, K. A. Dick, E. Lind, C. Thelander and L.-E. Wernersson, Electron Device Letters, IEEE **34**, 211-213 (2013).

A. Ali, H. Madan, A. Kirk, D. Zhao, D. Mourey, M. Hudait, R. Wallace, T. Jackson, B. Bennett and J. Boos, Appl Phys Lett **97**, 143502-143502-143503 (2010).

3:20pm **EM+2D-TuA4 Combined Wet HF and Dry Atomic H Cleaning of SiGe followed by Passivation of the Clean Surface via H₂O₂(g) Dosing, Sang Wook Park, T. Kaufman-Osborn, E.A. Chagarov, A.C. Kummel, University of California at San Diego**

Silicon Germanium (SiGe) is a well-known material for its high mobility and useful applications in strain engineering. Its advantages can be utilized to overcome the challenges when scaling down silicon-based devices. As the interest in introducing new kinds of materials increases, the cleaning and passivation methods also become more significant in order to provide uniform and clean surfaces, which would result in improved electrical properties such as high mobility and low interface trap density (Dit). In this

study, combined wet and dry cleaning and passivation of SiGe(100) surface is discussed, using scanning tunneling microscopy (STM), scanning tunneling spectroscopy (STS), and x-ray photoelectron spectroscopy (XPS).

Wet cleaning using 2% hydrofluoric acid (HF) was implemented to strip the native oxide off the SiGe sample but left residual carbon contamination on the surface. Although the oxide layer was removed, additional oxygen adsorbed to the surface during transfer from the HF solution to vacuum chamber. This residual oxygen can be eliminated by keeping the SiGe sample covered in the HF cleaning solution until the sample is introduced to the vacuum chamber or by transferring the sample in an inert environment. Dry in-situ atomic hydrogen cleaning was then implemented to remove the carbon contamination on the surface. A post deposition anneal at 550°C was used to obtain an atomically clean, flat, and ordered SiGe surface and this was verified using STM. The oxygen and carbon contaminant levels were monitored after each cleaning procedure using a monochromatic XPS. The clean SiGe sample was dosed at room temperature with a saturation dose of H₂O₂(g). STM and XPS measurements indicate that H₂O₂(g) dosing leaves the SiGe surface, which is mostly Ge atoms due to surface segregation, terminated with an ordered monolayer of Ge-OH sites. STS measurements of the Ge-OH sites show the conduction band edge dangling bond states are eliminated due to the passivating Ge-OH bonds, but the Fermi level is pinned near the valence band edge due to the large surface dipole. When the surface is annealed to 310°C, XPS measurements indicate that the -OH species on the surface break bonds with the Ge atom and bond instead to the Si atoms, raising Si atoms towards the surface. XPS also verifies that no oxygen leaves the surface due to the 310°C anneal. Instead, the oxygen remains on the surface in the form on Si-OH or SiO_x species. TMA is subsequently dosed on the surface forming and ordered monolayer of Al-O-Si bonds. STS indicates this unpins the Fermi level, leaving an electrically passive ordered layer which serves as an ideal template for further high-k ALD.

4:20pm **EM+2D-TuA7 Interfacial and Electrical Study of Crystalline Oxidation Passivation for AlGaIn/GaN HEMTs, Xiaoye Qin, H. Dong, J.Y. Kim, R.M. Wallace, University of Texas at Dallas**

AlGaIn/GaN high electron mobility transistors (HEMTs) are of significant interest for high power, high frequency and high temperature devices. However, these are known to experience significant surface related effects, such as large leakage currents and frequency dependent current collapse. Oxidation has been found to have a variety of effects on the atomic and electronic structure of nitride surfaces. Therefore, the oxidation layer and the device performance are closely related. Typically, GaN and AlN are found to form a disordered oxide layer related to high density of states when exposure to with O₂. Miao *et al.*¹ reported that oxidation of AlN and GaN surface change the density of surface states based on density functional theory (DFT). In their work, a 2 ML crystalline oxide can cause the lowest density of surface states within the band gap. However, experimental evidence of a 2 ML crystalline oxide remains to be established.

In this study, we investigate O₂ plasma- exposed AlGaIn surfaces at 300 °C and 550 °C by *in situ* X-ray photoelectron spectroscopy (XPS), low energy electron diffraction (LEED). The results indicate that a 500°C O₂ remote plasma exposure is able to generate a thin 2 ML ordered oxide on AlGaIn surface and the oxide is stable during subsequent ALD processing, in contrast to arsenide surfaces.² The capacitance- voltage (C- V) results indicates that the 2 ML crystalline oxide reduces the D_{it} and shifts the threshold voltage to positive voltages. The I-V and gate leakage current characteristics for crystalline oxide MOSHEMTs will also be presented. This work is supported by the AFOSR Asian Office of Aerospace Research and Development (AOARD) under Grand No. FA2386- 11- 1- 4077.

References

¹ M.S. Miao, J.R. Weber, and C.G. Van de Walle, J. Appl. Phys. **107**, 123713 (2010).

² D. M. Zhernokletov, P. Laukkanen, H. Dong, R. V. Galatage, B. Brennan, M. Yakimov, V. Tokranov, J. Kim, S. Oktyabrsky, and R. M. Wallace, Appl. Phys. Lett., **102**, 211601 (2013)

4:40pm **EM+2D-TuA8 Investigating Electrically Active Defects in High-k/InGaAs MOS System using MOS Capacitors and MOSFETs, Paul Hurley, Tyndall National Institute, Ireland, V. Djara, IBM Research - Zurich, Switzerland, E. O'Connor, S. Monaghan, I.M. Povey, J. Lin, Tyndall National Institute, Ireland, M.A. Negara, Stanford University, B. Sheehan, K. Cherkaoui, Tyndall National Institute, Ireland** **INVITED**

As silicon devices reach the limit of dimensional scaling there is a growing interest in the use of high electron mobility channels, such as In_xGa_{1-x}As, in conjunction high dielectric constant (high-k) gate oxides for n-channel Metal-Oxide-Semiconductor Field Effect Transistors (MOSFETs) and tunnel FET (TFETs) based devices. The understanding and control of electrically active defect states at the high-k/In_xGa_{1-x}As interface and of charges within the atomic layer deposited (ALD) high-k films will be

essential for the successful implementation of high mobility channel materials. The objective of this presentation will be to provide an overview of the current understanding of the density and distribution of electrically active defects at the high- k /InGaAs interface both within the InGaAs energy gap and extending into the InGaAs conduction band. The presentation will focus on InGaAs with a 53% Indium concentration. The electrically active interface state density distribution is determined from fully fabricated InGaAs MOSFET structures based on the full gate capacitance in conjunction with the Maserjian Y-function and Poisson-Schrodinger simulations. Very significant progress has been made in recent years in the passivation and intrinsic elimination of high- k /In_{0.53}Ga_{0.47}As interface defects to the point where genuine surface inversion for n and p type InGaAs MOS structures can be achieved and this research will be reviewed. The characteristic signatures of capacitance and conductance for an InGaAs MOS structure in inversion will also be discussed.

Electrically active defects with energies aligned with the InGaAs conduction band are significant for surface inversion mode MOSFETs and can result in a partitioning of charge between free carriers and trapped charge for devices biased above the threshold voltage. The presence of such defect also complicates the extraction of free charge and carrier mobility from device analysis. In this presentation we will also review a new approach where the technique of inversion charge pumping (initially developed for silicon MOSFETs) is applied to InGaAs MOSFETs to determine the free carrier concentration. Results will also be presented which indicate that the duty cycle of the inversion charge pumping technique can be used to discriminate between fast interface states and traps within the oxide for InGaAs MOSFETs biased beyond the threshold voltage.

5:20pm **EM+2D-TuA10 XPS Study of High- k Gate Stack and Interaction with Different Channel Materials and Metal Gate, Malcolm Bevan, Applied Materials Inc. INVITED**

Deposited high- k dielectrics with metal gates have replaced SiON gate with poly electrodes for several Logic nodes and rapidly followed with integration changes from planar to 3D FINFET structures. Performance is no longer through just scaling, and next generation devices have gaps that are being addressed with channel engineering using high mobility materials such as SiGe, Ge and III-V compound semiconductors. Gate stacks now involve several thin films of dissimilar material whose interfaces need to be precisely controlled as well as being conformal around the fin and between the spacers. The stack usually involves the channel material followed by a thin interface layer (iL), high- k dielectric and metal gate cap (MG cap) and each layer range from 0.5 to 2nm. In addition several layers may need plasma or thermal treatment to improve reliability and BTI of the gate stack. To understand performance of these stacks, XPS has been applied to compliment device results. In Fab XPS is a powerful tool to provide in short time information on stack thickness, composition and changes in bonding. Examples will be given to show how XPS has been used to optimize and compare high- k stack on Si, SiGe and Ge. In addition iL/high- k /TiN cap has been studied and further examples given and related to electrical device results.

6:00pm **EM+2D-TuA12 Reliability of nc-CdSe Embedded ZrHfO High- k Dielectric Nonvolatile Memory – Temperature Effects, Shumao Zhang, Y. Kuo, Texas A&M University**

Previously, it was reported that by adding the third element into the high- k film, the bulk and interface material and electrical properties can be improved [1]. For example, the Zr-doped HfO₂ film (ZrHfO) shows the higher crystallization temperature, a lower interface state density, and a larger effective k value than those of the un-doped HfO₂ film [1,2]. Furthermore, nanocrystals have been embedded into this kind of high- k film for the nonvolatile memory (NVM) application to replace the conventional floating-gate flash memory due to the improved device characteristics and reliability [3]. The nanocrystalline cadmium selenide (nc-CdSe) embedded ZrHfO MOS capacitor has shown excellent charge trapping and retention capabilities [4]. However, most studies on the nanocrystals embedded high- k memory devices are done at the room temperature. Since the temperature in the high density integrated circuit can be much higher than room temperature, it is imperative to study the reliability at a raised temperature [5]. In this paper, the temperature effects on memory functions were investigated on the nc-CdSe embedded sample in the range of 2 °C to 120°C. Compared with the fresh $C-V$ curve, the flat band voltage (V_{FB}) of $C-V$ curve shifts to the negative or positive gate voltage (V_g) direction after being stressed at -6 V or +6 V for 10 s, respectively. With the increase of the temperature, the magnitude of the V_{FB} shift increases at -6 V stress but decreases at +6 V stress. With the increase of the temperature, the hole-trapping is enhanced due to the increase of injection and retention of holes to the trapping sites. However, at the high temperature, electrons are possibly transferred through the whole high- k stack with minimum trapping to the high- k stack. In addition, at the high temperature, the nc-CdSe

embedded sample has the large relax current with the high discharge rate due to the increasing release of the trapped charges with large thermal energy. The charge retention capability of the device decreases with the increase of the temperature. For example, the device stressed at -6 V for 20 s will retain 30% of the original trapped holes at 20°C, 23% at 70°C, and 15% at 120°C, respectively, after 10 years. This is because the stored charges gain the high thermal energy and the bulk high- k film is more conductive at the high temperature.

Energy Frontiers Focus Topic

Room: 315 - Session EN+EM+NS-TuA

Charge Storage Materials and Devices

Moderator: Susanna Thon, Johns Hopkins University

2:20pm **EN+EM+NS-TuA1 Spatiotemporal Investigation of Li-Air Battery under Operating Condition: Understanding the Cathodic and Anodic Electrochemical Processes and their Interdependence, Di-Jia Liu, Argonne National Laboratory INVITED**

Li-O₂ battery has generated a great deal of interests due to its high theoretical energy storage capacity for vehicular application. Many studies were carried out in attempt to understand the fundamental chemical processes inside of Li-O₂ battery. The reports so far have been segmented into the investigation on the individual regions of the battery, cathode, anode and separator, mostly at the post mortem state due to the limitation of the characterization methods used.

We adopted a holistic approach in studying electrochemical processes and mechanism of the Li-O₂ battery using operando methods. Particularly, we introduced the microfocused synchrotron X-ray diffraction (μ -XRD) and tomographic (μ -CT) techniques for the spatiotemporal study on the phase and structural changes in Li-O₂ battery. These tools offered some unique capabilities to probe battery properties under the actual discharge-charging condition. For example, the μ -XRD has a spatial resolution at the micron scale of with a complete side penetration to the battery, rendering it feasible to study battery's composition layer-by-layer without the interruption of battery operation. In this presentation, we will discuss our recent investigation of the Li-O₂ batteries under cycling condition in real time using the cells fabricated with the most representative design and materials. We were able not only to reveal individually the changes at anode, cathode and separator, but also to provide a comprehensive view between the regional chemical processes and their interdependence to the overall battery performance during the multiple discharge-charge cycles. More importantly, the finding of this study provides new insights on the catalytic process inside of Li-O₂ cell and calls for new design and materials which could lead to high capacity and longer battery life.

The work performed at Argonne is supported by DOE under Contract No. DE-AC02-06CH11357 by UChicago Argonne, LLC.

3:00pm **EN+EM+NS-TuA3 Insights into Ionic vs. Electronic Transport in Nanostructured Battery Electrodes Enabled by Microfabrication and Spatially Resolved XPS, Alexander Pearse, E. Gillette, S.B. Lee, G.W. Rubloff, University of Maryland, College Park**

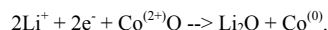
Nanostructured battery electrodes provide a design opportunity to achieve high power at high energy density, using thin active storage layers whose short ion diffusion pathways assure fast transport throughout the layers. However, this must be coupled with fast electron transport through current collectors to all regions of the ion storage layers, posing a design challenge in balancing and optimizing both charge transport components. Spatial inhomogeneity in the utilization of active material due to electronic or ionic transport limitations may lead to decreases in performance, but characterizing this effect with bulk electrochemical measurements is difficult. We address this challenge with a new state-of-charge (SOC) measurement scheme utilizing a patterned ultra-thin film battery electrode and spatially resolved XPS, and focus on the case of limited electronic transport by examining SOC as a function of distance from the current collector.

We fabricate electrode test structures by evaporating metallic strips as current collectors on an electrically insulating substrate. A patterned thin film of active material (V₂O₅) is then deposited using atomic layer deposition (ALD) and mechanical masking so that only a small fraction of the active material is in contact with the current collector. The use of ALD allows for an ultrathin (\leq 30nm) pinhole-free film. We discharge these electrodes in a liquid electrolyte under different rates and conditions and directly measure the state of charge as a function of distance from the current collector using small spot XPS, achieving a lateral resolution of better than 20 μ m. We find that a rate-dependent SOC gradient develops in

the electrodes, with the SOC decreasing with distance from the current collector. Unlike microspot Raman or XRD, XPS provides a direct quantitative measurement of the SOC through the concentration of inserted ions and/or reduced vanadium ions. Additionally, in the ultrathin films relevant to nanostructured storage, XPS becomes a “quasi-bulk” measurement, because the escape depth of photoelectrons becomes a significant fraction of the film thickness. We also explore the depth dependence of the SOC using angle resolved XPS and ion beam depth profiling. We compare our observations with simulations using COMSOL Multiphysics, and attempt to resolve discrepancies between the two. We believe this approach can provide design guidance for heterogeneous nanostructures applied to electrical energy storage, and we anticipate it to be broadly applicable to other electrode materials and active ions.

3:20pm EN+EM+NS-TuA4 The Lithium-Induced Conversion Reaction of CoO Thin Film Battery Materials in Ultra-High Vacuum as Studied by ARXPS and STM, Ryan Thorpe, S. Rangan, A. Howansky, R.A. Bartynski, Rutgers, the State University of New Jersey

Li-ion conversion batteries can store 2-3 times more charge than intercalation batteries by utilizing the full range of oxidation states of their constituent divalent or trivalent transition metal compounds during discharge. A prototypical conversion compound is CoO, which follows the reaction



Cobalt oxide and other transition metal oxides are attractive for use as Li-ion anodes in portable electronics due to their high charge storage capacity and moderate voltage versus Li^+/Li^0 . However, the cycling stability of conversion electrodes is poor, and capacity losses have thus far prevented their implementation.

In order to understand phase progression during the conversion reaction of CoO, high-purity CoO thin films grown in UHV were sequentially exposed to atomic lithium. The electronic structure of the pristine films and of the products of lithiation was studied using x-ray photoemission spectroscopy (XPS), UV photoemission spectroscopy, and inverse photoemission spectroscopy. The crystal structure and film reorganization were probed in parallel with transmission electron microscopy (TEM) and scanning tunneling microscopy.

The amount of CoO reduction for a given Li dose was observed to be highly dependent upon the temperature at which lithiation was performed. At 150°C, Li mobility in the active material was sufficient to allow full reduction of the CoO film as confirmed by XPS. Consistent with electrochemically lithiated CoO electrodes, precipitation of Co nanoparticles in a Li_2O matrix was observed in TEM images. However, at room temperature, the Li-rich overlayers that formed on the CoO film after initial lithiations inhibited further Li diffusion. This could be due to the intrinsically poor kinetic properties of Li_2O or to the formation of Li_2O_2 and/or LiOH passivating films.

The reactivity of CoO films was also found to depend on the orientation of the film. CoO(100) films exhibited a higher degree of conversion for a given Li exposure than polycrystalline films. STM and angle-resolved XPS of these films have been used to investigate the differences between these two film morphologies upon exposure to Li.

4:20pm EN+EM+NS-TuA7 Controlled Cathode/Catalyst Architectures for Li-O₂ Batteries, Malakhi Noked, M.A. Schroeder, A.J. Pearce, C. Liu, A.C. Kozen, S.B. Lee, G.W. Rubloff, University of Maryland, College Park

Electrochemical power sources based on metal anodes have specific energy density much higher than conventional Li ion batteries, due to the high energy density of the metal anode (3842mAh/g¹ for Li). Rechargeable Li-O₂ batteries consume oxygen from the surrounding environment during discharge to form Li oxides on the cathode scaffold, using reactions

- (1) [anode] $\text{Li}(s) \leftrightarrow \text{Li}^+ + \text{e}^-$
- (2) [cathode] $\text{Li}^+ + \frac{1}{2} \text{O}_2(g) + \text{e}^- \leftrightarrow \frac{1}{2} \text{Li}_2\text{O}_2(s), \sim 2.959 \text{ V vs Li/Li}^+$
- (3) [cathode] $\text{Li}^+ + \text{e}^- + \frac{1}{4} \text{O}_2(g) \leftrightarrow \frac{1}{2} \text{Li}_2\text{O}(s), \sim 2.913 \text{ V vs Li/Li}^+$

The cathode reaction requires large over-potentials for charging due to the mass transfer resistance of reagents to the active sites on its surface, decreasing the round trip efficiency, making recharge of the Li-O₂ cell difficult. To overcome these problems, the cathode needs good electrical conductivity and a porous structure that enables facile diffusion of oxygen and can accommodate the reduced oxygen species in the pores.

Two significant challenges exist in the use of the traditional activated carbon material as the cathode of the Li-O₂ system. First, in the presence of Li_2O_2 the carbon electrode becomes relatively unstable even at low voltages (~3V). Second, cathode structures must be porous to accommodate a substantial amount of Li-peroxide (Li_2O_2) without blocking ion transport channels in the cathode. While a few studies have been reported on the

effect of catalyst on the onset potentials for the oxygen evolution reaction (OER) and oxygen reduction reaction (ORR) in the Li-O₂ cell, the results were inconclusive due to the lack of systematic study in a single system and conditions.

We report here results from a model cathode system which enable determination of the effects of various catalysts on the OER/ORR reactions in the non-aqueous Li-O₂ cell. Mesoporous CNT sponge is used as the model cathode material, decorated with catalyst nanoparticles by nucleation-controlled atomic layer deposition (ALD) of Ru, RuO₂, MnO₂, and Pt catalyst components whose loading and composition are controlled by manipulating the ALD conditions. Using a custom Li-O₂ battery cell, we have studied the effect of different catalysts on the voltage of the OER and ORR, and on the cycling performances of the cell. We demonstrate a Li-O₂ cell that sustains >3000 mAhg⁻¹ over more than 15 cycles at current density of 200 mA_g⁻¹. To our knowledge, this is the first comparison of a variety of catalysts with a well-defined morphology (controlled by ALD and monitored by TEM), and under the same electrochemical conditions.

4:40pm EN+EM+NS-TuA8 Vertically Aligned Carbon Nanotubes on Ni Foam as a 3D Li-O₂ Battery Cathode, Marshall Schroeder, M. Noked, A.J. Pearce, A.C. Kozen, S.B. Lee, G.W. Rubloff, University of Maryland, College Park

The Li-O₂ battery system is one of the prime candidates for next generation energy storage. Like other metal-O₂ systems, this technology is known for its impressive theoretical specific energy due to use of metallic anodes and because the cathode active material (oxygen) is not stored in the battery, but is available in the cell environment. A typical cell consists of a pure lithium metal anode, an organic electrolyte (in this study), and a porous positive electrode (usually made of carbon or oxides) which acts as a reaction scaffold for oxygen reduction to Li_2O_2 or Li_2O during discharge. Despite remarkable scientific challenges within every component of the cell, the positive electrode is particularly complicated by its role in the oxygen evolution (OER) and reduction (ORR) reactions, leading to strict requirements for electrode architecture and physicochemical stability for optimal performance. We present herein one of the first experimental realizations of a controlled macroscale 3D carbon nanotube architecture with a practical carbon loading of 1mg/cm² in an attempt to satisfy these requirements.

The O₂ cathode highlighted in this work features a macroporous nickel foam current collector coated with dense forests of vertically aligned carbon nanotubes (VACNT). This freestanding, hierarchically porous system is the first to feature VACNT robustly and electrically connected to a 3D current collector without a binder, and without requiring delamination of the CNT from the growth substrate. Grown via LPCVD with an Fe catalyst on a thin ALD interlayer, the micron-length VACNT provide a very promising electrode material due to their high electrical conductivity, physicochemical stability, and a high surface area architecture that is conducive to ionic mobility and storage of the reduced oxygen discharge product. As a result, this structure exhibits significant capacity (>2Ah/g-carbon) at high ORR voltages (>2.76V) without requiring a catalyst.

Electrochemical performance results as a scaffold for oxygen reduction in various non-aqueous electrolytes will be presented with SEM/TEM/XPS of pristine/discharged electrodes.

5:00pm EN+EM+NS-TuA9 Solid Micro-supercapacitor using Directed Self-Assembly of Tobacco Mosaic Virus and RuO₂, Markus Gnerlich, E.I. Tolstaya, J. Culver, D. Ketchum, R. Ghodssi, University of Maryland, College Park

The 3D micro-supercapacitor reported here utilizes a novel bottom-up assembly method that combines genetically modified Tobacco mosaic virus (TMV-1Cys) with deposition of RuO₂ on multi-metallic microelectrodes. The nanostructured RuO₂ coating is selectively deposited on the electrodes due their unique composition, which is a significant advantage for microfabrication process integration. Test results show electrode capacitance as high as 18 mF/cm² in 1.0M H₂SO₄ electrolyte and 7.2 mF/cm² in solid Nafion electrolyte.

The device fabrication involves the photolithographic patterning of titanium nitride (TiN) microelectrodes with Au cap on top of polyimide micropillars supported by a silicon wafer. A schematic cross section of the device is shown in Figure 1 and a photograph of the fabricated chip in Figure 2. The complexity of the self-assembly process in multiple chemically reactive solutions required the development of a special kind of micro-electrode. The TiN functions as a chemically resistant current collector, the Au cap as an adhesion layer for the TMV-1cys, and the Ni pad as a sacrificial material during the RuO₂ deposition process. After microfabrication, each chip is submerged in TMV-1Cys solution for 24 hours and then transferred to a 0.5% solution of RuO₄. A nanostructured coating of RuO₂ forms on all exposed electrode areas as the Ni is sacrificed in a galvanic displacement reaction. EDX spectral imaging of the constituent elements on the electrode

demonstrates selective RuO₂ coating (Figure 3), and SEM images of the electrodes before and after TMV/RuO₂ coating shows the TMV-1Cys/RuO₂ nanostructures (Figure 4).

Cyclic voltammetry (CV) was performed from 0-800mV versus Ag/AgCl at 10 mV/s in 1.0M H₂SO₄ electrolyte. Figure 5 shows the CV curves, and Figure 6 shows the associated capacity fading, which was insignificant after 100 cycles for electrodes annealed at 150°C. Separately prepared chips were coated with Nafion dispersion and tested in a controlled humidity environment. The measured capacitance drops from 18 to 7.2 mF/cm² per electrode due to ionic conductivity limitations, but 80% capacity is retained after 12,000 cycles (Figure 7). Associated rate capability (Figures 8-9) shows 60% capacity is retained when comparing 3 uA/cm² to 3000 uA/cm², and the low leakage current of only 5 nA (Figure 10) enables use in a wide variety of energy storage applications.

The primary challenge of nanomaterials is often integration into microfabrication processes. The RuO₂ electrode developed here is optimized for compatibility with standard microfabrication steps by using a novel bottom-up assembly approach for manufacturing micro-supercapacitors.

5:20pm **EN+EM+NS-TuA10 Characterization of Tobacco Mosaic Virus-templated Ni/NiO Electrodes for Solid Flexible Supercapacitors, Sangwook Chu, K.D. Gerasopoulos, M. Gnerlich, J. Culver, R. Ghodssi, University of Maryland, College Park**

Characterization of nickel oxide supercapacitor electrodes utilizing *Tobacco mosaic virus* (TMV) nanotemplates is presented. NiO was formed on Ni coated TMV nanotemplates by annealing at high temperatures (Figure 1). The resulting electrode showed excellent electrochemical performance with remarkable cycle stability. The TMV/Ni/NiO nanostructured electrodes were also integrated with a solid electrolyte to demonstrate their potential application as solid flexible supercapacitors.

NiO supercapacitor electrodes have been prepared in literature using various methods, and it has been found that the crystallinity of the NiO is critical for its electrochemical charge capacity [1]. The NiO electrode presented in this work was thermally grown on Ni coated TMVs. Gold electrodes (0.5cm²) were immersed in TMV solution for virus self-assembly followed by electroless deposition of Ni uniformly coating the TMV nanostructure [2]. TMV/Ni electrodes were annealed in a furnace at three different temperatures (200°C, 300°C, and 400°C) and the NiO formation on TMV/Ni surface was characterized by XPS (Figure 2). The results indicate that thermal growth of NiO layer on TMV/Ni electrodes starts at temperatures higher than 300°C, in good agreement with previously reported results.

Electrochemical testing was performed in aqueous 2M KOH electrolyte in a three-electrode configuration. The electrodes annealed at 300°C showed the highest areal capacitance (148mF/cm²) measured by a galvanostatic (2mA/cm²) charge/discharge test shown in Figure 3a. The redox charge storage mechanism was confirmed by cyclic voltammetry (CV) with good rate capability up to 100mV/s (Figure 3b). Excellent cycle stability was measured with little degradation over 500 cycles as shown in Figure 4. This is attributed to the conformal layers of Ni/NiO over the TMV nanostructure, and the stabilizing effect of KOH on NiO. The continuous electrical contact between the Ni and NiO layers ensures an optimized current collector configuration.

A PVA-KOH-H₂O polymer was prepared to study the performance of the nanostructured electrodes with a solid electrolyte. Polymer electrolyte solution was poured onto the nanostructured NiO electrodes and the Pt foil was assembled on top as an anode. The polymer electrolyte film formed after 24hours was flexible and strong enough to support both electrodes. Figure 5 shows CV curves measured with the assembled cell, verifying proper operation of the nanostructures in both liquid and solid electrolytes. The successful integration of TMV/Ni/NiO electrodes with polymer electrolytes highlights the potential of this approach to develop flexible solid-state supercapacitor devices.

5:40pm **EN+EM+NS-TuA11 Charged Particles Micro-Penning-Malmberg Trap: An Approach to Store High Densities with Substantially Lower End Barrier Potentials, Alireza Narimannezhad, J. Jennings, C. Minnal, M.H. Weber, K.G. Lynn, Washington State University**
Among devices that have been used to store antimatter, Penning-Malmberg trap has become the device of choice because of its simplicity and versatility. However, the challenge involved in these traps is when the number of particles increases inside the trap to the densities of energy harvesting interest, the confining fields rise to unpractical values. One of the authors has proposed a design of microtube arrays with much lower end barrier potentials. The microtraps are designed for non-neutral plasma storage such as positrons. Here, we present fabrication, simulation studies, and trapping milestones so far. The fabrication involved advanced MEMS techniques including photolithography, deep reactive ion etching of silicon

wafers, sidewalls smoothing, gold sputtering, wafers aligning, and thermo-compression gold bonding. Alignment of less than 2 microns was achieved using a micro-machined jig and precision ground sapphire rods. Simulation using a WARP Particle-In-Cell code showed that density of $1.6 \times 10^{11} \text{cm}^{-3}$ is achievable with the new trap design while the end barrier potentials are several order of magnitudes smaller compared to the conventional traps. However, positron losses occur in experimentation by both trap imperfections such as misalignment of wafers, asymmetries, and physical imperfections on the surface, and also field misalignment and perturbations. The loss rates were also compared to the results from simulation in order to study and distinguish each effect. This project will open the door to a wide range of new and exciting research areas. The size of these traps along with the low confining potentials is a big step to make them portable. It could be used as a source of energy or in propulsion system where alternate sources are not feasible.

Exhibitor Technology Spotlight

Room: Hall ABC - Session EW-TuA

Exhibitor Technology Spotlight Session

Moderator: Chris Moffitt, Kratos Analytical Limited, UK

4:00pm **EW-TuA6 What's New in AFM for Nanoelectrical and Nanomechanical Characterization, Keith Jones, Oxford Instruments Asylum Research**

Oxford Instruments Asylum Research will present the latest AFM innovations for nanoelectrical characterization that provide new information that was inaccessible by previous techniques: • Scanning Microwave Impedance Microscopy (sMIM) for conductivity and permittivity mapping on insulators, semiconductors and conductors • Nanoscale time dependent dielectric breakdown (NanoTDDb) with the spatial resolution of an AFM tip • Dual Gain CAFM to measure current from 1 pA to 10 μA with sub-pA sensitivity on samples with widely varying conductivity We'll also present an overview and the latest results of AFM mapping modes that calculate both the elastic and loss modulus: • AM-FM Viscoelastic Mapping Mode for quantitative nanomechanics with the resolution, ease of use and speed of tapping mode • Contact Resonance Viscoelastic Mapping Mode for quantitative nanomechanics on materials from 1 GPa to 100's Gpa

In-Situ Spectroscopy and Microscopy Focus Topic

Room: 313 - Session IS+AS+MC+SS-TuA

Environmental Electron Microscopies

Moderator: Jorge Boscoboinik, Brookhaven National Laboratory

2:20pm **IS+AS+MC+SS-TuA1 Nanocrystal Shape Evolution during Growth, Haimei Zheng, Lawrence Berkeley Lab, University of California, Berkeley** **INVITED**

An understanding of nanocrystal shape control mechanisms during growth is critical for the design of novel functional materials with surface-enhanced properties. However, the atomic level shape evolution of nanocrystals during growth is mostly unknown due to the lack of direct observation. We use liquid cells under transmission electron microscope (TEM) to study the growth of Pt or Pt-alloy nanoparticles in situ, where growth either by nanoparticle attachment or by monomer attachment has been observed. First, I will present Pt-Fe nanorods formation by shape-directed nanoparticle attachment under the electron beam. Winding polycrystalline nanoparticle chains are achieved at the early stage then they are straightened to yield single-crystal nanorods. Tracking their growth trajectories allows us to distinguish the force fields exerted by single nanoparticles and nanoparticle chains. Second, I will show the observation of platinum nanocube growth and the facet development. By in situ imaging with high spatial and temporal resolution, we have identified unique growth mechanisms that cannot be predicted by Wulff construction or other existing growth theorems. We found layer-by-layer growth of the {100} and {111} facets while the {110} facets show steps. We also found that the growth rates of these facets are similar until the {100} facets stop growth. Hence, the distance from {100} facets to the crystal center is fixed throughout the subsequent growth. The {110} facets are eliminated when two adjacent {100} facets meet. Lastly, the growth of {111} facets fills the corners to complete a nanocube. Our calculation suggests oleylamine ligand mobility on the facet is responsible for the arresting of {100} growing facets. References:

1. Liao et al. "Facet Development during Platinum Nanocube Growth" Science in review.
2. H. G. Liao, L. Cui, S. Whitlam, H. Zheng, "Real time imaging Pt3Fe nanorod growth in solution." Science 336, 1011 (2012).
3. We used TEM facility at National Center for Electron Microscopy of Lawrence Berkeley National Laboratory (LBNL), which is supported by the Office of Basic Energy Sciences, Division of Materials Sciences and Engineering of the U.S. Department of Energy under Contract #DE-AC02-05CH11231. H.Z. thanks the support of DOE Office of Science Early Career Research Program.

3:00pm IS+AS+MC+SS-TuA3 Microfluidic Cell for In Situ Scanning Electron Microscopy of Hydrated Dynamic Systems, Christopher Brown, A. Yulaev, A. Kolmakov, National Institute of Standards and Technology (NIST)

The ability to conduct nanoscale imaging of fluid hydrated dynamic systems is a long sought goal within the scientific community. While improvement of commercial instrumentation and environmental cells has enabled in situ imaging of fluid hydrated systems using transmission electron microscopy (TEM) at the nanoscale, additional opportunities exist in implementing in situ techniques within scanning electron microscopy (SEM) instruments equipped with fluidic cells. Factors that motivate this work include: ubiquity and reduced cost of SEM instrumentation compared to TEM, drastically reduced restrictions on the sample size, and greater flexibility of systems and detectors designed for the SEM compared to TEM.

In this communication we report on development of the microfluidic environmental cell designed for in situ studies of fully hydrated dynamic objects. We describe strategies and experimental results that enable improved in situ imaging using the SEM, including development of electron transparent graphene windowed devices that increase signal-to-noise ratio of images of fluid hydrated objects. Limiting factors of in situ imaging of hydrated samples within the SEM are discussed including radiolysis and decreased electron beam penetration into liquid cells compared to higher acceleration voltage electron microscopy modalities.

3:20pm IS+AS+MC+SS-TuA4 Liquid Jet -X-ray Photoelectron Spectroscopy and MD Simulations indicate that Li Cations in Aqueous Solutions Exhibit High Surface Propensity, Kathryn Perrine, M.H.C. Van Spyk, M.J. Makowski, A.C. Stern, K. Parry, D.J. Tobias, University of California Irvine, A. Shavorskiy, H. Bluhm, Lawrence Berkeley National Laboratory, B. Winter, Helmholtz-Zentrum Berlin für Materialien und Energie/Elektronenspeicherung BESSY II, Germany, J.C. Hemminger, University of California Irvine

Ions impact chemistry at the aqueous liquid/vapor interface in environmental chemistry, electrochemistry and biomolecular chemistry. Ions are characterized as structure makers or breakers for protein mixtures, and the trend is known as the Hofmeister series.¹ The Born electrostatic model of ions at interfaces has shown that ions should be repelled from the liquid/vapor interface due to a decrease in free energy when solvation by water occurs.² Molecular dynamic (MD) simulations and recent experimental studies have shown that anions tend to adsorb to the liquid interface in an inverse Hofmeister trend.^{3, 4} Our synchrotron based XPS studies carried out over the last five years have provided experimental evidence that most cations follow classical ionic solution behavior and are repelled from the liquid/vapor interface, whereas some anions exhibit significant propensity for the surface. In this talk we present our recent experiments on Li salt solutions. Our experiments indicate that unlike larger cations, Li⁺ is not repelled from the interface and has a significant surface propensity.

Liquid jet-X-ray photoelectron spectroscopy (LJ-XPS) is used to explore the relative ion concentrations at different depths in aqueous salt solutions. Low photoelectron kinetic energies are used to probe the surface of solutions yielding relative ionic concentrations that are present at the liquid/vapor interface. Higher photoelectron kinetic energies probe deeper into the bulk of aqueous solutions. The relative ionic concentrations of solutions prepared from lithium halide salts are compared to potassium halide solutions at different depths. MD simulations support our studies and suggest that Li⁺ cations have interfacial propensity due to factors such as the tight water solvation shell on the Li⁺ ions. Density profiles reveal anion and Li⁺ ion adsorption to the liquid/vapor interface. In addition, we also compare various concentrations of KI and LiI aqueous solutions to determine ion adsorption at the aqueous interface.

1. K. D. Collins and M. W. Washabaugh, *Quarterly Reviews of Biophysics*, 1985, **18**, 323-422.
2. M. Born, *Zeitschrift Fur Physik*, 1920, **1**, 45-48.
3. P. Jungwirth and D. J. Tobias, *Journal of Physical Chemistry B*, 2002, **106**, 6361-6373.

4. D. J. Tobias, A. C. Stern, M. D. Baer, Y. Levin and C. J. Mundy, *Annual Review of Physical Chemistry*, Vol 64, 2013, **64**, 339-359.

4:20pm IS+AS+MC+SS-TuA7 Complementary Microscopy and Spectroscopy Investigations of the Initial Oxidation Stages of Binary Alloy Thin Films, Judith Yang, University of Pittsburgh INVITED

The transient stages of oxidation – from the nucleation of the metal oxide to the formation of the thermodynamically stable oxide – represent a scientifically challenging and technologically important terra incognita. These issues can only be understood through detailed study of the relevant microscopic processes at the appropriate length scale in situ. We are studying the dynamics of the initial and transient oxidation stages of a metal and alloys with complementary in situ methods - ultra-high vacuum (UHV) transmission electron microscopy (TEM) and X-ray photoelectron spectroscopy (XPS). We have previously demonstrated that the formation of epitaxial Cu₂O islands during the transient oxidation of Cu and Cu-Au thin films bear a striking resemblance to heteroepitaxy, where the initial stages of growth are dominated by oxygen surface diffusion and strain impacts the evolution of the oxide morphologies. We are presently investigating the early stages of oxidation of binary alloys where both elements compete to oxidize. Specifically, we are studying Cu-Ni and Ni-Cr single crystal thin films as a function of relative concentration, oxygen partial pressures and temperatures. For Cu-Ni oxidation, the addition of Ni causes the formation Cu₂O and/or NiO where the oxide type(s) and the relative orientation with the film depend on the Ni concentration, oxygen partial pressure and temperature. For Ni-Cr model alloys containing 4, 8 and 16 at.% Cr and isothermally oxidized at 600°C and 10⁻⁷ to 10⁻³ torr O₂ pressure, our XPS experiments reveal that after 2 min of oxidation only Cr₂O₃ forms on the surface of all three alloys. However, with further exposure (i.e., 30 min or 2 h), a competitive growth between Cr₂O₃ and NiO under all the tested conditions is clear. These XPS data are remarkable results, since prior studies reported in the literature suggest that NiO + internal Cr₂O₃ or NiO/NiCr₂O₄/Cr₂O₃+ internal Cr₂O₃ should form at least for the lower Cr content (4 and 8%) alloys. These experiments will be complemented with electron microscopy of scale cross sections to better understand the competitive nucleation and growth processes as a function of the oxygen partial pressure.

5:00pm IS+AS+MC+SS-TuA9 Direct Observation of Structure Controlled Carbon Growth by Environmental TEM, J. Kling, T.W. Hansen, Jakob Wagner, Technical University of Denmark INVITED

In order to meet the increasing demand of faster and more flexible electronics and optical devices and at the same time decrease the use of the critical metals, carbon based devices are in fast development. Furthermore, the rich resource of carbon element limits the need for recycling and the material supports the friendly environment approach.

Layered carbon structures spanning from graphene to few layered graphite are used for extremely compact devices with outstanding performance [1,2]. A relative cheap and easy way to produce layered carbon structures on the large scale is via chemical vapor deposition (CVD) growth on catalysts like copper and nickel. However, the exact growth mechanism is still under debate and is most likely dependent on precursor pressure and growth temperature.

Here, we have used environmental transmission electron microscopy (ETEM) to follow the growth of layered structures directly at the atomic level and thereby coupling growth rate and quality of the material on the local scale to the growth parameters. Acetylene and methane are exposed to the catalyst (Ni or Cu) in situ in the microscope at pressures ranging from 0.1Pa 100Pa at temperatures ranging from 500-700C. Following the subsequent appearance of carbon layers allows for determination of instant growth rates under controlled conditions.

Single walled carbon nanotube (SWCNT) based electronics is another way of addressing the environment friendly approach of faster and better electronics. In order to exploit the potential of SWCNTs in the electronic industry fully, selective growth of either conducting or semiconducting tubes is of high importance. Growing the tubes in situ in the ETEM under relevant growth conditions gives fundamental insight in the parameters controlling the chirality and thereby the electronic properties of the SWCNTs.

References:

- [1] K. S. Novoselov, S. V. Morozov, T. M. G. Mohinddin, L. a. Ponomarenko, D. C. Elias, R. Yang, I. I. Barbolina, P. Blake, T. J. Booth, D. Jiang, J. Giesbers, E. W. Hill, and a. K. Geim, *Phys. Status Solidi* **244**, 4106 (2007).
- [2] F. Schwierz, *Proc. IEEE* **101**, 1567 (2013).

5:40pm **IS+AS+MC+SS-TuA11 *In Situ* Energy Loss Spectroscopy, A Novel Approach to the Characterization of Surfaces during MBE Growth, Philippe Staib**, Staib Instruments, Inc.

A new energy analyzer for Auger Electron Spectroscopy (AES), the Auger Probe, is able to operate in growth vacuum chambers to measure *in-situ during growth* the composition of the surface [1,2,3]. The primary beam is provided by the RHEED electron gun at a very grazing incidence angle (2 to 3 degrees). The analyzer is also used in EELS mode to measure Characteristic Energy Losses (CEL). The use of a grazing incidence angle strongly enhances the strength of the energy losses peaks, which become more prominent than the elastic line

EELS data from the Auger Probe are presented showing the evolution of the CEL distributions during oxidation (ZnO), during thermal de-oxidation of GaSb, and during growth of binary and ternary materials (GaAsSb). Surprisingly, even during deposition of homoepitaxial layer, the CEL distributions show a marked dependence upon the flux of material to the sample which can reflect the formation of physio- rather than chemisorbed layers and the smoothness of the surface [4].

The CEL spectra cannot be interpreted simply, due to the strong overlapping of multiple excitations of single energy losses. A model is presented that takes into account the probability distribution for multiple losses, and allows extraction of the elementary energy loss lines from the distribution. Using this model, accurate energy loss values can be measured and an effective electron density can be calculated. The intensity of the extracted energy losses versus the intensity of the elastic peak is a measure of the ratio d/l between the electron path length d and mean inelastic free path l of the specific loss. The inelastic mean free path for each loss line can be deduced using d values from monte-carlo simulation of the electron trajectories and the intensity ratio of the loss peak vs. elastic peak.

Special thanks to S. Svensson and W. Sarney of ARL for their collaboration during measurements used in this work.

This work is funded in part by ARO (STTR Phase I - W911NF-13-P-0021A13A-011-0305).

[1] P. Staib, J. Vac. Sci. Technol. B 29(3), (2011).

[2] W.L. Calley, et al. J. Vac. Sci. Technol. B, (2013).

[3] P. Staib in "*In situ* Characterization of Thin Film Growth", Edited by G. Koster and G. Rijnders, Woodhead Publishing In Materials, (2011)

[4] Strawbridge B., Shih RK., Beach C., Mahajan S., Newman N., J. Vac. Sci. Technol. A 24 (5) 1776 (2006).

6:00pm **IS+AS+MC+SS-TuA12 Selective Staining for Enhanced Spectroscopic Identification of Domains in Immiscible Polymer Blends by Micro-Raman Spectroscopy, Nicholas Heller, C.R. Clayton**, SUNY Stony Brook, S.L. Giles, J.H. Wynne, Naval Research Laboratory, M.J. Wytiaz, M.E. Walker, Sherwin-Williams Company

Blends of incompatible polymers combined with fillers and pigments were used to produce unique low reflectance thermoset coatings. Understanding the origins of low reflectance from the coatings was approached through microscopy, thermal analysis and spectroscopic analysis of both pigmented and control clear coatings. Polymeric phase separation was confirmed by the presence of two distinct glass transition temperatures. Microscopy revealed random surface features for the pigmented coatings. Therefore, the pigments and fillers were removed to observe the polymer-polymer interactions within the blend under curing conditions. Identification of the polymeric domains was obtained using Raman spectroscopy mapping of cross-section samples embedded within a polyester resin. Cross-section samples of coatings were utilized to isolate encapsulated polymer domains from the continuous polymer network to minimize spectral averaging from both domains. Raman analysis of the blends was compared to cured films generated using the individual resins. The embedding process produced a marker peak in one phase and in one individual resin. The marker peak was found to be from styrene monomer and was found to selectively bind to one component of the polymer blend, based on polar and hydrogen bonding characteristics.

Accelerating Materials Discovery for Global Competitiveness Focus Topic

Room: 302 - Session MG-TuA

Multi-scale Modeling in the Discovery of Advanced Materials

Moderator: Alberto Roldan, University College London, Veena Tikare, Sandia National Laboratories

2:20pm **MG-TuA1 Search for Substitutes of Critical Materials with Targeted Properties by Scale-Bridging and High-Throughput Modelling and Simulation, Christian Elsässer**, Fraunhofer Institute for Mechanics of Materials IWM, Germany **INVITED**

In this lecture three case studies will be addressed on how sustainable substitutes for materials, which have outstanding functionalities but also constraining criticalities, can be discovered and developed efficiently by employing multi-scale-coupling and high-throughput-screening concepts.

In the first case, a multi-scale chain from atomic-level first-principles theory to microstructure-level phase-field theory for ferroelectric piezoelectrics is set up for the still best material $\text{Pb}(\text{Zr,Ti})\text{O}_3$ (PZT), which contains the biomedically health-critical element Pb, and then transferred to $(\text{K,Na})\text{NbO}_3$ (KNN), which is a potential substitute for PZT. [1]

The second case is on the modelling of structure-property relationships for transparent and conductive oxides (TCO), which are free of the geologically resource-limited element Indium and therefore potential substitutes for the still best TCO material Indium Tin Oxide (ITO) for front electrodes on, e.g., smart phones or solar cells. [2]

In the third case, a combinatorial high-throughput-screening approach is employed to search for crystal structures and chemical compositions of intermetallic phases of transition-metal (TM) and rare-earth (RE) elements, which have sufficiently good intrinsic ferromagnetic properties for permanent magnets but contain less amounts of the geopolitically supply-critical RE elements than, e.g., the still best permanent magnets based on $(\text{Nd,Dy})_2\text{Fe}_{14}\text{B}$. [3]

References:

[1] B. Völker, P. Marton, C. Elsässer, and M. Kamlah, *Multiscale modeling for ferroelectric materials: a transition from the atomic level to phase-field modelling*, Contin. Mech. Thermodyn. **23**, 435-451 (2011); S. Körbel and C. Elsässer, *Alignment of ferroelectric polarization and defect complexes in copper-doped potassium niobate*, Phys. Rev. B **88**, 214114 (2013).

[2] W. Körner, P. Gumbsch, and C. Elsässer, *Analysis of electronic subgap states in amorphous semiconductor oxides on the example of Zn-Sn-O systems*, Phys. Rev. B **86**, 165210 (2012); W. Körner and C. Elsässer, *DFT study of stability and subgap states of crystalline and amorphous Zn-Sn-O*, Thin Solid Films **555**, 81-86 (2014).

[3] N. Drebov, A. Martinez-Limia, L. Kunz, A. Gola, T. Shigematsu, T. Eckl, P. Gumbsch, and C. Elsässer, *Ab-initio screening methodology applied to the search for new permanent magnetic materials*, New J. Phys. **15**, 125023 (2013).

3:00pm **MG-TuA3 Monte Carlo Simulations of Nanoscale Focused Electron Beam Induced Etching, R. Timilsina, Philip Rack**, The University of Tennessee Knoxville, K. Wolff, M. Budach, K. Edinger, Carl Zeiss SMS, Germany

Focused beam (electron-ion-photon) induced processing has long been utilized as a micro-/nano-scale direct synthesis method for both additive (via deposition) and subtractive (via etching) machining for a variety of editing and prototyping applications. Nanoscale lithography mask editing is one critical area which is pushing the limits for these beam induced processing methods. Beam damage associated with liquid gallium and the recently developed gas field ion source limits their utility in lithography mask repair due to the stringent optical requirements. Thus, electron beam induced processing for mask repair of both clear and opaque defects is the method of choice. To understand the fundamental electron-solid-precursor interactions, a Monte Carlo electron-solid simulation has been developed with a dynamic precursor gas routine which emulates adsorption/desorption, surface diffusion and electron stimulated reactions. The simulation was recently modified to handle electron beam induced etching. The electron beam induced etching of silicon dioxide is studied at low and high energies, short and long dwell times and various etch precursor gas conditions to elucidate important rate limiting regimes. Furthermore, the temporal behavior of the high-aspect ratio etch process is demonstrated. In this presentation we will overview the Monte Carlo simulation and will illustrate how various parameters affect the resolution and etch rate of the electron beam stimulated etch process. We will demonstrate how beam

parameters (beam energy, current, and dwell and refresh time) precursor parameters (flux, residence time, surface diffusion coefficient, dissociation cross-section) and material (secondary electron yield, density) all contribute to the nanoscale etching process.

4:20pm **MG-TuA7 Advances in Multiscale Mathematical Modeling of Materials: From Phase Diagrams to Interface Dynamics**, *Maria Emelianenko*, George Mason University **INVITED**

This talk will survey recent developments in two areas critical for advancing materials design. First is the mesoscale kinetic modeling of polycrystalline materials, focused on the task of understanding how statistical distributions develop in the process of coarsening of materials microstructure and how these distributions in turn relate to materials properties. The challenges here include the design of reliable benchmarks for curvature-driven growth, vertex and Monte Carlo grain growth simulation codes, as well as the development of coarse-grained kinetic theories capable of capturing realistic materials behavior. These and other questions will be discussed in the context of nonlocal evolution theory and particle gas dynamics, and unexpected connections with other fields of science will be revealed. The other part of the talk will be concerned with phase diagram calculation methods, where robust and accurate numerical optimization methods are required to prevent costly mistakes. A universal Gibbs energy minimization formulation will be discussed that allows to link traditional Calphad codes and databases to state-of-the-art optimization engines, paving the road to a more intelligent automated phase data exploration.

5:00pm **MG-TuA9 Discrete All-Atom Simulations: Predicting Fit-for-Purpose Properties of Fuels**, *M.T. Knippenberg*, High Point University, *Barbara L. Mooney*, *J.A. Harrison*, United States Naval Academy

Hydrotreated renewable fuels are complex blends of hydrocarbons produced by catalytic treatment of oils from such materials as corn, algae, and tallow. These fuels are of potential interest to the US Navy for use in their fleet, but due to their complexity it is not obvious which blends are suitable, and which are not. To this end, we use computational modeling for the prediction, based upon chemical composition, of the fit-for-purpose (FFP) properties of these alternative fuels. Low-cost, high-throughput assessment of fuel space from molecular dynamics (MD) simulation accelerates fuel discovery by: 1) identifying suitable candidate fuels out of a large phase space of possible fuel mixtures and environmental conditions; 2) providing an informed starting point for experimental investigations; and 3) reducing waste by eliminating the need to perform expensive, time-consuming measurements on unviable candidates. We are able, through MD with the modified-AIREBO potential, to obtain excellent agreement with experimental measurements of density, enthalpy of vaporization, and bulk modulus for a range of example surrogates containing up to 12 hydrocarbon components, as well as for binary mixtures of the straight-chain alkane *n*-dodecane with the branched 2,2,4,4,6,8,8-heptamethylnonane over the full range of mole fractions.

Magnetic Interfaces and Nanostructures

Room: 311 - Session MI+MG-TuA

Development of Multiferroic Materials (2:20- 5:00PM)

MIND Panel Discussion (5:00-6:30 pm)

Moderator: Peter Fischer, Lawrence Berkeley National Laboratory

2:20pm **MI+MG-TuA1 Versatile Abilities of Lattice Instabilities: New Design Strategies for Emergent Ferroics**, *James Rondinelli*, Drexel University **INVITED**

I describe in this talk the design methodology and theoretical discovery of a new class of "rotation-induced" ferroelectric materials. By tailoring the instabilities of the BO_6 octahedral rotations common to ABO_3 perovskites oxides, I show these lattice distortions provide a new structural "sand box" from which to design and discover such ferroic phases. Bottom-up engineering of the transition metal octahedra at the unit cell level, is applied to realize ferroelectricity in artificial perovskites superlattices formed by interleaving two bulk materials with no tendency to such behavior. This emergent, chemistry-independent, form of ferroelectricity – octahedral rotation-induced ferroelectricity – offers a reliable means to externally address and achieve deterministic electric-field control over magnetism. I discuss the required crystal-chemistry criteria, which are obtained from a combination of group theoretical methods and electronic-structure computations, to select the compositions and stoichiometries giving polarizations comparable to the best known ferroelectric oxides. Much rarer

in crystalline materials with an electric polarization, however, is the appearance of a ferri-electric (FiE) state, vis-à-vis ferrimagnetism, where local electric dipoles of different magnitude are anti-aligned to yield a net non-zero electric polarization. The underlying reason is that the long-range Coulomb forces in oxide-based dielectrics favor the cooperative alignment of all electric dipoles in the crystal through cation displacements that occur against an oxygen ligand framework. I conclude by describing our recent discovery of a first-order, isosymmetric, transition between a ferrielectric (FiE) and ferroelectric (FE) state in A-site ordered perovskite superlattices and offering new areas for ferroic discovery

3:00pm **MI+MG-TuA3 Voltage-controlled Exchange Bias and Exchange Bias Training**, *Christian Binek*, *W. Echtenkamp*, University of Nebraska-Lincoln **INVITED**

Voltage-controlled exchange bias (EB) is a seminal achievement in nanomagnetism. It enables dissipationless electric control of interface magnetic states with major implications for room temperature spintronic applications. Numerous prototypical solid-state spintronic devices rely on switchable interface magnetism, enabling spin-selective transmission or scattering of electrons. Controlling magnetism at thin-film interfaces, preferably by purely electrical means, i.e. in the absence of electric currents, is a key challenge to better spintronics. Currently, most attempts to voltage-control magnetism focus on potentially large magnetolectric (ME) effects of multiferroics.

Here, we report on the use of antiferromagnetic (AF) ME Cr_2O_3 (chromia) for voltage-controlled magnetism [1,2]. Electrically switchable boundary magnetization (BM) can overcome the weak linear ME susceptibility of room temperature bulk ME antiferromagnets. BM is a roughness insensitive equilibrium property of ME antiferromagnets which is in sharp contrast to the surface magnetic properties of conventional antiferromagnets. Voltage-controlled BM is the key property enabling isothermal voltage-controlled switching of exchange bias (EB) which emerges at the interface of adjacent ferromagnetic (FM) and the ME antiferromagnetic (AF) thin film. The inter-layer exchange alters the magnetization reversal shifting the FM hysteresis loop along the magnetic field axis. In this presentation I introduce voltage-control of EB and EB training [2]. Electric switching between stable EB fields is investigated in heterostructures based on single crystal $Cr_2O_3(0001)/PdCo$ heterostructures and compared with recent results in MBE grown thin film EB heterostructures. In addition to voltage-switching of EB we electrically and isothermally tune chromia into distinct AF multi-domain states. As a result, EB training, which originates from triggered rearrangements of the AF interface magnetization during consecutively cycled hysteresis loops, is tuned between zero and sizable effects. We quantify and interpret the peculiar voltage-controlled training effect in $Cr_2O_3(0001)/PdCo$ by adapting our recently developed theory which is based on a discretized Landau-Khalatnikov dynamic equation [3].

We acknowledge the Center for NanoFerroic Devices, C-SPIN, part of STARnet, a SRC program sponsored by MARCO and DARPA for partial funding of this work.

[1] Xi He, Yi Wang, N. Wu, A. N. Caruso, E. Vescovo., K. D. Belashchenko, P. A. Dowben, and Ch. Binek, *Nature Mater.* **9**, 579 (2010).

[2] W. Echtenkamp, Ch. Binek, *Phys. Rev. Lett.* **111**, 187204 (2013).

[3] Ch. Binek, et al., *Phys. Rev. Lett.* **96**, 067201 (2006).

4:20pm **MI+MG-TuA7 Multiferroic Z_6 Vortices in Hexagonal $ErMnO_3$** , *Y. Geng*, *X.-Y. Wang*, *S.-W. Cheong*, *Weida Wu*, Rutgers University

Multiferroics are materials with coexisting magnetic and ferroelectric orders, where inversion symmetry is also broken [1-5]. The cross-coupling between two ferroic orders can result in strong magnetolectric coupling. Therefore, it is of both fundamental and technological interest to visualize cross-coupled topological defects in multiferroics. Indeed, topological defects with six interlocked structural antiphase and ferroelectric domains merging into a vortex core were revealed in multiferroic hexagonal manganites [6, 7]. Numerous Z_6 vortices are found to form an intriguing self-organized network, and may be used to test Kibble-Zurek model of early universe [8, 9]. Many emergent phenomena, such as enhanced conduction and unusual piezoelectric response, were observed in charged ferroelectric domain walls protected by these topological defects [10, 11]. In particular, alternating uncompensated magnetic moments were discovered at coupled structural antiphase and ferroelectric domain walls in hexagonal manganites using cryogenic magnetic force microscopy (MFM) [12], which demonstrates the coupling between ferroelectric and spin orders (B_2 phase). The appearance of correlated net moments at the coupled domain walls is in excellent agreement with a phenomenological Landau theory [13], suggesting that the 120° antiferromagnetic order (B_2 phase) rotates 4π in each Z_6 vortex. This is further corroborated by the magnetic field dependence of domain wall moments.

*This work is supported by NSF grant # DMR-0844807.

Reference

- [1] N. A. Spaldin, and M. Fiebig, *Science* **309**, 391 (2005).
- [2] W. Eerenstein, N. D. Mathur, and J. F. Scott, *Nature* **442**, 759 (2006).
- [3] S. W. Cheong, and M. Mostovoy, *Nat. Mater.* **6**, 13 (2007).
- [4] R. Ramesh, and N. A. Spaldin, *Nature Materials* **6**, 21 (2007).
- [5] N. A. Spaldin, S.-W. Cheong, and R. Ramesh, *Physics Today* (2010).
- [6] T. Choi *et al.*, *Nature Materials* **9**, 253 (2010).
- [7] T. Jungk *et al.*, *Appl. Phys. Lett.* **97**, 012904 (2010).
- [8] S. M. Griffin *et al.*, *Phys. Rev. X* **2**, 041022 (2012).
- [9] S. C. Chae *et al.*, *Phys. Rev. Lett.* **110**, 167601 (2013).
- [10] E. B. Lochocki *et al.*, *Appl. Phys. Lett.* **99**, 232901 (2011).
- [11] W. Wu *et al.*, *Phys. Rev. Lett.* **108**, 077203 (2012).
- [12] Y. Geng *et al.*, *Nano Letters* **12**, 6055–6059 (2012).
- [13] S. Artyukhin *et al.*, *Nat Mater* **13**, 42 (2013).

4:40pm **MI+MG-TuA8 Two-Dimensional Manganese Gallium Quantum Height Islands on Wurtzite GaN (000-1)**, Jeongihm Pak, A. Mandru, A.R. Smith, Ohio University

We describe the spontaneous formation of five and six-monolayer quantum height manganese gallium islands on gallium-rich, nitrogen polar GaN(000 $\bar{1}$). From ex-situ MOKE measurements at room temperature, we expect these MnGa islands to be ferromagnetic. The structural evolution is followed from the beginning of growth using reflection high energy electron diffraction, in which a dotted 2 \times pattern is observed to form. In-situ scanning tunneling microscopy is also used to investigate the islands' structures with atomic resolution. Based on all the observations, we propose the possible bulk and surface models for the islands. A possible bonding structure at the substrate/island interface is also discussed in which Mn atoms substitute for Ga atoms on the Ga adlayer thus making the MnGa islands bonded to the GaN substrate. Atomic chains are observed only on the six-layer island surface and the model for the chains is also discussed. STM observations of atomic-chain interconnection on the six-layer island surface indicate a dynamic system at room temperature. The models presented here should serve as useful starting points for theoretical calculations.

5:20pm **MI+MG-TuA10 Current Topics in Magnetism: The Importance of Interfaces**, Mark Stiles, National Institute of Standards and Technology

Interfaces play a crucial role in many magnetic systems. As magnetoelectronic devices shrink, this role is becoming more and more important. Unfortunately, many times these interfaces are not well enough characterized to allow measurements to constrain physical models of the behavior in these systems. In this talk, I give several examples from my own experience of systems of both historical and current interest in which the interfaces play a dominant role but for which very little is known. A historical example is exchange bias, the study of systems in which the behavior of a ferromagnetic film is modified by coupling to it to an antiferromagnet. In spite of decades of study on a wide variety of systems, structural characterization of the interfaces has only been done several times on model systems, despite the fact that all of the coupling occurs at this interface. A topic of recent interest is the study of current induced torques in magnetic bilayers consisting of ferromagnetic thin films coupled to non-magnetic materials with strong spin-orbit coupling. The spin orbit coupling dramatically affects the current induced torques in these systems. An outstanding question is what role the interfacial spin-orbit coupling plays. This can be addressed theoretically by first-principles calculations, but these necessarily assume ideal interfaces between perfectly coherent lattices for material pairs with lattice mismatch on the order of ten percent. Without real characterization of the structure of these interfaces, it is almost impossible to definitively determine which parts of the system are playing important roles. Both of these topics are useful or potentially useful for applications, a characteristic that tends to drive research focused on achieving dramatic results rather than doing the time intensive work necessary to characterize the samples adequately to support a deeper understanding of the underlying physics.

5:40pm **MI+MG-TuA11 Optical Spectroscopy of Nanomaterials within Magnetic Fields**, Angela Hight Walker, NIST

Transition-metal dichalcogenides are a new system in which to study the effect of temperature and magnetic field on optical properties. Recent experiments will be discussed from a novel set up which couples a confocal optical microscope into fields up to 9 Tesla and temperatures down to 3.5 K, with several laser sources throughout the visible range. As these

dichalcogenides or 2D materials are certainly under study for use in nanoelectronic devices they are of general interest to the Magnetic Interfaces and Nanostructures (MIN or MI) Division. Other areas where MIND members see as future foci will be explored. Methods to ensure that the Division draw upon the widest possible spectrum of talented individuals from all segments of society will also be discussed.

MEMS and NEMS

Room: 301 - Session MN+NS-TuA

Multi-Scale Phenomena and Bio-Inspired MEMS/NEMS

Moderator: Philip Feng, Case Western Reserve University, Meredith Metzler, Cornell University

2:20pm **MN+NS-TuA1 MEMS-Enabled Multiscale Nanolaminated Magnetics**, Mark Allen, University of Pennsylvania **INVITED**

The manufacture of materials with bulk volumes and precisely controlled nanostructure has led to the creation of materials with surprising and useful mechanical and electrical properties. Recently we have developed a 'top-down' fabrication technique that allows the creation of highly-structured multilayer metallic materials, with precisely designed characteristic lengths in the hundreds of nanometers scale, but volumes of manufactured material in the macro range. The fabrication relies on automated and repeated multilayer electrodeposition of multiple metallic materials, followed by sacrificial etching of one metal. The resultant structure consists of individualized high-lateral-aspect-ratio sub-micron metallic films. The application of these multiscale materials to ultracompact energy conversion is investigated. Metallic magnetic materials have desirable magnetic properties, including high permeability and high saturation flux density, when compared with their ferrite counterparts. However, eddy current losses preclude their use in many switching converter applications due to the challenge of simultaneously achieving sufficiently thin (100-500 nm) laminations such that eddy currents are suppressed while simultaneously achieving overall material thicknesses (0.1-1 mm) such that substantial power can be handled. Sequential electrodeposition of multiple nanoscale 'sheets', or laminations, of magnetic materials such as permalloy and NiFeCo offers an approach to fabricate the desired nanostructured magnetic core. Tests of toroidal inductors with nanolaminated cores showed negligible eddy current loss relative to total core loss even at a peak flux density of 0.5 T and a frequency of 10 MHz. The ability to operate at such high flux levels offers the possibility of dramatically shrinking the physical size of power inductors in energy converters. DC-DC converters with efficiencies of up to 93% and power handling of approximately 40W have been achieved in ultracompact form based on these materials.

3:00pm **MN+NS-TuA3 Fabrication and Electrical Performance of Through Silicon Via Interconnects Filled with a Copper/Carbon Nanotube Composite**, Y. Feng, Susan Burkett, The University of Alabama

Three-dimensional integrated circuit (3D-IC) technology has been developed using copper (Cu) filled through silicon vias (TSVs). The vertical interconnects pass through a set of stacked die and enable many applications that benefit from increased bandwidth, reduced signal delay, and improved power management. However, the reliability of Cu interconnects is a serious concern since the performance is affected by electromigration and stress associated with mismatch in thermal expansion coefficients. Carbon nanotubes (CNTs) are nanoscale materials which possess a high Young's modulus, a low coefficient of thermal expansion, and high thermal conductivity. Compared to Cu, CNTs exhibit low resistivity due to the existence of ballistic conduction and they are capable of carrying a higher current density. In this work, we fabricated TSVs using a novel materials system consisting of a composite of Cu and CNTs as a possible solution to the problems encountered in Cu-based interconnects. First, blind TSVs were fabricated using a Bosch process. After etching, an insulating layer, a metallic seed layer, and a catalyst layer were deposited previous to CNT growth. Vertically aligned CNTs were grown by chemical vapor deposition method. Finally, Cu was deposited by periodic reverse pulse electroplating inside the vias to form a Cu/CNT composite. Polishing completed the fabrication and allowed measurement of electrical performance for TSV interconnects. The experimental results were compared for interconnects filled with Cu and those filled with the Cu/CNT composite. The results are encouraging for the Cu/CNT composite having potential application as a TSV interconnect material.

3:20pm **MN+NS-TuA4 Meso Scale MEMS Motion Transformer and Amplifier Electrostatically Actuated by Parallel Plate Electrodes**, Y. Gerson, S. Krylov, Tel Aviv University, Israel, **Tali (T.) Nahmias**, R. Maimon, Microsystems Design Center, RAFAEL LTD, Israel

Meso scale microelectromechanical structures found on the upper scale of microelectromechanical systems (MEMS) can potentially replace conventional mechanical devices produced by common for the macro-engineering approaches such as machining and assembly of individual parts. When realized as a compliant mechanism containing a single flexible member rather than multiple parts attached by joints they provide smooth frictionless motion without backlash and exhibit improved reliability and robustness. Batch fabrication using micromachining processes established in MEMS allows improved yield and significantly lower cost. However, actuation of these devices remains challenging. Electrostatic actuation, which is the most widely used in smaller MEMS devices, is viewed to be less suitable for the actuation at the meso scale due to unfavorable scaling laws, namely quadratic reduction of the actuating force with the distance between the electrodes. For this reason, most of the meso scale micro devices are actuated by thermal transducers, distinguished by slow response and high power consumption or by piezoelectric or magnetic motors, which cannot be integrated within the device and require post-fabrication assembly.

In this work we report on the design, fabrication and characterization of an electrostatically actuated meso scale microelectromechanical motion transformer and amplifier. The actuator incorporate a transducer with multiple parallel plate electrodes and is realized as a compliant mechanism relying on flexible pseudo hinges. The $5000\ \mu\text{m} \times 4000\ \mu\text{m}$ device converts linear motion of the transducer into mechanically amplified angular motion of a rotating lever. By combining a highly efficient small-gap parallel plate electrode and a motion amplification the device is designed to provide a lever tip displacement of $60\ \mu\text{m}$, an initial blocking force of 0.001N at zero displacements and a blocking force of 0.012N in the maximal displacement configuration when the parallel plate actuator is in its closed position. The devices were fabricated using DRIE from a SOI wafer with (111) front surface orientation and a $150\ \mu\text{m}$ thick device layer. The devices were operated in ambient air conditions and the functionality of the device was demonstrated experimentally. The voltage-displacement dependence and resonant curves were built using image processing procedure implemented in Matlab. Excellent agreement between the results provided by the Finite Elements models and the experimental data was observed. The results of the work demonstrate an ability to achieve both large displacements and high blocking forces in an electrostatically actuated meso scale compliant mechanism.

4:20pm **MN+NS-TuA7 Bio-Inspired Microlenses and Their Biomedical Applications**, **Hongrui Jiang**, University of Wisconsin - Madison **INVITED**

Optical detection and imaging have wide applications in biomedicine and biological and chemical analyses. With continuing miniaturization effort to realize integrated microsystems, micro-scale optical components become more and more important. For any optical system, lenses are critical elements. In this talk, I will present our work on liquid microlenses. I will first introduce a few types of microlenses and microlens arrays, including tunable liquid microlenses actuated by temperature-, pH- and infrared light-responsive hydrogels, microlens arrays for light-field imaging, microcamera arrays mimicking compound eyes, and artificial reflecting superposition compound eyes. Then, I will discuss about potential applications of these lenses in medical instruments. I will describe miniaturized cameras capable of multiple viewpoints, prototype flexible endoscopes implementing infrared-light responsive liquid microlenses at their distal ends, and prototype multiple-camera laparoscopes.

5:00pm **MN+NS-TuA9 The Development of a Valve Based Microfluidic Biofilm Reactor for Biofilm Studies with Reliable Controls**, **Sowmya Subramanian**, M.T. Meyer, Y.W. Kim, W.E. Bentley, R. Ghodssi, University of Maryland, College Park

We present a multi-experiment PDMS based biofilm analysis platform using a valve-actuated microfluidic system, designed to reduce growth variance of *in-vitro* biofilms to less than 10%. This was achieved by integrating hydraulic push-down valve actuators to section a uniform biofilm grown in a channel by maintaining a single source of bacterial suspension [1, 2]. In this work, we establish a simplified process flow for the fabrication of a multi-depth device mold and demonstrate the high throughput capability of the microfluidic biofilm reactor.

Bacterial biofilms are the primary cause of infections in medical implants and catheters. The widespread use of high doses of antibiotics to treat biofilm infections is leading to the emergence of antibiotic resistant strains, necessitating the development of alternative methods of treatment [3]. However, the experimental evaluation of new treatment techniques is

strongly hindered by the stochastic nature of biofilm growth [1]. Therefore, it is required to develop a microsystem that can not only facilitate multi-experiment studies for new treatment evaluation but also enable the growth of uniform biofilms that can be used as reliable controls.

Figure 1 shows a single uniform biofilm grown in the horizontal center channel of the device is sectioned into multiple sections, by hydraulically actuating the push-down valves thereby enabling multi-experiment studies on the same biofilm. Figure 2 shows the schematic of the operation of a "push-down" valve [4], the schematic of the CAD layout of the two-level microfluidic device and its two modes of operation. The two-step photolithography of the molds (Figure 3) using negative photoresists, SU8-2015 and KMPR1050, allows for the patterning of the multi-depth microfluidic mold without the need for additional passivation of the first resist layer, thereby simplifying fabrication. The mold can be reused to produce multiple devices; a photograph of the valve region of a used multi-depth mold is shown in Figure 4. Photographs of the device operating in different modes are shown in Figure 5.

The unique capability of this valved microfluidic biofilm reactor to section uniform biofilms can facilitate high-throughput biofilm studies, including new drug discovery. The push-down valve configuration allows for easy integration of electrodes for the study of alternative treatment methods like electric fields. Furthermore, the integration of the biofilm reactor with a real-time measurement system will enable high-throughput continuous analyses on uniform biofilms while ensuring tight and reliable controls.

5:20pm **MN+NS-TuA10 Multimode Silicon Carbide (SiC) Microdisk Resonator in Liquid**, **Hao Jia**, P.X.-L. Feng, J. Lee, Case Western Reserve University

We experimentally demonstrate, for the first time to our knowledge, the operation of silicon carbide (SiC) microdisk resonators in fluidic and viscous environments (particularly in water) with robust multiple flexural-mode resonances in the high and very high frequency (HF/VHF) radio band. We observe ~ 8 resonance modes in a $20\ \mu\text{m}$ -in-diameter SiC microdisk resonator with resonance frequencies up to ~ 120 MHz and quality Q factors as high as ~ 40 in water.

SiC is a highly attractive material for microelectromechanical systems (MEMS) due to its superior mechanical (e.g. high elastic modulus, $E_Y \sim 450$ GPa), optical (wide bandgap, $>2.3\text{eV}$) and thermal properties (thermal conductivity of $320\text{--}490\ \text{W}/[\text{m}\cdot\text{K}]$) [1]. These advantages make SiC especially suitable for sensing applications in liquid for its transparency from visible to mid-infrared light and high optical power handling ability, facilitating efficient laser actuation and detection. Meanwhile, two dimensional (2D) microdisk structure exhibits multiple flexural-mode resonance characteristics, which can enhance sensing performances in liquid with the additional degrees of freedom and larger sensing area. Further, the unique biocompatibility of SiC allows potential in-liquid biosensing applications be developed.

In this study, we demonstrate the operation of high frequency SiC microdisk resonators in liquid. The SiC microdisk resonators are completely immersed in water, and are optically driven by an amplitude-modulated 405nm laser. The multimode resonances are detected with optical interferometry using a 603nm He-Ne laser. We observe ~ 8 resonance modes up to ~ 120 MHz with Q_s as high as ~ 40 in water. To our best knowledge, both the number of resonance modes and Q_s measured are the highest among flexural-mode resonators operating in water reported to date [2],[3],[4],[5]. Such high frequency SiC microdisk resonators with robust multimode resonances and high Q_s in water may provide an appealing platform for particle and biological sensing applications in liquid.

[1] X. Lu, J. Y. Lee, P. X.-L. Feng, and Q. Lin, *Opt. Lett.* **38**, 1304 (2013).

[2] S. S. Verbridge, L. M. Bellan, J. M. Parpia, and H. G. Craighead, *Nano. Lett.* **6**, 2109 (2006).

[3] S. Sawano, T. Arie, and S. Akita, *Nano. Lett.* **10**, 3395 (2010).

[4] J. H. Park, T. Y. Kwon, D. S. Yoon, H. Kim, and T. S. Kim, *Adv. Func. Mater.* **15**, 2021 (2005).

[5] C. Vancura, Y. Li, J. Lichtenberg, K.-U. Kirstein, A. Hierlemann, and F. Josse, *Anal. Chem.* **79**, 1646 (2007).

5:40pm **MN+NS-TuA11 Development of CMOS-based Capacitive Micromachined Ultrasonic Transducers Operated in Collapsed Mode**, **Wei-Cheng Chung**, M.-C. Tsao, P.-C. Li, W.-C. Tian, National Taiwan University, Taiwan, Republic of China

In this work, experimental results of complementary metal-oxide-semiconductor (CMOS)-based capacitive micromachined ultrasonic transducers (CMUTs) operated in the collapsed mode will be reported. Our CMUT is fabricated by TSMC $0.35\ \mu\text{m}$ two poly Si and four metal layer (2P4M) CMOS-MEMS standard process followed by a post customized wet

etching. Conventionally, the applied DC bias is 80% of the collapse voltage during the CMUT operation. Compared to the conventional operation, the CMUT membrane will be snapped-down on the bottom electrode and this will change the center frequency of the transducers. The collapsed voltage of our CMUT is designed at approximately 40V. The center frequency (in immersion) of our CMUT in conventional mode operation is 2.89MHz while the frequency is shifted to 9.12MHz in collapsed-mode operation. The sensitivity is proved to be 4-times larger in the collapse-mode operation because the increased electrical-mechanical coupling efficiency.

The comparison of single-electrode and double-electrode design will be reported as well. With the double-electrode design, the collapse voltage is first applied to the center electrode while a separated DC bias is applied to the side electrode to actuate our CMUTs. The maximum displacement of the CMUT membrane will be appeared on the side electrode. It is proved that CMUTs with the double-electrode design can transmit a higher output pressure and receive signals with a higher sensitivity compared to CMUTs with the single-electrode design. It is believed that the our CMUTs with standard CMOS-based process will broaden the application spaces such as in biomedical imaging and nondestructive evaluation.

6:00pm MN+NS-TuA12 Development of Micro Gas Preconcentrator Using Electroless Gold Deposition for Human Breath Analysis, ChunYen Kuo, C.-L. Hsu, National Taiwan University, Taiwan, Republic of China, H.-Y. Kuo, C.-J. Lu, National Taiwan Normal University, Taiwan, Republic of China, W.-C. Tian, National Taiwan University, Taiwan, Republic of China

The detection of the volatile organic compounds (VOCs) in human breath can be analyzed by gas chromatograph (GC) as a non-invasive diagnosis for lung diseases. However, the gas concentration of the VOCs in human breath is low, approximating in the ppb to sub ppb range, and thus a gas preconcentrator (PCT) must be placed before a GC to collect and preconcentrate trace compounds. Early μ PCTs using commercially available adsorbents and microheaters were demonstrated. However, the heating efficiency of the device is limited either by a large thermal mass or a poor heat transfer.

In this study, we present a gas PCT using a simple one-photomask micromachined process and the electroless gold deposition method to form the gold film, serving as a thin film microheater, on the inner surface of the microchannel. An amorphous and porous carbon film that functions as an adsorbent is grown on microheaters inside the microfluidic channel followed by the electroless gold deposition. The developed gas PCT can be heated to $>300^{\circ}\text{C}$ by applying a constant electrical power of $\sim 5\text{W}$ with a heating rate of $60^{\circ}\text{C}/\text{sec}$. Four suspected lung cancer biomarkers, acetone, benzene, toluene and xylene, are collected through the proposed gas PCTs and separated successfully using a 17-m-long gas chromatography (GC) column. Compared with previous works, the more simple fabrication process, more stable heating element, more uniform temperature distribution and more efficient heating rate of the micro gas preconcentrator are developed demonstrated.

Nanometer-scale Science and Technology

Room: 304 - Session NS+AS+SS-TuA

Nanowires and Nanotubes: Advances in Growth and Characterization

Moderator: Lincoln Lauhon, Northwestern University

2:20pm NS+AS+SS-TuA1 Surface Chemical Choreography of Nanowire Synthesis, Michael Filler, S.V. Sivaram, N. Shin, I.R. Musin, Georgia Institute of Technology **INVITED**

This talk will provide an overview of our recent efforts to understand the chemical phenomena underlying semiconductor nanowire growth. The vapor-liquid-solid technique – where a liquid “catalyst” droplet collects atoms from the vapor and directs crystallization of individual solid layers – is a ubiquitous method for the synthesis of these quintessential nanoscale building blocks, but a lack of atomic-level design rules prevents robust programming of structure. Long-standing challenges in the control of heterostructure, dopant profile, atomic stacking sequence, kinking, and even simple axial growth restrict the accessible property space and highlight the pitfalls of an overreliance on empirical process optimization. We couple in-situ or operando infrared spectroscopy with post-growth high-resolution electron microscopy to connect specific surface chemical bonds present during synthesis with nanowire structure. Studies of Si and Ge nanowires demonstrate the fundamental, and previously unrecognized, role of adsorbed hydrogen atoms. The surface coverage of these precursor (e.g., Si_2H_6 or Ge_2H_6) decomposition intermediates, which we quantitatively

determine as a function of pressure and temperature, can change over a narrow range and strongly influence growth. Our findings show, for example, that adsorbed hydrogen is essential for stabilizing the catalyst or driving elongation in new crystal directions for Ge and Si nanowires, respectively. We leverage these insights to rationally design precursors that choreograph nanowire structure on multiple length scales, permitting the fabrication of user-defined defect, kinking, and diameter-modulated superstructures.

3:00pm NS+AS+SS-TuA3 Atom Probe Tomography Analysis of GaAs-AlGaAs Core-Shell Nanowire Heterostructures, Nari Jeon, Northwestern University, S. Morkötter, G. Koblmüller, Technische Universität München, Germany, L.J. Lauhon, Northwestern University

GaAs-AlGaAs planar heterostructures have various electronic and optoelectronic applications such as solar cells and light-emitting diodes.^{1,2} This is due to a small lattice mismatch between GaAs and AlAs providing wider opportunities in bandgap tuning. Moreover, modulation doping scheme is well-known to be effective in enhancing electron mobility in the heterostructures by minimizing electron scattering from ionized impurities. Since growth of GaAs-AlGaAs core-shell nanowires was demonstrated in 2005,³ there has been a growing number of papers reporting novel (opto)electronic transport properties, which are originated from the nonparallel geometry of GaAs-AlGaAs interfaces and its related compositional fluctuations.⁴ In fact, compositional structures are more complex in the core-shell nanowires compared to the planar counterparts. For example, there are six Al-rich bands along the corners of $\{110\}$ sidewall facets in the AlGaAs shell.⁵ While most of the previous studies were based on transmission electron microscopy on cross-sectioned samples, we exploited the atom probe tomography (APT) to explore compositional fluctuations in three dimensions. The focus of the presentation will be APT sample preparation and composition characterization of Si delta-doped GaAs-AlGaAs core-shell nanowires. Molecular beam epitaxy reactor was used to grow the core-shell nanowires and the GaAs-AlGaAs superlattice planar samples as a reference to the nanowires. Individual nanowires were mounted on tungsten tips using micromanipulator for APT and planar samples were fabricated into tip-shaped APT samples by the lift-out and sharpening method using focused ion beam (FIB). Carefully designed structures of the superlattice with varied thickness and spacing in planar samples enabled us to estimate the range of possible ion beam damage from FIB. The atom probe conditions such as laser pulse energy and target detection rate were also optimized to achieve high spectral and spatial resolutions, which are critical for APT of III-V compound semiconductors where preferential detection loss and surface diffusion for III and/or V group elements are possible depending on the APT conditions. Intermixing at GaAs-AlGaAs interface and stoichiometric fluctuation in AlGaAs shell were mainly studied along with the detection limit of Si dopants in the delta doping layer.

1 K. Takahashi et al. *Solar Energy Materials and Solar Cells* **66** 517-524 (2001).

2 D. Ban et al. *Journal of Applied Physics* **96** 5243-5248 (2004).

3 J. Noborisaka et al. *Applied Physics Letters* **87** 093109-3 (2005).

4 S. Funk et al. *Nano Letters* **13** 6189-6196 (2013).

5 M. Heiss et al. *Nature Materials* **12** 439-444 (2013).

3:20pm NS+AS+SS-TuA4 Scanning Tunneling Microscopy of Semiconductor Nanowire Surfaces and Devices, R. Timm, J. Knutsson, M. Hjort, S. McKibbin, O. Persson, J.L. Webb, Anders Mikkelsen, Lund University, Sweden

III-V semiconductor nanowires (NWs) offer tremendous possibilities for device application in solid-state lightning, energy conversion, and information technology [1]. With their small diameter and their very large surface-to-volume ratio, the NW device behavior is strongly determined by their surface structure. Thus, it is both essential and challenging to investigate their atomic surface structure and to combine this information with electrical measurements on individual NWs.

Recently, we have managed to clean InAs NWs from their native oxide and revealed the atomic arrangement of their side surfaces with scanning tunneling microscopy (STM). Here, we present STM images of various NW surfaces of both wurtzite and zincblende crystal structure [2], including InAs, GaAs, InP, and InSb NWs. By combining STM imaging with scanning tunneling spectroscopy (STS) measurements, we simultaneously study the surface structure and local electronic properties across the interfaces of NW heterostructures [3].

For correlating local structural and electronic characterization with transport measurements of NW devices, we have developed a novel STM-based setup: We are using combined atomic force microscopy (AFM) and STM/S on individually contacted NWs for mapping the surface structure and the local band alignment along the NW heterostructure under device

performance. We show initial results of this unique approach on InAs-GaSb nanowire tunnel diodes, where we could prove Esaki behavior of a NW while it was investigated by STM/AFM. From a set of STS spectra we determined the position of the Fermi level along the nanowire for different applied biases, showing an abrupt drop directly at the material interface. In a reverse experiment, we used the STM/AFM tip as local gate and measured the resulting source-drain current through the nanowire for different biases [4].

In some cases it is desirable to measure the conductivity of individual as-grown nanowires in an upright-standing configuration without any sample processing. Here we have developed an alternative setup where the STM tip is used to first image free-standing nanowires from top and then form a point contact [5]. We will demonstrate the reproducibility of this method in establishing low-resistive Ohmic contacts to individual InP and InAs nanowires [6], and we will show initial results on the I-V properties of individual InP NW solar cells.

- [1] J. Wallentin *et al.*, *Science* **339**, 1057 (2013)
- [2] M. Hjort *et al.*, *Nano Lett.* **13**, 4492 (2013)
- [3] M. Hjort *et al.*, *ACS Nano* **6**, 9679 (2012)
- [4] J. L. Webb *et al.*, *Nano Res.*, in print
- [5] D. B. Suyatin *et al.*, *Nature Commun.* **5**, 3221 (2013)
- [6] R. Timm *et al.*, *Nano Lett.* **13**, 5182 (2013)

4:20pm NS+AS+SS-TuA7 Poly-Aromatic Hydrocarbon Nanostructure Growth on Single and Multi-Layer Graphene, Alexander Yulaev, CNST/UMD Graduate Student Researcher, A. Kolmakov, NIST

Poly-aromatic hydrocarbons (PAH) are known as potential hazardous organic pollutants, which can be found in soil, air, meat, fish and etc. Carbon based materials are routinely used for environmental remediation. Graphene has ultrahigh surface area and can be seen therefore as an “ultimate carbon filter”. In our communication we report PAH nanostructure nucleation and growth on a single and multi-layer graphene CVD grown on a copper substrate. The PAH deposition was performed by thermal evaporation in vacuum, and resultant morphology of a PAH was studied by means of SEM as a function of time, rate, substrate temperature and graphene thickness. We found that PAH predominantly grows in a form of nanowires which have a good vertical alignment with respect to a graphene plane. It was shown that temperature of a substrate, deposition rate of PAH, and number of graphene layers were the key parameters to control the PAH morphology such as a nucleation density and diameter of PAH nanowires. We relate the orthogonal growth of PAH nanowires to the discotic nature of PAH molecules forming weak VDW interactions with a graphene basal plane and lamella like structures due to favorable face-to-face intermolecular interaction. We envision PAH nanostructures grown on a graphene substrates may help optimize PAH filters.

4:40pm NS+AS+SS-TuA8 Using Surface Chemistry to Direct the In Situ Synthesis and Placement of Nanowires, A.A. Ellsworth, J. Yang, Z. Shi, Amy Walker, University of Texas at Dallas

Nanoscale one-dimensional materials, commonly called nanowires, have properties that differ significantly from their bulk counterpart materials, and thus have applications in areas including sensing, energy conversion, electronics and optoelectronics. One of the major challenges in the practical use of nanowires is their integration into complex functional structures in a predictable and controlled way. We have recently introduced two promising new techniques by which to direct the growth of metallic and semiconducting nanowires. ENDOM, or Electroless Nanowire Deposition On Micropatterned substrates, employs electroless deposition (ELD) to form metallic nanowires on substrates. SENDOM, or Semiconductor Nanowire Deposition on Micropatterned surfaces, uses chemical bath deposition (CBD) to deposit semiconductor nanowires. SENDOM and ENDOM are generally applicable to the preparation of metallic, semiconducting, and even insulating nanostructures on many technologically relevant substrates. These techniques have several advantages over existing *in situ* synthesis and placement methods: it is fast, and it does not require expensive lithographic equipment or a clean room.

Using ENDOM or SENDOM we are able to create nanowires that are ultralong (centimeters) and follow complex paths such as a right-angle or a curve. We illustrate ENDOM by deposition of Ni, Cu, Pd and other nanowires on patterned -OH/-CH₃ SAMs. We exploit the different deposition rates electroless deposition of metals using dimethylamine borane (DMAB) on -CH₃ and -OH terminated SAMs to deposit nanowires. We illustrate SENDOM by deposition of CuS nanowires on patterned -COOH/-CH₃ SAMs. In this case, the deposition is controlled by the interaction of thiourea (sulfur source) with the SAM surface. In this paper we discuss the reaction pathways involved in the formation of these nanowires including the nucleation sites and the dependence of the nanowire growth on pH and deposition temperature.

5:20pm NS+AS+SS-TuA10 Development of New Nanocatalysts through Restructuring of Co₃O₄ Nanorods Anchored with Pt Atoms, Shiran Zhang, University of Notre Dame, A. Frenkel, Brookhaven National Laboratory, F. Tao, University of Notre Dame

Low-temperature water-gas shift (WGS) reaction is crucial for low-temperature fuel cell technology as it provides a solution for on-board hydrogen purification near operational temperature. Design of catalysts with lower activation energy and higher activity is critical for a practical application. Significant effort has been devoted to development of new WGS catalysts with high activity at low temperatures. Most of them are metal nanoparticles supported on reducible oxides such as CeO₂ or TiO₂.

Here we reported two nanocatalysts, PtCo_n/Co₃O₄ and Pt_mCo_m/CoO_{1-x} that are highly active for low-temperature WGS reaction. They were prepared by restructuring singly dispersed Pt atoms supported on Co₃O₄ nanorods through a controlled reduction. The single dispersion of Pt atoms on cobalt oxide nanorods was confirmed with high-angle annular dark-field scanning transmission electron microscopy (HAADF-STEM). Photoemission features of Co2p and Pt 4d_{5/2} of these catalysts during catalysis were tracked with ambient pressure x-ray photoelectron spectroscopy (AP-XPS) using monochromated Al K α . Coordination environment of Pt atoms was tracked with in-situ extended x-ray absorption fine structure spectroscopy (EXAFS). These ex-situ and in-situ studies show that two new active phases, PtCo_n/Co₃O₄ and Pt_mCo_m/CoO_{1-x} were formed in the temperature ranges of 150 °C – 200 °C and 280 °C – 350 °C in the mixture of 3 Torr CO, 1 Torr H₂O, respectively. The formation of singly dispersed bimetallic sites PtCo_n anchored on Co₃O₄ was confirmed with in-situ EXAFS studies. The formed Pt_mCo_m nanoclusters supported on CoO_{1-x} in the temperature range of 280 °C – 350 °C was identified with HAADF-STEM. Kinetics studies in the gas mixture of carbon monoxide and water vapor with a ratio of 3:1 revealed that activation barriers for PtCo_n/Co₃O₄ at 150-200 °C and Pt_mCo_m/CoO_{1-x} at 150-250 °C are 50.1±5.0 kJ/mol and 29.6±4.0 kJ/mol, respectively. Turn-over frequencies (TOFs) of the two new catalysts PtCo_n/Co₃O₄ and Pt_mCo_m/CoO_{1-x} at 150 °C are larger than those of Pt and Au nanoparticles supported on CeO₂ and TiO₂ catalysts by one magnitude. The excellent activities of the new catalytic phases PtCo_n/Co₃O₄ and Pt_mCo_m/CoO_{1-x} formed through restructuring the singly dispersed Pt atoms on Co₃O₄ suggest a method of developing new catalysts through restructuring singly dispersed catalyst atoms such as noble metals on an oxide support.

5:40pm NS+AS+SS-TuA11 A Study of Single-Walled Carbon Nanotubes Coated with Iron Oxide (Fe₂O₃) Nanoparticles for Enhanced Magnetic Properties, Suman Neupane, D. Seifu, Morgan State University

Carbon nanotubes (CNTs) continue to attract significant interest due to their extraordinary thermal, electrical, optical, and mechanical properties. The preparation of CNTs coated with magnetically sensitive Fe₂O₃ nanoparticles has implications to the development of advanced heat transfer nanofluids and high capacity lithium ion batteries. In this report, single-walled carbon nanotubes (SWNTs) were uniformly coated with Fe₂O₃ nanoparticles through solution mixture. Scanning and transmission electron microscopy were used to compare the surface morphology of pristine SWNTs and as-prepared SWNTs coated with Fe₂O₃ nanoparticles. Raman spectroscopy and thermo gravimetric analysis presented the extent of defects and the amount of Fe₂O₃ nanoparticles present in the sample. Near edge X-ray absorption fine structure spectroscopy was used to probe the electronic band structure of as-prepared core-shell structures. Magnetization measurements indicate that the coercive field of SWNTs coated with Fe₂O₃ nanoparticles was twice that of pristine SWNTs.

One of the authors, D. S., acknowledges funding from ARL W911NF-12-2-0041 and from NSF MRI-DMR-1337339

**Plasma Science and Technology
Room: 308 - Session PS-TuA**

**Advanced BEOL/Interconnect Etching
Moderator: Toshihisa Nozawa, Tokyo Electron Ltd.**

2:20pm PS-TuA1 Highly-Selective Etch Gas Chemistry Design for Precise DSAL Dry Development Process, Hisataka Hayashi, T. Imamura, H. Yamamoto, I. Sakai, M. Omura, Toshiba Corporation Center for Semiconductor Research & Development, Japan

INVITED
To meet the needs of the device scaling trend, patterning technologies for critical dimension control less than 20 nm is required. For 1X nm pattern formation beyond the conventional optical lithography limit, it is necessary to use double (or multiple) patterning process which increases the process cost. Directed-self assembly (DSA) of block copolymer is one of the most attractive candidates for 1X nm pattern formation process and 12.5 nm hp

patterns were formed using polystyrene-block-poly(methyl methacrylate) (PS-b-PMMA) [1]. DSA lithography (DSAL) process using PS-b-PMMA needs selective removal of PMMA to PS, which is called "development process". A wet development process was applied successfully for contact hole shrink process [2]. Although this method can remove PMMA selectively, pattern collapse will occur for line and space pattern resulting from surface tension of developer solvent.

On the other hand, although a dry development process is expected to solve this problem, selective removal of PMMA is difficult because PMMA is a similar organic polymer to PS. Dry development processes using Ar plasma and O₂ plasma have been reported and their selectivities were 3.9 and 1.7, respectively [3]. However in our case, higher selectivity is needed for etching the underlayer with PS as mask.

In this study, we focused on differences of material composition of PS and PMMA. Our results concluded that the control of ion energy and design of gas chemistry were key factors for the selective etch.

The aromatic group in PS is more durable than the carbonyl group in PMMA for ion bombardment. A selectivity of around 8 was achieved by the control of ion energy in xenon plasma.

PMMA has more oxygen in the film than in PS, so we designed the gas chemistry to realize the selective PMMA etch by using this difference of the oxygen content. We studied carbon containing gas plasma, because carbon radical will deposit on PS which does not contain oxygen. On the other hand, carbon radical will react with the oxygen in the PMMA to make volatile CO_x, therefore selective PMMA etch to PS can be realized. A selectivity of over 20 was realized using CO gas plasma [4].

DSA lithography dry development was successfully realized by controlling ion energy and designing the etching gas chemistry based on the difference of material composition of PS and PMMA.

References

- [1] C. Bencher et al., Proc. SPIE 7970, 79700F (2011)
- [2] Y. Seino et al., Proc. SPIE 8323, 83230Y (2012)
- [3] M. Satake et al., Proc. SPIE 8685, 86850T (2013)
- [4] H. Yamamoto et al., Japanese Journal of Applied Physics 53, 03DD03 (2014)

3:00pm PS-TuA3 Plasma Etch Considerations for Roughness Improvements during EUV and DSA Pattern Transfer using Mid Gap CCP, Vinayak Rastogi, H. Matsumoto, A. Metz, A. Ranjan, N. Mohanty, A. Ko, Y. Chiba, TEL Technology Center, America, LLC, X. Hu, L. Wang, E. Hosler, R. Farrell, M. Preil, GLOBALFOUNDRIES U.S. Inc.

As the semiconductor manufacturing industry is gearing toward sub-30nm technology nodes, there are continuous efforts to establish alternative patterning strategies other than optical lithography. Extreme Ultraviolet (EUV) Lithography, 193nm Immersion augmented with multiple patterning schemes ('Self Aligned Double Patterning - SADP', 'Self Aligned Quadruple Patterning - SAQP') and 'Directed Self Assembly - DSA' are considered to be promising candidates. However, these methodologies come with challenges posed in the form of polymer to polymer selectivity, mask budget, incoming defectivity, mask shape, critical dimension control, line edge roughness (LER) and line width roughness (LWR) of ever decreasing feature sizes. These issues can be addressed by using spatially uniform low density plasma obtained in a dual frequency mid-gap capacitively coupled plasma etcher.

Here, the unique advantages of TEL Etch Systems and parametric considerations is demonstrated to reduce LER and LWR during plasma etch pattern transfer for two example cases, EUV resist patterning for contact hole patterning and Directed Self Assembly of PS-b-PMMA system for line space patterning. Since mask thickness is much thinner as compared to currently used deep ultraviolet lithography (DUV) resist, both systems require high resist/polymer selectivity during plasma etch of patterns. Also, fine ion/radical flux ratio tunability is required to maintain the pattern profile. Direct current superposition (DCS) on capacitive-coupled plasma (CCP) can enhance the etch resistance of resist and it can improve contact edge roughness (CER). In the case of an applied DCS cure, we confirmed EUV resist etch resistance enhancement and CER improvement. Additionally, we investigated which parameter is dominant for EUV resist cure. For DSA related etching, we have successfully demonstrated pattern transfer into metal hard mask for BEOL application and non-metal hard mask for FEOL applications using TEL Etch Systems. Specifically, the effect of deposition rich gases is investigated for preferential passivation of mask during etching of PS-PMMA films in an oxidizing plasma. This work was performed by the research teams of Tokyo Electron and GLOBALFOUNDRIES at Albany Nanotech Development Facilities.

4:20pm PS-TuA7 Interactions between the Plasma and the Mask Material during Contact Etching, Mokrane Mebarki, STMICROelectronics, France, M. Darnon, LTM - MINATEC - CEA/LETI, France, C.J. Jenny, D. Ristoiu, STMICROelectronics, France, N. Posseme, Cea-Leti, Minatec, O. Joubert, LTM - MINATEC - CEA/LETI, France

The reduction of device dimension at the sub-15nm technological node requires the use of double patterning for contact etching. Line and space patterns are defined first in a thin TiN layer. Then, a trilayer stack with Si-containing anti reflection coating (SiARC) and organic planarizing layer (OPL) is used to define open areas. The mask is defined by the intersections of both hard mask of TiN and OPL patterns and is used to etch contacts into silicon oxide (TEOS).

The OPL mask must conserve straight profiles during the different etching steps and TiN is exposed to the plasma during silicon oxide etching. The OPL can be etched by different plasmas (N₂/H₂, O₂/SO₂, O₂/CO₂) that may induce a passivation layer on the sidewalls via different passivation elements such as CN, CS, CO. Such passivation layers, as well as the presence of TiN during contact etching, can interfere with the SiO₂ etching process and change the final pattern profile. In this study, we investigated the OPL mask etching in COS/O₂ plasma in comparison with N₂/H₂ plasma.

The XPS analyses are performed into Theta300 angle resolved XPS system from Thermo Scientific, ellipsometry measurements are done with spectra FX 200th multiwavelength ellipsometer from KLA-Tencor and OES spectra are recorded with a SD1024 spectrograph detector from SpectraView.

Electronic microscopy observations of OPL patterns etched in N₂/H₂ or in COS/O₂ with various COS/O₂ ratios show that straight profiles without undercut can be obtained. After SiO₂ etching using a fluorocarbon-based plasma, we observe strong profiles variations in the SiO₂ depending on the OPL etch process. After the COS/O₂ OPL open, during the first seconds of the SiO₂ etching, strong emission lines originating from CS species are observed by OES. In addition, EDX analyses after COS/O₂ OPL etching reveal a large amount of sulfur on OPL sidewalls and TiN surface. TiN mask profile is also degraded during the over etch of the OPL and Ti residues are redeposited on all the surfaces. To precise the interaction mechanisms, XPS analyses are performed on TiN, OPL and TEOS after exposure to the various OPL etching processes. We evidenced that the contact profile is influenced by both the process used during OPL opening and the presence of TiN on the wafer. Degradation of masks profiles leads to Ti or S containing residues formation which tends to block the SiO₂ etching. These effects can be reduced by an increase of COS/O₂ ratio during OPL etching.

4:40pm PS-TuA8 Contact Level Patterning Challenges for Sub 22-nm Architecture, Jeffrey Shearer, J. Dechene, S. Kanakasabapathy, IBM Corporation, N. Mohanty, B. Messer, H. Cottle, A. Metz, TEL Technology Center, America, LLC, J. Lee, Samsung Electronics

As gate pitch scaling continues past the 22nm node, we are approaching gate and contact pitches below the threshold of single-exposed lithography. One has to decompose the contact layer into multiple reticles and integrate them on the wafer to achieve an effective pitch less than this threshold. Such integration schemes bring with them issues with substrate damage and gate-contact shorts. Although exercised in BEOL patterning schemes, multicolor integration schemes require customization for the contact module. Damage from plasma exposure to the gate sidewall and source/drain in multiple color integration schemes can detract from gate to contact short yield and device yield. This paper will present innovative etch-integration cooptimization options to minimize plasma induced damage. We also highlight the process challenges in pattern fidelity that the industry has to surmount to make these manufacturable as well as RIE strategies that will help overcome these challenges. Hard mask memorization will be discussed for contact level integration as well as how material selection and etch process optimizations are needed to ensure pattern robustness. Specifically, data will show that multicolor processing causes earlier colors to have degraded device performance. A metal hard mask memorization scheme will be discussed as a way to alleviate multiple source/drain plasma exposures during product processing, thereby improving device yield.

5:00pm PS-TuA9 Method for Preferential Shrink Ratio Control in Elliptical Contact Etch, Hongyun Cottle, A. Lisi, A. Metz, K. Kumar, D. Koty, A. Mosden, P. Biolsi, TEL Technology Center, America, LLC

Sub-22nm logic technology requires contact level etch to meet aggressive critical dimension (CD) shrinks as ArF immersion patterning has mostly reached its resolution limit. Utilization of elliptical contacts brings new constraints to CD shrink. Controlling the 2-D aspect ratio of oval contacts is critical to both device performances and yield. One challenge is that conventional plasma etch shrink methods can induce more shrinkage in the major (Y axis) direction than the minor (X axis), which can cause line-end shortening and feature tip-to-tip spacing control problems.

This paper presents a unique dry etch process that yields a Y to X shrink ratio range ≤ 1 concurrent with a 50% CD reduction from lithography. By utilizing a direct current superposition (DCS) technology, along with CxHyFz chemistry to cure a negative tone developed photoresist (NTD), this method creates a controllable *in-situ* hydrocarbon deposition, which is mainly responsible for the Y to X shrink ratio range ≤ 1 . This is not seen with conventional fluorocarbon etch based shrink where Y/X shrink ratio is typically > 1 , as a result of the larger collection angle for gas phase deposition along the major axis. The Y/X shrink ratio range can be modulated through process condition such as gas ratio, pressure, time, etc. After the controllable hydrocarbon deposition, multiple mask defining transferring steps can be executed anisotropically to complete the pattern transfer. Reported is the structural characterization pre and post etch detailing shrink ratio control. In addition, a mechanistic model will be proposed based on optical emission spectroscopy (OES), thin film compositional analysis, and mass spectrum data.

5:20pm **PS-TuA10 Novel Fluorocarbons Chemistries to Enable 3D NAND High Aspect Ratio Etching**, R. Gupta, B. Lefevre, Venkateswara Pallem, N. Stafford, American Air Liquide, J.M. Kim, K. Doan, S. Nemani, Applied Materials Inc.

The development of high aspect ratio etch processes is one of the challenges that must be overcome for the next generation devices such as 3D NAND. In addition to tool improvements a new variable for optimization of the process is the fluorocarbon chemistry (FC) that is used. The study presented here examines the effect of different FC on high aspect ratio etch processes. In this study several novel fluorocarbons chemistries have been tested using a 200mm dual frequency CCP etch tool. Novel chemistries are used to etch planar film of SiO₂, amorphous carbon, and SiN for which etch rates are measured as well as the deposition rate on bare Si. The O₂ flow rate is varied in order to find the optimum ratio of etch gas to O₂. High aspect ratio structures with oxide/nitride stack are etched using optimum condition. SEM cross-sections of pattern structures were analyzed to determine chemistry effect on etch profile, selectivities and mask preservation. By varying F:C ratios and molecular structures, high aspect ratio structure (> 25) were obtained with sub 100nm features with improved profile compared to standard FC chemistry. Mass spectrometry was also performed on pure etch gas. Variation of the electron energy from 10 to 100eV gives fragments concentration which can help to predict fragmentation of the molecules under plasma condition and etch performance of molecules. The most promising chemistry was tested on Applied Materials 300mm Dielectric Etch tool.

5:40pm **PS-TuA11 LER/LWR Improvements in Dual Frequency CCPs for Advanced Node Patterning**, Mingmei Wang, N. Mohanty, S. Nakamura, A. Ko, A. Ranjan, TEL Technology Center, America, LLC

One of the key parameters in semiconductor mass production control is Line Edge Roughness (LER) / Line width roughness (LWR) owing to its direct contribution to gate length variation, edge placement error, line resistance variation and others. Due to the resolution-line edge/width roughness-sensitivity (RLS) trade-off for photoresists (PR), photolithography has reached its limit to further improve PR LER/LWR for advanced technology nodes (1xnm and beyond). Thus post lithography roughness reduction treatments have become critical in meeting the ITRS targets for LER/LWR. Vacuum Ultra Violet (VUV) treatment has been showing promising results with photochemical modification based smoothing of PR surface using gases like Ar, H₂, HBr etc. which can produce VUV radiation. While several studies have been published over the past decade for improving PR LER/LWR using VUV, most do so by analyzing the results post-VUV-treatment at resist level (before etch transfer). To get good LER for final pattern, pattern transferring from PR is also critical.

CCP chambers, by design, have advantages to achieve good LER/LWR due to the relatively low plasma density and high deposition/etch radical ratio. CCPs with a wide gap are able to well decouple top and bottom RF powers so that we have either low plasma density with high ion energy incident onto the wafer surface or vice versa. In this presentation, post etch LER/LWR data will be discussed with various approaches, such as different treatment duration, different gas combination, ratio plus DC superposition, PR margin, and different plasma parameter settings etc. We will demonstrate that in-order to meet the ITRS targets for LER/LWR for 1x nm and beyond requires co-optimization of the resist roughness with resist profile; thickness; and the subsequent pattern transfer process onto underlying stack.

Novel Trends in Synchrotron and FEL-Based Analysis Focus Topic

Room: 312 - Session SA-TuA

Free Electron Laser and Synchrotron Studies at the Molecule-Surface Interfaces

Moderator: Zahid Hussain, ALS-LBNL

2:20pm **SA-TuA1 FEL-Based Techniques to Explore Photochemistry and Transient States of Molecules on Surfaces**, Wilfried Wurth, Universität Hamburg, Germany **INVITED**

New light sources based on linear accelerators such as the free-electron laser FLASH at DESY in Hamburg in the extreme ultraviolet, the Linac Coherent Light Source LCLS in Stanford as the world's first x-ray laser or FERMI at ELETTRA in Trieste as the first fully externally seeded free-electron laser provide ultrashort, extremely powerful short wavelength pulses with unprecedented coherence properties.

With these new sources it is possible to extend the well-established x-ray spectroscopic techniques for the investigation of the static electronic structure of matter like e.g. photoelectron and x-ray emission spectroscopy to probing the evolution of the electronic structure after controlled excitation in the time domain. The talk will review recent time-resolved x-ray spectroscopy experiments illustrating the opportunities for the study of ultrafast dynamics at surfaces. I will mainly discuss results which have been obtained in the framework of a large international Surface Science Collaboration at LCLS including groups from the US (SLAC in Stanford), from Sweden (University Stockholm), from Denmark (Danish Technical University), and from Germany (Fritz-Haber Institute and Helmholtz Center Berlin, and the Center for Free-Electron Laser Science (CFEL) at the University of Hamburg). These results show that with the new sources it is possible to characterize transient intermediates in surface reactions. Furthermore first steps towards monitoring surface reactions in real-time will be illustrated.

This work has been supported by German Ministry for Education and Science through the priority program FSP-301: "FLASH: Matter in the Light of Ultrashort, Extremely Intense X-ray Pulses"

References:

M. Dell'Angela et al., *Real-Time Observation of Surface Bond Breaking with an X-ray Laser*, *Science* 339, 1302 (2013)

M. Beye et al., *Selective Ultrafast Probing of Transient Hot Chemisorbed and Precursor States of CO on Ru(0001)*, *Phys. Rev. Lett.* 110, 186101 (2013)

T. Katayama et al., *Ultrafast soft X-ray emission spectroscopy of surface adsorbates using an X-ray free electron laser*, *Journal of Electron Spectroscopy and Related Phenomena* 187, 9 (2013)

3:00pm **SA-TuA3 Real-time X-ray Photoelectron Spectroscopy Studies of Electronic Dynamics at Molecule-Semiconductor Interfaces**, Oliver Gessner, Lawrence Berkeley National Laboratory **INVITED**

Interfacial charge transfer processes in molecular and nanoscale systems play an increasingly important role in emerging concepts for renewable energy technologies. Rational design decisions, however, rely on our capability to monitor the pathways of charge carriers on an atomic scale and with a temporal resolution that is commensurate with the timescales of interfacial electron motion. We introduce a new approach to characterize the location of a migrating electron at a molecule-semiconductor interface with sub-nanometer spatial sensitivity and sub-picosecond temporal resolution. Employing the unique capabilities of the Linac Coherent Light Source (LCLS) X-ray Free Electron Laser we use femtosecond time-resolved X-ray photoelectron spectroscopy (tr-XPS) to monitor the nature of an intermediate state that precedes free charge carrier generation in dye-sensitized ZnO nanocrystals after photoexcitation with visible light. Using the element specificity of inner-shell photoemission lines and, in particular, their sensitivity to transient local valence electronic structures, tr-XPS employs the Ru center of the dye molecule as a local reporter atom to provide a unique perspective on ultrafast interfacial charge flow. The underlying physics are explored in a concerted effort with constrained density functional theory (CDFT) calculations of the interfacial electronic structure. The results are discussed with respect to a significantly reduced rate of free charge carrier generation in N₃/ZnO systems compared to other material combinations such as N₃/TiO₂.

Femtosecond time-resolved experiments at the LCLS are complemented by a new picosecond time-resolved XPS effort at the Advanced Light Source (ALS). Using a novel time-stamping technique in combination with a high-power picosecond laser system, tr-XPS experiments on dye-sensitized semiconductor substrates can be performed with up to MHz repetition rates

in all operating modes of the ALS (multi-bunch and two-bunch). The measurements simultaneously monitor chemical shifts of particular photolines and transient surface photovoltages of the semiconductor substrate. Results will be discussed with respect to a possible correlation between intramolecular electron dynamics and transient interfacial charge carrier concentrations in the semiconductor. Routes and first steps toward the implementation of *in operando* X-ray studies of interfacial photoelectrochemical processes will be outlined.

4:20pm **SA-TuA7 Unraveling Topological Properties of Spintronic Materials Using Coherent X-rays**, *Sujoy Roy*, Lawrence Berkeley National Laboratory **INVITED**

Understanding new topological states in condensed matter systems is a current research topic of tremendous interest due to both the unique physics and their potential in device applications. The topological magnetic phases have exotic spin texture, and in some cases can be moved coherently over macroscopic distances with very low currents. Recently discovered skyrmions is an example of such a topological phase that manifest in magnetic systems as a hexagonal lattice of spin vortices. In this talk we will discuss our observation of the skyrmions using resonant soft x-ray scattering in Cu_2SeO_3 and demonstrate the unexpected existence of two distinct skyrmion sub-lattices that arise from inequivalent Cu sites with chemically identical coordination numbers and valency. The skyrmion sublattices are rotated with respect to each other implying a long wavelength modulation of the lattice. The coupled response of these sublattices to external magnetic field suggests a secondary interaction term that has not been predicted. We will also describe an artificial spin ice system whose origin lies in geometrical frustration that comes from the topology of a well-ordered structure rather than from disorder. We observed that under certain applied magnetic field the spin ice exhibits a magnetic structure that can impart orbital angular momentum into the photon beam thereby creating a vortex beam. Further, the vortex beam can be manipulated by an applied magnetic field. Creating an x-ray vortex beams may enable new x-ray based techniques such as coherent control of excitations in quantum material, trapping and rotation of quasiparticles or biomolecules with free electron laser x-ray sources.

Work is funded by U.S. DOE.

5:00pm **SA-TuA9 Where are the Electrons? Charge Transfer and Dissociation from a Femtosecond Electronic-Structure Perspective**, *Philippe Wernet*, Helmholtz-Zentrum Berlin (HZB), Germany **INVITED**

Molecular structure and chemical bonding determine the dynamic pathways of molecules in their multidimensional landscapes and hence define the outcome of chemical reactions. Characterizing chemical bonding in short-lived reaction intermediates and transient states of molecules is hence the key to understanding chemical selectivity. Spectroscopy with femtosecond light pulses with energies ranging from the ultraviolet to the x-ray regime enables a unique approach to the atomic-scale chemical dynamics as it allow for a complete mapping of the electronic structure of atoms and molecules during chemical reactions [1]. Time-resolved femtosecond x-ray spectroscopy in particular reveals chemical bonding both in real time of the reaction and from the atom's perspective in an element-selective way [2].

Here we present our view on charge-transfer and dissociation reactions both in the gas phase and in solution from a femtosecond electronic-structure perspective. We apply femtosecond laser pulses from laboratory laser sources and from large scale x-ray free-electron lasers to map the electronic structure evolution in prototypical systems. Our results reveal how the transient electronic structure and the nuclear dynamics are coupled and they elucidate the role of the solvent from a chemical-bonding perspective.

Detailed insight into the various cases is discussed and an outlook for the investigation of chemical reaction dynamics with x-ray laser spectroscopy is given.

References

- [1] Ph. Wernet, M. Odelius, K. Godehusen, J. Gaudin, O. Schwarzkopf, W. Eberhardt, "Real-time evolution of the valence electronic structure in a dissociating molecule", *Phys. Rev. Lett.* 103, 013001 (2009).
- [2] Ph. Wernet, "Electronic structure in real time: Mapping valence electron rearrangements during chemical reactions", *Phys. Chem. Chem. Phys.* 13, 16941 (2011).

5:40pm **SA-TuA11 Layer Speciation and Electronic Structure Investigation of Hexagonal Boron Nitride Thin Film by Scanning Transmission X-ray Microscopy**, *Jian Wang*, Canadian Light Source Inc., Canada, *Z. Wang*, University of Western Ontario, Canada, *H. Cho, M.J. Kim*, Korea Institute of Science and Technology, Republic of Korea, *T.-K. Sham*, University of Western Ontario, Canada, *X. Sun*, Soochow University, China

Thin films of hexagonal boron nitride (hBN) exhibit a honey cone structure similar to that of graphene, with sp^2 hybridized boron and nitrogen atoms alternately bonded in the basal plane. This unique structure leads to some excellent properties such as high chemical and thermal stabilities, enhanced thermal and electrical conductivity in the basal plane, and versatile doping capabilities. Thus hBN thin films have attracted increasing attentions in many fields. However, unlike graphene, the partly ionic B-N bond in hBN reduces electron-delocalization and creates a large band gap (5.2 eV) in the ultraviolet (UV), making hBN a wide band gap semiconductor and a promising deep UV light emitter. Therefore, an in depth understanding of the morphology and the electronic structure of individual hBN thin films will be of great importance in the development of sophisticated technologies. Synchrotron based scanning transmission X-ray microscopy (STXM) using a nanoscaled focused soft X-ray beam (~30 nm) provides an excellent combination of microscopic examination and chemical/electronic structure speciation via XANES spectroscopy for individual nanomaterials. In this work, chemical imaging, thickness mapping and layer speciation have been performed on a multilayered CVD hBN film with thickness from single layer up to 9 layers by STXM. Spatially-resolved XANES directly from discrete layers have been extracted and compared. Notably a double feature σ^* exciton state and a stable high energy σ^* state were observed at the boron site, and the boron projected σ^* DOS, especially the first σ^* exciton, is sensitive to surface modification, particularly in the single layer regions which show detectable contaminants and defects. Nitrogen site has shown no exciton character. The distinct exciton effect on boron and nitrogen was interpreted to the partly ionic state of hBN. Bulk XANES spectroscopy of hBN thin films was also measured to confirm the spectro-microscopic STXM result. Finally, we compare the XANES (i.e. unoccupied electronic structure) of hBN with that of graphene to elucidate the similarities and origins of the corresponding spectroscopic features.

6:00pm **SA-TuA12 Reference-free, In-depth Characterization of Nanoscaled Materials by Combined X-ray Reflectivity and Grazing Incidence X-ray Fluorescence Analysis**, *Philipp Hönicke, M. Müller*, Physikalisch-Technische Bundesanstalt, Germany, *B. Detlefs*, CEA-LETI, France, *C. Fleischmann*, IMEC, Belgium, *B. Beckhoff*, Physikalisch-Technische Bundesanstalt, Germany

The accurate in-depth characterization of nanoscaled layer systems is an essential topic for today's developments in many fields of materials research. Thin high-k layers [1], gate stacks and ultra-shallow dopant profiles are technologically relevant for current and future electronic devices. Nanolaminate composites, consisting of alternating layers of different materials with a nanometer scale thickness, are being developed for energy storage and memory applications [2]. However, the metrological challenges to sufficiently characterize such complex systems require a further development of the current analytical techniques.

Synchrotron-based Grazing Incidence X-ray Fluorescence (GIXRF) analysis has already been shown to be capable of contributing to the in-depth analysis of nanoscaled materials [3,4]. Essential for the quality of the results obtained with GIXRF is the calculation of the underlying X-ray standing wave field. This requires accurate knowledge of the optical properties of the system under investigation. Usually, this cannot be obtained from tabulated data due to the complexity of the sample in terms of layer thicknesses and material combinations and because of the fundamentally different material properties at the nanoscale.

The combination of GIXRF with X-Ray Reflectometry (XRR), provides access to the optical properties of the sample and has been shown to improve the characterization reliability of GIXRF [3]. Employing the novel in-house built instrumentation [5] and radiometrically calibrated detectors at the laboratory of the Physikalisch-Technische Bundesanstalt at the BESSY II synchrotron radiation facility, this combined method allows for reference-free quantitative in-depth analysis [3,4,6]. The capabilities of the combined XRR-GIXRF method are demonstrated by means of several nanoscaled layer systems as well as ultra-shallow dopant profiles.

- [1] R.D. Clark, *Materials* 7(4), (2014), 2913.
- [2] J. Azadmanjiri et al., *J. Mater. Chem. A* 2, (2014), 3695.
- [3] P. Hönicke et al., *J. Anal. At. Spectrom.* 27, (2012), 1432.
- [4] M. Müller et al., *Materials* 7(4), (2014), 3147.
- [5] J. Lubeck et al., *Rev. Sci. Instrum.* 84, (2013), 045106.
- [6] P. Hönicke, M. Müller, B. Beckhoff, *Solid State Phenomena* 195, (2013), 274.

Surface Science

Room: 309 - Session SS+NS-TuA

Nanostructures: Growth, Reactivity and Catalysis

Moderator: Judith Harrison, United States Naval Academy, Greg Kimmel, Pacific Northwest National Laboratory

2:20pm **SS+NS-TuA1 Building Nanostructured Nanowires via Sequential Catalyst Reactions, Frances Ross, IBM T.J. Watson Research Center** **INVITED**

By exposing catalytic nanoparticles to reactive source gases, nanowires can be grown with excellent control over length, diameter, crystal structure and composition. Here we discuss the degree to which this vapour-liquid-solid growth mechanism can be augmented by “programming” a sequence of reactions in the catalyst. Our aim is to produce complex structures in which quantum dots and quantum wells of precise dimensions are incorporated into single nanowires. We supply different species to nanowire catalysts, either as reactive gases or by evaporation, triggering the formation of new phases that become incorporated into the nanowires as they grow. *In situ* transmission electron microscopy allows us to view this process, identify phases and measure kinetics. As an example, we discuss the formation of silicide quantum dots within Si nanowires. Supplying metals such as Co and Ni to catalysts composed of liquid AuSi results in the formation of faceted silicide nanocrystals. These floating nanocrystals subsequently attach at the AuSi/Si interface. Further growth of Si incorporates these quantum dots into the nanowire. We discuss the generality of this phenomenon and the control of silicide structure and dimensions. The formation of narrow quantum wells, such as Ge layers within Si nanowires, can also benefit from understanding the sequential changes in the catalyst. We describe the relationship between catalyst properties and quantum well compositional abruptness, strain and stability. We finally consider the possibilities of combining quantum dots and quantum wells in single nanowires. We suggest that control of reaction pathways within the catalyst provides exciting opportunities for the growth of complex nanostructures.

3:00pm **SS+NS-TuA3 Ar/O₂ and H₂O Plasma Modified SnO₂ Nanomaterials for Gas Sensing Applications, Erin Stuckert, E.R. Fisher, Colorado State University**

Tin oxide (SnO₂) is an excellent material for gas sensing applications. The sensing mechanism of SnO₂ is controlled through gas interactions with adsorbed oxygen, which alters the charge flow through the sensing material. By measuring changes in charge flow, sensitivity and selectivity of a gas sensor can be determined. Sensitivity is improved by increasing surface-gas interactions of high surface area materials, SnO₂ nanoparticles and nanowires, combined with surface modification. One surface modification method that can achieve greater oxygen adsorption is plasma treatment; with an expansive parameter space, plasmas allow for greater control of the modification process. In this work, commercial SnO₂ nanoparticles and chemical vapor deposition (CVD)-grown SnO₂ nanowires were plasma modified to create oxygen vacancies with the aim of increasing oxygen adsorption during sensing. Specifically, we employed Ar/O₂ and H₂O plasmas because they can etch materials like SnO₂ to increase oxygen adsorption by creating surface oxygen vacancies. Ar/O₂ plasma treatment of SnO₂ nanoparticles and nanowires showed increasing oxygen adsorption with increasing plasma power and treatment time without changing Sn oxidation state or morphology, as measured by X-ray photoelectron spectroscopy (XPS) and powder X-ray diffraction (PXRD). With low power H₂O plasma treatments, however, greater oxygen adsorption was observed with nearly complete Sn reduction as well as significant morphological changes evidenced in XPS, PXRD, and scanning electron microscopy (SEM). Plasma treated materials were evaluated for their sensitivity and selectivity for a variety of gases including ethanol, formaldehyde, and benzene. Results for both Ar/O₂ and H₂O plasma treated SnO₂ nanoparticles and nanowires will be presented and discussed with respect to their sensing capabilities, including changes in selectivity and sensitivity.

Keywords:

Plasma treatment

Gas sensor

Tin oxide

Nanowire

Nanoparticle

3:20pm **SS+NS-TuA4 Interaction of D₂O on the Surface Grown ZnO(0001) Nanostructures, Xingyi Deng, D.C. Sorescu, J. Lee, C. Matranga, National Energy Technology Laboratory**

D₂O on the ZnO nanostructures grown on Au(111) has been investigated using a combination of experimental and theoretical methods as to probe the reactivity of model ZnO catalysts at the atomic level. We performed a series of D₂O temperature programmed desorption (TPD) experiments on two distinctive surfaces, one consisting of single layer Zn(0001) nanostructures, and the others consisting of mixtures of single and bilayer ZnO(0001) nanostructures. On the basis of our TPD data and in comparison with the ZnO structural characteristics, we are able to assign each D₂O TPD peak to a specific site existing on the ZnO nanostructures. Specifically, desorption peaks at 150 and 200 K are assigned to sublimation of D₂O multilayers and desorption of D₂O adsorbed directly on the ZnO surfaces, respectively; and D₂O adsorbed on the edges of either single or bilayer ZnO desorbs at a slightly higher temperature ~260 K. More importantly, we identify that D₂O binds to the steps between the single and bilayer ZnO much stronger than any other sites, desorbing around 400 K. Computational modeling based on density functional theory (DFT) calculations provides detailed adsorption geometry and energetics of the D₂O-ZnO(0001)/Au(111) system, further supporting our TPD assignments. Implications of our fundamental results for ZnO based catalysts will be discussed.

4:20pm **SS+NS-TuA7 2014 AVS Medard Welch Award Lecture: Quasicrystals to Nanoclusters: It's All on the Surface, Patricia Thiel*, Iowa State University** **INVITED**

Surface science continues as an exciting frontier—perhaps more so now than in the past—for at least two reasons. First, powerful new tools are emerging, and second, a broad and robust body of knowledge has been established which is serving as a springboard for new breakthroughs, and is critically guiding other fields. In this talk I will present some of the contributions that I and my coworkers have been privileged to make in this field, particularly in the area of quasicrystal surfaces, and in the area of growth and stability of nanoclusters and thin films at surfaces. Metallic quasicrystals have a remarkable atomic structure that engenders unusual properties, including surface properties, and our goal has been to establish the structure-property relationship at the surface. One of our achievements was to show that quasicrystal surfaces are generally bulk-terminated. This laid the groundwork for showing that one of the characteristics of quasicrystals—low friction—derives (at least in part) from the quasiperiodic atomic structure. It also allowed us to understand unusual features of thin film nucleation and growth on these surfaces, and facilitated efforts of other groups to exploit quasicrystals and complex metallic alloys as catalysts. Nucleation and growth of nanoclusters and thin films also shows surprising features on more conventional (crystalline metal) surfaces, and has been a topic of investigation in my group for some time. We discovered that unusual smooth growth at low temperature, and associated non-monotonic temperature dependence of roughness, reflects a process now called “downward funneling”. In addition to non-equilibrium growth morphologies, we have also explored the relaxation of these morphologies towards equilibrium. We found that two-dimensional homoepitaxial metal nanoclusters can diffuse significant distances, leading to coarsening (a reduction in the cluster density) via agglomeration. Nanocluster destabilization and coarsening can also occur via Oswald ripening, but the identity of the mass carriers may not be obvious. The presence of even trace amounts of adsorbates can lead to formation of additive-metal complexes which more efficiently transport mass than metal atoms. We have searched for these complexes under conditions which have rarely been investigated in the past, i.e. very low temperature and very low coverage, with some surprising results.

5:00pm **SS+NS-TuA9 Photodeposited Pt Nanoparticles on Iron Oxide Nanoparticles Supported on Highly Oriented Pyrolytic Graphite, Jayde Kwon, J.C. Hemminger, University of California Irvine**

Metal-semiconductor hybrid systems have been of great interest due to their unique photocatalytic properties. In metal-semiconductor hybrid systems, semiconductors are used as light absorbing components. They absorb photons and create electron holes localized at the semiconductor, which are formed by excited electrons that move through the heterointerface. Fe₂O₃ is a promising semiconductor photocatalyst due to its visible light absorption ($E_g = 2.2$ eV), abundance, non-toxicity, and stability against photo corrosion. However, Fe₂O₃ suffers from short hole diffusion length, low electrical conductivity and high rate of electron hole recombination. To overcome these barriers, different transition metals (e.g. Au, Si, Pt) have been deposited on Fe₂O₃. Particularly, Pt on Fe₂O₃ is an ideal heterogeneous catalyst that has a variety of uses such as photoelectrochemical water splitting and CO oxidation. Importantly, Pt on Fe₂O₃ provides an

* **Medard W. Welch Award Winner**

improvement in photocatalytic properties on the degradation of dyes, such as methylene blue. Although many studies deposit Pt on various forms of Fe_2O_3 (e.g. films, nanorods, and cores/shells), Pt nanoparticles on discrete Fe_2O_3 nanoparticles on highly oriented pyrolytic graphite (HOPG) has not been studied. The deposition of Pt on Fe_2O_3 has been studied using various methods such as electrodeposition and solution based synthesis. However, photodeposition of Pt on Fe_2O_3 has not yet been studied. In this work, we demonstrate photodeposition of Pt nanoparticles selectively on Fe_2O_3 nanoparticle arrays formed by physical vapor deposition on HOPG. We find that the Fe_2O_3 nanoparticles are in the range of 7-20 nm in diameter. Ongoing studies of the catalytic properties of these unique materials will be presented.

5:40pm **SS+NS-TuA11 Formation and Stability of and Surface Chemistry on Dense Arrays of Au Nanoclusters on Hexagonal Boron Nitride/Rh(111)**, *M.C. Patterson, Phillip Sprunger, J.R. Frick, Y. Xu, Louisiana State University, B.F. Habenicht, University of California Merced, R.L. Kurtz, Louisiana State University, L. Liu, Texas A&M University*

We have studied the nucleation and growth of Au clusters at sub-monolayer and greater coverages on the h-BN nanomesh grown on Rh(111) by means of scanning tunneling microscopy (STM), X-ray photoelectron spectroscopy (XPS), and density functional theory (DFT). STM reveals that sub-monolayer Au deposited at 115 K nucleates within the nanomesh pores and remains confined to the pores even after warming to room temperature. Whereas there is a propensity of mono-atomic high islands at low temperature, upon annealing, bi- and multilayer Au clusters emerge. Deposition of higher coverages of Au similarly results in Au confined to the nanomesh pores at both 115K and room temperature. XPS analysis of core-level electronic states in the deposited Au shows strong final-state effects induced by restricted particle size dominating for low Au coverage, with indications that larger Au clusters are negatively charged by interaction through the h-BN monolayer. DFT calculations suggest that the structure of the Au clusters transitions from monolayer to bilayer at a size between 30 and 37 atoms per cluster, in line with our experiment. Bader charge analysis supports the negative charge state of deposited Au. Using vibrational EELS, CO and O_2 are used to probe the activity of these gold model catalysts.

6:00pm **SS+NS-TuA12 Collective Multi-Atom Diffusion in Ag/Ge(110) 1D Nanoisland Growth**, *Shirley Chiang, C.H. Mullet, University of California, Davis, M.C. Tringides, Iowa State University and Ames Lab-USDOE, M.S. van Zijl, B.H. Stenger, E.S. Huffman, D.J. Lovinger, E.C. Poppenheimer, University of California, Davis*

The growth of Ag deposited on Ge(110) was studied with low energy electron microscopy (LEEM) and scanning tunneling microscopy (STM). The LEEM studies showed the formation of long, one-dimensional (1D) multi-height islands over the temperature range 430C-530C. During deposition, the length of the islands increases at a constant rate ($\sim 10^6$ atoms/sec reaching ~ 20 microns) and constant width (100-200nm) for 9ML total deposition. Stochastic diffusion cannot account for these very high island growth rates. When smaller islands decay, the rate is $\sim 2 \times 10^7$ atoms/sec, which is also exceedingly fast, based on the Ag diffusion and detachment barriers. These high rates are not consistent with independent adatom events and imply multi-atom correlated diffusion. Such collective mass transport must be related to the mobility of the wetting layer. STM images show the crystalline structure of the 1D Ag islands and also indicate that the reconstructed regions between the islands consist of bare Ge. These data are corroborated by LEEM IV curves. Together, they confirm that the wetting layer provides the material for the islands to grow at these high rates.

Thin Film

Room: 305 - Session TF+AS+EM-TuA

Thin Film: Growth and Characterization II

Moderator: Mark Davidson, University of Florida

2:20pm **TF+AS+EM-TuA1 A Statistical Optimization of Perpendicular Anisotropy and Damping for Ta-Inserted Double CoFeB/MgO Interface MTJ's**, *S. Gupta, Samuel Schwarm, B. Clark, University of Alabama*

A statistical Design of Experiments was conducted on double-interface Ta-inserted CoFeB-MgO magnetic tunnel junctions (MTJ's). These MTJ's were deposited using a Shamrock planetary sputtering system. The thicknesses of the inserted Ta and the CoFeB electrodes were varied using Response Surface Methodology. The responses measured using magnetometry and ferromagnetic resonance were a) effective

magnetization, b) damping constant and c) perpendicular anisotropy. The effect of annealing on the perpendicular anisotropy was also observed for these devices. As the Ta thickness is increased for fixed CoFeB thickness, the M-H loops indicate that the anisotropy is becoming perpendicular. After annealing, both magnetometry and FMR results show that the MTJ's indicate full perpendicular anisotropy. Interfacial perpendicular anisotropy, which can be extracted from the FMR measurements, scales with the inserted Ta thickness for both as-deposited and annealed samples.

2:40pm **TF+AS+EM-TuA2 1D Matlab Modeling of the Reaction-Diffusion System during the Selenization Process in the Two-Step CIGS Solar Cells Production Process**, *Jurjen Emmelkamp, A. Mannheim, TNO Technical Sciences, Netherlands*

Introduction

In the two-stage fabrication process of CIGS thin-film solar cells first copper, indium and gallium precursor layers are deposited, followed by the selenization process where selenium vapor is provided at high temperature to form CIGS. Despite of the literature, many stages of the reaction-diffusion process are still a mystery. Several experimental techniques exist to analyze the selenization process, however, most of them are only useful to analyze the post-selenization product. In-situ XRD can be used to analyze the crystal structure during the selenization process, but the information is limited because depth profiles and amorphous intermediates are not measured. Modeling of the reaction-diffusion system during the selenization process can result in deeper understanding of the process and in a predictive model for the optimal process conditions that can lead to cheaper and more efficient CIGS solar cells.

The model

A relative simple 1D mathematical Matlab model is developed. Since many intermediate products and the CIGS end-product are crystals, and thus 3D systems, an 1D approach is very simplified. Intensive evaluation with experimental in-situ XRD and cross section EDX, as well as literature values, are used to tune the model specific parameters. Main parameters include diffusion and reaction constants of the different elements and binaries/ternaries, as well as the sticking factor at the surface for the uptake of selenium from the vapor phase. Using these parameters the (intermediate) reactions can be derived and fitted to the data from experiments and literature studies.

First the process temperature profile is calculated as function of time, followed by the calculating the uptake of selenium from the vapor phase. Additionally, the diffusion and reactions are modeled, using Fick's second law, error functions and multiple reflections at the solid interfaces. Based on phase diagrams the reaction kinetics of the most important reaction products are derived and are included into the model.

For reasons of memory limitations, the time and spatial mesh need to be relative coarse. For the spatial mesh this requires adaptive meshing, in order to adapt to small spatial variations and to mimic the overall and the specific layer growth well at small time changes.

Conclusions

The development of the model is still in progress, but the first results show good approximation of the selenium uptake and the formation of the first binaries and ternaries, such as $\text{Cu}_{11}\text{In}_9$, Cu_{23}Se , In_4Se_3 and InSe . This can be expanded easily to other intermediates, CIS, CGS and CIGS. However, further parameter fitting is required to mimic the experimental data better.

3:00pm **TF+AS+EM-TuA3 TiSiO Thin Films Deposited by Plasma Enhanced Chemical Vapor Deposition for Optical and Electrical Applications**, *Antoine Goullet, S. Elisabeth, D. Li, M. Carette, A. Granier, IMN, France*

INVITED

TiO_2 thin films are good candidates for the development of passive optical or electrical integrated devices. They exhibit high optical refractive index ($1.8 < n < 2.7$ at 633 nm) in combination with high transparency in the visible range and high dielectric constant ($50 < k < 100$). They are compatible with semiconductor technologies and can be synthesized at low temperature by plasma processes such as plasma enhanced chemical vapor deposition (PECVD). This technique is very attractive to tune film composition and properties such as film refractive index. PECVD is also known for its ability to prepare good quality amorphous or partially crystalline films at low temperature.

Titanium-silicon mixed oxide (TiSiO) materials can overcome some of the limitations given by TiO_2 material, e.g. columnar morphology and relatively low band gap energy.

In this study, TiSiO thin films are prepared without any intentional heating in low pressure inductively coupled discharges from titanium tetraisopropoxide (TTIP- $\text{Ti}(\text{OC}_3\text{H}_7)_4$) and hexamethyldisiloxane (HMDSO - $\text{SiO}_2(\text{CH}_3)_6$) precursors mixed with oxygen.

Structure and chemical composition of the films are investigated by X-ray diffraction (XRD) and X-ray photoelectron spectroscopy (XPS). Information about film chemical bonds is also obtained from Fourier transform infrared spectroscopy (FTIR). Film morphology is characterized by scanning electron microscopy (SEM) and atomic force microscopy (AFM). Optical properties are mainly investigated by spectroscopic UV-Visible ellipsometry.

Capacitance-voltage ($C-V$) and current-voltage ($I-V$) measurements are performed by using MIS capacitors for evaluation of the mixed oxide film electrical performances.

TiO₂ thin films characteristics are investigated as a function of the plasma ion energy in the 25 – 175 eV range. Increasing the ion energy leads to more homogeneous and organized films with the transformation from anatase to rutile. To account for the columnar morphology of TiO₂ films, a gradient optical layer model was developed. The thin layer dispersion functions were described satisfactorily with the Tauc-Lorentz dispersion law.

TiSiO have been deposited by varying the HMDSO flow rate in the plasma operated in continuous or pulsed mode.

The thin films can be described as a mixture of silicon and titanium oxide at the atomic scale rather than two separate SiO₂ and TiO₂ phases. These mixed oxide layers are basically amorphous and exhibit good morphological properties provided the titanium content is lower than the silicon one.

On the whole these TiSiO layers offer a good compromise in terms of morphological, optical and electrical properties.

4:20pm TF+AS+EM-TuA7 Kinetically-Limited Lattice Relaxation in Linearly- and Non-Linearly- Compositionally-Graded In_xGa_{1-x}As/GaAs (001) Metamorphic Heterostructures, *Tedi Kujofsa, J.E. Ayers*, University of Connecticut

Metamorphic buffer layers allow tremendous flexibility to design novel InGaAs/GaAs semiconductor heterostructures for application in various microelectronic and optical devices. However, device fabrication, reliability and performance are limited by dislocation defects associated with the growth of highly mismatched systems such as InGaAs on GaAs substrate. Thus, understanding kinetically-limited lattice relaxation and development of a plastic flow model applicable to multilayered and compositionally graded heterostructure is desirable to provide guidance in designing InGaAs/GaAs devices. Previously, we reported a plastic flow model for Zn_ySe_{1-y}/GaAs (001) heterostructures which predicts the non-equilibrium strain relaxation as well as misfit dislocation and threading dislocation densities. Here, we have extended our model to In_xGa_{1-x}As/GaAs (001) metamorphic buffer layers with arbitrary compositional grading profile. In addition, we have investigated the evolution of the kinetically limited in-plane strain of In_xGa_{1-x}As/GaAs (001) heterostructures with an emphasis on grading schemes employing a step, linear-, S- and power-law- lattice mismatch compositional profile. For each structure, we have studied the thickness and grading coefficient dependence on the average and surface kinetically-limited in-plane strain. In addition, we show that the use of compositionally graded buffer layers enables the design of In_xGa_{1-x}As/GaAs (001) heterostructures with high surface strain values which enhance the sweeping of threading defects and therefore yielding device structures with minimal defect.

5:00pm TF+AS+EM-TuA9 Superconducting Properties of NbN and NbTiN Thin Films, *Matthew Burton, M.R. Beebe, R.A. Lukaszew, D. Beringer*, College of William and Mary

Thin films of NbN and NbTiN are promising materials currently researched for improvements in superconducting radio frequency (SRF) technology and applications. At present, bulk niobium SRF accelerating cavities suffer from a fundamental upper limit in maximally sustained accelerating gradients; however, a scheme involving multi-layered superstructures consisting of superconducting-insulating-superconducting (SIS) layers has been proposed to overcome this fundamental material limit of 50 MV/m [1]. The SIS multi-layer paradigm is reliant upon implementing a thin shielding material with a suitably high H_{c1} which may prevent early field penetration in a bulk material layer and consequently delay the high field breakdown. It has been predicted that for thin superconducting films — thickness less than the London penetration depth (~200 nm in the case of NbN) — the lower critical field H_{c1} will be enhanced with decreasing thickness. Thus, NbN thin films with a high H_{c1} value are possible candidates for such SIS structures. We note though that since the intrinsic resistivity of NbN is rather large, efforts are also devoted to NbTiN which has similar superconducting properties but much lower intrinsic resistivity which is preferable for this application. Here we present our study on the structure and superconducting properties of a series of NbN and NbTiN thin films and correlate the effects of film microstructure and surface morphology on

relevant superconducting properties such as the critical temperature, T_c, the lower critical field, H_{c1}, and the residual resistance ratio.

[1] A. Gurevich, Appl. Phys. Lett., 88, 012511 (2006).

5:40pm TF+AS+EM-TuA11 High-Throughput Assessment of the Composition Dependence of Initial Passivating-Al₂O₃-Scale Establishment in Al_xFe_yNi_{1-x-y} Alloy Thin Films, *Matthew Payne, J. Miller, A.J. Gellman*, Carnegie Mellon University, DOE - National Energy Technology Laboratory

AlFeNi-containing alloys capable of forming passivating Al₂O₃ scales are designed for high-temperature structural applications requiring robust oxidation resistance. Mechanical considerations typically dictate that Al content be minimized, but a critical concentration, N_{Al}^* , is minimally required to promote the initial establishment of a continuous Al₂O₃ layer. Current understanding of how N_{Al}^* evolves across multi-component composition spaces is limited, being based largely on experiments that are constrained by the need for meticulous preparation and characterization of large numbers of single-composition samples. The study of properties across alloy composition space can be greatly accelerated using composition spread alloy films (CSAFs), materials libraries comprised of continuous lateral composition gradients. Properly designed CSAFs can contain every possible composition of a ternary alloy. In this work, ~120 nm-thick Al_xFe_yNi_{1-x-y} CSAFs spanning the entire ternary range ($x = 0 \rightarrow 1$, $y = 0 \rightarrow [1-x]$) over an area of ~1 cm² were prepared. A variety of spatially resolved techniques were developed for effective, high-throughput characterization of early oxidation behaviors in the CSAFs. Energy-dispersive X-ray spectroscopy was used to measure changes in CSAF oxygen content as a function of both alloy composition and oxidation time. Raman spectroscopy allowed specific oxide phases formed in different regions of the composition space to be identified. X-ray photoemission depth profiling was performed at select locations of interest to determine composition and chemical state in CSAF cross-sections. These methods were used to study oxidation across Al_xFe_yNi_{1-x-y} composition space in both dry and moist air at 700 K, and have enabled the identification of continuous boundaries separating regions of phenomenologically unique oxidation behaviors, including the $N_{Al}^*(x,y)$ boundary for each environment. The results enhance fundamental understanding of early-stage Al_xFe_yNi_{1-x-y} oxidation and can contribute to the accelerated design of next-generation alloys.

6:00pm TF+AS+EM-TuA12 Structural, Electrical, and Optical Characterization of Impurity-Dependent, Ultra-Low-Dislocation-Density Ge Epitaxially Grown on Si and Characterization of MOSFETs Fabricated on Ge-on-Si, *Swarnadip Ghosh, S.M. Han*, University of New Mexico

Building on a simple two-step MBE growth technique, we have investigated possible dislocation locking mechanisms by dopant impurities, coupled with artificially introduced oxygen (O). In the case of n-type Ge grown on Si, our materials characterization indicates that the dislocation density (DD) can reach the ~10⁵ cm⁻² level, compared to p-type and undoped Ge on Si (GoS). We note that our Ge film covers the entire underlying Si substrate at the wafer scale without mesas or limited-area growth. In this presentation, we will focus on the use of n-type impurity (phosphorus) diffusion from the Si substrate and the introduction of O at the Ge-Si interface. The O is introduced by growing a thin chemical SiO₂ layer on top of the Si substrate before Ge epitaxy begins. Z-contrast cross-sectional TEM images suggest the presence of O precipitates in n-type Ge, whereas these precipitates appear absent in p-type Ge. These O precipitates are known to lock the dislocations. Supporting the argument of precipitate formation, the TEM shows Moiré fringes due to various phase boundaries that exist at the precipitate/Ge-crystal interface. We speculate that the formation of phosphorus (P) segregation resulting from slow diffusion of P through precipitates at the precipitate/Ge-crystal interface facilitates dislocation locking. Impurity segregation in turn suppress O concentration in n-type Ge leading to the reduced DD that appears on the top surface of n-Ge compared to p-Ge film. The O concentrations (10¹⁷ to 10¹⁸ cm⁻³) in the n- and p-type GoS films are measured using secondary ionization mass spectroscopy. We have then compared the structural and electrical characteristics of n-type Ge films with its p-type counterparts. In n-type Ge, the DD decreases from ~10⁹ cm⁻² near the Ge-Si interface to ~10⁵ cm⁻² at the film surface. In contrast, we observe 5×10⁷ cm⁻² DD at the film surface in p-type Ge. The full width at half-maximum for our n-type Ge(004) XRD peak is 100 arcsec, compared to 230 arcsec of p-type Ge. As a stringent test of the dislocation reduction, we have also fabricated and characterized high-carrier-mobility MOSFETs on GoS substrates. We also report p- and n-MOSFETs with μ_{eff} of 401 and 940 cm²/V-s and a subthreshold slope of 100 and 200 mV/decade, respectively. These effective mobilities show an exceptional 82 and 30% improvement over that of conventional Si channel MOSFETs. We also investigate the optical quality of ultra-low DD GoS film by measuring photoluminescence (PL). Then-type Ge PL main peak

shows pronounced tensile-strain ($\times 0.8\%$) than that of p-type, which is an indicator of direct bandgap shrinking at the Γ band-edge.

Thin Film

Room: 307 - Session TF+EN+PS-TuA

ALD for Energy

Moderator: Erwin Kessels, Eindhoven University of Technology, Netherlands

2:20pm **TF+EN+PS-TuA1 Li-Based ALD Solid Electrolytes for Beyond-Li-Ion Batteries, Alexander Kozen*, A.J. Pearse, M.A. Schroeder, C. Liu, M. Noked, C.F. Lin, G.W. Rubloff**, University of Maryland, College Park

Solid Li-based inorganic electrolytes offer profound advantages for energy storage in 3-D solid state batteries: (1) enhanced safety, since they are not flammable like organic liquid electrolytes; and (2) high power and energy density since the solid electrolyte can support interdigitated nanostructured electrodes, avoiding binders, separators, and much larger spacing (tens of mm's) between fully separated electrodes. The quality of thin solid electrolytes – even in planar form – is currently a major obstacle to solid state batteries[1] restricting electrolyte thickness to >100 nm to control electronic leakage, consequently slowing ion transport across the electrolyte and impeding interdigitated 3-D nanostructure designs that offer high power and energy. Furthermore, the ion-conducting, electron-insulating properties of solid electrolytes are promising for their use as passivation or protective layers on metal anodes (Li, Na, Mg) and on cathodes in proposed “beyond-Li-ion” battery configurations such as Li-O₂ and Li-S.

Atomic layer deposition (ALD) is well suited to the challenge of solid electrolytes, providing ultrathin, high quality films with exceptional 3-D conformality on the nanoscale. We have developed ALD processes for Li₂O, Li₃PO₄, and LiPON from LiO^tBu, H₂O, and N₂, exploiting spectroscopic ellipsometry, downstream mass spectrometry, and XPS surface analysis, all *in-situ*. Post-ALD XPS reveals for the first time carbon-free electrolytes and their intrinsic surface chemistry. E.g., ALD Li₂O grown at 250C is reversibly transformed to LiOH upon exposure to H₂O, but transforms back upon annealing. LiOH is completely and irreversibly converted to Li₂CO₃ by CO₂ exposure. These kinds of observations are essential to developing process sequences for fabricating 3-D solid batteries.

We then demonstrate the impact of this solid electrolyte synthesis in several examples. For solid state batteries, we employ the electrolytes in planar and nanostructured battery configurations to determine their Li diffusivity and electrochemical performance. For beyond-Li-ion configurations with organic electrolytes, we show the use of ALD Li₂O at controlled mass loading in high aspect ratio Li-O₂ cathodes to elucidate the Li-O₂ charging chemistry, and we demonstrate the use of the ALD solid electrolytes in passivating Li anodes in Li-S batteries.

[1] D. Ruzmetov, V. P. Oleshko, P. M. Haney, H. J. Lezec, K. Karki, K. H. Baloch, A. K. Agrawal, A. V. Davydov, S. Krylyuk, Y. Liu, J. Huang, M. Tanase, J. Cumings, and A. A. Talin, “Electrolyte Stability Determines Scaling Limits for Solid-State 3D Li Ion Batteries,” *Nano Lett*, vol. 12, no. 1, pp. 505–511, Jan. 2012.

2:40pm **TF+EN+PS-TuA2 Engineering Lithium-Containing Ionic Conductive Thin Films by Atomic Layer Deposition for Lithium-ion Battery Applications, Jea Cho, T. Seegmiller, J. Lau, L. Smith, J. Hur, B. Dunn, J.P. Chang**, University of California at Los Angeles

Lithium (Li)-ion batteries have drawn much attention for their outstanding performance in portable electronics applications. These batteries have the potential to function as miniaturized power sources for microelectromechanical (MEMS) devices through the fabrication of 3-dimensional configurations. To fabricate a fully functional 3D Li-ion microbattery, however, an ultra-thin and highly conformal electrolyte layer is required to coat the 3D electrodes. The solid oxide Li-ion conductor, lithium aluminosilicate (Li_xAl_ySi_zO, LASO), synthesized by atomic layer deposition (ALD) is a promising electrolyte material for 3D battery applications owing its adequate ionic conductivity as well as improved electrode stability.

The self-limiting characteristic of ALD allows for precise control of thickness and composition of complex oxides and results in a highly conformal and pinhole-free coating even on highly complex structures such as high aspect ratio 3D electrodes. The metal precursors, lithium t-butoxide

(LTB), trimethylaluminum (TMA), tris(tert-butoxy)silanol (TTBS), and tetraethylorthosilicate (TEOS) were used to form Li_xAl_ySi_zO via ALD. *In-situ* FTIR was implemented to study the incubation time and growth mechanisms for each oxide deposited on the other to improve the controllability of the films. *In-situ* FTIR studies revealed that the growth mechanism of silicon oxide is strongly affected by the underlying oxide layer, exhibiting different surface reaction mechanisms during the incubation stage.

Li-ion conductivities and the activation energy for conduction of as-deposited LASO/LAO/LSO films were determined for different lithium contents and film thickness. The LASO ALD coating on 3D carbon array posts were confirmed to be conformal and uniform using transmission electron microscopy (TEM) imaging. A Li-ion half-cell consisting of LASO coated on 3D carbon array electrode showed reversible electrochemical behavior. Lithiation cycling tests of thin LASO/LAO/LSO films were found to be functions of both composition and thickness. The reversibility and kinetics of insertion as well as the effect on the cycling stability from the direct deposition of LASO/LAO/LSO on potential anode materials, SiNWs were also investigated using *in-situ* TEM observations during lithiation.

3:00pm **TF+EN+PS-TuA3 Applications of ALD for Li ion Batteries and Low Temperature Fuel Cells, Xueliang (Andy) Sun**, University of Western Ontario **INVITED**

Atomic layer deposition (ALD) is a novel and unique coating technique with many applications in energy storage and conversion [1]. In this talk, I will present our recent work on exploring the applications of atomic layer deposition (ALD) in both fuel cells and Li ion batteries [2-7].

In the first part, we will report of use of ALD for Pt catalysts used in low temperature fuel cells. In particular, atomic Pt or clusters prepared by ALD show ten times higher methanol oxidation properties compared with ETK commercially-used catalysts [2].

In the second part, we will focus on employing ALD as a surface-modification method to enhance the performance of LIBs. Different materials for surface-modification (such as Al₂O₃, ZrO₂, TiO₂ and AlPO₄) [3,4] were first developed by ALD. Then systemic studies were carried out by using those materials to modify the anode (Li₄Ti₅O₁₂, SnO₂) [5] and the cathode (commercial LiCoO₂, NMC) [6]. The effects of different coating materials on the LIB performance of the anode and cathode were investigated in details. In addition, the potential application of ALD as a powerful technique for preparing solid-state electrolyte will be demonstrated [7]. We will discuss further development of ALD for fuel cells and Li ion batteries.

Reference:

- [1] X. Meng, X.-Q. Yang, X. Sun. *Adv. Mater.* 2012, 24, 3589-3615.
- [2] S. Sun, G. Zhang, N. Gauquelin, N. Chen, J. Zhou, S. Yang, W. Chen, X. Meng, D. Geng, M. Banis, R. Li, S. Ye, S. Knights, G. Botton, T.-K. Sham, X. Sun, *Scientific Reports* 3 (2013) 1775.
- [3] J. Liu, X. Meng, Y. Hu, D. Geng, M.N. Banis, M. Cai, R. Li, X. Sun. *Carbon* 2013, 52, 74-82.
- [4] J. Liu, Y. Tang, B. Xiao, T.K. Sham, R. Li, X. Sun. *RSC Adv.* 2013, 3, 4492-4495.
- [5] X. Li, X. Meng, J. Liu, D. Geng, Y. Zhang, M. Banis, Y. Li, R. Li, X. Sun, M. Cai, M. Verbrugge, *Adv. Funct. Mater.* 22 (2012) 1647-1654.
- [6] X. Li, J. Liu, M. Banis, A. Lushington, R. Li, M. Cai, X. Sun, *Energy Environ. Sci.* 7 (2) (2014) 768-778
- [7] J. Liu, M. Banis, X. Li, A. Lushington, M. Cai, R. Li, T.-K. Sham, X. Sun, *J. Phys. Chem. C* 117(2013) 20260-20267

4:20pm **TF+EN+PS-TuA7 ALD for a High Performance “All-in-One” Nanopore Battery, Chanyuan Liu, X. Chen, E. Gillette, A.J. Pearse, A.C. Kozen, M.A. Schroeder, K. Gregorczyk, S.B. Lee, G.W. Rubloff**, University of Maryland, College Park

A self-aligned nanostructured battery fully confined within a single nanopore presents a powerful platform to determine the performance and cyclability limits of nanostructured storage devices. We have created and evaluated such structures, comprised of nanotubular electrodes and electrolyte confined within anodic aluminium oxide (AAO) nanopores as “all-in-one” nanopore batteries. The nanoelectrodes include metal (Ru or Pt) nanotube current collectors with crystalline V₂O₅ storage material on top of them, penetrating part way into the AAO nanopores to form a symmetric full storage cell, with anode and cathode separated by an electrolyte region.

* TFD James Harper Award Finalist

The unprecedented thickness and conformality control of atomic layer deposition (ALD) and the highly self-aligned nanoporous structure of anodic aluminum oxide (AAO) are essential to enable fabrication of precision, self-aligned, regular nanopore batteries, which display exceptional power-energy performance and cyclability when tested as massively parallel devices (~ 2 billion/cm²), each with $\sim 1 \mu\text{m}^3$ volume (~ 1 fL).

To realize these “all-in-one” nanopore batteries, we focused on the precise control of Ru and Pt thin film conformality inside very high aspect ratio (300:1) AAO nanopores by thermal ALD process. 7.5 nm thick Ru and Pt are optimized to be 15 μm deep at both sides of 50 μm long AAO pores in order to provide fast electron transport to overlying V₂O₅ at both anode and cathode sides, while keeping them spatially and electrically isolated. Active storage layers of 23 nm thick crystalline V₂O₅ were deposited inside the metal nanotubes to form core-shell nanotubular structures at low temperature (170 °C) using O₃ as the oxidant, with <001> direction perpendicular to tube surface and RMS roughness ~ 4 nm. Then the V₂O₅ was prelithiated at one end to serve as anode while pristine V₂O₅ without Li at the other end served as cathode, enabling the battery to be cycled between 0.2 V and 1.8 V and to achieve full theoretical Faradaic capacity of the V₂O₅. Capacity retention of this full cell at high power (relative to 1 C rates) is 95% at 5 C and 46% at 150 C rates (i.e., 24 sec charge/discharge time). At 5 C rate (12 min charge-discharge cycle), 81.3% capacity remains after 1000 cycles. These performance metrics are exceptional, exceeding those of most prototypes reported in the literature. These results demonstrate the promise of ultrasmall, self-aligned/regular, densely packed nanobattery structures as a building block for high performance energy storage systems.

4:40pm TF+EN+PS-TuA8 Pseudocapacitive Manganese Oxide Grown by Atomic Layer Deposition, Matthias Young, C.D. Hare, A.S. Cavanagh, C.B. Musgrave, S.M. George, University of Colorado, Boulder

Pseudocapacitive supercapacitors are a class of energy storage materials that are midway between lithium ion batteries and capacitors in terms of both power and energy densities. Manganese oxide is a well-known pseudocapacitive material with particular appeal due to its earth abundance and low cost. In previous work, we have demonstrated that MnO ALD produced using bis(ethylcyclopentadienyl)manganese (Mn(CpEt)₂) and water can be electrochemically oxidized to produce pseudocapacitive MnO₂ in aqueous electrolytes. However, recent results have shown that the electrochemical oxidation of MnO ALD films results in partial dissolution and delamination. To avoid these problems, we have worked to grow pseudocapacitive MnO₂ by ALD that requires no post-processing. We have grown manganese oxide ALD films using ozone as the coreactant with Mn(CpEt)₂. We have also used intermediate ozone doses during Mn(CpEt)₂ and water exposures during ALD growth. The use of ozone results in more oxidized manganese oxide films. Another issue is that the alpha-MnO₂ crystal structure of MnO₂ which exhibits high pseudocapacitance contains open channels that are only stable in the presence of cations such as Na⁺ or K⁺. Consequently, directing the ALD growth toward alpha-MnO₂ pseudocapacitive crystal structures requires the incorporation of an alkali metal into the MnO₂ ALD films.

5:00pm TF+EN+PS-TuA9 Excellent Chemical Passivation of p⁺ and n⁺ Surfaces of Silicon Solar Cells by Atomic Layer Deposition of Al₂O₃ and SiO₂/Al₂O₃ Stacks, Bas van de Loo, H.C.M. Knoops, Eindhoven University of Technology, Netherlands, G. Dingemans, ASM, Netherlands, I.G. Romijn, ECN Solar Energy, Netherlands, W.M.M. Kessels, Eindhoven University of Technology, Netherlands

Thin films of Al₂O₃ provide excellent passivation of heavily p-doped (p⁺) silicon surfaces and are therefore often applied in silicon solar cells to reach high efficiencies. The high level of passivation by Al₂O₃ can be attributed to its low interface defect density and high negative fixed charge density Q_f. However, the negative fixed charge density of Al₂O₃ can be detrimental for the passivation of n⁺ surfaces [1]. Furthermore, in advanced cell architectures such as interdigitated back-contact (IBC) solar cells, both n⁺ and p⁺ surfaces are adjacent and are preferably passivated simultaneously. To this end, we systematically study the surface passivation by SiO₂/Al₂O₃ stacks prepared by atomic layer deposition (ALD), which exhibit excellent chemical passivation while the effective fixed charge density can be tuned to zero by carefully tuning the SiO₂ thickness.

Al₂O₃ and SiO₂/Al₂O₃ film stacks with varying ALD SiO₂ thickness (0-12 nm) were prepared by plasma-enhanced ALD at 200 °C, with H₂Si(N(C₂H₅)₂)₂ and Al(CH₃)₃ as metal-organic precursors and O₂ plasma as oxidant. Moreover, a SiO₂ ALD process using ozone was developed as this oxidant is more suitable for batch ALD. The relevant process parameters for surface passivation, such as ozone exposure time, were identified. The passivation of n⁺ and p⁺ doped surfaces was studied in detail, and results were compared with industrial passivation schemes, including PE-CVD SiN_x and similar SiO₂/Al₂O₃ stacks from a high-volume manufacturing ALD batch reactor.

A superior level of passivation of n⁺ surfaces (R_{sheet} = 100 Ω/sq) was obtained by SiO₂/Al₂O₃ stacks as compared to single layer Al₂O₃, significantly reducing the recombination current density (J₀) from (81±10) to (50±3) fA/cm². On p⁺ surfaces (R_{sheet} = 60 Ω/sq), J₀ increases with increasing SiO₂ thickness. The results can be explained by an excellent level of chemical passivation, combined with a strongly reduced negative fixed charge density when increasing the SiO₂ thickness. To fully exploit the virtues of ALD, the concept of using SiO₂/Al₂O₃ stacks for the passivation of both the n⁺ and p⁺ doped surfaces in a single deposition run was demonstrated on (completed) n-type bifacial solar cells, reaching conversion efficiencies >19%. The results are promising for IBC solar cells, where n⁺ and p⁺ surfaces are adjacent and care must be taken to achieve a low surface recombination, high shunt resistance and industrial feasibility.

[1] B. Hoex *et al.*, *Phys. status solidi - Rapid Res. Lett.*, vol. 6, no. 1, pp. 4-6, (2012).

5:20pm TF+EN+PS-TuA10 Opportunities for Transparent Conductive Oxides Prepared by ALD for Silicon Heterojunction Solar Cells, Bart Macco, S. Smit, Y. Wu, D. Vanhemel, W.M.M. Kessels, Eindhoven University of Technology, Netherlands

In silicon heterojunction (SHJ) solar cells, transparent conductive oxides (TCOs) serve as the top window layer which provides lateral charge transport to the metal contacts whilst maintaining a high optical transparency. Commonly-employed TCO materials include Sn-doped indium oxide (In₂O₃:Sn), Al-doped zinc oxide (ZnO:Al) and more recently also H-doped indium oxide (In₂O₃:H)¹, which are typically deposited by sputtering. In this work, atomic layer deposition (ALD) is explored as an alternative deposition technique for the abovementioned materials. Three salient features of the ALD process will be addressed. Firstly, the applicability of these ALD TCOs is evaluated in terms of their optoelectronic performance. It is shown that through controlled ALD doping cycles the carrier density can be accurately tuned and a low resistivity (<0.5 mΩcm) required for SHJ solar cells can be obtained. Secondly, it is shown that a thermal ALD process does not induce damage to the underlying a-Si:H passivation layers found in a SHJ solar cell. This is a distinct advantage over the conventional sputtering technique, in which plasma-related (UV, ions) damage is known to reduce the passivation level of the a-Si:H layers.² This perk of ALD is put to use in bilayers of ALD ZnO:Al/sputtered In₂O₃:Sn, where a thin ALD TCO layer (<15 nm) can very effectively protect the a-Si:H layers from sputter damage. TEM and *in-situ* spectroscopic ellipsometry measurements show that the protective properties are strongly correlated with the TCO surface coverage, as the initial ALD TCO growth on the a-Si:H layer suffers from a nucleation delay and associated island-like growth.³ Finally, the accurate control over the doping (profile) of the TCO offered by ALD opens up ways to optimize the band alignment of a SHJ solar cell. At the interface of the TCO and the p-type a-Si:H, a high doping of the TCO is unfavorable for the band alignment and results in a reduced fill-factor.³ On the other hand, the conductivity requirement of the TCO sets a lower bound to the doping level. In this respect, graded doping of the TCO by ALD allows for effective decoupling of the conductivity requirements of the TCO with the optimization of the interface contact formation.

¹ Barraud *et al.*, *Solar Energy Materials and Solar Cells*, **115**, 151–156 (2013)

² Demarex *et al.*, *Applied Physics Letters*, **101**, 171604 (2012)

³ Macco *et al.*, *Applied Physics Letters* (submitted)

5:40pm TF+EN+PS-TuA11 Study of the Surface Passivation Mechanism of c-Si by Al₂O₃ using In Situ infrared spectroscopy, R.P. Chaukulkar, Colorado School of Mines, W. Nemeth, A. Dameron, P. Stradins, National Renewable Energy Laboratory, Sumit Agarwal, Colorado School of Mines

The quality of Si surface passivation plays an integral role in the performance of c-Si-based solar cells. Recently, Al₂O₃ films grown by atomic layer deposition (ALD) have been shown to be an effective passivant for c-Si surfaces with surface recombination velocities (S_{eff}) that are <5 cm/s. The chemical passivation of the c-Si surface via Al₂O₃ is achieved by a reduction in the defect density at the interface, while field-effect passivation is attributed to the fixed negative charge associated with the Al₂O₃ films. However, a post-deposition annealing step is required to achieve this high level of passivation. We have investigated the mechanism of chemical passivation during the annealing step using *in situ* attenuated total reflection Fourier transform infrared (ATR-FTIR) spectroscopy. Specifically, we have studied the role of residual H- and O-atom migration from the ALD Al₂O₃ films to the c-Si/Al₂O₃ interface. Using Al(CH₃)₃ and O₃ as the ALD precursors, Al₂O₃ films were deposited directly onto high-lifetime float-zone c-Si internal reflection crystals (IRCs) followed by thermal annealing at 400 °C in different atmospheres. Specifically, we have used D-terminated c-Si IRCs to differentiate the residual H atoms that may

migrate from ALD Al_2O_3 films versus the residual D atoms present at the $\text{Al}_2\text{O}_3/c\text{-Si}$ interface after ALD. Within the sensitivity of the ATR-FTIR spectroscopy setup of $\sim 10^{12} \text{ cm}^{-2}$ for Si-H bonds, we do not detect any migration of H from Al_2O_3 to the $c\text{-Si}$ interface. Therefore, we conclude that the migration of O, and the subsequent restructuring of the interface during the annealing step, primarily contributes towards the chemical passivation of the $\text{Al}_2\text{O}_3/c\text{-Si}$ interface. The ATR-FTIR spectroscopy measurements are complemented by the minority carrier lifetime, interface defect density, and built-in charge density measurements on $\text{SiO}_2/\text{Al}_2\text{O}_3$ stacks on $c\text{-Si}$, which enable us to isolate chemical passivation from field-effect passivation. The stacks were annealed in different atmospheres to better understand the role of O versus H atoms in the chemical passivation mechanism.

We gratefully acknowledge the support from the NCPV Fellowship Program and U.S. Department of Energy, Office of Energy Efficiency and Renewable Energy, under Contract No. DE-AC36-08-GO28308 with the National Renewable Energy Laboratory.

6:00pm TF+EN+PS-TuA12 Low Temperature Plasma-assisted Atomic Layer Deposition of TiO_2 Blocking Layers for Flexible Hybrid Mesoscopic Solar Cells, *V. Zardetto*, Eindhoven University of Technology, Netherlands, *F. di Giacomo, T.M. Brown, A. di Carlo, A. D'Epifanio, S. Licocchia*, University of Rome "Tor Vergata", Italy, *W.M.M. Kessels, Mariadriana Creatore*, Eindhoven University of Technology, Netherlands

Atomic Layer Deposition (ALD) is widely acknowledged in the field of $c\text{-Si}$ and thin film PV technologies, for the fabrication of ultra-thin, uniform and conformal layers.[1] Thermal ALD has been applied also in the case of more challenging interfaces, e.g. dye-sensitized solar cells (DSCs) and the novel hybrid organo-lead-halide perovskite solar cells. Particularly, TiO_2 blocking layers have been developed on glass/TCO substrates with the aim of decreasing the charge recombination processes at the interface between the ITO and the mediator. Recently, we have explored the benefit of plasma-assisted ALD (PA-ALD) in terms of low temperature processing applied to flexible DSCs for the development of highly transparent Pt counterelectrodes on ITO/PEN. [2] In this work, we further explore PA-ALD for the deposition of ultra-thin, highly compact TiO_2 blocking layers on ITO-polymer substrates for DSCs and perovskite solar cells. The layers were prepared in a remote plasma reactor (FlexALTM) at 150 °C using an heteroleptic alkylamido precursor $\text{Ti}(\text{Cp}^{\text{Me}})(\text{NMe}_2)_3$ alternated with an O_2 plasma. For DSCs with an iodide-based electrolyte, the introduction of the blocking layer is essential at low light intensity, in order to increase the indoor performance of the cell. It is found that the presence of ultra-thin (6 nm) TiO_2 layers slightly affects the performance of the cell under sun simulator, whereas it definitely improves the generated power (+40%) under low level illumination (300 lux). The blocking behaviour of the PA-ALD deposited TiO_2 towards the tri-iodide reduction has been investigated by electrochemical impedance spectroscopy and Tafel plot analysis. We pinpointed that an increase in the TiO_2 layer thickness above 6 nm leads to a decrease of the recombination processes at the TCO/electrolyte interface, as well as to a dramatic reduction of the electron collection at the TCO, accompanied by a decrease in cell performance. For mesostructured perovskite ($\text{CH}_3\text{NH}_3\text{PbI}_2\text{Cl}$ -based) solar cells, the application of a TiO_2 blocking layer is essential for the performance of the device, due the higher current exchange at the interface TCO-hole transport material, i.e. Spiro-OMeTAD, typically used in this architecture. The application of a 11 nm-thick TiO_2 layer resulted in an efficiency of 7.4%. In conclusion, ALD is a valid approach for controlling electrochemical charge-transfer processes in mesoscopic solar cells.

[1] J.A. van Delft, D. Garcia-Alonso, W. M. M. Kessels, *Semicond. Sci. Technol.*, 27, 74002 (2012)

[2] D. Garcia-Alonso, V. Zardetto, A.J.M. Mackus, F. De Rossi, M.A. Verheijen, T.M. Brown, W.M.M. Kessels, M. Creatore, *Adv. En. Mater.* 4, 1300831 (2014)

Vacuum Technology

Room: 303 - Session VT-TuA

Vacuum Quality Analysis, Outgassing, and Control

Moderator: James Fedchak, National Institute of Standards and Technology (NIST), Marcy Stutzman, Thomas Jefferson National Accelerator Facility

2:20pm VT-TuA1 Our Present Understanding of Outgassing, *Manfred Leisch*, Graz University of Tech., Austria **INVITED**

Outgassing means basically the diffusion of atoms usually hydrogen through the bulk material, entering the surface and desorbing from it. The important consequence is it limits the lowest achievable pressure in a

vacuum chamber and is a central issue in vacuum science with respect to ultra high (UHV) and extreme high vacuum (XHV). Stainless steel (SS) is one of the most commonly used constructional materials for vacuum chambers and components. A considerable body of work is documented on the hydrogen outgassing behaviour of SS. For the description of the outgassing rate basically two models common as diffusion limited model (DLM) and recombination limited model (RLM) have been discussed so far. Experimental studies in the last decade show that the real situation on the complex SS surface cannot be fully described by DLM or RLM. Hydrogen atoms approaching the surface from the bulk are desorbing in a second-order process. The rate of recombination depends strongly on the atomic structure of the surface and is e.g. generally higher on stepped surfaces than on flat close packed planes. A new insight was gained by atomic level studies on the real morphology of SS with atomic force microscopy (AFM) and the scanning tunnelling microscopy (STM).

Beside surface morphology surface composition additionally controls the desorption kinetics. Auger electron spectroscopy (AES) gives reason for a composition change. Since the information depth of AES covers several atomic layers complementary atom probe analysis were performed, measuring the chemical composition on the surface atomic layer by layer. Energy calculations using the ASED method (Atom superposition and Electron Delocalization) result in lower energy levels in Fe vacancies. It supports the picture that surface and subsurface defects form traps with different energetic levels. They may control the recombinative desorption process and give explanation for the observed outgassing behaviour of stainless steel. From this results a more complete description of the outgassing process may be given by a more or less dynamic equilibrium between diffusion, sojourn in different level traps and recombinative desorption.

This work was supported by the Austrian „Fonds zur Förderung der wissenschaftlichen Forschung“ P 12099 and “Zukunftsfonds Steiermark“ P 119.

3:00pm VT-TuA3 Hydrogen Traps in the Outgassing Model of a Stainless Steel Vacuum Chamber, *Robert Berg*, National Institute of Standards and Technology (NIST)

The outgassing model accounts for the geometry of the chamber components, the hydrogen dissolved in those components, and the processes of diffusion, recombination, and trapping. Strongly bound or “trapped” hydrogen, which occurs at heterogeneities such as dislocations and grain boundaries, can hold most of the dissolved hydrogen even though those locations comprise fewer than 0.1% of all lattice sites. Four simplifications allowed practical use of the model: (1) Each component was described as a one-dimensional object. (2) The hydrogen initially dissolved in each component was described as a uniform concentration. (3) Accurate, consistent values were used to describe diffusion and recombination in stainless steel types 304 and 316 [Grant et al., *J. Nucl. Mater.* 149, 180 (1987); 152, 139 (1988)]. (4) Only one type of hydrogen trap was considered, and trapping was ignored in components made from vacuum remelted stainless steel. The simple model was developed and validated by comparing it to outgassing measurements. Traps were required to describe the outgassing from a component made of drawn stainless steel 304. The initial hydrogen concentration in that component was comparable to concentrations found elsewhere by thermal desorption and almost 100 times larger than in the components made of vacuum remelted 316 stainless steel. The model’s usefulness is illustrated by using it to predict the outgassing of a vacuum chamber made of type 304 stainless steel.

3:20pm VT-TuA4 A Mild Steel Ultrahigh Vacuum Chamber Appropriate for Magnetic Shielding, *B. Cho, S.J. Ahn*, Korea Research Institute of Standards and Science (KRISS), Republic of Korea, *C.D. Park, Taekyun Ha*, POSTECH, Republic of Korea

Mild steel, i.e. low carbon steel, is a soft magnetic material and widely used for shielding sensitive experimental apparatuses from stray magnetic field because of its relatively low price and high magnetic permeability. Mild steel vacuum chambers are usually nickel-plated in order to prevent corrosion and improve the vacuum. For example, electron microscopes employ nickel plated mild steel for constructing their specimen vacuum chambers in which the electron beam propagates and interacts with specimens; presence of stray magnetic field deteriorates proper propagation of the electron beam, degrading the resolution of the electron microscope.

The mild steel has not been employed, to the best of authors’ knowledge, for ultra-high vacuum (UHV) use because its outgassing rate has been known to be too high; reported values were on the order of $10^{-8}\sim 10^{-9} \text{ mbar l s}^{-1} \text{ cm}^{-2}$ or higher [1]. Ishimori *et al.* [2] reported that the outgassing rates of a mild steel (carbon $\sim 0.15\%$), a chromium-plated mild steel and a stainless steel were $2\sim 3\times 10^{-11} \text{ mbar l s}^{-1} \text{ cm}^{-2}$, $7\sim 9\times 10^{-11} \text{ mbar l s}^{-1} \text{ cm}^{-2}$ and $2\sim 3\times 10^{-12} \text{ mbar l s}^{-1} \text{ cm}^{-2}$, respectively, after baking at 300 °C for 3 hours. The

outgassing rate of UHV chambers are normally on the order of 10^{-12} mbar / $s^{-1} \text{ cm}^2$ or less after baking at $100 \sim 200$ °C.

The outgassing rates of a mild steel and a stainless steel 304 chamber were measured by using the so-called rate-of-rise (RoR) method [3]. We present that the outgassing rate of the mild steel purchasable on the market is much smaller than that of a stainless steel type 304L which is most widely used as a UHV vacuum chamber material. The ultimate pressure of a vacuum chamber made of the mild steel was 2.7×10^{-11} mbar, and its outgassing rate was of $< 3 \times 10^{-14}$ mbar / $s^{-1} \text{ cm}^2$, which indicates the mild steel is even appropriate for extreme high vacuum use. Vacuum annealing of the mild steel at 850 °C reduced the outgassing rate further.

[1] B. B. Dayton : 6th Nat. Symp. Vac. Tech. 101 (1959).

[2] Yoshio Ishimori, Nagamitsu Yoshimura, Shuzo Hasegawa, and Hisashi Oikawa, SHINKU 14(8), 295(1971).

[3] C. D. Park, S. M. Chung, Xianghong Liu and Yulin Li, J. Vac. Sci. Technol. A 26(5), 1166(2008).

4:20pm VT-TuA7 Ultimate Limits in the Gas Composition Determination Within Small Sealed Volumes by Quadrupole Mass Spectrometry, Vincenc Nemanič, Jozef Stefan Institute, Slovenia INVITED

Miniaturization of modern sealed vacuum devices and higher demands for their stable operation on the long-term scale require accurate determination of the gas composition in the early stage of their operation, as well as after a long operating period. Since particular gases may have detrimental effect on the device performance even at low concentrations, accurate quantification of the gas mixture is an important as well as a challenging task. Among a few highly gas-sensitive methods capable to detect quantities below 10^{-4} mbar L, the quadrupole mass spectrometry seems to be the most appropriate one for this task.

A two-step procedure, consisting of sample puncture inside an expanding chamber, followed by opening the leak valve to the quadrupole mass spectrometer, kept in the analytical chamber at $\sim 3 \times 10^{-11}$ mbar, is proposed. A limited number of ion current readings are used for the reconstruction of the original total pressure and gas composition. Calibration of such instruments at particular partial pressure is regularly achieved at stable gas influx and constant pumping speed. Several discrete points have to be recorded to get the sensitivity of the instrument expressed in A/mbar.

In this presentation, a systematic approach for preparing the instrument for routine quantification of small gas amounts is described. In the first stage, the instrument was calibrated as the precise partial gas flow meter by an innovative *in-situ* calibration procedure by three different gases, hydrogen, argon and nitrogen. Each gas was admitted into the expanding chamber, having a precisely determined volume of 0.312 L and equipped by a capacitance manometer. By opening the leak valve, ion currents versus gas flux were recorded over three orders of magnitude, expressing the partial flux sensitivity in As/(mbar L). In the second stage, known gas quantities $\sim 10^{-4}$ mbar L of pure gas were admitted at different leak valve conductance to determine the instrument's response. This data enabled minimizing the error by searching for a compromise between the number of the readings and the level of recorded ion currents. In the third stage, gas mixtures with various contents of three gases were prepared and analyzed. This evaluation enabled a much better prediction of the ultimate limits in reconstructing of the unknown gas mixture in a real device. Anyhow, uncertainty in evaluation increases by lowering the gas amounts as ion currents become indistinguishable from the background readings of the instrument.

5:00pm VT-TuA9 The Importance of Competitive Langmuir Adsorption Kinetics for Vacuum Cleanliness, Richard Versluis, TNO Technical Sciences, Netherlands

There are numerous examples of systems that rely on a very clean vacuum. Gaseous contamination and surface contamination may influence the process or even damage the machine (such as beam scattering accelerators and e-beam equipment or background contamination in gas analyzers) or may contaminate samples (XPS, SEM, HIM etc) or may contaminate sub-components of the machine (such as mirror contamination in EUV systems, space systems, spectral analyzers etc). The usual methods of contamination inspection are measurement of the residual gas compositions (RGA's) or the use of witness plates to determine surface contamination. The requirements on residual contamination (either gaseous or adsorbed on surfaces) are becoming more stringent with the development of equipment that is becoming more sensitive for contamination. A good understanding of the kinetics of contamination transport and gas-surface interaction is crucial when developing or using these requirements. This is important for both equipment users and equipment developers.

This talk will highlight some important aspects of gas-surface interaction in vacuum chambers by focusing on the dynamical behavior of gas species competing for adsorption sites. We will show how the adsorption energies

and concentrations influence the equilibrium that is reached, but we will also show how the adsorption energies and the concentrations determine the kinetic behavior before equilibrium is reached and how they influence surface coverage by different species during non-equilibrium. A simple model solving the coupled kinetic equations is able to predict the time dependent behavior, which can be used to determine for instance outgassing times and sampling times and the relationship between measured gas concentrations and surface coverage during non-equilibrium.

5:20pm VT-TuA10 Diagnostic Tool to Identify Volatile Molecules in Vacuum, Freek Molkenboer, A. Van de Runstraat, J.A. Van der Meer, T. Van Groningen, O. Kievit, TNO Technical Sciences, Netherlands

Residual gas analyzers (RGAs) are commonly used in ultra-high vacuum applications to measure vacuum quality. The RGA fragments and ionizes the molecules that are present in the gas phase in the vacuum system. These fragments of all the molecules make up the RGA spectrum. The RGA spectrum has to be interpreted to identify the contaminants that are present in the vacuum system. This is complicated and often impossible in case of complex mixtures of organics in the vacuum atmosphere.

The goal of this project is to develop a simple-to-use diagnostic tool that is able to identify the contaminant molecules in vacuum directly. After a trade-off of various options, we selected a removable cold trap in combination with an off-line gas chromatography-mass spectrometry (GC-MS) system for analysis of the samples.

The cold trap is installed on a vacuum flange. A removable sample tube is positioned inside the cold trap in connection with the vacuum system. The cooling of the cold trap is achieved with Peltier elements, which makes it simple to operate as well as independent of supply of coolants such as liquid nitrogen. After sampling, the sample tube can be removed without venting the vacuum system and a new sample tube can be installed to continue measurements if required.

After sampling of the vacuum vessel, the sample tube is connected to a GC-MS system for analysis of the sample and identifying and partly quantify the organic molecules present.

The first results are promising and we continue to improve the system. In this presentation we will present our sampling method and the results of vacuum quality measurements using the new diagnostic tool.

5:40pm VT-TuA11 Quantitative Gas Analysis of Small Batch Samples by Quadrupole Mass Spectrometer, Lily Wang, Los Alamos National Laboratory

In our studies of static gas release properties of various solid materials at low temperatures ranging from 25 to 80 °C, we find the amounts of gas collected from the experimental samples in sealed vacuum vessels over extended times (weeks to months) are only a few to less than 100 torrs in a free volume of 10 - 50 cc. In order to analyze these small batch gas samples, a quantitative method was developed using a quadrupole mass spectrometer. This method involves introducing a small pulse of the gas with a custom-designed sample manifold into a quadrupole mass spectrometer and analyzing the gas component quantity in a few seconds. The method is relatively quick and is particularly suitable for gas components that have low sticking coefficients to stainless steel surfaces. This method was evaluated for hydrogen, methane, and argon. In this presentation, the setup, the calibration and measurement procedures, and the performance of the method are presented and discussed.

6:00pm VT-TuA12 A Novel Vacuum Mini-Environment Design For Thin Film Sputter Deposition Apparatus, Jun Xie, R.L. Ruck, C. Liu, P. Leahey, T. Bluck, Intevac, Inc.

In microelectronics manufacturing, many critical process steps are carried out in high vacuum apparatus. Trace quantities of residual gaseous species, such as hydrogen and water (H₂O), are always present within such system, which are of great concern to state-of-the-art device fabrication. In the hard-disk drive industry, for example, metallic thin films of a magnetic recording disk are especially susceptible to H₂O, which could affect film growth adversely and compromise the device performance. It becomes a top priority to prevent the trace contaminants in the vacuum system, especially H₂O, from interacting with these metallic thin films during a sputter deposition process. The goal of this study is to create a pristinely clean mini-environment inside a general vacuum apparatus for ultrapure thin film sputter deposition. The approach consists of two innovative features. The first is a retractable enclosure that seals off a volume around the sputter target and the substrate. The second is a series of pumping channels of pre-determined sizes and shapes through the wall of the enclosure that facilitate the evacuation of the gases or byproducts from the enclosure in a controlled manner while minimizing the probability of outside contaminants entering the enclosure. Experiments were conducted by sputter-depositing chromium thin films in such an enclosure to getter contaminants and assess its

effectiveness with secondary ion mass spectrometry (SIMS) and X-ray photoelectron spectroscopy (XPS) analysis.

Tuesday Evening Poster Sessions

Electronic Materials and Processing

Room: Hall D - Session EM-TuP

Electronic Materials and Processing Poster Session

EM-TuP1 Growth of AlN Nanowires on Sapphire and Silicon using the Pulsed Electron Beam Deposition (PED) Process. *N. Arefin, P. Larson, University of Oklahoma, Matthew Kane, Texas A&M University, M.B. Johnson, P.J. McCann, University of Oklahoma*

This poster will describe results recently obtained with pulsed electron beam deposition (PED) of AlN on sapphire and silicon substrates. The PED technique is potentially useful for growth of III-nitrides at lower substrate temperatures, a capability that can allow use of new buffer layer materials, integration of chemically dissimilar materials, and help solve wafer bowing issues. In addition, PED has the advantage to deposit materials that are transparent to the Kr-F excimer lasers used in pulsed laser deposition and would thus be suitable for ultra-wide bandgap materials. Systematic studies are needed to explore the growth regimes for various materials as a function of processing conditions and sample preparation techniques. AlN was deposited on sapphire and silicon (111) at a substrate temperature of 500°C and 550°C, respectively, in a UHP N₂ (15 mTorr) environment (without any surface pre-treatment, i.e., pre-nitridation). A high power electron gun pulse was used to ablate the AlN target (1" dia. x 0.250" thick, 99.8% pure) stationed at 5 cm vertical distance from the substrate. The electron pulses were generated at 15KV, 0.3 J/pulse at 1 Hz for one hour. No post growth processing was performed following the growth. Scanning electron microscopy (SEM), Electron back scattered diffraction (EBSD), and X-ray diffraction (XRD), and various optical characterization techniques were performed on the as-grown material. SEM imaging confirms hexagonal faceted high aspect ratio AlN nanowires on both sapphire and silicon substrates. The nanowire lengths ranged from 10-100 μm with average diameter of 2.5 μm on the sapphire substrate, while on the silicon (111) substrate the nanowire dimensions ranged from 200 nm-10 μm in length, and the average diameter was 0.5 μm. EBSD scan over the nanowires identified the structures as c-plane oriented AlN. XRD θ-2θ scans from 2θ = 30° to 2θ = 50° showed only one peak other than those from the sapphire substrate, at 2θ = 37.56°. We had insignificant contribution from the AlN NWs in the XRD scan due to limited quantity of the NWs on the sample. The obtained peak at 2θ = 37.56° represents Al (111) suggests that during the initial growth phases Al was accumulated as metal on the substrate which acted as a precursor in initiating the nanowire growth afterwards. This finding was also verified with EBSD scans, as it also detected presence of Al crystallites on the sample surface as well as highly c-axis oriented AlN nanowires.

EM-TuP2 Passivation of InSb(100) with 1-Eicosanethiol Self-Assembled Monolayers. *Y.D. Contreras, Pablo Mancheno, A.J. Muscat, University of Arizona*

III-V semiconductors have the potential to replace Si to make faster computer processors due to their higher charge mobility. In particular, the bandgap of InSb (0.17 eV, the smallest of the III-V group) makes this semiconductor an absorber and emitter in the infrared region, suitable for infrared detectors. III-V semiconductors oxidize rapidly when exposed to air after etching, and have complex oxide layers. It has been shown that sulfur-containing molecules can passivate and enhance the electrical properties of III-V semiconductors. In this study, InSb(100) was chemically passivated for 3 min after native oxide etching by liquid-phase deposition of an alkanethiol self-assembled monolayer (SAM) on the surface of the semiconductor. The SAM contained 1-eicosanethiol (ET, 20 C atoms). The passivated surface was characterized with atomic force microscopy (AFM), spectroscopic ellipsometry, X-ray photoelectron spectroscopy (XPS) and FTIR. Tapping Mode AFM images of InSb native oxide showed that the starting surface was rough (RMS 2.25 nm), which could limit the formation of a dense and ordered alkanethiol SAM. The thickness of the overlayer (both InSb oxides and ET) measured by spectroscopic ellipsometry was 35 Å immediately after passivation. XPS analysis showed that the passivation process with a 1.0 M HCl last step and 20 h passivation yielded no detectable oxygen in the Auger region for 3 min of air exposure, but the surface was completely oxidized after 4 h of exposure. As a comparison, passivation of GaAs(100) (bandgap of 1.4 eV) with an ET SAM maintained oxygen below detection limits after 30 min, but the surface still oxidized after 4 h. When the passivation of InSb(100) was performed with different preparation conditions (HCl and thiol concentrations, solvent type, and deposition time), the largest bulk InSb to Sb₂O₃ 3d + O 1s XPS peak area ratio (minimum Sb oxidation) was achieved by using 1.0 M HCl in the oxide etching steps, 0.1 mM ET in ethanol and long thiol deposition times

(~20 h). FTIR analysis of an InSb sample passivated for 20 h in 0.1 mM ET showed the presence of peaks characteristic of methyl and methylene stretches at 2963 cm⁻¹, 2925 cm⁻¹ and 2847 cm⁻¹. The position and width of these peaks indicates the presence of a partially ordered alkanethiol layer. These results demonstrate that physically blocking O₂ diffusion with alkyl chains is possible on the surface of a narrow band-gap semiconductor, even on a surface with a relatively high average roughness.

EM-TuP3 Electric Measurements of RF SOI MOSFET using CMOS Technology. *William Mariano, UNICAMP, Brazil*

The aims of this work is the development of a 2 μm SOI CMOS process. The manufacturing of the devices was carried out using processes based on SOI CMOS technology. The characteristics of the fabricated devices in a SOI Silicon are compared in order to obtain its parameters, as well as with the results published in the literature. Besides is to present the electric measurements of n and p channel RF MOSFET fabricated on Silicon substrates of type SOI – Silicon On Insulator. The different structures of the devices had been fabricated and their physical and electrical characterizations performed. In addition, there will be a sequence of the process steps involved in building the CMOS chips. The devices are part of an academic chip, which will be used in disciplines of engineering courses and in research activities of the Microelectronics area.

EM-TuP5 Fabrication of Inverse Opal Structures by Langmuir-Blodgett Silica Microsphere Assembly and Germanium Back Filling by Molecular Beam Epitaxy. *M. Zhou, Sarun Atiganyanun, S. Ghosh, J. Chavez, S.E. Han, S.M. Han, University of New Mexico*

Photonic crystals give rise to a variety of applications such as absorbers, waveguides, and light filters. One of the common examples is an inverse opal structure made of semiconductors. This structure, unlike its counterpart opal structure, exhibits a complete photonic band gap. In this study, we investigate a low-cost and scalable fabrication of an inverse opal structure via self-assembly of colloidal silica microspheres and Ge molecular beam epitaxial (MBE) back filling, followed by buffered HF etching. First, silica microspheres are functionalized with allyltrimethoxysilane and dispersed in chloroform. Langmuir-Blodgett (LB) method is then used to self-assemble silica microspheres with a diameter of ~800 nm onto Si(100) substrates. By optimizing the pulling speed of the substrate and surface pressure within the trough, a hexagonally closed-packed opal structure is achieved. Scanning electron microscopy (SEM) images have shown domain size of the monolayer assembly to be approximately 10 μm by 10 μm. By repeating LB coating for *n* times, an *n*-multilayer assembly is formed, creating an opal template structure. After assembling silica microspheres on Si substrates, Ge MBE is used to back fill the voids between microspheres. The effusion cell temperature ranges from 1150 to 1000°C, which corresponds to the Ge flux of 6.44*10¹⁴ to 1.83*10¹³ Ge atoms/cm²-sec, respectively. When the substrate temperature is held constant at 580°C, the SEM characterization shows that the low Ge flux at 1000°C reduces random nucleation on top of the microspheres by approximately one order of magnitude compared to the high Ge flux at 1150°C. Following the backfill, the silica microspheres are removed by immersing the substrate in a buffered HF solution, creating a single-crystalline Ge inverse opal structure. In this presentation, we will further discuss the optimization of Ge flux and substrate temperature, examination of crystal quality of Ge by X-ray diffraction and Ge/Si interface by transmission electron microscopy, and the structure's optical properties with Fourier transform infrared spectroscopy.

EM-TuP7 Formation of AlN Thin Films by Direct Nitridation of Aluminum Thin Films and Their Visible Photoluminescence Property. *Shun Kajihara, M. Hamasaki, H. Katsumata, Meiji University, Japan*

AlN has the widest band-gap of 6.3 eV among the direct band-gap semiconductors and is therefore suitable for shorter wavelength light emitting devices and power devices. AlN thin films have been prepared by MOCVD and reactive sputtering with the deposition rate of about 0.1-10 nm/min. Meanwhile, AlN powders and AlN bulks have been prepared by reducing nitridation and direct nitridation methods. In this study, AlN thin films were formed by direct nitridation (DN) of Al thin films and their properties were compared with those formed by reactive sputtering (RS). For photoluminescence (PL) measurements, doping of Eu into AlN was performed to observe visible PL from Eu ions in AlN films.

Al thin films with a thickness of 150 nm were deposited on c-axis sapphire substrates by radio frequency (RF) magnetron sputtering using an Al target (φ4 inch, Koujundokagaku, Japan) in constant Ar (8.0 sccm) flow. Co-sputtering of Eu₂O₃ and Al was performed by placing 2 pieces of Eu₂O₃ tablets on the Al target for PL measurements. The films were subsequently annealed at 900°C for 15 sec in N₂ or NH₃ gas using a conventional electric quartz tube furnace, which can form AlN films with a theoretical thickness

of 300 nm. On the other hand, AlN thin films with a thickness of 500-700 nm were deposited on c-axis sapphire substrates by RS using an Al target in constant N₂ (5.6 sccm) and Ar (2.4 sccm) flow. Co-doping of Eu₂O₃ and Si during the formation of AlN films by RS was performed by placing several pieces of Eu₂O₃ and Si tablets on the Al target. Doping of Si was to observe the blue luminescence from Eu²⁺ in AlN by replacing Al atoms by Si atoms in AlN, which can prevent the formation of Eu³⁺. RF sputtering power was set at 200 W through this study. The films were subsequently annealed at 900°C for 30 min in N₂ with rapid thermal annealing system. Growth time of AlN films with a thickness of 300 nm by RS was approximately 30 times longer than that by DN. These samples were analyzed by X-ray diffraction (XRD), PL, optical transmittance and energy dispersive X-ray spectrometry. The wurtzite AlN (002) XRD peak appeared from the samples formed by DN. PL spectra of Eu₂O₃ doped AlN films formed by DN exhibited broad emissions at 400 nm and 530 nm, which were assigned to oxygen defect and Eu²⁺, respectively. The optical direct band-gap of AlN films doped with Eu₂O₃ was calculated to be 5.85 eV from their optical transmission spectra. These results were also obtained from the samples formed by RS. It is interesting to note that the PL spectral features of Eu₂O₃ doped AlN films formed by DN resembles those of Eu₂O₃ and Si co-doped AlN films formed by RS.

EM-TuP8 Improvement of Effective Work Function and Transmittance of ITO/Ultra-Thin In_{1-x}Ru_xO_y Stack Structure, Ippei Yamamoto, Shibaura Institute of Technology, Japan, *T. Kattareeya,* Chulalongkorn University, Thailand, *T. Chikyo, K. Tsukagoshi,* NIMS, Japan, *T. Ohishi,* Shibaura Institute of Technology, Japan, *T. Nabatame,* NIMS, Japan

The indium tin oxide (ITO), which is one of most attractive anode materials in organic electroluminescent, has a big issue of low work function (WF) of 4.7 eV. Several approaches have been proposed to improve the WF of ITO and/or develop new anode materials. We pay attention to RuO₂ material because of high WF (> 5 eV) and low resistivity. In this paper, we systematically investigate the characteristics of the In_{1-x}Ru_xO_y films. We also compare characteristics of ITO/ultra-thin RuO₂ (3 nm) and ITO/ultra-thin In_{1-x}Ru_xO_y (3 nm) stack structures.

The In_{1-x}Ru_xO_y films were prepared under Ar/O₂ (25 vol. %) by co-sputtering using Ru and In₂O₃ targets. The Ru composition ratio of the In_{1-x}Ru_xO_y films was varied from 0 to 1.0 by changing each sputtering power. A 150-nm-thick ITO film was deposited on RuO₂ (3 nm) or In_{1-x}Ru_xO_y (3 nm) film to fabricate ITO/RuO₂ or ITO/In_{1-x}Ru_xO_y stack structure by RF sputtering using an In_{0.9}Sn_{0.1}Ox target, respectively. The SiO₂ metal-oxide-semiconductor (MOS) capacitors with ITO/RuO₂ or ITO/In_{1-x}Ru_xO_y gate electrode were fabricated to obtain effective work function (EWF).

The In_{1-x}Ru_xO_y film consists of amorphous structure in x range from 0.3 to 0.83. The In_{0.38}Ru_{0.62}O_y film shows a lowest specific resistivity and smooth surface of small RMS (0.69 nm) value using atomic force microscopy. The maximum transmittance increased more than 80 % by reducing thickness less than 3 nm.

The ITO/RuO₂ (3 nm) stack structure shows a high EWF value (5.3 eV) and a slightly low transmittance (77 % in 600 nm) because the RuO₂ film has tetragonal crystal structure. On the other hand, the transmittance (80 % in 600 nm) of ITO/In_{0.38}Ru_{0.62}O_y (3 nm) is superior to that of ITO/RuO₂ stack structure. Furthermore, the ITO/In_{0.38}Ru_{0.62}O_y stack structure shows a high EWF (5.3 eV) and a low specific resistivity (9.2 × 10⁻⁵ Ω·cm). This suggests that the interface between ITO and In_{0.38}Ru_{0.62}O_y is kept to be clear because of same dominant element of indium and amorphous structure of In_{0.38}Ru_{0.62}O_y film.

EM-TuP9 Solid Phase Growth of Mg₂Si Thin Films on Poly-Si/Glass Substrates Prepared by Aluminum Induced Crystallization, Satoru Kawaguchi, A. Kusunoki, S. Yoshida, H. Katsumata, Meiji University, Japan

Aluminum induced crystallization (AIC) is a method of crystallizing amorphous Si (a-Si) by the interaction of Al and Si during the heat treatment. Polycrystalline Si (poly-Si) can be formed at lower temperature by AIC compared to solid phase growth techniques, since AIC can crystallize amorphous Si below the eutectic temperature of Al and Si at 577 °C. Poly-Si formed by AIC usually exhibits p-type conductivity with a high carrier concentration due to existence of residual Al. On the other hand, it has been difficult to form n-type poly-Si by metal induced crystallization using n-type doping materials as Sb. The purpose of this study is to fabricate a pn junction for light-receiving device consisting of AIC p-type poly-Si and n-type Mg₂Si. Mg₂Si (Eg: 0.6-0.7 eV) was selected as a candidate of n-type layers because Al atoms are considered to act as an n-type dopant in Mg₂Si.

The substrates used in this study were glass or p-Si (100) substrates. Al films with a thickness of 500 nm were deposited on the glass substrate by resistive evaporation. After deposition, they were exposed in the air for

more than 2 hours to form native Al oxide films. Subsequently, a-Si films with a thickness of 500 nm were deposited on the Al films by radio frequency (RF) magnetron sputtering. These samples were annealed at 450-500 °C for 3-12 hours in N₂ for AIC. After the AIC, Al top layer was removed with diluted HCl. Then, Mg films with a thickness of 100-300 nm were deposited either on AIC poly-Si films or p-type Si (100) substrates by resistive evaporation. These samples were annealed at 400 °C for 5 hours in Ar for solid phase growth of Mg₂Si.

Optical microscope images of surface of AIC poly-Si showed that the grain size of poly-Si increased with increasing AIC temperature. All sample showed Si (111) XRD peaks at 2θ = 28 degrees and Si Raman peaks at 520 cm⁻¹, which can be an evidence of formation of (111) preferentially oriented poly-Si by AIC. We investigated the correlation between grain size of poly-Si observed with optical microscope and FWHM of Raman peak at 520 cm⁻¹. As a result, it was found that the AIC at higher temperature decreased grain size and increased FWHM, while the AIC for longer time increased grain size and decreased FWHM. Optical band-gap of AIC poly-Si formed at 500 °C for 12 hours was determined to be 1.1 eV from optical transmittance spectra. Hall effect measurements of AIC poly-Si showed p-type conductivity with a hole concentration of 4.0×10¹⁷ cm⁻³ and a hole mobility value of 1.56 cm² · V⁻¹ · s⁻¹. Mg₂Si films formed both on AIC poly-Si/glass and p-Si (100) substrates showed Raman peaks at around 256 cm⁻¹, which originate from Mg₂Si.

EM-TuP11 The Effect of Vacuum-Ultraviolet Irradiation on Copper Diffusion into Low-k Dielectrics, Xiangyu Guo, University of Wisconsin-Madison, *Y. Nishi,* Stanford University, *J.L. Shohet,* University of Wisconsin-Madison

Cu diffusion into low-k dielectrics can cause serious reliability issues in on-chip interconnect systems. A considerable attention in the research community had been devoted to understanding the effect of Cu diffusion in the electrical breakdown properties of low-k dielectrics, while Cu-induced diffusion from vacuum-ultraviolet (VUV) irradiated low-k dielectrics has received only minimal attention. This work is aimed at determining the nature of copper interactions with VUV irradiated low-k dielectrics in integrated circuits. The effects of VUV irradiation on the Cu diffusion into low-k organosilicate glass (SiCOH) dielectric films were investigated. X-ray photoelectron spectroscopy depth profiling was used to assess Cu diffusion in the dielectric in the presence of a bias-temperature stress. After 12-eV photon irradiation under bias-temperature stressing at 3.5 MV/cm and 225°C respectively, Cu penetrates farther into the SiCOH, compared to that of an unirradiated sample. Further examination of the VUV photon-exposed SiCOH shows that the Cu distribution profile in the dielectric after bias-temperature stressing is different from the profile after the same temperature annealing but without electrical bias. In addition, no such enhanced phenomenon was observed in unexposed dielectrics, suggesting that Cu ion drift can occur in VUV-irradiated SiCOH. The implication of these findings on time-dependent dielectric breakdown in Cu/VUV irradiated low-k dielectrics is discussed.

This work has been supported by the Semiconductor Research Corporation under Contract No. 2008-KJ-1871 and the National Science Foundation under Grant No. CBET-1066231.

EM-TuP12 Electronic and Vibrational Structures in Photoemission Spectra for Dibenzopentacene on Au(111), Masaru Aoki, A. Suzuki, H. Sato, The University of Tokyo, Japan, *K. Shudo,* Yokohama National University, Japan, *S. Masuda,* The University of Tokyo, Japan

Electronic properties of dibenzopentacene (DBP) thin films on Au(111) were examined by ultraviolet photoemission spectroscopy (UPS), metastable atom electron spectroscopy (MAES),^{1,2} and first-principles DFT calculation. The UPS and MAES spectra for DBP multilayer show four bands near the Fermi level (E_F) due to π-derived 8b_g(HOMO), 7b_g+7a_u, 6a_u, and 6b_g states, in agreement with an earlier study.³ The corresponding bands emerge in the monolayer region, but the bandwidth of the HOMO band is much narrower than that in the multilayer. Furthermore, the HOMO band consists of three peaks with interval of ~160 meV, which is attributed to the vibrational structure of the CC stretching modes of DBP⁺ ion produced by photoionization. A similar vibronic coupling has been reported for organic molecules on inert surfaces such as phthalocyanine on graphite⁴ and pentacene on graphite,⁵ but to our knowledge there is no report in the organic-metal system. In the conference, we will introduce the weak interactions between DBP and Au(111) based on our DFT calculation, temperature-dependent (50-273 K) vibronic structure, and lifetime of photohole in organic-metal system.

References

- [1] Y. Harada, S. Masuda, H. Ozaki, *Chem. Rev.* **97**, 1897 (1997).
- [2] S. Masuda, *Appl. Surf. Sci.* **256**, 4054 (2010).

[3] B. Mahns, F. Roth, A. König, M. Grobosch, M. Knupfer, T. Hahn, *Phys. Rev. B* **86**, 035209 (2012).

[4] S. Kera, H. Yamane, I. Sakuragi, K. K. Okudaira, N. Ueno, *Chem. Phys. Lett.* **364**, 93 (2002).

[5] H. Yamane, S. Nagamatsu, H. Fukagawa, S. Kera, R. Friedlein, K. K. Okudaira, N. Ueno, *Phys. Rev. B* **72**, 153412 (2005).

EM-TuP13 Evolution of Gap States in Potassium-Doped Dibenzopentacene, *Hirofumi Sato, S. Mihara, M. Aoki*, The University of Tokyo, Japan, *K. Shudo*, Yokohama National University, Japan, *K. Akimoto*, University of Tsukuba, Japan, *S. Masuda*, The University of Tokyo, Japan

Electronic properties of potassium-doped dibenzopentacene (DBP) thin films on Au(111) were studied by ultraviolet photoemission spectroscopy (UPS), metastable atom electron spectroscopy (MAES),^{1,2} and first-principles DFT calculation. The UPS and MAES spectra for K_xDBP (0 ≤ x ≤ 3.5) films show three types of gap state (GS1~GS3) in the HOMO-LUMO gap of pristine DBP. The GS1 and GS2 emerge at the initial stage of deposition and are attributed to the modified HOMO state and partially-filled LUMO state, respectively. The threshold of electron emission for K₁DBP is located ~0.1 eV below the Fermi level (E_F) with no metallic feature, suggesting that K₁DBP is a Mott-Hubbard insulator. At the formation of K₂DBP, the GS1 and GS2 saturate in intensity and shift to the higher binding energy. This indicates that the native LUMO state is fully occupied by electron transfer, resulting in a wide-gap insulator. Upon further deposition, the GS3 appears near E_F and is attributed to partial electron filling in the LUMO+1~LUMO+3 states. For K_{3.5}DBP, the leading edge of GS3 is located ~0.1 eV below E_F without a metallic feature. Therefore, the heavily doped species transfers to a Mott-Hubbard insulator again. The GS3 plays a key role in superconductivity of K₃DBP at low temperature.³

The interaction of alkaline-metal atoms with aromatic hydrocarbons could be classified into three categories, i.e., weak interaction,⁴ simple charge transfer,⁵ and heavy mixing of mutual wave functions. The K-doped DBP belongs to third category, and the detail will be discussed in the conference.

References

[1] Y. Harada, S. Masuda, H. Ozaki, *Chem. Rev.* **97**, 1897 (1997).

[2] S. Masuda, *Appl. Surf. Sci.* **256**, 4054 (2010).

[3] M. Xue, T. Cao, D. Wang, Y. Wu, H. Yan X. Dong, J. He, F. Li, G. F. Chen, *Sci. Rep.* **2**, 1 (2012).

[4] M. Sogo, Y. Sakamoto, M. Aoki, S. Masuda, *J. Chem. Phys.* **133**, 134704 (2010).

[5] F. Bussolotti, S. Kera, N. Ueno, *Phys. Rev. B* **86**, 155120 (2012).

EM-TuP15 In Situ Metrology during GaN and InGaN Growth by Remote Plasma-assisted MOCVD, *Daniel Seidlitz, R.L. Samaraweera*, Georgia State University, *I.T. Ferguson*, University of North Carolina at Charlotte, *A. Hoffman*, Technical University Berlin, Germany, *N. Dietz*, Georgia State University

Using real-time optical diagnostics during the GaN and InGaN growth progress in a remote plasma-assisted Metal Organic Chemical Vapor Deposition (RPA-MOCVD) reactor provides details in the precursors' decomposition processes and epitaxial layer growth mechanisms. Growth process control provisions in the RPA-MOCVD reactor enable a temporal and spatial controlled injection of metal organics (MO) as well as ammonia (N₂) plasma activated hydride precursors such as hydrogen (H₂) or ammonia (NH₃). Remote activated hydride precursor fragments (e.g. N*/NH*/NH₂*) are generated using a hollow cathode driven by a tunable radio frequency (rf) power source up to 600W. The radicals are directed to the substrate surface by the remote plasma afterglow regime. Plasma Emission Spectroscopy (PES) and UV-Absorption spectroscopy (UV-AS) are used to identify the active species in the plasma and determine their concentrations in dependence of the injected precursors N₂, H₂ and NH₃. Plasma emission spectroscopy during the growth run allows also a time dependent recording of the quantitative behavior of the reactive particles inside the plasma. In addition, real-time measurements and analysis of reflection spectroscopy at normal incidence on the growth surface contribute sub-monolayer growth rates for GaN and InGaN. In this report we will present and discuss results of in-situ Plasma emission spectroscopy, UV-Absorption spectroscopy and Normal incidence reflection spectroscopy (NI-RS). The combination of these real-time characterization methods provides qualitative and quantitative identification of active species in the gas phase and determination of growth rates at the growth surface. The in-situ obtained growth rates are compared with ex-situ thickness measurements (e.g. Transmission and reflection spectroscopy) and results of layer structural characterization methods (Raman spectroscopy, PL). These studies will aid our understanding of how process growth parameter such as substrate

temperature, plasma-assisted precursor generation/defragmentation, or the quantity of active species concentrations influence the growth and properties of binary and ternary group III-nitride alloys.

EM-TuP16 AFM Study on the Structural Properties of Gold Thin Films by RF Magnetron Sputtering, *Moniruzzaman Syed*, Lemoyne-Owen College, *C. Glaser, M. Schell, I. Senevirathne*, Lock Haven University

Gold (Au) thin films offer a wide range of applications in many fields such as memory storage, energy harvesting and storage, nanosensors, optics, biosensing devices and catalysis. Au film is paying more attention in many critical applications as it is highly conductive and is not easily oxidized. Therefore, it is necessary to understand the growth mechanism of film on various substrates. The structural properties of gold thin films are also playing very important role on the film quality which may affect optical properties as well as the sensing capabilities of the devices. In this study, Gold (Au) thin films were deposited on both glass and Si (100) substrates at room temperature (RT) with Ar gas atmosphere as a function of deposition time. The structural properties and surface morphology of Au thin film has been studied using Atomic Force Microscope (AFM). The deposition rate was found to be increased with increasing time of those films deposited on glass substrate. The effect of annealing temperature on the structural properties of Au film deposited on various substrates will also be discussed.

EM-TuP17 Influence of Plasma-Activated Nitrogen Species in MOCVD Grown GaN/GaN Epilayers, *Rasanga Samaraweera, D. Seidlitz*, Georgia State University, *B. Hussain*, University of North Carolina at Charlotte, *M.K.I. Senevirathna*, Georgia State University, *I.T. Ferguson*, University of North Carolina at Charlotte, *N. Dietz*, Georgia State University

This contribution will present results on the influence of remote plasma activated nitrogen containing precursor species on the physical properties of GaN and ternary GaInN layers grown by plasma-assisted metal organic chemical vapor deposition (PA-MOCVD). A hollow cathode rf-plasma source (13.65 MHz, 50-500 W) was used to generate reactive nitrogen plasma species in which hydrogen (H₂) and ammonia (NH₃) are added downstreams to tailor the reactive nitrogen species (N*/NH* etc.) interacting at the growth sites.

Growth parameters such as: H₂, N₂, NH₃ flows, metalorganic (MO) flows, plasma power, reactor pressure, and/or substrate temperature have been varied to assess their influence on the physical layer properties. The plasma species and its compositions have been analyzed using plasma emission spectra and absorption spectra. The structural and optoelectronic properties of the epilayers have been studied by x-ray diffraction (XRD), Raman spectroscopy, Fourier transform infrared reflectance (FTIR) and Photoluminescence (PL) spectroscopy. The optical analysis of the GaN layers by Infrared (IR) reflectance reveals the optical dielectric function around ε_∞= 5.35, which is comparable with the reported bulk values. The growth rates vary up to 200 nm/hour for GaN.

EM-TuP18 The Electrical Properties of a Bimodal Nb Nanocluster Distribution Formed Through Plasma Gas Condensation, *Kevin Bray, C.Q. Jiao*, UES, Inc., *J.N. DeCervo, J.N. Merrett*, Air Force Research Laboratory

Nanocluster growth and characterization is an expanding field of research due to the promising catalytic, electrical, magnetic, mechanical, and optical properties exhibited by these materials. The properties of nanoclusters vary from the bulk material and can be tuned by varying the nanocluster size. The ability to obtain desired nanocluster sizes and distribution is an important step in effectively utilizing these materials. Transition metal clusters have received considerable interest due to their wide range of applications. Niobium has attracted attention due to observations of ferroelectric properties at low temperature. In this work, Nb nanoclusters are deposited using a plasma gas condensation process which involves the sputtering of a Nb target to create a dense metallic vapor where clusters are formed. Changes in the nanocluster nucleation and growth are influenced through modifications of the process parameters such as carrier gas composition and flow rate, sputter source ion current, and aggregation length. The formation of a bimodal cluster distribution under select process conditions has been observed, with the smaller cluster diameter near 1 nm and the larger cluster diameter varying from 2 to 10 nm. The larger cluster forms as a simple condensation product while the smaller cluster appears to arise from a different nucleation and growth mechanism. The effects of differing argon and helium carrier gas ratios on cluster formation in conjunction with varying sputter source currents and aggregation lengths will be discussed. The effect of the cluster size on the electrical properties will be examined.

EM-TuP20 Electron-Hole Exchange Energy in PbS and PbSe Nanocrystals, Joseph G. Tischler, E.E. Foos, D. Placencia, W. Yoon, J.E. Boercker, Naval Research Laboratory

Lead chalcogenides (PbS, PbSe and PbTe) nanocrystals (NC) possess outstanding optical properties such as broad optical absorption from the ultraviolet to the near infrared (NIR), bandgap tunability in the NIR, efficient multiple exciton generation and relatively high quantum yield luminescence. Such properties can be exploited in a variety of optoelectronic applications including biological tags, lasers, photodetectors, LEDs and photovoltaics. Thus, the electron-hole pair (or exciton) ground state electronic structure and dynamics is of particular interest. In particular, it has been reported that the luminescence of PbS nanocrystals is produced by two electronic states. A higher energy state with a lifetime of the order of tens of nanoseconds and a lower energy state with a lifetime of a few microseconds. Competition between these two levels has been reported in dynamics as a function of temperature and nanocrystal size. Furthermore, these two states have been invoked to explain the seemingly large Stokes shift dependence with nanocrystal size. Although there has been a lot of consensus on these observations, the origin of these states has been highly controversial. Some of the explanations utilized to explain the observed structure and dynamics include: a dark-exciton state, a hybrid state consisting of a trapped electron and hole in the conduction band, a trapped exciton state, an exciton state split-off due to the intervalley interaction, and shallow trap surface states.

In this work, we show that both the Stokes shift and splitting between the two energy states scale as d^3 , where d is the diameter of the NC. These findings imply that these two states correspond to the singlet "bright" state and the triplet "dark" state respectively. Furthermore we demonstrate that the Stokes shift is mainly given by the electron-hole exchange energy, and that opposite to what it was previously believed, the exchange energy is determined by the short-range interaction instead of the long-range interaction. Also, from these measurements we determined for the first time the bulk exchange interaction strength constant (J) for both PbSe and PbS.

EM-TuP22 Ultrasound Treatment Influence on the Si-SiO₂ interface defects structure, Daniel Kropman, Tallinn University of Technology, Estonia, *T. Laas,* Tallinn University, Estonia

The effect of ultrasonic treatment (UST) on the defect structure of the Si-SiO₂ system by means of electron spin resonance (ESR), selective etching, MOS capacitance technique and secondary ions mass spectroscopy is presented. The non-monotonous dependence of the defect densities on the US wave intensity has been observed. The influence of the UST frequency on the ESR signal intensity of the defect centres depended on the defects type and may be caused by vibration energy dissipation, which are a function of defect centres type. In the ESR spectra of Si samples a signal with $g=1.9996$ (P a centers) connected with vacancy complexes is observed. After UST appears another signal with $g=2.0055$ (broken bonds of Si atoms). The influence of the US frequency and sample orientation on the ESR signal intensity varies for different centres. The frequency and orientation dependence of the ESR signal with $g=1.9996$ and the lack of this dependence for the centres with $g=2.0055$ show that vibration energy dissipation depends on the type of defect centers. Defect density at the interface grows with an increase of US wave intensity or changes non-monotonously depending on the oxide thickness and crystallographic orientation. In the samples with thick oxide there is a maximum in the dependence of the charge carriers lifetime on the US wave amplitude and in the samples with thin oxides there is a minimum. This shows that the structural defects form electrically active centers and their density can be varied by US. The density of point defects and absorbed impurities at the Si-SiO₂ interface can be reduced and its electrical parameters improved by an appropriate choice of the UST and oxidation condition. US is widely used not only for materials treatment but in medicine as well (cancer treatment).

References:

[1] D.Kropman, V.Poll, L.Tambek, T.Karner, U.Abru. Ultrasonics 36(1998)1021-1025.

[2] D.Kropman, S.Dolgov. Physica status Solidi (c) v.9, issue 10-11, pp.2173-2176, 2012.

EM-TuP24 Low Temperature Growth of High-Quality SiO₂ Gate Dielectric by Atomic Layer Deposition, Sangram Pradhan, E. Tyani, A.K. Pradhan, Norfolk State University

A novel as well as simple method preparation of atomic layer deposited high quality SiO₂ gate dielectrics were fabricated using highly reactive ozone and tris (dimethylamino) silane. Small frequency dispersion and hysteresis behavior of SiO₂ MOS capacitor shows an ideal C-V behavior, suggesting excellent interfacial quality as well as purity of SiO₂ film. The flat-band voltage of the samples shifted from negative to positive sweep voltage region with increase in TDMAS pulse from 0.2 to 2 seconds. Based

on EOT point-of-view, the ALD SiO₂ has gate leakage current density as well as electrical fields of all ALD SiO₂ samples are nearly very good and more than (~ 10 MV/m) which is better comparable to that of thermal silicon oxide grown at temperatures above 800°C. The appealing electrical properties of thin ALD SiO₂ enable its potential applications as high-quality gate insulators for thin-film MOS transistors, and insulators for sensor structures and nanostructures on non-silicon substrates.

EM-TuP25 Surface Temperature and Kinetic Energy Dependence of SiGe Growth, Sang Choi, NASA Langley Research Center, *H.J.K. Kim,* National Institute of Aerospace

Silicon-germanium (SiGe) is an important semiconductor alloy for high-speed field effect transistors (FETs), high-temperature thermoelectric devices, photovoltaic solar cells, and photon detectors.[1] Semiconductor chipsets and devices require a single-crystalline phase of material without defects, while thermoelectric materials need granulated domains of poly crystalline structure with an interfacing boundary electrically connected but causing phonon scattering.[2] The structural formation between SiGe and substrate can be tailored for either single crystal or twin lattice structure.

Highly ordered single crystals with rhombohedral epitaxy using an atomic alignment of the [111] direction in cubic SiGe with the [0001] direction in the sapphire basal plane (c-plane) have been successfully grown at the NASA Langley Research Center. The changes in the growth temperature (from 820°C to 890°C) strongly influence the shape, size and density of the SiGe nuclei in the early growth stage and eventually the film morphology and defect density in the final growth stage. Annular bright field (ABF) and high angular dark field (HAADF) scanning transmission electron microscopy (STEM) were used to investigate the atomic structure and chemistry of SiGe and sapphire (Al₂O₃) interfaces, sapphire substrate reconstruction, and defects for studying the film growth mechanism. The best growth condition can be achieved by choosing the suitable substrate temperature and kinetic energy of impinging Si and Ge atomic flux. By controlling the kinetic energy of the surface atoms, either a dominant twin crystal or dominant single crystal was steadily formed. The kinetic energy of surface atoms is determined at the growth temperature between 820°C and 890°C.

[1] D. L. Hareme and B. S. Meyerson, IEEE Transactions on Electron Device, 48 (11), 2555 (2001).

[2] C. Gui, M. Elwenspoek, N. Tas, and J. G. E. Gardeniers, J. Appl. Phys. 85 (10), 7448 (1999).

EM-TuP26 TiN/Ag Multilayers made by dc Magnetron Sputtering for Patch Antennas Applications, José Ampuero, A.F. Talledo, V. Peña, C. Benndorf, Universidad Nacional de Ingeniería, Peru, *M. Yarlequé, R. Cerna,* Pontificia Universidad Católica del Peru

Titanium nitride has excellent physical properties such as high hardness, high abrasion wear resistance, as well as, high corrosion resistance, however, its electrical conductivity is poor compared to that of noble metals such as copper, silver or gold. On the other hand, silver films show excellent conductivity but in contact with normal atmosphere they are spoiled rapidly.

We have found that multilayers of silver and titanium nitride show high conductivity, high hardness and high corrosion resistance which make them useful for electrical and electronic applications.

In this paper we report (i) the production of silver-titanium nitride multilayers made by dc magnetron sputtering, (ii) structural and stoichiometry characterization made by X-ray diffraction and Auger electron spectroscopy. We also report the performance of patch antennas made of TiN/Ag multilayers deposited by dc magnetron sputtering on alumina plates. The analysis was made by using a Vector Network Analyzer. Typical bandwidth was in the range 3.3-3.4 GHz.

EM-TuP28 Quantum Effects Produced by Silicon Nanoparticles Embedded in Stacks of Silicon Rich Oxide Obtained by Low Pressure Chemical Vapor Deposition, Karim Monfil-Leyva, Benemerita Universidad Autónoma de Puebla, Mexico, *M. Aceves-Mijares,* Instituto Nacional de Astrofísica Óptica y Electrónica, *A.L. Muñoz-Zurita,* Universidad Autónoma de Coahuila, *J.A. Luna-López,* Benemerita Universidad Autónoma de Puebla, *R.C. Ambrosio-Lázaro,* Universidad Autónoma de Ciudad Juárez

Currently, new electronic and optoelectronic applications are using stacked arrays of different films, like superlattices, multilayers, tandem solar cells, etc. This work shows results and discussion of the structural and electrical properties from stacks of silicon rich oxide (SRO) films with different silicon excess. SRO films were deposited on *n*-type silicon (Si) substrate with low resistivity ($2\sim 3 \Omega\cdot\text{cm}$) using the low pressure chemical vapor deposition (LPCVD) technique. Two different stacks of SRO (SSRO) were formed varying the flow ratio (Ro) between N₂O and SiH₄ with Ro=10

(SRO₁₀) and Ro=30 (SRO₃₀). Also, low and high Si-implantation, 5×10^{15} and 2×10^{16} at/cm² doses respectively, were applied to SSRO. A thermal annealing was applied to all SSRO at 1100°C for 3 hours. Metal-oxide-semiconductor (MOS) structures were fabricated using the SSRO as dielectric layer with Aluminium (Al) on top and back contacts obtained by thermal evaporation. Cross section images of the Al/SSRO/Si structures were obtained by Transmission Electron Microscopy (TEM). The thickness of SSRO and diameters of embedded Si-nanoparticles (Si-Np's) were calculated from TEM images. The Si-implantation increases the size and density of Si-Np's in the SSRO. Current vs. Voltage ($I-V$) measurements of the Al/SSRO/Si structures showed current oscillations, staircases and bumps at room temperature. High frequency Capacitance vs. Voltage ($C-V$) measurements exhibited little jumps in the accumulation region due to charge trapping and de-trapping effect produced by the presence of Si-nPs. A group of SSRO structures showed a large hysteresis related to traps density in the SRO₁₀ films. The current oscillations and the other anomalies from electrical characterization were related with quantum effects like tunneling and Coulomb blockade between on and off states of the conductive paths as a result of Si-nPs embedded in the SSRO.

EM-TuP30 Tuning A Strong Photoluminescence Using Thin Silicon Rich Oxide And Silicon Rich Nitride Films Obtained By Low Pressure Chemical Vapor Deposition. *K. Monfil-Leyva*, Benemerita Universidad Autónoma de Puebla, Mexico, *A. Morales-Sánchez*, Centro de Investigación en Materiales Avanzados, S.C., *A.L. Muñoz-Zurita*, Universidad Autónoma de Coahuila, *F.J. Flores-Gracia*, Benemerita Universidad Autónoma de Puebla, *M. Moreno-Moreno*, Instituto Nacional de Astrofísica Óptica y Electrónica, *Esteban Ojeda-Durán*, Benemerita Universidad Autónoma de Puebla

Luminescent process in materials based on silicon nanostructures has attracted a great effort to overcome the intrinsic disadvantages of bulk-Si to develop optoelectronic devices. Nowadays, the Silicon Rich Oxide (SRO) and Silicon Rich Nitride (SRN) arise as a cheap and effective alternative to develop ultraviolet absorbers or silicon-based light emitters. SRO and SRN films can be deposited by several techniques but homogeneous layers can be easily obtained by low pressure chemical vapor deposition (LPCVD) using N₂O and NH₃ respectively mixed with SiH₄ as reactive gases. Silicon excess in SRO and SRN is well controlled by $Ro = N_2O/SiH_4$ and $Ro_n = NH_3/SiH_4$.

In this work, we report a wide study of the optical properties of thin SRO and SRN films obtained by LPCVD where silicon excess was changed by the pressure ratio Ro in the range of 15 and 45 (SRO15 to SRO45) and Ro_n in the range of 4 to 80 (SRN4 to SRN80). The effect of annealing at high temperature was studied at 1100 °C. Ellipsometry measurements were done on each sample to calculate the thickness and the refractive index. Fourier transform infrared (FTIR) measurements were applied on SRO and SRN films to confirm a change on stoichiometry. Absorbance spectra of SRO films showed the four characteristic peaks of non-stoichiometric silicon dioxide (SiO_x) after annealing. The as-deposited SRN films showed the characteristic peaks of a hydrogenated SiN_x matrix. However, the Si-H and N-H stretching peaks (2210 and 3315 cm⁻¹) disappeared after applying the annealing. SRN films showed a transmittance of 40 up to 90 % in the visible to near infrared region (400 to 900 nm). SRO films showed a strong photoluminescence (PL) at room temperature (RT) on two bands, a blue band from 400 to 550 nm or a red band from 575 nm to 875 nm depending on Ro. Blue and red emission bands were related to donor acceptor decays between traps promoted by defects. SRN films with high Si excess showed a wide PL from 450 to 850 nm. PL intensity from SRN was reduced when annealing temperature was increased, then the PL was also related to defects in the SiN_x matrix.

EM-TuP31 High Spatial Resolution Mass Spectrometry Imaging of Electronic Devices by Femtosecond Laser Desorption. *Yang Cui*, *M. Majeski*, *L. Hanley*, University of Illinois at Chicago

A variety of methods beyond secondary ion mass spectrometry are now available to molecularly image electronic devices and materials structures. Previous studies have shown the advantages of femtosecond laser desorption by removing sample without damaging remaining material, potentially allowing three dimensional imaging of molecular species [S. Milasinovic, et al., Anal. Chem. 84 (2012) 3945; Ibid, J. Phys. Chem. C (2014) <http://dx.doi.org/10.1021/jp504062u>]. Vacuum ultraviolet radiation has been added to femtosecond laser desorption to facilitate molecular detection [Y. Cui, ACS Appl. Mater. Interf. 5 (2013) 9269]. Nonlinear excitation by 800 nm, <100 fs laser pulses may also allow sampling of an analyte within a region smaller than the laser focus size. We explore this strategy to demonstrate mass spectrometry imaging by operating laser just above the ablation threshold. A USAF resolution test target and organic compound pattern were used for testing resolution. A simulated organic electronic device structure was then analyzed by depositing pentacene through a 1500 mesh electron microscopy grid onto a silicon wafer. The

sample was analyzed after the grid was removed, allowing collection of a mass spectrometric image of the pentacene grid as represented by signal from the intact pentacene ion. Overall, the method demonstrated a ~2-4 micron spatial resolution with the capability to maintain significant molecular information on an intact electronic device structure.

Energy Frontiers Focus Topic Room: Hall D - Session EN-TuP

Energy Frontiers Poster Session

EN-TuP2 Mini-band Formation in a Strain-balanced InGaAs/GaAsP MQW Solar Cell Structure Investigated by a Photoreflectance and a Surface Photovoltage Spectroscopy. *Tetsuo Ikari*, *A. Fukuyama*, *K. Nishioka*, *T. Aihara*, *H. Kuradome*, University of Miyazaki, Japan, *K. Toprasertpong*, *M. Sugiyama*, *Y. Nakano*, University of Tokyo, Japan

Embedding of multi quantum well (MQW) structures in an absorption layer of GaAs solar cell is a promising idea for developing higher efficient solar cell devices. Extension of the absorbing region to longer wavelength side enhances the short-circuit current. When the mini-band forms between the QW, further developing of the conversion efficiency would be expected in term of a carrier tunneling without recombination of the photo excited carriers. However, recombination at the QW interface still leads to the degradation of the efficiency. Therefore, we fabricated a strain-balanced InGaAs/GaAsP layer in the intrinsic region of the GaAs *p-i-n* solar cell [1]. The mini-band formation for the samples with different thickness of the barrier region from 5.3 to 1.9 nm was studied by using a photoreflectance (PR) and a surface photovoltage (SPV) spectroscopy at room temperature.

The energies at the Brillion zone edges were detected from the Kramers-Kronig analysis of the PR spectra for estimating the mini-band width as a function of barrier thickness. When the mini-band formed, the ratio of carriers escaped thermally from each QW may change. SPV spectra were, then, measured to know the carrier escaping rate and how this component affects the absorption spectra of the solar cell structures.

The observed PR spectra for the sample with thinnest barrier width of 1.9 nm show two critical energies at 1.274 and 1.312 eV. The energy difference of these critical energies was around 0.038 eV and this energy difference reduces from 0.020 to 0.009 eV for the samples with barrier thickness of 2.7 and 3.6 nm, respectively. Supposing that such energy difference shows the mini-band width, the reduction of the energy with increasing the thickness of the barrier can be understood. The theoretical estimation using a Kronig-Penny model calculation for the width suggests that the mini-band width in the QW is 70 and 0 meV for e1 and topmost hh1 sub-bands. Therefore, the observed mini-band width is smaller than expected. The reason is not clear at present. For the SPV spectra, two broad peaks were observed at 1.29 and 1.32 eV. The energy difference also decreases with increasing the thickness of the barriers. Smaller critical energies for SPV may be explained that these signals detect the maxima energy of the joint-density of states which is larger than the band edge energies. Since the carrier escaping from the QW and radiative and non-radiative recombination rates may be strongly temperature dependent, estimation of the relevant activation energies for carrier escaping from these measurements were useful for further discussion.

[1] M. Sugiyama, *et al.*, J. Cryst. Growth 315 (2011) 1.

EN-TuP5 Cu(In,Ga)Se₂ Absorber Layer Deposited by Radiofrequency Magnetron Sputtering. *Romain Meunier*, *M.-P. Besland*, *P.Y. Jouan*, *A. Lafond*, Université de Nantes, France, *P.Y. Thoulon*, *M. Ricci*, Crosslux Company, France

In the last decades, the deposition of CIGSe thin films by sputtering has seldom been investigated. Besides, the sputtering of a single quaternary CIGSe target would be a real advantage for industrial development. Indeed, sputtering technique exhibits a good compatibility with industrial up-scaling and limits selenium use with respect to toxicity issues. In 1992, Hernandez et al¹ early published on CIGSe layers deposited by sputtering of a single quaternary CIGSe target.

The improvement of plasma discharges at lower working pressures in the last years had allowed news possibilities for CIGS thin films deposited by sputtering. In 2010, Frantz et al² succeeded to obtain a CIGSe solar cell with an efficiency of 8.9%.

At IMN laboratory, a dedicated chamber has been home-designed for CIGSe thin films deposition using one step sputtering. CIGSe thin films were deposited on SLG/Mo substrates by radio-frequency magnetron sputtering at ambient temperature. The deposition parameters like pressure or power density have been investigated. Then, CIGS thin films have been annealed at various temperatures in a furnace under Ar flow. The evolution

of chemical composition and structural properties of CIGS thin films as-deposited and annealed will be presented.

References

1. *Hernández Rojas, J. L. et al. Appl. Phys. Lett. 60, 1875–1877 (1992)*
2. *Frantz, J. A. et al. Thin Solid Films 519, 7763–7765 (2010).*

EN-TuP6 Developments in Power Efficient Dissociation of CO₂ using Non-Equilibrium Plasma Activation, Waldo Bongers, A.P.H. Goede, M.F. Graswinckel, S. Welzel, Dutch Institute for Fundamental Energy Research, The Netherlands, *M. Leins, J. Kopecki, A. Schulz, M. Walker,* Universität Stuttgart, Germany, *M.C.M. van de Sanden,* Dutch Institute for Fundamental Energy Research, The Netherlands

In the framework of an emerging Solar Fuel program the first and essential CO₂ dissociation step of CO₂ into CO and O₂ has been studied. The focus was thereby on high energy efficiency of the process using non-thermal (non-equilibrium) microwave plasmas without the use of rare materials. The plasma was generated by tangentially injecting CO₂ gas in a quartz tube placed inside a low loss 915 MHz TM₀₁₀ circular waveguide mode cavity. Powers were used up to 10 kW. The feed gas expanded supersonically after the cavity to quench the plasma and prevent vibrational-translational relaxation losses. These experiments resulted in power efficient conversion (more than 50%) of large CO₂ flows (up to 75 standard liter per minute) with 11% conversion yield. The product formation was measured downstream the plasma at the expansion in a calibrated mass spectrometer.

The research at the plasma Solar Fuels facilities of DIFFER concentrates on optimization of power efficient selective vibrational CO dissociation. This can be achieved by means of several novel methods: like tuning the optimal kinetic energy range of the electrons by controlling the reduced electric field in the microwave cavity or make use of the relaxation time difference of translational and vibrational modes of CO controlled by modulating the microwave field. First results were obtained with a 2.45 GHz 1kW microwave plasma source. The source consists of a quartz tube with a tangential gas injection system placed inside a circular TEM mode coaxial cavity coupled to a TE₁₀ rectangular waveguide mode cavity. The configuration of the coaxial cavity allows control of the electric field. With an input of 7 standard liter per minute of CO₂ energy efficiencies 15% to 36% were obtained (based on CO₂ depletion) in the pressure range from 1Bar (atmospheric) till 0.2 Bar. An update on these new research developments will be shown.

EN-TuP8 GLAD & SAD-GLAD Nanorod Array Catalyst Electrodes for Polymer Electrolyte Membrane Fuel Cells, Fatma Yurtsever, M. Begum, M. Yurukcu, M.F. Cansizoglu, A.U. Shaikh, University of Arkansas at Little Rock, *W.J. Khudhayer,* University of Babylon, Iraq, *N. Kariuki, D.J. Myers,* Argonne National Laboratory, *T. Karabacak,* University of Arkansas at Little Rock

Polymer electrolyte membrane (PEM) fuel cell technology is one of the promising alternative

energy systems for an environmentally friendly, sustainable energy economy. However, PEM

fuel cells require an expensive platinum catalyst which raises the cost of the fuel cell. In this

study we investigated the electrocatalytic oxygen reductive reaction (ORR) activities of Pt and

Pt-Ni alloy catalyst thin film coated on Cr and Ni base nanorod arrays, respectively, and also

ORR of Pt-Ni alloy nanorods. Cr and Ni nanorods were used as low cost, high surface area

metallic supports for the conformal Pt and Pt-Ni alloy thin film, respectively. Nanorods were

grown on glassy carbon electrodes using a magnetron sputtering glancing angle deposition

(GLAD) technique and conformal coating of catalyst thin film on the base nanorods were

achieved using a small angle deposition (SAD) technique. Pt-Ni alloy nanorods were also grown

using GLAD. The electrocatalytic ORR activity of the nanostructured electrodes were

investigated using cyclic voltammetry (CV) and rotating disk electrodes (RDE) in a 0.1M

aqueous perchloric (HClO₄) acid solution. The electrochemical active surface area (ECSA),

surface area specific activity (SA), and mass activity (MA) values were determined and

compared to the Pt and Pt-Ni alloy catalyst results in the literature. The results from GLAD Pt-Ni

alloy nanorods exhibit higher values of ECSA compared to geometric area of the nanorods. The

MA of the Pt-Ni nanorods was found to be a factor of 2.3 to 3.5 higher than that of pure Pt

nanorods of the same dimensions and increasing with increasing Ni contents. However, the SA

enhancement was only observed for the nanorods with the highest Pt contents. In addition, both

the SAD-Pt/GLAD-Cr and GLAD-Pt-Ni alloy nanorods were found to have higher stability

against loss of ECA during potential cycling in the acidic electrolyte. Our preliminary results on

the SAD-Pt-Ni/GLAD-Ni nanorod arrays will also be presented

EN-TuP9 XPS Study of Ternary Chalcogenide Semiconductors Deposited by a Solution-based Method for Solar Cells Applications, Francisco Aguirre-Tostado, R. Garza-Hernandez, CIMAV-Monterrey, Mexico, *R. Mayen-Mondragon,* UNAM-Punta, Mexico, *E. Martinez-Guerra,* CIMAV-Monterrey, Mexico

The use of solution-based methods for semiconducting thin film deposition is of great importance for large area photovoltaics applications, enabling as well the deposition on flexible substrates. Chalcogenide semiconductor materials present p- and n-type characteristics that are attractive for photovoltaics applications. The optimization of device structure for a solar cell requires an atomistic understanding of the structure and chemical reactions taking place during deposition and post-deposition processes. In this regard, X-ray photoelectron spectroscopy (XPS) is uniquely suited for tracking chemical reactions occurring at the surface and interface of sub-nanometric layers. The chemical analysis and thermal stability for surface and interface reactions of binary and ternary chalcogenide semiconductors is presented. CuS, ZnS, SnS₂, CdS thin films and some of its combinations were deposited by the successive ionic layer absorption and reaction method (SILAR) under controlled environment next to the XPS analysis load-lock chamber. Step by step XPS analysis of the SILAR process reveals an incubation period that depends on temperature and ion concentrations. The stability of the heterostructures is discussed in terms of chemical reactivity and inter-diffusion.

EN-TuP10 Enhanced Photovoltaic Response of Pb_{0.95}La_{0.05}Zr_{0.54}Ti_{0.46}O₃ Thin Film Based Solar Cells, Vaishali Batra, G. Cabot, S. Kotru, University of Alabama

Ferroelectrics materials have generated considerable interest in the field of ferroelectric photovoltaic (FE-PV) in recent years and are still being researched as potential alternative material for future photovoltaic applications. However, the PV response from these FE-PV devices is still very low. In this work, various approaches were adopted to improve the PV response from the FE-PV devices. The ferroelectric material used for fabricating the capacitor type solar cells was Pb_{0.95}La_{0.05}Zr_{0.54}Ti_{0.46}O₃ (PLZT) in thin film form, prepared using chemical solution deposition method. In one approach, a thin layer of lead titanate (PTO) was introduced as a seed layer to control the (001)/(100) orientation and to suppress the (110) orientation of the PLZT films. Presence of seed layer was seen to show a remarkable effect on the ferroelectric and the photovoltaic properties of the devices. Another approach used was the incorporation of silver nanoparticles (SNPs) in PLZT matrix. The narrow band gap nanoparticles (NP) embedded in PLZT films enhances the optical absorption in Pt/PLZT/Pt by extending the absorption spectra from ultraviolet to a fraction of the visible light spectrum. Results showing the effect of seed layer and incorporation of NP on PLZT devices will be presented.

EN-TuP11 Influence of Orientation and Size in Crystallite on Various Properties in Al-doped ZnO Films for Solar Cell Transparent Electrode Applications, T. Minami, Toshihiro Miyata, T. Yamanaoka, Kanazawa Institute of Technology, Japan

We have recently reported that impurity-doped ZnO thin films appropriate for transparent electrode applications in thin-film solar cells were related more to the content rather than the kind of impurity doped into the films as well as to the deposition method used [1]. This paper describes the influence of the orientation and size in crystallite on the resulting optical absorption and the obtainable surface texture structure and carrier mobility in Al-doped ZnO (AZO) thin films prepared with different types of magnetron sputtering deposition (MSD) methods. The AZO thin films were prepared with a thickness of 500-3500 nm on OA-10 glass substrates at a sputter Ar gas pressure of 0.2-12 Pa and a temperature of room temperature (RT)-350°C by d.c. MSD or r.f. power superimposed d.c. MSD. The surface

texture formation was carried out as a result of MSD under the appropriate deposition condition or by wet-chemical etching (in a 0.1% HCl solution at 25°C). For example, when the AZO films were prepared with increasing a sputter gas pressure from 0.4 to 12 Pa at a deposition temperature of 350°C, the films exhibited the red shift with tailing in both the absorption edge and plasma edge as the sputter pressure was increased. With increasing the sputter gas pressure, the deposited films exhibited the increase of etching rate and the decrease of etch pit size obtained from the etching, whereas the pyramid type textured surface was formed at a pressure above approximately 6 Pa. It was also found that both in the c-axis orientation and the crystallite size as well as the carrier mobility in the deposited films were decreased by increasing the sputter gas pressure. It should be noted that the sputter gas pressure dependence described above was strongly dependent on the thickness of deposited films and MSD method used. In addition, the result described above was considerably affected by after heat-treatment with rapid thermal annealing (RTA) in air. Consequently, observed sputter gas pressure dependences such as the expanded tailing of absorption coefficient, etching characteristics and decrease of mobility were mainly correlated to the degradation of crystallinity as evidenced by the c-axis orientation and the crystallite size.

[1] T. Minami, T. Miyata, and J. Nomoto, *Materials Science and Engineering*, **34**, 012001 (2012).

EN-TuP13 Surface Analytical Investigation on Organometal Triiodide Perovskite, *Yongli Gao, C.G. Wang, C.C. Wang*, University of Rochester, *X.L. Liu*, Central South University, Changsha, China, *J.S. Huang*, University of Nebraska Lincoln

In a little over a year, there has been an unexpected breakthrough and rapid evolution of highly efficient solid-state hybrid solar cells based on organometal trihalide perovskite materials. This technology has the potential to produce solar cells with the very highest efficiencies while retaining the very lowest cost. We have measured the electronic density of states of $\text{CH}_3\text{NH}_3\text{PbI}_3$ using ultraviolet photoelectron spectroscopy (UPS), inverse photoemission spectroscopy (IPES), and x-ray photoelectron spectroscopy (XPS). The valence band maximum (VBM) and conduction band minimum (CBM) positions are obtained from the UPS and IPES spectra, respectively, by linear extrapolation of the leading edges. With the Fermi level close to the VBM, the sample is slightly p-type, with the $E_{\text{VBM}}=0.76$ eV, $E_{\text{CBM}}=-0.9$ eV, and transport energy gap 1.7 eV. The ionization potential (IP) of 6.16 eV can be obtained from the sum of the UPS measured E_{VBM} and the work function of 5.40 eV. The XPS spectra reveal an obvious deficiency of N is, whereas the concentrations of I and Pb are close to the expected values. The existence of O and excessive C indicate that the surface is contaminated, and the contamination is reduced by 12-20% by thermal annealing in vacuum. The interface between $\text{CH}_3\text{NH}_3\text{PbI}_3$ and TiO_2 is also investigated. As $\text{CH}_3\text{NH}_3\text{PbI}_3$ layer thickness increases, one sees a gradual shift of the vacuum level cut-off. At the $\text{CH}_3\text{NH}_3\text{PbI}_3$ thickness of 8.2 nm, the shift saturates, signaling the end of the interface dipole formation. The evolution of the VB is even more gradual, and it appears to mature only at the thickest layer. Given the UPS probing depth of ~1.5 nm and the typical interface formation in other systems, the saturation of the vacuum level cut-off at 8.2 nm in $\text{CH}_3\text{NH}_3\text{PbI}_3/\text{TiO}_2$ is surprisingly large. It points at the possibility that the films are not truly uniform. On the other hand, the interface dipole of 0.7 eV $\text{CH}_3\text{NH}_3\text{PbI}_3$ and TiO_2 is important for further understanding of the energy level alignment and charge transfer across the interface.

EN-TuP14 Synthesis, Characterization and Hydrogen-Storage Performance of Nanoporous Graphene-based Adsorbents, *Claus Rebholz, N. Kostoglou*, University of Cyprus, *V. Tzitzios, C. Tampaxis, G. Charalambopoulou, T. Steriotis, K. Giannakopoulos*, National Center for Scientific Research Demokritos, *Y. Li, K. Liao, K. Polychronopoulou*, Khalifa University of Science, Technology & Research

In the present work, we synthesized and systematically characterized two novel graphene-based nanomaterials, a reduced graphene oxide sponge and a microwave-exfoliated graphene oxide. Their textural properties were determined by N_2 adsorption/desorption at 77 K, while additional characterization techniques were employed in order to elucidate further their structure, surface chemistry and morphology such as X-Ray Diffraction (XRD), Fourier-Transform Infrared Spectroscopy (FT-IR), Field-Emission Scanning Electron Microscopy (FE-SEM) and High-Resolution Transmission Electron Microscopy (HR-TEM). Both nanomaterials were additionally evaluated for their H_2 storage performance and were critically compared to commercially available carbons (e.g. graphene nanoplatelets, carbon nanotubes) based on systematic H_2 adsorption/desorption measurements at 77K between 0-1 bar. Maximum H_2 gravimetric capacities ~0.5 wt% and ~0.7 wt% were recorded at 77 K and 1 bar for the reduced GO sponge and the microwave-exfoliated GO, respectively. A linear relationship was found between the H_2 uptake values and the BET specific surface area of the materials included in this study.

EN-TuP15 Vacuum Deposition Of Photosystem 1 Films In P-Doped Silicon Surface To Improve The Efficiency Of Bio-Photovoltaic Cells, *CarlosFelipeRezende Facchini, L.T. Manera, P. Mazzafera, R.V. Ribeiro, E. Kiyota*, University of Campinas, Brazil

The high efficiency which some organisms perform photosynthesis and its abundance around the globe, coupled with high world energy demand in the coming years and the low competitiveness of current photovoltaic devices in comparison with other forms of energy, inspired us to build a Bio-photovoltaic device composed of a heavily p-doped silicon substrate and a tandem of protein complex called Photosystem 1 (PS1) found in the thylakoid of leaves.

The process extraction of PS1 complexes from spinach essentially consists of two general steps: the extraction of thylakoid membranes from the spinach leaves and the isolation and purification of PS1 complexes from the thylakoids.

For the deposition of PS1 films onto silicon substrates we use a simple and straightforward method. The procedure entails depositing a volume (100 μL) of an aqueous PS1 suspension on to a silicon surface modified with 3-aminopropyl-triethoxysilane (APTS) and applying a negative pressure (~70 mTorr) to remove the solvent from the PS1 solution via vacuum deposition process. The thermodynamic driving force for the formation of these films arises from hydrophobic interactions between neighboring protein complexes in the film and by tuning the silicon Fermi energy by doping. This promotes the alignment of silicon bands with redox active sites of PS1, which leads to the formation of dense and resilient films.

Iterative depositions were similarly performed and for two deposition steps, a thickness of ~600nm was achieved, thereby increasing the efficiency of the bio-hybrid cell.

These results represent significant progress toward affordable, biologically-inspired renewable energy conversion platforms.

EN-TuP16 Cross Sectional Mapping of CdTe PV Devices with Scanning Capacitance Microscopy, *Gilad Zorn, B.A. Korevaar, J.R. Cournoyer, K. Dovidenko*, GE Global Research Center

Scanning capacitance microscopy (SCM) is a powerful method for mapping dopant variation in semi-conductor and PV devices. In SCM a conducting AFM tip is used to scan the surface in contact mode. The tip and sample surface form a metal-insulator-semiconductor structure. Simultaneous with the topography data collection, an AC bias is applied to the sample while the tip is grounded. The resulting oscillation of carriers near the tip, leads to a modulated capacitance (dC/dV), which is measured by a capacitance-sensing circuit. The capacitance measured by the SCM sensor varies as the carriers move towards (accumulation) and away from (depletion) the probe. When the sample is fully depleted the measured capacitance is that of the oxide plus the depletion layer. When carriers are accumulated at the surface, the measured capacitance is that of the oxide layer. The magnitude of the change in capacitance (dC) for a given change in voltage (dV) depends on the carrier concentration. For heavily doped materials the carriers do not move far. Hence, the measured capacitance variation between accumulation and depletion is small. The opposite is true for lightly doped semiconductors which yield a large capacitance change. The sign of the measured dC/dV signal changes between n-type and p-type. In p-type semiconductors, as the sample voltage becomes more negative relative to the tip, the width of the surface depletion layer will increase. Hence, the total capacitance will decrease. If the sample voltage is positive, accumulation will occur, and the capacitance measured will be that of the oxide layer only. For n-type samples the effects are opposite.

This work describes SCM cross-sectional mapping of CdTe devices, focusing on the role of the various processing steps during the device fabrication. These steps include CdTe deposition, CdCl_2 -treatment, and a copper-step. Generally it is accepted within the CdTe community that as deposited CdTe is lightly doped and could be both n-type or p-type depending on the deposition temperature and process. The effect of the CdCl_2 treatment is typically presented as a way to create so-called A-centers, which dope the CdTe p-type. The final copper-step then fills the A-centers and creates Cu on Cd-sites, which further dopes the CdTe p-type to levels in the range of 5×10^{13} to 5×10^{14} cm^{-3} . Here SCM is used to demonstrate the role of the various processing steps with regards to carrier density. SCM dopant map could clearly distinguish n and p-type CdTe as well as the p-n transition across the interface. It was found that the doping distribution across the CdTe layer depends on the type of the copper treatment.

Materials Characterization in the Semiconductor Industry Focus Topic

Room: Hall D - Session MC-TuP

Poster Session for all areas of Materials Characterization in the Semiconductor Industry

MC-TuP1 Volumetric and Surface Chemistry of SF₆/C₄F₈/Ar Gas Mixture, Robert Bates, M.J. Goeckner, P.L.S. Thamban, L.J. Overzet, University of Texas at Dallas

While plasmas using mixtures of SF₆, C₄F₈ and Ar are widely used in deep silicon etching, very few studies have linked the discharge parameters to etching results. We measured the optical emission intensities of lines from Ar, F, S, SF_x, CF₂, C₂, C₃ and CS as a function of the percentage C₄F₈ in the gas flow, the total gas flow rate and the bias power. In addition, the ion current density and electron temperature were measured using a floating Langmuir Probe. For comparison, trenches were etched of various widths and the trench profiles were measured. The addition of C₄F₈ to an SF₆/Ar plasma acts to reduce the availability of F as well as increase the deposition of passivation film. Sulfur combines with carbon in the plasma efficiently to create a large optical emission of CS and suppress optical emissions from C₂ and C₃. At low fractional flows of C₄F₈, the etch process appears to be controlled by the ion flux more so than by the F density. At large C₄F₈ fractional flows the etch process appears to be controlled more by the F density than by the ion flux or deposition rate of passivation film. CF₂ and C₂ do not appear to cause deposition from the plasma, but CS and other carbon containing molecules as well as ions do.

Financial Support Acknowledgement: TI/SRC Award #2261.001

MC-TuP3 SIMS Measurements of Impurities and Alloying Elements in Cu Films used for BEOL Processes, Steven Novak, T. Laurssen, SUNY College of Nanoscale Science and Engineering, M. Rizzolo, IBM Albany Nanotech Center, B. O'Brien, SUNY College of Nanoscale Science and Engineering

Significant recent work has concentrated on the impurity contents of electroplated copper and how they affect the crystallization of copper interconnects. Plating bath additives cause elevated impurity contents in electroplated Cu films that have been thought to pin grain boundaries and strongly affect the recrystallized grain structure of the Cu. SIMS is among the most utilized technique to measure impurity contents in electrochemically deposited Cu however SIMS data is typically only given as relative comparative data. We present quantitative measurements for C, O, S and Cl contents in ECD Cu using both TOF-SIMS (IonToF V) and quadrupole (Phi 6650) SIMS instruments. Using ion-implanted standards we have found that detection limits for impurity elements are typically well below the required limit for ECD Cu. Detection limits are typically one order of magnitude lower using dynamic SIMS compared to TOF-SIMS. The high mass resolution available for TOF-SIMS allows unambiguous quantitative measurement of impurities like S, which experiences mass interference from the O₂ molecular ion. Quantitative SIMS analyses show linear increases in impurity contents within plated Cu films as the additive content increases in the plating bath. Although impurity elements are commonly cited as a major effect on the grain size of recrystallized Cu films, recent experiments with intentionally layered Cu samples, having impurity content differences of 2-3X, show that the impurity content has little effect on ultimate crystallite size. Impurity measurements in Cu trenches have been a goal for SIMS for some time. Ion imaging of Cu trenches 450-35nm wide has been carried out using the Bi LMIG gun of the IonToF V instrument. This instrument is capable of 200nm image resolution. Depth profile analysis of Cu trenches show higher impurity contents within clearly-resolved 450nm wide trenches and suggest even higher contents within smaller trenches, when compared to the Cu overburden. Detection limits in image mode are at least one order of magnitude higher than standard depth profile mode. Alloying Cu with other metals has been proposed as a means of minimizing electromigration within plated Cu lines. Presently Mn is used as an alloy element in seed Cu layers. In addition to Mn, we have studied ion implants of Ag, Co and Ni in Cu as standards for quantifying these elements in seed Cu layers. The alloying element will be present below 1 at percent, less than can be reliably measure with other surface analytical techniques. SIMS analytical methodology and detection limits will be presented for each of these elements in Cu.

MC-TuP4 Growth and Characterization of β -Tungsten Films, Avyaya Jayanthinarasimham, M. Medikonda, A. Matsubayashi, A.C. Diebold, R. Matyi, V.P. LaBella, SUNY Albany, P. Khare, H. Chong, College of Nanoscale Science and Engineering

The giant spin Hall effect (GSHE) is caused by spin orbit interactions in a semiconductor^[1] or metal^[2] that result in a spin current that is transverse to charge current. Recent spin Hall effect studies in the beta phase of metals such as Ta and W produce transverse spin currents strong enough to switch an adjacent magnetic layer^[3]

The metastable β -W is known to exhibit giant spin Hall effect^[8]. Deposition conditions selective to β phase of W need to be understood for the large scale fabrication of devices that utilize GSHE. The growth of α and β phases of Tungsten are strongly governed by thickness^[4], base pressure^[5] and oxygen availability^{[6][7]}.

This poster will present our work on fabricating and characterizing tungsten films, dominated by the β -phase over a large thickness range by adjusting the oxygen content during the growth. Resistivity measurements as well as x-ray photoelectron spectroscopy and x-ray analysis are performed to determine the phase of the tungsten films.

Reference:

- [1] Dyakonov, M.I. Perel, V.I.: Phys. Lett. A 35, 459 (1971)
- [2] J.E. Hirsch, arXiv:cond-mat/9906160
- [3] Luaiao Liu et al. Science 336, 555 (2012)
- [4] D. Choi, et al. J. Vac. Technol. A 29, 051512 9 (2011)
- [5] S.M. Rossnagel et al. J. Vac. Sci. Technol. B20, 2047 (2002)
- [6] S. Basavaiah Appl. Phys. Lett. 12, 259 (1968)
- [7] T. Karabacak et al. Thin Solid Films 493 (2005) 293-293
- [8] C.F. Pai et al. [http://arxiv.org/abs/1208.1711]

MC-TuP6 Some Experience in Characterizing Thin Films on Next Generation 450mm Wafer with Spectroscopic Ellipsometry, Richard Sun, N. Sun, Angstrom Sun Technologies Inc.

Under guidance of International SEMATECH Manufacturing Initiative (ISMI), Angstrom Sun Technologies Inc developed the first tabletop spectroscopic ellipsometer for 450mm wafer application. A few challenges regarding wafer handling and small edge exclusion requirement will be discussed. With improved modeling, spectroscopic ellipsometry could also be used to determine EBR profile of photoresist by linear line scan near the wafer edge.

MC-TuP7 The Effect of Aberration Coefficients on Phase Shift in Electronic Optics, Chien-Nan Hsiao, J.S. Kao, F.Z. Chen, J.L.A. Yeh, ITRC, NARL, Taiwan, Republic of China

The epitaxial SiGe/Simultiple quantum wells (MQWs) were grown by ultra-high vacuum chemical vapor deposition (UHV-CVD) on a single crystalline silicon (111) substrate. Aberration corrected scanning transmittance electron microscopy equipped the high bright electron gun, DCOR aberration corrector, high angle annular dark field (HAADF) detector, and EDS was used to analysis the atomic structure of SiGe/Si interface. The defocus (C1) and aberration coefficients of electronic optics system such as astigmatism (A1, A2, A3, A5), coma (B2, B4), spherical aberration (C3, C5), and star aberration (S3) were corrected precisely by changing the convergence angle of electron beam probe (18 and 25 mrad). It was found that the distance between dumbbell Si and Ge atoms could be directly measured by the HRSTEM HAADF image. The corresponding FFT shows the point resolution was shown higher point resolution. In addition, the effect of aberration coefficients on phase shift in electronic optic (phase plate) was investigated. Furthermore, the experimental results also demonstrated that simultaneously complementary atomic-resolution EDS line-scan signal in HRSTEM HAADF image. These results provide an effective approach to investigate structural chemical element image in real space at the atomic resolution.

MC-TuP8 Modification of Density of States in Iron Chloride Intercalated Epitaxial Graphene with Electric Bias, Taurean Groover, M.D. Williams, Clark Atlanta University

Graphene, an atomic thick layer of carbon in a hexagonal lattice, has received a large amount of attention from researchers across many different scientific disciplines. Within the condensed matter physics community it is fairly well agreed that the electronic, optical, as well as structural properties of graphene are poised to revolutionize the semiconductor industry. This unique collection of properties proves promising but there are some obstacles that need to be addressed before these properties can be fully exploited. Graphene is a semimetal, which means that the conduction and valence bands touch at the Dirac point leaving no band gap to be utilized in semiconductor and optoelectronic devices. In this work we seek to

investigate the electronic characteristics of epitaxial graphene, stage one and stage three ferric(III) chloride intercalated epitaxial graphene. We investigate the opening of a band gap in graphene through intercalation and in conjunction with the application of an appropriate electrical bias normal to the sample surface. Through theoretical calculations, we show that the electrical bias normal to the surface not only tunes the carrier concentration but also has the ability to switch the majority carriers from electrons to holes. The Walt de Heer Confinement Controlled Sublimation method was employed for the production of the epitaxial graphene samples and the two zone vapor transport method was employed for the intercalation of the samples. With the Confinement Controlled Sublimation growth method used, graphene is grown on SiC substrates which make these materials uniquely suited for a smooth integration into existing silicon based electronics. We observe, compare, and interpret the alteration of the density of states as well as the work functions of these samples upon the application of the electric field normal to the sample surface. Analyzing the band structure of these samples, we witness a change of the band structure from that of the AB stacking configuration to that of the decoupled AA stacking configuration. In conjunction with Raman spectroscopy, this confirms the electronic decoupling of graphene layers. Auger spectroscopy was employed to investigate the chemical environment of the near surface region of the samples and may be a viable method for stage number determination in intercalated materials. When intercalated with FeCl₃, the optical transparency of the sample is conserved and the resistivity drops tremendously which makes this material, in particular, uniquely suited for the production of transparent electrodes that can be utilized to improve the performance of Li-Ion batteries.

Magnetic Interfaces and Nanostructures

Room: Hall D - Session MI-TuP

Magnetic Interfaces Poster Session

MI-TuP3 Fabrication and Magneto-Optical Properties of Co-doped ZnO Hollow Nanospheres, Da-Ren Liu, C.J. Weng, ITRC, NARL, Taiwan, Republic of China

Diluted magnetic semiconductors (DMS) have recently attracted considerable attention due to their potential applications for spintronic devices. ZnCoO is one of the most promising diluted magnetic semiconductors materials due to its room temperature ferromagnetism. In this study, Al₂O₃ layer was conformally deposited on the surface of polystyrene (PS) nanosphere with different diameter (300nm~800nm) by atomic layer deposition (ALD). After removal of PS nanosphere by heating, Al₂O₃ hollow nanospheres were formed. Then the Zn_{1-x}Co_xO (x=0.03, 0.05, 0.07) coatings were grown on Al₂O₃ hollow nanospheres by pulsed laser deposition (PLD). According to the results of high-resolution x-ray diffraction, Co-doping does not change the wurtzite structure of ZnO and the Zn_{1-x}Co_xO hollow nanospheres are polycrystalline. The surface and cross-section morphologies of the hollow nanospheres were analyzed using a field-emission scanning electron microscope (FE-SEM). Photoluminescence spectra demonstrate ultraviolet emission peaks which have shift with the increase of Co ion concentration. The magneto-optical properties of the nanospheres were measured by micro-MOKE and x-ray magnetic circular dichroism (XMCD) spectroscopy. The results show the magnetic properties of Zn_{1-x}Co_xO hollow nanospheres strongly depend on the Co composition fraction.

MI-TuP4 Study of Structural, Electronic and Magnetic Properties of (Fe₂O₃)_n Clusters Using Density Functional Theory, Sholeh Alaei, S. Erkoç, Middle East Technical University, Turkey, S. Jalili, Computational Physical Sciences Research Laboratory, School of Nano-Science, Institute for Research in Fundamental Sciences (IPM), Iran (Islamic Republic of)

In this paper, the electronic, magnetic and structural properties of (Fe₂O₃)_n (n = 2-5) clusters were studied using Density Functional Theory. It came out that the most stable structures for n = 2, 3 and n = 4, 5 were ferrimagnetic and antiferromagnetic, respectively. The states with completely geometrical symmetry were spin-symmetric also, i.e. had equal atomic magnetic moments. It was found that by increasing 'n', the binding energy (E_b) increased, while such an observation was not seen for n = 4 and n = 5 and the binding energies were equal in these cases. An interesting result was that one of the states for n = 4 (n4-1) was a half-metallic antiferromagnet, which is important in spintronics applications. The most of the considered clusters were semi-metal or half-metal due to presence of Fe atoms.

Plasma Science and Technology Room: Hall D - Session PS-TuP

Plasma Science and Technology Poster Session

PS-TuP3 Optical Emission Spectroscopy of CH₃F/CO₂ Plasmas and Etching of SiN_x and p-Si, Qiaowei Lou, S. Kaler, D.J. Economou, V.M. Donnelly, University of Houston

CH₃F plasmas are widely used in selective SiN_x etching over Si or SiO₂ with additives like O₂ or CO₂. In this work, inductively coupled CH₃F/CO₂ discharges were studied by optical emission spectroscopy (OES), with rare gas actinometry, as a function of feed gas composition and power (5–400 W), at a constant pressure of 10 mTorr. SiN_x(300 nm on Si) and Si (10 nm on Ge) etching was also studied in "plasma beams" created from both CH₃F/CO₂ and CH₃F/O₂ feed gases. Surfaces and film thicknesses were characterized *in situ* by vacuum-transfer XPS, and *ex situ* by spectroscopic ellipsometry. An abrupt transition in H, F, and O number densities was observed when the CO₂ feed gas was increased above 74-80 vol. %, similar to the enhancement in the number densities of these species above 48% O₂ in CH₃F/O₂ plasmas. These step changes were ascribed to the transition from polymer-covered to polymer-free reactor walls as increasing O₂ or CO₂ additions cause the film etching rate to exceed the deposition rate. Absolute H, F, and O number densities increased with power in CH₃F/CO₂ (20%/80%) plasmas, reaching 0.24, 0.81 and 1.92 × 10¹³/cm³, respectively, at 300W. This gas composition results in polymer-free wall conditions. Compared with CH₃F/O₂ (50%/50%) plasmas, the F and H number densities were lower and the O number density was higher in CH₃F/CO₂ plasmas. A maximum SiN_x etching rate (no bias) of 75 Å/min was observed using a plasma beam effusing from a 50%/50% CH₃F/O₂ compact ICP. A lower maximum SiN_x etching rate of 34 Å/min was found for CH₃F/CO₂ at 25%/75% composition.

PS-TuP5 Simulation and Diagnostic Study on the Large Area Magnetized Inductively Coupled Ar/O₂/CF₄ Plasma, Ho-Jun Lee, E.-J. Son, Y.-G. Kim, Pusan National University, Republic of Korea

Scaling up of inductively coupled plasma (ICP) and capacitively couple plasma (CCP) is important and urgent task for future 450 mm semiconductor wafer processing. A weakly magnetized inductively coupled plasma (MICP) have been introduced as an effort to improve efficiency, stability of low pressure operation and density uniformity of ICP. MICP is a source utilizing cavity mode of low frequency branch of right hand circularly polarized wave.⁽¹⁾ In the previous study, results on the simulation and optical multi-port diagnostics of Ar MICP have been presented.⁽²⁾ In this study we present simulation and experimental results on the properties of ICP and MICP with Ar/CF₄, Ar/O₂/CF₄ chemistry. Flow field calculation of feed gas was included in the self-consistent plasma simulation. Electron density and energy was measured with tuned langmuir probes. Spatially resolved emission spectra were taken with a home-made, wafer type multi-channel optical emission measurement system. In 5 mtorr, Ar/CF₄(5~20%) discharge condition, electron density uniformity of MICP was improved about factor of two compared with that of ICP. Electron density of MICP in Ar/CF₄ discharge was increased by 40 % due to improved power transfer efficient. However electron temperature became more non-uniform in MICP. Simulation results showed that density distribution of neutral species such as CF, CF₂, CF₃ were primarily affected by flow field. Highest density was observed on the top of electrode where the flow velocity was lowest.

PS-TuP6 Molecular Dynamics Simulation Study on Polymer Formation during Silicon Oxide (SiO₂) and Silicon Nitride (SiN) Etching by Fluoro/Hydrofluorocarbon Plasmas, Satoshi Hamaguchi, M. Isobe, K. Miyake, K. Karahashi, Osaka University, Japan, M. Fukasawa, K. Nagahata, T. Tatsumi, Sony Corporation, Japan

For the past several years we have been working on molecular dynamics (MD) simulation on silicon dioxide (SiO₂) and silicon nitride (SiN) etching by fluorocarbon (FC) or hydrofluorocarbon (HFC) ion beams such as CF_x⁺ or CF_xH_y⁺ in order to understand surface reactions and mechanisms of selective etching processes of SiO₂ and SiN by FC/HFC plasmas [1]. In our study, the sputtering yields and surface chemical compositions after etching obtained from MD simulations are compared with those obtained from beam experiments. Recently we have improved the predictive capability of our simulation code and successfully obtained sputtering yields from MD simulation that are in reasonable agreement with those observed in the corresponding beam experiments. In this presentation, we shall discuss what aspects of MD simulation techniques need to be most carefully designed in order for the simulator to reproduce realistic beam-surface interactions.

Selective etching of SiN over SiO₂ or vice versa is widely used in the microelectronics industry. It has been known that, at relatively low incident energy, FC or HFC ions such as CF_x⁺ or CF_xH_y⁺ incident upon a SiO₂ or

SiN surface from the plasma can etch the material surface while forming a thin polymer film on it. The thickness and chemical compositions of such a polymer film sensitively affect the etch rate (i.e., sputtering yield) of the material underneath. Therefore, for an MD simulation to represent beam-surface interactions with high accuracy, the simulation needs to correctly reproduce physical processes of polymer formation. It has been demonstrated that highly accurate carbon (C)-fluorine (F) interatomic potential models including electronegativity of F and an efficient thermostat algorithm to remove excess heat from incident ions are the key for better representation of ion-surface interactions by MD simulation.

[1] K. Miyake, T. Ito, M. Isobe, K. Karahashi, M. Fukasawa, K. Nagahata, T. Tatsumi, and S. Hamaguchi, *Jpn. J. Appl. Phys.* **53** 03DD02 (2014).

PS-TuP7 Development of a Compact Microwave Plasma Density Sensor for Processing Plasma Monitoring. *JinSheng Chiou, W.C. Chen, C.H. Hsieh, K.C. Leou*, National Tsing Hua University, Taiwan, Republic of China

Plasma density is a key parameter that control the property of processing plasmas and hence the processing results. It is thus of great interest to develop a sensor not only for characterization of the plasmas but also for monitoring of the plasma based processes. In this study, a compact microwave plasma density probe was developed and the effect of plasma sheath and pre-sheath was also investigated. The principle of the probe is based on the resonant absorption of microwave of a coaxial antenna immersed in the plasma. In this study, the probe has a outer diameter 0.9 mm, designed to minimize the perturbation to the plasma. It consists of a monopole antenna formed by a short section of the center conductor of a semi-rigid coaxial cable and a glass enclosure. Experimental measurements were carried out in an inductively coupled plasma and the results show that the resonance frequency increase linearly with the source rf power, as expected. The results are also consistent with that from measurements by a Langmuir probe. The compact probe was also investigated numerically by employing a full wave electromagnetic simulation using a finite element code (COMSOL). In the simulation analysis, a coaxial line was attached to the probe head and the "driven mode" was adopted, i.e., the wave was fed into the coaxial line and the absorption spectrum, reflection coefficient vs frequency, was then analyzed. The plasma surrounding the probe was characterized by the collisional electromagnetic plasma permittivity, determined by plasma density, wave frequency and momentum transfer collisional frequency. The simulation results show that the absorption spectrum exhibits a resonance, occurring between the plasma frequency and the surface plasma wave resonance frequency [1]. The effect of plasma sheath and presheath was also studied by the numerical simulation where the sheath (floating) was modeled by an air gap of thickness twice the Debye length while a linear plasma density distribution was assumed for the presheath region. The resonance frequency was also found to be dependent of the probe diameter and antenna length. These results are consistent with the results obtained by experimental measurements. This indicates that one can use the result from numerical simulation as a calibration for the plasma resonance probe measurement.

1. H. Kokura, et al, *Jpn. J. Appl. Phys.*, Pt 1, 38, 5262, 1999.

* Work supported by the National Science Council and the National Center for High Performance Computing of R. O. C. (Taiwan).

PS-TuP8 Impact of Magnetic Neutral-Loop Discharge Plasma on Low-k Dielectrics. *Weiyi Li, S-H. Kim, J. Blatz*, University of Wisconsin-Madison, *B.H. Moon, Y.M. Sung*, Kyungshung University (Korea), *S. Banna, AMAT, Y. Nishi*, Stanford University, *J.L. Shohet*, University of Wisconsin-Madison

The magnetic neutral-loop discharge (NLD) plasma was proposed by Uchida in 1994. We developed an NLD plasma reactor using a stainless-steel chamber, instead of commonly used quartz chamber in previous work. In order to examine the usefulness of this NLD reactor, low-k dielectric films are exposed to the NLD plasma under various conditions.

The structure of the NLD plasma reactor is described as follows. A cylindrical chamber lies in the middle of three sets of magnetic coils. With DC currents flowing in opposite direction in the middle set against side sets of coils, a circle on which magnetic field is zero, i.e. neutral loop(NL), can be produced in the middle of the chamber. In order to generate plasma, 13.56 MHz RF is inductively coupled into the chamber with a spiral antenna, through a quartz window on one end of the chamber. The reactor can be operated at two modes, NLD mode when there are opposite direction DC currents in the magnetic coils, or ICP mode when there are no DC currents or same direction DC currents in the magnetic coils. In NLD mode, the plasma was observed to be brighter near the NL than in the center. This difference was further confirmed with a measurement of optical spectrum using an OceanOptics spectrometer, which shows the relative plasma glow brightness at the NL is as twice high as near the center of the chamber, and about 10% higher than a non-NLD ICP plasma.

By adjusting the ratio of the DC currents running in the magnetic coils, the position of the NL can be changed. Both experiment and simulation show that the glow follows the change of NL, especially at low pressure (<1 mTorr), due to much less collision.

Low-k dielectrics are widely used in modern back-end processing, in order to reduce the R-C delay in interconnection. During processing, low-k dielectrics are often subjected to plasma exposure. The consequent damage to low-k dielectric films is presented and compared with other types of plasma reactors.

This work has been supported by Semiconductor Research Corporation under Contract No. 2008-KJ-1781 and by the National Science Foundation under Grant CBET-1066231.

PS-TuP9 Characterization and Simulation of a VHF Remote Plasma Source. *Scott Polak, D. Carter*, Advanced Energy Industries, *A. Bhoj, A. Roy*, ESI US R&D Inc.

This paper describes a novel, remote source technology using capacitively coupled, VHF energy to produce a flexible and unique plasma generator. The electrode design and internal construction are compatible with most processing chemistries, allowing generation of very low to very high plasma densities across extensive flow and pressure regimes. Furthermore, Langmuir and IEDF probe measurements have illustrated a competency of the remote source to deliver plasma well beyond the output of the apparatus, into large downstream chambers. This ability makes both neutral-radical and downstream ion enhanced processing possible. Due to the enhanced efficacy of this remote plasma source, optimization and characterization across the wide operating range becomes challenging. To facilitate characterization of the remote source and to augment empirical testing, plasma simulation techniques are employed. Commercially available, multi-physics code, CFD-ACE+, is used to simultaneously solve for the electromagnetics, fluid flow, heat transfer, species chemistry and transport equations for non-equilibrium discharges. A summary of the important remote source design elements will be reviewed along with a comparison of actual and simulated results, illustrating details of the plasma generation and distribution from this new technology.

PS-TuP10 Temporally and Spatially Resolved Optical Emission Spectroscopy of Capacitively Coupled Pulsed Plasmas. *John Poulouse, L.J. Overzet, M.J. Goeckner*, University of Texas at Dallas

Pulsed plasma provides a method to 'independently' control ion and neutral fluxes. Temporal and spatial evolutions of the pulsed plasmas have been studied to provide a better understanding of transitory behavior in such systems. The optical emission intensities (OEIs) of various lines (atomic and molecular) from pulsed plasmas through Ar, O₂, and N₂ gases have been collected. The RF power was turned on and off at frequencies of 1, 10 and 100 kHz with a 50% duty cycle. The OEIs measured from argon plasma have shown a longer turn on/off time than those measured from O₂ or N₂ pulsed plasmas. Specifically, the OEIs measured from pulsed argon plasmas are still rising at the end of the on-time and do not completely extinguish at the end of the off-time at 100 kHz. This is in comparison to pulsed plasmas through both O₂ and N₂ in which the OEIs completely extinguish during the off-time and reach an apparent steady state level during the on-time. Additionally, the OEIs contract radially just after the start of the on-time for pulsed plasmas through argon, but a similar radial contraction phase is not found in the other gases. The radial extent of the OEIs in O₂ and N₂ remains essentially constant. We will present these results and the effects of other parameter and gases on the transitory behavior of pulsed discharges.

This material is based upon work supported by the National Science Foundation under Grant No. NSF IIP1338917.

PS-TuP11 Laser-induced Incandescence Diagnostic for In Situ Monitoring of Synthesis of Nanoparticles in Plasma. *James Mitrani, B. Stratton, Y. Raites*, Princeton Plasma Physics Laboratory

A DC arc discharge with a consumed graphite, anode electrode is commonly used for synthesis of carbon nanoparticles, including buckyballs, nanofibers, and nanotubes [1-3]. The graphite electrode is vaporized, leading to nanoparticle synthesis in a low temperature (0.1 – 1 eV), atmospheric pressure plasma. The formation of nanoparticles in this plasma is poorly understood. For example, it is not clear where nanoparticles nucleate and grow in the arc discharge. To tackle this problem, a laser-induced incandescence (LII) diagnostic for in situ monitoring of the nanoparticles' spatial distribution in the plasma is currently being constructed. The LII diagnostic involves heating the particles with a short-pulsed laser, and measuring the resulting spatial and temporal incandescence profiles on longer timescales [4]. By appropriately modeling the spatiotemporal incandescence profiles, one can measure the particle diameters and volume fraction. LII diagnostics have been extensively used to study soot particles in various backgrounds, including laboratory flames, smokestacks, and engines. However, LII has only recently been applied to

study engineered nanoparticles, and has never been applied in a strongly coupled plasma background, such as a carbon arc discharge. Even though the spatial scale-lengths for soot and nanoparticles are similar (10-100 nm), great care is needed in developing an LII diagnostic for monitoring nanoparticles in an atmospheric pressure plasma. Therefore, we will initially calibrate our LII diagnostic by measuring spatiotemporal incandescence profiles of known, research grade carbon particles, including soot and nanoparticles. Preliminary results of this study will be discussed. [1] C. Journet et al. *Nature* 388, 756-8 (1997); [2] A. J. Fetterman et al. *Carbon* 46 1322-6 (2008); [3] M. Keidar et al. *Phys. Plasmas* 17, 057101 (2010); [4] C. Schultz et al. *Appl. Phys B* 83, 333-54 (2006).

PS-TuP12 Influence of Porosity on Electrical Properties of Low-k Dielectrics Irradiated with Vacuum Ultraviolet Radiation. *F.A. Choudhury*, University of Wisconsin-Madison, *J.-F. de Marneffe*, *M. Baklanov*, IMEC, KU Leuven Belgium, *Y. Nishi*, Stanford University, **Leon Shohet**, University of Wisconsin-Madison

During plasma processing, low-k dielectric films are exposed to high levels of vacuum ultraviolet (VUV) radiation emitted from the plasma. To reduce the dielectric constant of organosilicate (OSG) low-k materials, porosities (up to 50%) are introduced in the dielectric layer. The porous structure of these materials makes them even more sensitive to VUV modification due to their low density and deep penetration of photons into the film¹. The effects of VUV photons on the chemical modification of OSG low-k materials as a function of porosity has been reported recently¹ and showed that OSG films having high porosities undergo higher Si-CH₃ depletion and severe chemical degradation. In this work, we investigate the changes to the electrical properties of porous low-k dielectrics as a function of porosity after VUV irradiation. VUV irradiation introduces defect states and generates trapped charges within the dielectric that can degrade the electrical properties of the film². In order to investigate the influence of the porosity on the electrical properties after VUV exposure, organic low-k films of porosities between 15 and 50% were exposed to synchrotron VUV radiation of energies ranging from 6 to 15 eV and fluences up to 5×10^{14} photons/cm² to find the most damaging photon energies. CV measurements showed an increase in the dielectric constant along with a flat-band voltage shift and the presence of hysteresis after VUV irradiation. Initial IV and TDDB measurements indicate an increase in leakage currents along with lower breakdown fields after VUV irradiation. It is likely that these effects will be a function of VUV photon energy.³

This work has been supported by the Semiconductor Research Corporation under Contract No. 2012-KJ-2359 and the National Science Foundation under Grant No. CBET-1066231.

References:

¹ T. V. Rakhimova, A. T. Rakhimov, Yu. A. Mankelevich, D. V. Lopaev, A. S. Kovalev, A. N. Vasil'eva, O. V. Proshina, O. V. Braginsky, S. M. Zyryanov, K. Kurchikov, N. N. Novikova, and M. R. Baklanov, *Applied Physics Letters*, **102**, 111902 (2013)

² H. Sinha, J. L. Lauer, M. T. Nichols, G. A. Antonelli, Y. Nishi, and J. L. Shohet, *Appl. Phys. Lett.* **96**, 052901 (2010).

³ H. Sinha, H. Ren, M. T. Nichols, J.L. Lauer, M. Tomoyasu, N. M. Russell, G. Jiang, G. A. Antonelli, N.C. Fuller, S.U. Engelmann, Q.Lin, V. Ryan, Y. Nishi, and J. L. Shohet, (Focused Review), *Applied Physics Reviews*, *Journal of Applied Physics* **112** 11101 (2012)

PS-TuP13 Ink Cap to Preserve Nanostructure during Sample Preparation for Electron Microscopy. *Brian Krist*, *J.S. Chawla*, *M. Chandhok*, *S.R. Cook*, *H.J. Yoo*, Intel Corporation

Transmission electron microscopy (TEM) imaging of narrow critical dimension (CD) features patterned in low-k materials is critical for functional validation of the patterning process steps. For interconnect applications in particular, low-k porous dielectrics can be mechanically weak and suffer structural damage from plasma processing due to higher carbon content.

Cross-section TEM sample lamellae prepared by focused ion beam (FIB) milling using conventional in-situ protective cap materials like insulator deposition (IDep, eg. TEOS), Pt, and W alter the low-k material line width, edge/surface roughness, and profile due to stress and high energy secondary electron interaction during localized capping. In addition, the conventional cap materials cannot gap fill features trenches that are less than 20 nm wide. Gapfill defects can cause poor mechanical stability during TEM sample preparation and imaging. These defects can also lead to ion beam damage during TEM sample preparation.

In this paper, we investigate the ability of the ex-situ liquid inks as cap material for TEM cross-section sample lamellae to replace conventional in-situ cap materials. The use of ink fill protects the surface from the secondary electron beam damage that occurs using conventional in-situ FIB dual beam capping methods. Ink fill capped samples have undistorted ILD

patterns that hold to zone axis. The ink to Pt FIB mill is matched unlike high dense high stress IDep so both sample thickness and stress are more consistent. Several inks were reviewed and down selected for lack of high aspect ratio fill, or inability to cure out solvents in ink. Cross-section images in this work use either hand dispensed *BIC Mark it*, or automate dispensed using *GenesisEcono-Jet* printer 3440BK INK.

We also demonstrate how ink fill capping enables imaging of the smallest features in interconnect process technology having low-k ILD.

PS-TuP15 Surface Modification to Improve Chemical Resistance of Coatings. *Gregory Peterson*, *W.O. Gordon*, Edgewood Chemical Biological Center, *E.M. Durke*, Excet, Inc.

Coatings are required to demonstrate chemical resistance in order to protect material, vehicles, and personnel. In addition, numerous other requirements for the development of new coatings often involve substantial reformulation efforts in order to adapt to changing conditions and applications. One method to improve chemical resistance of coatings is to modify the surface of the paint to reduce surface energy without changing the bulk; ensuring any bulk properties remain unaltered. Plasma-based chemical vapor deposition (PCVD) of perfluorinated compounds has been used for years to improve resistance of fabrics and materials to water and other chemicals. For example, there are several reports in the literature of superhydrophobic fabrics developed using PCVD. Here we report the application of a PCVD method that not only induces superhydrophobicity to a real world coating, but dramatically improves the resistance of the coating to the spreading and absorption of the chemical warfare agents, HD and VX. Over the 30 min age time, droplets remained pinned and are therefore more easily decontaminated or removed physically. Surface analysis confirms modification of the surface with fluorinated species and also shows etching of the organic components of the paint. This treatment suggests that surface modification strategies may be effective in improving chemical resistivity, without changing the bulk properties, or requiring a significant reformulation effort.

PS-TuP16 The Effect of Electron-Molecule Collision Cross Sections on Plasma Models. *Sebastian Mohr*, Quantemol Ltd, UK, *J.R. Hamilton*, *A. Asokan*, *J.C. Tennyson*, University College London, UK

Discharges in reactive gases such as SF₆ and C₄F₈ are commonly used for industrial etching and deposition processes. The necessary surface reactions are induced by the free radicals in these discharges which are created by electron impact and heavy particle collisions. The process speed is thus usually determined by the densities of the free radicals, a prior knowledge of these densities and their dependence on parameters such as the pressure, input power or the gas composition is desired.

Numerical simulations of reactive gas discharges are employed to systematically study the chemical reaction rates and particle densities as functions of the aforementioned parameters. Furthermore, a reliable set of rate coefficients or cross sections for the included reactions are needed.

Quantemol-N, which provides full accessibility to the well-known UK molecular R-matrix codes [1], is used to model electron polyatomic molecule interactions including those with radicals. A wide range of cross-sections, otherwise not available experimentally are calculated for the required plasma chemistries. An expert system, Quantemol-VT, based on the Hybrid Plasma Equipment Model (HPEM) [2] is then used to model plasma tool on a reactor scale.

We provide results of a systematic study of a C₄F₈ discharge which is commonly used for deposition during the Bosch process. This study further compares the effect of including cross sections calculated with Quantemol-N against use of datasets comprising only known and commonly used cross sections taken from experimental studies. A plasma model of the discharge in a GEC cell is provided for a plasma chemistry containing C_xF_y radical reactions (calculated with Q-N) and without. The two models are compared and the role of C_xF_y radicals in plasma processing is highlighted.

[1] Tennyson, J., Brown, D., Munro, J., Rozum, I., Varambhia, H. and Vinci, N. (2007). Quantemol-N: an expert system for performing electron molecule collision calculations using the R-matrix method. 86(1), p.012001.

[2] Kushner, M. (2009). Hybrid modelling of low temperature plasmas for fundamental investigations and equipment design. *Journal of Physics D: Applied Physics*, 42(19), p.194013.

PS-TuP17 Development of Microwave-driven 1- and 2-Dimensional Microplasma Arrays and Tests of Atmospheric-Pressure Film Deposition. *Alan Hoskinson*, *H.C. Thejaswini*, *J. Hopwood*, Tufts University

Microwave-driven microplasmas allow for the generation of cold atmospheric-pressure plasmas at higher time-averaged electron densities (~10¹⁴ cm⁻³) than most other techniques. These high densities may open unique regimes for high-pressure materials processing. The low ion

energies (due to the short mean free paths at atmospheric pressure) may be partially compensated for by extremely large fluxes of ions and energetic metastable species while maintaining low gas temperatures. We present data from exploratory experiments showing rapid deposition of diamond-like carbon films at atmospheric pressure using a single microplasma. The development of one- and two-dimensional arrays of such microplasmas demonstrates a path towards film deposition on moderate-area substrates.

This work was partially supported by the DARPA Microscale Plasma Devices program (Dr. Dan Purdy, Program Manager) under awards FA9550-12-1-0006, managed by Dr. John Luginsland through AFOSR, and N00014-13-1-0619 managed by Stephen Pappert through ONR.

PS-TuP18 Mechanical Property of Polyurethane Nanocomposite Film with Carbon Nanotubes Functionalized by Atmospheric Dielectric Barrier Discharge. *D. Ogawa, Keiji Nakamura*, Chubu University, Japan
Polymers composited with carbon nanotubes (CNTs) have been researched for many years to modify their material properties. This is because a polymer is mechanically soft and electrically insulated. The mix of CNTs is a good idea because CNTs can compensate the weakness of the polymer by making composites.

The functionalization of CNTs is a common technique for their applications due to chemical inertness of CNTs. This is why CNTs are generally difficult to disperse well in a liquid, while CNTs can disperse well after a functionalization. Nitric acid (HNO₃) is commonly used to functionalize carboxyl group on CNTs. The functional group is modified to the functional group to fit one's application. It is reported that plasma can also functionalize CNTs without using the acid by making reactive species generated in plasma.[1]

We want to enhance the mechanical property of polyurethane (PU) film (approximately 100µm thickness) through functionalized multi-wall CNTs (MWCNTs). In order to achieve our goal, we created a dielectric barrier discharge (DBD) above the CNTs that is located at the bottom of a quartz test tube. The discharge was created with the peak-to-peak voltage at 9 kV, the frequency at 10 kHz, and the discharge pressure at atmospheric pressure. Our process gas was made with a certain combination among argon, nitrogen, hydrogen, and oxygen gas depending on the functionalized group we want to attach on the CNTs. Here, Fourier transform infrared (FTIR) spectrometer was used to identify the functional groups attached by plasma discharge. After the plasma treatment, the CNTs were dispersed into a tetrahydrofuran (THF) solvent. The solvent is so versatile because the solvent is miscible to water and dissolvable even to non-polar solution. Some parts of the CNTs were dispersed in a THF solvent so that the concentration of the CNTs in the solvent was found from the transmission of the light at 600 nm. The PU film formed after drying out the mixture of the solvent and the PU solution over night.

In order to evaluate the strength of the PU film, the PU film was rubbed with a sand paper for hours. Here, we compared the wearing rate of the PU film that is defined by dividing the film thickness over the time when the PU film was completely rubbed out. The mechanically stronger the PU polymer is, the more wearing rate was observed.

In the presentation, we will show our recent progresses of the PU film that contains the CNTs functionalized with atmospheric DBD plasma.

[1] A. Felten, C. Bittencourt and J. Pireaux, *Nanotechnology* 17 (2006) 1954–1959

PS-TuP20 Development of a Low Cost and Portable Needle Type DBD Jet Operated under Atmospheric Pressure. *Chieh-Wen Chen, Y.J. Yang, C.C. Hsu*, National Taiwan University, Taiwan, Republic of China

A low cost and portable needle-type DBD jet operated under atmospheric pressure is developed. The plasma jet is comprised of an inner grounding electrode made of stainless steel rod, a quartz tube serving as the dielectric layer, and an outer powered ring electrode that is attached to the outer surface of the quartz tube. The quartz tube is 6-cm long with inner and outer diameters of 6 and 8 mm, respectively. A needle (25G) is attached to one side of the quartz tube that serves as the exit nozzle. This jet is powered by a low cost portable power that is commercially available (PVM 12, Information Unlimited, USA). Helium with a flow rate below 2 slm is used as the plasma gas. With this arrangement, a jet approximately 2 mm long can be extended out of the needle tip. The key features of this jet are (i) low cost: less than USD\$100 per system, (ii) portable, and (iii) equipped with a robust needle. Diagnostic studies of this plasma jet and using it for materials processing with a spatial resolution down to 1 mm will be presented.

PS-TuP21 Development of Low Cost and Flexible Microplasma Generation Devices Operated under Atmospheric Pressure. *Chih-Ming Wang, T.H. Lin, Y.J. Yang, C.C. Hsu*, National Taiwan University, Taiwan, Republic of China

Microplasmas are plasmas with geometric dimension less than 1 mm. Due to its miniature size, fabrication of microplasma generation devices frequently involves high cost materials and/or processes, such as semiconductor manufacturing processes. In this work, we present the development of two types of low-cost flexible microplasma generation devices: devices made on paper substrates and on flexible printed circuit board (PCB). The former is made of paper, conductive carbon paste, and tape, while the latter is fabricated using commercially available process that makes printed circuit board. We examine the stability of the discharge and the lifetime of the devices. When the paper-based device is assembled as a dielectric barrier discharge (DBD)-type device, stable array of discharges can be sustained for tens of minutes. When it is assembled as a micro-hollow cathode discharge (MHCD)-type system, no array of discharge can be obtained and the device lifetime is no longer than 3 min. For the PCB-based device, stable array of discharges can be sustained for longer than one hour. The use of the PCB-based device to perform gas conversion is also demonstrated. CO₂ decomposition forming CO and O₂ is chosen as the system to test. It is shown that the power efficiency above 7% can be obtained under selected conditions.

PS-TuP22 A Low Cost and Flexible Microplasma Generation Device to Create Hydrophobic/Hydrophilic Contrast on Nonflat Surfaces. *Yao-Jhen Yang, C.C. Hsu*, National Taiwan University, Taiwan, Republic of China

This work presents a cost-effective (less than a quarter per device) and easy-to-fabricate dielectric-barrier-discharge-type (DBD-type) microplasma generation device for maskless surface patterning. This device was made of double-side copper laminate. A process to define circuit patterns on printed circuit board was utilized to define the electrodes required for the microplasma generation device. This device was then utilized for maskless surface patterning, either creating hydrophobic patterns on hydrophilic surfaces or hydrophilic patterns on hydrophobic surfaces. The former patterns were obtained by plasma polymerization of *c*-C₄F₈ precursor under He atmosphere to form fluorocarbon on designated regions on glass surfaces. The optical emission spectrum shows the CF₂ emission (250 nm–380 nm), suggesting the dissociation of precursor molecules. The FTIR spectrum of the deposited film shows strong CF₂ absorption peak at 1250 cm⁻¹. The contact angle of the film ranges from 102 to 105 degree. The hydrophilic patterns on hydrophobic surfaces were obtained by treating a fluorocarbon-coated surface using this plasma-generation device under ambient air. Non-flat surface patterning using this device will be demonstrated. (This work was supported by National Science Council of Taiwan, the Republic of China 101-2221-E-002-163-MY2)

PS-TuP23 Control of Plasma in Solution Using Bipolar Pulsed Voltage. *Fei-Hung Huang, C.Y. Chou, H.W. Chang, C.C. Hsu*, National Taiwan University, Taiwan, Republic of China

This work presents control of plasmas in saline solution using bipolar pulsed DC power. It is known that plasma of such a type generates inside the gas-phase that composes of water vapor, oxygen, and hydrogen through joule heating and/or electrolysis. We use a 1-ms-wide positive pulse of 550 V to ignite the plasma. Prior to this positive pulse, a 10-ms-wide pre-pulse is applied to generate electrolytic gas. By changing polarity the pre-pulse, namely positive pre-pulse (mode++), negative pre-pulse (mode-+), or without the pre-pulse (mode0+), the gas composition can be tailored. Optical emission spectroscopy shows OH, H, and O emissions, which implies that the plasma generates hydroxyl, H, and O radicals. We used a chemical probe, disodium salt of terephthalic acid, to quantify the formation rate of OH radicals using photoluminescence spectroscopy. To assess how the power type influences the efficiency in organic degradation, acid orange 7 (AO7) was chosen as the model organic materials. AO7 decolorization was quantified using ultraviolet-visible adsorption spectroscopy. AO7 degradation kinetics was fitted using 1st order kinetics. It is shown that mode-+ has a higher AO7 degradation rate constant as well as higher OH radical formation rate.

PS-TuP24 The Effect of the Electrode Diameter on the Behavior of Plasmas in Saline Solution. *Shen-Chieh Lin, C.C. Hsu*, National Taiwan University, Taiwan, Republic of China

In this presentation, the effects of the electrode diameter on the discharge behavior of plasmas in saline solution are studied. The plasma is driven by a bi-polar DC pulse power source with an applied voltage up to 700V and a pulse width above 0.05 ms. The driving electrode is a platinum wire covered by a glass tube to precisely define the area exposed to the solution. Platinum wires of four different diameters, namely 0.1 mm, 0.3 mm, 0.5 mm, and 1 mm, were used. The grounding electrode is a bare platinum wire

0.5 mm in diameter and it is immersed in 0.1 M NaCl solution. Current and voltage probes are used to monitor the current and voltage waveforms across the electrode surface. A high speed camera is used to capture the bubble behavior and plasma appearance. An optical emission spectrometer is used to analyze plasma emission light. It is found that the breakdown voltage decreases with the electrode diameter. At a given applied voltage, the current peak value and the emission time delay upon the onset of the voltage pulse both increase with the electrode diameter, while the power density increases with the decrease in the electrode diameter.

PS-TuP25 Surface Treatment Using Portable Dielectric Barrier Discharge Device, Yao-Yi Kuo, W.S. Zseng, C.M. Wang, C.C. Hsu, National Taiwan University, Taiwan, Republic of China

A portable dielectric barrier discharge device operated under one atmosphere is developed and the use of this device for surface treatment is performed. This device consists of a powered electrode made of a copper plate, a ground electrode made of stainless steel woven wire mesh, and a quartz plate 1 mm in thickness that serves as dielectric barrier between powered and ground electrode. This device is driven by a portable power source that is commercially available. This power source supplies voltages up to 20 kV with a frequency of 20-50 kHz. This plasma system is compact and low cost. Surface treatment under air, argon, and nitrogen atmosphere on PET, glass, and PTFE substrates to enhance hydrophilicity is performed. It is found that the water contact angle of the glass surface decreases from 40° to below 10° after treated using this device for 5 min operated in air and argon. For PET surface treatment under argon atmosphere, the contact angle decreases from 70° to 20° after 5 min of treatment. Due to its low cost and compact size, this portable DBD device shows great potential in various applications where portable devices are desired.

PS-TuP27 RF Pulsing Technology on Commercial CCP(Capacitively Coupled Plasma) Dielectric Etcher and ICP(Inductively Coupled Plasma) Conductor Etcher., Taeho Shin, SEMES, Republic of Korea

RF pulsing technology in dry etcher had been developed about 20 years ago. But recently as the device node falls below 20nm (pitch size) many etch problems such as profile distortion, poor uniformity control, etc. become critical issue to be cleared. Many commercial dry etchers are currently introducing various pulsing technologies on their process chamber to overcome those process issues. They have claimed many process merits with RF pulsing. However one of the main problems in RF pulsing in mass production fabs lies in slower etch rate and unstable plasma. We also have developed RF pulsing technology on our CCP type dielectric etcher and ICP type conductor etcher. We have tested and optimized many different RF configurations such as RF frequencies pulsing, DC(Direct Current) pulsing and secondary electrode pulsing. One of tested configurations, we have found that secondary electrode DC pulsing with 3 different RF frequencies biased wafer electrode showing higher etch rate with improved mask selectivity as well as controlled bottom CD(critical dimension). Those results might be due to the fact that higher density plasma with higher ion energy is generated by enhanced electron energy distribution function(EEDF) and narrowed high energy ion density with DC pulsing.

PS-TuP28 Plasma Damage Characterization in Backbone Carbon Organosilicate Glass Low-k Films - with Backbone Chains (-Si-R-R-Si-) and (-Si-R-Si-), Haseeb Kazi, R. James, S. Gaddam, J.A. Kelber, University of North Texas

X-ray photoelectron spectroscopy (XPS) and FTIR data indicate that organosilicate glass (OSG) films with backbone carbon (-Si-(CH₂)_x-Si-) exhibit significantly enhanced resistance to carbon loss upon exposure to O₂ plasma, atomic oxygen (O³P) and vacuum ultraviolet photons (VUV+O₂) at 10⁻⁴ Torr O₂ compared to films with terminal methyl groups (Si-CH₃). Two different low-k films with backbone structures (-Si-(CH₂)₂-Si-) and (-Si-CH₂-Si-) were investigated separately. Films incorporating backbone ethyl groups (-Si-(CH₂)₂-Si-) were deposited from 1,2 bis (triethoxysilyl) ethane (BTESE) precursor by ebeam or plasma cross-linking with achievable dielectric constant (k) ~3.00. XPS spectra for PECVD and ebeam cross-linked films are similar. The effects of (O³P) on ebeam cross-linked film indicates negligible carbon loss or Si oxidation, combined with C-O bond formation, under conditions where OSG films with terminal methyl groups exhibit > 80% carbon loss within the surface region of the film. C-O bond formation is never observed for terminal CH₃ groups. Further, backbone carbon (-Si-(CH₂)₂-Si-) films exposed to VUV+O₂ exhibit self-limiting, minimal net carbon loss and formation of C-O bonds within the surface region. In separate experiments, low-k films with methylene bridging unit (-Si-CH₂-Si-) were investigated which contains a mixture of (-Si-CH₂-Si-) and (-Si-CH₃) bonding environments in the final deposited film (k=2.55). Data indicate these backbone carbon (-Si-CH₂-Si-) films when exposed to O₂ plasma exhibit higher carbon removal rate for terminal groups (-Si-CH₃) whereas carbon in the linking chain (-Si-CH₂-Si-) undergo relatively slower removal rate, with Si-O, C-O bond formation.

This indicates that O₂ plasma-induced Si-C bond rupture still occurs in the linking unit, but with a low probability of simultaneous rupture of both Si-C bonds required for abstraction of an in-line methylene bridging group. The data thus demonstrate that OSG films containing backbone carbon groups exhibit greatly reduced rates of carbon loss in the presence of O₂ plasma, atomic O or VUV+O₂ compared to films with terminal carbon groups due to fundamentally different patterns of Si-C bond scission. The results reported here demonstrate the potential for OSG films with backbone carbon to resist O₂ plasma damage.

Acknowledgement: This research was supported by Semiconductor Research Corporation under Task ID: 2561.001. Authors acknowledge Dr. Alfred Grill for providing the carbosilane based backbone low-k films and also acknowledge Dr. Geraud Dubois for stimulating discussions.

PS-TuP29 A Continuous Plasma-Liquid Interface formed by a Laminar Flow Liquid Water Jet and Atmospheric-pressure Microplasma, BrittanyPaige Bishop, S. Ghosh, I. Morrison, D. Scherson, R. Akolkar, R.M. Sankaran, Case Western Reserve University

Reactions at the interface of a plasma and a liquid surface have recently become important for applications in wastewater treatment, materials synthesis, and therapy. These experiments are typically carried out between an atmospheric-pressure plasma jet and a static liquid surface (i.e. liquid bath or film). Here, we present a continuous plasma-liquid interface formed by an atmospheric-pressure microplasma and an open air, laminar flow liquid water jet.

A vertically falling water jet is formed in open air by pumping liquid water through a microcapillary. The stability of the water jet is explained by the Plateau-Rayleigh instability. At low flow rates, surface tension leads to the breakup of the jet into droplets. At high flow rates, the jet becomes turbulent and again breaks up. The water jet is found to be highly stable at intermediate flow rates where the water jet is laminar, with a relatively constant diameter of 500 μm over lengths of more than 30 mm. This allows the microplasma to be stably formed at the surface of the water jet and current to flow across the plasma-liquid interface to a counter electrode. The system is characterized with the microplasma operating by current-voltage measurements. We find that the overall resistance is strongly influenced by the inter-electrode distance and the ion concentration in solution, suggesting that solution conductivity dominates the electrical conductivity of our system. This is explained by a simple model based on a geometrical approximation for the water jet which shows that the resistance of the water jet is large because of the confined volume.

We have applied this newly developed system to the synthesis of metal nanoparticles. Aqueous solutions of silver nitrate are formed as a liquid water jet and pumped through the plasma-liquid interface. A distinct color change is observed as the silver nitrate is reduced by the microplasma to silver nanoparticles. The solutions are characterized by ultraviolet-visible (UV-vis) absorbance spectroscopy and transmission electron microscopy (TEM) which confirm crystalline, nanometer-sized silver particles. We find that the particle production rate depends on the plasma current and the liquid water jet flow rate, the latter of which is consistent with a space time approximation for the reactor.

PS-TuP30 Anomalous Electron Cross-Field Transport in a Low Pressure Magnetized Plasma For Material Processing Applications, Yevgeny Raitses, Princeton Plasma Physics Laboratory

The application of the magnetic field in a low pressure plasma can cause a spatial separation of cold and hot electron groups. This so-called magnetic filter effect is used for many plasma applications, including ion and neutral beam sources, plasma processing of semiconductors and nanomaterials, and plasma thrusters. In spite of successful practical applications, the magnetic filter effect is not well understood. In this work, we explore this effect by characterizing the electron and ion energy distribution functions in a plasma column with crossed electric and magnetic fields. Experimental results revealed a strong dependence of spatial variations of the plasma properties across the magnetic field on the gas pressure. In particular, the results showed the existence of the gas pressure threshold below which the increase of the magnetic field leads to a more uniform profile of the electron temperature. This surprising result is due to anomalously high electron cross-field transport that causes mixing of hot and cold electrons. For xenon and argon gases, this threshold is ~ 1 motrr. At higher gas pressures, a stronger separation of cold and hot electrons, which is favorable for the above applications, was observed.

Novel Trends in Synchrotron and FEL-Based Analysis

Focus Topic

Room: Hall D - Session SA-TuP

Synchrotron Analysis Poster Session

SA-TuP1 Soft X-ray Spectroscopy Reveals Chemical Information beneath the Surface of Organic Photovoltaic Devices, Claudia Fleischmann, IMEC, Belgium, P. Hönicke, M. Müller, B. Beckhoff, Physikalisches Technische Bundesanstalt (PTB), Germany, E. Voroshazi, J. Tait, T. Conard, IMEC, Belgium, W. Vandervorst, IMEC, KU Leuven Belgium

While inorganic photovoltaic devices (PV) remain the main choice for large-scale energy production, *organic photovoltaic devices* (OPV) show great potential for future, environmentally friendly energy sources. Their semi-transparency, light-weight and unique opto-electrical properties combined with the possibility to shape OPV devices at will enable new applications where PV has never been used before. Similar to their inorganic counterparts, the underlying physical mechanisms and hence the performance and efficiency of organic devices is directly linked to their physicochemical properties. Revealing these properties is often very challenging due to the limited sensitivity and specificity of standard analytical techniques used for inorganic semiconductor characterization. In addition, it is highly desirable to probe the device structure as close as possible to a real one, which typically comprises organic-inorganic interfaces, intermixed phases being based on the same constituent atoms, or multilayer structures of a few tens to hundreds of nanometer thickness.

In this contribution we will examine the capabilities of *Near-Edge X-ray Absorption Fine Structure Spectroscopy* (NEXAFS) for the chemical characterization of (complete) bulk-heterojunction OPV device structures based on conjugated polymers and fullerene derivatives including P3HT, PCDTBT, DPP and PCBM. We will show that the high chemical sensitivity of the carbon K-edge (~290eV) NEXAFS permits to distinguish between the common organic semiconductors in these devices, providing a tool for compositional analysis and miscibility studies. By using fluorescence yield detection the information depth is extended far beyond the surface, in contrast to electron yield detection, allowing to probe non-destructively the bulk properties of (buried) layers in the OPV structure. In this context, we will also illustrate the remaining metrology challenges and investigate the sensitivity of the sulfur and nitrogen K-edge NEXAFS to be used for degradation studies. Finally, we will discuss the stability of these organic materials under x-ray irradiation, which is particularly critical for synchrotron radiation-based methods.

SA-TuP2 Exact, Efficient Calculation of Synchrotron Radiation-Proximity and Angle Effects, Eric Shirley, NIST

We evaluate synchrotron radiation for a circular orbit using Graf's addition theorem for Bessel functions. Using Debye's and Olver's asymptotic expansions, the exact radiation fields can be calculated without recourse to assuming large distance from the tangent point and without using truncations as in Schwinger's work. Thus, the present results should be both numerically robust and efficient, requiring no numerical integration. The results are applied to assessing the accuracy of the Schwinger formula for radiometric applications. The formulas are particularly well suited for long wavelengths and for measurements at end stations close to the storage ring. Application areas are typically UV and x-ray instrument calibration for such purposes as found on environmental satellites. By carrying out this work, we can gain a quantitative sense on the accuracy of various approximations that can be made, and hence their consequential suitability.

Advanced Surface Engineering

Room: Hall D - Session SE-TuP

Advanced Surface Engineering Poster Session

SE-TuP1 Oxidation and Nanopatterning of Thin Metal Films on Flexible Substrates via Oxygen Directed Irradiation Synthesis, Zachariah Koyn, B. Holybee, S.N. Srivastava, J.P. Allain, University of Illinois at Urbana-Champaign

Ion bombardment of polycrystalline thin metal films is known to induce nanometer-scale surface patterning, including ripples and dots^{1,2}. Additionally, the irradiation of metals with oxygen ions has been shown to induce surface oxidation, with a state dependence on fluence³. This work seeks to unravel the directed irradiation synthesis of oxide-based thin-films, in particular ZnO thin-films, with low-energy irradiation-driven

mechanisms on dissimilar material substrates, such as polymer-based systems. This examines the dual effects of oxygen irradiation as a method of both oxidizing and patterning metal thin-films at ambient temperatures. This represents a scalable process in growing and functionalizing metal-oxide thin-films on polymers, which are sensitive to the high temperatures required in thermal oxidation processes. Ion-beam sputtering (IBS) is known to induce surface nanopatterning in multi-component systems⁴ with simultaneous modification of surface chemistry. Irradiation with O⁺ is performed at grazing incidence near 70° with particle energies between 25-1000 eV at ambient temperatures. X-ray photoelectron spectroscopy investigates the resulting oxidation states as a function of fluence from early-stage nanopattern formation near 10¹⁵ cm⁻² up to fluences nearing a coarsening regime. Atomic force microscopy examines pattern formation under similar conditions. These results are then adapted to nanostructured thin-films on flexible substrates, namely polydimethylsiloxane (PDMS) about 1-mm thick and 1-cm². The ability to fabricate heterostructures on transparent, flexible substrates offers exciting applications in areas such as gas sensors, biosensors, and photonics⁵. Additional benefits of an oxygen ion beam are the chemical changes (formation of SiO groups, introduction of water and gaseous byproducts) induced in the PDMS substrate as the active thin-film is nanostructured. Oxidation of this polymer has been shown to induce significant temporary hydrophilicity⁶ and thus provide for an effective bioactive nanostructured biointerface for in-situ endovascular protocols.

¹ D. Ghose, J. Phys. Condens. Matter **21**, 224001 (2009).

² P. Gailly, C. Petermann, P. Tihon, and K. Fleury-Frenette, Appl. Surf. Sci. **258**, 7717 (2012).

³ N. V. Alov, Nucl. Instruments Methods Phys. Res. Sect. B Beam Interact. with Mater. Atoms **256**, 337 (2007).

⁴ O. El-Atwani, S. Ortoleva, A. Cimaroli, and J.P. Allain, Nanoscale Res. Lett. **6**, 403 (2011).

⁵ I.-S. Hwang, Y.-S. Kim, S.-J. Kim, B.-K. Ju, and J.-H. Lee, Sensors Actuators B Chem. **136**, 224 (2009).

⁶ H. Hillborg, J.F. Ankner, U.W. Gedde, G.D. Smith, H.K. Yasuda, and K. Wikstro, Polymer (Guildf). **41**, 6851 (2000).

Surface Science

Room: Hall D - Session SS-TuP

Surface Science Poster Session

SS-TuP1 Visible Light Photocatalytic Degradation of Methylene Blue using Ag₂O Nanostructures, Z.-H. Yang, Szetsen Lee, Chung Yuan Christian University, Taiwan, Republic of China

Various kinds of Ag₂O nanostructures were prepared by a precipitation reaction of silver nitrate, ammonium nitrate, and sodium hydroxide with different mixing ratios and temperatures. The band gap values of Ag₂O nanostructures were measured using diffuse uv-visible reflectance spectroscopy. The photocatalytic activity of Ag₂O nanostructures was tested with the degradation reaction of methylene blue (MB) in aqueous solutions. A halogen lamp with a cut-off filter (> 400 nm) was used as the visible light source. The intensity variation of the 664 nm absorption peak of MB was monitored. The photocatalytic degradation rate of MB varies with the shapes of Ag₂O nanocrystals. The degradation rates of MB were correlated with the measured band gap values of Ag₂O. The efficiency of visible-light photocatalytic performance of Ag₂O nanostructures is discussed.

SS-TuP3 Formation of Copper Nanoparticles on a Surface of OH-terminated ZnO Powder Material, Hsuan Kung, A.V. Teplyakov, University of Delaware

Cu/ZnO catalyst is one of promising catalysts commonly used in industry for methanol synthesis, methanol steam reforming, and hydrogen production reactions. Two typical methods to prepare this catalyst are wet chemistry or vacuum-based techniques. In this study, we grew Cu nanoparticles on zinc oxide (ZnO) powder at room temperature using common chemical vapor deposition precursors, such as hexafluoroacetylacetonate copper(I) vinyltrimethylsilane, (Cu(hfac)(VTMS)) under high vacuum conditions. Before deposition, exposing ZnO powder to the gas-phase water to form a hydroxyl-terminated monolayer was able to enhance the growth of copper nanoparticles. In-situ FTIR studies showed that the intensity of the infrared signatures of hydroxyl groups decreased following exposure to copper precursor and confirmed copper deposition. X-ray photoelectron spectroscopy and Auger electron spectroscopy studies determined that Cu(I) species are the dominant products present on the surface. Cu nanoparticles grown on ZnO(000-1), ZnO (10-10) and defect sites were visualized by Scanning

electron microscopy. This Cu/ZnO surface covered with strongly bound hfac ligands was then annealed to different temperature to remove surface contamination. The thermal chemistry involved in this process and the chemical stability of the surface-bound ligands will be discussed.

SS-TuP4 Radical Reactions with Organic Surfaces, Robert Chapleski, D. Troya, Virginia Tech

Motivated by recent ultra-high-vacuum surface experiments, we have used electronic structure methods, quantum mechanical/molecular mechanical calculations, and molecular dynamics simulations to investigate the structure and reactions of radicals with organic surfaces.

For the first reaction being studied, that of ozone with C60 fullerene, we have characterized stationary points in the potential energy surface for the reactions of O₃ with C60 that include both the formation of primary ozonide and subsequent dissociation reactions of this intermediate that lead to C–C bond cleavage. We have also investigated the addition of multiple O₃ molecules to the C60 cage to explore potential reaction pathways under the high ozone flux conditions used in recent experiments. The lowest-energy product of the reaction of a single ozone molecule with C60 that results in C–C bond breakage corresponds to an open-cage C60O₃ structure that contains ester and ketone moieties at the seam. This open-cage product is of much lower energy than the C60O + O₂ products identified in prior work, and it is consistent with IR experimental spectra. Subsequent reaction of the open-cage C60O₃ product with a second ozone molecule opens a low-energy reaction pathway that results in cage degradation via the loss of a CO₂ molecule. Our calculations also reveal that, while full ozonation of all bonds between hexagons in C60 is unlikely even under high ozone concentration, the addition of a few ozone molecules to the C60 cage is favorable at room temperature.

We have also investigated the reaction of nitrate radicals with functionalized self-assembled monolayer surfaces. Specifically, using quantum mechanical/molecular mechanical calculations, we have calculated vibrational modes of nitrate-SAM products that are consistent with IR experimental spectra. Also, using molecular dynamics simulations, we are able to describe the orientation of the alkanethiol chains that form the surface in order to provide insight into reaction mechanisms under further experimental study.

SS-TuP5 Degenerate Phases of Iodine on Pt(110) at Half-Monolayer Coverage, N. Oberkalmsteiner, M. Cordin, Stefan Duerrbeck, E. Bertel, University of Innsbruck, Austria, J. Redinger, Vienna University of Technology, Austria, C. Franchini, University of Vienna, Austria

Iodine-surface interactions are of considerable interest in sustainable-energy research. For instance, Iodine is used as redox shuttle in dye-sensitized solar cells and serves as a promoter in photocatalytic water splitting. In most of these applications, Pt is involved either as an electrode or as co-catalyst or both. As part of a general study of Pt-halogen interaction we discuss here the adsorption of Iodine on Pt(110) at a coverage (Θ) of 0.5 monolayers (ML). The I/Pt(110) adsorbate system was investigated by scanning tunneling microscopy (STM), low-energy electron diffraction (LEED) and by density functional theory (DFT) calculations using both, the LDA and the GGA approximation. Remarkably, three different phases involving occupation of two different binding sites were found to coexist at $\Theta = 0.5$ ML. While the observed phases are similar to the ones reported for Br on Pt(110)^{1,2}, the preferred binding sites are different. The structure of defects in the adsorbate layer as well as the dynamics at the transition between the nearly degenerate phases is not the same as the one in a Br layer indicating a shifted balance of adsorbate-substrate binding and inter-adsorbate repulsion. The $c(2 \times 2) \rightarrow (3 \times 2)$ phase transition shows evidence for a long-range interaction. The latter phase also involves a surprisingly strong buckling in the Pt surface amounting to 15% of the interlayer distance. While the DFT calculations reflect the energetic details of the $c(2 \times 2)$ phase with stunning precision, they only partially reproduce the experimental results from the (3×2) phase. Comparison with literature data shows that the iodine adlayer is almost floating on Au(110) and uniaxially compressible on Pd(110), while on Pt(110) Iodine adsorption is tied to specific adsorption sites, precluding the formation of compression structures.

¹ E. Doná, T. Loerting, S. Penner, et al., Physical Review Letters **98**, 186101 (2007).

² M. Cordin, B. A. J. Lechner, S. Duerrbeck, et al., Sci. Rep. **4** (2014).

SS-TuP6 Reaction of Hydrazine with Cl-terminated Si(111) Surface, Fei Gao, A.V. Teplyakov, University of Delaware

This work focuses on obtaining well-defined surface of silicon functionalized with hydrazine to produce an oxygen-free platform for further functionalization. Single crystalline Si(111) surface has been prepared using modified RCA procedure to produce a well-defined H-terminated Si(111) surface. Next, Cl-terminated Si(111) surface is prepared

from H-terminated Si(111) surface using PCl₅ in chlorobenzene solvent with trace amount of benzoyl peroxide as a reaction initiator under nitrogen atmosphere following previously established procedures. Hydrazine-functionalized Si(111) sample is obtained from Cl-Si(111) surface with anhydrous hydrazine at 35°C under Ar atmosphere. To confirm the presence of Si-N bonds following this procedure and to establish the structures of surface species produced, we followed the reaction by Fourier-transform infrared spectroscopy, X-ray photoelectron spectroscopy, and time-of-flight secondary ion mass spectrometry. To study the configuration of Si-NH_x groups on the surface, result was compared with the results of phenylhydrazine reactions on Cl-terminated silicon surface by wet chemistry method and also on clean silicon surface under ultrahigh vacuum (UHV) condition. Density functional theory (DFT) calculations were performed to infer the mechanisms of surface reactions and to compare the predicted vibrational spectra and core-level energies with the results of experimental studies.

SS-TuP8 Synthesis of Formate Species on Cu Surface using CO₂ Molecular Beam, Tetsuya Ogawa, Q. Jiamei, T. Kondo, J. Nakamura, University of Tsukuba, Japan

The methanol synthesis by hydrogenation of CO₂ attracts a great deal of attention because this process can realize the direct conversion of CO₂ into a useful chemical feedstock. In a present industrial process using Cu/ZnO-based catalyst, however, the reaction requires high pressure (50-100 bar) and high temperature (200-300°C). If this reaction proceeds at a mild reaction condition, it would be a very attractive process to convert CO₂. But the detailed process of the reaction is not well understood. We focus on the formate synthesis on Cu surfaces, which is the first step of the methanol synthesis reaction. Our previous studies suggest that this process proceeds by the translational and vibrational energy of CO₂ molecules. The kinetic analysis of formate synthesis suggests that the mechanism of the reaction can be an Eley-Rideal type, in which gaseous CO₂ directly reacts with hydrogen atoms on Cu surfaces [1]. DFT calculation also suggests that the activation barrier can be overcome by supplying energy to CO₂ molecules [2]. In this work, we conduct formate synthesis with translationally and vibrationally hot CO₂ molecules to prove the mechanism of formate synthesis on Cu surfaces.

The translational and vibrational energy of CO₂ molecules is controlled by the supersonic molecular beam technic. Firstly hydrogen atoms are pre-adsorbed on Cu single crystal with hot tungsten filament. Then CO₂ molecular beam is irradiated to H/Cu surface. The relation between the energy of incident CO₂ molecules and the formation of formate are investigated using temperature programmed desorption and infrared reflection absorption spectroscopy.

[1] H. Nakano, I. Nakamura, T. Fujitani, and J. Nakamura, *J. Phys. Chem. B* **2001**, 105, 1355

[2] G. Wang, Y. Morikawa, T. Matsumoto, and J. Nakamura, *J. Phys. Chem. B* **2006**, 110, 9

SS-TuP9 Chemical and Electronic Structure of (Y_{1-x}Ca_x)CrO₃, (0.00 ≤ x ≤ 0.15) in Core Levels and Valence Band by XPS and DOS, Lazaro Huerta, R. Escamilla, M. Cruz, A. Duran, Universidad Nacional Autónoma de México

Polycrystalline samples of (Y_{1-x}Ca_x)CrO₃ with 0.00 ≤ x ≤ 0.15 were synthesized by combustion method. The samples were studied by X-ray diffraction (XRD) and photoelectron spectroscopy (XPS). Results of refinement of Rietveld shows that the cell volume decrease occurs through the change from Cr(III) to Cr(IV) as a result of the charge compensation of the Ca doping. XPS was used to investigate the binding energies of the Y 3d, Cr 2p, Ca 2p, and O 1s core level and Y 4d, Cr, 3d Ca 3d and O 2s contributions of valence band. The valence band measurement is consistent with the calculations of the band structure calculated near the Fermi level.

SS-TuP10 Wettability of MgO-P₂O₅ Glasses: Relation between Bulk and Surface Properties, Naoya Yoshida, N. Masuda, M. Yamada, T. Okura, Kogakuin University, Japan

MgO-P₂O₅ glass system shows anomalous changes in bulk properties, such as density, with changing in its composition; density does not simply

increase with increase of MgO composition, and significantly decreases at around meta composition (50MgO-50P₂O₅). This phosphorus oxide anomalies derive from local structural changes between tetrametaphosphate and pyrophosphate structures. Wettability, one of the important surface properties, depends on surface energy and surface roughness, therefore, with samples of constant surface roughness, wettability simply reflects surface energy, which relates with chemical composition and structure of the surface.

Here, we prepared MgO-P₂O₅ glasses with changing composition from 35MgO-65P₂O₅ to 55MgO-45P₂O₅, and studied the relation between their

bulk properties (density and solubility in water) and wettability. As a result, simple relation was found among wettability, density, and

solubility in water. Of course, wettability is only a surface phenomenon, however, the results suggested that bulk properties are possibly estimated by measurements of wettability. We will discuss the results of other glass systems such as $\text{Na}_2\text{O-B}_2\text{O}_3$.

SS-TuP11 Preparation and Characterization of Photocatalytic Thin Films of Zn-doped Calcium Phosphate, Yuji Nakamura, N. Yoshida, T. Okura, Kogakuin University, Japan

Ti-doped hydroxyapatite (TiHAP), partially substituted Ca^{2+} with Ti^{4+} , exhibits photocatalytic activities such as decomposition of organic compounds similar to that of TiO_2 , as our group has reported. Oxidation power of TiHAP seems to be weaker than that of TiO_2 , and, it shows excellent adsorption ability derived from hydroxyapatite structure. The mechanism of photocatalytic activities of TiHAP is still unknown, however, Ti-doping and/or defects derived from Ti-doping are thought to play an important role in photocatalytic reactions. Here, we tried to fabricate thin films of Zn-doped calcium phosphate, and to evaluate those photocatalytic activities.

Transparent and homogeneous thin films of Zn-doped calcium phosphate were successfully fabricated from a solution of zinc nitrate, calcium nitrate, and phosphorus oxide by spin-coating on glass substrates and following calcination. Several characterizations, such as UV-vis transmission and reflection spectroscopy, X-ray diffraction analysis, and surface structural analysis by atomic force microscope, were carried out. Methylene blue decomposition tests under irradiation of UV light suggested that photocatalytic activity was improved by Zn-doping.

SS-TuP12 Critical Review and Recommended Values of Work Functions for Low Index Faces of Clean Metal Surfaces, Gregory Derry, Loyola University Maryland

Despite the fundamental interest and technological importance of the work function, the standard reference tables of this quantity used by the surface science community are outdated, incomplete, and include flawed experimental information. In this work, a thorough critical review of the entire literature is undertaken, with both the cleanliness and characterization of the surfaces and the reliability of the experimental techniques examined. Unreliable data is rejected and realistic uncertainty estimates are made for the all of the comparatively reliable data. Based on this information, recommended values of the work functions and their uncertainties are presented for all clean metal surfaces with low index crystal faces for which good data exists, along with updated tables that include all of the primary references and relevant information needed to evaluate each surface and generate such recommended values. Details of the evaluation protocols employed are also presented. It is anticipated that the information presented here will be useful both in technological applications (such as electrochemistry and microelectronics) and in the testing of theoretical models for electrons at metal surfaces.

SS-TuP13 Unveiling Hidden Information in Temperature-Programmed Desorption-Reaction Data: Identification of Desorbing Compounds by Their Desorption and Fragmentation Patterns, JuanCarlos Rodríguez-Reyes, Universidad de Ingeniería y Tecnología, UTEC, Peru, J.-M. Lin, J. Zhao, A.V. Teplyakov, University of Delaware

Temperature-programmed desorption/reaction (TPD/R) experiments are very powerful for providing information in several fields related to surface science, including heterogeneous catalysis, thin film precursor analysis and thermal treatments. Data can be, however, very complex and difficult to extract, especially when competing reaction pathways yield products with similar spectrometric features. We present a mathematical method for analyzing TPD/R data, which is able to extract, for each desorbing compound, its desorption pattern and its fragmentation pattern. This method is called multivariate curve resolution (MCR) and, briefly, requires the organization of data (e.g. "n" m/z traces followed over "t" temperature points) as a (n x t) matrix, which can be seen as the product of two matrices, (n x k) and (k x t), where k is calculated by considering variations and correlations between m/z traces. Interestingly, k turns out to be the number of components (compounds desorbing from a surface), and its value is limited not only by correlations between data points, but also by the fact that intensities in the two matrices cannot be negative. Therefore the two matrices correspond to the fragmentation pattern, (n x k) matrix, and to the desorption pattern, (k x t) matrix. Since it is a mathematical method, MCR is applicable even when no previous knowledge of the system under investigation is available. However, any available information can be used as constraints that guide the outcome, increasing the accuracy of the resolution. The usefulness of this method is demonstrated using datasets from a variety of surface reactions, including the reaction of ethyl halides

with a Si(100) surface and the thermal decomposition of the TiN precursor tetrakisdimethylamido titanium, TDMAT.

SS-TuP14 Dependence on an O₂ Gas Flow Rate of NiO Thin Films Prepared by Reactive Magnetron Sputtering, Tomokazu Tsuchiya, I. Takano, Kogakuin University, Japan

As one solution to the power shortage and global warming, a renewable energy such as solar cells is desired. Silicon-based solar cells having over 30% in the theoretical efficiency are the present mainstream, however the single crystal-silicon has a problem on the manufacturing cost. Further more the high purity silicon that is the main raw material for solar cells is insufficient worldwide, and so a new solar cell without silicon that is replaced silicon-based solar cells has been required. Practical application of oxide-based thin film solar cells is expected in reduction of energy costs or environmental loads.

Generally a typical oxide-based thin film solar cell is a wet dye-sensitized solar cell composed of an electrolyte, an electrode of titanium oxide and a sensitizing dye. Recently a solid-state dye-sensitized solar cell which uses metal oxides instead of an electrolyte has been studied.

In our previous study on $\text{TiO}_2/\text{Cu}_2\text{O}$ solid-state dye-sensitized solar cells, the problem was Cu diffusion from underlayer Cu_2O . The diffusion of Cu induced collapse of p-n junction. In this study, we used NiO as a next p-type oxide semiconductor instead of Cu_2O . The NiO thin film is used as the transparent oxide semiconductor. Most of the transparent oxide semiconductors are an n-type semiconductor, while NiO is a p-type semiconductor. The NiO thin films prepared by changing an oxygen gas flow rate were evaluated by crystallinity, optical properties, semiconductor properties, surface morphology in comparison with Cu_2O thin films.

NiO thin films were fabricated by reactive magnetron sputtering. As substrates, the glass (Corning#1737) and ITO-film coated glass were ultrasonically cleaned. The NiO thin film was deposited on those substrates using pure metallic nickel (99.99%) as a sputtering target material in an oxygen gas atmosphere. The flow rate of an argon gas for sputtering was 20 sccm. The flow rate of an oxygen gas was changed at 2.0 sccm, 2.7 sccm, 3.2 sccm, 3.7 sccm and 4.4 sccm. A thickness of the NiO thin films was kept at about 200 nm.

The NiO thin films were successfully fabricated by reactive magnetron sputtering. The XRD pattern of the NiO thin film showed the stronger peak at the (012) crystal plane of NiO, when the flow rate of an oxygen gas was lower. The resistivity of NiO thin films showed a higher value than that of Cu_2O thin film and the mobility of NiO thin films showed a lower value than Cu_2O .

SS-TuP15 Properties of Cu/Ti Thin Films on the Biodegradable Resin Irradiated by an Ar⁺ Ion Beam, Ryosuke Tan, I. Takano, Kogakuin University, Japan

Recently, biodegradable resin attracts attention as one of the effective use of resources on environmental measures. PGA (Polyglycolic acid) used in this study is categorized to a kind of polyester resin and is composed of hydrogen, carbon and oxygen. PGA shows a high gas barrier property, a high hydrolysis property and high mechanical strength. These characteristics are applied for sutures of surgery or multi-layer PET bottles, while there is hardly application in an electronic field. The usage of PGA in electronic parts such as a printed circuit board has the important role in environmental measures, however there are some problems that have to be overcome.

In this study, the surface of PGA was modified by using an ion beam so that the durability of the PGA coated with metal films was improved. The ion beam cut off the bonding of molecules and as a result the surface of PGA turned to a carbon layer which was stable against heating or humidity. Double layer films of Cu/Ti were deposited on the modified PGA by vacuum evaporation. The Ti layer between the Cu film and the modified PGA (carbon layer) improved adhesion and electrical conductivity. The ion beam irradiation and vacuum evaporation were performed using the high current ion implanter with an electron beam evaporator. The ion beam was extracted from the bucket-type ion source with multi-aperture electrodes of 100 mm in diameter.

The Ar^+ ion irradiation conditions were controlled at a current density of 20 $\mu\text{A}/\text{cm}^2$, an acceleration voltage of 1 kV and irradiation time of 50 s. The deposition conditions of Ti were kept at a deposition rate of 0.3 nm/s and were changed a film thickness of 0-200 nm. The deposition conditions of Cu were kept at a deposition rate of 0.3 nm/s and a film thickness of 200 nm. The kind of prepared samples was the metal coated PGA sample, the ion irradiated PGA sample and the metal coated sample on the irradiated PGA. The sample hardness was measured by a load-unloading method using a micro-hardness tester with a Knoop indenter. Electrical conductivity of metal films was calculated from V-I characteristics measured using the

four probe method. A surface chemical-bonding state was investigated by X-ray photoelectron spectroscopy.

The Ti layer between the Cu film and the carbon layer improved adhesion and electrical conductivity of samples. Those properties showed the maximum value at 50 nm in a Ti thickness, while the excess Ti-layer thickness decreased those properties. The measurement results of electrical conductivity suggested the possibility of PGA used as a printed circuit board.

SS-TuP17 Understanding the Growth and Activity of Monometallic and Bimetallic Clusters on TiO₂(110), Randima Galhenage*, University of South Carolina, *H. Yan*, Brookhaven National Laboratory, *D.A. Chen*, University of South Carolina

The study of metal clusters on single-crystal oxide supports has garnered much attention as model systems for fundamental investigations of surface activity that can guide the rational design of new catalyst. We have studied the growth and activity of monometallic and bimetallic clusters on TiO₂(110) for metals such as Au, Co, Pt and Re, since these metals are known to have desirable properties for alcohol reforming and oxidation reactions. Scanning tunneling microscopy studies show that the cluster size and number of nucleation sites for these metals depend on the mobility of each metal on the titania surface. In general, the diffusion length decreases with increasing metal-titania bond strengths, and DFT studies show that the metal-titania bond strengths can be predicted directly from metal-oxygen bond strengths. Bimetallic clusters (Au-Co, Pt-Co, Pt-Re) were prepared from sequential deposition by growing the metal with the lower mobility first, followed by the more mobile metal. In general, exclusively bimetallic clusters are formed when the number of seed clusters generated from the deposition of the first metal provides a sufficient number of nucleation sites for the second metal. Surface compositions for the clusters were investigated by low energy ion scattering spectroscopy; for metals that do not alloy in the bulk, like Co and Au, core-shell structures are formed, and the surface composition is determined by the relative surface free energies. For metals that are bulk miscible, like Co-Pt and Pt-Re, both metals exist at the surface, regardless of the relative surface free energies. The chemical activity of the bimetallic clusters for CO adsorption and methanol reaction were investigated by temperature programmed desorption experiments. The addition of Au and Pt to Co clusters increased the thermal stability of the surface intermediate by inhibiting C-H bond scission and resulted in H₂ and CO desorption at higher temperatures.

SS-TuP18 Conductivity of Graphene as a Function of its Lattice Orientation Relative to Substrate Layers, Hyunsoo Lee, KAIST, Republic of Korea, *Y. Qi*, Okinawa Institute of Science and Technology Graduate University, Japan, *S. Kwon*, KAIST, Republic of Korea, *M.B. Salmeron*, Lawrence Berkeley National Laboratory, *J.Y. Park*, KAIST, Republic of Korea

We report strongly varying electrical transport properties of graphene layers on graphite that depend on the relative lattice orientation of the surface and subsurface layers. Employing the pressure dependence of conductance on the surface of highly ordered pyrolytic graphite (HOPG) using the conductive tip of an atomic force microscope as an electrode, we found that the electrical conductivity of graphite terraces separated by steps can vary by large factors of up to 100. This effect can be attributed to interlayer interactions when stacked commensurately in a Bernal sequence (ABAB...), which opens a band gap, while rotational misaligned layers behave as graphene. Small angular misorientations of a few degrees were found to give rise to large increases in the conductivity of the top layer, with the maximum occurring at around 30°. In addition, two types of steps were encountered on HOPG surface: external steps where the edge C atoms have dangling or broken bonds, and internal steps where the bonds are only broken in the second layer or deeper. Accordingly, graphite layers covering several underlying terraces and steps retain the same conductivity across the terraces. Top layer terraces have higher friction on the edges, making it easy to distinguish them from subsurface steps where no friction changes occur. These results suggest new applications for graphene multilayers using stacked layers at various angles to control the resistance of connected graphene ribbons in devices.

* Morton S. Traum Award Finalist

SS-TuP19 Electron Percolation via In-Gap States in Semiconductor Quantum Dot Arrays, Yingjie Zhang, University of California, Berkeley and Lawrence Berkeley National Laboratory (LBNL), *D. Zherebetsky*, *S. Barja*, *L. Lichtenstein*, LBNL, *N.D. Bronstein*, University of California, Berkeley, *P. Alivisatos*, University of California, Berkeley and LBNL, *L.-W. Wang*, LBNL, *M.B. Salmeron*, University of California, Berkeley and LBNL

Charge hopping and percolation in disordered semiconductors has been widely studied, but the microscopic nature of the percolation process is not understood and has never been determined. Here we directly image the charge percolation pathways in 2-D PbS quantum dot (QD) arrays using Kelvin probe force microscopy. We showed that the electrons percolate via in-gap states (IGS) instead of the conduction band, while holes percolate via valence band states. This exotic transport behavior is explained by the electronic structure and energy level alignment of the individual QDs, which was measured by scanning tunneling spectroscopy. Density functional theory and spectroscopic analysis show that the IGS are induced by oxygen molecules adsorbed on the QDs' surface. These states are partially hybridized with the valence band states, enabling inter-IGS coupling and electron transport via IGS. Surface chemical treatments open the way of defect engineering, achieving tunable electronic structure and transport properties by controlling the IGS.

SS-TuP20 Mechanisms of CO Oxidation on Well-defined Pd Oxide Films on Pd(111), Feng Zhang, T. Li, University of Florida, *L. Pan*, *A. Astagiri*, The Ohio State University, *J.F. Weaver*, University of Florida

The surface chemistry of late transition-metal oxides has attracted significant attention due largely to observations that the formation of metal oxide layers can drastically alter the catalytic performance of parent metals in applications of oxidation catalysis. For example, previous *in situ* studies have shown that CO oxidation over palladium undergoes a significant rate increase when the palladium surface becomes oxygen rich. This observation has been attributed to the formation of various types of palladium oxide layers or surface oxygen phases, though the reaction mechanisms have not been determined in detail. In this presentation, I will show results of recent experiments and density functional theory (DFT) calculations in which we studied CO oxidation on well-defined Pd oxide surfaces. In the experiments, we utilized mass spectrometry to investigate the CO oxidation kinetics on both surface and bulk Pd oxides during TPRS and under isothermal conditions and used reflection absorption infrared spectroscopy (RAIRS) to monitor the evolution of CO binding states and hence the formation of new surface phases as the oxides undergo reduction.

In direct rate measurements under isothermal condition, we find that the initial reaction rates are nearly ten times larger on PdO(101) compared with the Pd₅O₄ surface oxide, demonstrating that PdO(101) has a much higher intrinsic activity toward CO oxidation compared with the surface oxide. The measurements also show that the reactions occur on both oxide surfaces in an autocatalytic fashion, where the CO₂ generation rate increases as oxygen on the surface is consumed. The RAIRS data shows that the reduction of PdO(101) by CO initially creates oxygen vacancies and that CO preferentially binds to atop-Pd sites located next to the O-vacancies. This atop CO-species yields a characteristic IR peak between 2090 cm⁻¹ and 2060 cm⁻¹. DFT results agree very well with the measured C-O stretching frequencies, and further show that CO achieves significantly stronger binding on an atop-Pd site located next to an oxygen vacancy vs. on the pristine PdO(101) surface. In addition to oxygen vacancies, we also find that surface metal domains develop during the early stages of isothermal reaction of CO on PdO(101) and the Pd₅O₄ surface oxide, except that on the Pd₅O₄ surface CO reaction only leads to the creation of metallic domains without producing oxygen vacancies. Thus, the autocatalytic kinetic behavior observed for both oxides arises from a similar mechanism wherein surface reduction during CO oxidation continually creates sites that bind CO strongly and thus facilitate the adsorption and subsequent reaction of CO.

SS-TuP21 Surface Structure and Chemistry of Rh(110) Model Catalyst under Reaction Condition and during CO Oxidation, Luan Nguyen, *L. Liu*, *S. Zeng*, *F. Tao*, University of Notre Dame

Heterogeneous catalysis is a chemical process performed at a solid/gas or solid/liquid interface. An elevated pressure of a reactive environment could cause materials surface likely to restructure geometrically and electronically to adapt to the surroundings. Since catalytic performance (activity, selectivity, promotion effect, deactivation, etc.) depends on the surface structure of a catalyst during the reaction, it is necessary to study the surface under reaction condition (a reactant) and during catalysis (a mixture of all reactants).

Since a high pressure of a reactant gas typically results in high adsorbate coverage, one alternative approach to mimic the gas environment of a high pressure is to increase coverage of adsorbate by lowering the catalyst

temperature. However, decreasing of catalyst temperature in low pressure environment is only valid when entropy effects are negligible and the relevant adsorption structure is not kinetically hindered. In fact, the magnitudes of entropy contribution to the surface free energy in ultrahigh vacuum (UHV) and under an ambient pressure of a reactant gas are actually different by about 0.3 eV or even larger. Therefore, pressure-dependent entropy can lead to large restructuring of catalyst surfaces. It is difficult to predict how a system will respond to the change of pressures of gases and temperatures of catalysts. Here we will present an in-situ investigation of a model catalyst surface Rh(110) which revealed interesting restructuring of Rh(110) surface in pure CO and a mixture of CO and O₂ in the temperature range of 25°C-130°C.

In UHV environment clean Rh(110) surface exhibits a (1x1) structure. However, upon O₂ adsorption at elevated temperature (approximately 500 °C), the surface reconstructs to an O-covered (1x2) missing row structure, namely Rh(110)-(2x2)p2mg-O. High pressure STM and ambient pressure XPS were used in in-situ studies of surface chemistry and structure of Rh(110) in the mixture of CO and O₂. Initially, the Rh surface exhibits a (1x2) missing row structure. During CO (0.08 Torr) oxidation with O₂ (0.02 Torr) at room temperature, the (1x2) structure reconstructs to form (1x1) islands. Interestingly, no surface reconstruction was observed when Rh(110)-(2x2)p2mg-O surface was exposed to only one reactant gas, CO or O₂ at room temperature, or in the mixture of CO and O₂ at in the pressure range of 10⁻⁷ Torr. The surface chemistry and structure of Rh(110) in pure CO, O₂ and mixture of CO and O₂ at different temperatures and pressures will be presented. A correlation between surface chemistry and structure of this catalyst during CO oxidation and its catalytic activity will be discussed.

SS-TuP22 Mechansim of Formation of Zinc Oxide Nanostructures Synthesized by Photon Irradiation, Rupali Nagar, Symbiosis Institute of Technology (SIT), Symbiosis International University (SIU), India, *A. Praveen, S. Ramaprabhu*, Indian Institute of Technology Madras, India

Zinc oxide (ZnO) is a wide bandgap semiconductor with strong room temperature luminescence, high electron mobility and good transparency. These properties make it an attractive transparent conducting oxide rendering it suitable for optical and photovoltaic applications. It is imperative to devise synthesis techniques that are quick, safe, economical, and easy to implement. In this direction, ZnO nanostructures were synthesized by photon irradiation technique by using different sets of precursors and reducing agents. The synthesized nanostructures were characterized by X-ray diffraction, scanning and transmission electron microscopy, and optical properties investigated by UV-Visible and Raman spectroscopy. Various aspects of the synthesis procedure are compared to understand the mechanism of formation of nanostructures, and the effects of pH, irradiation time that impact the morphology and yield of ZnO nanostructures are discussed.

SS-TuP23 Crystallization and Phase Separation Kinetics of Organic Molecules from Solution on Si(111) Substrates, Miriam Ceza, R.J. Phaneuf, University of Maryland, College Park

Understanding the underlying science behind the arrangements of small organic molecules in mixtures is important for numerous technological applications, among which organic solar cells (OSCs) are especially noteworthy, given the drive toward alternative energy sources. An important process on which organic solar cells depend is the phase separation of organic small molecules. The spontaneous formation of a particular morphology during phase separation from a solvent-based, bimolecular solution onto a substrate depends on several parameters, including relative molecular concentrations, solubilities of each type of molecule in the solvent, mutual interaction between molecules of the same species, interaction of individual molecules with the substrate surface, solvent evaporation rate, and annealing conditions. In this work, we carry out a study of molecular mixtures consisting of tetranitro zinc-phthalocyanine (tn-ZnPc) and [6,6]-phenyl-C₆₁-butyric acid methyl ester (PCBM) using chloroform as a solvent, and native oxide-covered Si(111) substrates. We investigate the role that the solvent evaporation rate during deposition, followed by solvent vapor annealing (SVA), plays on the formation of phase separated mixtures and their crystallization and phase transformation. We also investigated the relative concentration of individual molecules in the mixtures. We found that the PCBM molecules alone undergo several phase transformations as the evaporation rate of the solvent decreases and upon SVA, while the tn-ZnPc molecules alone are very stable. Moreover, the concentration of the phthalocyanine molecules in the mixture with the PCBM highly affects the crystallization process of the latter.

Vacuum Technology

Room: Hall D - Session VT-TuP

Vacuum Technology Division Poster Session and Student Poster Contest

VT-TuP2 Performance Evaluation of Scroll Pump, Fan-Chun Hsieh, P.H. Lin, C.S. Yu, F.Z. Chen, National Applied Research Laboratories, Taiwan

Scroll pumps are widely used in solar-optic and semiconductor industry for backing purpose. The performance of scroll pump could affect the operation of production line significantly. Here, we compared the performance of scroll pump before and after maintenance. The ultimate pressure and acceleration were measured. The ultimate pressure decreases slightly from 5x10⁻¹ Torr to 2x10⁻² Torr. The RMS magnitude of acceleration shows a maximum peak which occurs at about 30 Hz. Moreover, small peaks were also observed in the spectrum. The small peaks were high before maintenance compared to after maintenance. We speculated that this trend is due to the damage of ball bearing and wear of tip seal. The proposed measurements provide a considerable advancement in maintenance of pump.

VT-TuP3 Reliability Engineering Study of TMPs and Cryopumps, JongYeon Lim, K.M. Choi, K.M. Baik, Korea Research Institute of Standards and Science, Republic of Korea, *S.Y. In*, Korea Atomic Energy Research Institute, Republic of Korea, *S.K. Lim*, National Nano Fab Center, Republic of Korea, *D.Y. Koh*, Korea Institute of Machinery and Materials, Republic of Korea, *W.S. Cheung*, Korea Research Institute of Standards and Science, Republic of Korea

Methods of the characteristics evaluation of vacuum pumps are well-defined in the international measurement standards such as ISO, PNEUROP, DIN, JIS, and AVS. HV pumps such as TMPs and cryo-pumps, essential equipment in the advanced industry, require very objective engineering reliability for ascertaining their performance estimation.

Developmental effort for establishing reliability engineering evaluation infra-structure of TMPs and cryo-pumps has been conducted in the manner of component level test, characteristics evaluation and field tests in KRISS.

Until now reliability study for vacuum pumps is not well developed since there are so many unknown factors are prevailing in vacuum industry. However, the increasing needs for the reliability engineering in real field are continuously rising. In this reason we have currently developed the partial reliability engineering evaluation system of high vacuum pumps. In the case of TMPs and cryo-pumps, we shortly try to remark the developmental flow of reliability chain in the fields as follows;

TMPs:

1. Characteristics evaluation – pumping speed, ultimate pressure, etc.
2. Endurance evaluation – Continuous starting and stopping operation (10 % to 90 % RPM)
3. Field Test – NNFC Etcher system
4. Quality assurance evaluation – magnetic field tolerance valuation system
5. Destructive test,

Cryo-pumps:

1. Component evaluation – Refrigerator evaluation
2. Characteristics evaluation – pumping speed, ultimate pressure, etc.
3. Field Test – NNFC Sputter system
4. Quality assurance evaluation .

In this presentation we suggest the methodological approach to the completion of high vacuum pump development through a reliability engineering study

Acknowledgements: Results are partially attributed to two national project (Contract No. 10031836) sponsored by the Korean Ministry of Knowledge Economy, and KRISS main project 14011016.

VT-TuP4 Improved Threshold Ionisation Mass Spectrometry, D.L. Seymour, S. Davies, Alan Rees, P. Hatton, Hidden Analytical, UK

Threshold ionisation mass spectrometry (TIMS) is well established as a technique for improving on standard methods of residual gas analysis, particularly when the dominant peaks in the mass spectrum occur at very nearly the same mass/charge ratio. The mass peaks are then difficult to separate using standard quadrupole mass spectrometric methods. We have described elsewhere several applications in which TIMS has proved to be very effective. More recently, we have examined ways in which the

interpretation of TMS measurements can be improved by fitting to the experimental data trend lines calculated from theoretical expressions.

VT-TuP5 The XHV Cathode Preparation System of the "High Current High Polarization" Electron Gun for the Proposed eRHIC Project. *Omer Rahman, I. Ben-Zvi, E. Wang, T. Rao, J. Skaritka,* Brookhaven National Laboratory

A very compact cathode preparation chamber for the high current high polarization gun for the proposed Erhic project has been designed and assembled at the Brookhaven National Laboratory. This preparation chamber is used to prepare GaAs cathodes to be used to extract electron beam in the multi-cathode gun. Preparation of GaAs strictly requires XHV environment and this system is able to achieve that in a consistent way. In this paper, the construction of the vacuum system including different components, the procedure and pressure results over more than a year of study will be discussed.

Wednesday Morning, November 12, 2014

2D Materials Focus Topic

Room: 310 - Session 2D+EM+NS+SS+TF-WeM

Novel 2D Materials

Moderator: Evan Reed, Stanford University

8:00am **2D+EM+NS+SS+TF-WeM1 Silicene and Germanene: Novel Graphene-like Artificial Silicon and Germanium Allotropes, Guy Le Lay, Aix-Marseille University, France** **INVITED**

Silicene, graphene's cousin, and germanene, a new born in Terra Plana, are predicted to combine the unique electronic properties of graphene associated to quasiparticles behaving as massless Dirac fermions to a character of two-dimensional topological insulators, and, even, possibly, high temperature superconductors. In this talk, I will present fundamental results on these novel synthetic 2D materials, which do not exist in nature, but which might open the way to practical applications, because of their expected direct compatibility with the current nano/micro electronic technologies.

8:40am **2D+EM+NS+SS+TF-WeM3 Silicon Growth at the Two-Dimensional Limit on Ag(111), Andrew Mannix, B.T. Kiraly, Northwestern University, B.L. Fisher, Argonne National Laboratory, M.C. Hersam, Northwestern University, N.P. Guisinger, Argonne National Laboratory**

Bulk silicon has played a dominant role in the growth of microelectronics over the past 50 years. Considering the immense interest in two-dimensional (2D) materials (e.g., graphene, MoS₂, phosphorene, etc.), the growth of Si in the 2D limit is of high relevance to the evolution of electronic materials. Utilizing atomic-scale, ultra-high vacuum (UHV) scanning tunneling microscopy (STM), we have investigated the 2D limits of Si growth on Ag(111). In agreement with previous reports of *sp*²-bonded silicene,^{1,2} we observe the evolution of ordered 2D phases, which we attribute to apparent Ag-Si surface alloys. At sufficiently high Si coverage, we observe the precipitation of crystalline, *sp*³-bonded Si(111) domains. These domains are capped with a $\sqrt{3}$ honeycomb phase that is indistinguishable from the $\sqrt{3}$ honeycomb-chained-trimer (HCT) reconstruction of Ag on Si(111).^{3,4,5} Additional evidence suggests that silicon intermixing with the Ag(111) substrate is followed by the precipitation of crystalline, *sp*³-bonded silicon nanosheets. These conclusions are supported by *ex-situ* atomic force microscopy (AFM), Raman spectroscopy, and X-ray photoelectron spectroscopy (XPS). Even at the 2D limit, scanning tunneling spectroscopy shows that the *sp*³-bonded silicon nanosheets exhibit semiconducting electronic characteristics.

[1] Vogt, P., *et al.* Silicene: Compelling Experimental Evidence for Graphene-like Two-Dimensional Silicon. *Phys. Rev. Lett.*, 108(15), 155501 (2012).

[2] Feng, B., *et al.* Evidence of silicene in honeycomb structures of silicon on Ag(111). *Nano Lett.*, 12(7), 3507–11 (2012)

[3] Le Lay, G. Physics and electronics of the noble-metal/elemental-semiconductor interface formation: A status report. *Surf. Sci.*, 132(1-3), 169–204 (1983).

[4] Aizawa, H., Tsukada, M., Sato, N., & Hasegawa, S. Asymmetric structure of the Si(111)- $\sqrt{3}\times\sqrt{3}$ -Ag surface. *Surf. Sci.*, 429 (0–5) (1999).

[5] Ding, Y., Chan, C., & Ho, K. Structure of the ($\sqrt{3}\times\sqrt{3}$) R30° Ag/Si(111) surface from first-principles calculations. *Phys. Rev. Lett.*, 67(11), 1454–1458 (1991).

9:00am **2D+EM+NS+SS+TF-WeM4 Growth, Structure, and Properties of 2D SiO₂ Polymorphs, Eric Altman, J. Götz, X. Zhu, A. Sonnenfeld, U.D. Schwarz, Yale University**

Recently it has been shown that SiO₂ can form closed 2D bilayers; because the layers have no dangling bonds they are expected to interact solely through van der Waals interactions. Despite the expected weak interactions, hexagonal crystalline bilayers on Pd(100) are stretched 4% to match the lattice constant of the substrate. Both electron diffraction and STM reveal that the size of the crystalline domains is limited along Pd[011] and one of the other bilayer close-packed directions but was long along the third one. The formation of regular domain boundaries on the square Pd substrate is attributed to stress relief in the crystalline layer. *Ab initio* calculations indicate that much of the remaining strain energy can be relieved by allowing the film to relax along the incommensurate direction. In this way the square substrate actually aids the templating of the overlayer despite the severe geometric mismatch. The calculations also indicate that the bilayer is surprisingly compliant, explaining the lattice matching despite the weak

interaction and poor match. Amorphous bilayers could also be prepared on Pd(100). Atomic-scale features in STM images of the amorphous film could be associated with 4-9 membered rings of corner-sharing SiO₄ tetrahedra. In addition to the structural heterogeneity, spectroscopic STM imaging revealed electronic heterogeneity with oxygen sites joining larger rings of corner-sharing SiO₄ tetrahedra fading at low bias; spectra revealed two distinct electronic states responsible for this phenomenon. MBE growth of silica bilayers on graphene layers grown on epitaxial Ru on sapphire will also be discussed.

9:20am **2D+EM+NS+SS+TF-WeM5 Layer-dependent Electronic and Vibrational Properties of SnSe₂ and SnS₂ 2D Materials, Joseph Gonzales, R. Schlaf, I.I. Oleynik, University of South Florida**

Layered metal chalcogenides possess a wide range of unique electronic properties, which are currently explored for applications as novel two-dimensional electronic materials. SnS₂ and SnSe₂ layered materials consist of covalently bonded S-Sn-S (Se-Sn-Se) sheets bonded together by weak van der Waals interactions. The atomic, electronic and vibrational properties of SnS₂ and SnSe₂ thin films are investigated using first-principles density functional theory (DFT). The accurate prediction of electronic and optical properties of SnS₂ and SnSe₂ layered 2D materials is achieved by applying state of the art many-body perturbation theory in GW approximation followed by solving the Bethe-Salpeter equation (BSE) to take into account excitonic effects. The evolution of the thickness-dependent band structure, optical and Raman spectra are discussed. The strain effects due to interactions with the substrate are also considered. The first-principles results are compared with available experimental data.

9:40am **2D+EM+NS+SS+TF-WeM6 Synthesis and Properties of Large Scale, Atomically Thin Tungsten Diselenide (WSe₂), Sarah Eichfeld, Y.C. Lin, L. Hossain, The Pennsylvania State University, A. Piasecki, The Pennsylvania State University, A. Azcatti, University of Texas, Dallas, S. McDonnell, R.M. Wallace, University of Texas at Dallas, J.A. Robinson, The Pennsylvania State University**

Transition metal dichalcogenides (TMDs), such as tungsten diselenide (WSe₂) are of interest due to their intriguing properties including the transition from indirect gap to direct gap as the material is thinned to a single atomic layer. Stacking of these layered TMDs also allows for the possibility of bandgap tuning. These properties can suit a large range of flexible and low temperature electronic and optoelectronic devices. Current methods of WSe₂ research involve exfoliation or vaporization of WO₃ and Se powder, which limits industrial scalability. This work is focused on development of a metal-organic chemical vapor deposition process that can controllably produce highly-crystalline, atomically thin WSe₂ on large area substrates.

Growth of controlled monolayer tungsten diselenide (WSe₂) was carried out using chemical vapor deposition in a cold wall vertical reactor. Tungsten hexacarbonyl (W(CO)₆) and dimethylselenium (DMSe) served as the tungsten and selenium precursors, respectively. Use of MOCVD precursors provides a means to independently control the W and Se precursors allowing for more precise control of the individual species during growth. Process variables including temperature (500-950°C), pressure (100-700 Torr), and carrier gas, which were correlated with grain size, growth rate, and nucleation density of the WSe₂ to identify optimal parameters for atomically controlled synthesis. Increasing the growth pressure from 100-700 Torr results in a decrease in growth rate and nucleation density, leading to a >50x increase in grain size. Increased growth temperatures yield an increase in grain size, however, it was found that above temperatures of 800 °C the sapphire substrate begins to decompose in the growth environment, resulting in a degradation of WSe₂ above 800°C. Synthesis using 100% hydrogen, and also hydrogen/nitrogen mixtures was carried out. It was found that 100% hydrogen was necessary in order to achieve low carbon incorporation in the WSe₂ films. Characterization of these samples via Raman and photoluminescence spectroscopy verified that high quality, monolayer WSe₂ is readily achievable. Additional characterization (i.e. scanning electron microscopy, atomic force microscopy, etc.) verify the quality, grain size, and nucleation density of the atomic layers. Finally, we will discuss the impact of substrate choice on the quality of the WSe₂ atomic layers, as well as providing direct evidence that synthesis on graphene results in highly textured films, with nearly 100% commensurability to the underlying graphene.

11:00am **2D+EM+NS+SS+TF-WeM10 Growth of Transition Metal Dichalcogenides and their Alloys and on Flat and Patterned Substrates.** *E. Preciado, A. Nguyen, D. Barroso, V. Klee, S. Bobek, I. Lu, S. Naghibi, G. Von Son Palacio, T. Empante, K. Brown, K. Yang, A. Nguyen, J. Mann, Ludvig Bartels*, University of California - Riverside

The use of organic chalcogen precursors permits the CVD growth of $\text{MoS}_{2(1-x)}\text{Se}_{2x}$ alloys of any composition between pure MoS_2 and MoSe_2 on SiO_2 . Spatially resolved vibrational and photoluminescence (PL) spectroscopy is used to characterize our samples: while we observe a continuous transition of the PL maximum with S: Se ratio, the vibrational modes behave in a more complicated, 2-mode fashion. Depending on growth conditions, compositional homogeneous and heterogeneous films can be prepared.

We present details of our growth processes and show to which extend patterns on the substrates can affect the resultant structures. The patterns range from simple hole and pillar arrays to complex waveguide structures. We find that holes to an underlying reducing substrate (silicon) are effective in seeding growth. In contrast, protrusions on the substrate have little effect, so that complex devices can be overgrown.

Ref: Mann et al., 2-Dimensional Transition Metal Dichalcogenides with Tunable Direct Band Gaps: $\text{MoS}_{2(1-x)}\text{Se}_{2x}$ Monolayers, *Advanced Materials* 26, 1399 (2014)

11:20am **2D+EM+NS+SS+TF-WeM11 Synthesis, Characterization and Radiation Response of Boro-Carbon-Oxy-Nitride: A Heterogeneous 2D Material.** *GaneshRahul Bhimanapati, M. Wetherington, M. Kelly, J.A. Robinson*, The Pennsylvania State University

Since graphene, there have been many other two-dimensional materials systems (e.g., boron nitride (hBN), borocarbon nitride (BCN), transition-metal dichalcogenides) that provide an even wider array of unique chemistries and properties to explore future applications. In fact, these other 2D materials, are sometimes far better suited for many optoelectronic and mechanical applications. Specifically, tailoring graphene/boron nitride heterostructures, which retain the character of single-atom thick sheets that can withstand large physical strains, are easily functionalized, and have entirely different optical and mechanical properties compared to graphene can provide the foundation for entirely new research avenues. In recent years, it has been shown that because of the similar crystal structure, carbon, boron, and nitrogen can coexist as atomic sheets in a layered structure. Thus, combining these materials to form a new heterogeneous material system known as boro-carbon-oxy-nitride (BCON) for potential nano-mechanical and electronic applications and to study its fundamental property relations is necessary. Here, we present the fundamental property relations of BCON and its structural response to various radiation sources such as alpha, beta and gamma particles thereby providing a means for potential radiation sensing applications.

We have developed a facile method of integrating boron nitride and graphene oxide (GO) via chemical exfoliation. Chemical exfoliation of graphene oxide and boron nitride powders is accomplished via oxidation in strong acids, as we find previous methods of sonication in polar solvents does not yield stable solutions of hBN. Upon exfoliation, GO and hBN are mixed, and the resulting BCON material can be suspended in DI water, with suspension stability depending on the pH of the GO. The study of the stability of this material at different pH conditions indicates a stable and a uniform solution is achievable at pH 4-7. Fourier transform infrared spectroscopy (FTIR) indicates the B-N-B bending in the BCON is decreased as an effect of parent GO. Further, radiation response of this material to various radiation sources such as alpha, beta and gamma radiation are studied using In-Situ X-Ray Photoelectron Spectroscopy (XPS). The structural changes of carbon 1s peak in the BCON even for very low doses of radiation energy indicate potential applications in radiation sensing.

11:40am **2D+EM+NS+SS+TF-WeM12 The Structure of 2D Glass.** *Christin Büchner*, Fritz-Haber-Institut der Max-Planck-Gesellschaft, Germany, *L. Lichtenstein*, Lawrence Berkeley National Laboratory, *M. Heyde, H.-J. Freund*, Fritz-Haber-Institut der Max-Planck-Gesellschaft, Germany **INVITED**

For the first time, the structure of an amorphous network is imaged in real space.[1] Through a thin film approach, silica is made accessible for investigation with scanning tunneling microscopy (STM) and atomic force microscopy (AFM). Physical vapor deposition with subsequent annealing is employed to create an atomically flat bilayer of SiO_2 , supported on a Ru(0001) single crystal. Atomic positions of oxygen and silicon can be visualized, as well as ring structures with their distributions and local neighborhoods. All atomic species on the surface can be directly assigned with chemical sensitivity imaging.[2] This allows for statistical analysis of the building units, comparing amorphous to crystalline regions, as well as experiment to theory. Pair correlation functions of the 2D film structure are

set against diffraction data of bulk silica, revealing very similar bond distributions.

Coexisting crystalline and amorphous areas allow imaging of a topological transition region.[3] The understanding of glassy structures gained from these experiments is the starting point for more in-depth structural investigations[4], but also for investigating thin films with modified composition. Al-doping or Fe-doping can be employed to create 2D-Aluminosilicates or 2D-Clays, respectively.[5] Adsorption properties of the film can be probed using single metal atoms which migrate through the film, exhibiting ring-size-selectivity.[6]

[1] L. Lichtenstein, et al., *Angew. Chem., Int. Ed.* 51, 404 (2012)

[2] L. Lichtenstein, et al., *J. Phys. Chem. C* 116, 20426 (2012)

[3] L. Lichtenstein, et al., *Phys. Rev. Lett.* 109, 106101 (2012)

[4] C. Büchner, et al., *Z. Phys. Chem.*, DOI: 10.1515/zpch-2014-0438 (2014)

[5] J. A. Boscoboinik, et al., *Angew. Chem. Int. Ed.* 51, 6005 (2012)

[6] W. E. Kaden, et al., *Phys. Rev. B* 89, 115436 (2014)

Applied Surface Science

Room: 316 - Session AS+BI+MC-WeM

Chemical Imaging in 2D and 3D

Moderator: Jeffrey Fenton, Medtronic, Inc., Kathryn Lloyd, DuPont Corporate Center for Analytical Sciences

8:20am **AS+BI+MC-WeM2 Expanded Approaches for Single Cell Analysis by SIMS.** *Christopher Szakal*, National Institute of Standards and Technology (NIST)

Secondary ion mass spectrometry (SIMS) has been increasingly utilized for single cell imaging owing to its unique combination of spatial resolution and chemical differentiation by mass. Depending on the instrument type, subcellular lateral resolution between 10's and 100's of nanometers can be obtained, sometimes with both elemental and organic information obtained simultaneously, and sometimes with highly precise isotopic ratio measurements being attainable. However, imaging at the limits of the technique requires sufficient counts per pixel, which can be limited by analyte concentrations, competitive ionization pathways, and cumulative cluster ion beam damage accumulation. This work focuses on the advantages and disadvantages of combining focused ion beam (FIB) milling of single cells with subsequent ToF-SIMS imaging, as well as using large geometry (LG)-SIMS for high mass resolution analysis of single cell components that would otherwise not be easily detectable in other instrumental configurations. Such developments expand the research areas that are possible for single cell SIMS analyses, including cell differentiation without relying on multivariate analyses and targeted cell uptake studies.

8:40am **AS+BI+MC-WeM3 3-Dimensional Chemical Imaging on the Nanoscale with Cluster-SIMS.** *Nicholas Winograd*, Penn State University **INVITED**

Bombardment of molecular solids with polyatomic projectiles allows interrogation of the sample with reduced chemical damage accumulation. Hence, it is now possible to perform depth profiling experiments with a depth resolution of less than 10 nm. In our hands, the projectile of choice is C_{60} due to the fact that the ion beam can be focused to a 250 nm spot size, and erosion of the sample can be performed with minimal chemical damage, especially at low temperature. With this combination of properties, it is feasible to think about creating 3-dimensional molecule-specific images.

A basic impediment to accomplishing this goal involves the fact that the SIMS images provide only chemical information and no direct depth information. The measurable quantity is the incident ion beam fluence, which can indirectly be related to depth, but independent measurements are required. The formation of topography and differential sputtering effects across the sample surface can also degrade the quality of the 3-D rendering when 2-D images are stacked. We have employed AFM in combination with SIMS imaging to develop protocols for correcting for these phenomena. Here, examples are shown using a patterned trehalose thin film and an Irganox delta layer reference material provided by NPL in the U.K. The idea is to provide chemical information with SIMS, and the depth information, acquired at each pixel in the image, using AFM. In addition to examining eroded craters directly, we have also developed a wedge-beveling technique that allows sputtering yield and topography to be determined with a single SIMS measurement and a single AFM measurement.

The long term aim of developing these protocols is to be able to acquire high resolution chemical images of single biological cells. So far, it appears that differential sputtering effects are not too serious for these samples. The combined SIMS/AFM strategy developed here will be important for verifying these initial observations. Finally, there is an emerging interest in gas cluster ion sources, namely Ar₄₀₀₀, since even less chemical damage than C₆₀ is observed, and the depth resolution during erosion appears to be less than 5 nm. Here we show that the combination of C₆₀ imaging and Ar₄₀₀₀ sputtering provides an even more powerful protocol. In general, we show that the AFM/SIMS combination is a powerful tool for 3-dimensional chemical imaging.

9:20am **AS+BI+MC-WeM5 SIMS 2D and 3D Characterization of Organic/Inorganic Surfaces by FIB Crater Wall Imaging and Tomography**, *Felix Kollmer, R. Möllers, D. Rading, S. Kayser*, ION-TOF GmbH, Germany, *N. Havercroft*, ION-TOF USA, Inc., *E. Niehuis*, ION-TOF GmbH, Germany

Information on the chemical composition, physical properties and the three dimensional structure of materials and devices is of major importance. Time-of-Flight Secondary Ion Mass Spectrometry (TOF-SIMS) is known to be an extremely sensitive surface imaging technique which provides elemental as well as comprehensive molecular information on all types of solid surfaces. In the so-called dual beam mode the pulsed analysis beam is combined with a low energy sputter ion beam for the removal of material. This allows depth profiling of multilayers with high depth resolution as well as three-dimensional analysis.

However, the analysis of structures at greater depth (> 10µm) requires long measurement times and the build-up of surface roughness at the crater bottom limits the achievable spatial resolution. Moreover, extremely rough samples, samples with voids, and material that exhibits strong local variations in density or sputter yield are unsuitable for conventional depth profiling. Not only that the initial surface topography is unknown but it is also modified and in many cases even roughened by the sputtering process.

In order to overcome these limitations we used a combined SIMS/FIB setup. Either a Bi cluster beam or a mono-atomic Ga beam is used to FIB mill a crater into the sample. Subsequently, a 2D TOF-SIMS image of the vertical crater wall is acquired. Since the crater wall is hardly affected by the aforementioned roughening problems this approach allows the in-depth distribution of elements to be determined by analyzing a plane perpendicular to the surface at high lateral resolution (DI<50nm) [1].

Moreover, by serial slicing of the crater wall followed by intermediate analysis steps this approach can be extended in order to provide the full 3D characterization of the analyzed volume. We will present 2D and 3D data of reference material, multilayer samples and technically relevant real world samples such as fuel cells and battery electrodes. For thin multilayer samples the FIB process can be performed under grazing incidence in order to bevel the surface and hence magnify and accentuate thin layers in the plane of the analyzed crater wall.

However, the FIB/SIMS approach fails when analyzing organic surfaces since the molecular structure is almost completely destroyed by the sputtering process. We will discuss methods to maintain the molecular structure under high dose sputtering conditions by performing the FIB milling with massive argon clusters.

[1] F. Kollmer, W. Paul, M. Krehl, E. Niehuis, SIMS XVIII proceedings paper, Surf. Interface Anal., 2012

9:40am **AS+BI+MC-WeM6 Multivariate Imaging: A New Approach towards Chemical State Identification of Novel Carbons in XPS Imaging**, *Anders Barlow, N. Sano, P.J. Cumpson*, NEXUS, Newcastle University, UK

The differentiation between various forms of carbon in XPS spectra is made difficult by the subtle changes in C1s spectra that one would typically analyse. This is ideally demonstrated by a comparison of sp² and sp³ carbon, such as graphite and diamond, where the variation in the C1s peak is less than 1eV. When applied to 'real' samples, such as a diamond like carbon coating, or a graphene surface, this difference can be even less. This presents a real problem for XPS imaging, where typically the analyst would sacrifice energy resolution in favour of signal intensity and spatial resolution. Such subtle differences are then completely lost when performing XPS imaging of novel carbon surfaces, where there may be discrete boundaries or layers between materials that are chemically very different, yet appear the same when the C1s peak energy is used in imaging.

We report a method of elucidating these differences in XPS imaging through shifting the focus from the C1s feature, to the X-ray induced Auger feature, a method we call Multivariate Auger Feature Imaging (MAFI). The carbon Auger feature can be studied and through the extraction of the so-called D-Parameter¹, chemical states of carbon can be clearly identified, with little ambiguity between sp² and sp³ states. Extension of this method to

XPS imaging, and the generation of 3-Dimensional images (2 spatial, 1 kinetic energy), we have shown that imaging of the Auger feature of graphite on polymers can identify multiple states of carbon-carbon bonding domains, where the imaging of the C1s feature alone yields no distinguishable differences or spatial features. We have also shown that PCA analysis of the carbon Auger feature also yields clear and distinguishable differences in the XPS images. The result is two independent methods of distinguishing novel carbon materials from one-another in XPS imaging. With modern instrumentation capable of a spatial resolution down to the few micron level, this greatly enhances the capability of XPS instrumentation to image novel carbon surfaces and devices.

¹ Lascovich, J.C. et al., App. Surf. Sci., 47(1), pp. 17-21 (1991).

11:00am **AS+BI+MC-WeM10 Multivariate Analysis Approaches for Image De-noising and Image Fusion**, *Bonnie Tyler*, National Physical Laboratory (NPL), UK **INVITED**

Image fusion has become widely used in both medical diagnostics and optical remote sensing and there is growing interest in using these methods in applied surface science research. The goal of data fusion is to combine measurements from complementary techniques in order to aid in the analysis of the data and enhance information content. Recently, pan-sharpening techniques developed for optical remote sensing have received considerable interest in the surface science community because of their ability to improve spatial resolution and image contrast. Although image fusion can produce dramatic improvements in image sharpness and contrast, it can also lead to significant artefacts and care must be taken to ensure reliable results. These artefacts can be quite severe if the spectra have sharp bands, high background, or low signal-to-noise, features that are common in ToF-SIMS and XPS imaging. For optical remote sensing, a wide variety of methods have been developed for pan-sharpening, including approaches based on wavelet transforms, high pass filters, intensity hue saturation, Gram-Schmidt transforms, and Principal Components Analysis. Each of these methods offers advantages for certain applications but all are prone to artefacts when applied under non-optimal conditions. In order to minimize artefacts and produce reliable results, the methods must be adapted to account for the unique characteristics of different imaging modes. Of the methods in the literature, PCA image fusion is the most readily adapted for use with ToF-SIMS and XPS images. Methods for adapting PCA fusion for optimal use with ToF-SIMS and XPS images will be presented, including statistically based preprocessing of the data, target factor rotations and histogram matching. PCA image fusion can be a valuable technique for reducing noise, improving image contrast, and spatial resolution in ToF-SIMS and XPS data. With appropriate attention to the unique characteristics of each spectrometry, this can be done without significant artefacts or distortion of the spectral detail.

11:40am **AS+BI+MC-WeM12 Global Analysis Peak Fitting for Imaging NEXAFS Data**, *Mark H. Van Benthem, J.A. Ohlhausen*, Sandia National Laboratory

We will present a method of analyzing NEXAFS image data to extract chemical information from the complex elemental peak structure in the material under analysis. The method, known as global analysis, fits emission bands to peaks described by nonlinear functions using nonlinear and linear optimization techniques. It can fit multiple types of peaks simultaneously, such as those found in NEXAFS spectra: Gaussian, Lorentzian, Voigt, asymmetric Gaussian and Lorentzian, and step edge with decay. Typically, peak fitting of NEXAFS data is very complex and somewhat arbitrary. Our method takes advantage of the high dimensionality of the image space to yield peaks with potentially greater reliability than single spectrum fitting. The method also employs data compression with principal component analysis (PCA) to rapidly complete the analysis. A discussion of the algorithm along with several examples of its application will be presented.

Sandia is a multiprogram laboratory operated by Sandia Corporation, a wholly owned subsidiary of Lockheed Martin Corporation, for the U.S. Department of Energy's National Nuclear Security Administration under contract DE-AC04-94AL85000.

12:00pm **AS+BI+MC-WeM13 Visualizing Pharmaceutical Compounds in Single-cells with label-free 3D Mass Spectrometry Imaging**, *Melissa K. Passarelli, C. Newman*, National Physical Laboratory, UK, *A. West*, University of York, UK, *C.T. Dollery, I.S. Gilmore*, National Physical Laboratory, UK, *J. Bunch*, National Physical Laboratory

Drug-induced phospholipidosis is an adverse side-effect that hinders the therapeutic value of some pharmaceutical compounds. In this report, three-dimensional secondary ion mass spectrometry (SIMS) imaging was used to investigate the cellular uptake of phospholipidosis-inducing pharmaceutical compounds. A fast and simple sample preparation method, frozen dehydrated, was used to extract the drug compound to the surface layers of

individual cells. Although the native localization of drug compound within the cell is lost, the compound was isolated to the confines of the individual cells and matrix-related effects were no longer a concern. With this method we were able to successfully detect intact-unlabeled drug compound at therapeutic dosages in macrophages. Relative quantification of the drug compound in individual cells was achieved. Overall, this approach provides a platform for studying cellular uptake of pharmaceutical compounds at the single cell level. This system also provides a model for studying metrology of cell imaging using SIMS. The effects of sample preparation and limitations of current technologies will be discussed along with new possibilities for the future.

Biomaterial Interfaces

Room: 317 - Session BI+AS-WeM

Nonlinear Optical & Vibrational Spectroscopy

Moderator: Luke Hanley, University of Illinois at Chicago

8:40am **BI+AS-WeM3 Characterizing Adsorbate Structure at the Solid-Liquid Interface through Nonlinear Vibrational Spectroscopy and Modelling Approaches**, *S. Roy, P.A. Covert, K.-K. Hung, U. Stege, Dennis Hore*, University of Victoria, Canada **INVITED**

Even-order nonlinear spectroscopies such as second harmonic (SHG) and sum frequency generation (SFG) are valued for their sensitivity to interfacial structure as they are capable of discriminating from adjacent bulk phases based on symmetry. Visible-infrared SFG spectroscopy additionally harnesses the sub-molecular structural probe of a vibrational spectroscopy by tuning the infrared laser over molecular resonances. As a result, over the past two decades, SFG spectroscopy has been successfully applied to a wide variety of solid, liquid, and vapor interfaces, revealing signatures of the molecular organization that provide clues to the surface structure. Our group has been working on techniques to assist in the molecular interpretation of the SFG response. For small molecules, this includes grid computing-based searches to validate candidate orientation distributions based on the experimental data. For larger molecules with additional conformational flexibility, we employ molecular dynamics simulations to further refine our efforts to interpret the SFG data. Our most recent efforts explore the use of phase-resolved SFG spectra in order to develop more sensitive functions for scoring trial molecular orientation distributions. Our goal is to develop tools that are scalable to molecules of arbitrary complexity. This talk will provide some examples to illustrate our path towards this direction.

9:20am **BI+AS-WeM5 Vibrational Spectroscopy Investigation of the Giant Surface Potential of Organic Semiconductors**, *Laura Kraya*, Princeton University, *C. Krekeler, C. Weigel*, Technical University Braunschweig, Germany, *P. Zhao*, Princeton University, *W. Kowalsky*, Technical University Braunschweig, Germany, *C. Lennartz*, BASF, *A.L. Kahn, B. Koel*, Princeton University

A phenomenon known as the giant surface potential (GSP), where the surface potential of organic films display linear growth with increasing film thicknesses in the absence of light was first reported by Ito et al. on (8-hydroxyquinoline)aluminum (Alq_3), a prototypical fluorescent material used in OLEDs. It has been shown that the surface potential of Alq_3 has reached 28 V for a 560 nm thick film by Kelvin probe measurements in vacuum in the absence of light. Since then this phenomenon has been observed for a broad range of molecules thermally evaporated on varying substrates under similar conditions. The effect is independent of the substrate, dependent on film thickness and decays quickly with illumination at the normal mode of the respective molecule. The spontaneous buildup of the GSP cannot be explained by any classical interfacial phenomena. Investigations into the cause of GSP, including the analysis of light and heat on the surface potential, are not yet understood.

In this study we use vibrational spectroscopy to understand the nature of the GSP buildup, where we have found a significant change in the vibrational structure of the organic material in thick films where the GSP is present as compared to thin films. The vibrational spectra of the most commonly studied light-emitting material, Alq_3 , on indium tin oxide (ITO) is investigated as a function of thickness using high resolution energy electron loss spectroscopy (HREELS), Raman spectroscopy, high resolution x-ray photoelectron spectroscopy (HR-XPS), attenuated total reflectance infrared spectroscopy (ATR-IR), and density functional theory (DFT) calculations. In order to provide a holistic understanding of the GSP, the results are compared to the vibrational spectra of 1,3,5-tris(N-phenylbenzimidazole-2-yl)benzene (TPBi) on ITO, an electron transporter host material with a measured GSP of 0.07 V/nm, and bis(triphenylsilyl)-dibenzofuran (BTDF) on ITO, a typical electron-conducting host used in combination with hole-

conducting deep-blue emitter with a measured GSP of 0.08V/nm. The observed spectra show significant changes with the presence of the GSP in the organic material on ITO, which can be explained in terms of different symmetries of the isomers as well as between complexes and isolated anions. Additionally, it has been found that the surface phase differs from the bulk phase, where a structured layer is evident at the interface of the organic semiconductor, and this layer shifts with increasing thickness and in the presence of the GSP. The present work has provided direct evidence that a different molecular orientation exists at the interface than in the bulk, where the GSP exists.

9:40am **BI+AS-WeM6 Diatom Biom mineralization at the Molecular Level Probed by SFG Spectroscopy**, *H. Lutz*, Max-Planck-Institute for Polymer Research, Germany, *J.E. Baio*, Oregon State University, *V. Jaeger, A. Roehrig, G. Drobny, J. Pfaendner*, University of Washington, *Tobias Weidner*, Max-Planck-Institute for Polymer Research, Germany

Specialized mineral proteins control the growth of biogenic hard tissue. Using specific recognition motifs, proteins bind and release mineral facets and grow the intricate mineral morphologies found in Nature. Particularly fascinating examples of biom mineralization are the high fidelity silica nanostructures in the shells of diatoms. Within the unicellular algae *Cylindrotheca fusiformis*, proteins called silaffin play a crucial role in the molecular biom mineralization machinery. In order to harness the concepts used by Nature to efficiently fabricate mineral nanostructures we aim to understand the underlying protein-silica interactions. We found that artificial peptides consisting of lysine and leucine (LK peptides) can mimic silaffin's capability of forming various biosilica nanostructures. These peptides were designed to adopt helical or beta-sheet structures due to their hydrophobic periodicities and represent simple model systems to study the effect of protein folding on mineralization. Using surface sensitive sum frequency generation (SFG) vibrational spectroscopy we have studied the interactions of LK peptides with biosilica surfaces and within biosilica composites. We monitored how different LK peptides fold at the silica-water interface and we found that interfacial folding is crucial for the silica morphology: spheres, rods and flakes were produced by LKs – depending on their surface folding. Side chains also actively participate in the mineralization process. We probed the side chain structure of LKs in contact with silicic acid solution and observed increased ordering of charged lysine side chains during the formation of biosilica, indicating their involvement in silica nucleation. Combined with cryo-TEM measurements and MD simulations of different stages of nanoparticle nucleation the SFG studies provide important details of peptide-driven silica formation.

11:00am **BI+AS-WeM10 Water, Charge and Membrane Interface Stability**, *Sylvie Roke*, Ecole Polytechnique Fédérale de Lausanne (EPFL), Switzerland **INVITED**

Life occurs in three dimensional turbid aqueous systems. A cell consists for ~60 % of water and contains many organelles and interfaces. The average distance between two molecules, or a molecule and a membrane interface is approximately 1 nm. The molecular, structural, dynamic, and biological properties of water, aqueous systems and aqueous interfaces are essential in understanding the complexity of life, and our ability to harness its features for novel (nano)technologies.

Here, I will introduce nonlinear light scattering methods that can be used to gain label-free molecular level information about model membrane interfaces in liquid aqueous nanoscopic systems. The use of these methods will be illustrated around the following questions:

- Does water behave charge asymmetrically?
- What is the role of water in determining the stability of amphiphilic interfaces?
- Is the molecular structure of model membranes influenced by the above considerations?

11:40am **BI+AS-WeM12 Second Harmonic Scattering: Characterizing the Interaction between Lipid Membranes and Water**, *Cornelis Lütgebaucks*, *C. Macias-Romero, S. Roke*, Ecole Polytechnique Fédérale de Lausanne (EPFL), Switzerland

Lipid membranes are essential for all organisms by separating functional compartments and mediating cellular signaling. Dioleoylphosphatidylcholine (DOPC) and Dioleoylphosphatidylserine (DOPS) are the main constituents of mammalian cell membranes. Molecular level understanding of cell membrane architecture often involves supported lipid membranes and invasive methods. We designed a second harmonic scattering (SHS) instrument that allows for investigating the molecular properties of interfaces from lipid vesicles in aqueous solution, label-free, and substrate independent. Characterizing DOPC:DOPS composed liposomes, we find that the water-lipid interaction is mainly responsible for the SHS signal. Moreover, the SHS signal increases up to a

lipid mixing ratio of 9:1 and remains unchanged at lower ratios. This value coincides with the saturation value of DOPS in the outer leaflet of the mammalian membrane, when spontaneous apoptosis occurs.

12:00pm BI+AS-WeM13 Analyzing the Structure of Amyloid Fibrils in Bacterial Biofilms *In Vitro* and in Real Time Using Sum-Frequency-Generation Spectroscopy, P. Johansson, R. Francisco, J. Bryers, Patrick Koelsch, University of Washington

Curli fimbriae are thin, needle-like structures formed by proteins. These so-called amyloid fibrils are typically associated with neurodegenerative conditions such as Alzheimer and Parkinson's disease; however, they can also play a beneficial role in various other processes in nature. *Curli fimbriae* have been shown to be involved in e.g. the colonization of abiotic surfaces, biofilm formation, and internalization of bacteria into eukaryotic cells. The structure of amyloid fibrils has been studied by IR spectroscopy, far UV CD spectroscopy, NMR, scanning probe techniques, and fluorescent probes that bind to fibrils. What is common to those approaches is the need for labelling or an *ex vitro* character, typically involving purification steps. Here we show how to use sum-frequency-generation (SFG) spectroscopy to study early stages of amyloid fibrillar formation within biofilms formed by a *Pseudomonas* strain of the *P. fluorescens* group. Studies have been performed *in vitro*, over several days of biofilm formation, under defined environmental conditions, and in real time - without the need for labels or any other disruptive sample preparation. In addition to the wild-type strain, genetically modified *P. fluorescens* were studied that are either overexpressing fibrils, or for which the fibrillar formation was suppressed. Furthermore, SFG spectra from purified amyloids were used to correlate *in vitro* and *ex vitro* results.

**Electronic Materials and Processing
Room: 311 - Session EM1-WeM**

Materials and Devices for High Power Electronics (8:20-11:00 am)/Two Dimensional Electronic Materials & Devices (11:00 am - 12:20 pm)

Moderator: Andrew Antonelli, Lam Research, Rachael Myers-Ward, U.S. Naval Research Laboratory

8:00am EM1-WeM1 Commercialization of High Voltage GaN HEMT, P. Parikh, Rakesh Lal, Transphorm Inc. INVITED

With its proven ability to reduce size (improved form factor) and save energy (improved efficiency) Gallium Nitride (GaN) is now no longer a nice to have, it is a must have for power conversion. In applications have emerged ranging from sub 100 watt ultra-compact high frequency adapters to multi kilowatt highly efficient PV Inverters, GaN makes it possible to do what Silicon cannot. High voltage GaN on Silicon HEMT switches are now a reality, following successful completion of JEDEC qualification as well as establishment of a high voltage lifetime of 100M hours. A large area (6inch) Silicon substrate, epitaxial processes that promise to leverage the commercial success of the well established GaN LED & lighting products and the ability to manufacture in existing high volume Silicon foundries makes GaN commercially attractive. Successful companies need to deliver high quality product with a deep understanding of how the GaN switch is best utilized in applications. We will discuss the commercialization of the GaN power HEMT by Transphorm - enabled by execution on the above fronts, a strong intellectual property across the full value chain and a strong team with deep rooted experience in GaN technology and business. Ultimately GaN is expected to significantly reduce conversion losses endemic in all areas of electricity conversion, ranging from power supplies to PV inverters to motion control to electric vehicles, enabling consumers, utilities and Governments to contribute towards a more energy efficient world.

8:40am EM1-WeM3 Progress and Future Challenges in SiC Material for High-Voltage Power Devices, Tsunenobu Kimoto, Kyoto University, Japan INVITED

Silicon carbide (SiC) is an emerging wide bandgap semiconductor, by which high-voltage, low-loss power devices can be realized owing to its superior properties. SiC unipolar devices such as Schottky barrier diodes and MOSFETs will replace Si unipolar/bipolar devices in the blocking-voltage range from 600 V to about 6500 V. Regarding SiC power MOSFETs, the authors developed vertical trench MOSFETs in collaboration with ROHM. The trench MOSFETs with cell miniaturization exhibited extremely low on-resistances of 0.79 mΩcm² and 1.4 mΩcm² for 630 V and 1260 V devices, respectively, with normally-off characteristics

[1]. After reliability tests, all-SiC power modules (1200 V – 180 A) are now commercial products.

For ultrahigh-voltage applications above 6500 V, SiC bipolar devices such as PiN diodes and IGBTs are promising. Major technological challenges include fast epitaxy of thick (> 100 μm) and high-purity epilayers, stress control, reduction of basal-plane dislocations and stacking faults, enhancement and control of carrier lifetimes. The authors succeeded in fast epitaxial growth of 100-200 μm-thick SiC at a growth rate of 40-85 μm/h with a high purity (1x10¹³ cm⁻³) and reduced density of basal-plane dislocations. Through elimination of the Z_{1/2} center, a lifetime killer in SiC, via thermal oxidation, the authors obtained about 200 μm-thick, Z_{1/2}-free n-type SiC epilayers, where the bulk lifetime reaches 30 μs or even longer [2]. The carrier lifetimes can be controlled by low-energy electron irradiation, which can preferentially generate the Z_{1/2} center (carbon vacancy) in SiC.

Ultrahigh-voltage PiN diodes were fabricated by using lightly-doped (2-3x10¹⁴ cm⁻³) SiC epilayers with different thicknesses (50-260 μm). The breakdown voltage was scaled with increasing the epilayer thickness, as simulated. The maximum breakdown voltage experimentally obtained exceeded 27 kV, which is the highest blocking voltage among any solid state devices. The differential on-resistance was remarkably reduced by enhancement of carrier lifetimes, being 2 mΩcm² and 10 mΩcm² for 13 kV and 27 kV devices, respectively. A SiC bipolar junction transistor with a blocking voltage over 21 kV and current gain over 60 was also demonstrated [3].

This work was supported by the Funding Program for World-Leading Innovative R&D on Science and Technology (FIRST Program) and a Grant-in-Aid for Scientific Research from JSPS. The authors acknowledge Dr. T. Nakamura with ROHM for the MOSFET collaboration.

[1] T. Nakamura et al., Tech. Digest. 2011 IEDM, 26.5.1.

[2] S. Ichikawa et al., Appl. Phys. Exp., **5**, 101301 (2012).

[3] H. Miyake et al., IEEE Electron Device Lett., **33**, 1598 (2012).

9:20am EM1-WeM5 4H-SiC Epilayers Grown on 2° Offcut Substrates, Rachael Myers-Ward, Z.R. Robinson, V.D. Wheeler, P.B. Klein, N.A. Mahadik, R.E. Stahlbush, C.R. Eddy, Jr., D.K. Gaskill, Naval Research Laboratory

Silicon carbide is a material of interest for high-voltage, high-power switching device applications. Basal plane dislocations (BPDs) are a major concern for SiC bipolar devices as they source Shockley-type stacking faults in the presence of an electron-hole plasma and reduce minority carrier lifetimes [1]. Many researchers have investigated methods to reduce BPD densities by experimenting with pre-growth treatments [2-4], substrate orientation [5], growth parameters [5, 6] and growth interrupts [7]. This work investigates extended defects, morphology and lifetime in 4H-SiC epilayers grown on substrates offcut 2° toward the [11-20].

Epilayers were grown in a horizontal hot-wall reactor using silane (2% in H₂) and propane. Hydrogen etching was conducted to determine the morphology of the substrate during the ramp to growth temperature; temperatures explored were 1400, 1450 and 1500 °C. Epilayers were grown at various growth rates of 1, 5 and 10 μm/hr and C/Si ratios from 1.0 to 1.55. The influence of doping with ultra-high purity nitrogen was investigated. Ultraviolet photoluminescence (UVPL) imaging was used to identify BPDs in low doped epilayers. Time resolved photoluminescence measurements were performed to determine the minority carrier lifetime of the layers and Raman spectroscopy was used to analyze polytype inclusions. Surface roughness was measured by atomic force microscopy and Nomarski microscopy was also used to characterize morphology.

No step bunching was found when the temperature was raised to 1400 °C in H₂ and cooled down immediately. However, intermittent step bunching formed when the temperature was raised to 1500 °C. When a 15 μm epilayer was introduced, step bunching was observed and the surface roughness was 6.0 nm RMS. For comparison, a standard 4° offcut sample typically has 3.0 nm RMS for a 20 μm epilayer. Using UVPL, it was found that after 4 μm of epi, 90% of the BPDs had converted in the epilayer as compared to 70% in a 4° offcut sample, indicating the conversion is faster in the lower offcut material. Epilayers without any BPDs were observed; however, 3C-SiC inclusions were present as verified by Raman spectroscopy. BPD densities and carrier lifetimes of the epilayers will also be reported.

[1] J.P. Bergman, et al. Mater. Sci. Forum Vol. **353-356**, 299 (2001).

[2] Z. Zhang, et al., Appl. Phys. Lett. **89**, 081910 (2006).

[3] J.J. Sumakeris, et al., Mater. Sci. Forum **527-529**, 529 (2006).

[4] H. Tsuchida, et al., Mater. Sci. Forum **483-485**, 97 (2005).

[5] W. Chen and M.A. Capano J. Appl. Phys. **98**, 114907 (2005).

[6] T. Ohno, et al., J. Cryst. Growth **271**, 1 (2004).

[7] R.E. Stahlbush, et al., Jr., Appl. Phys. Lett. **94**, 041916 (2009).

11:00am **EM1-WeM10 Recent Progress in Graphene and Heterostructure RF Electronics**, *Jeong-Sun Moon, H.-C. Seo, K.A. Son, B. Yang, M. Antcliffe, A. Schmitz, D. Le*, HRL Laboratories, LLC, *L.O. Nyakiti, V.D. Wheeler, R.L. Myers-Ward, C.R. Eddy, D.K. Gaskill*, Naval Research Laboratory, *K.-M. Lee, P. Asbeck*, University of California at San Diego

INVITED

Graphene is a truly 2D electronic material with a very high intrinsic saturation velocity (V_{sa}) of $\sim 5 \times 10^7$ cm/sec, which has great potential for high-speed RF applications. In addition, graphene offers unique properties, such as high mobility, excellent scalability, symmetry in electron or hole channel, its ability to be integrated into any substrate, and its potential compatibility with CMOS.

The material quality and fabrication process for graphene have improved with sheet resistance of ~ 200 ohm/sq, ohmic contact resistance of ~ 0.03 W \times mm, the lowest on-state resistance of 0.13 W \times mm, and the highest saturated source-drain current of ~ 3 A/mm at $V_{ds} = 1$ V. Recently, graphene FETs (GFETs) demonstrated zero-bias resistive FET mixer operation up to 20 GHz [1] with 10 times improvement in the mixer quality factor (IP3/total power) over state-of-the-art (SOA) resistive FET mixers; these GFETs also demonstrated zero-bias in power detectors and radiometers (up to 220 GHz) [2] with linear-in-dB dynamic range with >20 dB improvement over SOA FETs. Graphene heterostructure-based FETs have been developed as enhancement-mode FETs with an Ion/Ioff ratio of $>10^5$ and excellent pinch-off and I-V saturation [3]. Graphene varactors have been demonstrated on glass substrates, expanding graphene's potential to be integrated with arbitrary substrates, and potentially enabling active and tunable antenna surfaces beyond wafer-scale.

In this talk, we present recent progress in graphene material, GFETs, graphene heterostructure FETs, circuit applications for mixers, radiometers, detectors, varactors, and progress toward integrating graphene with active antennas. Continuous development of this emerging material would potentially enable RF systems on nonconventional surfaces.

This material is partially based upon work supported by the Government under Contract No. N66001-08-C-2048. Any opinions, findings and conclusions or recommendations expressed in this material are those of the author(s) and do not necessarily reflect the views of the Contracting Agency.

[1] J.S. Moon et al., IEEE Electron Device Letters., vol 34, p465, 2013; J. S. Moon and D. Kurt Gaskill, IEEE Trans. Microwave Theory and Tech., vol. 52, pp 1014-1024, 2011.

[2] J. S. Moon et al., IEEE Electron Device Letters., vol 33, p1357, 2012.

[3] J.S. Moon et al., IEEE Electron Device Letters., vol 34, p1190, 2013

11:40am **EM1-WeM12 High-Field and Thermal Transport in 2D Atomic Layer Devices**, *Eric Pop, C.D. English*, Stanford University, *V.E. Dorgan, A. Behnam*, University of Illinois at Urbana-Champaign, *Z. Li*, Stanford University, University of Illinois, Urbana-Champaign, *S. Islam*, University of Illinois at Urbana-Champaign

INVITED

Two-dimensional (2D) materials like graphene and transition metal dichalcogenides (TMDs) are uniquely suited for nanoscale field-effect transistors (FET) due to sub-nm channel thickness and lack of dangling surface bonds. Thus, unlike three-dimensional (3D) materials such as Si, FETs based on 2D materials would be more resilient to short-channel effects and would suffer less mobility degradation from carrier-surface scattering. Nevertheless, most existing studies of 2D materials have focused on large devices and low-field transport. By contrast, highly scaled 2D-FETs will require very good understanding of electric transport at high fields and thermal transport as relevant for large scale device integration.

In this talk we will describe our recent progress in optimizing transport at 2D-3D material contacts, examining high-field transport, FET scaling and thermal measurements at sub-100 nm device dimensions. For instance, we have recently uncovered transport physics at TMD and 2D graphene contacts with metal electrodes, including the roles of metal deposition conditions during fabrication and that of thermoelectric (Peltier) effects during transistor operation [1,2]. We will also describe our understanding of high-field transport in MoS2 and graphene, including the importance of self-heating effects on various substrates such as SiO2, BN and HfO2 [3,4]. Finally, we will describe our thermal measurements in suspended graphene [5] and in graphene devices with dimensions comparable to the electron and phonon mean free paths (~ 100 nm) [6]; the former yield the intrinsic behavior of this material, while the latter show quasi-ballistic thermal transport near room temperature, as well as significant phonon-edge scattering in narrow devices. The results are of importance for both electronic and thermal applications of 2D materials.

References

[1] K.L. Grosse, M.-H. Bae, F. Lian, E. Pop, W.P. King, Nature Nano. 6, 287 (2011)

[2] C.D. English, V.E. Dorgan, G. Shine, K. Saraswat, E. Pop, IEEE Device Research Conf. (2014)

[3] M.-H. Bae, S. Islam, V.E. Dorgan, E. Pop, ACS Nano 5, 7936 (2011)

[4] S. Islam, Z. Li, V.E. Dorgan, M.-H. Bae, E. Pop, IEEE Electron Device Lett. 34, 166 (2013)

[5] V.E. Dorgan, A. Behnam, H. Conley, K. Bolotin, E. Pop, Nano Lett., 13, 4581 (2013).

[6] M.-H. Bae, Z. Li, Z. Aksamija, P.N. Martin, F. Xiong, Z.-Y. Ong, I. Knezevic, E. Pop, Nature Comm. 4, 1734 (2013)

Electronic Materials and Processing

Room: 314 - Session EM2-WeM

High-K Dielectrics from Non-Classical Channels

Moderator: Christopher Hinkle, University of Texas at Dallas

8:00am **EM2-WeM1 The Influence of Surface Preparation pre-Atomic Layer Deposition of Al₂O₃ on GaN Metal Oxide Semiconductor Capacitors**, *Dmitry Zhernokletov*, Stanford University

High- κ gate dielectrics have been proposed as a means of producing high performance field effect devices with low gate leakage on GaN-based substrates for low static power consumption, improved transconductance, and higher output power capabilities [1-3]. However, because the surface of GaN may contain defects such as dangling bonds and contaminants [4], understanding the effect of varying surface preparation prior to atomic layer deposition (ALD) of the high- κ gate dielectrics on GaN is of great importance for the advancement of field effect devices. Surface defects and contaminants such as carbon and oxygen may have detrimental effects on optical quality and device performance of GaN based devices. Several methods to improve GaN surface and interface quality have been proposed [4-8]. They include surface cleaning procedures using aqueous (NH₄)₂S, and acid/base treatments such as HCl, HF, NaOH and NH₄OH.

We present a detailed study on the influence of surface preparations pre-atomic layer deposition of Al₂O₃ on GaN metal oxide semiconductor capacitors. The electrical, chemical, and luminescence characteristics of MOS structures prepared on both chemically treated and as-received GaN substrates are reported. Aqueous NH₄OH cleaning shows promise for providing an enhanced starting surface for atomic layer deposition of Al₂O₃ layers on GaN.

[1] P.D. Ye et al., Appl. Phys. Lett. 86, 063501 (2005).

[2] O.I. Saadat et al., IEEE Electron. Dev. Lett. 30 1254-1256 (2010).

[3] D.J. Meyer et al., Solid-State Electron. 5 1098 (2010).

[4] R.D. Long et al., Materials. 5, 1297-1335 (2012).

[5] Diale et al., Appl.Surf.Sci. 246, 279–289 (2005).

[6] Lee et al., J. Electrochem. Soc. 147, 3087–3090 (2000).

[7] Hattori et al. Surf. Sci. 2010, 604, 1247–1253.

[8] Y. Koyama et al., Solid State Electron. 43, 1483–1488 (1999).

8:20am **EM2-WeM2 Low Voltage Nonlinearity Metal-Insulator-Insulator-Metal (MIIM) Capacitors using Plasma Enhanced Atomic Layer Deposition of SiO₂ and Al₂O₃**, *Dustin Austin*, Oregon State University, *D. Allman, D. Price, S. Hose*, On Semiconductor, *J.F. Conley*, Oregon State University

Back end of line (BEOL) metal-insulator-metal (MIM) capacitors reduce the need for discrete off-board components and have become a core passive device in integrated circuits. Applications include analog-to-digital converters, analog noise filters, DC voltage decoupling, and electrostatic discharge (ESD) protection. To enable continued scaling, capacitance density must be increased, either by introducing higher dielectric constant (κ) materials or by reducing the insulator film thickness. However decreasing insulator film thicknesses increases both leakage current density and voltage nonlinearity (characterized by the quadratic voltage coefficient of capacitance or αVCC). In addition high- κ materials typically have a large positive αVCC . Although a promising route to simultaneously meeting these competing requirements is to use a nanolaminate of insulators, which allows for combining of layers with complementary properties. Previous work has demonstrated nanolaminate MIIM devices with high capacitance density, low leakage current density, and low αVCC using PECVD SiO₂ or uncommon materials.¹⁻³

In this work, MIIM capacitors using bilayers of Al₂O₃ and SiO₂ were deposited sequentially using plasma enhanced atomic layer deposition

(PEALD). PEALD allows for low deposition temperatures, precise thickness control, and conformal coverage over high aspect ratio structures. Al_2O_3 and SiO_2 are attractive due to their common usage in IC fabrication, large metal-insulator barrier heights, and high dielectric breakdown strength. In addition SiO_2 is one of the few materials that exhibits a negative αVCC . Spectroscopic ellipsometry was used to characterize the growth rate and nucleation delay on TaN and Si substrates. The dielectric constants of Al_2O_3 and SiO_2 were found to be 4.6 and 8.7, respectively. αVCC values were plotted as a function of thickness and fit with a power law. Appropriate layer thicknesses were chosen to offset the negative αVCC of SiO_2 with the positive αVCC of Al_2O_3 in order to minimize the effective αVCC for a given capacitance density. The initial results for 8 nm Al_2O_3 / 3.5 nm SiO_2 MIIM devices show capacitance density of 5.4 $\text{fF}/\mu\text{m}^2$, 2 nA/cm^2 leakage at 1V, and αVCC of 70 ppm/V^2 , simultaneously meeting the ITRS 2014 requirements for capacitance density ($> 5 \text{ fF}/\mu\text{m}^2$), leakage current density ($< 10 \text{ nA}/\text{cm}^2$ at 1V), and voltage nonlinearity ($< 100 \text{ ppm}/\text{V}^2$). Current work is underway to optimize this nanolaminate to meet the ITRS 2017 requirements.

¹ S. Van Huynenbroeck et al, Electron Device Lett. IEEE 23, 191 (2002).

² S.J. Kim et al, Electron Device Lett. IEEE 25, 538 (2004).

³ T.H. Phung et al, Electrochem. Soc. 158, H1289 (2011).

8:40am **EM2-WeM3 Metal-Insulator Transitions, Resistive Switches and Oxide Electronics, Shriram Ramanathan, Harvard University INVITED**

There is growing interest in the exploring complex oxide semiconductors as functional elements in solid state devices. This is in part created by the inevitable limits to use of traditional semiconductors in highly scaled devices and also expanding interest in integrating multiple functionalities at the chip-level. Dielectrics with engineered defects and correlated oxides could be potentially interesting in this regard as switchable, adaptive materials for interconnects, logic and memory. There are a number of fundamental issues from the materials and interface aspects that remain poorly understood. For example, how can we develop a quantitative understanding of the electrical aspects of the high-k / correlated oxide interface where in almost all cases, such phase change materials show drastic frequency dependent properties? How can we design gate stacks to modulate carrier density approaching that of metallic state in such oxides? In this presentation, I will address these problems, with emphasis on studies conducted in our laboratory on rutile (e.g. VO_2) and perovskite (e.g. SmNiO_3) structured oxide thin films that undergo insulator-metal transitions.

9:20am **EM2-WeM5 Complex Oxide Devices, Suman Datta, Penn State University INVITED**

Strongly correlated electronic phases encountered in complex oxides exhibit collective carrier dynamics that if properly harnessed can enable novel functionalities and perhaps even new computation paradigms. In this talk, we will present our recent understanding of electronically triggered charge oscillations in a prototypical metal insulator transition (MIT) system, vanadium dioxide. We show that the key to such oscillatory behavior lies in the ability to stabilize a spontaneously reversible phase transition in the complex oxide devices using a negative feedback mechanism. We also explore the synchronization dynamics of such oscillators via experiment and simulation, and investigate its potential for coupled oscillator based non-Boolean associative computing.

11:00am **EM2-WeM10 Ferroelectric Devices, Alexander Demkov, The University of Texas at Austin INVITED**

Novel methods of deposition developed over the past decade or so, enabled fabrication of thin films of ferroelectric materials, such as BaTiO_3 (BTO), of very high crystal quality. This has resulted in renewed interest in ferroelectric field effect transistors and in addition, led to new device architectures, such as negative capacitance devices. Thanks to very high Pockels coefficient, thin films of BTO may find applications in Si nanophotonics.

In this talk I will describe our recent efforts on integration of BTO (and other ferroic oxides) on semiconductors using a SrTiO_3 (STO) buffer. More specifically, I will describe integration of BaTiO_3 on Si (001) and Ge (001) using molecular beam epitaxy (MBE) and atomic layer deposition (ALD). We employ first principles modeling to both guide the crystal growth and analyze the characterization data. By modeling core level spectroscopy and comparing it with the x-ray photoemission data we are able to identify the Zintl growth template for STO on Si and Ge. Comparing theoretical spectral functions with the angle resolved photoemission spectra (ARPES), provides us with a better understanding of the SrTiO_3 buffer surface. Using this strategy we stabilized ferroelectric state with out-of-plane polarization in BaTiO_3 (BTO) grown on Si with an STO buffer. And we demonstrate both

out-of-plane in-plane polarized BTO growth on Ge (001). Annular dark field microscopy is used to elucidate the atomic structure of the semiconductor/oxide interface that is used in subsequent first principles calculations of the band alignment at the interface. We use a combination of polarization force and microwave impedance microscopies to investigate the ferroelectric response and field effect in our structures.

This work is done in collaboration with Patrick Ponath, Kurt Fredrickson, Agham Posadas, John Ekerdt, David Smith, Martin Frank, Vijay Narayanan, Catherine Dubourdieu, Sergei Kalinin and Keji Lai. It is supported by the Air Force Office of Scientific Research under grant FA9550-12-1-0494, Office of Naval Research (ONR) under grant N000 14-10-1-0489, National Science Foundation under grant DMR- 1207342, and Texas Advanced Computing Center.

11:40am **EM2-WeM12 Enhanced Performance Metal/Insulator/Insulator/Metal (MIIM) Tunnel Diodes, N. Alimardani, John F. Conley, Jr., Oregon State University**

Thin film metal-insulator-metal (MIM) tunnel devices are gaining interest for applications such as hot electron transistors, diodes for optical rectenna based IR energy harvesting, IR detectors, large area macroelectronics, and selector diodes to avoid the sneak leakage in RRAM crossbar arrays. For many of these applications, figures of merit include high asymmetry and strong nonlinearity of current vs. voltage (I-V) behavior at low turn on voltages (V_{ON}). The common strategy to achieving rectification in MIM devices relies on Fowler-Nordheim tunneling (FNT) conduction in conjunction with the use of dissimilar work function metal electrodes to produce an asymmetric, polarity dependent electron tunneling barrier. The properties of single layer MIM diodes are dominated by the choice of insulator. Performance is limited by the workfunction difference that can be achieved between the electrodes as well as the metal-insulator band offsets. Wide bandgap oxides are limited by high V_{ON} . Narrow bandgap dielectrics such as Ta_2O_5 and Nb_2O_5 are attractive because the small barrier heights allow for low turn-on voltages. However, because conduction in these materials is based on emission rather than tunneling, they may not be suitable for high speed rectification. Recently, we showed that a nanolaminate pair of insulators ($\text{Al}_2\text{O}_3/\text{HfO}_2$) can be used to form MIIM diodes with enhanced performance over single layer MIM diodes and demonstrated that observed enhancements in low voltage asymmetry are due to "step tunneling," a situation in which an electron may tunnel through only the larger bandgap insulator instead of both.¹

In this work, we show that MIIM diodes may require only one of the insulators to be dominated by tunneling and thus allow use of narrow band gap insulators for tunnel devices. Atomic layer deposition (ALD) was used to deposit nanolaminate insulators on smooth amorphous metal bottom electrodes. We demonstrate that Ta_2O_5 , a narrow bandgap dielectric dominated by thermal emission, may be combined with Al_2O_3 , a wide bandgap dielectric dominated by tunneling, to achieve high asymmetry, low V_{ON} MIIM diodes whose overall performance is dominated by tunneling. The performance of a variety of other bilayer MIIM diodes ($\text{HfO}_2/\text{Ta}_2\text{O}_5$, $\text{ZrO}_2/\text{Ta}_2\text{O}_5$, $\text{Al}_2\text{O}_3/\text{ZrO}_2$, and $\text{HfO}_2/\text{ZrO}_2$) will be discussed as well. These results advance the understanding needed to engineer thin film tunnel devices for microelectronics applications.

1. N. Alimardani and J.F. Conley, Jr., Appl. Phys. Lett. 102, 143501 (2013).

12:00pm **EM2-WeM13 Assessment of Barrier Heights between ZrCuAlNi Amorphous Metal and SiO_2 , Al_2O_3 , and HfO_2 using Internal Photoemission Spectroscopy, Tyler Klarr, Oregon State University, L. Wei, N.V. Nguyen, O.A. Kirillov, National Institute of Standards and Technology (NIST), J. McGlone, J. Wager, J.F. Conley, Oregon State University**

As scaling of Si based devices approaches fundamental limits, thin film metal-insulator-metal (MIM) tunnel diodes are attracting interest due to their potential for high speed operation. Because operation of these devices is based on tunneling, electrode / interfacial roughness is critical. Recently, we showed that combining ultra-smooth bottom electrodes with insulators deposited via atomic layer deposition (ALD) enabled reproducible fabrication of MIM diodes with stable I-V behavior.¹ Key performance parameters of MIM diodes include high I-V asymmetry and low turn-on voltage. The standard way to achieve asymmetry relies on the use of non-equivalent workfunction metal electrodes to induce a built-in field that creates polarity dependent electron tunneling barrier.² Assessment of metal-insulator barrier heights is therefore critical for predicting diode performance.

In this work, we report the first use of internal photoemission spectroscopy (IPE) to measure barrier heights between an amorphous ZrCuAlNi (ZCAN) metal bottom electrode and several high-k dielectrics. MIM stacks were fabricated on Si substrates capped with 100nm of thermally grown SiO_2 and a 150nm thick ZCAN amorphous metal bottom electrode deposited via DC magnetron sputtering. Al_2O_3 and HfO_2 were deposited via thermal ALD at

250°C using H₂O and TMA or TEMA-Hf, respectively. SiO₂ was deposited using plasma-enhanced ALD (PEALD) at 200°C using O₂ and bis-diethylaminosilane (BDEAS). For IPE measurements, semitransparent top electrodes were formed by electron beam evaporation of Al (0.04mm²) and patterned by a multistep photolithography process. In IPE, the conduction band offset between two materials is characterized by measuring the additional current created by photo-excitation of carriers under an applied bias (V_{app}). Devices were tested in a custom built IPE system in which incident photon energy (E_{ph}) from a broadband 150W xenon lamp source was swept from 1.5 to 5eV while the increase in current (photoemission yield) was monitored. The V_{app} polarity was such that photoemission occurs at the ZCAN/insulator interface. The photoemission yield^{1/2} was plotted vs. E_{ph} to determine the spectral threshold at each V_{app}. Finally, a Schottky plot of spectral threshold vs. V_{app}^{1/2} was used to estimate the zero field barrier heights from the y-axis intercept. Initial analysis indicates barriers of 3.4, 3.2, and 2.7 eV for SiO₂, Al₂O₃, and HfO₂, respectively. Additional dielectrics and metals are under investigation. IPE results will be compared to electrical methods of barrier extraction.

1. N. Alimardani et al, JVSTA 30, 01A113 (2012).

2. J.G. Simmons, JAP 34, 2581 (1963); JAP 34, 1793 (1963).

Energy Frontiers Focus Topic

Room: 315 - Session EN+AS+EM+SE-WeM

Thin Film Photovoltaics

Moderator: Rachel Morrish, Colorado School of Mines

8:20am **EN+AS+EM+SE-WeM2 Epitaxy and Nanochemistry of CdS on Cu(In,Ga)Se₂ for Photovoltaic Devices**, *X. He*, University of Illinois at Urbana Champaign, *H. Tellez, J. Druce*, Kyushu University, Japan, *K. Demirkan, Miasole, P. Ercius*, Lawrence Berkeley National Laboratory, *V. Lordi*, Lawrence Livermore National Laboratory, *J. Kilner*, Imperial College London, UK, *T. Ishihara*, Kyushu University, Japan, **Angus Rockett**, University of Illinois at Urbana Champaign

Cu(In,Ga)Se₂ (CIGS) photovoltaics are very promising candidates for high-performance energy generation from sunlight. They typically include a heterojunction between CdS and CIGS. The nature of that heterojunction is critical to the performance of the devices. We present experimental results on the nanochemistry of CIGS and CIGS/CdS heterojunctions and the nanostructure of the junctions. In particular we present low energy ion scattering (LEIS) results on epitaxial single crystal CIGS and CIGS/CdS heterojunctions formed by chemical bath deposition of CdS. Also shown are results of high-resolution transmission electron microscopy (TEM) studies of the CIGS/CdS heterojunction where the junction is formed by physical vapor deposition. LEIS has single-atomic-layer chemical sensitivity that provides a unique ability to distinguish the nanochemical nature of CIGS surfaces and heterojunctions. TEM provides both nanostructural information and the possibility to determine the chemistry of the junction on the nanoscale by energy dispersive spectroscopy and energy filtered imaging. Complete epitaxy of the CdS throughout its ~50 nm thickness is observed in the physical-vapor-deposited CdS. Domains of cubic zincblende and hexagonal wurtzite structure CdS have been observed. Twins in the CIGS grains were found to propagate into and often through the CdS layer, resulting in a twin or grain boundary in the CdS. The CdS epitaxial relationship and the effect of surface steps on the CIGS surface are shown. The nanochemical analysis results show significant penetration of Cu into the CdS layer, although no alteration in the CdS nanostructure is observed. The other elements show an abrupt nanochemical junction. LEIS results show the presence of segregated layers on the CIGS surface and further refine the nature of the nanochemical intermixing across the interface.

8:40am **EN+AS+EM+SE-WeM3 Microstructure Development in Cu₂ZnSn(S_xSe_{1-x})₄ Thin Films During Annealing of Colloidal Nanocrystal Coatings**, *B.D. Chernomordik, M. Ketkar, K. Hunter, A.E. B elard, Eray Aydil*, University of Minnesota

A potentially high-throughput and inexpensive method for making Cu₂ZnSn(S_xSe_{1-x})₄ (CZTSSe) thin film absorber layers for solar cells is annealing of coatings cast from colloidal dispersions of CZTS nanocrystals (NCs). The nanocrystal coatings can be annealed in sulfur or selenium atmosphere to make CZTS or CZTSSe, respectively. During annealing, the nanocrystal films can transform into polycrystalline thin films with micrometer size grains. Understanding the roles of key annealing parameters in the development of microstructure in CZTSSe thin films is critical for achieving inexpensive and high-efficiency CZTSSe solar cells. In this presentation, we will discuss the effects of parameters such as selenium vapor pressure, annealing temperature, substrate, and heating

ramp-rate on the microstructure development in CZTSSe films and contrast the results with films annealed in sulfur. By using a closed system, rather than a flow furnace, we can quantify and systematically control selenium pressure. Annealing films at high selenium pressure (450 Torr) leads to the formation of a layer of 2-5 μm size CZTSSe grains on top of a nanocrystalline layer that is rich in carbon. This segregation of carbon at the CZTSSe-substrate interface is commonly ascribed to the immediate formation of a capping/blocking layer of CZTSSe grains, which trap the carbon, originating from the ligands on NC surfaces, beneath these grains. However, we found that a continuous layer of CZTSSe grains is not necessary to observe carbon segregation to the film-substrate interface. In contrast, films annealed with sulfur do not show such distinct carbon-rich layers and most of the carbon volatilizes from the film during annealing. Increasing the heating ramp-rate to the annealing temperature eliminates the formation of the carbon-rich layer and results in grains that are approximately 500 nm. We will discuss the results of a series of experiments which led us to conclude that Se condensation during annealing may play a key role in grain growth and carbon segregation.

9:00am **EN+AS+EM+SE-WeM4 Effect of Chemical Wet Cleaning on Surface Composition and Work Function of Thin Film CZTS,Se**, *Kasra Sardashti*, University of California at San Diego, *E.A. Chagarov, T. Kaufman-Osborn*, University of California, San Diego, *S.W. Park*, University of California San Diego, *R. Haight, W. Wang, D.B. Mitzi*, IBM T.J. Watson Research Center, *A.C. Kummel*, University of California at San Diego

Polycrystalline Copper-tin-zinc-sulfide/selenide (CZTS,Se) compounds have received wide research interest due to their potential as inexpensive absorber materials composed earth-abundant elements. Photovoltaic devices fabricated on CZTS,Se has reached the highest (or record) conversion efficiency of the 12.6 %. One of the key parameters to further boost the conversion efficiency is to control the concentration of recombination sites at the surface, in the grain boundaries, and in the bulk. Surface states formed on the sample surface as a result of carbon and oxygen contamination can act as non-radiative recombination sites which limit the ultimate cell efficiency. Therefore, a surface-cleaning method which can effectively reduce the amount of surface oxygen and carbon is necessary for CZTS,Se processing. In this work, 2 μm thick CZTS,Se films were prepared by spin coating hydrazine-based precursor solutions onto Mo-coated soda lime glass substrates in a nitrogen-filled glove box. To clean the CZTS,Se surfaces, three different wet cleaning recipes were used: a) NH₄OH only; b) HCl followed by NH₄OH; 3) H₂O₂ followed by NH₄OH. The effect of the wet cleaning on the surface composition including carbon and oxygen content has been studied via X-ray photoelectron spectroscopy (XPS) and femtosecond ultraviolet photoelectron spectroscopy (fs-UPS). Spatial variation of work function over the surface upon surface cleaning was measured via Kelvin Probe Force Microscopy (KPFM). The stability of the clean surface against reoxidation in ambient was modeled by density functional theory (DFT). The H₂O₂/NH₄OH recipe showed the best result reducing the amount of surface O and C down to 5% and 20%, respectively. This is due to the oxidizing effect of H₂O₂ which converted the carbonaceous surfaces contaminants into oxides which were later removed by NH₄OH. DFT calculations are consistent with a group VI surface being stable against oxidation by ambient moisture. KPFM measurements showed strongly non-homogeneous surfaces after both NH₄OH-only and H₂O₂/NH₄OH clean. Areas with work function different from CZTS could be the binary chalcogenides formed during the growth and were covered by the native oxide. NH₄OH etch successfully removed the covering oxide and made those phases visible to KPFM.

9:20am **EN+AS+EM+SE-WeM5 Phase Transformation, Surface States, and Electronic Structures of Pyrite Thin Films Under In Situ Heating and Oxygen Gas Exposure**, *Yu Liu, N. Berry, Y.N. Zhang*, University of California Irvine, *C.-C. Chen*, Argonne National Laboratory, *H. Bluhm, Z. Liu*, Lawrence Berkeley National Laboratory, *R.Q. Wu, M. Law, J.C. Hemminger*, University of California Irvine

Iron pyrite (cubic FeS₂) with its exceptional optical absorption and suitable band gap is a promising earth-abundant semiconductor for thin film solar cells. Using ambient pressure synchrotron x-ray spectroscopies, we report the nanoscale depth profiles of surface and electronic structures for phase-pure pyrite thin films under *in situ* heating and oxygen gas exposure. Polarized x-ray absorption spectra show that the absorption edge of Fe L₂-edge shifts closer to the Fermi surface with increasing temperature. The XAS line shapes of Fe and S L-edge provide the information of ligand crystal field environment and the phases of the FeS₂ particles. We also report the non-destructive photoemission depth distributions of sulfur defects, vacancies, impurities and oxide as a function of temperature and oxygen dose. Valence band spectra indicate a band gap narrowing related to the creation of surface states at elevated temperature. An irreversible phase transition from pyrite (FeS₂) to pyrrhotites (Fe_{1-x}S) occurs above 430 °C. In

addition, our results under *in situ* oxygen gas exposure suggest that the surface monosulfide species is oxidized first, and the reduction in the total density of states near the Fermi surface is caused by oxide layers of sulfate like and iron oxide products on the top ~2 nm.

9:40am **EN+AS+EM+SE-WeM6 Improvement of SnS-based Photovoltaic Devices via Reverse Engineering of the V_{oc} and Study of Optimal n-Type Material**, *Rona Banai, N.J. Tanen, J.J. Cordell, J.R. Nasr, R.E. Urena, H. Lee, J.R.S. Brownson, M.W. Horn*, Penn State University

Tin (II) Monosulfide (SnS) has theoretical promise as a new material for thin film photovoltaics (PV). Despite a full decade of rigorous research to develop SnS-based devices, improvement beyond single-digit percent efficiencies seems unattainable. Engineering this material into a usable device is crucial for future development. Our group has been investigating the optical and structural properties of magnetron sputtered SnS_x thin films [1,2,3]. This work will investigate the properties that govern open-circuit voltage, including band gap, series resistance, carrier concentration and built-in potential. Some of these parameters are directly related to the junction material paired with SnS. Several partner materials will be presented with p-SnS including, but not limited to highly doped n-ZnO and n-SnS. Current work is underway to produce n-type SnS as well which would have potential to produce a homojunction.

The optoelectronic properties of SnS make it a suitable material for PV. Its high absorption coefficient, greater than 10⁴ cm⁻¹, and band gap near 1.3 eV are well matched with the solar spectrum. SnS also has a carrier concentration greater than 10¹⁵ cm⁻³ and potential to be both n-type and p-type. Our group is able to produce dense SnS thin films with optimal electronic properties. Sputtering the material gives great control over the material properties and recent work optimizing post-deposition heat treatment has shown great promise for improving the material.

Tin sulfide thin films were sputtered on glass and oxidized silicon substrates at varying substrate-to-target distances, substrate temperature, target power, and chamber pressure. The sputter target was a 3" SnS₂ with 99.999% purity (LTS Research Laboratories, Inc.). These sulfur-rich samples were then annealed under medium vacuum (<2x10⁻⁶ Torr) in the deposition chamber at 400°C to produce a uniform α-SnS, which is most likely to be p-type. Producing n-type SnS is possible via annealing of the films in a methanol/SnCl₄ solution. Production of homojunction SnS-based thin film devices is not found in the literature. Our work aims to produce these devices for the first time and compare them to a well-known partner material such as ZnO.

- [1] R. E. Banai, et al., in *Proceedings of 2012 38th IEEE Photovoltaics Specialists Conference*, Austin, 2012, pp. 164-169.
- [2] R. E. Banai, et al., *IEEE Journal of Photovoltaics*, vol. 3, no. 3, pp. 1084-1089, 2013.
- [3] R. E. Banai, et al., in *Proceedings of 2013 39th IEEE Photovoltaic Specialists Conference*, Tampa, 2013, pp. 2562-2566.

11:00am **EN+AS+EM+SE-WeM10 Advanced Contacts for High Efficiency CdTe Solar Cells**, *D. Meysing, J.J. Li, J. Beach, T.R. Ohno*, Colorado School of Mines, *M.O. Reese, T.M. Barnes*, National Renewable Energy Laboratory, *Colin Wolden*, Colorado School of Mines

Record CdTe device efficiency has recently surpassed 20%, and it is the leading thin film photovoltaic technology in terms of commercial installation with current manufacturing capacity exceeding 1 GW/year. However, with a Shockley-Queisser limit of ~33% there remains substantial room for additional improvements in efficiency. The quality of both the front and back contacts has substantial influence on CdTe solar cells device efficiency, impacting the current and voltage respectively. This talk will focus on recent work directed at understanding the materials science of both the front and back contact interfaces and optimizing their performance.

Cadmium sulfide is the most commonly employed window layer in the front contact, and its properties can greatly affect cell performance through optical absorption and the quality of the CdS-CdTe junction. In this work, we develop reactive sputtering as an alternative to chemical bath deposition (CBD) for the production of oxygenated cadmium sulfide (CdS:O) to enable high efficiency CdTe solar cells. The intrinsic properties of CdS:O as well as their impact on device performance were studied by varying the oxygen content in the Ar sputtering ambient over the range of 0-10%. XRD, RBS, XPS, and spectrophotometry were used to measure the crystal structure, composition, bonding, and optical properties, respectively. The variation in properties is unsurprisingly non-linear, and optimal performance is attributed to a compromise between optical transmission, which improve monotonically with oxygen content, and band alignment which sharply attenuates device performance beyond a critical threshold.

It is notoriously difficult to make a good ohmic contact to CdTe using conventional metals, because this requires a work function of greater than 5.7 eV. Copper-doped zinc telluride (ZnTe:Cu) is one of the most commonly employed buffer layers to mitigate this issue. ZnTe was identified due to its valence band alignment and compatibility with CdTe. Copper has both positive and deleterious effects and it is critical to precisely control both its amount and spatial distribution in order to obtain high efficiency. We have developed a back contacting procedure that employs rapid thermal processing (RTP) to deliver precise control over the activation and distribution of Cu. The RTP process is coupled with atom probe tomography and advanced optoelectronic characterization to improve our understanding of the structure-property-performance relationships in this system. The advances achieved here using commercially scalable processes are combined to produce devices with $V_{oc} > 850$ mV and efficiencies exceeding 16%.

11:20am **EN+AS+EM+SE-WeM11 Structural Variations and their Effects on the Fundamental Bandgap of ZnSnN₂**, *Nathaniel Feldberg*, University at Buffalo-SUNY, *Y. Yang*, University of Michigan, *W.M. Linhart, T.D. Veal*, University of Liverpool, UK, *P.A. Stampe, R.J. Kennedy*, Florida A&M University, *D.O. Scanlon*, University College London, UK, *L.F.J. Piper*, Binghamton University, *N. Senabulya, R. Clarke*, University of Michigan, *R.J. Reeves*, University of Canterbury, New Zealand, *S. Durbin*, Western Michigan University

In recent years Zn-IV-N₂ compounds have seen increased interest as potential earth abundant element semiconductors for photovoltaic and solid state lighting applications. Several reports of successful growth for the Ge and Si containing compounds are extant as well as more recent publications on the Sn containing member of the family. This material offers a possible alternative to indium containing materials which have experienced large price fluctuations due to limited domestic supply, lack of recycling and heightened demand. Our films were grown by plasma assisted molecular beam epitaxy on (111)-yttria stabilized zirconia. In the case of an ordered lattice, density functional theory (DFT) predicts an orthorhombic structure; however, the disordered lattice is predicted to be pseudo-hexagonal. Reflection high energy electron diffraction patterns for these films indicate single crystal structure with hexagonal symmetry, consistent with X-ray diffraction measurements. Hall effect indicates carrier concentrations in the 3-10x10²¹ cm⁻³ range for which we would expect a significant Burstein-Moss shift. Contrary to expectations, optical measurements of absorption onset occur at higher energy in films with lower carrier concentrations. As in ZnSnP₂, the bandgap is expected to narrow with the introduction of disorder for this material; this narrowing behavior is consistent with observed variations in absorption spectra. Of practical interest is the possibility of a material with a tunable bandgap without the need for traditional alloying. Zn-Sn-N₂ is expected to have a bandgap varying from 1.1 to 2 eV controlled by the continuous degree of order in the cation sublattice. Although hard X-ray diffraction measurements of these films do not show any variation from a hexagonal structure, Hall measurements of carrier concentrations compared with absorption data indicates that our samples vary their absorption onset, not as would be expected from Burstein-Moss Shift, but in a manner consistent with a variation in the lattice order. DFT calculations indicate that there is a variation in the Density of States between the ordered and disordered films. Films which were consistent with increased order absorption are also consistent with an increased order density of states measured by HAXPES.

This project is supported by NSF grant DMR1244887 (Program Director Charles Ying), and EPSRC grant EP/G004447/2.

11:40am **EN+AS+EM+SE-WeM12 Inhomogeneity of p-n Junction and Grain Structure of Thin Film CdTe Solar Cells Studied by Electron Beams**, *Heayoung Yoon, P. Haney*, NIST, *P. Koirala*, University of Toledo, *J.I. Basham, Y. Yoon*, NIST, *R.W. Collins*, University of Toledo, *N.B. Zhitenev*, NIST

Thin film CdTe solar cells are a promising photovoltaic (PV) technology in today's market due to their high optical absorption and inexpensive fabrication processes. However, the current module efficiency is well below the theoretically estimated maximum efficiency (13 % vs. 30 %). Recent studies have suggested that inhomogeneity of the PV materials is mainly responsible for the low power conversion efficiency. In this work, we investigate the variation of local PV properties of CdTe solar cells, focusing on grain bulk, grain boundaries, and n-CdS / p-CdTe junctions. The window (≈ 120 nm thick CdS) and absorber (≈ 2.2 μm thick CdTe) layers were sputtered on a TCO (transparent conductive oxide) coated glass substrate followed by CdCl₂ treatment. The back contact metals (3 nm Cu / 30 nm Au) were deposited and annealed, creating 256 devices in a 15 cm by 15 cm solar panel. Following light and dark current-voltage measurements, we performed local characterizations using electron beams for high (> 13 %) and low efficiency (< 6 %) devices within the panel. Electron beam induced current (EBIC) was used to measure the local carrier collection

efficiency with a spatial resolution of ≈ 20 nm exciting carriers either from the top surface or the cross-sections of the devices. Cross-sectional EBIC data reveals that the peak of efficiency is in the middle of CdTe layer in the low efficiency devices, while the carrier collection is maximal near the *p-n* junction in the high efficiency devices. The EBIC contrasts at grains/grain boundaries in these devices are also compared. The measured local electronic properties are correlated to microstructural morphology (Transmission Electron Microscopy), orientation (Electron Back Scattered Diffraction), and chemical composition (Energy Dispersive X-ray spectroscopy). We perform 2D model drift-diffusion simulations to determine the magnitude of downward band-bending near grain boundaries (with typical magnitude of 0.2 eV). We will discuss the impact of carrier generation rate (high level injection vs. low level injection) in EBIC analysis.

12:00pm **EN+AS+EM+SE-WeM13 Micro-Structural Activation Mechanisms in Thin Film CdTe Photovoltaic Devices**, *John Walls, A. Abbas, J.W. Bowers, P.M. Kaminski*, Loughborough University, UK, *K. Barth, W. Sampath*, Colorado State University

Thin Film CdTe photovoltaics is a commercially successful second generation technology now used extensively in solar energy generation at the utility scale. Although the cadmium chloride treatment is a process that is essential to produce high efficiency devices, the precise mechanisms involved in the re-crystallization and associated improvement in electronic properties have not been fully understood. In this paper we report on the application of advanced micro-structural characterization techniques to study the effect of the cadmium chloride treatment on the physical properties of the cadmium telluride solar cell deposited by both close space sublimation (CSS) and magnetron sputtering and relate these observations to device performance. In particular, High Resolution Transmission Electron Microscopy (HRTEM) reveals that the untreated material contains high densities of planar defects which are predominantly stacking faults and that the optimized cadmium chloride treatment removes these completely with only twins remaining. Parallel theoretical studies using Density Functional Theory (DFT) shows that certain types of stacking fault are responsible for the poor performance of the untreated material. Extending the treatment time or increasing the annealing temperature above $\sim 400^\circ\text{C}$ improves the microstructure but results in lower efficiency devices. Composition –depth profiling using XPS and SIMS reveals that this deterioration in performance is linked with chlorine build up at the CdS/CdTe junction. These experiments and parallel theoretical studies have improved our understanding of the mechanisms at work in the cadmium chloride assisted re-crystallization of CdTe and could lead to further increases in device efficiency

Exhibitor Technology Spotlight

Room: Hall ABC - Session EW-WeM

Exhibitor Technology Spotlight Session

Moderator: Chris Moffitt, Kratos Analytical Limited, UK

10:20am **EW-WeM8 Product Advancements to Reduce Semiconductor Manufacturing Contamination**, *J. Legare, Mark Heller*, Dupont™ Kalrez® and Vespel

Sealing materials can degrade in harsh semiconductor manufacturing processes. Advancements in elastomeric sealing materials and their components help reduce the risk of contamination from sealing materials. This presentation will highlight the latest DuPont Kalrez® sealing products and their test results.

10:40am **EW-WeM9 Wet Cell II for Analysis at the Liquid Vacuum Interface**, *Junhang Luo, Rodek*, SPI Supplies

The liquid interfaces chemistry plays a key role in environmental, biological, and industrial processes. However, in-situ analyzing liquid surface is an extreme challenge because of the rapid liquid evaporation especially in vacuum. Wet Cell II makes it possible and simple for scientists and researchers to directly analysis of liquids at the molecular level in a vacuum environment with minor cost. As a lab-on-a-chip device, Wet Cell II can be straightforwardly adaptable to many different analytical platforms, including scanning electron microscopy (SEM) and time-of-flight secondary ion mass spectrometry (TOF-SIMS). Wet Cell II only consumes a few drops of liquid and requires little or no sample preparation. Typical applications include microbiology, liquid surface chemistry, drug delivery & reaction, and energy storage, etc.

In-Situ Spectroscopy and Microscopy Focus Topic

Room: 313 - Session IS+AS+MC+SS-WeM

In-Situ X-ray Absorption and Raman Spectroscopy

Moderator: Hirohito Ogasawara, SLAC National Accelerator Laboratory

8:00am **IS+AS+MC+SS-WeM1 In Situ Studies on the Behavior of Metal/Oxide Catalysts during the Water-gas Shift Reaction**, *Jose Rodriguez, D. Stacchiola, S. Senanayake, J. Hanson*, Brookhaven National Laboratory

INVITED
In this talk, it will be shown how a series of *in-situ* techniques [X-ray diffraction (XRD), pair-distribution-function analysis (PDF), X-ray absorption spectroscopy (XAS), environmental scanning tunneling microscopy (ESTM), infrared spectroscopy (IR), ambient-pressure X-ray photoelectron spectroscopy (AP-XPS)] can be combined to perform detailed studies of the structural, electronic and chemical properties of metal/oxide catalysts used for the production of hydrogen through the water-gas shift reaction (WGS , $\text{CO} + \text{H}_2\text{O} \rightarrow \text{H}_2 + \text{CO}_2$). Under reaction conditions most WGS catalysts undergo chemical transformations that drastically modify their composition with respect to that obtained during the synthesis process. The active phase of catalysts which combine Cu, Au or Pt with oxides such as ZnO, CeO₂, TiO₂, CeO_x/TiO₂ and Fe₂O₃ essentially involves nanoparticles of the reduced noble metals. The oxide support undergoes partial reduction and is not a simple spectator, facilitating the dissociation of water and in some cases modifying the chemical properties of the supported metal. Therefore, to optimize the performance of these catalysts one must take into consideration the properties of the metal and oxide phases. IR and AP-XPS have been used to study the reaction mechanism for the WGS on the metal/oxide catalysts. Data of IR spectroscopy indicate that formate species are not necessarily involved in the main reaction path for the water-gas shift on Cu-, Au- and Pt-based catalysts. Thus, a pure redox mechanism or associative mechanisms that involve either carbonate-like (CO₃, HCO₃) or carboxyl (HOCO) species should be considered. In the last two decades, there have been tremendous advances in our ability to study catalytic materials under reaction conditions and we are moving towards the major goal of fully understanding how the active sites for the production of hydrogen through the WGS actually work.

8:40am **IS+AS+MC+SS-WeM3 Tuning Catalytic Performance of Bimetallic Nanoparticle Catalysts through a Single or Sequential Post-Synthesis Reaction in a Gas Phase**, *F. Tao, J. Shan, S. Zhang, L.T. Nguyen*, University of Notre Dame, *A. Frenkel*, Yeshiva University, *J. Greeley*, Purdue University, *Shibi Zeng*, University of Notre Dame

Besides a sophisticated synthesis of bimetallic nanocatalysts in a colloidal solution, a post-synthesis reaction in a gaseous phase is a complementary method to tailor the surface structure and composition of a bimetallic nanocatalyst to tune its catalytic performance. Here we illustrate the capability of creating a new catalyst surface exhibiting a lower activation barrier through segregation of a bimetallic catalyst in a post-synthesis reaction in a reactive gaseous environment. In-situ surface chemistry of bimetallic nanocatalysts were analyzed with AP-XPS. Coordination environment of Pt and Cu atoms under different reaction conditions was tracked with in-situ EXAFS. The surface restructuring was simulated with DFT calculation from thermodynamic, *ci* point of view. The composition and geometric structure of the newly formed surface of the bimetallic nanocatalysts strongly depend on the reactant gas used in the post-synthesis reaction. A further sequential reaction in a different gas after the initial post-synthesis reaction in a gas forms a different catalyst surface. A post-synthesis reaction of a Pt-Cu regular nanocube (Pt-Cu RNC) in hydrogen forms a near surface alloy (NSA) which exhibits an activation barrier of 39 kJ/mol for CO oxidation, much lower than pure Pt nanocubes. These studies demonstrate a method of tuning catalytic performances and generate another catalytic phase through a post-synthesis reaction in a gas phase.

9:00am **IS+AS+MC+SS-WeM4 In Situ Characterization of Metal-Based Ionic Liquids using X-ray Spectroscopy**, *Robert Meulenber*, University of Maine, *C. Apblett, H. Pratt, T. Anderson*, Sandia National Laboratories

Energy storage for vehicles is advancing rapidly, and one of the possible contenders for a battery that can quickly be recharged is a redox flow battery, which uses liquids that are pumped into the battery to be charged or discharged, and then removed to storage containers. This makes the chemistry roughly analogous to liquid fuels employment, where the charged chemistry is pumped into the battery, discharged, and then pumped into a waste container, similar to fuel pumped into an engine, ignited, and then expelled through the tailpipe. Unlike internal combustion engines, however, the discharged product is retained on the vehicle, and can be subsequently

either recharged on the vehicle, or pumped off the vehicle to be recharged at a filling station, while replacing with freshly charged material.

To date, however, the concentrations of most redox flow battery chemistries have been low, below the 1-2M concentration level. Recently, a new type of ionic liquid (IL) redox flow chemistry has been developed that raises this to 5-6M, and improves the energy density of the system. However, little is known about the structure of the molecule in the charged and discharged states. The current understanding of the structure of the IL, primarily the Fe IL, comes from primarily from FTIR, Raman, and TGA/DSC data, as traditional methods such as NMR to probe surface chemistry are limited due to the paramagnetic Fe center. It is believed the coordination of the ligand to the metal center occurs primarily through the alcohol groups. Cyclic voltammetry of the FeIL exhibits behavior associated with Fe(III)/Fe(II) reduction/oxidation, with some evidence that the ligands are coordinating to adjacent Fe atoms, resulting in antiferromagnetic coupling between the metal centers. A complete, fundamental understanding of the local coordination and ligand environment is not known and is the primary goal of our research. To further understand this structure, we have constructed a new electrochemical cell to be used for *in situ* transmission Fe K-edge x-ray absorption fine structure (XAFS) spectroscopy. We conduct our measurements at various states of charge, and the structure of the molecule in these various states is determined using this from analyzing both the XANES and EXAFS. Effects of electrochemical cell potential on local structure of the FeIL will be discussed.

9:20am **IS+AS+MC+SS-WeM5 Monitoring Catalysts during Catalytic Reactions with *In Situ* Raman Spectroscopy, Israel Wachs, Lehigh University** **INVITED**

The surfaces of heterogeneous catalysts in reactive environments are dynamic and require *in situ* characterization studies under reaction conditions to fully understand their fundamental structure-activity relationships. This presentation will focus on the application of Raman spectroscopy to determine the nature of the catalytic active sites in different reaction environments. Emphasis will be placed on investigating heterogeneous supported metal oxide catalysts containing multiple catalytic active sites and determining the roles of each of the sites. Some of the examples to be presented will be the metathesis of $H_2C=CHCH_3$ to $H_2C=CH_2$ and $H_3C-CH=CHCH_3$ by supported ReO_x/Al_2O_3 catalysts, polymerization of $H_2C=CH_2$ by supported CrO_x/SiO_2 and methane conversion to aromatic liquids by supported $MoO_x/ZSM-5$ catalysts.

11:00am **IS+AS+MC+SS-WeM10 Photoelectron Spectroscopy on Ice, Mineral Oxides and Aqueous Solutions of Atmospheric Relevance, Markus Ammann, Paul Scherrer Institut, Switzerland** **INVITED**

Aerosol particles and ice are key in atmospheric chemistry as many chemical and physical processes occurring on and within them are relevant for air pollution and climate. The fundamental understanding of these processes increasingly relies on a molecular level description of structures and mechanisms. This requires tools to access condensed phase – air interfaces with structural and chemical selectivity. Recent advances in pushing the pressure limits of ultrahigh-vacuum surface science methods such as photoelectron spectroscopy have allowed the investigation of environmentally relevant surfaces under nearly ambient conditions and have thereby significantly contributed to the advancement of our understanding of interfaces in the atmosphere. In this overview, recent results on the interaction of acidic gases with ice surfaces, of chemical and photochemical processes on mineral oxides, and of the structure of aqueous solution surfaces will be presented. These examples also demonstrate the instrumental requirements for such *in situ* experiments, and our recent developments of sample environments to facilitate experiments with environmental substrates will be presented.

11:40am **IS+AS+MC+SS-WeM12 *In Situ* Analysis of Materials Under Mechanical Stress: A Novel Instrument for Simultaneous Nanoindentation and Raman Spectroscopy, Chris Michaels, Y.B. Gerbig, R.F. Cook, NIST**

Instrumented indentation or “nanoindentation” is a method that is widely used in the study of the mechanical deformation of materials on small length scales (~ micrometer). Raman spectroscopy is a technique that provides insight into the molecular or crystallographic level processes involved in the mechanical deformation of materials, such as strain build-up, phase transformations and variations in crystallinity. Typically these approaches have been used separately wherein the spectroscopic analysis of the material might take place prior to and after the end of a mechanical transformation. Of course, there is significant interest in *in situ* analyses of materials during mechanical transformation as such an approach promises a richer understanding of the underlying physics than is likely possible with analysis limited to pre- and post-transformation. For example, the ability to follow the path of phase transformations rather than just the endpoints is

certainly desirable. Consequently, significant effort has been directed toward the coupling of indentation instruments with various *in situ* analysis capabilities.

This talk describes the design and operation of a nanoindentation instrument that is coupled with a laser scanning Raman microscope to conduct *in situ* spectroscopic analyses of mechanically deformed regions of optically transparent materials under contact loading. The force transducer of the device allows adjustment of crucial experimental parameters, such as indentation loads and loading rates. An incorporated displacement sensor allows for collection of force-displacement curves comparable to conventional nanoindentation instruments. The device is mounted on the sample stage of an inverted optical microscope that is configured for Raman microscopy, allowing optical access to the mechanically deformed regions of transparent samples. The capabilities of this novel instrument will be demonstrated by *in situ* studies of the indentation-induced phase transformations in an epitaxial silicon-on-sapphire (SoS) thin film, in both a microspectroscopy and a laser scanning Raman imaging configuration.

Accelerating Materials Discovery for Global Competitiveness Focus Topic Room: 302 - Session MG-WeM

Design of New Materials

Moderator: Christian Elsässer, Fraunhofer Institute for Mechanics of Materials IWM, Susan Sinnott, University of Florida

8:20am **MG-WeM2 Hydrogen Molecules Distribution in Multi-Cathodes Funnelling Gun, Erdong Wang, I. Ben-Zvi, J. Skaritka, T. Rao, Brookhaven National Laboratory, R. Bothell, J. Bothell, A. Henry, Atlas Technologies**

The high average current polarized electron source for future electron ion collider (EIC) requires extremely high vacuum. Currently, we have constructed a DC gun based on principle of beams funneling and this gun is under commissioning. Superlattice GaAs cathodes will be used as our electron source. The lifetime of these cathodes is dependent on ion back bombardment which caused by the residual gas pressure. Multiple GaAs cathodes with almost same lifetime are extremely crucial for the operation of this gun. Therefore, produce a uniform extremely high vacuum environment is essential in gun design. We studied residual molecules distribution in funneling gun by Molflow+ and a python based Monte-Carlo simulator. Twenty cathodes testing is under planning. Cathodes lifetime changes will give us indication on vacuum distribution inside the gun. This articles describes our coding and modeling for the gun vacuum, analyzes the residual gas distribution on the gun and discusses on multiple cathodes lifetime measurement test. We also discusses the XHV achievement in our gun test.

8:40am **MG-WeM3 Tailored Functionality of Wide Band Gap Semiconductors, B.E. Gaddy, Z.A. Bryan, I.S. Bryan, R. Kirste, North Carolina State University, J. Xie, R. Dalmau, B. Moody, Hexatech Inc., Y. Kumagai, Tokyo University of Agriculture and Technology, Japan, T. Nagashima, Y. Kubota, T. Kinoshita, Tokuyama Corporation, Japan, A. Koukitu, Tokyo University of Agriculture and Technology, Japan, R. Collazo, Z. Sitar, Douglas Irving, North Carolina State University**

Semiconductors obtain new functionality by the incorporation of dilute concentrations of impurities. This principle has been utilized to tailor the properties of narrow gap semiconductors, such as Si or GaAs, but tailoring the properties of wide band gap materials for optical or high power applications has been extremely challenging. As a result, there has been slow progress in identifying *new material* combinations (bulk material + dilute dopants) to enable *novel functionality*. To help overcome these obstacles, we have developed and implemented a point defects database in which we store formation, ionization, and optical transition energies determined by hybrid exchange-correlation density functional theory methods. These predictions from first principles are then strongly coupled with synthesis and characterization efforts to identify troublesome point defects and also suggest routes to realizing desired properties if particular defect cannot be removed. The stored data is also used to solve mass balance equations to determine the number of carriers and compensating defects. In this talk, I will present our recent efforts in applying these tools to determine solutions for unwanted optical absorption in AlN grown by PVT. With our data we have demonstrated that substitutional carbon on the nitrogen site is a deep acceptor. When ionized it is the source of unwanted optical absorption. This was confirmed by PL, SIMS, and HVPE. Solution of mass balance equations reveals that the compensating defect is a singly

ionized nitrogen vacancy for relevant growth conditions. The presence of this defect has been confirmed by an optical emission predicted to originate from a donor acceptor pair recombination and measured by PLE spectroscopy. When carbon cannot be removed from the growth process, we have used our database to determine mechanisms important to removing unwanted optical absorption in high carbon samples. In total, this approach has accelerated the design of new materials and also led to deeper understanding of the important mechanisms, which will impact future efforts to tailor properties of AlN and its alloys.

9:00am **MG-WeM4 Substitution and Strain Control of Polarization in Multifunctional Materials**, *M. Ashton, A. Chernatynskiy, Susan Sinnott*, University of Florida

Density functional theory (DFT) calculations are used to analyze the combined effects of substitution and strain on spontaneous polarization in multiferroic perovskites, such as BiFeO₃. In particular, DFT calculations are used within the Vienna Ab-initio Simulation Package (VASP) to examine the macroscopic spontaneous polarization in BiFeO₃ systems with varying percentages of substitution and epitaxial strain. Substitutional elements considered for the A-site (Bi), B-site (Fe), and A/B co-substitution combination include Ba and La (A-site), Co, Cr, and Ni (B-site), and Ca/Mn and La/Ru (A/B site combination). In addition, strain values between +/- 2% are considered for each system. The results provide new insights into the roles of each of these factors on polarization and will be analyzed with data mining techniques to extrapolate design principles for high-T_c perovskites with controllable polarization. This work is supported by the National Science Foundation (DMR-1307840).

9:20am **MG-WeM5 Manipulation of Site Reactivity at the Au Nanoparticle – Titania Interface through Alloying: Insights from Density Functional Theory**, *Sampyo Hong, T.S. Rahman*, University of Central Florida

It has been shown that in methanol decomposition, as in CO oxidation, on titania supported Au nanoparticle, the interfacial atoms are the most reactive [1]. When we replace the Au atom, to which methoxy is bonded at the interface of Au₁₃/TiO₂(110), by other 3d (Cr, Ni, Cu) and 5d (Pt, W) atoms, we find that the dopant atoms at the interface become more cationic than the original Au atom and the relevant activation energies for a H-C bond scission of methoxy bonded to them is reduced as compared to that for methoxy bonded to the original Au atom. On the basis of these results we propose that the activity of Au/TiO₂ interface for reactions involving C-H scission of hydrocarbons would be enhanced by increasing the density of interfacial atoms with higher oxidation state than that of gold at the interface. Work supported in part by DOE Grant No. DOE-DE-FG02-07ER15842 [1] S. Hong and T. S. Rahman, *J. Am. Chem. Soc.* **2013**, *135*, 7629.

9:40am **MG-WeM6 Structural Descriptors for Hole Traps in Hydrogenated Amorphous Silicon Revealed through Machine Learning**, *Tim Mueller*, Johns Hopkins University, *E. Johlin, J.C. Grossman*, Massachusetts Institute of Technology

The discovery and design of new materials can be accelerated by the identification of simple descriptors of material properties. However the identification of the most relevant descriptors and how they relate to the properties of interest is not always obvious. We demonstrate how machine learning, in the form of genetic programming, can be used to identify relevant descriptors for predicting hole trap depths in hydrogenated nanocrystalline and amorphous silicon. Amorphous silicon is an inexpensive and flexible photovoltaic material, but its efficiency is limited by low hole mobility. We have evaluated 243 structural descriptors of amorphous silicon to identify those that are most indicative of the hole trap depth. Our calculations reveal three general classes of structural features that influence hole trap depth and predict that multiple interacting defects may result in deeper traps than isolated defects. These results suggest a possible mechanism for the Staebler-Wronski effect, in which exposure to light degrades the performance of amorphous silicon over time.

11:00am **MG-WeM10 Integration of Meso-scale Microstructural Modeling for Engineering Materials Development**, *Veena Tikare*, Sandia National Laboratories **INVITED**

The meso-scale materials modeling community, over the last two decades, has developed vast capabilities in microstructurally-based modeling of complex ceramic and metals. While several modeling techniques have been developed, the Potts kinetic Monte Carlo model and the phase-field model form the foundation of most materials modeling efforts for a variety of microstructural evolution processes experienced by ceramics and metals during fabrication and engineering service. Harnessing these modeling capabilities and applying them to design materials to tailor their microstructure for optimal engineering performance properties and

designing fabrication processes to obtain the desired microstructure can greatly accelerate development and optimizing of materials for a large number of technologies. This presentation will give a general overview of the core capabilities of the microstructural evolution modeling capabilities by reviewing the two most commonly used methods, Potts and phase-field. The former is a discrete, statistical-mechanical model that has been successfully used to simulate many microstructural evolution processes, such as grain growth, sintering, coarsening in the presence of mobile and immobile pinning phase, and recrystallization. The phase-field model is a continuum, thermodynamic model that has been used to successful simulation solidification, phase transformation and coarsening processes. The capabilities and limitation of each model will be reviewed and appropriate application of the models to different materials microstructural evolution processes will be discussed. The presentation will also demonstrate how these two models can be applied to understand and predict materials processes including coarsening, sintering and phase transformations. Specific examples of microstructural modeling and their application to design materials microstructure for optimal performance will be presented and discussed. Examples will included simulation of microstructural evolution during sintering of complex powder compacts; the generation, transport and release of fission gases from nuclear fuels during service in a reactor; and development of grain shapes and sizes during welding processes. Finally, the current trends in microstructure model development will be discussed.

Sandia National Laboratories is a multi-program laboratory managed and operated by Sandia Corporation, a wholly owned subsidiary of Lockheed Martin Corporation, for the U.S. Department of Energy's National Nuclear Security Administration under contract DE-AC04-94AL85000.

11:40am **MG-WeM12 Insights on the CO₂ Reduction Mechanism on Bio-inspired Iron Sulphide**, *Alberto Roldan, N.H. de Leeuw*, University College London, UK **INVITED**

Carbon dioxide capture and utilisation is gaining attention, driven not only by environmental factors but also by the potential to use it as chemical feedstock. One plausible utilisation route is its conversion to form small organic molecules, however, CO₂ is thermodynamically very stable and its reduction is energy intensive. The CO₂ conversion takes place under mild conditions in chemoautotrophic bacteria catalysed by enzymes.¹ These enzymes often contain Fe₄S₄ clusters (cubanes), which have been shown to act as electron-transfer sites^{2,3} but they can also be catalytically active centres for molecule transformations.⁴ An iron thiospinel mineral is structurally similar to the cubane,⁵ fact that brings us to suggest it as a novel heterogeneous catalyst. We present a theoretical investigation using the iron sulphide greigite mineral (Fe₃S₄) as a catalyst to transform CO₂ into small organic molecules. In agreement with the experiments, the adsorbed species depends on the solution pH as well as both concentration and actual products formed. The reduction consists of a sequential hydrogenation steps that we studied by the common Langmuir-Hinshelwood mechanism. We have identified ~170 steady states describing the different reaction pathways where the most favourable ones lead to formate and carboxyl intermediates yielding two different products, HCOOH and CH₃OH, also identified experimentally under conditions of room temperature and pressure.

References

- (1) Huber, C.; Wachtershauser, G. *Science* 1997, *276*, 245.
- (2) Nicolet, Y.; Amara, P.; Mouesca, J. M.; Fontecilla-Camps, J. C. *Proc. Natl. Acad. Sci. U. S. A.* 2009, *106*, 14867.
- (3) Hayashi, T.; Stuchebrukhov, A. *Abstracts of Papers of the American Chemical Society* 2012, 243.
- (4) Seino, H.; Hidai, M. *Chemical Science* 2011, *2*, 847.
- (5) Martin, W.; Russell, M. J. *Philosophical Transactions of the Royal Society of London Series B-Biological Sciences* 2003, *358*, 59.

Optomechanics, Photonics, and Quantum Nanosystems

Moderator: Susan Burkett, The University of Alabama,
W.K. Hiebert, University of Alberta and The National
Institute for Nanotechnology

8:40am **MN-WeM3 Diamond Quantum Nanophotonics and Nanomechanics, Marko Loncar**, Harvard University **INVITED**

Diamond possesses remarkable physical and chemical properties, and in many ways is the ultimate engineering material - "the engineer's best friend!" For example, it has high mechanical hardness and large Young's modulus, and is one of the best thermal conductors. Optically, diamond is transparent from the ultra-violet to infra-red, has a high refractive index ($n = 2.4$), strong optical nonlinearity and a wide variety of light-emitting defects. Finally, it is biocompatible and chemically inert, suitable for operation in harsh environment. These properties make diamond a highly desirable material for many applications, including high-frequency micro- and nano-electromechanical systems, nonlinear optics, magnetic and electric field sensing, biomedicine, and oil discovery. One particularly exciting application of diamond is in the field of quantum information science and technology, which promises realization of powerful quantum computers capable of tackling problems that cannot be solved using classical approaches, as well as realization of secure communication channels. At the heart of these applications are diamond's luminescent defects—color centers—and the nitrogen-vacancy (NV) color center in particular. This atomic system in the solid-state possesses all the essential elements for quantum technology, including storage, logic, and communication of quantum information.

I will review recent advances in nanotechnology that have enabled fabrication of nanoscale optical devices and chip-scale systems in diamond that can generate, manipulate, and store optical signals at the single-photon level. Examples include a room temperature source of single photons based on diamond nano wires [1] and plasmonic apertures [2], as well as single-photon generation and routing inside ring [3] and photonic crystal resonators fabricated directly in diamond [4]. In addition to these quantum applications I will present our recent work on diamond based on-chip frequency combs [5], diamond nano mechanical resonators [6].

- 1 TM Babinec, et al, "A bright single photon source based on a diamond nanowire," *Nature Nanotechnology*, 5,195 (2010)
- 2 JT Choy, et al, "Enhanced Single Photon Emission by Diamond-Plasmon Nanostructures," *Nature Photonics*, 5,738 (2011)
- 3 BJM Hausmann, et al, "Integrated Diamond Networks for Quantum Nanophotonics", *Nano Letters*, 12,1578 (2012)
- 4 MJ Burek, et al, "Free-standing mechanical and photonic nanostructures in single-crystal diamond", *Nano Letters*, 12,6084 (2012)
- 5 B Hausmann et al, "Diamond Nonlinear Photonics", *Nature Photonics*, 8,369 (2014)
- 6 M Burek et al, "Nanomechanical resonant structures in single-crystal diamond", *Appl. Phys. Lett.*, **103**,131904 (2013)

9:20am **MN-WeM5 A Compact Footprint Nano-Opto-Mechanical System with Evanescent Interaction, Marcel Pruessner, D. Park, T.H. Stievater**, Naval Research Laboratory, *D.A. Kozak*, NRC Postdoc (Naval Research Lab), *W.S. Rabinovich*, Naval Research Laboratory

We present a compact footprint, fully-integrated nano-opto-mechanical system with strong evanescent field interaction. Silicon nitride films with sub-wavelength thickness ($t_{\text{Si}_3\text{N}_4} < \lambda/4n_{\text{Si}_3\text{N}_4}$) enable low-loss waveguides [1] as well as complex photonic circuits [2], e.g. directional couplers, Mach-Zehnder interferometers, microring cavities [3], nanobeam cavities [4], etc. Furthermore, the thin core layer and air top cladding allow access to the waveguide's evanescent field, which can be tailored by simply varying the Si_3N_4 core layer deposition thickness. We previously demonstrated evanescent field interactions in these structures using a tapered fiber as an *off-chip* perturber [2] and by performing absorption spectroscopy on a number of chemical analytes present near the waveguide [3].

We now build upon our previous work [2,3] by fabricating a suspended tensile microbridge (SiN_x) just above the waveguide surface ($\text{gap} \approx 100\text{-}300\text{nm}$) to achieve strong interactions between optical and mechanical structures in a *fully-integrated* device. For example, displacement of the mechanical perturber (microbridge) modifies the waveguide's effective index so that the nano-opto-mechanical system acts as a high-resolution displacement sensor in which determination of the change in effective index is a measurement of displacement. At the same time, the change in the

waveguide effective index as a function of displacement implies an optical force that acts on the microbridge [5].

Our nano-opto-mechanical system is compact and occupies a footprint that is essentially determined only by the waveguide since the mechanical structure is suspended directly above it. This vertical architecture enables us to optimize the optical and mechanical structures independently. Although simple, the opto-mechanical system enables complex interactions with a variety of potential applications including displacement sensing, optical-force reconfigurable photonics, and opto-mechanical oscillators. The compact footprint enables large-scale integrated opto-mechanical systems on a chip.

We will present the basic approach of our nano-opto-mechanical system, design and fabrication details, simulations to support strong evanescent field interaction, and initial experimental results demonstrating a strong interaction in chip-scale opto-mechanical structures.

9:40am **MN-WeM6 GaAs Disks Optomechanical Resonators in Liquid, I. Favero, Eduardo Gil-Santos**, Université Paris Diderot, CNRS, France

Vibrating nano or micromechanical structures, such as cantilevers, have been the subject of extensive research for the development of ultrasensitive mass sensors for mass spectrometry, chemical sensing and biomedical analysis. In liquids, the energy losses due to viscous damping, acoustic losses and squeeze film effects are high and the mass sensitivity diminishes dramatically. Additionally, viscous damping in a fluid is often larger when the devices are miniaturized.

To circumvent these problems, novel structures have been proposed, such as microchannels, where the liquid is placed directly inside the resonator. They have indeed shown lower energy losses, but they can hardly be miniaturized. External feedback loops have been applied as well in order to diminish artificially energy losses [4]. Besides this, another technique to reduce mechanical losses in a liquid has been to use higher order modes or contour/extensional modes. On one hand, these modes indeed show lower dissipation, on the other hand the related displacement is extremely small, making it more difficult to detect, especially in a liquid.

Here we study the potential of GaAs disk resonators in this context, in particular focusing on mechanical radial breathing modes. GaAs mechanical disks, with their high mechanical Q even in air ($>10^3$), their low mass (pg) and high mechanical frequency (GHz), have been shown to be potential powerful sensors. Their use in liquids has been never investigated or even suggested, and it is still uncertain what energy losses and sensitivity they will present in such environment. GaAs disks support optical whispery gallery modes (WGMs), with high optical quality factor (several 10^5). This fact, together with the outmost optomechanical coupling that they possess (up to 4 MHz), provide them with an extremely high displacement sensitivity in the 10^{-18} m/ $\sqrt{\text{Hz}}$ range, allowing measuring the thermomechanical noise of the resonator even in a liquid.

We measure for the first time a GaAs mechanical disk vibrating in a liquid, directly in the Brownian motion regime. Employing finite element simulations and an analytical fluid-structure model, we investigate the mechanical damping mechanisms at play in this situation. We study the fluidic dissipation as a function of disk's dimensions and of the physical properties of the liquid, such as density and viscosity, performing experiments in a family of different liquids. We finally analyze the sensing capabilities of this object and compare it to other existing approaches.

11:00am **MN-WeM10 Photonic Actuation and Detection of Higher Order Modes in Nanomechanical Resonators, Jocelyn Westwood, V.T.K. Sauer**, University of Alberta and The National Institute for Nanotechnology, Canada, *Z. Diao*, National Institute for Nanotechnology and University of Alberta, Canada, *W.K. Hiebert*, University of Alberta and The National Institute for Nanotechnology, Canada

All-optical actuation and detection of nanomechanical devices has recently emerged as a high-bandwidth technique with high displacement sensitivity [1],[2],[3],[4],[5]. We explore optical actuation and detection of higher order vibrational modes, including even modes, in nano-optomechanical doubly clamped beams. Higher order modes have increased resonance frequencies, thereby increasing the mass sensitivity for sensing purposes and increasing the measurement bandwidth [6], [7]. Currently, higher order modes are not well studied since the symmetry of the modes causes a zero effective index shift over the vibrating beam, limiting the sensitivity of the all-optical technique. We demonstrate the fabrication of doubly clamped beams with the symmetry broken, due to a step in the substrate height under the doubly clamped beam. The doubly clamped beams are embedded in an optical racetrack resonator. This allows for the all-optical actuation and detection of the first through fifth modes of the doubly clamped beams. Additionally, the thermomechanical noise floor of the first few modes is observed.

- [1] F. Marquardt and S. Girvin, *Physics*, vol. 2, pp. 40, 2009.
- [2] T. J. Kippenberg and K. J. Vahala, *Science*, vol. 321, pp. 1172–6, 2008.
- [3] J. Chan et al., *Opt. Express*, vol. 17, no. 5, pp. 3802–3817, 2008.
- [4] M. Li et al., *Nature*, vol. 456, pp. 480–4, 2008.
- [5] V. T. K. Sauer et al., *Appl. Phys. Lett.*, vol. 100, no. 26, pp. 261102, 2012.
- [6] K. L. Ekinici, Y. T. Yang, and M. L. Roukes. *J. Appl. Phys.*, vol. 95, no. 5, pp. 2682–2689, 2004.
- [7] M. K. Ghatkesar et al., *Nanotechnology*, vol. 18, no. 44, pp. 445502, 2007.

11:20am **MN-WeM11 Dynamic Range Effect on the Mass Sensitivity of Optomechanically Transduced NEMS Devices with a Poorer Q Value.** *S.K. Roy, V.T.K. Sauer, W.K. Hiebert*, University of Alberta and The National Institute for Nanotechnology, Canada

Suitable control over the oscillatory properties and tunable nonlinearities has made nanomechanical resonators attractive to the research community not only for their ultra-sensing ability but also for rich physics behind their optomechanical properties. Optomechanical transduction of these devices has become promising for optimizing device applications. The present work is aimed at studying the interplay between dynamic range (DR), mass sensitivity, and mechanical quality factor (Q), and measurement bandwidth in state-of-the-art optomechanical NEMS devices. While poorer Q is normally assumed to lead to degradation in mass sensing performance, there are situations where performance can be recovered, and even improved, through the dynamic range dependencies on Q. This is welcome news for applications at atmospheric pressure such as sensitive gas sensing. In quest of an appropriate mass or gas sensor, nonlinear oscillatory behaviour was studied on a doubly clamped beam of $8.75\mu\text{m}\times 220\text{nm}\times 160\text{nm}$ which is 160 nm away from a racetrack resonator optical cavity. To get the upper end of DR, the resonator was driven close to nonlinearity, i.e. to the amplitude where 1dB compression was observed. Thermomechanical noise signals were measured to achieve the bottom end of the DR. At high vacuum ($<10^{-5}$ torr), 6 torr and 1atm the obtained experimental DR values are 53, 64 and 55 respectively. The corresponding Q values are 2866, 944 and 26. According to these experimental results, calculated mass sensitivity for the device were found 0.3, 0.2 and 28 Zepto g at high vacuum, 6 torr and 1atm respectively. An atmospheric pressure room temperature mass sensitivity of 28 zeptogram for Q value of 26 is an intriguing value. Such a surprising result of better mass sensitivity with poorer Q can be explained based on existing theories.

12:00pm **MN-WeM13 Scanning Optical Interferometric Spectromicroscopy for Mapping Multimode Resonant Motions in Planar Silicon Carbide (SiC) Micromechanical Resonators with $f\times Q$ Approaching 10^{13}Hz .** *Zenghui Wang, J. Lee, P.X.-L. Feng*, Case Western Reserve University

Higher-order and multiple modes in vibrating micro/nanomechanical resonators are of great interest and promise for both fundamental research such as exploring and understanding quantum mechanics in these man-made structures, and for technological applications such as signal processing and multi-modality sensing (e.g., simultaneously detecting mass and position of a physisorbed particle on resonator surface)[1][2]. It is therefore important to understand such multimode behavior in micro/nanomechanical resonators down to their fundamental limits, i.e. in their completely-undriven Brownian motions, at all conditions (e.g., ranging from cryogenic to elevated temperatures). This demands ultrasensitive motion transduction schemes that would allow us to attain more comprehensive information from the devices, far beyond what can be extracted from the conventional frequency-domain resonance curves.

Over the recent few decades, various motion transduction technologies (e.g., electrostatic, piezoelectric, piezoresistive, optomechanical, etc.) have been developed to read out small displacements in micro/nanomechanical resonators. While the commonly-used motion readout schemes have their respective advantages and have achieved many milestones, they lack multimode capabilities, and particularly, experimental visualizations of these multiple modes. For example, optomechanical technique has demonstrated excellent displacement sensitivity (better than $\text{fm}/\text{Hz}^{1/2}$), but is unable to experimentally determine the spatial mode shapes of 2D planar resonators, which is highly desired for determining and engineering high-order modes.

Optical interferometric techniques have been continuously advancing over the recent years [3][4]. Here, we report on the design and implementation of a scanning laser interferometry and spectromicroscopy technique, and we demonstrate direct visualization of multimode resonances in SiC micromechanical resonators with various geometries, including membranes, plates, trampolines, torsional resonators, and center-supported disks, with many resonances up in the VHF and UHF bands. Besides setting a new

record of $f\times Q$ product in all SiC flexural-mode resonators ($\sim 1.0\times 10^{13}$), our devices effectively enable high-order resonances with clearly distinguishable mode shapes through their 2D nature and high-aspect-ratios.

- [1] Dohn, S., Sandberg, R., Svendsen, W. & Boisen, A. *Appl. Phys. Lett.* **86**, 233501 (2005).
- [2] Hanay, M. S. et al. *Nature Nanotech.* **7**, 602 (2012).
- [3] Hiebert, W. K., Vick, D., Sauer, V., & Freeman, M. R. *J. Micromech. Microeng.* **20**, 115038 (2010).
- [4] Lee, J., Wang, Z., He, K., Shan, J., & Feng, P. X.-L. *ACS Nano* **7**, 6086 (2013).

Nanometer-scale Science and Technology Room: 304 - Session NS-WeM

Nanoscale Catalysis and Surface Chemistry

Moderator: Jeremy Robinson, Naval Research Laboratory

8:00am **NS-WeM1 Single Atom Alloys as a Strategy for Selective Heterogeneous Hydrogenations.** *Charles Sykes*, Tufts University
INVITED

Hydrogenation reactions are central to the petrochemical, fine chemical, pharmaceutical, and food industries and are of increasing interest in energy production and storage technologies. Typical heterogeneous catalysts often involve noble metals and alloys based on platinum, palladium, rhodium and ruthenium. While these metals are active at modest temperature and pressure, they are not always completely selective and are expensive. We have demonstrated that single palladium atoms can convert the otherwise catalytically inert surface of an inexpensive metal into an ultrasensitive catalyst. We used high resolution imaging to characterize the active sites and temperature programmed reaction spectroscopy to probe the chemistry. The mechanism involves facile dissociation of molecular hydrogen at individual palladium atoms followed by spillover onto the copper surface, where ultrasensitive catalysis occurs by virtue of weak binding. The reaction selectivity is in fact much higher than that measured on palladium alone, illustrating the unique synergy of the system.

8:40am **NS-WeM3 In Situ FTIR Spectroscopic Observation of the Formation of Gold Ketenyldene during Carboxylic Acid Oxidation on a Au/TiO₂ Nanoparticle Catalyst.** *Monica McEntee, W. Tang, M. Neurock, J.T. Yates, Jr.*, University of Virginia

Gold nanometer diameter particles supported on reducible oxide supports exhibit catalytic activity at temperatures as low as 90 K.[1] Numerous studies[2-4] have theorized that the catalytic activity occurs at the metal-support interfacial sites. In 2011, Green et al.[5] discovered, using infrared (IR) spectroscopy, a dual catalytic site for molecular oxygen adsorption and subsequent activation with one O atom bonded to the Au and the other O bonded to the Ti⁴⁺ site of the TiO₂ support. Here I show, using IR spectroscopy and density functional theory (DFT), the oxidation of three carboxylic acids (acetic, propionic and butyric acid) on a Au/TiO₂ catalyst with ~3 nm diameter Au nanoparticles producing gold ketenyldene, Au₂C=C=O, species. The initial step in all three acid oxidation processes is the dissociation of O₂ at the Au-Ti⁴⁺ dual site to form reactive O adatoms at the interface. Next, in sequential steps, α -CH and β -CH bonds specifically next to the COO group in each acid are oxidatively dehydrogenated to produce unsaturated, C=C, species. C-C and C-O bond scission occur next yielding adsorbed ketenyldene, Au₂C=C=O, an exotic species formed just before full oxidation. Control oxidation experiments on the TiO₂ support alone produce no Au₂C=C=O species verifying the reaction occurs at the Au/TiO₂ interface. Also, isotopically-labelled O₂ and acid experiments confirm the Au₂C=C=O is composed of specifically α -C and β -C atoms and O atoms from the acid.

References

- Haruta, M.; Kobayashi, T.; Sano, H.; Yamada, N. Novel gold catalysts for the oxidation of carbon monoxide at a temperature far below 0 °C. *Chem. Lett.* **1987**, 405-408.
- Rodriguez, J.; Ma, S.; Liu, P.; Hrbek, J.; Evans, J.; Perez, M. Activity of CeO_x and TiO_x nanoparticles grown on Au (111) in the water-gas shift reaction. *Science* **2007**, *318*, 1757-1760.
- Molina, L.; Rasmussen, M.; Hammer, B. Adsorption of O₂ and oxidation of CO at Au nanoparticles supported by TiO₂(110). *J. Chem. Phys.* **2004**, *120*, 7673.
- Camellone, M. F.; Zhao, J.; Jin, L.; Wang, Y.; Muhler, M.; Marx, D. Molecular Understanding of Reactivity and Selectivity for Methanol

Oxidation at the Au/TiO₂ Interface. *Angew. Chem., Int. Ed.* **2013**, *52*, 5780 – 5784.

5. Green, I. X.; Tang, W.; Neurock, M.; Yates Jr., J. T. Spectroscopic observation of dual catalytic sites during oxidation of CO on a Au/TiO₂ catalyst. *Science* **2011**, *333*, 736-739.

9:00am **NS-WeM4 Fabrication and Photocatalytic Activity of Metal-loaded TiO₂ Nanometer Scale Particles**, *Paolo Reyes, Y. Liu, J.C. Hemminger*, University of California Irvine

We will describe methods to generate TiO₂ nanoparticles supported on HOPG substrates. We then utilize photoelectrochemical deposition to selectively decorate the TiO₂ particles with metal nanoparticles. These samples are easily amenable to characterization with SEM and TEM imaging as well as electron spectroscopy surface analysis methods. The introduction of noble metals adsorbed on TiO₂ substrates can affect the intrinsic catalytic properties of the metal oxide, however previous research has been focused on single species of adsorbed noble metals (e.g. Pt, Au, Co, etc.) and the result impact on the photocatalytic activity. Typical effects from noble metals include lowering the band-gap requirement of TiO₂ (3.2 eV) in order for electron excitation from the valence band to the conduction band to occur. Our current research focuses on the fabrication and study of two or more noble metal nanoparticle species loaded onto TiO₂ particle arrays and to observe the impact on the catalytic activity, chemistry, electromagnetic field enhancements. The presence of two or more noble metal species may affect the catalytic properties of TiO₂ in interesting ways, such as Au nanoparticles allowing visible light to be absorbed, and Pt particles allowing more efficient photo-chemistry in degrading pollutants. In this work, we photodeposit Pt and Au particles onto TiO₂ particles situated on highly oriented pyrolytic graphite (HOPG). Au and Pt particles are found to be on average 4.7 nm in diameter. Preliminary experiments on bi-metallic loaded particles have been conducted in order to study photocatalytic properties via pollutant degradation rate. Methylene Blue (MB), a common organic dye, is used to observe photocatalytic activity of these particles through UV-induced photo-degradation. Bare TiO₂ particles are known to be photoactive, however the introduction of noble metal species show an increase of MB degradation over time. We are currently observing MB degradation rates with dual-loaded TiO₂ nanoparticles. Previous work in our group has proven that polarized Raman spectroscopy performed on Ag nanoparticle arrays yields a significant increase in signal

1. Wei Luo, W. Van der Veer, P. Chu, D. L. Mills, R. M. Penner, and J.C. Hemminger, *Journal Of Physical Chemistry C*, 2008. : p. 11609-11613.

This work is supported by the U.S. Department of Energy, Office of Basic Energy Sciences through grant number: DE-FG02-96ER45576

9:20am **NS-WeM5 Size-dependent Trends in CO and O₂ Adsorption on Pd Nanoparticle Catalysts**, *Hemma Mistry, L.K. Ono*, University of Central Florida, *B. Roldan Cuenya*, Ruhr-University Bochum, Germany

Due to the striking dependence of many catalytic reactions on particle size and shape, a thorough understanding of structure-dependent reactivity trends in the interaction of adsorbates with model nanoparticles (NPs) is key to designing highly active and selective catalysts. Palladium NPs are highly active for important reactions such as CO oxidation and methane combustion. However, conflicting reports exist in the literature on the change in CO and O₂ adsorption strength on Pd NPs of different size. In this study, temperature programmed desorption (TPD) was used to investigate the binding strength of O and CO on Pd NPs supported on SiO₂/Si(111). A range of clusters with Pd deposition thicknesses between 1.5 and 15 Å were investigated and compared to Pd(111). Our results indicate that both O and CO binding strength increase dramatically with decreasing particle size, and the presence of distinct binding sites on the smaller NPs was revealed by CO TPD.

9:40am **NS-WeM6 Mixed Structures of CO and H on Ru(0001) as Precursor States for Fischer-Tropsch Synthesis**, *Barbara Lechner, X. Feng, S. Carenco*, Lawrence Berkeley National Laboratory, *P.J. Feibelman*, Sandia National Laboratories, *M.B. Salmeron*, Lawrence Berkeley National Laboratory

The Fischer-Tropsch reaction is of great importance in the industrial synthesis of hydrocarbon fuels and as such has motivated a large number of studies on the microscopic processes underlying the reaction. However, while the adsorption and interaction of the two reactants, carbon monoxide and hydrogen, on model catalyst surfaces has been investigated in detail for decades, several fundamental questions still remain, in particular that of the nature of the precursor species [1]. In addition, CO and H have been shown to segregate into different domains on single crystal surfaces [2-4], raising the question whether the reaction only takes place at the interface of these domains.

Here we investigate the co-adsorption of CO and H on Ru(0001) using scanning tunneling microscopy (STM), X-ray photoelectron spectroscopy (XPS) and density functional theory calculations with the goal of a more detailed understanding of the forces driving the formation of the precursor state in the Fischer-Tropsch reaction. CO and H co-adsorbed at 77 K show a largely unordered structure in STM, while subsequent annealing to 150-300 K results in dense CO islands compressed and separated by H atom regions that decrease in size with increasing annealing temperature. Unexpectedly, further annealing to 300-350 K gives rise to a mixed phase of CO and H in a 1:1 ratio. XPS measurements confirm a change in bonding geometry upon annealing. We believe that studying the transition from a segregated to a mixed phase is an important step toward tracing the microscopic reaction pathway.

[1] R. A. van Santen, A. J. Markvoort, I. A. W. Filot, M. M. Ghouri, E. J. M. Hensen, *Phys.Chem. Chem. Phys.* **15**, 17038 (2013).

[2] D. E. Peebles, J. A. Schreifels, J. M. White, *Surf. Sci.* **116**, 117 (1982).

[3] B. Riedmuller, D. C. Papageorgopoulos, B. Berenbak, R. A. van Santen, A. W. Kleyn, *Surf. Sci.* **515**, 323 (2002).

[4] I. M. Ciobica, A. W. Kleyn, R. A. van Santen, *J. Phys. Chem. B* **107**, 164 (2003).

11:00am **NS-WeM10 In Situ Investigation of Oxidation State and Reactivity of a Cu Model Catalyst by Simultaneous Mass Spectrometry and Indirect Nanoplasmonic Sensing**, *Hans Fredriksson, H.J.W. Niemantsverdriet*, Eindhoven University of Technology, Netherlands

The activity of a catalyst depend on a wide range of factors such as elemental composition, particle dispersion and the oxidation state of the active material. All of these properties can change during operation, reversibly or irreversibly, thereby severely influencing the catalysts performance. It is therefore of great importance to learn how the fundamental properties of a catalyst change during use and to correlate these changes with changes in activity and selectivity. This requires simultaneous, in-situ measurements of both fundamental catalyst properties and activity, a far from trivial task. Here we present a novel quartz-tube micro flow-reactor in which optical spectroscopy and mass spectroscopy can be performed simultaneously. The optical setup is based on indirect nanoplasmonic sensing, which utilizes the localized surface plasmon resonances of Au-discs embedded in Si₃N₄ to detect subtle changes in the oxidation state of a material. We investigate CO-oxidation on a model catalyst consisting of Cu nanoparticles formed by thin film evaporation and subsequent annealing. From these measurements we demonstrate the correlation between oxidation state of the Cu-catalyst and onset temperature for CO₂ formation in gas mixtures with various CO/O₂ ratios. The changes in oxidation state were then confirmed by XPS.

11:20am **NS-WeM11 Controlling Surface Reactivities of TiO₂ (110) by Nanoscale Strain Field**, *Zhisheng Li, D.V. Potapenko, R.M. Osgood*, Columbia University

Strain is found to be an ubiquitous quantity in nanostructured surfaces and on supported catalysts. Therefore, understanding the influence of strain on surface properties is crucial for rational design of catalytic materials. The study of the interaction of nanoscale strain and adsorbate reactivity presents two experimental challenges, generating an intense strain field and differentiating strain effects from effects induced by change in other surface properties. In this work, we generate a patterned, nanoscale strain field on TiO₂ (110) surface by low energy bombardment of single crystal TiO₂ samples with argon ions at 1000°C. The interstitial argon diffuses so as to self-assemble into highly pressurized argon clusters and distort the surrounding lattice a few nanometers below the surface. As a result, the top surface layers of the crystal have a convex morphology while retaining their unstressed surface structures, thus introducing nanometer-size surface protrusions. The strain level obtained on the protrusions can be as large as ~4%. The locally varying strain field across the protrusion is ideal for strain effects study. By combining scanning tunneling spectroscopy (STM) imaging and continuum model, we show that the adsorption energy of hydrogen binding to surface bridge-bonded oxygen (BBO) is significantly altered by local lattice strain. In particular, strain causes, oxygen vacancies (BBOv) to be absent from the strained area. Our results thus provide direct evidence of the influence of strain on atomic-scale surface properties and thus help guide future research in catalysis materials design

11:40am **NS-WeM12 NSTD Recognition Award Lecture: Probing Local Optoelectronic Properties of Porphyrin-Gold Molecular Interfaces with STM/STS**, *X. Chen, E.H. Morales, T.-H. Park*, University of Pennsylvania, *M.J. Therien*, Duke University, **Dawn Bonnell***, University of Pennsylvania **INVITED**

Porphyrim molecules are a group of organic compounds that exist extensively in natural biological systems, and they manifest rich electronic and photonic properties, raising the possibility of optoelectronic device applications. In this research thiolated Zinc-porphyrin oligomer molecules were linked to Au(111) surface in a vertical device configuration, embedded within an alkanethiol self-assembled monolayer. Spectroscopic measurements were done to determine the electronic orbital structures of different Zinc-porphyrin oligomer single molecules via scanning tunneling microscope. With lasers of different wavelength coupled to the tunneling junction, both ground state and excited state electronic orbital structures of Zinc-porphyrin single molecule were measured.

Plasma Science and Technology Room: 305 - Session PS1-WeM

Plasma Based Ion Implantation and Ion-Surface Interactions

Moderator: Aseem K. Srivastava, Applied Materials, Inc.

8:00am **PS1-WeM1 Dosimetry Challenges for Plasma Doping and Ion Implantation**, *Bo Vanderberg, L.M. Rubin, A.M. Ray*, Axcelis Technologies, Inc. **INVITED**

Plasma doping been described as a fledgling technology to complement and replace ion beam based implantation, due to its advantage in productivity given by the much higher average ion current delivered to work pieces. While productivity is an important factor in industrial applications, each technology also has to deliver appropriate dose control, and thus relies on advanced dosimetry systems to provide accurate dosage, high dose uniformity across the work piece, precise ion placement, i.e. energy and angle control, low contamination of undesired energetic and environmental species, and reliability and exception handling capability.

For commercial semiconductor manufacturing applications in particular, simultaneous compliance to each of these requirements is critical. Modern ion beam based implantation systems can provide dosimetry to meet these requirements, and we will describe some of the new technologies developed specifically for ion implantation of the most advanced semiconductor devices: fast data acquisition of multiple Faraday systems with parallel current collection, and measurement of spatial ion beam properties such energy and two-dimensional spatial and angle distribution, as well as their time dependence to monitor drift and intermittent failures.

For plasma doping to meet these standards, obstacles in terms of lack of mass-resolution, simultaneous implantation, deposition and etching, and lack of in situ beam monitoring during the plasma doping process represent formidable challenges. While some of the inherent shortcomings of plasma doping are fundamental, some techniques have been developed to address these issues, including novel Faraday systems as well as model based dosimetry with either theoretical or empirical modeling of plasma physical and chemical processes, some of which we will review.

The most difficult challenge for plasma doping is matching of dopant depth profiles of existing ion beam based implantation, where implanted dopant profiles as presented in the literature are different from their equivalent ion beam produced profiles. Without this capability, plasma doping of semiconductors is confined to a niche application space, covering less sensitive doping processes in semiconductor manufacture.

8:40am **PS1-WeM3 Ion Implantation Challenges and Applications for Future Memory Devices**, *Allen McTeer*, Micron Technology **INVITED**

For many years memory manufacturers resisted the need to adopt implant steps that were considered mainstream in logic manufacturing in order to keep cost down. In the last few years this approach has had to change to address scaling issues. Pre-amorphization, carbon, germanium and indium implants have been adopted by most memory manufacturers for dopant profile and silicide growth control. At the same time, plasma doping was adopted to address productivity issues seen with high dose, low energy beamline implants. These changes reflect the realization that technology challenges and cost mitigation are becoming more divergent with shrinking geometries. The introduction of emerging and vertical memory devices is expanding the applications of both beamline and plasma doping techniques.

This talk will discuss some of the new implant applications that could be introduced in upcoming memory devices to address process needs. This will include discussion and data review of applications related to stress control, implant damage, silicon cracking, high aspect ratio implants, hydrogenation, surface modification, dopant profile control and interface cleaning.

9:20am **PS1-WeM5 Challenges in Ion Implantation**, *Joseph Olson, S. Chennadi, G. Gammel, N. Pradhan, F. Sinclair, S. Todorov, M. Welsch, R. White*, Applied Materials, Varian Semiconductor Equipment **INVITED**

Requirements on commercial ion implantation equipment grow increasingly stringent as device nodes progress. In the face of these tightening requirements the implanter designer is faced with the challenge of designing and building apparatus to measure and control process properties and then to validate improved performance. Recent examples of this process in action are discussed. (1) Precise control of the incidence angles of ions on a substrate is required for accurate placement of dopant atoms. Development to meet this need lead to advanced measurement and control systems and a powerful new technique (the 2D V curve) that produces a map of incident angles over an entire 300 mm Si substrate. The 2D V curve is explained in detail. (2) The current density in beamline implantation has potential process consequences on microuniformity, substrate charging and amorphization. The development of a beam density measurement, beam size control system and validation by examination of implanted wafers is discussed.

11:00am **PS1-WeM10 Plasma Doping Process Monitoring Diagnostics**, *Yuuki Kobayashi*, Tokyo Electron Limited, Japan, *P. Ventzek*, Tokyo Electron America, Inc., *K. Yamashita, S. Nishijima, M. Oka, H. Ueda, Y. Sugimoto, M. Horigome, T. Nozawa*, Tokyo Electron Limited, Japan

Plasma doping is an emerging technology for the doping of next generation topographic structures such as Fin-FET extensions. Typically a dopant precursor such as arsine is injected into a plasma source where the dopants are freed from the precursor and injected into a surface that is initially amorphized by the ion flux incident on the topographic structure. As the doping process is impacted by the precursor, ion and energy flux to the substrate, it is important to have diagnostics to measure these quantities. Knowing the dose as a function of the critical measureable plasma parameters allows a model to be developed for dose monitoring and control. The model need not be physically based but could also be statistical. The challenge is coming up with simple enough diagnostics that integrate in a non-contaminating way with the plasma. Independent measurement of plasma parameters is also important as a monitor of plasma source and process stability which also impact dose. We have developed a hybrid sensor set comprising of an in-situ current and optical emission (OES) monitors that are used to correlate with dose measurements corresponding to a radial line slot antenna plasma doping process. The in-situ current monitor enables measurement of plasma density and OES provides measurement of dopant radicals. Both monitoring methods, when used together, permit detection of previously immeasurable process drift affecting doping performance. In this presentation, we describe the sensors and typical results. The relationship between dose, plasma and optical measurements is discussed in terms of a descriptive model. A physical interpretation of the results is aided by simulations of the plasma for which we present summary results.

11:20am **PS1-WeM11 Control over the Ion Flux Obtained by Sawtooth-like Waveforms in Radiofrequency Capacitively Coupled Plasmas**, *Bastien Bruneau†*, *T. Novikova, T. Lafleur, J.-P. Booth, E.V. Johnson*, Ecole Polytechnique, France

The use of Tailored Voltage Waveforms (TVWs) to manipulate the Electrical Asymmetry Effect (EAE) in a capacitively coupled plasma (CCP) chamber has been shown to be an effective technique for varying ion bombardment energy (IBE) at the surface of an electrode. It stems mainly from an amplitude asymmetry, i.e. from waveforms with different maximum and minimum. We present herein a new plasma asymmetry, obtained by sawtooth-like waveforms.

We use Particle-in-Cell (PIC) simulations to study an argon plasma excited by sawtooth-like waveforms. Using a waveform with slow rise and fast fall, we show that a fast fall leads to fast sheath expansion in front of the powered electrode, and therefore high ionization at this sheath edge. On the other hand, the slow fall leads to slow sheath expansion in front of the grounded electrode, and therefore to weak ionization at this sheath edge. This ionization asymmetry subsequently leads to an ion flux asymmetry, with up to twice higher flux on powered electrode. Because of this ion flux asymmetry, a positive self-bias develops in this plasma, leading to smaller IBE on the powered electrode compared to the grounded electrode.

* NSTD Recognition Award

† Coburn & Winters Student Award Finalist

Therefore, the high-flux electrode also corresponds to the low-energy electrode. This property is unique, as it cannot be obtained with any of the geometrical asymmetry, amplitude asymmetry or with any mono-frequency RF excitation. We show that the ion flux asymmetry effect increases both with the number of frequencies composing the waveform, as the slope-asymmetry of the waveform then increases, and with pressure, as diffusion from one electrode to the other is hindered at high pressure. Waveforms optimizing the slope-asymmetry effect and allowing a fine and continuous control over the asymmetry are presented.

This slope asymmetry effect can be of great interest for any process using RF-CCP plasma, as one can control independently the ion flux on each electrode. For instance, one can imagine using a sawtooth-like waveform in a deposition (or etching) process. The deposition (or etching) rate can then be increased on the substrate of interest, while benefitting from a low IBE, and while keeping the up-time of the reactor high by keeping the maintenance-time low, thanks to the low deposition (or etching) rate on the other electrode.

11:40am **PS1-WeM12 Surface Roughening Mechanisms and Roughness Suppression during Si Etching in Inductively Coupled Cl₂ Plasmas**, Nobuya Nakazaki, H. Matsumoto, K. Eriguchi, K. Ono, Kyoto University, Japan

As ULSI device dimensions continue to be scaled down to << 100 nm, increasingly strict requirements are being imposed on plasma etching technology. The requirements include the precise control of profile, critical dimension, roughness, and their microscopic uniformity (or aspect-ratio dependence), together with that of etch rate, selectivity, and damage. Atomic- or nanometer-scale surface roughness has become an important issue to be resolved in the fabrication of nanoscale devices, because the roughness at the feature bottom affects the uniformity of bottom surfaces, which in turn leads to a recess and thus a damage to transistors in gate fabrication. Moreover, the roughness on feature sidewalls is responsible for the line edge roughness (LER) and linewidth roughness (LWR), which affect the variability for gate or channel lengths and thus the variability in transistor performance. The formation of such surface roughness is stochastic and three dimensional, which are assumed to be affected by a number of factors during processing including plasma etching.

Experimental investigations of the surface roughness of planer substrate of Si etched in inductively coupled Cl₂ plasmas have been performed, including several surface and plasma diagnostics, to gain a deeper understanding the mechanisms for surface roughening and then to find a way for suppressing the roughness during plasma etching. The experiments indicated that as the rf bias power or incident ion energy E_i is increased, the etch rate continues to increase, while the surface roughness increases and then substantially decreases at high E_i . In addition, the surface roughness at low E_i increases with etching time, while does not depend on etching time at high E_i . The analysis of the etch rate as a function of E_i and etching time, with the help of Fourier transform infrared (FTIR) absorption spectroscopy, quadrupole mass spectrometry (QMS), and classical molecular dynamics (MD) simulation, implied that by-product ions of silicon chlorides SiCl_x⁺, whose concentration is increased in the plasma at increased E_i , play a critical role in surface roughening as well as etching at increased E_i through competitive etching and deposition. [1,2] Moreover, the pulse-bias etching through a repetitive on/off of the rf bias power also have been demonstrated to be one promising way of reducing the surface roughness during plasma etching.

[1] H. Tsuda, N. Nakazaki, Y. Takao, K. Eriguchi, and K. Ono: J. Vac. Sci. Technol. B (2014) in press.

[2] N. Nakazaki, Y. Takao, K. Eriguchi, and K. Ono: Jpn. J. Appl. Phys. 53 (2014) 056201.

12:00pm **PS1-WeM13 Ion Induced Electron Emission from Semiconductors: An Investigation into Fermi Level and Surface Electric Field Effects**, David Urrabazo, M.J. Goeckner, L.J. Overzet, University of Texas at Dallas

A few recent publications point to the possibility of controlling the ion induced electron emission (IIEE) yield from semiconductor surfaces in real time through controlling the numbers of electrons in the semiconductor's conduction band ($n_{e,CB}$). Of course, ion bombardment induced electron emission also occurs in the plasma processing of semiconductors, and should cause differences between processing n- and p-type wafers if it truly depends upon $n_{e,CB}$. Hagstrum's Auger neutralization theory for semiconductors¹ assumes that the IIEE yield should NOT depend upon $n_{e,CB}$, and as a result most models make the assumption that the IIEE yield is independent of $n_{e,CB}$ (and the position of the Fermi level as well as temperature). To our knowledge, no one has investigated this assumption! Therefore, we have experimentally and theoretically investigated it by using and extending Hagstrum's theory as well as by measuring the IIEE yield from semiconductor samples versus doping density and type. Our results for

Si demonstrate good agreement with the assumption both theoretically and experimentally. The IIEE yields of p-type, intrinsic and n-type samples are essentially the same. In direct contradiction to the theory/assumption, however; the IIEE yield for p-type Ge was measured to be 2.5 times greater than that of intrinsic and n-type samples. Precisely the opposite of what one might first expect! This result indicates that there can be other significant factors controlling the IIEE yield. One likely factor is a surface electric field. (It could have been induced by Fermi level pinning in the case of our Ge measurements, and in plasmas it could be induced by the sheath.) As a result, the new principle question becomes: Can a moderate surface electric field control the IIEE yield from semiconductors? To our knowledge, there are no unambiguous measurements answering this question either. Therefore, we will introduce a device we have designed, modeled, and begun fabricating for measuring the IIEE yield while allowing independent control over the ion flux to the surface and electric field imposed on that surface.

Acknowledgement: This material is based upon work supported by the Department of Energy under Award Number DE-SC-0009308.

¹H.D. Hagstrum, Phys. Rev. 122 83 (1961)

**Plasma Science and Technology
Room: 308 - Session PS2-WeM**

Plasma Modeling

Moderator: Steven Shannon, North Carolina State University

8:00am **PS2-WeM1 Self-Consistent Modeling of Capacitive Coupling in Inductively Coupled Plasmas**, Ankur Agarwal, S. Rauf, K. Collins, Applied Materials Inc.

Plasma etching of microelectronic structures at advanced technological nodes (< 1x nm) places great emphasis on process uniformity.[1] Antenna designs have become more complicated in industrial inductively coupled plasma (ICP) tools to improve uniformity.[2] The antenna region in ICPs also contain auxiliary systems for gas flow, temperature control, etc. which influence the antenna electrical characteristics. Plasma equipment models typically employed to investigate ICP sources have used a circuit model to compute voltage and current along the coils to capture the antenna-plasma coupling self-consistently.[3,4] However, the approach is limited to simple coil structures which is not necessarily the case for next-generation ICP tools. For example, Applied Materials' AdvantEdge chamber utilizes a two-coil structure fed through the same power supply.[5]

In this work, we discuss results from a two-dimensional plasma equipment model, HPEM[6], which has been modified to compute the voltage and current (amplitude and phase) in the coils by solving the equivalent circuit of the coils and the plasma in the frequency domain. The plasma is treated as the secondary coil of an air-core transformer. The amplitude of the driving voltage is adjusted in the circuit model such that the sum of inductive, capacitive and resistive powers is maintained constant. Capacitive coupling is calculated by including the voltage on the coils in the Poisson's equation. The coil currents from the circuit model are used as driving terms in the solution of the wave equation and to compute resistive losses in the coils.

Results will be discussed for an Ar/Cl₂ plasma and the consequences of varying electronegativity of the feedstock gas mixture, varying current ratios between the two-coils and the phase of current between the coils on capacitive coupling will be assessed over a pressure range of 5 – 150 mTorr. We found that inductive component of the power coupled increases with pressure from 5 to 30 mTorr as the increase in electron density supersedes the rise in collision frequency. While, power is dominantly coupled inductively for electropositive gas mixture, the pressure at which transition to capacitive mode occurs decreases as electronegativity increases.

[1] K. Ahmed and K. Scheugraf, IEEE Spectrum **48** (11), 50 (2011).

[2] Ch. Hollenstein, et al., Plasma Sources Sci. Technol. **22**, 055021 (2013).

[3] M.J. Kushner, et al., J. Appl. Phys. **80**, 1337 (1996).

[4] T. Panagopoulos, et al., J. Appl. Phys. **91**, 2687 (2002).

[5] A. Agarwal, et al., Trans. Plasma Sci. **39**, 2516 (2011).

[6] M.J. Kushner, J. Phys. D **42**, 194013 (2009).

8:20am **PS2-WeM2 Experimentally Guided Development of a Dielectric Etch Plasma Model**, *Ajit Balakrishna, S. Rauf, K. Collins*, Applied Materials Inc.

Smaller technology nodes in the semiconductor industry place increased emphasis on etch productivity requirements, such as etch rate and critical dimension. Modeling and simulation play a central role in new developments (design of new hardware and exploration of novel processing options) to address the concurrent demand for improved performance and shorter development cycle. Validation against experimental data is a critical step in making these models a mature development tool. In this study, we have developed, refined and validated a dielectric etch process model based on blanket wafer etching results.

In an earlier study, we tested a 2-dimensional model for capacitively coupled plasmas (CCP) in combination with a surface mechanism model against experimental data for etching of blanket SiO₂ wafers in a dual-frequency CCP plasma etcher. The process parameters for this c-C₄F₈/O₂/Ar plasma were varied over a wide range of pressures (25-150 mTorr), bias powers (500-1500 W), and c-C₄F₈ and O₂ flows. The etch rate increased with bias power and c-C₄F₈ flow rate, weakly decreased with increasing O₂ flow rate, and moderately increased with pressure. The reactor simulations were performed using CRTRS, a 2/3-dimensional fluid plasma model. The plasma simulations provided fluxes of various fluorocarbon polymerizing species, atomic oxygen and atomic fluorine. We also calculated fluxes and energies of the ions impacting the wafer. Based on comparisons to the experimental data, we selected a coverage based etch mechanism. This mechanism described center-point etch rates well but indicated that the model needed some improvements to predict the radial etch rate profile and to capture the sensitivity to pressure.

Closer examination of the fluid plasma modeling results revealed that the electron density, and consequently the etch reactants, peaked near the wafer edge. The experimental profiles, on the other hand, showed a slight center-high profile. In the fluid plasma model, the electrons absorbed power at the wafer edge and increased reaction rates close to this power-absorption region. At lower pressures (with fewer collisions), this model was not capturing the non-local behavior of high-energy electrons. A Monte Carlo model provided better spatial representation of electron kinetics and this was coupled with the fluid plasma model. This hybrid plasma model significantly improved the experimental match. Both coverage and thickness based dielectric etching mechanisms were tested. In addition to these improvements, careful accounting for the power going into DC and RF modes gave greater model fidelity to the observed pressure sensitivity.

8:40am **PS2-WeM3 Insights to Critical Dimension Control Through 3-Dimensional Profile Simulation For Plasma Etching**, *Yiting Zhang*, M.J. Kushner*, University of Michigan, *S. Sriraman, A. Paterson*, Lam Research Corp

Plasma assisted etching is a necessary process for pattern transfer in microelectronics fabrication. In prior technology nodes, 2-dimensional feature profile models served very well to help optimize features and connect reactor scale properties to feature scale critical dimensions (CDs). The current technology nodes utilize 3-dimensional structures such as FinFETs and Tri-Gate transistors, whose optimization is considerably more difficult and not well represented by 2D profile simulators. For example, etching of 3D structures typically require longer over-etch to clear corners, which then places additional challenges on selectivity to maintain CD. Prior CD control techniques are evolving to address these issues.

In this paper, we report on development of a 3-dimensional profile simulator, the Monte Carlo Feature Profile Model (MCFPM-3D). The MCFPM-3D builds upon the 2D MCFPM modeling platform that has many advanced features such as charging, mixing, implantation and photon stimulated processes. The same reaction mechanism used for the 2D model can be used in MCFPM-3D. The MCFPM-3D uses a rectilinear mesh in 3 dimensions having fine enough resolution that, for example, circular vias can be resolved. Each cell within the mesh may represent a different solid material or a mixture of materials. The model addresses reaction mechanisms resulting in etching, sputtering, mixing and deposition on the surface to predict profile evolution based on fluxes of radical, ions and photons provided by an equipment scale simulator. In these studies, energy and angularly resolved fluxes are provided by the Hybrid Plasma Equipment Model (HPEM).

To address evolving CD control issues, results from the model will be used to compare etching of 2D and 3D structures. Ar/Cl₂ and Ar/CF₄/O₂ plasmas are used for Si and SiO₂ etching in representative 2D and 3D feature topographies relevant to etch applications in advanced technology nodes. Phenomena such as line-edge roughness, reactive ion etch lag and aspect ratio dependent etching will be discussed.

* **Coburn & Winters Student Award Finalist**

9:00am **PS2-WeM4 3-Dimensional Model for Electron-Beam Generated Plasma**, *Shahid Rauf, A. Balakrishna, A. Agarwal, J. Kenney, L. Dorf, K. Collins*, Applied Materials Inc.

Plasmas generated using energetic electron beams have unique properties that make them attractive for emerging plasma processing applications. In the pioneering work done at the Naval Research Laboratory, [1] it has been demonstrated that electron temperature (T_e) in the electron-beam generated plasmas is typically < 0.8 eV while electron densities are comparable to those obtained in radio-frequency (RF) inductively and capacitively coupled plasmas. In addition, the ions and radicals are primarily produced by highly energetic electrons (few keV) instead of electrons in the tail of a low energy distribution. The plasma chemistry in electron-beam generated plasmas is therefore significantly different to RF plasmas with a much higher ion to neutral radical density ratio. As feature dimensions shrink below 20 nm in microelectronics devices with atomic level precision required during manufacturing, the unique properties of electron-beam generated plasmas (low T_e , low ion energy and unique chemistry) are increasingly becoming attractive for plasma processing in the semiconductor industry.

For typical gas pressures used in electron beam generated plasmas (~ 50 mTorr), self-induced electric field and collisions can quickly broaden the electron beam. A relatively strong magnetic field parallel to the beam direction has therefore been employed to confine the electron beam. [1] Many complex mechanisms effect uniformity of a magnetized plasma, especially if the magnetic field is inhomogeneous and near the edges of the plasma. We have developed a 3-dimensional plasma model to better understand the spatial characteristics of electron-beam generated magnetized plasmas. The bulk plasma electrons are treated as a fluid and the model includes continuity equations for charged and neutral species, momentum equation for ions, and energy conservation equation for electrons. A Monte Carlo model is used for electron beam transport through the vacuum and plasma regions, which includes gas phase collisions and the effect of magnetic field and electric fields on electron motion.

The 3-dimensional plasma model is used to understand the spatial characteristics of electron beam generated Ar, N₂ and O₂ plasmas. These simulations have been done for a plasma chamber with radius < 30 cm, and several magnet designs. The impact of magnetic field, beam electron energy, and gas pressure on uniformity of important plasma properties (electron and ion densities, radical densities, T_e) is examined. Modeling results are also validated against probe measurements. [1]

[1] E. H. Lock *et al.*, Plasma Sources Sci. Technol. 17, 025009 (2008).

9:20am **PS2-WeM5 From Nonlocal Electron Kinetic Theory to Practical Applications**, *Igor Kaganovich*, Princeton Plasma Physics Laboratory, *D. Sydorenko*, University of Alberta, Canada, *A. Khrabrov, Y. Raitses*, Princeton Plasma Physics Laboratory, *P. Ventzek, L. Chen*, Tokyo Electron America, Inc.

The purpose of the talk is to describe recent advances in nonlocal electron kinetics in low-pressure plasmas. Partially-ionized, bounded, and weakly-collisional plasmas demonstrate nonlocal electron kinetic effects, nonlinear processes in the sheaths, beam-plasma interaction, collisionless electron heating, etc. Recently Physics of Plasmas published special topic of collected papers dedicated to "Electron kinetic effects in low temperature plasmas" in memory of the pioneer and leader of this field, Professor Lev D. Tsendin [1]. The plethora of kinetic processes supporting the non-equilibrium plasma state is an invaluable tool, which can be used to adjust plasma parameters to the specific needs of a particular plasma application. We report on recent advances in nonlocal electron kinetics in low-pressure plasmas where a non-Maxwellian electron velocity distribution function was "designed" for a specific application: in dc discharges with auxiliary biased electrodes for plasma control [2], hybrid DC/RF unmagnetized [3] and magnetized plasma sources [4], and Hall thruster discharges [5]. We show using specific examples that this progress was made possible by synergy between full-scale particle-in-cell simulations, analytical models, and experiments. Initial "academic" studies paved the way to understanding of modern plasma devices that are being developed for future plasma technology. One example is so-called non-ambipolar electron plasma, where an electron beam is extracted through a small aperture [6]. Our previous studies of extraction system [2] and collective interaction of electron beam with the plasma aides understanding and optimization of this device [6]. Another example is modeling of high power plasma switch for electric grid system [7].

References

[1] I. D. Kaganovich, V. Godyak, and V. I. Kolobov, Phys. Plasmas 20, 101501 (2013).

[2] A. S. Mustafaev, V. I. Demidov, I. D. Kaganovich, M. E. Koepke, and A. Grabovskiy, "Sharp transition between two regimes of operation of dc discharge with two anodes and thermionic emission from cathode", to be published in Rev. Scient. Instr. (2014).

- [3] K. Denpoh and P. L. G. Ventzek, *J. Vac. Sci. Technol. A* **26**, 1415 (2008).
- [4] S. Abolmasov, *Plasma Sources Sci. Technol.* **21** 035006 (2012).
- [5] Y. Raitsev, I.D. Kaganovich, A. V. Khrabrov, D. Sydorenko, N.J. Fisch, and A. Smolyakov, *IEEE Trans. Plasma Sci.* **39**, 995 (2011).
- [6] L. Chen, Zh. Chen and M. Funket, *Plasma Sources Sci. Technol.* **22**, 065015 (2013).
- [7] D. M. Goebel, *Rev. Sci. Instr.* **67**, 3136 (1996).

9:40am **PS2-WeM6 Electromagnetic Modeling of Inductively-Coupled Plasma Sources with Realistic Plasma Loads**, *Jason Kenney, S. Rauf, K. Collins*, Applied Materials, Inc.

Design of inductively-coupled plasma (ICP) sources for industrial tools is a challenging process, often relying on multiple classes of models owing to differing design goals and model limitations. A basic progression may include two-dimensional (2D) plasma modeling to fix the source architecture; three-dimensional (3D) electromagnetic (EM) modeling to investigate feed structures, current requirements, and azimuthal uniformity; and thermal modeling of source components using heat loads from the plasma and EM modeling. For the 2D plasma simulation, a typical approach assumes that power is coupled into the plasma volume purely inductively [1], reducing the source calculation to computation of azimuthal electric fields arising from coil currents. This can be enhanced by modifying the equivalent circuit of coils and plasma to account for capacitive and resistive powers.[2]

The computational expense of a coupled 3D plasma and EM model—which would require a fine mesh to capture source details along with a large number of computational cycles to allow the plasma properties to reach steady-state—is generally avoided through appropriate assumptions. In the 3D EM model, the simplest assumption is to represent the plasma as a conductive medium with conductivity matching that of a plasma with assumed density (or density profile) similar to the plasma simulation. However, in this work, we consider the impact of a more realistic treatment of a plasma load in a 3D finite-element time-domain (FDTD) EM model. In this method, the Maxwell Equations are solved in a leapfrog manner, updating electric and magnetic field vectors in turn. Rather than assume the plasma is a fixed medium with assumed conductivity, we consider the plasma current through solving the linearized momentum conservation equation for electrons, which is coupled to the Maxwell equations. It is assumed that ions are fixed. In addition, we consider methods to capture the nonlinear sheath dynamics by treating the sheath as a nonlinear circuit element and embedding these elements at the plasma – material interfaces in the mesh.

Discussion will be focused on impact of ICP source frequency and power for low pressure conditions (~20 mT) typical of ICP operation.

- [1] M.J. Kushner, et al., *J. Appl. Phys.* **80**, 1337 (1996).
- [2] A. Agarwal, et al., AVS Symposium (2014).

11:00am **PS2-WeM10 Two Dimensional Simulations of the Impact of Weak Magnetic Fields on the Plasma Properties of a Planar Slot Antenna Surface Wave Driven Plasma Source**, *Jun Yoshikawa*, Tokyo Electron Ltd., *Y. Susa*, Tokyo Electron Miyagi Limited, *P. Ventzek*, Tokyo Electron America, Inc.

The radial line slot antenna plasma source is a type of surface wave plasma source driven by a planar slotted antenna. Microwave power is transmitted through a slot antenna structure and dielectric window to a plasma characterized by a generation zone adjacent to the window and a diffusion zone that contacts a substrate. The diffusion zone is characterized by a very low electron temperature. This renders the source useful for soft etch applications and thin film deposition processes requiring low ion energy. Another property of the diffusion zone is that the plasma density tends to decrease from the axis to the walls under the action of ambipolar diffusion. A previous simulation study [1] predicted that the anisotropy in transport parameters due to weak static magnetic fields less than 50 Gauss could be leveraged to manipulate the plasma profile in the radial direction. These simulations motivated experimental tests in which weak magnetic fields were applied to a radial line slot antenna source. Plasma absorption probe measurements of electron density and etch rate measurements showed that the magnetic fields remote from the wafer were able to manipulate both electron density and etch rate. The presentation includes a brief recap of the first simulations, a summary of the experimental results and new simulation results that mate to these experiments. [1] *J. Vac. Sci. Technol. A* **31**, 031306 (2013)

11:20am **PS2-WeM11 Analytical Model of Plasma Sheaths at Intermediate Radio Frequencies**, *Mark Sobolewski*, NIST

Analytical models of plasma sheaths provide physical insight and are useful in 2-d and 3-d plasma simulations, where numerical solution of the sheath equations at each boundary point is too time-consuming to be practical. Analytical models have long been known for the high-frequency and low-frequency limits, where the time it takes ions to cross the sheath, t_i , is either much greater than or much less than the rf period, T . At intermediate frequencies, where $t_i \approx T$, sheath behavior is more complicated. In addition to the well-known narrowing of ion energy distributions (IEDs) there are other, lesser known effects at $t_i \approx T$, including changes in the ion current — which becomes strongly time-dependent within the sheath — and in IED peak intensities, average ion energy, sheath impedance, and sheath power. Existing analytical models of collisionless sheaths based on the "damped potential" formalism yield accurate predictions for IED widths and peak energies, but not for any of the other phenomena. Here, we describe a different approach for modeling intermediate-frequency, collisionless sheaths. It captures the essential elements of ion dynamics yet still provides analytical expressions for most sheath properties. Others require minimal numerical effort, such as a single numerical integration of an analytical expression. Predictions of the analytical model are compared to previous analytical results, complete numerical solutions of the relevant partial differential equations, and, where possible, experimental data. The model yields new insights into ion dynamics and may serve to increase the accuracy of 2-d and 3-d plasma simulations, in particular, their predictions for power and average ion energy.

11:40am **PS2-WeM12 Plasma Prize Invited Lecture: Simulations of Plasma Processes and Equipment for Semiconductor Device Fabrication**, *Peter Ventzek*, Tokyo Electron America, Inc. **INVITED**

For decades, simulation and theory has been applied to the design and analysis of semiconductor process and fabrication equipment development. Simulation technology has advanced from predictions of the electron energy distribution function and plasma chemistry to multidimensional simulations of plasma equipment. Multidimensional plasma source models have been used to predict (and sometimes post-predict) many important phenomena. Prediction of the consequence of augmentation of sources with weak magnetic fields is used to illustrate this. Progress in surface topography evolution models and sub-surface property prediction has been similarly impressive. Complemented with classical force field molecular dynamics simulations have been used to address critical problems related to patterning and atomic layer etching. While fully integrated equipment-feature scale models have been demonstrated, they remain less than tightly coupled because of difficulties dealing with plasma and plasma-surface chemistry. While this presentation will not reveal closing of gaps between models, progress in coupling can be reported. Advances in quantum chemistry and molecular dynamics methods permit insights to be gained from existing simulations of plasma sources. We will use the example of plasma doping using microwave plasma sources as an example. Techniques that complement equipment simulations such as highly resolved particle-in-cell simulations and test particle methods help reveal how the physics of the plasma source is related to phenomena at the surface and sub-surface. Once akin to "Imagineering," Modeling and simulation is now pervasive in the semiconductor industry. Globally this is manifested through direct activity in industry or through interactions with consortia or academia. The presentation will provide a perspective on future directions in the field.

Selective Deposition as an Enabler of Self-Alignment

Focus Topic

Room: 318 - Session SD-WeM

Fundamentals of Selective Deposition

Moderator: James Engstrom, Cornell University, Florian Gstrein, Intel Corporation

8:00am **SD-WeM1 Utilizing Inhibitor Molecules in Low Temperature CVD to Control Thin Film Nucleation, Surface Morphology and Conformality in Deep Features**, *John R. Abelson*, University of Illinois at Urbana-Champaign **INVITED**

When performed at low substrate temperature, the growth of thin films by chemical vapor deposition can be strongly *inhibited* by the reversible adsorption of precursor, byproduct, or neutral molecule species on the active surface. The microscopic mechanism is typically that of site blocking: as the surface coverage of inhibitor species increases, the reaction probability of arriving precursor molecules drops, and can reach values as low as 10^{-6} under realistic growth conditions. In specific cases, the

mechanisms of associative precursor desorption or coverage-dependent film growth rate also occur.

We will show that site blocking by the precursor itself can afford extremely conformal film growth in structures with aspect ratio $> 100:1$, and that the addition of a neutral molecule inhibitor to a 'non-conformal' precursor can provide good step coverage in features with aspect ratio $\sim 10:1$. We also solve the diffusion-reaction equation to predict the regimes of precursor pressure and substrate temperature that afford conformal growth, and map the boundaries onto a *conformal zone diagram*. Under conformal conditions the surface roughness is exceptionally low due to the smoothing effect of precursor re-emission, which mitigates the 'shadowing' of the incident flux by peaks in the surface morphology.

We then show that an inhibitor molecule can be used to control the film nucleation step. The inhibitor molecule must have a greater adsorption energy on the deposited material than on the bare substrate surface, or vice versa, such that the equilibrium coverage of inhibitor is large only on the strongly binding surface. For strong binding to the film, the deposit consists of a high density of nm-scale nuclei that coalesce into an ultra-smooth film; we give the example of HfB_2 growth on SiO_2 using NH_3 as the inhibitor. Conversely, when the inhibitor slows the nucleation rate, the deposit consists the sparse distribution of islands in a narrow size distribution that may be useful in photonic or catalytic applications; we give the example of Cu growth using VTMC as the inhibitor.

The use of inhibitors may provide a pathway towards selective deposition if film growth can be completely shut off on the surface that is intended to remain bare. Systems in which the inhibitor can drive associative desorption of the precursor are predicted to be especially useful, in that they remove unwanted precursor molecules. Another possibility is the use of activated species such as atomic H, generated by a remote plasma, that fully passivate covalently bonded surfaces but recombine rapidly (and therefore have no effect) on metallic surfaces.

8:40am SD-WeM3 Metrology of Selective Functionalization of Semiconductor, Oxide and Nitride Surfaces, *L. Liu, W.J.I. DeBenedetti, S. Karakaya, T. Peixoto*, University of Texas at Dallas, *R. Hourani, D.J. Michalak*, Intel Corporation, *Yves Chabal*, University of Texas at Dallas
INVITED

There is an increasing need to develop selective functionalization of surfaces. This goal requires careful control over surface cleaning, intermediate passivation, and chemistry (either vapor phase or wet) on oxide, semiconductor, and/or metal surfaces, many of which have not been well-studied in the past. It is therefore critical to bring to bear a number of characterization techniques that can provide sufficient information to fully understand each of these three steps (cleaning, passivation, functionalization).

This talk will illustrate the role of characterization in examining surfaces such as silicon nitride, silicon oxide, and metallic surfaces with a unique cluster tool equipped with *in-situ* infrared (IR), X-ray photoelectron spectroscopy (XPS) and low-energy ion scattering (LEIS) for bonding, elemental, chemical and spatial characterization. These techniques are coupled with *ex-situ* AFM, spectroscopic ellipsometry, and SEM for full characterization of interesting surface species and products. Following a goal to achieving chemical selectivity between Si_3N_4 and SiO_2 surfaces, we first focus on the surface chemistry after cleaning and etching with aqueous HF. While H or NH_x is typically believed to be the chemical termination of HF-etched silicon nitride surfaces, we find that such surfaces not only require careful preparation to remove salt byproducts, but are also essentially fluorine terminated. Despite the clear difference in surface termination between nitrides and oxides, both surfaces display surprisingly similar reactivity and bonding upon exposure to chloro- and ethoxysilane molecules: both surfaces display the formation of Si-O-Si bonds but the nitride surfaces show little removal of fluorine. We propose a novel concept for surface reaction involving the activation of surface atoms back-bonds, such as Si-N/Si-O in the case of F-terminated Si_3N_4 . While such a process does not lead to selective chemistry of silicon oxide and nitride surfaces, its understanding opens the way for the selection of appropriate molecules for selectivity.

9:20am SD-WeM5 First Principles Calculations of Substrate-Specific Reactions in ALD, *Simon Elliott, M. Shirazi, S. Klejna*, Tyndall National Institute, Ireland

Selective-area atomic layer deposition (ALD) requires a new level of understanding of how to activate and deactivate substrates towards precursors and film growth, beyond the rather brute-force approach taken to date towards nucleation of ALD films. We present a review of substrate-specific interactions in ALD as determined by first principles calculations (mostly density functional theory). The substantial body of calculations in the literature of ALD onto oxide and H-terminated semiconductor substrates is introduced briefly as a baseline [S. D. Elliott, *Semicond. Surf. Techn.* 27,

074008 (2012)]. Our new results reveal at an atomic level why ALD reactions can be self-limiting on oxides [M. Shirazi et al., *Chem. Mater.* 25, 878 (2013)]. This is contrasted with computed mechanisms for reactions that do not self-limit and indeed where substrate oxides are consumed by precursors [Klejna et al., *Chem. Mater.* 26, 2427 (2014)]. Differences have also been computed for precursor adsorption and ligand reactions on metallic substrates (Cu, Ru) and these are discussed.

9:40am SD-WeM6 Surface Chemistry during ALD of SiN_x from BTBAS and N_2 Plasma, *C.K. Ande, K. de Peuter*, Eindhoven University of Technology, Netherlands, *H.C.M. Knoops*, Eindhoven University of Technology, *S.D. Elliott*, Tyndall National Institute, Ireland, *Erwin Kessels*, Eindhoven University of Technology, Netherlands

There is an urgent need for a scalable, low-temperature ALD process for the deposition of high-quality silicon nitride (SiN_x). However the development of such process by thermal ALD has been challenging, particularly when the use of halide-free precursors is required. Plasma-enhanced ALD processes can provide a solution as we have recently demonstrated by the development of an ALD process based on $\text{SiH}_2(\text{NH}^t\text{Bu})_2$ (BTBAS) precursor and N_2 plasma. This process yields high-quality SiN_x with a low wet etch rate and a good conformality on surface features with an aspect ratio of < 5 . In this contribution the surface chemistry during the SiN_x ALD process will be addressed. On the basis of mass spectrometry and optical emission spectroscopy, the surface reactions during precursor adsorption will be discussed as well as the interaction of the N_2 plasma species with the growth surface. In particular, the question will be addressed why the ALD process is feasible when using a pure N_2 plasma but not when using a H_2 - N_2 plasma or a NH_3 plasma. On the basis of carefully-designed experiments involving multiple plasma and gas exposures of the surface during an ALD cycle, it will be shown that the presence of under-coordinated N atoms at the surface is key for precursor adsorption. This will be supported by first-principles simulations in which the interaction of a $\text{Si}_3\text{N}_4(0001)$ surface with precursor molecules and various co-reactants (atomic H, atomic N and NH_3) was probed. These atomic scale simulations reveal that atomic H and NH_3 passivate the under-coordinated N and Si atoms on the surface rendering it unreactive towards the BTBAS precursor. N atoms on the other hand bind to under-coordinated surface N and Si atoms, but still leave behind under-coordinated N atoms on the surface. This understanding is vital to advance the precursor design for SiN_x ALD as well as for further development and improvement of the SiN_x ALD processes and material properties.

11:00am SD-WeM10 Enhanced Area-Selective Atomic Layer Deposition of TiN on HfO_2 , *Sonali Chopra, A.P. Lane, C.G. Willson, J.G. Ekerdt*, The University of Texas at Austin

This research targets the selective deposition of TiN onto HfO_2 for use as the word line in an STT-RAM (spin-transfer torque random access memory) device. It focuses on scalable technologies that are compatible with all steps in STT-RAM fabrication. Previous work has shown that chlorosilane and methoxysilane molecules can effectively block the HfO_2 surface from TiN deposition by area selective atomic layer deposition (AS-ALD). Other research has demonstrated the blocking efficiency of these organic layers declines with increasing number of cycles of atomic layer deposition. This deficiency has been attributed to imperfectly formed self-assembled monolayers during deposition or degradation of the organic layer due to the high temperatures of the ALD process. The decline in performance of the organic blocking layer limits the thickness of the material that can be deposited in unblocked regions without loss of selectivity. In this presentation, we will reveal methods to improve the blocking characteristics of these organic layers. We will demonstrate how specially functionalized macromolecules such as dendrimers and sequential chemical vapor deposition reactions using bifunctional molecules can be used to achieve enhanced blocking characteristics. Using x-ray photoelectron spectroscopy, water contact angle measurements, atomic force microscopy, and x-ray reflectivity, we examine the nucleation of TiN on the organic blocking layer and the limits (temperature, number of ALD cycles) of these passivants. Finally, we report the effectiveness of these organic layers to block TiN deposition on substrates with pre-formed features and explore their potential for device applications.

11:20am SD-WeM11 Selective Area Deposition of Short Cycle-Time ALD for Patterned-by-Printing Electronics, *CarolynR. Ellinger, S.F. Nelson*, Eastman Kodak Company

In this talk we will review our current understanding of the process space of spatial ALD and selective area deposition – including ALD cycle time, process temperature, precursors and choice of inhibitor. Data will be presented on inhibition of the precursors useful for making all of the layers necessary for thin film transistors over a temperature range of 100°C to 250°C , namely DEZ, DMAI, and H_2O . Our devices are composed of conductive aluminum-doped ZnO (AZO), semiconducting ZnO, and electrically insulating aluminum oxide.

We use selective area deposition as an alternative approach to printed electronics. We print an inhibiting polymer ink, and deposit active materials via spatial atomic layer deposition (ALD), thereby separating the ink requirements from the active materials requirements. We have previously shown a process flow using this methodology to make simple bottom gate ZnO thin film transistors (TFTs) that have the same device performance as TFTs using the same materials but patterned by more conventional photolithographic means. Here, we will present new data highlighting the advantages of the additive patterning allowed by selective area deposition. We demonstrate devices having architectures that are easily achievable with this approach, that are correspondingly difficult to achieve through subtractive processing methods.

In addition to providing design freedom, the patterned-by-printing process flow allows for high throughput and fast process speeds. The atmospheric spatial ALD system enables the use of very short cycle times, with single gas exposure times between 25 and 200 ms (cycle times of 100 to 800 ms). In addition, since there is no time penalty for pumping down a reaction chamber to vacuum levels, the process time is approximately the number of cycles required times the cycle time. Additional gains in process speed are to be had by using selective area deposition and printing, because there are no inorganic etch steps and no need for exposure or development of a photoresist. The process time is simply determined by the print rate and the time necessary to remove the inhibitor at the end of spatial ALD deposition. For our typical conditions, we complete a full pattern process cycle in less than 20 minutes, and can build functional circuits only hours after completing the layout of a new design. These studies show that the patterned-by-printing method offers a rapid cycle time approach to high quality electronics on a variety of supports.

11:40am **SD-WeM12 Self-limiting CVD of a Silicon Monolayer for Preparation of Subsequent Silicon or Gate Oxide ALD on InGaAs(001)-(2x4)**, *Mary Edmonds, T. Kent*, University of California, San Diego, *R. Droopad*, Texas State University, *E.A. Chagarov, A.C. Kummel*, University of California, San Diego

A broader range of channel materials allowing better carrier confinement and mobility could be employed if a universal control monolayer (UCM) could be ALD or self-limiting CVD deposited on multiple materials and crystallographic faces. Si-OH is a leading candidate for use as the UCM, as silicon uniquely bonds strongly to all crystallographic faces of InGa_{1-x}As, In_xGa_{1-x}Sb, In_xGa_{1-x}N, SiGe, and Ge enabling transfer of substrate dangling bonds to silicon, which is then passivated by atomic hydrogen. The surface may subsequently be functionalized with an oxidant such as HOOH(g) in order to create the UCM terminating Si-OH layer. This study focuses on depositing a saturated Si-H seed layer via two separate self-limiting and saturating CVD processes on InGaAs(001)-(2x4) at substrate temperatures of 250°C and 400°C. XPS in combination with STS/STM were employed to characterize the electrical and surface properties of the saturated silicon seed layers on InGaAs(001)-(2x4).

The 250°C self-limiting CVD procedure includes a decapped In_{0.53}Ga_{0.47}As(001)-(2x4) surface dosed with 300 MegaLangmuir of Si₃H₈ at sample temperature of 250°C. The 400°C self-limiting CVD procedure includes a decapped surface dosed with 21 MegaLangmuir of Si₂Cl₆, followed by a 500 Langmuir dose of atomic hydrogen at sample temperature of 400°C, leaving the silicon surface hydrogen terminated. The XPS spectra following the saturated Si₃H₈ and Si₂Cl₆ doses shows the increase of the silicon 2p_{3/2} peak and decrease in the gallium 3p_{3/2} substrate peak, indicative of saturating coverage. Complete saturation is determined to occur once further dosing with Si₃H₈ or Si₂Cl₆ leads to no further increase in the silicon 2p peak or further decrease in the gallium 3p peak areas. STM images of the decapped surface following Si₃H₈ CVD at 250°C and post annealing shows high surface order. STM images of the saturated Si₂Cl₆ surface followed by 500 Langmuir atomic hydrogen at 400°C show silicon absorbs in a commensurate structure with average row spacing nearly identical to the (2x4) surface at 1.5 nm, consistent with III-V dangling bond elimination. Both CVD processes employ high pressure CVD pulses, which protect from unwanted carbon and oxygen contamination. The hydrogen terminated silicon surface achieved by both CVD procedures show identical STS results with the surface Fermi level remaining at the same location as the n-type clean (2x4) surface and conduction and valance band edges lining up, indicating both processes do not pin the Fermi level nor degrade the surface density of states.

Surface Science

Room: 309 - Session SS+AS+EN-WeM

Dynamic Processes of Single Atoms and Molecules at Surfaces

Moderator: Arthur Utz, Tufts University, Andrew Gellman, Carnegie Mellon University

8:00am **SS+AS+EN-WeM1 Construction and Manipulation of Individual Functional Molecules: from Reversible Conductance Transition to Reversible Spin Control**, *Hong-Jun Gao*, Chinese Academy of Science, China **INVITED**

Control over charge and spin states at the single molecule level is crucial not only for a fundamental understanding of charge and spin interactions but also represents a prerequisite for development of molecular electronics and spintronics. While charge manipulation has been demonstrated by gas adsorption and atomic manipulation, the reversible control of a single spin of an atom or a molecule has been challenging. In this talk, I will present a demonstration about a robust and reversible spin control of single magnetic metal-phthalocyanine molecule via attachment and detachment of a hydrogen atom, with manifestation of switching of Kondo resonance. Low-temperature atomically resolved scanning tunneling microscopy was employed. Using density functional theory calculations, the spin control mechanism was revealed, by which the reduction of spin density is driven by charge redistribution within magnetic 3d orbitals rather than a change of the total number of electrons. This process allows spin manipulation at the single molecule level, even within a close-packed molecular array, without concern of molecular spin exchange interaction. This work opens up a new opportunity for quantum information recording and storage at the ultimate molecular limit.

References:

1. L.W. Liu, K. Yang, Y.H. Jiang et al., Scientific Report 3, 1210 (2013).
2. L. Gao et al., Phys. Rev. Lett. 99, 106402 (2007).

*In collaboration with Liwei Liu, Kai Yang, Yuhang Jiang, Boqun Song, Wende Xiao, Linfei Li, Haitao Zhou, Yeliang Wang, and Shixuan Du, Institute of Physics, Chinese Academy of Sciences, Beijing 100190, China

8:40am **SS+AS+EN-WeM3 Single Molecule Origins of Electronic Disorder: Random Conformations of α -NPD Molecules on Au(111)**, *Daniel Dougherty, J. Wang, J. Wang*, North Carolina State University

Disorder is an important aspect of modeling organic and polymeric electronic materials. Proper accounting of the effects of disorder both in active layers and at interfaces with contacts determine the detailed current-voltage characteristics in organic thin film devices [1]. Our study seeks to visualize and statistically quantify the disorder in α -NPD films at the single molecule scale. This molecule is a common hole transport material in organic LED's and has been found to exhibit strong disorder in thin film diode geometries [2]. We used scanning tunneling microscopy and spectroscopy to observe numerous surface structures of α -NPD on the (111) surface of Au. These structures are distinguished by different lateral order as well as different local molecular conformations. Random molecular conformations on the surface lead to an statistical distribution of hole transport states that is consistent with the distribution inferred from device analysis. *This work was funded by an NSF CAREER award through DMR-1056861. [1]Tessler et al., Adv. Mater. 21, 2741 (2009) [2] van Mensfoort et al., J. Appl. Phys. 107, 113710 (2010)

9:00am **SS+AS+EN-WeM4 Pt-Cu Single Atom Alloys for the Selective Partial Hydrogenation of Butadiene**, *Felicia Lucci, M. Marcinkowski, E.C.H. Sykes*, Tufts University

Butene is a common feedstock for polymerization reactions; however, butadiene is a minority impurity that poisons the polymerization catalyst. The selective hydrogenation of butadiene to butene serves to increase the purity of the feedstock without reducing the overall concentration of butene. Therefore, catalysts that selectively hydrogenate butadiene to butene and prevent the hydrogenation of butene to butane are of great interest. Using scanning tunneling microscopy (STM) and temperature programmed desorption/reaction (TPD/R), we show that Pt-Cu single atom alloys catalyze hydrogenation of butadiene to butene with 100% selectivity. The addition of small amounts of Pt (~1%) into Cu reduces the barrier for H₂ dissociation, allowing for the low temperature dissociation of H₂. H atoms spill-over onto the Cu sites increasing the concentration of weakly bound H atoms available for the hydrogenation reaction. The weakly bound H atoms readily hydrogenate butadiene to butene. TPD of co-adsorbed H and butadiene shows the exclusive desorption of reactively formed butene, where the reaction extent is limited by the availability of H on the surface.

While the individual, isolated Pt atoms in the Cu terrace activate molecular H₂, they do not induce the decomposition of butadiene as observed on Pt(111) surfaces. The ability to control geometries of atomic ensembles and hence the extent of hydrogenation reactions using *single atom alloys* allows for the production of new and efficient catalysts.

9:20am **SS+AS+EN-WeM5 Toward a Dynamical Understanding of Chemistry at Metal Surfaces**, *Alec Wodtke*, Max Planck Institute for Biophysical Chemistry **INVITED**

One of our most fundamental scientific challenges is to develop predictive theories of chemistry rigorously grounded in the laws of physics. In 1929, Dirac identified the problem famously in a comment about the importance of quantum mechanics to chemistry... *"The underlying physical laws necessary for the mathematical theory of... ..the whole of chemistry are thus completely known, and the difficulty is only that the exact application of these laws leads to equations much too complicated to be soluble."* Despite electrifying advances in computational power, Dirac is still right. The theory of chemistry requires approximate methods for practical computations.

For the theory of surface chemistry, three central approximations are made, involving the use of: 1) classical mechanics for describing nuclear motion, 2) density functionals for calculating electronic states and the Born-Oppenheimer approximation to separate electronic and nuclear degrees of freedom.

The growing importance of computational surface chemistry motivates us to design rigorous experimental tests of these assumptions. Many fundamental questions arise. Can we trust the Born-Oppenheimer approximation for calculating potential energy surfaces for reactions at metal surfaces? Can we characterize and overcome the weaknesses of density functional theory, for example by developing new wave-function based methods for the solid-state? For all of these reasons, it is important to carefully design experimental tests of the capabilities of modern computational surface chemistry.

Using modern molecular beams methods in state-to-state scattering experiments, we obtain a wealth of observational data characterizing the interactions of molecules with metal surfaces. Emphasizing quantitative comparison to first principles theories, we find that energy conversion can occur by unexpected mechanisms, where the electronically adiabatic approximation separating the time scales of electronic and nuclear motion is found to be invalid. The simplicity of the systems under study provides opportunities for developing new theories that go beyond the Born-Oppenheimer approximation. One important outcome of this is the realization that Born-Oppenheimer breakdown can be induced by simple electron transfer events that are common in surface chemistry.

11:00am **SS+AS+EN-WeM10 Steric Effect in O₂ Chemisorption on Al(111)**, *Mitsunori Kurahashi, Y. Yamauchi*, National Institute for Materials Science (NIMS), Japan

O₂ adsorption on Al(111) has been investigated intensively as the most representative system of surface oxidation. The dynamical process happening on the surface, however, remained unclear. An STM study by Brune et al.[1] has proposed that adsorbed O-atoms are atomic and are well separated each other. Initially, this has been ascribed to the transient mobility driven by the O₂ chemisorption energy ("hot-atom" mechanism)[1], but this mechanism has been found to be unlikely. The abstraction mechanism, in which one O-atom is bound to the surface while the other is ejected, has been proposed alternatively based on the resonance enhanced multi-photon ionization measurement.[2] It is however not evident whether or not the abstraction process is the dominant event at low translational energies (E₀). In addition, the STM study by Schmid et al.[3] has suggested that the adsorbates consist of two O-atoms locating at nearby sites. This cannot be explained by the abstraction mechanism.

In this study, we focused attention to the alignment dependence in the O₂ sticking to clarify the reaction mechanism. A single spin-rotational state-selected [(J,M)=(2,2)] O₂ beam, for which we can specify both the molecular alignment and spin direction relative to the magnetic field, was adsorbed on an Al(111) surface. The results show that O₂ molecules parallel to the surface have much higher sticking probabilities than those perpendicular to the surface at E₀ < 0.2 eV. The E₀ dependence of the sticking probability indicates that the dissociation barrier at the perpendicular geometry is about 0.1 eV higher than at the parallel geometry. The present results reveal that the abstraction process, which occurs at the perpendicular geometry, is a minor event at low E₀. [4]

[1] Brune et al., Phys. Rev. Lett., 68, 624 (1992). [2] Komrowski et al., Phys. Rev. Lett., 87, 246103 (2001). [3] Schmid et al., Surf. Sci., 478, L355 (2001). [4] Kurahashi et al., Phys. Rev. Lett., 110, 246102 (2013)

11:20am **SS+AS+EN-WeM11 Surface Temperature Effects in Methane Dissociation on Ni and Ir Surfaces**, *Arthur Utz, E. Peterson, E. Dombrowski, E. High, E. Nicotera*, Tufts University

Recent transition state and quantum dynamics calculations have suggested an important role for surface atom motion in promoting methane dissociation on transition metals including Ni, Pt, and Ir. Here, we describe state-resolved gas-surface scattering measurement of methane dissociation on Ni(111), Ir(111), and Ir(110)-(1x2). Infrared laser excitation prepares methane in a single excited rotational and vibrational state with a precisely defined internal energy. A supersonic molecular beam provides tight control over the translational energy of the methane molecules. The methane molecules, with their well-defined energy, accentuate the role of surface temperature, and the resulting thermal motion of surface atoms, on reactivity.

The presentation will focus on recent experimental results. On the Ir(110)-(1x2) surface, we observe both precursor-mediated and direct reaction channels for the vibrationally excited (v₃, v=1) molecules at surface temperatures of 300K or higher. For v=0 molecules, a precursor-mediated pathway appears for surface temperatures above 500K, but not for temperatures of 500K or lower. The abrupt disappearance of the precursor-mediated reaction path correlates with a surface reconstruction to (331) facets that was previously reported to occur at 500K. We will report on measurements that extend the temperature range for the vibrationally excited (v₃, v=1) molecules to temperatures between 100 and 300K on the Ir(110) surface. We will also report on more recent studies that explore the surface temperature dependence of more highly vibrationally excited methane molecules.

11:40am **SS+AS+EN-WeM12 Activation of C₁-C₉ Alkanes on Pt(111): Importance of Dynamics, van der Waals Interactions, and Gas-Surface Energy Transfer**, *Jason Navin, S.B. Donald, G. Cushing, I.A. Harrison*, University of Virginia

A variety of dissociative sticking coefficients (DSCs) were measured for alkanes varying in size from methane to nonane on Pt(111) using an effusive molecular beam technique. Thermal equilibrium (T_g = T_s) and non-equilibrium (T_g ≠ T_s) DSC measurements provided information about the gas-surface reactivity and energy transfer. Angle-resolved DSCs, S(700 K; θ), measured for methane, ethane, and propane on Pt(111) were used to define thermal DSCs, S(T), and discern dynamical behavior. Methane and ethane DSCs were sharply peaked around the surface normal and were found to have similar dynamical biases away from statistical behavior. Precursor-mediated microcanonical trapping (PMMT) models were used to both analyze and predict DSCs over a wide range of experimental conditions and experiments. It was found that the activation energy for dissociative chemisorption of an alkane scales linearly with its molecular desorption energy from the physisorption well in front of the surface. The molecular desorption energy should be proportional to the van der Waals stabilization energy for the products of dissociative chemisorption. The gas-surface energy transfer increased as the alkane size increased from C₁ to C₉. For alkanes larger than C₄, the gas-surface energy transfer was apparently sufficient to fully thermalize the impinging molecule to the temperature of the surface before reaction such that, S(T_g=300K, T_s) = S(T).

12:00pm **SS+AS+EN-WeM13 Shining light on an Important Intermediate Step in Photocatalysis: Probing Polarons in ZnO using Infrared Reflection Absorption Spectroscopy**, *Fabian Bebensee, H. Sezen*, Karlsruhe Institute of Technology, Germany, *A. Nefedov, C. Wöll*, Karlsruhe Institute of Technology

ZnO is a wide-bandgap metal oxide exhibiting various highly desirable physico-chemical properties, among them high photocatalytic activity. As such, it has been widely studied employing virtually all available techniques over the past 50 years.^[1] In the context of photoexcitations, primarily excitons have been studied extensively including their very recently reported ultrafast formation dynamics.^[2] In photocatalysis, dissociation of excitons into free electrons and holes takes place and therefore the binding energies of the polaronic states become crucial for the subsequent steps on the way to finally transferring an electron or hole onto an adsorbed molecule. Despite their importance in photochemistry (see recent work on TiO₂^[3]), very little work has been devoted to these trap states in ZnO. Here, we report a novel approach to study polarons in ZnO single crystal substrates: the polaron traps are populated via UV-light irradiation and then probed using infrared reflection absorption spectroscopy (IRRAS). Upon irradiation, a number of previously unobserved, well-defined and sharp absorption bands appear in the IR-spectra. Among these new features is an absorption-edge like feature that we assign to excitations of electrons from the conduction band into hole polaronic trap states. From their time-dependent intensity, we infer a (temperature-dependent) life time of 25 seconds at 75 K. The implications of these findings for ZnO photochemistry will be discussed.

- [1] C. Klingshirn, *physica status solidi (b)* **2007**, 244, 3027-3073.
- [2] J.-C. Deinert, D. Wegkamp, M. Meyer, C. Richter, M. Wolf, J. Stähler, *Physical Review Letters* **2014**, 113, 057602.
- [3] H. Sezen, M. Buchholz, A. Nefedov, C. Natzeck, S. Heissler, C. Di Valentin, C. Wöll, *Sci Rep-Uk* **2014**, 4, 3808.

Surface Science

Room: 312 - Session SS+AS-WeM

Atomistic Modeling of Surface Phenomena

Moderator: Carol Hirschmugl, University of Wisconsin Milwaukee, Eddy Tysøe, University of Wisconsin-Milwaukee

8:00am **SS+AS-WeM1 Oxidation of Cu Surfaces with Step-Edge Defects: Insights from Reactive Force Field Simulation**, *Qing Zhu, W.A. Saidi, J. Yang*, University of Pittsburgh

Defects on metal surfaces can induce non-canonical oxidation channels that may lead to the formation of novel nanostructures. Cu surfaces have been actively researched in the surface science community due to their wide range of applications in many fields. Recently, *in situ* TEM experiments showed that the oxidation of stepped surfaces promotes the formation of a flat metal-oxide interface through the Cu adatoms detachment from steps and diffusion across the terraces. In order to better understand these results, and to provide a tight bridge between the experiment and theory, we have investigated the Cu (100) oxidation using ReaxFF method as implemented in Large-scale Atomic/Molecular Massively Parallel Simulator (LAMMPS). Using models for both defect-free flat and stepped surfaces, our study shows that the step-edge defects induce markedly different oxidation dynamical behavior compared to the flat surface. Additionally, on the stepped-surfaces, we show that the oxidation of the upper-terrace are more favored than the lower-terrace, which we validated by depositing oxygen homogeneously on the surface or by using a biased-mechanism where the oxygen atoms target either the top or lower terraces. This favoring of the oxidation of the top terrace drives Cu diffusion flux from the upper-terrace to the lower-terrace that explains the recent TEM experiments. We additionally show that the oxidation behavior of the stepped Cu (100) bears many similarities with the formation of the metal-oxygen "added-row" structures on the (110) surfaces of several metals. Future studies include the investigation of vicinal surfaces with different morphologies and different metals.

8:20am **SS+AS-WeM2 The Role of Time-scale Analysis in Simulation of ALD and CVD Surface Reaction Kinetics**, *Raymond Adomaitis, E. Remmers, C.D. Travis, D. Arana-Chavez*, University of Maryland, College Park

In this paper, we will describe our research on the mathematical structure of atomic layer deposition (ALD) and chemical vapor deposition (CVD) surface reaction kinetics models. Our primary objective is to investigate the mathematical structure of the differential-algebraic (DAE) systems of equations describing surface reaction species dynamics during these thin-film deposition processes. The research is motivated by the challenges presented by writing a well-posed DAE model for surface reaction species dynamics as well as the difficulties encountered when numerically solving these systems. Using a perturbation analysis approach, we demonstrate that the deposition kinetics decomposes naturally into slow (deposition reactions), fast (equilibrium reactions), and instantaneous (conserved quantities) time scales. A key contribution of our work is the development of a reaction network factorization procedure that partitions the surface reaction and deposition species dynamic balances into the distinct time scale ranges described. Under what conditions this procedure works, understanding the implications of fixed points for dynamic ALD processes, interpreting reaction fluxes, and extending the methods to spatially distributed processes in the context of representative thin-film application domains will be discussed. Physical interpretation of DAE system initial conditions for these surface processes constitutes another important research direction in this project; results will be presented which illuminate alumina ALD growth surface dynamics at the start of each exposure (TMA and water) and purge period.

8:40am **SS+AS-WeM3 Hydrogen Production from Formic Acid on Transition Metals and Alloys: A Selectivity Challenge**, *Manos Mavrikakis, J. Scaranto, J.A. Dumesic, S. Singh, S. Li, J.A. Herron, R. Carrasquillo, L. Roling, B. O'Neill, G. Peng*, University of Wisconsin - Madison **INVITED**

Formic acid (HCOOH) is a simple molecule that is an abundant product of biomass processing and can serve as an internal source of hydrogen for oxygen removal and upgrading of biomass to chemicals and fuels. In addition, HCOOH can be used as a fuel for low temperature direct fuel cells. We present a systematic study of the HCOOH decomposition reaction mechanism starting from first-principles and including reactivity experiments and microkinetic modeling. In particular, periodic self-consistent Density Functional Theory (DFT) calculations are performed to determine the stability of reactive intermediates and activation energy barriers of elementary steps. Pre-exponential factors are determined from vibrational frequency calculations. Mean-field microkinetic models are developed and calculated reaction rates and reaction orders are then compared with experimentally measured ones. These comparisons provide useful insights on the nature of the active site, most-abundant surface intermediates as a function of reaction conditions and feed composition. Trends across metals on the fundamental atomic-scale level up to selectivity trends will be discussed. Finally, we identify from first-principles alloy surfaces, which may possess better catalytic properties for selective dehydrogenation of HCOOH than monometallic surfaces, thereby guiding synthesis towards promising novel catalytic materials.

9:20am **SS+AS-WeM5 Elucidating Atomic-scale Wear Processes in Hydrocarbon-based Materials via Molecular Dynamics and AFM**, *Judith Harrison*, United States Naval Academy, *T.D.B. Jacobs*, University of Pennsylvania, *P.L. Keating, M. Fallet*, United States Naval Academy, *J.D. Schall*, Oakland University, *Y. Jiang, K.T. Turner, R.W. Carpick*, University of Pennsylvania, *K.E. Ryan*, United States Naval Academy

Molecular dynamics (MD) simulations are unique in their ability to elucidate atomic-scale phenomena because the positions, velocities, and forces of all atoms in the system are known as a function of time. Atomic-scale wear in nanoscale contacts is of particular importance for tip-based nanomanufacturing applications. As a result, wear resistant materials, such as diamond-like carbon (DLC), have been used to coat AFM tips to improve the lifespan and reliability of AFM probes. We have performed atomic force microscope (AFM) experiments and MD simulations aimed at examining adhesion and wear in diamond, ultrananocrystalline diamond (UNCD), and amorphous carbon (a-C:H) materials. Specifically, we examined the normal and sliding contact of differently shaped axisymmetric tips, composed of a-C:H and UNCD, with hydrocarbon-based substrates. Specific attention was paid to elucidating specific atomic-scale wear mechanisms and their dependence on tip shape, material, surface termination, impact point, and roughness. To examine the effect of the potential energy function on wear mechanisms, identical simulations were performed with the AIREBO potential and the REBO+S potential. The AIREBO potential is based on the reactive empirical bond-order potential (REBO), which was developed to model CVD growth of diamond. Recently, it was demonstrated that the short-range cut-off for covalent bonding in the REBO potential resulted in bond-breaking forces that are an order of magnitude larger than those predicted by DFT calculations. A screening function was added to the REBO potential (REBO+S) to alleviate this situation. Simulations were carried out using each potential, and wear mechanisms identified in each set of simulations were compared.

9:40am **SS+AS-WeM6 Theoretical Investigation of the Structure and Properties of Titania/Graphene Hybrid Materials**, *Ivan Iordanov, C.J. Karwacki*, Edgewood Chemical And Biological Center, *G.M. Mogilevsky*, Booz Allen Hamilton

We are using modeling to understand the properties of complex materials that show promise for catalysis, filtration and decontamination. These materials are of interests both for chemical defense, as well as in many industrial applications. The main focus of our modeling so far has been determining the structure and properties of mixtures of TiO₂ nanoparticles (NPs) and small sheets of graphene. The synthesis technique for these materials was pioneered at ECBC. It involves synthesizing graphene from alizarin molecules in close contact with TiO₂ NPs. This was expected to create a close connection between the graphene and TiO₂ NPs, and improve their catalytic properties. However, the exact structure of the small graphene patches and how and where they bind to TiO₂ is difficult to characterize experimentally. Our models have shown that the binding between graphene TiO₂ is quite weak (on the order of 0.01eV/Carbon atom), and that it is not strongly dependant on the addition of O and OH to the surface of the graphene, or to the size of the graphene patches. This appears to confirm the experimental finding that the surface graphene can be removed from the TiO₂ particles simply by rubbing. We also modeled the case where graphene is surrounded by TiO₂ on both sides, and the

binding in this case increases by nearly 2x, suggesting that graphene would prefer to bind between TiO₂ NPs. This may be the explanation for the disappearance of the smallest (~5nm) sized pores from the TiO₂ NP agglomerates upon addition of graphene. We also find that there is a non-trivial degree of charge transfer between graphene and TiO₂, which can be expected to improve TiO₂'s photo catalytic properties.

11:00am **SS+AS-WeM10 Real-Time Ab-Initio KMC Simulation of the Self-Assembly and Sintering of Bimetallic Epitaxial Nanoclusters: Au+Ag on Ag(100)**, James Evans, Y. Han, D.-J. Liu, Iowa State University
Far-from-equilibrium shape and structure evolution of bimetallic epitaxial nanoclusters during formation by deposition or during post-assembly sintering is extremely sensitive to the details of periphery diffusion and intermixing kinetics. Precise characterization requires accurate determination of distinct barriers for many possible local environments (compositions and periphery configurations) of the diffusing adatom. This is achieved for epitaxial nanoclusters using DFT to assess adsorption energies and lateral pair- and trio-interactions both conventionally with adatoms at adsorption at adsorption sites, and unconventionally with an adatom at the transition state for hopping. KMC simulation incorporating these barriers then captures structure evolution on the appropriate time-scale. The approach is applied for unstrained Au-Ag nanoclusters on Ag(100) where these can be assembled with either 2D core-ring by sequential codeposition or intermixed structures by simultaneous codeposition or annealing. This ab-initio level approach replaces typical heuristic analyses, often resorting to macroscopic concepts, e.g., for intermixing kinetics.

11:20am **SS+AS-WeM11 Progress in Characterizing Submonolayer Island Growth: Capture-Zone Distributions, Growth Exponents, and Hot Precursors**, Theodore L. Einstein, J.R. Morales-Cifuentes, University of Maryland, College Park, A. Pimpinelli, Rice Quantum Institute

We review previous results for using the capture-zone [island proximity cell] distribution (CZD) in island growth to extract information about the critical nucleus size i^* . Over the experimentally accessible region, the CZD is well described by the generalized Wigner distribution $P_p(s) = a_p s^\beta \exp(-b_p s^2)$, dependent only on the exponent β . For diffusion-limited aggregation (DLA), $\beta \approx i+2$. We discuss recent experimental applications. For comparison with this approach, we consider the corresponding dependence of the growth exponent χ (stable island density $N \sim F^\chi$, where F is the flux) for both DLA and attachment-limited aggregation (ALA). In either case, $\chi\beta = i$, so that for ALA, where $\chi = 2i/(i+3)$, we find $\beta = (i+3)/2$.² We compare with experiments depositing pentacene (5A) and p-hexaphenyl (6P) on sputtered mica.

Furthermore, recent experiments³ studying 5A on amorphous mica gave evidence of nucleation via a hot precursor state, with an unusual relationship between N and substrate temperature. Thus motivated, we examine a model of such behavior.⁴ We use rate equations and Walton's relation. We take deposited monomers to be hot initially, traveling ballistically with temperature-independent speed v until a time τ , when they thermalize. For the dimensionless combination $z := v \tau N^{1/2} \ll 1$ rapid thermalization occurs, with consequent DLA nucleation. For $z \gg 1$ we find the novel behavior for hot-monomer aggregation (HMA): χ has, unexpectedly, the same form as for ALA. We scrutinize behavior in both limits as well as in the crossover regime $z \sim 1$, in which behavior can be described using an effective χ . At low temperatures, the behavior becomes markedly non-Arrhenius, insensitive to temperature. We conclude a discussion of more general applications of this framework.

¹T.L. Einstein, A. Pimpinelli, Diego Luis González, J. Crystal Growth (2014), <http://dx.doi.org/10.1016/j.jcrysgro.2014.01.053>.

²A. Pimpinelli, L. Tumbek, A. Winkler, J. Phys. Chem. Lett. 5 (2014) 995.

³A. Winkler, L. Tumbek, J. Phys. Chem. Lett. 4 (2013) 4080.

⁴A. Pimpinelli, J.R. Morales-Cifuentes, T.L. Einstein, preprint.

11:40am **SS+AS-WeM12 Molecular Dynamics Simulation of Ge Deposition and Islanding on Amorphous Silica Substrates**, C.Y. Chuang, University of Pennsylvania, S.M. Han, University of New Mexico, Talid Simno, University of Pennsylvania

Selective epitaxial growth (SEG) of Ge on Si substrates has proven to be a versatile pathway for producing Ge substrates to enable III-V device integration on Si. However, persistent problems remain, including dislocation formation and high stresses due to lattice parameter and thermal expansion coefficient mismatches between Si and Ge. Further optimization of the SEG process may be significantly assisted by atomistic simulation. Here, we present an atomistic analysis of Ge deposition on SiO₂. We begin by describing a validation process for a Tersoff-based model for the ternary Si-Ge-O system [1,2], in which we compare simulation predictions to detailed experimental data [3,4] for a variety of properties. Using this

validated interatomic potential, Ge deposition and islanding on an amorphous SiO₂ surface is studied with direct molecular dynamics and the results are compared to experimental measurements [4] of island size distributions as a function of deposition rate and temperature. A key aspect of our modeling approach is a procedure to accelerate the simulations. While direct molecular dynamics simulations of Ge deposition on SiO₂ are able to capture Ge island nucleation, growth and coarsening, the very fast deposition rates necessary makes difficult direct comparison to experimental measurements of island density and size distributions. In particular, we show that direct molecular dynamics simulations are able to approach, but not quite reach, the deposition conditions in experiment. The accelerated simulations are based on "equation-free" coarse projective integration [5]. Here, measures of the island size distribution dynamics are obtained from short molecular dynamics simulations and then used to evolve numerically the size distribution over large time intervals. The new island size distribution is then used to reconstruct consistent atomic configurations that are subsequently evolved further with molecular dynamics and the process is repeated. Here, we show that the reconstruction of atomic configurations from size distribution moments represents the key challenge in deposition simulations and we propose approaches for achieving this in a computationally tractable manner.

[1] J. Tersoff, *Phys. Rev. B* **39**, 5566 (1989).

[2] S. Munetoh, T. Motooka, K. Moriguchi and A. Shintani, *Comput. Mater. Sci* **39**, 334 (2007).

[3] Q. Li, J. L. Krauss, S. Hersee, and S. M. Han, *J. Phys. Chem. C* **111**, 779 (2007).

[4] D. Leonhardt and S. M. Han, *Surf. Sci.* **603**, 2624 (2009).

[5] M.E. Kavousanakis, R. Erban, A.G. Boudouvis, C.W. Gear, I.G. Kevrekidis, (2007) 382-407.

12:00pm **SS+AS-WeM13 Dimerization Induced Deprotonation of Water on RuO₂(110)**, R. Mu, D.C. Cantu, V.-A. Glezakou, Z. Wang, I. Lyubimetsky, R. Rousseau, Zdenek Dohnalek, Pacific Northwest National Laboratory

RuO₂ has proven to be indispensable as a co-catalyst in numerous systems designed for photocatalytic water splitting. Here we present a first mechanistic study of water adsorption, dissociation, and diffusion on the most stable RuO₂ surface, rutile RuO₂(110). Variable temperature scanning tunneling microscopy (STM) and ab initio molecular dynamics based density functional theory calculations (DFT) are employed to follow the behavior of small water clusters. We show that water monomers adsorb molecularly on Ru sites, become mobile above 240 K, and diffuse along the Ru rows. The monomers readily pair up and form dimers that are immobile below 273 K. Finally, the dimers deprotonate and form Ru-bound H₂O-OH and bridging OH species. This is in a sharp contrast with the molecular binding of water dimers observed on isostructural TiO₂(110). The onset for diffusion of H₂O-OH pairs on RuO₂(110) is observed at ~273 K, indicating a significantly higher diffusion barrier than that for water monomers. The experimentally determined diffusion barriers are in agreement with those obtained from the DFT calculations. The diffusion of H₂O-OH pairs is found to proceed via a rollover mechanism, with a water molecule moving over OH, followed by hydrogen transfer from H₂O to OH. At high water coverages, water dimers are found to be the building blocks of longer water chains on Ru rows. The observed behavior of water monomers and dimers is compared and contrasted with that previously reported on isostructural rutile TiO₂(110).

Thin Film

Room: 307 - Session TF+MS+PS-WeM

Applied ALD: Nanoelectronics and Emerging Applications

Moderator: Jesse Jur, North Carolina State University

8:00am **TF+MS+PS-WeM1 ALD and Beyond CMOS Materials**, Robert Wallace, University of Texas at Dallas **INVITED**

Two-dimensional layered materials, such as graphene and transition metal dichalcogenides (TMDs), have been recently proposed for a number of novel device concepts due to their interesting materials properties. For example, the possibility of low surface defect densities due to an anticipated dearth of surface defects and dangling bonds raises the prospect of improved performance for low power tunnel field effect logic devices that switch on and off very rapidly due to the anticipated steep subthreshold slope characteristic. However, for ALD processes, such surfaces present significant challenges for nucleation and growth. This talk will review our

recent work on in-situ characterization of 2D materials for such device applications. This research is supported in part by the STARNet Center for Low Energy Systems Technology, sponsored by the Semiconductor Research Corporation (SRC) and DARPA, the SWAN Center sponsored by the SRC Nanoelectronics Research Initiative and NIST, and by an IBM Faculty Award.

9:00am TF+MS+PS-WeM4 Combining Gas Phase Aerosol Deposition with Atomic Layer Deposition for Fast Thin Film Deposition: A Case Study of Transparent Conducting ZnO, Elijah Thimsen, Washington University, St. Louis, *M. Johnson, A. Wagner, A. Mkhoyan, U.R. Kortshagen, E.S. Aydil,* University of Minnesota

Atomic layer deposition (ALD) has emerged as a powerful and scalable technique for a variety of applications where layer-by-layer control over film properties and conformal deposition in tight geometries are needed. One common criticism of ALD is that it is slow and may become uneconomical when thick films and high deposition rates are needed. In fact, deposition rate is often an issue even with physical vapor deposition methods such as sputtering and also chemical vapor deposition. One way to deliver material onto a substrate at high rates is through deposition of nanoparticles. Gas phase aerosol deposition is particularly attractive because rates as high as 100 nm/s are possible even at low temperatures. However, aerosol deposition often yields porous films unsuitable for optoelectronic applications. In this talk, we describe a new two-step strategy for depositing dense thin films at high rates. Our strategy combines the high rates of aerosol deposition with advantages of ALD. In the first step nanoparticles are synthesized in the gas-phase and deposited onto suitable substrates by aerosol deposition. In the second step, the space between the nanoparticles is infilled by ALD. This is a versatile approach since there are many material options for forming both the nanoparticle network and the ALD coating. In the specific example that will be discussed in this talk, the crystalline nanoparticles are synthesized in a nonthermal plasma containing the precursors that lead to nucleation and growth of the desired material. These nanocrystals are deposited on suitable substrates through supersonic expansion and inertial impaction. Using this approach, we demonstrate fast deposition of nanocrystalline ZnO films, an earth-abundant, nontoxic, low cost material that can be used as a transparent conducting oxide (TCO), from a plasma containing Ar, O₂ and diethylzinc. The space between the particles is filled either by Al₂O₃ or Al-doped ZnO (AZO) to give continuous TCO films. After annealing in H₂ and coating with Al₂O₃, the ZnO nanocrystal network becomes conductive with Hall effect electron mobilities as high as 3.0 cm² V⁻¹ s⁻¹. Depending on the combination of the nanocrystals, ALD coating, and post processing, we have obtained transparent films with resistivity values as low as 3.8 x 10⁻³ Ohm cm. The lowest resistivity films were obtained with undoped ZnO nanoparticles coated with AZO. The resistivity can be improved by doping the nanocrystals, which has proven to be challenging. We will discuss the effects of nanocrystal size, doping of nanocrystals in the gas phase, and film porosity on electrical conductivity.

9:20am TF+MS+PS-WeM5 Detecting Order in the Molecular Layer Deposition of Polymer Films by X-Ray Diffraction, David Bergsman, R.W. Johnson, R. Britto, S.F. Bent, Stanford University

The deposition of highly ordered, thin, organic films is of great importance to a variety of fields. The development of biological sensors, organic solar cells, and optical devices relies on the ability to grow thin layers of organic material with various thicknesses, compositions, functionalities, and levels of crystallinity. One promising method of creating such films is molecular layer deposition (MLD), which uses an alternating sequence of self-saturating reactions by vapor-phase organic precursors at the substrate to grow films in a layer-by-layer fashion. This technique has been demonstrated with a variety of precursor chemistries and has been shown capable of growing films on high aspect ratio features with low surface roughness and high conformality. But despite the growing use of MLD, many questions still remain as to the orientation of the molecular chains within the deposited films and the packing of these chains. Many different factors may contribute to varying degrees of crystallinity during growth, such as chain-chain steric repulsion, Van der Waals forces, chain growth angle, and inter-chain hydrogen bonding. Here, we demonstrate that some MLD chemistries can form nanoscale organic films that exhibit well-ordered packing. Polyurea MLD films with different thicknesses and backbone chemistries were grown in an MLD reactor and then examined with x-ray diffraction (XRD) using synchrotron radiation at the Stanford Synchrotron Radiation Lightsource (SSRL). Spectroscopic ellipsometry was used to observe film thickness, while x-ray photoelectron spectroscopy and Fourier transform infrared spectroscopy monitored for film degradation. XRD results for the polyurea MLD films show peaks at q-values of 1.5/Å, corresponding to a d-spacing around 4.2 Å. Changing the precursor from a more rigid to a more flexible backbone leads to variations in d-spacing and diffraction intensity. Growth on substrates with different surface chemistries

and roughness, as well as the effect of heating and re-cooling the films, is also explored. These results suggest that thin organic films with varying levels of packing order can be grown using MLD by tuning the precursor chemistry.

9:40am TF+MS+PS-WeM6 Native Oxide Diffusion and Removal During the Atomic Layer Deposition of Ta₂O₅ on InAs(100) Surfaces, Alex Henegar, T. Gougousi, University of Maryland, Baltimore County

The use of high-κ dielectrics on III-V semiconductors in place of Si/SiO₂ structures in metal oxide semiconductor devices has been perpetually hindered by poor quality native oxides at the substrate/film interface. A promising solution for the removal of these oxides is the atomic layer deposition (ALD) growth technique which has shown the ability to remove native oxides during deposition without additional processing for certain chemistries.¹⁻⁴

In this work, Ta₂O₅ thin films were deposited on InAs(100) by ALD using pentakis dimethyl amino tantalum (PDMAT) and H₂O to study the effects of film deposition on the native oxides. 3 and 7 nm films were grown at 150-300 °C on InAs substrates covered with native oxides and substrates chemically etched in NH₄OH. Analysis of the film deposited on native oxide covered substrates by x-ray photoelectron spectroscopy (XPS) shows arsenic and indium oxides are readily removed during deposition of 3 nm Ta₂O₅ at 250 and 300 °C, temperatures very close to the optimal ALD temperature for the specific chemistry. At lower temperatures both oxides persist with indium oxides generally being harder to remove.

Depth profiling by argon-ion sputtering data of 7 nm films shows that indium oxides have diffused into the Ta₂O₅ film. The sharp decrease in oxide signal after the first sputter cycle indicates that the majority of the indium oxide is located near the surface suggesting the migration of indium oxides to the film surface during deposition. Arsenic oxides, however, are detected in smaller amounts and generally speaking remain at the interface. For depositions on etched InAs no arsenic oxides were detected but a small amount of indium oxides remain even at the optimal deposition temperatures. Films grown on etched substrates always contain less indium and arsenic oxides than their equivalents deposited on native oxide surfaces. Mixing of indium oxide in the films may have a significant negative effect on their insulating properties negating any gain from a sharper interface.

¹ P.D. Ye, G.D. Wilk, B. Yang, J. Kwo, S.N.G. Chu, S. Nakahara, H.-J.L. Gossman, J.P. Mannaerts, M. Hong, K.K. Ng, and J. Bude, Appl. Phys. Lett. **83**, 180 (2003).

² M.M. Frank, G.D. Wilk, D. Starodub, T. Gustafsson, E. Garfunkel, Y.J. Chabal, J. Grazul, and D.A. Muller, Appl. Phys. Lett. **86**, 152904 (2005).

³ M.L. Huang, Y.C. Chang, C.H. Chang, Y.J. Lee, P. Chang, J. Kwo, T.B. Wu, and M. Hong, Appl. Phys. Lett. **87**, 252104 (2005).

⁴ C.-H. Chang, Y.-K. Chiou, Y.-C. Chang, K.-Y. Lee, T.-D. Lin, T.-B. Wu, M. Hong, and J. Kwo, Appl. Phys. Lett. **89**, 242911 (2006).

11:00am TF+MS+PS-WeM10 ALD in High Aspect Ratio Structures and Nanoporous Materials, C. Detavernier, Jolien Dendooven, University of Ghent, Belgium **INVITED**

Atomic layer deposition (ALD) is known to be an excellent technique for the deposition of thin films with uniform thickness over micro- and nanoscale 3D structures. The superior conformality of ALD is a direct consequence of the self-saturating surface reaction control and makes the technique increasingly useful in the rapidly growing field of nanotechnology. The successful ALD-based processing of nanostructured materials requires however a careful optimization of the growth parameters. In this work, we present an extensive study on the conformality of ALD in high aspect ratio structures and nanoporous materials.

A first experimental approach was based on the use of macroscopic, trench-like structures in combination with low precursor pressures. In this way, the transport of the precursor molecules in the test structures was governed by molecular flow, as in microscopic trenches under standard ALD conditions. This method allowed us to quantify the conformality of the trimethylaluminum (TMA)/H₂O process as a function of the aspect ratio and the TMA exposure time. Our experimental data indicated that the sticking probability is a determining factor in the conformality of ALD [1]. A better understanding of the effect of this parameter on the conformality was obtained via kinetic modeling and Monte Carlo modeling.

As a second substrate, porous titania thin films with pore sizes in the low mesoporous regime (< 10 nm) were considered in order to get insights on the minimum pore diameter that can be achieved by ALD. Novel in situ characterization techniques were developed to monitor the pore filling by ALD. Synchrotron-based x-ray fluorescence and scattering techniques provided cycle-per-cycle information on the material uptake and densification of the porous film, while ellipsometric porosimetry was used to quantify the pore size reduction. This study nicely demonstrated the

ability of ALD to tune the diameter of nanopores down to the molecular level [2].

Finally, we performed ALD of TiO₂ into a 3D ordered silica powder with two types of mesopores [3]. By varying the Ti-precursor exposure time, we investigated the introduction of TiO₂ into the differently sized mesopores. A TEM study revealed the diffusion limited nature of the TiO₂ ALD process, leading to anisotropic penetration profiles in this specific pore structure. We observed a systematic deeper penetration of the deposition front along the main channels compared to the narrower mesopores. These results were corroborated by modeling work.

[1] J. Dendooven et al., *J. Electrochem. Soc.* 156, P63, 2009. [2] J. Dendooven et al., *Chem. Mater.* 24, 1992, 2012. [3] S. P. Sree et al., *Chem. Mater.* 24, 2775, 2012.

11:40am TF+MS+PS-WeM12 Pyrolysis of Alucone MLD Films to Form Electrically Conducting and Nanodomained Al₂O₃/C Composite Films, J.J. Travis, J.W. DuMont, Steven George, University of Colorado, Boulder

Alucone is an aluminum alkoxide polymer grown using molecular layer deposition (MLD) techniques with trimethylaluminum and organic diols or triols as the reactants. Alucone films can be pyrolyzed under inert atmosphere or vacuum to yield electrically conductive Al₂O₃/C composite films. This pyrolysis provides a pathway to deposit ultrathin, conformal and conducting Al₂O₃/C films on high surface area substrates. Our recent results have shown that the electrical conductance of the Al₂O₃/C films is dependent upon the amount of carbon in the film. The initial alucone films are non-conducting. After pyrolysis to 850°C, alucone films grown using glycerol, with three carbons, or hydroquinone, with six carbons, display high electrical conductivity of ~1-3 S/cm. In contrast, pyrolyzed alucone films grown using ethylene glycol, with only two carbons, remain non-conducting. In situ transmission Fourier transform infrared (FTIR) spectroscopy was used to monitor the pyrolysis of the alucone films. The C-H, C-O and C-C vibrational features were lost from the alucone films between 300-450°C. The vibrational spectra also showed prominent carboxylate features at 400-450°C. Carboxylate features are consistent with COO⁻ - Al³⁺ complexes at the interfaces between the Al₂O₃ and carbon regions of the composite. High resolution transmission electron microscopy (HRTEM) images are consistent with a highly interfacial nanodomained Al₂O₃/C composite. These Al₂O₃/C composite films may provide electrical conductivity and oxidation resistance during electrochemical processes on metal and carbon electrodes.

12:00pm TF+MS+PS-WeM13 Atomic Layer Deposition of Metal Oxides on Ultra-High Aspect Ratio, Vertically Aligned Carbon Nanotube Arrays, Kelly Stano, M. Carroll, R.P. Padbury, J.S. Jur, P. Bradford, North Carolina State University

Atomic layer deposition (ALD) is commonly used to coat high aspect ratio structures, including vertically aligned carbon nanotube arrays (VACNTs). Previous studies, however, have demonstrated precursor diffusion depths of only 60 µm for long exposure times, leading to a "canopy effect" where preferential coating takes place at the top of arrays. In this research we report the first example of conformal Al₂O₃ ALD on 1.5 mm tall VACNTs with uniform coating distribution from CNT base to tip. Large-scale CNT arrays with free volume aspect ratios ~15,000 were able to be uniformly coated by manipulating sample orientation and mounting techniques, as confirmed by cross-sectional energy dispersive x-ray spectroscopy. Conformal coating was achieved through modification of CNT surface chemistry via vapor phase techniques including pyrolytic carbon deposition and atmospheric pressure oxygen plasma functionalization. Thermogravimetric analysis revealed that arrays which were functionalized prior to ALD coating were more stable to thermal degradation compared to untreated, ALD coated arrays. Interestingly, CNTs could be easily removed during thermal oxidation to yield arrays of continuous, high surface area, vertically aligned Al₂O₃ nanotubes. Additionally, functionalized and ALD coated arrays exhibited compressive moduli two times greater than pristine arrays coated for the same number of cycles. Al₂O₃ coated arrays exhibited hydrophilic wetting behavior as well as foam-like recovery following compressive strain. These processing techniques have been successfully applied to other ALD precursors to yield CNT arrays uniformly coated with ZnO and TiO₂ as well.

Vacuum Technology

Room: 303 - Session VT-WeM

Accelerator and Large Vacuum Systems I

Moderator: Marcy Stutzman, Thomas Jefferson National Accelerator Facility

8:00am VT-WeM1 Vacuum Technology Developments at Daresbury Laboratory for Modern Accelerators, Keith Middleman, A.N. Hannah, J.D. Herbert, O.B. Malyshev, R. Valizadeh, STFC Daresbury Laboratory, UK

INVITED

The Vacuum Science group at the STFC Daresbury Laboratory has a unique position in that it has the capability to operate and design the vacuum systems for new accelerators whilst maintaining a very active research laboratory looking at many new facets of vacuum design for accelerators. This gives the group the opportunity to develop ideas in the laboratory before implementing them on the accelerator. This paper will present some of the latest accelerator ideas and machines at Daresbury and provide an insight into how some of our laboratory developments are helping improve the vacuum design.

A range of topics will be covered such as:

- 1) Machine developments – VELA, CLARA and ALICE
- 2) NEG coatings – a new quaternary alloy with a reduced activation temperature
- 3) Photocathode research – metal and semiconductor cathode developments
- 4) Bakeout – a new permanent thin film heater coating for in-situ bakeout
- 5) XHV – optimising the process to routinely achieve 10⁻¹² mbar
- 6) Thin films – SRF coating developments

8:40am VT-WeM3 First Year Operation of NSLS-II Vacuum Systems with Beam, Hsiao-Chaun Hseuh, W. DeBoer, S. DiStefano, C. Hetzel, S. Leng, K. Wilson, D. Ziggrosser, H. Xu, Brookhaven National Laboratory

National Synchrotron Light Source II is a new synchrotron radiation facility, consisting of a 200-MeV Linac, a 3-GeV Booster and a 3-GeV storage ring. The Linac and the Booster were completed and commissioned in 2012 and 2013, respectively. The 792m storage ring was completed in January. Commissioning with electron beam is underway in the last few months. The performance of these ultrahigh vacuum systems with intense electron and X-ray beams will be described. The reliability and usefulness of over 1500 vacuum pumps and instruments will be summarized. Experience with NEG coated narrow gap chambers, in-vacuum undulators and superconducting cavity will also be presented.

*Work performed under the auspices of U.S. Department of Energy, under contract DE-AC02-98CH10886.

9:00am VT-WeM4 APS-Upgrade Storage Ring Vacuum System Conceptual Design, Herman Cease, B. Stillwell, B. Brajuskovic, J. Nudell, J. Carter, Argonne National Laboratory

A conceptual design is being developed for a storage ring vacuum system at the Advanced Photon Source (APS) which is compatible with a seven-bend achromat lattice under consideration by the APS Upgrade (APS-U) project. The required proximity of the magnet poles to the beam, quantity and stability of beam position monitors, synchrotron radiation loading, beam physics considerations, and installation duration place a challenging set of constraints on the vacuum system design. These requirements can be satisfied with a hybrid system which combines NEG-coated copper chambers with conventional extruded aluminum chambers housing mechanically-mounted NEG strips and discrete absorbers. The hybrid design, expected outgassing and thermal loads, and preliminary vacuum pressure analysis is described.

9:20am VT-WeM5 APS-Upgrade Vacuum System Pressure Using a 3-D Simulation Tool, Jason Carter, H. Cease, Argonne National Laboratory

A conceptual design is being developed for a storage ring vacuum system at the Advanced Photon Source (APS) which is compatible with a seven-bend achromat lattice under consideration by the APS Upgrade (APS-U) project. The design features a hybrid vacuum system to address outgassing and thermal loads which will combine discrete pumping, NEG-coated copper chambers, and NEG strip pumping in conventional extruded aluminum chambers. A preliminary 3D vacuum pressure analysis is described which uses the SynRad/MolFlow+ 3D vacuum analysis package developed at CERN to determine if the system can meet pressure requirements. The analysis uses the software package to predict photon stimulated desorption loads and then determine the resulting vacuum system pressure.

9:40am **VT-WeM6 For Some Results Solving Key Issues of Vacuum Systems in Electron Storage Rings, Hiroshi Saeki**, Japan Synchrotron Radiation Research Institute, Japan, *T. Momose*, Emeritus Professor of Miyagi National College of Technology, Japan

From 1980's to 2000's in Japan, electron storage rings had some key issues of their vacuum systems. To overcome two key issues especially, we observed dust trapping phenomena as a key issue, using lead-glass counters at first.^{1,2} Dust particles collected in beam ducts were analyzed³ and simulation experiments to trap dust particles were carried out using these collected dust particles.^{2,4,5} As the results, the mechanism of the phenomena was found clearly and we knew how to prevent these phenomena occurring.^{6,7} We review and discuss the phenomena using published and unpublished data.

As the other key issue, it was that ionization gauges misread due to radiation-induced currents.⁸ A hot-cathode-ionization gauge with correcting electrode was developed and tested in simulation experiments^{9,10,11} and in actual radiation environments.^{12,13} The pressure-measurement error of the developed vacuum gauge was about 20%. We also review and discuss the vacuum gauge and other devices¹⁴ to overcome other issues using latest data.

References

- ¹Hiroshi Saeki, Takashi Momose, and Hajime Ishimaru, *Rev. Sci. Instrum.* 62(4), 874 (1991).
- ²Hiroshi Saeki, Takashi Momose, and Hajime Ishimaru, *Rev. Sci. Instrum.* 62(11), 2558 (1991).
- ³TAKASHI MOMOSE, HIROSHI SAEKI, and HAJIME ISHIMARU, *VACUUM* 43(3), 189 (1992).
- ⁴Hiroshi Saeki, Takashi Momose, and Hajime Ishimaru, *Rev. Sci. Instrum.* 62(11), 2568 (1991).
- ⁵Hiroshi Saeki, Takashi Momose, and Hajime Ishimaru, *Rev. Sci. Instrum.* 65(11), 3479 (1994).
- ⁶Hiroshi Saeki, Takashi Momose, and Hajime Ishimaru, *Rev. Sci. Instrum.* 67(4), 1475 (1996).
- ⁷Hiroshi Saeki, Takashi Momose, *J. Vac. Sci. Technol. A* 18(2), 492 (2000).
- ⁸Hiroshi saeki, Takashi Momose, *J. Vac. Sci. Technol. A* 18(1), 244 (2000).
- ⁹Hiroshi Saeki, Tamotsu Magome, and Tsuyoshi Aoki, Nobuaki Gotoh, Takashi Momose, *Rev. Sci. Instrum.* 75(12), 5152 (2004).
- ¹⁰Hiroshi Saeki, and Tamotsu Magome, *Rev. Sci. Instrum.* 79(5), 055102-1 (2008).
- ¹¹Hiroshi Saeki, and Tamotsu Magome, *J. Vac. Sci. Technol. A* 29(6), 061601-1 (2011).
- ¹²Tamotsu Magome, and Hiroshi Saeki, *J. Vac. Sci. Technol. A* 23(4), 725 (2005).
- ¹³Hiroshi Saeki, and Tamotsu Magome, Yoshihiko Shoji, *J. Vac. Sci. Technol. A* 24(4), 1148 (2006).
- ¹⁴For example, Hiroshi Saeki, Hiroyasu Ego, Takahiro Watanabe, Katsuya Ishibashi, Takafumi Satoh, Kazuo Miyamoto, *Vacuum* 85(10), 975 (2011).

11:00am **VT-WeM10 Progress in Thin Film Technology for Superconducting RF Applications, Anne-Marie Valente-Feliciano**, Thomas Jefferson National Accelerator Facility **INVITED**

Bulk Nb has so far been the material of choice for Superconducting RF (SRF) applications. With RF cavity performance approaching the theoretical limit for bulk niobium, alternative routes for the future of superconducting structures used in accelerators are explored. Over the years, Nb/Cu technology has positioned itself as an alternative route for the future of superconducting structures used in accelerators, but has suffered shortcomings due to the commonly used magnetron sputtering. The recent developments in ionized PVD coating techniques (i.e. vacuum deposition techniques using energetic ions) such as Electron Cyclotron Resonance (ECR) and High Power Impulse Magnetron Sputtering (HiPIMS) are opening avenues for the production of thin films tailored for SRF applications based on Nb and alternative materials.

This contribution reports the on-going efforts pursued at Jefferson Lab and in different institutions to exploit the potential of novel film technologies to produce bulk-like Nb films and go beyond Nb performance with the development of film systems, based on other superconducting materials and multilayer structures.

11:40am **VT-WeM12 Modeling and Measurement of a Tesla-like Cage Cavity, John Noonan, M.J. Virgo, T.L. Smith**, Argonne National Laboratory

The cage cavity is an RF cavity fabricated by forming tubes to follow the surface contour of a cavity design, e.g. a TESLA cavity, and assembling the

tubes to form a closed cavity. Computer simulations demonstrated that the cage cavity had the potential to be a cost effective alternative to solid wall cavities. However, early RF spectrum measurements did not agree with the simulations. The cage cavity can approach RF properties of a solid wall cavity by using a coupled cavity design: The cage cavity is mounted in a large RF cavity in which this cavity's Eigen frequencies are decoupled from the cage cavity's Eigen frequencies. Computer models of the coupled cavity system will be presented to show that the quality factor of the cage cavity can be ~90% of the Q for a solid wall, superconducting cavity. The simulations also demonstrate several advantages of the cage cavity over a solid wall cavity, i.e. high order harmonic suppression, power coupling, and tuning. A prototype coupled cavity system has been fabricated and measurements of a cage cavity in a coupled cavity will be presented.

12:00pm **VT-WeM13 e-Cloud Activity of DLC Coated Chamber at FNAL Main Injector, Shigeki Kato**, KEK-High Energy Accelerator Research Organization, Japan, *J. Eldred*, Indiana University, *C.Y. Tan, M. Backfish, B. Zwaska*, FNAL

Carbon material that has a low mass density (resulting a long electron penetration depth in bulk), a low δ_{\max} and a low secondary electron yield is of good option to mitigate electron cloud activity in particle beam chambers. In addition to this, diamond-like-carbon (DLC) coating on beam chambers would give advantages of a large deposition rate (a couple of $\mu\text{m/h}$), inexpensiveness (~US\$800.- /m for coating of 100m), a good uniformity ($\pm 5\%$) and coating applicability on any type of beam chamber (even bent one) and on any material without requirement of magnetic field. A DLC coated stainless steel chamber and a reference stainless chamber were installed into the FNAL main injector simultaneously in order to investigate e-cloud activity in the chambers with three retarding field analyzers (RFAs). Preliminary results at the low beam intensity showed RFA signals in the DLC coated chamber showed only 1/100 of that in the steel chamber. The e-cloud activity at the higher beam intensity and comparison of e-cloud activity at usually prepared surface (smooth surface) with roughed surface to aim further reduction of the activity will be also reported in the presentation.

Wednesday Lunch, November 12, 2014

Exhibitor Technology Spotlight

Room: Hall ABC - Session EW-WeL

Exhibitor Technology Spotlight Session

Moderator: Chris Moffitt, Kratos Analytical Limited, UK

12:40pm **EW-WeL2 An Auger Electron Analyzer System for *In Situ* Growth Monitoring.** *W.Laws Calley III, P.G. Staib*, Staib Instruments, Inc.

The Auger Probe is a specially designed electron analyzer engineered for in situ growth monitoring [1]. To avoid shadowing a growing surface, the Probe is designed to operate at extended working distances (tested between 50mm to 82mm) with a tapered, small diameter tip. The Probe can utilize a grazing incidence RHEED gun or a near normal incidence electron gun. Figure 1 shows a typical Probe configuration in an MBE system.

AES is a surface sensitive technique capable of detecting nearly all elements. The Probe has detected low-Z elements like Li, figure 2, as well as high-Z elements like Dy [2], figure 3, during real time deposition of the respective element.

The Probe has been implemented in a wide variety of growths environments, from more traditional MBE III-V growths, to III-Nitrides and Oxides, figure 4, as-well-as metal alloy growths.

The Probe has proven reliable in all the tested growth environments, including systems with Li, O, Cl, Ga, As, and Sb. It has not failed in any tested growth environment after hundred of hours of exposure during growth. It has not been shown to interfere with any growth process that it has been operated.

The Probe is easy to operate, requiring simplified alignment when compared to traditional AES. Coupled with automated data acquisition software, it is easy to implement in real time growth monitoring.

The Probe has been used to detect and identify several contaminants in growth environments including. C, O, and Cl. It has also been used to monitor the oxide removal from substrates prior to growth.

The Probe has been used to monitor the growing surfaces in all of the previously mentioned growth environments. This real time monitoring of growing films allows the user to construct an AES growth profile of the grown film.

The Probe provides real time N(E) auger spectra enabling quantification of the Auger data. This allows the user to track the elemental concentration throughout the growth.

The Probe has been used in a wide variety of growths environments. The Probe has not failed in any of the environments in which it has been installed. The Probe can detect elements as light as Li to heavy elements through the Lanthanide system. In addition to AES, the analyzer provides REELS spectra of the distribution of characteristic energy losses [3]. Due to its robust and unique design, the Probe can be used in a variety of growth environments to provide real time elemental analysis during growth.

[1] P. G. Staib, J. Vac. Sci. Technol. B 29, (2011).

[2] W. Laws Calley, et al., J. Vac. Sci. Technol. B 31, (2013).

[3] P. G. Staib, at this conference. Abstract #5115

1:00pm **EW-WeL3 Safe and Efficient - Dry Bed Exhaust Gas Abatement of Toxic Gases I.** *Sam Yee*, CS Clean Systems Inc.

The NOVAPURE® series offers a safe, efficient and reliable solution for treatment of hazardous process gases and by-products.

This unique system uses chemisorptive granulate technology to treat process gases in a negative pressure environment ensuring only inbound flows. Continuous gas monitoring assures total point-of-use gas treatment below TLV levels. In the event of a power outage, the NOVAPURE system will continue to treat the inflows.

The built-in 90% depletion feature provides warning of breakthrough when the granulate is 90% consumed. The remaining capacity allows the current process to run-to-finish and time to schedule a shutdown for canister replacement.

Chemisorptive technology provides irreversible reactions with process gases and their byproducts, forming non-volatile solids. The spent canister can be easily and safely disposed of or incinerated. Air pollution regulations, employee health concerns, and growing awareness of toxic agents from semiconductor processes demand increased improvements in exhaust gas conditioning.

The NOVAPURE® Dry Scrubber reduces the hazards associated with flammable, toxic or corrosive gases and vapors.

NOVAPURE® effluent gas scrubbers offer an extremely safe and efficient way to treat toxic and corrosive gases resulting from hazard processes. This scrubber is a technologically advanced dry chemical scrubber containing approximately 32 or 37 gallons of scrubbing media. The scrubber is suitable for use in production and general laboratory environments. Operating passively at ambient temperature, chemical resins in the canister react on contact with process gases and by-products, converting them to non-volatile inorganic solids.

Applications include: Ion Implant, Etch, ALD, CVD, III-V, and MOCVD. Flow limit is 240slpm. The unit is equipped with built in bypass, end point detector.

1:20pm **EW-WeL4 The Workstation For Your 2D Characterization Needs - The First Low Temperature MultiProbe SPM-NSOM System Integrated with Raman.** *David Lewis*, Nanonics Imaging Ltd.

The Nanonics CryoView MP is the ideal SPM platform for studying mechanical, optical, and electrical nanoscale properties of 2D materials at low temperature. Materials such as graphene, hexagonal boron nitride (h-BN), dichalcogenides (e.g.) MoS₂, etc. The CryoView MP is uniquely suited to conduct studies in dynamics, photoconductivity, electrical conductivity, and other phenomenon of such materials. Very sensitive and stable tip- sample interaction control through the tuning fork feedback mechanism allows for high resolution SPM measurements. The open optical access allows for a variety of optical integrations including near-field, Raman, TERS and fluorescence measurements. Multiple probes allows for a variety of electrical measurements including MFM, EFM, KPM and thermal measurements. The CryoView MP opens up many new possibilities for exciting research in your 2D materials.

1:40pm **EW-WeL5 Trends and Solutions of Control Electronics for Surface Analysis and Science.** *Jacek Latkowski*, PREVAC sp. z o. o.

Any electronics, magnetic and electrostatic field distortions give rise to unwanted effects, especially in sensitive electron microscopy measurement techniques such as XPS and UPS. The electronics utilised in these techniques require special consideration in order to minimise the influence of such distortions. We will describe, based on practical experience, how important these considerations are.

Wednesday Afternoon, November 12, 2014

2D Materials Focus Topic

Room: 310 - Session 2D+AS+EM+MI+MN+NS+TF-WeA

Properties of 2D Materials

Moderator: Guy Le Lay, Aix-Marseille University

2:20pm **2D+AS+EM+MI+MN+NS+TF-WeA1 Tuning Excitons in Two-Dimensional Semiconductors**, Kirill Bolotin, Vanderbilt University
INVITED

Monolayer molybdenum disulfide (MoS₂) is a two-dimensional crystal comprising a single layer of molybdenum atoms sandwiched between two layers of sulfur atoms. Monolayer MoS₂ differs from its celebrated all-carbon cousin, graphene, by the presence of a direct band gap leading to robust light absorption and by strong electron-electron interactions leading to formation of rightly bound excitons. In this talk, we demonstrate that both electrical and optical properties of MoS₂ can be widely tuned via external influences.

In the first part of the talk, we study changes in the bandgap and phonon spectra in strained MoS₂. We investigate the transition from direct to indirect band gap in MoS₂ under uniaxial strain. The experimental signatures of this transition include strain-induced changes in the PL wavelength and intensity.

Second, we examine the influence of the environment of MoS₂ on its properties. We demonstrate substrate-induced scattering is suppressed in suspended MoS₂ specimens. We use photocurrent spectroscopy to study excitons in pristine suspended MoS₂. We observe band-edge and van Hove singularity excitons and estimate their binding energy. We study dissociation of these excitons and uncover the mechanism of their contribution to photoresponse of MoS₂.

3:00pm **2D+AS+EM+MI+MN+NS+TF-WeA3 Electron-Phonon Coupling and Photoluminescence in Single Layer Transition Metal Dichalcogenides**, Neha Nayyar, V. Turkowski, D.T. Le, T.S. Rahman, University of Central Florida

Single layer MoS₂ and other transition metal dichalcogenides have been the subject of numerous investigations because of their unusual optical, electronic and transport properties. To understand and thereby tune their photoluminescent properties, we have analyzed the role of electron-phonon interactions. Density functional perturbation theory is used to calculate the dispersion of system phonons, while electron-phonon coupling is obtained using the Eliashberg approach. Time-dependent density-functional theory based calculations using the density-matrix approach is employed to study the exciton and trion excitations which are found to appear as peaks in the absorption spectrum in the visible range with binding energy ~0.5 – 1 eV and ~0.02-0.03 eV, correspondingly. The emission peak is found to also lie in the visible spectrum and is sensitive to the value of the electron-phonon coupling, which depends on the nature and extent of doping. The position of the spectral peaks may thus be manipulated by doping. Calculations of the self-energy and spectral functions of doped systems show excitations to have 10-100 fs lifetime, which makes the system interesting for ultrafast applications. Comparison will be made of these optical properties of several single layer dichalcogenides and contact will be made with available experimental data. Work supported in part by DOE Grant No. DOE-DE-FG02-07ER46354

3:20pm **2D+AS+EM+MI+MN+NS+TF-WeA4 Temperature Dependent Photoluminescent Spectroscopy of MoS₂**, Michael Watson, J.R. Simpson, Towson University & NIST, R. Yan, H. Xing, University of Notre Dame, S. Bertolazzi, J. Brivio, A. Kis, EPFL, Switzerland, A.R. Hight-Walker, NIST

We report temperature and power dependent photoluminescence (PL) of molybdenum disulfide (MoS₂). Mechanical exfoliation of MoS₂, from bulk provides single-layer flakes which are then transferred either to sapphire substrates or suspended over holes in Si/Si₃N₄. We measure temperature dependence from ~100K to 400K and power dependence from ~6μW to ~7mW using an Argon laser at 514.5nm and a HeNe laser at 632.8 nm. The PL spectrum exhibits a main excitonic peak(A) at ~1.87eV which consist of both neutral excitons and charged trions (A- or A+) [1]. The A exciton peak and the A- exciton peak redshift and broaden with increasing temperature and power. Along with the A peak, we observe a lower energy bound exciton (BE) that is likely related to defects. The BE, a broad peak centred at ~1.7eV, linearly redshifts and narrows with increasing power. The power dependence of both the main and bound peak saturates above 0.5mW. Raman temperature and power dependence will also be discussed [2].

[1] K.F. Mak et al. Nat. Mat 12,207(2013)

[2] R.Yan and J.R.Simpson, S. Bertolazzi and J. Brivio, M. Watson, X.Wu and A. Kis, T.Luo, H.G.Xing, A.R. Hight Walker, ACS Nano 8,1 (2013)

4:20pm **2D+AS+EM+MI+MN+NS+TF-WeA7 Effects of Dimensionality on the Raman and Photoluminescence Spectra of and TaSe₂ and TaS₂ Dichalcogenides**, Danilo Romero, University of Maryland, College Park, M. Watson, J.R. Simpson, Towson University, H. Berger, Ecole Polytechnique Federale de Lausanne, Switzerland, A.R. Hight Walker, NIST

We investigate the effects dimensionality on the electronic properties through the optical spectra of the transition-metal dichalcogenides 2H-TaSe₂ and 1T-TaSe₂, and 1T-TaS₂. In bulk, these materials exhibit electronic states from Mott insulator, commensurate and incommensurate charge-density phases, and superconducting ground state as function of temperature. We explore the evolution of these properties as the materials approach a few layers, achieved via mechanical exfoliation of bulk single-crystals. Raman and photoluminescence spectroscopy of 2H-TaSe₂ and 1T-TaSe₂, and 1T-TaS₂, carried out over a wide-range of temperature, were used as a probe of the change of the electronic properties from the bulk to single-layer phases of the materials. Comparison of the phonon and excitonic transitions as a function of temperature and dimensionality will be presented.

4:40pm **2D+AS+EM+MI+MN+NS+TF-WeA8 Few-Layer and Symmetry-Breaking Effects on the Electrical Properties of Ordered CF₃Cl Phases on Graphene**, Josue Morales-Cifuentes, T.L. Einstein, Y. Wang, J. Reutt-Robey, University of Maryland, College Park

An effective potential mechanism for breaking the inherent sublattice symmetry of graphene has been studied using DFT calculations on hexagonal boron nitride.¹ Electrical detection of CF₃Cl phase transitions on graphene shows the existence of a commensurate ordered phase in which this can be tested.² We study the electronic properties of similar phases varying coverage and orientation of CF₃Cl with respect of the graphene substrate using VASP ver 5.3.3, with ab initio van der Waals density functionals (vdW-DF1, vdW-DF2).^{3,4} Consistent with a physisorbed phase, binding energies are calculated to be on the order of 280meV, and insensitive to coverage and orientation of the CF₃Cl molecules. Charge transfer was calculated to be sensitive with coverage, but not orientation, which is qualitatively consistent with experiment. For low coverages, sublattice symmetry breaking effects are responsible for gap openings in the order of 4meV, whereas for large coverages it is the formation of ordered overlayers that opens gaps of 15meV. Furthermore, in bilayer graphene at low coverage we estimate an enhanced gap of 20meV.

[1] Gianluca Giovannetti et al. , PRB **76**, 073103(2007)

[2] Yilin Wang et al. , APL **103**, 201606 (2013)

[3] Jiri Klimes et al. , PRB **83**, 195131 (2011)

[4] Kyuho Lee et al. , PRB **82**, 081101(R) (2010)

5:00pm **2D+AS+EM+MI+MN+NS+TF-WeA9 Optical Anisotropies in Layered Nanomaterials**, Jon Schuller, UC Santa Barbara
INVITED

In nanomaterials optical anisotropies reveal a fundamental relationship between structural and optical properties. In layered materials, optical anisotropies may result from in-plane and out-of-plane dipoles associated with intra- and inter-layer excitations respectively. In this talk, I describe a novel method wherein we resolve the orientation of luminescent excitons and isolate photoluminescence signatures from distinct intra- and inter-layer excitations, respectively. We compare photoluminescence anisotropies in materials with weak or strong interlayer coupling, MoS₂ and the organic semiconductor PTCDA respectively. We demonstrate that photoluminescence from MoS₂ mono-, bi- and trilayers originates solely from in-plane excitons, whereas PTCDA supports distinct in-plane and out-of-plane exciton species with different spectra, dipole strengths and temporal dynamics. The insights provided by this work are important for understanding fundamental excitonic properties in layered nanomaterials and designing optical systems that efficiently excite and collect light from exciton species with different orientations.

5:40pm **2D+AS+EM+MI+MN+NS+TF-WeA11 Mechanical Properties of 2D-Materials**, J.M. Gonzales, University of South Florida, R. Perriot, Los Alamos National Laboratory, Ivan Oleynik, University of South Florida

Graphene and other two-dimensional (2D) materials possess extraordinary mechanical properties, which are currently being explored in various novel applications. Atomic force microscopy (AFM) nanoindentation experiments

on both pristine and polycrystalline samples of 2D materials, while being successful in measuring overall mechanical performance of graphene, require some theoretical input to extract the important mechanical properties. Large-scale atomistic molecular dynamics simulations are used to predict the mechanical properties of 2D materials, such as the elastic moduli, breaking strength, stress/strain distributions, and mechanisms of fracture under conditions of AFM nanoindentation experiments. Perfect, defective, and polycrystalline samples are investigated using large-scale molecular dynamics simulations with a screened environment-dependent bond order (SED-REBO) potential. The mechanisms of crack propagation in both perfect and defective samples will also be presented.

6:00pm 2D+AS+EM+MI+MN+NS+TF-WeA12 Mechanical Control of Structural Phase Transitions in Two-Dimensional Mo- and W-Dichalcogenide Monolayers, Evan Reed, K.-A.N. Duerloo, Y. Li, Stanford University

Mo- and W- dichalcogenide compounds have a two-dimensional monolayer form that differs from graphene in an important respect: it can potentially have more than one crystal structure. Some of these monolayers exhibit tantalizing hints of a poorly understood structural metal-to-insulator transition with the possibility of long metastable lifetimes. If controllable, such a transition could bring an exciting new application space to monolayer materials beyond graphene. Here we discover that mechanical deformations provide a route to switching the thermodynamic stability between a semiconducting and a metallic crystal structure in these monolayer materials. We employ density functional and hybrid Hartree-Fock/density functional calculations including vibrational energy corrections to discover that single layer MoTe₂ is an excellent candidate phase change material. We identify a range from 0.3% to 3% for the tensile strains required to transform MoTe₂ under uniaxial conditions at room temperature. We elucidate the appropriate thermodynamic constraints for monolayers, which can differ from bulk materials. The potential for mechanical phase transitions is predicted for all six studied compounds. The potential application space ranges from catalysis to information storage and nanoscale electronics.

Applied Surface Science

Room: 316 - Session AS+BI+MC-WeA

Practical Surface Analysis I

Moderator: Alexander Shard, National Physical Laboratory, Christopher Szakal, National Institute of Standards and Technology (NIST)

2:20pm AS+BI+MC-WeA1 The Application of XPS to Study Corroded Stainless Steel Surfaces, Helen Brannon, S.J. Coultas, J.D.P. Counsell, S.J. Hutton, A.J. Roberts, C.J. Blomfield, Kratos Analytical Limited, UK, J. Morrison, The University of Birmingham, UK

The corrosion of structural materials in contact with hot, pressurised water, which is heavily dependent on the condition of the exposed surface, is a common problem in nuclear power processes. This side reaction is undesirable due to the reduced heat transfer efficiency which is caused by the deposited oxide layers.

X-ray photoelectron spectroscopy (XPS) is demonstrated as a quantitative surface analysis technique which can be used to determine the type of corrosion chemistry that occurs.

Stainless steel (316L) substrates containing 70% Fe, 18% Cr, 8% Ni and 2% Mo (as well as a low concentration of impurities) are suspended in water at 300 °C for 1000 hours. A metal oxide double layer is found to develop over time on the stainless steel surface: the top layer is a mix of magnetite (Fe₃O₄) and Nickel Ferrite (NiFe₂O₄) and the bottom layer is a mix of magnetite and chromite (FeCr₂O₄) (below is the base metal).

A high energy, medium sized argon gas cluster source is shown to be advantageous compared to a conventional monatomic argon ion source when depth profiling such layered structures, causing reduced structural and chemical damage from the ion beam sputtering process.

Data acquisition at small analysis areas gives well resolved spectra, revealing the multi-layered oxide structures produced from the corrosion process.

[1] Depth profiling of the Passive Layer on Stainless Steel using Photoelectron Spectroscopy, Wendy Fredriksson, Uppsala University

[2] Applied Surface Science, 257, (2011), 2717–2730

[3] The Radiochemistry of Nuclear Power Plants with Light Water Reactors, By Kark-Heinz Neeb

2:40pm AS+BI+MC-WeA2 Molecular Characterization of Lubricant Degradation Produced in a Tribological Wear Test Using TOF-SIMS and Scanned Microprobe XPS Imaging, Gregory Fisher, S.S. Alnabulsi, Physical Electronics Inc., T. Le Monge, Ecole Centrale de Lyon - LTDS, France, J.S. Hammond, Physical Electronics Inc.

Scanning Auger microscopy (SAM) and x-ray photoelectron spectroscopy (XPS) are today the most widely used surface analysis techniques for quantitative elemental and chemical analysis in tribology. Modern SAM instrumentation allows the elemental and chemical analysis of features at spatial resolutions down to 10 nm while modern scanning x-ray microprobe XPS instrumentation can provide even more complex chemical state surface characterization at a sub-10 μm spatial resolution. The use of a scanned x-ray microprobe enables chemical state imaging at a low x-ray fluence to minimize disturbance of the surface chemistry. Notwithstanding the aforesaid capabilities, the elucidation of molecular chemistry and lubricant degradation that occurs via tribological wear remains intractable by SAM and XPS analysis alone.

This study focuses on the application of time-of-flight SIMS (TOF-SIMS), with supporting XPS analysis for quantification, to determine the molecular decomposition and metal-organic reaction products of lubricants used in bio-diesel fuel. The test specimens were produced on a reciprocating cylinder-on-flat tribometer to simulate the piston / cylinder contact geometry and dynamics that are typical of internal combustion engines. The lubricant used in the bio-diesel fuel consists of C₁₈ fatty acids at a concentration in the high part-per-million (ppm) range. The TRIFT mass spectrometer of the PHI nanoTOF provides an advantage for this study in that the wear track topography is effectively decoupled from the molecular characterization and imaging. The HR² imaging mode of the PHI nanoTOF, simultaneously achieving a spatial resolution < 400 nm and a mass resolution of ≈ 10,000 m/Δm, is an important asset in molecular identification and imaging.

3:00pm AS+BI+MC-WeA3 Surfaces and Interfaces of Real-World Products: What Do We Really Need to Know and What Are The Best Ways to Find Out?, Anna Belu, L. LaGoo, W. Theilacker, Medtronic, Inc. INVITED

Real world components and products come in many shapes, sizes and materials, and their surface properties are critical for performance in many areas including adhesion, biocompatibility, corrosion, lubricity, and welding. Surface analysis tools are often employed to gain a fundamental understanding of surface properties of products in development, as well as to evaluate properties of surfaces and interfaces of products that are not performing as specified. This presentation will discuss best practices for analysis of real world samples in an industrial, mainly R&D, environment.

The culture of industry is typically fast paced with the goal being to get product into the hands of consumers as soon as possible. In this environment, the surface analyst is faced with the challenge of providing high quality information from a variety of materials and issues in a short amount of time. The requestor often wants a simple answer and is unaware that the analyst progresses through a series of questions such as What is the issue? What are the best tools to find the answer to the issue? Are the tools up to the task? Is the lab up to the task? What types of results are necessary? What types of samples are helpful? What is the most efficient way to obtain the data? Is it OK to use one tool and analyze one point on one sample? What are efficient ways to analyze data? Do the results solve the problem? This presentation will discuss the consideration that goes into providing high quality data in a short amount of time and include several examples of surface analysis from real world products.

4:20pm AS+BI+MC-WeA7 Forensic XPS Surface Characterization of Cosmetic Trace Evidence, Brian Strohmeier, Thermo Fisher Scientific, R. Blackledge, Independent Consultant

X-ray photoelectron spectroscopy (XPS) has a long distinguished history of providing important information on the surface chemistry of a wide variety of materials including: catalysts, ceramics, coatings, fibers, glass, metals, oxides, polymers, powders, semiconductors, thin films, and many others. In addition, studies involving the use of XPS have addressed numerous complex materials problems in a multitude of diverse fields such as: adhesion science, chemical surface treatments, corrosion, electronics, medical devices, oxidation, solar cells, and so on. Despite its many advantages and unique capabilities as a surface analytical technique, XPS has not been widely used in forensic science for the examination of specimens gathered at the scene of a crime. The main reasons for the lack of forensic studies involving XPS are: 1) the lack of standard forensic XPS methods and standard samples for comparison to real world samples; and 2) the historical long analysis times (hours per sample) and large analysis areas (several square millimeters) compared to other common forensic techniques such as Raman microscopy and scanning electron microscopy combined with energy dispersive X-ray spectroscopy (SEM/EDS). Advances in XPS

instrumentation over the last decade have now improved analysis times to minutes per sample and analysis areas down to the range of tens to hundreds of micrometers. Also, recently developed argon cluster ion sources now allow "soft" depth profiling of organic and polymeric species with minimal ion beam damage, thus preserving the chemical state information available from XPS. XPS, therefore, has increased potential for new forensic science applications involving the surface characterization of trace evidence materials. Previous work has demonstrated the potential of XPS for revealing unique surface chemical information for gunshot residue (GSR) and textile fibers. This presentation will describe the use of XPS for forensic characterization of cosmetic materials such as hair chalks, shimmer, and glitter. These types of cosmetic materials have a high probability of transfer and retention if a victim struggles with an assailant during an abduction or sexual assault and could help support an association between an assailant, a victim, and a specific crime scene in a specific case circumstance. XPS is an excellent technique for characterizing residues of these cosmetic materials.

4:40pm **AS+BI+MC-WeA8 Industrial Applications of Surface Analysis**, *William Stickle, M.D. Johnson, G.A. DeHaan, J.A. Burgess*, Hewlett Packard

Using surface analysis has been a mainstay of industrial research and corporate analytical labs for more than thirty years. The applications of surface chemical analysis in an industrial setting range from the investigation of the composition and chemistry of buried interfaces of single molecule memory devices created in the R&D lab to the routine analysis of plasma treated polymer surfaces on the production line. Some analyses are performed to provide a 'yes' or 'no' answer to question such as 'Has the oxide been removed?' or 'Was the surface plasma treated?'. Other analyses are much more complicated and often require the application and correlation of several analytical methods. This correlation between techniques often occurs in the characterization of, for example, fab processes where a process may be characterized by x-ray photoelectron spectroscopy to understand the chemistry; but then the analysis needs to correlate to the information obtained by Auger electron spectroscopy or ToF SIMS which are the techniques of choice when the process is scaled to dimensions where XPS is not practical. Further, simple data processing, such as calculating atomic concentrations, is often not the end of the analytical story. Examples of using numerical methods such as linear least squares fitting or the application of Tougaard backgrounds to clarify an analysis will also be discussed. More detailed analyses can also be achieved by applying modeling methods such as SESSA or using simple overlayer models to describe a material. This presentation will cover these different aspects of surface chemical analysis in an industrial laboratory with practical examples of using XPS, AES and ToF SIMS for process characterization, materials development and failure analysis.

5:00pm **AS+BI+MC-WeA9 Peter Sherwood Mid-Career Award Talk: Chemical Analysis of Cells and Tissues with Imaging ToF-SIMS**, *Lara J. Gamble, B. Bluestein, D. Graham*, University of Washington **INVITED**

The ability to image cells and tissues with chemical and molecular specificity could revolutionize our understanding of biological processes. It would increase our understanding of chemical changes in cells and tissues as a function of an applied stress or as a result of disease, and enable tracking the spatial distribution of metabolites and lipids. Chemistry of tumor microenvironments, lipid metabolomics relationship to cancer, delivery of nanoparticles to cells, and tissue repair could be visualized on a cellular and sub-cellular level. The sub-cellular resolution mass spectral imaging capability of ToF-SIMS holds the potential to achieve this possibility. ToF-SIMS analysis of biological samples from 2D images of tissue biopsies to 3D images of nanoparticles in cells will be presented including multivariate analysis of the ToF-SIMS image data. The ToF-SIMS images are also combined with optical images of the same samples (same slices and serial biopsy slices). This combination of images allows researchers to visualize a molecular map that correlates with specific biological features or functions. The potential to combine the ToF-SIMS images with other techniques will also be discussed.

5:40pm **AS+BI+MC-WeA11 Characterization Strategies for the Detection of Carbon Nanotubes within an Epoxy Matrix**, *Justin Gorham, J. Woodcock, W.A. Osborn, J. Heddleston, K. Scott*, National Institute of Standards and Technology (NIST)

Carbon nanotubes (CNT) have been widely incorporated into composite systems due to the enhanced properties that they add to new and existing products, especially with respect to mechanical strength. X-ray photoelectron spectroscopy (XPS), in conjunction with SEM and Raman spectroscopy, has been employed in efforts to characterize several CNT: epoxy composite systems. This characterization approach was applied to composite systems with (1, 4 and 5) CNT weight percentages. Additionally, imaging XPS results will be presented to provide further insight into the

dispersion quality on the micron scale. Challenges associated with overlapping spectral features, charging and a variety of other considerations regarding the surface and the bulk of the sample will be discussed.

6:00pm **AS+BI+MC-WeA12 Measuring Schmutz: Accounting for Adventitious Carbon Contamination in X-ray Absorption Spectra of Carbon-Based Materials**, *Filippo Mangolini, J.B. McClimon, J. Hilbert, R.W. Carpick*, University of Pennsylvania

Near-edge X-ray absorption fine structure (NEXAFS) spectroscopy is one of the most powerful weapons in the surface-analysis arsenal, since it provides insights into the local ordering, bonding configuration, oxidation state, and hybridization of the elements present in the near-surface region (information depth: ~5 nm). NEXAFS analyses are commonly performed under the assumption of chemical and structural homogeneity within the nanometer-depth scale probed. Unfortunately, this does not hold for the vast majority of solid surfaces due to the presence of complex surface and near-surface structures (e.g., natural oxides, contamination) and can lead to large errors when analyzing elements that are simultaneously present in multiple layers. This is particularly challenging for carbon-containing materials previously exposed to air, as their carbon K-edge NEXAFS spectra are a convolution of the spectrum of the material under investigation and that of the adventitious carbon contamination. While analysis methods for determining the composition and thickness of each layer in a multilayer system without applying any destructive technique have been developed for X-ray photoelectron spectroscopy, no corresponding methodology has ever been reported for NEXAFS spectroscopy.

Here, we present a novel, non-destructive, and generally-applicable method for accounting for the contribution of thin overlayers (with thickness smaller than the information depth) from NEXAFS spectra of two-layered systems (constituted by a substrate covered by a surface layer) to give the corrected NEXAFS spectrum of the substrate. The new methodology is applied to NEXAFS data acquired on air-exposed hard carbon-based materials (ultranano-crystalline diamond and hydrogenated amorphous carbon) and allowed for the removal of the contribution of adventitious carbon contamination from the as-acquired spectra to give the intrinsic photo-absorption NEXAFS spectra of the materials under investigation. The results demonstrated that, in the case of amorphous carbon-based materials, significant errors, between 5% and 20%, could be introduced in the computation of the fraction of carbon atoms in different hybridization states if the contribution from the carbonaceous contamination layer is not removed from the as-acquired NEXAFS spectra. We also extract information about the composition and bonding found in the contamination layer.

The development of this novel methodology has important implications for the thorough investigation of the near-surface region of carbon materials as well as of the phenomena occurring in them in response to different energetic inputs (e.g., temperature, mechanical stress).

Biomaterial Interfaces

Room: 317 - Session BI+MG-WeA

Design and Discovery: Biointerfaces

Moderator: Morgan Alexander, The University of Nottingham, UK

2:20pm **BI+MG-WeA1 Discovery of Materials for Stem Cell Control using Polymer Microarrays**, *Morgan Alexander*, The University of Nottingham, UK

Polymer micro arrays have proven to be useful tools for the discovery of new synthetic materials which control cells.¹ This high throughput (HT) materials discovery approach is attractive because the paucity of understanding of the cell-material interface hinders the *ab initio* rational design of new materials.² The large number of polymer chemistries that can be investigated on a single polymer micro array act as a wide "net" in the search for materials that can achieve a certain cell response. Micro array *hits* are the starting point from which new materials may be developed.

Combinatorial acrylate libraries formed on standard glass slides were presented as a HT platform by Anderson and Langer of MIT.³ To complement materials screening, we developed the approach of *HT surface characterisation* employing a range of analytical techniques in collaboration with the MIT group.⁴ This surface characterisation step is necessary to directly relate the effect of the material on attached cells to the actual surface on which they sit, and to enable effective scale up from micro array to culture ware dimensions. Application of chemometrics, to handle the large amounts of complex data, reveals the importance of certain surface

moieties, guiding the process of materials discovery and increasing our understanding of the cell-material interface.

We have applied this approach to the identification of materials which resist bacterial attachment and biofilm formation with application in the reduction of medical device centred infection.^{5,6} In the mammalian cell field, we have identified materials which show promise as synthetic substrates for pluripotent stem cell culture.^{7,8} These materials require pre-treatment with expensive proteins such as vitronectin, a constraint which limits their commercialisation.⁹

In this talk, screening of arrays with greater chemical diversity than ever before, incorporating up to 140 monomers¹⁰, is reported which leads to the identification of materials which support pluripotent stem cell expansion without pre-treatment of the substrate with protein. Materials which support differentiation to mature cardiomyocytes which have potential application in *in vitro* toxicology screening have also been discovered.

- 1 Hook, A. L. **Biomaterials** (2010).
- 2 Kohn, J., **Nature Materials** (2004).
- 3 Anderson et al. **Nature Biotechnology** (2004).
- 4 Urquhart, A. et al. **Advanced Materials** (2007).
- 5 Hook, A. L. et al. **Nature Biotechnology** (2012).
- 6 Hook, A. L. et al. **Advanced Materials** (2013)
- 7 Mei, Y et al. **Nature Materials** (2010).
- 8 Saha, K. et al **PNAS** (2011).
- 9 Celiz, A. D et al. **Nature Materials** (2014).
- 10 Celiz, A. et al. **Biomaterials Science** (2014).

3:00pm **BI+MG-WeA3 Interfacial Force Field Parameterization in CHARMM for the Accurate Molecular Dynamics Simulation of Peptide Adsorption on High-Density Polyethylene**, *Tigran Abramyan, J.S. Snyder, J.Y. Yancey, S.S. Stuart, R.A. Latour*, Clemson University

A fundamental molecular-level understanding of protein-surface interactions (PSIs) is crucial for many applications in biotechnology and bioengineering. All-atom molecular dynamic (MD) simulation methods hold great promise as a valuable tool for understanding and predicting PSIs. However, current MD force fields have not been validated for this application. In this study, adsorption free energy (ΔG_{ads}) of small TGTG-X-GTGT host-guest peptides (T = threonine, G = glycine, and X = variable amino acid residue) on a high-density polyethylene (HDPE) surface (110 crystalline plane) using the CHARMM force-field were calculated and compared with experimental results in order to find inaccuracies. In order to accurately calculate ΔG_{ads} in our simulation studies, advanced sampling methods such as umbrella sampling and replica-exchange MD were used to provide adequate conformational sampling of the peptides over the HDPE surface. Results revealed substantial discrepancies between the simulation and the experimental ΔG_{ads} values (i.e., differences exceeding 1.0 kcal/mol). To correct the adsorption behavior, an *in-house-developed* interfacial force-field (IFF) was incorporated into the simulation program with IFF parameters adjusted until satisfactory agreement with the experimental data set was achieved. Subsequent studies are planned to apply the tuned IFF to simulate the adsorption behavior of lysozyme and ribonuclease A proteins to HDPE, for which synergistically matched experimental studies have also been conducted to validate the developed method for protein-adsorption simulations.

3:20pm **BI+MG-WeA4 Degradable Silica Nanoshells for Ultrasonic Imaging and Therapy**, *Alexander Liberman, C. Barback, R. Viveros, S.L. Blair, D. Vera, L. Ellies, R. Mattrey, W. Trogler, A.C. Kummel*, University of California at San Diego

As a safe alternative to intrasurgical guidewires and implantable radioactive seeds, gas-filled hollow Fe-doped silica particles have been developed, which can be used for ultrasound-guided surgery for multiple foci. The function of the Fe doping is to render the silica shells biodegradable. The particles are synthesized through a sol-gel method on a polystyrene template, and calcined to create hollow, rigid nanoshells. The Fe-doped silica shell is derived from tetramethyl orthosilicate (TMOS) and iron ethoxide, which forms a rigid, nanoporous shell upon calcination. The nanoshells are filled with perfluoropentane (PFP) vapor or liquid. The flouros phase is contained within the porous shell due to its extremely low solubility in water. *In vitro* studies have shown that continuous particle imaging time is up to approximately three hours non-stop. *In vivo* particle injection longevity studies have been performed in tumor bearing mouse models show signal presence with color Doppler imaging up to ten days post injection. To study biodistribution, nanoshells were functionalized with DTPA and radiolabeled with Indium-111 and then imaged by gamma scintigraphy over 72 hours. Scintigraphic imaging and gamma counting confirm that particles undergoing IV delivery to tumor bearing mice will

passively accumulate in the tumors which may allow for tumor detection and therapeutic applications. Additionally, long term biodistribution studies in mice have shown a steady decrease in silicon content over the course of 10 weeks by inductively coupled plasma optical emission spectroscopy (ICP-OES).

These silica shells break under acoustic excitation to release uncovered gas pockets which increase acoustic energy absorption and reduce acoustic cavitation threshold locally. Therefore they may also be employed as a sensitizing agent in high intensity focused ultrasound (HIFU) therapy. Traditional ultrasound agents which can be used as a HIFU sensitizing agent pose several potential drawbacks such as poor *in vivo* persistence (minutes) and high risk during continuous perfusion. Preliminary *in vivo* HIFU ablation studies show that very few particles are needed in order to develop a sensitizing effect to HIFU thereby substantially reduce the amount of HIFU exposure necessary to achieve an ablative effect. It was found that nanoshells systemically administered to breast tumor bearing mice could be cavitated by HIFU 24 hours after administration. This mechanical cavitation caused liquefaction within the focal volume of the HIFU which contained the nanoshells within seconds of the HIFU application. This may potentially allow for a larger area to be ablated in less time with less power.

4:20pm **BI+MG-WeA7 An Encapsulation Technique for Adenovirus to Enhance Viral Gene Therapy**, *Natalie Mendez, V. Herrera, L. Zhang, F. Hedjran, W. Trogler, S.L. Blair, A.C. Kummel*, University of California at San Diego

Oncolytic viruses (OVs) constitute a promising class of cancer therapeutics which exploit validated genetic pathways known to be deregulated in many cancers. To overcome an immune response and to enhance its potential use to treat primary and metastatic tumors, a method for liposomal encapsulation of adenovirus has been developed. The encapsulation of adenovirus in anionic 140-180nm diameter PEG containing non-toxic liposomes has been prepared by self-assembly of lecithin around the viral capsid. The encapsulated viruses retain their ability to infect cancer cells. Furthermore, an immunoprecipitation (IP) technique has shown to be a fast and effective method to extract non-encapsulated viruses and homogenize the liposomes remaining in solution. 76% of adenovirus plaque forming units were encapsulated and retained infectivity after IP processing. Additionally, encapsulated viruses have shown enhanced transfection efficiency up to 4X higher compared to non-encapsulated Ads. Extracting non-encapsulated viruses from solution may prevent an adverse *in vivo* immune response and may enhance treatment for multiple administrations.

4:40pm **BI+MG-WeA8 Sequential and Competitive Adsorption of Peptides at Pendant PEO Layers**, *X.W. Wu, M.R. Ryder, J.M. McGuire, Karl Schilke*, Oregon State University

A more quantitative understanding of peptide entrapment and elution from otherwise protein-repellent polyethylene oxide (PEO) brush layers will provide direction for development of new strategies for drug storage and delivery. Here we describe criteria for peptide integration and structural change within the PEO brush, and discuss the reversibility of peptide entrapment with changing solvent conditions. For this purpose, three cationic peptides were used: the arginine-rich amphiphilic peptide WLBU2, the chemically identical but scrambled peptide S-WLBU2, and the non-amphiphilic homopolymer poly-L-arginine (PLR). Circular dichroism (CD) was used to record the adsorption and conformational changes of WLBU2 and S-WLBU2, and polyarginine peptides at PEO-coated silica nanoparticles. UV spectroscopy and a quartz crystal microbalance with dissipation monitoring (QCM-D) were used to quantify changes in the extent of peptide elution. Peptide conformation was controlled between disordered and α -helical forms by varying the concentration of perchlorate ion. We show an initially more ordered (α -helical) structure promotes peptide adsorption into the PEO layer. Peptide interaction with the PEO chains resulted in entrapment and conformational change that was irreversible to elution with changing solution conditions in the case of the amphiphilic peptide. In contrast, the adsorption and conformational change of the non-amphiphilic peptide was reversible. We also evaluated the effects of peptide surface density on the conformational changes caused by peptide-peptide interactions, and using CD, QCM-D, and UV spectroscopy, showed that these phenomena substantially affect the rate and extent of peptide elution from PEO brush layers. Specifically, for amphiphilic peptides at sufficiently high surface density, peptide-peptide interactions result in conformational changes which compromise their resistance to elution. In contrast, elution of a non-amphiphilic peptide is substantially independent of its surface density, presumably due to the absence of peptide-peptide interactions.

The sequential and competitive adsorption behavior of WLBU2, S-WLBU2 and PLR at pendant PEO layers was studied by optical waveguide lightmode spectroscopy (OWLS), time-of-flight secondary ion mass spectrometry (TOF-SIMS), CD and UV spectroscopy. Results strongly indicate that amphiphilic peptides are able to displace non-amphiphilic

peptides that are adsorbed in PEO layers, while non-amphiphilic peptides cannot displace amphiphilic ones. In summary, peptides of high amphiphilicity are expected to dominate the competitive adsorption with less amphiphilic peptides in PEO layers.

5:00pm **BI+MG-WeA9 Moulding Cells and Materials in High Throughput**, *Clemens van Blitterswijk, R. Truckenmuller, L. Moroni, N. Rivron, P. Habibovic, J. De Boer*, Maastricht University, The Netherlands
INVITED

The interaction of cells and materials at their interface is crucial for the performance of devices that are applied in regenerative medicine. In general the approach to optimize interaction is characterized by a mechanistic low throughput research cycle where researchers try to move forward by improving performance based on fundamental insights and related small volume *in vitro/in vivo* experiments. Although this approach has successes it has its disadvantages. First as the field of regenerative medicine is young we currently lack fundamental insights into many of aspects that are relevant to our field. Second, the research cycle is slow, so if our experiments do not give the anticipated results we may lose several years. Third, the conventional approach only allows us to test a maximum of ca. 10 experimental conditions in one cycle forces us to leave out many other possibly equally interesting, opportunities.

In our lab we are convinced on how influential surface geometry of material can be on cell behavior and *in vivo* response by recently inducing prominent bone formation in muscle tissue in large animals by modulating the biomaterial surface in the submicrometer range. The effects of these instructive materials are equivalent to the use of growth factors while no biological agents or cultivated cells were applied. As we have no complete insight in the underlying mechanism, a conventional low throughput mechanistic approach does not seem the method of choice for further optimizing this performance and applying it to other tissue types.

Therefore, we developed multiwell screening systems that allow us to test a selection of thousands of surfaces from a truly designed high throughput library of 150 million different surface features in a single run. We have shown that this method allows us to modify cell shape and function in a remarkable way, both as far as cell attachment, proliferation and differentiation are concerned. As the above topochip platform is focused on 2D single cell performance and actual tissues are 3D and multicellular we have developed alternative platforms that allow us to build 3D mesoscale complex tissues in the thousands, while we have also generated so called 2.5 D multiwell systems that present convex surface features. Applying such systems allowed us to demonstrate that the mechanism of function follows form not only holds for individual cells but equally for millimeter scale cell aggregates. We are currently applying these technology platforms to create deeper insights in formation of tissues for regenerative medicine by introducing very early (embryonic) tissues in these systems while actively collaborating with developmental cell biologists.

6:00pm **BI+MG-WeA12 The Influence of Structural Array of Polymorphic hIAPP fibrils to its Mechanical Properties**, *HyunJoon Chang, M. Lee*, Korea University, Republic of Korea, *G. Yoon*, Boston University, *S. Na*, Korea University, Republic of Korea

Amyloid proteins are misfolded, denatured proteins that are responsible for causing several degenerative and neuro-degenerative diseases, such as type II diabetes, Alzheimer's disease, Huntington's disease, and so on. Determining the mechanical stability of these amyloids is crucial for understanding the disease mechanism, which will allow us to provide guidance in treatment. Furthermore, many research groups also recognized amyloid proteins as a functional biological materials that can be used in nano sensor, bacterial biofilms, coatings, etc. There have been many *in vitro* studies to determine the material characteristics via force spectroscopy methods, Atomic Force Microscopy and Optical Tweezers to exemplify. However, computational methods (e.g. Molecular Dynamics (MD) and Elastic Network Model) not only reveal the mechanical properties, but also provide a more in-depth information on the amyloids by visualizing the conformation. In this study, we have discovered the material properties of four different polymorphic structures of Human Islet Amyloid Polypeptide (hIAPP) by using MD simulations under tensile Steered Molecular Dynamics (SMD) conditions. Also, from our results, we have observed how these mechanical properties may differ in respect of their structural formation. This study will help us to take a step forward for treating degenerative disease and also establish a template for the functional biological materials.

Electronic Materials and Processing Room: 311 - Session EM+EN+TF-WeA

Thin Films and Materials for Energy Storage

Moderator: Christopher Hinkle, University of Texas at Dallas

2:20pm **EM+EN+TF-WeA1 Investigation of Composite Dielectric Materials for Energy Storage**, *Kimberly Cook-Chennault, U. Sundar, W. Du*, Rutgers, the State University of New Jersey

Electrical energy storage plays a key role in electronics, stationary power systems, hybrid electric vehicles and pulse power applications. Traditionally, bulk ceramic dielectric oxides are used for these applications, though they suffer from inherently low breakdown field strength, which limits the available energy density and increases the dielectric loss. On the other hand, polymers have high break down field strengths, low dielectric losses and can be readily processed into thin films, but suffer from relatively low dielectric permittivity, and thus low energy densities. As a result, contemporary materials have become a limiting factor to the realization of miniaturized devices, due to Moore's Second law, in terms of size, cost and parasitic impedances. Realization of micrometer to sub-micrometer scale commercial and industrial devices such as, high density DRAM (dynamic access memory), non-volatile memory (NRAM) and capacitors, require advanced materials that can both accumulate and deliver vast amounts of energy nearly instantaneously with minimal dielectric losses. This work focuses on examination of piezoelectric-epoxy based composites for dielectric materials, and explores the interrelationship processing plays on realized electrical and dielectric properties. Materials under investigation include lead-zirconate-titanate, and barium titanate – epoxy composites.

2:40pm **EM+EN+TF-WeA2 Preparation and Characterization of ZnO Nano Rods**, *P. Thamaraiselvan*, Selvam Arts and Science College, India, *M. Saroja, M. Venkatachalam, P. Gowthaman*, Erode Arts and Science College, India, *S. Ravikumar*, Sengunthar Arts and Science College, India, *S. Shankar*, Erode Arts and Science College, India

ZnO nano rods were prepared using chemical bath deposition technique. ZnO seed layer thin films were deposited on glass substrates by dip coating method. Subsequently, ZnO seed-coated glass substrates were immersed in aqueous solution of zinc nitrate and hexamethylenetetramine (HMT) at three different growth time of 3, 4 and 5 hours at low temperature of 90°C. 0.02 mol of Zinc nitrate and 0.2 mol of Hexamethylenetetramine (HMT) on 1:10 molar concentration were used for the growth of Zinc oxide nano rods. The structure and surface morphology of the ZnO nano rod were studied using X-ray diffraction Scanning Electron Microscopy (SEM), respectively.

3:00pm **EM+EN+TF-WeA3 Rational Design of Energy Storage Materials from Earth Abundant Elements**, *Kyeongjae Cho*, UT Dallas
INVITED

As a part of global scale renewable energy technology solutions, large scale energy storage system (ESS) would be critical in mediating the gaps between cycles of energy demands and intermittent solar and wind energy generations. Furthermore, electric vehicles (EV) require significantly larger energy storage capacity compared to the batteries used electronic device applications. There are significant challenges in extending the current Li ion battery (LIB) technology (based on graphite anode, organic liquid electrolyte, and Co oxide cathode) to EV and ESS applications. Many different approaches are currently investigated to overcome the capacity, safety and cost issues of LIB in EV and ESS applications, and new battery technology researches include Si anode, Na and Mg batteries, metal-air batteries, over-lithiated-oxide (OLO) [1] and silicate cathodes [2] for LIB. OLO and silicate cathode materials provide two times larger charge storage capacity (~300 mAh/g) compare to current commercial LiCoO₂ (LCO) or Li(Ni,Co,Mn)O₂ (NCM) cathodes. Both Li₂MnO₃ and Li₂FeSiO₄ are based on earth abundant transition metals of Mn and Fe so that a successful development of these cathode materials would improve cathode capacity and cost problems. In order to achieve the short term goal of OLO and silicate cathode development and the long term goal of EV and ESS material development, we have applied the rational material design and development framework developed for pollution control technology in which Pt catalysts are replaced by PdAu alloy and Mn-mullite catalysts. [3-5] In this talk, we will discuss the current status of OLO and silicate cathode material research based on the integrated material design-synthesis-characterization framework.

This work was supported by Samsung GRO project.

1. R. C. Longo et al., "Phase stability of Li-Mn-O oxides as cathode materials for Li-ion Batteries: insights from ab initio calculations" (submitted)
2. R. C. Longo, K. Xiong and K. Cho, "Multicomponent Silicate Cathode Materials for Rechargeable Li-ion Batteries: An ab initio study," *Journal of the Electrochemical Society* 160, A60 (2013).
3. X. Hao et al., "Experimental and Theoretical Study of CO Oxidation on PdAu Catalysts with NO Pulse Effects," *Top. Catal.* 52, 1946 (2009).
4. B. Shan et al., "First-principles-based embedded atom method for PdAu nanoparticles," *Phys. Rev. B* 80, 035404 (2009).
5. W. Wang, G. McCool, N. Kapur, G. Yuan, B. Shan, M. Nguyen, U. M. Graham, B. H. Davis, G. Jacobs, K. Cho, X. Hao, "Mixed-Phase Oxide Catalyst Based on Mn-Mullite (Sm, Gd)Mn₂O₅ for NO Oxidation in Diesel Exhaust," *Science* 337, 832-835 (2012).

4:20pm **EM+EN+TF-WeA7 Transferring Environmentally Sensitive Battery Materials between GloveBox and UHV Surface Analysis Chamber: Composition Study of Model Battery Interfaces and their Controlled Oxidation, Hugo Celio**, University of Texas at Austin

Environmentally sensitive battery materials prepared in an inert environment (e.g., Argon filled glovebox containing trace levels of water and oxygen at ~1 part-per-million) are often difficult to transfer to an ultra-high vacuum (UHV) chamber for surface analysis. While minimizing additional oxidant(s) exposure, three challenging factors arise from transferring environmentally sensitive materials: 1) Engineering a pump-down load-lock to transition from atmospheric pressure to UHV regime, 2) developing a method to generate a set of figures of merit (FOMs) that allows a user to evaluate transfer reliability, and 3) evaluating of the amount of material that subsequently undergoes, due to reaction with trace ppm levels of oxidants in the Argon gas, oxidation during transfer. To target these issues a novel transfer load-lock/capsule was built and directly coupled to a UHV surface analysis chamber, equipped with X-ray photoelectron spectrometer (XPS). This new load-lock/capsule has led to a new capability to study the composition of model battery materials (e.g., silicon anode and metal oxide cathode) at the solid electrolyte interfacial (SEI) layer, including their controlled oxidation post-transfer.

4:40pm **EM+EN+TF-WeA8 Development of Thin Film Si-C Based High Temperature Microsupercapacitor Devices, J.P. Alper, C.-H. Chang, C. Carraro, Roya Maboudian**, University of California at Berkeley

On-chip integrated energy storage and delivery at high power is an important aspect in realizing the full potential of microsystems technology such as remote mobile sensor platforms. One promising high power device which has garnered much attention is the supercapacitor. Energy is stored in SC's at the electrode-electrolyte interface, making the high specific surface area of thin films of 1-d materials particularly attractive for application to these devices. However many operations such as in the chemical process industries which could benefit from remote sensor deployment reach temperatures beyond current electrode and electrolyte material constraints. Here we report on the use of bottom-up chemical vapor deposition based silicon carbide (SiC) nanowires and top-down chemically etched SiNWs passivated with an ultrathin carbon sheath as thin film micro-SC electrodes. The electrochemical performance of the two nanowire types in high temperature compatible electrolytes such as ionic liquids and yttria stabilized zirconia (YSZ) are presented. The materials are stable during cycling and achieve specific capacitance values comparable to or better than previously reported carbon electrodes. Operation at temperatures above those attainable with standard electrode-electrolyte systems is also demonstrated. Current challenges for the methods presented and strategies for overcoming them are discussed.

5:00pm **EM+EN+TF-WeA9 Rate Capability of Silicon Carbon Nanotube Anodes for Lithium Ion Batteries, Lawrence Barrett, R. Fan, R.C. Davis, K. Hinton, R.R. Vanfleet**, Brigham Young University

Research has shown stable high capacity lithium ion battery anodes can be made from silicon deposited on carbon nanotubes (CNTs). However, rate capability remains a challenge. We have explored two potential limiting factors: diffusion from the top of the forest down and diffusion into the silicon coating. To probe top down diffusion, we compared a uniform CNT forest to a forest with an array 10 um holes spaced 10 um apart to allow channels for faster top down diffusion and found rate capability was unaffected, indicating top down diffusion is not a limiting factor. We also probed diffusion through the silicon coating by changing the thickness and morphology of the coating.

5:20pm **EM+EN+TF-WeA10 Characterization and Optimization of Interface Engineering on Li Metal Anode Using Atomic Layer Deposition and In Situ Electrochemical AFM, Chuan-Fu Lin, A.C. Kozen, A.J. Pearse, M. Noked, M.A. Schroeder, S.B. Lee, G.W. Rubloff**, University of Maryland, College Park

Rechargeable Li-metal anode batteries could be considered the holy grail of energy storage systems because Li offers extremely high theoretical specific capacity (3860 mAh/g), low density (0.59 g/cm³), and the lowest negative electrochemical potential (-3.040 V vs. standard hydrogen electrode). However, Li is thermodynamically unstable with organic solvents, inviting serious capacity degradation as well as safety concerns such as Li dendrite growth. The prognosis for Li anodes would be profoundly enhanced for next generation batteries if suitable passivation schemes could be developed to protect Li anodes without significantly reducing ion transport between Li and electrolyte.

In our laboratory, we use atomic layer deposition (ALD) to precisely deposit very thin layer of aluminum oxide (Al₂O₃) on Li foils, using glove box and UHV environments to avoid air exposure while depositing passivation layers on the Li metal surface. We then characterize the surface morphology of the passivated Li by AFM at varying stages of electrochemical reaction and as a function of time and film thickness. We observed the growth of defects on ALD-passivated Li metal surface, decorated by AFM structures indicative of localized electrochemical reactions. The resulting defect density decreased as the film thickness increased.

For thinner ALD protection layers, EC-AFM showed bubble-like structures decorating the steps and boundaries of ALD/Li metal surface in electrochemical system, suggesting mechanisms associated with volatile products. While thin ALD layers suppress charge transfer processes which lead to electrolyte decomposition and formation of solid electrolyte interphase (SEI) [1-2], defects in the ALD passivation layer may cause localized SEI formation, which in turn involves volatile products (e.g., C₂H₄, CO). Alternatively, trace H₂O in the propylene carbonate electrolyte may react with Li metal through pinholes in the ALD layer, leading to LiOH and volatile H₂ products. We are working to differentiate between these by applying in-situ mass spectroscopy to monitor the gas formation in the cell as a function of controlled water content and ALD film thickness. The identification of passivation layer degradation mechanisms and the development of robust approaches to metal anode protection have profound benefit to a variety of beyond-Li-ion batteries.

References:

1. Kevin Leung, *J. Phys. Chem. C*, 2012, 117, 1539-1547.
2. Kevin Leung et al., *JACS*, 2011, 133, 14741-14754.

5:40pm **EM+EN+TF-WeA11 The Road to Next-Generation Energy Storage is Paved with Zinc, Joseph Parker, C.N. Chervin**, Naval Research Laboratory, I.R. Pala, National Research Council postdoc working at Naval Research Laboratory, E.S. Nelson, Pathways Student working at Naval Research Laboratory, J.W. Long, D.R. Rolison, Naval Research Laboratory

While Li-ion batteries presently dominate the energy-storage landscape, zinc-based batteries offer a compelling alternative due to the earth-abundance of zinc, innate safety and cost advantages that arise from using aqueous electrolytes, and device-realized specific energy that is comparable to or higher than Li-ion. Yet the performance of present-day Zn-based batteries is hindered by suboptimal Zn utilization (typically <60% of theoretical capacity) and poor rechargeability—a consequence of the complex dissolution/precipitation processes that accompany Zn/Zn²⁺ cycling and the ad hoc construction of conventional powdered-bed Zn anodes. We address these limitations by designing and fabricating highly conductive, porous, and 3D-wired Zn "sponge" electrodes from emulsion-cast, consolidated Zn powders that are thermally treated to produce rugged monolithic forms. With this 3D Zn architecture, we achieve >90% Zn utilization when discharged in primary Zn-air cells with retention of the 3D framework of the Zn sponge and uniform deposition of charge/discharge products at the surfaces of the Zn sponge, as verified by scanning electron microscopy and impedance spectroscopy. We further show that the structural characteristics of the Zn sponge promote greater rechargeability when cycled in prototype Ag-Zn and Ni-Zn cells. Our results demonstrate that all Zn-based chemistries can now be reformulated for next-generation rechargeable batteries.

Electronic Materials and Processing

Room: 314 - Session EM-WeA

High-K Dielectrics for 2D Semiconductor

Moderator: Andrew C. Kummel, University of California at San Diego

2:20pm **EM-WeA1 Adding New Functionalities to CMOS Integrated Circuits Via Directed Self-Assembly**, *Theresa Mayer*, Penn State University **INVITED**

With CMOS nearing the physical limits of scaling, the future of the semiconductor industry is at a critical point. The International Technology Roadmap for Semiconductors identifies the growing need to interface new nanoscale materials and devices with Si CMOS architectures to sustain nanoelectronic circuit scaling (more-of-Moore) and to discover entirely new electronic systems (more-than-Moore). This talk will describe new directed self-assembly process to position large, diverse, and interchangeable arrays of nanowire sensors or sheets of alternative electronic materials onto fully-processed Si CMOS circuits. The wires or sheets are fabricated off-chip from many different materials tailored for a specific function. Electric-field forces are then used direct different populations of these materials to specific regions of the chip, while also providing accurate registry to a predefined feature on the chip. Following assembly, conventional lithographic processes can then be used to define the nanodevices and connect them to the Si circuit. Several material and device integration examples will be discussed, including the directed assembly of metal-oxide nanowire device arrays as well as monolayer 2D transition metal dichalcogenide crystal materials.

3:00pm **EM-WeA3 Band Gap Engineering of 2D Semiconductor Materials via Atomic Layer Deposition of TiOPc on Graphene and MoS₂**, *Pabitra Choudhury*, New Mexico Institute of Mining and Technology, *A.C. Kummel*, University of California at San Diego

Metal phthalocyanine (MPc) molecules are composed of a metal atom and a surrounding phthalocyanine ligand ring. The metal-ligand interaction and molecule-surface interaction are the two most important parameters, which controls the various physical and chemical properties of this adsorption system of MPc molecules onto the substrate. MPc molecules can potentially be employed for electrostatic doping of non-reactive substrates (for example 2D semiconductor materials), will lead to various applications such as sensors and electronics, and hence MPc become a model system for surface chemistry and nanotechnology. Tytanyl phthalocyanine (TiOPc) is another interesting molecule of phthalocyanine family having anisotropic intermolecular interactions. In this study, TiOPc electrostatic interactions with two nonreactive 2D semiconductor substrates, graphene and MoS₂, were studied. We have carried out first principle density functional theory (DFT) calculations and theoretical analysis to explore the structural and electronic properties of mono- and bi-layer of TiOPc molecule on both graphene and MoS₂. The adsorption of mono- and bi-layer films of TiOPc on graphene shows that there is a net 0.047 electrons and 0.016 electrons per TiOPc molecule charge transfer takes place from the graphene surface, respectively. Conversely, a net amount of 0.058 electrons and 0.029 electrons per TiOPc molecule charge transfer take place to the MoS₂ surface in case of mono- and bi-layer of TiOPc, respectively. Moreover, we find that the bandgaps of graphene/TiOPc(mono-and bi-layer) and MoS₂/TiOPc(mono-and bi-layer) heterostructures decrease with increasing number of TiOPc layers. Our results suggest that the band gap of 2D semiconductors, MoS₂/TiOPc and graphene/TiOPc heterostructures, could be engineered with atomic layer precision by controlling the number of TiOPc layer deposited on the 2D substrate, which could serve as a potential candidate for both sensor and advanced electronics applications.

3:20pm **EM-WeA4 HfSe₂ Thin Films: 2D Transition Metal Dichalcogenides Grown by MBE**, *Ruoyu Yue, A. Barton, X. Peng, N. Lu, R. Addou, S. McDonnell, L. Chen, J.Y. Kim*, University of Texas at Dallas, *L. Colombo*, Texas Instruments, *M. Kim, R.M. Wallace, C.L. Hinkle*, University of Texas at Dallas

The growth of high-quality, layered HfSe₂ thin films by molecular beam epitaxy (MBE) on a variety of substrates is demonstrated for the first time. The cross-section of HfSe₂ thin films on highly ordered pyrolytic graphite (HOPG) shows the layered structure of crystalline HfSe₂ with an atomically sharp interface between the HfSe₂ and HOPG, verifying the van der Waals epitaxy. Crystalline HfSe₂ thin films with preferred orientation and hexagonal top surface symmetry are characterized by RHEED, STM, and XRD with a measured lattice constant consistent with the theoretical prediction of the 1-T phase. The stoichiometry (Hf: Se) of crystalline HfSe₂ on HOPG, measured by XPS, is very close to 1:2 and the in-plane and out-of-plane vibration mode peaks of the 1-T structure of HfSe₂ is confirmed by

Raman spectroscopy. It is also noted that the crystal quality of the HfSe₂ changes as a function of substrate with the best growth results obtained on inert, hexagonal symmetry surfaces. These results indicate that the growth of novel TMDs by MBE is achievable and opens the possibility for exciting new 2D heterostructures and devices.

4:20pm **EM-WeA7 Phonons, Scattering, and Semiclassical Transport Studies in 2D Materials and Devices**, *Massimo Fischetti, W.G. Vandenberghe*, The University of Texas at Dallas **INVITED**

Basic ideas from pseudopotentials and semiclassical-transport will be used to discuss the properties of some novel 2D materials considered for post-Si-CMOS applications. First, it will be shown that in order to scale devices to 5 nm, simple electrostatic scaling laws demand the use of these two-dimensional materials, despite the daunting processing challenges they pose. Graphene will be considered discussing how its outstanding electronic properties become much less interesting when used as a component of some non-ideal structure, such when supported and gated and/or in nanoribbon form. A couple of very interesting ideas will be discussed next: 1. The Bose-Einstein condensation in bilayer systems (motivating UT-Austin's BiSFETs) as an example of how issues of practical implementation may regrettably transform an excellent idea into a pure academic exercise; and 2. Monolayer tin ("stannane") as a 2D topological insulator with potential applications in spintronics and low-power high-performance devices. Besides discussing its potential electronic properties, the likelihood of actually fabricating such a material will be discussed on the basis of *ab initio* thermodynamics.

5:00pm **EM-WeA9 In Situ Transmission Electron Microscopy of Oxides on TMDs**, *Moon Kim, N. Lu, J. Oviedo, X. Peng, J. Wang, G. Lian, A. Azcatl, S. McDonnell, R.M. Wallace*, The University of Texas at Dallas, *S. Vishwanath, H. Xing*, University of Notre Dame **INVITED**

Over the past two years, transition metal dichalcogenide (TMD) materials, as 2-D crystals, have attracted much interest for a wide range of electronic and optoelectronic device applications. Yet, uniform deposition of sub-10 nm dielectrics on 2-D materials remains challenging. There is a great demand for the visualization and analysis of interfaces and defects in 2-D crystals and gate oxides, which play an important role in the growth and properties of heterostructures. Site-specific cross-sectional TEM imaging and associated techniques have become essential in providing detailed atomic scale information. High angle angular dark field (HAADF)-scanning transmission electron microscopy (STEM) can be used to investigate the atomic structure and chemistry of TMD-oxide interfaces and defects. *In-situ* TEM techniques such as heating and electrical/mechanical probing can also provide information regarding the dynamic behavior of the materials/devices of interest.

Herein, we report our results on HfO₂ and Al₂O₃ thin films deposited on MoS₂ by atomic layer deposition and SnSe₂ FETs with an Al₂O₃ gate oxide. Our *in-situ* TEM work on 2-D materials will also be presented. Based on our study, a possible growth mechanism of oxides on TMD with different surface treatments has been proposed [1,2]. These unique and effective site-specific and *in-situ* analysis tools can be widely applied to other gate oxides of interest.

This work was supported in part by the Center for Low Energy Systems Technology (LEAST), one of six centers supported by the STARnet phase of the Focus Center Research Program (FCRP), a Semiconductor Research Corporation program sponsored by MARCO and DARPA.

[1] ACS Nano, 7, 10354–10361, 2013.

[2] Applied Physics Letters, 104, 111601, 2014.

5:40pm **EM-WeA11 Effects of Neutron Irradiation of Ultra-Thin HfO₂ Films**, *Kai-wen Hsu*, University of Wisconsin-Madison, *H. Ren*, Applied Materials, *R.J. Agasie*, University of Wisconsin-Madison, *L. Zhao, Y. Nishi*, Stanford University, *J.L. Shohet*, University of Wisconsin-Madison

In order to investigate neutron-induced effects on HfO₂ resistive random-access memory (RRAM), HfO₂ films are subjected to irradiation by neutrons with energies above 1 MeV. Changes in the defect state concentrations of HfO₂ may lead to changes in the states of memory which has the potential to convert a "0" into a "1" in RRAM or vice versa.

Electron-spin resonance (ESR) is used to detect defect-state concentrations of the HfO₂ film deposited on high-resistivity substrates. Additionally, leakage currents of HfO₂ films are also measured to support the ESR data.¹

Neutron irradiation at low fluence decreases the Pb-type and E' defect levels in ultra-thin HfO₂ films because electrons can fill existing states. These electrons come from electron-hole pairs generated by neutron interactions with silicon and oxygen. Thus, a low fluence of neutrons "anneals" the sample. However, when neutron fluence increases, more neutrons collide with oxygen atoms and cause them to leave the lattice or to transmute into different atoms. This causes the E' state concentration to

increase. The changes in the number of defect states lead to changes in leakage currents.

This work was supported by the Semiconductor Research Corporation under Contract 2012-KJ-2359 and by the National Science Foundation under Grant CBET-1066231.

¹K-W Hsu, H. Ren, R.J. Agasie, S. Bian, Y. Nishi, and J.L. Shohet, *Applied Physics Letters* **104** 032910 (2014)

6:00pm EM-WeA12 Nucleation of Low Temperature HfO₂ Atomic Layer Deposition on InGaAs using Various Native Oxide Removal Techniques, Tyler Kent, University of California at San Diego, K. Tang, Stanford University, S. Lee, C.Y. Huang, V. Chobpattana, University of California at Santa Barbara, K. Sardashti, M. Edmonds, University of California at San Diego, R. Droopad, Texas State University, P.C. McIntyre, Stanford University, A.C. Kummel, University of California at San Diego

One of the major obstacles impeding the advancement of III-V MOSFETs is the large density of interfacial trap states (D_{it}) at the high-k/III-V interface. Poor nucleation of the gate oxide can lead to dangling bonds, strained bonds, and metallic bonds which contribute to D_{it} ; additionally, low nucleation density requires a thicker oxide to avoid pinholes which increase gate leakage. The nucleation of HfO₂ was studied using tetrakis(ethylmethylamino)hafnium (TEMAH) and H₂O on the InGaAs (001) and InGaAs (110) surfaces at low temperature, 120 °C, using atomic layer deposition (ALD). Low temperature ALD reduces subcutaneous oxidation of the channel when this is an activated process. The pulse and purge times of the oxidant and reductant were varied and their impact on the nucleation of HfO₂ were studied by fabricating MOSCAPs and extracting the D_{it} using the full interface surface state model. All samples had 10 cycles of an in-situ pre-ALD surface clean developed by Choptabanna and Carter which utilizes atomic H and TMA. The effectiveness of the ex-situ buffered oxide etch (BOE) was examined by fabricating samples with and without this clean. The BOE was more effective on the (001) samples since the non-BOE samples had a larger D_{it} and a higher C_{max} indicating poor nucleation of the HfO₂. The dispersion in accumulation remained constant indicating the BOE had an immediate effect on the interface, rather than deep traps in the oxide. The BOE and non-BOE (110) samples had a nearly identical C_{max} , D_{it} , and dispersion in accumulation indicating the nucleation of HfO₂ is not as dependent on the BOE as the (001) surface. This result obviates the need for the BOE allowing an all dry process on InGaAs(110) and is likely a result of the inherent stability of the (110) surface compared to the (001) surface.

Energy Frontiers Focus Topic

Room: 315 - Session EN+AS+EM-WeA

Organic-Inorganic Interfaces for Energy

Moderator: Ramana Chintalapalle, University of Texas at El Paso

2:20pm EN+AS+EM-WeA1 Towards Efficient Solution Processed Organic Photovoltaic Devices, Elsa Reichmanis, Georgia Institute of Technology **INVITED**

Solution-processed π -conjugated semiconductors exhibit potential in the development of low-cost, light-weight and large-area flexible plastic optoelectronics, particularly photovoltaics (OPVs). However, one drawback to current OPVs is their limited efficiency. We have explored the use of donor-acceptor (D-A) hybridization to tailor HOMO/LUMO energy levels and thus the band gap. Materials exhibiting high charge carrier mobility and strong low-energy absorption profiles have been synthesized and characterized. Coupled with materials structure, the performance of devices fabricated using polymeric semiconductors depends critically upon alignment of the polymer chains at the nano- through meso- and macro-scales. Significant structure-process-property relationships that allow for enhancement of long-range order will be discussed. For instance, a lyotropic liquid crystalline (LC) phase has been observed in poly-(3-hexylthiophene) (P3HT) via solvent-evaporation induced self-assembly. The lessons learned through these studies may allow for simple, controllable, and cost-effective methodologies for achieving high performance flexible plastic electronic devices.

3:00pm EN+AS+EM-WeA3 Understanding Carrier Dynamics in Cu₂ZnSn(S,Se)₄ Using Time-Resolved Terahertz Spectroscopy, G.W. Guglietta, Drexel University, K. Roy Choudhury, J.V. Caspar, DuPont Central Research and Development, **Jason Baxter**, Drexel University

We have used time-resolved terahertz spectroscopy (TRTS) to measure lifetimes and determine recombination mechanisms in Cu₂ZnSn(S,Se)₄ (CZTSSe) thin films fabricated from nanocrystal inks. TRTS probes photoconductivity on femtosecond to nanosecond time scales that are relevant for recombination in thin film photovoltaics. Terahertz frequencies (0.2-2.5 THz) correspond to typical scattering rates in semiconductors, enabling determination of carrier density and mobility. Ultrafast time resolution permits tracking the evolution of carrier density to determine recombination mechanisms. By manipulating the photoexcitation wavelength and fluence, we can tailor the generation profile of photoexcited carriers to distinguish between surface, Shockley-Read-Hall (SRH), and Auger recombination mechanisms and determine rate constants.

TRTS experiments and modeling were used to understand the role of recombination mechanisms and their contribution to CZTSSe photovoltaic performance. TRTS photoconductivity shows an instrument-limited onset within 1 ps of an ultrafast pump pulse, followed by a slow decay over nanoseconds. Photoconductivity decay kinetics were fit with a bi-exponential model with two time constants and a weight fraction. The short time constant is typically ~200 ps and roughly corresponds to diffusion to and recombination at the surface. The long time constant is typically ~2 ns and is attributed to SRH recombination. Assignment of these mechanisms is supported by the dependence of kinetics upon excitation fluence and wavelength. Normalized kinetics are independent of fluence over a range of 40x, indicating that no Auger recombination is occurring. Without Auger recombination, we can distinguish between surface and SRH rates by tuning the pump wavelength. As the excitation wavelength is shifted towards the blue, carriers are generated nearer to the front surface and the photoconductivity kinetics are sensitive to the surface recombination velocity. With blue excitation, we see that a larger fraction, ~0.5, of carriers recombine with a short time constant. With redder excitation wavelengths, the carriers are generated more evenly throughout the film and the kinetics are dominated by SRH recombination with the long time constant having a majority of the weight fraction, ~0.8. TRTS provides a pathway to determine performance-limiting recombination mechanisms and measure key parameters like SRH lifetime and surface recombination velocity, helping to direct the design of efficient thin film photovoltaics.

3:20pm EN+AS+EM-WeA4 Comparative Study of the Doping Effects of Titanium and Nitrogen into Tungsten Oxide (WO₃) Thin Films for Photovoltaic Device Applications, Mirella Vargas, C.V. Ramana, The University of Texas at El Paso

Tungsten oxide (WO₃) is a technologically important n-type semi-conductor that is extensively studied in the fields of electronic and opto-electronic devices. Due to its unique properties such as a high work function and high-coloration efficiency, WO₃ is attractive for electrochromic and memory devices including large area information displays, smart-windows, and optical heat-mirrors. Low-dimensional structures of WO₃ coupled with an ideal band gap ($E_g \sim 2.8$ eV) have been employed as materials for the photocatalyst driven by visible light irradiation in dye-sensitized solar cells. In addition, WO₃ has also become a strong contender to replace indium-doped tin oxide or ITO thin films in transparent electrode applications. The present work is focused on WO₃ thin films characterized as promising transparent conducting oxide (TCO) materials by investigating doping effects on the structural, chemical, and optical properties. The incorporation of titanium (Ti) was achievable by depositing the films through co-sputtering of W and Ti metal targets. The sputtering powers to the W and Ti were kept constant at 100 W and 50 W, respectively, while varying the growth temperature (T_s) in the range of 25-500 °C. While all the samples are optically transparent, the structural quality of Ti-doped WO₃ films is dependent on T_s . Ti-doped WO₃ films grown at $T_s < 400$ °C were amorphous. A temperature of 400 °C is critical to promote the structural order and formation of nanocrystalline films in the monoclinic phase. The optical constants and their dispersion profiles determined from spectroscopic ellipsometry indicate that there is no significant inter-diffusion at the film-substrate interface for W-Ti oxide film growth of ~40 nm. The index refraction (n) at $\lambda = 550$ nm vary in the range of 2.15-2.40 with a gradual increase in growth temperature. Nitrogen (N₂) incorporation was made through a post-deposition anneal in an ammonia environment on WO₃ films. The un-doped WO₃ films grown by variable growth temperature will be annealed at high temperatures for various rates to accommodate a strong N₂ incorporation. The tungsten oxynitride films will be characterized by various analytical techniques to compare the doping effects of Ti and N₂ on the structural, electronic, and optical properties of WO₃ thin films.

5:00pm **EN+AS+EM-WeA9 Engineering Exciton Recombination in Organic Light-Emitting Devices, Russell Holmes, University of Minnesota** **INVITED**

While capable of realizing very high peak efficiency, many organic light-emitting devices (OLEDs) suffer a significant reduction in efficiency under large injected current densities. This efficiency roll-off can limit device brightness and potentially compromise operational stability. Much previous work has identified the key contributing factors to the efficiency roll-off in phosphorescent OLEDs as triplet-triplet annihilation and triplet-polaron quenching. Here, the parameters associated with these quenching processes are independently measured, and the impact of the exciton recombination zone width on the quenching processes in various OLED architectures is examined directly. In high efficiency devices employing a graded-emissive layer (G-EML) architecture the roll-off is due to both triplet-triplet annihilation and triplet-polaron quenching, while in devices which employ a double-emissive layer (D-EML) architecture, the roll-off is dominated by triplet-triplet annihilation. Overall, the roll-off in G-EML devices is found to be much less severe than in the D-EML device. This result is well accounted for by the larger exciton recombination zone that is experimentally measured in G-EML devices, serving to reduce exciton density-driven loss pathways. Indeed, a predictive model of the device efficiency based on the quantitatively measured quenching parameters shows the role a large exciton recombination zone plays in mitigating the roll-off.

5:40pm **EN+AS+EM-WeA11 Interface Engineering to Control Magnetic Field Effects of Organic-based Devices by using a Self-Assembled Monolayer, Hyuk-Jae Jang, NIST & WFU, S.J. Pookpanratana, NIST, A.N. Brigeman, Wake Forest University, R.J. Kline, NIST, J.I. Basham, NIST & PSU, D.J. Gundlach, C.A. Hacker, O.A. Kirillova, NIST, O.D. Jurchescu, Wake Forest University, C.A. Richter, NIST**

Magnetic field effects (MFEs) in non-magnetic organic semiconductors provide a non-contact approach to control electronic and optoelectronic properties of organic-based devices by using a sub-tesla magnetic field and thus they have been of great interest to industry as well as academia around the world.^{1,2} However, there is no consensus on the physical mechanism(s) causing the MFEs in organic semiconductors even though a variety of fundamental models have been proposed to explain the effects.³ Studies on many different organic semiconductors and organic-based structures have shown that the magnitude and even the sign of the MFEs can vary by changing the measurement and fabrication conditions such as bias voltage, film thickness, and temperature. Therefore, it is suggested that there can be multiple origins inducing the MFEs and the outcome may result from a competition between different MFE mechanisms.²

In this presentation, we report a novel method of manipulating the MFEs on electrical resistance of organic semiconductors, namely organic magnetoresistance in Alq₃ (tris-(8-hydroxyquinoline) aluminum) – based devices by simply adding a molecular self-assembled monolayer (SAM) between a metal electrode and an organic semiconductor. SAMs have been known for their versatile use in various technological applications.³ Particularly, SAMs can alter the physical property of an inorganic solid surface and thus modify the interface between an electrode and an organic thin film when a SAM is inserted between them.³ We show for the first time that the interfacial modification by simply inserting a fluorinated SAM (heptadecafluoro-1-decanethiol [CF₃(CF₂)₇(CH₂)₂SH] or F-SAM) in organic-based devices changes the sign of organic magnetoresistance due to the change in relative strength of different MFE mechanisms coexisting in organic-based devices. In addition, we utilize different MFE mechanisms coexisting in organic-based devices by adding a thin TPD (N,N'-Bis(3-methylphenyl)-N,N'-diphenylbenzidine) layer to create a system whose organic magnetoresistance can be tuned by an external bias voltage.

References

1. J. Kalinowski, M. Cocchi, D. Virgili, P. Di Marco, and V. Fattori, *Chem. Phys. Lett.* vol. 380, pp. 710-715, 2003.
2. W. Wagemans, P. Janssen, A. J. Schellekens, F. L. Bloom, P. A. Bobbert, and B. Koopmans, *SPIN* vol. 1, pp. 93-108, 2011.
3. J. C. Love, L. A. Estroff, J. K. Kriebel, R. G. Nuzzo, and G. M. Whitesides, *Chem. Rev.* vol. 105, pp. 1103-1169, 2005.

6:00pm **EN+AS+EM-WeA12 Study on the Correlation between Electrode-Active Layer Interfaces and Performance of Polymer Solar Cells, Huanxin Ju, J.F. Zhu, University of Science and Technology of China**

The PSCs were fabricated with different cathodes (Ca/Al and Al) as the electron-collection layers and with PCDTBT (poly[N-9"-hepta-decanyl-2,7-carbazole-alt-5,5-(4',7'-di-2-thienyl-2'',1'',3''-benzothiadiazole)]) and PC70BM ([6,6]-phenyl-C71-butyric acid methyl ester) as the active layers.

The Ca/Al interlayer significantly improves the open circuit voltage (VOC), short circuit current (JSC), fill factor (FF) so as to improve the PCE in comparison with Al as the cathode. In order to understand how the electrodes affect the device performance, the Ca/PCDTBT and Al/PCDTBT interfaces were investigated by transient photovoltage (TPV), charge extraction (CE) and synchrotron radiation photoemission spectroscopy (SRPES). The TPV and CE measurements were used to determine the charge carrier lifetime and density. Charge carrier recombination rate constant was found to be much smaller in the device with Ca/Al cathode as compared to that with Al cathode. Energy band diagrams and interfacial chemical reactions were characterized using high-resolution SRPES. The results indicate that the Ca interlayer can induce the stronger dipole moment, which facilitates electrons collection and drives holes away at the cathode/polymer interface. The device performance was improved because of the lower recombination.

Exhibitor Technology Spotlight

Room: Hall ABC - Session EW-WeA

Exhibitor Technology Spotlight Session

Moderator: Chris Moffitt, Kratos Analytical Limited, UK

4:00pm **EW-WeA6 FOCUS beyond PEEM and NanoESCA, Dieter Pohlenz, M. Escher, M. Weber, FOCUS GmbH, Germany**

FOCUS is an owner-managed German company situated in Hünstetten close to Wiesbaden. Since its establishment in 1990, FOCUS has been engaged in the field of electron beam evaporation, electron spectroscopy and electron microscopy and in scientific apparatus construction generally. Most recent developed products are the focused VUV-source HIS 14 HD and the universal UHV Ion Source FDG 150. The HIS 14 HD source delivers a spot diameter of 300µm for angle resolved photoemission spectroscopy using technology developed at synchrotron beam lines. We list the mounting requirements and show first ARPES results. The FDG 150 is designed for depth profile analysis in XPS- and Auger Spectroscopy and charge neutralization (ESCA). Further applications are sample cleaning and sensor cleaning in scanning probe microscopy and the use as excitation source for ISS/LEIS analysis. The FERRUM spin polarization detector is the latest FOCUS product for spin analysis which can be combined with state of the art electron spectrometers.

In-Situ Spectroscopy and Microscopy Focus Topic

Room: 313 - Session IS+2D+MC+NS+SP+SS-WeA

In-Situ Scanning Microscopy

Moderator: Markus Ammann, Paul Scherrer Institut

2:20pm **IS+2D+MC+NS+SP+SS-WeA1 In Situ Studies of Model Fuel Cells, Zhi Liu, Lawrence Berkeley National Laboratory** **INVITED**

The ambient pressure x-ray photoelectron spectroscopy (AP-XPS) endstations based on differentially pumped electron energy analyzers have been recognized by scientific communities as an important in-situ tool to study water, environmental science, catalysis and many other important fields. Multiple new AP-XPS endstations are currently under planning or development at US and international synchrotron light sources. Recently we have installed a new hard x-ray AP-XPS endstation at ALS Beamline 9.3.1 (2.5keV- 5keV). By using X-ray up to 5KeV, we can perform AP-XPS at a pressure up to 110 torr. The probing depth of photoelectrons also increases to >10 nm, which will allow us to study not only the gas/solid interface but also the liquid/solid interface. In this talk, I will give an overview of science projects at ALS BL9.3.2 in heterogeneous catalysis and electro-chemistry using these new systems. Furthermore, I will present results of our in-situ study on the electrolyte/electrode interface of a working model electrochemical cell at ALS BL9.3.1. We believe the successful development of soft and hard X-ray APXPS endstations will provide energy research community a powerful in-situ tool to directly study the electrolyte/electrode interface of many important electrochemical devices.

3:00pm **IS+2D+MC+NS+SP+SS-WeA3 Probing of Nanoscale Objects in Reactive Liquids through Membranes using Near-Field Microwave Microscopy, Alexander Tselev, Oak Ridge National Laboratory, A. Komakov, National Institute of Standards and Technology (NIST)**

Many functional objects (and interfaces) have to be studied in situ when the object is immersed in liquid environment. In addition, for energy, chemical, (bio-) medical and other applications, there is a need to study the

encapsulated objects, which otherwise can be chemically reactive or toxic. These samples are often mesoscopically small or exist in minuscule quantities. Recently, we have developed a process for preparation of liquid-filled cells sealed with ultrathin membranes. Such cells can be implemented for in-situ studies using, for example, electronor soft x-ray microscopy due to a high transparency of these membranes to electron beams. However, in many cases electron microscopy is an invasive technique due to various electron beam induced parasitic effects (e.g. radiolysis or beam induced deposition). To overcome these impediments, we demonstrate the scanning microwave impedance microscopy (sMIM) to image different nanoscale objects immersed in the liquid environment through 30 nm SiN membranes. In the sMIM, microwaves of a frequency of 3 GHz are sent through a coaxial cable connected to a shielded cantilever probe fully compatible with an AMF microscope. The sharp probe tip provides "focusing effect" for the electric component of the microwave. For imaging, the tip is brought into gentle mechanical contact with a membrane. Amplitude and phase of microwaves reflected from the probe are monitored. Since the wave reflection is dependent on the tip-sample system impedance, reflected waves carry information about sample local properties. The effective distance into the sample depth, where the tip-induced field enhancement takes place, is approximately equal to the tip apex radius. Since the membrane thickness is smaller compared to the tip radius of a typical probe (about 50 nm for a fresh tip), the tip-sample impedance is dependent on the dielectric properties of the material beneath membrane, and therefore, it is possible to "see" through the membrane. We demonstrate imaging of different combinations of model liquids and nanoparticles: water and water-based solutions ($\epsilon \sim 80$), organic solvents ($\epsilon \sim 10-25$), and oils ($\epsilon \sim 2-3$) containing Ni metal, polystyrene ($\epsilon \sim 2.5$) and PbO ($\epsilon \sim 25$) particles. This technique can be further implemented for a broad range of objects in confined liquids, and can be used to monitor interfacial electrochemical reactions. Imaging with sMIM was performed at CNMS, which is sponsored at ORNL by the SUFD, BES, US DOE.

4:20pm **IS+2D+MC+NS+SP+SS-WeA7 Caught in the Act! Live Observations of Catalysts Using High-Pressure Scanning Probe Microscopy, Irene Groot, Huygens-Kamerlingh Onnes Laboratory, Leiden University, Netherlands** **INVITED**

Recently it has become clear that essential differences can exist between the behavior of catalysts under industrial conditions (high pressure and temperature) and the (ultra) high vacuum conditions of traditional laboratory experiments. Differences in structure, composition, reaction mechanism, activity, and selectivity have been observed. These observations indicated the presence of the so-called pressure gap, and made it clear that meaningful results can only be obtained at high pressures and temperatures. However, most of the techniques traditionally used to study catalysts and their reactions were designed to operate under (ultra) high vacuum conditions. To bridge the pressure gap, the last years have seen a tremendous effort in designing new instruments and adapting existing ones to be able to investigate catalysts *in situ* under industrially relevant conditions.

This talk focuses on the development of scanning probe microscopy for *operando* observations of active model catalysts. In our group, we have developed set-ups that combine an ultrahigh vacuum environment for model catalyst preparation and characterization with a high-pressure flow reactor cell, integrated with either a scanning tunneling microscope or an atomic force microscope. With these set-ups we are able to perform atomic-scale investigations of well-defined model catalysts under industrial conditions. Additionally, we combine the structural information from scanning probe microscopy with time-resolved mass spectrometry measurements on the gas mixture that leaves the reactor. In this way, we can correlate structural changes of the catalyst due to the gas composition with its catalytic performance.

This talk highlights a short overview of the instruments we developed and illustrates their performance with results obtained for different model catalysts and reactions. As a proof of principle, results for the fruit fly of surface science, *i.e.* CO oxidation, will be shown. But additionally, results for more complex reactions such as NO reduction, Fischer-Tropsch synthesis, desulphurization, and production of chlorine will be discussed.

5:00pm **IS+2D+MC+NS+SP+SS-WeA9 X-ray Photoelectron Spectroscopy Studies of H₂O Dissociation on Pre-oxidized Al (111) and Cu (111) Single Crystal Surface, Qianqian Liu, SUNY, Binghamton University, X. Tong, Brookhaven National Laboratory, G.W. Zhou, SUNY, Binghamton University**

Dissociation of H₂O molecules on ultrathin oxide overlayers formed on metal surfaces plays a critical role in many catalytic reactions. However, the effects of chemical states and thickness of oxide overlayers on the microscopic process of H₂O dissociation are still poorly understood. In this work, X-ray photoelectron spectroscopy (XPS) is employed to study H₂O dissociation on oxidized Al (111) and Cu (111) surfaces with controlled

chemical states and thicknesses of the oxide films. For Al (111), the experiment was performed under two water vapor pressures (10⁻⁶ Torr and 5 Torr) on aluminum oxide films with the thicknesses varying from 2.47 Å to 5.14 Å; for Cu (111), the experiment was performed by varying the water vapor pressure from 10⁻⁷ Torr to 10⁻⁵ Torr and temperature from 100°C to 450°C on the oxide film with a constant thickness. Al (2p), Cu (2p), Cu (LMM) and O (1s) spectra were monitored by XPS after each oxygen exposure followed by subsequent H₂O exposure. Upon exposing the oxide to water vapor, the O (1s) peak shifts to a higher energy and becomes broader. A detailed analysis of the spectra indicates that H₂O molecules dissociate into OH groups for both oxidized Al and Cu surfaces. However, the subsequent reaction of OH groups with the oxide films on Cu (111) and Al (111) surfaces are dramatically different. On the oxidized Al(111) surface, OH is further incorporated into the aluminum oxide that results in the thickening of the oxide film, whereas on the oxidized Cu (111) surface, OH works as a reducing agent to remove oxygen from the oxide film that results in the thinning of the Cu oxide film. The microscopic processes underlying the differences in H₂O dissociation on oxidized Al (111) and Cu (111) will be described in detail.

5:20pm **IS+2D+MC+NS+SP+SS-WeA10 Operando APXPS of the Liquid-Solid Interface: Au Oxidation, Ethan Crumlin, S.A. Axnanda, P.N.R. Ross, Z.L. Liu, Lawrence Berkeley National Laboratory**

Interfaces play an important role for many reaction processes and are essential for electrochemistry. Electrochemical systems ranging from high temperature solid oxide fuel cells (SOFC) to lithium ion batteries to capacitors have a wide range of important interfaces between solids, liquids, and gases which play a pivotal role in how energy is stored, transferred, and/or converted. Previous capabilities of ambient pressure X-ray Photoelectron Spectroscopy (APXPS) have primarily only been able to observe the gas-solid and gas-liquid interfaces. However, recent enhancements now enable new APXPS systems to work at pressures larger than 20 Torr, and utilize 'Tender' X-rays (2.5 – 7 keV). These features provide new capabilities and opportunities for probing the liquid-solid and solid-solid interfaces. Using synchrotron X-rays at Lawrence Berkeley National Laboratory, the Advanced Light Source and our 'Tender' X-ray APXPS endstation that is outfitted with various *in situ/operando* features such as electrical leads to apply electrical potentials and operates at pressures >20 Torr, to observe the liquid-solid interface of a gold foil electrode that has been immersed and partially removed from a liquid electrolyte. This talk will provide details on how we used this technique to probe liquid-solid interface and in real-time observe the oxidation of the gold foil electrode under varying applied potentials and different electrolyte solutions.

5:40pm **IS+2D+MC+NS+SP+SS-WeA11 Water on ZnO(10-10) Investigated by Ambient Pressure X-ray Photoelectron Spectroscopy, Chris Goodwin, University of Delaware, A. Boscoboinik, Brookhaven National Lab, C. Arble, J.T. Newberg, University of Delaware**

The extent to which ZnO hydroxylates under ambient conditions can significantly influence catalytic properties. Thus, it is critical to understand the composition of different ZnO terminations as a function of relative humidity (RH) in order to elucidate the true interfacial surface terminations. In this talk we present results of ambient pressure XPS (APXPS) for water exposures to a ZnO(10-10) single crystal. It will be shown that ZnO(10-10) extensively hydroxylates at the interface, and both molecular and dissociative water increase as the RH increases. These results are consistent with simulations in the literature that highlight the efficacy for ZnO(10-10) to dissociate water.

MEMS and NEMS

Room: 301 - Session MN+PS-WeA

Emerging Materials and Fabrication Technologies for MEMS/NEMS

Moderator: Sushma Kotru, The University of Alabama, Meredith Metzler, Cornell University

2:20pm **MN+PS-WeA1 Organic Sensors and Actuators Patterned by Inkjet Printing, Tse Nga (Tina) Ng, PARC (Palo Alto Research Center), a Xerox Company, J. Kim, W.S. Kim, Simon Fraser University, Canada, K.S. Kwon, Soonchunhyang University, South Korea** **INVITED**

Organic materials have been demonstrated as good candidates for large-area sensors, because they allow wide tolerance of sensor geometry and thickness, which would ease fabrication problems such as strain induced cracking on deformable plastic platforms. Organic electronic materials can

be deposited and patterned by low-cost printing tools such as inkjet printers. Notably, the printing process is compatible with many substrates ranging from plastics to fibers, to potentially integrate electronics on any surface. At Palo Alto Research Center, we have developed processes for printed electronics that enable new form factors and applications in flexible sensors and circuits. In conjunction with university collaborators, here we present examples of organic mechanical sensors and actuators fabricated by facile solution processes.

The first example is a capacitive pressure sensor patterned by block copolymers. Different microstructures (hemisphere, cones, nano-needles) are explored for the dielectric film, and the dielectric with nano-needles showed the highest sensitivity, with the relative capacitance change up to 176%/kPa. The capacitor with the nano-needle filler was integrated with an inkjet printed OTFT to provide current output. The device sensitivity is comparable to the sensitivity of human skin and will be useful for tactile sensing applications on a wide range of surfaces.

In a second example, we have fabricated a bimorph actuator from electroactive polymer blends with ionic liquid. The polymer blends allow low-voltage operation, and we found that the actuator displacement increases with larger gradient difference in ionic liquid content. A maximum strain of 0.48% was observed. The electroactive polymers are compatible with extrusion printing and have the potential to be patterned through layer-by-layer printing for incorporation into 3d structures.

3:00pm MN+PS-WeA3 Microfabrication by Etching for Carbon Nanotube Composite Sheets, Nathan Boyer, J. Rowley, D.D. Allred, Brigham Young University, S. Liddiard, Moxtek, Inc, R.R. Vanfleet, R.C. Davis, Brigham Young University

We have prepared extremely smooth carbon nanotube (CNT)/polymer composite sheets and patterned them with holes and trenches using a process of photolithography and plasma etching. The high strength patterned CNT/polymer composite could be used in MEMS applications. A CNT sheet was impregnated with polyimide and the composite was cured in a vacuum hot press at 400°C. A film of amorphous silicon nitride was deposited on the composite sheet and patterned to act as a hard mask during oxygen plasma etching. Structural and mechanical testing of the CNT composite sheets will be presented along with plasma etching results.

3:20pm MN+PS-WeA4 High Aspect Ratio Magnetic MEMS Fabricated using Carbon Nanotube Templated Microfabrication, Robert Davis, L. Barrett, D. Barton, R.R. Vanfleet, D.D. Allred, Brigham Young University

We have fabricated nickel microstructures with aspect ratios greater than 20-1, and feature sizes as small as 5 μm . The process involves growing a forest of carbon nanotubes in the desired pattern, and coating the tubes with an additional layer of carbon by CVD. Then the remaining space in the forest, approximately 90%, is filled with nickel by pulsed electroplating. Because the resulting composite has a magnetic response, it is ideal for MEMS magnetic sensors and actuators. To demonstrate this, we constructed a simple MEMS scale sensor with a frame, two flexures and a proof mass. Optical measurement of the proof mass's displacement as a function of applied magnetic field will be shown.

4:20pm MN+PS-WeA7 Sub-100nm Thin Polycrystalline Diamond Nanomechanical Torsional Resonators, Rui Yang, Z. Wang, J. Lee, C.A. Zorman, P.X.-L. Feng, Case Western Reserve University

We report experimental demonstration of high-frequency (HF) torsional nanomechanical resonators based on nanoscale polycrystalline diamond thin films. We fabricate devices with tethers as thin as 100nm \times 50nm in cross section, measure their multi-mode resonances with frequency (f_{res}) into the HF band (up to \sim 10MHz, while most existing sensitive torsional devices are at kHz or low-MHz), and quality (Q) factors exceeding 2000 at room temperature. We also perform temperature-varying measurements, and observe strikingly different temperature coefficients of frequency (TCf) between the torsional and flexural resonant modes.

Diamond is particularly interesting for micro/nanoelectromechanical systems (MEMS/NEMS), because of its exceptional mechanical properties (Young's modulus greater than 10^{12} Pa), relatively low mass density (3500kg/m³), very high thermal conductivity (22W/(cm-K)), and excellent wear/corrosion resistivity¹. Especially, its high sound velocity is attractive for making high frequency mechanical resonators². Resonators based on diamond thin films from microwave plasma chemical vapor deposition have been demonstrated, showing mechanical properties comparable to single crystal. However, *torsional resonators* based on diamond thin films showing resonance in HF band and exceptional force and torque sensitivities have not been explored. While we demonstrated torsional resonators using 1.2 μm -thick SiC film³, *much thinner and smaller devices* are required for higher sensitivities.

Here we fabricate torsional resonators on 50 to 100nm thin polycrystalline diamond films with focused ion beam. We perform Raman spectroscopy to confirm the nanocrystalline diamond nature of the membrane. The mechanical resonances are measured by driving the mechanical motion with a modulated laser (405nm), and detecting the resonant motion with laser interferometry (633nm). These devices show force sensitivity down to the sub-fN/ $\sqrt{\text{Hz}}$ range, and torque sensitivity on the order of 10^{-22} (N $\cdot\text{m}$)/ $\sqrt{\text{Hz}}$, which is similar to the best reported results in other materials⁴. This opens up the possibility for fabricating ultrasensitive devices for force/torque, inertia, and thermal sensing, based on nanocrystalline diamond platform. TCf measurement shows clear and intriguing anti-crossing behavior, which vividly illustrates cross-mode mechanical coupling.

¹ O. Auciello, *et al.*, *J. Phys.-Condens. Mat.* **16**, R539 (2004).

² L. Sekaric, *et al.*, *Appl. Phys. Lett.* **81**, 4455-4457 (2002).

³ R. Yang, P. X.-L. Feng, *et al.*, *Appl. Phys. Lett.* **104**, 091906 (2014).

⁴ X. C. Zhang, *et al.*, *Nano Lett.* **13**, 1528 (2013).

4:40pm MN+PS-WeA8 Temperature Compensated Graphene Nanomechanical Resonators, Jaesung Lee, Case Western Reserve University, H.-Y. Chiu, University of Kansas, P.X.-L. Feng, Case Western Reserve University

Graphene-based atomically-thin two-dimensional (2D) nanostructures have emerged as new building blocks for novel nanoelectromechanical systems (NEMS) [1], which can enable nanodevices with unprecedented performances such as ultrasensitive detectors and highly tunable oscillators [2]. In addition to its excellent mechanical properties, such as ultralow areal density ($r_A=0.74\text{fg}/\mu\text{m}^2$), ultrahigh strain limit (\sim 25%), and large Young's modulus ($E_Y\sim$ 1TP), graphene has superior thermal properties, which can enable large temperature range operations and ultra-stable high temperature performances. In addition, the unique negative thermal expansion coefficient of graphene can be employed to tune the device tension and thus its resonance behavior through controlling the device temperature. To date, most experimental investigations of graphene resonators are at room temperature or below, with high temperature operation remaining largely unexplored.

In this work, we experimentally study graphene resonators from room temperature to \sim 600K and study their resonance characteristics by measuring the thermomechanical noise. Our graphene resonators show relatively small frequency shifts from 300K to 600K due to natural temperature compensation from the different thermal expansion coefficients of graphene and other structural metals. We further examine temperature profile in graphene resonators, and establish resonator models with wide range temperature operation, elucidating temperature compensation mechanisms in graphene resonators. This study will help improve the understanding and development of both temperature-sensitive and insensitive 2D NEMS resonators, which can lead towards future large temperature range and high temperature application of 2D NEMS.

References:

[1] J. Lee, P. X.-L. Feng, *IEEE International Frequency Control Symposium (IFCS'12)*, DOI: 10.1109/IFCS.2012.6243742 (7 pages), Baltimore, MD, May 21-24 (2012).

[2] C. Chen, J. Hone, *Proc. IEEE* **101**, 1766-1779 (2013).

[2] C. Chen, S. Rosenblatt, K. I. Bolotin, W. Kalb, P. Kim, I. Kymissis, H. L. Stormer, T. F. Heinz, and J. Hone, *Nature Nanotech.* **4**, 861- 867 (2009).

5:00pm MN+PS-WeA9 A Porous Material for Improving Cantilever Q in Air and Liquid for Resonant Mechanical Sensing, Steven Noyce, R.C. Davis, R.R. Vanfleet, Brigham Young University, H.G. Craighead, Cornell University

Nanoporous cantilever resonators have potential performance advantages for cantilever based sensing. For porous cantilevers a high surface area leads to a high adsorbed mass which is independent of the cantilever dimensions. Larger cantilever dimensions can lead to higher quality (Q) factors in air and liquid sensing environments. Here we present work on the fabrication of nanoporous carbon/carbon nanotube composite cantilevers. Our results include characterization work on tuning the composite materials properties and cantilever geometries for high Q in fluid.

5:20pm MN+PS-WeA10 XPS to Investigating Spatial and Temporal Modification of PDMS Platforms for Micro-Fluidic Devices, Marshal Dhayal, CSIR- Centre for Cellular and Molecular Biology, India

Spatial and temporal changes in surface chemical composition silicon (Si), carbon (C) and oxygen (O) of polydimethyl siloxane (PDMS) surfaces before and after plasma treatment were estimated from quantitative elemental analysis of X-ray photoelectron spectroscopy (XPS) wide scan

spectra. Theoretical ratio of Si/C/O in repeating unit $[-Si-(CH_3)_2-O]_n-$ of PDMS were calculated and were compared to experimentally obtained ratio for Si/C/O obtained from untreated and plasma PDMS surfaces used for micro-fluidic devices. The contact angle measurements have shown that (PDMS) surfaces treated by air plasma can recover up to about 50% of its hydrophobic nature in less than 30 min of air exposure. These plasma modified surfaces were functionalized with poly(ethylene glycol) (PEG) silane to obtain PDMS surface as hydrophilic in nature for micro fluidic application. The surface chemistry of PEG-functionalized PDMS substrate has been studied using XPS. These different types of surfaces were used fabricate micro-fluidic devices and effects of surface nature of micro channels on fluid velocity were observed in PEG grafted micro channel in PDMS base micro fluidic devices. The effect of different pH of the fluids on the fluid velocity in PDMS-based micro channel was also studied.

5:40pm **MN+PS-WeA11 A Microplasma-based Sputtering System for Direct-Write, Micropatterning of Metal Structures**, *Edwin Burwell, A.C. Barnes, P.X.-L. Feng, M. Sankaran, C.A. Zorman*, Case Western Reserve University

Patterning metal as a contact or interconnect is a critical processing step for device fabrication in a wide range of applications ranging from conventional electronics on silicon chips to implantable biosensors on flexible polymeric substrates. Traditionally, physical vapor deposition is combined with photolithography to deposit patterned metal films. Although this subtractive approach produces high pattern fidelity and conductivity, low throughput, materials wastage, and need for vacuum lead to high production costs and limited scalability. The emergence of flexible devices has stimulated the desire for additive approaches such as ink-jet printing for depositing patterned conductive materials. Ink-based printing is carried under ambient conditions and can be integrated with roll-to-roll systems for large-scale manufacturing. However, the inks can be expensive and the variety of materials that are available as printable inks is very small. In addition, the organic capping agents that are used to stabilize the particles are difficult to remove, which can compromise conductivity and mechanical integrity. Removal of the organics requires high annealing temperatures that limit the usage of certain polymers and other temperature-sensitive substrates. Adhesion of the printed structures to the substrates can also be a significant issue, especially in flexible applications.

In this paper, we describe a microplasma-based process to deposit patterned structures with micro- to nanoscale dimensions on rigid or flexible conducting and insulating substrates. This direct-write, additive process uses plasma-based sputtering to generate a physical vapor comprised of the material of interest. The plasma is generated within a small capillary tube that is capped with a micron-sized orifice. The sputtering target consisting of a micron-sized wire is positioned inside the capillary. Forced Ar flow aids in the ejection of the resulting physical vapor through the orifice, which is positioned in close proximity to the substrate. The process is performed at atmospheric pressure, thereby addressing the most significant limitation associated with conventional magnetron sputtering and thermal evaporation, and is low temperature, allowing deposition on temperature-sensitive substrates such as polymers and paper. To date, we have successfully deposited patterned Au structures that are submicron in thickness and 150 microns in width on glass substrates. Our presentation will detail the apparatus, the principal of operation, and the most current results in creating and characterizing micropatterned metal structures on insulating substrates.

Manufacturing Science and Technology

Room: 302 - Session MS+TF-WeA

Overview: Applications and Manufacturing of Devices on Paper and Textiles

Moderator: Liangbing Hu, University of Maryland, College Park, Bridget R. Rogers, Vanderbilt University

2:20pm **MS+TF-WeA1 Challenges and Opportunities in the Production of Cellulose Nanomaterials**, *Junyong Zhu*, USDA Forest Products Lab **INVITED**

Cellulose nanomaterials has attracted great attention in the scientific community due to its unique optical and mechanical properties along with its renewability and abundance. However, the production process is very costly using current technologies, which limited its use to high value products. This created a market mismatch, i.e., a very large amount natural cellulose are available. In this presentation I will outline the challenges in reducing the cost of cellulose nanomaterials. At the same time, I provide some opportunities to reduce the cost. I will specifically outline a few

process innovation in our laboratory for both cellulose nanocrystal and cellulose nanofibril productions

3:00pm **MS+TF-WeA3 Engineering Cellulose Nanomaterial Substrates for Flexible Electronics**, *Y. Zhou, C. Fuentes-Hernandez, T. Khan*, Georgia Institute of Technology, *J.-C. Liu, J. Diaz*, Purdue University, *J. Hsu, J. Shim, A. Dindar*, Georgia Institute of Technology, **Robert Moon**, US Forest Service-Forest Products Laboratory, *J. Youngblood*, Purdue University, *B.J. Kippelen*, Georgia Institute of Technology **INVITED**

Fabrication of flexible electronics (e.g. solar cells) on recyclable and biodegradable substrates are attractive for the realization of a sustainable technology, but significant advances are required to make the technologies economically viable and, from a life-cycle perspective, environmentally friendly, and consequently scalable. One of the key areas of research for making this a reality is in the design/engineering of suitable substrate materials that can: mechanically and chemically support the given electronics, have sufficient surface features (low roughness, surface chemistry, etc) to facilitate the process of the electronics, have similar thermal expansion characteristics of the electronics to minimize stress at the substrate-device interface, have the desired optical transmittance for device performance or application of product, and facilitate the recovery of the electronic components during the recycling process, to name a few. Our recent work has focused on the development cellulose nanocrystals (CNCs) based substrates for such applications. Cellulose nanomaterials (CNM) are emerging high-value nanoparticles extracted from plants that are abundant, renewable, and sustainable. CNCs are rod-like nanoparticles of about 4-10 nm in diameter and 50-400 nm in length and through solvent casting of aqueous suspensions, transparent substrates suitable for electronic devices can be produced. By adjusting the suspension composition, pH, application of shear (control CNC alignment), drying conditions and heat treatment, have been identified as relevant factors affecting the final film/substrate properties.

This talk will provide a general introduction and review of the current state of art in cellulose nanomaterials, their use as substrate materials for flexible electronics, and summarize our work on the measurement of thermo-mechanical properties of CNC-based substrate materials and the development of efficient polymer solar cells fabricated on optically transparent CNC substrates.

4:20pm **MS+TF-WeA7 Circuits on Cellulose: From Transistors to LEDs, from Displays to Microfluidics on Paper**, *Andrew Steckl*, University of Cincinnati **INVITED**

Organic electronics is a rapidly growing field due to a combination of strong performance from improving materials with the low fabrication cost associated with large area printing technology. Recently, the incorporation into organic electronic technology of natural biomaterials that are renewable and biodegradable is being increasingly investigated with the goal of producing "green" electronics that is environment-friendly.

In this presentation, a review is given on the use of cellulose-based paper as a material in a variety of electronic (and related) applications, including transistors, light emitting diodes, displays, microfluidics. Paper is a very attractive material for many device applications: very low cost, available in almost any size, versatile surface finishes, portable and flexible. From an environmental point of view, paper is a renewable resource and is readily disposable (incineration, biodegradable). Applications of paper-based electronics [1,2] currently being considered or investigated include biochips, sensors, communication circuits, batteries, smart packaging, electronic displays. The potential advantages of paper-based devices are in many cases very compelling. For example, lab-on-chip devices fabricated on paper for bio/medical applications [3] use the capillary properties of paper to operate without the need of external power sources, greatly simplifying the design and reducing the cost. Specific examples of paper-based devices will be discussed, including organic light emitting diodes [4] (OLED) and field effect transistors [5] (OFET) on flexible and transparent paper, medical diagnostic devices utilizing lateral capillary flow on paper.

1. D. Tobjork and R. Osterbacka, "Paper electronics". *Adv Mater* **23**, 1935, doi:10.1002/adma.201004692 (2011).
2. A. J. Steckl, "Circuits on Cellulose", *IEEE Spectrum* **50** (2) 48, doi:10.1109/MSPEC.2013.6420146 (2013).
3. Rolland, J. P. & Mourey, D. A. "Paper as a novel material platform for devices", *MRS Bulletin* **38**, 299, doi:10.1557/mrs.2013.58 (2013).
4. S. Purandare, E. F. Gomez and A. J. Steckl, "High brightness phosphorescent organic light emitting diodes on transparent and flexible cellulose films", *IOP Nanotechnology*, **25**, 094012, doi 10.1088/0957-4484/25/9/094012 (March 2014).
5. A. Zocco, H. You, J. A. Hagen and A. J. Steckl, "Pentacene organic thin-film transistors on flexible paper and glass substrates", *IOP*

5:00pm **MS+TF-WeA9 Cellulose Nanostructures for Energy Devices and Flexible Electronics**, *H.L. Zhu, W. Bao, F. Shen, Y. Li, Z. Fang, Liangbing Hu*, University of Maryland, College Park **INVITED**

I will discuss our recent results and the fundamental science of novel transparent paper with tailored optical and mechanical properties, and applications in flexible electronics, origami devices and solar cells. I will also discuss the fundamental advantages of using mesoporous, soft wood fibers for low-cost Na-ion batteries.

5:40pm **MS+TF-WeA11 Designing Functional Paper for Emerging Electronics and Energy Devices**, *Hongli Zhu, L.B. Hu*, University of Maryland, College Park

The natural wood fiber has a hierarchical structure with one regular fiber consisting of numerous smaller fibers, and these small nanofibers can be disintegrated from the microfiber with chemical and mechanical treatment. By integrating electronically conductive material, we apply the low cost and sustainable biomaterial in the electronics and energy storage devices. In the first part, we will introduce a novel transparent paper made of wood fibers that displays both ultrahigh optical transparency (~96%) and ultrahigh haze (~60%), thus delivering an optimal substrate design for solar cell devices. We will also introduce the flexible transparent organic field-effect transistors (OFETs) and organic light emitting diode (OLED) device fabricated on nanopaper. These studies are important for the future development of flexible electronics based on new transparent substrates made from sustainable cellulose instead of plastic. In the second part, we will discuss wood fiber based batteries. The wood fibers are intrinsically porous and soft. Thin film Sn anodes deposited onto wood fibers sustain more than 400 charging/discharging cycles, a new record for Sn anodes in Na-ion batteries. Additionally, dual ion transport pathways within the mesoporous structure of wood cellulose fibers significantly improve the traditionally slow ion transport in Na-ion batteries.

6:00pm **MS+TF-WeA12 Transparent Films of Cellulose Nanocrystals Derived from Waste Cotton T-shirts**, *Nasim Farahbakhsh, J.S. Jur, R.A. Venditti*, North Carolina State University

The hierarchical structure of cellulosic materials is a renewable building block for a wide range of novel applications, including electronic devices. In this work we present on the fabrication of the transparent cellulose nanocrystal (CNC) thin films for flexible electronic applications. The CNC platforms were manufactured from waste cotton T-shirts fibers using sulphuric acid at optimum reaction temperature and acid concentration. The derivation of nanocellulose from cotton fibers beneficial due to a high cellulose content (~95%) and high crystalline structure which results in high yield without any intensified purification process. The resultant CNC particles, with an average diameter of 25 nm with average length of 200 nm, are used to produce transparent free-standing films and spun-cast films on silicon. Opportunities related device fabrications are presented.

Nanometer-scale Science and Technology

Room: 304 - Session NS+AS-WeA

Nanoscale Imaging and Materials Characterization

Moderator: Craig Prater, Anasys Instruments, Paul Sheehan, Naval Research Laboratory

2:20pm **NS+AS-WeA1 2014 AVS Albert Nerken Mark Award Lecture - Brilliant Nanodiamond Particles**, *Olga Shenderova**, Adamas Nanotechnologies Inc., *G.E. McGuire*, International Technology Center **INVITED**

Despite that nanodiamond (ND) particles were discovered more than 50 years ago and were mass produced in the early 80s, for a long time they were in the shadow of their more famous sp² carbon cousins. Two recent major breakthroughs, production of individual 4-5nm particles and particles containing colour centres exhibiting stable luminescence and unique spin properties have brought ND particles to the forefront of materials research.¹ Nanometer size particles are produced by detonation of carbon-containing explosives or by grinding of microdiamond powders. Besides well-known outstanding mechanical and thermal properties, diamond particles have remarkable optical properties in combination with biocompatibility, high specific surface area, and tuneable surface structure. Applications of ND

which have captivated the imagination of scientist in areas which have broad societal impact, such as energy preservation and biomedical imaging, will be briefly illustrated and a more in-depth review of their optical properties provided.

The optical emission, scattering and attenuation of ND are finding unique applications. In life sciences nanoparticles are increasingly used as fluorescent probes to monitor cellular interactions and study cellular dynamics at the single molecular level. Foreign atoms can be incorporated into the lattice of ND particles providing photostable particles as well as systems for quantum sensing that may be used to probe the intracellular environment at the nanoscale. Development of multimodal imaging probes based on 5-10nm ND and doping of ND with different elements to generate photoluminescence at alternative wavelengths are future directions for this field. Carbon dot-decorated ND is another means of generating photoluminescent nanoparticles with tuneable emission over the visible to near-infrared portion of the electromagnetic spectrum. The photoluminescent ND is increasingly being viewed as a means of drug delivery. Encapsulating ND in a porous silica shell is a means of achieving stable fluorescent imaging with nanoparticles with a high loading capacity for bioactive molecules.

Due to its high refractive index, wide bandgap and crystalline lattice, ND highly attenuates and scatters ultraviolet radiation. High attenuation and scattering in combination with large surface area has been shown as a means of increasing the radiation resistance of polymer nanocomposites. This can be beneficial in sunscreens as well as in polymers used in the construction of satellites to be placed in low Earth orbit.

¹V.Mochalin, O.Shenderova, D.Ho and Y.Gogotsi, "The properties and applications of nanodiamonds", (2012) *Nature Nanotechnology*, 7 (1) 11-23.

3:00pm **NS+AS-WeA3 Oxidation State Sensitive Imaging of Ceria Nanoparticles**, *Aaron Johnston-Peck*, National Institute of Standards and Technology (NIST)

Scanning transmission electron microscopy (STEM) coupled with electron energy loss spectroscopy (EELS) has been successfully applied to track changes to composition as well as bonding environment with atomic resolution. These measurements impose exacting experimental and instrumentation requirements that include aberration-corrected optics, electron sources with narrow energy spreads, and extremely stable room environments. Therefore it seems prudent when possible that other techniques with less demanding experimental requirements supplement EELS measurements. Imaging or diffraction techniques greatly relax these aforementioned requirements as the need for corrective optics and narrow energy spreads can be eliminated. Moreover the possibility of beam induced artifacts is reduced because the total electron dose needed to form an image or diffraction pattern is less than an EELS spectrum image.

Low angle annular dark field (LAADF) STEM is presented as an alternative to EELS measurements to identify changes to local changes of oxidation state in ceria (CeO₂) nanoparticles. This relationship was established through the use of EELS, *in-situ* measurements, and image simulations. Ceria has numerous energy related applications due to the ability of ceria readily store and release oxygen. The formal charge of the cerium ions transition from 4+ to 3+ as oxygen vacancies are formed. These oxygen vacancies cause local distortions to the crystal and subsequently produces additional diffuse scattering to low angles. The LAADF STEM signal is sensitive to this change in scattering and contrast variations in the image become resolved. Additionally, preliminary experiments on other metal oxide nanoparticles suggest that this approach may be applied to other material systems and processes as well.

3:20pm **NS+AS-WeA4 Shape and support interaction of size-selected Pd and Pt NPs on TiO₂(110)**, *Mahdi Ahmadi, F. Behafarid*, University of Central Florida, *B. Roldan Cuenya*, Ruhr-University Bochum, Germany

The shape and the support interaction of 3D palladium and platinum nanoparticles (NPs) deposited on TiO₂(110) was investigated using scanning tunneling microscopy (STM). The NPs were synthesized using inverse micelle encapsulation. In spite of the initial random location of the micelle-prepared NPs on the support, step edge decoration was observed after annealing at high temperature (>1000°C). In general, resolving the shape of 3D NPs using STM is very challenging due to the tip-convolution effects. However, a combination of ultra-sharp STM tips and samples containing structurally well-defined NPs allowed us to resolve the NP shape, with the highest features on the NPs being unaffected by tip artifacts. It was found that all NPs had a truncated octahedron shape, with {111} top and interfacial facets. Furthermore, the alignment of the NP edges (or symmetry axes) with the TiO₂(110)-[001] atomic rows evidenced the epitaxial relationship with support achieved after annealing. The STM data were analyzed following the Wulff-Kaischew theorem, and a MATLAB code was used to reconstruct the NP shape, eliminating overestimations in

* Albert Nerken Award Winner

the lateral size inherent to the STM technique due to tip effects. The surface energy ratio $\gamma_{100}/\gamma_{111}$ was calculated for each Pd NP with an average value of 1.12 ± 0.07 , which is in good agreement with theoretical values. Moreover, the adhesion energy was found to display a size-dependence, with larger NPs having smaller adhesion energy. This phenomenon can be explained based on the minimization of the interfacial strain by reducing the contact area. Following similar analysis of Pt NPs on $\text{TiO}_2(110)$, a higher $\gamma_{100}/\gamma_{111}$ ratio of 1.18 ± 0.1 was obtained as compared to Pd. Also, the rate of decrease in the adhesion energy with increasing NP height was lower for Pt as compared to Pd.

4:20pm NS+AS-WeA7 Nanoscale Imaging and Spectroscopy of Plasmonic Hot Spots and Dark Modes with the PTIR Technique, Andrea Centrone, National Institute of Standards and Technology (NIST) INVITED

Localized surface plasmon resonances couple propagating light with nanoscale volumes of matter (hot-spots), enabling new applications in sensing and therapeutics. Surface-Enhanced Infrared Absorption (SEIRA) Spectroscopy exploits such hot-spots for sensitive chemical detection. Calculations predict large SEIRA enhancement factors but the diffraction of long IR wavelengths ($2 \mu\text{m} - 16 \mu\text{m}$) has hindered the experimental determination of SEIRA enhancements with nanoscale resolution.

Photo Thermal Induced Resonance (PTIR) combines the chemical specificity of IR spectroscopy with the lateral resolution of Atomic Force Microscopy (AFM). PTIR circumvents the limitations of light diffraction by employing an AFM tip as a local detector for measuring the transient thermal expansion induced by the absorption of light pulses in the sample. Local IR spectra and composition maps are obtained recording the amplitude of the tip deflection as a function of the laser wavelength and position, respectively. Notably, the PTIR signal is proportional to the absorbed energy (not scattering) and the PTIR spectra are directly comparable with IR spectral libraries, enabling materials identification.

In this work, the PTIR technique is applied to image the dark plasmonic resonance of gold Asymmetric Split Ring Resonators (A-SRRs) in the mid-IR with nanoscale resolution. Additionally, the chemically-specific PTIR signal is used to map the local absorption enhancement of PMMA coated A-SRRs, revealing hot-spots in the resonators' gaps with enhancement factors up to ≈ 30 .

The local information gathered with in the PTIR experiments can provide insightful information and possibly help to engineer nanomaterials for greatest efficacy. As an additional example the PTIR technique will be applied to image phase separated domains in Metal-Organic Frameworks single crystals, a novel class of materials that find application in catalysis, sensing and separation.

5:00pm NS+AS-WeA9 AFM-based Infrared Spectroscopy—Nanoscale Chemical Analysis with Sensitivity Down to Single Monolayers, Craig Prater, K. Kjoller, M. Lo, E. Dillon, R. Shetty, Anasys Instruments, C. Marcott, Light Light Solutions, F. Lu, M. Jin, M. Belkin, University of Texas at Austin, A. Dazzi, Université Paris-Sud, France

The ability to perform chemical analysis at the nanoscale has been considered one of the "holy grails" of the scanning probe microscope community. Many techniques have been developed to provide material contrast in SPM images based on a variety of properties (electronic, optical, mechanical, etc.), but there had not been the ability to perform broadly applicable chemical analysis on diverse samples. We have developed AFM-based infrared spectroscopy (AFM-IR)¹ that enables broadly applicable chemical analysis on samples with nanoscale spatial resolution and with sensitivity down to the scale of individual molecular monolayers. The AFM-IR technique illuminates a sample with light from a tunable infrared laser source and then uses the tip of an AFM to measure the sample's local photothermal expansion due to the absorption of infrared light at specific wavelengths.² Measuring absorption as a function of wavelength creates an IR absorption spectrum that acts as a chemical fingerprint to characterize and identify chemical components. Mapping IR absorption spatially over a sample at different wavelengths can be used to create maps of nanoscale chemical composition. Recently we have implemented two techniques to extend both the applicability and sensitivity of the AFM-IR technique. First, we implemented top side illumination to enable AFM-IR on a much wider array of samples and sample substrates. Second, we developed a resonance enhanced mode³ where the IR laser pulses are synchronized to a contact resonance of the AFM cantilever. Combined with "lightning rod" enhancement of the incident IR light, the resonance enhanced technique can achieve chemical analysis with single monolayer sensitivity⁴ and spatial resolution ~ 25 nm. We will describe the AFM-IR technique, recent innovations and applications in materials, life sciences, photonics, and semiconductors.

References:

1. A. Dazzi, R. P., F. Glotin, and J. M. Ortega. *Opt. Lett.* 2005, 30, 2388-2390.
2. Dazzi, A.; Prater, C. B.; Hu, Q.; Chase, D. B.; Rabolt, J. F.; Marcott, C. *Appl. Spectrosc.* 2012, 66, (12), 1365-1384.
3. Lu, F.; Belkin, M. A. *Opt Express* 2011, 19, (21), 19942-19947.
4. Lu, F.; Jin, M.; Belkin, M. A. *Nat Photon* 2014, 8, (4), 307-312.

5:20pm NS+AS-WeA10 Schottky Barrier Height Mapping of Nanoengineered Metal/Semiconductor Interfaces, Robert Balsano, C. Durcan, University of Albany-SUNY, A. Matsubayashi, V.P. LaBella, University at Albany-SUNY

Metal/semiconductor junctions form rectifying contacts known as Schottky diodes, which have an energy barrier determined by charge transfer and bonding at the interface. Current-voltage and capacitance-voltage spectroscopy measurements yield a spatially averaged barrier height. Ballistic electron emission microscopy (BEEM) is a scanning tunneling microscopy (STM) technique that can measure transport of hot electrons through materials and interfaces locally with high spatial and energetic resolution due to the precise positioning of the STM tip. This presentation details work done to map the Schottky barrier height with nanoscale resolution at several metal/semiconductor interfaces. These maps can give insight into the homogeneity of the barrier height as well as the spatial distribution of individual metal species. Potentially this technique can be used to image nanoengineered interfaces.

5:40pm NS+AS-WeA11 Scanning Electron Microscopy to Probe Electron Transport of Working Nanodevices under Realistic Operation Conditions, Ana Stevanovic, A. Kolmakov, National Institute of Standards and Technology (NIST)

The interplay between the electron transport and chemical status of the surface of working nanodevices can be affected by local electroactive inhomogeneities (defects), presence of near surface depletion regions and Schottky contacts. In spite of tremendous progress achieved in understanding of semiconductor chemical sensors, very little experimental data are available on aforementioned interplay in working devices under realistic operation conditions. Ambient pressure electron microscopy is used in this work to address *in situ* imaging of a formation of electroactive inhomogeneities inside a model SnO_2 nanowire device as a function of gas environment and temperature under realistic operating conditions. In addition, using scanning photoelectron and Auger microscopy with the lateral resolution of ca 80 nm, we are able to access spectroscopically the fine changes in surface condition of an individual SnO_2 nanowire during their operation. It is possible to monitor the changes in a conductance of the SnO_2 nanodevice in operando mode upon exposures to different redox gases and relate them to the formation of the specific surface groups.

**Plasma Science and Technology
Room: 305 - Session PS+2D-WeA**

Plasma Processing for 2D Materials, Coating, and Surface Modification

Moderator: Colin Wolden, Colorado School of Mines

2:20pm PS+2D-WeA1 Hydrogen Plasmas Processing of Graphene, Emilie Despiau-Pujo, A.O. Davydova, G. Cunge, LTM, Univ. Grenoble Alpes/CNRS/CEA-Leti Minatoc, France, L. Magaud, Institut Neel, Univ. Grenoble Alpes/CNRS, France, D.B. Graves, University of California at Berkeley INVITED

The successful development of graphene-based technologies relies on our capability to grow and integrate this new material into sophisticated devices. Since the presence of multilayers or defects/contaminants on the graphene surface can significantly degrade its intrinsic properties, the development of new techniques to clean graphene surfaces from polymer residues, etch graphene films layer-by-layer or pattern graphene nanoribbons (GNRs) with minimal edge disorder, are major challenges. ICP H_2 plasmas seem promising to specifically treat graphene films but little is known about the fundamental mechanisms of plasma-graphene interaction. We therefore develop Molecular Dynamics (MD) simulations, coupled with experiments, to assist the development of plasma processes to clean, dope and pattern graphene layers in a controlled way. We more specifically investigate the interactions between hydrogen plasmas and various types of graphene surfaces (monolayers, multilayers, nanoribbons). Except for impacts at GNRs edges or defects location, H species are shown to experience a repulsive force which prevents any species with less than $\sim 0.6\text{eV}$ to adsorb on the graphene surface. H^+ bombardment in the $[1-10]$ eV range does not damage the graphene basal plane while irreversible

damages are expected for $E_i > 12$ eV (penetration of atomic H through the layers or C-C bond breaking) [1]. As a first step to model graphene cleaning, we investigate the mechanisms of CH_3 groups (a crude approximation for resist residues) removal from graphene by atomic hydrogen. Depending on the incident energy range and the surface temperature, MD shows the possibility for chemical etching of the methyl radical without damaging the graphene basal plane [2]. Recent experiments and XPS/AFM/Raman measurements confirm that H_2 plasmas are promising to clean PMMA residues from graphene with almost no damage after annealing. Simulations of GNRs trimming show that lateral etching is maximum for surface temperatures ~ 600 K and occurs via a specific mechanism limiting the edge roughness, as also observed experimentally. Finally, energetic H^+ or H_2^+ bombardment of stacked multilayer graphene (s-MLG) is investigated and the possibility to store hydrogen (trapped as H_2 molecules) between adjacent layers or etch a full single graphene sheet is discussed. [1] Despiau-Pujo, Davydova, Cunge et al, *J.Appl.Phys.*113, 114302 (2013) [2] Delfour, Davydova, Despiau-Pujo et al, submitted to *Phys.Rev.B* (2014)

3:00pm PS+2D-WeA3 Plasma Synthesis of WS_2 Films, Rachel Morrish, C.D. Sentman, T. Haak, C.A. Wolden, Colorado School of Mines

Two-dimensional metal dichalcogenides (WS_2 , MoS_2) have attracted great interest due to their extraordinary optical properties, catalytic performance, and electronic structure. Synthesis of WS_2 has been accomplished by a variety of methods, but the high temperature (> 800 °C) and/or harsh S atmosphere required by many of these procedures precludes deposition onto conductive layers and low-temperature glass substrates needed for many applications. Previously we demonstrated the advantages of plasma processing for low temperature synthesis of a related metal dichalcogenide, pyrite (FeS_2). It was shown that stoichiometric FeS_2 films could be fabricated either by plasma-assisted sulfurization of hematite [1] or by direct deposition using pulsed plasma-enhanced chemical vapor deposition (PECVD) with mixtures of H_2S and $\text{Fe}(\text{CO})_5$. [2] In this talk we describe how these two approaches may be readily extended to the synthesis of WS_2 using WO_3 and $\text{W}(\text{CO})_6$, respectively.

Thin tungsten disulfide (WS_2) films were prepared on FTO coated glass substrates by H_2S plasma sulfurization of sputtered WO_3 . The reactive environment provided by the plasma enabled the complete transformation of oxide films to stoichiometric WS_2 within one hour at 500 °C. An apparent activation energy of 63.6 ± 1.9 kJ/mol was calculated for the plasma conversion process, which is less than half the barrier reported for the reaction of WO_3 with H_2S . The conversion followed Deal-Grove behavior, with the growing WS_2 overlayer hindering diffusion to/from the reactive interface. Calibrated light absorption and relative intensity of the second order Raman 2LA(M) peak were identified as two additional methods to progressively monitor the thickness of the WS_2 . The semiconducting WS_2 layers exhibited *n*-type behavior with an indirect band gap at 1.4 eV and an absorption coefficient of $\sim 5 \times 10^4$ cm^{-1} . Self-limiting growth of WS_2 thin films was accomplished by pulsed PECVD with continuous delivery of tungsten hexacarbonyl diluted in a mixture of H_2S and argon. The growth rate per cycle was controlled between 0.1 – 1 Å/pulse by adjusting the precursor flowrate. It was found that the morphology and orientation of the films was a complex function of film thickness, substrate temperature, and plasma parameters. Preliminary electrochemical measurements showed that these WS_2 films reduced the overpotential required for the hydrogen evolution reaction by several hundred mV relative to FTO while displaying good stability.

[1] R. Morrish, R. Silverstein and C. A. Wolden, *JACS*134 17854 (2012).

[2] C. D. Sentman, M. O'Brien and C. A. Wolden, *JVSTA*32 021201 (2014).

3:20pm PS+2D-WeA4 Decoration of Graphene with Gold Alloy Nanoparticles Synthesized in Solution Plasma, Maria Antoaneta Bratescu, Aichi Science and Technology Foundation, Nagoya University, Japan, T. Ueno, N. Saito, Nagoya University, Japan

In order to be used in electronics and optics, graphene must be in contact with other materials, which can change its electrical and optical properties. The substrate, charge impurities, doping with chemical functional groups, and metal contacts can shift the position of the Fermi level of graphene. Furthermore, graphene with plasmonic nanoparticles (NPs) can offer a new perspective for light conversion systems, by optimization of visible light absorption via the SPR of the NPs, followed by electron exchange between graphene and NPs and electron transport through graphene.

In this work we present a facile, one-step, and surfactant-free method for the synthesis and loading of stable gold and gold-alloy NP on large-area graphene without NP deterioration using an electrical discharge in a liquid solution, termed solution plasma (SP). We investigated the charge transfer process between graphene and gold-alloy NPs by Raman spectroscopy and electron energy loss spectroscopy (EELS) in high resolution transmission electron microscopy (HRTEM).

The excess charge on graphene caused by transferred electrons or holes from the NPs to graphene was calculated from the change of the Fermi level relative to the initial position and the shift of the G band. In the case of graphene with gold NPs a decrease of the surface charge concentration with -3.5×10^{12} cm^{-2} , and a movement of Fermi level with -0.06 eV.

In the case of the AuIn and AuGa NPs the transfer of electrons from graphene to the gold-alloy NPs produces an increase of the surface charge with 1.3×10^{12} cm^{-2} and 1.9×10^{12} cm^{-2} , which correspond to a raising of Fermi level with 0.02 eV and 0.03 eV, respectively.

The EELS results were consistent with Raman spectroscopy results, i.e. the electrons and holes are transferred from the gold and gold-alloy NPs to graphene, respectively.

M.A. Bratescu, et al., *J. Phys. Chem. C* 115 (2011) 24569

S.P. Cho, et al., *Nanotechnology* 22 (2011) 455701.

M.A. Bratescu, et al., *J. Alloys and Compounds* 562 (2013) 74

M.A. Bratescu, et al., *J. Phys. Chem. C* 117 (2013) 26804

4:20pm PS+2D-WeA7 Generation and Stabilization Mechanisms of Free Radicals in Plasma Polymers, S. Ershov, F. Khelifa, P. Dubois, Rony Snyders, University of Mons, Belgium

Cladded aluminum alloys are widely used in many applications being protected by a conversion coating based offering some self-healing properties nowadays based on the use of toxic chromate compounds. For both environmental and work safety reasons it is necessary to identify an alternative to this chromate-based conversion coating (CBCC).

In this context, in the framework of a collaborative project, we are working on the replacement of the CBCC by a multilayer combining, among others, plasma polymer films (PPF) and conventional polymers. The key features of this multilayer is grafting of a conventional polymer on the alloy surface by using the free radicals present in the as-deposited PPF as initiating sites for a radical-based polymerization reaction. It is therefore necessary to get a complete understanding on the generation and stabilization of the PPF radicals in order to control the grafting procedure.

The aim of this work is to contribute towards the understanding of the free radicals generation mechanism in the PPF and on their stabilization by comparing the plasma polymerization of different precursors namely isopropanol, benzene and cyclohexane. *In situ* FTIR spectroscopy and a combination of XPS and chemical derivatization measurements are used to quantitatively evaluate the plasma and thin films chemistry, respectively. Grafting experiments with 2-ethylhexyl acrylate (EHA) allows to cross-check the relevance of the XPS results.

Our results reveal that, for isopropanol PPF, the surface density of free radicals is about $\sim 1.6 \cdot 10^{14}$ spin/ cm^2 and depends strongly on the injected power in the plasma. On the other hand, a significant effect of the presence of resonant structure in the plasma polymer on the radical stability is highlighted.

4:40pm PS+2D-WeA8 Simulation of Direct Current Microplasma Discharge in Carbon Dioxide at High and Intermediate Pressures, N. Hasan, P.R. Fernandez, Bakhtier Farouk, Drexel University

Direct current (DC) micro-plasma discharges in intermediate to high pressure (10–200 kPa) carbon dioxide are investigated for potential applications in carbon dioxide decomposition and thin film deposition. Numerical simulations are performed using a hybrid CFD model. The model contains detailed reaction mechanisms for the gas-phase discharge and the surface reactions to predict the species densities in the discharge and the deposition characteristics and its growth rate. Sixteen species and a seventy-six step reaction mechanism are considered for the gas-phase carbon dioxide discharge. A simplified surface chemistry consisting eleven reaction steps are considered in the model. The simulations are carried out for a DC pin-to-plate electrode configuration with an inter-electrode gap of 500 μm . An external circuit is also considered along with the discharge model and surface reactions. Basic plasma properties such as electron and species density, electric field, electron temperature and gas temperature are studied. Special attention is devoted to study the influence of operating pressure and discharge current on the plasma characteristics and the deposition characteristics and its rate. The CO_2^+ and O- concentrations are found to be the dominant ions in the plasma. The simulations indicated significant gas heating in the entire regime of operation. Ion Joule heating was found to be dominant in the sheath whereas Franck-Condon heating and heavy particle reaction induced heating was dominant in the volume. The results presented here can be utilized for the development of computational models for plasma discharge in supercritical conditions which can be used to investigate processes such as carbon nanotube synthesis, biological reaction catalysis and carbon dioxide decomposition.

5:00pm **PS+2D-WeA9 The Impact of Ambient Gas Chemistry on Lipopolysaccharide Deactivation and Polymer Modification by Plasma-Generated Radicals at Atmospheric Pressure**, *Elliot Bartis, A.J. Knoll, P. Luan, C. Hart*, University of Maryland, College Park, *D.B. Graves*, University of California, Berkeley, *I.V. Adamovich, W. Lempert*, The Ohio State University, *J. Seog, G.S. Oehrlein*, University of Maryland, College Park

In this study, lipopolysaccharide (LPS) -coated silicon substrates were exposed to the effluent of an atmospheric pressure plasma jet (APPJ) under a controlled environment to examine the effect of plasma-generated reactive species on the surface chemistry and biological activity. The goal of the present work is to understand the role of plasma-environment interactions in biodeactivation and surface modifications by regulating both the proximity of the plasma to the environment and the environmental gas chemistry. The APPJ is mounted inside a vacuum chamber that can be evacuated and refilled with any gas chemistry. By changing the APPJ geometry, the plasma plume can be either exposed or protected from the ambient. By adding small N₂/O₂ admixtures to Ar, we find that the O₂ admixture in the APPJ is a major determining factor for both deactivation and surface modification as measured by an enzyme-linked immunosorbent assay and x-ray photoelectron spectroscopy, respectively. N₂ admixture without O₂ causes minimal deactivation, while N₂/O₂ admixtures deactivate more with increasing O₂ content. For identical O₂ feed gas flows, less deactivation occurs when N₂ is also added, which demonstrates that nitrogen-based species quench reactive oxygen species (ROS) responsible for biodeactivation. After plasma treatments, a new chemical species was detected on LPS surfaces that was stoichiometrically verified as NO₃. To determine if this species forms due to nitrogen and oxygen found naturally in LPS, we treated model polymer films of polystyrene, polypropylene, and poly(methyl methacrylate), as these materials contain solely carbon or only carbon and oxygen. We find that the formation of NO₃ is generic to all surfaces even with no N₂ in the feed gas. Thus, the reactive interaction of oxygen-based species with ambient N₂ takes place, indicating that plasma-environment interactions create this moiety and providing insight into the mechanisms by which the APPJ modifies surfaces. For polystyrene films, oxygen uptake is dramatic with O/C ratios as high as 0.47 at the near surface. The oxygen uptake results in a variety of moieties including C-O, O-C-O, C-O-NO₂, O-C=O, and O-(C=O)-O. APPJ treatments are also compared with a corona discharge to examine the role of long lived species such as ozone and NO_x. Results from gas-phase characterization will also be discussed. The authors gratefully acknowledge financial support by the US Department of Energy (DE-SC0005105 and DE-SC0001939) and National Science Foundation (PHY-1004256).

5:20pm **PS+2D-WeA10 Modification of LDPE Induced by an Ar/H₂O Plasma: Comparison between a Post-Discharge Treatment and a DBD Treatment**, *Stephanie Collette*, Université Libre de Bruxelles, Belgium, *V. Cristaudo*, Université catholique de Louvain, Belgium, *T.R. Dufour*, Université Libre de Bruxelles, Belgium, *P. Viville*, Université de Mons, Belgium, *A. Delcorte*, Université catholique de Louvain, Belgium, *F.A.B. Reniers*, Université Libre de Bruxelles, Belgium

The study of the water reactivity in plasma was achieved by injecting water vapor in the post-discharge of an RF plasma torch and in a dielectric barrier discharge (DBD), both supplied in argon as carrier gas.

The RF plasma torch operates at atmospheric pressure. Optical emission spectroscopy (OES) and mass spectrometry evidenced the production and the consumption rates of Ar, O, OH, O₂⁺ and N₂ species. These species could be quantified as a function of the water vapor flow rate, the treatment time and the gap (distance separating the post-discharge from a solid surface) to have a better understanding of the reactivity. Some chemical reactions occurring within the post-discharge could be evidenced and their importance was determined according to their kinetic constants. The reactivity of H₂O in the post-discharge was also carried out using an indirect method: the exposure of low density polyethylene (LDPE) samples to the plasma torch, in order to correlate the amount of oxygenated radicals resulting from water vapor dissociation reactions with the amount of oxygenated functions (C-O, C=O, COO) grafted on the surface. The modified LDPE surfaces were characterized by X-ray photoelectron spectroscopy (XPS), with a special emphasis on the deconvolution of the spectral envelope of the C1s peak. For longer treatment times, we showed that the decrease in the oxygen concentration observed by XPS could result from a competition between the LDPE surface etching and its functionalization. Besides, depth profiles achieved with XPS evidenced the diffusion of O in the subsurface, thus proving the efficiency of the plasma treatment. Those results were correlated with WCA measurements indicating a decrease of the angle from 100° to 35° and with AFM showing an increase of the RMS roughness value from 30 nm to 90 nm. ToF-SIMS analyzes were also achieved on LDPE surfaces. To compare the impact of the plasma treatment to the influence of water contained in the atmosphere, D₂O was injected in the plasma torch. The use of D₂O permits to selectively

probe the presence of fragments from the injected water grafted on the LDPE surface.

Those results were compared to those obtained with a second plasma source, namely a DBD operating at atmospheric pressure. In this case, LDPE samples were placed directly between the two dielectric barriers. Similar species as those described in the post-discharge have been evidenced by OES and MS with however slightly different reactive mechanisms, thus explaining why the treated LDPE surfaces present a different hydrophilic state.

This work was supported by PSI-IAP 7(plasma surface interactions (Belgian Federal Government BELSPO agency)).

5:40pm **PS+2D-WeA11 Atmospheric Plasma Polymerization of Fluorinated Precursor : Comparison of Various Liquid Precursors and Plasma Types (AC and Pulsed DC)**, *J. Hubert, Nicolas Vandecasteele*, Université Libre de Bruxelles, Belgium, *C. Poleunis*, Université catholique de Louvain, Belgium, *J. Mertens*, Université Libre de Bruxelles, Belgium, *A. Delcorte, P. Bertrand*, Université catholique de Louvain, Belgium, *F.A.B. Reniers*, Université Libre de Bruxelles, Belgium

The deposition of PTFE like films by argon atmospheric plasma using various precursors, liquid at room temperature, is presented. Those compounds are: Perfluorohexane (C₆F₁₄), a fully saturated monomer, perfluoro(2-methylpent-2-ene) (C₆F₁₂) containing one unsaturated bond and Perfluorotributylamine (C₁₂F₂₇N), containing a central nitrogen atom to which 3 fully saturated perfluorobutyl chains are attached. The influence of the monomer structure as well as the electrical parameter of the plasma (AC or pulsed DC) on the films chemistry and deposition rate is studied.

PTFE like films are of interest because of their low surface energy which gives them interesting properties such as easiness of cleaning etc.

The surface composition of the films is studied by X-Ray Photoelectron Spectroscopy (XPS) and Time of Flight Secondary Ion Mass Spectrometry (ToF-SIMS). The surface energy of the films is studied by Water Contact Angle (WCA). The films thickness is determined by profilometry, and the composition of the plasma phase is analyzed by atmospheric Mass Spectrometry (atm-MS) and Optical Emission Spectroscopy (OES).

Results

Very similar atomic composition and surface energies are obtained for the tested range of experimental parameters. Difference in composition, depending on the precursor used, can however be detected in the high resolution C1s peak (XPS). The signature of the precursor can also be detected in the atm-MS results of the plasma phase. OES measurements on the other hand do not allow to easily differentiate the various precursors. The main species detected other than Ar are F and CF₂. The combination of the gas phase analysis and the films composition suggest a small fragmentation of the monomer in the plasma. Indeed as the initial structure of the precursor can still be detected in the deposited films we can conclude that the chemical structure of the polymerizing species must be close to the one of the initial molecule.

Differences in deposition speed depending on the precursor type and/or the plasma type (AC or DC) are evidenced by profilometry measurements. As expected the precursor containing the unsaturated bond has a higher deposition rate. Thicker films exhibit slightly higher contact angle values (~140°) than thinner ones (~130°). This cannot be attributed to the chemical composition of the films as they are very similar but can be explained by the increased roughness of the thicker samples.

The overall composition of the films can only be slightly modified by changing the precursor structure or the plasma parameters. The deposition speed is the main parameters linked to both the precursors structure and the plasma parameters.

6:00pm **PS+2D-WeA12 Surface Modification of Nafion Membranes Exposed to an atmospheric He-O₂ and He-H₂ Post-Discharge**, *Thierry Dufour, D. Merche, H. Julie, R.F. François*, Université Libre de Bruxelles, Belgium

Nafion is commonly used as a proton-conducting polymer membrane to separate the anode and cathode compartment of proton exchange membrane fuel cells (PEMFC) and water electrolyzers. The use of plasma based technology has contributed to lower catalyst loadings, thus decreasing the production costs. In this framework, our researches have been focused on a simple and robust technique to modify Nafion surface properties, using the post-discharge of an atmospheric RF plasma torch supplied in helium as carrier gas and H₂ or O₂ as reactive gas. The modifications achieved on Nafion samples have been compared with those of common polymers such as polyethylene, PVF and PTFE. Contrarily to these polymers, the Nafion presents more complex etching mechanisms, that may be correlated with the complexity of its molecular formula: (i) its hydrophobic region is a continuous semi-crystalline region which is Teflon®-like, being made up of main chain TFE segments, while (ii) its hydrophilic region (sulfonate

group) allows water and proton/ion transport but can also swell and change in size and/or shape with water uptake (eventually forming a continuous network). We have already demonstrated that the chemical nature of the fragment species (ejected from the Nafion film) depends on the exposure time because the fluorinated backbone is not etched as efficiently as the perfluorovinyl ether groups terminated with sulfonate groups.

The morphological and chemical structural changes of the Nafion films during exposure to the post-discharge have been characterized using scanning electron microscopy (SEM), atomic force microscopy (AFM) and X-ray photoelectron spectroscopy (XPS) as well as WCA (Water Contact Angle) measurements. Moreover, a characterization of the proton conductivity and of the methanol permeability will also be introduced.

This work is supported by PSI-IAP 7 (plasma surface interactions) from the Belgian Federal Government BELSPO agency.

Plasma Science and Technology

Room: 308 - Session PS-WeA

Plasma Diagnostics, Sensors, and Control

Moderator: Jean-Paul Booth, LPP-CNRS, Ecole Polytechnique, France

2:20pm **PS-WeA1 Diagnostics of Cl₂/O₂ Inductively-Coupled Plasmas by Ultra-High Sensitivity Broad-Band Absorption Spectroscopy.** *Mickaël Foucher*, LPP-CNRS, Ecole Polytechnique, France, *E. Carbone*, LTM - MINATEC - CEA/LETI, France, *J.-P. Booth*, LPP-CNRS, Ecole Polytechnique, France

Inductively-coupled plasmas (ICP) containing O₂ and Cl₂ (and often HBr) are widely used for etching, for example of silicon transistor gate. Simulations, including global and two-dimensional fluid models have been developed over the years, but validation against experimental measurements of absolute densities remains sparse.

Absorption spectroscopy is a powerful diagnostic for reactive plasmas, providing absolute density measurements of numerous atoms, molecules and free radicals in ground and various excited states. The sensitivity is determined in practice by the characteristics of the light source used: spectral range, stability and intensity. Previously Xe arc lamps have been used but they suffer from spatiotemporal fluctuations, limiting the sensitivity to about 10⁻³ in absorption. More recently UV light-emitting diodes have been used, giving greatly increased stability, but these have very limited spectral ranges (a few 10's of nm), necessitating the use of specific diodes for each species detected.

We have constructed a new absorption bench that overcomes these difficulties. The light from a broad-band (200-1000) nm laser-induced plasma source (Energetiq-LDLS EQ-99) is collimated and steered with reflective (achromatic) optics. After passing through the reactor the beam is analyzed with an aberration-corrected spectrograph (Acton SCT-320) equipped with a 1024 element photodiode array detector. Three gratings allow spectral ranges of 32, 63 or 250 nm to be analyzed at one time. This setup gives spectra in minutes with random noise and baseline stability better than 10⁻⁴, allowing detection of species which only show weak absorption bands over wide spectral ranges.

The gases (O₂, Cl₂ and mixtures) are flowed through a cylindrical aluminum chamber (55 cm diameter, 10 cm height). The plasma is excited at 13.56 MHz by a 4-turn planar coil through a dielectric window. We observed molecular absorption bands from ground state Cl₂, vibrationally excited O₂ and of various O₂Cl₂ reaction products, allowing the densities, vibrational and rotation temperatures to be determined. As far as we know this is the first time oxychlorides densities have been measured in plasmas. This data is complemented by measurements of absolute atom densities (Cl and O) by TALIF and hairpin probe measurements of electron density. The interpretation of this data set will be discussed.

2:40pm **PS-WeA2 Diagnostics in Pulsed Hydrogen Plasmas.** *Jerome Dubois*, *G. Cunge*, LTM - CEA/LETI, France, *N. Posseme*, CEA-LETI, France, *M. Darnon*, LTM - CEA/LETI, France, *L. Vallier*, CNRS-LTM, France, *O. Joubert*, LTM - CEA/LETI, France

Hydrogen plasmas have been used for decades in the microelectronic industry with applications in the fields of deposition (PECVD, Plasma Enhanced Chemical Vapor Deposition) [1], etching [2] and surface treatment (reduction of the photoresist roughness in the lithography step [3]). However hydrogen is a very peculiar element due to his low mass and his electronegative character, and the mechanisms at stake in low pressure hydrogen plasma aren't well understood yet. A complete fundamental study with reliable diagnostics would be highly valuable for many applications

[4]. Moreover, hydrogen plasmas present a great potential interest for the treatment of new materials such as graphene [5] or carbon nanotubes [6]. To modify the surface of such ultrathin layers without damaging the material, very low ion energy bombardment is required (conditions such as those obtained in pulsed ICP reactor [7]). By contrast, for other applications such as etching of several nanometer thick layers, the ion energy must be very high to get a significant etch rate. To assist the development of innovative processes in H₂ plasmas, we have thus analyzed systematically CW and pulsed H₂ plasmas both with and without RF bias power. In particular, we carry out time-resolved ion flux, and time-averaged ion energy measurements in different pulsing configurations. A large variety of ion energies and shapes of IVDF are reported depending on pulsing parameters. The IVDF are typically very broad (due to the low ion transit time of low mass ion through the sheath) and either bi or tri-modal (H⁺, H₂⁺ and H₃⁺ contributions). The time variations of the ion flux in pulsed plasmas also presents peculiar features that will be discussed.

References

1. W. A. Lanford, and M. J. Rand, *Journal of Applied Physics*, **49**, 2473-2477 (1978)
2. A. Efremov, N. K. Min, J. Jeong, Y. Kim, and K. H. Kwon, *Plasma Sources Science and Technology*, **19** (2010)
3. E. Pargon, L. Azarnouche, M. Fouchier, K. Menguelti, R. Tiron, C. Sourd, and O. Joubert, *Plasma Processes and Polymers*, **8**, 1184-1195 (2011)
4. M. Sode, T. Schwarz-Selinger, and W. Jacob, *Journal of Applied Physics*, **113** (2013)
5. E. Despiau-Pujo, A. Davydova, G. Cunge, L. Delfour, L. Magaud, and D. B. Graves, *Journal of Applied Physics*, **113** (2013)
6. A. Hassanien, M. Tokumoto, P. Umek, D. Vrbancic, M. Mozetic, D. Mihailovic, P. Venturini, and S. Pejovnik, *Nanotechnology*, **16**, 278 (2005)
7. C. Petit-Etienne, M. Darnon, P. Bodart, M. Fouchier, G. Cunge, E. Pargon, L. Vallier, O. Joubert, and S. Banna, *Journal of Vacuum Science & Technology B*, **31** (2013)

3:00pm **PS-WeA3 The Role of Diagnostics in Plasma Etch Reactors in Enabling the Information Age.** *Alex Paterson*, *J. Holland*, *S. Sriraman*, *E. Hudson*, *H. Singh*, *V. Vahedi*, Lam Research Corp **INVITED**

Over the last decade, semiconductor industry growth has been driven chiefly by the demand for consumer electronics: the move to mobile smart devices such as phones and tablet PC's. It is now common place for hand-held mobile devices to have 32 Gb of memory and processor speeds of over 1 GHz, a truly remarkable feat that would have been unthinkable 10 years ago. This capability has been enabled by the continuation of IC scaling to smaller and smaller features sizes with the present technology being mass produced by 28 nm node technology and smaller nodes down to 10 nm currently being developed by IC manufacturers. The limitations of lithography to keep up with the decrease in dimensions required for these smaller nodes has resulted in new challenges for plasma etch to enable patterning at these small feature sizes. Device performance requirements also drive critical dimension (CD) non-uniformity to less than one nanometer across the entire 300 mm wafer for sub-20 nm features and yield requirements extend this patterning region to within 1.5 mm of the wafer edge. Wafer fabrication production also relies on plasma etch solutions to be stable at these levels across long periods of time and capable of flexibility in multiple applications. The realization of all of these goals has been greatly facilitated by a much better understanding of the basic chemical, physical, and electromagnetic processes that occur during the plasma etch of semiconductor devices.

In this paper we will discuss the crucial role diagnostics play in achieving this understanding and in the development of state of the art plasma etch chamber technology that allow the continuation of Moore's Law. Diagnostics are essential not only to understand etch mechanisms and chamber characteristics but to also accelerate hardware development in order to meet customer time critical needs. We will review the different types of diagnostics commonly used in plasma etch chamber development with reference to findings from literature and augment this with diagnostic work undertaken at Lam Research. Finally, we will discuss the suitability of diagnostics in main stream production and give some thoughts on future diagnostics that may be required for production enhancement and also angstrom level etching.

4:20pm **PS-WeA7 Ion Angular Distributions Measured with a Planar Retarding Field Analyzer.** *Shailesh Sharma*, Impedans Ltd., Ireland

In microelectronics fabrication the angular distribution of the bombarding ions can impact the process outcome. The ion energy distribution as a function of ion angle at specific locations on the substrate or wafer surface need to be controlled in certain anisotropic etching and conformal

deposition plasma processes. We report a novel method for the measurement of ion energy distributions as a function of ion angle, at the substrate location, using a planar retarding field analyser.

Planar retarding field analyzers are commonly used to measure ion energy distributions but provide no information about the angular distribution of ions bombarding the substrate surface. Here, we report on a novel planar retarding field analyser design capable of resolving the angular distribution of the energetic ions. The design has three active grids, a collector plate and an aperture with variable aspect ratio (height / diameter) to control the angular spread of the ions allowed through the device for detection. First, the potential of the ion energy discriminating grid is modulated to select ions with a specified energy resolution for analysis. Then, the aspect ratio of the aperture is varied from large acceptance angle to narrow acceptance angle with specified angle resolution - predetermined from the aperture geometry. The ion current is recorded for each acceptance angle to give an integral form of the ion angular distribution at a given ion energy where the angular distribution can be recovered by taking a first derivative. The procedure is then repeated for each ion energy. Once the angular distribution is determined as a function of ion energy, the energy distribution as a function of ion angle is easily calculated.

The analytical theory used to define ion current as a function of incident ion angle, ion energy and aperture aspect ratio is presented. The method used to vary the aspect ratio of the additional aperture is also discussed. This novel method allows ion angular distributions to be determined using a compact planar retarding field analyser.

With the modified retarding field analyzer design and advanced analytical technique, ion angular distributions with angle resolution as low as 3° have been measured and resolution up to 1° can be achieved. This technique adds important functionality to the retarding field analyser technology - which has become one of the most important technologies in the field of plasma diagnostics in recent years.

4:40pm PS-WeA8 Quantitative Analysis of Neutral Species Generated in Styrene Low Pressure RF Plasma, as a Function of Plasma Power, X. Gillon, J.-J. Jean-Jacques, Laurent Houssiau, University of Namur, Belgium

Plasma polymerization processes enable unique polymer coatings unattainable with conventional wet chemistry. Among them, plasma polystyrene (pPS) deposition has been intensively studied, but very few studies report on plasma diagnostics of styrene discharges, which is however a necessary step to understand the fundamental mechanisms of plasma polymerization. In this work, pPS was produced from pure styrene vapor injected in a vacuum chamber at 50 mTorr (6.7 Pa) and 28 sccm. An inductively coupled plasma was ignited by a planar coil delivering a continuous wave RF power ranging from 30 W to 210 W. Plasma diagnostics was achieved by means of a mass spectrometer (MS) located in the post-discharge region, enabling only the detection of neutral species. A problem associated with electron impact MS is the cracking of organic molecules, which hampers species identification and quantification in the plasma phase. However, by reducing the electron energy as low as 12 eV, much below the standard 70 eV energy, we were able to suppress most of the molecular cracking, so that species measured by MS could be unambiguously assigned to neutral species existing in the plasma. The assignment was further confirmed by measuring the appearance potentials of all ions in the MS. This procedure revealed the existence of 55 neutral species in the styrene plasma, which is five times more than what has been reported so far. Their relative intensities in the MS spectrum help understanding the formation pathways of these species, either by direct fragmentation of the styrene molecule, or by recombination of small molecules. The most abundant species generated in the styrene plasma were H_2 , methane, acetylene, ethylene, benzene, toluene and naphthalene. In order to quantify the partial pressure of those species in the plasma, we determined their sensitivity factors by injecting them pure in the plasma reactor and measuring the molecular ion peak intensity at 50 mTorr pressure. The MS intensities measured in the styrene plasma were subsequently converted into partial pressures. The sum of partial pressures from the main species present in the plasma, including styrene, was found to match remarkably well with the measured pressure in the reactor, confirming the quantitativity of the procedure. The main features observed in the plasma chemistry when the power was raised are: a decrease of styrene pressure (monomer consumption) along with a strong production of acetylene and hydrogen. A very sharp drop of the plasma pressure was measured around 185 W, corresponding to the disappearance of the monomer and a sudden increase of the deposition rate.

5:00pm PS-WeA9 Comparison of Commercial Plasma Probe Systems, Valery Godyak, RF Plasma Consulting, B.M. Alexandrovich, Plasma Sensors

Electrostatic (Langmuir) probes are powerful instruments for diagnostics of non-equilibrium plasmas in experimental and industrial plasma reactors. There are three levels of the probe diagnostics comprising different equipment complexity and having different accuracy of obtained the plasma parameters. These three approaches are based on inferring the plasma parameters from: *i* - the ion part of the probe characteristic, *ii* - the electron part of the probe characteristic (classical Langmuir probe method), and *iii* - by differentiation of the probe characteristic to obtain an Electron Energy Distribution Function, EEDF. Then, the electron temperature T_e and plasma density N_e , as well as, the rates of collisional processes and transport coefficients are found as corresponding integrals of the measured EEDF. Methods *i* and *ii* assume Maxwellian EEDF which is not valid for most cases of non-equilibrium plasmas. This and many others questionable assumptions in methods *i* and *ii* make actual EEDF measurements the only reliable contemporary probe diagnostics. Langmuir probes in plasma processing reactors are often subjected to the probe surface contamination and high level of rf and low frequency noise. Reliable EEDF measurements require the probe system capable of efficient mitigation of these environmental distortions. The presentation main subject is comparison of EEDF measurement results obtained with different commercial probe systems. It is shown that the measurement accuracy of the plasma parameters in many commercial probe systems is compromised by heavily distorted EEDF in low and high energy region. Low energy distortions make impossible to detect low energy electrons (comprising the majority of electron population), thus leading to underestimation of the plasma density, while high energy distortions make undesirable detection of fast electrons producing excitation and ionization. Therefore, some commercial probe systems yielding distorted EEDFs are unable to reveal any additional valid information to that obtained with classical Langmuir procedure.

5:20pm PS-WeA10 Systematic Diagnostic Approach for Fabricating High Quality SiNx:H Film using UHF Assisted Capacitively Coupled Plasma Source, J.G. Han, B.B. Sahu, Kyung S. Shin, Sungkyunkwan University, Republic of Korea, K. Ishikawa, M. Hori, Nagoya University, Japan

Silicon nitride thin films have shown many useful applications in microelectronic and optoelectronic industries. Fabrication, of these films at low temperature, is done typically by PECVD using a mixture of silane (SiH_4) and ammonia (NH_3). Recent trend shows that the most practical deposition of low-hydrogen-content-silicon-nitride-films ($SiNx:H$) is to use N_2 instead of NH_3 as the main nitrogen source. However, N_2 has an inherently much higher bonding energy than NH_3 , which makes N_2 more difficult to dissociate into free nitrogen active species, thus nitrogen deposition rate is significantly reduced. But if low hydrogen nitride films can be obtained, which may give better device performance, the deposition rate may not be an important factor and PECVD of silicon nitride by little addition of SiH_4 and NH_3 to the N_2 is still an attractive process. Moreover, the important deposition parameters for any PECVD process are RF power, working pressure, substrate temperature, the gas flow ratio of the reactant gases and the electrode spacing (for CCD or parallel plate system). All these parameters have significant role on the deposition and etch rates along with other physical and optical properties of film depending on device applications.

Although PECVD processes have shown as an emerging method for achieving good quality $SiNx:H$ films for the industry, still there are lack of understanding in correlation between the properties of the plasmas and the characteristics of the synthesized films. In the present work, a deposition parameter matrix is constructed for $N_2-SiH_4-NH_3$ PECVD process and the effect of variation of above parameters on deposition is studied. The present study investigates PECVD process with different plasma processing conditions by utilization of different plasma sources, e.g., RF, which is capacitively coupled plasma (CCP) source at 13.56 MHz and UHF, a 320 MHz very high frequency (VHF) RF source. The goal of the UHF source is to assist and enhance the dissociation of nitrogen radicals along with the RF. One of the major goals of this work is also to investigate dissociation of the nitrogen radicals, which controls the $SiNx:H$ film deposition process. To understand the fundamental plasma surface interactions in this process, basic plasma diagnostics such as Langmuir probe (LP), optical emission spectroscopy (OES), and vacuum ultraviolet absorption spectroscopy (VUVAS), etc., are used. Thus, the investigations, of high quality $SiNx:H$ film synthesis described in this paper, focus predominantly on the plasma diagnostics and film synthesis. This also reports about high quality film having transmittance about 90 %.

5:40pm **PS-WeA11 Electron Beam Generated Plasmas in Fluorine Chemistries**, *David Boris, R.F. Fernsler, G.M. Petrov, Tz.B. Petrova, S.G. Walton*, Naval Research Laboratory

Electron beam generated plasmas are characterized by high plasma densities and very low electron temperatures, making them well-suited for next-generation processing techniques where high fluxes of low energy ions are desirable. In this work, we focus on plasma generation in fluorine containing gas backgrounds due to their relevance to a number of industrial plasma applications. In particular, we focus on the effect of fluorine-containing gas dilution on the plasma properties of electron beam generated plasmas including electron density, total plasma density, electronegativity, and electron temperature. These parameters are measured through a combination of Langmuir probe, and RF impedance spectroscopy techniques.

6:00pm **PS-WeA12 Characterization of Hydrogen Recombination at the Wall and its Effect on Hydrogen Source Performance**, *Shaun Smith*, MKS Instruments, Inc.

There is ongoing interest in using remote plasma sources for on wafer processing with hydrogen radical based chemistries. Yet there has been limited availability of reliable measurements for recombination rates, as they pertain to semiconductor processing. Presented here are diagnostics and some insight to understating of how process responds to material choice or the surface condition of the plasma facing wall. The impact that surface recombination of radical species has on the discharge is discussed and the impact that surface material choice and condition has on source operation and process performance is examined. As well as a discussion of factors that can effect that recombination rate. These parameters are explored in the 1-10torr 1-5slm and 1-10kW regime

Atomic hydrogen recombination rate is measured for a range of materials. Toroidal plasma sources are then built with these materials as the plasma facing wall and are characterized for their discharge parameters and atomic hydrogen output. The discussion will include a description of the diagnostic tools used in this study; a comparison of modeled source discharge parameters running in Ar and H₂ with experiment along with a brief comparison of the impact of volumetric and surface recombination of radical species is presented.

This work was specifically targeted for the use of radicals produced by a toroidal remote plasma sources for semiconductor applications but is generalizable to discharges in hydrogen independent of excitation or application.

Surface recombination of the hydrogen radical is shown to be a dominant mechanism in determining process parameters for semiconductor applications.

Selective Deposition as an Enabler of Self-Alignment

Focus Topic

Room: 318 - Session SD-WeA

Process Development for Selective Deposition and Self-Aligned Patterning

Moderator: Paul Ma, Applied Materials, Inc., John Smythe, Micron Technology

2:20pm **SD-WeA1 Material Requirements for Self-Aligned Patterning – a Lithographer's Perspective**, *Charles Wallace*, Intel Corporation
INVITED

As feature sizes shrink in semiconductor processes, overlay control is quickly becoming the most significant source of variation. Physical limitations of lithography equipment are constantly pushed beyond their capability in order to meet device requirements. This presentation will discuss past, current and future methods of decreasing overlay and critical dimension errors using self-alignment and selectivity. Self-aligned processes in logic-product manufacturing reduce edge-placement-errors (EPE) which improve yield and device performance. Self-aligned VIAs, self-aligned double patterning (SADP) and directed self-assembly (DSA) are some recent examples of complementary patterning techniques to conventional lithography. These processes enable scaling beyond the resolution limits of conventional lithography. In addition to addressing fundamental physical limitations of optical lithography, these techniques can help to reduce costs because of shorter patterning process flows and the use less expensive equipment. Now is the time for material design and selectivity (selective etch, deposition and removal) to start playing a major role in patterning in order to reduce and eliminate overlay error.

3:00pm **SD-WeA3 Controlling Selective Area Atomic Layer Deposition of Metals and Metal Oxides without the use of Organic Blocking Layers**, *Gregory Parsons, B. Kalanyan, S.E. Atanasov*, North Carolina State University
INVITED

Selective area CVD has been heavily studied, and several strategies for selective growth are known, including sacrificial reactions, surface activation, nucleating species removal and passivation of non-growth surfaces. However, the success of selective deposition processes in manufacturing has been limited. Atomic layer deposition allows the partial pressure and exposure sequence of individual reactants to be independently adjusted, providing additional control in surface reaction sequence. Surface passivation layers can promote selective area ALD of metals and dielectrics, but integration into manufacturing can be a challenge. Recently, we have studied modified ALD process sequences as a means to control nucleation, without the need for pre-deposited nucleation blocking layers. For example, tungsten ALD using WF₆/SiH₄ onto SiO₂ proceeds when surface Si-H (from SiH₄) begins to form, allowing WF₆ reduction to W and elimination of SiF₄. We hypothesized that the introduction of a H₂ or H-plasma exposure into the ALD sequence after the SiH₄ dose may help remove Si from the SiO₂, which could extend the nucleation delay on SiO₂, while not affecting W growth on Si. Using ellipsometry, XPS, high resolution SEM and in-situ quadrupole mass spectrometry we found that a H₂ exposure step after SiH₄ during W ALD on ex-situ prepared SiO₂ decreased the rate of W nucleation compared to growth without the H₂ step, effectively increasing the selectivity window. At 220°C, one ALD cycle produced nm-scale nuclei on Si-H surfaces, and film coalescence after ~10 cycles, whereas growth on SiO₂ showed no W nuclei after 10 cycles. After some nucleation, growth proceeded readily on the nuclei, with few new nuclei forming, producing rough surfaces that coalesced after 40 cycles. Including the H₂ exposure step after SiH₄ delayed nucleation by 5-10 cycles on SiO₂, with no noticeable effect on Si-H. However, we found that removing surface carbon from the SiO₂ prior to growth had a similar effect, indicating that C helped aid nucleation. Recent work with H₂-plasma exposure also shows enhanced nucleation on SiO₂, which likely depends on the extent of H exposure. In other studies, we are examining metal oxide nucleation using metal/metal alkoxide reaction sequences and comparing to similar reactions with water as a reactant. These results will help to define ALD nucleation sequences that are distinct from steady-state film growth, to achieve reliable selective area deposition.

4:20pm **SD-WeA7 Selective Deposition through Organic Blocking Layers**, *Rami Hourani, S.B. Clendenning, G.M. Kloster, A. Basu, F. Gstrein*, Intel Corporation

With the ever increasing complexity of lithography and associated patterning techniques, pattern overlay has become a critical limiter for the continued scaling of integrated circuits. Self-alignment of patterns through area selective deposition, or area-selective etch is an attractive way of addressing pattern overlay and edge placement challenges. Inherently, surface-selective deposition techniques are rare in the fields of chemical vapor deposition (CVD) and atomic layer deposition (ALD). This is particularly true for the selective deposition of dielectrics. Tuning the chemical properties of precursors to achieve inherent substrate-dependent selectivity is thus a key enabler. In the face of poor inherent selectivity, using organic layers such as self-assembled monolayers (SAMs) as blocking layers for subsequent CVD and ALD deposition is an attractive way of achieving selective growth and controlling defectivity. In this paper we will present a joint experimental and theoretical investigation (Density Functional Theory based calculations with semi-empirical dispersion correction) aimed at assessing the stability of a variety of SAMs and their ability to block the deposition of a dielectric thin film. Simple line space patterns will be used to assess the defectivity of this approach. The critical parameters to achieve area-selective deposition will be discussed including proper surface pre-treatment, optimization of the SAM deposition through judicious choice of SAM terminal group and carbon chain length, and optimization of the deposition process through ALD precursor choice. Finally, obstacles to making selective deposition processes manufacturable will be discussed.

4:40pm **SD-WeA8 Selective Deposition and Selective Etching of Patterned Dielectric Films**, *FatemehSadat Minaye Hashemi, C. Prasittichai, S.F. Bent*, Stanford University

Planar and 3-D electronic structures such as those found in FinFETs contain metal/dielectric patterns, for which selective deposition processes may facilitate the fabrication of device features on the length scale of nanometers. The ultimate adoption of selective deposition approaches in device fabrication will require a technique that can provide for deposition of different materials with a variety of thicknesses while maintaining the selectivity even at high thickness limits. Atomic layer deposition (ALD) is a good choice for selective deposition because it is based on self-limiting reactions between gas phase precursors and specific functional groups at the

growth surface. This chemical specificity provides a means to achieve selectivity in ALD on a spatially patterned substrate.

In our previous studies, we have demonstrated area selective ALD of dielectric-on-dielectric by selectively depositing an organic self-assembled monolayer (SAM) of octadecylphosphonic acid (ODPA) as the blocking layer on metal parts of a metal/dielectric (Cu/SiO₂) pattern. This approach provided the ability to carry out selective deposition for film thicknesses above 10 nm. However, the deposition time of a well-packed ODPA passivation layer required to achieve such selectivity was over 40 hours. Also, it is desirable to remove the organic ODPA molecules from the metal surface after the process of area selective ALD. Moreover, due to the diverse chemical nature of different dielectric precursors, when using very reactive precursors the selectivity achieved using an ODPA passivation layer can be limited to dielectric film with thicknesses less than 10 nm. Here we propose a new strategy to resolve these issues by performing selective deposition combined with selective etching of dielectric films on metal/dielectric pattern.

In this approach, we first selectively deposit ODPA SAMs on a Cu/SiO₂ pattern for a reduced deposition time. Subsequent ALD processes of dielectric material on the substrate results in poor or no selective deposition on the substrates. Then we use a mild etchant to selectively remove the deposited dielectric film on Cu surface without affecting the film grown on neighboring SiO₂. X-ray photoelectron spectroscopy (XPS) and Auger electron spectroscopy (AES) measured after applying the etchant confirm no residual dielectric film on Cu, while ellipsometry and XPS results show metal oxide growth on SiO₂. We thus show that using this method, not only the area selective ALD is achievable with more rapid processing but also high selectivity can be reached for deposition of a variety of high-k dielectric materials, opening up the possibility for new applications.

5:00pm SD-WeA9 All-Dry Etching Strategy for Self-Assembly Block Copolymers PS-b-PMMA, Philippe Bézard, G. Cunge, E. Latu-Romain, A. Tavernier, LTM, France, R. Tiron, CEA-LETI, France, X. Chevalier, Arkema, France, O. Joubert, LTM - CEA/LETI, France

Vertically aligned cylinder block copolymers are often considered to be used as etching masks for hole patterning with very aggressive critical dimensions (CD) – typically sub-15nm. PS-b-PMMA, as a di-block copolymers configuration, has been thoroughly studied in the past decade [1]. The transfer strategy with PS-b-PMMA features [2] is to remove PMMA by wet or dry processes and to use PS as a mask for etching. A combination of UV and acetic acid bath has shown good results [3] but requires several specific steps as PMMA residues removal in addition to brush layer [4] and hard mask opening. An all-dry strategy would consist of trading three steps (UV, wet, PMMA residues plasma etching) with a single PMMA cylinder etching one without additional CD dispersion, providing a substantial process flow simplification for industrial purpose.

A deep understanding of both PMMA and PS etching mechanisms under various plasma conditions in terms of chemistry and ion energy is then required to overcome this challenge. Rigorous material- and plasma characterisations lead to the use of H₂-based plasma chemistry rather than O₂-based plasmas. Conventional oxygen-based plasmas result indeed in a poor selectivity (around 2) due to similar material composition, leading to CD degradation. Selectivity in H₂-based plasma benefits from PMMA-exclusive C-O and C=O bonds which are easily broken (weakening the material) when PMMA is exposed to H₂ (as evidenced by XPS and MIR results).

We will present results obtained both in synchronously-pulsed [5] and continuous wave low pressure Inductively Coupled Plasmas (ICP) in H₂-based chemistry. While synchronously-pulsed ICP plasmas allow efficient brush layer opening [3], best selectivity is achieved in continuous wave ICP plasmas.

As a result, transfer of sub-15nm 60nm-deep nanoholes into silicon with about 2nm CD dispersion has been achieved without using any hard mask strategy.

- [1] K.W. Guarini & al., J. Vac. Sci. Technol. B **19**, 2784 (2001)
- [2] R.Tiron & al., Proc. SPIE 8680, Alternative Lithographic Technologies V, 868012 (2013)
- [3] P.Bezard & al., Plasma etching of sub-14nm holes in silicon using PS-b-PMMA block-copolymer masks, PESM (2014)
- [4] X.Chevalier & al., Proc. SPIE 8680, Alternative Lithographic Technologies V, 868006 (2013)
- [5] S.Banna & al., Journal of Vacuum Science & Technology A **30**, 040801 (2012)

5:20pm SD-WeA10 Selective CVD Cobalt Capping Advanced-Groundrule Cu Interconnects : Electromigration Study, Andrew Simon, IBM Microelectronics Division, T. Bolom, GLOBALFOUNDRIES Inc., C. Niu, ST Microelectronics, F.H. Baumann, IBM Microelectronics Division, C.-K. Hu, IBM Research Division, C. Parks, J. Nag, IBM Microelectronics Division, J.-Y. Lee, GLOBALFOUNDRIES Inc., C.-C. Yang, S. Nguyen, IBM Research Division, D. Priyadarshini, D. Kioussis, IBM Microelectronics Division, T. Nogami, IBM Research Division, S. Guggilla, J. Ren, J. Aubuchon, Applied Materials, Inc.

A key requirement in scaling of Cu interconnects to groundrules at 14nm is maintaining electromigration (EM) performance. Adhesion of the Cu to the capping layer is a major reliability limitation, and adhesion-promotion schemes involving self-segregation of alloy components (e.g., Al, Mn) and selective metal capping (most often Co) have been developed. A parallel development is the use of seed-enhancement liner layers, (e.g. CVD Co), to improve conformality and Cu wettability while maintaining compatibility with established polishing processes. In this study, we compare the EM performance of CuMn self-capping to selective CVD Co capping on 22nm-Groundrule Cu interconnects, with and without the use of a CVD Co seed-enhancement layer.

Dual-damascene 22nm-groundrule interconnects were etched in a k=2.5 dielectric. Deposition of the PVD Ta(N) barrier, CVD Co liner layer and PVD Cu or CuMn seed layers was done on a clustered mainframe. After plating and CMP, capping was done either with SiC_xN_yH_z alone, or with selective CVD-Co followed by SiC_xN_yH_z.

SIMS studies [1] comparing Mn-depth profiles of CuMn-seeded samples with a PVD Ta(N)-only liner vs a Ta(N)/CVD Co liner were done on wires capped only with SiC_xN_yH_z. The PVD TaN/Ta liner shows a spike in Mn-concentration at the cap-layer interface of ~8e20 atoms/cm³, consistent with enhanced EM. In contrast, the CVD Co seed-enhancement layer results in a ~5x suppression of Mn self-capping due to the presence of the carbonyl CVD Co layer (Fig.1).

Further studies compared PVD TaN/Ta liner / CuMn seed samples vs. selective CVD Co capped-samples with either (a) PVD TaN/Ta / Cu seed - or- (b) PVD Ta(N) / CVD Co-liner / PVD Cu liner/seed schemes. Fig. 2 shows TEM/EDX images of selective-CVD Co capped samples with both PVD Ta(N)-only or PVD Ta(N) / CVD Co liners. The full-encapsulation of the Cu wire with the CVD Co liner and selective CVD Co cap is apparent in the lower-right EDX image, with strong Co signals around the entire periphery. In contrast, the sample with Co only in the selective capping layer (upper right) shows a strong Co signal only in the cap layer.

Median downstream EM lifetimes at 300C for PVD Ta(N)/ Liners with either Co caps or CuMn seedlayers were in the range of 15-40 hours (Fig.3), consistent with previously-reported activation energies of 1.0eV[2]. However, the CVD Co Liner / selective Co cap samples showed median failure times of >150 hours at 400C and >3000 hours at 340C (Fig. 4), indicating an exceptionally high activation energy of 1.7 eV. **Acknowledgements:** This work was performed by the Research and Development Alliance Teams at various IBM Research and Development Facilities

5:40pm SD-WeA11 Growth and Characterization of Ultra-Thin Silicon Dioxide Layers for Low-k Dielectrics on HOPG and Graphene, Antonio Lucero, L. Cheng, Y.G. Lee, H.H. Hwang, X. Qin, R.M. Wallace, J.Y. Kim, University of Texas at Dallas

Despite graphene's excellent electrical properties, little progress has been made in developing a successful, high performance logic device due to the difficulty of creating a band gap. A proposed device which side steps this issue is the graphene bilayer pseudo-spin field effect transistor (BiSFET)[1]. It has been suggested that a low-k, ultra-thin (<3 nm) tunneling dielectric is needed for the operation of the BiSFET. The inert surface of graphene presents challenges for the scaling that is necessary to grow this ultra-thin layer. This work focuses on the development of a SiO₂ deposition process which can be used as a low-k tunneling barrier. Additionally, we investigate the inclusion self-assembling monolayers (SAM) to further reduce the dielectric constant. To this aim, two growth techniques well-known for their thin film growth capabilities are compared: molecular beam epitaxy (MBE) and atomic layer deposition (ALD).

Growth using MBE and ALD is studied on both highly ordered pyrolytic graphite (HOPG) and transferred graphene. For MBE growth, silicon deposition is carried out in a UHV cluster tool and the films are subsequently oxidized to form SiO₂. Film growth has been scaled from 3 to 1 nm in thickness while maintaining uniform coverage. The ALD process uses tris(dimethylamino)silane and ozone at room temperature for growth. *In-situ* static ozone treatment is used to encourage nucleation similar to previous work [2]. The static ozone cycle is repeated from 3 to 10 times in order to study the scalability of the process. Thickness varies from 2 to ~1 nm, depending on the number of cycles. Growth rate is calculated using x-ray photoelectron spectroscopy (XPS) attenuation of substrate peaks and

confirmed with transmission electron microscope. Surface morphology is intensively studied using an atomic force microscope (AFM) to ensure films are continuous and uniform. Morphology for MBE and ALD films is good even when scaled to 1 nm. Raman spectroscopy confirms that no significant defects form during the growth process. Metal-insulator-metal (MIM) capacitors are fabricated in order to evaluate the effectiveness of the ultra-thin silicon dioxide films as tunneling dielectrics both as-is and with octadecyltrichlorosilane SAM functionalization. Results indicate that both MBE and ALD SiO₂ are effective tunneling dielectrics with and without OTS.

We would like to thank the Toshiba Mitsubishi-Electric Industrial Systems Corporation (TMEIC) for providing the ozone generator used in this study and SWAN for their financial support.

References:

- [1] S. K. Banerjee, et al., *Electron Device Lett.* **30**, 158 (2009).
- [2] S. Jandhyala, et al., *ACS Nano*, **6**, 2272 (2012)

Scanning Probe Microscopy Focus Topic

Room: 312 - Session SP+AS+BI+NS+SS-WeA

Advances in Scanning Probe Microscopy

Moderator: Tae-Hwan Kim, Pohang University of Science and Technology, Jewook Park, Oak Ridge National Laboratory

2:20pm **SP+AS+BI+NS+SS-WeA1 Majorana Mode in Vortex core of Bi₂Te₃/NbSe₂ Topological Insulator-Superconductor Heterostructure.** *Jinfeng Jia*, Shanghai Jiao Tong University, China **INVITED**

Majorana fermions have been intensively studied in recent years for their importance to both fundamental science and potential applications in topological quantum computing^{1,2}. Majorana fermions are predicted to exist in a vortex core of superconducting topological insulators³. However, they are extremely difficult to be distinguished experimentally from other quasiparticle states for the tiny energy difference between Majorana fermions and these states, which is beyond the energy resolution of most available techniques. Here, we overcome the problem by systematically investigating the spatial profile of the Majorana mode and the bound quasiparticle states within a vortex in Bi₂Te₃/NbSe₂⁴ by using *in situ* ultra-low temperature STM/STS. While the zero bias peak in local conductance splits right off the vortex center in conventional superconductors, it splits off at a finite distance ~20nm away from the vortex center in Bi₂Te₃/NbSe₂, primarily due to the Majorana fermion zero mode. While the Majorana mode is destroyed by reducing the distance between vortices, the zero bias peak splits as a conventional superconductor again. This work provides strong evidences of Majorana fermions and also suggests a possible route to manipulating them.

References:

1. J. Alicea, *Rep. Prog. Phys.* **75**, 076501 (2012).
2. C. W. J. Beenakker, *Annu. Rev. Con. Mat. Phys.* **4**, 113 (2013).
3. L. Fu, C. L. Kane, *Phys. Rev. Lett.* **100**, 096407 (2008).
4. M. X. Wang et al., *Science* **336**, 52 (2012)

* In cooperation with Jin-Peng Xu, Mei-Xiao Wang, Zhi Long Liu, Jian-Feng Ge, Xiaojun Yang, Canhua Liu, Zhu An Xu, Dandan Guan, Chun Lei Gao, Dong Qian, Ying Liu, Qiang-Hua Wang, Fu-Chun Zhang, Qi-Kun Xue

3:00pm **SP+AS+BI+NS+SS-WeA3 Robust Protection from Backscattering in the Topological Insulator Bi_{1.5}Sb_{0.5}Te_{1.7}Se_{1.3}.** *Fumio Komori, S. Kim, S. Yoshizawa, Y. Ishida*, University of Tokyo, Japan, *K. Eto, K. Segawa*, Osaka University, Japan, *S. Shin*, University of Tokyo, Japan, *Y. Ando*, Osaka University, Japan

Three-dimensional (3D) topological insulators (TIs) are accompanied by gapless surface states due to a nontrivial Z₂ topology of the bulk wave functions. The topological surface state (TSS) of a 3D TI is helically spin polarized, which leads to a suppression of electron scatterings due to spin mismatch between the eigenstates before and after the scattering. The suppression has been inferred from the measurements of quasiparticle interference (QPI) using scanning tunneling microscopy. No QPI was observed for intraband scatterings within unwarped TSSs. However, it has not been clear to what extent the scattering is suppressed within TSS.

In the present study, we have elucidated how the elastic scattering is suppressed as a function of the scattering angle and electron energy in the helically-spin-polarized surface electrons in a single and unwarped upper

Dirac cone of Bi_{1.5}Sb_{0.5}Te_{1.7}Se_{1.3}. In this material [1], E_F is located very close to the Dirac energy E_D. We compared the scattering wave vectors observed at 5 K with the diameters of the constant-energy contours of the unoccupied TSS which was measured by using time-resolved ARPES implementing a pump-probe method. Moreover, the inelastic scattering time of unoccupied TSS was directly obtained by this method.

At the energy above E_D, we found that there is a sharp threshold for the length of the scattering vector, above which the observed QPI intensity is abruptly diminished [2]. Such a threshold indicates the existence of a well-defined critical scattering angle beyond which elastic scattering is suddenly suppressed. The observed protection from backscattering in the TSS occurs not only for 180° but also for a wide range of angles between 100° and 180°. Such a wide angle range for the protection from backscattering is found to be essentially independent of the energy up to 300 meV above E_D until the Dirac cone becomes warped and/or the bulk scattering events intervene. At energies higher than 300 meV, we found hexagonal patterns in the FT-QPI images that come from warping of the TSS Dirac cone. In this energy range, the critical scattering vector was not clearly observed, indicating a different mechanism of the protection from backscattering in the warped Dirac cone. The observed inelastic scattering lifetime of TSS is longer than 10 psec just above E_F. The robust protection from the backscattering and long inelastic scattering in the TSS strongly support the possible applications for electronics and spintronics using weak electron scattering of TSS at E_F.

References

1. A. A. Taskin *et al.*, *Phys. Rev. Lett.* **109**, 066803 (2012).
2. S. Kim, *et al.*, *Phys. Rev. Lett.* **112**, 136802 (2014).

3:20pm **SP+AS+BI+NS+SS-WeA4 Measurements and Analysis of Sub Nanometer Stepped Surfaces Using a Traceable Atomic Force Microscope.** *Ndubuisi Orji*, National Institute of Standards and Technology (NIST), *S. Gonda*, AIST, Japan, *R.G. Dixson*, National Institute of Standards and Technology (NIST)

Although scanning probe microscopes are used in a wide variety of nanoscale measurements, the issue of instrument characterization, accuracy and calibration, continue to be a limiting factor in interpreting the resulting data. In order to accurately characterize dimensional linearity and accuracy at the sub-nanometer range, samples and robust analysis techniques suited to measurements at this range should be used.

Using Al₂O₃ surfaces on the c(0001), a(110), and r(102) planes, and robust analyses techniques, we evaluate stepped surfaces for linearity characterization at the nanoscale. Measurements were performed using a traceable atomic force microscope (T-AFM) with displacement interferometry in all three axes. The T-AFM, which has a metrology scanning stage monitored in six axes, is housed in a mini environment with a long term temperature range of less than 2 mK, and serves as a stable platform to develop calibration standards.

The smallest of the features Al₂O₃ c(0001) with a height of 0.22 nm shows a combined uncertainty of 0.01 nm, with a linearity of 0.009%. The intrinsic traceability of the T-AFM (through displacement interferometer to the SI meter) provides additional verification to the size naturally occurring steps of the Al₂O₃ and other samples used. The results show that robust and stable linearization and calibration procedures could be developed for sub nanometer SPM characterization with low uncertainty. This will enable and support accurate dimensional characterization of scientifically relevant surfaces.

4:20pm **SP+AS+BI+NS+SS-WeA7 Direct Observation of Edge States of 1D and 2D Topological insulators.** *Han Woong Yeom*, Institute for Basic Science, Republic of Korea **INVITED**

1D and 2D topological insulators (TIs) are characterized by 0D and 1D edge states of exotic spin-charge characteristics. In this talk, we introduce the first direct real space observations of such 0D and 1D edge channels of 1D and 2D TIs by scanning tunneling microscopy/spectroscopy. The 1D TI utilized is the charge density wave phase of In atomic wires formed on the Si(111) surface, which we discovered in 1999. We clearly identified, topographically and spectroscopically, two different soliton excitations along the wires. The unique features of these solitons, theoretically unraveled as chiral solitons of the Z₄ topology, are discussed. On the other hand, a Bi(111) bilayer was theoretically predicted as a 2D TI in 2005. We have grown Bi(111) bilayer nanoislands with zigzag edges on the surface of Bi₂Te₂Se. Along those edges, we identified the edge localized electronic state in accordance with first principle calculations. The unexpected electronic structures of the epitaxial Bi(111) bilayer and the Bi/Bi₂Te₂Se interface are discussed. These two findings pave the avenue towards the microscopic study and the nanoscale utilization of topological solitons and quantum spin Hall states.

5:00pm **SP+AS+BI+NS+SS-WeA9 Controlling Charges of the Dipole Layer at Metal-Semiconductor Interfaces**, *Tae-Hwan Kim*, Pohang University of Science and Technology, Republic of Korea, *H.W. Yeom*, Pohang University of Science and Technology and Institute for Basic Science, Republic of Korea

Metal-semiconductor interfaces have drawn a lot of interest in the field of semiconductor surface and interface science, and have been one of the most essential parts in semiconductor electronic and optoelectronic devices. For example, the Schottky-barrier height experimentally observed at the metal-semiconductor interface appears to be nearly independent of the work function of the metal. Since the time of Bardeen, interface gap states seem to have been a primary mechanism of the Schottky-barrier height causing Fermi level pinning at metal-semiconductor interfaces. Recently, polarized chemical bonds at metal-semiconductor interfaces have been recognised to lead to the apparent Fermi level pinning effect. When these interface bonds are formed underneath thin metal islands grown on a silicon substrate, a spontaneous charge transfer across the semiconductor-metal interfaces occurs as a result of the difference in the Fermi level positions between the metal and the semiconductor. These polarized chemical bonds can form a dipole layer. This dipole layer can play an important role in many areas of technology, for instance, in organic light emitting diodes. However, some of the fundamental aspects of the charge injection process into/from the interface dipole layer at the Schottky contact are yet not explored in any real detail.

In this work, we report the use of scanning tunneling microscopy (STM) to form a double-barrier tunneling junction (DBTJ) with thin metallic nanoislands grown on Si(111) and to control charges of the interface dipole layer formed between the metallic nanoislands and the Si(111) substrate. Reversible hysteric switchings in their $I-V$ and differential conductance spectra are observed due to the charging and discharging of the interface dipole layer in a similar fashion to molecular DBTJs. STM images clearly visualize the distinct charge states and scanning tunneling spectroscopy (STS) spectra reveal that quantum well states (QWSs) of the ultrathin islands act as the charging/discharging channels in analogy to the molecular orbitals in the case of the molecular DBTJs. This work demonstrates that the charges of the interface dipole layer at the nanoscale Schottky contact can be controlled by the electron transfer via the QWSs of the metallic islands.

5:20pm **SP+AS+BI+NS+SS-WeA10 Advances in Imaging and Quantification of Electrical Properties at the Nanoscale using Scanning Microwave Impedance Microscopy (sMIM)**, *Stuart Friedman*, *Y. Yang*, *O. Amster*, PrimeNano, Inc, *S. Johnston*, Stanford University

Scanning Microwave Impedance Microscopy (sMIM) is a novel mode for AFM-enabling imaging of unique contrast mechanisms and measurement of local permittivity and conductivity at the 10's of nm length scale. Custom shielded AFM probes enable the system to use microwaves to probe the impedance of the tip sample interface and extract information on local electrical properties of the sample. After introducing the theory of operation, we will review the state of the art, including imaging studies of microelectronic devices as well as novel materials and nanostructures, such as graphene and patterned optical crystals and ferro-electrics. These studies reveal novel information about doping distributions, domains, domain walls and other features. In addition to imaging, the technique is suited to a variety of metrology applications where specific physical properties are determined quantitatively. We will present research results on quantitative measurements of dielectric constant (permittivity) and conductivity (e.g. dopant concentration) for a range of materials. For samples where properties such as dielectric constant are known the technique can be used to measure film thickness.

5:40pm **SP+AS+BI+NS+SS-WeA11 Scanning Photocurrent Microscopy on MoS₂, MoS_{2(1-x)Se_{2x}}, and MoSe₂ Monolayer Islands and Films Grown by CVD**, *Velveth Klee*, *D. Barroso*, *E. Preciado*, University of California - Riverside, *K. Erickson*, Sandia National Laboratories, *M. Triplett*, University of California - Davis, *C. Lee*, *A. Nguyen*, *I. Lu*, *S. Bobek*, *J. Mann*, University of California - Riverside, *A. Talin*, *F. Leonard*, Sandia National Laboratories, *L. Bartels*, University of California - Riverside

We presents scanning photocurrent measurements on CVD-grown monolayer films of molybdenum disulfide, molybdenum diselenide and the alloys of these materials. Our experiments reveal a pronounced effect of the current on excitation in the gap region between contacts, as opposed to directly at the electrodes. Measurements at different irradiation intensity, irradiation position and bias shed light on the charge transfer processes in this material system. Thermal effects are ruled out by complementary measurements of thermal transport using infrared imaging.

Surface Science

Room: 309 - Session SS-WeA

Chirality and Enantioselectivity on Surfaces

Moderator: Melissa A. Hines, Cornell University, Andrew Teplyakov, University of Delaware

2:20pm **SS-WeA1 Simple Rules and the Emergence of Chirality at Surfaces**, *Rasmita Raval*, University of Liverpool **INVITED**

Chiral surfaces can be created by the adsorption of intrinsically chiral molecules, with the handedness defined by the molecule [1-4]. Additionally, a second manifestation of chirality may arise due to the molecule-substrate interaction in the form of chiral adsorption footprints. Recent advances have allowed both levels of chirality to be determined at the single-molecule level [5-8] and, surprisingly, reveal a wide range of chiral orderings. How both these aspects unfold and express themselves in organized molecular layers at surfaces is little understood. This talk will illustrate how the emergence of chirality in organised assemblies of amino-acids on a Cu(110) surface can be understood in terms of simple generic rules.

[1] *M.Ortega-Lorenzo, C.J.Baddeley, C.Muray and R.Raval, 'Extended Surface Chirality from Supramolecular Assemblies of Adsorbed Chiral Molecules', Nature, 404 (2000) 376.*

[2] *N. Liu, S. Haq, G. R. Darling and R. Raval, 'Direct Visualisation of Enantiospecific Substitution of Chiral Guest Molecules into Heterochiral Molecular Assemblies at Surfaces' Angewandte Chemie Int.Ed., 46 (2007) 7613.*

[3] *P. Donovan, A. Robin, M. S. Dyer, M. Persson, R. Raval, 'Unexpected Deformations Induced by Surface Interaction and Chiral Self-Assembly of Co(II)-Tetraphenylporphyrin adsorbed on Cu(110): A combined STM and Periodic DFT study'. Chemistry, A European Journal, 16 (2010) 11641.*

[4] *S.Haq, N. Liu, V.Humblot, A.P.J.Jansen, R.Raval, 'Drastic Symmetry Breaking in Supramolecular Organization of Enantiomerically Unbalanced Monolayers at Surfaces'. Nature Chemistry, 1 (2009) 409-414.*

[5] *M. Forster, M. Dyer, M. Persson and R.Raval, 'Probing Conformers and Adsorption Footprints at the Single-Molecule Level in a Highly Organized Amino Acid Assembly of (S)-Proline on Cu(110)'. J. Am. Chem. Soc., 131 (2009) 10173-10181.*

[6] *M. Forster, M. Dyer, M. Persson and R.Raval, '2-D Random Organization of Racemic Amino-Acid Monolayers Driven by Nanoscale Adsorption Footprints: Proline on Cu(110)', Angewandte Chemie Int. Ed., 2010 (49), 2344-47.*

[7] *A.G. Mark, M. Forster, R. Raval, Recognition and Ordering at Surfaces: The Importance of Handedness and Footedness. ChemPhysChem 2011, 12, 1474.*

[8] *M.Forster, M.S. Dyer, M. Persson, R.Raval, Tailoring Homochirality at Surfaces: Going Beyond Molecular Handedness. J. Am. Chem. Soc. 2011, 133, 15992.*

3:00pm **SS-WeA3 Exploring Enantioselectivity on Chirally Modified Surfaces in Ultrahigh Vacuum**, *Wilfred T. Tysoe*, University of Wisconsin-Milwaukee

The mode of operation of heterogeneous chiral modifiers can be classified into those operating as templates, where several modifier molecules act in concert to define a chiral adsorption site, or one-to-one modifiers that form a docking complex between the modifier and a prochiral reactant. Enantioselectivity is measured by adsorbing chiral probe molecules onto chirally modified surfaces. Templating is illustrated using amino acids on Pd(111). Scanning tunneling microscopy (STM) reveals that some amino acids form tetrameric units, and others form dimers. Only those amino acids that form tetramers are enantioselective implying that the tetramers act as templates.

Naphthylethylamine (NEA) is proposed to acts as a one-to-one modifier. The interaction between NEA and a prochiral reactant, methyl pyruvate, is explored using STM. Possible docking complexes are identified using density functional theory and the simulated images are compared with experimental images.

3:20pm **SS-WeA4 The Structure Sensitivity of L and D Tartaric Acid Explosive Decomposition on Copper Surface Structure Spread Single Crystals**, *Aaron Reinicker*, *B.S. Mhatre*, *B.S. Holsclaw*, Carnegie Mellon University, *E.C.H. Sykes*, Tufts University, *A.J. Gellman*, Carnegie Mellon University

There are many catalytic reactions that are sensitive to the surface structure of the catalyst. Surface Structure Spread Single Crystals (S⁴Cs) expose a

continuous distribution of crystal planes across their surfaces. Each point on the S^4C s has a different local crystallographic orientation that can be determined from the shape of the S^4C s and the orientation of its bulk crystal lattice vectors. Crystal planes on these S^4C s contains terraces, monatomic steps, and kinks and can be described as chiral with an R or an S orientation. When coupled with spatially resolved surface analysis techniques, S^4C s can be used to study the effects of surface structure and chirality on surface chemistry across a broad, continuous distribution of crystal planes. In this work, the structure sensitivity of L and D tartaric acid explosive decomposition was studied using a $Cu(111)\pm 10^\circ S^4C$. Isothermal Temperature Programmed Desorption (TPD) was used in which each sample was held at a temperature >20 K below the temperature of peak decomposition observed in a standard (TPD) experiment until the decomposition reaction occurred. Spatially resolved X-ray Photoelectron Spectroscopy (XPS) was performed to determine which crystal planes on the $Cu(111)\pm 10^\circ S^4C$ had undergone explosive decomposition after quenching the temperature of the sample at the decomposition peak during an isothermal TPD. Quenching the sample at different times during the isothermal TPD decomposition peak was implemented to visualize the stages of reaction on the $Cu(111)\pm 10^\circ S^4C$ surface. It was found that both D-tartaric acid and L-tartaric acid reacted on crystal planes with (100) steps before crystal planes with (111) steps and the surface structure had more of an effect on the explosive decomposition of tartaric acid than the surface chirality.

4:20pm **SS-WeA7 Ordering of L-alaninate Superstructures on Cu(001)**, *Erkan Ciftlikli, B.J. Hinch*, Rutgers University

Multiple domains of a $c(4\times 2)$ superstructure are produced following dissociative L-Alanine adsorption on Cu(001) at temperatures of $0^\circ C$ and above. The anticipated structure at 0.25ML relies on stabilization of a tridentate surface species, in ordered arrays, held together with intermolecular H bonding. He atom diffraction is benign, and the films can be investigated over the course of days. The saturated $c(4\times 2)$ structure is stable up to $\sim 200^\circ C$. In contrast the subsaturation surfaces are thermally unstable and a slow relaxation occurs after nucleation of $c(4\times 2)$ domains. He-surface bound state resonances are seen to affect the symmetries of the He diffraction intensities and the inelastic He-phonon cross sections observed from the chiral adsorbate. The enhanced inelastic scattering intensities are used to compare the vibrational characteristics of saturated and sub-saturation L-Ala/Cu(001) surfaces.

4:40pm **SS-WeA8 Quantitation of Enantiospecific Adsorption on Chiral Nanoparticles from Optical Rotation**, *Nisha Shukla, N. Ondeck, N. Khosla, A.J. Gellman*, Carnegie Mellon University

Au nanoparticles modified with enantiomerically pure D- or L-cysteine have been shown to serve as enantioselective adsorbents of R- and S-propylene oxide [1]. A simple adsorption model and accompanying experimental protocol have been developed to enable optical rotation measurements to be analyzed for quantitative determination of the ratios of the enantiospecific adsorption equilibrium constants of chiral species on the surfaces of chiral nanoparticles, $(K^S_L / (K^S_D)) = (K^R_D) / (K^R_L)$. This analysis is robust in the sense that it obviates the need to measure the absolute surface area of the absorbent nanoparticles, a quantity that is somewhat difficult to obtain accurately. This analysis has been applied to optical rotation data obtained from solutions of R- and S-propylene oxide, in varying concentration ratios, with D- and L-cysteine coated Au nanoparticles, in varying concentration ratios [2].

[1] N. Shukla, M.A. Bartel, A.J. Gellman "Enantioselective separation on chiral Au nanoparticles" *Journal of the American Chemical Society*, 132(25), (2010), 8575–858.

[2] N. Shukla, N. Ondeck, A.J. Gellman "Quantitation of Enantiospecific Adsorption on Chiral Nanoparticles" *Surface Science*, (accepted-2014).

5:00pm **SS-WeA9 Low-Temperature STM Observation of Asymmetrical Adsorption and Chirality of Ga Adatoms on Wurtzite GaN(000-1)**, *Khan Alam, A. Foley, J. Corbett, Y. Ma, J. Pak, A.R. Smith*, Ohio University

A sample with atomically flat terraces having the $c(6\times 12)$ reconstruction on GaN(000-1) surface is grown by molecular beam epitaxy and studied at liquid helium temperature using scanning tunneling microscopy. Being the most Ga-rich reconstruction (corresponding to the Ga stability limit) occurring on the N-polar GaN surface, [1] low-temperature STM imaging reveals new details of the $c(6\times 12)$, although not inconsistent with the early model. [2] Unexpectedly however, a dilute concentration (0.0031 ML) of single atomic adsorbates not seen at room temperature is found covering the terraces. The coverage is stable with time and increases with Ga flux during growth. These adsorbate features are thus attributed to the condensation of Ga adatoms which at room temperature would be in a 2D gas-like state at the surface. Surprisingly, the Ga adsorbates manifest at ~ 2.5 V sample bias

as distinct L-shapes which are always in one of two possible orientations with respect to $\langle 10-10 \rangle$. Furthermore, on any given atomic terrace, the probability of finding one of the two L-shape orientations is 80%, reversing across a step. However, no in-plane rotation will result in the opposite handed-ness of an L-shape, on either terrace. The L-shaped adsorbates thus reveal broken chiral symmetry linked to adsorption probability, which is attributed to symmetry breaking of the $c(6\times 12)$ reconstruction.

5:20pm **SS-WeA10 Enantioselectivity and Auto-Amplification by Adsorption**, *Andrew Gellman, Y. Yun*, Carnegie Mellon University

Metal surfaces can be rendered chiral by cleavage along low symmetry planes of the bulk metal lattice. Their chirality results in the enantioselective adsorption of chiral molecules from racemic mixtures. This work has developed and applied a ^{13}C isotopic labeling method for mass spectrometric detection and quantification of enantiospecific adsorption on chiral surfaces. Enantiomerically pure chiral compounds in which one enantiomer is available in an isotopically labelled form allow the design of experiments in which one can expose chiral or achiral surfaces to mixtures of varying enantiomeric excess in the gas phase (ee_g) and then use mass spectrometry to determine enantiomeric excess on the surface (ee_s).

Exposure of a racemic mixture of D-aspartic acid and ^{13}C -L-aspartic acid to the chiral $Cu(3,1,17)^{R\&S}$ surfaces results in the adsorption of a non-racemic monolayer because of the selective adsorption of one enantiomer over the other. ^{13}C -labeling allows mass spectrometry to distinguish the two enantiomers during desorption from the surface.

These measurements have been used to quantify the enantiospecific adsorption equilibrium constants and the enantiospecific difference in the free energies of adsorption of D- and L-aspartic acid on the chiral $Cu(3,1,17)^{R\&S}$ surfaces.

Not surprisingly, exposure of a racemic mixture of D- and ^{13}C -L-aspartic acid to the achiral Cu(111) results in the adsorption of a racemic mixture; in other words, a gas phase mixture with $ee_g = 0$ results in an adsorbed mixture with $ee_s = 0$. However, exposure of the achiral Cu(111) surface to a gas phase mixture with $ee_g = 0.2$ results in an adsorbed phase with $ee_s = 0.4$. In spite of the fact that the surface is achiral adsorption results in auto-amplification of enantiomeric excess. Although the mechanism of auto-amplification has not been confirmed, one can show that this can be a simple consequence of adsorption of gas phase monomers in the form of homochiral clusters L_n or D_n .

In general, during adsorption on chiral surfaces, the phenomena of enantiospecific adsorption and auto-amplification must be occurring and either competing or augmenting one another.

Thin Film

Room: 307 - Session TF+EM+EN-WeA

Thin Film and Nanostructured Coatings for Light Trapping, Extraction, and Plasmonic Applications

Moderator: Tansel Karabacak, University of Arkansas at Little Rock

2:20pm **TF+EM+EN-WeA1 Enhanced Light Trapping by Glancing Angle Deposited Semiconducting and Metallic Nanostructure Arrays**, *Hilal Cansizoglu, R. Abdulrahman, M.F. Cansizoglu*, University of Arkansas at Little Rock, *M. Finckenor*, NASA Marshall Space Flight Center, *T. Karabacak*, University of Arkansas at Little Rock

Management of light trapping in nano materials has recently got attention owing to altering optical properties of materials commonly used in potential applications such as photovoltaics and photonics. Trapping the light inside the semiconducting nanostructure coating can increase optical absorption capacity of the material dramatically. Meanwhile, metallic nanostructures can serve as individual back reflectors if the light is achieved to be trapped among metallic nanostructures, which results in enhanced optical absorption of the possible surrounding absorber material around metallic structures. In this study, we examine light trapping in arrays of zig-zags, springs, screws, tilted rods, and tapered vertical rods of indium sulfide (In_2S_3) and aluminum (Al) as the model semiconducting and metallic materials, respectively. Nanostructures of different shapes were produced by glancing angle deposition (GLAD) technique. We investigated the effect of size and shape of the arrays on light trapping properties using ultraviolet-visible-near-infrared (UV-VIS-NIR) spectroscopy and finite difference time domain (FDTD) simulations. Optical characterization results show that light trapping by GLAD nanostructures can strongly depend on their shapes. Under normal incidence of light, 3D geometries of semiconducting nanostructures such as springs, screws, and tapered vertical rods can

provide an enhanced optical absorption compared to zigzags, and tilted rods. In addition, total reflectance measurements reveal that reflectance is inversely proportional to metallic nanorod length in the wavelength range of 200-1800 nm. Meanwhile, FDTD optical modelling indicates an enhanced diffuse light scattering and light trapping through uniform distribution of diffracted light within the 3D In_2S_3 nanostructure geometries such as springs, screws and vertical rods. On the other hand, zigzags and tilted rods show light absorption at relatively low level similar to the experimental results. In addition, simulations reveal that average reflectance of Al nanorods can drop down to as low as ~50%, which is significantly lower than the ~90% reflectance of conventional flat Al film at similar wavelengths. Our results demonstrate that GLAD nanostructures can provide efficient light trapping through the control of their shapes and size.

2:40pm TF+EM+EN-WeA2 Enhanced Photoresponsivity of Conformal TiO_2/Ag Nanorod Arrays Fabricated via (Successful) Glancing Angle and Atomic Layer Deposition, Ali Haider, N. Biyikli, A.K. Okyay, Bilkent University, Turkey, T. Karabacak, H. Cansizoglu, University of Arkansas at Little Rock, B. Teckcan, Bilkent University, Turkey, M.F. Cansizoglu, University of Arkansas at Little Rock

Improved charge carrier collection and optical absorption are two main techniques to enhance the photocurrent of a nanostructured photodetector. In a nanostructured photodiode, longer carrier life time and shorter transit time of the photo-generated carriers provides efficient charge carrier collection while the nanostructured device architecture contributes towards trapping the light by diffuse light scattering and enhancing optical absorption. However, efficient charge carrier collection is limited by the random and non-uniform nano-network. For nanostructured Schottky photodetectors, uniform nanostructured geometries with larger aspect ratio can enhance the interface of the Schottky junction which in turn decreases the transit time of generated carriers. In addition, most of the nanofabrication methods that can produce uniform nanostructure geometries are limited to certain materials. Therefore, it is an overwhelming demand to develop innovative low-cost nanostructured photodetector fabrication methodologies which enables the use of a variety of semiconductor alloy families with uniform and optimized geometries for improving photoresponsivity performance. In this work, we demonstrate a proof-of-concept nanostructured Schottky photodiode fabrication method combining glancing angle deposition (GLAD) and atomic layer deposition (ALD) to fabricate metal-semiconductor radial junction nanorod arrays, which offers significantly enhanced photoresponse compared to conventional planar counterpart. Firstly, silver (Ag) nanorod (NR) arrays were deposited on Ag thin film/Si templates by utilizing glancing angle deposition (GLAD) technique. A conformal and thin titanium dioxide (TiO_2) coating was deposited on silver nanorods via ALD. ALD emerge as highly attractive deposition technique for coating of nanorods due to its remarkable conformality and uniformity on the densely packed NR structures. Moreover, ALD also facilitates the ultra-precise control of deposited film thickness in the sub-nm scale. Following the growth of TiO_2 on Ag NRs, aluminum (Al) metallic top contacts were deposited by thermal evaporation to complete the fabrication of NR-based Schottky photodiodes. Due to the improved charge carrier collection and optical absorption, the resulting nanostructured detector exhibits a more-than two orders of magnitude photoresponsivity enhancement factor (3.8×10^2) under 3V reverse bias when compared to the corresponding thin film counterpart device with the same TiO_2 thickness. Our preliminary structural, optical, electrical, and photoresponse characterization results are presented.

3:00pm TF+EM+EN-WeA3 Nanostructured Photonic Materials for Light-Trapping and Photon Management in Solar Energy Conversion, Koray Aydin, Northwestern University INVITED

Nanophotonics, the emerging field of photon-material interactions at the nanoscale, poses many challenges and opportunities for researchers both in the basic and applied sciences. In this talk, I will describe our efforts in designing, realizing and characterizing nanostructured photonic materials including metals, transparent conductive oxides and inorganic semiconductors. By shaping materials at the nanoscale, one can drastically increase absorption in and/or scattering from nanostructures that could provide significant performance enhancements in solar energy conversion processes including photovoltaics and photocatalysis. First, I will discuss our research efforts on realizing broadband plasmonics absorbers enabled by nanophotonic light-trapping approaches in metal-insulator-metal resonators. By using reflective metals and transparent dielectrics, we have achieved significant absorption enhancement in the metallic parts opening routes for spectrally and spatially selective light-absorbing devices that could find use in thermophotovoltaics and hot-electron collection devices. Then, I will describe light-trapping in nanostructured inorganic silicon ultrathin films which results in drastic absorption enhancement over the entire solar spectrum and over the wide range of incident angles. This approach does not involve any plasmonic components and based solely on

localized and delocalized resonances in semiconductor nanostructures. This novel resonant light absorption phenomenon in semiconductors could find use in photocatalytic and photovoltaic applications of inorganic semiconductors. Finally, I will talk about our results on nanostructured transparent conductive oxide contacts, which is capable of light trapping over broad range of wavelengths. Nanostructured TCO contacts could benefit both organic and inorganic photovoltaic materials, offering significant absorption and short circuit enhancements.

4:20pm TF+EM+EN-WeA7 Porous Solid Phase Microextraction (SPME) Fibers by Oblique Angle Deposition, Anubhav Diwan, B. Singh, Brigham Young University, M. Kaykhani, Sistan & Baluchestan University, Iran (Islamic Republic of), B. Paul, P. Nesterenko, University of Tasmania, Australia, M.R. Linford, Brigham Young University

Solid phase microextraction (SPME) is a solvent-free technique used for extracting organic compounds from matrices such as air or wastewater. It involves a fiber coated with a liquid or solid stationary phase that extracts target compounds directly from a solution or from the head space above a solution or material. Solid stationary phases provide faster extraction than liquid phases, but exhibit lower capacities. Porous solid phases have been able to overcome these issues by providing large surface areas for analyte adsorption. Commercial SPME fibers are rather expensive, swell in many solvents, and often extract limited numbers of compounds (show limited selectivity). Herein, we discuss the preparation of porous SPME fibers by oblique angle deposition (OAD) of sputtered silicon or other materials onto a fiber. OAD involves deposition of materials onto substrates placed at steep angles with respect to the direction of the incoming species, creating porous structures. The resulting nanoporous coatings can be modified with different functional groups to enhance selectivity of the phase towards target compounds. If normalized for thickness, our fibers show ca. three times the capacity of a commercial, 7 μm PDMS fiber. To confirm their morphologies, new OAD-based fibers have been characterized by scanning electron microscopy (SEM). Various silane coatings can be applied to our fibers, which will offer a range of selectivities. These coatings, e.g., a C18 silane, have been characterized on model planar substrates by X-ray photoelectron spectroscopy (XPS) and contact angle goniometry (wetting).

4:40pm TF+EM+EN-WeA8 Chiral Patchy Particle Arrays: A Simple Fabrication Method to Achieve Plasmonic Circular Dichroism in the Visible Region, George Larsen, Y. He, W. Ingram, Y.P. Zhao, University of Georgia, Athens

An object is said to be "chiral" if it cannot be made superimposable upon its mirror image solely by rotations and translations. That is, chiral objects do not exhibit reflective symmetry. By combining self-assembled colloid monolayers and glancing angle deposition (GLAD), we can create chiral patchy particle thin films that exhibit plasmonic activity in the visible region. Due to their chirality, these patchy particle films exhibit circular dichroism, i.e., they absorb right- and left-circular polarized light to different degrees. Interestingly, we find that the GLAD method relaxes requirements on the template quality, allowing for the production strongly chiral films from polycrystalline colloidal monolayers with randomly oriented domains. It is determined that the rotation direction during GLAD breaks the racemic symmetry of the templates by creating a chiral distribution of material which enhances the chirality of one set of enantiomers relative to the other. Microscopic analysis and geometric chirality calculations confirm that the optical chirality of the bulk film results from incomplete cancellations of even stronger local chiralities. By improving the quality of the colloidal monolayers and intentionally creating a chiral material distribution, we seek to use these chiral patchy particle arrays as plasmonic biosensors that are sensitive to the handedness of the target molecule.

5:00pm TF+EM+EN-WeA9 Tunable Three-Dimensional Helically Stacked Plasmonic Layers on Nanosphere Monolayers, Yizhuo He*, G.K. Larsen, W. Ingram, Y.P. Zhao, University of Georgia, Athens

Chiral metamaterials are artificial materials designed to interact with left- and right-handed circularly polarized light in different ways. Such a unique optical property enables applications such as negative refractive index, circular polarization, enantiomer sensing, etc. Practical applications usually require the fabrication of large-area chiral metamaterials on substrates with tunable chiroptical properties, especially in visible to near infrared wavelength region. We report a simple and scalable method to fabricate three-dimensional chiral metamaterial combining glancing angle deposition and self-assembled colloidal monolayers. Ag and SiO_2 are deposited alternately on colloidal monolayers. By controlling the azimuthal rotation of substrates between depositions, Ag and SiO_2 layers can be helically stacked in left-handed and right-handed fashions to form continuous

*** TFD James Harper Award Finalist**

helices. These helically stacked plasmonic layers (HSPLs) exhibit localized surface plasmon resonances (LSPR) and strong chiroptical responses in visible to infrared region, which is also confirmed by finite-difference time-domain simulations. The most important feature of HSPLs is the great tunability of chiroptical spectra. By increasing the nanosphere diameter from 200 nm to 500 nm, the HSPL structure can be scaled up and thus the LSPR peak redshifts from 520 nm to 1000 nm. Since the chiroptical response originates from the strong interaction of metal layers with light, i.e. LSPR, the chiroptical spectra also redshifts accordingly without a significant change in magnitude. With such flexibility in the design, HSPLs may act as tunable chiral metamaterials, as well as serve as different building blocks for chiral assemblies.

5:20pm TF+EM+EN-WeA10 Co-deposition of Mixed-Valent Oxides of Molybdenum and Germanium ($\text{Mo}_x\text{Ge}_y\text{O}_z$): A Route to Tailored Optical Absorption, Neil Murphy, Air Force Research Laboratory, L. Sun, General Dynamics Information Technology, J.G. Jones, Air Force Research Laboratory, J.T. Grant, General Dynamics Information Technology

Mixed-valent oxides of molybdenum and germanium were deposited simultaneously using reactive magnetron co-deposition within an oxygen-argon environment. The films' stoichiometry, optical and physical properties were varied through changes in oxygen partial pressure induced by systematic variation of the potential applied to the molybdenum cathode. The oxygen partial pressure was determined from the drop in pressure as measured by a capacitance manometer, assuming constant argon partial pressure. To facilitate deposition, a constant power of 100 W DC was applied to the germanium cathode, while power was applied to the molybdenum target using a modulated pulse power supply. Modulated pulse power magnetron sputtering was used due to its ability to generate high target power densities, allowing for rapid reduction of oxygen on the surface of the "oxygen poisoned" molybdenum cathode, as well as for its highly metallic plasma resulting in increased oxygen-gettering capability. Changes in the modulated pulse power supply's capacitor bank charge, stepped from settings of 300 to 380 V, resulted in films ranging from mixtures of transparent GeO_2 (Ge^{4+}) and MoO_3 (Mo^{6+}) to the introduction of various absorptive ionic species including Mo^{5+} , Mo^{4+} , Ge^{2+} and Ge^0 , as determined from X-ray photoelectron spectroscopy. The presence of each of the aforementioned ions results in characteristic changes in the films' band energies and optical absorption, measured using UV-VIS-NIR optical spectroscopy. As deposited $\text{Mo}_x\text{Ge}_y\text{O}_z$ thin films grown using this method have been shown to have band gaps that are able to be tailored between 2.8 eV and 0.6 eV, spanning useful ranges for devices operating in the visible and near-infrared.

5:40pm TF+EM+EN-WeA11 Permanent Optical Tape and Solid State Data Storage Devices, Hao Wang, R. Gates, N. Madaan, J. Bagley, A. Diwan, A. Pearson, S. Jamieson, K. Laughlin, Brigham Young University, Y. Liu, Lehigh University, B. Lunt, M. Asplund, Brigham Young University, V. Shutthanandan, Pacific Northwest National Laboratory, R.C. Davis, M.R. Linford, Brigham Young University

Recently we have prepared novel write–once–read–many (WORM) optical stacks on Mylar for archival data storage in an optical tape format.¹ Here, a nanoscale, co-sputtered bismuth–tellurium–selenium (BTS) alloy was employed as the write layer with carbon protective layers on both the top and bottom of the BTS film. We have successfully written information (matrix of marks) on the C/BTS/C optical stack using a 532 nm laser. Both the optical stack structure (film thickness) and writing conditions (laser power and laser spot size) have been optimized. Films were characterized by X-ray diffraction, X-ray photoelectron spectroscopy, time-of-flight secondary ion mass spectrometry, scanning electron microscopy, spectroscopic ellipsometry, and atomic force microscopy.^{2,3}

We have also recently developed novel WORM solid-state memory elements. These consisted of nanoscale, bowtie-like sputtered carbon films to which a voltage (ca. 10 V) is applied. These fuses have been successfully blown, and the carbon fuse shape, thickness of the carbon layer, and writing voltage have been optimized. Other aspects of the device are currently being optimized.

References

- [1] Wang, H.; Lunt, B.M.; Gates, R.J.; Asplund, M.C.; Shutthanandan, V.; Davis, R.C.; Linford, M.R. Carbon/ternary alloy/carbon optical stack on Mylar as an optical data storage medium to potentially replace magnetic tape, *ACS Appl. Mater. Interfaces*, **2013**, 5, 8407-8413.
- [2] Wang, H.; Diwan, A.; Lunt, B.M.; Davis, R.C.; Linford, M.R. XPS and SIMS characterization of a BiTeSe write layer for permanent optical tape storage, *Proceedings of ISOM 2013*, ISOM 2013 International Conference, Incheon, South Korea, 2013.
- [3] Wang, H.; Lunt, B.M.; Davis, R.C.; Linford, M.R. Simulation of laser writing on Bi-Te-Se alloy/carbon/Mylar permanent optical storage tape, ISOM 2013 International Conference, Incheon, South Korea, 2013.

Vacuum Technology

Room: 303 - Session VT-WeA

Accelerator and Large Vacuum Systems II

Moderator: James Fedchak, National Institute of Standards and Technology (NIST)

2:20pm VT-WeA1 Load locks, Transfer arms, and other In-Vacuum Motions in the Cornell DC Photoelectron Gun Development Project, Karl Smolenski, X. Liu, B. Dunham, L. Cultrera, J. Conway, Cornell University

INVITED

The Cornell DC photoelectron guns pose a series of challenging vacuum engineering problems. These high brightness electron sources have produced the highest currents (0.075A) yet achieved from a photocathode source and are prototypes for future state of the art accelerators. The guns operate in the XHV (<1e-11 Torr) with massive NEG pumping and require exchange of the photocathode wafer periodically for continuous operation. The scale of the vacuum vessel, set by the extreme high voltages, requires the use of meter scale transfer arms to load and extract the photocathode holder with minimal disruption to the vacuum level and without particulate generation. These transfers are required to be rapid and simple to minimize operational downtime.

We have developed a series of mechanisms to retain the photocathodes, magnetic and bellows-coupled transfer arms to move samples between chambers, and load locks to introduce cathodes into the vacuum systems. More recently vacuum suitcases have been employed to move photocathodes from remote labs to our accelerators and to other laboratories for testing. This talk will present our experiences maintaining large scale systems with extensive in-vacuum motions under extreme requirements.

3:00pm VT-WeA3 Vacuum Performance of 5-mm Undulator Chamber for Cornell High-Energy Synchrotron Source, Yulin Li, X. Liu, A. Lyndaker, A. Temnykh, Cornell University

To significantly enhance the X-ray beam performance at Cornell High-Energy Synchrotron Source (CHESS), a 3.9-m long, 5-mm vertical aperture undulator vacuum chamber were designed, constructed and tested at Cornell Electron Storage Ring (CESR). The vacuum chamber is constructed of aluminum (Type 6061-T6) extrusions with an electron beam aperture (with nominal 5-mm vertical and 90-mm horizontal apertures), a pump antechamber and a cooling channel. To minimize the undulator magnet pole gap, pockets were machined on top and bottom of the extrusion in the middle portion. With the top and bottom wall thickness of 0.6 mm, the effective beam vertical aperture is reduced to 4.5mm owing to deflection from the atmospheric pressure. The undulator vacuum chamber was tested at its final designated location in CESR near a strong dipole magnet, intercepting high synchrotron radiation (SR) power and flux. To handle very high distributed gas load due to SR-induced desorption, six non-evaporable getter/ion pumps (NexTorr D100-5, SAES Getters) were installed along the undulator chamber. The test chamber was equipped with four cold cathode ionization gauges (CCGs) and a residual gas analyzer (RGA) to monitor vacuum performance. In this talk, we will present the construction, mechanical and vacuum qualifications, and the beam conditioning history of the undulator vacuum chamber. We will summarize the experiences learnt from the successful week-long beam tests.

3:20pm VT-WeA4 Near-XHV Pressure Characterization for the Jefferson Lab Polarized Electron Source, Marcy Stutzman, P. Adderley, Thomas Jefferson National Accelerator Facility, M.A. Mamun, A.A. Elmustafa, Old Dominion University, M. Poelker, Thomas Jefferson National Accelerator Facility

Long operational lifetime at the Jefferson Lab high polarization electron source requires vacuum approaching XHV (1×10^{-10} Pa). Determining the ultimate pressure in a chamber requires minimizing outgassing rate, maximizing pumping, and accurately measuring pressure. Two systems were used to study the ultimate pressure that could be achieved: test chambers that were fabricated to characterize the effects on outgassing of different chamber material processing and coatings, and a cryopumped electron source sized chamber. This paper presents both the characterization of XHV gauges and the ultimate pressure achieved in the various chambers. The extent to which temperature dependent outgassing rate can be exploited to improve ultimate pressure will also be discussed. Finally, progress on reconciling the persistent discrepancies between calculated and measured pressure will be presented.

4:20pm **VT-WeA7 Design Optimization and Fabrication Progress of ITER's Large Custom Vacuum Pumps**, *Robert Pearce, M. Dremel, L. Worth*, ITER Organisation, France, *L. Baylor, S. Meitner*, Oak Ridge National Laboratory

INVITED

ITER is under construction in the south of France in order to demonstrate the feasibility of fusion as a clean power source. It is one of the world's largest scientific and engineering collaborations. The civil structures, to house the ITER machine, are progressing, and the key systems and components are moving from design to manufacturing.

The ITER vacuum system will be one of the largest, most complex vacuum systems ever to be built. There are a number of large volume systems including: the cryostat (~ 8500m³), the torus (~1330 m³), the neutral beam injectors (~180m³ each) and a number of lower volume systems including: the service vacuum system, diagnostic systems, and electron cyclotron transmission lines. In total there are more than 400 vacuum pumps of 10 different technologies required to pump the systems. The most demanding vacuum pumping applications are served by 18 large cryogenic pumps of 3 distinct custom designs.

The ITER vacuum vessel and cryostat are to be pumped by a total of 8 cylindrical cryo-sorption pumps with integral 800 mm all metal vacuum valves. The "build-to-print" design of these pumps has been optimised and finalised and the first pump is being manufactured.

The ITER neutral beam systems are each pumped by a pair of open structure panel style cryo-sorption pumps with a length of 8 m, and height of 2.8 m. They should achieve a pumping speed of 4500 m³/s for hydrogen. The final design of these pumps has involved development of new fabrication methods so as to significantly reduce the cost and manufacturing time for the thousands of cryo-panels and thermal shields within the pumps. The design is ready for manufacture, with the first pump destined for the ITER neutral beam test facility (MITICA).

During plasma operations, to pump the mixture of gasses originating from the regenerations of torus and neutral beam cryo-pumps, the roughing system will utilize 6 cryogenic viscous flow compressors (CVC). The principle of the CVC is that it will cryogenically condense hydrogen isotope mixtures, while providing first stage compression of helium ash originating from the fusion process. Each CVC is designed for throughputs of 200 Pam³/s and consists of a tube heat exchanger housed in a cryostat of diameter ~1 m and height 2.5 m. The very novel nature of this pump requires a full size prototype, which has been manufactured and will go through a test campaign.

In this paper an overview is given of the ITER construction. Examples of the cryo-pump 'value engineering' and design optimization for manufacturing are given. Progress and challenges in the "First of a Kind"(FOAK) vacuum pump manufacturing are given.

5:00pm **VT-WeA9 Commissioning of the KATRIN Main Spectrometer**, *Joachim Wolf*, Karlsruhe Institute of Technology, Germany

The objective of the Karlsruhe Tritium Neutrino experiment (KATRIN) at the Karlsruhe Institute of Technology (KIT) is the measurement of the electron neutrino mass with an unprecedented sensitivity of 200 meV by using electrons from the beta-decay of tritium. A central component is the electro-static main spectrometer (MS), where the energy of the beta-electrons (18.6 keV) will be measured with high precision. It consists of a large ultra-high vacuum vessel with a volume of 1240 m³ and a surface of 690 m², instrumented with a complex inner wire-based electrode system, which almost doubles the inner surface of the MS.

The pumping system of the MS consists of 6 turbo-molecular pumps (10 000 l/s), a large-scale getter pump (3000 m NEG strips, St707, 10⁶ l/s) and three cryo-baffles (6.8 m²) at LN₂ temperature. The vacuum system has three major tasks: (I) the ultimate pressure, dominated by H₂, has to be kept in the range of 10⁻¹¹ mbar in order to maintain a low background rate. (II) In conjunction with a differential pumping section and a cryogenic pumping section of the electron beam line, which connects the gaseous tritium source with the spectrometer, it has to keep the partial pressure of tritium in the MS below 10⁻²¹ mbar. (III) The NEG strips are known to emanate a small amount of radon atoms, increasing the intrinsic background rate. Therefore cryogenic baffles at LN₂ temperature have been installed in front of the NEG pumps, which are expected to capture most of the radon atoms, before they can enter the sensitive volume of the MS. This paper describes the design of the vacuum system and reports on measurements of the vacuum performance during the first commissioning of the whole spectrometer system.

This work has been supported by the German BMBF (05A11VK3 and 05A11PM2).

2D Materials Focus Topic

Room: 310 - Session 2D+AS+HI+NS+SS-ThM

Nanostructures including 2D Heterostructures, Patterning of 2D Materials

Moderator: Kirill Bolotin, Vanderbilt University

8:00am 2D+AS+HI+NS+SS-ThM1 **Stitching and Stacking for Atomically Thin Circuitry**, Jiwoong Park, Cornell University INVITED

The development of large scale growth methods based on chemical vapor deposition (CVD) has enabled production of single-atom-thick films with diverse electrical properties, including graphene (conductor), h-BN (insulator), and MoS₂ (semiconductor). Precise vertical stacking and lateral stitching of these 2D materials will provide rational means for building ultrathin heterostructures with complex functionality. However, large scale production and control of these structures requires new characterization and fabrication approaches. In this talk, I will first discuss the structure and physical properties unique to CVD graphene in single and bilayers. Using the atomic-resolution imaging as well as a dark-field transmission electron microscopy (TEM) technique, our group investigated the structure of grain boundaries in CVD graphene and its impact on the mechanical, electrical, and chemical properties. This allowed us to produce CVD graphene with optimized electrical properties. We also reported a new patterned regrowth method to fabricate 2D lateral heterojunctions entirely made of graphene and h-BN, which enables the development of atomically thin integrated circuitry. If time allows, I will also discuss our recent results on the large scale growth of high quality single layer MoS₂ as well as graphene film with a uniform lattice orientation. Our characterization and growth approach would ultimately allow the fabrication of electrically isolated active and passive elements embedded in continuous, one-atom-thick sheets, which could be manipulated and stacked to form complex devices at the ultimate thickness limit.

8:40am 2D+AS+HI+NS+SS-ThM3 **Vertical and Lateral Heterostructures of Carbon Nanomembranes (CNMs) and Graphene**, Andreas Winter, University of Bielefeld, Germany, M. Woszczyna, R. Stosch, T. Weimann, F. Ahrelrs, Physikalisches Bundesanstalt, Germany, A. Turchanin, University of Bielefeld, Germany

Heterostructures of graphene with other 2D materials are of great interest for nanoscience and nanotechnology. However, their fabrication is still not a trivial task. Here we present the engineering and characterization of (i) vertical and (ii) lateral heterostructures of molecular thin (~1 nm) dielectric carbon nanomembranes (CNMs) made of aromatic molecules [1] and single-layer (SLG) graphene sheets. (i) The vertical CNM/SLG heterostructures with terminal amino-groups (NH₂-) are assembled via the mechanical transfer onto oxidized silicon wafers. We show by complementary spectroscopy and microscopy techniques as well as by electric transport measurements that functional amino groups are brought into close vicinity of the SLG sheets and that electric transport of the SLG is not impaired by this assembly, leading to the non-destructive chemical functionalization of graphene [2]. (ii) *The lateral heterostructures* are engineered using electron-irradiation-induced crosslinking of SLG sheets with CNMs. We demonstrate reliable production of well-defined laterally patterned CNM-SLG heterostructures of various sized and architectures on solid substrates and as free-standing sheets, and characterize their properties by Raman spectroscopy and helium ion microscopy.

[1] A. Turchanin and A. Götzhäuser, Carbon nanomembranes from self-assembled monolayers: Functional surfaces without bulk. *Prog. Surf. Sci.* 87, 108-162 (2012)

[2] M. Woszczyna et al., All-carbon vertical van der Waals heterostructures: Non-destructive functionalization of graphene for electronic applications. *Adv. Mater.* 26 (2014) DOI: 10.1002/adma.201400948

9:00am 2D+AS+HI+NS+SS-ThM4 **Gate Tunable Carbon Nanotube - Single Layer MoS₂ p-n Heterojunctions**, Deep Jariwala*, V.K. Sangwan, C.-C. Wu, P.L. Prabhumirashi, M.L. Geier, T.J. Marks, L.J. Lauhon, M.C. Hersam, Northwestern University

The isolation of graphene and the subsequent reports on its electronic properties have spurred tremendous interest in a variety of two dimensional (2D) materials for electronic device applications. Layered semiconducting transition metal dichalcogenides (TMDCs) of Mo and W have emerged as

promising alternatives to graphene for optoelectronic applications due to their finite band gap in the visible portion of the electromagnetic spectrum.¹ The atomically thin structure of these 2D materials coupled with van der Waals bonding between adjacent layers allows their stacking into atomically sharp heterostructures with defect-free interfaces, in contrast to epitaxially grown III-V semiconductor heterostructures where the material choices are constrained by lattice matching. Additionally, the few atom thickness of the individual layers enables doping modulation of the overlying layers in a heterostructure using a global back gate. While a large number of heterostructure devices employing graphene have been reported, it's gapless band structure prevents the formation of a large potential barrier for charge separation and current rectification. Consequently, a p-n heterojunction diode derived from ultrathin materials is notably absent and significantly constrains the fabrication of complex electronic and optoelectronic circuits. Here we demonstrate a gate-tunable p-n heterojunction diode using semiconducting single-walled carbon nanotubes (s-SWCNTs) and single-layer molybdenum disulfide (SL-MoS₂) as atomically thin p-type and n-type semiconductors, respectively. The vertical stacking of these two direct band gap semiconductors forms a heterojunction with electrical characteristics that can be tuned with an applied gate bias over a wide range of charge transport behavior, ranging from insulating to rectifying with forward-to-reverse bias current ratios exceeding 10⁴. In addition, the gate-dependent characteristics of this diode exhibit a unique 'anti-ambipolar' behavior with two off-states at either extremes of the gate voltage range and a maximum on-state current between them. This heterojunction diode also responds to optical irradiation with photoresponse time < 15 μs.² We anticipate that the novel properties and characteristics of this p-n heterojunction can be widely generalized to other atomically thin materials systems.

REFERENCES:

1. Jariwala, D. et al. Emerging Device Applications for Semiconducting Two-Dimensional Transition Metal Dichalcogenides. *ACS Nano* 2014 , 8, 1102-1120.
2. Jariwala, D. et al. Gate-Tunable Carbon Nanotube-MoS₂ Heterojunction p-n Diode. *Proc. Natl. Acad. Sci. U.S.A.* 2013 , 110, 18076-18080.

9:20am 2D+AS+HI+NS+SS-ThM5 **Graphene Transfer onto sub 1nm Al₂O₃/TiOPc/Graphene Gate Stacks**, Ijfo Kwak, J.H. Park, University of California at San Diego, H.C.P. Movva, University of Texas at Austin, E.K. Kinder, H.L. Lu, University of Notre Dame, A.C. Kummel, University of California at San Diego

A novel transfer method with chemically controlled interfacial adhesion is reported for the fabrication of novel logic devices. This method allows direct transfer onto gate stacks and eliminates the possibility of Au electrodes deposition could shorting the thin oxide prior to transfer. The top graphene layer was grown on a Cu layer on a SiO₂/Si substrate by CVD. Au electrodes were deposited on top of the graphene by e-beam evaporation. To transfer the graphene layer, PIB (Polyisobutylene) were drop cast on top of graphene prior to bonding of the Au/graphene/Cu to a PDMS (Polydimethylsiloxane) film. The PIB serves to moderate the adhesion between the PDMS (Polydimethylsiloxane) and the Au electrodes. The PDMS provides mechanical support. Afterwards, the PDMS/PIB/Au/graphene/Cu/SiO₂/Si stack was immersed in ammonium persulfate solution to dissolve the Cu, releasing the top graphene stack. The bottom gate stack was HOPG (highly ordered pyrolytic graphite) with a sub-nano Al₂O₃ film on a monolayer TiOPc(titanyl phthalocynine) film. The monolayer TiOPc was deposited via MBE at 100C and annealed to 250C to insure a monolayer film. The TiOPc acts as a nucleation layer for the oxide ALD. The Al₂O₃ layer was deposited by ALD using TMA (Trimethylaluminum) and H₂O at 100 C. The PDMS/PIB/Au/Graphene stack was placed on the gate stack, and PDMS was removed. Using hexane solution, the rePIB layer was dissolved, leaving clean graphene surface. To measure the oxide characteristics, an AFM was converted into a capacitance meter. This measurement allows non-destructive probing of Au/graphene/Al₂O₃/TiOPc/graphene structure while conventional probe station could damage the oxide or electrodes.

9:40am 2D+AS+HI+NS+SS-ThM6 **Effect of Monolayer Substrates on the Electronic Structure of Single-Layer MoS₂**, Alfredo Ramirez-Torres, D.T. Le, T.S. Rahman, University of Central Florida

We have performed first-principles calculations based on density functional theory (DFT) utilizing the optB88-vdW functional to study structural and electronic properties of a single layer of MoS₂ deposited on single-layer substrates of hexagonal boron nitride (BN), graphene and silicene. All have a honeycomb structure; hence the formation of heterostructures is expected. Since the lattice mismatch between MoS₂ and these substrates is large, we

* NSTD Student Award Finalist

have considered different periodicities among layers to reduce as far as possible the incommensurability between lattices. Our results show that BN barely affects the electronic structure of isolate single-layer MoS₂; the DFT gap remains proximately unchanged. Graphene and silicene severely modify the electronic structure introducing additional states within the optical gap. Adsorption on graphene produces that the system turns like a zero band gap semiconductor bringing the conduction bands of MoS₂ down to the Fermi level of graphene. Adsorption on silicene shifts both valence and conduction bands of MoS₂, towards the Fermi level of silicene, in addition to inducing a gap of about 50 meV in the silicene itself.

This work was partially supported by CONACYT (México) Postdoctoral Fellowship Program (number 204065) and DOE grant DE-FG02-07ER46354

11:00am **2D+AS+HI+NS+SS-ThM10 Ballistic Transport in Epitaxial Graphene Nanoribbons**, *Walt de Heer*, Georgia Institute of Technology
INVITED

Graphene nanoribbons are essential components in future graphene nanoelectronics. However, in typical nanoribbons produced from lithographically patterned exfoliated graphene, the charge carriers travel only about 10 nanometers between scattering events, resulting in minimum sheet resistances of about 1 kW. In contrast 40 nm wide graphene nanoribbons that are epitaxially grown on silicon carbide are single channel room temperature ballistic conductors on greater than 10 μm length scale, similarly to metallic carbon nanotubes. This is equivalent to sheet resistances below 1W surpassing theoretical predictions for perfect graphene by at least an order of magnitude. In neutral graphene ribbons, we show that transport is dominated by two modes. One is ballistic and temperature independent; the other is thermally activated. Transport is protected from back-scattering, possibly reflecting ground state properties of neutral graphene. At room temperature the resistance of both modes abruptly increases non-linearly with increasing length, one at a length of 16 μm and the other at 160 nm. Besides their importance for fundamental science, since epitaxial graphene nanoribbons are readily produced by the thousands, their room temperature ballistic transport properties can be used in advanced nanoelectronics as well.

11:40am **2D+AS+HI+NS+SS-ThM12 Solution-Synthesized Graphene Nanoribbons**, *Alexander Siniitskii*, University of Nebraska - Lincoln

In this talk I will discuss a recently developed bottom-up approach for gram quantities of narrow graphene nanoribbons that are less than 2 nm wide and have atomically precise armchair edges. These graphene nanoribbons have been characterized by a number of microscopic (STM, AFM, SEM, TEM) and spectroscopic (XPS, UPS/IPES, UV-vis-NIR, IR and Raman spectroscopy) techniques. The properties of graphene nanoribbons could be tuned by incorporation of nitrogen atoms in their edges. Narrow graphene nanoribbons have a large electronic bandgap, which makes them promising for applications in field-effect transistors with high on-off ratios, as well as bulk applications, including coatings, composites and photovoltaic devices.

12:00pm **2D+AS+HI+NS+SS-ThM13 Graphene Silicon Interfaces at the Two-Dimensional Limit**, *Brian Kiraly, A.J. Mannix, M.C. Hersam*, Northwestern University, *N.P. Guisinger*, Argonne National Laboratory

Artificial van der Waals heterostructures have demonstrated both significant improvements of graphene's intrinsic properties and entirely new properties of their own. Early interest in these structures was based on nearly ideal carrier mobility in graphene on two-dimensional (2D) hexagonal boron nitride. Although exfoliation and reassembly of bulk vdW solids has yielded impressive initial results, this method inherently limits the geometry and constituent materials of these structures. Growth of 2D heterostructures has been demonstrated, but mainly limited to the prototypical graphene/hBN system. Adding new constituent materials, particularly those with electronic heterogeneity, to these 2D heterostructures allows them to be engineered with a variety of new properties.

We present the growth and characterization of interfaces between an atomically thin silicon layer and graphene. First, graphene is grown on Ag(111) via atomic carbon deposition at temperatures from 600°C -700°C. Following the growth of graphene, atomic silicon is evaporated on the graphene-covered Ag(111) substrate at 320°C-360°C. The resulting silicon growth results in faceted domains capped with a honeycomb lattice with periodicity 6.4 Å; Raman spectroscopy reveals peaks at 520 cm⁻¹ and 900-1000 cm⁻¹ that coincide precisely with bulk diamond cubic silicon, indicating these domains are comprised of sp³ bonded crystalline Si. These 2D sheets of silicon demonstrate both semiconducting character and a honeycomb lattice is attributed to a silver-based reconstruction of the Si(111) surface. The resulting silicon domains grow in two different configurations with respect to the dendritic graphene: (1) silicon domains appear to grow directly on the Ag(111) surface and terminate at the graphene boundaries.

These in-plane interfaces are atomically-precise and clearly resolved via scanning tunneling microscopy. Electronically, the density of states of both isolated constituent materials persist to these interfaces within the resolution of the measurement, indicating little interaction at the border. (2) The silicon growth is observed *underneath* the existing graphene flakes. The vertically stacked silicon graphene domains are identified via atomically resolved imaging *through* the graphene domains at larger biases where graphene is transparent under STM. Furthermore, the vertical materials interfaces demonstrate distinct electronic signatures from either constituent material. The resulting interfaces represent atomically pristine interfaces between graphene and a sp³ bonded semiconducting Si film, demonstrating a significant step forward in the diversification of van der Waals heterostructures.

Atom Probe Tomography Focus Topic
Room: 301 - Session AP+AS+MC+NS+SS-ThM

APT Analysis of Semiconductors, Magnetic and Oxide Materials

Moderator: Paul Bagot, Oxford University, UK, Daniel Perea, Pacific Northwest National Laboratory

8:00am **AP+AS+MC+NS+SS-ThM1 A Vision for Atom Probe Tomography**, *Thomas F. Kelly*, CAMECA Instruments Inc **INVITED**

Atom Probe Tomography has undergone revolutionary changes in the past two decades. It is tempting to think that these changes are likely to be followed by a period of adjustment and maturation but not continued innovation. However, there are still many active opportunities for development of atom probe tomography. Some of these new technologies are already upon us. There are recent major developments in data reconstruction, detector technology, data mining, and correlative microscopy. Furthermore, application areas are evolving at a rapid pace. The equipment needed to serve some applications will necessarily be developing alongside the more fundamental operating components of atom probes.

This talk with review some recent developments that are just emerging and will offer a vision for where the field is headed. Some of the unproven concepts needed to reach this vision will be highlighted.

8:40am **AP+AS+MC+NS+SS-ThM3 Interfaces in Semiconductors: Application to Photovoltaic Materials**, *Oana Cojocaru-Mirédin*, Max Planck Institut für Eisenforschung GmbH, Germany, *R. Würz*, Zentrum für Sonnenenergie- und Wasserstoff-Forschung Baden-Württemberg, Germany, *D. Raabe*, Max Planck Institut für Eisenforschung GmbH, Germany
INVITED

Cu(In,Ga)Se₂ (CIGS), Cu₂ZnSnSe₄ (CZTSe), and multicrystalline Si (mc-Si) solar cells possess a high efficiency [1], despite the polycrystalline structure of the absorber layer. One of the major factors controlling the cell efficiency is the diffusion of the impurities during the fabrication process into the absorber layer and to the p-n junction [2]. However, the interaction between the defects and the impurities at the internal interfaces is not completely understood. This is due to a lack of information on the local chemical changes across the internal interfaces at the nanoscale.

As a step towards a better understanding of the impurity redistribution at the internal interfaces, we have developed novel approaches of preparing site-specific atom probe specimens using combined focused ion beam (FIB), (scanning) transmission electron microscopy ((S)TEM) and electron backscattered diffraction (EBSD). These approaches allow selected GBs in polycrystalline CIGS, CZTSe and mc-Si layers to be studied by atom probe tomography (APT).

Several examples of correlative EBSD-TEM-APT (see Figure 1) and STEM-APT (see Figure 2) studies will be presented in this work. Using APT, segregation of impurities at the GBs was directly observed. APT data of various types of GBs will be presented and discussed with respect to the possible effects on the cell efficiency.

[1] Empa [Internet]. Empa.ch: A new world record for solar cell efficiency, 2013. Available from: <http://www.empa.ch/plugin/template/empa/3/131438/---/l=2> [cited 2013 January 18].

[2] J. L. Shay, S. Wagner, H. M. Kasper, Appl. Phys. Lett. 27 (1975) 89, S. Yip and I. Shih, Proceedings of the 1st World Conference on Photovoltaic Energy Conversion (IEEE, Piscataway, 1994), p.210.

9:20am **AP+AS+MC+NS+SS-ThM5 Analysis of Discontinuous InGaN Quantum Wells by Correlated Atom Probe Tomography, Micro-Photoluminescence, and X-ray Diffraction**, *J. Riley, X. Ren*, Northwestern University, *D. Koleske*, Sandia National Laboratories, *Lincoln Lauhon*, Northwestern University

In(x)Ga(1-x)N quantum wells are the foundation of solid-state lighting, with excellent quantum efficiencies despite high densities of defects. While there is as yet no universally accepted explanation for the high-efficiency, it is clear that carrier localization plays a role. Consistent with this picture, the quantum efficiencies of some samples can be improved by annealing and hydrogen gas to produce discontinuous quantum wells. However, the standard analysis of quantum well widths and composition by high-resolution x-ray diffraction is complicated by such complex morphologies. Specifically, the influence of surface roughness, and interfacial diffuseness, and planar continuity may be difficult to deconvolve. We will describe correlated analysis of continuous and discontinuous InGaN quantum wells by atom probe tomography, micro-photoluminescence, high-resolution x-ray diffraction, and atomic force microscopy. We find that precise composition profiles extracted from atom probe analysis enable refinement of x-ray diffraction peak fitting in the case of continuous quantum wells, and a better estimate of indium mole fraction and quantum well width. For discontinuous quantum wells, atom probe analysis enables simple models to be integrated into routine x-ray diffraction modeling to enable reliable extraction of indium mole fraction and better correlation with photoluminescence spectra. Correlation of atomic force microscopy tomographic images and micro-photoluminescence spectra over common sample areas, together with site-specific lift out techniques, will be presented to explore the surprising coexistence of high quantum efficiency and inhomogeneous broadening due to the complex underlying quantum well morphology.

9:40am **AP+AS+MC+NS+SS-ThM6 Atom Probe Tomography Characterization of Doped Epitaxial Oxide Multi-Layered Structures**, *Nitesh Madaan, A. Devaraj, Z. Xu, M.I. Nandasiri, S.A. Thevuthasan*, Pacific Northwest National Laboratory

Atom probe tomography is the state of the art 3D microscopy technique with sub-nanometer scale spatial resolution and ppm level mass sensitivity. For complex heterogeneous materials the accurate artifact-free reconstruction of collected data is quite a challenging task due to varying local evaporation fields leading to non-hemispherical evolution in the tip shape during the APT analysis. In this work we utilized laser assisted APT to analyze alternate multilayer oxide thin film structure of Samaria doped ceria (SDC) and Scandia stabilized zirconia (ScSZ), grown epitaxially on sapphire substrate, which is potentially useful for solid oxide fuel cells due to their high ionic conductivity. By analyzing the sample in different orientations (top-down, side-ways, and back-side) and comparing with dynamic tip shape evolution using level set simulations for similar geometries, an attempt was made to understand and decouple the APT evaporation artifacts from the real physical sample features. This study would help provide insights to improve the APT reconstruction process for complex multi-layered thin film materials.

11:00am **AP+AS+MC+NS+SS-ThM10 Atom Probe Tomography and Field Evaporation of Insulators and Semiconductors: Theoretical Issues**, *Hans Kreuzer*, Dalhousie University, Canada **INVITED**

After reviewing the physics and chemistry in high electrostatic fields and summarizing the theoretical results for Atom Probe Tomography of metallic tips, we turn to the new challenges associated with insulators and semiconductors with regard to local fields inside and on the surface of such materials. The recent (theoretical) discovery that in high fields the band gap in these materials is drastically reduced to the point where at the evaporation field strength it vanishes will be crucial in our discussion.

11:40am **AP+AS+MC+NS+SS-ThM12 Atom Probe Tomography Investigation of the Microstructure of Multistage Annealed Nanocrystalline SmCo₂Fe₂B Alloy with Enhanced Magnetic Properties**, *Xiujuan Jiang, A. Devaraj*, Pacific Northwest National Laboratory, *B. Balamurugan*, University of Nebraska-Lincoln, *J. Cui*, Pacific Northwest National Laboratory, *J. Shield*, University of Nebraska-Lincoln

Permanent magnets have garnered great research interest for energy applications. The microstructure and chemistry of a permanent magnet candidate—SmCo₂Fe₂B melt-spun alloy—after multistage annealing was investigated using high resolution transmission electron microscopy (HRTEM) and atom probe tomography. The multistage annealing resulted in an increase in both the coercivity and magnetization as is desired for permanent magnets design. The presence of Sm(Co,Fe)_xB (1:4:1) and Sm₂(Co,Fe)₁₇B_x (2:17:x) magnetic phases were confirmed using both techniques. Fe₂B at a scale of ~ 5 nm was found by HRTEM precipitating within the 1:4:1 phase after the second-stage annealing. Ordering within the 2:17:x phase was directly identified both by the presence of antiphase

boundaries observed by TEM and the interconnected isocomposition surface network found in 3D atom probe results in addition to radial distribution function analysis. These observed variations in the local chemistry after the secondary annealing were considered pivotal in improving the magnetic properties.

12:00pm **AP+AS+MC+NS+SS-ThM13 Detector Dead-time Effects on the Accurate Measurement of Boron in Atom Probe Tomography**, *Frederick Meisenkothen*, National Institute of Standards and Technology (NIST), *T.J. Prosa*, CAMECA Instruments Inc., *E.B. Steel*, NIST, *R.P. Kollie*, University of Maryland, College Park

The atom probe tomography (APT) instrument uses a time-of-flight (TOF) mass spectrometer to identify ions that are field ionized and evaporated from the apex of a needle-like nano-tip specimen. A pulse event, either laser or voltage, is used to trigger field evaporation and to initiate the timing sequence for the mass spectrometer. Ideally, a single atom is field evaporated during a single pulse event. However, it is also common to have multi-hit detection events where more than one ion strikes the detector between pulses. For reasons not completely understood, some elements, such as boron, are prone to field evaporate in multi-hit detection events when compared to other elements, and a large fraction of the boron signal is reportedly lost during acquisition. Obtaining an improved understanding of the field evaporation behavior of boron at different concentration levels, in view of the limited ability of the detection system to resolve multi-hit detection events, may lead to new ways to compensate for the boron signal loss.

A nominally pure boron sample was chosen as a high boron concentration material while the boron implanted silicon, NIST-SRM2137, (1E15 atoms cm⁻² retained dose) was chosen as the low boron concentration material. A dual-beam FIB/SEM instrument, with an *insitu* lift-out system, was used to prepare the APT specimen tips from the bulk materials. A laser pulsed LEAP 4000X Si* instrument was used to acquire APT data sets for each of the specimen tips. Custom software scripts were used to filter the data sets and extract the ion information associated with specific search criteria, e.g. event multiplicity, which is the number of ions within a given multi-hit event. Ion correlation analysis was used to graphically demonstrate the detector dead-time effect. In the present work, more than 60% of the detected boron signal resided within the multi-hit detection events, for both the high and low boron concentration samples.

* Certain commercial equipment, instruments, or materials are identified in this paper in order to specify the experimental procedure adequately. Such identification is not intended to imply recommendation or endorsement by the National Institute of Standards and Technology, nor is it intended to imply that the materials or equipment identified are necessarily the best available for the purpose.

Conservation Studies of Heritage Materials Focus Topic Room: 313 - Session CS-ThM

Conservation Studies of Heritage Materials

Moderator: David S. McPhail, Imperial College London, UK, Naoko Sano, NEXUS, Newcastle University, UK

8:00am **CS-ThM1 Complementary Ion and Electron Microscopy Studies for Heritage Conservation**, *Barbara Shollock*, Imperial College, London **INVITED**

Heritage conservation is an ever-growing discipline, fuelled by factors such as environmental pollution, and the issues surrounding conservation are not always clear. Defining the conservator's needs and the information required to address them can stimulate scientists to apply analytical techniques to new and unconventional challenges.

In this presentation, we will review some of the key issues faced in heritage conservation and the boundaries imposed by the ethics of conservation. Understanding these ethical considerations can guide the dialogue between conservator and analytical scientist to form a research approach that can satisfy both the scientific questions and the ethics of conservation. The application of electron and ion beam techniques will be considered in terms of conservation studies, and case studies will be used to illustrate the advantages and limitations of these techniques.

8:40am **CS-ThM3 Conservation Science at the National Archives: Science in Support of the Preservation of the Records of the Federal Government**, *Jennifer Herrmann*, National Archives and Records Administration **INVITED**

The National Archives and Records Administration (NARA) is the repository of the permanently valuable records of the United States

Government, including the Charters of Freedom, and a wide range of records that document the working of federal agencies and the rights and privileges of citizens. These materials range from Civil War-era pension files to immigration records and from homestead records to logs of Navy ships. NARA has the mission of preserving all of these records for future generations to access. Conservators and conservation scientists work together at NARA to support this dual mission of preservation and access. The Research and Testing Lab (R&T) works closely with the exhibits program and facilities across NARA to ensure that the products and materials used to display and store records will not contribute to their deterioration. In order to answer these questions as well as help preserve individual NARA holdings, R&T uses many standard analytical techniques. FTIR is the first non-destructive analytical technique we use to identify unknowns in the laboratory, including deteriorating films which could be cellulose nitrate or acetate. If FTIR cannot give us enough information, we often rely on the non-destructive XRF and also SPME-GC-MS, which is useful for monitoring off-gassing of records or materials used around records. For example, XRF has been useful in determining if a forgery of a date on a Lincoln Pardon could be reversed safely. This technique has also been used to study platinum photographs of different known recipes and processing conditions to see if the ghost image phenomenon that often occurs with historic platinum images could be better understood. DART MS, XPS, SEM, and FTIR have all been attempted for this photographic research project, as well as accelerated aging tests, microfading experiments, and fiber and paper analysis. The most visible R&T project that supports the dual mission has been the re-encasement and monitoring of the Charters of Freedom (the Declaration of Independence, Constitution, and Bill of Rights) and the Rubenstein Magna Carta. Instrumentation to monitor leaks and oxygen content, as well as air tight connections and plumbing are required in order to determine the conditions within these high tech encasements. As can be seen, the field of conservation science has many great tools from analytical chemistry to help preserve our important records and art.

9:20am **CS-ThM5 Advanced Spectroscopy for Traditional and Modern Heritage Materials**, *Fenella France*, Library of Congress **INVITED**

The conservation of art and cultural heritage objects requires advances in non-invasive, non-destructive analytical techniques to characterize cultural heritage materials, including substrates (paper, parchment) and media (inks, pigments, colorants). Spectral imaging systems developed for astronomical imaging and remote sensing have been adapted and customized for libraries and museums. The Library of Congress (LC) is using hyperspectral imaging to support preservation of cultural heritage materials with a range of capabilities. With an integrated 39 MegaPixel camera and LED illumination panels to capture high-resolution images in ultraviolet, visible and near infrared spectrum, researchers can create a spectral map of a manuscript or object that can be linked with other non-invasive analyses. Hyperspectral imaging captures non-visible and visible information in registered high resolution digital images, with further capabilities including identification of materials through spectral response, and monitoring of degradation or changes due to environmental conditions and conservation treatments.

The Library utilizes this system to address challenges associated with characterizing manuscript materials, including: early Portolan (nautical) Charts, L'Enfant Plan of Washington D.C., Jefferson's handwritten draft of the Declaration of Independence, and Herblock political cartoons. It has been used to illustrate non-invasive characterization of materials, deterioration, and detection of non-visible changes due to exhibition and storage. Assessing the long-term effects of treatments on collection materials is a growing area of research at LC. The conservation of a 1513 hand-colored Ptolemy Geographia posed interesting challenges in terms of the treatment of select maps in poor condition, due to the presence of verdigris, and a later restoration treatment. Analysis for treatment to stabilize these seven maps included a combination of quantitative X-ray fluorescence, spectral imaging, and Raman spectroscopy. Development of reference databases and integration of data from other analytical techniques allows a more complete mapping of collection materials. Linking this mapping data with other spectroscopic techniques allows for more data from single-point analyses, and provides a greater depth of information. Scriptospatial mapping of data enables direct sharing and visualization of data, with capture of standardized instrumentation parameters and object metadata. The scriptospatial interface enhances interaction between a range of professions, allowing multidisciplinary collaboration for integration of preservation, scientific and cultural information.

11:00am **CS-ThM10 Building a Case for the Future: Design and Construction of an Encasement and Monitoring System to Protect the US Bill of Rights for the Next 100 Years**, *Jacob Ricker, J.H. Hendricks, N.J. Brandenburg, G.F. Strouse*, NIST

NIST has been working to revolutionize the way we monitor and protect our historical documents by designing and constructing the next generation of document encasement. While the encasement "operates" at atmospheric pressure, to protect important documents it must perform like an ultra-high vacuum (UHV) system in terms of purity requirements, outgassing rate, permeation and leak rates. It has long been known that documents degrade overtime, but archivists and historians have been working to slow this process down through limiting exposure to damaging agents (oxygen, dust, excess humidity, mold, etc.) while still allowing visibility of the document for the public. NIST's design is innovative due to its ability to seal the document in a humidified Argon environment using a custom designed chamber with a double o-ring seal to reduce oxygen permeation through the second viton o-ring seal. This system required several innovative solutions to reduce differential pressure on the display glass and to improve and leak test the o-ring sealing.

The Encasement also features a custom designed sensor suite to monitor the status of the internal environment. The NIST design monitors and wirelessly transmits differential pressure, barometric pressure, temperature, humidity, oxygen content, and GPS location. All of the sensors were designed to be vacuum compatible with metal seals to ensure integrity of the encasement. The talk will feature discussions on oxygen permeation rates and measurement along with monitoring sensor performance.

11:20am **CS-ThM11 Parylene Coating for Paper/Book Strengthening**, *Lei Pei, M. Pollei, S. Jordan-Mowery, J. Baty*, Johns Hopkins University

Parylene, the generic name for a class of polymers with the base monomer para-xylylene, has been used to strengthen papers via chemical vapor deposition. The deposited monomers polymerize *in situ*, forming a thin conformal coating that adds strength. Compared to other paper strengthening techniques, such as lining and paper splitting, which are mostly based on individual sheet treatment, parylene coating has the unique ability to treat all the pages of a book simultaneously. Parylene as a paper strengthening technique, however, has had limited recognition within the conservation community since the pioneering research was completed in the 1990s. The major conservation concerns centered at that time on how well Parylene coatings improve the durability of brittle papers and how well the treatment would enable future conservation intervention. One of the earliest criticisms revolved around reversibility of the treatment. No one would reasonably argue that it is desirable to return an embrittled book back to a state of embrittlement, which prevents its being used and/or its ability to accept other traditional repair techniques. Given that we cannot readily correct depolymerization of cellulose at this stage, the real value in parylene is the extent to which it will impart adequate material strength and be receptive to the range of traditional repair techniques as would be used on a non-embrittled book, and all other things being equal, how long the strength will last.

To answer these concerns and highlight the potential of this paper strengthening technique, we present the results obtained from mechanical testing and the behavior of parylene coated paper in standard paper conservation treatments. These results show that Parylene-treated groundwood pulp book papers from 1951 reveal many of the characteristics of a new wood pulp paper, in term of rattle, turn radius, and general tactile experience. The treated paper has over 30% improvement in tear resistance and more than three times higher folding endurance (based on a log scale of the number of double folds via an MIT folding endurance tester). Additionally, parylene treated paper is receptive to conventional paper conservation treatments such as traditional wheat starch paste and Japanese paper tear mending, guarding, washing and resizing. We will also discuss moisture content measurements to clarify concerns about the vacuum treatment involved in the Parylene coating process and its effect upon the treated paper.

11:40am **CS-ThM12 Iron Gall Ink Chemistry and Corrosion of Historical Documents Probed by XPS and Raman**, *Karen Gaskell, A.A. Ponce, S. Gibbons, P. Zavalij*, University of Maryland, College Park, *L. Brostoff*, Library of Congress, *B. Eichhorn*, University of Maryland, College Park

Iron gall inks were the major writing medium from the middle ages through the 19th Century in the Middle East and Europe, and are present in hundreds of thousands of important cultural heritage objects worldwide, including books, manuscripts and artistic drawings. Iron gall ink depending on its preparation is well known for its potentially corrosive effect on paper or other writing medium, over time, changes in temperature and humidity can accelerate this degradation resulting in the worst case, complete loss of documents. The major ingredients of iron gall ink are iron salts, most often

iron sulfate, tannic acids derived from vegetable sources such as gall nuts and gum arabic used as a binder. In this study, X-Ray Photoelectron Spectroscopy (XPS), is used to probe the chemistry of iron gall ink and to study the effect of common preservation techniques such as deacidification and phytate treatment. Despite much research in this area the chemistry of iron gall ink is still poorly understood, including the structure of the complex itself, resulting from the reaction between iron sulfate and gallic acid. The two most widely accepted structures in literature have been proposed by Kreckel and Wunderlich, these structures will be discussed and compared to XPS, Raman, FTIR and X-ray crystallography data obtained from model compounds.

Spectroscopic Ellipsometry Focus Topic

Room: 304 - Session EL+AS+EM+EN+SS-ThM

Spectroscopic Ellipsometry for Photovoltaics and Instrument Development

Moderator: Mariadriana Creatore, Eindhoven University of Technology, Netherlands, Tino Hofmann, University of Nebraska-Lincoln

8:00am **EL+AS+EM+EN+SS-ThM1 Spectroscopic Ellipsometry Characterization in the Photovoltaic Device Configuration, Nikolas Podraza**, University of Toledo **INVITED**

Thin film large area photovoltaics (PV) are a maturing field, yet challenges remain in manufacturing and fundamental research. Even the simplest thin film PV devices consist of multiple layers of doped or undoped semiconductors, transparent conducting front contacts, and metal back contacts. Characteristics of each layer, along with the interfaces between layers, all have an impact upon device performance. Within each layer, the material may evolve with thickness or exhibit spatial non-uniformity. Furthermore, studies of each thin film material can be difficult, as fundamental property measurements on special substrates may not accurately represent the characteristics of the material in the final device configuration. Spectroscopic ellipsometry (SE) data, collected over the infrared to ultraviolet, is sensitive to layer thicknesses, interface formation, and surface roughness as well as the optical response of each component in the form of the complex dielectric function spectra ($\epsilon = \epsilon_1 + i\epsilon_2$) for samples deposited on arbitrary reflective substrates. Variations in ϵ for a given layer can be linked to order (amorphous vs. crystalline, grain size, crystal phase), composition, and characteristics of opto-electronic response (band gap, dc electrical properties). In situ real time SE (RTSE) is now often applied to study the growth evolution of component materials within device configurations for hydrogenated silicon (Si:H), cadmium telluride (CdTe), and copper indium gallium selenide (CIGS) PV. This utilization of RTSE provides a means of monitoring layer characteristics as materials are being processed in the device structure and generates appropriate structural models for analysis of similar samples when only ex situ SE measurements are available. Appropriate structural models derived from RTSE have been applied to analyze ellipsometric spectra collected over 6 inch x 6 inch rigid substrates and assess the spatial uniformity in characteristics of each layer in the sample. These maps of optically derived material properties can be compared to electrical device performance (efficiency, open circuit voltage, short circuit current, fill factor) and used to guide PV optimization principles. The optical (ϵ) and structural (layer thickness) information gained from SE is input into quantum efficiency simulations for comparison with experimental PV device measurements. These comparisons are used to assess both opto-electronic performance of devices and validity of models used in SE data analysis as well as further guide device development by identifying sources of optical and electrical losses.

8:40am **EL+AS+EM+EN+SS-ThM3 Application of Pseudo-Bulk Approach in Ellipsometric Studies of Polycrystalline Photovoltaic Thin Films, Sukgeun Choi**, National Renewable Energy Laboratory, J. Li, University of Toledo, I. Repins, National Renewable Energy Laboratory

Fundamental band gap is one of the key properties of semiconducting materials, which directly influences the functionality and performance of many photonic and photovoltaic (PV) devices. Photoluminescence (PL) and optical absorption spectroscopies are widely used to determine the band-gap energy E_g . For polycrystalline thin-film PV materials, however, it is often challenging to unambiguously interpret PL data owing to the presence of multiple peaks associated with various types of defect structures. To estimate E_g from optical absorption spectrum, on the other hand, a straight segment of the absorption coefficient curve needs to be chosen. But this selecting procedure is somewhat arbitrary, which leads to an inaccurate E_g value.

Spectroscopic ellipsometry (SE) accurately determines material's optical function spectra over a wide spectral range. For semiconductor thin-film structures, a multilayer analysis is generally used to extract the optical information from SE data. Although mainly surface overlayer artifacts need to be corrected for SE data well-above the band gap in the analysis, several contributions should be considered for those near (and below) the band gap, such as the optical characteristic of substrate, presence of interfacial layers, and finite thickness of film in addition to the artifacts from surface overlayers. As a result, the obtained optical function spectrum and E_g value become somewhat model dependent with an increased uncertainty.

To reduce complications in mathematical modeling of SE data and improve the accuracy of resulting near-band-gap optical function spectrum, we introduce the *pseudo-bulk* approach, where SE measurements are performed on thin films grown on macroscopically roughened substrate surface. The essence of this approach is in suppressing the reflection of probing light from the film/substrate interface and below. Thus, no thickness fringes appear in the SE data, despite the thin-film nature of sample, and the band-gap onset can be clearly observed with a post-growth chemo-mechanical polishing of the film surface. We apply the *pseudo-bulk* approach to study near-band-gap optical properties of $\text{Cu}_2\text{ZnSnSe}_4$ and related PV absorber materials. We present a non-monotonic temperature-dependence of E_g for $\text{Cu}_2\text{ZnSnSe}_4$ and the clear band-gap onset of Cu_2SnSe_3 at around 0.45 eV for the first time. SE results are explained by the results from the electronic structure calculations. The applicability and limit of this approach are also discussed.

9:00am **EL+AS+EM+EN+SS-ThM4 Real-Time and Through-the-Glass Mapping Spectroscopic Ellipsometry for Analysis and Optimization of CdS:O Window Layers of CdTe Superstrate Solar Cells, Xinxuan Tan, R.W. Collins, P. Koirala, J. Li, N.J. Podraza**, University of Toledo

In-situ real-time spectroscopic ellipsometry (RT-SE) has been applied for the analysis of CdS:O films sputter deposited on c-Si substrates from a CdS target using different flow ratios of $\text{O}_2/(\text{Ar}+\text{O}_2)$ from 0 to 0.05. RT-SE studies of the CdS:O layers from the film side provide the complex dielectric function spectra of each the layers over a spectral range of 0.75 to 6.5 eV and its dependence on oxygen content in the material as deduced by energy dispersive X-ray spectroscopy (EDS). Ex-situ infrared ellipsometry of these samples enables extension of the dielectric function data to ~ 0.04 eV and provides information on free carrier conduction and chemical bonding in the material. In similar RT-SE studies, data acquired during the growth of CdS:O/CdTe layers on transparent conducting oxide (TCO) coated glass superstrates have been analyzed to determine the structural evolution of the layers in the configuration used for CdTe solar cells, with the CdS:O serving as an n-type window layer for the p-type CdTe absorber. The results of this analysis assist in the development of a realistic optical model for the multilayer structure of the solar cell. Using this optical model ex-situ through-the-glass spectroscopic ellipsometry (TG-SE) has been implemented toward the analysis of glass/(TCO-stack)/CdS:O/CdTe solar cells in the superstrate configuration.

For the solar cells, CdS:O layers with different oxygen contents were deposited on 15 cm x 15 cm TCO coated glass superstrates. A 16 x 16 array of dot cells each with an area of 0.125 cm² was fabricated on the superstrate in order to optimize efficiency improvements through combinatorial methods. Because the as-deposited superstrate/film-structure undergoes additional processing steps during device fabrication, three sets of TG-SE mapping data were acquired on (i) as-deposited, (ii) CdCl₂-treated (an activation step), and (iii) back-contact coated device structures. With an optical database that has been established for both as-deposited and CdCl₂ treated CdS:O, CdTe, and back contact materials, each of the TG-SE mapping data sets were analyzed based on an optical model deduced from RT-SE studies of the CdS:O and CdS:O/CdTe depositions. Thickness and compositional non-uniformity observed over the area by mapped by TG-SE enables correlations between solar cell performance and basic property parameters of the component layers including layer thicknesses and compositions. The resulting correlations provide a pathway to expedite solar cell optimization.

9:20am **EL+AS+EM+EN+SS-ThM5 Combined Optical Emission Spectroscopy and Spectroscopic Ellipsometry Collected During Thin Film Deposition, Anna Barnes, M.M. Junda, N.J. Podraza**, University of Toledo

Plasma processes are commonly used to deposit thin film layers for a variety of optical, electronic, and coating applications. Two common processes widely used in the fabrication of thin films are physical vapor deposition (sputtering) and plasma enhanced chemical vapor deposition (PECVD). Non-contacting optical probes, such as spectroscopic ellipsometry (SE) and optical emission spectroscopy (OES), are particularly attractive techniques to study these deposition processes in situ during film growth. Connecting studies involving SE and OES offers the ability to

observe and interpret the growth of thin films from plasma over time using variant parameters, though in different ways. Real time SE (RTSE) provides a means of monitoring the deposited material itself, while OES can be used to track variations in the plasma employed for the deposition. Tracking the time dependence of both film and plasma properties is desirable as variations in material properties resulting from changes in plasma conditions may impact the final device performance. In this particular study, we look at the growth evolution of semiconductor, transparent conducting oxide (TCO), and metal contact layers commonly used in thin film photovoltaic devices. Case studies involve undoped, n-type, and p-type hydrogenated amorphous silicon prepared by PECVD, as well as zinc oxide, indium tin oxide, and silver prepared by magnetron sputtering on either smooth test substrates (glass, crystal silicon wafers) or in the full device configuration. Variations in thin film structure (bulk layer thickness, surface roughness) and optical properties in the form of the complex dielectric function spectra ($\epsilon = \epsilon_1 + i\epsilon_2$) are obtained as a function of time by RTSE. Results from RTSE (ϵ , structure) are interpreted to determine order (grain size, amorphous vs. nanocrystalline), electronic transitions (band gap, free carrier absorption characteristics), and morphology evolution as appropriate for the given material layer. OES indicates the presence and relative strength of plasma emission peaks, which correspond to the species present in the plasma and their relative concentrations. Analysis of RTSE and OES data collected simultaneously is sought to identify links present between these plasma and film characteristics.

9:40am **EL+AS+EM+EN+SS-ThM6 Optical Insights into Graphene Functionalized by Atoms, Biomolecules and Metal Nanoparticles**, *Maria Losurdo, M. Giangregorio, G.V. Bianco, P. Capezzuto, G. Bruno*, CNR-IMIP, Italy

New opportunities for energy production and storage, catalysis, biosensing, drug delivering and plasmonics are offered by graphene-based materials. In order to make all those applications viable technologies, it is mandatory to functionalize graphene for modulating reproducibly its properties and for better understanding the surface and interfacial electronic phenomena in graphene hybrids.

To this aim, this contribution discusses the optical properties measured by spectroscopic ellipsometry in the 0.6-6.5 eV of graphene functionalized by:

- (1) the covalent attachment of hydrogen, nitrogen, oxygen, and fluorine atoms, which strongly affect the optical properties of graphene through a partial sp²-to-sp³ conversion of carbon.
- (2) the non-covalent interaction with organic molecules such as porphyrins that interact with graphene through p-systems.
- (3) a variety of metals nanoparticles, like Au, Ag, Ga, to create a versatile graphene-based platform for plasmonics in frequency range from the terahertz to the visible .
- (4) plasmonic nanoparticles and subsequent proteins to create an electro-optical sensing graphene platform.

The graphene is grown by chemical vapor deposition (CVD) and transferred to glass substrates with coverage higher than 98%. This assures large area graphene samples that can easily accommodate the ellipsometric probing light spot avoiding uncontrolled effects due to undefined substrate/graphene boundaries. With the availability of high quality samples, effect of thickness and anisotropy, which have been debated for a while, are clarified.

Data on the real time monitoring of graphene optical properties by spectroscopic ellipsometry that allows for an unprecedented control over the degree of functionalization will also be presented.

The perspective of this work is twofold. From the fundamental point of view, in the investigated spectral range, the band structure of graphene has saddle van Hove-like singularities at the M points of the Brillouin zone, with possible excitonic effects. Focusing on the analysis of these singularities, many-body effects for all the graphene-derivates mentioned above are described.

From the technological point of view, it will be shown how the optical measurements can serve to clarify and explain the occurrence and stability of the doping of graphene by the various heteroatoms and molecules, the electron transfer between graphene and metals and molecules, and finally the sensitivity of the-graphene-platform in sensing gases and biomolecules.

Spectroscopic ellipsometry data of functionalized graphene are corroborated by Raman spectroscopy, microscopies and electrical characterizations.

11:00am **EL+AS+EM+EN+SS-ThM10 Enhanced Sensitivity to Surface-Normal Dielectric Function of Uniaxial-Anisotropic Materials via Attenuated Total Reflection Ellipsometry**, *Thomas Tiwald, J.A. Woollam Co., Inc., J. VanDerslice, Z. Xiao, J.S. Huang*, University of Nebraska Lincoln

It is often difficult to determine the surface-normal dielectric functions of anisotropic materials, because to lack of sensitivity to optical properties out

of the surface plane[1][2]. The primary cause is the large angle of refraction that occurs as the light enters from low index medium like air. In these circumstances, the penetrating light beam bends strongly towards surface normal, resulting in electric fields that are oriented primarily in the surface plane. This is a particular problem for absorbing films, since most of the light collected by the detector is reflected from the ambient/film interface. We use a total internal reflection method to enhance ellipsometric sensitivity to optical properties of uniaxial absorbing materials in the out-of-plane direction. This non-destructive technique is illustrated using a P3HT poly(3-hexylthiophene) film on fused silica, and the results are compared to the standard air/film/substrate method.

[1] D.E. Aspnes. *J. Opt. Soc. Am.*, **70**, 10, 1275 (1980).

[2] G. E. Jellison Jr. and J. S. Baba, *J. Opt. Soc. Am. A23*, 2 468 (2006).

11:20am **EL+AS+EM+EN+SS-ThM11 Infrared to Ultraviolet Optical Properties of Gadolinium Gallium Garnet (Gd₃Ga₅O₁₂) and Bismuth Germanate (Bi₄Ge₃O₁₂) Single Crystals**, *Kiran Ghimire, H. Haneef, N.J. Podraza*, University of Toledo

The optical properties of commercially available oxide single crystals gadolinium gallium garnet (Gd₃Ga₅O₁₂) and bismuth germanate (Bi₄Ge₃O₁₂) have been studied over a maximum spectral range of 0.034 to 6.5 eV by multiple spectroscopic ellipsometry and transmittance measurements, via a multichannel ellipsometer from the near infrared to ultraviolet, a Fourier transform infrared (FTIR) ellipsometer, and a spectrophotometer. Spectroscopic measurements from each instrument and over the respective spectral ranges have been analyzed differently yet yield optical properties over the full measured range. Near infrared to ultraviolet ellipsometric spectra are analyzed using a divided spectral range procedure whereby information below and above the band gap are fit to models with separate physically realistic parameterizations of the complex dielectric function spectra ($\epsilon = \epsilon_1 + i\epsilon_2$) that share the same structural parameters—surface roughness thickness in these cases. The surface roughness thicknesses are then fixed and direct numerical inversion is used to determine ϵ over the continuous spectral range. Analysis of transmittance and FTIR ellipsometric spectra also relies upon fixing surface roughness from near infrared to ultraviolet spectroscopic ellipsometry analysis and either direct numerical inversion or parametric models to determine ϵ . In the vicinity of the band gap, the absorption coefficient (α) obtained from ϵ is then combined with low values of ϵ obtained from transmittance below the absorption edge, where ellipsometry lacks sensitivity. The combined α from transmission and ellipsometry is used to determine the band gap of the materials. Unlike Gd₃Ga₅O₁₂, the band gap of the Bi₄Ge₃O₁₂ is sufficiently within the measured spectral range so critical point analysis has been performed on Bi₄Ge₃O₁₂ by extending the measured spectral range up to 6.5 eV, where the material was found to have additional critical points. FTIR ellipsometric spectra are analyzed with a parametric model combining Gaussian and Lorentzian broadened resonance features to represent modes attributed to chemical bonding and lattice vibrations. The results of these analysis procedures yield ϵ from the infrared to ultraviolet, from which information on the band gap, electronic transitions, and vibrational modes are obtained.

11:40am **EL+AS+EM+EN+SS-ThM12 Cu surface reactions in hydrochloric solution probed on the atomic scale by polarization optical methods and STM**, *Christoph Cobet, Gh. Barati, V. Solokha, K. Hingerl*, Johannes Kepler University, Austria

Electrochemical reactions on metal electrodes have been in the focus of many scientific studies and Cu is probably the most investigated example. Mainly, the interest on Cu is motivated by by questions concerning e.g. the corrosion behavior or the optimization of electro-polishing procedures. Classical electrochemical approaches contain usually a description of the occurring reaction products and concentrations. However, it is evident that a fundamental understanding also requires knowledge about the microscopic occurrence of the metal-electrolyte interface. Desirable is a fundamental knowledge as it is obtained already for surfaces in UHV. But unfortunately, most of the classical surface sensitive techniques cannot be applied in liquid environments. Thus it is not surprising that many fundamental issues in electrochemical reactions are still unsolved.

In our work we combine reflection anisotropy spectroscopy, spectroscopic ellipsometry, and a homemade electrochemical scanning tunneling microscope to study Cu single crystals in hydrochloric solutions. With these methods we enabled monitoring of the local appearance as well as the dynamics of interface transformations/reactions on the atomic scale. In particular it was possible to explain for the (110) surface in more detail the correlation of Faraday-current and structural transformation. Here, the Cl adsorption minimizes the surface energy by a formation of monoatomic steps parallel to the [001] direction which finally ends in a faceting of the surface. It turns out that characteristic redox peaks in cyclic voltammograms correlate with the stabilization of certain arrangements of these steps. The structures are formed first by Cu dissolution and at higher anodic potentials

by rearrangement of Cu atoms in the surface. It is remarkable that the latter process compares nicely with oxide/chloride induced surface transformations which are observed in UHV. The comparison with the UHV results in turn is used to achieve a more comprehensive model for the processes in electrochemical environment.

Electronic Materials and Processing

Room: 311 - Session EM1-ThM

Materials for Light Management

Moderator: Sang M. Han, University of New Mexico

8:40am **EM1-ThM3 Thin Film c-Si Solar Cells – Detailed Understanding from Light Trapping to Carriers Collection**, *M.S. Branham, W.-C. Hsu*, Massachusetts Institute of Technology, *S. Yerci*, Middle East Technical University, Turkey, *Gang Chen*, Massachusetts Institute of Technology **INVITED**

Crystalline silicon (c-Si) is the dominant material in photovoltaic industry. However, it contributes ~40% of the total module cost of c-Si solar cells, and a thin-film device has been one strategy to reduce the usage of material. Here, we demonstrate experimentally that an inverted nanopyramid light-trapping scheme for a 10 μ m-thick c-Si thin-film solar cell can achieve an absorbance value comparable to that of a 300 μ m-thick planar device and its efficiency higher than 13%. To reach the high efficiencies necessary for a commercial product, we constructed a multi-physics optimization tool incorporating both optical absorption and electronic carrier collection to understand in detail loss mechanisms including incomplete photonic absorption, contact losses, surface, Schottky-Read-Hall and Auger recombination. Our model predicts that a 10 μ m-thick thin-film c-Si solar cell with an inter-digitated back contact scheme can have an efficiency higher than 20%. Finally, we calculated the optimum height to period ratio of light-trapping structures around 0.7 for a fixed period of 700nm. This structure can be obtained in crystalline silicon using a well-known potassium hydroxide anisotropic etching. These multi-physics simulation results can provide design insights for flexible and high efficiency thin silicon solar cells.

9:20am **EM1-ThM5 Symmetry-Breaking in Light Trapping Nanostructures on Silicon for Solar Photovoltaics**, *SangEon Han, S. Ghosh, T. Cai, B.R. Hoard, S.M. Han*, University of New Mexico

In thin-film photovoltaics, highly absorptive materials are conventionally used. However, these materials except gallium arsenide have achieved efficiencies that are not comparable to those of thick crystalline silicon (c-Si) photovoltaics and, in some cases, suffer from their toxicity and low supply. A viable solution to these problems would be to use c-Si for thin-film photovoltaics. However, thin c-Si films absorb sunlight weakly because of its indirect band gap, and highly efficient light-trapping should be provided to achieve high efficiency. For thin-film photovoltaics, nanoscale structures are typically involved for light trapping because the film thickness becomes comparable to the wavelength of sun light. While diverse nanostructures have been studied to break the light-trapping limit of geometric optics, known as the Lambertian limit, highly efficient nanostructures that can be easily manufactured have not been demonstrated. We have previously predicted that symmetry-breaking in light-trapping periodic nanostructures on thin films can approach the Lambertian limit very closely. Herein, we will present how the systematic symmetry-lowering increases light-trapping in thin-film photovoltaics. Further, we will demonstrate the experimental realization of such low-symmetry structures using simple wet etching methods on c-Si(100) wafers without any off-cut, tilt angle.

9:40am **EM1-ThM6 Suppressing Optical Absorption in Nanostructured Metal Electrodes in Photovoltaics**, *Samuel Clark, S.E. Han*, University of New Mexico

Electrodes are ubiquitously used in optoelectronic devices such as solar cells, infrared detectors, and light emitting diodes. Typically, metals exhibit good electrical conductivity due to their free electrons and are suitable for electrodes in these devices. However, metal electrodes cause inefficiency in the devices by absorbing light as their free electrons suffer from collisions. To circumvent this problem, nanostructured metals are being explored to realize low optical losses while maintaining large electrical conductivity. Here, we study optical absorption in helical metal nanocoils and find that absorption can be dramatically decreased when the metal is suitably nanostructured. Theoretical modeling showed that this effect is due to the increase in effective mass of free electrons in nanostructured metals. Heavy electrons suffer a decreased rate of collision and emulate dielectric materials where optical losses are negligible. Calculations showed that, when metal

electrodes are used in semiconductor devices, suitably chosen nanostructures can increase the fractional absorption in semiconductors more than 60 times by reducing losses in the metal. Further, we show that a two-dimensional analogue to nanocoil, namely serpentine structure, exhibits optical losses of less than 7 % in the infrared even at a large metal area fraction of 0.3. We will discuss the different physics of optical losses between the coil and the serpentine structures.

11:00am **EM1-ThM10 High Efficiency Si Cells and the Challenges to Integrate the Light Management**, *Paul Stradins, B.G. Lee*, National Renewable Energy Laboratory **INVITED**

In this talk, we discuss the stringent requirements that enable the high efficiency, industrially relevant, Si solar cells, and show that the light management approaches need to be developed integral to the whole device. The highest efficiencies known today are obtained with PERL (UNSW), IBC (SunPower) and IBC Heterojunction (Panasonic) device architectures. The challenge is to balance the excellent bulk, surface, and contact passivation leading to high Voc, with light management features leading to high Jsc. For example, pyramid-texturing the front of the cell leads to an excellent visible range response and near-Lambertian light trapping in near-infrared, but the associated 1.7x increase in the front surface area increases the recombination current prefactor. The IBC approaches significantly restrict any light management structures on the back of the cell (e.g. plasmonics, gratings). Novel passivated contact approaches currently pursued by NREL [1] and others [2] show promise to significantly enhance cell efficiencies in an industrially relevant way. In particular, we have developed [1] high performance tunneling passivated full area back contact for the n-CZ based cell. Because of the high-low junction induced by a deposited n+ poly-Si contact layer, there is no P-doping involved in BSF formation. The contact itself provides better BSF passivation than currently used nitride-passivated BSF surface, has low contact resistance, and does not need patterning as in PERT or PERL structures. We then discuss of how advanced optics and light trapping can fit into this device architecture and are there viable alternatives to the near-Lambertian pyramid texturing. With near-perfect bulk and surface/contact passivation, the importance of light management increases. However, it becomes increasingly more challenging to justify much thinner wafer cells even with perfect Lambertian light trapping. For high efficiency, passivated contact wafer cells, additive light management structures provide potential efficiency improvements and will be discussed. Finally, we will briefly discuss numerous light management approaches examined in the course of our previous Si program that focused on <10 micron thin c-Si devices (small pyramids, black Si, dielectric nanoparticle backscatterers), and their potential to high efficiency Si cells.

1.D. L. Young et al., SiliconPV conference proceedings 2014.

2.F. Feldmann et al, Sol. En. Mat. Sol. Cells (2014) 120, pp. 270-274.

11:40am **EM1-ThM12 Developing Periodically Oriented Gallium Nitride for Frequency Conversion**, *Jennifer Hite, R. Goswami, J.A. Freitas, Jr., M.A. Mastro, I. Vurgaftman, J.R. Meyer, U.S. Naval Research Laboratory, C.G. Brown, Sotera Defense Solutions, S.R. Bowman, C.R. Eddy*, U.S. Naval Research Laboratory

Gallium nitride is a semiconductor widely used in both optical and electronic devices. The polarity of GaN (+/- c-direction) influences many properties of the resultant material, including chemical reactivity and electric field in these 'spontaneously polarized' materials. By engineering inversion layers, we have demonstrated control of GaN polarity on both polar faces of GaN. By employing a selective growth method to deposit the IL, the lateral polarity of the GaN can be alternated, thus enabling structures referred to as periodically oriented (PO) GaN.

In previous work on N-polar substrates, we demonstrated that optimization of the MOCVD growth rates resulted in sharp, vertical interfaces and smooth surfaces. The present work has moved the technology substantially closer to practical non-linear optic emitters by using HVPE to extend the PO GaN templates on N-polar substrates to total thicknesses of up to 80 μ m, while faithfully maintaining the pattern of alternating polarity. Additionally, cross-sectional cathode-luminescence (CL) imaging of such an extension shows that the large initial dislocation densities occurring in the original inversion layers greatly decreased after about 25 μ m of regrowth.

For growth on Ga-polar substrates, we have demonstrated that inversion layers can be created using atomic layer deposition (ALD) of Al₂O₃. This new capability is especially relevant because Ga-polar films are more prominent in devices, as they result in lower impurities, higher quality and smoother films. In this case, GaN grown over the inversion layer is N-polar. This inversion layer was used to form laterally-patterned stripes of alternating Ga- and N-polar films. We find that annealing the ALD films crystallizes the Al₂O₃, thereby allowing N-polar GaN to be grown over the new sapphire-like surface. Transmission electron microscopy shows that the inversion layer in a PO GaN structure is crystalline, a-plane oriented, and a-phase. TEM characterization further indicates that the GaN layers, both

above and below the Al₂O₃ inversion layer, are c-oriented without any rotation between them. The optimization of this process has enhanced the surface smoothness.

These methods of GaN polarity inversion offer the promise of engineered materials with custom lateral and vertical polarity variations for applications in novel electronic and optoelectronic devices, a subset of which are expected to be suitable for non-linear optics.

12:00pm **EM1-ThM13 White-Light Emission from Amorphous ZrHfO_x/AlO_x/ZrHfO high-k Stack**, C.-C. Lin, Yue Kuo, Texas A&M University, X. Zhang, Xi'an Jiaotong University, China

LEDs has the low energy consumption, compact size, and long-lifetime [1]. Since the white light cannot be emitted from a single LED, a combination of red, green, and blue LEDs or an UV or blue LED with a yellow phosphor has to be used. Kuo and Lin proposed a new type of single-chip, white-light emission LED that is made of the amorphous high-k dielectric thin film on a Si wafer [2-5]. The light emission is from the thermal excitation of nano-size conductive paths formed during the dielectric breakdown, which is similar to the principle of the incandescent device. Its energy efficiency is expected to be much higher than that of the incandescent light bulb because of the small size conductive path. The emission light intensity and wavelength range of the LED were enhanced with the embedding of a nanocrystal layer in the high-k film paths [2]. Authors investigated optical and electrical characteristics of the ZrHfO_x/AlO_x/ZrHfO LED.

The following results were obtained from this study. First, the AlO_x embedded ZrHfO LED emits the broad band light including the visible to near IR wavelengths. Second, the emitted light falls into the warm white light region of the CIE 1931 color chart with a high color rendering index (CRI) of ~98. Third, the LED has a larger leakage current than the control sample, i.e., ZrHfO without the embedded AlO_x layer, which is due to the stress mismatch between these two materials film [6]. Fourth, both the emission light intensity and the number of the bright dots increase with the inclusion of the AlO_x layer and the increase of the magnitude of the stress voltage (V_g). These phenomena can be explained by the mechanism of thermal excitation of the conductive path. The large current density causes the high thermal excitation efficiency of the conductive path for the high intensity light emission. The larger number of conductive paths also contribute to the high emission intensity. Fifth, light emission was studied with the pulsed V_g driving method, i.e., at 1 kHz and -40 V, at various duty cycles (DCs). The spectrum wavelength range was independent of the change of DC. However, the peak height decreases with the decrease of the DC. It can be explained by the fast thermal excitation process of the extremely short conductive path, i.e., ~8.7 nm. The new LED can be an important white light source for many industrial, medical, etc. applications.

[1] N. Kimura, APL 90 051109 (2007)

[2] Y. Kuo et al., APL 102, 031117 (2013).

[3] Y. Kuo et al., Electrochem. Solid-State Lett. 2, Q59 (2013).

[4] Y. Kuo et al., Solid-State Electron. 89, 120 (2013).

[5] C.-C. Lin et al, JVSTB 32, 011208 (2014).

[6] C.-C. Lin et al, JVSTB 32, 03D116 (2014).

Electronic Materials and Processing

Room: 314 - Session EM2-ThM

High-K Dielectrics for ReRAM and RAM

Moderator: John Conley, Oregon State University

8:00am **EM2-ThM1 Challenges and Materials Solutions for Memristive Devices (ReRAM)**, Jianhua(Joshua) Yang, HP Labs
INVITED

Memristive devices (also known as RRAM when used for memory) are electrical resistance switches that can retain a state of internal resistance based on the history of applied voltage or current, which can be used to store and process information for computing systems beyond CMOS technologies. These devices have shown great scalability, switching speed, non-volatility, analogue resistance change, non-destructive reading, 3D stack-ability, CMOS compatibility and manufacturability. However, there are still a number of challenges facing memristive devices for real applications, including device variability and isolation in a crossbar array. This talk will discuss and address these challenges from the materials perspective.

8:40am **EM2-ThM3 Physical Mechanisms and Scaling of the Resistive Memory (ReRAM)**, Daniele Ielmini, S. Balatti, S. Ambrogio, Politecnico di Milano, Italy
INVITED

The resistive memory (ReRAM) is attracting strong interest from the industry and academia for its low-power, high-speed and nonvolatile behavior. ReRAM properties are compatible with many of the requirements of storage (e.g., the solid state drive, or SSD) and memory (e.g., SRAM or DRAM), thus ReRAM may potentially revolutionize computing architectures in the future. While ReRAM has been recently introduced in the ITRS, the industrial programs for device development, volume production and commercial exploitation are still challenged by the lack of understanding about device physics, reliability and scaling.

This work will discuss the recent progress on the understanding of ReRAM physics. First, a numerical model for ReRAM switching will be described, highlighting the primary role of defect migration driven by Joule heating and electric field. The model will be tested under several conditions of voltage and currents, showing the model capability to identify new operation modes for self-select ReRAM and enhanced multilevel operation. Finally, the scaling issues will be addressed, explaining the device variability data with the aid of a Monte Carlo model for discrete defect migration. The fundamental tradeoff between power reduction and device reliability will be finally discussed.

9:20am **EM2-ThM5 Variability of Metal Oxide Based RRAM: Challenges and Opportunities**, An Chen, GLOBALFOUNDRIES
INVITED

Recently, metal-oxide based resistive-RAM (RRAM) has emerged as a promising nonvolatile memory (NVM) candidate. However, it is also recognized that the stochastic RRAM switching mechanisms inevitably introduce large variability in device parameters, which impose severe challenges for memory applications especially in high-density arrays. RRAM variability can be attributed to the microscopic variation of dimension and/or composition of the filamentary conductive paths during the switching process. Variability in switching voltage/current reduces safe operation margin and resistance variation degrades sensing margin. Cell-to-cell and cycle-to-cycle variability has different origins and needs to be differentiated in RRAM characterization. Resistance variability measured by σ/μ (deviation/mean) has to be controlled within target ranges determined by device and array specifications. Mechanism and typical characteristics of RRAM variability will be reviewed in this presentation. Although variability is undesirable for memory arrays, security applications embrace truly random variations. Pervasive and ubiquitous computing requires robust light-weight security technologies at low cost. Physical unclonable functions (PUF) exploit physical randomness and variability as security primitives. RRAM variability may be utilized for PUF implementation, which may achieve much smaller footprint than existing PUF solutions. Feasibility of PUF designs based on RRAM variability will be analyzed based on measured device properties

11:00am **EM2-ThM10 High-K Development for DRAM, NAND, and ReRAM Applications**, Nirmal Ramaswamy, Micron Technology
INVITED

DRAM, NAND and ReRAM utilize high-K oxides to enable high performance devices. High-K oxides are deployed as capacitor dielectrics in DRAM, blocking dielectrics in NAND and solid state electrolytes to enable ion motion in ReRAM. The material and electrical properties required to enable these different technologies are widely different. Several critical parameters such as dielectric constant, band offset, trap density, modulus, crystallinity and texture have to be simultaneously optimized for each technology. This talk highlights the performance requirements of advanced memory devices and the high-K materials engineering required to enable these devices.

11:40am **EM2-ThM12 Resistive Switching Characteristics and Mechanism in Oxide Conductive-Bridge RAM**, Ming Liu, Q. Liu, H.B. Lv, S.B. Long, Chinese Academy of Sciences, China
INVITED

Conductive bridging RAM (CBRAM) has been intensively investigated for the application of next generation nonvolatile memories due to its excellent scalability and superior switching performances [1-2]. Generally, the device forms by an ion-conducting insulator sandwiched between an oxidizable electrode (i.e. Cu or Ag) and an inert electrode (i. e. Pt or W). The resistance switching is based on the the formation and annihilation of nanoscale metallic conductive filament (CF) in the ion-conducting insulator under the external power. This kind of filament utilizes composition of metal ions transferring from the oxidizable electrode to the inert electrode due to cation redox reaction [2]. Deep understanding of the CF dynamic growth mechanism and development of controllable CF growth method will help to guide the design of CBRAM devices with desirable properties. Using binary oxide, such as ZrO and HfO, we successfully

obtained some CBRAM devices with excellent resistive switching performances [3-4]. Based on the variable temperature testing and the advanced SEM and TEM analysing, some fundamental issues related to the resistive switching effect, including the morphologies, chemical compositions and dynamic growth/dissolution of CFs were directly addressed in various CBRAM systems [5]. In addition, using “electrical engineering”, we demonstrated that the CF growth process can be controlled by modulating distribution electric field inside ion-conducting insulator, which greatly improving the uniformity of the CBRAM device [6].

Reference:

- [1]. R. Waser, M. Aono, Nat. Mater. 2007, 6, 833.
- [2]. J. J. Yang, D. B. Strukov, D. R. Stewart, Nat. Nanotechnol. 2013, 8, 13.
- [3]. Q. Liu, S. Long, W. Wang, S. Tanachutiwat, Y. Li, Q. Wang, M. Zhang, Z. Huo, J. Chen, M. Liu, IEEE Electron Device Lett. 2010, 31, 1299.
- [4]. Y. Li, H. Lv, Q. Liu, S. Long, M. Wang, H. Xie, K. Zhang, Z. Huo, M. Liu, Nanoscale 2013, 5, 4785.
- [5]. Q. Liu, J. Sun, H. Lv, S. Long, K. Yin, N. Wan, Y. Li, L. Sun, M. Liu, Adv. Mater. 2012, 24, 1844.
- [6]. Q. Liu, S. long, H. Lv, W. Wang, J. Niu, Z. Huo, J. Chen, M. Liu, ACS Nano 2010, 4, 6162.

Exhibitor Technology Spotlight

Room: Hall ABC - Session EW-ThM

Exhibitor Technology Spotlight Session

Moderator: Chris Moffitt, Kratos Analytical Limited, UK

10:20am **EW-ThM8 An Entirely New Generation of Cold Cathode Gauges**, *Martin Wüest*, INFICON Ltd., Liechtenstein

The cold cathode gauge is a robust vacuum gauge used in many applications. INFICON has introduced an entirely new generation of the inverted magnetrons shedding the issues that plagued performance of the past and now allow its use even in domains that have traditionally been occupied by hot ionization gauges. An innovative and patented magnet design produces the first sensor conforming to Semi S2 specifications regarding ultra-low external magnetic stray field. Together with its small dimensions and low magnetic stray field, it can even be used within analytical devices without impact on surrounding instrumentation. First customer data received demonstrates that the gauge lasts approximately four times longer in a process environment than its predecessor. A unique interchangeable dual chamber facilitates maintenance. It takes only moments to exchange the sensor and return it to normal functional performance. Additional significant features will be discussed, as well.

10:40am **EW-ThM9 Raman Imaging Microscopy Characterization of Carbon Nano Material**, *Alex Rzhetskii, M.H. Wall*, Thermo Fisher Scientific

Over the last few years carbon nano materials have been the focus of many investigations due to their unique electronic, mechanical, and chemical, properties. These materials are being investigated as routes towards more efficient batteries, stronger lighter polymer composites, and faster electronics, to name a few. However, it is necessary to solve several challenges regarding quality uniformity and scalability before these applications are fully realized. Raman imaging microscopy offers a means to address these challenges. This presentation will highlight the Thermo Scientific DXRxi Raman imaging microscope and its application to the characterization of carbon nano materials. Specific examples will be discussed that demonstrate the enhanced speed, intuitive operation, and the simultaneous data acquisition/data analysis capabilities of this new Raman imaging microscope. See how highly detailed Raman chemical images gives comprehensive insight into the nature of carbon nano materials.

Helium Ion Microscopy Focus Topic

Room: 316 - Session HI+2D+AS+BI+MC-ThM

Fundamental Aspects and Imaging with the Ion Microscope

Moderator: Gregor Hlawacek, Helmholtz-Zentrum Dresden - Rossendorf, Stuart Boden, University of Southampton

8:00am **HI+2D+AS+BI+MC-ThM1 He+ and Ne+ Ion Beam Microscopy and Microanalysis**, *David C. Joy*, University of Tennessee, Oak Ridge National Laboratory **INVITED**

After one hundred years of use the electron microscope is now being overtaken by ion beam systems because of their many advantages. A wide variety of different ions are available, each of which has its own particular strengths, but the two most commonly used at present are Helium (He+) and Neon (Ne+). Changing from one to the other takes only a couple of minutes to complete. For operation at beam energies between 20 and 50kV both He+ and Ne+ generate ‘ion induced secondary electrons’ (iSE) which yield images which are comparable with those from a conventional SEM but offer image resolutions of 0.4nm or less even on bulk samples, a much greater depth of field, and an enhanced signal to noise ratio. At typical imaging currents between 10-12 to 10-14Amps damage to most samples is very limited for He+ although more severe for Ne+ but at higher beam currents both He+ and Ne+ can pattern, deposit, or remove, a wide range of materials. In such applications He+ provides the best resolution, but Ne+ is much faster.

The production of X-rays depends on the speed of the incident particle, not on its energy. At typical operating energies the He+ or Ne+ ions are traveling too slowly to generate X-rays so another approach is required for chemical microanalysis. The most promising option is “Time of Flight-Secondary Ion Mass Spectrometry” (TOF-SIMS). Here the incoming ion “splashes” material from the top few layers of the specimen surface. These fragments are then characterized by determining their mass to charge ratios. The chemical data this generates is much more detailed than the bare list of elements that is produced by X-ray microanalysis.

8:40am **HI+2D+AS+BI+MC-ThM3 Gas Field Ion Sources**, *Jason Pitters, R. Urban*, National Institute for Nanotechnology, Canada, *R. Wolkow*, University of Alberta and The National Institute for Nanotechnology, Canada **INVITED**

Single atom tips (SATs) prepared by the spatially controlled field assisted etching method are proving to have utility as ion sources, electron sources and in scan probe applications.

As Gas Field Ion Sources (GFISs), there is potential for operation in scanning ion microscopes (SIMs) and our efforts to prepare and characterize SAT ion emission will be discussed. It will be shown that etching to a single atom tip occurs through a symmetric structure and leads to a predictable last atom. SATs can be prepared reproducibly with emission along a fixed direction for all tip rebuilds. It will also be shown that the emission properties of the SAT can be altered by shaping of the tip shank during the etching procedure. In this manner, the operating voltage can be controlled and a lensing effect of the tip base is demonstrated. During formation, the tip shape can be evaluated by using both helium and neon ionizing gases. The stability of helium and neon ion beams generated by SATs will also be demonstrated and compared to other tip orientations. The remarkable robustness of these tips to atmosphere exposure will also be shown and the ability to prepare SATs from material other than tungsten will be demonstrated.

SATs also have utility in electron emission. By shaping the tip appropriately, electron emission characteristics can also be tailored and the coherence properties of an SAT will be presented as deduced from holographic measurements in a low-energy electron point source microscope. Initial utility in scan probe experiments including atomic force microscopy and scanning tunneling microscopy will also be discussed.

9:20am **HI+2D+AS+BI+MC-ThM5 Ion Beam Profiles Generated by W(111) Single Atom Tips**, *Radovan Urban, R. Wolkow*, University of Alberta and The National Institute for Nanotechnology, Canada, *J.L. Pitters*, National Institute for Nanotechnology, Canada

Single atom tips (SATs) gained significant attention over the past decade because they serve as high brightness, field emission electron sources and gas field ion sources (GFISs). Small virtual source size makes these attractive candidates for advanced scanning imaging applications such as SEM, TEM, and scanning ion microscopy (SIM) as well as for non-staining ion beam writing applications.

The ion beam diameter σ , together with total ion current I generated by a single surface atom of W(111) nanotip, are crucial parameters which determine angular current density and brightness of gas field ion sources. It is, therefore, essential to understand underlying mechanisms that govern beam width. Furthermore, mapping both σ and I to a large parameter space of tip temperature, imaging gas pressure, and extraction voltage is necessary to optimize gas field ion source operation. In this contributions we will explore both σ and I as a function of temperature and extraction voltage at different imaging gas pressures using a field ion microscope (FIM) to monitor beam shape and total current. The qualitative model of our results will be also discussed. Finding “the best imaging voltage” for a SAT will be briefly discussed.

9:40am **HI+2D+AS+BI+MC-ThM6 Defect Observation by using Scanning Helium Ion Microscopy**, *Hongxuan Guo, L. Zhang, D. Fujita*, National Institute for Materials Science (NIMS), Japan

Scanning helium ion microscopy (HIM) is an innovative method to characterize surface of various materials. With a secondary electron detector (SED) and a micro plate detector (CPD), Orion Plus system can obtain surface information including morphology, composition, and crystal orientation. [1, 2] Improve the abilities of characterization of materials with HIM will benefit the develop of new materials, such as structure materials including metals, ceramics and others.

In this presentation, we will show the investigation of the crystal structure of metal with HIM. We prepared an sample stage with a reflector that can be used to obtain the transmission helium ions intensities in the samples. With this sample stage, we observed the Ni-Co base super alloy and aerogel composed with hollow nanosphere. The Rutherford backscattered image (RBI) of metal surface show different orientation of poly crystal. The nano-twins and other defects in Ni-Co base superalloy were investigated by HIM in scanning and transmission mode. The nano-twins also be observed by other techniques, such as transmission electron microscopy and electron backscatter diffraction. The scattering of helium ions with different energy was analyzed. This work provide some new methods to improve the research on defects and structure of crystal.

[1]. H. X. Guo, D. Fujita, Scanning helium ion microscopy, Characterization of Materials, 2nd Edition(Wiley, New York, 2012)

[2]. H. X. Guo, J. H. Gao, M. S. Xu, D. Fujita, Applied Physics Letters, 104, 031607, 2014

11:00am **HI+2D+AS+BI+MC-ThM10 Helium Ion Microscopy (HIM) for the Imaging of Biological Samples at Sub-nanometer Resolution**, *James Fitzpatrick*, Salk Institute for Biological Studies **INVITED**

Scanning Electron Microscopy (SEM) has long been the standard in imaging the sub-micrometer surface ultrastructure of both hard and soft materials. In the case of biological samples, it has provided great insights into their physical architecture. However, three of the fundamental challenges in the SEM imaging of soft materials are that of limited imaging resolution at high magnification, charging caused by the insulating properties of most biological samples and the loss of subtle surface features by heavy metal coating. These challenges have recently been overcome with the development of the Helium Ion Microscope (HIM), which boasts advances in charge reduction, minimized sample damage, high surface contrast without the need for metal coating, increased depth of field, and 5 angstrom imaging resolution. We demonstrate the advantages of HIM for imaging biological surfaces as well as compare and contrast the effects of sample preparation techniques and their consequences on sub-nanometer ultrastructure.

11:40am **HI+2D+AS+BI+MC-ThM12 Helium Ion Microscopy of Biological Cells**, *Natalie Frese, A. Beyer, M. Schürmann, B. Kaltschmidt, C. Kaltschmidt, A. Götzhäuser*, University of Bielefeld, Germany

In this presentation HIM images of biological cells are presented. The presented study focuses on neuronal differentiated human inferior turbinate stem cells, mouse neurons and mouse fibroblasts. The cells were prepared by critical point drying or freeze drying and a flood gun was used to compensate charging, so no conductive coating was necessary.

Therewith, extremely small features at native cell surfaces were imaged with an estimated edge resolution of 1.5 nm. Due to the size of the structures and the preparation methods of the cells the observed features could be an indicator for lipid rafts. This hypothesis will be discussed.

12:00pm **HI+2D+AS+BI+MC-ThM13 Helium Ion Microscopy Analysis of Ag Nanoparticle Implanted Biological Samples for MILDI-MS (Matrix Implanted Laser Desorption/Ionization) Imaging**, *S. Shubeita*, Rutgers University, *L. Muller*, NIDA-IRP, *H.D. Lee*, *C. Xu*, Rutgers University, *D. Barbacci*, Ionwerks Inc., *K. Baldwin*, NIDA-IRP, *J.A. Schultz*, Ionwerks Inc., *L. Wielunski*, *Torgny Gustafsson*, *L.C. Feldman*, Rutgers University, *A.S. Woods*, NIDA-IRP

MILDI mass spectrometry is an emerging tool for detecting changes in brain tissue. An ~20 nm thick region of rat brain tissue implanted with $10^{13}/\text{cm}^2$ $\text{Au}_{(400)}^{4+}$ nanoparticle (NP) ions at 40 keV, produces analytically useful signals of lipids, peptides and proteins using a pulsed nitrogen laser [1]. When a dose of $10^{12}/\text{cm}^2$ 500 eV AgNP (approximately 6 nm diameter) is implanted as a matrix, only lipids are detected [2]. To understand this it is essential to measure the spatial distribution of the nanoparticles. We have used Rutherford Backscattering and Helium Ion Microscopy imaging to determine the Ag NP distributions and areal densities in an implanted coronal rat brain section. We then correlate the ion beam analysis and imaging with individual lipid intensities from several hundred MILDI mass distributions. The results show a high degree of uniformity of the Ag atomic and particulate distribution on a sub-micron scale among different regions of the tissue. Helium Ion Microscopy provides verification of NP matrix uniformity, validating the use of MILDI for quantitative mass analysis.

This work is partially supported by NSF (DMR 1126468), NIH (R44DA030853-03) and IAMDN.

[1] A. Novikov et al, *Analytical Chemistry* 76 (2004) 7288. [2] S. N. Jackson et al, *Analyt. and Bioanal. Chem.* (e-pubed Dec 2013).

Manufacturing Science and Technology Room: 302 - Session MS+PS+TF-ThM

Processes for Mesoscale Structure on Paper and Textiles Moderator: Jesse Jur, North Carolina State University

8:00am **MS+PS+TF-ThM1 High-Performance Composites Based on Wood Cellulose Nanofibrils**, *Qi Zhou*, KTH Royal Institute of Technology, Sweden **INVITED**

With increasing concerns for the climate and environment, it has been recognized globally that paradigm-shifting research is required to improve the performance of materials based on renewable resources. Attempts to develop very high performance natural cellulosic fibers based composite materials using intact cells from hemp, flax and cotton have failed mainly due to the inherent imperfections of the secondary cell walls of natural fiber cells. These issues have been recently addressed by replacing with cellulose nanofibrils (CNFs), which are three orders of magnitude smaller than the intact fiber cells. The extraction process of CNFs from renewable resource has been extensively investigated in the past decade. A critical challenge in the fabrication of high performance products based on CNFs is to tailor their surface structure and functionality in an efficient and environmentally friendly fashion, thus to accommodate a wider range of applications and sustainability requirements for the next generation of materials. In this talk, I will present our recent work on the fabrication of functional composite materials based on CNFs. In particular, several novel surface modification techniques of CNFs and their effects on nanostructure and material properties of CNFs based composites will be discussed.

8:40am **MS+PS+TF-ThM3 Manufacturing and Applications of Carbon Nanotube Textiles**, *Philip Bradford*, North Carolina State University **INVITED**

Carbon nanotubes (CNTs) are short nanofibers that are usually produced in the form of a black powder. This powder is then incorporated into other materials to produce a wide array of multifunctional products. Processing raw CNTs into materials that look and behave like traditional textiles is a growing area of interest, however the CNTs are often processed in solution and the end products look more like papers than textiles. There are currently only a couple of options for creating fabrics out of CNTs which preserve the high surface area of the individual tubes and retain high porosity. This presentation covers the work of my research group to make this type of fabric from a special type of CNT structure called drawable CNT arrays. These arrays are synthesized in a low pressure chemical vapor deposition process and then utilized for CNT nonwoven fabric formation. My group is also exploring many novel applications for the use of these unique fabrics.

The nonwoven CNT fabrics produced in our lab contain millimeter long CNTs, have a preferential CNT alignment, low CNT bundling and high porosity. These features make them attractive for use in: composites reinforcement, battery electrodes, sensing, filtration and barrier fabrics. Of particular interest to the AVS community may be our recent work with

collaborator Dr. Jesse Jur at NC State, to study the atomic layer deposition (ALD) of thin inorganic layers into CNT arrays and fabrics. Through optimization of CNT pretreatment, ALD parameters and sample orientation, we have been able, for the first time, to uniformly coat CNT structures whose characteristic aspect ratios are extremely large. Due to the unbundled nature of the CNT fabrics we have the ability to uniformly coat CNTs along their entire millimeter length, making for some very unique hybrid CNT structures.

9:20am MS+PS+TF-ThM5 Carbonized Cellulose Fibers for Low-Cost Energy Storage, Fei Shen, L.B. Hu, University of Maryland, College Park

A low-cost but scalable carbon film was successfully obtained via cellulose fiber carbonization. This cellulose derived film can be also applied as an alternative anode for lithium or sodium ion battery due to its natural mesoporous structure of the starting material which was excellent for ion storage. Furthermore, this new type of carbonized cellulose possesses electrically interconnected three-dimensional framework with advanced dual properties of anode material and current collector, afford to result in a higher energy density by eliminating the extra mass of inactive materials such as binder and carbon black in conventional designs. Electrochemical studies showed the film achieved a high capacity of 800mAh/g for lithium ion battery and a moderate capacity of 200mAh/g for sodium ion battery at C/10.

9:40am MS+PS+TF-ThM6 Traditional, 20th, and 21st Century Strengthening Techniques for Cultural Heritage Papers Weakened by Cellulose Depolymerization, L. Pei, M. McGath, John Baty, Johns Hopkins University

Cellulose depolymerization leading to paper brittleness can occur throughout the sheet, or be localized to where a corrosive substance is present. Uniform brittleness is associated with mass-produced, inexpensive, and acidic papers. Rendering millions of books and unbound papers useless, paper brittleness impairs scholarly communication and destroys historic and artistic works. Localized brittleness is most commonly associated with corrosive pigments and inks, including iron gall ink. It visually alters and can also physically destroy paper-based works. In the absence of techniques to restore the cellulose polymer to its initial condition, diverse techniques have been developed to strengthen paper. Traditional conservation techniques vary from conceptually simple ones, such as backing the sheet with a reinforcing layer, to complex ones, such as splitting the sheet into two plies to adhere a reinforcing sheet in-between. 20th century techniques include the widespread lamination of documents with a cellulose acetate film, the present condition of which we have studied and discuss along with its successor, the encapsulation of papers within a polyester film envelope to which the sheet is only electrostatically attracted. Both of these techniques involve the addition of a visible film, altering the look and feel of the artifact. Therefore, we are studying chemical vapor deposition (CVD) using Parylene to deposit a thin, conformal, barely perceptible coating to add strength to brittle papers. We conclude that, here as elsewhere, scientific research can improve traditional conservation techniques by making additional tools available to the conservator; that both cellulose acetate lamination and polyester film encapsulation have achieved a greater preservation benefit than they are credited for; and that CVD is a useful tool for both single-item as well as batch treatments to preserve cultural heritage papers weakened by cellulose depolymerization.

11:00am MS+PS+TF-ThM10 Visualizing the Interface in Strained Cellulosic Nanocomposites, Chelsea Davis, J. Woodcock, A.M. Forster, M. Zammarano, I. Sacui, N. Chen, S.J. Stranick, J.W. Gilman, National Institute of Standards and Technology (NIST)

In fundamental composite theory, the nature of the interface is often the key parameter which determines the strength of the resulting composite structure. While it is possible to observe interfacial failure and characterize the areal coverage of the matrix on the surface of the reinforcement phase in conventional composite materials, directly quantifying interfacial strength and contact area in a nanocomposite becomes far more difficult. A novel solution developed at NIST has been to utilize Förster resonance energy transfer (FRET) imaging^[1,2] by preferentially labeling the interface within a nanocomposite system, allowing direct imaging of the interface with an optical microscope.^[3] Zammarano et al. have shown that the incorporation of a FRET dye pair onto the surface of a cellulosic nanoreinforcement phase (dye 1) and within a polymer matrix (dye 2) allows visualization of the nanoscopic interphase region as the two dyes transfer energy on the same scale as the interphase depth (1 nm-100 nm).^[3,4]

Building upon this FRET-based interfacial characterization technique, our goal is to develop a globally nondestructive measurement system that allows the quantitative characterization of key interfacial properties; first, the wetting and surface contact formed between the nanocellulose and an epoxy matrix and second, the deformation of the interface on the nanoscale

upon application of small mechanical strains. We are constructing a suite of mechanical strain tools to enable *in situ* mechanical interrogation with simultaneous FRET imaging. The development of the first of these tools, uniaxial tensile test will allow a preliminary observation of small strain effects on the interphase region regarding the fluorescent response of the FRET dye pair. As a first proof of concept, it has been shown that FRET can be used to observe nanoscopic interfacial fracture and to determine local (microscopic) stress concentration zones before macroscopic failure of the nanocomposite is observed.

This *in situ* FRET/mechanical deformation approach allows the use of an optical microscope to probe nanoscale features in a powerful way, enabling characterization of nanomaterials which will complement measurements made by electron microscopy and standard mechanical property testing methods.

Topic Area: Novel nanocomposites, Multi-technique characterization of nanostructured materials

[1] T. Förster, *Ann. Phys.* **1948**, 248.

[2] E. a Jares-Erijman, T. M. Jovin, *Nat. Biotechnol.* **2003**, 21, 1387.

[3] M. Zammarano, P. H. Maupin, L.-P. Sung, J. W. Gilman, E. D. McCarthy, Y. S. Kim, D. M. Fox, *ACS Nano* **2011**, 5, 3391.

[4] C. Berney, G. Danuser, *Biophys. J.* **2003**, 84, 3992.

11:20am MS+PS+TF-ThM11 SERS-based Chemical and Biological Analytics on Inkjet-fabricated Paper Devices, Ian White, University of Maryland

SERS-based chemical and biological analytics on inkjet-fabricated paper devices

Abstract. As a bio/chemical sensing technique, surface enhanced Raman spectroscopy (SERS) offers sensitivity comparable to that of fluorescence detection while providing highly specific information about the analyte. The high sensitivity of SERS detection results from the localized plasmons generated at the surface of noble metal nanostructures upon excitation by resonant electric fields at optical frequencies. Although single molecule identification with SERS was demonstrated over a decade ago, today a need exists to develop practical solutions for point-of-sample and point-of-care SERS systems. Recently, we demonstrated the fabrication of SERS substrates by inkjet printing silver and gold nanostructures onto paper and other similar membranes. Using a low-cost commercial inkjet printer, we deposited silver nanoparticles with micro-scale precision to form SERS-active biosensors. Using these devices, we have been able to achieve detection limits comparable to conventional nanofabricated substrates. Furthermore, we have leveraged the fluidic properties of paper to enhance the performance of the SERS devices while also enabling unprecedented ease of use, which is critical for extending chemical and biological analytics from central labs out into the field.

In this presentation we will review the capabilities of inkjet-fabricated paper SERS devices as chemical and biological sensors. We will introduce the fabrication of paper-based fluidic SERS devices using inkjet printing, and we will review results for chemical detection with paper SERS devices, including the use of the paper substrates as swabs and dipsticks for pesticide detection, as well as chromatography SERS on PVDF membranes for the detection of melamine in infant formula. We will then present the results of the fluidic paper SERS devices for biomolecule detection, including paper SERS dipsticks that leverage the chromatographic separation properties of paper to distinguish the outcome of multiplexed TaqMan PCR from a single reaction. In particular, we have utilized this technique to detect the presence of two drug resistance biomarkers for methicillin-resistant *S. Aureus* (MRSA).

11:40am MS+PS+TF-ThM12 NSF Scalable Nanomanufacturing (SNM) Program, Khershed P. Cooper INVITED

Abstract: Nanomanufacturing involves the fabrication of nano-scale building-blocks (nanomaterials, nanostructures), their assembly into higher-order structures such as nanodevices and nanosystems, and the integration of these into larger scale structures and systems such that both heterogeneity and complexity are possible with manipulation and control at nano-scale. In 2010, following a review of the NNI, PCAST recommended greater emphasis be put on commercialization of nanotechnologies by doubling Federal Government investment in nanomanufacturing R&D. In 2011, the inter-Agency NNI Signature Initiative (NSI) in Sustainable Nanomanufacturing was announced. In response to the NSI, the NSF Scalable Nanomanufacturing (SNM) Program was launched. SNM's emphasis is on research to overcome the key scientific and technological barriers that prevent the production of useful nanomaterials, nanostructures, devices and systems at an industrially relevant scale, reliably, and at low cost and within environmental, health and safety guidelines. The SNM program's objective is to address challenges presented at the various stages of the nanomanufacturing value chain of nano-scale building-blocks to

nano-enabled products. It sponsors fundamental scientific research in well-defined technical areas that are strongly justified as approaches to overcome critical barriers to scale-up and integration. It seeks discovery of scalable processes and methods for large-area or continuous manufacturing at the nano-scale. It encourages the study of design principles for production systems leading to nanomanufacturing platforms, identification of metrology, instrumentation, and standards, and development of methodologies needed for process control and assessing quality and yield. SNM encourages an inter-disciplinary approach, industry collaboration and integration of research and education. SNM projects are studying a variety of building-blocks—CNT, graphene, membranes, BCPs, DNA, nanowires, nanofibers, QDs, etc., a variety of top-down and bottom-up processes—thermal, vapor-based, solution-based, lithography, patterning, bio-inspired, etc., targeting applications across the board—energy, environmental, electronics, sensors, structural, etc. Many projects are investigating roll-to-roll processing systems, some are studying in-line metrology and quality control. Moving ahead, SNM seeks to explore new research opportunities in processing (hierarchical nanomanufacturing, cyber-enabled nanomanufacturing, etc.), in materials (graphene, MoS₂, etc.), in devices (plasmonics, ultrafine vias, etc.), and in manufacturing platforms (3D printing, bio-enabled assembly, etc.). SNM encourages an inter-disciplinary approach involving the disciplines of engineering, physical sciences and mathematics. The ultimate goal is to create a knowledge base for the reliable production of nano-enabled systems and products.

Plasma Science and Technology

Room: 305 - Session PS1+TF-ThM

Plasma Deposition and Plasma Assisted ALD

Moderator: Sumit Agarwal, Colorado School of Mines

8:00am **PS1+TF-ThM1 Sputtering Growth of High-Quality ZnO-based Semiconductors for Optoelectronic Applications, Naho Itagaki,** Kyushu University, Japan

INVITED

ZnO and its related semiconductors are remarkable multi-functional materials with a huge range of existing and emerging applications including transparent conducting oxides (TCO) and light emitting diodes (LED). In order to obtain physical properties required for such applications, control of the crystallinity (grain size, crystal axis alignment, crystal defects) is of great importance. We have recently developed a new fabrication method based on magnetron sputtering, "Impurity mediated crystallization (IMC)", where crystal nucleation and the growth are controlled by impurity atoms adsorbed on the film surface [1,2]. Here we demonstrate sputtering deposition of two kinds of ZnO films by utilizing buffer layers fabricated via IMC method. One is polycrystalline TCO films fabricated on glass substrates, and the other is single crystalline films on sapphire substrates for LED applications. Effects of impurity during the crystal growth of ZnO are studied by observing the evolution of film morphology by means of atomic force microscopy (AFM).

IMC-ZnO buffer layers have enabled fabrication of single-crystalline ZnO films even on large lattice-mismatched (18%) sapphire substrates by a conventional sputtering method. The ZnO films have atomically-flat surfaces with steps of 0.26nm-high, corresponding to a half of c-axis length of ZnO. AFM observation of IMC-ZnO buffer layers revealed that impurity atoms inhibit the crystal growth and thus increase in the grain density, which reduce the strain energy caused by the large lattice mismatch between ZnO and sapphire. IMC-ZnO buffer layers have also improved the film quality of ZnO based TCO fabricated on glass substrates. The most remarkable effect is a reduction in the resistivity of the films thinner than 100 nm. The resistivity of ZnO:Al films fabricated by conventional sputtering increases substantially from $6.3 \times 10^{-4} \text{ W}\cdot\text{cm}$ to $1.5 \times 10^{-3} \text{ W}\cdot\text{cm}$ with decreasing the film thickness from 100 nm to 20 nm, while the resistivity of ZnO:Al films with IMC buffer layers is low of $2.8\text{-}3.2 \times 10^{-4} \text{ W}\cdot\text{cm}$ in the thickness range 20-100 nm. The role of impurity here is to suppress the nucleation and allow the crystal growth with larger grains from the very early stage of deposition.

We believe that IMC method will not only accelerate the commercialization of ZnO in optoelectronic devices but also open up a new pathway for development of other oxide semiconductors, some examples of which including In₂O₃:Sn will be presented at the conference.

This work was partially supported by JSPS (25630127), JST-PRESTO, and AOARD.

[1] N. Itagaki, et al., Appl. Phys. Express 4 (2011) 011101. [2] K. Kuwahara, et al., Thin Solid Films 520 (2012) 4507.

8:40am **PS1+TF-ThM3 Novel Composite Materials Fabricated by Plasma-enhanced CVD of Carboranes and Pyridine or Benzene, Robinson James, U. Chiluwal,** University of North Texas, *E. Echeverria,* University of Nebraska-Lincoln, *R. Gafpzi, J. Tae,* University of North Texas, *P.A. Dowben,* University of Nebraska-Lincoln, *J.A. Kelber,* University of North Texas

Altering the electronic structure of carborane-derived boron carbides by incorporating aromatic compounds is of scientific and technological interest in neutron detection and microelectronics. The fabrication of novel composite materials derived from ortho-carborane or meta-carborane with benzene or pyridine by plasma enhanced chemical vapor deposition (PECVD) at room temperature may lead to improved device performance over conventional boron carbides. The chemical composition and electronic structure of the resulting films were studied using in-situ x-ray and ultraviolet photoelectron spectroscopy (XPS, UPS) respectively. XPS of composite films of carboranes with pyridine shows the evidence of B-N bond formation during the PECVD process. Pyridine incorporation in the boron carbide materials resulted in the improved adhesion of physical vapor deposited Cu (PVD Cu) overlayers on the surface. XPS indicates that no thermal induced diffusion/dewetting of Cu was observed in the ortho-carborane and pyridine composite films even after annealing up to 1000K in UHV. In contrast, pure boron carbide films exhibited poor adhesion of Cu overlayers on the surface resulted in the significant dewetting during 400-600 K annealing although no diffusion of Cu was observed even after annealing up to 1000 K. Composite films of ortho-carborane or meta-carborane with benzene were also grown on Si substrates by PECVD. These carborane: benzene composite films exhibit augmented B-C bond formation due to linking of benzene with the icosahedral carborane units as evidenced by XPS.

9:00am **PS1+TF-ThM4 Engineering High-k Dielectric Gate Stacks using In Situ Spectroscopic Ellipsometry, Yuanxia Zheng,** Penn State University, *G.B. Rayner,* Kurt J. Lesker Company, *A. Agrawal, S. Datta, R. Engel-Herbert,* Penn State University

The development of Ge-based field effect devices requires the integration of a high quality dielectric that forms an electrically well behaved semiconductor dielectric interface. Although GeO₂/Ge has been found promising, the thermodynamic instability as well as the relatively low dielectric constant of GeO₂ requires an alternative approach. The utilization of an ultrathin Si layer to move the semiconductor/dielectric interface from Ge into Si has been successfully demonstrated; however, the introduction of a planar thin layer into the gate stack is incompatible with a 3D FinFET manufacturing process flow. It is thus desirable to develop a multilayer gate stack by atomic layer deposition process, where an ultrathin GeO₂ layer can be thermodynamically stabilized and combined with a high-k dielectric film to meet the stringent requirement of low interface trap density and large capacitance density while maintaining a low gate leakage.

In this talk, we will present an approach of developing a multilayer gate-stack of HfO₂/Al₂O₃/GeO₂ for Ge using in-situ processing control in plasma-enhanced atomic layer deposition (PEALD) by utilizing real-time monitoring capabilities of in-situ spectroscopic ellipsometry (SE). Pristine Ge-surface is obtained by removing native GeO_x using H-plasma and an ultrathin GeO₂ layer is grown thereafter by O-plasma anneal; in-situ SE is used to monitor the process and to control GeO₂ thickness. An ultrathin bilayer of alumina and hafnia is subsequently grown using thermal ALD and large capacitance densities with equivalent oxide thicknesses (EOT) below 1 nm and gate leakages below $1 \times 10^{-4} \text{ A}/\text{cm}^2$ at -1V (EOT=0.7 nm) are demonstrated. The impact of the thickness of the individual dielectric layers on interface trap density, determined by the conductance and the Terman method, leakage current and EOT is discussed. We will further discuss how in-situ SE is used to optimize process-relevant parameters for native oxide etching, intentional oxidation and deposition of high-k dielectrics. The potential of this in-situ real-time process metrology is projected for the development of high quality high-k dielectrics on other high mobility low band gap semiconductor materials.

9:20am **PS1+TF-ThM5 Impact of Low Frequency Addition to RF Power in PECVD Process: Case of TiN and GeTe, Christophe Vallee, F. Piallat, M. Aoukar, P.D. Szkutnik,** LTM - CEA/LETI, France, *R. Gassilloud, P. Noé, P. Michallon,* CEA, LETI, MINATEC Campus, France

In Dual Frequency plasma etching, one frequency is chosen to be much higher than the other in order to achieve an independent control of ion bombardment and electron density (i.e. ion flux). It is assumed that high frequency control the density and low frequency (LF) the energy. Recently, many groups have simulated the effect of LF addition to RF source. Depending on the model, it has been reported that the plasma density may be reduced due to sheath width variation as well as it may be increased due to highly energetic secondary electrons. Donko *et al* have shown how the γ coefficient of the secondary electrons may be used to interpret contradictory published papers [1] and they concluded that there is only a small pressure

process window for which the effect of secondary electrons on the ionization compensates the effect of the frequency coupling.

The interest of adding LF to RF plasma in order to enhance the deposition reaction mechanisms is demonstrated here. An in depth investigation of plasma by Optical Emission Spectroscopy shows that the plasma density increases when adding LF (350 Khz) in a RF (13.56 Mhz) metal deposition process. In this case, the plasma enters a γ -mode due to secondary electron heating. This mode is not obtained when depositing semiconductors (GeTe) or dielectric, i.e. depending on the biased nature of the surface of showerhead electrode during the process. Adding LF to RF also modifies the sheath thickness of the plasma and increases the electron temperature of the gas [2]. In our experiments, all the deposited materials show different properties and new emission peaks are observed by OES for all precursors. Carbon content, density and growth rate are strongly modified by adding LF. For example, in case of TiN we found that the deposition rate is increased by a factor of two while in the same time the resistivity is strongly reduced (50%) and the density is going from 3.4 to 3.8 g.cm⁻³[3]. We also studied the plasma impact on the Equivalent Oxide Thickness (OET) regrowth of a TiN/HfO₂ integrated MOS capacitors. For phase change material (PCM) applications, very different cycles (amorphous to crystalline) are observed for devices with RF GeTe or LF+RF GeTe. All the deposition processes are performed in 200 (GeTe) and 300 mm (TiN) pulsed liquid injection PEMOCVD chambers from AltaCVD Advanced MaterialsTM, located in CEA-LETI cleanroom.

[1] Z. Donkó, *et al*, Appl. Phys. Lett. **97** (2010) 081501

[2] W-J Huang *et al*, Phys. Plasmas **16** (2009) 043509

[3] F. Piallat *et al*, J. Phys. D: Appl. Phys. **47** (2014) 185201

11:00am **PS1+TF-ThM10 Surface Reactions during Ammonia-Plasma-Assisted Atomic Layer Deposition of Silicon Nitride**, *Dennis Hausmann*, Lam Research Corporation, *R. Ovanesyan, S. Agarwal*, Colorado School of Mines

The advent of FinFETs with high-aspect-ratio 3-D geometries increases demands on conformality of the SiN_x films. These stringent requirements on conformality and low thermal budget can be simultaneously met using atomic layer deposition (ALD). While there are a few reports in the literature that show that SiN_x can be conformally deposited via ALD at <400 °C, these films are not sufficiently dense to serve as moisture or oxidation barriers. Hence, improvements in this area are needed via a fundamental understanding of the surface reaction processes. Recently, we have developed a novel ALD processes for the growth of Si₃N₄ thin films using trisilylamine (Si(NH₃)₃, TSA) and silane precursors, and an NH₃ plasma. This ALD process with TSA provides dense films with a conformal coverage over aspect ratios typical for the applications; 10:1. To understand the underlying film growth mechanism, the specific surface reactions involved during each half-reaction cycle of this ALD process were monitored with *in situ* attenuated total reflection Fourier transform infrared (ATR-FTIR) spectroscopy. ZnSe internal reflection crystals were used as substrates since ZnSe is transparent in the infrared up to 700 cm⁻¹. This spectral range, combined with the high sensitivity achieved with ATR-FTIR spectroscopy, allows us to identify and monitor in real time the different surface species generated and consumed due to sequential exposure of the growth surface to Si-containing precursors and an NH₃ plasma. The vibrational modes that were monitored include the surface SiH_ν and NH_ν stretching modes in the 2100 and 3400 cm⁻¹ region, respectively, and Si₃N₄ phonon modes, which appear in the 800-900 cm⁻¹ region. The corresponding surface reaction products were monitored using quadrupole mass spectrometry. Further, these films were extensively characterized using a suite of *ex situ* diagnostic tools.

11:20am **PS1+TF-ThM11 Plasma Assisted Atomic Layer Epitaxy of III-N Ternaries for Next Generation Devices**, *Neeraj Nepal, J.K. Hite, V.R. Anderson, V.D. Wheeler, S. Qadri, C.R. Eddy*, Naval Research Laboratory

III-Ns (InN GaN and AlN) and their alloys have been attractive semiconductor materials for application in a wide range of device technologies. The most common growth methods of this material system are CVD and MBE, but these conventional growth techniques have challenges in achieving alloys without phase separation over the entire stoichiometric range, ultimate thickness control at the atomic level, and the ability for *in situ* growth of complete device structures. Plasma-assisted atomic layer epitaxy (PA-ALE) is a promising method to grow III-N alloys and incorporate them into device structures as it allows low temperature growth and precise control of thickness, stoichiometry and uniformity. Recently, PA-ALE has been used for the growth of III-N binaries at low temperatures (<500°C)[1,2]. Ternary growth at these low temperatures could eliminate miscibility gaps, which has been an issue for conventional growth methods.

We present the growth and characterization of III-nitride ternaries by PA-ALE over a wide stoichiometric range including the range where phase

separation has been an issue for MBE and CVD. Using our previously reported optimal growth conditions for GaN, InN [1], and AlN [2], Al_xGa_{1-x}N, In_xAl_{1-x}N and In_xGa_{1-x}N (0≤x≤1) alloys were grown at 250–500 °C. Group III-B metal contents in these alloys were varied with binary cycle ratios and the alloy compositions were determined by XPS and XRD and reflectivity measurements. Since the growth rate (GR) of InN is slower than that of AlN, a digital alloy produced from 3 cycles of InN for every cycle of AlN results in an Al_{0.83}In_{0.17}N film. The GaN GR, however, is slower than InN, and In_{0.54}Ga_{0.46}N alloy was grown for every alternating cycle of GaN and InN. Additionally, 4 cycles of GaN for every cycle of AlN gave Al_{0.5}Ga_{0.5}N alloy and the measured concentration was confirmed optically. By this digital alloy growth method, we are able to grow In containing ternaries by PA-ALE in the spinodal decomposition region (15-85%). The surface roughness of III-N alloys on GaN were the same as the starting roughness of 0.4 nm. Optimal ternary growth conditions were used to synthesize III-N based device structures on GaN and demonstrated 2DEG at the interface. We will present electrical and optical data on ALE III-N heterojunctions on GaN templates.

These early efforts suggest great promise of PA-ALE for addressing miscibility gaps issue encountered with conventional growth methods and realizing high performance optoelectronic and electronics devices involving ternary/binary heterojunctions, which are not currently possible.

[1] N. Nepal *et al.*, JCGS **13**,1485 (2013).

[2] N. Nepal *et al.*, APL **103**, 082110 (2013).

11:40am **PS1+TF-ThM12 Plasma-enhanced Atomic Layer Deposition: Prospects and Challenges**, *Hyungjun Kim*, Yonsei University, Korea
INVITED

Due to various benefits such as atomic level thickness control and excellent conformality, atomic layer deposition (ALD) is expected to play an important role in future device fabrication. Especially, plasma enhanced ALD (PE-ALD) allows deposition at significantly lower temperatures with better film properties than conventional thermal ALD. This low temperature process makes PE-ALD more attractive for emerging nanoscale device fabrication. In addition, since ALD is surface-sensitive deposition technique, surface modification by plasma exposure can be used to alter nucleation and adhesion. In this presentation, the basic characteristics and several examples of PE-ALD processes for various applications such as semiconductor/display devices fabrication will be presented. The PE-ALD is a valuable tool to deposit very thin metal layers with good properties including little nucleation delay and high purity. Co, Ni, Ru films with good conformality was deposited by PE-ALD using NH₃ plasma. Film properties as well as applications for emerging electronic devices of the metal PE-ALD will be discussed. Also, the use of plasma for ALD enables improvements in electrical properties of next generation semiconductor devices. Various high k oxides including HfO₂, CeO₂, La₂O₃ and doped high k oxides were deposited by PE-ALD from metal organic precursors and oxygen plasma. Especially, comparative study between PE-ALD and thermal ALD has shown that the interface defect density and leakage current are better for PE-ALD. Also, PE-ALD of ZnO thin films was investigated for thin film transistors. We studied the modulation of device parameters of PE-ALD ZnO based TFTs using UV light exposure. Finally, PE-ALD TiO₂ thin films have shown high photocatalytic effects on various substrates. These indicate that the PE-ALD processes are versatile methods enabling nano scale manufacturing in emerging applications.

Plasma Science and Technology
Room: 308 - Session PS2+TF-ThM

Atomic Layer Etching (ALE) and Low-Damage Processing

Moderator: Geun Young Yeom, Sungkyunkwan University, Republic of Korea

8:00am **PS2+TF-ThM1 Fluorocarbon Assisted Atomic Layer Etching of SiO₂ and Selectivity over Si Using Cyclic Ar/C₄F₈ Plasma**, *Dominik Metzler**, University of Maryland, College Park, *S.U. Engelmann, R.L. Bruce, E.A. Joseph*, IBM T.J. Watson Research Center, *V.A. Godyak*, University of Michigan, *G.S. Oehrlein*, University of Maryland, College Park

There is great interest in establishing directional etching methods capable of atomic scale resolution for fabrication of highly scaled electronic devices. Recently, controlled etching of SiO₂ at the Angstrom-level based on steady-

*** Coburn & Winters Student Award Finalist**

state Ar plasma, periodic injection of a defined number of C_4F_8 molecules, and synchronized plasma-based Ar^+ ion bombardment has been shown [1]. Controlled etching is based on deposition of a thin (\sim several Å) reactive fluorocarbon (FC) layer on SiO_2 enabled by precise C_4F_8 injection. For low energy Ar^+ ion bombardment conditions, the physical sputter rate of SiO_2 vanishes, whereas SiO_2 can be etched when FC reactants are present at the surface. In this work, plasma conditions have been characterized in real time during cyclic exposure using a Langmuir probe. Changes in plasma potential, electron density, and electron temperature are measured throughout each cycle and compared to continuous precursor addition. Continuous precursor addition has a higher C_4F_8 concentration than periodic injection. The C_4F_8 injection has a short, significant impact on the plasma properties within each cycle and a small impact for longer time scales, i.e. from cycle to cycle. Observed trends in plasma properties agree with continuous precursor addition. Additionally, this cyclic approach was used to investigate the transition from SiO_2 to Si etching employing SiO_2 -Si- SiO_2 layers. Si etching and the selectivity of SiO_2 over Si is investigated as a function of FC surface coverage, ion energy (20 to 30 eV), and etch step length using *in situ* ellipsometry. Time-dependent etch and deposition rates are compared for Si and SiO_2 . The etch behavior during the cyclic approach is compared to continuous precursor addition etching of SiO_2 and Si. X-ray photoelectron spectroscopy is used to investigate surface chemistry at various stages of the cyclic etching and will be reported.

The authors gratefully acknowledge financial support of this work from National Science Foundation (CBET-1134273) and US Department of Energy (DE-SC0001939).

References:

[1] D. Metzler, R. Bruce, S. Engelmann, E. A. Joseph, and G. S. Oehrlein, *J Vac Sci Technol A* **32**, 020603 (2014)

8:20am **PS2+TF-ThM2 Highly Selective Atomic Layer Etching of Silicon Dioxide Using Fluorocarbons**, *Eric Hudson, V. Vidyarthi, R. Bhowmick, R. Bise, H.J. Shin, G. Delgadino, B. Jarivala, D. Lambert, S. Deshmukh*, Lam Research Corporation

As microelectronics advancements require smaller device features, masking layers are becoming thinner. Additionally, there are tighter requirements on allowable loss of films during processing. This leads to exacting requirements for etch, where a target film must be removed with very high selectivity to a mask and/or substrate film. For etching of SiO_2 or similar materials, this high selectivity is typically achieved using very polymerizing fluorocarbon-based combinations of gases. However this approach can introduce problems with etch rate loading, such that the oxide in features with larger critical dimension (CD) tends to etch more slowly due to excessive passivation.

A novel approach for oxide etching has been developed which addresses this tradeoff between selectivity and etch rate loading. The etch process is based on repeated cycles of fluorocarbon deposition and etch reaction activation, similar to the process described by Metzler et al [1]. In each cycle there are two different phases of plasma conditions in which (1) a thin film of fluorocarbon polymer is deposited and (2) the polymer film is bombarded by noble gas ions to activate the etch reaction. Under the right conditions, oxide films are incrementally etched in each cycle. This atomic layer etch approach is less susceptible to etch rate loading because under properly adjusted conditions, the oxide etch front remains clear of polymer buildup after each cycle. Under the same conditions, polymer can build up on the mask or substrate surface with successive cycles, protecting the film and resulting in minimal loss. The process times for the deposition and activation phases of the cycle are the primary parameters for process control. A comparison of model and experiment is presented to characterize the effect of these two time parameters upon process results.

[1] Metzler, et al *JVST A* **32**, 020603 (2014).

8:40am **PS2+TF-ThM3 Electron Beam Plasma Tool for Atomic Precision Etching**, *Leonid Dorf, S. Rauf, M.-F. Wu, Y. Zhang, F. Tavassoli, K. Ramaswamy, K. Collins*, Applied Materials Inc.

As the node size diminishes, microelectronics fabrication progressively requires atomic layer precision, so it becomes critical to accurately control ion energy during plasma processing. Damage caused by conventional plasma technologies (capacitively or inductively coupled plasmas) is becoming unacceptable for critical etch and clean applications. Using electron sheet beam parallel to the substrate surface to produce plasma in a processing chamber provides an order of magnitude reduction in electron temperature T_e (\sim 0.3 eV) and ion energy E_i ($<$ 2 eV without applied bias) compared to conventional plasma technologies, thus making electron beam plasmas an ideal candidate for processing features at 5 nm and below. In this presentation, we report processing results for a range of advanced plasma etching applications tested using the electron beam generated low T_e plasma. Using patterned wafers, we have developed low-bias power (0 – 10 W) processes resulting in infinite selectivity (as per high-resolution TEM

images) of silicon nitride to silicon oxide and poly-silicon in fluorocarbon based chemistries. Such high selectivity can be attributed to the two phenomena: (1) at very low bias power, ion energy is sufficiently small to allow processing near the etch threshold, and (2) plasma ions and radicals in the electron beam generated plasma are produced by highly energetic (\sim 2000 eV) electrons, such that the ratio between dissociation and ionization cross-sections for most gases differs considerably from that in conventional tools with chemical processes determined by 10-15 eV electrons. The latter results in weak dissociation of the fluorocarbon gas (CH_2F_2) and relatively low free fluorine concentration, which in turn leads to very low silicon etch rate. We have also investigated a nitride spacer application, in which 20 nm nitride layer deposited conformally over a silicon fin needs to be etched away to produce straight side walls for further double patterning (as one application). Our results indicate that using the electron beam plasma provides suitably small footing with a reasonably small slant angle of the shoulder, at the same time being selective to the underlying silicon layer. Accurate analysis of several time-series of TEM images allowed characterization of lateral and vertical etch processes over a range of operating conditions, such as the bias power and the beam current. Initial studies also indicate excellent loading characteristics, even at high bias power, which again can be attributed to unique chemical composition of the processing gas in the electron beam generated plasma.

9:00am **PS2+TF-ThM4 Precise Theoretical Calculation of Neutral Beam Generation Efficiency by Collision of Chlorine Against Graphite Surface**, *Tomohiro Kubota*, Tohoku University, Japan, *N. Watanabe, S. Ohtsuka, T. Iwasaki, K. Ono, Y. Iriye*, Mizuho Information & Research Institute, Japan, *S. Samukawa*, Tohoku University, Japan

We investigated the generation mechanism of neutral particles in high efficiency neutral beam source developed by Samukawa et al [1], by collision of positive and negative chlorine ions against graphite surface. It is already known experimentally that neutralization efficiency of negative ion (Cl^-) is much higher than that of positive ion (Cl_2^+) [2]. However, the mechanism has not been clarified. Recently we investigated the neutralization mechanism by using numerical simulations based on quantum mechanics [3] and succeeded in explaining higher neutralization efficiency of negative ions than positive ions.

In this study, collision process of a chlorine particle (Cl , Cl^- , Cl_2 , or Cl_2^+) against graphite surface was simulated by calculation based on time-dependent density functional theory (TD-DFT). Neutralization efficiency was calculated from the number of the valence electrons on the particle after the collision. By using a unit cell with enough size, dispersion of electron density into vacuum was suppressed and quantitative interpretation became possible.

Also, dependence on incident angle and energy of the particle was investigated. It was found that experimental result of energy dependence of the neutralization efficiency was quantitatively reproduced by the calculation. It suggests we have achieved a precise simulation of the neutralization process.

A part of this work was supported by the New Energy and Industrial Technology Development Organization (NEDO).

[1] S. Samukawa et al., *Jpn. J. Appl. Phys.* **40**, L779 (2001).

[2] S. Samukawa, *Jpn. J. Appl. Phys.* **45**, 2395 (2006).

[3] N. Watanabe et al., *Phys. Rev. E* **65**, 036705 (2002).

[4] <http://www.mizuho-ir.co.jp/solution/research/semiconductor/nano>

[5] T. Kubota et al., *J. Phys. D: Appl. Phys.* **45**, 095202 (2012).

9:20am **PS2+TF-ThM5 Achieving One Tenth of a Nanometer Precision in Etching of SiO_2 Over Silicon: Challenges and Opportunities**, *Gottlieb Oehrlein*, University of Maryland, College Park
INVITED

We discuss use of low pressure plasma surface interaction mechanisms aimed at achieving atomic scale precision in etching materials. Using a steady-state Ar plasma in conjunction with periodic injection of a defined number of C_4F_8 molecules and synchronized plasma-based Ar^+ ion bombardment, we have shown that one tenth of a nanometer precision in etching of SiO_2 is possible.¹ For low energy Ar^+ ion bombardment conditions giving a maximum ion energy of about 20eV, the physical sputter rate of SiO_2 vanishes whereas for an FC-coated SiO_2 surface, chemical modifications of the SiO_2 surface take place and SiO_2 etching is initiated. Precise management of C_4F_8 supply enables control of the deposited fluorocarbon (FC) layer thickness in the 1 to several Ångstrom range. We will discuss the temporal variation of the chemically enhanced etch rate of SiO_2 for Ar^+ ion energies below 30 eV as a function of fluorocarbon surface coverage which enables controlled removal of Ångstrom-thick SiO_2 layers per process cycle. We will also discuss silicon underlayer etch rate measurements and challenges connected with this approach.

¹ D. Metzler, R. Bruce, S. Engelmann, E. A. Joseph, and G. S. Oehrlein, *J Vac Sci Technol A* **32**, 020603 (2014)

* Based on collaborations with D. Metzler, C. Li, S. Engelmann, R. Bruce, E. Joseph, E. Godyak, and M. Kushner. We gratefully acknowledge funding from National Science Foundation (CBET-1134273) and US Department of Energy (DE-SC0001939).

11:00am **PS2+TF-ThM10 Numerical Simulation of Atomic Layer Etch via FPS3D**, *Paul Moroz*, Tokyo Electron US Holdings

Atomic layer etching (ALE) and atomic layer deposition (ALD) are becoming more attractive processing methods primarily due to their higher control of profiles and less induced damage to materials. They require multi-step processing, with each time-step having its own chemistry, incoming fluxes, and energy distribution of species. In this work, we simulated ALE of Si by employing a cycle of two main steps: chlorination of Si surface layer by Cl₂ gas and then removal of the chlorinated layer with Ar neutral beam of low energy and narrow energy spectrum, so the sputtering of Si could be neglected. Feature scale simulator FPS3D [1,2] is well designed for the multi-step operations and allowed us to replicate main results of the corresponding experiments [3]. Each step in ALE processing was self-limiting, and we have used the same conditions and parameters as reported for the experiment. The intermediate gas-purge steps were excluded, as simulations allow instantaneous change of chemistry and fluxes, which is not possible in actual processing. We will demonstrate simulation of ALE processing with clear time resolution of chlorination and removal steps and with etch rate corresponding to experiments.

[1] P. Moroz, *IEEE Transactions of Plasma Science*, 39 (11) 2804 (2011).

[2] P. Moroz, D.J. Moroz, *ECS Transactions*, 50(46) 61 (2013).

[3] J.K. Kim, et al, *J. Vac. Sci. Tech. A* 31, 061310 (2013).

11:20am **PS2+TF-ThM11 Low Damage Etch Residue Removal of CoFeB Material using CO/NH₃ Reactive Ion Beam for STT-MRAM Device**, *MinHwan Jeon, K.C. Yang, D.H. Yun, J.Y. Youn, G. Yeom*, Sungkyunkwan University, Republic of Korea

Spin transfer torque magnetic random access memory (STT-MRAM) is a promising candidate for the next generation memory device due to high density, nonvolatile storage, fast switching speed, etc. comparing to conventional memory devices. For the nano scale STT-MRAM device fabrication, the dry etch process is one of the critical issues due to difficulty in the formation of volatile compounds between MTJ materials such as CoFeB, CoPt, MgO, NiFe and etch gases. The MTJ materials have been etched using conventional reactive ion etching (RIE) system with noncorrosive gases such as CO/NH₃, CH₃OH so as to increase the volatile compounds. However, the relatively low etch selectivity over hard mask material and etch residue still remain on the etched pattern sidewall. In this study, reactive ion beam etching (RIBE) system has been applied to effectively remove the etch residues remaining after the main etch of CoFeB material in the conventional ICP system. The CO/NH₃ gas mixtures was also used for the removal of the etch residues on the sidewall of etched MTJ features. After the optimized RIBE, the etch residue was effectively removed, the surface composition was restored, and the surface roughness of the etched CoFeB thin film after the etching in the RIBE system was decreased indicating the effective removal of redeposited etch residue by the RIBE. The other characteristics of CoFeB substrate after the residue removal by the RIBE were also investigated and will be reported in the presentation.

11:40am **PS2+TF-ThM12 Effects of Cryogenic Cooling on Gallium Nitride Film in Argon Plasma**, *Daisuke Ogawa, Y. Nakano, K. Nakamura*, Chubu University, Japan

We have developed the technique to reduce the damage that is induced by argon plasma to the surface of a gallium nitride (GaN) film. Our technique especially reduces the damage relating to the band gap more than 2.5 eV. Our in-situ monitoring showed that a GaN film cooled with liquid nitrogen (LN₂) has a different pattern of the damage induced by the plasma.

In order to make the in-situ monitoring of the GaN surface, we made real-time measurements with photoluminescence (PL) spectrum emitted from the GaN film. Here, the GaN film was excited with a light illumination generated from a xenon lamp passing through a 313 nm band pass filter. This configuration allows us to monitor the volume-averaged material condition from the surface to ~75 nm depth. M. Chen previously found that the ratio of the blue luminescence (BL) band over the near-band edge (NBE) band is effective to make the in-situ monitoring of the damage induced by plasma.[1] The ratio basically gets larger as the film gets more damages. However, our result showed that the ratio stayed almost constant only when the film was cooled with LN₂. This means that the damage induced by the argon plasma was likely avoided by using LN₂ cooling.

To find the effect of the cooling with LN₂, we made X-ray photoelectron spectroscopy (XPS) measurements for three samples (pristine, LN₂, and no LN₂) after the plasma exposures. We sputtered the film with argon ion beam for 3 minutes in vacuum every cycle of the XPS measurements to obtain the depth profile. The XPS spectrum from the GaN film that was exposed in argon plasma *with LN₂ cooling* was matched well with the spectrum from the pristine GaN film after the first sputtering. On the other hand, the XPS spectrum from the GaN film that was exposed in argon plasma *without LN₂ cooling* showed a chemical shift at the gallium line and a decrease at a nitrogen line. All three spectra matched well after the second sputtering. This profile indicates that the plasma-damaged layer thicker than ~30 nm was formed in the case of no LN₂ cooling. (Assumed the sputtering rate at 5 nm/min.)

Our in-situ temperature monitoring on the GaN surface that was exposed in the argon plasma showed that the temperature stayed below 150 °C with LN₂ while the temperature exceeded over 300 °C without LN₂. This is the indication that we should be able to reduce the damage by controlling the GaN film temperature during the plasma processing.

In this presentation, we will show the evolution of the PL spectrum, connecting with the surface temperature, XPS results supporting with more details.

[1] M. Chen et al., *App. Phys. Lett.* 101, 071105 (2012)

Fundamentals & Biological, Energy and Environmental Applications of Quartz Crystal Microbalance Focus Topic

Room: 317 - Session QC+AS+BI+MN-ThM

Fundamentals and Method Development of QCM

Moderator: Ralf Richter, CIC biomaGUNE & MPI for Intelligent Systems, W.K. Hiebert, University of Alberta and The National Institute for Nanotechnology

8:40am **QC+AS+BI+MN-ThM3 High-Frequency Contact Mechanics Studies with a QCM**, *Diethelm Johannsmann*, Clausthal University of Technology, Germany

INVITED

Studying particulate objects with a QCM is challenging with regard to interpretation, but also of outstanding interest. Potential samples would be (bio-) colloids, vesicles, granular matter, bacteria or technical multi-contact interfaces. The analysis must build on the small-load approximation, which states that the shifts in resonance frequency and resonance bandwidth are proportional to the in-phase and the out-of-phase component of the area-averaged stress at resonator surface. For realistic modeling, a numerical code is needed which predicts this stress field from the geometry and all materials parameters involved. There is such a model in two dimensions, building the finite element method.

On a simpler level, the behavior of particles on a resonator surface can also be understood from the coupled resonance model. The particles in contact form small resonators of their own, where the “particle resonance frequency” is determined by the mass and the stiffness of the contact. If the particle resonance frequency is in the range of frequencies amenable to the QCM one observes a coupled resonance, meaning that the shifts of resonance frequency and resonance bandwidth themselves form a resonance curve when plotted versus overtone order. Depending on whether the particle resonance frequency is higher or lower than the QCM frequency, the frequency shift can be positive or negative. From the particle resonance frequency, one can assess the stiffness of the contact between the particle and the surface.

The detailed investigation of the coupled resonance picture reveals a problem, though. FEM models of the corresponding geometries reveal two coupled resonance, occurring at different frequencies. They correspond to a rotation of the particle about the point of contact (the “rocking mode”) and a rotation about the center of mass (the rotational mode”). The problem complicates the interpretation of experimental data, but it points to an intriguing analogy between QCM experiments a vibrational spectroscopy. A QCM experiment amounts to a vibrational spectroscopy on surface-attached colloids.

The last part of the talk is concerned with a novel sensing dimension of the QCM, which is the dependence of frequency and bandwidth on amplitude. Such dependences are ubiquitous in contact mechanics experiments and can be understood in terms of partial slip. The contacts behave nonlinearly. Nonlinear behavior can also be observed in liquids, where it is caused by the nonlinear term in the Navier-Stokes equation. The nonlinear term drives

a steady flow of liquid along the direction of oscillation towards the center of the plate.

9:20am **QC+AS+BI+MN-ThM5 Study of Water Adsorption and Capillary Bridge Formation for SiO₂ Nanoparticle Layers by Means of a Combined *In Situ* FT-IR Reflection Spectroscopy – QCM-D Set-up**, *Boray Torun, C. Kunze*, University of Paderborn, Germany, *C. Zhang, T.D. Kühne*, Johannes Gutenberg University Mainz, Germany, *G. Grundmeier*, University of Paderborn, Germany

During the past decade nanoparticles attracted a great deal of attention and found many applications in various fields ranging from pigments and antibacterial agents to highly effective catalysts. In this context, the handling and processing of nanoparticle powders play an important role. In contrast to macroscopic particles, nanoparticle flow properties are mainly governed by the particle-particle interactions. The forces determining these interactions strongly vary not only with the material properties but also with surface chemical composition as well as the environmental conditions. Hence, a fundamental understanding of the processes and forces involved plays a key role for the prediction of nanoparticle powder behavior.

In the presented study^[1], water adsorption and capillary bridge formation within a defined layer of SiO₂ nanoparticles was studied by means of a novel *in-situ* analytical setup allowing for combined quartz crystal microbalance with dissipation analysis (QCM-D) and Fourier transformation infrared reflection absorption spectroscopy (FT-IRRAS). On the one hand, the QCM-D gave insights on both, mass change (Δf) and changes in the contact mechanics, indicated by dissipation changes ($\Delta \Gamma$), whereas on the other hand FT-IRRAS allowed for the characterization of the adsorbed water structure. Employing peak deconvolution to the OH-signal in the region of 3400 cm⁻¹, “ice-like” and “liquid-like” water structures could be clearly identified.

Combined measurements show that for a monolayer of monodisperse SiO₂ particles with a diameter of about 250 nm the adsorption of water leads to a linear increase in dissipation for relative humidity (RH) values up to 60%. Subsequently, the strong increase in dissipation between 60% and 80% RH was attributed to the actual liquid bridge formation. This result was supported by the predominant growth of “liquid-like” water during the bridge formation phase indicated by the corresponding FT-IR data. Furthermore, for RH > 90% a decrease in dissipation was detected indicating the merging of capillaries and the onset of a water film formation. Overall, our results indicate that combined *in-situ* QCM-D and FT-IRRAS analysis enables the qualitative and quantitative analysis of water adsorption and capillary bridge formation in particle layers.

[1] Torun, B. et al., *Phys. Chem. Chem. Phys.*, **2014**, 16, 7377-7384

9:40am **QC+AS+BI+MN-ThM6 On the Role of Acoustic Streaming in Particle Detachment Events at a QCM Surface**, *Rebekka König, A. Langhoff, D. Johannsmann*, Clausthal University of Technology, Germany

A steady flow of liquid was observed above the surface of a quartz crystal microbalance (QCM) under conditions, where the oscillation amplitude exceeded 10 nanometers. The streaming flow occurs parallel to the displacement vector and is directed towards the center of the plate. It is expected to have applications in acoustic sensing, in microfluidics, and in micromechanics in a wider sense. The flow is caused by the nonlinear term in the Navier-Stokes equation, which can produce a nonzero time-averaged force from a periodic velocity field. Central to the explanation are the flexural admixtures to the resonator's mode of vibration. Unlike pressure-driven flows, the acoustically driven steady flow attains its maximum velocity at a distance of a few hundred nanometers from the surface. It is therefore efficient in breaking bonds between adsorbed particles and the resonator surface. As a side aspect, the flow pattern amounts to a diagnostic tool, which gives access to the pattern of vibration. In particular, it leads to an estimate of the magnitude of the flexural admixtures to the thickness-shear vibration.

[1] R. König, A. Langhoff, D. Johannsmann, *Physical Review E* **2014**.

11:00am **QC+AS+BI+MN-ThM10 QCM for Particle Sizing and Beyond**, *Adam Olsson, I.R. Quevedo, D. He, M. Basnet, W. Lee, N. Tufenkji*, McGill University, Canada **INVITED**

The dissipative energy loss of a quartz crystal microbalance (QCM) sensor is typically ascribed to the viscoelastic nature of the adsorbed material. While such an interpretation is suitable for thin homogeneous films, it is not *a priori* valid for discrete objects. As demonstrated recently, dissipation due to nanoparticle deposition can be described by the relative movement of the particles attached to the oscillating sensor surface. This particular dissipation behavior of nanoparticles gives rise to new experimental approaches to study colloidal transport, particle-surface interactions and particle properties.

In this presentation, we focus on QCM-D as a method to determine the size of deposited nanoparticles. The approach involves analysis of the change in dissipation per attached mass (i.e., the “ $\Delta D/\Delta f$ -ratio”) to predict a hypothetical full particle surface coverage that can be used to calculate an effective layer thickness of the particulate film; and this quantity, in turn, can be related to the average particle diameter. To validate the approach, we determined particle sizes using various types of nanoparticles with diameters ranging from ~ 5 nm to ~ 110 nm and compared the results with sizes obtained from dynamic light scattering (DLS) and transmission electron microscopy (TEM). We found that accurate particle sizing is possible, but requires firm coupling between the particle and the sensor surface. Hence, if the particle size is known, the approach can also be used to investigate the strength of the nanoparticle-surface interaction.

We will also describe our ongoing work where we are studying the QCM-D response to the deposition of anisotropic bacteriophage to determine their orientation on the surface. Bacteriophages are viruses that bind to and infect bacteria with high specificity and, thus, can be exploited in antimicrobial and biosensor applications. One challenge in functionalizing surfaces with bacteriophages is to control their orientation such that their binding sites remain exposed to the ambient medium. By studying how dissipation changes with phage surface coverage, it is possible to identify at which surface coverage phage-phage interaction occurs. This event compromises the phages ability to bind to bacteria, as evidenced by subsequent bacterial “capture” experiments and imaging, and thus is crucial for the performance of QCM-D based biosensors that utilize bacteriophage as a biorecognition element.

11:40am **QC+AS+BI+MN-ThM12 Full Experimental Proof of the Relationship between the Intrinsic Viscosity of DNA and the Acoustic Ratio of SAW and TSM Sensors**, *Achilleas Tsortos*, IMBB-FORTH, Greece, *G. Papadakis*, NCSR-Demokritos, Greece, *E. Gizeli*, IMBB-FORTH & Univ. of Crete, Greece

Acoustic wave sensors are extensively used in biotechnology and biophysics in order, for example, to detect molecules in a solution, study an antibody-antigen interaction or the hybridization of DNA. Today, data analysis includes (a) the use of the Sauerbrey equation, in order to calculate the mass of the molecules attached on the surface of the acoustic device by use of frequency data and (b) the use of complicated mathematical models of the assumed ‘film’ formed by the attached molecules. In the second case information such as the rigidity modulus and viscosity of the ‘film’ can be calculated and comments can be made on the softness (viscoelasticity) of the added layer.

Here, we present an entirely different approach. Based on a theory developed earlier^{1,2} we correlate the acoustic ratio R , to the intrinsic viscosity $[\eta]$ of the attached molecule. The acoustic ratio is the ratio of the amount of energy loss per attached unit mass – this is given as $(\Delta D/\Delta f)$ in the TSM acoustic mode notification, or as $(\Delta A/\Delta Ph)$ in the SH-SAW mode and is readily obtained in each experiment. The *intrinsic* viscosity on the other hand, is a hydrodynamic quantity directly related to the size and shape of a biomolecule and can be determined independently through viscometry. In this study we present collected experimental data from a variety of case studies proving for the first time the semi-empirically assumed relationship $R \sim [\eta]$ in a general form. Data are presented for various shapes and sizes of DNA and other systems of biological interest. The case is made for two acoustic modes (thickness shear and surface horizontal) and for various frequencies in the range of 5-155 MHz.

Our analysis presents a paradigm shift and challenge; we claim that (label-free) structure probing is a much more improved method offering higher flexibility in design and interpretation of experimental assays. Detecting and monitoring in real time processes that involve structural changes but not necessarily mass changes and/or ‘film’ formation is a novel concept that can be readily applied in anything from DNA, RNA hybridization and detection of mutations to molecular machines (e.g. DNA Holliday junction) and protein/DNA/RNA interactions in the broad areas of biophysics, structural DNA nanotechnology and diagnostics.

Acknowledgement: the REGPOT-InnovCrete/EU-FP7 (Contract No. 316223) for financial support.

References:

1. A. Tsortos, et al., *Biophys. J.* 2008, **94**:2706
2. A. Tsortos, et al., *Biosens. Bioelectron.* 2008, **24**:836

12:00pm **QC+AS+BI+MN-ThM13 Characterization of the Conformation of Linker-Suspended Proteins at Surfaces through Acoustic Ratio Measurements**, *Electra Gizeli*, IMBB-FORTH & Univ. of Crete, Greece, *D. Milioni*, IMBB-FORTH, Greece, *G. Papadakis*, NCSR-Demokritos, Greece, *A. Tsortos*, IMBB-FORTH, Greece

Characterization of protein shape and orientation following surface binding is an area of great interest in biophysics with many applications in

chemistry and nano/biotechnology. Techniques such as ellipsometry and AFM have been extensively used for providing such information. A lot of effort has also been put with acoustic sensors; results in this case though depend greatly on the data interpretation model employed. An important question is always the preservation of protein integrity/form.

In this work we employ acoustic devices based on a QCM geometry at 35 MHz. The acoustic ratio $\Delta D/\Delta F$, i.e., the dissipation over frequency change of the shear wave has been employed in our analysis. We have previously shown¹ that as a tool, this ratio provides valuable information regarding the conformation of surface attached DNA molecules; we have also employed this approach in the design of DNA assays for diagnostic purposes, including detection of sequence targets in real samples².

Here we expand this methodology in proteins; streptavidin is used as a case study for characterizing spherical protein immobilization on an acoustic device. Good control of the binding mode was achieved by changing the distance of the protein from the surface, ranging from zero (direct physisorption) to several nm, using anchor molecules. In this way we can manipulate the degree of surface interference to the protein structure. Our results clearly show that direct protein adsorption is a multistep process resulting in very low acoustic ratio, in agreement with the literature. However, we show for the first time that suspending the protein away from the surface from a single point through a variable-length linker, gives an entirely different picture; the process is a single-step event, as judged from D-F plots, and the resulting acoustic ratio is much higher (order of magnitude) than that obtained in physisorption. The effect of the linker length on the apparent acoustic ratio is analyzed. This approach gives more reliable and different information regarding the protein shape than do simple physisorption protocols and interpretation models involving notions such as 'film' formation etc.

References:

1. A. Tsortos, et al., *Biosens. Bioelectron.* 2008, **24**:836; A. Tsortos et al., *Biophys. J.* 2008, **94**:2706

G. Papadakis et al., *Anal. Chem.* 2012, **84**:1854; G. Papadakis et al., *Scientific Rep.* 2013, **3**:2033

Surface Modification of Materials by Plasmas for Medical Purposes Focus Topic

Room: 315 - Session SM+AS+BI+PS-ThM

Plasma Processing of Antimicrobial Materials and Devices

Moderator: Heather Canavan, University of New Mexico, Morgan Hawker, Colorado State University

8:00am **SM+AS+BI+PS-ThM1 Plasma Polymers: Dogma, Characterisation and Challenges, Sally McArthur**, Swinburne University of Technology, Australia **INVITED**

Plasma polymers, the dogma tells us are densely cross-linked, pinhole free films that adhere to virtually any dry surface. But when you are working at low power and trying to retain specific functional groups within your films, is this still true? How does environment (pH, salt concentration) effect film behaviour and what do responses to change in environment tell us about the nature of these films? This talk will explore methods for studying the physicochemical behaviours of plasma polymer films and discuss how these films can be manipulated address specific biomaterials challenges.

8:40am **SM+AS+BI+PS-ThM3 The Role of Plasma Surface Modification in Antimicrobial Thin Films and Strategies, Renate Foerch**, FhG-ICT-IMM, Germany **INVITED**

"Delivery on demand" has become a key issue in the development of solutions for bacterial infection and the evolution of resistance. Antimicrobial bioactive coatings may be thin layers, scaffolds or hybrid materials with chemically immobilized or physically embedded antimicrobial substances that act while tethered to a surface or that are released either passively or upon a stimulus. Examples include burst release systems of an antimicrobial from plasma polymerised thin films that have fed into a recent efforts aiming to develop, characterize and evaluate nanocomposite coatings consisting of thin films, nanoparticles and nanocarrier systems. The nanocomposite coatings are formulated to respond to specific changes in the surrounding environment. The work to be described is part of a European-Australian effort to investigate new strategies to combat microbial infection; it draws expertise from plasma assisted technologies and wet chemical post plasma attachment of responsive nanocontainers carrying an antimicrobial to treat bacterial infection.

9:20am **SM+AS+BI+PS-ThM5 Plasma Modification of Drug-Eluting Materials for Localized Action at Medical Device Interfaces, J. Joslin, A. Pegalajar-Jurado, M.J. Hawker, E.R. Fisher, Melissa Reynolds**, Colorado State University **INVITED**

To direct protein and cellular behavior at the surface of synthetic materials, both localized chemical signaling and control over surface properties are required. To achieve requisite drug delivery dosages, hydrophobic polymers are often employed that slowly elute a therapeutic agent from the bulk material into systemic circulation. However, the surface free energy of the hydrophobic material can lead to deposition of undesired proteins and activation of the clotting. To overcome these challenges, advanced material platforms are needed to achieve localized therapeutic action and customizable surface properties. Herein, we present the development of H₂O(v) plasma-treated PLGA-nitric oxide (NO) releasing materials. NO is a well-established anti-platelet and anti-microbial agent, and the NO release rate can be controlled by the hydrophobic nature of the bulk material where it was incorporated. Plasma treatment conditions were optimized to maintaining the NO release function while rendering the surface hydrophilicity. Despite the plasma conditions employed, the material retained 80-90% of the S-nitrosothiol content, while the NO release profiles were unaltered compared to the control. The change in the surface wettability was confirmed by water contact angle measurements. Extensive surface (XPS) and bulk (ATR FT-IR) chemical characterization demonstrated that the changes in wettability was due to the implantation of O-containing surface functional groups such as carbonyl and hydroxyl groups. In addition, optical profilometry analysis confirmed no statistically significant changes in the surface roughness compared to the control. Furthermore, the materials show minimal hydrophobic recovery after several days stored at -20°C. By combining both chemical signaling and surface treatments into one material, we expect to reduce activation of clotting cascade and enhance the biocompatibility of the materials.

11:00am **SM+AS+BI+PS-ThM10 Plasma Treated Substrates Reduce Protein Adsorption, Marvin Mecwan, J. Stein, W. Ciridon**, University of Washington, X. Dong, Eli Lilly and Company, B. Ratner, University of Washington

Proteins irreversibly adsorb onto surface, causing losses from solution, denaturation, as well as aggregation. Hence, there have been recent efforts in the pharmaceutical industry to addressing the manufacture, packaging and delivery of protein-based pharmaceuticals. We propose the use of radio-frequency (RF) plasma deposition to create coatings on substrates relevant to the pharmaceutical industry—glass, stainless steel and cyclic olefin polymer (COP). The monomers of choice were acrylic acid (AA) and tetraglyme (TG) (hydrophilic), and perfluoropropylene (C3F6) and perfluoromethyl vinyl ether (C3F6O) (hydrophobic). All monomers were successfully plasma coated on all substrates, and did not delaminate as was determined from survey and detailed ESCA scans. Furthermore, no peaks associated with the substrates were seen in the scans, which indicate that the plasma coating are at least 100Å thick. Protein adsorption studies were carried out using 0.1mg/mL solution of I-125 tagged bovine IgG by adsorbing the tagged protein on the plasma treated substrates for an hour. All hydrophilic monomer plasma treated substrates had lesser protein adsorbed on their surfaces (< 2ng/cm²) as compared to hydrophobic plasma treated substrates (10-14 ng/cm²). This is in comparison to untreated controls that had 200-300 ng/cm² protein adsorbed on the surface. Furthermore, following ISO 10993-5 guidelines, by performing cytotoxic studies using NIH-3T3 fibroblasts all plasma treated substrates were determined to be non-cytotoxic. Hence, these results indicate that radio-frequency plasma treatment could lead to a new generation of surfaces that will be particularly effective for protein manufacture, storage and delivery. Future studies will be aimed at determining plasma coating thickness, protein aggregation assessment as well as studying the bonding strength of the proteins to the plasma treated surfaces.

11:20am **SM+AS+BI+PS-ThM11 Modification of Porous Materials by Low Temperature Plasma Treatment to Achieve Low-Fouling Membranes, Adoracion Pegalajar-Jurado, B.D. Tompkins, E.R. Fisher**, Colorado State University

Artificial porous polymeric membranes are used in many applications including water filtration systems and devices to treat blood for a broad variety of therapeutic purposes. In water filtration systems, membranes are used to remove colloidal particles and organic molecules from the watercourse and, in medical treatments, they function primarily to eliminate toxins from the blood before it is returned to the patient's body. Although these are very different applications, both are affected by membrane fouling from proteins, toxins, bacteria, and cells, which significantly decrease flow through the porous material. Surface modification techniques that retain the desired bulk properties are the ideal method for obtaining low-fouling membranes, thus extending their life-time in applications where they are exposed to fouling conditions. Here, we will present the properties of

polysulfone ultrafiltration membranes subjected to H₂O plasma and their performance when exposed to proteins and bacteria. Plasma treated membranes showed enhanced hydrodynamic characteristics (i.e. increase in water flux) as a result of their high hydrophilicity. Notably, hydrophilic characteristics were retained for more than six months, ensuring top-shelf stability of the surface treatment. In terms of protein fouling performance, treated membranes show less bovine serum albumin adsorption than untreated membranes and cleaning of treated fouled membranes yields 70-90% flux recovery depending on plasma treatment time. This surface modification provides a mechanism for extending the life-time of the membranes.

11:40am **SM+AS+BI+PS-ThM12 Immobilized Laminin Concentration Gradients on Electrospun Fiber Scaffolds for Controlled Neurite Outgrowth**, *Nicole Zander*, US Army Research Laboratory, *T. Beebe Jr.*, University of Delaware

Neuronal process growth is guided by extrinsic environmental cues such as extracellular matrix proteins (ECM). Recent reports have described that the growth cone extension is superior across gradients of the ECM protein laminin compared to growth across uniformly distributed laminin. In this work, we have prepared gradients of laminin on aligned electrospun nanofibers for use as substrates for neuronal growth. The substrates therefore presented both topographical and chemical guidance cues. Step gradients were prepared by the controlled robotic immersion of plasma-treated polycaprolactone fibers reacted with N-hydroxysuccinimide into the protein solution. The gradients were analyzed using x-ray photoelectron spectroscopy and confocal laser scanning microscopy. Gradients with a dynamic range of protein concentrations were successfully generated and neurite outgrowth was evaluated using neuron-like PC12 cells. After 10 days of culture, PC12 neurite lengths varied from $32.7 \pm 14.2 \mu\text{m}$ to $76.3 \pm 9.1 \mu\text{m}$ across the protein concentration gradient. Neurite lengths at the highest concentration end of the gradient were significantly longer than neurite lengths observed for cells cultured on samples with uniform protein coverage. Gradients were prepared both in the fiber direction and transverse to the fiber direction. Neurites preferentially aligned with the fiber direction in both cases indicating that fiber alignment has a more dominant role in controlling neurite orientation, compared to the chemical gradient.

Scanning Probe Microscopy Focus Topic

Room: 312 - Session SP+2D+AS+EM+MC+NS+SS-ThM

Probing Electronic and Transport Properties

Moderator: An-Ping Li, ORNL, Corentin Durand, ORNL

8:00am **SP+2D+AS+EM+MC+NS+SS-ThM1 Investigation of the Electronic and Structural Properties of Metal Free Naphthalocyanine Vapor Deposited on Au(111)**, *Bryan Wiggins*, University of Chicago, *K.W. Hipps*, Washington State University

Naphthalocyanines (Ncs) are promising candidates for future components in electronic devices and applications. To maximize the efficiency of Nc devices, it is critical to understand their structural and electronic properties and how these are impacted by deposition methods. The formation of a metal free naphthalocyanine (H₂Nc) self-assembled monolayer on a Au(111) crystal was investigated by scanning tunneling microscopy under ultra-high-vacuum conditions at room temperature. A rigorous purification and processing procedure was developed to produce high purity, low defect, and well-ordered monolayers. High-resolution STM images reveal epitaxial growth of H₂Nc on Au(111) with the observed structure having a molecular spacing of $1.6 \pm 0.05 \text{ nm}$, with molecules orientated slightly off (roughly 2.5°) the low density packing direction of Au(111). A commensurate structure having 4 molecules per unit cell and unit cell parameters of $A = 3.25 \pm 0.05 \text{ nm}$, $B = 3.17 \pm 0.05 \text{ nm}$, and $\alpha = 87.5 \pm 2^\circ$ is proposed. Orbital-mediated tunneling spectroscopy was used to examine the electronic properties of individual molecules within the thin film. The first ionization potential and electron affinity of H₂Nc adsorbed on Au(111) were measured to be -0.68 ± 0.03 and $1.12 \pm 0.02 \text{ eV}$, relative to the Fermi energy.

8:20am **SP+2D+AS+EM+MC+NS+SS-ThM2 The Fundamentals of Charge Transport at Oxide and Ferroelectric Interfaces**, *Ramsey Kraya*, *L.Y. Kraya*, University of Pennsylvania

Here we investigate how charge transport properties at metal-semiconductor interfaces scale down to the nanoscale regime, comparing the properties to macroscopic interfaces and providing a perspective on what it means to device manufacturing. Strontium titanate - the prototypical oxide material - has been widely studied for applications in thermoelectrics, nanoelectronics, catalysis, and other uses, and behaves as an n-type semiconductor when doped. We investigated how charge transport is effected at interfaces to

strontium titanate under a wide range of conditions - by varying contact size, interface shape, dopant concentration, and surface structure and in various combinations. The results of the analysis have wide ranging implications, especially for ferroelectric oxide materials and serves as the basis for understanding and controlling switching effects - both polarization and oxygen migration based switching.

8:40am **SP+2D+AS+EM+MC+NS+SS-ThM3 Epitaxial Graphene on Nanostructured Silicon Carbide**, *Phillip First*, Georgia Institute of Technology

INVITED

Graphene grown epitaxially on silicon carbide conforms to nanofaceted step edges, even for step heights of many nanometers. The "sidewall" nanoribbons that result show astounding transport characteristics (~15 um ballistic length at room temperature), as demonstrated by others,¹ but the physical basis for these results is still not certain. In our STM measurements of sidewall nanoribbons, we find an extended 1D region with electronic structure much different than 2D graphene. Spectroscopic results on graphene near nanofacet corners indicate a strain gradient and a rapid change in the doping. Such strong gradients may be key to understanding the ballistic transport in this system. P

¹J. Baringhaus, M. Ruan, F. Edler, A. Tejada, M. Sicot, AminaTaleb-Ibrahimi, A.-P. Li, Z. Jiang, E. H. Conrad, C. Berger, C. Tegenkamp and W. A. de Heer, "Exceptional ballistic transport in epitaxial graphene nanoribbons," *Nature*, **506**, 349 (2014).

9:20am **SP+2D+AS+EM+MC+NS+SS-ThM5 Conductivity of Si(111) - 7 × 7: The Role of a Single Atomic Step**, *B. Martins*, University of Alberta and The National Institute for Nanotechnology, Canada, *M. Smeu*, *H. Guo*, McGill University, Canada, *Robert Wolkow*, University of Alberta and The National Institute for Nanotechnology, Canada

The Si(111) - 7 × 7 surface is one of the most interesting semiconductor surfaces because of its

complex reconstruction and fascinating electronic properties. While it is known that the Si - 7 × 7 is

a conducting surface, the exact surface conductivity has eluded consensus for decades as measured

values differ by 7 orders of magnitude. Here we report a combined STM and transport measurement

with ultra-high spatial resolution and minimal interaction with the sample, and quantitatively determine the intrinsic conductivity of the Si - 7 × 7 surface. This is made possible by the capability of

measuring transport properties with or without a single atomic step between the measuring probes:

we found that even a single step can reduce the surface conductivity by two orders of magnitude.

Our first principles quantum transport calculations confirm and lend insight to the experimental

observation.

9:40am **SP+2D+AS+EM+MC+NS+SS-ThM6 Asymmetric Electron Transport Revealed at Monolayer-Bilayer Graphene Junctions by Atomic-Scale Scanning Tunneling Potentiometry**, *K. Clark*, *X. Zhang*, *J. Park*, Oak Ridge National Laboratory, *G. Gu*, University of Tennessee, *G. He*, *R.M. Feenstra*, Carnegie Mellon University, *An-Ping Li*, Oak Ridge National Laboratory

The quest for novel two-dimensional (2D) materials has led to the discovery of hybrid heterostructures of graphene and other 2D atomic films [1]. These heterojunctions provide us fascinating playground for exploring electronic and transport properties in 2D materials. Even in graphene itself, there usually exist large amount of extended topological defects, such as grain boundaries, changes in layer thickness, and substrate steps, which divide graphene into grains and domains. These interfaces and boundaries can break the lattice symmetry and are believed to have a major impact on the electronic properties, especially the transport, in 2D materials.

Here, we present our recent study on an asymmetric electron transport upon bias polarity reversal at individual monolayer-bilayer (ML-BL) boundaries in epitaxial graphene on SiC (0001), revealed by multi-probe scanning tunneling potentiometry [2,3]. A greater voltage drop is observed when the current flows from monolayer to bilayer graphene than in the reverse direction, and the difference remains nearly unchanged when bias exceeds a threshold. A thermovoltage is measured across the boundary due to the thermopower difference between the two sides, which however is too small to account for the observed asymmetry. Interestingly, this asymmetry is not from a typical nonlinear conductance due to electron transmission through an asymmetric potential. Rather, it indicates the opening of an energy gap at the Fermi energy. Our theoretical analysis finds that Friedel charge

oscillation opens a gap for electrons with wave vectors perpendicular to the boundary. The Friedel gaps are different on the monolayer and bilayer sides, which can shift under bias and lead to asymmetric transport upon reversing the bias polarity. A quantitative agreement is seen between experiment and theory on both the sign and the magnitude of the asymmetry.

1 “Heteroepitaxial Growth of Two-Dimensional Hexagonal Boron Nitride Templated by Graphene Edges”, L. Liu, J. Park, D. A. Siegel, K. F. McCarty, K. W. Clark, W. Deng, L. Basile, J.-C. Idrobo, A.-P. Li, G. Gu, *Science* **343**, 163-167 (2014).

2 “Spatially Resolved Mapping of Electrical Conductance around Individual Domain (Grain) Boundaries in Graphene”, K. W. Clark, X.-G. Zhang, I. V. Vlassiounk, G. He, R. M. Feenstra, and A.-P. Li, *ACS Nano*. **7** (9), 7956-7966 (2013).

3 “Friedel Oscillation-Induced Energy Gap Manifested as Transport Asymmetric at Monolayer-Bilayer Graphene Boundaries”, K. W. Clark, X.-G. Zhang, G. Gu, G. He, R. M. Feenstra, and A.-P. Li, *arXiv*: 1401.1796, *Physical Review X* **4** (1), 011021 (2014).

11:00am **SP+2D+AS+EM+MC+NS+SS-ThM10 Defect-mediated Transport in CVD-grown Monolayer MoS₂**, *Corentin Durand, J. Fowlkes*, Oak Ridge National Laboratory, *S. Najmaei, J. Lou*, Rice University, *A.P. Li*, Oak Ridge National Laboratory

Transition metal dichalcogenides like molybdenum disulphide (MoS₂) have attracted great interest as candidate to fill the need of 2 dimensional semiconductor materials. By controlling the thickness, the bandgap of MoS₂ thin films can be tuned from 1.2 eV (bulk material, indirect bandgap) to 1.8 eV (monolayer film, direct bandgap). Recently, researchers succeeded in growing monolayered MoS₂ by chemical vapor deposition (CVD) on silicon dioxide (SiO₂) substrate, showing the possibility of low cost scalable device fabrication. However, the mobility reported on exfoliated MoS₂ monolayers exceeds 200 cm².V⁻¹.s⁻¹, whereas the measurements realized on CVD growth MoS₂ monolayers reveal a mobility value that is usually 1-2 orders of magnitude lower. Here, we study the transport properties of CVD-grown monolayer on SiO₂/Si substrate. We directly measure the resistivity and the mobility of the material with a field-effect transistor architecture by using a cryogenic four-probe scanning tunneling microscope (STM), the Si substrate being used as back-gate. In order to ensure reliable electrical contacts, we fabricate platinum pads (4x4 μm²) on individual MoS₂ crystal domains by using an electron-beam induced deposition technique. The combination of the STM scanners and a scanning electron microscope (SEM) enables us to connect the STM tips on those pads and thereby establish the contacts on this material without any subsequent lithography process, avoiding contaminations introduced by other technological steps. An electron hopping process in localized charge trapping states appears to dominate the transport behavior. We performed temperature-dependent measurements in the range of 82 K to 315 K which demonstrate a variable range hopping (VRH) transport with a very low mobility. Furthermore, the effects of electronic irradiation are examined by exposing the film to electron beam in the SEM in an ultra-high vacuum environment. We found that the irradiation process affect the mobility and also the carrier concentration of the material, with conductance showing a peculiar time-dependent relaxation behavior. It is suggested that the presence of defects such as vacancies and antisites create charge trapping states, leading to the low mobility. This is consistent with recent density functional theory calculations where these defects are shown to create localized gap states that can act as scattering centers and thereby reduce the mobility.

11:20am **SP+2D+AS+EM+MC+NS+SS-ThM11 Coherent One Dimensional Boundaries in Graphene and Hexagonal Boron Nitride Heterostructures**, *Jewook Park*, Oak Ridge National Laboratory, *L. Liu*, The University of Tennessee Knoxville, *D.A. Siegel, K.F. McCarty*, Sandia National Laboratories, *L. Basile, J.-C. Idrobo, K. Clark*, ORNL, *W. Deng*, The Univ. of Tennessee Knoxville, *C.P. Durand*, ORNL, *G. Gu*, The Univ. of Tennessee Knoxville, *A.P. Li*, ORNL

The quest for novel two-dimensional (2D) materials has led to the discovery of hybrid heterostructures where graphene and other atomic layer films such as monolayer hexagonal boron nitride (hBN) form phase-separated domains or both materials grow epitaxially onto a common crystalline substrate. By implementing the concept of epitaxy to 2D space, we developed and applied a new growth technique to hybrid isostructural but electrically dissimilar materials, such as the 2D epitaxial growth of hBN templated by graphene edge [1]. Scanning tunneling microscopy and spectroscopy measurements revealed a single-atomic-layer, in-plane heterostructure between graphene and hBN, as well as an abrupt 1D zigzag oriented boundary. In addition, the dI/dV conductance map unveiled the 1D interfacial states that are extended along, but localized at the boundary. We investigated spatial and energetic distributions of 1D boundary states. Also, low-energy electron microscopy and micro low-energy electron diffraction confirmed the heterostructure at

mesoscopic scale and established that the graphene edge solely determines the crystallography of the hBN regardless of underlying the Cu(100) lattice. The Z-contrast scanning transmission electron microscopy further indicates an atomically sharp interface with a transition width of ~0.5 nm. We suggest that the graphene-hBN epitaxial heterostructure provides an excellent platform to explore heteroepitaxy in 2D space, and the unique functionalities at the 1D interface. [1] Lei Liu *et al. Science* **343** 163 (2014)

11:40am **SP+2D+AS+EM+MC+NS+SS-ThM12 Charge and Spin Density Waves in Quasi One-Dimensional Atomic Wires**, *Herbert Pfnür*, Leibniz Universität, Germany **INVITED**

Although free one-dimensional (1D) objects should exist only at T=0, atomic single wires or arrays embedded into a two- or three-dimensional environment exist even at room temperature and above, since they are stabilized by lateral interactions. These interactions not only stabilize, but also strongly modify the properties of the wires. Their 2D or 3D coupling, however, does not generally prevent observation of 1D properties with their complex variety of instabilities. Furthermore, these coupling can result in special 1D behavior not predicted by standard theories either in 1D or 2D. I will show several examples how atomic wires and wire arrays grown by self-assembly on semiconducting surfaces of Si and Ge acting as insulating substrates can be used to study in detail fundamental aspects of low-dimensional physics, such as charge density waves [1] and Luttinger liquid behavior [2], partially under explicit control of the atomic structure. Due to the low symmetry in these structures, large Rashba-type spin-orbit coupling is expected to lift the spin degeneracy of the metal-induced surface states. In this context new types of spin order were proposed, e.g. for Au/Si(553) [3] and found to be consistent with experiment. As a further example, the Pb/Si(557) system close to monolayer coverage turned out to be an intriguing model system that demonstrates the wealth of phenomena to be expected in quasi-1D physics. Adsorbate induced electronic stabilization leads to (223) refaceting of the (557) surface, to opening of a band gap, to Fermi nesting normal to the steps [4], and to the formation of a charge density wave. Rashba splitting is so large that it causes in-plane anti-ferromagnetic spin polarization along the steps with twice the step periodicity resulting in a combined spin-charge density wave. New superstructures are formed by an excess Pb coverage up to 0.1ML due to ordered step decoration indicating strong electron-electron correlation across steps. This leads to new long range ordered states and formation of a sequence of 1D charge density waves up to a concentration of 1.5 ML, but also, as very recent angular and spin resolved photoemission studies show, to new ordered spin states.

[1] T. Tanikawa *et al.* Phys. Rev. Lett. **93**, 016801 (2004).

[2] C. Blumenstein *et al.* Nat. Phys. **7**, 776 (2011).

[3] S.C. Erwin, F. J. Himpsel, Nature Communications **1**, 58 (2010); J. Aulbach *et al.* Phys. Rev. Lett. **111**, 137203 (2013)

[4] C. Tegenkamp, D. Lükermann, H. Pfnür, B. Slomski, G. Landolt H. Dil, Phys. Rev. Lett. **109**, 266401 (2012).

Surface Science

Room: 309 - Session SS+TF-ThM

Organic Layers on Surfaces

Moderator: Edmund Seebauer, University of Illinois at Urbana Champaign

8:00am **SS+TF-ThM1 Orbital Tomography: Imaging the Wavefunctions of Adsorbed Molecules with Angle Resolved Photoemission**, *Michael Ramsey*, University of Graz **INVITED**

Here it will be shown that the apparently complex angular distribution of valence band photoemission can be simply and quantitatively predicted from a Fourier transform of initial state wavefunctions. This will be demonstrated for a variety of orbitals of the proto-typical pi conjugated molecules pentacene, sexiphenyl and PTEDA on a number of substrate surfaces. For adsorbate monolayers it will be shown how this orbital tomography can be used to determine molecular geometries, unambiguously determine the orbital energy ordering, gain insight into the nature of the surface chemical bond and image the orbitals in real space.

8:40am **SS+TF-ThM3 Chemical Pathways for Surface Functionalization: From Surface-“Stapled” Nanostructures to Layered Materials**, *Andrew Teplyakov*, University of Delaware

One of the important venues in designing novel interfaces and materials is based on the complementary functionalization of surfaces, modified

molecules, and nanostructures, so that combining them would lead to layers and materials with novel chemical and physical properties. This presentation will focus of the molecular-level view of surface functionalization and extending the molecular approach to nanostructures and nanostructured layers with three-dimensional control. Classical organic reactions will be used to first build a nearly perfect layer of chemically functionalized nanoparticles on a flat surface and then the approach will be extended into the third dimension. The work will combine "click chemistry" with chemical functionalization approach and utilize surface analytical techniques including XPS, infrared spectroscopy, microscopic techniques combined with focused ion beam (FIB) sample preparation and will be complemented with the DFT studies. The spectroscopic techniques combined with DFT modeling will support the chemistry of deposition, while the electron microscopy techniques will confirm the growth of layered structures.

9:00am SS+TF-ThM4 Observation and Trapping of Organic Reaction Intermediates for the Reaction of $O(^3P)$ with Oligo(Phenylene Ethynylene) Thiolate Self Assembled Monolayers on Au(111), Wenxin Li, G. Langlois, N.A. Kautz, S.J. Sibener, The University of Chicago

We have taken steps to develop a methodology for observing and trapping organic reaction intermediates by exposing well-ordered self assembled monolayers (SAM) to supersonic beams of atomic oxygen. The use of a SAM stabilizes highly energetic intermediates formed from bimolecular reactions at the interface due to rapid thermal equilibration with the SAM matrix. In this presentation we will discuss the elucidation of the mechanistic details for the fundamental reaction between $O(^3P)$ and alkyne bonds by monitoring chemical and structural changes in an oligo(phenylene ethynylene) SAM reacting with $O(^3P)$ under collision conditions having specified initial reaction orientation. Utilizing time-resolved reflection-absorption infrared spectroscopy (RAIRS) and scanning tunneling microscopy (STM) under ultrahigh vacuum conditions, we have directly observed electrophilic addition of $O(^3P)$ onto the alkyne moieties, resulting in formation of a ketene intermediate via phenyl migration. Under single-collision conditions in the gas phase the vibrationally-excited ketene intermediate cleaves to release CO. In contrast to this, herein we have directly observed the formation of the condensed-phase stabilized singlet ketene by RAIRS. Moreover, we have also observed that the phenyl ring at the vacuum/film interface significantly cants towards the substrate plane as a result of this reaction. STM images of the SAM taken before and after $O(^3P)$ exposure show an expansion of the ordered lattice resulting from formation of the new nonlinear molecular structures within the adsorbed film. This approach of using pre-oriented reactive molecules in ordered self assembled monolayers in combination with angle and velocity selected energetic reagents provides a general approach for probing the geometric constraints associated with the reaction dynamics for a wide range of chemical reactions.

9:40am SS+TF-ThM6 Relative Stability of S-Au and Se-Au Bonding in Aromatic and Aliphatic Self-Assembled Monolayers – Exchange and Ion Desorption Experiments, Jakub Ossowski, A. Noworolska, Jagiellonian University, Poland, S. Schuster, University of Heidelberg, Germany, J. Rysz, Jagiellonian University, Poland, A. Terfort, University of Frankfurt, Germany, M. Zharnikov, University of Heidelberg, Germany, P. Cyganik, Jagiellonian University, Poland

Self-assembled monolayers (SAMs) are considered a model system in many areas on nanotechnology.¹ However, potential use of SAMs strongly depends on stability of their chemical bonding to the substrate. Most of the studies of SAMs have been performed using S-Au bonding.¹ More recently the Se-Au bonding is considered as an interesting alternative. However, as documented by the recent review,² there is still missing information which of these head group provides higher stability binding to the Au(111) substrate and whether or not this relative stability depends on the type of molecular backbone i.e. aliphatic or aromatic. A meaningful comparison of S-Au and Se-Au stability requires that respective molecules not only have the same carbon backbones, but also should form ordered structures with very similar molecular packing. Only under such conditions, not fulfilled by the most of previous studies, the contribution of the molecule-substrate bonding on the film stability can be elucidated. Following this idea, we will present a new data obtained for naphthalene based SAMs bound to the Au(111) substrate via S or Se atoms.³ After presenting detailed microscopic (STM) and spectroscopic (XPS, NEXAFS) characterization of these SAMs, which exhibit very similar well-ordered structure, we will show results of two independent experiments probing the stability of their bond to the Au(111) substrate using an exchange method as well as ion-induced desorption (SIMS). We will compare these results with our previous exchange⁴ and recent ion-desorption experiments⁵ of aliphatic based systems. Irrespective of the type of molecular backbone our results clearly demonstrate much higher stability of the Se-Au bond as compared to the S-Au bond.

References

- [1] C. Love, G. et al. **2005**, *Chem. Rev.*, 105, 1103.
- [2] L. V. Romashov and V. P. Ananikov, **2013**, *Chem. Eur. J.*, 19, 17640.
- [3] J. Ossowski, A. Noworolska, S. Schuster, J. Rysz, A. Terfort, M. Zharnikov, P. Cyganik, **2014**, *in preparation*.
- [4] K. Szelagowska-Kunstman, P. Cyganik, B. Schüpbach, A. Terfort, **2010**, *Chem. Phys. Phys. Chem.*, 12, 4400.
- [5] J. Ossowski, J. Rysz, M. Krawiec, D. Maciazek, Z. Postawa, A. Terfort, P. Cyganik **2014**, *submitted*.

11:00am SS+TF-ThM10 CuPc:C₆₀ Composite Films: From Sub-Monolayer to Multi-Layer Growth, Taylor Stock, J. Nogami, University of Toronto, Canada

CuPc:C₆₀ composite films of various compositions and thicknesses grown on the Cu(111) surface have been studied using room temperature scanning tunneling microscopy (STM) and scanning tunneling spectroscopy (STS). At coverages below two monolayers (ML), phase segregated, ordered films, or well mixed, disordered films can be produced depending on the particular deposition sequence. This compositional variability is achieved by exploiting the differences in the relative strengths of the various molecule-substrate and molecule-molecule interaction forces. In thicker films, the CuPc-C₆₀ intermolecular interaction dominates the growth, and for a range of concentrations these films are found to be well mixed, amorphous and thermally stable. These results provide a rationale for improvements that have been seen for organic light emitting diode (OLED) performance associated with C₆₀ doping of CuPc molecular layers. [1]

- [1] Y. Y. Yuan, S. Han, D. Grozea, and Z. H. Lu, *Appl. Phys. Lett.* **88**, 093503 (2006).

11:20am SS+TF-ThM11 2D Co-Crystallization of Organic Ferroelectrics, Axel Enders, D.A. Kunkel, A. Sinitzki, University of Nebraska-Lincoln, S. Simpson, University at Buffalo-SUNY, J. Hooper, Jagiellonian University, Poland, E. Zurek, University at Buffalo-SUNY

We will present an experimental study on the self-assembly and electronic properties of the organic ferroelectrics, croconic acid (CA), 3-hydroxyphenalenone (3-HPLN), and the related compound rhodizonic acid (RA) on crystalline metal surfaces. Importantly, the bond polarization of the selected organics is highly planar. This provides the foundation for the development of 2D polarization patterns by design, including rather complex ones like the honeycomb pattern recently discovered by our group [1]. What is remarkable about those honeycomb networks of CA, is that the interaction with the substrate is key to ferroelectric switching barriers. Also the structurally related 3-HPLN forms linear chains on surfaces that are expected to exhibit 2D polarization ordering within the plane of the 2D organic layer. The molecular arrangement can be manipulated through the use of the substrate and growth conditions, and we have also identified a new, chiral phase of hydrogen-bonded trimers of 3-HPLN. This surface-science approach was key to the first reported synthesis of RA crystalline structures [2]. Here we present an overview over the structural phases of select organic ferroelectrics on surfaces and how ordered 2D polarization states can emerge. Importantly, we discovered by co-deposition of CA and 3-HPLN that they form ordered 2D co-crystalline phases. The structure of the resulting networks can be tuned by varying the relative concentration of the organics. Namely, for equal ratios of CA and 3-HPLN two polymorphs are observed, while for 2/1 CA/3-HPLN ratio, only a single structure is found. Transitions from CA rich structures to CA poor structures can be induced through weak annealing, in which the smaller CA desorbs before 3-HPLN. We expect that important ferroelectric properties of organic ferroelectrics, such as their ordering temperature and switching fields, can be manipulated through co-crystallization. We will highlight how surface science studies, specifically STM, can help accelerate co-crystal discovery.

References:

- [1] D. A. Kunkel, et al. *Phys. Rev. B* **87**, 041402 (2012).
- [2] D. A. Kunkel, et al. *J. Phys. Chem. Lett.* **4**, 3413 (2013).

11:40am SS+TF-ThM12 Phenol Adsorption on TiO₂(110): Evidence for Temperature Dependent Radical Formation, Matthew Patterson, M.F. DiTusa, C.A. Thibodeaux, Louisiana State University, RW. Hall, Dominican University of California, O. Kizilkaya, R.L. Kurtz, E.D. Poliakov, P.T. Sprunger, Louisiana State University

We have examined the electronic structure of phenol on rutile TiO₂(110) using angle resolved photoelectron spectroscopy (ARPES), electron energy loss spectroscopy (EELS), and density functional calculations on model phenoxy/TiO₂ clusters. Previous electron paramagnetic resonance studies have shown that exposure of titania powder to phenol at 250°C results in the

formation of environmentally persistent free radicals (EPFRs), which have lifetimes on the order of dozens of hours and have been shown to exacerbate negative health effects caused by particulate matter. The proposed chemisorption model of radical formation from aromatic species on metal oxides involves electron transfer from the adsorbed organic to the metal oxide, locally reducing the oxide. Resonant ARPES shows direct evidence of charge transfer from high-temperature adsorbed phenol to electronic states of TiO₂ (110) usually associated with the accumulation of charge at surface oxygen vacancies, providing direct evidence of the hypothesized reduction mechanism. Electronic EELS reveals there is an associated decrease of phenol HOMO-LUMO gap. Electronic structure calculations using model phenoxy-TiO₂ clusters give insight into the changes induced in the occupied molecular orbitals of the chemisorbed phenoxy radical. Results will be discussed in light of other metal oxide systems

12:00pm **SS+TF-ThM13 Adsorption behavior of Zinc Tetraphenylporphyrin Molecules on a Au(111) Surface**, Charles Ruggieri, S. Rangan, R.A. Bartynski, E. Galoppini, Rutgers, the State University of New Jersey

The interaction between Zinc Tetraphenylporphyrin (ZnTPP) molecules and the Au(111) surface is investigated using scanning tunnel microscopy (STM), from initial adsorption sites to monolayer organization, with a particular emphasis on its relation to the surface atomic structure and reorganization. When adsorbed at room temperature, ZnTPP molecules initially decorate step edges at low coverage. As the coverage approaches 0.5 monolayer (ML), ZnTPP molecules self-organize into islands of molecules in a rectangular array that is in registry with the underlying Au(111) lattice. The molecules are oriented with their macrocycles parallel to the surface, and form islands in areas delimited by herringbone reconstruction domain walls. As the coverage approaches one ML, the adsorption geometry of the self-organized molecular layer can be fully characterized with respect to the atomic structure of Au(111) surface atoms. Moreover, ZnTPP adsorption alters the Au(111) herringbone reconstruction domain size, most likely caused by anisotropic adsorbate-induced surface stress. However, when a monolayer is prepared from desorption of a ZnTPP multilayer, a different molecular organization is observed at the surface. It is proposed that this reconstruction is enabled by the particular reconstruction of the Au(111) surface. In this configuration, the domain size of the Au reconstruction is closer to that of clean Au, due to smaller adsorbate-induced surface stress.

Thin Film

Room: 307 - Session TF+PS-ThM

Advanced CVD and Chemical Vapor Infiltration Methods

Moderator: Robert Davis, Brigham Young University

8:00am **TF+PS-ThM1 Industrializing Single Wall Carbon Nanotubes by Water-Assisted CVD**, Don Futaba, AIST, Japan **INVITED**

Since the discovery of the carbon nanotube (CNT) 20 years ago, extensive effort has been made to utilize their exceptional intrinsic properties toward industrial applications. However, availability has significantly thwarted these endeavors. In one section of my presentation, I will describe our efforts toward the economical mass-production of single-walled carbon nanotubes (SWCNT) based on the water-assisted chemical vapor deposition technique, from which highly efficient synthesis of vertically aligned SWCNTs grow from substrates (SWCNT forests). These SWCNT forests form through the self-assembly of individual SWCNTs when grown in sufficient density and have been shown to be useful templates for various applications from energy device electrodes to MEMS materials due both the continuous nature and high porosity. Further, I will describe the forest, and present a few examples of how we have infiltrated these material to create a new material with enhanced properties.

8:40am **TF+PS-ThM3 Organoboranes as Single Precursors for Low Temperature CVD of Boron Carbide Thin Films for Neutron Detectors**, M. Imam, Linköping University, Sweden, C. Höglund, European Spallation Source (ESS AB), J. Birch, Henrik Pedersen, Linköping University, Sweden

The world-wide shortage of the ³He isotope has led to a need for novel designs of neutron detectors. A detector based on the isotope ¹⁰B, in the form of thin films, has been suggested by the European Spallation Source (ESS). The detector design uses ¹⁰B₄C films, ≥1 μm, deposited on both sides of neutron transparent substrates such as Al blades.[1] The melting point of Al (660 °C) sets a strict upper temperature limit for CVD of the ¹⁰B₄C films.

Also, metallic Al will be badly affected by corrosive by-products, like HCl. This means that traditional B₄C CVD routes based on BCl₃ and CH₄ cannot be used. An alternative CVD route is to use organoboranes, i.e. molecules with direct B-C bonds, as such molecules are very reactive and do not produce corrosive by-products.

We have demonstrated the synthesis of thin, X-ray amorphous, boron-carbon films at low temperature (400-600 °C), by thermally activated CVD using triethylboron, B(C₂H₅)₃, (TEB) as single precursor on both single crystalline Si (100) and Al substrates.[2] Films with B/C-ratio of 4.6 with density 2.42 g/cm³ (bulk B₄C density 2.52 g/cm³) and 3.6 with density 2.14 g/cm³ were deposited at 600 °C in hydrogen and argon ambient respectively, the impurity levels in the films was about 4 at.% of H at 600 °C. Further studies of TEB as precursor at higher temperatures (700-1200 °C) on Si substrates show that films with a B/C ratio of 4.5 and 3 were obtained from films deposited at 700 °C in hydrogen and argon ambient respectively with < 0.24 at.% of H. A threshold temperature of 1000 °C for the deposition is identified above which the B content decreases dramatically. Based on our results, a chemical mechanism for boron-carbon films from TEB, where the TEB molecule is decomposed to BH₃ and hydrocarbons, is suggested.

Plasma Enhanced CVD using trimethylboron, B(CH₃)₃, (TMB) is also explored to further lower the deposition temperature. Results from CVD and PECVD will be compared with state of the art PVD of ¹⁰B₄C.

[1] R. Hall-Wilton et al. IEEE NSS/MIC conference record, 4283 (2012)

[2] H. Pedersen et al. *Chem. Vapor Deposition* 18, 221-224 (2012)

9:00am **TF+PS-ThM4 High-Quality ZnO Thin Films Grown by a New CVD Method using Catalytically-generated High-energy Precursors**, T. Nakamura, Y. Ohashi, N. Yamaguchi, E. Nagatomi, T. Kato, Kanji Yasui, Nagaoka University of Technology, Japan

ZnO is useful for many applications, and various growth techniques, including MBE [1-2], PLD [3, 4], and MOCVD [5], have been used to prepare ZnO films. Despite the advantages of MOCVD in industry, ZnO deposition by conventional MOCVD consumes a lot of electric power to react the source gases and raise the substrate temperature. To overcome this, a more efficient means of reacting oxygen and metalorganic source gases is needed.

In this paper, a new CVD method for ZnO film growth using the reaction between dimethylzinc (DMZn) and high-temperature H₂O produced by a catalytic reaction on Pt nanoparticles is presented [6]. H₂ and O₂ gases were admitted into a catalyst cell containing a Pt-dispersed ZrO₂ catalyst, whose temperature increased rapidly to over 1300 K due to the exothermic reaction of H₂ and O₂ on the catalyst. The resulting high-temperature H₂O molecules were ejected from a fine nozzle into the reaction zone and allowed to collide with DMZn ejected from another fine nozzle. ZnO epitaxial films were grown directly on a-plane sapphire substrates at substrate temperatures of 773-873 K with no buffer layer. Growth rates were 0.02-0.13 μm min⁻¹, and film thicknesses were 2-8 μm. X-ray diffraction patterns exhibited intense (0002) and (0004) peaks. The smallest FWHM value of the ω-rocking curve of ZnO(0002) was less than 0.1° (194 arcsec). The Hall mobility and residual carrier concentration of the epilayers were in the ranges 140-197 cm²V⁻¹s⁻¹ and 5.8×10¹⁶-6.0×10¹⁷ cm⁻³ at 300K, respectively. This Hall mobility is very large compared with ZnO films grown directly on sapphire by other deposition methods. PL spectra at 10 K showed a strong emission peak at 3.360 eV, attributed to the neutral donor-bound exciton D⁰_x. The FWHM was as low as 0.9 meV, which is smaller than that previously reported for ZnO obtained by MBE (5.5 meV) [4], and by PLD on a sapphire(0001) substrate (1.7 meV at 2K) [3].

[1] M. Sano et al., *Jpn. J. Appl. Phys.*, **42** (2003) L1050. [2] H. Tampo et al., *Appl. Phys. Lett.*, **84** (2004) 4412. [3] E. M. Kaidashev et al., *Appl. Phys. Lett.*, **82** (2003) 3901. [4] A. Ohtomo et al., *Semicond. Sci. Technol.*, **20** (2005) S1. [5] J. Dai et al., *J. Cryst. Growth*, **290** (2006) 426. [6] K. Yasui et al., *MRS Symp. Proc.*, **1494** (2013) 127

9:20am **TF+PS-ThM5 Filling High Aspect Ratio Features: A Ballistic Transport Model**, Wenjiao Wang, J.R. Abelson, University of Illinois at Urbana-Champaign

The ability to fill a high aspect ratio feature with a thin film material enables the fabrication of many nanoscale devices. Examples include shallow trench isolation or inter-metal dielectric in microelectronics. One approach is to use chemical vapor deposition under conformal coating conditions. However, as film builds up on the sidewalls the width of the feature shrinks and the aspect ratio increases sharply. This often results in incomplete filling, leaving a narrow void or 'seam' of low-density material along the central axis. One solution is to taper the feature into a 'V' shape, such that uniform deposition causes the apex of the V to move smoothly upwards.

To achieve complete filling, the flux of deposition precursor down the axis of the feature must be sufficient to maintain a uniform growth rate. Precursor transport is typically modeled using the diffusion equation under quasi-static conditions. We show that for high aspect ratio features, the diffusion equation significantly under-estimates the flux of material that is deposited deep in the feature. This occurs because the diffusion formalism assumes a mean transport distance between collisions that is proportional to the feature size. However, in molecular flow some of the transport events occur at glancing angles to the feature sidewall and afford very long flight paths. These events move precursor species to the bottom of the feature, an effect that enhances filling.

We have developed a ballistic transport model based on computing the emission/capture probability between all points on the surface and coding the result as a matrix. Species transport from a starting distribution is found by matrix multiplication to afford the distribution of final positions. We first show how the results of this model compare with the diffusion formalism: the bulk of the transport is similar, but the ballistic model predicts a 'tail' of long-range events. We then simulate the filling of V-shaped features as a function of the apex angle and sticking coefficient. The result is a prediction of regimes that can afford complete filling.

Finally, we consider the effect of growth rate saturation under high precursor flux, an effect that is physically significant and vastly improves conformal growth. We derive from the ballistic model the total flux arriving at each position, and self-consistently calculate the effective sticking probability. We simulate the coating profiles on rectangular and V-shaped features and determine that rate-saturated growth conditions, in combination with long-range precursor transport, greatly expand the regime that affords complete filling.

9:40am **TF+PS-ThM6 Ozone Pretreatment's Effect on Infiltration of Carbon Nanotube Forests**, *Richard Vanfleet, L. Barrett, J. Rowley, K. Hinton, R.C. Davis, D.D. Allred*, Brigham Young University

Thin films deposited on carbon nanotubes (CNTs) appear to be enabling materials for a variety of applications including: capacitive and electrochemical energy storage, chromatography and filtration chemical separations media, chemical sensing, and MEMS. Using CNT forests as a substrate creates new challenges to traditional thin film deposition techniques because of the need to penetrate into the forest and the chemical inertness of the CNT surface. We have explored the effect ozone pretreatment has on film morphology in two different deposition regimes: amorphous silicon deposited by low pressure chemical vapor deposition and nickel deposited by electroplating. TEM and SEM images of the forests after deposition show increased nucleation density on forests that were pretreated with ozone.

11:00am **TF+PS-ThM10 A Novel Gap Fill Technology to Address the Current and Future Scaling Challenges of the Semiconductor Industry**, *A. Mallick, Jingmei Liang, B. Underwood, K. Thadani, N. Ingle, T. Mandrekar*, Applied Materials Inc.

Gap fill has been a continuous challenge for the semiconductor industry driving innovation in the field of chemical vapor deposition. Applied Materials has continuously met this challenge by developing and refining CVD technologies to address the challenges of void-free gap fill in features of narrowing opening dimension and increasing aspect ratio. Technologies including Applied's HARP™ sub-atmospheric CVD and Ultima™ high density plasma established themselves as workhorses of the semiconductor industry. These technologies enabled dielectric materials including silicon dioxide, nitrides, carbides, and carbon in narrow gap. While these technologies see continued use in the manufacture of Logic and Memory device at <20nm node and below, gap fill of the narrowest and highest aspect ratio features required a new technical approach. As structure CD drops below 30nm, the sidewall angle approaches or exceeds 90° presenting a shape that promotes void or seam formation with conventional gap fill approaches including CVD and ALD.

To address these challenges Applied Materials has developed a new CVD technology we call FCVD™ to enable synthesis of high quality dielectric films including silicon oxides, silicon nitrides, silicon carbo-nitrides, silicon, low-k dielectrics, and carbon with a mechanism of film growth that promotes void-free fill irrespective of structure dimension and shape; this technology demonstrates capability to fill re-entrant structures with opening size <5nm and aspect ratio >20, flexibility to address multiple material systems and has been productized to address volume manufacturing requirements. In this paper we will demonstrate that we can achieve a void-free, profile-insensitive gap fill with multiple materials in a CVD reactor.

11:20am **TF+PS-ThM11 Comparison of Carbonaceous Thin Films Deposited on Ru-capped Multilayer Mirrors via Extreme-Ultraviolet Light and Electrons**, *Michael Barclay*, Johns Hopkins University, *N.S. Faradzhev, S.B. Hill, T.B. Lucatorto*, National Institute of Standards and Technology (NIST), *D.H. Fairbrother*, Johns Hopkins University

This presentation focuses on comparing growth characteristics of carbonaceous thin films produced by irradiation of Ru-capped multilayer surfaces with either extreme-ultraviolet light or electrons in the presence of hydrocarbon vapors. This work is motivated by the likelihood that extreme-ultraviolet lithography (EUVL) will be the next step in improving chip production for the semiconductor industry. Using a shorter (13.5 nm) wavelength of light, manufacturers can mass-produce microchips with feature sizes (< 10nm) that are impossible to achieve with current lithographic techniques. Since all materials strongly absorb 13.5 nm light, EUVL must be carried out under vacuum. Ultimately, this makes certain that the delicate multilayer optics and chemical photoresists, used in the EUVL process, cannot be completely isolated from one another. As a corollary, volatile organics released from resist-outgassing have the ability to be deposited via EUV- induced reactions, resulting in degradation of the multilayer optics. To protect the delicate optics, industry has established a resist-outgas testing protocol to determine the outgas-contamination risk of each resist before introducing it to the EUVL tool. This qualification procedure determines a resist's rate of contamination as well as the cleanliness of its outgas products. Unfortunately, a key component of this protocol is the use of a dedicated, bright, EUV source. To mitigate the large capital investment necessary for such a source, electron beams are often used as a proxy. It is therefore important to correlate the carbon deposition processes induced by electron and EUV irradiation. To this end, we have exposed Ru-capped multilayer optics to both electron and EUV irradiation in the presence of admitted hydrocarbon vapors of two model species: benzene and tetradecane. Multiple exposures were performed with varying doses of EUV and electron irradiation for various hydrocarbon partial pressures; then subsequently characterized using scanning X-Ray Photoelectron Spectroscopy and small-spot spectroscopic ellipsometry. Electron exposures utilized the electron beam from a Perkin-Elmer 10-155 Cylindrical-Auger Electron Optics System; calibrated and characterized using a ThorLabs DCC1645c camera in conjunction with a Ce:YAG scintillator. EUV exposures utilized the Synchrotron Ultraviolet Radiation Facility at NIST. We find that the carbon growth rates for both exposure methods have sub-linear pressure dependence at low irradiance which transitions to linear scaling at higher irradiance. The growth rates at which this transition occurs, however, are different for EUV and e-beam irradiation.

11:40am **TF+PS-ThM12 Production and Characterization of Thin Film Group IIIB, IVB and Rare Earth Hydrides by Reactive Evaporation**, *James Provo*, J.L. Provo Consulting

A recent short history of reactive evaporation by Mattox (1) described various methods for producing oxides, nitrides, carbides, and some compound materials using this special process. However, no mention was made producing hydrides using this method. A study was performed in the mid 1970's at the General Electric Company (GE) Neutron Devices Department (GEND) in Largo, FL, by the author to study preparation of thin film hydrides using reactive evaporation and to determine their unique characteristics and properties.

Films were produced of scandium (Sc), yttrium (Y), titanium (Ti), zirconium (Zr), and the rare earth praseodymium (Pr), neodymium (Nd), gadolinium (Gd), dysprosium (Dy) and erbium (Er) hydrides by hot crucible filament evaporation in atmospheres of deuterium and tritium gas. All metal vacuum systems were used and dedicated for this special processing. Thin film test samples ~ 5,000Å thick were prepared on half-inch diameter molybdenum disk substrates for each occluder material.

Loading characteristics (i.e., gas to-metal atomic ratios), oxidation characteristics, film structure, and stress properties were determined and showed near maximum gas-to-metal atomic ratios, variable oxidation properties, platelet type film structures and minimum film stress levels as determined by a double resonator technique. Also, stress aging characteristics were determined for some hydride films prepared in a radioactive tritium gas atmosphere.

The timeless data obtained showed gas-to-metal atomic ratios varied from 1.8 to 2.0, surface oxide levels varied from ~ 80Å to over 1,000Å, and initial normalized differential (tensile) stress levels were (1.0 to 4.0) x 10⁸ dyne/cm² for tritium loaded samples and (1.0 to 2.0) x 10⁹ dyne/cm² for deuterium loaded samples. Tritium loading, however, had the undesirable characteristic of having to dispose of the internal processing system fixtures, but the method generally produced desirable thin films.

† Formerly, Principal Member of the Technical Staff at Sandia National Laboratories,

Albuquerque, NM (Retired).

(1) Mattox, D.M., "History Corner- A Short History of Reactive Evaporation", SVC Bulletin, p.50 – 51, Spring 2014.

12:00pm **TF+PS-ThM13 Cathodic Cage Plasma Deposition of TiN and TiO₂ Thin Films on Silicon Substrate**, *R.R.M. de Sousa*, IFPI, Brazil, *P.S. Sato*, UFSCar, Brazil, *B.C. Viana*, UFPI, Brazil, *C. Alves Jr*, UFRSA, Brazil, *A. Nishimoto*, Kansai University, Japan, *Pedro Nascente*, UFSCar, Brazil

A new technique called cathodic cage plasma deposition (CCPD) was used for growing TiN and TiO₂ films on silicon substrate. In this technique, the samples are positioned inside a cage having uniformly distributed round holes with fixed diameter, and onto an alumina insulator disk, so that the plasma acts on the cage and not on the sample surface, eliminating possible defects usually formed during the conventional plasma deposition. The CCPD technique produces films with high uniformity and permits a good control of roughness and crystallinity. The main advantages of this technique are the uniformity, tri-dimensionality, and high rate of deposition of the deposited films, as well as low cost of production.

TiN coatings increase the surface hardness and decrease the friction coefficient, thus enhancing the lifetime of components and tools employed in the metalworking industries. Thin films of TiO₂ have attracted considerable attention because of different applications on many fields due to their unique properties, such as chemical stability, no toxicity, low cost, high refraction index, high permittivity, wide valence band, etc. The TiO₂ main crystalline phases are: anatase, brookite, and rutile. The TiO₂ thin films can have a mixture of these phases showing hybrid properties. Many studies have focused on relationship of the different phases as dependent of the deposition method and parameters. Each one of these phases has its own characteristic properties, leading to different applications.

In this work, the influence of the parameters (temperature and gas atmosphere) in the characteristics of the deposited films was investigated. The TiN and TiO₂ thin films were characterized by X-ray diffraction (XRD), scanning electron microscopy (SEM), and Raman spectroscopy in order to identify their crystalline phases and estimate their thicknesses. The combination of XRD and Raman spectroscopy results indicates that only a TiN crystalline phase was detected for the TiN films, and mainly the anatase phase was detected for the TiO₂ film. High crystallinity and uniformity of the films were observed by XRD, Raman, and SEM, confirming that this low cost technique is effective in producing high quality TiN and TiO₂ films.

Tribology Focus Topic

Room: 303 - Session TR+NS-ThM

Bridging Scales in Tribology

Moderator: J. David Schall, Oakland University

8:00am **TR+NS-ThM1 Temporal and Spatial Multiscale Simulations of Low-Velocity Frictional Sliding**, *Woo-Kyun Kim*, University of Cincinnati **INVITED**

As the size of mechanical systems of technological interest such as micro electro-mechanical systems (MEMS) decreases, the need to develop experimental and theoretical tools to investigate micro/nanometer scale phenomena has been growing rapidly. Since its invention in 1986, the Atomic Force Microscope (AFM) has been a primary tool to study the atomic-scale friction and wear and atomistic simulation methods such as molecular dynamics (MD) have also been widely used because these simulations can provide direct access to atomic-scale mechanisms which cannot be observed experimentally. However, there is a great disparity in length and time scales between the simulated systems and the real experimental systems. One of the significant artifacts of these scale differences is that systems are loaded at by several orders of magnitudes larger rates in simulations than in experiments, which may completely distort the underlying mechanisms. Recently, a novel multiscale method, called hyper-QC, which can span both length and time scales simultaneously has been developed. Hyper-QC combines quasicontinuum (QC), a spatial multiscale method, and hyperdynamics, an accelerated MD scheme, in a single platform. In this talk, the hyper-QC simulation results of AFM experiments will be presented. Hyper-QC enables the reduction in the sliding rate by two or three orders of magnitudes from that of the conventional MD scheme as well as the reduced effective number of atoms that is achieved through the QC coarse-graining.

8:40am **TR+NS-ThM3 Crystal-Amorphous and Amorphous-Amorphous Transitions in Carbon under Tribological Load**, *Lars Pastewka*, Karlsruhe Institute of Technology, Institute for Applied Materials IAM, Germany **INVITED**

Diamond and amorphous carbon (aC) are prototypical examples of wear resistant materials. Yet, these materials wear down, but little is known about the atomic scale processes that cause wear. Molecular dynamics is ideally suited to gain a deeper understanding of the underlying wear processes [1]. Such atomic-scale simulations reveal that both, mechanical and oxidative wear actions are active. Mechanical action transforms the material to a weaker state that is then easily oxidized. For diamond, we find a transition to an aC, while we find a high-density—low-density aC-aC transition for amorphous thin films. The velocity of the diamond/aC interface depends crucially on the diamond surface orientation with the highest speed found for (110) surfaces that are rubbed in the (001) direction, while the lowest interface speed was observed for the diamond (111) surface. High-density aC itself transforms even faster to a low density state than succumbs to wear [2]. We relate the aC-aC transition to shear-banding in plasticity of amorphous materials, and argue that the formation of shear-bands is crucial for the wear resistance of carbon based hard coating. These findings are in perfect agreement with a 600 years old experimental knowledge of diamond polishers, and with recent experiments comparing wear in diamond and amorphous carbon thin films.

[1] L. Pastewka, S. Moser, P. Gumbsch, M. Moseler, Nat. Mater. 10, 34 (2011)

[2] T. Kunze, M. Posselt, S. Gemming, G. Seifert, A.R. Konicek, R.W. Carpick, L. Pastewka, M. Moseler, Tribol. Lett. 53, 119 (2014)

9:20am **TR+NS-ThM5 A Molecular Dynamics Investigation of the Atomic-Scale Wear of Carbon-Based Materials Upon Repetitive Contact**, *Kathleen Ryan*, United States Naval Academy, *V. Vahdat*, University of Pennsylvania, *P.L. Keating*, United States Naval Academy, *Y. Jiang*, *K.T. Turner*, *R.W. Carpick*, University of Pennsylvania, *J.A. Harrison*, United States Naval Academy

Amplitude modulation atomic force microscopy (AM-AFM) involves hundreds of thousands of contacts between a tip and surface per second. Each contact can result in the formation and breakage of chemical bonds causing wear to the tip. Atomic-scale wear hinders the quality and reproducibility of structures created by tip-based nanomanufacturing processes. However, wear cannot be analyzed at the single-atom level using existing experimental methods. Continuum mechanics models can be used to estimate stresses, deformations, and the work of adhesion. However, these models can break down at the nanoscale as they rely upon assumptions about the tip shape and material properties, and ignore the discrete atomic structure of the materials. Molecular dynamics (MD) simulations allow the nanoscale behavior to be modeled by resolving the positions, velocities, and forces of all atoms in the system. Here, MD simulations are used to model the repeated contact of an axisymmetric, hydrogenated amorphous carbon (a-C:H) tip with a 3-dimensional ultrananocrystalline (3D UNCD) surface. Using a finite element method to select the smallest portion of the tip that should be modeled atomistically, the tip radius could be set at 15 nm, much larger than previous simulations of this type and in the range of experimental AFM tip sizes. Tip/surface material and tip shapes were also chosen to closely mimic those used in comparable experiments. The wear processes, including adhesive forces, material transfer, and changes to material hybridization are examined following multiple contact cycles. We observe discrete atomic bonding and transfer events, as opposed to plastic deformation or fracture of multi-atom clusters. This is consistent with interpretations of experimental wear behavior and adds significant new detail to the possible pathways for the wear process.

9:40am **TR+NS-ThM6 The Buried Interface: In Situ Methods for Tribology**, *Brandon Crick*, Lehigh University, *K.G. Rowe*, *A.I. Bennett*, *D.W. Hahn*, *W.G. Sawyer*, University of Florida

Tribological phenomena occur at interfaces which are often difficult to directly observe or access. *In situ* techniques are rapidly emerging to probe surfaces buried at an interface, illuminating the physical, mechanical and chemical interactions between two surfaces in intimate contact. In this presentation, we discuss several *in situ* techniques, including optical microscopy of the real area of contact, thermal imaging of contact temperature, and Surface Plasmon Resonance of molecular transfer of a solid lubricant during sliding.

Utilizing an optical *in situ* microtribometer, we can explore the real area of contact and near contact surface topography of contacting surfaces; this technique has been used to visualize adhesive-elastic contact between a rigid sphere and a thin elastic foundation as well as randomly rough elastomer surface in contact with an infinitely stiff and flat (by comparison) surface. Similarly, an forward looking infrared (FLIR) microscope camera

can reveal interface temperatures with microscopic resolutions. Finally, an *in situ* Surface Plasmon Resonance (SPR) tribometer is used to measure molecular-scale transfer of solid lubricants during sliding. For some systems, such as PTFE, transfer is detected as early as the first cycle of sliding, while minimal transfer is observed in other systems such as UHMWPE.

11:00am **TR+NS-ThM10 Contact and Friction Between Rough Adhesive Surfaces: From Atomic to Micrometer Scales, Mark Robbins,** Johns Hopkins University, *L. Pastewka*, Fraunhofer Institute for Mechanics of Materials IWM, Germany **INVITED**

Experimental surfaces typically have roughness on a wide range of length scales. This roughness greatly reduces the fraction of the area that is in intimate molecular contact and thus can contribute to friction and adhesion. The talk will first describe recent numerical calculations of elastic contact between rough surfaces with nominally flat or spherical geometries on large scales. An efficient Greens function approach allows calculations for systems with roughness on nanometer to micrometer scales to be performed with atomic resolution in the contact. Results for a wide range of geometries can be collapsed using simple scaling relations that depend on the root mean squared surface slope, sphere radius, elastic modulus, and work of adhesion. The scaling relations explain why adhesive interactions have little effect unless the surfaces are extremely smooth or soft. The traditional Fuller-Tabor model for adhesion of rough surfaces is shown to be qualitatively inconsistent with the simulations. The effect of atomic scale plasticity on contact and adhesion is surprisingly small. The talk will conclude by considering how forces in the contact area give rise to friction at larger scales.

11:40am **TR+NS-ThM12 Scaling Properties of Measured Frictional Parameters in Microscale Contacts, Brian P. Borovsky,** St. Olaf College

We present a study of the frictional properties of microscopic contacts (radius $\sim 1 \mu\text{m}$) in the high-speed regime ($> 1 \text{ m/s}$) during the initiation of full slip. Energy dissipation, lateral contact stiffness, and amplitude of motion are measured for a transverse-shear quartz resonator in contact with a small spherical probe. Averaged values for the elastic and dissipative forces are derived as functions of shearing amplitude, at constant normal loads in the range from $10 \mu\text{N}$ to 8 mN . We observe a transition from partial to full slip at a threshold amplitude of motion, characterized by a maximum elastic force. Kinetic friction in the full-slip regime is observed to be about a factor of two smaller than this elastic force limit. Data from tests at various normal loads can be collapsed onto common curves by normalizing the forces and amplitudes according their characteristic values. We discuss the observed scaling of these frictional parameters with the size of the contact and the extent of agreement with current theories of microslip.

12:00pm **TR+NS-ThM13 Scale Effects in Single-Asperity Friction, Tristan Sharp,** Johns Hopkins University, *L. Pastewka*, Fraunhofer Institute for Mechanics of Materials IWM, Germany, *M.O. Robbins*, Johns Hopkins University

Simulations are used to examine the static friction in model single-asperity contacts between a rigid sphere and a flat elastic substrate. The sphere radius R and the contact radius a are varied from nanometers to micrometers. First the case of commensurate contact between identical aligned surfaces with repulsive interactions is considered. For small contacts all contacting atoms move coherently and the friction coefficient μ is independent of contact radius and load. In larger contacts, interfacial slip is mediated by localized dislocations. At first μ decreases with increasing contact radius: $\mu \sim (Ra_0)^{1/2}/a$, where a_0 is the nearest-neighbor spacing. At even larger contact sizes, μ begins to drop more slowly. The results are in sharp contrast to Cattaneo-Mindlin continuum theory where μ is independent of contact size. Separate simulations are performed to connect the results to the dislocation-based models of contact-size effects due to Hurtado and Kim, and Gao, which assume adhesive interactions between surfaces and find $\mu \sim (a_0/a)^{1/2}$. The talk will conclude with discussions of the effect of changes in the relative alignment of crystalline axes.

Thursday Afternoon, November 13, 2014

2D Materials Focus Topic

Room: 310 - Session 2D+EM+MI+MN+NS+SS+TF-ThA

Novel Quantum Phenomena in 2D Materials

Moderator: Alexander Sinitskii, University of Nebraska-Lincoln

2:20pm **2D+EM+MI+MN+NS+SS+TF-ThA1 Optoelectronics of Two-Dimensional Semiconductors, Xiaodong Xu**, University of Washington
INVITED

Two dimensional transition metal dichalcogenides are a recent addition to the 2D electronic materials family. They have shown outstanding electrical and optical properties for new optoelectronic device concepts. In this talk, we will first discuss the unique interplay between spin, valley, and layer pseudospins in bilayer WSe_2 . Such coupling effects lead to electrical control of spin states and optical generation of valley coherence through interlayer triions, where electrons and holes are localized in different layers. We will then talk about optoelectronic devices based on monolayer WSe_2 , including p-n junctions as light emitting diodes and hybrid monolayer semiconductor/photonic crystal cavity devices. We will conclude the talk with a discussion of the optoelectronic properties of MoSe_2 - WSe_2 heterostructures.

3:00pm **2D+EM+MI+MN+NS+SS+TF-ThA3 Theory of Graphene Transport Barriers in the Specular Limit, Daniel Gunlycke, C.T. White**, Naval Research Laboratory

Offering room-temperature ballistic electron transport well over one micron, while being atomically thin and planar, graphene is undeniably a promising material for future nanoelectronic devices. Presently, however, switchable devices have normally low on-off ratios, a reflection of the challenge of selectively blocking electron and hole carriers from propagating across the graphene surface. This has stimulated a lot of research on different methods for making graphene nanoribbons that exhibit suitable band gaps. An alternative way to obtain a controllable gap takes advantage of resonant tunneling across a pair of transport barriers. For the latter approach, the key is to find a barrier that is fairly reflective but not so much as to effectively cut off all transport across it.

In this presentation, we present a model for straight transport barriers in graphene in the specular limit. Using the Lippmann-Schwinger equation, we obtain the wave function, from which we derive the reflection and transmission probabilities, as well as the local density of itinerant states. This local density of states exhibits fluctuations arising from quantum interference between incoming and outgoing matter waves that allow the transport properties of a barrier to be estimated without explicitly probing the current across the barrier. Our model is tested against exact multi-channel, tight-binding quantum transport calculations for graphene with weak local potentials, local strain, local adsorption, and a locally defective structure. As the model parameters are related to observable quantities, they could be obtained from theory and/or experiment, allowing the model to be adopted even when the precise details of the barrier are unknown.

3:20pm **2D+EM+MI+MN+NS+SS+TF-ThA4 Tip-induced Potential Confinement on Graphene in Scanning Tunneling Microscopy Measurement, Yue Zhao, J. Chae, J.E. Wyrick, NIST/CNST, F.D. Natterer, Ecole Polytechnique Fédérale de Lausanne (EPFL), France, S. Jung, Korea Research Institute of Standards and Science (KRISS), A.F. Young, C.R. Dean, L. Wang, Y. Gao, Columbia University, J.N. Rodrigues, Graphene Research Centre, NUS, Singapore, K. Watanabe, T. Taniguchi, National Institute for Materials Science (NIMS), Japan, S. Adam, Graphene Research Centre, NUS, Singapore, J.C. Hone, K. Shepard, P. Kim, Columbia University, N.B. Zhitenev, J.A. Stroscio, NIST/CNST**

Graphene is a two-dimensional-electron-gas(2DEG) system with exposed surface, which allows scanning tunneling microscopy (STM) to investigate the electron-electron interaction associated with the Dirac nature on a local scale, with a variety of tuning knobs, such as carrier density, spatially varying disorder potential, and applied magnetic field. However, the electron-electron interaction in graphene is sensitive to the disorder details. Moreover, tip induced potential confinement can significantly complicate the interpretation of STM experiment. Utilizing a high mobility graphene device with low residual disorder, we can minimize the effect of local potential fluctuation, to better understand the role tip-induced potential plays in the measurement. We observed the emergency of large spectra gaps, modification to graphene Landau levels (LLs), and quantum dots with changing size due to the spatially inhomogeneous tip gating.

4:00pm **2D+EM+MI+MN+NS+SS+TF-ThA6 Topological Phase Transitions and Spin-orbit Density Waves, Hugo Dil, Ecole Polytechnique Fédérale de Lausanne (EPFL), Switzerland**
INVITED

In recent years systems where the spin-orbit interaction (SOI) is not just a perturbation but the main energy scale have received increasing attention. In combination with a broken inversion symmetry in the crystal structure or at interfaces, SOI will lift the spin degeneracy and induce a complex Fermi surfaces and spin textures with spin momentum locking [1,2]. Furthermore, the SOI can drive the system through a phase transition to a so-called topological insulator. Being an insulator in the bulk these systems are characterized by spin-polarized, topologically protected interface states.

After a short introduction to the role of topology in the band structure of solids I will give an overview of our main spin- and angle-resolved photoemission (SARPES) results on a variety of non-interacting topological insulators [3]. One of the questions is how the spin texture evolves around a topological transition. We explored the occurrence of spin polarized states around a SOI driven topological transition [4] and around a structure driven topological transition [5]. In both cases we observe spin-polarized precursor states, which indicate that although the topological transition is sharp, the response of the system is more gradual.

From a fundamental point of view the truly interesting aspect of non-trivial spin textures lies in their combination with other interactions. This can result in a variety of phenomena, cumulating in the creation of the elusive Majorana Fermion. An example of a combination of interactions is our recent verification with SARPES of Sb_2Te_3 as a topological Kondo insulator [6]. In topologically trivial systems, interactions can lead to the formation of a so-called spin-orbit density wave. I will show how the combination of a large spin-splitting and Fermi nesting leads to the formation of such a state and can explain the anisotropic behavior of Pb nanowires [7]. Furthermore, I will present our recent SARPES results for transition metal oxide surfaces where a subtle interplay between ferroelectricity and magnetic order results in the formation of a single spin-polarized energy contour. The occurrence of superconductivity in such systems could render it a 2D Majorana platform.

[1] J.H. Dil, J. Phys: Cond. Mat. 21, 403001 (2009)

[2] G. Landolt et al. Phys. Rev. Lett. 109, 116403 (2012)

[3] D. Hsieh et al. Science 323, 919 (2009); D. Hsieh et al. Nature 460, 1101 (2009); S.Y. Xu et al. Science 332, 560 (2011); S. Ereemeev et al. Nature Comm. 3, 635 (2012)

[4] S.Y. Xu et al. arXiv:1204.6518

[5] G. Landolt et al. Phys. Rev. Lett. 112, 057601 (2014)

[6] N. Xu et al. Nature Materials (2014)

[7] C. Tegenkamp et al. Phys. Rev. Lett. 109, 266401 (2012)

4:40pm **2D+EM+MI+MN+NS+SS+TF-ThA8 The Symmetry Dependent Band Structure of MoS_2 , Duy Le, University of Central Florida, T. Komesu, University of Nebraska-Lincoln, Q. Ma, University of California, Riverside, E.F. Schwier, H. Iwasawa, Hiroshima University, Japan, M. Shimada, Higashi-Hiroshima, Japan, T.S. Rahman, University of Central Florida, L. Bartles, University of California, Riverside, P.A. Dowben, University of Nebraska-Lincoln**

We will present results of density functional theory (DFT) based calculations of symmetry dependent band structures of single crystal $\text{MoS}_2(0001)$ surface together with symmetry-polarized angle resolved photoemission spectroscopy (ARPES) derived experimental band structure. The good agreement of the DFT band structure with the experimentally derived bands with even and odd symmetries, attests to the reliability of the results. We performed ARPES at the Hiroshima Synchrotron, determining the MoS_2 band structure separately for both p- and s-, polarized to distinguish even and odd symmetry, and the experimentally determined dispersion, in accordance with expectations and experimental confirmation of C_{3v} symmetry, argues in favor of an experimental band structure obtained from single domains. The comparison of theory and experiment provides strong indications that the bands at the top of the valence band are dominated by Mo 4d states. These states and indeed placement of the valence band can be perturbed by adsorbates. Indeed, we find that, under the effect of Na adsorption, the changing placement of the valence band structure of MoS_2 clearly indicate the Na atoms donate electrons to MoS_2 and that the Fermi energy level shifts as much as 0.5 eV with respect to the top of MoS_2 's valence band. Surprisingly, Na adsorption does not perturb the MoS_2 band dispersion significantly. We will discuss these results in the light of those obtained for single layer MoS_2 for insights and clarity.

5:00pm **2D+EM+MI+MN+NS+SS+TF-ThA9** **CuIn₁₁₁P₂S₆ - Room Temperature Layered Ferroelectric**, *Alex Belianinov, P. Maksymovych, Oak Ridge National Laboratory, A. Dziugys, Vilnius University, Lithuania, Q. He, Oak Ridge National Laboratory, E. Eliseev, National Academy of Sciences of Ukraine, A. Borisevich, Oak Ridge National Laboratory, A. Morozovska, NAS of Ukraine, J. Banys, Vilnius University, Lithuania, Y. Vyschanskii, Uzhgorod University, Ukraine, S.V. Kalinin, Oak Ridge National Laboratory*

We have utilized ambient and Ultra High Vacuum Scanning Probe Microscopy tools to explore ferroelectric properties in cleaved 2D flakes of copper indium thiophosphate, CuIn₁₁₁P₂S₆ (CITP), and report on size effect and presently achievable limits of ferroelectric phase stability. CITP is an unusual example of a layered, anti-collinear, uncompensated, two-sublattice ferroelectric system. These are the only materials known to display “2-D” ferroelectric semiconductor behavior in a van-der-Waals crystal. The material exhibits a first-order phase transition of order–disorder type from the paraelectric to the ferroelectric phase at T_c = 315 K. Our observations suggest the presence of stable ferroelectric polarization as evidenced by domain structures, rewritable polarization, and hysteresis loops. These observations suggest that flakes above 100 nm have bulk-like polarization and domain structures, whereas below 50 nm polarization disappears. Furthermore, the materials have measurable ionic mobility, as evidenced both by macroscopic measurements and by formation of surface damage above tip bias of 4 V, likely due to copper reduction. We ascribe this behavior to well-known instability of polarization due to depolarization field, along with internal screening by mobile Cu ions, as suggested by their high ionic mobility.

Acknowledgement:

Research for (AB, PM, QH, AB, SVK) was supported by the US Department of Energy, Basic Energy Sciences, Materials Sciences and Engineering Division. Research was conducted at the Center for Nanophase Materials Sciences, which is sponsored at Oak Ridge National Laboratory by the Scientific User Facilities Division, Office of Basic Energy Sciences, US Department of Energy.

5:20pm **2D+EM+MI+MN+NS+SS+TF-ThA10** **Doping Efficiency and Mechanisms of Single and Randomly Stacked Bilayer Graphene by Iodine Adsorption**, *Hokwon Kim, A. Tyurnina, Univ. Grenoble Alpes/CEA, LETI, France, J.-F. Guillet, J.-P. Simonato, J. Dijon, Univ. Grenoble Alpes/CEA, LITEN, France, D. Rouchon, D. Mariolle, N. Chevalier, O.J. Renault, Univ. Grenoble Alpes/CEA, LETI, France*

The precise control of graphene's conductivity and work function is crucial in developing practical applications of graphene based electronics. In order to enhance the conductivity of graphene, we employed a simple doping method where graphene films produced by chemical vapor deposition and transferred onto SiO₂, Al₂O₃, and WO₃ substrates are p-doped with iodine vapor through physisorption at temperature of ~ 100 °C [1-3]. The work function values and iodine to carbon ratios of the one-layer (1L) and two-layer (2L) folded regions were analyzed by high spatial- and energy resolution X-ray photoelectron emission microscopy (XPEEM) on a *NanoESCA* instrument. After the iodine doping, the work function values were significantly increased up to ~0.4 eV and ~0.5 eV, respectively, for 1L and 2L graphene on SiO₂/Si. This higher degree of doping by iodine was corroborated by I 3d_{5/2} core level imaging of the same area where the 2L graphene exhibited significantly larger concentration of iodine (2 at. % versus 1 at. %) likely due to the intercalation of iodine at the inter-layer space.

The main iodine species identified by high resolution core level X-ray photoemission spectroscopy and Raman spectroscopy were I₃⁻ and I₅⁻ polyiodide anionic complexes with slightly higher concentration of I₅⁻ in 2L than 1L graphene possibly due to different doping mechanisms. Temperature dependent ultra-high-vacuum, in-situ annealing of the doped films has demonstrated that most of iodine is removed above 300 °C for the both 1L and 2L regions, although a significant removal of iodine is observed for 2L graphene at temperature as low as 100 °C. Surprisingly, after the complete removal of iodine by annealing, the work function value did not return to the original one before the doping treatment and remained at a much higher value. This can be ascribed to the residual hydrocarbon contaminations interacting with the atomic defects within the graphene layer that lead to unintentional n-type doping in our samples[4].

Acknowledgement: The XPEEM and KFM measurements were performed at the Nanocharacterization Platform (PFNC).

References

- [1] L. Grigorian, K.A. Williams, S. Fang, G.U. Sumanasekera, A.L. Loper, E.C. Dickey, S.J. Pennycook, P.C. Eklund, *Phys. Rev. Lett.*, (1998) 5560-5563.
- [2] A.B. Kaiser, *Rep. Prog. Phys.*, (2001) 1.

[3] S.W. Chu, S.J. Baek, D.C. Kim, S. Seo, J.S. Kim, Y.W. Park, *Synth. Met.*, (2012) 1689-1693.

[4] B.H. Kim, S.J. Hong, S.J. Baek, H.Y. Jeong, N. Park, M. Lee, S.W. Lee, M. Park, S.W. Chu, H.S. Shin, J. Lim, J.C. Lee, Y. Jun, Y.W. Park, *Sci. Rep.*, (2012).

5:40pm **2D+EM+MI+MN+NS+SS+TF-ThA11** **Use of XPS for Device Characterization**, *P. Aydogan, E.O. Polat, C. Kocabas, Sefik Suzer, Bilkent University, Turkey*

A noncontact chemical and electrical measurement technique of XPS is utilized to investigate a number of devices made of graphene. The main objective of the technique is to trace chemical and location specific surface potential variations as shifts of the XPS peak positions under operating conditions. Devices consisting of graphene; (i) acting as a simple resistive element between two gold electrodes, (ii) a semiconducting sheet controlled by a back-gate, and (iii) between the source and the drain metal electrodes in a full transistor geometry, have been analyzed by recording the Au4f of the metal electrodes, the C1s of the graphene layer, and the O1s (or N1s) peaks of the silicon oxide (or nitride) of the substrate. The advantage of this technique is its ability to assess element specific surface electrical potentials of devices under operation based on the deviations of the core level peak positions in surface domains/structures. Detection of the variations in electrical potentials and especially their responses to various stimuli gives unprecedented information about the chemical nature as well as the location of structural and/or other types of defects as a result of doping, oxidation, reduction, etc.

Atom Probe Tomography Focus Topic

Room: 301 - Session AP+AS+EN+NS+SS-ThA

APT and FIM Analysis of Catalysts and Nanomaterials

Moderator: David Diercks, Colorado School of Mines, David Larson, CAMECA Instruments Inc.

2:20pm **AP+AS+EN+NS+SS-ThA1** **In Situ Study of Gas - Solid Reactions via Environmental APT**, *Krishna Rajan, Iowa State University*
INVITED

In this presentation we describe the design and examples of applications of the use of an environmental cell integrated into a LEAP atom probe. The use of such a cell helps to open up the field of in-situ gas-solid reactions by permitting one to study surface and near surface reactions which are closer to ambient conditions than is possible in traditional surfaces science studies. The implications for this experimental approach in the context of the study of catalysts and nanomaterials are discussed.

3:00pm **AP+AS+EN+NS+SS-ThA3** **Propagation of Chemical Waves: A Field Emission Microscopy Study**, *Cédric Barroo, Y. De Decker, N. Kruse, T. Visart de Bocarmé, Université Libre de Bruxelles, Belgium*

The catalytic hydrogenation of NO₂ over platinum field emitter tips has been investigated by means of field emission techniques. Field emission microscopy (FEM), as well as field ion microscopy (FIM), has been proved to be an efficient method to study the dynamics of catalytic reactions occurring at the surface of a nanosized metal tip, which represents a good model of a single catalytic nanoparticle. These studies are performed during the ongoing reaction which is imaged in real time and space. Nanoscale resolution allows for a local indication of the instantaneous surface composition.

The presence of adsorbates modifies the value of the local work function. These variations are expressed by modulations of the brightness of field emission patterns. A qualitative investigation of the local surface composition is then possible as function of time.

The microscope is run as an open nanoreactor, ensuring that the system is kept far from thermodynamic equilibrium. Under these conditions, chemical reactions can induce time and space symmetry breaking of the composition of a system, for which periodic oscillations and target patterns are well-known examples.

Self-sustained periodic oscillations have been reported for the NO₂ reduction. By increasing the time resolution of the system, it is now possible to study the emergence of these oscillations and to observe the propagation of chemical waves at the nanoscale, on a single facet of a nanocrystal. The velocity of wave propagation is estimated to be in the μm/s range, which is in accordance with previous studies of catalytic reaction at the mesoscale.

3:20pm **AP+AS+EN+NS+SS-ThA4 3D Nanoscale Chemical/Structure Analysis in Mineral Carbon Sequestration Study using Atom Probe Tomography**, *Jia Liu, D.E. Perea, R.J. Colby, L. Kovarik, B. Arey, O. Qafoku, A. Felmy*, Pacific Northwest National Laboratory

Mineral carbon sequestration is one of the important means to store CO₂ in order to mitigate the environmental concern regarding ever-growing anthropogenic CO₂ emissions. Olivines, X₂SiO₄ where X = Mg and Fe, hold promise as potential media to sequester carbon due to its broad availability in basalt deposits and reactivity to form stable metal carbonates. Site-specific reactivity of olivine with supercritical CO₂ is of great interest in understanding the fundamental elementary reaction mechanisms, where the presence of impurities within the bulk mineral may affect reaction kinetics. A combination of atom probe tomography (APT) and scanning transmission electron microscopy (STEM) is being used to map the complex composition and nanoscale structure across various site-specific regions. APT analysis of unreacted natural fayalite indicates the presence of 2-3-nm-thick hydrated iron oxide layers. In addition, Na impurities were found to concentrate within the hydrated layers while Mg and Mn were depleted from these regions. With the ability of APT to detect the chemical/structural heterogeneity at nanometer-scale, we find that APT will provide a means to correlate with ongoing experimental reaction studies and also provide guidance into models of the heterogeneous phase formation and reaction rates at precisely defined interfaces within minerals.

4:00pm **AP+AS+EN+NS+SS-ThA6 Catalyst Nanomaterials Analysis via Atom Probe Tomography**, *P.A.J. Bagot*, Oxford University, UK, *Q. Yang*, University of Oxford, UK, *K. Kruska*, Pacific Northwest National Laboratory, *D. Haley*, University of Oxford, UK, *E. Marceau, X. Carrier*, Université Pierre et Marie Curie, France, *Michael Moody*, University of Oxford, UK **INVITED**

Heterogeneous catalytic materials play an increasingly critical, yet largely unnoticed, role underpinning countless modern technologies. Their active components are generally transition group metals, each of which offers different catalytic properties in terms of selectivity, yield and stability under demanding operating conditions. The need to develop more efficient catalysts that meet industrial demands and comply with environmental legislation targets requires better understanding how different catalysts may alter at the atomic scale in terms of structure or surface composition under their respective operating environments. Further, many catalysts take the form of nanoparticles, the performance of which can be strongly correlated to size, shape, chemistry and structure. However, discerning the nature of nanoparticles scale poses significant challenges to conventional microscopy.

Recently, atom probe tomography (APT) techniques have been developed to provide unique insight into the behaviour of catalyst alloys subject to conditions like those experienced in service [1–3]. This study is aimed at more accurate and insightful analyses comprising unique 3D atomistic descriptions of the evolving alloy nanostructure which can then be correlated to catalyst performance. Here, APT results are presented for characterization of oxidation-induced segregation in a Pt-Pd-Rh gauze and Fe-Ni alloy catalysts. Progress in the development of new approaches for the analysis of nanoparticles via APT is also presented.

[1] T. Li et al., Atomic engineering of platinum alloy surfaces. *Ultramicroscopy* 132, 205 (2013).

[2] T. Li et al., Atomic Imaging of Carbon-Supported Pt, Pt/Co, and Ir@Pt Nanocatalysts by Atom-Probe Tomography. *ACS Catalysis* 4, 695 (2014).

[3] P. Felfer et al, Long-Chain Terminal Alcohols through Catalytic CO Hydrogenation. *Journal of the American Chemical Society* 135, 7114 (2013).

Conservation Studies of Heritage Materials Focus Topic Room: 313 - Session CS-ThA

Conservation Studies of Heritage Materials 2

Moderator: H. Frederick Dylla, American Institute of Physics, Robert Opila, University of Delaware

2:20pm **CS-ThA1 A Conservator's Perspective of Technical Studies and Scientific Analysis**, *Patricia Favero*, The Phillips Collection **INVITED**

The nature of technical studies is necessarily interdisciplinary as they address various questions about works of art and artifacts: What materials did the artist use; how did he use his materials; and most importantly, what is the significance of this information for a greater understanding of the artist and his work? What is learned in technical studies often both augments art historical research and informs conservation treatment

decisions. Collaboration between conservators, scientists, and art scholars is becoming ever more common in the study of works of art. Results of in-depth studies are now featured in exhibitions and scholarly publications, and their importance is increasingly recognized within larger art historical studies of an artist's oeuvre.

In this light, this presentation will consider two recent technical studies carried out at The Phillips Collection in Washington, D.C. The first, a study of a group of Georges Braque's mid-career paintings, was conducted in collaboration with conservation scientists from Harvard Art Museums and curators at the Phillips and the Kemper Art Museum in St. Louis. The results of the study were featured in the exhibition *Georges Braque and the Cubist Still Life, 1928-1945* and in the related publication. The second study focuses on one painting, *The Blue Room* (1901), an early Blue Period picture by Pablo Picasso in the collection at the Phillips. Ongoing research of this picture is being conducted in collaboration with independent Picasso scholars and scientists from the Winterthur Museum in Delaware, Cornell University, and the National Gallery of Art.

Both studies began in the conservation studio with the conservator carefully examining each painting in good light and under magnification, considering each artist's technique and how it may have influenced their material choices. Other examination techniques, such as UV-induced fluorescence, infrared imaging, and x-radiography were also employed.

In both studies, paint samples were taken and analyzed to positively identify the artists' materials and understand them in context. In the Braque study, the increasingly wide-spread use by conservators of portable x-ray fluorescence (pXRF) spectroscopy allowed for comparative pigment analysis of eight paintings from five different collections. For the Picasso, three non-invasive techniques—reflectance imaging spectroscopy, fiber optic reflectance spectroscopy (FORS), and XRF intensity mapping—were used.

The presentation will consider the collaborative nature of both studies and evaluate what made them successful in addition to discussing the process and outcome of each project from the conservator's perspective.

3:00pm **CS-ThA3 State of the Art: Probing Complexity in Paint**, *Francesca Casadio, F. Pozzi, L. Chang*, The Art Institute of Chicago, *D. Kuroski, S. Zaleski, N.C. Shah, R.P. Van Durne*, Northwestern University, *V. Rose*, Argonne National Laboratory **INVITED**

In recent years, the scientific analysis of painted surfaces has made a giant leap forward. At the same time as innovative standoff macro-scale imaging modalities have been developed to deliver elemental mapping (using macro X-ray fluorescence spectroscopy) and molecular imaging (with Ultra-Violet/ Visible, Near Infrared, Mid-Infrared reflectance, fluorescence, and Raman imaging), our ability to probe local paint chemistries and mechanical properties at the nanoscale has grown exponentially. These recent developments have fundamentally changed the way conservators, curators and conservation scientists approach the study of works of art, leading to cutting-edge research on pigment degradation phenomena and enabling us to retrieve otherwise lost information on altered colors or hidden compositions that make up the original aspect of masterpieces.

This talk will present recent research employing high resolution nanoprobe synchrotron X-ray fluorescence (XRF) mapping of metallic impurities with 30 nm resolution in single grains of zinc oxide pigments used in early 20th century paints formulated for artists and other commercial uses and widely employed by Pablo Picasso (1881-1973). Such highly detailed chemical characterization of paints at the nanoscale opens the path to a better understanding of their historical fabrication and chemical reactivity.

For the characterization of organic molecules used in paintings Surface-Enhanced Raman Spectroscopy (SERS) has recently been developed into a robust, reliable and highly sensitive technique to detect and unambiguously identify minute quantities of organic colorants. SERS has seen the field of cultural heritage become one of its foremost research and application areas, resulting in improved analytical protocols applicable to several other fields such as pharmaceuticals and forensic analysis. In particular, our efforts to develop methods to identify more than one colorant on a single sample using combined Thin Layer Chromatography / SERS and microfluidics SERS approaches will be discussed. Pushing the envelope of in-situ SERS analysis, first results on the use of Tip-Enhanced Raman spectroscopy (TERS) for the high spatially resolved, highly sensitive and non-invasive investigation of dyes used on paper supports will be discussed and preliminary results presented. This first demonstration of TERS spectral acquisition directly on a paper substrate confirms the analytical potential of TERS to identify organic colorants in artworks with high sensitivity, high spatial resolution, and minimal invasiveness opening the way to future developments for the nano-scale mapping of organic constituents of works of art.

4:00pm **CS-ThA6 The Degradation Mechanisms of Cadmium Pigments in Works by Henri Matisse, Edward Munch, and Their Contemporaries, Jennifer Mass**, Winterthur Museum, *E. Pouyet*, ESRF, France, *F. Meirer*, Utrecht University, Netherlands, *M. Cotte*, ESRF, France, *A. Mehta*, Stanford Synchrotron Radiation Lightsource **INVITED** Cadmium carbonate (CdCO_3) has for several years been identified in the altered cadmium yellow (CdS) paints found Impressionist, early modernist, and post-Impressionist works. When it is concentrated at the surface of the painting, CdCO_3 appears to be a result of the photo-alteration of CdS, likely through a CdSO_4 -containing phase. However, in other cases CdCO_3 is distributed throughout the paint layer. This is significant because CdCO_3 is highly insoluble (K_{sp} of 1.0×10^{-12}), and if it were formed solely as a result of photo-alteration it would not be expected to migrate away from the painting's surface. In cadmium yellow paints in works such as Edvard Munch's c. 1910 *The Scream* (The Munch Museum, Oslo), Plahter et al. have recently proposed that CdCO_3 is present because this compound was used in the indirect wet process synthesis of CdS (through, for example, the reaction of CdCO_3 and Na_2S). This would mean that the CdCO_3 is a residual starting reagent rather than a photo-alteration product. Such an interpretation is supported by the identification of CdCO_3 in the unaltered cadmium yellow paints of early modernist works such as Pablo Picasso's *The Blue Room* (The Phillips Collection, 1901) and Henri Matisse's *Flower Piece* (The Barnes Foundation, 1906).

To address this question of CdCO_3 's role, a flake of apparently nondegraded cadmium yellow paint was removed from Henri Matisse's *Flower Piece* so that the distribution of CdCO_3 could be studied, both as a function of depth in the paint layer and in individual pigment particles.

X-Ray microspectroscopy and microdiffraction were respectively carried out at ESRF ID21 and Petra III, supplemented by light microscopy, backscattered electron microscopy with X-ray microanalysis, and Fourier transform infrared spectroscopy. This presentation will focus on results from X-ray microspectroscopy: μ -X-ray fluorescence (XRF scanning) allowed precise mapping of local elemental distribution, and Full Field X-ray Near-Edge Absorption Structure (FF-XANES) for mapping the chemical speciation using the Cd-L₃ and S-K edges.

FF-XANES imaging of a 15 micrometer thin section at CdL₃-edge revealed the presence of three Cd-based phases: CdS, CdSO_4 , and CdCO_3 . The CdSO_4 was concentrated on only one surface of the sample, suggesting its role as a photo-alteration product. Cadmium carbonate was found to comprise the bulk of the individual pigment particles, suggesting that it is a synthesis starting reagent. CdS was found to be concentrated on the surface of these CdCO_3 particles. CdSO_4 could also be observed to surround some of the CdCO_3 particles, suggesting the beginnings of photo-oxidation of the thin CdS coating.

4:40pm **CS-ThA8 Characterisation of Modern Watercolour Paints using XPS, HIM, ToF-SIMS and Principal Component Analysis Techniques, Naoko Sano, P.J. Cumpson**, NEXUS, Newcastle University, UK, *E. Cwiertnia*, *B.W. Singer*, Northumbria University, UK

To conserve old masterpieces is, of course, critical but modern fine/contemporary arts also need preservation as future cultural heritage. Therefore, nowadays many modern artistic works have been studied using scientific techniques to preserve their condition. As with easel oil paintings, modern watercolour paintings represent some of our great cultural heritage from artists such as J.M.W. Turner, Paul Klee or Georgia O'Keeffe. For conservation scientists, the characterization of the binder and pigments in modern paintings is especially important yet problematic in terms of conservation treatments and environmental conditions for display or storage.

In investigation of modern paintings it is often critical to identify the origin of organic molecules in the paintings, since modern paintings have commonly used artists' paints containing synthetic organic pigments due to their greater selection of colours. In addition, in terms of watercolour paints, commonly used binders such as gum arabic, gum tragacanth or honey are not straight forward to identify due to their organic content.

To contribute to a better understanding of modern artists' paints for conservation, this study presents a scientific investigation into commercially prepared watercolour cakes and binders from the 20th century. Analysis focuses on the characterisation of commercial watercolour paints (red colour) that may contain quinacridone and/or saccharide materials, and shows different surface chemistries of the paint between powder and cake types. Moreover, we attempt the identification of the synthetic organic pigments and the plant gum binder from the watercolour paint using surface analysis techniques and principal component analysis (PCA). Especially, we feel surface analysis techniques such as x-ray photoelectron spectroscopy (XPS), helium ion microscopy (HIM) and time of flight secondary ion mass spectrometer (ToF-SIMS) are powerful techniques for cultural heritage preservation.

5:00pm **CS-ThA9 The Analysis of Egg-Oil Binding Media by Time-of-Flight Secondary Ion Mass Spectrometry, Zachary Voras, K. DeGhetaldi, D. Clark**, University of Delaware, *J.L. Mass*, Winterthur Museum, *T.P. Beebe, Jr.*, University of Delaware

Time-of-Flight Secondary Ion Mass Spectrometry (ToF-SIMS) is quickly becoming a critical tool in the field of art conservation. This technique provides high-resolution spatial maps of both inorganic and organic components located across and below the surface of a paint cross-section or other art object. With recent advancements in surface analysis, ToF-SIMS can now be used to identify specific amino acids present in protein-containing materials as well as fatty acids present in drying oils. For example, the detection of the ion fragment associated with the amino acid hydroxyproline can be used to confirm the use of animal glue in a paint sample. As an analytical technique, ToF-SIMS avoids the need for derivatization/silylation reagents, with no interference by the presence of reactive or unreactive pigments. Furthermore, the layered systems that are often encountered in historical paint samples remain intact throughout the analytical procedure. This allows for the co-localization of organic and inorganic species in specific layers (e.g., egg yolk paint atop a glue ground). Because of this ability to localize the analytical signal to approximately 1 μm or less, the mass spectral information can be used to produce mass-resolved and spatially resolved images which can be correlated to previous studies of the same preserved samples. In this study, ToF-SIMS was used to analyze paint cross-sections obtained from various time periods. A focus will be on works by Italian artists such as Raphael (from the Walters Art Museum) with additional mentions of a painting by Matisse (from the Barnes Foundation) and Henry Ossawa Tanner (from the Smithsonian American Art Museum).

5:20pm **CS-ThA10 The Right Snuff? A Technical Study of Two Snuff Boxes from the Winterthur Museum Collection, Marlene Yandrisevits**, Winterthur/ University of Delaware Program in Art Conservation, *J.L. Mass*, *C. O'Grady*, *C. Matsen*, Winterthur Museum Scientific Research and Analysis Laboratory, *E. Torok*, Winterthur/ University of Delaware Program in Art Conservation

The nasal inhalation of snuff tobacco stored in vanity boxes was a fashionable custom among the colonial European elite. From the late 18th to the early 19th century, small decorative enameled boxes were manufactured in England to supply a bourgeois demand for stylish, but less expensive, imitative snuff boxes. The utilization of traditional materials and techniques for later 19th/ early 20th century repair and revival fabrication of enameled boxes introduces a serious challenge in distinguishing the original from the copy or the heavily restored. This study examines two enameled boxes at the Winterthur Museum with the goal to contribute technical data to provenance and dating discussions. Ultraviolet-induced visible fluorescence surface examination, x-radiography, energy dispersive x-ray fluorescence spectroscopy, microRaman spectroscopy, cross-sectional microscopy with visible and UV illumination, scanning electron microscopy – energy dispersive x-ray spectroscopy/ back-scattered electron imaging, Fourier transform infrared spectroscopy, and gas chromatography – mass spectrometry were used to characterize the composition and stratigraphy of the materials comprising the boxes, followed by comparison to period materials and techniques reported in historical sources and to the findings of previous research. As characterized in this study, aluminosilicates were inferred as the enamel network forming agent combined with lead arsenate and tin oxide opacifiers and potash flux on both boxes, with soda flux additionally on one box. Enamel colorants were metal-based (including iron oxides in red, pink and purple overglazes; colloidal gold in pink and purple overglazes; cobalt oxides/ glass in blue and green overglazes; and Pb-Sb-Sn oxides in yellow and green overglazes). Findings suggest that, while significant titanium-containing restoration overpaint and synthetic coatings are present on both boxes, the enamel and mount materials of one box are consistent with the early production. The majority of materials on the other are also consistent with the early stage of enameled snuff box production in England, with the possible exceptions of chromium-based green enamels, iron oxide pink and purple enamels, and brass-based imitation gilding in localized areas which may represent an early restoration campaign. The materials identified on both boxes are consistent with the findings of previous analyses, excluding a yellow colorant identified in previous research as Naples yellow ($\text{Pb}(\text{SbO}_3)_2/\text{Pb}_3(\text{Sb}_3\text{O}_4)_2$) now detected in this study and recharacterized as a related Pb-Sn-Sb triple oxide ($\text{Pb}_2(\text{SnSb})\text{O}_6$), which may suggest further research towards a reliable dating scheme.

Spectroscopic Ellipsometry Focus Topic

Room: 304 - Session EL+AS+EM+MC+SS-ThA

Optical Characterization of Nanostructures and Metamaterials

Moderator: David Aspnes, North Carolina State University, Mathias Schubert, University of Nebraska-Lincoln

2:20pm **EL+AS+EM+MC+SS-ThA1 The Optical Properties of Metallic Nanostructures, Bruno Gompf**, Universität Stuttgart, Germany **INVITED**

The entire optical response of a homogenous reciprocal sample can be characterized by eight basic physical properties: mean absorption, mean refraction, circular birefringence and circular dichroism, linear birefringence and linear dichroism (0° , 90°), linear birefringence and linear dichroism ($+45^\circ$). Always two out of the three main birefringence-dichroism pairs (basic anisotropies) are sufficient to jump from any point of the Poincare-sphere to any other. A common example is the Soleil-Babinet compensator. This implies that always two of the basic anisotropies generate artificial signals of the third [1]. Therefore even for perfect crystals it is hard to judge, what optical property lead to an observed polarization change.

In the case of inhomogeneous materials the permittivity additionally becomes k -dependent $\epsilon_{ij}(\omega, k)$; it exhibits spatial dispersion. For most artificial nanostructures, dubbed metamaterials, the building blocks are in the range $l/10 < P < l/2$. During the last couple of years it has become clear that in general it is not possible for these kinds of materials to define *effective* optical parameters, which are independent of the angle of incidence of the probing light. There optical response is intrinsically k -dependent.

With Mueller-matrix spectroscopic ellipsometry the entire optical response of artificial nanostructures can be characterized. For this the Mueller-matrix elements $m_{ij}(\theta, \alpha, \omega)$, which depends on the angle of incidence q , the azimuth orientation α and the energy, had to be measured over the complete angular and a wide frequency range. Visualizing the results in polar contour plots enables a detailed analysis of how nanostructures influence the polarization state of light [2-4]. Most importantly, immediate experimental evidence is obtained for deviations from pure dielectric behaviour; i.e. the optical response cannot be explained by an effective $\epsilon_{ij}(\omega)$ alone but requires spatial dispersion.

In the talk the entire optical response of a some artificial nanostructures will be presented and some generalizations will be discussed, when spatial dispersion becomes important and how it can be distinguished from other optical properties leading to a mixing of polarization states, like birefringence and optical activity.

[1] J.Schellman and H.P.Jensen, Chem. Rev., 87, 1359 (1987.)

[2] B. Gompf, J. Braun, T. Weiss, H. Giessen, M. Dressel, U. Huebner, Phys.Rev.Lett. **106**, 185501 (2011).

[3] B.Gompf, B. Krausz, B. Frank, M. Dressel, Phys.Rev.B. **86**, 075462 (2012).

[4] A. Berrier, B. Gompf, Liwei Fu, T. Weiss, H. Schweizer, Phys.Rev.B. in print

3:00pm **EL+AS+EM+MC+SS-ThA3 Mueller Matrix Ellipsometry As a Powerful Tool for Nanoimprinted Grating Structure Metrology, Xinguo Chen, C.W. Zhang, S.Y. Liu**, Huazhong University of Science and Technology, China

Compared with conventional ellipsometric scatterometry, which only obtains two ellipsometric angles, Mueller matrix ellipsometry (MME, sometimes also referred to as Mueller matrix polarimetry) based scatterometry can provide up to 16 quantities of a 4 by 4 Mueller matrix in each measurement. Consequently, MME can acquire much more useful information about the sample and thereby can achieve better measurement sensitivity and accuracy. In this talk, we will demonstrate MME as a powerful tool for nanoimprinted grating structure metrology. We will show that MME-based scatterometry at least has the following three aspects of advantages over conventional ellipsometric scatterometry.

(1) More accurate characterization of line width, line height, sidewall angle, and residual layer thickness of nanoimprinted grating structures can be achieved by performing MME measurements in the optimal configuration. In contrast, conventional ellipsometric scatterometry can only be conducted in the planar diffraction configuration, i.e., with the plane of incidence perpendicular to grating lines, which is not necessarily the optimal measurement configuration for nanostructures in general.

(2) Not only further improvement in the measurement accuracy and fitting performance can be achieved, but also the residual layer thickness variation over the illumination spot can be directly determined by incorporating depolarization effects into the interpretation of measured data. The depolarization effects, which are demonstrated to be mainly induced by the finite bandwidth and numerical aperture (NA) of the instrument, as well as the residual layer thickness variation of the nanoimprinted grating structures, can be only handled by MME.

(3) Conventional ellipsometric scatterometry has difficulties measuring asymmetric grating structure due to the lack of capability of distinguishing the direction of profile asymmetry. In contrast, MME not only has good sensitivity to both the magnitude and direction of profile asymmetry, but also can be applied to accurately characterize asymmetric nanoimprinted gratings by fully exploiting the rich information hidden in the measured Mueller matrices.

3:20pm **EL+AS+EM+MC+SS-ThA4 Vector Magneto-Optical Generalized Ellipsometry on Sculptured Thin Films with Forward Calculated Uniaxial Response Simulation, Chad Briley, T. Hofmann**, University of Nebraska-Lincoln, *D. Schmidt*, National University of Singapore, *E. Schubert, M. Schubert*, University of Nebraska-Lincoln

We present the vector magneto-optical generalized ellipsometric (VMOGE) response and forward calculated simulations of ferromagnetic slanted columnar thin films. Directional hysteresis magnetization scans were performed with an octu-pole vector magnet at room temperature on slanted columnar thin film samples of permalloy grown by glancing angle deposition passivated by an atomic layer deposited Al₂O₃ conformal coating. Model analyses of the measured Mueller matrix ellipsometric data through a point-by-point best match model process determines the magneto-optical (MO) dielectric tensor. Three dimensional rendering of the anti-symmetric off-diagonal elements of the MO dielectric tensor reveal a uniaxial magnetic response of the thin film along the long axis of the columns. The magnetic response was subsequently modelled by a best match model process with uniaxial hysteretic response governed by the shape induced anisotropy from the physical geometry and orientation of the nano-columns. By using model parameters for normalized saturation $||M_s||=1$, coercivity $||H_c||=50$ mT, and remanence $||M_r||=0.9999*||M_s||$ the forward calculated magnetic simulations described the observed magneto-optical response for all measured orientations of the nano-columns with respect to all magnetizing field directions generated by the vector magnet.

1) D. Schmidt, C. Briley, E. Schubert, and M. Schubert Appl. Phys. Lett. **102**, 123109 (2013)

4:00pm **EL+AS+EM+MC+SS-ThA6 In Situ Generalized Ellipsometry Characterization of Silicon Nanostructures during Lithium-ion Intercalation, Derek Sekora, R.Y. Lai, T. Hofmann, M. Schubert, E. Schubert**, University of Nebraska-Lincoln

Nanostructured silicon has emerged as a leading candidate for improved lithium-ion battery electrode design. The combined highly accessible surface area and nanoscale spacing for volumetric lattice expansion of nanostructured thin films have shown improved cycle lifetime over bulk-like silicon films. Additionally, ultra-thin passivation layers have been reported to increase the longevity and stability of silicon thin film electrodes. Very little *in-situ* information has been reported on silicon films during the complicated lithiation process. Furthermore, what information available has been limited to the study of bulk-like thin films. The advantageous geometry of glancing angle deposited (GLAD) thin films allows for the strain from lithiation to affect individual nanostructures in comparison to the bulk response. For this reason, alumina passivated GLAD silicon films were grown for use as working electrodes in half cell electrochemical experiments.

The spatially coherent silicon GLAD nanostructures have intrinsic biaxial optical properties. Therefore, generalized ellipsometry was employed to investigate the silicon film's physical response to lithium intercalation during an electrochemical cyclic voltammogram cycled against pure lithium metal in a conductive anhydrous electrolyte solution. *In-situ* ellipsometric monitoring of directional optical constant changes determined by the homogeneous biaxial layer approach are presented. The optical response expresses a morphologic conversion from a highly anisotropic film to a pseudo-isotropic lithium concentrated form and subsequently, its return to the original anisotropic state. The ability to nondestructively monitor complex nanostructured thin films during lithium-ion processes provides new avenues for high storage battery electrode design.

4:20pm **EL+AS+EM+MC+SS-ThA7 Characterization of SiO₂ Nanoparticle Layers on a Glass Substrate by Spectroscopic Imaging Ellipsometry and AFM**, Peter H. Thiesen, Accurion GmbH, Germany, G. Hearn, Accurion Inc., C. Röling, Accurion GmbH, Germany

The well-directed organization of nanoparticles is of increasing technical and scientific interest. One approach is the organization of nanoparticles at the air/water interface for applications, like producing 2D colloidal crystals or nanowires. For example, Gil et al. (2007) monitored the formation of 2D colloidal crystals by Langmuir-Blodgett technique. They used Brewster angle microscopy to observe the film quality. Zang et al. (2009) have also studied silica nanoparticle layers at the air/water interface by multiple angle of incidence ellipsometry. For data interpretation, a two-layer model was introduced. With this model, the radius of interfacial aggregates and the contact angle of the nanoparticle surface at the air/water interface were obtained.

In this paper different line shaped pattern of SiO₂ nanoparticles were characterized by spectroscopic imaging ellipsometry in the wavelength range between 360 and 1000 nm and by AFM. The samples were provided by the research group of Professor Y. Mori, Doshisha University, Japan.

The work shows the unique capability of imaging ellipsometry in characterizing patterned surfaces. We started with a pre inspection of the surface by imaging ellipsometric contrast microscopy. Tiny regions of interest (ROIs) were placed on interesting areas like on different steps of the stripes and Delta and Psi spectra were recorded. The next step in characterization was the mapping of Delta and Psi with pixel resolution of the detector. The same samples were also characterized with an AFM. The results optical modelling are in good agreement with the results of the scanning method.

A. Gil, M. Vaupel, F. Guitiana, D. Möbius (2007) *Journal of Materials Chemistry* 17: 2434–2439.

D. Zang, A. Stocco, D. Langevin, B. Weib, B.P. Brinks (2009) *Phys. Chem. Chem. Phys.* 11: 9522–9529.

5:00pm **EL+AS+EM+MC+SS-ThA9 Dielectric Tensor Model for Inter-Landau-level Transitions in Highly Oriented Pyrolytic Graphite and Epitaxial Graphene – Symmetry Properties, Energy Conservation and Plasma Coupling**, Philipp Kühne, Linköping University, Sweden, T. Hofmann, M. Schubert, University of Nebraska-Lincoln, C.M. Herzinger, J.A. Woollam Co., Inc., V. Darachieva, Linköping University, Sweden

We report on polarization sensitive, magneto-optic, reflection-type Landau level (LL) spectroscopy at low temperatures by using the integrated optical Hall effect instrument¹ in the mid-infrared spectral range (600 – 4000 cm⁻¹) on highly oriented pyrolytic graphite (HOPG) and epitaxial graphene grown on C-face silicon carbide by thermal decomposition. In both sample systems we observe a multitude of inter-LL transitions. Inter-LL transitions in HOPG possess polarization mode mixing polarization selection rules characteristics, while polarization mode conserving and polarization mode mixing inter-LL transitions are observed in epitaxial graphene which can be assigned to single- and Bernal stacked (ABA) multi-layer graphene, respectively.² We present a new dielectric tensor model for inter-LL transitions which explains all experimentally observed line-shapes. For inter-LL transitions in multi-layer graphene and HOPG we employ this new model together with energy conservation considerations, to show that these polarization mode mixing inter-LL transitions couple with a free charge carrier plasma. Finally, inter-LL transition energy parameters are determined and discussed.

¹) P. Kühne, et. al., *Rev. Sci. Instrum.*, accepted (2014)

²) P. Kühne, et. al., *Phys. Rev. Lett.* 111, 077402 (2013)

5:20pm **EL+AS+EM+MC+SS-ThA10 Characterization of Exfoliated 2D Nano Materials with Imaging Spectroscopic Ellipsometry**, P.H. Thiesen, Accurion GmbH, Germany, Greg Hearn, Accurion Inc., B. Miller, Technische Universität München, Germany, C. Röling, Accurion GmbH, Germany, U. Wurstbauer, Columbia University, E. Parzinger, A.W. Holleitner, U. Wurstbauer, Technische Universität München, Germany

In the initial period of graphene research, the issue was to identify and characterize crystallites of microscopic scale. Imaging ellipsometry is a nondestructive optical method in thin film metrology with a lateral resolution down to 1 µm. In a number of papers, imaging ellipsometry has been applied to characterize graphene flakes of few micrometer size. Ellipsometric contrast micrographs, delta and Psi maps as well as wavelength spectra [1],[2] and single layer steps in multilayer graphene/graphite stacks [3] have been reported.

Molybdenum disulfide is a layered transition metal dichalcogenide. From the point of current research, 2D-nano materials based on MoS₂ are very promising because of the special semiconducting properties. The bulk material has an indirect 1.2 eV electronic bandgap, but single layer MoS₂ has a direct 1.8 eV bandgap. The monolayer can be used in prospective

electronic devices like transistors (MOSFETs) or photo detectors. Delta and Psi Spectra of MoS₂ monolayers as well as maps of the ellipsometric angles will be presented. The practical aspect of single layer identification will be addressed and the capability of ellipsometric contrast micrographs as a fast tool for single layer identification will be demonstrated.

An additional focus will be on the modelling of the optical properties of 2D nanomaterials.

[1] Wurstbauer et al., *Appl. Phys. Lett.* 97, 231901 (2010)

[2] Matkovic et al. *J. Appl. Phys.* 112, 123523 (2012)

[3] Albrektsen O. *J. OF Appl. Phys.* 111, 064305 (2012)

Electronic Materials and Processing

Room: 311 - Session EM1-ThA

Materials for Quantum Computation

Moderator: Sang M. Han, University of New Mexico

2:20pm **EM1-ThA1 Mos Quantum Bits for Adiabatic and Non-Adiabatic Quantum Computing**, Malcom Carroll, Sandia National Laboratories **INVITED**

This talk will describe silicon nanostructures that confine electrons at the SiO₂/Si interface and produce quantum dot behavior. These structures combined with single ion implantation provide a platform for silicon quantum bits. Application of these structures towards circuit model and ground state quantum computing approaches will be discussed. We acknowledge the research funding support provided by the laboratory directed research and development (LDRD) program at Sandia National Laboratories. Sandia National Labs is a multi-program laboratory operated by Sandia Corporation, a Lockheed Martin Company, for the United States Department of Energy's National Nuclear Security Administration under contract DE-AC04-94AL85000.

3:00pm **EM1-ThA3 ²⁸Si Enriched In Situ to 99.9998 % for Quantum Computing Devices**, Kevin Dwyer, University of Maryland, College Park, J. Pomeroy, D. Simons, National Institute of Standards and Technology (NIST)

We are enriching *in situ* and depositing epitaxial thin films of ²⁸Si in support of quantum computing devices. Highly enriched ²⁸Si is a critical material for quantum computing as removal of ²⁹Si spins provides a non-interacting “semiconductor vacuum” medium for qubits such as ³¹P donors which have electron and nuclear coherence (T₂) times of seconds and minutes respectively even up to room temperature. ³¹P donors can also be addressed optically due to hyperfine transitions not normally resolvable in natural Si. Starting with natural abundance silane, we have used mass filtered ion beam deposition to produce ²⁸Si films enriched to > 99.9998 % with a residual ²⁹Si isotope fraction < 1 ppm (40 times less than previously reported ²⁸Si sufficient for optical addressing). Using our ion beam system we have grown crystalline ²⁸Si films and are pursuing characterization of their structural properties using *in situ* reflection high energy electron diffraction (RHEED), *in situ* scanning tunneling microscopy (STM), and transmission electron microscopy (TEM). Secondary ion mass spectrometry (SIMS) is used to determine enrichment of crystalline ²⁸Si films. As we move away from silane towards a solid sputtering source, enrichment may be improved even further and the use of additional materials such as Ge can become possible. Numerous experimental systems can take advantage of ²⁸Si as a medium for qubits including STM based hydrogen lithography devices, single donors coupled to single electron transistors, and quantum wells. We have demonstrated the ability to produce isotope heterostructures with applications including fully enriched ²⁸Si/²⁸Si⁷⁴Ge quantum wells. The importance of ²⁸Si to quantum information systems and the scarcity of such material make clear the critical need for an alternate source of enriched silicon such as the one we demonstrate.

3:20pm **EM1-ThA4 Computational Analysis of Interdiffusion in Silicon-Germanium Alloy Films Subject to Patterned Stress Fields**, Daniel Kaiser, University of Pennsylvania, S. Ghosh, S.M. Han, University of New Mexico, T.R. Sinno, University of Pennsylvania

In this talk we present a multi-element computational approach for quantitatively describing atomic interdiffusion within a random-alloy SiGe wafer subject to a patterned stress field imposed by an indenter array applied to its surface. The model, and the associated parametric investigations we carry out, are motivated by a recently-proposed approach for forming ordered arrays of heteroepitaxial Ge quantum dots (QD) on semiconductor substrates in a scalable and robust manner. In this approach, patterned compositional redistribution of Si and Ge atoms is driven by an applied stress field under thermal annealing. The resulting compositional

heterogeneity is shown to induce an internal stress field in the SiGe substrate wafer that persists after the indenter array is removed, thereby effectively “transferring” the stress pattern of the indenter into the substrate. The transferred stress pattern, which we study in detail as a function of several parameters including indenter geometry and thermal annealing schedule, is then used to drive patterning in a subsequent Ge deposition step.

The interdiffusion model is based on a combination of lattice kinetic Monte Carlo (LKMC) and static energy minimization. The LKMC simulation is propagated using rates for atomic diffusion that depend explicitly on local values of stress, composition, and temperature. The dependence of atomic diffusion on composition is regressed to experimental data while the stress dependence is described using the theory of activation volumes [1]. The stress field is updated quasi-statically using a separate energy minimization routine with forces computed based on a Tersoff interatomic potential for the Si-Ge system [2]. The atomic stresses and identities are then smoothed to generate continuous fields that are used as input into the LKMC simulation.

Using our model, we establish that atomic redistribution is feasible for reasonable indenter forces and annealing times and temperatures. We compute the corresponding internal stresses in the compositionally patterned film for several different annealing conditions and show that these stresses are likely to be large enough to influence subsequent Ge quantum dot nucleation and growth. We also compare our results to recent experimental measurements.

References:

- [1] M. J. Aziz, Applied Physics Letters 70, 2810 (1997).
- [2] J. Tersoff, Physical Review B 39, 5566 (1989).

4:00pm EM1-ThA6 Scanning Capacitance Microscopy of Atomically-Precise Donor Devices in Si, Shashank Misra, E. Bussmann, M. Rudolph, S.M. Carr, G. Subramania, G. Ten Eyck, J. Dominguez, M.P. Lilly, M. Carroll, Sandia National Laboratories

Recently, a scanning tunneling microscopy (STM) technique to fabricate atomically-precise dopant-based nanoelectronics in Si has been developed. Phosphorus donors are placed via an atomic-precision template formed by STM H-depassivation lithography, then capped with epi-Si and lastly metal contacts are made to the buried donor layer using conventional microfabrication. New challenges are introduced with this approach that center around difficulties to locate and characterize the pattern of buried donors. In this talk, we show that scanning capacitance microscopy (SCM) can image these buried donor nanostructures with sub-100-nm tip-limited resolution. The technique is used to successfully locate and characterize buried donor nanostructures relative to surface alignment marks. This approach relaxes alignment requirements for the STM lithography step and can offer improved alignment of subsequent metallization steps. The SCM technique is also used to nondestructively image the shape of the electronic carrier distribution and characterize the relative doping levels. This work, performed in part at the Center for Integrated Nanotechnologies, a U.S. DOE Office of Basic Energy Sciences user facility, was supported by Sandia's Lab Directed Research and Development Program. Sandia is a multi-program lab operated by Sandia Corp, a Lockheed-Martin Company, for U. S. DOE under Contract DE-AC04-94AL85000.

4:20pm EM1-ThA7 SiGe on sSOI: Nanoscale Engineering of Structures and Devices on Surfaces, Esmeralda Yitamben, E. Bussmann, Sandia National Laboratories, R. Butera, Laboratory for Physical Sciences, S. Misra, M. Rudolph, S.M. Carr, M. Carroll, Sandia National Laboratories
The relentless increase in both density and speed that has characterized microelectronics, and now nanoelectronics, will require a new paradigm to continue beyond current technologies. One proposed such paradigm shift demands the ultimate control over the number and position of dopants in a device, which includes quantum information processing and variety of semiconductor device materials and architectures aimed at solving end-of-Moore's law issues.

Such a work requires the development of a tool for the design of atomically precise devices on silicon and other surfaces, in hope of studying the effect of local interactions between atomic-scale structures, their microscopic behavior, and how quantum mechanical effects might influence nano-device behavior in very small structures. Demonstrations of remarkable 2D nanostructures down to single atom devices are reported here thanks to the development of scanning tunneling microscopy (STM) as an imaging and patterning tool. These include atomic-scale depassivation of a hydrogen terminated surface with an STM, toward the incorporation of dopants in silicon, and SiGe growth on strained silicon on insulator (sSOI). sSOI has been shown to be relatively insensitive to thermal relaxation and thereby provides a starting material that satisfies the requirements of both enabling high temperature surface preparation steps combined with providing a

strained layer that can be capped with relaxed SiGe forming a high quality interface for gate tunable channel formation. In this talk we will present, STM and other characterization results on cleaning, hydrogen lithography, dopant incorporation and SiGe growth on sSOI.

Acknowledgments: This work was performed, in part, at the Center for Integrated Nanotechnologies, a U.S. DOE, Office of Basic Energy Sciences user facility. The work was supported by the Sandia National Laboratories LDRD Program. Sandia National Laboratories is a multi-program laboratory operated by Sandia Corporation, a Lockheed-Martin Company, for the U. S. Department of Energy under Contract No. DE-AC04-94AL85000.

4:40pm EM1-ThA8 Creating a Responsive SiGe Substrate to Form 2D Array of Ge Quantum Dots Using Stress-induced Near-surface Compositional Redistribution, S. Ghosh, University of New Mexico, D. Kaiser, T.R. Sinno, University of Pennsylvania, Sang M. Han, University of New Mexico

A well-defined array of Ge quantum structures possesses unique electronic properties for a variety of applications, including quantum-computers and infrared photodetectors. Herein, we use simulation to predict and experiment to demonstrate the compositional redistribution of Si and Ge in the near-surface region of $\text{Si}_{0.8}\text{Ge}_{0.2}$ substrates by applying a spatially structured compressive stress to the substrate and thermally annealing the substrate under stress. The primary advantage of the proposed approach is that a single, reusable template is used to induce the compositional variation for multiple substrates. The compositional redistribution of Ge is predicted under purely elastic deformation, using a lattice kinetic Monte-Carlo simulation that accounts for the influence of composition, temperature, and stress on the diffusion kinetics of Ge in SiGe alloy. Atomistic stress field in a SiGe slab is computed using the Tersoff empirical potential and static relaxation. This compositional variation in turn can be used to selectively grow a 2D array of Ge quantum dots upon Ge exposure. To complement the computational prediction, the compressive stress is applied by pressing a 2D array of Si pillars against the $\text{Si}_{0.8}\text{Ge}_{0.2}$ substrate. Hertz contact model is used to calculate the compressive stress applied to the $\text{Si}_{0.8}\text{Ge}_{0.2}$ substrate under the Si nanopillars. We observe that the magnitude of compressive stress and annealing temperature determine the nature of deformation (elastic or plastic) in the $\text{Si}_{0.8}\text{Ge}_{0.2}$ substrate. Corresponding energy dispersive x-ray spectroscopy (EDS) shows that the compositional redistribution of Si and Ge in the near-surface region of $\text{Si}_{0.8}\text{Ge}_{0.2}$ substrates results from elastic deformation within a thermal annealing temperature range of 950 to 1000 °C and an applied stress range of 15 to 18 GPa. Based on nano-probe EDS, the elastically deformed compressed region shows near-complete Ge depletion and Si enrichment in atomic concentration. However, the temperature and stress exceeding the aforementioned ranges result in plastic deformation with no compositional variation. The plastic deformation depth is ~30 nm according to scanning transmission electron microscope images. We attribute the plastic deformation to (1) the localized pressure applied to the substrate under the contact area, (2) the near-surface substrate stiffness at substrate temperature, and (3) the tensile biaxial stress under the compressed region due to different thermal expansion rates of Si vs. $\text{Si}_{0.8}\text{Ge}_{0.2}$.

5:00pm EM1-ThA9 DFTMD Modeling of Atomic Scale Structure Requirements for amorphous Sub 0.5 EOT Gate Oxides, T. Kent, T. Kaufman-Osborn, M. Edmonds, S.W. Park, J.H. Park, L.J. Kwak, E.A. Chagarov, University of California, San Diego, P. Choudhury, New Mexico Institute of Mining and Technology, R. Droopad, Texas State University, Andrew C. Kummel, University of California, San Diego
For EOT scaling below 0.5 nm on FinFETs, it is necessary to nucleate the ALD in 99% of the unit cells on multiple crystallographic faces to obviate the requirement that the oxide overgrow non-reactive unit cells. (1) DFTMD calculations of high-k/InGaAs stacks annealed at 700K show that oxide bonding to each InGaAs surface atom in each cell is critical to avoid dangling bonds creating conduction band edge states; this requires high ALD nucleation by a metal precursor density follow by oxidation of any metal-metal bonds formed during nucleation. For III-V semiconductors, experimental STM and STS studies show the in-situ exposure of just a few hundred Langmuirs of atomic H readily removes both group V and group III oxides from 001 and 110 surfaces allowing high nucleation density of metal ALD precursors. Concurrent MOSCAP studies show demonstrate sub 0.5 nm EOT gate oxides with low defect densities on InGaAs after in-situ cleaning and high nucleation density ALD. (2) DFTMD studies of the $\text{a-Al}_2\text{O}_3/\text{SiGe}(001)$ stack show that the $\text{SiGe}(001)$ interface with Si termination ($\text{a-Al}_2\text{O}_3/\text{Si-SiGe}(001)$) has a superior electronic structure to the interface with Ge termination ($\text{a-Al}_2\text{O}_3/\text{Ge-SiGe}(001)$). Silicon termination of SiGe should also be highly favorable for forming gas passivation of dangling bonds. For $\text{SiGe}(001)$ a novel technique has been developed to produce surface which will mimic the good passivation properties of $\text{Si}(001)$ by terminating the surface in a monolayer of Si-OH which will

react with nearly any metal ALD precursor. (3) While group IV and III-V semiconductors can be nucleated by covalent bonds, 2D semiconductors require a different approach. DFTMD simulation studies show the metal coordination complexes can readily chemisorb on 2D semiconductor via non-bonding interaction and they can covalent bond multiple TMA molecules consistent with a submolecular nucleation density. A technique has been developed for functionalize 2D semiconductors with a phthalocyanine, and it has been demonstrated it can nucleate insulation sub 1nm gate oxide growth.

5:20pm EMI-ThA10 Crystalline SrHfO₃ Grown Directly on Ge (001) by Atomic Layer Deposition as a Gate Oxide for High-Mobility Ge-based Transistors, Martin McDaniel, T.Q. Ngo, A.B. Posadas, C. Hu, S.N. Chopra, E.T. Yu, A.A. Demkov, J.G. Ekerdt, The University of Texas at Austin

Crystalline strontium hafnate, SrHfO₃ (SHO), is an ideal candidate to study as a suitable high-*k* gate dielectric on Ge. SHO (*a* ~ 4.069 Å) has a reasonable lattice match to the Ge (001) surface (*a*/√2 ~ 3.992 Å), yielding a ~1.9% compressive strain in the epitaxial film. SHO shows a high permittivity (*k*~20) with appropriate band alignment (~1 eV offset) to Ge. In addition, the crystalline nature of the SHO film is expected to drastically reduce the interface trap density at the oxide-Ge interface. We will report our recent results on the growth, characterization, and electrical performance, of epitaxial SHO films and heterostructures for next-generation high-*k* dielectrics on Ge.

In our recent publication, we reported on the direct growth of crystalline strontium titanate, SrTiO₃ (STO), on Ge via atomic layer deposition.^[1] Electrical measurements of a 15-nm thick undoped STO film show a large dielectric constant (*k*~90), but high leakage current (~10 A/cm² at +1 eV). In the present work, the unfavorable conduction band offset (and high leakage current) of STO on Ge is circumvented by growing the Hf-based perovskite, SHO. For the growth of SHO, we employ the commercially available strontium bis(triisopropylcyclopentadienyl) and hafnium formamidate precursors. After thermal deoxidation, the Ge substrate is transferred *in vacuo* to the deposition chamber where a thin film of SHO (2-4 nm) is deposited by ALD at 225 °C. Following post-deposition annealing at 700 °C, the perovskite film becomes crystalline with epitaxial registry to the underlying Ge (001) substrate. *In situ* x-ray photoelectron spectroscopy confirms stoichiometric to Sr-rich films with no GeO_x formation or carbon impurities.

Ex situ x-ray diffraction confirms the perovskite structure and orientation of the SHO film. Thicker SHO films (above 2 nm) appear to show a relaxed lattice constant, indicating relaxation of the epitaxial film above the critical thickness. The electrical performance of several SHO films and heterostructures will be presented. In general, the leakage current is reduced by several orders of magnitude for the SHO films versus STO on Ge. The current work demonstrates the promise for crystalline oxides grown by ALD on Ge for advanced semiconductor devices, including high-mobility Ge-based transistors.

[1] M. D. McDaniel *et al.*, "A Chemical Route to Monolithic Integration of Crystalline Oxides on Semiconductors," accepted to *Adv. Mater. Interfaces* (2014), doi: 10.1002/admi.201400081.

5:40pm EMI-ThA11 The Influence of Carbon Incorporation into Gd₂O₃ High-k Gate Dielectric on the Electronic Behavior of the MOS Stack, Pini Shekhter, Technion Israel Institute of Technology, Israel, A.R. Chaudhuri, Leibniz University, Germany, A. Laha, Indian Institute of Technology Bombay, India, H.J. Osten, Leibniz University, Germany, M. Eizenberg, Technion Israel Institute of Technology, Israel

High *k* dielectric materials receive great attention in recent years due to the downscaling of metal-oxide-semiconductor (MOS) devices leading to the need in replacing the traditionally used SiO₂ gate oxide. Rare earth oxides are leading candidates as high-*k* dielectrics. Introduction of different elements into the bulk of such oxides can drastically alter the behavior of the MOS stack.

Here we present the results of incorporation of carbon into the bulk of Gd₂O₃ on the electrical properties of the Pt/Gd₂O₃:C/Si stack. Crystalline layers of stoichiometric Gd₂O₃ were MBE deposited together with elemental C on Si (100) substrates. Four samples with different concentration of elemental C were prepared: 0%, 0.10%, 0.67% C and 1.89%. MOS capacitors were prepared by *in-vacuo* (in the MBE tool) evaporating Pt through a shadow mask.

Capacitance voltage (C-V) measurements revealed an increase in the flatband voltage (*V_{fb}*) for the carbon rich sample. While the three samples with the lower carbon content all showed *V_{fb}* voltages of -0.1 ± +0.2 V, the sample with 1.89% carbon presented a significant increase to 2.25 V.

X ray diffraction (XRD) revealed that all the layers hold the same structure and that no orientation differences are present in the layers, ruling out the option of structural differences leading to such a change in *V_{fb}*. Time of flight secondary ion mass spectroscopy (ToF-SIMS) depth profiles revealed an uneven concentration profile for the carbon in the 0.67% and 1.89% samples. For both samples, the same concentration was found in the bulk of the layer, indicating the existence of a certain solubility limit that had been exceeded. This led to some segregation for the 0.67% sample to the inner interface while substantial segregation was observed in the 1.89% sample to the inner interface and some to the outer surface. Transmission electron microscope (TEM) micrographs show a thin amorphous interface layer that is formed between the Gd₂O₃ and Si that most likely plays a role in the capturing of the segregating carbon atoms.

We propose that the carbon segregation causes a modification of *V_{fb}* which is an important property of the MOS stack. By using carbon incorporation it might be possible to develop an effective method for controlling *V_{fb}* without changing the process or materials for any of the MOS gate components.

Electronic Materials and Processing Room: 314 - Session EM2-ThA

Hybrid and Organic Electronics

Moderator: Sean King, Intel Corporation, Rachael Myers-Ward, U.S. Naval Research Laboratory

4:00pm EM2-ThA6 Innovating Organic Electronics and Photonics, Bernard Kippelen, Georgia Institute of Technology INVITED

Printed organic electronics, a technology based on organic semiconductors that can be processed into thin films using vacuum processing or conventional printing and coating techniques, has been the subject of active research and development over the past decades. A range of solid-state devices, including organic light-emitting diodes (OLEDs), organic field-effect transistors (OFETs), photodiodes, and solar cells, have been demonstrated with this new class of materials. However, despite a steady progress in performance, many challenges remain and further scientific and technological advances are required before this emerging technology can unleash its full potential.

In this talk, we will review recent advances both in materials and device architectures in a series of organic semiconductor devices. First, we will present progress in organic light-emitting devices with an unconventional architecture that yield current efficiencies of 200 cd/A at a luminance of 1000 nits and 100 cd/A at 100,000 nits. Next, we will discuss a new organic field-effect transistor geometry that yield unprecedented environmental stability and allows for continuous reversible sensing in aqueous media. In a third part, we will discuss recent advances in organic photovoltaic devices. A new method to produce air-stable low work function electrodes as a substitute for Ca will be presented. This method is based on surface modification by water-soluble polymers that physisorb to the surface of various conductors and lead to large surface dipoles that shift the vacuum level (> 1 eV) reducing the injection or collection barrier for electrons. We will show that these advances in interface modification can be used to design organic solar cells with novel architectures that can overcome some of the economic hurdles of current approaches and accelerate the deployment of these technologies. We will show that the current-voltage characteristics of organic solar cells can be modeled with engineering-inspired equivalent circuit models. Strategies based on transfer lamination will be presented that allow for a drastic reduction of parasitic shunt effects, enabling solar cells with unprecedented dynamic range. Finally, we will discuss how to minimize the environmental footprint of organic electronic technologies.

4:40pm EM2-ThA8 Role of Light Scattering in Hybrid Solar Cells, James Dorman, M. Noebels, T. Pfadler, J. Weickert, L. Schmidt-Mende, University of Konstanz, Germany

Hybrid solar cells, with an inorganic/organic interface for charge separation, have been extensively investigated in the past decade in order to replace the expensive Si based technology with an inexpensive alternative. Typically, these devices incorporate a mesoporous TiO₂ film which is decorated with dye molecules and filled with a hole transport material, to conduct the electrons and holes, respectively. Recently, devices with an liquid electrolyte have been able to reach up to 13% conversion efficiency. However, the TiO₂ mesoporous films used for solid state dye sensitized solar cells and hybrid solar cells have a limited light absorption due to thickness of the film (500 nm – 2 μm) required for efficient charge transportation. An elegant approach to increase the light absorption is to induce "defects" within the mesoporous film, causing light to scatter within

the active layer of the device. In this work, we combine the commonly used 25 nm particles with other nanostructures, including 200 nm TiO₂ particles, TiO₂ nanowires, and Sn doped nanowires, all of which produce light scattering due to their dimensions and disorder within the active layer. Through this approach, we are able to correlate an improvement in conversion efficiencies of around 25 % to the light scattering. Furthermore, the incorporation of these nanowire structures increases the mobility of the electrons, allowing for increased charge extraction and reduced recombination. These two phenomena can be simultaneously engineered due to the crystallinity of the “defects” within the films and the cascading conduction bands produced with the incorporation of the doped TiO₂ wires. The extent of the reduction in recombination is quantified through photovoltage decay and impedance spectroscopy measurements and compared to the standard mesoporous TiO₂ devices.

5:00pm **EM2-ThA9 The Structure and Energetics of the Calcium / Phenyl-C₆₁-butyric Acid Methyl Ester Interface**, *James Lownsbury, C.T. Campbell*, University of Washington

The vapor deposition of metal films onto the surfaces of organic semiconductors, especially fullerene derivatives and π -conjugated polymers, plays an important role in the fabrication and long-term stability of organic electronic, optoelectronic and photovoltaic devices. Nevertheless, the strength and structural details of metal-organic bonding at such interfaces is not well known. We report here measurements of the interface structure and adsorption energies of calcium metal films grown by vapor deposition on phenyl-C₆₁-butyric acid methyl ester (PCBM). PCBM is a much studied electron acceptor material used in a vast array of organic electronic devices, most notably organic photovoltaics, and Ca metal is often used as the cathode material for such devices due to efficient electron collection at the cathode-active layer interface. Structural details of the interface and the morphology of the evolving metal film were measured using low-energy ion scattering spectroscopy and X-ray photoelectron spectroscopy. The energetics of interfacial bonding were measured using an adsorption microcalorimeter which is unique in the world, and which has been applied previously to the adsorption of Ca on common and well-researched electron donor materials including derivatives of poly(phenylene-vinylene), polyfluorene, and polythiophene. Spin-cast PCBM samples were prepared under nitrogen environment and transferred to our ultrahigh vacuum chamber without exposure to atmosphere. There, a pulsed beam of calcium atoms was directed at the sample surface. By simultaneously measuring the heat of adsorption and the sticking probability of the metal atoms as a detailed function of metal coverage, we obtain interfacial bonding energies for Ca on PCBM.

Work supported by the National Science Foundation under grant CHE-1010287

5:20pm **EM2-ThA10 Controlling the Electronic Structure of Organic Semiconductors via Doping**, *Antoine Kahn*, Princeton University **INVITED**

Typical organic (molecular and polymer) semiconductors (OSC) used in organic light emitting diodes, field-effect transistors or photovoltaic cells have energy gaps upwards of 1.5-2 eV and have very low conductivity due to the exceedingly small density of “free” carriers and the localized nature of these carriers. Chemical doping has proven to be an extremely powerful tool for controlling the electronic structure of these materials, in particular for improving charge carrier injection at contacts. This talk will review recent developments in the area of chemical doping of OSCs [1,2]. The reducing or oxidizing power of a number of n- and p-type organic dopants are reviewed, along with their impact on the electronic structure and conductivity of both vacuum- or solution-processed OSC films. In particular, the talk will outline recent work aimed at passivating, or compensating, deep electronic gap states, or traps, which are due to structural or chemical imperfections and profoundly affect interface energetic and carrier transport [3]. The process implies the control of ultra-low concentrations of dopants just sufficient to fill traps states and render them inactive, without adding significant densities of “free” carriers in the system. Impact on device characteristics will be reviewed [4].

[1] C. K. Chan et al. *Org. Elect.* **9**, 575 (2008)

[2] G. Song et al. *Adv. Mat.* **24**, 699 (2012)

[3] S. Olthof et al., *Phys. Rev. Lett.* **109**, 176601 (2012)

[4] S. Olthof et al., *Appl. Phys. Lett.* **101**, 253303 (2012)

Helium Ion Microscopy Focus Topic Room: 316 - Session HI+2D+AS+MC-ThA

Nanoengineering with Helium Ion Beams

Moderator: Armin Götzhäuser, University of Bielefeld, Germany, David C. Joy, University of Tennessee, Oak Ridge National Laboratory

2:20pm **HI+2D+AS+MC-ThA1 Helium Ion Microscopy (HIM) Technology for Imaging, Characterization, and nano-Fabrication for nano-Device Materials and Structures**, *Shinichi Ogawa*, NeRI, AIST, Japan **INVITED**

Several unique applications of a helium ion microscopy (HIM) technology have been studied. In comparison with electron, helium ion has larger cross section, and it realized HIM observation with less current because of higher efficiency of secondary electron generation with maximum distribution energy of 1 eV [1], a few eV in a SEM case, for imaging, which results in less power implant (less thermal damage input) into samples. Utilizing these features, a low dielectric constant material pattern of 70 nm line with less deformation (thermal damage) and a Cu metal line underneath a 130 nm dielectric of band gap of a few eV were imaged [2]. Luminescence from a SiO₂ sample was detected at imaging conditions [3], in which no damage was observed by a transmission electron microscopy (TEM) - electron energy loss spectroscopy method [4]. As one of nano-fabrication applications, we found that a helium ion irradiation using the HIM functionalizes a gate control of carrier conduction in a single-layer graphene at an appropriate amount of helium ion dose to graphene which enable gate bias control of current with an on-off ratio of two orders of magnitude at room temperature [5], [6]. A few nm diameter tungsten particles were deposited onto a TEM sample under the helium ion beam irradiation in W(CO)₆ gas atmosphere with high special resolution accuracy, which realized precise electron tomography and re-construction [7], and tungsten pillars of a few nm height with 40 nm diameter were formed with a straight hole of a few nm diameter through a center of the pillars [8]. The research on graphene material is granted by JSPS through FIRST Program initiated by CSTP.

References: [1] Y. V. Petrov, O.F. Vyvenko, and A. S. Bondarenko, *J. Surface Investigation*, 792 (2010), [2] S. Ogawa, W. Thompson, L. Stern, L. Scipioni, L. Notte, L. Farkas, and L. Barriss, *Jpn. J. Appl. Phys.*, 49 04DB12 (2010), [3] S. Ogawa, T. Iijima, S. Awata, S. Kakinuma, and T. Kanayama, *Proc. of International Interconnect Technology Conference* (2011), [4] Y. Otsuka, Y. Shimizu, N. Kawasaki, S. Ogawa, and I. Tanaka, *Jpn. J. Appl. Phys.*, 49 111501 (2011), [5] S. Nakaharai, T. Iijima, S. Ogawa, H. Miyazaki, S. Li, K. Tsukagoshi, S. Sato, and N. Yokoyama, *Appl. Phys. Express*, 5 015101 (2012), [6] S. Nakaharai, T. Iijima, S. Ogawa, S. Suzuki, S. Li, K. Tsukagoshi, S. Sato, N. Yokoyama, *ACS Nano*, 7 (2013) 5694-5700, [7] M. Hayashida, T. Iijima, T. Fujimoto and S. Ogawa, *Micron* 43, 992-995 (2012), [8] K. Kohama, T. Iijima, M. Hayashida, and S. Ogawa, *J. Vac. Sci. Technol. B* 31 (3), 031802 (2013)

3:00pm **HI+2D+AS+MC-ThA3 MEMS Temperature Controlled Sample Stage for the Helium Ion Microscope**, *Jose Portoles, P.J. Cumpson*, Newcastle University, UK

The Helium microscope allows the imaging of samples with magnifications beyond those of electron microscopes with the added advantages of directly imaging insulators without being so critically dependent on a need to conductive coating the samples. This facilitates the imaging of for instance organic structures without the need of surface modification. The large depth of focus allows simultaneously focusing details of the sample at different depths. When using a temperature controlled stage this allows the samples to stay focused as thermal expansion produces vertical displacements of the sample surface, however due to the large magnifications in-plane thermal expansions are still an issue. We have investigated a solution based on a thermally actuated X-Y MEMS stage by exploiting the ability of MEMS actuators to provide smooth electronic control of lateral displacements in the micron range in order to compensate for lateral thermal expansion at the point of observation. The difficulties involved in producing relatively large out of plane displacements with a MEMS device can be neglected due to the large instrumental depth of focus. The device we present has been fabricated using a “silicon on insulator” (SOI) MEMS process, and can be driven at low voltages and currents using a standard vacuum feedthrough to the instrument's analysis chamber and compensate lateral thermal expansion in order to keep any spot on a small specimen in the field of view at high magnifications. The small size of the heating stage makes it rapid in its thermal response.

3:20pm **HI+2D+AS+MC-ThA4 Monte Carlo Simulations of Focused Neon Ion Beam Induced Sputtering of Copper**, *Rajendra Timilsina, P.D. Rack*, The University of Tennessee Knoxville, *S. Tan, R.H. Livengood*, Intel Corporation

A Monte Carlo simulation has been developed to model the physical sputtering and nanoscale morphology evolution to emulate nanomachining with the Gas Field Ion Microscope. In this presentation, we will present experimental and simulation results of copper vias milled by a focused neon ion beam. Neon beams with a beam energy of 20 keV and a Gaussian beam profile with full-width-at-half-maximum of 1 nm were simulated to elucidate the nanostructure evolution during the physical sputtering of high aspect ratio features. In this presentation we will overview our simulation attributes which includes an evolving real-time sputtered via profile considering both the sputtered and re-deposited material. The sputter yield and sputter profile vary with the ion species and beam parameters and are related to the distribution of the nuclear energy loss in the material. We will also illustrate how the effective sputter yield is aspect-ratio dependent due to the change in the effective escape angle of the sputtered species. Quantitative information such as the sputtering yields, dose dependent aspect ratios and resolution-limiting effects will be discussed. Furthermore, we will show that the calculated nuclear energy loss and implant concentration ahead of the sputtering front correlates to observed damage revealed by transmission electron microscopy.

4:00pm **HI+2D+AS+MC-ThA6 Circuit Edit Nanomachining Study using Ne+ & He+ Focused Ion Beam**, *Richard Livengood, S. Tan*, Intel Corporation **INVITED**

FIB nanomachining has been used extensively for over 20 years for the purpose of rewiring integrated circuits to validate design changes, isolate process faults, and generate engineering samples. During this time frame, the minimum feature size of an IC (Moore's Law) has scaled from 500nm to 14nm (36X) compared with ~6X scaling of Ga+ FIB. As a result FIB nanomachining capabilities have been steadily eroding over the last several generations, limiting the types of circuit modifications that can be successfully completed. There are however, several promising new ion beam scaling R&D initiatives that provide hope of enabling further nanomachining scaling into the sub 10nm process node.

One such technology is GFIS (gas field ion source) technology. He+ GFIS based FIBs have been successfully used to image with sub 0.5nm resolution and nanomachine sub 10 nm structure in Au, Graphene, and other thin film structures.[1, 2, 3] More recently He+ and Ne+ GFIS sputtering properties have been studied for nanomachining in bulk semiconductor films.[4] In this paper, we will show our latest results on GFIS FIB GAE (gas assisted etch) nanomachining and IBID properties and electrical invasiveness impact.

References

- [1] J. Notte, M. Rahman, L. Farkas, S. Tan, and R. Livengood, *Scanning* 33, 1 (2011).
- [2] D. S. Pickard, V. Viswanathan, M. Bosman, J. Dorfmüller, H. Giessen, Z. Ai, H. Hao, M. Mahmoudi, Yue Wang and Chao Fang, Invited talk, EIBPN-HIM Session (2012)
- [3] V. Sidorkin, E. v. Veldhoven, E. v der Drift, P. Alkemade, H. Salemink, D. Mass, *J. Vac. Sci. Technol. B* 27 (4) (2009)
- [4] S. Tan, R. Livengood, D. Shima, P. Hack, R. Hallstein, J. Notte, and S. McVey, *JVST B*, 29 (6), 06F604 (2011).

4:40pm **HI+2D+AS+MC-ThA8 Evaluation of EUV Resist Performance below 20-nm CD using Helium Ion Lithography**, *D.J. Maas*, TNO Technical Sciences, Netherlands, *Nima Kalthor*, TU Delft, Netherlands, *W. Mulckhuysse, E. van Veldhoven*, TNO Technical Sciences, Netherlands, *A. van Langen-Suurling, P.F.A. Alkemade*, TU Delft, Netherlands, *S. Wuister, R. Hoefnagels, C. Verspaget, J. Meessen, T. Fliervoet*, ASML, Netherlands
For the introduction of EUV lithography, development of high performance EUV resists is of key importance. This development involves studies into sensitivity, resolving power and pattern uniformity. We have used a sub-nanometer-sized 30 keV helium ion beam to expose chemically amplified (CAR) EUV resists.

There are remarkable similarities in the response of resists to He⁺ ions and EUV photons. Both primary particle beams traverse the resist and meanwhile interact with the target atoms. The low backscattering of the He⁺ ions results in ultra-low proximity effects, which is similar to EUV exposure. Absorption of an EUV photon creates a high-energy electron that relaxes by the excitation of Secondary Electrons (SEs). A collision of a 20-30 keV helium ion with a target atom directly releases low-energy SEs. Each ion scatters several times in the resist layer, thus enabling resist exposures at very low doses per CH. The energy spectra of SEs generated by EUV and He⁺ are remarkably alike. These SEs, in turn, activate the resist.

In this paper we show 30 keV He⁺ ions exposures of contact holes and lines with a CD of 8 – 30 nm at 20 nm half-pitch in a chemically amplified EUV resist. We will demonstrate the potential of using He⁺ ion lithography [1,2] in the study of EUV resists.

[1] V. Sidorkin et al., *Sub-10-nm nanolithography with a scanning helium beam*, *J. Vac. Sci. Technol. B* 27, L18 (2009)

[2] D. Maas et al., *Evaluation of EUV resist performance below 20nm CD using helium ion lithography*, *SPIE Proc.* 9048, 90482Z (2014)

5:00pm **HI+2D+AS+MC-ThA9 Helium Ion Beam Lithography for Nanoscale Patterning**, *X. Shi*, University of Southampton, UK, *D.M. Bagnall*, University of New South Wales, UK, *Stuart Boden*, University of Southampton, UK

Electron beam lithography (EBL), the modification of thin films of resist by a focused beam of electrons to create a pattern that is subsequently transferred into the substrate, is a key technology in the development of nanoscale electronic devices. However, with the demand for ever smaller features and pattern dimensions, new lithographic techniques are required to extend beyond existing limits of EBL. One such emerging technology is helium ion beam lithography (HIBL), driven by the development of the helium ion microscope, a tool capable of producing a high intensity beam of helium ions focused to a sub-nanometer spot [1]. Preliminary studies on HIBL using typical EBL resist materials such as PMMA and HSQ have shown that HIBL has several advantages over EBL, including a smaller spot size (potentially leading to higher resolution patterning) and a decrease in the exposure dose required and so the potential for faster pattern definition and therefore higher throughput. Furthermore, proximity effects, which are caused by beam scattering leading to inadvertent exposure of surrounding material, and are problematic when producing high density patterns in EBL, are massively reduced in HIBL [2], [3].

Here, the latest results from an experimental investigation into the HIBL technique will be presented. Areas of PMMA films of various thicknesses are exposed to different helium ion doses. After subsequent development in MIBK/IPA, atomic force microscopy is used to measure residual layer thickness in order to generate exposure response curves for different initial thicknesses of resist. High sensitivity is confirmed with full exposure of 50 nm thick layers achieved with a helium ion dose of only ~2 μC/cm². Experiments to characterise minimum feature size and proximity effects are currently underway. The use of other high resolution resists will also be investigated with the aim of providing a thorough assessment of the capabilities and limitations of this emerging nano-patterning technique.

[1] L. Scipioni, L. A. Stern, J. Notte, S. Sijbrandij, and B. Griffin, "Helium Ion Microscope," *Adv. Mater. Process.*, vol. 166, pp. 27–30, 2008.

[2] D. Winston, B. M. Cord, B. Ming, D. C. Bell, W. F. DiNatale, L. A. Stern, A. E. Vladar, M. T. Postek, M. K. Mondol, J. K. W. Yang, and K. K. Berggren, "Scanning-helium-ion-beam lithography with hydrogen silsesquioxane resist," *J. Vac. Sci. Technol. B.*, vol. 27, no. 6, pp. 2702–2706, 2009.

[3] V. Sidorkin, E. van Veldhoven, E. van der Drift, P. Alkemade, H. Salemink, and D. Maas, "Sub-10-nm nanolithography with a scanning helium beam," *J. Vac. Sci. Technol. B.*, vol. 27, no. 4, p. L18, 2009.

5:20pm **HI+2D+AS+MC-ThA10 Sub-100nm Nanofabrication using Helium and Neon Ion Beams**, *James Sagar, C. Nash, N. Braz, T. Wootton, M.J.L. Sourribes, T.-T. Nguyen, R.B. Jackman, P.A. Warburton*, London Centre for Nanotechnology, UK

Sub-100nm Nanofabrication using Helium and Neon Ion Beams

J. Sagar¹, C. R. Nash¹, N. Braz^{1,2}, T. Wootton^{1,2}, M. J. L. Sourribes^{1,2}, T.-T. Nguyen^{1,2}, R. B. Jackman^{1,2}, and P. A. Warburton^{1,2}

¹London Centre for Nanotechnology, University College London, 17-19 Gordon Street, London, WCH1 0AH, UK

²Department of Electrical and Electronic Engineering, University College London, London, WC1E 7JE, UK

Using a Zeiss Orion NanoFab we have created sub-100nm devices for experiments in quantum electronics and nanophotonics. The Orion NanoFab has the ability form an ion beam with either helium or neon gas. This makes the NanoFab a much more versatile instrument for nanofabrication since large area mills can be performed using Ne without the need for a Ga FIB column. The use of a Ne gas field ion source (GFIS) in the Orion NanoFab allows fabrication of sub-100nm devices on timescales comparable to that of conventional liquid Ga FIB but with considerably enhanced fidelity due to an increased sputter yield (ten times greater than that of He) whilst retaining a small probe size (≤ 5nm). Using a Ne ion beam we have fabricated two kinds of nanoscale superconducting devices: a superconducting nanowire based on a compound low-T_C superconductor; and an array of nanoscale Josephson junctions based on a compound oxide high-T_C superconductor. The use of an inert-gas ion species in these devices

is extremely important as Ga implantation into superconducting materials has previously been shown to suppress superconductivity. The extremely small probe size of the He GFIS has allowed us to create sub-20nm apertures in a variety of materials. Sub-20nm apertures in InAs nanowires and in graphene have been fabricated for experiments in quantum coherent electronics and quantum nanophotonics respectively.

Manufacturing Science and Technology

Room: 302 - Session MS+PS+TF-ThA

Functionalization of Paper and Textiles & Their Applications

Moderator: Jack Rowe, North Carolina State University, Bridget R. Rogers, Vanderbilt University

2:20pm **MS+PS+TF-ThA1 Vapor-Phase Infiltration of Cellulose and Cotton**, *Mato Knez, K. Gregorczyk, M. Garcia, I. Azpitarte*, CIC nanoGUNE, Spain, *D. Pickup, C. Rogero*, Centro de Fisica de Materiales (CSIC-UPV-EHU), Spain **INVITED**

There is a significant interest in using inexpensive biological materials as substrates and scaffolds for emerging applications due to their natural occurrence. Of particular importance is the use of paper based materials and substrates for potential applications in energy storage, catalysis, solar cells, etc. Atomic layer deposition (ALD) has been proven to be the technique of choice to modify paper and other cellulose based materials due to its low reaction temperatures, extreme thickness control, and conformality. Furthermore, vapor phase infiltration techniques, which are a recent modification to ALD, have allowed infiltration of metal-organic precursors into a variety of organic materials including spider silk, porphyrins, and polytetrafluoroethylene (PTFE), leading to a more detailed understanding of the reaction between these organic substrates and the metal-organic precursors, as-well-as surprising changes in bulk properties. Understanding the chemical interactions between precursors and substrates are crucial in order to approach applications. We modified cellulose and cotton with common ALD precursors and monitored the chemical changes after the reaction a semi-*in-situ* XPS experiments. Our findings show that the precursors induce small, but important changes to the biopolymer upon chemical interaction and that the precursors indeed react different to each other. The experiments also compare well to the final results of standard *ex-situ* XPS. Changes in the bulk mechanical properties of the substrates were studied through use of tensile testing. The ultimate tensile strength (UTS), Young's modulus (YM), and toughness are shown to be a non-linear function of both the precursor used and the number exposure cycles.

3:00pm **MS+PS+TF-ThA3 Patterned Photoreduction of Metal Atoms on Polymeric Substrates for Flexible Electronic Applications**, *Halil Akyildiz, J.C. Halbur*, North Carolina State University, *A.T. Roberts*, Redstone Arsenal, *H.O. Everitt*, Duke University, *J.S. Jur*, North Carolina State University

Flexible electronics are of interest for displays, sensors, and health monitoring systems. Polymeric substrates, being flexible, easy to manufacture and inexpensive, are wanted for such applications. However, polymers, aside from good properties usually require alteration of electronic and optical properties. Sequential vapor infiltration (SVI) is a technique that modifies polymer properties by formation of hybrid materials via infiltration of organometallic precursors into bulk polymers. In this work we present how SVI tailors the optical properties of polyethylene terephthalate (PET) fibers by infiltration of trimethylaluminum (TMA) precursors to form PET-Alumina hybrid structures. Photoluminescence (PL) spectroscopy showed an order of magnitude increase in photoluminescence as compared to the pristine PET fibers which is attributed to the increased interactions between polymer chains by formation of alumina polymer coordination complexes. Furthermore metal ions out of a metal salt solution were reduced onto the modified substrates by photo catalytic effect. Patterned silver lines on PET fabric were successfully achieved by selective excitation of the fabric using a laser source showing promising results for integration of electronic devices.

3:20pm **MS+PS+TF-ThA4 Multifunctional Fabrics via Tungsten ALD on Kevlar**, *Sarah Atanasov, B. Kalanyan, G.N. Parsons*, North Carolina State University

Multifunctional materials combine two or more distinct capabilities into a single article unit. Kevlar is a high strength fiber used for personal protection and other mechanically demanding applications. Adding conductivity to Kevlar creates a new multifunctional protective/electronic material for electromagnetic shielding, communications, and erosion

resistant, anti-static fabrics and cables for space and automotive technologies. For this study, we coated Kevlar fibers and woven mats with ALD tungsten, using WF_6 and dilute silane (SiH_4 , 2% Ar) at 220°C. Kevlar's thermal stability makes it a very amenable polymer for ALD coating at relatively high temperatures. Before W ALD, we deposited a TiO_2/Al_2O_3 bilayer by ALD onto the Kevlar, at various temperatures (50-220°C). The Al_2O_3 layer promotes W nucleation. The TiO_2 layer is important because previous mechanical analysis indicates that the TMA precursor degrades the Kevlar polymer backbone, whereas TiO_2 ALD using $TiCl_4$ and H_2O was less damaging. XPS analysis confirms the presence of TiO_2 , Al_2O_3 and W on the fibers after each coating step. After W ALD, the yarns and mats are highly conductive (~3000 S/cm) and remain flexible. Tensile testing shows that upon coating with 20 ALD cycles, the strength of the Kevlar decreases from 3.32 GPa to 3.02 GPa. The ability to create highly conductive Kevlar with mechanical strength within 90% of the original mechanical performance could open new areas of application for large area low temperature ALD processing.

4:00pm **MS+PS+TF-ThA6 Direct and Self-Assembly of Nanocellulose Cleaved from Fiber Cell Walls and Integration in Device Manufacture**, *Orlando Rojas*, North Carolina State University **INVITED**

We introduce our work related to the application of surface and colloid science in the development of cellulose nanomaterials. These efforts take advantage of the process by which nature assembles fibers in a highly hierarchical structure encompassing a wide range of sizes, from the nano to the meter scales. A number of materials cleaved from the cell wall have been the subject of intensive research, including, nanofibrillar cellulose and cellulose nanocrystals, i.e., defect-free, rod-like crystalline residues after acid hydrolysis of cellulose fibers. Interest in nanocellulose originates from its appealing intrinsic properties: nanoscale dimensions, high surface area, unique morphology, low density, chirality and mechanical strength. Directing their assembly back to different hierarchical structures is a quest that can yield useful results in many revolutionary applications. As such, we will discuss the use of non-specific forces to create ultrathin films of nanocellulose at the air-solid interface for applications in nanocoatings, sensors, etc. Assemblies at other interfaces will be introduced as means to produce Pickering emulsions. Methods common in biophysics and employed to control the packing density of nanocellulose at the air-liquid and air-solid interfaces will be presented. A convective assembly setup assisted by shear and electric fields will be discussed as a suitable method to produce highly ordered structures. Concepts related to piezoelectric cellulose nanocrystal films, organic-inorganic hybrid materials with magnetic and other properties. Overall, the prospects of such novel materials will be explained in light of the unique properties of cellulose and its nanostructured assemblies.

5:20pm **MS+PS+TF-ThA10 Van der Waals Materials on Nanostructured Paper -- Aqueous Gating and Sensing Application**, *Wenzong Bao, Z. Fang, J. Wan, L.B. Hu*, University of Maryland, College Park

We report the first aqueous transistors on a bilayer-structured paper with a nanoscale smoother surface. Such transistors have a planar structure with source, drain and gate electrodes on the same surface of paper, and the mesoporous paper is used as an electrolyte container. Such transistors are enabled by a bilayer-structured all-cellulose paper with nano-fibrillated cellulose on the top surface that leads to an excellent surface smoothness, while the rest of micro-sized cellulose fibers can absorb electrolyte effectively. Based on 2D Van der Waals materials such as graphene and MoS_2 , we demonstrate high-performance transistors with large on-off ratio. Our devices also show excellent bending flexibility. Such planar transistors with absorbed electrolyte gating can be used as sensors integrated with other components towards paper microfluidic systems.

5:40pm **MS+PS+TF-ThA11 Mechanistic Understanding of Anomalous Scaling Law of Mechanical Properties of Nano-Cellulose Paper**, *S. Zhu, Z. Jia, Y. Li, Z. Fang, S. Parvinian, N.J. Weadock, O. Vaaland, Y.C. Chen, L.B. Hu, Teng Li*, University of Maryland, College Park

The quest of both strength and toughness is perpetual in advanced material design; unfortunately, these two mechanical properties are generally mutually exclusive. A general and feasible mechanism to address the conflict of strength vs. toughness still remains elusive. Here we demonstrate an anomalous but highly desirable scaling law of the mechanical properties of cellulose nanopaper: both its strength and toughness increase simultaneously (40 & 130 times, respectively) as the size of the constituent cellulose fibers decreases (from a diameter of 27 microns to 10 nm). Our theoretical mechanics modeling and molecular dynamics simulations reveal the underlying mechanistic understanding of such an anomalous scaling law. These stimulating results suggest a fundamental bottom-up strategy generally applicable for other material building blocks, and thus hold the promising potential toward a new scaling law: the smaller, the stronger

AND the tougher. There are abundant opportunities to utilize the fundamental bottom-up strategy to design a novel class of functional materials that are both strong and tough.

Plasma Science and Technology Room: 308 - Session PS+SE-ThA

Atmospheric Pressure Plasma Processing; Fundamental and Applications

Moderator: Richard van de Sanden, DIFFER, Stefan Welzel, FOM Institute DIFFER

2:20pm **PS+SE-ThA1 Insights into the Chemistry of Atmospheric Pressure Plasma Deposition Processes, Fiorenza Fanelli**, Institute of Inorganic Methodologies and Plasmas - National Research Council, Italy, P. Bosso, A.M. Mastrangelo, F. Fracassi, University of Bari 'Aldo Moro', Italy **INVITED**

Over the last decade there have been considerable advances in the utilization of atmospheric pressure cold plasmas for thin film deposition. Intense research efforts have been made to develop a large variety of processes which exploit different types of atmospheric pressure discharges for the direct and remote deposition of thin films from monomers in gas, vapor and aerosol form [1]. However diagnostic studies of the plasma chemistry and mechanistic investigations of thin film growth are still scarce, while being crucial prerequisite for further process optimization. The research should be addressed to detect the film precursors, to identify the main reaction pathways (both homogeneous and heterogeneous processes) and to clarify the plasma-surface interaction.

In this contribution, our studies on thin film deposition by dielectric barrier discharges (DBDs) will be presented to provide insights into the chemistry of atmospheric pressure plasma processes. Examples discussed will include the investigation of the role of the monomer chemical structure in the plasma-enhanced chemical vapor deposition of organosilicon coatings from different methylsiloxanes [2], and the study of the influence of air and water vapor feed gas impurities in the deposition of fluorocarbon coatings from argon-hexafluoropropene fed DBDs [3]. Our recent work on the deposition and characterization of organic-inorganic hydrocarbon polymer/ZnO nanoparticles nanocomposite coatings by a DBD fed with helium and the aerosol of a dispersion of oleate-capped ZnO nanoparticles in hydrocarbon solvents will be presented [4]. Results from the plasma jet co-deposition of acrylic acid and ethylene towards water-stable coatings containing carboxylic functionalities will be also shown.

The overall deposition mechanisms will be outlined on the basis of the results from the chemical and morphological characterization of the coatings, the optical emission spectroscopy investigation of the plasma phase, the analysis of the exhaust gas by means of gas chromatography-mass spectrometry. The latter is a powerful *indirect* diagnostic technique of the gas phase which allows the assessment of the monomer depletion and the qualitative-quantitative determination of stable byproducts formed by plasma activation.

[1] F. Massines, C. Sarra-Bournet, F. Fanelli, N. Naudé, N. Gherardi, *Plasma Process. Polym.*, 9, 1041 (2012).

[2] F. Fanelli, S. Lovascio, R. d'Agostino, F. Fracassi, *Plasma Process. Polym.*, 9, 1132 (2012).

[3] F. Fanelli, R. d'Agostino, F. Fracassi, *Plasma Process. Polym.*, 8, 557 (2011).

[4] F. Fanelli, A. M. Mastrangelo, F. Fracassi, *Langmuir*, 30, 857 (2014).

3:00pm **PS+SE-ThA3 Understanding Charge Transfer Reactions at a Plasma-Liquid Interface, Paul Rumbach***, University of Notre Dame, R.M. Sankaran, Case Western Reserve University, D.M. Bartels, D.B. Go, University of Notre Dame

The interaction of atmospheric-pressure plasma jets with liquids is becoming increasingly important for medical and materials applications. Despite empirical evidence of reactions occurring both in the bulk plasma and liquid phases, a basic understanding of the chemistry, particularly at the interface of the plasma and liquid, remains poorly understood. Previous studies have shown that species produced in the plasma phase such as nitric oxide (NO) and hydroxyl radicals (OH) can solvate in the liquid, yielding products such as nitrous acid (HNO₂) and hydrogen peroxide (H₂O₂) in the bulk solution [1]. In addition, we have recently shown that charge can be transferred from a DC microplasma jet into an aqueous solution to promote

electrolytic reduction reactions [2]. However, it remains unclear how these charge transfer reactions occur and, in particular, if plasma electrons solvate in the liquid before subsequently reducing solution species.

To clarify the role of electrons solvating at a plasma-liquid interface, we have designed and built an experiment to detect solvated electrons using optical absorption spectroscopy. Electrons solvated in aqueous solutions are well known to absorb strongly in the red. Initial models suggest that because of the short lifetime of solvated electrons in aqueous solutions (~1 μs) and anticipated solvation depths on the order 10 – 100 nm, optical absorption will be on the order of one part in 10⁶, making this an inherently challenging measurement. In this presentation, we will give an overview of our experimental method and present preliminary findings on direct measurements of electron solvation.

[1] P. Rumbach, M. Witzke, R. M. Sankaran, and D. B. Go, *J. Am. Chem. Soc.* **135** 16264-16267 (2013).

[2] M. Witzke, P. Rumbach, D. B. Go, and R. M. Sankaran, *J. Phys. D: Appl. Phys.* **45** 442001 (2012).

3:20pm **PS+SE-ThA4 A Novel Atmospheric Pressure Plasma Application for Fuel Tank Inerting, Matthew Price, A. Srivastava**, Interspace, Inc.

Aircraft fuel tanks have traditionally been protected from ballistic threats caused from explosive vapors by filling the area above the fuel with suppressant foam or inert gas. More recently fuel tank inerting systems have been developed for commercial transport aircraft. Inert gas is the preferred method since foam is heavy, reduces fuel tank capacity and is expensive to maintain. Current solutions consist of Onboard Inert Gas Generation Systems (OBIGGS) to reduce oxygen content in fuel tanks through the use of nitrogen-air separators. These membrane-based separators require high-powered pumps to flow air through small pores in the membranes. OBIGGS systems are bulky and too power hungry to be practical for smaller aircraft with multiple fuel tanks and limited electrical power. INTERSPACE has developed an innovative and efficient inerting system that does not rely on a pre-stored inerting agent or bleed air and is scalable to support multiple independent tanks. The system requires minimal electrical power and is capable of inerting to trace oxygen concentration levels without contaminating the fuel.

Our solution uses a getter material to readily sequester oxygen as surface oxides. A non-thermal, atmospheric pressure plasma then combines hydrocarbons in the tank with the getter to reduce the oxide and reverse the process to form water vapor. No consumable inerting product is used. Experimental data shows the getter absorbs 20 times its volume in oxygen before saturation. Scaling up this reaction would inert a 500 gallon fuel tank in 11.4 minutes with one liter getter at standard temperature and pressure conditions. Time-to-inert decreases at higher altitudes due to lower pressure. Time-to-inert curves were calculated for the typical aircraft flight envelope based on this model. We have successfully demonstrated the feasibility of our inerting system in a laboratory environment. Our inerting system is highly selective to oxygen, and eliminates the membranes and high power pumps used in existing systems. The next step will be to evaluate a prototype system through demonstration testing on the replica of a military aircraft fuel tank system. A customized plasma source will be developed optimized in size and weight competitive with aircraft applications.

4:00pm **PS+SE-ThA6 In Situ Diagnostic Studies of CO₂ containing Dielectric Barrier Discharges, Stefan Welzel**, FOM Institute DIFFER; Eindhoven University of Technology, Netherlands, F. Brehmer, Eindhoven University of Technology; AFS GmbH, Germany, B.L.M. Klarenaar, Eindhoven University of Technology, Netherlands, M.C.M. van de Sanden, FOM Institute DIFFER; Eindhoven University of Technology, Netherlands, R. Engeln, Eindhoven University of Technology, Netherlands

Carbon dioxide will be a key enabler for the integration of renewable energy into a future CO₂ neutral energy system as well as into chemical industry. The application of non-equilibrium plasmas offers a promising route to overcome the initial energy-demanding CO₂ dissociation step. Through subsequent hydrogenation of the CO produced, gaseous or liquid hydrocarbon(ate)s are synthesised. Dielectric barrier discharges (DBDs) are known as useful tools in plasma-assisted gas conversion. The main objective was to unravel main reaction mechanisms in CO₂ containing DBDs through combination of several *in-situ* diagnostic techniques.

Optical emission spectroscopy, (infrared) absorption spectroscopy along with rotational Raman scattering were employed to study the CO₂ conversion and deduce gas temperatures in mid-frequency (kHz) driven DBDs at elevated pressures. To study the kinetics of CO formation the DBD was additionally operated in pulsed mode. Absolute densities of CO, O₂ and O₃ were established downstream the plasma reactor. The CO yield was typically below 5% for gas flow rates that would allow reasonable throughput. The generally weak emission of electronically excited species

* Coburn & Winters Student Award Finalist

(CO₂⁺, CO) was monitored during individual AC cycles. Additionally, phase- and time-resolved signals of ro-vibrational absorption lines of CO and CO₂ in their (electronic) ground state were detected by quantum cascade laser absorption spectroscopy. In contrast to emission, the CO absorption remained constant throughout individual AC cycles. The modulation of CO absorption signals during pulsed operation can be successfully modelled by considering the power density of the DBD, the reactor wall and gas temperatures (up to 550 K), and the residence time of the gas along with the reactor geometry.

The results suggest electron-impact CO₂ excitation and ionisation followed by potentially surface enhanced recombination. The stoichiometric CO:O₂ ratio is described by a uniform trend as function of the number of charges transferred during the residence time of CO₂ in the active plasma zone.

4:20pm PS+SE-ThA7 Effect of the Nature of the Plasma Gas on the Resulting Chemistry of Atmospheric Plasma Deposited Coatings and of Plasma Treated Gases, D. Merche, N. Vandencastele, A. Ozkan, J. Hubert, François Reniers, Université Libre de Bruxelles, Belgium

In atmospheric plasma processes, the use of a main gas, usually considered as inert, to sustain the plasma is common. Nitrogen, argon and helium are the most regularly used gases. If the nature of the gas has a strong influence in the breakdown discharge voltage (due to Paschen Law), it also leads to plasmas which are optically and electrically different. This has drastic consequences on the chemistry and structure of plasma deposited coatings and on the chemistry of plasma treated gases. In this study, we compare, and try to explain, the results obtained on different topics using either argon or helium as main plasma gas.

All experiments have been conducted in dielectric barrier discharge reactors, powered with sinusoidal AFS generators, operating at frequencies lower than 40 kHz. For all the studies the reactors have been pumped down to evacuate contaminations and then backfilled with the plasma gas (Ar or He). The precursor is then injected in the DBD through the appropriate flow of the carrier gas.

Internal chemistry of coatings :

Through a combined XPS, FTIR and SIMS study, it is shown that the degree of cross-linking, the branching and the number of insaturations of plasma-polymerized polystyrene or sulfonated polystyrene (for fuel cell applications) is higher with argon than with helium, whereas the density of aromatics exhibits the opposite behavior.

Surface roughness of coatings

Similarly, for all the organic coatings synthesized by a dielectric barrier discharge (PS, CF_x from C₆F₁₂, PA), the roughness, determined by AFM is always higher with argon than with helium.

Conversion of CO₂ by DBD

Finally, the conversion rate of CO₂ into CO in atmospheric plasma conditions (DBD), is higher when argon is the main plasma gas than with helium.

It is suggested that all these effects are strongly related to the plasma operating mode and to the energy distribution inside the plasma.

This work is supported by PSI-IAP 7 (plasma surface interactions) from the Belgian Federal Government BELSPO agency

4:40pm PS+SE-ThA8 Diagnostics of an Atmospheric-Pressure dc Glow Plasma in Contact with Solution: Insight into Plasma-Liquid Interaction, Koichi Sasaki, Hokkaido University, Japan INVITED

The interaction between an atmospheric-pressure plasma and a liquid attracts much attention in conjunction with plasma-aided medical treatments and plasma-assisted agriculture. Major interests are the production and the transport of OH radicals in plasmas in contact with liquids. In this work, we examined the spatial distribution of the OH radical density in the gas phase of a dc glow plasma produced between a stainless-steel nozzle as the anode and electrolyte of NaCl solution as the cathode by laser-induced fluorescence (LIF) imaging spectroscopy. We were careful about the influence of collisional quenching and the rotational temperature in deducing the spatial distribution of the OH radical density from the LIF images.

The maximum rotational temperature was approximately 3000 K, which was observed in the plasma column in contact with the electrolyte surface. The frequency of collisional quenching was also high in the contacting region to the electrolyte surface, suggesting that the dominant quencher of the excited state of OH was water vapor. The absolute density of water vapor was evaluated from the quenching frequency and the rate coefficient of collisional quenching. It was found that the partial pressure of water vapor was more than five times higher than the saturated vapor pressure of water at room temperature.

The OH radical density was high in the neighboring region to the electrolyte surface, suggesting that water vapor produced from the electrolyte is the parent of OH radical. However, the peak of the OH radical density was separated from the electrolyte surface, and also the OH radical density on the electrolyte surface was not zero. It is noted that, if OH radicals are not reactive on the electrolyte surface, the decrease in the OH density toward the electrolyte surface would not be observed. On the other hand, if OH radicals are too reactive in the gas phase, the OH radical density on the electrolyte surface would become zero (Note that the production of OH in the cathode sheath is negligible), and in this case we cannot expect the interaction of OH radicals with the electrolyte. The axial distribution of the OH density observed in this work indicates that the electrolyte surface interacts with OH radicals as their sink. In other words, OH radicals are lost on the electrolyte surface. A possibility of the loss process is recombination to form hydrogen peroxide and water. In addition, we can also expect the transport of OH radicals into the inside of the electrolyte.

5:20pm PS+SE-ThA10 Absolute Measurements of Short Lived Reactive Species in Cold Atmospheric Pressure Plasmas, Deborah O'Connell, K. Niemi, J. Dedrick, S. Schroeter, J. Bredin, A. West, E. Wagenaars, T. Gans, University of York, UK

Low temperature plasmas are emerging as an exciting development for therapeutics. The unique properties of cold non-equilibrium plasmas have enormous potential in disease therapeutics and plasma pharmacology as drug alternatives. Applications of these plasmas include surface sterilization and bacterial decontamination, biofilm inactivation, antimicrobial treatment in food preservation, wound healing, to cancer treatment.

Non-equilibrium plasmas, operated at ambient atmospheric pressure and temperature, are very efficient sources for highly reactive neutral particles e.g. reactive oxygen and nitrogen species (RONS) (such as atomic oxygen, atomic nitrogen, hydroxyl radical, superoxide, singlet delta oxygen, nitrogen oxides), charged particles, UV-radiation, and electro-magnetic fields. Individually many of these components have been implicated in therapeutics. RONS are known to play a crucial role in biological systems, such as signalling, and generating oxidative damage to a variety of cellular components, which can ultimately lead to cell death. Plasmas have the advantage of delivering these simultaneously providing potentially superior processes.

Transport of the plasma components to the target is complex. In the core plasma production region a large, but defined, number of species can be created (including for example O, N, NO, O₂). As the plasma interacts with ambient air new reactions and components are formed. Upon interaction with either humidity or liquid layers on biological samples new species of varying lifetimes can be created (e.g. OH, H, H₂O₂, ONOO). Energy dissipation at these interfaces is important and to date unclear.

In order to understand the chemical kinetics and plasma-liquid-biological interaction mechanisms measurements of the relevant RONS are key. Measurements and simulations under this atmospheric pressure environment are challenging, primarily due to the multi-phase (solid, liquid, gas and plasma), strongly non-equilibrium with large gradients (e.g. in electric field), high collisionality, thus requiring extremely high temporal (picosecond to nanosecond) and spatial (microns) resolution.

Two advanced optical diagnostic techniques are applied, and will be presented, to measure absolute radical densities: Pico-second two-photon absorption laser induced fluorescence (ps-TALIF) and high-resolution synchrotron VUV absorption spectroscopy will be presented. Radicals measured in an atmospheric pressure plasma operated in helium with varying admixtures of oxygen, nitrogen and water vapour will be presented.

5:40pm PS+SE-ThA11 Recent Progress in the Diagnostics of Microwave Discharges for Optimization of CO₂ Dissociation, Tiago Silva, N. Britun, T. Godfroid, R. Snyders, University of Mons, Belgium

The increase in global emissions of carbon dioxide (CO₂) due to fossil-fuel combustion and other energy-related human activities is strongly related with the global warming issue. Due to this effect, the study of CO₂ dissociation process is a highly demanding topic, which requires attention and efficient solutions. Among the proposed strategies, one possible way to limit CO₂ emission is to use plasma technology to break the CO₂ molecule into oxygen (O) and carbon monoxide (CO), which can be later used for production of valuable chemicals, e.g. for the fuel synthesis (syngas).

Recently, energy-efficient powerful plasma-chemical systems have been developed based on microwave plasmas. These discharges are often generated using electromagnetic waves in the range of 300 MHz to 10 GHz, and can operate over a wide range of conditions of pressure and power. In particular, microwave surfaguide discharges (MSGD) where the gas flow in the discharge tube is perpendicular to the waves propagation, are proven to be good solution for an efficient molecular dissociation of di- or multi-atomic species [1].

In this work, the recent results on CO₂-containing MSGD operating at 0.9 GHz and 2.45 GHz in pulsed and continuous regimes are presented. The plasma is sustained in CO₂ and CO₂+N₂ flowing gas mixtures in a quartz tube crossing a copper waveguide. The microwave discharges are characterized in terms of various plasma parameters using various optical emission spectroscopy (OES) methods. In particular, the characteristic plasma temperatures, such as the gas temperature (via CO rotational spectra), and vibrational temperature (via N₂ vibrational bands) are determined as a function of time at different axial positions along the gas flow in the discharge tube. The CO₂ conversion rate in the discharge volume, along with the measurements of plasma energetic efficiency of such conversion is performed by means of optical emission actinometry. The results of the time- and space- resolved OES measurements demonstrate a non-uniform dissociation rate of CO₂ along the gas propagation direction in the discharge. As a result, the dissociation degree can be substantially modified by varying the power balance and the composition of the gas mixture [2]. In addition, in order to get a complete picture of the process, gas chromatography measurements were performed in the post discharge region. The obtained integrated results allow better understanding of the μ wave plasma-based dissociation of CO₂.

[1] T. Godfroid, J. P. Dauchot and M. Heq, *Surf. Coating Technol* **174-175** 1276-1281 (2003)

[2] T. Silva, N. Britun, T. Godfroid, R. Snyders *Plasma Sources Sci. Technol* **23** 025009 (2014)

Plasma Science and Technology

Room: 305 - Session PS-ThA

Plasma Processing of Nanoparticles and Nanomaterials

Moderator: Mohan Sankaran, Case Western Reserve University

2:20pm **PS-ThA1 Raman Spectroscopy as Diagnostics for Size Distribution and Surface Chemistry of Remote Plasma Synthesized Silicon Nanocrystals**, *I. Dogan*, Eindhoven University of Technology, Netherlands, *R. Gresback*, *T. Nozaki*, Tokyo Institute of Technology, Japan, *Mauritius C.M. van de Sanden*, Dutch Institute for Fundamental Energy Research (DIFFER), Netherlands

The possibility to realize advanced photon management in solar cells and ultrahigh capacity charge storage in Li-ion batteries with silicon nanocrystals (Si-NCs) have boosted the interest on them, thanks to their size dependent optical properties and surface reactivity. To promote the use of these properties of Si-NCs in solar cells and batteries in an optimized manner, particle size control and surface engineering are the critical requirements. Therefore, accurate analysis of the size distribution is essential to optimize the process parameters to reach an ultimate control on nanocrystal size, which raises the requirement of a suitable diagnosis and post-analysis route. The analysis technique to be used is expected to provide quantitative data of size and morphology related features in a fast and non-destructive manner. Common techniques, such as X-ray diffraction (XRD), transmission electron microscopy (TEM) and photoluminescence spectroscopy (PL) are time consuming and only provide qualitative data of the size distribution especially when the Si-NC size distribution is not monodisperse, which is hardly achievable in most of the nanocrystal processing tools. Thus, these techniques are far from being considered as ideal tools for effective size analysis. Our aim in this work is to demonstrate that, Si-NCs with multimodal size distributions can be quantitatively analysed in a fast and non-destructive way by using Raman spectroscopy (RS). Free standing densely packed Si-NCs are synthesized in Ar/SiH₄ and Ar/SiCl₄ gas mixtures by using a remote expanding thermal plasma and a ultra-high frequency non-thermal plasma. Synthesized Si-NCs have a multimodal size distribution with peak sizes of 5 nm and 70 nm, respectively. Experimental Raman spectra are deconvoluted for separate analysis of the sub-distributions by using the size dependent phonon confinement model. Comparison of the extracted size distributions with the distributions obtained from TEM and PL show that RS provides highly reliable, quantitative information of size distribution and volume fraction. Analysis of the surface chemistry of Si-NCs is performed by depositing a monolayer of Si-NCs on a 10 nm thick Ag. Using a 514 nm laser enhances the Raman signal by two orders of magnitude, which reveals the presence of Si-H_x, Si-O_x and Si-Cl_x bonds on Si-NC surface. In addition, disappearance of Si-H_x signal with oxidation is observed. With this observation, we show that, Raman spectroscopy can be used for probing the surface chemistry of Si-NCs. These results propose that Raman spectroscopy has the potential to become a standard diagnostic tool for the size and surface chemistry analysis of Si-NCs.

2:40pm **PS-ThA2 High Rate Production of Silicon Nanoparticles Through a Microwave Torch Production Process**, *David Oakes, M.A. Costolo, J.D. Lennhoff*, Physical Sciences Inc.

Nanometer sized aluminum particles are currently utilized as an energetic additive in propellant, pyrogen, and explosives formulations. Nano-silicon is potentially an attractive replacement for nano-aluminum in these applications since it has a similar energy density while being less sensitive, and thus safer to handle. In addition silicon forms a thin passivation layer which makes it a stable additive compared to aluminum which can oxidize in-depth. Incorporating nano-silicon into energetic formulations is currently limited by the high cost of the material which is generally formed in low production rate, batch processes.

This paper describes the development of a scalable, continuous (non-batch) high production rate method for nano-silicon utilizing a microwave driven plasma torch-based process. Silane (SiH₄) is injected near the throat of the supersonic output nozzle of the torch where it dissociates in the near atmospheric pressure nitrogen plasma formed by the microwave discharge. The local gas temperature in the torch plenum is approximately 2800 K which is sufficient to produce greater than 0.9 moles of silicon atoms for each mole of SiH₄ (>90% efficiency). The resulting silicon atom rich gas is rapidly quenched (~2x10⁸ K/s) in a supersonic expansion into a vacuum chamber (~ 50 torr) producing the seed particles that then grow to 10 – 20 nm in approximately 0.1 ms. The process meets the criteria specified by Kodas and Frielander for producing monodisperse particles in a flow reactor by namely: 1) Separating seed particle production in the supersonic expansion from subsequent growth of the seeds downstream of the nozzle, 2) Providing a flat velocity profile in the growth region enabling a uniform residence time for the particles in the growth region, and 3) Utilizing a high velocity jet which results in a short residence time in the growth region to minimize particle agglomeration.

Growth conditions will be described that produce 6 g/min of 10 -20 nm diameter silicon particles with a 140 m²/g surface area from a 2 kW microwave discharge. Material analysis will be described including SEM and TEM to assess the particle morphology and size distribution, single point and BET surface area measurements, and EDX, differential scanning calorimetry, and electrochemical performance to assess purity and energetic characteristics of the material. Future efforts will extend the growth region of the process to enable larger particle sizes and scale up the microwave system to 5 kW to enable 15 – 30 g/min production rates.

3:00pm **PS-ThA3 Plasma-Produced Nanomaterials for Energy Recovery and Storage**, *Lorenzo Mangolini*, University of California, Riverside **INVITED**

Despite being heavily utilized in industry, the unique capabilities of non-thermal plasmas with respect of materials processing have yet to be fully realized. In this talk we will describe our effort in understanding the nucleation and growth of silicon nanoparticles in non-thermal plasmas and we will discuss their application for energy-related applications.

Several research groups have focused on nanoparticle nucleation and growth in silane-containing plasmas. Yet a clear understanding of the correlation between plasma parameters and the properties of silicon particles is missing. There is no theory explaining how a non-thermal process can produce nanocrystals of a material with a relatively high melting point within few milliseconds of reaction time. We have performed *in-situ* FTIR measurements and aerodynamically extracted particles along the length of a flow-through reactor similar to the one described in [1], and have found that silane is rapidly consumed and converted into amorphous particles with size close to their final one. Crystallization takes place after the precursor is fully consumed and within few milliseconds. An independent measurement of the crystallization rate of small silicon particles [2] suggests that their crystallization kinetics exceeds that of bulk amorphous silicon films. Despite this the current models describing the plasma-nanoparticle interaction [3,4] cannot justify the substantial heating necessary to achieve crystallization in such short time. Results from our ongoing efforts in this area will be presented.

By leveraging the processing capabilities of non-thermal plasmas it is possible to provide improvements in the performance of devices that are relevant for energy-related applications. By sintering plasma-produced nanocrystals it is possible to fabricate bulk samples with precise control of grain size and grain size distribution. These samples show some of the lowest thermal conductivities ever reported for the case of bulk nanostructured silicon. This is a promising step towards the development of highly efficient waste-heat recovering devices that do not require alloying with expensive materials such as germanium. Furthermore, plasma-produced silicon particles can also be integrated into anodes for lithium-ion batteries. Their excellent dispersibility into polymer matrices allows achieving stable operation over hundreds of charge-discharge cycles.

[1] L. Mangolini et al., *Nano Letters* **5** (2005) 655.

[2] T. Lopez and L. Mangolini, *Nanoscale* **6** (2014) 1286.

- [3] L. Mangolini and U. Kortshagen, *Physical Review E* 79 (2009) 026405.
 [4] N. J. Kramer et al., *Journal of Physics D: Applied Physics* 47 (2014) 075202.

4:00pm **PS-ThA6 Atmospheric-Pressure Microplasma Synthesis of Colloidal Metal Nanoparticles**, *Caroline De Vos, J. Baneton, J. Dille, S. Godet*, Université libre de Bruxelles, Belgium, *M. Sankaran*, Case Western Reserve University, *F.A.B. Reniers*, Université libre de Bruxelles, Belgium
 Microscale plasmas are electrical discharges where at least one geometrical dimension is sub-millimetric. In consequence, they present a remarkable stability at high pressure as reducing the size of the plasma allows keeping breakdown voltages sufficiently low to avoid the glow-to-arc transition. [1] The development of non-thermal atmospheric pressure microplasmas facilitates the coupling with the liquid phase and offers new potential applications in water treatment, medicine and material synthesis. [2]

This study focuses on the synthesis of silver and gold nanoparticles in aqueous solution. The plasma, supplied with argon, is initiated at the surface of silver nitrate or chloroauric acid solution. The electrons from the discharge lead to electrochemical reactions and reduction of the metal cations. Different stabilizers such as polyvinyl alcohol and sodium dodecyl sulfate are mixed with the solution to prevent uncontrolled particle growth.

X-ray photoelectron spectroscopy (XPS) spectra exhibit the metallic nature of the Ag and Au nanoparticles and particles growth is monitored by ultraviolet-visible absorbance spectroscopy. The two plasmon bands, characteristic of spherical Ag and Au nanoparticles, can be observed at 415 and 530 nm respectively. The morphology and the size of as-grown colloidal metal nanoparticles are evaluated by transmission electron microscopy (TEM). For silver nanoparticles, the average size rises from 10 to 20 nm when the discharge current increases from 2 to 5 mA. Moreover, bigger nanoparticles are observed at higher concentration and reaction times. For gold experiments, particles about 10 nm in diameter are synthesized at higher current than for silver experiments. Lower precursor concentration is necessary to avoid aggregates formation. In both cases, particles below 20 nm are spherical whereas at larger diameters, various shapes such as triangle, hexagon, appear.

In the project continuity, a comparison of the reduction mechanisms is performed for the two studied metals. At first, the proportion of reduced metal cations is quantified by potentiometric analyzes. Thereafter, the active species involved in the reduction process (e.g., H₂O₂, electrons) are discriminated. Finally, a bimetallic synthesis is studied to help the comprehension of the fundamental mechanisms. Indeed, metal ratio and alloy formation provide information about the reduction kinetic of both metals.

This work is supported by PSI-IAP 7 (plasma surface interactions) from the Belgian Federal Government BELSPO agency.

References

- [1] D. Mariotti, *Appl. Phys. Lett.* **92** (2008) 151505.
 [2] D. Mariotti, R. M. Sankaran, *J. of Phys. D: Appl. Phys.* **44** (2011), 174023.

4:20pm **PS-ThA7 Gas Chromatography and Mass Spectrometry Characterization of Nanoparticle-Producing Atmospheric-Pressure Microplasmas**, *Jonathan Cole, R.M. Sankaran*, Case Western Reserve University

Plasma processes are becoming increasingly important for the production of nanoparticles by homogeneous nucleation.^{1,2} The high-purity conditions that have made plasmas essential for thin film etching and deposition in the semiconductor industry similarly allow nanoparticles to be synthesized without organic stabilizers or other types of contaminants. In addition, high temperature and/or pressure materials such as silicon and diamond can be produced in plasmas because of non-equilibrium conditions. A novel class of plasmas for nanoparticle synthesis is microplasmas. Microplasmas operate stably at atmospheric pressure as a result of pd scaling (p being the gas pressure and d the electrode gap), eliminating the need for vacuum infrastructure. In addition, particle nucleation, growth, and agglomeration are controlled by the rapid quenching that results from the small volume and flow-through geometry.

Here, we present gas chromatography and mass spectrometry measurements of atmospheric-pressure microplasmas with reaction chemistries relevant to nanoparticle synthesis by homogeneous nucleation. We focus on two different gas chemistries that are used to produce nanoparticles: 1) metal-organic vapors that allow the synthesis of metal nanoparticles, such as Ni and Fe, and 2) hydrocarbon gases that allow the synthesis of carbon nanoparticles, including nanodiamonds. Measurements are performed on the effluent at the exit of the microplasma. To sample gases at high pressure (>1 atmosphere), we have built a mass spectrometry system consisting of an open ion source, quadrupole trap, 1-300 AMU detection range RGA (Dycor

Technologies, Ltd.) and capillary inlet. The gas chromatography system (Shimadzu, Inc.) is equipped with a recently developed barrier ionization discharge detector, which is capable of universal detection of molecular gases with sensitivity at the ppm and ppb levels. The results are thus comprehensive, but restricted to the neutral vapor or gas molecule reaction products because of the high sampling pressure. Important insight is nonetheless obtained about reactant conversion, gas product selectivity, process efficiency, and influence of plasma characteristics. The gas chemistry studies are complemented by optical emission spectroscopy (Ocean Optics, Inc.) and scanning mobility particle sizer spectrometry (TSI, Inc.) of the nanoparticle aerosol. Materials analysis of collected product by high resolution transmission electron microscopy is also carried out in support of the in situ measurements.

References

- U. Kortshagen, *J. Phys. D* **42**, 113001 (2009).
²D. Mariotti and R. M. Sankaran, *J. Phys. D* **43**, 3223001 (2010).

4:40pm **PS-ThA8 Top-down InGaAs/GaAs Nanopillars Fabrication using a Bio-Nano-Process and a Neutral Beam Etching Process**, *Cédric Thomas, K. Yoshikawa, C.Y. Lee, Y. Tamura, A. Higo*, Tohoku University, Japan, *T. Kiba, A. Murayama*, Hokkaido University, Japan, *I. Yamashita*, Nara Institute of Science and Technology, Japan, *S. Samukawa*, Tohoku University, Japan

Quantum dot (QD) lasers have been extensively studied in the last few decades due to their device characteristics benefits. However, fabrication of a high density and uniform two-dimensional array of QDs is still a big challenge. We have developed a damage-free top-down process for creating InGaAs QDs by combining a high-density bio-template [1] and a neutral beam (NB) etching process [2]. The bio-nano process consists of a high-density (up to $7 \times 10^{11} \text{ cm}^{-2}$), two-dimensional array of cage-shaped proteins called ferritins with encapsulated metal oxide nanoparticles (NPs). Ferritins can be functionalized with polyethylene glycol (PEG) to control distance between them and avoid QDs in-plane coupling. After removal of the protein shell, 7 nm in diameter iron oxide NPs were used as etching masks. The NB etching consists of an inductively coupled plasma chamber separated from the process chamber by a carbon electrode with a high-aspect-ratio aperture array. As a result, the charged particles are efficiently neutralized whereas almost no UV photons can reach the sample.

A self-assembled monolayer of PEG-ferritins was formed by spin coating on a GaAs cap surface with native oxide. Samples grown by metalorganic vapor phase epitaxy (MOVPE) with the following structure were used: 10-nm-thick GaAs cap, three 8-nm-thick In_{0.24}Ga_{0.76}As active layers separated by two 20-nm-thick GaAs barrier layers on top of a semi-insulating substrate. A low-temperature oxygen annealing in vacuum was used to remove protein shell and form etching mask with the iron oxide cores. Subsequently, a hydrogen radical treatment was performed during 30 min at 350°C to remove native oxide, followed by hydrogen passivation at room temperature. Nanopillars were etched by neutral beam etching process with a mixture of argon and chlorine. Substrate temperature, neutrals energy and mixture ratio were investigated to find the optimized conditions in term of etching profile and nanopillars density. It has been found that a mixture ratio of Ar:Cl₂ = 27:73 with a substrate temperature of 50°C were the best conditions to obtain high-density and anisotropic nanopillars, with diameters about 20 nm and height about 80 nm. After regrowth of the GaAs barrier layer by MOVPE, photoluminescence was observed. PL emission from InGaAs QDs could be detected. The results showed that III-V compound QDs can be realized by this damage free top-down nanoproces.

- [1] I. Yamashita et al., *Biochim. Biophys. Acta* **1800** (2010) 845
 [2] S. Samukawa et al., *Jpn J. Appl. Phys.* **40** (2001) L997

5:00pm **PS-ThA9 Nanostructuring of Metal Surfaces by Low Energy He Ions**, *Irem Tanyeli*, FOM Institute DIFFER, Netherlands, *L. Marot*, University of Basel, Switzerland, *M.C.M. van de Sanden*, FOM institute DIFFER, Netherlands, *G. de Temmerman*, ITER Organization, Netherlands
 The effect of low energy (<50 eV) helium ion irradiation on surface modifications of metals has been studied [1,2]. The most pronounced works have been done on tungsten and molybdenum surfaces [2]. Nanostructure formation on these surfaces by high fluxes of low energy helium ions is identified as a self-growth process of He bubbles. In this study, we provide a size-controlled nanostructure formation by surface temperature and plasma exposure time on iron surfaces consistently with the experiments on tungsten and molybdenum. Besides, various metal surfaces such as titanium, aluminum and copper are irradiated by low energy He ions. We investigated the behavior of these surfaces under the He ion irradiation as a function of surface temperature, plasma exposure time and He ion flux. Different surface morphologies are observed for these metals. Nanostructure growth kinetics shows dependency on surface temperature

and plasma exposure time. It has been shown that the nanostructured surfaces present high surface area and hence high light absorption [3]. The photo-catalytic activity of our metal surfaces will be presented.

[1] K. Tokunaga, et al., *J. Nucl. Mater.* 337–339, 887 (2005).

[2] G. De Temmerman, et al., *JVSTA*, 30 (2012).

[3] S. Kajita, et al., *Appl. Phys. Express.*, 3 (2011).

5:20pm PS-ThA10 Nucleation of Microcrystalline Silicon Thin Films on Nano-Imprint Textured Substrates, Jurgen Palmans, T. Faraz, W.M.M. Kessels, M. Creatore, Eindhoven University of Technology, Netherlands

Hydrogenated microcrystalline silicon ($\mu\text{c-Si:H}$) is important in thin-film silicon solar technology where it is combined with amorphous silicon ($a\text{-Si:H}$) in tandem cells for enhanced light absorption. However, efficient light absorption requires thick ($>1\ \mu\text{m}$) $\mu\text{c-Si:H}$ films compared to thin $a\text{-Si:H}$ ($\sim 350\ \text{nm}$). Since reduced absorber thickness is desired, the potential of light management, typically induced by texture-etched transparent conductive oxides (TCO), has been explored, demonstrating a strong dependence of absorber layer quality on TCO chemical nature and morphology. Generally, electrical, optical and structural properties require optimization. Due to parameter interdependence, nano-imprint lithography (NIL) was introduced to decouple electrical/optical and structural properties by inducing texture on glass prior to TCO deposition, allowing independent optimization of light diffraction and electrical/optical requirements. The potential of NIL textures has been demonstrated in this respect. However, such novel morphologies (periodic/random) impact absorber layer quality. Therefore, the nucleation of $\mu\text{c-Si:H}$ thin films ($\sim 100\ \text{nm}$), deposited under high power-high pressure conditions in a capacitively coupled plasma reactor, has been studied on various NIL textured substrates. To replicate a solar cell structure, NIL textured and flat glass have been coated with $\sim 500\ \text{nm}$ magnetron sputtered aluminum doped zinc oxide (AZO). Characterization through Raman spectroscopy and crystal grain analysis has been performed. For flat glass, the crystalline volume fraction (X_c) increased a factor 2 upon AZO addition joined by a narrower phase transition. This was related to a different microstructure evolution. Introducing a NIL texture increased nucleation delay on randomly textured compared to periodically textured substrates. Since nucleation depends on process conditions, i.e. silane flow rate (Φ_{SiH_4}), the role of ions and radicals is considered a determining factor. A reduced Φ_{SiH_4} enhances the ion-to-growth flux ratio and ion energy, promoting surface diffusion^[1]. However, on rough morphologies the ion contribution per unit area is reduced, therefore reducing X_c on NIL substrates. When shifting to the phase transition, preferential etching of $a\text{-Si:H}$ by atomic hydrogen dominates while the ion contribution is reduced. This is confirmed by the microstructure parameter (R^*) experiencing a transition from void-rich to (di)vacancy-dominated films. Furthermore, a direct correlation of R^* and X_c was obtained. The insights obtained as such directly impact process control when dealing with challenging morphologies.

^[1] J. Palmans et al., *J. Phys. D: Appl. Phys.* **47** (2014)

5:40pm PS-ThA11 Synthesis of AZO Film on Polymer by Nano-Process Control with Confined Magnetic Field Sputtering, J.G. Han, NU-SKKU Joint Institute for Plasma-Nano Materials, Republic of Korea, Subong Jin, B.B. Sahu, J.B. Kim, NU-SKKU Joint institute for plasma nano materials, Republic of Korea, K. Takeda, M. Hori, Plasma Nanotechnology Research Center, Japan

Al doped ZnO(AZO) film has been attracting as one of promising candidate film replacing ITO film for transparent conductive oxide film of next generation flexible digital electronics devices. The relatively low resistivity and transparency of AZO film deposited at low temperature are still hurdles to overcome for replacing ITO film even though its unique advantages in low cost and high toughness over those of ITO film. It is well known that resistivity is closely associated with carrier concentration and mobility which are controlled by stoichiometry, binding energy of atoms and lattice defects of film including oxygen vacancy as well as Al replacement in Zn atom sites.

The control of those atomistic structure and lattice defects is affected by surface energy accumulated with atoms and molecules deposited at top surface layer during film nucleation and growth depending on process parameters during deposition process. The surface energy is mostly comprised of kinetic energy of neutrals, electronic energy of activated neutral molecule and atoms and ions as well as flux density. We have investigated effect of those atomic and molecular level energy analysis on structure formation and related electrical property changes by in-situ diagnostics during sputtering process under confinal confined magnetic field. The kinetic energy and flux of sputtered atoms are controlled by independent variation of power density for direct sputtering and in-direct sputtering targets on polymer substrate at low temperature below 100 C. Optical emission spectroscopy and radical diagnostics as well as Langmuir

probe analysis have been performed to measure plasma parameters. Carrier concentration and mobility have been analyzed depending on microstructure changes including binding energy of atoms and Al replacement of Zn site etc.. The resistivity is significantly reduced with atomic level nano process control and can be reached less than $4\text{E-}4$ at low temperature.

This paper discusses on fundamental mechanism of film nucleation and growth with top surface energy accumulation with atomic and molecular energy diagnostics for AZO film synthesis by magnetron sputtering, and then illustrate control of resistivity associated with control of carrier concentration and mobility.

Fundamentals & Biological, Energy and Environmental Applications of Quartz Crystal Microbalance Focus Topic

Room: 317 - Session QC+AS+BI+MN-ThA

Applications of QCM

Moderator: Electra Gizeli, IMBB-FORTH, Heraklion, Crete, Greece, Adam Olsson, McGill University, Canada

2:20pm QC+AS+BI+MN-ThA1 Permeability of a Model Stratum Corneum Lipid Membrane, Daeyeon Lee, University of Pennsylvania

INVITED

The stratum corneum (SC), composed of corneocytes and intercellular lipid membranes, is the outermost layer of the epidermis, and its main function is the regulation of water loss from the skin. The major components of the SC lipid membranes are ceramides (CER), cholesterol (CHOL), and free fatty acids (FFA), which are organized in multilamellar structures between corneocytes. The intercellular SC lipid membrane is believed to provide the main pathway for the transport of water and other substances through the skin. While changes in the composition of the SC lipid membranes due to intrinsic and/or extrinsic factors have been shown to affect the organization of the lipid molecules, little is known about the effect of compositional changes on their water permeability. In this talk, I will present our results on the effect of composition on the permeability of a model SC lipid membrane consisting of ceramide, palmitic acid, and cholesterol using a quartz crystal microbalance with dissipation monitoring (QCM-D). The QCM-D method enables the direct determination of the diffusivity (D), solubility (S), and permeability (P) of water through the model SC lipid membranes. In the first part, I will discuss the effect of membrane composition on the water permeability of the model SC lipid membrane. We find that D and S weakly depend on the chain length of saturated fatty acids, while P shows no significant dependence. In contrast, the saturation level of free fatty acids and the structure of ceramide have significant influence on D and S, respectively, resulting in significant changes in P. In the second part of the talk, I will present our recent work on the effect of common anionic surfactants on the water permeability of the model SC lipid membrane. Particularly, the effect of sodium dodecyl sulfate (SDS) and sodium lauryl ether sulfate (SLES) with one or three ethoxy groups on the water permeability of the model SC lipid membrane is compared.

3:00pm QC+AS+BI+MN-ThA3 Investigation of Interaction between a Monoclonal Antibody and Solid Surfaces via Multiple Surface Analytical Techniques, Xia Dong, C.A.J. Kemp, Z. Xiao, Eli Lilly and Company

The interaction between proteins and surfaces is an important topic in the field of biomaterials. With the development of monoclonal antibody products, there is increasing interest in understanding the nature of the interactions between antibodies and the solid surfaces they contact during manufacturing processes and storage. In this study, a monoclonal antibody was introduced to quartz crystal microbalance (QCM) substrates coated with gold, stainless steel and silicon carbide. The samples were characterized by multiple surface analytical techniques, including TOF-SIMS and XPS. The preliminary XPS results suggest that the protein adsorbed at higher concentration on gold than on stainless steel and silicon carbide, while nitrogen concentration detected on stainless steel is slightly higher than on silicon carbide. This is generally consistent with the QCM results. TOF-SIMS spectra also suggest that the interaction between the antibody and three substrates is not the same. The fragmentation patterns detected in the TOF-SIMS spectra obtained from silicon carbide and stainless steel are similar to each other, but they are different from those detected on gold. The interaction between the antibody and stainless steel coupons will be further studied to understand the influence of surface morphology.

3:20pm **QC+AS+BI+MN-ThA4 Combining Spectroscopic Ellipsometry and Quartz Crystal Microbalance to Study Biological Hydrogels – Towards Understanding Nucleo-Cytoplasmic Transport.** N.B. Eisele, S. Ehret, R. Zahn, CIC biomaGUNE, Spain, S. Frey, D. Gorlich, MPI Biophysical Chemistry, Germany, Ralf Richter, CIC biomaGUNE & Université Grenoble Alpes & MPI Intelligent Systems, Spain

Nature has evolved hydrogel-like materials that are exquisitely designed to perform specific biological functions. An example of such a material is the nuclear pore permeability barrier, a nano-sized meshwork of intrinsically disordered proteins (so called FG nups) that fills the nuclear pores (i.e. the roughly 40 nm wide channels across the nuclear envelope) and controls the entry of macromolecules into the nucleus of eukaryotic cells. The permeability barrier exhibits a unique selectivity in transport: very small molecules can cross the barrier efficiently, while larger objects are delayed or blocked unless they are bound to specialized proteins, so called nuclear transport receptors (NTRs). How size and species selectivity are encoded in the hydrogel-like properties of the permeability barrier is currently not well understood.

We have developed monolayers of end-grafted FG nups as a nano-scale model system of the permeability barrier. The planar geometry of this well-defined biomimetic film affords detailed and quantitative characterization – not accessible for the native system – with a toolbox of surface-sensitive characterization techniques. In particular, we present the application of the *in situ* combination of quartz crystal microbalance (QCM-D) and spectroscopic ellipsometry (SE) to quantify film thickness, hydration and viscoelastic properties as a function of protein surface density.

We will present how this experimental data, combined with polymer theory, allows us to better understand the relationship between the supramolecular organization and dynamics of the permeability barrier, its physico-chemical properties and its biological function. We demonstrate that attractive interactions between FG nups play an important role in tuning the assembly and morphology of FG nup meshworks, and highlight that even rather weak interactions – typically a few *kT* per biopolymer chain – have functional importance. We show also how the interaction between NTRs and FG nup meshworks is tuned to afford strong enrichment and at the same time rapid entry and exit of NTRs in the permeability barrier, thereby facilitating NTR translocation.

Taken together, these studies contribute important information to understand the mechanism of size- and species-selective transport across the nuclear pore permeability barrier. The mechanistic insight gained should be useful towards the design of bioinspired species-selective filtering devices. Moreover, the presented procedures for the acquisition and analysis of combined QCM-D/SE data are broadly applicable for the characterization of ultrathin biomolecular and other polymer films.

4:00pm **QC+AS+BI+MN-ThA6 Probing Nanoparticle-Biofilm Interactions using Quartz Crystal Microgravimetry and Complementary Surface-sensitive Methods.** Kaoru Ikuma*, University of Massachusetts, Z. Shi, A.V. Walker, University of Texas at Dallas, B.L.T. Lau, University of Massachusetts

The environmental fate and transport of nanoparticles (NPs) have been a rising topic of concern due to the increased use of nanotechnology. Recent studies have shown that NPs are likely to interact readily with and accumulate in environmental biofilms. Biofilms are a ubiquitous form of microbial presence where cells attached on solid surfaces are surrounded by a sticky matrix of extracellular polymeric substances (EPS). The EPS matrix is considered to be highly heterogeneous and chemically complex. Polysaccharides and proteins are known to be major constituents of EPS and may greatly impact the likelihood of interactions occurring between NPs and biofilms.

In this study, we examined the deposition of NPs onto surface-immobilized proteins to determine the importance of protein-rich domains in the interfacial interactions between NPs and biofilms. Such interfacial processes are the initial and potentially rate-limiting step in NP-biofilm interactions. The deposition kinetics and extent of model hematite ($\alpha\text{-Fe}_2\text{O}_3$) NPs onto protein-coated silica surfaces were quantitatively measured by quartz crystal microbalance with dissipation (QCM-D). Model proteins including bovine serum albumin (BSA) and lysozyme as well as bacterial total proteins were used herein. The proteins were initially adsorbed onto either negatively-charged bare or positively-charged poly-L-lysine (PLL)-precoated silica sensors to assess the effects of the orientation of surface-immobilized proteins. In addition to QCM-D, other complementary surface-sensitive techniques such as Kelvin probe force microscopy and time-of-flight secondary ion mass spectrometry (TOF SIMS) were used to

characterize the mechanisms of interaction between the NPs and the protein-coated surfaces.

QCM-D results indicated that for all tested proteins, the total deposition extent of hematite NPs was significantly greater on protein layers that were adsorbed onto bare silica compared to PLL-precoated silica sensors. TOF SIMS results showed that the amino acid profiles of the topmost surface of the protein layers on bare and PLL-precoated silica sensors were distinctly different, suggesting that NP deposition was greatly influenced by the orientation of the surface-immobilized proteins. Both the extents and rates of NP deposition were also dependent on the type of model protein. Based on the surface charge, topography, and hydrophobicity characterization results, the observed interfacial interactions between hematite NPs and surface-immobilized proteins appeared not to be controlled by one dominant interaction force but by a combination of electrostatic, steric, hydrophobic, and other interactions.

4:20pm **QC+AS+BI+MN-ThA7 Association and Entrapment of Membrane-Targeted Nanoparticles with Different Binding Avidity: A QCM-D and Single Particle Tracking Study.** Anders Lundgren*****, B. Agnarsson, S. Block, F. Höök, Chalmers University of Technology, Sweden

Nanoparticles specifically targeted to receptors in the cell membrane are interesting for various applications such as intracellular delivery and visualization of diffusing membrane proteins, so-called single particle tracking. These diverse applications require particles optimized to display different binding properties: In this model study we investigated the effect of particle size and ligand density on the association rate and mobility/entrapment of biotin functionalized core-shell nanoparticles to supported lipid bilayers sparsely modified with streptavidin. Gold-PEG core-shell nanoparticles were synthesized with two different core sizes, 20 and 50 nm in diameter, and a shell (10 nm) of mixed uncharged, negatively charged and biotinylated PEG-ligands, the biotin content varied from one to several hundreds per particle. Particle binding was examined on the ensemble level using QCM-D and on single particle level using novel light scattering microscopy that will be detailed. At physiological salt conditions, binding of 50 nm particles were weakly dependent on the number of displayed biotin ligands, whereas the association of 20 nm particles were strongly attenuated in direct relation to the ligand density. At low salt conditions, binding of the larger particles resembled that of the smaller particles, with a strong dependence on ligand density. PEGylated particles without biotin-ligands did not bind at any condition. Thus, it was concluded that specific particle affinity is strongly attenuated by particle size and surface charge due to different interaction potential between the particle and the surface. On the contrary, no dependence on particle size was observed for the mobility of single particles displaying diffusion constants close to 0.4 or 0.8 $\mu\text{m}^2/\text{s}$ irrespective of particle size, which was similar to ensemble measurements using FRAP data on FITC-labelled streptavidin (0.5 $\mu\text{m}^2/\text{s}$). Only particles with a single surface tether show continuous diffusion; after formation of a second surface bond particles got quickly entrapped and formed additional bonds. In QCM-D measurements, this was manifested by a continuously decreasing dissipative response per particle for binding of particles with increasing ligand density. Together, QCM-D and particle tracking data indicates that two different mechanisms may lead to particle trapping and ultimately particle wrapping: For very high ligand densities membrane receptors in the membrane diffuse to and partly wraps around immobile particles, whereas for intermediate ligand densities the diffusion and dynamics of the particles themselves facilitate the formation of additional surface bonds and eventual wrapping.

4:40pm **QC+AS+BI+MN-ThA8 Complementary Chemiresistor and QCM Studies of Biomacromolecules as Sorptive Materials for Vapor Sensing.** Kan Fu, X. Jiang, B.G. Willis, University of Connecticut

Biomolecules are integral components of current sensing and diagnostic technologies including enzymatic glucose sensors, DNA microarrays, and antigen-antibody assays. The use of biomolecules in non-biological situations, however, is a burgeoning new field that may break the existing boundaries of biomolecule applications in exclusively biological context. Extensive studies have already been performed in bioelectronics using small biomolecules and biomacromolecules, revealing promising results regarding charge transport and conformation dependence. In the area of sorptive chemical sensors, biomacromolecules have inherent advantages over conventional synthetic polymers. DNA oligomers have precisely defined sequences through synthesis, they are monodisperse, and they can self-assemble into nanoscale structures. These features make them interesting for vapor sensing of small molecules.

In this work, a series of 8 custom-designed, single-strand DNA (ssDNA) were integrated with chemiresistors and QCM to make sensors. Chemiresistor sensors were made by depositing gold nanoparticles functionalized with ssDNA molecules onto microfabricated electrodes, and QCM sensors were made by depositing films of ssDNA on quartz crystals.

* QCM Focus Topic Young Investigator Award

While chemiresistors give high signal-to-noise ratios and significantly better limits of detection (LODs) and may eventually be the transducer for practical applications, QCM is a purely mass-sensitive technique that reveals fundamental absorption properties in terms of partition coefficients. By exposing these sensors to a series of organic vapors, the resistance change and mass change of the two sensor platforms can be compared. It is demonstrated that, similar to previous comparative studies of gold nanoparticles functionalized with small organic thiols and synthetic polymer modified QCM crystals, the nanoparticle-based chemiresistor response follows the QCM-traced mass change. The studies show that sorption and conductance modulation mechanisms of vapors on biomolecules are similar to sensors with small organic molecules, but the polarity preference is very different. A model relating partition coefficients K in and chemiresistor responses $\Delta R/R$ is thereafter suggested to account for the links between these 2 sensing systems. It needs to be noted that points which deviate from the modeled trends are likely the result of more complex vapor-material interactions. From here, we demonstrate that DNA oligomers are rich in diversity, which may qualify these materials for array-based and specific sensing applications. It also establishes QCM as a useful complementary tool for evaluating materials for various sensing systems.

5:00pm QC+AS+BI+MN-ThA9 The Evolution of Complex Artificial Cell Membranes: Combining Patterned Plasma Polymers and Supported Lipid Bilayers, Hannah Askew, S.L. McArthur, Swinburne University of Technology, Australia

Supported lipid bilayers (SLBs) have provided researchers with stable and reproducible platforms to recreate cell membrane environments. Such models are useful for studying a variety of processes including cell signalling and drug-membrane interactions. Unfortunately, current models are lacking in their ability to mimic complex micro and nanoscale architectures found within native cell membranes. Many methods of SLB patterning have emerged to form these complex structures. In particular pre-patterned substrates combined with vesicle collapse are of great interest as they eliminate complications associated with preserving membrane integrity during patterning. Plasma polymerisation provides a versatile, one step, dry method of creating thin films of different chemistries on almost any substrate. Successful bilayer formation on such coatings would be beneficial for promoting specific organisation in complex SLB systems using patterned surface chemistries. In the initial stages of this work we studied the effect of plasma polymer chemistry on the lipid structures formed using vesicle collapse. DOPC lipid vesicles were introduced to commonly used coatings formed from plasma polymerised allylamine (ppAAm) and acrylic acid (ppAAc). The coatings were characterised using X-Ray Photoelectron Spectroscopy (XPS), contact angle and Quartz Crystal Microbalance with Dissipation (QCM-D) techniques. Lipid interaction kinetics and lipid mobility were characterised using QCM-D and Fluorescence Recovery after Photobleaching (FRAP) respectively. It was shown that a variety of lipid structures including mobile bilayer can be formed on ppAAc using pH alone to control electrostatic interactions. ppAAm formed immobile vesicular layers under all conditions tested and could therefore be used as a barrier to confine fluid areas of bilayer. Work is now being undertaken to create single and dual plasma polymer patterns on both glass and silicon wafer. Standard photolithography and ion beam methods will be employed to pattern on both a micro and nanoscale. In this way plasma polymer patterns may enable the formation of increasingly complex SLB architectures.

5:20pm QC+AS+BI+MN-ThA10 Applications of QCM in Industrial R&D, Andrey Soukhovjak, The Dow Chemical Company

An overview of diverse applications of QCM enabled by its unparalleled sensitivity to mass and viscoelastic properties of thin samples in R&D of The Dow Chemical Company will be presented.

Surface Modification of Materials by Plasmas for Medical Purposes Focus Topic

Room: 315 - Session SM+AS+BI+PS-ThA

Plasma Processing of Biomimetic Materials

Moderator: Sally McArthur, Swinburne University of Technology, Adoracion Pegalajar-Jurado, Colorado State University

2:20pm SM+AS+BI+PS-ThA1 The Chemistry of Plasma Modified 3D Biomaterials, Eloisa Sardella, CNR-IMIP, Italy **INVITED**

Plasma processing has become a most powerful and versatile tool for surface functionalization of porous materials in biomedical field.

Non equilibrium plasmas have many advantages over wet chemistry approaches: they are highly eco-friendly, have high potentialities in developing surfaces with peculiar characteristics, are capable to be part of in-line material processing and most importantly, can be applied to any material. Consequently, it has opened many new opportunities for investigation of surface modification in various fields like tissue and organ regeneration and biosensing. In this talk, we shall give a brief review on the recent developments of plasma processing of porous materials. We shall describe our experience on non-equilibrium plasmas to modify materials of biomedical interest like: scaffolds for tissue engineering and 3D carbon nanotubes carpets for bio-sensing. This research is aimed to gain new insights on the potentialities of plasma processing of biomedical materials. This work is encouraged by a deep characterization of material's surface and investigation of the material/ bio-environment interface.

3:00pm SM+AS+BI+PS-ThA3 Advantages of Plasma Polymerized Surfaces for Cell Sheet Engineering over Other Deposition Techniques, Heather Canavan, M.A. Cooperstein, University of New Mexico, B. Bluestein, University of Washington, J.A. Reed, University of New Mexico **INVITED**

Poly(N-isopropyl acrylamide) (pNIPAM) undergoes a conformation change in a physiologically relevant temperature range: it is relatively hydrophobic above its lower critical solution temperature (LCST, $\sim 32^{\circ}\text{C}$), and mammalian cells are easily cultured on pNIPAM-grafted surfaces. When the temperature is lowered below the LCST, the polymer's chains rapidly hydrate, and cells detach as intact sheets capable of being used to engineer tissues ("cell sheet engineering"). This behavior has led to a great deal of interest from the bioengineering community, resulting in a variety of film deposition methods, substrate storage techniques, and cell release methods. Unfortunately, this has also resulted in widely varying responses (e.g., % of cells released, biocompatibility and stability of surfaces, etc.) from the resulting cell sheets. In this work, we present a comprehensive comparison of the surface chemistry, biocompatibility, and effect on reversible cell adhesion that results from pNIPAM substrates fabricated using the most common polymerization (free radical and plasma polymerization) and deposition (spin coating and plasma polymerization) techniques. The relative biocompatibility of different mammalian cells (e.g., endothelial, epithelial, smooth muscle, and fibroblasts) was evaluated using appropriate cytotoxicity tests (MTS, Live/Dead, plating efficiency). The pNIPAM-coated surfaces were evaluated for their thermoresponse and surface chemistry using X-ray photoelectron spectroscopy and goniometry. We find that plasma polymerized NIPAM substrates (ppNIPAM) are more stable under a variety of storage conditions prior to their use. Furthermore, when used for cell culture, ppNIPAM films exhibit no cytotoxicity toward any of the cell types tested and yield excellent cell detachment ($\sim 85\%$), which is an important consideration for their ultimate use in engineered tissues.

4:00pm SM+AS+BI+PS-ThA6 Biofunctionalization of Surfaces by Energetic Ion Implantation: Fundamentals and Recent Progress on Applications, Marcela Bilek, A. Kondyurin, E. Kosobrodova, G. Yeo, University of Sydney, Australia, S. Wise, Heart Research Institute, Australia, N.J. Nosworthy, C.G. dos Remedios, A.S. Weiss, D.R. McKenzie, University of Sydney, Australia **INVITED**

Despite major research efforts in the field of biomaterials, rejection, severe immune responses, scar tissue and poor integration continue to seriously limit the performance of today's implantable biomedical devices. Implantable biomaterials that interact with their host via an interfacial layer of active biomolecules to direct a desired cellular response to the implant would represent a major leap forward. Another, perhaps equally revolutionary, development that is on the biomedical horizon is the introduction of cost-effective microarrays for fast, highly multiplexed screening for biomarkers on cell membranes and in a variety of analyte solutions.

Both of these advances will rely on the availability of methods to strongly attach biomolecules to surfaces whilst retaining their biological activity. Radicals embedded in nanoscale carbon rich surface layers by energetic ion bombardment can covalently immobilize bioactive proteins [*Proc. Nat. Acad. Sci* **108**(35) pp.14405-14410 (2011)] onto the surfaces of a wide range of materials, including polymers, metals, semiconductors and ceramics. This new approach delivers the strength and stability of covalent coupling without the need for chemical linker molecules and multi-step wet chemistry. Immobilization occurs in a single step directly from solution and the hydrophilic nature of the surface ensures that the bioactive 3D shapes of the protein molecules are minimally disturbed.

This presentation will describe recently developed approaches that use energetic ions extracted from plasma to facilitate simple, one-step covalent surface immobilization of bioactive molecules. A kinetic theory model of the biomolecule immobilization process via reactions with long-lived, mobile, surface-embedded radicals and supporting experimental data will be presented. Progress on applications of this technology to create antibody

microarrays for highly multiplexed, simple analysis of cell surface markers and to engineer bioactive surfaces for implantable biomedical devices will be reviewed.

4:40pm **SM+AS+BI+PS-ThA8 Three-Dimensional Biopolymeric Scaffold Surface Modification Using Plasma Enhanced Chemical Vapor Deposition: The Effect of Functionality and Wettability on Cell and Bacterial Attachment**, *Morgan Hawker, A. Pegalajar-Jurado, E.R. Fisher*, Colorado State University

Three-dimensional (3D) bioresorbable polymeric materials, such as porous scaffolds made of poly(ϵ -caprolactone) (PCL), have desirable bulk properties for tissue engineering, wound healing, and controlled-release drug delivery applications. However, the surface properties (e.g., chemical functionality and wettability) are often undesirable for certain biomedical applications. Therefore, the ability to fabricate 3D materials with ideal bulk properties and customizable surface properties is a critical aspect of biomaterial development. Here, we demonstrate the deposition of conformal films throughout the 3D porous scaffold network using plasma enhanced chemical vapor deposition (PECVD). Resulting film properties can be tailored by using different precursor species. Octofluoropropane (C_3F_8) and hexafluoropropylene oxide (HFPO) precursors were chosen as model hydrophobic film PECVD systems, whereas a copolymerization system consisting of allylamine/allyl alcohol (allylNH/allylOH) precursors was chosen as a model hydrophilic, nitrogen containing PECVD system. To ensure the efficiency and reproducibility of the treatments, both the exterior and interior of the plasma treated scaffolds were characterized using contact angle goniometry, X-ray photoelectron spectroscopy (XPS), and scanning electron microscopy (SEM) to assess changes in wettability, chemical functionality, and scaffold architecture in comparison to untreated scaffolds. C_3F_8 and HFPO PECVD on scaffolds resulted in fluorocarbon films on the exterior of the scaffold, and the extent of deposition throughout the scaffold's 3D structure was controlled by treatment time. The nitrogen content of the allylNH/allylOH films was tailored by changing the feed gas composition of the copolymerized films. After surface modifications, modified PCL scaffold surface interactions with cells and bacteria were assessed to confirm the relevance of these coatings for the biomedical field. We also explored the effect of different plasma treatments on cell adhesion/proliferation using both human dermal fibroblasts and endothelial cells, bacterial attachment, and biofilm formation using *Escherichia coli*.

5:00pm **SM+AS+BI+PS-ThA9 Plasma Polymerized Bandages for Wound Healing**, *Jason Whittle, L.E. Smith, T.L. Fernandez*, University of South Australia

Wound healing is a multi-billion dollar drain on healthcare systems around the world. This is particularly true in developed countries as they deal with aging populations and conditions such as vascular disease and diabetes. More than 30% of the costs associated with treating diabetes can be attributed to management of chronic wounds. Dressings for the clinical management of wounds are constantly evolving to provide antimicrobial environments and optimal gas exchange, pH and hydration to facilitate wound healing. Ideally, the next generation of wound dressings will also provide a favourable surface for cell attachment, proliferation and migration to further promote the healing process. A number of approaches have been developed for healing chronic wounds, many of which involve culturing of explanted cells, or donor cells, and returning them to the wound site. In this paper, we have used plasma polymerisation to develop surfaces which influence the migration rate of primary cells (keratinocytes, fibroblasts and endothelial cells). A pro-migratory surface will enable cell transport into the wound bed. Earlier workers have concentrated on cell attachment as a key measurement of clinical potential, but we have observed that cell mobility exhibits a preference for different surface chemistry to attachment, and this preference depends on cell type. We show how plasma polymerization can be used to produce surfaces with controllable chemistry, and explore the effect of changing surface chemistry on the migration rate of primary fibroblasts and keratinocytes in vitro. We also investigate the effect of these surfaces on wound closure rate using an in-vitro wounding model based on an engineered skin composite. We also explore the application of plasma polymerized pro-migratory surfaces to electrospun scaffolds for use with deeper wounds.

Scanning Probe Microscopy Focus Topic
Room: 312 - Session SP+AS+BI+NS+SS-ThA

Probing Chemical Reactions at the Nanoscale

Moderator: Carl Ventrice, Jr., University at Albany-SUNY, Jun Nogami, University of Toronto, Canada

2:20pm **SP+AS+BI+NS+SS-ThA1 Surface Structures of Catalysts in Reactive Environments with Scanning Tunneling Microscopy**, *Franklin (Feng) Tao, L.T. Nguyen*, University of Notre Dame **INVITED**

Structure and chemistry of catalysts under a reaction condition or during catalysis are the key factors for understanding heterogeneous catalysis. Advance in ambient pressure photoelectron spectroscopy has taken place over the last decades, which can track surface chemistry of catalysts in gas environment of Torr or even tens of Torr pressure range. Environmental TEM has been developed for studying structures of catalysts while they are in a gas or liquid phase. In terms of environmental TEM, images at a pressure up to bars have been obtained although 1-10 Torr to one bar is the typical pressure range of in-situ studies of catalysts by E-TEM. Compared to structural and chemical information of catalyst particles offered from environmental TEM, packing of adsorbed molecules on a catalyst surface and arrangement of catalyst atoms of catalyst surface are complementary for the structure information provided by environmental TEM. High pressure scanning tunneling microscopy (HP-STM) is the most appropriate technique to achieve these pieces of important information. With the HP-STM the structures of surfaces of model catalysts under a reaction condition or during catalysis can be visualized. Surface structures of catalysts only formed under a reaction condition or during catalysis can be tracked. Such information is significant for understanding catalysis performed at solid-gas interfaces.

In this talk, I will present the historical development of HP-STM. Then, I will review the pressure-dependent packing of chemisorbed molecules; one type of pressure dependence is the change of packing of adsorbates from site-specific binding in UHV or a gas phase with a low pressure to non-specific binding in a gas phase at a relatively high pressure; the other type is a switch from one specific binding site to another specific binding site along the increase of the pressure of gas phase of the reactant. In addition, restructuring of a catalyst surface is another consequence of the increase of the gas phase pressure. The threshold pressure at which a restructuring is performed depends on the original surface structure and the intrinsic electronic state of the metal. I will review the surface restructurings of metal model catalysts including different vicinal surfaces in different reactant gases. In addition, the in-situ studies of Pt(110) and Rh(110) during CO oxidation will be taken as two examples to illustrate the in-situ studies of surfaces of metal model catalysts under reaction conditions (in a gas phase of one reactant) and during catalysis (in a mixture of all reactants of a catalytic reaction).

3:00pm **SP+AS+BI+NS+SS-ThA3 Numerical Analysis of Amplitude Modulation Atomic Force Microscopy in Aqueous Salt Solutions**, *P. Karayaylali, Mehmet Z. Baykara*, Bilkent University, Turkey

We present a numerical analysis of amplitude modulation atomic force microscopy in aqueous salt solutions, by considering the interaction of the microscope tip with a model sample surface consisting of a hard substrate and soft biological material through Hertz and electrostatic double layer forces (P. Karayaylali and M.Z. Baykara, *Applied Surface Science*, 2014, DOI: [10.1016/j.apsusc.2014.02.016](https://doi.org/10.1016/j.apsusc.2014.02.016)). Despite the significant improvements reported in the literature concerning contact-mode atomic force microscopy measurements of biological material due to electrostatic interactions in aqueous solutions, our results reveal that only modest gains of ~15% in imaging contrast at high amplitude set-points are expected under typical experimental conditions for amplitude modulation atomic force microscopy, together with relatively unaffected sample indentation and maximum tip-sample interaction values.

3:20pm **SP+AS+BI+NS+SS-ThA4 Surface Potential Investigation of AlGaAs/GaAs Heterostructures by Kelvin Force Microscopy**, *S. Pouch, Nicolas Chevalier, D. Mariolle, F. Triozon, Y.M. Niquet, T. Melin, L. Borowik*, CEA, LETI, MINATEC Campus, France

The Kelvin force microscopy (KFM) provides a spatially resolved measurement of the surface potential, which is related to the energetic band structure of a material. However, it depends strongly on the physical properties of the tip, e.g. width of the apex, the geometric shape and the stiffness of the cantilever as well as the surface sample state. The goal of this work is to investigate the surface potential measured by KFM on AlGaAs/GaAs heterostructures. For this study, we used a certified reference sample (BAM-L200), which is a cross section of GaAs and $Al_{0.7}Ga_{0.3}As$

epitaxially grown layers with a decreasing thickness (600 to 2 nm) and a uniform silicon doping ($5 \times 10^{17} \text{ cm}^{-3}$). The resulting stripe patterns are commonly used for length calibration and testing of spatial resolution in imaging characterization tools (ToF-SIMS, SEM, XPEEM...). The surface potential measurement is performed under ultra-high vacuum with an Omicron system by using two acquisition modes: the amplitude modulation (AM-KFM), sensitive to the electrostatic force and the frequency modulation (FM-KFM), sensitive to its gradient. Three kinds of tips have been used for this study: platinum or gold nanoparticles coated silicon tips and super sharp silicon tips.

We will present the measurements obtained with these different tips for the narrowest layers (typ. < 40 nm). The surface potential mapping reveals a contrast around 300 meV between $\text{Al}_{0.7}\text{Ga}_{0.3}\text{As}$ and GaAs layers. However, we observed that this contrast vanishes when layer thickness becomes thinner. This loss of contrast cannot be only explained by the resolution limit of the KFM technique. Indeed, we will discuss the effect of the band bending length scale at the AlGaAs/GaAs interface related to the dopant concentration. The contribution of band bending between the layers is evaluated by a self-consistent simulation of the electrostatic potential, accounting for the free carriers distribution inside the sample and for the surface and interface dipoles. We will show that the electric fields of the narrowest layers recover each other, resulting in the partial or total loss of the contrast between $\text{Al}_{0.7}\text{Ga}_{0.3}\text{As}$ and GaAs layers. The simulation results will be compared to the experimental results in order to emphasize that the surface potential contrast is not only influenced by the resolution limit.

4:00pm **SP+AS+BI+NS+SS-ThA6 Probing the Quantum Nature of Hydrogen Bonds at Single Bond Limit in Interfacial Water, Ying Jiang, Peking University, China** **INVITED**

Quantum behaviors of protons in terms of tunneling and zero-point motion have significant effects on water properties, structure, and dynamics even at room and at higher temperature. In spite of tremendous theoretical and experimental efforts, accurate and quantitative description of the quantum nuclear effects (QNEs) in water is still challenging, due to the difficulty of accessing the internal degrees of freedom of water molecules. Using a low-temperature scanning tunneling microscope (STM), we are able to resolve in real space the internal structure, that is, the O-H directionality, of individual water molecules adsorbed on a solid surface [1,2]. The key steps are decoupling electronically the water from the metal substrate by inserting an insulating NaCl layer and enhancing the molecular density of states of water around the Fermi level via tip-water coupling. These techniques allow us not only to visualize the concerted quantum tunneling of protons within the H-bonded network, but also to determine the impact of proton delocalization on the strength of hydrogen bonds by resonantly enhanced inelastic electron tunneling spectroscopy (IETS).

Key words: STM, IETS, water, QNEs, proton transfer, H-bonding strength

[1] J. Guo, X. Z. Meng, J. Chen, J. B. Peng, J. M. Sheng, X. Z. Li, L. M. Xu, J. R. Shi, E. G. Wang*, and Y. Jiang*, "Real-space imaging of interfacial water with submolecular resolution", *Nature Materials* 13, 184 (2014).

[2] J. Chen, J. Guo, X. Z. Meng, J. B. Peng, J. M. Sheng, L. M. Xu, Y. Jiang*, X. Z. Li*, E. G. Wang, "An unconventional bilayer ice structure on a NaCl(001) film", *Nature Communications* 5, 4056 (2014).

4:40pm **SP+AS+BI+NS+SS-ThA8 Resonant Enhanced Spectroscopy of Molecular Rotations with the STM and Field Effect Control of Molecular Dynamics, Fabian Natterer, F. Patthey, Ecole Polytechnique Fédérale de Lausanne (EPFL), Switzerland, Y. Zhao, J.E. Wyrick, J.A. Stroscio, NIST, H. Brune, Ecole Polytechnique Fédérale de Lausanne (EPFL), Switzerland**

Inelastic electron tunneling spectroscopy (IETS) with the scanning tunneling microscope (STM) has vastly fueled the study of magnetic, electronic and vibrational properties of individual atoms and molecules due to its unmatched spatial and excellent energy resolution. Recently [1,2], rotational excitations could be characterized with IETS for the first time and yielded valuable insights into surface dynamics, bond lengths, and, notably about the nuclear spin state of homonuclear molecules. In particular, the two alike nuclei induce symmetry constraints in consequence of the Pauli principle and a certain alignment of nuclear spins requires a specific set of rotational levels J . We demonstrate rotational excitation spectroscopy (RES) with the STM for hydrogen, its isotopes, and mixtures thereof, physisorbed on metal supported graphene and hexagonal boron nitride, as well as on exfoliated graphene devices. We observe excitation energies that are equivalent with rotational transitions ($\Delta J = 2$) of molecules in the gas phase for hydrogen, hydrogen-deuteride, and deuterium, respectively. Notably, these values represent the nuclear spin isomers *para*- H_2 and *ortho*- D_2 . For HD, an additional $J = 0 \rightarrow 1$ transition is discerned, which is allowed for heteronuclear diatomics. We discuss the excitation mechanism in the light of resonant enhanced tunneling [3,4], and illustrate how the

dynamics of molecules could be controlled by applying an electric field using a back gating graphene device geometry [5].

[1] F. D. Natterer, F. Patthey, H. Brune, *Phys. Rev. Lett.* **111**, 175303 (2013)

[2] Li *et al.*, *Phys. Rev. Lett.* **111**, 146102 (2013)

[3] F. D. Natterer, F. Patthey, H. Brune, *arXiv:1403.1312* (2014)

[4] B. N. Persson, A. Baratoff, *Phys. Rev. Lett.* **59**, 339 (1987)

[5] J. Chae *et al.*, *Phys. Rev. Lett.* **109**, 116802 (2012)

Funding from the Swiss National Science Foundation under project number 148891 is greatly appreciated.

Surface Science

Room: 309 - Session SS+AS+NS-ThA

Semiconductor Surfaces and Interfaces 1

Moderator: Ludwig Bartels, University of California - Riverside, Kurt Kolasinski, West Chester University

2:20pm **SS+AS+NS-ThA1 A Study of the InAs(001) Surface Electronic Structure, Jacek Kolodziej, N. Tomaszewska, P. Ciochon, Jagiellonian University, Poland**

Angle-resolved photoelectron spectroscopy (ARPES) is used to study electronic bands at the n-type InAs(001) surfaces, having several different reconstructions. Indium-rich $(8 \times 2)/(4 \times 2)$ and arsenic-rich $c(2 \times 8)/(2 \times 4)$ surfaces as well as sulphur passivated (2×1) surface are prepared and investigated. Measured electronic bands are identified by analysis of their symmetries in the k-space.

In InAs crystal bulk the conduction band minimum (CBM) is located very close to the Fermi level (FL). Downward band bending, typical for the studied surfaces, causes formation of two dimensional electron gas, confined in a subsurface well, also known as the electron accumulation layer. This is indicated by characteristic quantized subband states visible in the ARPES spectra.

It is shown that the band bending magnitude and the quantization (of the accumulated electron energies associated with the coordinate normal to the surface) depend on the surface reconstruction as well as on the crystal doping. In most cases the electron accumulation bands are found at the Fermi level and close to the Γ_{1x1} symmetry point in the center of the surface Brillouin zone. The most clear picture is observed for the sulphur passivated (2×1) surface, where three distinct subbands with minima at $E_1 = -0.276 \text{ eV}$, $E_2 = -0.096 \text{ eV}$ and $E_3 = -0.039 \text{ eV}$ with reference to Fermi level are found. Unexpectedly, for the indium rich surface, occupied conduction states are found also at Γ_{4x2} symmetry points indicating that, for this case, surface resonances mix with the electron accumulation states.

It is also shown that the observed surface bands are sensitive to surface treatment. Two surface preparation techniques have been used: cycles of ion beam annealing (IBA) and *ex situ* wet chemical treatment (WCT). Although low electron energy diffraction (LEED) indicates no increased disorder on the IBA surfaces they yield considerably worse electronic band images. This is most likely due to scattering of photoelectrons on the electrically active antisite defects.

We acknowledge financial support by Polish NCN (contract 2011/03/B/ST3/02070). The research was carried out with the equipment purchased thanks to European Regional Development Fund in the framework of the Polish Innovation Economy Operational Program (contract no. POIG.02.01.00-12-023/08).

2:40pm **SS+AS+NS-ThA2 Control of Point Defect Behavior in Metal Oxides via Surface Band Bending, M. Li, P. Gorai, Edmund Seebauer, University of Illinois at Urbana-Champaign**

Point defects within metal oxide semiconductors such as ZnO affect the material's performance in applications for nanoelectronics, gas sensing, photonics and photocatalysis. Past work in this laboratory has shown that the presence of a nearby surface can influence the concentrations and spatial distributions of defects deep within the semiconductor – often in a controllable way. One mechanism for this influence involves band bending near the surface. The present work employs the optical modulation technique of photoreflectance to measure the magnitude V_s of band bending at polar c-axis ZnO surfaces, and demonstrates that V_s can be manipulated over a significant range (roughly 0.23-0.44 eV) through variations of both temperature and the ambient partial pressure of O_2 . Separate modeling of charged oxygen interstitial motion within the ZnO indicates that the near-surface concentration of these defects scales quadratically with V_s , thereby pointing to a novel general approach by which bulk point defect concentrations can be controlled.

3:00pm **SS+AS+NS-ThA3 Evolution of Surface-Assisted Oxidation of GaAs by Gas-Phase N₂O, NO and O₂.** *Xueqiang Zhang, S. Ptasinaka, University of Notre Dame*

Interests in metal-insulator-semiconductor field effect transistors (MISFETs) have been re-ignited recently due to the approaching of the scaling limit of Si complementary metal-oxide-semiconductors (CMOS). The fate of the III-V semiconductors relies strongly on the availability of a suitable surface passivation technology for fabrication of high quality insulator/III-V semiconductor interface. Gallium oxides on GaAs represent one of contenders for suitable surface passivated oxide-based dielectrics that could produce device-quality electrical interfaces between the oxide and semiconductor. However, there has been a debate on possible GaAs oxidation mechanisms over years. A comparative study between O₂ and other reactive but heteronuclear molecules (such as NO and N₂O) near realistic conditions would provide new insights for a better understanding of the GaAs oxidation process.

A near-ambient pressure X-ray photoelectron spectroscopy (NAP XPS) study of interfacial chemistry between GaAs (100) and three oxidizing gases, N₂O, NO and O₂, are carried out in a wide range of pressures and temperatures. At room temperature, surface oxidation, involving the formation of both Ga₂O and Ga₂O₃ is observed with the extent of oxidation in the order of NO > O₂ > N₂O at elevated pressures. At elevated temperatures, the extent of oxidation is in the order of O₂ > NO > N₂O. Our experimental results show that the oxidation of GaAs (100) by N₂O and NO is primarily determined by the probability and nature of interactions at the gas/semiconductor interface, whereas the limiting factor in the case of O₂ is the energy requirement for O-O bond dissociation.

3:20pm **SS+AS+NS-ThA4 Morphology Dependence of Gas-Phase Molecule Interactions with GaAs Surfaces.** *Sylvia Ptasinaka, X.Q. Zhang, University of Notre Dame*

A great deal of progress has been made in understanding molecular interactions at the interface of two-dimensional GaAs systems under ultra-high vacuum (UHV) conditions. While research on understanding of such interactions with lower-dimensional GaAs-based structures, such as one-dimensional nanowires (NWs), has not been performed despite the potential importance of these structures for developing nano-electronic circuits. Moreover, surface characterization of GaAs under more realistic than the UHV studies, are critical in any attempt to correlate surface chemistry with device properties.

Nowadays, due to recent developments in the surface characterization techniques, and especially the development of Near Ambient Pressure X-ray Photoelectron Spectroscopy (NAP XPS) [1], we are able to track surface chemistry in-situ under elevated pressures and temperatures for different morphologies.

In our present study we used NAP XPS to investigate the interaction of a radically non-planar GaAs surface comprised of an ensemble of GaAs NWs with O₂ and H₂O molecules. In this study the evolution of O₂ and H₂O molecule dissociation on GaAs NWs is tracked under in-situ conditions as a function of temperature and gas pressure to establish whether these processes depend on surface morphology. In contrast to ideally flat GaAs single crystal surfaces that are previously studied [2], gas molecules experienced the enhanced dissociation on GaAs NW ensembles due to an increase in the surface area ratio and the presence of stepped edges, atom vacancies, and other defects on non-flat semiconductor surfaces [3].

[1] D. E. Starr, Z. Liu, M. Havecker, A. Knop-Gericke, and H. Bluhm, Investigation of solid/vapor interfaces using ambient pressure X-ray photoelectron spectroscopy, *Chem. Soc. Rev.* 42, 5833-5857 (2013)

[2] X. Zhang, S. Ptasinaka, Dissociative Adsorption of Water on an H₂O/GaAs(100) Interface-in-Situ near Ambient Pressure XPS Studies, *J. Phys. Chem. C* 118, 4259-4266 (2014)

[3] X. Zhang, E. Lamere, X. Liu, J. K. Furdyna, S. Ptasinaka, Morphology Dependence of Interfacial Oxidation States of Gallium Arsenide under near Ambient Conditions, *Appl. Phys. Lett.* DOI:10.1063/1.4874983 (2014)

4:00pm **SS+AS+NS-ThA6 STM Imaging of the Buried Interface Structures at Ultra-thin Ag Films/Si(111) Substrates.** *Y. Yoshiike, I. Kokubo, Y. Aoki, K. Nakatsuji, Hiroyuki Hirayama, Tokyo Institute of Technology, Japan*

The Schottky barrier height (SBH) has been reported to change sensitively to the variety of reconstructions at the Si substrates before depositing metal films in such systems as Pb/Si(111) and Ag/Si(111). Meanwhile, metal and Si do not mix, and the interfaces between the metals films and Si substrates are atomically abrupt in these systems. Thus, reconstructions at the Si(111) substrate are regarded to be preserved at buried interfaces under metal films, and have an influence on the SBH. In this respect, direct characterization of the buried interface structures in real space is required.

Scanning tunneling microscopy (STM) is a potentially promising method to achieve this, although it is conventionally considered to be useful only for exposed surfaces. Substantially, two different patterns, which were regarded to reflect the periodicity of the lattice at the buried interfaces, were observed on ultra-thin Pb films on the Si(111) substrates. However, the relation to the buried interface structures and the reason for the visualization were still not elucidated. With regard to these points, it is of significant interest to examine whether a different reconstruction on the Si(111) substrate could cause various periodic patterns in abrupt interface systems other than the Pb/Si(111). It is also of interest to investigate the origin of the new periodic pattern. From this perspective, we investigated the STM images of ultra-thin Ag films on Si(111) $\sqrt{3}\times\sqrt{3}$ -B and Si(111)7x7 substrates in this study.

As results, ripples were observed at the surface of ultra-thin Ag films on a Si(111) $\sqrt{3}\times\sqrt{3}$ -B substrate system in STM and dI/dV images. The ripples were faint, independent of the bias voltage, and had the 3x3 periodicity. These indicate that the ripples were geometric corrugations formed at the Ag film surface, which were induced by the commensuration of the Ag(111)1x1 and Si(111) $\sqrt{3}\times\sqrt{3}$ -B lattices at the buried interface. In the meantime, a different ripples were observed at the surface of ultra-thin Ag films on a Si(111)7x7 substrate. The ripples were less periodic, but the Fast Fourier Transform of the images revealed that they had the 7x7 periodicity. In contrast to the Pb/Si(111)7x7 system, the ripples were independent of the bias voltage. Thus, the 7x7 ripple was also regarded to reflect the interface commensuration-induced geometric corrugations at the Ag film surfaces. More detailed results and Synchrotron radiated X-ray diffraction data of these buried interfaces will be shown and discussed in the presentation.

4:20pm **SS+AS+NS-ThA7 Ge on Si Epitaxy: Formation of 3D Ge Islands on Si(100)-2x1 by Annealing of Ge Wetting Layers.** *Gopalakrishnan Ramalingam, P. Reinke, University of Virginia*

The epitaxial growth of Ge on Si(100)-(2x1) proceeds by Stranski-Krastanow (SK) mode where the formation of a wetting layer (WL) is followed by the emergence of quantum dots (QD). New growth modes have been reported recently which can lead to highly anisotropic Ge-wires and are achieved by annealing of the WL prior to the onset of QDs. The goal of the current work is to understand the atomistic processes involved in the transformation of the WL during annealing. We have investigated the WL structure during post-growth annealing at 400 to 600 C and report the transformation of epitaxial two dimensional Ge wetting layers into three dimensional islands, referred to here as pre-quantum dots (p-QDs). The p-QDs include hillocks with a stacked, wedding-cake type structure which show a progression to partial {105} faceting in case of thicker Ge WLs and longer anneal times. At low WL thickness (1-1.5 ML), the p-QDs have a stacked structure while thicker WLs (2-3.5 ML) lead to partial {105} faceted structures. All p-QDs, irrespective of the faceting or size, are characterized by an amorphous mound at the apex; this is strictly limited to p-QDs and not observed for regular QDs. The transition from the WL to p-QDs depends sensitively on the WL thickness (for a given annealing temperature): a six-fold increase in the island number density and a similar decrease in average island volume are observed when the initial WL thickness was increased from 1.2 to 3.5 ML. A small but notable increase in the island number density is observed when samples are annealed for longer durations (after the initial anneal to form the p-QDs) confirming that Ostwald ripening is not a dominant process in this system. Our observations will be integrated with a simulation of the growth process which will inform on the relevant mass transport and the role of strain on the WL transformation to p-QDs.

4:40pm **SS+AS+NS-ThA8 In Search of Nanopatterns: STM Provides Mechanistic Insights into Silicon Functionalization.** *Erik Skibinski, Cornell University, W.J.I. DeBenedetti, Y.J. Chabal, University of Texas at Dallas, M.A. Hines, Cornell University*

Functionalization reactions leave characteristic patterns on surfaces that can be read by STM, providing insight into reaction mechanisms. The functionalization of silicon surfaces with organic monolayers has attracted interest for applications ranging from chemical and biological sensing to renewable energy. A wide variety of surface functionalization reactions have been developed based on dehydration reactions that target surface -OH groups on oxidized silicon. Uniform functionalization therefore requires a uniform, high density of surface -OH groups. Hydroxylating silicon surfaces without concomitant oxidation of the substrate was long thought impossible; however, a novel three-step strategy was recently reported.¹ A hydrogen-terminated silicon surface is first methoxylated in methanol, and then the Si-OCH₃ sites are converted first to Si-F then to Si-OH by successive immersion in hydrofluoric acid and water. Original spectroscopic evidence suggested the creation of nanopatterned surface, in which every other site on the surface is functionalized. New STM and spectroscopic data show selective reaction at step edges and an unexpected functionalization pattern. The mechanistic implications of this pattern will be discussed.

5:00pm SS+AS+NS-ThA9 Benzene and Chlorobenzene Dissociation Pathways Involving Singlet-Triplet Crossing on the Si(100) Surface Modeled Using Small Clusters, Nicholas Materer, E. Butson, Oklahoma State University, Q. Zhu, University of Pittsburgh

The dimer rows in the Si(100) surface have di-radical character, which can be configured as a singlet or triplet. At the minimum energy crossing point of the singlet to triplet crossing for a single Si-dimer cluster, the spin-orbit coupling (SOC) coefficient was determined to be approximately 25 cm^{-1} . Using this SOC, the Landau-Zener spin-crossing probability at room temperature was computed to be approximately 0.5%. Similar computational methods were used to investigate possible adsorption and dissociation processes for benzene and chlorobenzene. The 1,2 product (a tilted configuration) for benzene adsorption was proposed to undergo C-H bond cleavage to form lower-energy products. However, this process requires a spin-crossing of the initial 1,2 bond product, followed by a transition state with large activation barriers. Chlorobenzene can adsorb on the Si(100) by breaking one double bond on the phenyl ring and forming two new carbon-silicon bonds with the dimer cluster. Again, for dissociation to occur, the system must undergo a spin crossing process from the singlet to the triplet state. After this spin crossing event, the carbon-chlorine bond is cleaved and a new silicon-chloride bond is formed. The final product is a dissociation product with chlorine and a phenyl ring attached directly to the (100) surface of silicon. Both cases illustrate that spin crossing could be more common than realized in the adsorption and dissociation of organic molecules on Si(100).

5:20pm SS+AS+NS-ThA10 Adsorption of Organic Triols on Ge(100)-2x1 Surface, Tania Sandoval, S.F. Bent, Stanford University

Organic functionalization of semiconductor surfaces can provide tunable control of interfacial properties in organic-inorganic hybrid devices. The key step toward applications in this area is to understand the selectivity in the reactions of organic molecules on these surfaces.

In this work, adsorption of 1,3,5-benzenetriol and 2-hydroxymethyl-1,3-propanediol on Ge(100)-2x1 surface was studied. Both molecules have three hydroxyl groups available for reaction with the Ge surface. While the reactions of these molecules with the surface may be similar, differences in reactivity can be expected due to their different backbone structures. The aim of this study is to investigate whether a difference in reactivity exists and how the reaction with the surface is affected by the structure of the molecules.

Energy diagrams for both molecules were calculated by density functional theory. In both cases, proton transfer reactions from two or three hydroxyl groups to the Ge dimer atoms are suggested as thermodynamically favored pathways. However, the reaction through 3 OH groups in 2-hydroxymethyl-1,3-propanediol is more than 15 kcal/mol more stable than the same reaction in 1,3,5-benzenetriol. This difference can be associated with strain of the aromatic ring.

Infrared spectroscopy (IR) and X-ray photoelectron spectroscopy (XPS) were performed to investigate the adsorption products. IR results show the presence of a $\nu(\text{Ge-H})$ mode for both molecules, suggesting the proton transfer reaction as the main pathway. XPS spectra of each molecule both chemisorbed and physisorbed on the surface were obtained. The differences between these two spectra can be used to indicate the reaction products. For both molecules, no change in the C(1s) spectra is observed, suggesting that carbon does not form a bond directly with Ge. On the other hand, clear differences between the chemisorbed and physisorbed O(1s) spectra are observed for both molecules. A second peak with a lower binding energy only in the chemisorbed spectra, assigned to a Ge-O bond confirms that both molecules react with the Ge surface through O-H dissociation. The ratio between O(1s) peaks indicates that about 80% of the total hydroxyl groups are involved in reaction with Ge, suggesting that a significant fraction of the adsorbates react with the surface through all 3 of their hydroxyl groups.

In conclusion, both 1,3,5-benzenetriol and 2-hydroxymethyl-1,3-propanediol react with the Ge(100)-2x1 surface through O-H dissociative adsorption. Little difference in reactivity was observed between these triols, suggesting that other factors besides backbone structure are governing the reactivity in these systems.

5:40pm SS+AS+NS-ThA11 The Chemistry of Adsorbed Water on Semiconductor Surfaces for Aqueous Photoelectrochemistry, Coleman Kronawitter, B. Koel, Princeton University

The surface chemistry of water molecules adsorbed on single crystals, model structures relevant to photoelectrode-water interfaces in solar photoelectrochemical systems, is discussed. In heterogeneous processes

relevant to photoelectrochemistry, the interaction of water with semiconductor and metal oxide surfaces is often a critical event whose character influences subsequent chemical pathways that ultimately dictate the reactions' efficiencies and selectivities. A surface science approach is used to characterize adsorbed water molecules on copper oxide and III-V semiconductor surfaces known to actively facilitate solar energy conversion in photoelectrochemical fuel synthesis devices. In this approach, ultrahigh vacuum conditions are used to facilitate the fabrication of highly characterizable adsorbate systems, and the use of single crystal substrates permits analysis of surface chemistry independent of sample grain boundaries and morphology. An understanding of the surface chemistry of adsorbed water is developed through core-level spectroscopies and scanning probe microscopy.

Thin Film

Room: 307 - Session TF-ThA

Thin Film for Permeation Barriers and Membranes

Moderator: Adriana Creatore, Eindhoven University of Technology

2:20pm TF-ThA1 Enhancing Water Desalination Membranes by Initiated Chemical Vapor Deposition (iCVD), Karen Gleason, Massachusetts Institute of Technology **INVITED**

The process of iCVD (initiated Chemical Vapor Deposition) is compatible with the fragile polymeric membranes utilized in seawater desalination, since no solvents or high surface temperatures are employed. The iCVD method is scalable over large areas (commercial reactors >1 m across) and to roll-to-roll processing. Over 70 different monomers have been successfully surface polymerized with iCVD.

Two applications of iCVD to water desalination membranes will be discussed. First, iCVD layers have been directly applied to reverse osmosis (RO) membranes for prevention of fouling by molecules and microbes. Second, iCVD enables the deposition of conformal hydrophobic fluoropolymers which are desired for fabricating high performance membranes for desalination by membrane distillation (MD).

The motivation for the antifouling layers is that with the build-up of scale and/or biofilms, system performance declines, resulting in increased operating costs. Fouling also necessitates periodic shutdown for cleaning and replacement of system components and expensive membranes, resulting in higher maintenance costs. Antifouling surface chemistries synthesized by iCVD include amphiphilic and zwitterionic copolymers. Ultrathin (~20 nm) iCVD coatings have been proved to significantly reduce fouling on commercial reverse osmosis (RO) membranes retaining their water permeation and salt rejection performance. The synthesis of iCVD polymer films starts from the membrane surface allowing chemical design strategies for forming grafted interfaces. These grafted interfaces greatly enhance the durability of iCVD surface modification layer which is essential for real-world implementation that would help ensure reliable and economical clean water production.

3:00pm TF-ThA3 Pulsed Plasma Enhanced Chemical Vapor Deposition for Nanoscale Control of the Size, Shape and Surface Properties of Asymmetric Membranes, Sanket Kelkar, D. Chivetta, C.A. Wolden, Colorado School of Mines

The objective of our research is to develop a simple and scalable approach for modification of size and geometry of model membrane supports to fabricate nanopores. In this work, we first employ relatively large template structures (~100 nm) produced by track-etching or e-beam lithography. The pore size is then reduced to the desired level by deposition of material using pulsed plasma enhanced chemical vapor deposition (PECVD). Pulsed PECVD has been developed as a high throughput alternative to atomic layer deposition (ALD) to deliver self-limiting growth of thin films. Pulsed PECVD has two growth components that act sequentially: ALD-like component during the plasma off step ($\gamma \sim 0$); and PVD-like growth component during the plasma on step ($\gamma \sim 1$), where γ is the reactive sticking coefficient. The ALD contribution is constant at $\sim 1 \text{ \AA/pulse}$ whereas the PVD contribution can be typically varied from 0.5 - 10 \AA/pulse by appropriate control of operating conditions. The degree of conformality in pulsed PECVD can thus be engineered by controlling the relative contribution of these 2 growth components. Like ALD, pulsed PECVD provides sub-nm resolution over the pore size. However, pulsed PECVD does not result in perfectly conformal deposition profiles, and as such control of the final nanostructure is more complicated. In this work we develop feature scale modeling tools to predict and design the fabrication of nanostructures, such as asymmetric nanopores, using pulsed PECVD. The

model is verified by systematic investigation of deposition profiles on patterned cylinders and trenches through cross-section electron microscopy. Polymeric track etched membrane supports (TEMS) are employed as model template structures to demonstrate the capability of pulsed PECVD for precise pore size reduction. Permeance and solute rejection measurements demonstrate that the pulsed PECVD coated TEMS exhibit higher selectivity without compromising on the flux due to their asymmetric structure. These nanoporous membranes will be utilized to study the effect of pore size and geometry on hindered transport of ions and macromolecules at the nanoscale. Furthermore, the hydrophobicity of polymeric supports will be mitigated by deposition of suitable oxide material.

3:20pm TF-ThA4 A Combined Microstructure Characterization of Moisture Permeation Barrier Layers by Means of Electrochemical Impedance Spectroscopy and Ellipsometric Porosimetry, Alberto Perrotta, Eindhoven University of Technology; Dutch Polymer Institute (DPI), Netherlands, S.J. Garcia, Delft University of Technology, Netherlands, J.J. Michels, Holst Centre / TNO, Netherlands, W.M.M. Kessels, M. Creatore, Eindhoven University of Technology, Netherlands

In engineering organic electronic devices, encapsulation layers are mandatory due to the sensitivity of active layers and low work function cathodes to moisture. The quality of the moisture permeation barriers is generally validated by means of water vapor transmission rate (WVTR, $\text{gm}^{-2}\text{day}^{-1}$) measurements as well as visual inspection/identification of the local defects (e.g. pinholes) acting as unhindered pathways for water molecules. Furthermore, it has been demonstrated that the water permeation through the nanoporosity - or free volume - of the bulk of the barrier layer can be 15-20 times higher than the one through local defects [1]. While several methods allow the identification of pinholes/defects, novel techniques able to characterize the barrier microstructure in the broad range of nano- and meso-porosity are sought. In a recent work [2], ellipsometric porosimetry has been demonstrated to be a valuable technique for nanopore characterization. Adopting different probing molecules (i.e. trivinyltrimethyl cyclotrisiloxane, $d_{\text{V3D3}} = 1 \text{ nm}$, and water, $d_{\text{H2O}} = 0.3 \text{ nm}$), a correlation has been found between the (residual) nanoporosity in PE-CVD and (PE-)ALD barriers and their *intrinsic* barrier properties. The pore size range of 0.3-1 nm and its relative content have been found to control the transition in WVTR in the regime of $10^{-4} - 10^{-6} \text{ gm}^{-2} \text{ day}^{-1}$. In order to further investigate this range, electrochemical impedance spectroscopy (EIS) has been adopted for the first time in the study of moisture permeation barriers. EIS allows to follow the diffusion of electrolytes through the barrier and cations having different hydrated shell sizes in the range 0.5-0.7 nm, i.e. Na^+ , Li^+ , K^+ and Cs^+ , have been selected. Changes in the barrier layer resistance have been attributed to the formation of conductive pathways due to the ion diffusion and allow to study differences in layer porosity in the above-mentioned pore diameter/cation size range. Moreover, it is possible to investigate the water permeation as a function of the variation of the barrier capacitance value upon immersion in the electrolyte solution. In this way, the water uptake (ϕ , the volume fraction of water in a coating) and diffusivity coefficient (D) of different moisture barriers are determined. ϕ and D values in the range of 0.8-4% and 10^{-13} - $10^{-15} \text{ cm}^2 \text{ s}^{-1}$ have been found, respectively. This demonstrates that EIS is a versatile tool for the characterization of moisture permeation barriers.

[1] J. Affinito *et al.* 47th Annual Technical Conference Proceedings (2004) 563

[2] A. Perrotta *et al.*, *Microporous and Mesoporous Materials* (2014) 163

4:00pm TF-ThA6 Influence of Surface Topography and Defects on the Performance of Nanoscale Thin Film Moisture Permeation Barriers, Sean King, D. Jacob, B. Colvin, D. Vanleuven, J. Kelly, Intel Corporation
Nanoscale moisture permeation barriers are needed for a wide range of applications including encapsulation of organic light emitting diodes, passivation of thin film photovoltaic devices, low dielectric constant Cu interconnect capping layers, hermetic food packaging, and protective coatings for biomedical devices. A variety of materials deposited by various methods have been proposed and successfully demonstrated for these diverse applications. However, it is well known (although not rigorously characterized) that surface roughness and surface particulates/defects can dramatically reduce the permeation barrier performance of all coating materials. In this presentation, we specifically investigate the impact that surface topography and defects can have on the moisture permeation barrier performance of various materials deposited by common methods such as atomic layer deposition (ALD), plasma-enhanced ALD (PEALD), and plasma-enhanced chemical vapor deposition (PECVD). We show that in the absence of significant surface topography a variety of different PECVD, PEALD, and ALD materials can serve as excellent moisture permeation barriers at thicknesses < 10 nm, but the controlled introduction of surface topography dramatically reduces the barrier performance in all cases. To simulate the presence of surface particulates and defects in a controlled manner, various barrier materials of interest were deposited on hanging

trenches etched into nano-porous inorganic silicates deposited on a thick moisture absorbing SiO_2 film used for moisture permeation detection. The aspect ratios and dimensions were varied to probe the impact of surface particulates of different size and geometry. It will be shown that increasing surface topography generally increases the minimum thickness for a given material and deposition method to serve as a robust moisture permeation barrier. Over all, the surface topography barrier performance is found to strongly correlate with the step coverage and conformality of the deposition process with ALD and PEALD films out performing PECVD films.

4:20pm TF-ThA7 Atomic Layer Deposition for Encapsulation and Barriers, F. van den Bruele, F. Grob, Paul Poedt, Holst Centre / TNO, Netherlands

Developments in the field of flexible electronics, such as organic light emitting diodes (OLEDs), organic photovoltaics (OPV) and other thin-film solar cells, are slowly but surely evolving from lab-scale to industrial production. Proper encapsulation of these moisture sensitive devices is critical, as exposure to moisture from the ambient will degrade these devices, reducing their efficiency, lifetime, or even lead to failure altogether. Especially for OLEDs, the barrier requirements are very challenging, with a Water Vapor Transmission Rate < $10^{-6} \text{ gm}^{-2}/\text{day}$. Encapsulation of flexible devices is even more challenging as the encapsulation should not affect the device flexibility too much. Various flexible thin film encapsulation techniques have been recently developed, often combining one or more thin inorganic diffusion barrier layers (e.g. SiN_x , Al_2O_3) with an organic layer. To achieve these very low WVTRs, very high quality barrier layers are required, being pinhole free over the entire device area.

One approach to make high quality inorganic barrier films is Atomic Layer Deposition (ALD). ALD is a deposition technique capable of producing ultrathin conformal films with control of the thickness and composition of the films at the atomic level. With thin (5-100 nm) Al_2O_3 films deposited by ALD, excellent barrier films (WVTR $\sim 10^{-6} \text{ gm}^{-2}/\text{day}$) can readily be obtained on lab-scale. The major drawback of ALD, however, is its low deposition rate making compatibility with industrial scale processing of devices challenging. The recent development of roll-to-roll and large-area Spatial ALD technology has however spurred the interest in ALD for encapsulation and barriers and the first commercially available electronic devices with ALD encapsulation are probably not far away.

The recent developments of ALD for thin-film encapsulation will be reviewed from a point of view of material- and process development, as well as ALD equipment, with a strong focus on spatial ALD. However, producing barriers with ALD is more complex than only the deposition step itself. For this reason, special attention will be given to aspects such as up-scaling, substrate handling and planarization, managing the effects of particles, characterization and costs of the process.

4:40pm TF-ThA8 Lifetime of Atomic Layer Deposited Al_2O_3 and Parylene Bilayer Encapsulation for Passive and Active Neural Interfaces, Loren Rieth, R. Caldwell, X. Xie, F. Solzbacher, University of Utah

Encapsulation of penetrating neural interfaces with complex geometries is one of the greatest challenges to achieve long-term functionality and stability need for therapeutic systems. We present results from testing a novel encapsulation scheme that combines atomic layer deposited (ALD) Al_2O_3 and Parylene-C for biomedical implants with integrated electronics. The ALD alumina is utilized for its very low water vapor permeation rate, and the Parylene acts as a kinetic barrier to prevent dissolution of the alumina and as a well-regarded biocompatible coating.

Our devices were first coated with a combination of 52 nm of Al_2O_3 deposited by PA-ALD at 120 °C. The organo-silane adhesion promoter A-174 was applied, followed by a 6- μm film of Parylene-C deposited using a CVD process. Acceleration conditions included temperature and/or voltage bias with interdigitated electrodes (IDEs) and Utah Arrays. IDE testing focused on the effects of additional topography on the encapsulation lifetime at acceleration temperatures up to 80 °C. Topography was added by attachment of 0402 surface mount capacitors and custom 5.5 mm wire-wound Au coils, both used in our fully wireless neural interfaces. A >50% decrease in lifetime from > 280 days to 140 days was measured with the addition topography. We are investigating the mechanism for the decreased lifetime to determine if it is associated with chemical degradation, contamination, or mechanical forces through a comparison with thermal cycling measurements.

In-vitro measurements of the impedance stability for passive UEAs have been used to test the encapsulation performance of these devices while soaking in phosphate buffered saline (PBS). The impedances of these arrays are widely reported to decrease during soak testing due to water ingress. Contrary to this trend, we saw an increase in the impedance of arrays from median impedances of 60 k Ω to 160 k Ω during soaking for 960 days of

equivalent time at 37°C. The mechanism for the increase impedance is likely the loss of tip metal.

The impact of voltage bias was also investigated using IDEs and fully-integrated wireless neural interface systems. These devices were maintained 37 °C or higher temperatures for acceleration, and a continuous 5 V bias. For the fully integrated wireless devices, the bilayer encapsulated devices continued to function for 140 days (37 °C equivalent) compared to > 1860 days of equivalent soaking for unpowered devices, indicating ~10 times shorter lifetimes. The lifetime is also more than 10x longer than devices only encapsulated with Parylene-C, indicating the bilayer encapsulation is a significant improvement for these very challenging conditions.

5:00pm TF-ThA9 Influence of Polymer Microstructure and Process Temperature on the Formation of Tailored ALD Coatings on Polymers, R.P. Padbury, Jesse Jur, North Carolina State University

Atomic layer deposition is a technique that is able to integrate nanoscale inorganic coatings to organic polymers. Through this process a number of different inorganic coating morphologies are able to form during ALD nucleation on a wide variety of polymers. In this work, we provide a systematic analysis of the ALD nucleation characteristics on polymers by investigating the influence of polymer microstructure and ALD process temperature. Specifically, in-situ quartz crystal microgravimetry is employed to understand the nucleation behavior of trimethyl aluminum (TMA) in a series of polyesters and poly-n-methacrylates. The data indicates that the glass transition temperature of the polymer, as influenced by variations in microstructure and process temperatures, has a significant impact on the absorption/desorption characteristics during TMA/water exposures. Finally, we propose potential growth mechanisms and demonstrate adjustments to the ALD process parameters that enable the ability to produce a customized interface for ALD materials growth on polymer substrates.

5:20pm TF-ThA10 Mechanisms of Moisture and Oxygen Transport through Thin Silica-like Barrier Films Deposited in Atmospheric Pressure Dielectric Barrier Discharge, Sergey Starostin, FOM Institute DIFFER, Netherlands, B.C.A.M. van der Velden-Schuurmans, S. Quan, FUJFILM Manufacturing Europe b.v., Netherlands, A. Meshkova, M.C.M. van de Sanden, H.W. de Vries, FOM Institute DIFFER, Netherlands

Atmospheric pressure plasma enhanced chemical vapor deposition (AP PECVD) is attracting steadily growing research interest by having clear benefits in terms of equipment costs, footprint size and possibilities for high throughput in-line processing. However the details of the deposition process and the properties of the synthesized coatings were not studied yet as well as for traditional low pressure PECVD. Recently we have reported that good performing moisture and oxygen silica-like barrier films can be fabricated in atmospheric pressure high current diffuse dielectric barrier discharge [1]. However little is known yet about the dominant gas permeation mechanisms through atmospheric pressure plasma deposited barrier films.

In the present contribution the rates of oxygen and moisture vapor permeation were studied as a function of temperature, film thickness and deposition rate. Activated rate theory was applied to analyze the mechanisms of oxygen and moisture transport through the bilayer system of silica-like film and polymer foil. The experimental value of the apparent activation energy E_a determines the degree of interaction between permeating gas and the barrier film. If the E_a values of the bilayer are close to the activation energy of the polymer (47 kJ/mol for moisture), this indicates that the gas transport is controlled by large pinholes with limited or no interaction with the silica film. A transition from polymer controlled moisture permeation to a transport through the silica-like film was observed by tracing an increase in the apparent activation energy from 47 kJ/mol to 80 kJ/mol with film thickness from 2 nm to 100 nm. The gas permeation measurements for the films with different thicknesses were complemented by a detailed morphological study carried out with atomic force microscopy (AFM). The evolution from a non-self-affine morphology of the polymeric substrate to a characteristic smooth surface of the deposited silica-like layer was observed as the film thickness increased from 2 nm to 20 nm. In addition film composition was analyzed by XPS and ATR-FTIR, showing inorganic silica-like character of the deposited layers.

[1] P. Antony Premkumar, S.A. Starostin, M. Creatore, H.W. de Vries, R.M.J. Paffen, P.M. Koenraad, M.C.M. van de Sanden Plasma Process. Polym., 7, 635-639 (2010)

5:40pm TF-ThA11 Scale Dependent Surface Energies Influence Wetting Behaviour on Ultimately Small Topographies, Jan Knauf, Advanced Molecular Films GmbH and RWTH Aachen University, Germany, L. Reddemann, Advanced Molecular Films GmbH and Universität zu Köln, Germany, K. Cheng, AMF GmbH, Germany, A. Böker, DWI-Leibniz-Institute for Interactive Materials, RWTH Aachen University; Lehrstuhl für Makromolekulare Materialien und Oberflächen, RWTH Aachen University, Germany, K. Reihls, Advanced Molecular Films GmbH, Germany

For the first time we observe the effect of scale dependent surface energies on a macroscopic wetting phenomenon. We have been able to produce surfaces structured with sub-nm topographies which exhibit liquid wetting deviating considerably from the behaviour expected from thermodynamic models.

It is known from grazing-incidence X-ray scattering experiments on planar liquid surfaces that surface energy is reduced at very small length scales [1,2]. By deliberately transferring this effect to solid-liquid interfaces it would be possible to create surfaces with distinct wetting characteristics. We have achieved this transfer by preparing defined monolayers of mixed compositions deposited from 1H,1H,2H,2H-perfluoroalkyl thiols of differing chain lengths. As an example, an equimolar binary mixed monolayer from 1H,1H,2H,2H-perfluorodecyl and 1H,1H,2H,2H-perfluorododecyl thiols shows an increase in advancing water contact angle of about 2° compared to the single component monolayers. This increase is considerably less than expected from simple thermodynamic models, as Wenzel's equation of wetting on rough surfaces predicts an advancing angle difference of 7°. We expected that with suitable contacting liquids and tailored topographies the effect of reduced surface energy could be enhanced or even be inverted towards increased surface energies. Thus, it would be possible to manipulate the apparent wetting behaviour of surfaces by creating well-defined ultimately small topographies.

As model system we prepare monolayers from various mixtures of 1H,1H,2H,2H-perfluoroalkyl thiols (FnH2SH, n = 6,8,10,12,14) of different chain lengths on gold, which have been proven to adsorb randomly on the substrate without forming separated domains. Another crucial feature is the stiff helical conformation that is adopted by fluoroalkyl chains. Thus, sub-nm surface topographies with distinct height differences of 1.2 Å per CF₂ group and chain distances of 5.8 Å are created, which have been characterized in detail by static secondary ion mass spectrometry, dynamic contact angle measurements and ellipsometry. Parameters governing the formation of the final monolayers could be obtained and were shown to vary systematically depending on the thiols employed.

[1] S. Mora *et al.*, Phys. Rev. Lett. **90**, 216101 (2003)

[2] C. Fradin *et al.*, Nature **403**, 871 (2000)

**Tribology Focus Topic
Room: 303 - Session TR-ThA**

**Tribology in Unique Environs
Moderator: Kathleen Ryan, United States Naval Academy**

3:00pm TR-ThA3 Molecular Mechanisms of Aqueous Boundary Lubrication by Mucinous Glycoproteins, Stefan Zauscher, Duke University

INVITED

In this talk I will focus on lubricin and surface zone protein, secreted, cytoprotective glycoproteins, encoded by the gene PRG4, that are essential to maintaining joint function and long-term integrity of synovial joints by providing boundary lubrication, preventing cartilage-cartilage adhesion, and mediating adsorption of cells and proteins. Specifically I will report on our results from nanotribo-mechanical measurements on model surfaces and cartilage, combined with other surface specific, physicochemical measurements that shed new light on the mechanisms by which PRG4 provides lubrication and wear protection in diarthrodial joints. Furthermore, I will report on the interaction of PRG4 with collagenous model surfaces. Taken together, our results suggest that the role of effective boundary lubricants in mediating friction in articular joints is largely one of wear protection of surface asperities, by maintaining the surfaces in a nonadhesive mode and causing shear dissipation in the biopolymeric boundary lubricant layer, even at the cost of attaining "high" coefficients of friction (COF ~ 0.15). Our results also contribute to the understanding of the conformation and physico-chemical function of mucinous glycoproteins on biological interfaces.

4:00pm **TR-ThA6 Unusual Friction and Wear Behavior of Graphene in Different Environments**, *Ali Erdemir, D. Berman, A.V. Sumant*, Argonne National Laboratory **INVITED**

Graphene is a remarkable 2D material made of one-atom-thick carbon layer. Its unusual electrical, thermal, optical, and mechanical properties make it a promising material for numerous industrial applications. Recently, graphene was also shown to exhibit unusual tribological properties when used at sliding contact interfaces. In our laboratory, we have been exploring friction and wear behavior of graphene using nano-to-macro-scale tribological test systems and out of our research, we have discovered that a few layers of graphene on sliding surfaces can last tens of thousands of sliding cycles and the rubbing surfaces where graphene is applied to suffer very little or in some instances no wear. Friction was also dramatically reduced. We have found that graphene works equally well in humid or dry test environments; thus contrasting the very high environmental sensitivity of other solid lubricants like graphite or molybdenum disulfide. Our more recent studies have confirmed that even one layer of graphene put on a steel surface has a lifetime of more than 6000 cycles in hydrogen and the rubbing surfaces show no sign of wear. When 2 to 3 layers of large graphene sheets were applied, the lifetime increases to more than 30,000 cycles. Furthermore, under the right test conditions or against the right kind of counterfaces, graphene has the ability to literally vanish friction. This and other tribological observations point to a unique lubrication mechanism for graphene. In this talk, we will provide a comprehensive overview of recent experimental findings regarding the unusual friction and wear behavior of graphene and try to explain why it is so effective in drastically reducing friction and wear despite being only one atom thick.

4:40pm **TR-ThA8 Tribological Properties and Effects of Water on Carbon-Based Materials using Molecular Dynamics Simulations**, *Marcel Fallet, K.E. Ryan*, United States Naval Academy, *M. Knippenberg*, High Point University, *P. Mikulski, J.A. Harrison*, United States Naval Academy

Tribological studies of C-based materials have come to the forefront of experimental and computational chemistry with applications for microfluidic devices and tip-based nano-manufacturing. The effects of humidity on friction and adhesion of some carbonaceous materials underscore the need to understand underlying mechanisms. Since it is difficult to determine atomic-scale behavior via experimental methods, molecular dynamics simulations have been employed to examine this behavior. Sliding simulations of non-hydrogenated, ultrananocrystalline diamond (UNCD) surfaces in the presence of water using the qAIREBO potential¹ have been performed. This reactive, bond-centric potential can model charge in C, H, and O systems. Hybridization changes, cross-sectional distributions of water, charge distributions, and other results will be presented to better understand the tribological impact of water in these systems.

5:00pm **TR-ThA9 An Atomistic Investigation of Tribological Performance of Solvated Nanodiamonds**, *Farshad Saberi-Movahed, D. Brenner*, North Carolina State University, *O.A. Shenderova*, International Technology Center

Nanodiamonds synthesized by detonation of explosives have emerged as a promising additive to base lubricants to reduce wear and friction. Several mechanisms have been suggested for this observation, including creation of protective surface films, surface roughness reduction by abrasion and by filling in surface regions between asperities and by acting as spacers that roll and slide between contacting surfaces.

To better understand the details of these various mechanisms, and how these details relate to nanodiamond and surface structure and properties, we have been carrying out molecular dynamics of solvated nanodiamonds between sliding interfaces. Our initial simulations have focused on understanding the role of particle shape (round versus faceted) on viscosity of base fluid, the motion of the nanodiamond (sliding versus rolling), and correlation time of the nanodiamond motion as a function of pressure, and the interface sliding speed and separation. For example, we have observed that at higher nanodiamond volumetric ratio, the viscosity of water increased. It was also observed that the viscosity of the nanofluid decreased as the temperature increased. Simulation results for nanodiamonds with different surface functional groups, agglomerated nanodiamonds and nanodiamonds reacting with metal surfaces during sliding will be discussed, as well as studies using non-aqueous solvents.

This material is based upon work supported by the G8 Research Council through the National Science Foundation under Grant No. CMMI-1229889

5:20pm **TR-ThA10 Quantitative Analysis by AES and XRD and Tribological Properties of Multilayers and Nanocomposites Based on Titanium Nitride**, *Arturo Talledo*, Universidad Nacional de Ingeniería, Peru, *J.A. Huaranga, J.L. Ampuero, J.J. Asmat, K. Paucar, C. Benndorf*, Universidad Nacional de Ingeniería, Perú

Multilayers and nanocomposites based on titanium nitride are widely investigated due to their high hardness and tribological properties. In this paper we report the production of coatings, on high speed steel, made by dc magnetron sputtering of multilayers TiN/VN, TiN/CrN and TiN/SiN as well as nanocomposites consistent in nanoparticles of SiN or CrN or VN embedded in matrixes of TiN. All these coatings were investigated by Auger Electron Spectroscopy and X-ray diffraction. Stoichiometry and structure were related to their respective Vickers hardness (measured by using Scanning Electron Microscopy), friction coefficient and abrasion wear measurements.

Thursday Evening Poster Sessions

2D Materials Focus Topic

Room: Hall D - Session 2D-ThP

2D Materials Poster Session

2D-ThP1 Extremely Low Impact Energy SIMS Characterization of Graphene, *Alexander Merkulov, F. Horreard, CAMECA, France, W. Strupinski, ITME, Poland, A. Davis, CAMECA Instruments Inc*

Characterization of graphene forms an important part of graphene research and involves measurements based on various microscopic and spectroscopic techniques. Characterization involves determination of the number of layers and the purity of sample in terms of absence or presence of defects or doping species.

A quantitative estimation of the layer thicknesses can be obtained using attenuated secondary electrons emitted from the substrate. Transmission electron microscopy (TEM) can be directly used to observe the number of layers on viewing the edges of the sample, each layers corresponding to a dark line. The information on the defectness of the graphene layer or presence of dopant species can be provided by surface sensitive technique such as XPS and SIMS (Secondary Ion Mass Spectrometry).

The extreme sensitivity of SIMS to any doping constituents in the surficial layer could provide the important information, difficult to obtain by other technique. Application of SIMS to graphene is not yet established. This work is having the goal to advance in finding an approach for graphene layers characterization.

SIMS is a destructive technique based on physical sputtering and consecutive ionization of sputtered atomic or molecular particles. All problems inherent to sputtering itself, such as recoil mixing and ion enhanced diffusion reduce the depth resolution necessary for monoatomic layers characterization. In order to avoid such effect, an Extremely Low Impact Energy (EXLIE) ion beam approach is employed in our experiments. Sputtering with different ionic species and under different angles is performed, targeting the best possible depth resolution in graphene layers.

These EXLIE SIMS measurements are among the first SIMS results obtained on such structures. SIMS as many of the characterization processes needs subsequent tests to determine the validity of the results, using different SG, FG and SLG structures. The SIMS quantification aspects will be also discussed.

2D-ThP3 Synthesis and Characterization of Large-Area and Highly Crystalline Molybdenum Disulfide Atomic Layers by Chemical Vapor Deposition, *Yooseok Kim, S.-H. Park, J.S. Kim, Y.H. Ko, Sungkyunkwan University, Republic of Korea, C. Jeon, Korea Basic Science Institute, Republic of Korea, C.-Y. Park, Sungkyunkwan University, Republic of Korea*

The Isolation of few-layered transition metal dichalcogenides has mainly been performed by mechanical and chemical exfoliation with very low yields. In particular, the two-dimensional layer of molybdenum disulfide (MoS_2) has recently attracted much interest due to its direct-gap property and potential application in optoelectronics and energy harvesting. However, the synthetic approach to obtain high-quality and large-area MoS_2 atomic thin layers is still rare. In this account, a controlled thermal reduction sulfurization method is used to synthesize large- MoO_x thin films are first deposited on Si/SiO_2 substrates, which are then sulfurized (under vacuum) at high temperatures. Samples with different thicknesses have been analyzed by Raman spectroscopy and TEM, and their photoluminescence properties have been evaluated. We demonstrated the presence of single-, bi-, and few-layered MoS_2 on as-grown samples. It is well known that the electronic structure of these materials is very sensitive to the number of layer, ranging from indirect band gap semiconductor in the bulk phase to direct band gap semiconductor in mono-layers. This synthetic approach is simple, scalable, and applicable to other transition metal dichalcogenides. The transferability of MoS_2 films onto other arbitrary substrates like SiO_2/Si makes our MoS_2 a perfect candidate for engineering a variety of applications in nanoelectronics and optoelectronics. Furthermore, this thermal reduction-sulfurization method of synthesizing large WS_2 could now be implemented for the synthesis of other TMDs such as WSe_2 , MOSe_2 , NbS_2 , NbS_2 , etc.

2D-ThP6 XPS Depth Profiling: A Viable Alternative to Secondary Ion Mass Spectrometry, *Michael Williams, Clark Atlanta University, B.R. Strohmeier, Thermo Fisher Scientific*

Secondary ion mass spectrometry (SIMS) is a workhorse for the depth profile characterization of epitaxial materials in the optoelectronics industry. Most notable is its parts-per-billion sensitivity and nm depth resolution for the III-V semiconductors. XPS depth profiling was used to study the effect of substrate temperature on the composition and growth rate of InGaAs/InP multiple layers grown by chemical beam epitaxy. The results are in excellent agreement with published results from SIMS analysis. We show that XPS with its characteristic sensitivity to the environment of the constituent elements in conjunction with argon ion sputtering yields depth profile information on layered systems that exceeds the utility of SIMS.

2D-ThP7 Investigation of Luminescent Properties of $\text{Ca}_5(\text{PO}_4)_3\text{OH}:\text{Gd}^{3+}, \text{Pr}^{3+}$ Phosphor for Application in Displays, Phototherapy Lamps and Thermoluminescence Dosimetry, *Puseletso Mokoena, University of the Free State, South Africa, L. Chithambo, Rhodes University, South Africa, H.C. Swart, O.M. Ntwaeaborwa, University of the Free State, South Africa*

Luminescent properties of calcium phosphate phosphors are being investigated today for many applications in different types of light emitting devices. We have investigated the photoluminescent (PL), cathodoluminescent (CL) and thermoluminescent (TL) properties of hydroxyapatite or $\text{Ca}_5(\text{PO}_4)_3\text{OH}:\text{Gd}^{3+}, \text{Pr}^{3+}$ phosphor for application in phototherapy lamps, information displays and TL dosimetry, respectively. This phosphor was prepared by co-precipitation method and the concentrations of Gd^{3+} and Pr^{3+} in the $\text{Ca}_5(\text{PO}_4)_3\text{OH}$ host were varied. The PL data were recorded in air under excitation by a monochromatized xenon lamp, the CL was measured in vacuum with a Gatan MonoCL4 attached to Jeol JSM-7800F field emission scanning microscope and the TL glow curves were recorded using a Riso TL/OSL reader (model TL/OSL-DA-20) system. In addition, the structure, particle morphology, and chemical states and composition of the phosphor were analyzed by x-ray diffraction, scanning electron microscopy and x-ray photoelectron spectroscopy respectively. The phosphor exhibited a narrowband ultraviolet B (UVB) emission located at 313 nm when excited with the xenon lamp or high energy electrons. This emission was attributed to the $^1\text{P}_{1/2} \rightarrow ^8\text{S}_{7/2}$ transition of Gd^{3+} and was shown to improve considerably by incorporation of Pr^{3+} suggesting that there was energy transfer from Pr^{3+} to Gd^{3+} . The TL glow curves were measured in order to investigate the nature of the electron trapping centers and to determine the related activation energy. A single prominent peak was observed at 347 K at a constant heating rate of 5 K.s^{-1} . The TL kinetic parameter (activation energy) was deduced by the initial rise method, peak shape method and variable heating rates method.

2D-ThP8 Influence of the Deposition Time in Optical and Electric Characteristics of Ge Nanoparticles Grown in SiO_2 by LPCVD Technique, *Melissa Mederos Vidal, S.N. Mestanza Muñoz, Federal University of ABC, Brazil, I. Doi, J.A. Diniz, University of Campina, Brazil*

Germanium nanoparticles (Ge-nps) have potential applications for electronic flash memories and light emitters in visible and near infrared wavelengths, with the main advantage of being compatible with actual device technology. It is known that, in floating gate devices, semiconductor nanoparticles are the charge-storage nodes placed in the gate oxide between the gate and de channel. Thus, as a result of the smaller bandgap, superior carrier mobilities, and higher excitonic Bohr radius compared to Silicon (Si), quantum confinement effects are much more obvious in Ge-nps, making this compound more ideal for memory devices. On the other hand, efficient light emission from Ge-nps in SiO_2 matrix has been already demonstrated being that this can be tuned by changing the size of the nanoparticle and their existence is attributed to the presence of oxide defects, nanoparticles interface, quantum effects, Ge oxygen deficient centers, etc. So, in this context, the present work proposes the study of the influence that the improvement of the Ge-nps quality grown in SiO_2 by LPCVD under different time of deposition, have on their photoluminescence and memory characteristics. For that, measurements as Raman Spectroscopy (RS), Atomic Force Microscopy (AFM) and photoluminescence spectroscopy (PL) were carried out. All samples were made on p-type Si (100) wafer covered by a 8 nm- SiO_2 -thermal-layer, using a vertical CVD reactor PMC 200 Phoenix Materials Corporation. The synthesis method was realized following a two-steps process: a first step, where took place the functionalization of SiO_2 surface by the deposition of Si nuclei from the SiH_4 pyrolysis, and a second step, where the selective growth of Ge nps over Si nuclei happens from GeH_4 pyrolysis. Fig 1 shows the Normalized PL spectra for different Ge-nps size where a shift in the PL

peak position towards longer wavelengths is observed with the increase of nanoparticle-size and, a raise in the intensity of the peak can be note with the enhance of the density of nanoparticle. For the memory characterization, circular MOS capacitors with 200 μm of diameter were fabricated containing these Ge-nps. Fig 2 shows the schematic of the MOS device (a) and the C-V curve comparison between a standard MOS capacitor and one containing the Ge NPs (b). According to this Fig., can be assumed that the major contribution to the memory property of the device comes from the nanoparticles in the gate dielectric since, for the capacitor without nanoparticles hardly hysteresis is observed.

2D-ThP9 Enhanced Electrical Conductivity of Transparent Carbon Nanotube Sheet by Acid Treatment, *J. Kim, JinHong Kim*, University of Texas at Dallas

Enhanced electrical conductivity of transparent carbon nanotube sheet by acid treatment

Jinhong Kim, Daewoong Jung, Maeum Han and Gil S. Lee*

Department of Electrical engineering, University of Texas at Dallas, Richardson, Texas, USA

Fax: +1-(972)-883-6839 E-mail address: gslee@utdallas.edu

Considerable efforts were dedicated to fabricate flexible transparent conductive films (TCFs) with high transmittance and low resistance for utilizing in various applications. To date, the most commonly used material for TCFs is indium tin oxide (ITO) due to its high transparency and low electrical resistance. However, there are several disadvantages with using ITO films in future applications, such as the brittleness and problems with polymer substrates. Recently, researches focused on developments in flexible TCFs, either through optimized structural configuration or exploring new materials to replace ITO films.

Carbon nanotubes (CNTs) have received increasing attentions as ITO replacement due to their excellent mechanical, electrical, thermal properties. Our previous work produced transparent, conductive CNT sheets by using a simple spinning method [1-2]. These CNT sheets had sheet resistances of 0.75-1 $\text{k}\Omega/\text{sq}$ and transmittances of ~85-90 %. However, there was a trade-off effect between sheet resistance and transmittance of TCFs during transferring process of CNTs. An increasing number of CNT layers in the TCFs can decrease the sheet resistance as well as the transmittance, simultaneously. Therefore, key challenge is how to realize the highly conductive CNT sheet without a degrading of transmittance.

Simple acid treatment was conducted to improve the electrical conductivity of the CNT sheets. The transferring CNT sheets on glass substrates were immersed in 60 % nitric acid for 1 hour. After the acid treatment, highly conductive CNT sheets were obtained with slightly increased transmittance. The acid treatment leads further inter-connection between the individual CNTs to form continuous electrical pathway, result in high conductivity of the CNT sheet. These results lead us to believe that the CNT sheets with low sheet resistance (450 Ω/sq) and high optical transmittance (90%) can be potential candidate for flexible TCF applications.

Reference

1. Jung et al, *Sens Actuators A199* (2013), 176.
2. Jung et al. *Jpn. J. Appl. Phys.*, **52** (2013), 03BC03

2D-ThP11 CVD Processes for the Growth of Single Layer Transition Metal Dichalcogenides and Alloys, *Ariana Nguyen, D. Barroso, E. Preciado, V. Klee, S. Bobek, C. Lee, S. Naghibi, I. Lu, G. Von Son Palacio, T. Empante, K. Brown, K. Yang, A. Nguyen, P. Rigas, W. Coley, L. Bartels*, University of California - Riverside

Transition metal dichalcogenides (TMD) present an exciting material system that provides tunable and direct π -bandgap semiconducting properties at the single-layer limit. While monolayer TMD materials can be fabricated through exfoliation, we demonstrate single layer films and islands of MoS_2 , MoSe_2 , WS_2 , etc. as well as their alloys that are grown in a CVD-like processes on SiO_2 and similar materials at process temperatures of $\leq 700^\circ\text{C}$. The resultant films can extend in a continuous fashion across cm-scale substrates and are composed of micron-scale rotational domains. By means of alloying, their band gaps can be tuned in a continuous fashion between 1.9 and 1.6 eV. We present how the use of organic chalcogen precursors allows more versatile alloying and homogeneous growth over extended areas. We also explore variations in the growth mode as a function of process pressure.

2D-ThP15 Studying Graphene & Other 2D Materials With A Multiprobe Cryogenic System That Provides For Simultaneous Raman & Other Optical Modalities With A Wide Variety of Functional SPM Probes, *J. Ernstoff*, Nanonics Imaging Ltd., Israel, *Aaron Lewis*, Hebrew University of Jerusalem, Israel, *O. Zinoviev, A. Komissar, E. Maayan*, Nanonics Imaging Ltd., Israel

This presentation will address the revolution that is occurring in 2D materials such as Graphene, MoS_2 , WSe_2 , etc., and the variety of measurement modalities that are needed to fully understand these materials at cryogenic temperatures.

It is a challenge to study such materials at temperatures down to 10°K when one considers the wide variety of physical phenomena that have to be applied to get a full picture of the functionality of the material under study. This involves questions of structure, nanometric photoconductivity, electrical properties, thermal properties, near-field optical in the apertured and scattering modes, Kelvin probe, and of course Raman. All of these phenomena are common not only to 2D materials but also to carbon nanotubes.

Today's scientific challenges demand a system where one can image these phenomena and correlate such images with the nanometric structure of the material under study. This requires a multiprobe scanned probe microscopy system working at such extreme temperatures, which allows for multiple SPM on-line while maintaining complete optical accessibility. More specifically, the probes which can investigate near-field photoconductivity and Kelvin probe have to be capable of being on-line at the same time and also come into contact with one another to obtain overlapping images of nanometric spaces while still allowing for reflection Raman. This is necessary as many of these systems are incorporated into opaque devices. Such a system will be presented in this presentation with results on graphene.

2D-ThP17 Development of Low-k Dielectric for Graphene device, *YoungGon Lee, L. Cheng*, University of Texas at Dallas, *Y. Kim*, Gwangju Institute of Science and Technology, *G. Mordi*, Samsung, *HH. Hwang, A. Lucero*, University of Texas at Dallas, *BH. Lee*, Gwangju Institute of Science and Technology, *J. Kim*, University of Texas at Dallas

Graphene bilayer pseudo-spin field effect transistor (BiSFET) has been suggested as one of the most promising nanoelectronics since it has a lot of advantages such as low power operation and good scalability.[1] For graphene based 2D devices like BiSFET, it is preferable to have an extremely thin insulator layer with a low-k dielectric constant conformally deposited on the graphene surface. In this work, the transport behavior of non 2D crystalline low-k dielectrics, 3,4,9,10-parylene tetracarboxylic dianhydride (PTCDA), has been investigated to apply the graphene based device as an interlayer tunnel barrier for BiSFET. PTCDA thin films were evaporated on highly ordered pyrolytic graphite (HOPG) and Si surfaces using the molecular beam deposition. Then, Ru/Al was deposited using E-beam evaporator for electrical measurement.

PTCDA devices grown on Si substrate exhibit a rectifying behavior because Schottky can be formed at interface between PTCDA layer and Si substrate. The dielectric constants around $\sim 1.6 - 2.2$ were extracted from capacitance at built-in potential. These results are consistent with previous papers about organic-inorganic Schottky diode.[2] However, as the PTCDA film thickness is scaled down from 20 to 5 nm, the reverse currents increase up to six orders of magnitude possibly because of the tunneling current. In order to explore the tunneling behavior of PTCDA layer on the graphene, the current behaviors of PTCDA layer on HOPG has been investigated. Similar to the current behavior of thin PTCDA layer on Si substrate, PTCDA device on HOPG exhibit tunneling behavior; the current increase linearly with the applied bias in low bias region, whereas it changes exponentially as a function of applied bias in high bias region. The tunneling current of PTCDA layer shows thickness dependence. These behaviors can be modeled by direct tunneling equation. [3] Capacitances around ~ 9 and ~ 16 pF in 3 and 1 nm PTCDA layer on HOPG, respectively, were identified using a time domain reflectometry (TDR) measurement, which are coincide with the value of PTCDA on Si substrate. In addition, there is a weak temperature dependence in current of thin PTCDA device.

In summary, non-2D crystalline low-k dielectric has been developed for the tunnel barrier of graphene based device. The thickness of PTCDA film was successfully scaled down to a few layers. It has also demonstrated that the devices fabricated with thin PTCDA films on HOPG exhibit feasibility of direct tunneling behaviors.

- [1] S. K. Banerjee et al., *Electron Device Lett.* **30**, 158 (2009).
- [2] S. R. Forrest et al., *J. Appl. Phys.* **56**, 543 (1984).
- [3] W. Wang et al., *Rep. Prog. Phys.* **68**, 523 (2005).

2D-ThP18 Charge Exchange and Energy Loss of Slow Highly Charged Ions Passing Through Carbon Nano Membranes, René Heller, R.A. Wilhelm, Helmholtz-Zentrum Dresden - Rossendorf, Germany, E. Gruber, R. Ritter, TU Wien - Vienna University of Technology, Austria, S. Facsko, Helmholtz-Zentrum Dresden - Rossendorf, Germany, F. Aumayr, TU Wien - Vienna University of Technology, Austria

The interaction of slow highly charged ions (HCI) with solid surfaces has been excessively investigated within the recent past. Numerous systematic experiments on the nano structure creation by HCI impact have been carried out and revealed in a variety of different models describing phenomena as the creation of nano hillocks, mono atomic deep pits and etch pits on different kind of (bulk) materials [1-5].

Recently, we have investigated the interaction of slow HCI with one nanometer thin carbon nano sheets. We could show that HCIs can efficiently induce the creation of nm-sized pores in these membranes [6]. However, the extremely small thickness of this kind of target offered us a second opportunity - the observation of the projectile right after the interaction process in terms of its energy loss and charge exchange.

The results of those measurements show an unexpected two-fold ion charge state distribution after passing the membrane comprising (a) ions with very high charge states (close to the initial one) that almost lost no kinetic energy as well as (b) very low charged ions that lost a significant amount of kinetic energy. The balance of both contributions was found to depend strongly on the initial ion charge state. From these findings we draw a microscopic picture of the interaction process that is presented in the present contribution.

References

- [1] A.S. El-Said, R. Heller, W. Meissl, R. Ritter, S. Facsko et al., *Phys. Rev. Lett.* (2008) 100, 237601
- [2] R. Heller, S. Facsko, R. A. Wilhelm and W. Möller, *Phys. Rev. Lett.*(2008) 101, 096102
- [3] A.S. El-Said, R. Heller, F. Aumayr and S. Facsko, *Phys. Rev. B*(2010) 82, 033403
- [4] A.S. El-Said, R. A. Wilhelm, R. Heller, S. Facsko et al., *Phys. Rev. Lett.*(2012) 109, 117602
- [5] F. Aumayr et al., *J. Phys.:Cond. Mat.*(2011) 23, 393001
- [6] R. Ritter, R. A. Wilhelm, M. Stöger-Pollach, R. Heller et al., *Appl. Phys. Lett.*(2013) 102, 063112

2D-ThP20 An Efficient Dry-Transfer Technique with Thermal Annealing for Enabling High-Performance Multilayer MoS₂ Transistors, Xuqian Zheng, R. Yang, Z. Wang, P.X.-L. Feng, Case Western Reserve University

We report the first dry-transferred pristine molybdenum disulfide (MoS₂) field-effect transistors (FETs) fabricated without any post-transfer lithographical and chemical processes, by using a facile, completely-dry-transfer technique with high throughput and high alignment precision. We show that the device performance can be greatly boosted by thermal annealing.

MoS₂ FETs have shown significant potential for enabling 2D electronic devices [1], by demonstrating increasingly competitive performance including high mobility, contact quality, and excellent On/Off ratios. All the MoS₂ FETs reported to date, however, are fabricated using electron-beam- or photo-lithography on top of MoS₂ flakes, and/or polymer-assisted transfer of MoS₂ sheets followed by dissolving the polymer [2], both of which involve multiple wet processing steps. Such processes may contaminate or even degrade the MoS₂ surface, and adversely affect device performance[3].

Here, we demonstrate multilayer MoS₂ FETs fabricated by using a completely-dry transfer method, which not only obviates the undesirable wet chemistry steps, but also has high device yield and more scalable device geometry. Using the technique, we fabricate the electrodes at wafer scale, aligning each flake to the electrodes during the transfer, which significantly improves the efficiency and yield, achieving nearly 100% success rate in obtaining pristine MoS₂ FETs. This dry-transfer process is readily applicable to substrates with much thinner high-k dielectric layers to attain low-threshold-voltage, low-power operations. Also, the performance of as-transferred devices can be further improved through vacuum annealing treatments. While experiments suggest that annealing may lead to dissolving of graphene into metal and thus improve contact [4], annealing effect on MoS₂ devices remains to be systematically explored. We find that the devices' performance typically exhibit noticeable improvement after initial annealing, and further enhancement can often be achieved via additional annealing. With annealing treatments at increasing temperatures, reliable reduction in device resistance is observed, together with consistent increase in mobility up to $\mu=76\text{cm}^2/(\text{V}\cdot\text{s})$, improvement in On/Off ratio exceeding 10^7 , and enhancement in transconductance. Furthermore, while

sometimes annealing can even convert non-Ohmic contacts into Ohmic, occasionally such conversion may not be completed, but still clear improvement can be observed.

- [1] B. Radisavljevic, et al., *Nat. Nanotechnol.* 6, 147 (2011).
- [2] D. Dumcenco, et al., arXiv:1405.0129 (2014).
- [3] Z. Cheng, et al., *Nano Lett.* 11, 767 (2011).
- [4] W. S. Leong, et al., *Nano Lett.* 14, 3840 (2014).

Atom Probe Tomography Focus Topic Room: Hall D - Session AP-ThP

Atom Probe Tomography Poster Session

AP-ThP1 Nanoscale Semiconductor and Oxide Characterization using Atom Probe Tomography, David Larson, M. Ulfig, D. Lenz, D. Lawrence, D. Olson, D.A. Reinhard, T.J. Prosa, P.H. Clifton, T.F. Kelly, CAMECA Instruments Inc.

Atom probe tomography (APT) is being used for an ever widening range of applications [1-3] and is now used by the majority of the leading semiconductor manufactures around the world for research and development [4]. The recent adoption of APT in studying complex semiconductor devices is driven by a combination of the need for nanoscale 3D dopant characterization [5] as well as the concurrent advances in sample preparation methods and advanced control of commercial APT systems [3]. Recent years have seen continued improvements such as flexible data acquisition control, signal-to-noise ratio improvement, compositional accuracy, and yield through improved control of software and hardware.

Yield in APT is often a limitation in extending the technique to non-traditional, material systems. Advanced proportional, integral, differential (PID) control algorithms have been developed to allow stable data collection at lower rates with very fast response times. This feature enables data collection at more optimal conditions to promote higher yield. Additionally, in laser mode, keeping the focussed laser spot optimally aligned with specimen apex is critical to both yield and data quality. Adaptive scan and focus algorithms with smart PID control have been shown to be especially useful in low data collection rate modes to achieve improved yield and accommodate changing environmental conditions. Examples of these advances will be shown.

The nature of APT requires that the entire region of interest (ROI) be captured within a volume roughly 200nm on a side. As applications of APT have expanded, analyses are often limited by the capability to isolate a given region within the bounds of an APT sample geometry. Recently, preparation techniques which allow for re-orientation and isolation of highly discreet ROIs have been developed. These techniques use a focused ion beam system to create markers (in this case holes) in a sample which delineate a specific region. Using this method (known as "targeted backside preparation" [6]), the region of interest is subsequently positioned in a specimen apex in a reversed orientation. This method improves often yield in many difficult materials cases, such as single device analysis or failure analysis.

- [1] T.F. Kelly, D.J. Larson, Annual Reviews of Materials Research, 42 (2012) p. 1.
- [2] E. A. Marquis et al, Current Opinions in Solid State and Materials Science 17 (2013) p. 217.
- [3] D.J. Larson et al, "Local Electrode Atom Probe Tomography", (Springer Science+Business Media, New York) 2013.
- [4] McClean Report, IC insights 17 (2013).
- [5] <http://public.itrs.net/> .
- [6] D. Lawrence et al, 7th Annual FIB SEM Workshop (2014).

Applied Surface Science Room: Hall D - Session AS-ThP

Applied Surface Science Poster Session

AS-ThP1 Formation of Pt, Rh, and Pd Nanoclusters on a Graphene Moire Pattern on Cu(111), Esin Soy, Z. Liang, M. Trenary, University of Illinois at Chicago

Formation and growth of Pt, Rh, and Pd nanoclusters on a graphene covered metal substrate has been investigated by ultrahigh vacuum scanning

tunneling microscopy (UHV-STM). For this purpose a graphene film was formed on the Cu (111) surface by the decomposition of ethylene at high temperatures. According to our results, isolated graphene islands were successfully grown on the Cu surface with different periodicities. Different rotational domains were observed as a result of weakly coupled Cu and graphene caused by the low C solubility in Cu. The most prevalent moire patterns have periodicity of 2.2, 4 and 6.6 nm with rotational angles of 0° and 1.4°, and 37°. Subsequently, nanoclusters were formed at room temperature on the template of a graphene moire pattern formed on Cu (111) surface. As confirmed by the height and size profiles, Rh and Pt clusters display similar planar structures with an average height of about 0.4 nm and average diameter of about 10 nm. The size and distribution of the metal clusters on the two types of Moirés seem to be different. The clusters on the smaller Moiré pattern show a narrow size distribution in both diameter and height. Additionally, these nanoclusters are found to be relatively stable and only undergo agglomeration at relatively high temperatures. These results demonstrate that the metal-C and metal-metal interactions may play a significant role in the cluster formation and it is possible to fabricate finely dispersed metal nanoclusters on the moire structure of graphene covered Cu (111).

AS-ThP2 Valence Band Offsets of Two Rare Earth Oxides on Al_xGa_{1-x}N (0 ≤ x ≤ 0.67) as Measured by Photoelectron Spectroscopy. *Michael Brumbach, A. Allerman, D. Wheeler, S. Atcity, J. Ihlefeld*, Sandia National Laboratories

Preparation of high quality gate oxides on wide bandgap semiconductors is a challenge for realizing efficient high performance devices. For GaN electronics there are a limited number of compatible oxides that have a sufficiently large bandgap to minimize electrical leakage. In this work, reactive molecular beam epitaxy was used to deposit rare earth oxides, Gd₂O₃ and La₂O₃, on GaN substrates. For Gd₂O₃, the valence band offset was tuned by altering the composition of the Al_xGa_{1-x}N substrate. Thin films were characterized using reflection high-energy electron and X-ray diffraction and valence band offsets were determined via X-ray photoelectron spectroscopy.

Sandia National Laboratories is a multi-program laboratory managed and operated by Sandia Corporation, a wholly owned subsidiary of Lockheed Martin Corporation, for the U.S. Department of Energy's National Nuclear Security Administration under contract DE-AC04-94AL85000.

AS-ThP3 Surface Electronics of Individual Si-doped GaN Wires Studied by Synchrotron-Radiation XPEEM Spectromicroscopy. *Olivier Renault, N. Chevalier, J.W. Morin*, CEA-LETI, France

Heavily Si-doped GaN wires are at the basis of innovative LEDs used in advanced solid-state lightning. Understanding how silicon incorporation influences the electronic properties and the measured electrical characteristics of recently emerged very high-conductivity GaN wires [1] is of prime importance for future device optimization.

Here, we have implemented photoemission microscopy with synchrotron radiation (XPEEM) [2] and scanning Auger nanoprobe microscopy (SAM) [3] to investigate the incorporation of Si at the surface of individual GaN wires of 2 μm diameter and the local work function. The high-resolution Si2p micro-spectra evidence complex incorporation of Si pointing on intentional (Si substitution in Ga sites) and un-intentional doping (Si substitution in N-vacancies). By combining elemental analysis from SAM and XPEEM core-level results, we can quantitatively discriminate these two contributions to the doping. Next, we have studied the influence of illumination flux on both the work function and Ga3d binding energies, the strong variations of which evidence surface band bending through the surface photovoltage effect.

This work was carried out at the NanoCharacterization Platform (PFNC) of MINATEC.

AS-ThP6 Characterization of Nanostructured Cu-Zn Oxides Used for Photocathodic Water Splitting. *Sankar Raman, J.F. Moulder*, Physical Electronics Inc., *S. Banarjee*, Washington University, St. Louis, *Y. Myung, H. Im, J. Park*, Korea University, *P. Banarjee*, Washington University, St. Louis

Metal alloys can be efficiently exploited, via controlled fabrication steps, to create mechanically robust and adherent, mixed metal oxide films with tunable photoelectrochemical (PEC) properties. Brass, an alloy of Cu and Zn is an inexpensive source of semiconducting Cu₂O, CuO and ZnO, which have all been used separately as photo-cathodes or photo-anodes respectively for solar water splitting. However, thermodynamics and free energy change predicts a prevalence of ZnO formation when brass is oxidized. We have co-fabricated Cu and Zn oxides to form a highly adherent, mixed metal oxide surface and investigated the relationship between structure property and performance in a PEC cell.

Structural and chemical characterization of the oxide layer was accomplished using an SEM and the PHI X-Tool Scanning XPS microprobe. SEM results show the presence of CuO nanowires interspersed with ZnO fibers and high energy resolution XPS provides detailed chemical state information for Cu and Zn on the surface as a function of sample treatment.

This study indicates that the thermal oxidation of metal alloys can lead to formation of highly interspersed, mixed oxide phases forming novel heterojunctions for use as economical and manufacturing-scalable energy harvesting devices.

AS-ThP8 Impact of a Mixed Oxide's Surface Composition and Structure on Its Adsorptive Properties: The Case of the α-(Fe,Cr)₂O₃(0001) Surface. *M.A. Henderson, Mark Engelhard*, Pacific Northwest National Laboratory

Characterization of an α-(Fe_{0.75},Cr_{0.25})₂O₃(0001) mixed oxide single crystal surface was conducted using x-ray photoelectron spectroscopy (XPS), secondary ion mass spectrometry (SIMS), low energy electron diffraction (LEED) and temperature programmed desorption (TPD). After sputter/anneal cleaning in ultra-high vacuum (UHV), the mixed oxide surface became terminated with a magnetite-(111) structure based on the presence of (2x2) spots in LEED and Fe²⁺ in XPS. The composition of the surface was close to that of M₃O₄ based on XPS, with the metal (M) content of Fe^{2+/3+} and Cr³⁺ being close to 1.4:1, despite the fact that the film's bulk was 3:1 with respect to the metal cations. The enrichment of the surface with Cr was not altered by high temperature oxidation in UHV, but could be returned to that of the bulk film composition by exposure to the ambient. Adsorption of various probe molecules (NO, O₂, CO₂ and H₂O) was used to identify the active cation sites present in the (Fe,Cr)₃O₄(111) terminated surface. Although XPS and SIMS both indicated that the near-surface region was enriched in Cr³⁺, no adsorption states typically associated with Cr³⁺ sites on a -Cr₂O₃ single crystal surfaces were detected. Instead, the TPD behaviors of O₂ and CO₂ pointed toward the main active sites being Fe²⁺ and Fe³⁺, with O₂ preferentially adsorbing at the former and CO₂ at the latter. NO was observed to bind at both Fe²⁺ and Fe³⁺ sites, and H₂O TPD looked nearly identical to that for H₂O on the Fe₃O₄(111) surface. Competition for adsorption sites between coadsorbed combinations of CO₂, O₂, H₂O and NO corroborated these assignments. These results indicate that the surface composition of a mixed oxide can vary significantly from its bulk composition depending on the treatment conditions. Even then, the surface composition does not necessarily provide direct insight into the active adsorption sites. In the case of the (Fe,Cr)₃O₄(111) termination of the α-(Fe_{0.75},Cr_{0.25})₂O₃(0001) surface, Cr³⁺ cations in the near-surface region appear to be fully coordinated and unavailable for adsorbing molecules.

AS-ThP9 Analysis of Metal Particles by Proximal Excitation of Al and Mg Kα X-rays. *C.F. Mallinson, James Castle*, University of Surrey, UK

In preliminary work [1] we have shown that use of an aluminium substrate to support a distribution of copper particles enables their characteristic photoelectrons to be observed within the Auger electron spectrum generated by an incident electron beam. This observation raises the possibility of the use of chemical shifts and the corresponding Auger parameter to identify the chemical states present on the surface of individual sub-micrometer particles within a mixture. In this context, the technique has an advantage in that, unlike conventional Auger electron spectroscopy, the electron beam does not dwell on the particle but on the substrate adjacent to it. Given the importance, for both medical and toxicological reasons, of the surface composition of such particles we have continued to explore the potential of this development.

In this contribution, we show that proximal excitation of x-rays is equally successful with magnesium substrates: In some regions of the XP spectrum the much larger Auger peaks generated by the electron beam can cause inconvenient clustering of Auger and photoelectron peaks. As in conventional XPS, the ability to switch between Al and Mg sources is useful in such situations. In this context, we have extended the studies to iron and nickel particles where we show that use of Al or Mg substrates, as necessary, can make a contribution to clear identification of individual components in the Fe and Ni 2p peaks.

For this development in electron spectroscopy to achieve its full potential it is necessary to optimise the beam conditions used to generate the local x-ray to give good selectivity of a given particle. Measurements made in support of this will be given. Of greater concern is a possible problem of local heating associated with x-ray generation. We continue to explore this problem and report some progress in minimising heating of the particle whilst maintaining the particle selectivity that is central to this exciting development.

References

1. J. E. Castle, R.Grilli and C.F. Mallinson, "XPS Analysis of Small Particles by Proximal X-Ray Generation" *Surface and Interface Analysis*. DOI 10.1002/sia 5452 (2014)

AS-ThP10 XPS Sputter Depth Profiling of Organometallic Multilayer Materials Using Massive Argon Cluster Ions, *Simon Hutton*, Kratos Analytical Limited, UK, *T. Bendikov*, Weizmann Institute of Science, Israel, *W. Boxford, S.C. Page, J.D.P. Counsell*, Kratos Analytical Limited, UK

Thin polymer films are found in an enormous range of devices and have many applications from use in semi-conductors, displays and solar cells to corrosion protection and packaging. New ion sources such as the multi-mode Ar gas cluster ion source (GCIS) have revolutionised the study of such organic thin films by depth profiling with techniques such as X-ray photoelectron spectroscopy (XPS). As reported elsewhere the chemical composition of organic thin films may now be determined as a function of depth by a combination of XPS analysis and etching using massive Ar ions.

In this study we present results from XPS gas cluster depth profiling of multi-layer organometallic thin films. The multi-layer structures are formed by sequential immersion of a pyridine-terminated template layer on silicon or ITO-coated glass substrates.

AS-ThP11 XPS of Liquids: Chemical Bonding in Ionic Liquids and on Tribo-Films Formed on Cast Iron, *Harry Meyer, J. Qu, H. Luo, W. Barnhill*, Oak Ridge National Laboratory

Parasitic friction in internal combustion engines accounts for 10-15% of the nearly 7 billion barrels of oil consumed by cars and trucks in the United States. Recently a new group of oil-miscible ionic liquids has been developed as next-generation lubricant additives. Among the many positive attributes of these IL-additives are thermal stability, excellent wettability, non-corrosive, and most importantly, they possess effective anti-scaffing/anti-wear and friction reduction characteristics. Since the idea of using ionic liquids (ILs) as lubricants was raised in 2001, many studies have been conducted in this area and results have demonstrated superior lubricating performance for a variety of ILs. It is widely believed that a protective tribo-boundary film is formed on the contact area by tribochemical reactions between the metal surface and the IL during the wear process and, as a result, reduces friction and wear. However, the study of this critical boundary film in the literature has been limited to two-dimensional topography examination and chemical analysis from the top surface. Several ionic liquids have been evaluated in both bench and engine tests at ORNL and have shown superior wear protection compared to conventional anti-wear additives. In this poster, two IL ([N888H][DEHP] and [P8888][DEHP]) have been used in scuff tests of cast iron samples (pin-on-disk arrangement) and are compared with zinc dialkyldithiophosphate (ZDDP), the most common anti-wear additive. X-ray photoelectron spectroscopy (XPS) was first used to examine chemical bonding in the ionic liquids and the ZDDP in their *liquid state*. This is possible due to the extremely low vapor pressure exhibited by these materials (including ZDDP). The scuff tests produce tribo-films on the cast iron samples. XPS depth profiling is used to determine the composition as a function of depth for these tribo-films. Chemical bonding within the tribo-film is compared and contrasted to the photoemission results obtained on the liquid forms of the IL's and ZDDP.

Research sponsored by the Vehicle Technologies Program, Office of Energy Efficiency and Renewable Energy, U.S. Department of Energy (DOE). Oak Ridge National Laboratory, managed by UT-Battelle, LLC, for the U.S. Department of Energy under contract number DE-AC05-00OR22725. #

AS-ThP12 X-ray Photoelectron Spectroscopy for Electronic Structure and Valence Information, *R.G. White*, Thermo Fisher Scientific, UK, *Thomas Levesque*, Thermo Fisher Scientific

X-ray Photoelectron Spectroscopy (XPS) is well known for its surface specificity and chemical selectivity. By studying the small binding energy shifts of core level spectra, the analyst may identify the chemical bonding environments of elements present in the surface. When electronic structure or valence information is required, however, many analysts will turn to Ultraviolet Photoelectron Spectroscopy (UPS). There have been many publications in the literature which demonstrate that XPS can also provide electronic and valence information, ranging from work function measurements to valence bonding information.

This work demonstrates the utility of XPS for such measurements and compares results from the same sample set using the complementary techniques of XPS and UPS.

AS-ThP13 Mapping Chemical and Mechanical Property Degradation in PV Modules, *Katherine Stika*, C.S. Westphal, DuPont Central Research and Development, *J. Kapur*, DuPont Packaging & Industrial Polymers, *R.G. Raty, J. Li*, DuPont Central Research and Development, *J. Kopchick, W. Gambogi, B. Hamzaviehary, A. Bradley*, DuPont Photovoltaic Solutions, *J.R. Marsh, B. Foltz*, DuPont Central Research and Development

An understanding of material interactions and degradation pathways in both fielded modules and modules used for accelerated testing is important for photovoltaic (PV) materials specification. As part of the effort to build this understanding, a suite of destructive and non-destructive testing protocols has been developed to compare material performance and reliability under the stresses of different service environments.

This presentation will describe our recent experience mapping the physical and chemical changes observed in degraded PV modules. Examples will include: a) the application of Laser Ablation-Inductively Coupled Plasma-Mass Spec (LA-ICP-MS) for the study of ion migration pathways in encapsulants after PID (Potential Induced Degradation); b) Time-of-Flight Secondary Ion Mass Spectrometry (ToF-SIMS) to follow chemical changes in cells extracted from modules following PID and Damp Heat exposure; and c) NanoHardness testing (NHT) to map mechanical property differences in backsheets removed from PV modules after field exposure.

AS-ThP14 Surface and Interface Studies of Flexible Front Sheets for PV Modules, *Lei Zhang, N.J. Glassmaker, B.B. Sauer*, DuPont Central Research and Development

To develop the next generation flexible front sheets for photovoltaic (PV) modules, FEP, a tetrafluoroethylene/TFE copolymer with ~10wt% hexafluoro propylene, has shown great promise due to its low refractive index and superior properties in light transmission. The chemical and photochemical inertness of FEP make it an ideal candidate for PV front sheets; FEP is expected to produce approximately ~1.5% to ~5% improvement in module power output over incumbent glass or poly(co-ethylene-TFE) (ETFE) front sheets.

Because FEP is a per-fluorinated polymer, the grand challenge in the development process is to achieve good adhesion between the FEP film and the underlying poly(co-ethylene-vinyl acetate) (EVA) encapsulant layer. The adhesion of glass and ETFE to EVA has been demonstrated to be durable to environmental effects. However, untreated FEP film has poor adhesion to EVA, especially after accelerated weathering test conditions at elevated temperature and humidity. In order to exploit the advantages that FEP can offer for improved module efficiency, we have developed a multi-step treatment process to modify FEP surfaces for enhanced adhesion of FEP to EVA. Integrated analytical techniques including XPS, contact angle, SEM, and others were applied to characterize the complex surfaces and interfaces of the modified fluoropolymer surfaces. These analytical results have enabled us to better understand the treatment induced functionality on the FEP surfaces, especially the possible mechanism and the locus of failure at the FEP-EVA interface. This presentation will focus on the studies of the modified FEP-EVA surfaces/interfaces and their correlation with adhesion performance.

AS-ThP15 Multi-technique Surface Analysis of Catalytic Systems with XPS, ISS and UPS, *Bill Sgammato*, Thermo Fisher Scientific, UK

Characterization of catalytic systems benefits from analysis with multiple surface analysis techniques. X-ray Photoelectron Spectroscopy (XPS), for example, is the ideal technique for identifying different chemical species present within the top 10nm of a catalyst surface, but if the elemental composition of the top monolayer is to be investigated then Ion Scattering Spectroscopy (ISS) is the preferred analytical technique. Additionally, if the surface electronic structure can be analyzed, using Ultraviolet Photoelectron Spectroscopy (UPS), then it may be possible to correlate catalytic activity with electronic structure enabling the analyst to identify the chemical species and active sites responsible for catalytic reactions.

This work demonstrates how a single, multi-technique surface analysis system can be used to comprehensively characterize a catalytic system. XPS, ISS and UPS data is presented.

AS-ThP16 Multifunctional Ultra-High Vacuum Apparatus for Studies of the Interactions of Chemical Warfare Agents on Complex Surfaces, *Wesley Gordon*, U. S. Army Edgewood Chemical Biological Center, *E.M. Durke*, Excet, Inc., *A.R. Wilmsmeyer*, Augustana College, *J.R. Morris*, Virginia Tech

A fundamental understanding of the surface chemistry of chemical warfare agents is needed to fully understand the interaction of these toxic molecules with militarily relevant materials. Knowledge of the surface chemistry of agents can be applied to the creation of next generation decontaminants, reactive coatings, and protective materials for the warfighter. Here, we describe a multi-functional ultra-high vacuum instrument for conducting

comprehensive studies of the adsorption, desorption, and surface chemistry of chemical warfare agents on model and militarily relevant surfaces. The system applies reflection-absorption infrared spectroscopy, x-ray photoelectron spectroscopy, and mass spectrometry to study adsorption and surface reactions of chemical warfare agents. Several novel components have been developed to address the unique safety and dosing issues that accompany the research of these toxic, often very low vapor pressure, compounds. Equipment and methods applied in order to safely work with chemical warfare agents will be detailed.

AS-ThP17 A New Transfer Vessel to Facilitate the Characterization of Air-Sensitive Materials, *Richard White, T.S. Nunnay*, Thermo Fisher Scientific, UK, *H.M. Meyer*, Oak Ridge National Laboratory

Analyzing key components of technologically significant devices such as OLED displays, Li-ion batteries and catalyst materials can present challenges to the surface analysts. Amongst the most critical issue is the air sensitivity of these materials. Small amounts of oxygen or water vapour can cause radical changes in the material, ultimately affecting the analysis results and leading to uncertainty in the validity of any conclusions drawn.

Transfer from the preparation environment to the instrument requires the samples to be loaded into a container that can be unloaded into vacuum in the analysis instrument without exposure to the ambient atmosphere. In this presentation we will show results obtained using a new transfer vessel, designed to make the introduction of samples into the vacuum system more automated. Data has been collected from samples covering a range of application areas in order to validate the system, and this will be used to illustrate the benefits of the design.

AS-ThP18 Large-Area Secondary Ion Mapping: An Essential Component of Industrial Problem-Solving, *Kathryn Lloyd, J.R. Marsh*, DuPont Corporate Center for Analytical Sciences

Secondary Ion Mass Spectrometry (SIMS), carried out with liquid metal primary ion sources and time-of-flight mass analyzers, has long been recognized as a means of obtaining lateral distributions of species at the surface via detection of chemically-specific molecular ions. As efforts continue to routinely achieve sub-micron lateral resolution from organic and electrically-insulating samples, it is worth noting that the technique easily lends itself to large-area (millimeters to centimeters) chemical mapping. This capability fills an important niche in the chemical mapping "toolbox" and is relevant to many industrial surface-related problems.

For small-area (less than $500 \times 500 \mu\text{m}^2$) mapping, the primary ion beam optics are (usually randomly) rastered across a pixel array spanning the area of interest, and secondary ion spectral data is collected at each pixel. In the simplest implementation of large-area mapping, the sample stage is moved in regular (essentially large pixel) intervals under an optically-stationary primary ion beam. A more optimal approach is to combine both small-area ion beam rastering with stage rastering in a so-called "patch" configuration.

These large-area mapping acquisitions typically take 30 minutes. Coupled with multivariate analysis, they provide a chemical view of the surface not easily obtainable from other techniques. Examples shown will include optimization of anti-stat coating, understanding fabric color streaking, and assessment of printing uniformity.

AS-ThP19 In Situ Ar Plasma Cleaning of Samples Prior to Surface Analysis, *Vincent Smentkowski, H. Piao*, General Electric Global Research Center, *C.A. Moore*, XEL Scientific

The surface of as received samples is often contaminated with adsorbed layers of hydrocarbons. These surface contaminants can attenuate or mask underlying species of interest, inhibiting or compromising accurate analysis. *In-situ* ion beam sputtering is often used to remove the outer layer of a sample surface and thus remove contaminants, however this erosion process is inherently destructive and can alter the surface of interest. Moreover there are also many materials that can not be cleaned using monoatomic ion beam sputtering as the material(s) may decompose and deposit a layer of fragments onto the outer surface of the material to be analyzed. Recently gas cluster ion beams (GCIB) have been developed^{1,2}, which allows for depth profile analysis of organic layers with minimal degradation³ (and references therein). GCIBs have also been used for low damage surface cleaning^{4,5,6}. A non line-of-sight protocol which is able to clean large (mm or greater) areas is desired. We recently demonstrated that ambient air plasma processing can be used to clean the outer surface of samples⁷, however ambient air plasma treatment can result in oxidation of the material. In this presentation we report our first attempts at *in-situ* plasma cleaning of samples using Ar prior to XPS and ToF-SIMS analysis. We compare Ar plasma cleaning with air plasma cleaning, and report key findings.

¹I. Yamada, J. Matsuo, N. Toyoda and A. Kirkpatrick, *Mater. Sci. Eng., R* **34**, 231 (2001).

²S. Ninomiya, K. Ichiki, H. Yamada, Y. Nakata, T. Seki, T. Aoki and J. Matsuo, *Rapid Commun. Mass Spectrom.*, **23**, 3264 (2009).

³V. S. Smentkowski, G. Zorn, A. Misner, G. Parthasarathy, A. Couture, E. Tallarek, and B. Hagenhoff, *J. Vac. Sci. Technol. A.*, **31**, 30601 (2013).

⁴M. Akizuki, M. Harada, Y. Miyai, A. Doi, T. Yamaguchi, J. Matsuo, G.H. Takoka, C.E. Ascheron, and I. Yamada, *Surface Review and Letters*, **03** (1), 891(1996).

⁵I. Yamada, J. Matsuo, Z. Insepov, D. Takeuchi, M. Akizuki, and N. Toyoda, *J. Vac. Sci. Technol. A* **14**(3) 780 (1996).

⁶I. Yamada, J. Matsuo, and N. Toyoda, *Nuclear Instruments and Methods in Physics Research B*, **206**, 820 (2003).

⁷V.S. Smentkowski, C.A. Moore, *J. Vac. Sci. Technol. A.* **31** (2013) 06F105.

AS-ThP20 Discrete Distribution Profile Model for Characterization of Ultra-Thin Surface Films, *Tatyana Bendikov, T. Toledano, H. Cohen*, Weizmann Institute of Science, Israel

Accurate characterization of ultra-thin surface films is a basic requirement for the successful development of the electronic devices. For example, electrical transport measurements in molecular electronics, often consisting of ultra-thin films, are extremely sensitive to the quality of the films and their associated interfaces. As an experimental technique, X-ray Photoelectron Spectroscopy (XPS) is uniquely suited for the direct characterization of thin films in terms of layer thicknesses, elemental composition and, frequently, the depth-distribution profile of elements across the film. However, interpretation of the raw experimental data requires a reliable theoretical modeling of the photoelectron attenuation; a mechanism that is usually addressed by considering a continuum medium with a phenomenological attenuation parameter. Such models impose severe limitations when self-assembled molecular layers (SAMs) are to be analyzed. In SAMs studies, calculations based on a Discrete Distribution Profile (DDP) are necessary for a proper accounting of atoms situated at the specific locations along the molecular backbone.

In this work, 1-undecane, 11-chloro monolayer deposited on Si substrate was used as a model system. XPS intensities of carbon, chlorine, oxygen and silicon were measured and their components (C_{Cl} , C_{Si} , Si_{ox} , Si_C) were quantified using curve fitting analysis. The intensity ratios (C_{tot}/Cl , C_{tot}/C_{Cl} , C_{tot}/C_{Si} , C_{tot}/Si_C , C_{Si}/Si_C) were then compared to DDP calculated ratios, yielding excellent agreement between experimental and calculated values. The detailed agreement points to the high quality of the studied layers and, more generally, supports the validity of the DDP model as a tool for thin films characterization.

AS-ThP24 Co-solvent Enhanced Zinc Oxysulfide Buffer Layers in Kesterite $Cu_2ZnSnSe_4$ Solar Cells, *Xerxes Steirer, R.L. Garris, J. Li*, National Renewable Energy Laboratory, *M. Dzara*, Rochester Institute of Technology, *P.F. Ndione, K. Ramanathan, I. Repins, G. Teeter, C.L. Perkins*, National Renewable Energy Laboratory

Thin film solar cells rely upon the efficient transfer of photocharge from the absorbing photovoltaic material to an external circuit via thin buffer junction layers. Problems such as low fill factor and current loss arise when the electron collecting contact (emitter) exhibits a large positive conduction band discontinuity with the absorber. This study shows evidence for one approach to circumvent this problem by taking advantage of electronic defects prominent with chemical bath deposition (CBD) of buffer layers. X-ray and ultraviolet photoelectron spectroscopy (XPS/UPS) of heterojunctions formed between CZTSe and CBD-ZnOS with two different buffer preparations exhibit clear differences in electronic properties yet we observe no discernable differences in composition. Structure of CBD-ZnOS made using the different preparation methods is measured with grazing incidence X-ray diffraction (GIXRD) and also exhibits no discernable differences in the peak positions or full widths. XPS/UPS derived band energy diagrams are presented for quasi-*in-situ* prepared CZTSe/CBD-ZnOS interfaces with both preparation methods yielding valence band offsets equal to -1.0 eV and conduction band offsets equal to 1.1 eV. However, comparison between water only and a water/dimethyl sulfoxide solvent mixture in device characterization and band offset measurements show increased band bending in accordance with higher n-type carrier density with water as the only solvent. Seemingly incongruous, the more strongly n-type buffer layer performs worse in solar cells and exhibits inflected current-voltage response under one-sun illumination. A proposed electron transport band for these buffer layers that seems to circumvent the large conduction band spike is estimated to have energies about 0.6 eV below the conduction band of the CBD-ZnOS. Hence, these defects appear to enable adequate band-lineup with the low-band gap absorber, CZTSe ($E_g = 0.96$ eV). These findings suggest that cosolvation approaches may allow for the manipulation of the electronic structure of ZnOS and enable a wider range of electronic applications where larger electron affinities are required.

AS-ThP25 Analysis of Metal Nanoparticles by Auger, XPS and TEM, *Wayne Jennings*, Case Western Reserve University, *C.V. Bishop*, The Best Mode Company, *J. Cowen*, Case Western Reserve University, *J.S. Hammond*, *D.F. Paul*, Physical Electronics USA

Nanoparticles of Pd and PdSn are important as catalysts for chemical reactions and metallization of polymeric materials. Metallization applications include nano-circuitry and automotive plating on plastic. Catalytic applications include the Heck and Suzuki reactions and a variety of other coupling reactions (hydrogenation, dehydrogenation and petroleum cracking). A common synthesis route for Pd nanoparticles is reduction of PdCl₂ with stannous compounds. The structure and purity of the resulting particles is critical to their performance. TEM has been used to examine PdSn nanoparticles for their compositional structure. For very small particles, EDS and EELS analyses become difficult due to the expanded excitation volume. Surface sensitive methods have utility for effective characterization of materials of this type. This work demonstrates the utility of scanning Auger analysis in characterization of particles of this type that effectively complements TEM methods.

Biomaterial Interfaces

Room: Hall D - Session BI-ThP

Biomaterial Interfaces Poster Session

BI-ThP2 Electroassembled Cell Populations in Microfluidic Gradient Generators for Biomolecule Screening, *Chris Wolfram*, University of Maryland, College Park, *X. Luo*, The Catholic University of America, *H.C. Wu*, *C.Y. Tsao*, *M. Guo*, *G.W. Rubloff*, *W.E. Bentley*, *H. Sintim*, University of Maryland, College Park

Laminar flow at the microscale has led to the development of novel new methods for the generation of stable, highly controllable gradients in microfluidic devices. These well-characterized devices have enabled the study of bacterial behavior in complex microenvironments, as well as quantifying the strength of their response to varying concentrations of small molecules. However, flow-based gradient generators subject bacterial cells to shear stress which can attenuate any observed response and make single cell tracking difficult. Static gradient generators eliminate this effect, but the established gradient decays as a function of time due to diffusion. Entrapping cell populations in hydrogels protect them from turbulent environmental conditions, allowing for the use of flow. Additionally, spatially constraining these cells in an array subjects individual cells to the same local concentration without continual gradient deterioration.

The use of electroaddressable hydrogels has been previously demonstrated as a platform for biofabricating "model biofilms." Entrapping populations of *E. coli* in these stimuli-responsive polysaccharide hydrogels enables bacterial signaling interrogation in microfluidic environments with high precision. This technique is integrated within a flow-based microfluidic gradient generator as a device for probing the comparative effects of signaling molecules and nutrients on *E. coli*. The entrapped cells express fluorescent proteins when exposed to a molecule of interest, dependent on the concentration of this molecule. This platform is used for screening the effects of several small molecules on bacterial populations through expression of fluorescent proteins, while mitigating interference from flow-based shear stress or gradient-flattening from diffusion. A concentration-dependent fluorescent response to the interkingdom signaling molecule Autoinducer-2 is demonstrated.

Spectroscopic Ellipsometry Focus Topic

Room: Hall D - Session EL-ThP

Spectroscopic Ellipsometry Poster Session

EL-ThP3 Indium Doped Zinc Oxide as a Transparent Conductor Oxide Replacement for Thin Film Solar Cells Applications, *Neville Sun*, *R. Sun*, Angstrom Sun Technologies Inc., *N.J. Alexander*, *H. Efstathiadis*, SUNY College of Nanoscale Science and Engineering

Indium doped Zinc Oxide as a transparent conductor oxide replacement for thin film solar cells applications

Neville Sun^a and Richard Sun^a

^aAngstrom Sun Technologies Inc., 31 Nagog Park, Acton, MA 01720

^bJ. Nicholas Alexander^b and Harry Efstathiadis^b

^bSUNY – College of Nanoscale Science and Engineering, 257 Fuller Road, Albany, NY 12203

Transparent conductors (TCs) are currently used in many applications, such as solar cells, displays, and electrochromic windows. TCs transparency is reduced in the infrared region due to their metallic property. Indium doped zinc oxide (InZnO) has been considered to be a substitute for the traditional indium tin oxide (ITO) to reduce indium consumption. In this work InZnO was deposited from a metallic indium target and a ceramic zinc oxide target via magnetron co-sputtering in a confocal configuration deposition tool. The films were deposited on soda-lime glass and silicon substrates and had their physical and optical properties measured. The mobility and carrier concentration was characterized by hall measurements, optical properties characterized through ultraviolet-visible-Near Infrared spectroscopy (UV-VIS-NIR), composition characterized by x-ray photoelectron spectroscopy (XPS) and band-gap characterized by spectroscopic ellipsometry.

EL-ThP4 An Innovative High-speed Spectroscopic Ellipsometry and its Novel Applications, *Gai Chin*, ULVAC Inc., Japan

We developed an innovative high-speed spectroscopic ellipsometer. It analyzes the spectrums obtained from the polarization interference occurring between two multiple-order retarders which snapshot the wavelength distribution of the sample's spectroscopic polarization parameters. This novel spectroscopic ellipsometer can measure the thickness and optical constants of thin films at a dramatically fast speed. Its acquisition time is as short as 10 ms. It does not require the conventional complex mechanical or active components for polarization-control, such as a rotating compensator and an electro-optical modulator. It can open great opportunities for new applications of the spectroscopic ellipsometry in which the compactness, the simplicity and the rapid response are extremely important. For example, it was integrated into the deposition tool and successfully measured thin films in the vacuum chamber.

This paper describes the principle, system configuration and our innovative efforts on developing the compact high-speed spectroscopic ellipsometer. Some of the novel applications will be also introduced, such as the ALD, EUV, OLED and other measurement data for the semiconductor, flat panel display and semiconductor industries.

EL-ThP5 Spectroscopic Ellipsometry Studies of Amorphous Silicon Based Photovoltaic Devices, *Maxwell Junda*, *L. Karki Gautam*, *R.W. Collins*, *N.J. Podraza*, University of Toledo

Strategies for improving thin film photovoltaics (PV) are largely dependent on the ability to effectively characterize the opto-electronic and structural properties of each layer and correlate these properties with electrical performance. The common approach of growing and characterizing each layer individually, outside of a complete device, is hindered by the fact that individually grown layers are often not representative of the same layer in a complete device due to substrate dependent growth processes. We have applied spectroscopic ellipsometry (SE) to extract layer thicknesses, interface composition, and optical response in the form of complex dielectric spectra ($\epsilon = \epsilon_1 + i\epsilon_2$) for all hydrogenated amorphous silicon (a-Si:H) layers grown via plasma enhanced chemical vapor deposition onto rough transparent conducting oxide (TCO) coated glass. These samples are processed into single junction p-i-n PV devices and electrically characterized. Real time SE (RTSE) is used in situ, during deposition to monitor the growth evolution of each a-Si:H layer. To accurately model the initial TCO/p-layer interface, a parameterized description of the TCO structure, morphology, and ϵ was developed. From RTSE collected in the early stages of a-Si:H growth, changes in structural and optical properties of the TCO due to plasma exposure are tracked. Characterizing these changes to the substrate material has proved essential to accurately modeling the overlying a-Si:H layers. Leveraging previous studies that determined functional relationships for ϵ of a-Si:H in terms of only the band gap, physically realistic optical and structural properties for each layer are determined by allowing a minimal number of free parameters to fit models to RTSE data. This technique is effective in providing sensitivity to otherwise inaccessible material properties such as ϵ of the thin p-layer and subtle band gap gradients within the i-layer. Models generated from RTSE have been applied to ex situ SE collected over a spectral range of 0.04 – 5.88 eV. This combination of RTSE and infrared extended SE utilized on PV devices enables study of free carrier absorption in the TCO layers, silicon-hydrogen vibrational modes, higher energy electronic transitions in each material, and identification of spectral ranges with enhanced sensitivity to different layers and interfaces.

EL-ThP6 High Speed Spectroscopic Ellipsometry Technique for On-line Monitoring in 600x1200mm Standard Sized Solar Panel Production, *C. Major*, *G. Juhasz*, *P. Petrik*, Mta Ttk Mfa, Hungary, *ZG. Horvath*, MTA Wigner, Hungary, *Miklos Fried*, Hungarian Academy of Science, Hungary

A macro imaging spectroscopic ellipsometer has been developed for high speed mapping of large area multilayer coated substrates. Non-contact or

touchless characterization techniques based on spectroscopic ellipsometry (SE) are widely used by the photovoltaic industry for process or quality control in production. The commercialization of thin film photovoltaic (PV) technologies and the related increasing surfaces lead to many key problems such as reduced efficiency caused by multiple non-uniformities of the layers properties over the entire panel resulting from the technological steps of individual layer components. Scanning methods, based on the conventional narrow beam spectroscopic ellipsometry measurements provides high accuracy but suffer from long mapping times as the polarization state of the reflected beam must be detected. Our new instrument provides a line image of SE ($\lambda=350-1000$ nm) data with a lateral resolution of ~ 20 nm, thus SE information of 1800 points can be collected less than 600 sec over a 600×1200 mm PV material and it could be several 10 times faster than a conventional scanning method. In this paper the calibration were carried out on SiO₂/c-Si structures and test measurements on a-Si films grown on soda lime glass (transparent samples) are presented.

Helium Ion Microscopy Focus Topic Room: Hall D - Session HI-ThP

Aspects of Helium Ion Microscopy Poster Session

HI-ThP1 Fabrication of Single Atom Tip and Characteristics of Gas Field Ion Source at Room Temperature, *In-Yong Park, B. Cho, C. Han, J. Kim, N.-K. Chung, S.J. Ahn*, KRIS, Korea

For a long time, scanning electron microscope (SEM) and transmission electron microscope (TEM) have been playing a significant role in research and industry, especially for high resolution imaging. However, both of them stand in need of sample preparation, such as coating with metal for non-conducting material and slicing for electron transmission, etc. Recently, helium ion microscope (HIM) shows that sub-nanometer imaging resolution could be possible regardless of conducting or non-conducting material without sample metal coating, including nanometer resolution patterning. HIM uses a gas field ion source (GFIS) which is different from tungsten filament, Schottky emitter and liquid metal ion source. In this work, we center around assessment of the characteristics and processes of GFIS in respect to temperature.

The needle like tip to which a high electric field is applied has a fundamental component in GFIS and much of the source physics of GFIS are very similar with field ion microscopy (FIM) [1]. When gases are introduced around the tip, polarized gases are attracted to tip and then ionized at an apex sites by transferring electron from gas to tip. If an ionization sites are confined to only a few atoms, then angular current density can be increased and adaptable to a charged particle microscope although the total current of ion beam is picoampere level. There are a lot of required conditions for generation of stable and high ion beam current. Among them, tip temperature which is related to stability, current density and energy spread is very important. Generally, in order to get an enough ion beam current, tip is cooled by refrigerant and maintained continuously. Supposing a source tip can be used for ion microscope at room temperature without cooling system, maintenance cost and price of apparatus will be reduced with simplified microscope. The aim of this study is to provide an overview of comparison of ion beam in cooled and uncooled tip. We observed the FIM of tungsten tip and fabricated the single atom tip through field assisted nitrogen etching [2]. Furthermore, to simplify the whole process, we did not anneal the tip for tip cleaning through resistive heating. We measured the total ion beam current generated from multi atom and single atom according to gas species, applying voltage, gas pressure and temperature. After that, we examined the potential to be an ion source, which generates ion beam at room temperature, for ion microscope by calculating an angular current density and stability.

[1] Müller, E.; Bahadur, K., Phys. Rev. 102, 624, 1956

[2] Rezeq, M., Pitters, J. and Wolkow, R, J Chem Phys. 124, 204716, 2006

HI-ThP2 Probing Structural Aspects of <10 nm-sized Young Soot, *M. Schenk*, University of Bielefeld, Germany, *S. Lieb*, University of Southern California, *H. Vieker, A. Beyer, Armin Götzhäuser*, University of Bielefeld, Germany, *H. Wang*, University of Southern California, *K. Kohse-Höinghaus*, University of Bielefeld, Germany

Because of its importance for climate, environment and health, detailed information on soot emission is needed. It is particularly important to understand how characteristic parameters, such as size, morphology, and chemical reactivity of soot particles depend upon the formation process. Small soot particles can be particularly dangerous since they can penetrate deeply into the respiratory tract and they may also be more reactive than more mature, larger particles [1]. Investigating the nature of <10 nm soot particles is thus of particular interest. We have studied the morphology of

nascent soot probed from previously well-characterized burner-stabilized ethylene flames [2] with Helium-Ion Microscopy (HIM). HIM allows unambiguous recognition of smaller nascent soot particles than those observed in previous transmission electron microscopy studies. With this technique, surface details are visible down to approximately 5 nm, and particles as small as 2 nm are detectable. The results demonstrate that nascent soot is structurally and chemically inhomogeneous, and even the smallest particles can have shapes that deviate from a sphere [3]. Structural details will be discussed.

[1] B. Frank, R. Schlögl, D.S. Su, Environ. Sci. Technol. 47, 3026-3027, 2013.

[2] A.D. Abid, N. Heinz, E.D. Tolmachoff, D.J. Phares, C.S. Campbell, H. Wang, Combust. Flame 154, 775-788, 2008.

[3] M. Schenk, S. Lieb, H. Vieker, A. Beyer, A. Götzhäuser, H. Wang, K. Kohse-Höinghaus, ChemPhysChem 14(14), 3248-3254, 2013.

HI-ThP3 Fabrication of Carbon Nanotube Nanogap Electrodes by Helium Ion Sputtering for Molecular Contacts, *C. Thiele*, Karlsruhe Institute of Technology, Germany, *H. Vieker, André Beyer*, Bielefeld University, Germany, *B.S. Flavel, F. Hennrich*, Karlsruhe Institute of Technology, Germany, *D.M. Torres, T.R. Eaton*, University of Basel, Switzerland, *M. Mayor, M.M. Kappes*, Karlsruhe Institute of Technology, Germany, *A. Götzhäuser*, Bielefeld University, Germany, *H.V. Löhneysen, R. Krupke*, Karlsruhe Institute of Technology, Germany

We use helium ion beam lithography to sputter nanogaps of 2.8 ± 0.6 nm size into single metallic carbon nanotubes embedded in a device geometry (1). The high reproducibility of the gap size formation provides a reliable nanogap electrode testbed for contacting small organic molecules. To demonstrate the functionality of these nanogap electrodes, we integrate oligo(phenylene ethynylene) molecular rods, and measure resistance before and after gap formation and with and without contacted molecules.

(1) C. Thiele, H. Vieker, A. Beyer, B.S. Flavel, F. Hennrich, D.M. Torres, T.R. Eaton, M. Mayor, M.M. Kappes, A. Götzhäuser, H.v. Löhneysen, R. Krupke: Fabrication of carbon nanotube nanogap electrodes by helium ion sputtering for molecular contacts, Appl. Phys. Lett., doi: 10.1063/1.4868097 (2014)

HI-ThP4 High Resolution UHV Helium Ion Microscopy of Work Function, Step Edges and Crystal Structure, *Gregor Hlawacek*, Helmholtz-Zentrum Dresden - Rossendorf, Germany, *M. Jankowski, R. van Gastel, H. Wormeester, H.J.W. Zandvliet, B. Poelsema*, University of Twente, Netherlands

Helium Ion Microscopy--in particular under UHV conditions--is well known for its high resolution imaging capabilities and the exceptional surface sensitivity. Here, we utilize both of these outstanding characteristics of this technology to visualize step edges, minute changes in composition and structural properties of a Ag/Pt alloy layer grown on Pt(111). A work function contrast of only a few tens of meV allows to distinguish between areas of different Ag content in the alloy layer. As a result step edges on the Pt(111) crystal overgrown by the alloy layer become visible. Furthermore, the regular arrangement of FCC and HCP areas in the alloy layer could be revealed using fast Fourier image analysis and dechanneling image contrast. The measured spacing of 6 nm agrees well with the expected value. Low energy electron microscopy has been used to cross check the results and further analyze the alloy layer.

This research is supported by the Dutch Technology Foundation STW, which is the applied science division of NWO, and the Technology Programme of the Ministry of Economic Affairs.

HI-ThP6 Ion Beam Analysis in a Helium Ion Microscope, *Nico Klingner, R. Heller, G. Hlawacek, S. Facsko, J. von Borany*, Helmholtz-Zentrum Dresden - Rossendorf, Germany

Helium ion microscopes (HIM) have become powerful imaging devices within the last decade. Their enormous lateral resolution of below 0.3 nm and the highest field of depth make them a unique tool in surface imaging. So far the possibilities to identify target materials (elements) are rather limited.

In the present contribution we will show concepts as well as preliminary studies on the capability, efficiency and the limits of applying (Rutherford) Backscattering Spectrometry (RBS) within a HIM device to image samples with target mass contrast and to analyze target compositions.

We will present different concepts of how to realize RBS in a HIM and point out mayor challenges and physical limitation.

In-Situ Spectroscopy and Microscopy Focus Topic Room: Hall D - Session IS-ThP

In-Situ Spectroscopy and Microscopy Poster Session

IS-ThP1 In Situ Synchrotron Radiation Photoemission Spectroscopy Study of Property Variation of Ta₂O₅ Film during the Atomic Layer Deposition. *SeungYoub Lee*, Sungkyunkwan University, Republic of Korea, *C. Jeon*, Korea Basic Science Institute, Republic of Korea, *Y. Kim*, Sungkyunkwan University, Republic of Korea, *J. Lee*, Korea Basic Science Institute, Republic of Korea, *C.-Y. Park*, Sungkyunkwan University, Republic of Korea

Atomic layer deposition (ALD) can be regarded as a special variation of the chemical vapor deposition method for reducing film thickness. ALD is based on sequential self-limiting reactions from the gas phase to produce thin films and over-layers in the nanometer scale with perfect conformality and process controllability. These characteristics make ALD an important film deposition technique for nanoelectronics. Tantalum pentoxide (Ta₂O₅) has a number of applications in optics and electronics due to its superior properties, such as thermal and chemical stability, high refractive index (>2.0), low absorption in near-UV to IR regions, and high-k. In particular, the dielectric constant of amorphous Ta₂O₅ is typically close to 25. Accordingly, Ta₂O₅ has been extensively studied in various electronics such as metal oxide semiconductor field-effect transistors (FET), organic FET, dynamic random access memories (RAM), resistance RAM, etc.

In this experiment, the variations of chemical and interfacial state during the growth of Ta₂O₅ films on the Si substrate by ALD was investigated using *in-situ* synchrotron radiation photoemission spectroscopy. A newly synthesized liquid precursor Ta(NⁱBu)(dmamp)₂Me was used as the metal precursor, with Ar as a purging gas and H₂O as the oxidant source. The core-level spectra of Si 2p, Ta 4f, and O 1s revealed that Ta suboxide and Si dioxide were formed at the initial stages of Ta₂O₅ growth. However, the Ta suboxide states almost disappeared as the ALD cycles progressed. Consequently, the Ta⁵⁺ state, which corresponds with the stoichiometric Ta₂O₅, only appeared after 4.0 cycles. Additionally, tantalum silicide was not detected at the interfacial states between Ta₂O₅ and Si. The measured valence band offset value between Ta₂O₅ and the Si substrate was 3.08 eV after 2.5 cycles.

IS-ThP2 Application of LEEM, PEEM and STM/ncAFM Techniques to Graphene on Metal Surfaces. *A. Thissen*, *Violeta Simic-Milosevic*, SPECS Surface Nano Analysis GmbH, Germany

Abstract Summary: We present recently obtained results in graphene-based systems as measured with LEEM / PEEM and STM / NC-AFM techniques. We highlight the latest state-of-the-art developments in these two techniques and show how these techniques are applied in the latest graphene research as well in other experimental systems.

Introduction: Eighty years ago, Ernst Brueche developed the first photoemission electron microscope (PEEM) in the AEG laboratories in Berlin. Today, the state-of-the-art Low Energy Electron Microscope (LEEM) is produced just a few kilometers away from Brueche's former laboratory carrying forward this groundbreaking developments into the SPECS FE-LEEM P90. This instrument - based on the sophisticated electron-optical design by Ruud Tromp - combines user friendly operation with highest stability and ultimate resolution measurements. Graphene monolayer step edges on Si-sublimated SiC measured using the aberration corrector show a spatial resolution of 1.6 nm, closely approaching theoretical limits.

One of the advantages of SPECS systems is their interconnectability, in this case, by combining the LEEM / PEEM with a SPECS SPM Aarhus 150 with KolibriSensor. The SPM is an ideal system for investigating lattice mismatched surfaces, with a focus in the present talk of SPM measurements on the graphene/Ir(111) system. Microscopy experiments were performed in constant current / constant frequency shift (CC/CFS) and constant height (CH) modes, exploiting a combination of the STM and NC-AFM capabilities of the system. We found that in STM imaging the electronic contribution is prevailing compared to the topographic one and the inversion of the contrast can be assigned to the particular features in the electronic structure of graphene on Ir(111). Contrast changes observed in constant height AFM measurements are analyzed on the basis of the energy, force, and frequency shift curves, obtained in DFT calculations, reflecting the interaction of the W-tip with the surface and are attributed to the difference in the height and the different interaction strength for high-symmetry sites within the moiré unit cell of graphene on Ir(111). The presented findings are of general importance for the understanding of the properties of the lattice-mismatched graphene/metal systems especially with regard to possible applications as templates for molecules or clusters.

IS-ThP3 Quantum Cascade Laser Cavity Ring Down Spectroscopy: New Method for the Characterization and Detection of Aerosols. *E.M. Durke*, *Angela Buonaugurio*, Excet, Inc./Edgewood Chemical Biological Center, *J.M. Edmonds*, Edgewood Chemical Biological Center

Aerosolized chemical warfare agents (CWAs) and toxic industrial chemicals (TICs) are potential threats for the warfighter, resulting in the need for aerosol identification and detection for further developments in protection and mitigation. One of the most reliable techniques for the identification of trace gas species is absorption spectroscopy. Cavity ring down spectroscopy (CRDS) is a highly sensitive and selective absorption method with the ability to detect trace levels of chemical species. Its advantage is based on the extremely long effective path length, providing precise detection of the rate of decay of light from a high finesse optical cavity to directly measure the absorption of the trace gas. The mid-wave (MWIR) and long-wave (LWIR) infrared regions are of particular interest due to the characteristic rovibrational absorption bands exhibited in these regions for identification of a species. Quantum cascade lasers (QCLs) have the capability of emitting both infrared wavelength regions, of 3-8 μm and 8-15 μm, respectively. During the first year of this multi year effort, we have developed a new method for the characterization of aerosols by combining the highly powerful spectroscopic method of cavity ring down spectroscopy and the ability to detect in the IR fingerprint region using quantum cascade lasers for identification. This novel technique results in *in-situ* investigations of chemical aerosols. The development of this method and preliminary data on accepted test vapors and simulants, leading up to aerosols of chemical warfare agents, are presented.

MEMS and NEMS

Room: Hall D - Session MN-ThP

MEMS and NEMS Posters

MN-ThP1 Study on Aspect Ratio Characterization of Polydimethylsiloxane (PDMS) Pillar Arrays for Mechanobiological Traction Forces. *Yu-Hsiang Tang*, National Applied Research Laboratories, Taiwan, Republic of China, *Y.H. Lin*, Instrument Technology Research Center, Taiwan, Republic of China

This paper describes a PDMS-based microchip, which consists of a uniform array of ordered arrangement, vertical, elastomeric micropillar(MP), to study the effects of substrate rigidity for mechanobiological traction forces. The PDMS substrates used have the advantage that their stiffness can be easily adjusted by altering their geometry and can precisely detect the biological activities. We developed the micropillar array substrates that a flexible polymer microfabrication technique was applied for manufacturing the elastomeric microstructures of various aspect ratios with height of 2, 4, 8, 12 mm and radius: period ratios of 1:4, 1:5, 1.5:7, and 2:7 mm. The PDMS micropillar was fabricated by replica molding technique for the standard and combines different steps including photolithography, deep reaction ion etching (DRIE) and soft lithography. The experiment result shows that the micropillar array is clean and in good situation. Meanwhile, more complex patterns of pillar rigidity will help us to study the physical and topographical effect of the substrate on mechanobiological behavior. This has significant implications when designing pillar arrays or comparing lateral forces measured on different pillar geometries. Furthermore, the results presented by this research are believed to be useful for biologists who are clarifying similar mechanobiological processes. Consequently, it was investigated how the substrate contribution to the total pillar deflection depends on the Poisson ratio of the material.

Keywords: PDMS, Soft lithography, Micropillar arrays, Aspect-ratio structure

MN-ThP2 Mixing Effect of PDMS Microchannel with Biaxial Orientation Entry and Various Arrangements of Microstructures. *Po-Li Chen*, *Y.H. Tang*, ITRC, NARL, Taiwan, Republic of China, *Y.S. Lin*, Hungkuang University, Taiwan, Republic of China, *C.N. Hsiao*, *M.H. Shiao*, *Y.H. Lin*, ITRC, NARL, Taiwan, Republic of China

Most active micromixers have the problem of high fabrication cost and low reliability since external actuators and stirrers were involved. In passive mixers, the mixing effect was obtained by changing channel geometry to enlarge the contact surface between different fluids, including serpentine, herringbone, zigzag, twisted, rotating, T-shape and Y-shape channels; and they were preferred due to their easy fabrication and integration in the actual micro system. However, most literatures focused on the studies for mixers with entries on the same plane (i.e. flow directions were all parallel to horizontal plane); in this study, we report a micromixer design with biaxial orientation entries (i.e. flow directions were parallel and vertical to horizontal plane) and investigate the mixing performance by placing various

arrangements of rectangular microstructures with Computational Fluid Dynamics (CFD) techniques.

This study aims on achieving good mixing by changing the arrangements of microstructures to activate the interaction between different fluids. In this paper, several major parameters, including the width and height of microstructures, and the inline or staggered arrangements of various rectangular obstacles on the overall mixing channel pressure drop and mixing efficiency all were well predicted and compared. Simulated and experimental results showed that the microstructures played an important part and resulting in good fluid mixing at low Reynolds numbers.

MN-ThP3 An Integrated Volatile Organic Compounds Sensing Module for Exhaled Air Analysis, Po-Kai Huang, C.-Y. Kuo, P.-H. Kuo, T.-H. Tzeng, S.-S. Lu, W.-C. Tian, National Taiwan University, Taiwan, Republic of China

The detection limit for the gas sensor has been an important factor for the low concentration compound measurement, especially for the detection of disease biomarkers from exhaled human breath air. In this study, we developed a CMOS-based volatile organic compounds (VOCs) sensor with either by a system on chip (SOC)-enabled negative feedback calibration (NFC) readout circuit or a custom-made voltage divider.

The sensor and the SOC-enabled NFC chip were both fabricated by the commercial TSMC 0.35 μ m two poly Si and four metal (2P4M) layer process. The sensing module included a stacked of interdigitated electrodes (IDEs) with polysilicon microheater and the sensing material of monolayer protected gold nanoclusters (MPCs) coated on the electrodes.

In order to conquer the sensor resistance variation created by the MPCs spraying process, the NFC readout circuit was used to overcome the resistance value fluctuation of the VOCs sensor. The sensitivity of our sensing module, consisting of the CMOS-based sensor and the SOC-enabled NFC readout circuit, was increased by approximately two times compared to the previous design. With our sensing module, a wide dynamic range of toluene detection from 30 ppm to 6000 ppm was demonstrated. The sensor responded rapidly, with the rising time and the recovery time both less than six seconds.

With this VOCs sensing module, the detection of lung disease biomarkers from exhaled human breath air could be achieved. Ultimately, the VOCs sensor and NFC readout circuit will be integrated on the same chip to further miniaturize the systems and to minimize the noises in the future.

Manufacturing Science and Technology Room: Hall D - Session MS-ThP

Manufacturing Science and Technology Poster Session

MS-ThP1 Development of Dispersed C₆₀-Molecules/Al Composite Materials Using Nanocrystalline Al Powder Synthesized by Pulsed Wire Evaporation Method, Daiki Muto, A. Matsumuro, Aichi Institute of Technology, Japan

Carbon dioxide reduction is global environmental issues are urgent for all over worlds. As one of the problem solving methods, it is necessary to develop innovative higher specific strength materials. From this viewpoint, we focused on synthesis of new C₆₀/Al composites materials.

In this study, C₆₀/Al composite materials were prepared by a usual press sintering method. We must prevent from aggregation of C₆₀ powders in composite materials because the aggregation parts would surely cause a loss of strength of the materials. In order to distribute C₆₀ molecules around Al powders, ultrasonic vibration was applied with isopropyl alcohol as a solvent for 1 h when both powders were mixed before sintering composite materials. The powder for press sintering was prepared to dry in a furnace at about 340 K for 10 minutes. The average diameter of Al powders and the crystal grain size were about 100 nm measured by SEM and several tens of nm estimated by X-ray diffraction method, respectively. The composite materials with uniform dispersion of C₆₀ were fabricated by press sintering process under the condition of the applied pressure of 1 GPa and the temperature of 723K for 4 hour in Ar gas atmosphere. We investigated the optimal condition of the composite materials as changing composition rates from 0 to 5.0 wt.%C₆₀.

In our results, we could not find remarkable aggregated parts of C₆₀ powders mixing powders up to 1.0 wt.%C₆₀ powders by SEM observations, and the microstructures must be considered to dispersion of C₆₀ molecules around Al powders. All specimens sintered were looked like uniform bulk materials. The densities of composite materials decreased according to the increase in the composition rate of C₆₀, and decreased from 2.7 $\times 10^3$ kg/m³ of Al to 2.36 $\times 10^3$ kg/m³ of 1.0 wt.%C₆₀. X-ray diffraction method showed only Al crystalline structure for all composite materials and FT-IR analysis

clarified the existence of C₆₀ molecules in composite materials. Vickers hardness of Al material showed drastic increase up to 300 Hv in comparison with about 60 Hv of commercial Al materials due to nanocrystallization effect. The composite material with 1.0 wt.%C₆₀ showed the maximum value of 340 Hv. The specific strength of 1.0wt.%C₆₀ was increased up to 5.4 times comparing with those of industrially Al materials. This maximum specific strength of this study clarified surprisingly enhancement of over 3 times in comparison with that of commercial Mg alloys. Therefore, dispersed C₆₀-molecules/Al-matrix composite materials with nanocrystalline powder give us dreams of development for innovative high specific strength materials.

MS-ThP2 Reliability Improvement in Metal Hard-mask based Cu/Ultra Low-K Interconnects by Damage Reduction, MingDa Hsieh, United Microelectronics Corporation, Taiwan, Republic of China

Among the several factors of the circuit reliability degradation, Low-k damage is one of the major factors. The purpose of this paper is to improve reliability by reducing the damage during etching. Low-k damage has been quantified by analysis of measured k value, Relief etch, Thermal Desorption Spectroscopy (TDS) and Leakage Current. Based on all the results, we can infer that Low dissociation Ash and low power PET reduces low-k damage and improves VRDB.

MS-ThP4 Electrical Contact Resistance Characteristics of 28nm HK/MG Gate-Last Process with Advanced Manufacture Technology, Ching-Pin Hsu, C.L. Lu, Y.C. Lin, F.Y. Chang, K.Y. Liao, C.L. Chen, United Microelectronics Corporation, Taiwan, Republic of China, L. Chen, C. Huang, C. Chen, Tokyo Electron Taiwan, Republic of China, J. Tsai, Y. Hsiao, A. Wang, Hermes Epitex, Taiwan, Republic of China

The High-k Metal Gate (HK/MG) Contact Rc is an extremely key factor to dominate the HK/MG MOS transistor device performance. Therefore the HK/MG Contact Rc stability and controllability become relatively important. However, the influence of HK/MG Contact Rc stability would come from the Contact etching process especially. This paper presents HK/MG Contact Rc performance evaluation to achieve the goal of mass production with the control of process flow time, and with several difference treatment methods of Dry and Wet process.

MS-ThP5 Double Patterning Critical Open of Dual Damascene Approach for 14nm Node Beyond, ShihChun Tsai, United Microelectronics Corporation, Taiwan, Republic of China

Double patterning lithography (DPL)

technologies have become a must for 32nm

nodes below. Currently have 2 approaches for DPL:

Self-aligned double patterning(SADP) and litho

etch litho etch(LELE).In this paper, we focus on

LELE induce issue, and present an etching solution

to solve this critical VIA open issue.

MS-ThP6 Vertical Poly Dimethylsiloxane (PDMS) Fluidic Channel Fabrication by Rapid Prototyping, Yu-Hsin Lin, P.L. Chen, NARL, Taiwan, Republic of China, Y.S. Lin, Hungkuang UniversityHungkuang University, Y.H. Tang, C.C. Yang, M.H. Shiao, C.N. Hsiao, NARL, Taiwan, Republic of China

This paper describes a rapid fabrication process in vertical poly dimethylsiloxane (PDMS) fluidic device for bio-applications by Rapid Prototyping (RP). Rapid Prototyping is fast, easy and mask-less process to build the 3-dimension structures. The process allows for the stacking of many PDMS channel layers to realize vertical fluidic device. In this paper, the vertical PDMS fluidic device is consisted two PDMS fluidic channel layer included top fluidic channel layer and bottom fluidic channel layer. The fluidic channel structures is manufactured by Rapid Prototyping then glued on a glass substrate with UV curing as a master. The Teflon-like film is coated on the surface of master. The PDMS is cast against the master producing molded channel layer. After curing process, the PDMS replica is easily peeled off from the master. The top and bottom fluidic channel layers are aligned and bonded together by oxygen treatment to form vertical fluidic device. The performance of vertical fluidic device prepared using this rapid prototyping technique has been demonstrated by fabricating a miniaturized bio-application system.

MS-ThP7 Fabrication of Deeply Striped Pattern Structures by ICP-RIE Technique on the Lithium Niobate Substrate, Chun-Ming Chang, M.-J. Huang, J.Y. Su, N.N. Chu, C.N. Hsiao, M.H. Shiao, ITRC, NARL Taiwan, Republic of China

In this study, striped pattern structures with linewidth of 5 μ m and 10 μ m on lithium niobate (LiNbO₃) substrate were fabricated by the inductively

coupled plasma reactive ion etching (ICP-RIE) technique for the waveguide applications. Pure nickel (Ni) thin film of 300 nm in thickness used as the etching mask and was deposited by sputtering technique on the LiNbO₃ substrate with a 20 nm adhesion layer of nickel-chrome (Ni-Cr) alloy with a composition ratio of 80/ 20. The LiNbO₃ substrates with the Ni etching mask was etched in the boron trichloride (BCl₃)/ Argon (Ar) mixed etching gas which flow ratio was controlled at 30/ 5 SCCM and the working pressures controlled at 30 mTorr, 40 mTorr, 50 mTorr, and 60 mTorr, respectively. The ICP powers were controlled from 100 W to 600 W and the RF powers were controlled from 100 W to 500 W during 45 minutes of each ICP-RIE process.

From the experimental results, it can be found that the DC bias (-V) decreases with the working pressure, and increases with the ICP powers and the RF powers. Under suitable ICP-RIE etching parameters, the structure with 6 μm in depth and the sidewall angle of 80° was successfully prepared on the the surface of LiNbO₃ substrate, which the etch selectivity ratio was 10 and the etching rate was 70 nm/ min.

MS-ThP9 Fabrication of Micro ring Resonators for Nonlinear Optics Applications using Silicon Nitride Film Deposited at Room Temperature Overcoming the Stress Limitation, Adriano Ricardo do Nascimento Jr., L.T. Tiago Manera, J.A. Alexandre Diniz, A.R. R. Silva, M.V. Vinicius Puydinger dos Santos, University of Campinas, Brazil, A.C. Cerqueira S. Jr., National Institute of Telecommunications, Brazil, L.A. A. M. Barea, N.C. C. Frateschi, University of Campinas, Brazil

Silicon nitride (Si_xN_y) films deposited by low-pressure electron cyclotron resonance plasma enhanced chemical vapor deposition (ECR-CVD) at room temperature are proposed for nonlinear optics applications in the telecommunications C-band. Due to the high silicon nitride nonlinearity, these films recently have also been used for nonlinear optics [1]. For nonlinear applications such as the generation of frequency combs, the waveguide needs a zero dispersion point in the middle of C-band, requesting large waveguide area. Unfortunately, these thick Si_xN_y films (>400 nm) have high stress and suffer from catastrophic cracking, which reduces the device efficiency [2]. Using numerical simulations it was demonstrated that for refractive index (n) values greater than 2, the area of the waveguide with zero dispersion point at λ = 1.55 μm is greatly reduced.

By varying deposition parameters, such as gas pressure (4-6 mTorr) and Si/N ratio (0.62-1.25), Si_xN_y films with high deposition rate and high refractive index was obtained. In many cases, for larger pressure values a considerable increase in the deposition rate is observed, and for lower N₂ flow was observed a large increase of η (due to high concentration of Si). However, increasing the gas pressure, a reduction of η due the incorporation of hydrogen in the film was also observed.

A Si-rich silicon nitride layer with 730 nm of thickness, refractive index of 2, high deposition rate, low hydrogen concentration and roughness average of 0.52 nm was deposited above a Si/SiO₂ wafer during 100 minutes using ECR-CVD and applied for fabrication of nonlinear microring resonators. Due to the low temperature deposition, no thermal stress was observed in the Si_xN_y film, allowing a large thickness (obtained with only one deposition process). The main advantage of higher Si concentration in this film is the higher values of η and the absence of losses caused by two-photon absorption, responsible for the introduction of additional losses in silicon based waveguides [3].

After experimental measurements, microring resonators having a radius of 60 μm, presented an equidistant Free Spectral Range and a Q-factor of 4x10³ was achieved, showing the high efficiency of the device. Finally, using the deposition process at low temperature and controlling the process parameters such as pressure and gas ratios, a remarkable free thermal stress silicon nitride film was obtained, overcoming the stress limitation of thick silicon nitride films.

[1] J. S. Levy *et al.*, Nat. Photonics, vol. 4, no. 1, pp. 37–40, 2009.

[2] K. Luke *et al.*, Opt. Express 21, 22829-22833, 2013.

[3] H. K. Tsang *et al.*, Appl. Phys. Lett., vol. 80, no. 3, p. 416, 2002.

Nanometer-scale Science and Technology

Room: Hall D - Session NS-ThP

Nanoscience Division Poster Session

NS-ThP1 Gallium Nitride Nanoparticle Synthesis using Non-Thermal Plasma with N₂ Gas and Ga Vapors, Jung-Hyung Kim, Korea Research Institute of Standards and Science, Republic of Korea, K.H. You, Korea Advanced Institute of Science and Technology, Republic of Korea, S.J. You, D.J. Seong, Y.H. Shin, Korea Research Institute of Standards and Science (KRISS), Republic of Korea

Compounds of Ga, such as gallium oxide(Ga₂O₃) and gallium nitride(GaN), are of interest due to its various properties in semiconductor application. In particular, GaN has the potentially application for optoelectronic device such as UV- to blue-light-emitting diodes(LEDs) and laser diodes(LDs).¹ Nanoparticle is an interesting material due to its unique properties compared to the bulk equivalents. While bulk-GaN exhibits a band gap of 3.3 eV to 3.5 eV, nanoparticles show a size-depending band gap if the particle size falls below 10.0 nm.²

In this report, we develop a synthesizing method for gallium nitride nanoparticle using non-thermal plasma. For gallium source, the gallium is evaporated by induction heating. Nitrogen radicals for GaN nanoparticle synthesis are supplied from inductively coupled plasma with N₂ gas. We use two plasma sources: one is for sufficient N radicals and the other is for in-situ plasma treatments. With this method, the post treatments such as annealing are not needed to get sufficient crystallinity. The synthesized nanoparticles are analyzed using field-emission scanning microscope(FESEM), transmission electron microscope(TEM) and x-ray photoelectron spectroscopy(XPS), and photo-luminescence(PL). The synthesized particles are investigated and discussed in wide range of experiment conditions such as flow rate, pressure and RF power.

References

1. D. Pile, Nat. Photonics 5, 394, 2011

2. H. Morkoc, S. Strite, G. B. Gao, M. E. Lin, B. Sverdlov and M. Burns, J. Appl. Phys., 76, 1363, Review. 1994

NS-ThP3 Imaging and Spectroscopy of Infrared Absorption Enhancement in the Near-Field of Plasmonic Array with the PTIR Technique, Jungseok Chae, B. Lahiri, G. Holland, A. Centrone, National Institute of Standards and Technology

Propagating light can interact efficiently with artificially fabricated metallic nanostructures through plasmonic excitations. In the infrared (IR) such light-matter interactions enables enhanced absorption in nanoscale volumes ("hot spots"), leading to sensitive IR detection. However, direct imaging of IR absorption hot spots is challenging because their size is several time smaller of the diffraction limit of the long IR wavelengths. Recently our group directly imaged and quantified the mid-IR absorption enhancement in polymer films coating asymmetric split ring resonators (ASSRs) using the photothermal induced resonance (PTIR) technique.[1] PTIR measures the transient thermal expansion caused by the absorption of light pulses in the sample with an atomic force microscope cantilever, leading to lateral resolution comparable to the AFM tip size P lasmonic arrays of different shapes (ASRR, C-shaped, crescent-shaped and U-shaped) and different lattices (square, hexagonal and rhombic) were fabricated by e-beam lithography on top of zinc selenide right angle prisms to enable PTIR characterization. Here I'll show how the different shapes and arrangements of the resonators impact the shape, distribution and intensity of IR absorption hot spots in the near-field. The experimentally and directly measured enhancement factors in PMMA film coating the plasmonic structures will be compared for the different cases and with the enhancements measured for a single resonator of each shape.

[1]. B. Lahiri, G. Holland, V. Aksyuk and A. Centrone, NanoLetters. 13, 3218 (2013).

NS-ThP5 A Novel Method for the Formation of Pt Metal Nanoparticle Array on Dimpled Ta using Nanosecond Pulsed Laser Dewetting, Ebenezer Owusu-Ansah, C. Horwood, University of Calgary, Canada, H.A. El-Sayed, Technische Universität, Germany, V. I. Birss, Y. Shi, University of Calgary, Canada

The unique properties of metal nanoparticle arrays (MNAs) depend on their sizes and geometries, and they differ considerably from the individual atoms and the bulk material. MNAs have been at the frontier in fabrication of materials with enhanced optical, magnetic, plasmonic, and mechanical properties, in biosensors as well as in catalysts with optimized selectivity. Lithographic techniques are the major conventional methods used to generate MNAs, however, the processes are sophisticated and time consuming. The formation of sub-50-nm nanoparticle sizes has become

increasingly difficult using lithography. Recently, thermal dewetting has been successfully used to form nanoparticle arrays of Au on dimpled Ta (DT) substrate, however, the major setback associated with this method is the deformation of the substrate when applied to high-melting point metals such as Pt. Pulsed laser dewetting is able to generate well-defined MNAs with the unique advantage of very little or no thermal damage to the substrate. Within the short width of the laser pulse, typically in the range of 7–12 ns, the laser energy is instantaneously converted into heat to dewet only the thin metal film with minimal or no heat transfer to the underlying substrate. We report here the results from our study on the formation of Pt MNAs using laser dewetting of Pt thin films on DT substrate under high vacuum condition. The DT substrate was fabricated using electrochemical anodization in highly concentrated H₂SO₄/HF solution. It has been demonstrated that dewetting occurs only at and beyond the threshold fluence. Beyond this threshold a single laser pulse was enough to achieve complete dewetting. The effect of several key parameters, including laser fluence, irradiation time, and film thickness, on the nanoparticle sizes and distribution was studied. To better characterize the MNA features, the percentage of dimples occupied by Pt nanoparticles was determined. As high as 80% of dimpled Ta occupancy can be achieved using pulsed laser dewetting. This study shows that laser dewetting is a novel method capable of annealing thin films of high-melting point Pt metal to achieve well-defined MNAs with narrow particle size distribution without subsequent damage to the DT substrate.

NS-ThP7 Dielectrophoretic Manipulation of Nickel Nanowires, *Marcos Vinicius Puydinger dos Santos, R. Mayer, K.R. Pirota, F. Beron, S. Moshkalev, J.A. Diniz,* University of Campinas, Brazil

Nanowires have received much attention because their high aspect ratio, shape anisotropy, relatively large surface area and particular electron transport properties. Furthermore, given to the low electrical current level usually present in the nanowires and their high sensitivity to the environment, they can be used as sensors devices. Dielectrophoresis (DEP) is a deposition method of electrically neutral particles based on the application of alternating electric field between electrodes. In this work, 80 nm-thick aluminum electrodes were deposited on a 300 nm-thick SiO₂ layer grown on n⁺-type silicon wafer using optical lithography and lift-off. After electrodes fabrication, nickel nanowires (NiNW) (length of 4 μm and diameter of 35 nm), obtained by electrodeposition, were manipulated and defined between the electrodes using DEP. Electrical parameters of DEP deposition – like frequency, electric potential, NiNW concentration and process time – as well as electrodes geometry were studied to investigate deposition efficiency. Preliminary results show best selection of electrical parameters and electrodes geometry that optimizes the nanowires deposition. For suitable parameters, the efficiency of DEP deposition is up to 90%. To characterize NiNW electrical properties, electrical current through the nanowires was measured as the voltage between electrodes. Initially, a Schottky-like contact is present and contact sintering under forming gas (92% of N₂ and 8% of H₂) at 450 °C was taken to reduce the electrodes-NiNW contact resistance down to the NiNW resistance (~ 1k Ω). Finally, this method for nanowire deposition and electrical contact reduction has a suitable throughput and is a key for electric characterization of nanowires and fabrication of nanowire-based devices.

NS-ThP9 Electron Tunneling in Weak Coupled Triple Quantum Dots: Sensitivity to Symmetry Violation, *Igor Filikhin, B. Vlahovic,* North Carolina Central University

The electron localization and tunneling in the triple quantum dots (TQD) is studied in relation to their spectral properties. Modeled are lateral InAs/GaAs TQDs using single sub-band effective mass approach with the effective potential simulating the strain effect [1]. As an approximation, two-dimension quantum wells (QW) are considered. Dynamics of electron localizations in TQD over whole spectrum is studied by varying the inter-dot distances. To consider tunneling between localized-delocalized states selected was a QD pair (DQD). In isolated DQD, such tunneling goes consecutively from high energy levels to the ground state when the inter-dot distance decreases [2]. The electron spectrum is separated by three parts: localized states, delocalized states, and states with different probability for localization in the left and right QDs. The electron localization demonstrates extreme sensitivity to small variations of DQD shape, which violate Left-Right symmetry. The effect of adding third quantum dot to DQD is considered for weak coupling triple system. We show that presence of the third dot increases tunneling in weakly coupled DQDs. The star and chain configurations of TQDs are considered. The effect of violation of reflexing symmetry in TQD was studied. We found that the tunneling is highly sensitive to a small violation of the geometry symmetry.

This work is supported by the NSF (HRD-0833184) and NASA (NNX09AV07A).

[1] I. Filikhin, V. M. Suslov and B. Vlahovic, *Phys. Rev. B* 73, 205332 (2006).

[2] I. Filikhin, S. Matinyan and B. Vlahovic, *Mathematical Modeling and Geometry*, Vol. 2, No 2, 1 (2014).

Fundamentals & Biological, Energy and Environmental Applications of Quartz Crystal Microbalance Focus Topic

Room: Hall D - Session QC+AS+BI+MN-ThP

Fundamentals & Biological, Energy and Environmental Applications of Quartz Crystal Microbalance Poster Session

QC+AS+BI+MN-ThP1 *In Situ* Toxic Nano-Material Sensing Method Using DNA Immobilized Quartz Crystal Microbalance, *Kuewhan Jang,*

S. Lee, J. You, C. Park, J. Park, S. Na, Korea University, Republic of Korea

Nano-material has grown from scientific interest to commercial products and there are more than 1600 nano-material products on the market. Among those nano-materials, single-walled carbon nanotube (SWNT) and silver ion have been shown great interest due to their extraordinary properties. Since SWNT and silver ion production capacity increases each year, its contamination to the environment water system will increase in the form of industrial waste. Moreover, toxicity assessment of those materials is required for human health and environmental issue since the toxicity of those materials has been reported. In this study, we propose the in-situ detection of SWNT and silver ion. The detection mechanism is based on the measurement of the resonance frequency shift arisen from the binding on the DNA immobilized quartz crystal microbalance. We are able to detect SWNT and silver ion less than an hour with the detection limit of 100 ng/ml of SWNT and 100 pM of silver ion, respectively. Moreover, the DNA immobilized quartz crystal microbalance enables the detection in real tap water. This work shows the potential of DNA immobilized quartz crystal microbalance as the in-situ toxic nano-material screening tool.

QC+AS+BI+MN-ThP2 Mechanics of Multicontact Interfaces Studied with a QCM, *R. König, S. Hanke, J. Vlachová, D. Johannsmann, Arne Langhoff,* Clausthal University of Technology, Germany

The contact stiffness and the contact strength at interfaces between rough surfaces are of outstanding relevance in many different fields, including mechanical engineering, bio-lubrication, and technical tribology.

Individual sphere-plate contacts have been previously investigated with a QCM and it was found that the contact stiffness can be inferred from the frequency shift, where the latter is positive because contact increases the overall stiffness of the composite resonator. At elevated amplitude of oscillation, the apparent contact stiffness decreases because of partial slip. Partial slip (also: “microslip”) describes the situation, where a contact partly sticks and partly slips. Sticking mostly is observed in the center. Slip is found at the edges, where the local stress is large.

The presentation describes the extension of this work to multicontact interfaces as well as the new results which were found with the single contacts. Generally speaking, multicontact interfaces differ from individual contacts by, firstly, a broad distribution of contact size and contact strength and, secondly, by an elastic coupling between neighboring load-bearing asperities.

Different materials (aluminum, PMMA) and different characteristic scales of roughness (all in the range of many microns) were studied. The focus is on polymer surfaces, which were treated with an abrasive paper. A novel geometry, where the resonator is symmetrically loaded with the same type of sample from both sides, has allowed to increase the normal force by a factor of 10, compared to previous experiments.

At small amplitudes, the frequency response of the QCM to a contact with rough PMMA surfaces is similar to the behavior observed with individual sphere-plate contacts. There is an increase in resonance frequency, which can be converted to an interfacial stiffness. Interesting, the contact stiffness observed with MHz excitation was found to be much higher than what has been found similar samples with excitation frequencies in the kHz range.

At elevated amplitudes, the behavior is variable. Often one finds partial slip. Occasionally, however, there is a sharp increase in contact stiffness at a certain threshold in amplitude. The bandwidth goes through a maximum at that same amplitude. The behavior is reversible; the threshold is the same for decreasing and increasing amplitude ramps. We tentatively associate the increased apparent stiffness with an oscillation-induced increase in contact area.

[1] S. Hanke, J. Petri, D. Johannsmann, *Phys. Rev. E* 2013, 88.

Scanning Probe Microscopy Focus Topic

Room: Hall D - Session SP+AS+EM+NS+SS-ThP

Scanning Probe Microscopy Poster Session

SP+AS+EM+NS+SS-ThP2 Fabrication of Single-Walled Carbon Nanotube Probe and Processing of Single Nanometer Scale Pit with High-Aspect-Ratio of Highly Oriented Pyrolytic Graphite Using by STM, *Syun Ohsumimoto, A. Matsumuro*, Aichi Institute of Technology, Japan

Our unique fabrication methods of high-aspect-ratio nanometer scale three-dimensional structures of pits, lines and convex parts using a multi-wall carbon nanotube (MWNT) with diameter of about 50 nm as a STM probe have been developed successfully. It turns out that this method has been applicable to surfaces of various conducting materials, such as noble metal thin films, low-resistivity single crystalline silicon wafer and highly oriented pyrolytic graphite (HOPG). We also have clarified that the physical origin of this nanometer-scale pit processing using STM must be the field evaporation mechanism by the results of TEM *in-situ* observations during fabrication process. In order to realize further ultra-precise three dimensional structures with high aspect ratio, it is surely required that an innovative ultimate ultra-precision processing technology needs fabrication size below several nm, i.e. single nanometer scale.

This study paid great attention to realize the ultimate processing of single nanometer scale structures using a single-wall carbon nanotube (SWNT) probe as our original STM processing. The most important problem was to overcome the difficulty in synthesis of SWNT probes with high probability. Then, the application of mixed dispersion liquid containing both MWNTs and SWNTs could be devised at the process of producing SWNT probes. In this process, it was clarified that the SWNT easily attached to the point of the MWNT, which was easily adhered to the apex of the conventional tungsten needle through the pulling method that we developed originally. The success rate for synthesis of the SWNT probes with diameters of about 2 nm and 10 nm were drastically increased up to about 10 % and 14 %, respectively. As compared with the case where the dispersion liquid of only SWNT is used, success fabrication rate has been nearly equal to 0 %. Single nanometer scale pits were actually fabricated on HOPG in atmosphere and room temperature condition. The SWNT probe with diameter of about 2 nm under the conditions of a bias voltage of 5 V, tunnel current of 1 nA and fabrication time of 60 s could realize a single nanometer scale pit with the diameter of 9 nm and the depth of 13 nm. The aspect ratio with SWNT probes increased up to about 5 times in the case of MWNT probes. These demonstrate that these STM fabrications by using SWNT probes with several diameters must give a remarkable effect in fabricating three-dimensional high-aspect-ratio structures with single nanometer-scale.

SP+AS+EM+NS+SS-ThP3 Probing the Electronic Structure of the Layered Electride Ca_2N , *Jeonghoon Ha*, NIST/Maryland Nano Center, University of Maryland, *H. Baek*, NIST & Seoul National University, Republic of Korea, *D. Zhang*, NIST/Maryland Nano Center, University of Maryland, *Y. Kim, S. Kim, Y.J. Song*, Sungkyunkwan University, Republic of Korea, *Y. Kuk*, Seoul National University, Republic of Korea, *J.A. Stroscio*, NIST

Electrides are electronic materials in which excessive electrons are confined into cavities defined by the crystal structure. These excessive electrons take the place of negatively charged ions in an ionic crystal. The geometry of the cavities confining these anionic electrons determines the electronic properties of the material and provides a platform to study various interaction physics [1]. A previous study reported the inorganic electride Ca_2N to have a layered structure with anionic electrons confined to 2-dimensional cavities between the cationic crystal layers [2]. In this previous study, transport measurements showed high electron mobility and long mean scattering time, and magneto-resistance measurements confirmed diffusive 2-dimensional transport in the electron layers.

In the present work, we use an ultra-low temperature scanning tunneling microscope to investigate the local electronic structure of a cleaved surface of a Ca_2N single crystal. An energy gap was observed in the tunneling spectrum with a gap size of 0.4 meV. The spectra contain multiple coherence-like peaks which are equally spaced in energy, suggestive of possible multi-band superconductivity or quantum confinement in the electron layers. Temperature-dependent tunneling spectroscopy measurements show a gradual suppression of the energy gap up to 2.5 K. An interesting observation is that the gap structure and the peak features do

not get suppressed in the presence of a perpendicular magnetic field up to 14.5 T, suggesting if the crystal is in a superconducting state, then the critical field is extremely large compared to the transition temperature. These observations and further discussion of possible unconventional superconductivity will be discussed in this presentation.

[1] J. Dye, Science **301**, 607 (2003)

[2] K. Lee *et al.*, Nature **494**, 336 (2013)

SP+AS+EM+NS+SS-ThP5 Improving the Accuracy of Atomic Force Microscopy in Nanometrology for Linewidth Measurements, *James Su, N.N. Chu, M.H. Shiao, C.N. Hsiao*, Instrument Technology Research Center, National Applied Research Laboratories, Taiwan, Republic of China

Atomic force microscopy (AFM) has an important role in dimensional metrology especially in the nanoscale. The morphology image processed by the AFM is the interaction between the tip and the sample surface. The result of the interaction may cause broadening of peaks and shrinking of valleys in the scanning process caused by tip effects. It would be impossible to differentiate the portion due to the tip and the portion due to the sample surface without determining the tip geometry which is a key role in AFM-image quality. As a case study, AFM measurements of nanowires (NW), carbon nanotubes (CNT) and nano-honeycombs fabricated by nanosphere lithography (NSL) technology are examined. Line width measurement results may expand up to 39.5% by adopting a conventional pyramid-shaped probe and 17.5% by using a conical-shaped one as the dimensions of the scanned features approaches to the order of magnitude of the tip apex. The uncertainty of measurement would expand if tip wear occurs during image scan. Calculation for surface reconstruction has been developed to extract the part related to the tip from the SPM image. The SPM used for these measurements is equipped with a highly accurate scanning system, which employs closed-loop capacitive feedback control to ensure outstanding linearity and position accuracy. To identify the geometry of the tip, a silicon tip characterization grating was imaged between the measurements. Deconvolution process were carried out for topography image corrections, and the results were further compared with the ones measured from the scanning electron microscope (SEM). This process is essential to derive accurate measurement results in the nanoscale region.

SP+AS+EM+NS+SS-ThP8 The Effect of Electrochemical Potential on Single Molecule Conductance, *Esteban Sanchez, R. Aguilar*, BUAP, Mexico, *S. Afsari*, Temple University, *Z. Li*, Ball State University, *E. Borguet*, Temple University

Porphyryns have been widely studied for their electrochemical properties to understand charge transfer. The related property of charge transport can be accessed by single molecule conductance (SMC) measurements. The most common SMC studies involve transport between different anchor groups at transversal positions in the molecule [1]. Few investigations have been made using porphyryns lying flat on the substrate in electrochemical environment [2]. Recent studies have shown that the templating effect of self-assembly can be exploited to orient molecules in metal-molecule-metal junctions, so that transport perpendicular to the molecular plane can also be easily accessed [3].

This goal research is to use self assembly, verified by scanning tunneling microscopy (STM), to measure charge transport in single porphyryns adsorbed flat on the Au (111) surface. 5,10,15,20-Tetra(4-pyridyl)porphyryn (TPyP) is a good candidate for this research because it has been demonstrated that this porphyryn has a strong interaction with, and can form ordered layers on, Au (111) in electrochemical environment [4]. This control of the orientation of the porphyryn by electrochemical potential enables us to make SMC measurements perpendicular to the molecular plane.

[1] Zhihai Li, Manuel Smeu, Mark A. Ratner, and Eric Borguet, Effect of Anchoring Groups on Single Molecule Charge Transport through Porphyryns, J. Phys. Chem. C, **117**, 14890–14898 (2013).

[2] Quirina Ferreira, Ana M. Braganca, Luis Alcacer, and Jorge Morgado, Conductance of Well-Defined Porphyryn Self-Assembled Molecular Wires up to 14 nm in Length, J. Phys. Chem. C, **118**, 7229–7234 (2014)

[3] Sepideh Afsari, Zhihai Li, and Eric Borguet, Orientation-Controlled Single-Molecule Junctions, Angew. Chem. Int. Ed. **53**, 9771–9774 (2014).

[4] Tao Ye, Yufan He, and Eric Borguet, Adsorption and Electrochemical Activity: An In Situ Electrochemical Scanning Tunneling Microscopy Study of Electrode Reactions and Potential-Induced Adsorption of Porphyryns, J. Phys. Chem. B, **110**, 6141–6147 (2006).

Thin Film

Room: Hall D - Session TF-ThP

Thin Films Poster Session

TF-ThP1 Synthesis of Multilayered MgO/Ag/MgO Thin Films in the (001) and (111) Orientations by Pulsed Laser Deposition, Daniel Velazquez, R. Seibert, Z. Yusof, L. Spentzouris, J. Terry, Illinois Institute of Technology

Crystalline, highly oriented MgO/Ag/MgO ultrathin films were grown in the crystallographic orientations (001) and (111) via pulsed laser deposition at 150 °C and 170 °C, respectively. Buffer Ag films ~40 nm thick on MgO(001) and Si(111) single crystal substrates were used to assist the epitaxial growth of the MgO/Ag/MgO multilayer structures in the corresponding orientation. The formation of multilayers was monitored in-situ via reflection high-energy electron diffraction. The physical and chemical structure of the films is further characterized via X-ray photoelectron spectroscopy and scanning tunneling microscopy.

TF-ThP2 Development of CNT/Ni Composite Plated Films with Excellent Mechanical Properties, Shoko Yamada, Aichi Institute of Technology, Japan, *H. Ito,* Aichi Institute of Technology, *A. Matsumuro,* Aichi Institute of Technology, Japan

Surface modification of forming many kinds of films must be one of the most important technologies. For especially many kinds of plating methods are already established and easy processing to the product of complicated forms. Furthermore, the composite plating which contains many kinds of small particles in the film are also fabricated and it contributes to the further improvement in the characteristic.

In this study, we focused on development of Ni composite plated films reinforced by dispersed multi-walled CNT with 50 nm in the diameter and several μm in the length using the ultrasonic vibration. An ordinary electroplating method was applied at room temperature. CNT/Ni composite plated film was examined under the conventional plating conditions of pH 4.5-4.7 using a Ni plate as an anode and a Cu plate as a cathode. The mixing weight concentrations of CNT were changed in the range of 0-0.1 wt.%CNT to the weight of the plating bath. It is necessary to prevent from aggregation of CNT in composite plated films because the aggregation parts of CNT must surely cause a loss of strength of the materials. In order to distribute CNT molecules in the plating solution, the ultrasonic vibrations was applied for 1 h before the plating process. The operation conditions was set constant as follows; the bias voltage of 3.7 V, the current density of 3.0 A/dm² and the plating time of 10 minutes. Thickness of plated film obtained was about 40 μm . Fabrication of CNT/Ni composite films of all mixing weight ratio plated on a Cu plate was confirmed with flat surfaces. But the remarkable condensation parts were observed at the surface at the weight ratio of 0.1 wt.%CNT. The X-ray diffraction experiments clearly indicated no formation of any compound between Ni metal and CNT, because only Ni crystalline diffraction patterns for all CNT concentrations were identified. Vickers hardness tests showed that the hardness increased with the increase of concentration up to 310 Hv of 0.07 wt.%CNT, and decreased after that. This maximum hardness was about twice of the value of the pure Ni plated film. The decrease of hardness over the concentration of 0.07 wt.%CNT should be due to existence of softer aggregate part CNT in the composite films. The friction and abrasion characteristics were also estimated using by a pin-on-disk tester under the load of 0.5 N with a stainless steel pin. It was clarified that the friction coefficient of the composite film with concentration of 0.07 wt.%CNT decreased to 0.5 in comparison with pure Ni coating of 0.8 and showed an unobservable abrasion mark.

From the above results, industrial validity of this study was surely able to be found out.

TF-ThP3 Fabrication of Dispersed C₆₀ Molecules/TiN Composite Film Using by Simultaneous Deposition Method with Both Heating Evaporation and Sputtering, Yuki Ishiyama, A. Matsumuro, Aichi Institute of Technology, Japan

We fabricated dispersed C₆₀ molecules/Al nano-composite thin films using by a conventional vacuum evaporation method. The microstructural characterization of the films obtained clarified the uniform dispersion of C₆₀ molecules in Al based film. Nano-indentation hardness of Al-1.0 wt.%C₆₀ showed increase up to 3 times larger than that of Al film. These results clearly indicated that dispersion of C₆₀ molecules in the conventional films contributes to drastic improvement in mechanical properties.

In this study, we tried to establish the synthesis technology of the composite thin films containing dispersed C₆₀ molecules in order to apply practical uses in the industry fields. We focused on conventional high hardness TiN

films fabricated using by RF magnetron sputtering method. For the purpose of evaporating C₆₀ molecules, the heating evaporator was equipped directly below the substrate of existing RF magnetron sputtering chamber due to prevent from the influence of plasma. It was possible to control the deposition rates of two kinds of evaporation sources to become the predetermined compositions separately.

TiN films with constant thickness of 100 nm were deposited on Si(100) water-cooled substrates using by the RF magnetron sputtering deposition method for 30 minutes. The concentration of C₆₀ molecule powder was changed in the range from 0.5 to 50 wt.%, and the evaporation temperature was controlled in the range of 473-673 K. The structure analyses of all nano-composite films prepared by X-ray diffraction method showed TiN crystalline structure, and FT-IR analysis clarified the existence of C₆₀ molecules contained in TiN films. Nano-indentation studies showed that the hardness of the composite film of 2.0 wt.%C₆₀/TiN showed the maximum hardness of 18 GPa and this value was increased up to 50 % larger than that of TiN film.

The present results clearly indicate that the conventional hard thin films prepared by RF sputtering should be also effective to synthesize remarkable hard composite thin films by dispersing C₆₀ molecules. Therefore, this study let us know the bright future view of development of the innovative high-hard composite thin films reinforced using by C₆₀ molecules.

TF-ThP4 Improved Reflectance of M/Si Bilayers for Extreme Ultraviolet Lithography Reflective Mirror, Chao-Te Lee, D. Chiang, P.-K. Chiu, H.-P. Chen, C.N. Hsiao, National Applied Research Laboratories, Taiwan, Republic of China

The periodic Mo/Si bilayers were deposited on Si substrate by RF magnetron sputtering with Mo and Si targets. The Mo/Si bilayers were designed for reflectivity at the wavelength of 13.5 nm. The effects of substrate temperature range (T=20 to 25 °C, and 20 to 55°C) on the microstructure, surface roughness and reflectance of Mo/Si bilayers were investigated by atomic force microscopy (AFM), high resolution transmission electron microscopy (HRTEM), and a spectrometer. The AFM measurements showed the Mo/Si bilayers to have a uniform morphology with a very low surface roughness value under 0.2 nm. It was found that the interface between Mo and Si film was clearly discriminated at substrate temperature range 20 to 25 °C by HRTEM. The reflectivity of Mo/Si bilayers was 47.9% at substrate temperature range 20 to 55 °C, and 63.3% at substrate temperature range 20 to 25 °C, respectively. The incident angle increased from 33.47o to 46.13o with substrate temperature range. The improved reflectance and incident angle shifted were attributed to form the clearly interface and vary the film thickness.

TF-ThP8 Characterization of Fluorine-doped Al₂O₃ Films Deposited by High-Power Impulse Magnetron Sputtering, Bohuei Liao, Instrument Technology Research Center, Taiwan, Republic of China, *C.N. Hsiao,* ITRC, NARL, Taiwan, Republic of China, *C.C. Lee,* National Central University, Taiwan, Republic of China

Fluorine-doped Al₂O₃ films were deposited by high-power impulse magnetron sputtering with an Al metal target at room temperature. In order to obtain better optical and mechanical properties, films were investigated under different duty cycle and different ratios of O₂ to CF₄ gas. The optical properties in deep ultraviolet range, microstructure, surface roughness, and crystalline structure, of fluorine-doped Al₂O₃ films have been studied. The fluorine-doped Al₂O₃ films deposited with 45/55 duty cycle and 0.6 sccm CF₄ has lowest extinction coefficient (5×10^{-4}) and highest refractive index (1.70) at 193 nm. Besides, the fluorine-doped Al₂O₃ films reveal a dense and amorphous structure.

TF-ThP9 Formation of ZnGaON Films Prepared by Two Types of co-Sputtering using ZnO or Zn Target and their Optical Properties, Junichi Iwata, Y. Hirano, H. Sase, H. Katsumata, Meiji University, Japan

ZnO is an interesting wurtzitic semiconducting material with a wide band-gap of 3.3 eV. It has been reported that the reduction of the optical band-gap down to 2.4 eV was observed from (ZnO)_x(GaN)_{1-x} powders with x = 0.81[1]. Moreover, optical band-gap of nitrogen doped ZnO (ZnON) films decreased from 3.26 to 0.9 eV with increasing the N concentration[2], while that of Zn_{1-x}Ga_xO films was reported to be engineered from 3.3 to 4.9 eV by varying the Ga content[3]. From these facts, we believe that the band-gap of ZnGaON can be widely controllable from 0.9 to 4.9 eV by changing their chemical composition. In these previous reports, however, there have been few observations on their luminescence properties. The purpose of this study is to form ZnGaON thin films with various optical band-gaps. The substrates used in this study were c-axis sapphire substrates or glass substrates. ZnGaON thin films were deposited on these substrates by two kinds of radio frequency (RF) magnetron co-sputtering methods. One is co-sputtering (a) of GaN tablets and a ZnO target in N₂/O₂ gas flow, in which the GaN tablets were placed on the ZnO target and the number of GaN

tablets (N_{GaN}) was varied from 0 to 3. The other is co-sputtering (b) of Ga_2O_3 tablets and Zn target in Ar/N_2 gas flow, in which the Ga_2O_3 tablets were placed on the Zn target. Samples were subsequently subjected to NH_3 treatment at 500 °C for nitridation in former co-sputtering (a) and N_2 annealing at 500 °C for improvement of crystallinity in latter co-sputtering (b). These samples were characterized by X-ray diffraction (XRD), energy dispersive X-ray spectrometry (EDS), optical transmittance and photoluminescence (PL). First of all, we show the characterization results of films prepared by co-sputtering (a). XRD analysis showed that the crystalline quality of ZnGaON films became worse with increasing N_{GaN} . EDS results revealed that nitrogen doping concentration in ZnGaON films was increased only by NH_3 treatment. Optical band-gap of ZnGaON films became wider from 3.29 to 3.51 eV with increasing N_{GaN} from 0 to 3 due to Burnstein-Moss shift. PL spectra of ZnO films showed band-to-band emission at 380nm, while those of ZnGaON films exhibited a broad and weak peak centered at 530 nm, which results from oxygen interstitial (O_i). On the other hands, optical band-gap of ZnON films prepared by co-sputtering (b) without Ga_2O_3 tablets decreased to 1.18 eV, probably due to formation of Zn_3N_2 .

[1] J. Wang et al., *J. Mater. Chem.*, **21**, 4562 (2011).

[2] L. Jensen et al., *J. Phys. Chem. C*, **112**, 3439 (2008).

[3] J. Zhao et al., *IEEE Trans Electron Devices*, **56**, 2995 (2009).

TF-ThP14 Growth and Characterization of Aluminum Oxide for M/I/S Junctions, Zachary Barcikowski, University of Maryland, College Park, *J. Pomeroy*, National Institute of Standards and Technology (NIST)

In progress towards spin polarization measurements, we are using a unique ultra-high vacuum (UHV) deposition chamber equipped with electron gun deposition sources, sputter deposition, and plasma oxidation to fabricate shadow-mask defined tunnel junctions. The formation of the tunnel barrier is one of the most crucial processes in junction fabrication which makes the development of an optimal growth recipe a vital step. While varying plasma oxidation process parameters, we will be growing aluminum oxide thin films as a tunnel barrier for metal/insulator/superconductor junctions. Optical spectra of the oxidation plasma and electrical characterization of the resulting junctions will be used to elucidate optimum growth conditions for our aluminum oxide tunnel barriers. The aforementioned data and experimental details will be discussed in this presentation.

TF-ThP15 Low-Temperature Thin Dielectric Films Obtained by ECR-CVD for Application in Non-Volatile Memories, David Mateos, J.A. Diniz, University of Campinas, Brazil, *S.N. Mestanza Muñoz*, Federal University of ABC, Brazil, *N. Nedeo, M.A. Curriel Alvarez*, Autonomous University of Baja California, Mexico, *M. Mederos Vidal*, Federal University of ABC, Brazil, *B. Valdez, G. Montero*, Autonomous University of Baja California, Mexico

In this work we present results for two types of thin films deposited by ECR-CVD: silicon oxide (SiO_2) and hydrogenated amorphous silicon (a-Si:H) with thicknesses of about 6–8nm and 3–4nm respectively. $\text{SiO}_2/\text{a-Si:H}$ and $\text{SiO}_2/\text{a-Si:H}/\text{SiO}_2$ structures for potential application in Non-Volatile Memories, were deposited on p-type (100) c-Si wafers under the following conditions: a gas pressure of 2.0mTorr, an applied ECR microwave (frequency of 2.45GHz) with power of 250Watts and a substrate temperature of 20°C. The precursor gases used for SiO_2 deposition were 2% of SiH_4 diluted in Ar, Ar and O_2 with flows of 125, 5 and 2.5sccm, respectively. The a-Si:H layers were deposited without oxygen using the same SiH_4 and Ar flows. The films were subjected to furnace annealing in N_2 at temperatures in the 800–1100°C range for 60min. Different oxygen and silicon incorporation into the films were extracted using Energy Dispersive X-ray (EDX) analysis (Fig1). Information for the layer thicknesses and optical properties was carried out by Single Wavelength Ellipsometry (SWE) λ -638nm. The thickness measured was 7–11nm and 9–20nm for two and three layers, respectively. Refractive index (n) values between 1.46–1.53 that were obtained are greater than stoichiometric silicon oxide (n=1.457) reported in the literature, indicating formation of thin films rich in silicon. MOS capacitors were fabricated by r.f. sputtering of Al as top (d=0.5 μm) and back contacts. These capacitors were sintered at 450°C in forming gas (92% N_2 and 8% H_2) for 5, 10 and 20min. Electrical characterization was carried out by Capacitance-Voltage (C-V) measurements. The increase of the low temperature annealing time, leads to an improvement of the SiO_2/Si interface seen as an increase of the slope of the high frequency C-V dependence. The capacitance variation in accumulation (C_{acc}) is in the range of 160–180pF for two layer capacitors which correspond to a thickness of 6–7nm (Fig2). In the same way for three layers the variation of C_{acc} is larger and the thickness calculated is 11–17nm (Fig3). The obtained values are in agreement with the expected thickness determined by SWE. Three-layer MOS capacitors annealing in forming gas for 20min showed hysteresis in their C-V measurements with ramps varying from negative to positive voltages and back. The flat-band Voltage

shift (ΔV_{FB}) obtained for capacitors annealed at 800°C and 1000°C were: -2.7V to -2.13V and -4.3V to -2.48V showing an hysteresis window of 0.57V and 1.82V, respectively (Fig4). By the other hand for two-region structures do not present hysteresis (Fig5) which means that three-layer structures could be a possible application as memory devices.

TF-ThP16 MOCVD Growth of 2-D MgZnO Wurtzite Thin Films for Solar-blind Detector Applications, Judith Reynolds, J.E. Rowe, L. Reynolds, D.E. Aspnes, North Carolina State University

We report the MOCVD growth of doped thin 2-D MgZnO films on c-plane sapphire substrates for solar-blind detector applications. Spectroscopic ellipsometry (SE), X-ray diffraction (XRD), and X-ray photoelectron spectroscopy (XPS) are used to determine the composition. The carrier gas is N_2 . For pure ZnO, the precursors are diethylzinc (DEZ) and nitrous oxide (N_2O). When growing p-type material, 3% nitric oxide (NO) in N_2 provides N ions in the +2 oxidation state needed for doping, and growth occurs as a two-step process monitored in real time by the SE. In the first step, we use a low Zn partial pressure to induce V_{Zn} formation. Because V_{Zn} energies are low for Fermi levels from mid-gap to the conduction band edge, and because the absorption energy for N_{Zn} is 0.08 eV for the hexagonal close packed site of the Zn-polar surface, this allows the N to incorporate at Zn sites as N_{Zn} . In the second step, we use a high Zn partial pressure to drive the formation of oxygen vacancies (V_{O}). Growth is then followed by an appropriate annealing sequence. While substitutional N on the O sublattice is a deep acceptor, we find that acceptor complexes involving N, H and V_{Zn} can provide p-type ZnO films with a hole concentration of $\sim 10^{18} \text{ cm}^{-3}$ at room temperature. For MgZnO growth, we use bis-cyclopentadienyl magnesium (BcMg) in addition to DEZ, N_2O , and NO. Although we deposit MgZnO, films of a quality that we consider acceptable have not yet been produced owing to the large parameter space of temperature, precursor flows, and gas pressure.

TF-ThP17 Investigation of RF-sputtered Tin Sulfide Thin Films with In Situ and Post-Deposition Heating for Photovoltaic Applications, R.E. Banai, Jacob Cordell, J.R. Nasr, R.E. Urena, N.J. Tanen, J.R.S. Brownson, M.W. Horn, Penn State University

Tin (II) Monosulfide (SnS) has become an interesting new material for thin film photovoltaics (PV). The optoelectronic properties indicate that SnS is a suitable material for PV. Its high absorption coefficient, greater than 10^4 cm^{-1} , and band gap near 1.3 eV are well matched with the solar spectrum. SnS also has a carrier concentration greater than 10^{15} cm^{-3} and potential to be both n-type and p-type. With recent success in achieving 4% efficiency, SnS -based devices demonstrated their potential. However, the success comes with extensive optimization of each layer in the device, suggesting that further understanding of SnS is crucial to improving performance.

Sulfur is more volatile than tin and despite strong Sn-S bonds in tin sulfide compounds, sulfur loss to the gas phase while annealing in a vacuum environment. Therefore, it is important to start with a sulfur-rich thin film prior to annealing. Annealing of sulfur-rich sputtered tin sulfide thin films has not been done before. This work will investigate the optoelectronic properties, composition and morphology of annealed, sputtered tin sulfide thin films. Specifically, we will investigate the change in phase and improvement in material quality as a result of post-deposition heat treatments.

Tin sulfide thin films are sputtered on glass and silicon substrates from a distance of 11.5 cm at 115 W with a Ar chamber pressure of 10 mTorr. The sputter target was a 3" SnS_2 with 99.999% purity (LTS Research Laboratories, Inc.). SnS_x samples are deposited at room temperature and 150°C. These samples are then annealed some under medium vacuum ($< 2 \times 10^{-6}$ Torr) in the deposition chamber without breaking vacuum at 200, 300, and 400°C.

Preliminary results show promise for high-quality SnS thin films. Significantly improved crystallinity was seen in sulfur-rich thin films annealed at 400°C for 30 minutes. Morphology is not the same for film deposited with and without substrate heating, although both film exhibit a uniform SnS phase as determined by X-ray diffraction. Longer anneal times are expected to further improve crystal quality. Reasonable resistivities are seen in these annealed thin films. The presentation will include details on producing high-quality SnS thin films as well as detailed results of optoelectronic properties, composition and morphology.

TF-ThP19 Sputter-Deposited Carbon Fuses in Long-Term Digital Data Storage, Jacob Bagley, H. Wang, A. Diwan, R.C. Davis, B. Lunt, M.R. Linford, Brigham Young University

Solid-state digital data storage devices with the capacity of storing data for 1000 years are being developed. One implementation of this effort is a device that employs a series of carbon fuses. This study explores whether sputtering can yield sufficiently conductive carbon for this application. We hypothesize that reducing the amount of oxygen in the sputtered carbon

may sufficiently improve its conductivity. Accordingly, carbon is deposited by DC magnetron sputtering. Sputtering conditions studied include argon pressures of 5 mTorr and 7 mTorr and powers of 250 W and 400 W. Titanium is also co-sputtered at 150 W with a closed shutter to act as an oxygen getter. The oxygen contents of the films were measured by X-ray photoelectron spectroscopy (XPS), and their conductivity was measured with a 500 V megaohmmeter. The oxygen content of the films slightly decreases with decreasing argon pressure and decreasing power on the carbon target. Use of the titanium getter significantly decreases the oxygen contents of the films. However, no significant increase in conductivity is observed, i.e., the deposited carbon is not conductive enough for our purposes. We conclude that sputtered carbon, as deposited with our current system, is not suitable for our devices.

TF-ThP20 Low Hydrogen Silicon Nitride Films Deposited by Plasma Enhanced Chemical Vapor Deposition, Erica Douglas, A. Starbuck, C. DeRose, Sandia National Laboratories

Due to exceptional material properties, such as refractive index and others, the use of silicon nitride (SiN) as an optical waveguide has become common. SiN films are used in many applications, from gate dielectrics to encapsulation layers. However, the use of SiN as a waveguide is greatly affected by hydrogen incorporation, particularly at telecommunication wavelengths of ~1550 nm.

Hydrogen incorporation for plasma enhanced chemical vapor deposition (PECVD) of SiN_x is a due to the Si-H species from the use of SiH₄ as well as the standard precursor NH₃ for the N component for SiN_x. The resulting hydrogen bonds, both Si-H species and N-H species, result in absorption and thus loss in the telecommunication spectrum. In particular, the N-H bond has high absorption around 1550 nm.

Previous studies have investigated the use of N₂ as a replacement precursor for NH₃ for low-hydrogen PECVD SiN_x.^{1,2} However, these studies have only investigated a few process parameters and their effect on the optical characteristics of the film. In our investigation, a detailed study was performed on a production PECVD system to look at the effect of SiH₄ flow, NH₃ flow, N₂ flow, ratios of all precursors, chamber pressure, and RF bias. The relative hydrogen content was measured for all process parameters through Fourier transform infrared spectroscopy (FTIR). Additionally, we measured the refractive index (from 375 nm to 1675 nm), deposition rate, uniformity, and stress of the SiN_x films. We are able to not only tune the relative hydrogen content of the film, but the uniformity, stress and refractive index independently, in order to fabricate SiN_x optical waveguides for photonic applications.

It was observed that although substituting N₂ in place of NH₃ for the source of N in SiN_x resulted in lower relative hydrogen content, it greatly affected the refractive index and stress of the film resulting in a film that is not ideal for photonic integrated circuits. In order to balance these film properties, we were able to exploit other process parameters, such as chamber pressure and RF bias, in order to tune the film. We also measured the insertion loss of SiN_x optical waveguides with select SiN_x films in order to further understand the role of different film properties.

Sandia National Laboratories is a multi-program laboratory managed and operated by Sandia Corporation, a wholly owned subsidiary of Lockheed Martin Corporation, for the U.S. Department of Energy's National Nuclear Security Administration under contract DE-AC04-94AL85000.

¹S. C. Mao, et al., *Opt. Express* **16**, 20809-20816 (2008).

²F. Karouta, et al., *J. Phys. D: Appl. Phys.* **45**, 445301 (2012).

TF-ThP21 Enhancing the Water Vapour Barrier Properties of Polymer Substrates with ALD Metal Oxide Films, Karyn Jarvis, G. Griffiths, Australian Nuclear Science and Technology Organisation (ANSTO), Australia, L. Hyde, Melbourne Centre for Nanofabrication (MCN), Australia, P. Evans, G. Triani, Australian Nuclear Science and Technology Organisation (ANSTO), Australia

Polymer substrates are used for flexible organic electronics due to being lightweight, cheap, transparent and printable in continuous roll to roll manufacturing technology. However, a significant disadvantage of these materials is their high gas/vapour permeability. A permeation barrier is therefore essential when using polymer substrates in organic electronics to reduce both oxygen and moisture ingress to an acceptable level. Films deposited by atomic layer deposition (ALD) have shown to improve the barrier properties of polymeric films [1-2]. In the present study, single alumina (Al₂O₃) films were deposited onto one surface of PET substrates (Mulptapex, biaxially oriented, 75 μm thick) using thermal and plasma enhanced ALD. Films with thicknesses in the range of 7 - 25 nm were deposited at 100 or 120°C. The water vapour transmission rate (WVTR) of the ALD films was determined predominately by tritium permeation, but was also measured using the MOCON and Ca-tests for comparison. Thermally grown 20 nm thick alumina films were also deposited onto PET

and PEN substrates with thicknesses of 75 and 125 μm to evaluate the effect of substrate type and thickness on WVTR. In addition, several mixed oxide structures such as alumina/hafnia and alumina/titania were also investigated to examine their potential for further decreasing the WVTR. Characterisation of the ALD grown films was carried out using X-ray photoelectron spectroscopy, atomic force microscopy and optical microscopy. For single Al₂O₃ layers, film thickness and deposition temperature influenced the WVTR. The WVTR decreased with increasing film thickness and deposition temperature. The deposition of ALD metal oxide films was successful in reducing water permeation through polymer substrates, demonstrating the potential of these coatings as a barrier technology for organic electronics over wide range of polymer based products.

[1] Groner MD, George SM, McLean RS, Carcia PF *Appl. Phys. Lett* **2006**, 88, 051907

[2] Dameron AA, Davidson SD, Burton BB, Carcia PF, McLean S, George SM *J. Phys. Chem. C* **2008**, 112(12), 4573

TF-ThP22 Sol-Gel Deposited TiO₂ Thin Films for Propane Gas Sensors, Ismael Garduño-Wilches, A. Maldonado Álvarez, CINVESTAV-IPN, México, D.R. Acosta-Najarro, Universidad Nacional Autonoma de México

Titanium-dioxide films are produced by the dip coating method, using a solution of 2-propanol and titanium isopropoxide in a concentration of 0.17M and an immersion speed of 0.122 cm/s. Films with different thickness are obtained by changing the number of immersion cycles. Analysis results indicate that the obtained films present the TiO₂ anatase structure when treated at 400 °C for 3 hrs, the film thickness ranged from 20nm to 150 nm and the rate deposition is of 18 nm/cycle.

Gas sensing studies indicate that at a work temperatures of 300 °C sensors present a significant change in electrical resistance. When analyzing sensors sensitivity as a function of propane concentration and film thickness a two-regime behavior is observed, being the sensitivity independent of the film thickness when partial pressures are above 400 ppm, and thickness dependant at lower partial pressures. The maximum sensitivity is obtained in the range from 5 ppm to 300 ppm for the film grown with 5 immersion cycles.

TF-ThP23 Investigation of Optical Property and Crystalline of the Silver Mirror in the 35 Krad Co-60 Radiation Environment, Po-Kai Chiu, D. Chiang, C.T. Lee, Y.W. Lin, C.N. Hsiao, Instrument Technology Research Center, National Applied Research Laboratories, Taiwan, Republic of China

This study investigated the optical design of silver mirror and effected of optical properties in the radiation environment. In different optical designed by Macleod software was studied in the same radiation environment. The optical properties were measured by the integrating sphere spectrophotometer and material properties by X-ray diffraction instrument. After the 35 Krad Co-60 radiation testing, the titanium dioxide film, silicon dioxide film, pure chromium and silver film could efficient reduce the damage of the B270 substrate by radiation. In the visible light, the titanium dioxide film had smaller spectral absorption about 0.5% at 450 nm and about 25 nm spectral drift. In the metal film, ΔT% in visible light of the silver film was about 0.5% and chrome film about 1.5%. So, the radiation resistance of silver film was better than chrome film. By X-Ray diffraction analysis showed that the crystalline of silver film would be slightly improved by exposure to radiation.

TF-ThP25 Effect of Mg Doping Concentration on Resistance Switching Behavior of Oxygen Deficient Mg-doped Al₂O₃ Films, Kyumin Lee, Y. Kim, T. Kim, H. Na, H. Sohn, Yonsei University, Korea

In this study, the effect of Mg doping concentration on the resistance switching behavior of Al₂O₃ films was investigated in conjunction with an analysis of the chemical bonding states. Mg doping concentration is increased from 0 to 8.6% with increasing Mg gun power. In micro-structure, the Al₂O₃ and Mg-doped Al₂O₃ films have amorphous structure in all conditions. In non-lattice oxygen, the concentration of non-lattice oxygen is increased with increasing Mg doping concentration in Al₂O₃ films. In order to identify the effect of only non-lattice oxygen concentration without crystal structure change, the resistance switching characteristics such as operating current, forming electric field, endurance, and retention was compared. The operating current and uniformity of endurance is increased with increasing Mg doping concentration. And also the conduction mechanism and activation energy from Poole-Frenkel equation of resistance switching characteristics of Mg-doped Al₂O₃ films was investigated. The activation energy is decreased with increasing non-lattice oxygen concentration because non-lattice oxygen is defect in Al₂O₃

films. From these findings, the resistance switching characteristics are influenced by non-lattice oxygen concentration.

TF-ThP26 Failure of Semiclassical Models to Describe Resistivity Size Effect in sub 15nm Films., *Daniel Yates*, University of Central Florida, *X. Liu*, Carnegie Mellon University, *D. Choi*, Korea Railroad Research Institute, Republic of Korea, *P. Schelling*, University of Central Florida, *K. Barmak*, Columbia University, *K.R. Coffey*, University of Central Florida

Previous work in copper thin films with thickness > 30nm demonstrated excellent agreement with the semiclassical models of the resistivity size effect. Using the same methodology developed for Cu, electron scattering at surfaces and grain boundaries in polycrystalline Ni, Ru, and W films was examined. 2-200 nm thick films were prepared via DC magnetron sputtering onto thermally oxidized silicon wafers. Films with thicknesses below 10nm were encapsulated in 0.5nm thick layers of Ta to improve film stability.

Films were annealed in the range of 200°C to 900°C in Ar+3% H₂. They were characterized using X-ray reflectivity, Rutherford backscatter spectrometry, and transmission electron microscopy with precession electron diffraction techniques to measure thickness, grain size, and film continuity. Resistivity was measured using the Van Der Pauw method.

The contributions of surface and grain boundary scattering were assessed using the semiclassical models of Fuchs-Sondheimer and Mayadas-Shatzkes. Systematic deviations from model predictions were observed for films less than approximately 15nm thick in all three metals. The complex Fermi surfaces of these metals result in a variety of Fermi velocities, as several bands cross the Fermi level. This complexity may be a likely cause for the failure of the semiclassical models, which consider only an average mean free path value. The deviations are most pronounced in the thinnest films.

Tribology Focus Topic

Room: Hall D - Session TR-ThP

Tribology Poster Session

TR-ThP2 Nanocomposite Hf-B-C Hard Coatings by Low Temperature CVD, *Elham Mohimi*, *J.R. Abelson*, *T. Ozkan*, *K. Walsh*, *S. Babar*, *P.J. Semprout*, *G.S. Girolami*, University of Illinois at Urbana Champaign, *A.A. Polycarpou*, Texas A&M University

Nanocomposite coating materials can afford an excellent combination of chemical, physical and mechanical properties, including high or super-hardness along with toughness. There is an extensive literature concerning the growth and properties of transition metal nitride, carbide and boride materials, as well as ternary (pseudo-binary) combinations. Our group previously reported the conformal growth and favorable mechanical properties of HfB₂ and Hf-B-N hard coatings by chemical vapor deposition (CVD) using the high vapor pressure precursor hafnium borohydride, Hf(BH₄)₄, at substrate temperatures below 300°C. Our objective is to extend the use of the HfB₂ system for tribological applications, for which a low coefficient of sliding friction is desirable. A useful analogue is C-alloyed TiB₂, which exhibits super-hardness and good thermal stability. However, there have been no previous reports of the growth and properties of Hf-B-C alloys.

We report the CVD of Hf-B-C nanocomposite coatings on Si and on steel discs using hafnium borohydride precursor with a co-flow of dimethylbutene (DMB), (CH₃)₃CCH=CH₂, as the carbon source. Depositions are performed in a high vacuum chamber with 0.1-0.5 mTorr of hafnium borohydride and 0.1-0.4 mTorr of DMB at a substrate temperature of 250-700 C. The resulting carbon contents are 10-33 at. %. DMB acts as growth inhibitor which reduces the film growth rate by a factor of 2-6 compared to growth using the precursor alone; for high temperature depositions, DMB also enhances the film density and decreases the surface roughness. XPS analysis indicates that Hf-B-C films consist of a mixture of HfB₂, HfC and B₄C phases. As-deposited films are XRD amorphous with hardness values of 8-10 GPa and reduced modulus of 92-120 GPa. Upon annealing at 700°C for 3 hrs, the films transform partially to a nanocrystalline structure, which increases the hardness and modulus. Multilayer films of (HfB₂ / Hf-B-C)_n afford a means to engineer the hardness and modulus to desirable values. The tribological properties of Hf-B-C films are superior to those of HfB₂ films. This system affords conformal coating at low growth temperature, suitable for complex structures such as MEMS.

TR-ThP3 Stress Analysis of TiSiN and TiAlN Coatings using Scratch Testing and Raman Spectroscopy, *Johans Restrepo*, Instituto de Investigaciones en Materiales - UNAM, Mexico, *E. Camps*, Instituto Nacional de Investigaciones Nucleares, Mexico, *S. Muhl*, Universidad Nacional Autónoma de México

The TiSiN and TiAlN coatings were deposited using Pulsed Laser Deposition. The films were characterized by SEM-EDS (chemical composition and surface morphology), X-ray diffraction (crystalline structure and grain size) and Nanoindentation (hardness and Young's modulus). The tribological properties of the coatings were evaluated using scratch testing, using two counter materials (1/16" balls of 100CR6 and Al₂O₃). To study the plastic deformation caused by the application of the load during the scratch measurements we used 3d profilometry. Finally, micro-Raman spectroscopy was employed to study any deformation-induced on the lattice and the chemical reactions produced, under the different loads, by the contact with the counterpart materials. The results show the TiSiN against alumina had the lower friction coefficient due to not showed reactive process on the surface for all load used just the movement of the Raman peak at lower wave numbers.

TR-ThP4 The Corrosion-Wear Mechanisms of CoCrMo Alloys Coated with TiAlN/TiAl Multilayer, *Martín Flores*, *O. Jimenez*, *E. Rodriguez*, Universidad de Guadalajara, Mexico, *E. Andtade*, Universidad Nacional Autonoma de Mexico

The tribocorrosion phenomenon is present in biomedical alloys that are used in artificial implants to replace natural joints. This damage limits the service life of such implants, the hard coatings can improve the resistance to wear and corrosion. The multilayers of TiAlN/TiAl were deposited on CoCrMo alloys by magnetron sputtering. In this work we study the wear mechanism of the coated alloy and without multilayer in a simulated body fluid with an ion concentration similar to that in the human blood. The structure of coatings was studied by means of XRD and the composition by RBS and EDS techniques. The tribocorrosion behavior of CoCrMo alloys alone and coated with TiAlN/TiAl multilayers was studied in simulated body fluid and distilled water. The tribocorrosion was performed using a tribometer with an geometry of ball on plate and reciprocating movement. The tests were conducted at 36 ± 1 °C of temperature. The loads used were 1N, 1.5, and 2N, the oscillating frequencies was 1Hz. The corrosion and tribocorrosion were studied using open circuit potential (OCP) in wear-corrosion tests and potentiodynamic polarizations in corrosion tests. In order to study the wear mechanisms, the topography and composition of worn surfaces were analyzed by means of SEM, EDS and profilometry. In the case of CoCrMo alloy it was found a transition from smooth wear to abrasive wear when the load was increased.

TR-ThP5 Improving the Surface Hardness of Plasma Nitrided 316L Stainless Steel, *Petros Abraha*, *S. Mikashima*, Meijo University, Japan

Stainless steels have very good corrosion resistance but the lower surface hardness poses marked limitation on the range of tribological applications that can be envisaged. Here plasma nitriding treatment was performed to modify the hardness without altering the corrosion resistance of austenitic 316L stainless steels.

In nitriding the 316L stainless steel, the passive Cr₂O₃ layer that protects the surface from corrosion is removed first as it hinders the diffusion of nitrogen ions and atoms into the bulk of the stainless steel material. The removal of the passive layer was done by argon sputtering and the subsequent plasma nitriding was performed in electron beam excited plasma apparatus under nitrogen atmosphere for three hours. The apparatus was driven at an acceleration voltage of 100 volts and a beam current of 3 amperes. The sample temperature was held constant at 450 degree centigrade. Treated and untreated samples were characterized by means of morphological analysis, Vickers hardness measurements, and corrosion tests in NaCl solutions.

The results of our experiments show that nitriding treatments performed in primarily ion and neutral enviros have increased hardness, slightly lower chrome concentration, and hence slightly higher quantity of rust. The measured hardness, chrome concentration, and quantity of rust for the non-treated samples were 230 Hv, 17 mass%, and 4 g/m², respectively. Ion nitriding in contrast largely increased the surface hardness of the stainless steel samples (more than 6 times), but decreased the corrosion resistance properties due to the CrN precipitation (15.8 mass %). Nevertheless nitriding treatments performed under neutral nitriding increased the surface hardness of the stainless steel samples (more than 3 times), avoid a large CrN precipitation (16.8 mass %) and rust quantity of 7.8 g/m² that is much lower than the 350 g/m² for ion nitriding. The above results indicate that stainless steels can be used as sliding or meshing mechanical parts in environments such as vacuum chambers and underwater machinery.

2D Materials Focus Topic

Room: 310 - Session 2D+EM+MS+NS-FrM

2D Materials: Device Physics and Applications

Moderator: Daniel Gunlycke, Naval Research Laboratory

8:20am **2D+EM+MS+NS-FrM1 1, 2, 3... Ripples, Gaps and Transport in Few-layer Graphene Membranes, ChunNing(Jeanie) Lau**, University of California, Riverside **INVITED**

Graphene, a two - dimensional single atomic layer of carbon, has recently emerged as a new model system for condensed matter physics, as well as a promising candidate for electronic materials. Though single layer graphene is gapless, bilayer and trilayer graphene have tunable band gaps that may be induced by out-of-plane electric fields or arise from collective excitation of electrons. Here I will present our results on mechanical manipulation and transport measurements in bilayer and trilayer graphene devices with mobility as high as 400,000 cm²/Vs. We demonstrate ripple formation due to thermally or mechanically induced strain, the presence of an intrinsic gapped state in bilayer and trilayer graphene at the charge neutrality point and evidence for quantum phase transition. Our results underscore the fascinating physics in these 2D membranes, and have implications for band gap engineering for graphene electronics and optoelectronic applications.

9:00am **2D+EM+MS+NS-FrM3 Photoinduced Doping in Heterostructures of Graphene and Boron Nitride, Jairo Velasco Jr., L. Ju**, UC Berkeley, *E. Huang*, Stanford University, *S. Kahn, C. Nosiola, H.-Z. Tsai*, UC Berkeley, *W. Yang*, Beijing National Laboratory for Condensed Matter Physics, Republic of China, *T. Taniguchi, K. Wantanabe*, National Institute for Materials Science (NIMS), Japan, *Y. Zhang*, Fudan University, Republic of China, *G. Zhang*, Beijing National Laboratory for Condensed Matter Physics, Republic of China, *M.F. Crommie, A. Zettl, F. Wang*, UC Berkeley

Van der Waals heterostructures (VDH) provide an exciting new platform for materials engineering, where a variety of layered materials with different electrical, optical and mechanical responses can be stacked together to enable new physics and novel functionalities. Here we report an emerging optoelectronic phenomenon (i.e. photo-induced modulation doping) in the graphene-boron nitride VDH (G/BN heterostructure). We find it enables flexible and repeatable writing and erasing of charge doping in graphene with visible light. We demonstrate that the photo-induced modulation doping maintains the remarkable carrier mobility of the G/BN heterostructure, and it can be used to generate spatially varying doping profiles like *pn* junctions. Our work contributes towards understanding light-matter interactions in VDHs, and innovates a simple technique for creating inhomogeneous doping in high mobility graphene devices. This opens the door for new scientific studies and applications.

9:20am **2D+EM+MS+NS-FrM4 Two-dimensional Resistance Map of Graphene p-n Junction in the Quantum Hall Regime, Nikolai N. Klimov, S. Le, C.A. Richter**, National Institute of Standards and Technology (NIST), *J. Yan*, University of Massachusetts, Amherst, *E. Comfort, J.U. Lee*, SUNY-University of Albany, *D.B. Newell*, National Institute of Standards and Technology (NIST)

Graphene, a two dimensional (2D) electronic system with a unique band structure, is a promising material for future electronic devices, especially for electrical metrology [1]. Currently, devices based upon GaAs heterostructures 2D electron gases (GaAs-2DEG) are used to realize a single quantum resistance standard value of $(\frac{1}{2})h/e^2 = 12,906.4035 \Omega$ with metrological accuracy. It is important to realize resistance values over a wider resistance scale to expand the technical relevance of quantum resistance standards.

In the past, attempts have been made by using parallel or series GaAs-2DEG Hall bars to achieve multiple or fractional resistance values of h/e^2 . However, the difficulties of fabricating ideal contacts and metal interconnects between the Hall bars severely limit the yield of properly operating devices. Graphene, with its ability to create both electron and hole 2D gases on a single Hall bar device without metal interconnects, is an ideal platform to overcome this difficulty [2].

We have fabricated a graphene FET p-n junction device in a Hall bar geometry and experimentally characterized it at large magnetic fields to determine the range of quantized resistance values that can be obtained. The device features two doped polysilicon split gates that are buried in a SiO₂ substrate within 100 nm-150 nm from the surface of graphene. The fabrication process achieves an atomically smooth dielectric surface, which is needed to preserve the intrinsic band structure of graphene. Independent

voltage control on these gates allows separate tuning of both type and concentration of charge carriers in the two parts of graphene conducting channel. In addition, a very narrow 150 nm gap between split gates gives a very sharp junction. Measurement of the sample's resistance at different gate values and measurement configurations in the quantum Hall regime allows us to fully characterize the device and to obtain multiples or fractions of the resistance value h/e^2 . We will show that our experimental results can be explained by the Landauer-Büttiker edge-state transport model with the assumption of a partial mixing at the p-n interface. Potential application of graphene p-n junction devices for resistance standards with a wide range of resistance values other than $h/2e^2$ will be discussed.

References:

[1] A. Tzalenchuk, *et al.*, Nature Nanotech., 5, 186 (2010)

[2] M. Woszczyzna, *et al.*, APL, 99, 022112 (2011)

9:40am **2D+EM+MS+NS-FrM5 Electrical Breakdown and Current Carrying Ability of Multilayer MoS₂ Transistors, Philip Feng, R. Yang, Z. Wang**, Case Western Reserve University

We report the first study of electrical breakdown of multilayer molybdenum disulphide (MoS₂) transistors through precision electrical measurements and simulation that shows the effect of varying the device size and conductivities on the breakdown limit. We demonstrate that the multilayer devices have better current carrying capabilities compared to thin layer devices. We also study the effect of varying MoS₂ thickness upon electron mobility in the channel.

MoS₂ has recently emerged as a new two-dimensional (2D) semiconducting crystal with attractive properties, such as the absence of dangling bonds, high thermal stability, and having a thickness-dependent bandgap [#_edn1]. While prototype single- and few-layer MoS₂ FETs and circuits have been demonstrated, in practice multilayer (up to 10s of nanometers) devices may be more desirable for certain applications: they can have higher carrier mobility and density of states under the same dielectric environment, greater mechanical strength, higher current limit and better manufacturability [#_edn2] [#_edn3]. While the breakdown of single layer MoS₂ transistors has been demonstrated [#_edn4], breakdown of multilayer devices has not been studied.

In this work, we study the electrical breakdown of devices with different thicknesses through experimental demonstration and simulation with finite element method (FEM). We observe that the breakdown process happens gradually with multiple voltage sweeping cycles, and thicker devices generally show higher breakdown current, which is also demonstrated in the simulation. The highest breakdown current in the measurement is 1.2mA, which is one of the highest current reported results so far for MoS₂ transistors. Simulation also shows that with higher conductivity channel, the breakdown current and breakdown current density both increase. The high field transport characteristics of multilayer MoS₂ transistors demonstrate that the devices could drive high loads in circuits and could be used for circuits that require high power or current. The thickness dependence of mobility shows that the device performance can be further improved by carefully tuning the device parameters.

[i] [#_ednref1] Q. H. Wang, *et al.*, Nat. Nanotechnol. 7, 699 (2012).

[ii] [#_ednref2] D. Jariwala, *et al.*, ACS Nano 8, 1102 (2014).

[iii] [#_ednref3] R. Ganatra, Q. Zhang, ACS Nano (2014), DOI: 10.1021/nn405938z.

[iv] [#_ednref4] D. Lembke, A. Kis, ACS Nano 6, 10070 (2012).

10:00am **2D+EM+MS+NS-FrM6 Lithography-free Fabrication of Graphene Devices, Nick Thissen, R.H.J. Vervuurt**, Eindhoven University of Technology, Netherlands, *J.J.L. Mulders*, FEI Electron Optics, Netherlands, *J.W. Weber, A.J.M. Mackus, W.M.M. Kessels, A.A. Bol*, Eindhoven University of Technology, Netherlands

Graphene device fabrication on large-area graphene typically involves several patterning steps using electron beam or optical lithography, followed by graphene etching and metallization for application of metallic contacts. However, the resist films and lift-off chemicals used in lithography introduce compatibility issues, such as the difficulty of removing the resist from the graphene. This resist residue has a negative influence on the thermal and electrical properties of the graphene and interferes with functionalization of the graphene. This motivates the development of a 'bottom-up', direct-write, lithography-free fabrication method.

In this work, a lithography-free fabrication method for graphene-based devices was developed. As a first step, the method involves direct

patterning of large-area graphene by focused ion beam (FIB) in order to isolate graphene from the bulk. The patterning of the graphene is performed in a DualBeam (SEM / FIB) system, in which a 30 kV FIB is used to locally remove graphene from the substrate. An *in situ* Raman microscope allows for direct observation of the graphene quality before and after FIB processing, from which it was determined that a low Ga-ion dose of 10 C/m² is sufficient for complete graphene removal. By optimizing the pattern design, the ion beam current and the background pressure in the DualBeam system, unintentional damage of the graphene by scattered ions is almost completely prevented.

After FIB patterning, as a second step a direct-write atomic layer deposition (ALD) technique is applied in the same system to locally deposit contacts to the isolated graphene. In the direct-write ALD technique, the patterning capability of electron beam induced deposition (EBID) is combined with the material quality of ALD. A thin seed layer consisting of small Pt grains in amorphous carbon is deposited on the graphene by EBID in the desired contact pattern. Subsequently, a selective ALD process purifies the seed layers and builds them into high-quality Pt contacts. This combined approach yields virtually 100% pure Pt (resistivity of 12 μΩcm) with a lateral resolution of 10 nm¹¹. This chemical approach to contact deposition is expected to yield lower contact resistances compared to conventional physical deposition techniques.

By combining patterning and direct contact deposition in the same system, graphene devices were fabricated from large-area graphene without the use of lithography. First results from sub-optimal devices demonstrate field-effect mobilities approaching 500 cm²/Vs and contact resistances as low as (40 ± 30) Ω.

[1] A.J.M. Mackus et al., *Nanoscale* 4, 4477 (2012)

10:40am **2D+EM+MS+NS-FrM8 Electronic Transport in Transition Metal Dichalcogenides, Joerg Appenzeller, Purdue University INVITED**
Since the discovery of graphene for electronic applications, there has been a substantial worldwide effort to explore other layered materials. Transition metal dichalcogenides (TMDs) like MoS₂, MoSe₂, or WSe₂, to just name a few, not only offer the desired ultra-thin body structure that translates into superior electrostatics as desirable for nanoelectronics applications, but also exhibit a sizable band gap. While to date the ideal application space for these materials has not been identified, it is obvious that only through a detailed understanding of the underlying transport in these layered materials intrinsic properties that lend themselves to particular applications can be uncovered.

In my presentation I will first discuss the benefits of an ultra-thin body structure for scaled tunneling FET applications including tunneling devices. Contacts play a particularly crucial role in this context and can easily mask the intrinsic performance of TMDs as will be discussed based on experimental Schottky barrier tunneling data obtained from MoS₂, MoSe₂ and WSe₂ field-effect transistors. A careful analysis of all these material systems reveals details about Schottky barrier heights for electron and hole injection as well as the band gap. These findings are then put into the context of channel length scaling and layer thickness dependence of three-terminal TMD devices based on MoS₂ transistors. Last, experimental data on the band-to-band tunneling in partially gated WSe₂ device structures will be discussed and projections about the potential usefulness of TMDs for tunneling device applications will be made.

11:20am **2D+EM+MS+NS-FrM10 Controlled Synthesis and Fuel Cell Application of Carbon Nanowalls, Hiroki Kondo, S. Imai, K. Ishikawa, M. Sekine, M. Hori, Nagoya University, Japan, M. Hiramatsu, Meiji University, Japan**

Carbon nanowalls (CNWs) are one of carbon nanomaterials and contain stacks of graphene sheets vertically standing on a substrate. Each wall with the top edge is continuous crystallographically through bending or branching and composed of nanographite domains. Recently, we have developed the formation method of the ultra-high-density over 10¹³ cm⁻² Pt nanoparticles on the whole surface area of the CNWs with a diameter of 2-3 nm employing metal-organic chemical fluid deposition (MOCFD) method in supercritical fluid (SCF). They are promising as a catalytic electrodes for a polymer electrolyte fuel cell because of its high-specific-surface-area and high aspect ratio. On the other hand, while it is known that Pt nanoparticles are poisoned by CO below 100°C, it is reported that Pt-Au nanoparticles are excellent candidate for a low-temperature anode electrocatalyst. In this study, supporting processes of Pt-Au nanoparticles on the CNWs using the SCF-MOCFD method and their catalytic properties were investigated.

We used the SCF-MOCFD system to support Pt and Au nanoparticles on the CNWs. Firstly, Pt nanoparticles were supported using 1wt% (CH₃C₂H₄)(CH₃)₃Pt solution (2 ml). Then, Au nanoparticles were subsequently supported using (CH₃)₂Au(CH₃COCHCOCH₃) solution (1 ml). Both precursors were diluted by n-hexane [CH₃(CH₂)₄CH₃].

According to the SEM images of the CNWs after the supporting processes of only Pt nanoparticles and, both Pt and Au ones, the nanoparticles are supported on the entire surface area of each CNWs in the both cases. It is also found that the diameter and its distribution of the nanoparticles decrease after the second Au supporting process, while its density increases. This means that the relatively large Pt nanoparticles are effectively removed and small Au nanoparticles are simultaneously supported at the second supporting process. On the other hand, we evaluated cyclic voltammetry (CV) characteristics using CNWs with different-density Pt nanoparticles, in which density of 3.0×10¹² cm⁻² and diameter of 1.1 nm obtained for 10 min supporting and, density of 8.3×10¹² and diameter of 1.5 nm obtained for 30 min supporting. Peaks related to adsorption and desorption of hydrogen were found in both cases. With increasing the supporting time, the specific surface area of Pt evaluated from the CV about twofold increased. However, according to the TEM images, the ratio of surface area of Pt nanoparticles are about fivefold. It is deduced that some parts of Pt nanoparticles are inactive. Therefore, these results indicate that not the crystallinity control of CNWs are essential to improve the catalytic performance.

Atom Probe Tomography Focus Topic

Room: 301 - Session AP+AS+NS+SS-FrM

Correlative Surface and Interface Analysis with APT

Moderator: Arun Devaraj, Pacific Northwest National Laboratory

8:20am **AP+AS+NS+SS-FrM1 Correlative Transmission Electron Microscopy and Atom Probe Tomography of Interfaces in CdTe, David Diercks, J.J. Li, C.A. Wolden, B.P. Gorman, Colorado School of Mines INVITED**

CdTe solar cells are a promising thin film technology, yet the highest reported efficiencies [1] remain well below the theoretical efficiency for such materials. For polycrystalline CdTe, interface contacts and grain boundaries along with impurities likely account for the majority of this underperformance.

Atomic scale analysis is an important feedback mechanism to relate the structure to both the device performance and the processing conditions. Through this, the atomic scale factors which improve or limit the performance can be ascertained. This then enables the development of materials and processing methods which best eliminate or mitigate the detrimental effects.

With these goals, atom probe tomography (APT) in conjunction with transmission electron microscopy (TEM) was used to study the contact interfaces and grain boundaries in CdTe devices. With the combination of time-of-flight mass spectrometry and point projection microscopy by controlled field evaporation, APT has the ability to obtain tens of ppm composition sensitivity along with near atomic-level spatial resolution. TEM provides crystallographic information along with other correlative information for guiding the reconstruction of the APT data.

It is demonstrated that the compositions measured for CdTe by APT are sensitive to the analysis conditions. Therefore, the APT analysis conditions for obtaining accurate measurements of the specimen stoichiometry were first ascertained. Following that, TEM and APT analyses of thin film devices consisting of a fluorine-doped tin oxide coated glass substrate subsequently coated with CdS, CdTe, Cu-doped ZnTe, and Au were performed. Using optimized values, APT analyses on the absorber layers and contact interfaces after different deposition and processing conditions were performed. These show significant changes in copper and sodium distributions as a result of the thermal processing.

[1] M. A. Green, K. Emery, Y. Hishikawa, W. Warta, and E. D. Dunlop, "Solar cell efficiency tables (version 42)," *Progress in Photovoltaics*, vol. 21, pp. 827-837, Aug 2013.

9:00am **AP+AS+NS+SS-FrM3 Atom Probe Compositional Analysis of Nanoscale Precipitates in Nb-Ti Micro-alloyed Steels, Monica Kapoor, G.B. Thompson, University of Alabama, R.M. O'Malley, Nucor Steel**

Composition of complex carbide and carbo-nitride precipitates in Ti-Nb micro-alloyed 80-ksi (0.06 wt. % Nb; 0.06 wt. % Ti) and 100-ksi (0.03 wt. % Nb; 0.12 wt. % Ti) steels was studied using atom probe tomography. Fine (~2 nm) and coarse (~8 nm) NbTiC precipitates were identified in the 100 ksi steel with the Fe content decreasing with increasing precipitate size. Both steels had coarse NbTiCN precipitates (~80 nm) having ~7 at. % and ~30 at. % Nb in the precipitates for the 100 ksi and 80 ksi steels respectively. Star-shaped TiC precipitates and parallel rows of interphase NbTiC clusters on and near grain boundaries were also identified in the 100

ksi steel. In the 80 ksi steels, uniformly distributed disk-shaped and spherical NbTiC clusters were observed along dislocations. The composition and phase stability of these precipitates are discussed in terms of Thermo-Calc solution thermodynamic modeling.

9:20am **AP+AS+NS+SS-FrM4 Nanoscale Imaging of Li and B in Glass Samples, a Comparison of ToF-SIMS, NanoSIMS, and APT**, *Zihua Zhu, Z.Y. Wang, J. Liu, J. Crum, J.V. Ryan, D.K. Schreiber, J.J. Neeway*, Pacific Northwest National Laboratory

A widely used method to immobilize nuclear wastes is fusing them into glasses. These proposed glass waste forms are multicomponent complex material with the common components of Li and B compounds. It is difficult for commonly-used surface analysis tools (e.g., X-ray photoelectron spectroscopy (XPS), Auger electron spectroscopy, scanning electron microscope/energy dispersive spectroscopy (SEM/EDX), and transmission electron microscope/energy dispersive spectroscopy (TEM/EDX)) to image the distributions of ultra-light elements like Li and B with sub-micron lateral resolutions. Time-of-flight secondary ion mass spectrometry (ToF-SIMS), NanoSIMS, and atom probe topography (APT) were used to image Li and B distributions in several representative glass samples. ToF-SIMS can provide ~100 nm lateral resolutions if using Li⁺ and BO₂⁻ images. However, both positive ion mode and negative ion mode are needed because neither B signals in positive ion mode nor Li signals in negative ion mode can provide adequate intensity to form qualified images. NanoSIMS can provide ~100 nm lateral resolutions if using Li⁻ and BO₂⁻ images, while the lateral resolution of positive ion mode of NanoSIMS is poor (~400 nm). APT can provide ~2 nm lateral resolution for Li⁺ and B⁺ in a 3-D mode and quantification of APT is better than that of SIMS. While APT can provide much better ultimate lateral resolution than ToF-SIMS and NanoSIMS, it has three drawbacks: limited field-of-view, time-consuming sample preparation, and frequent/unpredicted sample damage during measurement. As a comparison, field-of-view of SIMS is flexible, sample preparation is simple, and little unpredicted sample damage occurs during SIMS measurement. Therefore, SIMS and APT can be regarded as complimentary techniques in nanoscale imaging of Li and B in glass samples.

9:40am **AP+AS+NS+SS-FrM5 Application of (S)TEM and Related Techniques to Atom Probe Specimens**, *William Lefebvre, D. Hernandez-Maldonado, F. Cuvilly, F. Moyon*, University of Rouen, France **INVITED**
The geometry of atom probe tomography (APT) specimens strongly differs from standard scanning transmission electron microscopy (STEM) foils. Whereas the later are rather flat and thin, APT tips display a curved surface and a significantly larger thickness. As far as a correlative approach aims at analysing the same specimen by STEM and APT, it is mandatory to explore the limits and advantages imposed by the particular geometry of APT specimens to STEM.

High angle annular dark field (HAADF) in STEM provides a contrast related to atomic number and to the amount of atoms in a column. A complete analysis of a high resolution HAADF STEM image requires the identification of projected column positions, the calculation of integrated HAADF intensity for each column and, eventually, the estimation of a "background level" generated by the amorphous carbon or oxide layer present on the specimen surface. Then, by of a statistical analysis [1], the possibility of atomic counting in an APT specimen can be explored. For this purpose, we propose an image processing method which provides a complete analysis of HAADF STEM images, that was applied here to APT specimens. In order to estimate the advantages and limitations of the method for such a particular specimen geometry, simulations have been applied and confronted to experimental results. Illustrations will be given for specimens before and after field evaporation in APT.

[1] S. Van Aert et al. Phys. Rev. B 87 (2013) 064107

10:40am **AP+AS+NS+SS-FrM8 APT Analysis of Biological Materials**, *Daniel Perea, J. Liu, J.A. Bartrand, N.D. Browning, J.E. Evans*, Pacific Northwest National Laboratory **INVITED**

Biointerfaces play an essential role for the function of many biological materials and organisms. The behaviors of complex macromolecular systems at materials interfaces are important in the fields of biology, environmental biology, biotechnology, and medicine. An understanding of the chemical processes and physics, and ultimate the ability to engineer biomaterials and microorganisms with specific properties and functions, is aided by an atomic level understanding of the composition and morphology of biointerfaces. However, a great challenge exists to map the atomic level composition and morphology of biointerfaces using APT, precluding a complete understanding of the structure properties relationship. At the Environmental Molecular Sciences Laboratory (EMSL), the application of APT is being developed in combination with other microscopy and spectroscopic techniques to study interfaces in biologic materials. We are

developing methodologies and analyses that are allowing us to probe the ultimate limits of what APT analysis can confidently provide despite the complex thermally-assisted field evaporation behavior of soft materials. Advanced sample preparation techniques will also be discussed that further advance the application of APT into field of biology.

Applied Surface Science

Room: 316 - Session AS+MC+SS-FrM

Practical Surface Analysis II

Moderator: Steven Pachuta, 3M Company

8:20am **AS+MC+SS-FrM1 Vector Potential Photoelectron Microscopy**, *Raymond Browning*, R. Browning Consultants

Vector potential photoelectron microscopy (VPPEM) is a new class of synchrotron based analytic spectromicroscopy using NEXAFS and XPS spectroscopy. To optimize the spatial resolution VPPEM images very low energy photoelectrons which poses both challenges and opportunities. At low energies the NEXAFS signals have an information depth that is similar to that from total yield absorption (TAY) measurements, while the XPS signals have a variable information depth from the universal curve at low energies. VPPEM has a very high depth of focus, and immunity to many imaging artifacts such as surface charging, and magnetic state. This makes VPPEM suitable for analyzing real world samples, and we present some results from the prototype instrument at NSLS.

8:40am **AS+MC+SS-FrM2 Hydrogen and Chemical Quantification of an Organic Coating**, *Paul Mack*, Thermo Fisher Scientific, UK

Zinc-coated steel substrates often have an additional organic coating applied, protecting the steel surface or altering its appearance for decorative reasons. X-ray Photoelectron Spectroscopy (XPS) is an analysis technique which provides chemical bonding information from the top few nanometres of a surface down to many microns in depth. It is the ideal technique, for example, for identifying the carbon functional groups in these organic coatings. XPS cannot detect hydrogen, however, but the complementary technique of Reflection Electron Energy Loss Spectroscopy (REELS) is able to both detect and quantify hydrogen. REELS can also be used to discern between aliphatic and aromatic carbon in the organic coatings.

There is also a requirement for compositional profiling of these coatings, combining the excellent depth resolution and chemical specificity of XPS with some kind of ion beam sputtering. Traditional methods such as argon monomer ion profiling can result in a high degree of chemical modification during the acquisition of depth profiles for organic materials. Numerous studies over recent years, however, has shown that argon cluster beams may be used for depth profiling while preserving chemical information during analysis of organic materials.

This talk will present data from cluster profiling studies of an organic coating on steel. The data will be compared with an alternative method of profiling the coating, i.e. ultra low angle microtomy. A complete elemental compositional profile of the coating, including hydrogen, will be presented.

9:00am **AS+MC+SS-FrM3 Mechanical Strain Induced Tunable Reflective and Conducting Silver Nanorods Embedded PDMS Film**, *Pratibha Goel*, J.P. Singh*, Indian Institute of Technology, India

The formation of metallic films on both inorganic and organic polymeric substrate continues to be of substantial interest because of various applications.^{1,2} Polymeric supports offer the obvious advantages in weight, flexibility, elasticity, and fragile relative to inorganic support such as glasses, ceramics, or native metal. Silver is a metal of choice as a reflecting material because of its high reflection coefficient (0.93). Silver also has the highest electrical conductivity of all metals at 6.3×10^7 (Ωm)⁻¹. However, there are disadvantages of using silver as the reflecting metal. Firstly, silver is a relatively soft metal so that the face of a mirror needs to be carefully protected from mechanical abrasion. Secondly, silver tends to tarnish which diminishes its reflectivity. (Ambient sulfur-containing compounds are a particular problem.) Thirdly, and perhaps the most important, silver(0), as a more passive metal, does not interact strongly with organic functionalities, which means that adhesion of a silver layer on a polymer surface can be a substantial problem.

In this study we present a straightforward two step fabrication of highly adherent, reflective and surface conductive flexible films. First, the Ag nanorods were deposited on the Si (001) substrates by thermal evaporation of silver powder using oblique angle deposition (OAD).³ Then the thermal

* ASSD Student Award Finalist

curing of the PDMS on the Ag nanorods grown Si wafer leads to the copolymerization yielding a flexible, reflective and conductive silver surface approaching that of the native film. The Fig. 1 shows schematically the route followed for the fabrication of the sample. As prepared sample appear to be highly reflecting and conducting with the reflectance (R) of 64.17 % at 530 nm and sheet resistance (R_s) of 24.03 Ω /sq. Elongation of the sample up to 30% of its original length results into decrease in the reflectance and increase in R_s . Fig. 2 shows the tunability of the R at 531 nm and R_s with respect to the strain applied. Adhesion between the silver nanorods and the polymeric PDMS film was outstanding. No adhesive tapes removed any silver from the surface. Our sample may find potential applications in multifunctional devices where tunability of reflectance and conductivity is desirable through flexibility.

References: 1. N. Hubin, L. Noethe, Science 262 (1993), 1390.

2. L. Yan, X. M. Zhao, G. M. Whitesides, J. Am. Chem. Soc. 120 (1998), 6179.

3. P. Goel, K. Singh, J. P. Singh, RSC Advances 4 (2014), 11130.

9:40am **AS+MC+SS-FrM5 Surface Analysis of Electronic Materials**, R.L. Opila, Kevin Jones, J. Church, University of Delaware, R. Gupta, V. Pallem, B. Lefevre, Air Liquide, X. Lin, University of Delaware

Surface analysts at the University of Delaware have used a variety of surface analytical techniques to analyze films for electronic materials applications. These films were deposited by a variety of technique including plasma enhanced chemical vapor deposition, molecular organic chemical vapor deposition and atomic layer deposition using precursors synthesized at Air Liquide. Methods of analysis include x-ray photoelectron spectroscopy, scanning Auger electron spectroscopy, time-of-flight secondary ion spectrometry, nano-indentation and synchrotron-based hard x-ray analysis. The advantages of each technique for particular analyses will be discussed.

10:40am **AS+MC+SS-FrM8 Lewis Base Sites on the Nitrogen-Doped Graphite Surfaces Probed by CO₂ Adsorption**, Takahiro Kondo, R. Shibusya, S. Morohoshi, D. Guo, J. Nakamura, University of Tsukuba, Japan

Carbon materials have been reported to exhibit unique adsorption property and catalytic activity when they have received specific treatments such as nitrogen doping. For example nitrogen-doped graphene has been reported to show the superior catalytic activity for the oxygen reduction reaction (ORR) in fuel cell [1]. To understand the origin of such specific properties at the atomic scale, we are now trying to examine the relationship among the localized electronic states of the carbon atoms, the adsorption property of the molecule, and the catalytic activity towards ORR by using model catalyst of graphite with surface science techniques. Previously, we have reported based on the scanning tunneling spectroscopy (STS) that the carbon atoms around a pyridinic-nitrogen (N having two N-C bonds) in a highly oriented pyrolytic graphite (HOPG) have occupied localized states near the Fermi level [2]. We consider that such carbon atoms may act as Lewis base sites [2] and may relate to the ORR activity. In this work, we have examined this hypothesis by observing the carbon dioxide adsorption property with temperature programmed desorption (TPD), ORR catalytic activity measurement, and X-ray photoelectron spectroscopy (XPS).

To prepare the pyridinic-nitrogen-doped graphite (pN-HOPG) as the model catalyst, we have firstly cleaved the HOPG at atmosphere and then bombarded it by the nitrogen ion through Ni patterned mask to make edges with N-termination. After the bombardment, the sample was put into HNO₃ solution for 72 hours to remove Ni impurity. The sample was annealed at 900 K for 2 hours in ultrahigh vacuum. XPS spectrum shows that the nitrogen in the prepared sample consists of over 60 % pyridinic-nitrogen, suggesting that nitrogen atoms are dominantly doped at the edges.

In TPD measurements, CO₂ desorption peak was observed at around 370 K from pN-HOPG after the 1000 L CO₂ exposure at 300 K, while no CO₂ desorption peak was observed from clean HOPG. These results indicate that Lewis base sites are formed on pN-HOPG. The same CO₂-TPD results were reproducibly observed by sequential 4 time measurements. This means Lewis base sites on pN-HOPG does not change by the CO₂ adsorption and desorption. Details of CO₂ adsorption properties on pN-HOPG, the relationship with ORR activity and the influence of nitrogen configuration on the carbon atoms in pN-HOPG will be discussed.

[1] L. Qu et al., ACS Nano, 4 (2010) 1321.

[2] T. Kondo, S. Casolo, T. Suzuki, T. Shikano, M. Sakurai, Y. Harada, M. Saito, M. Oshima, M. Trioni, G. Tantardini and J. Nakamura, Phys. Rev. B 86 (2012) 035436.

11:00am **AS+MC+SS-FrM9 Towards Spin-FETs: Growth and Characterization of Magnetoelectric Chromium Oxide Films on Graphene**, Sean Stuart, E. Sachet, J.-P. Maria, J.E. Rowe, D.B. Dougherty, North Carolina State University, M. Ulrich, Army Research Office

Graphene has brought spintronic devices that depend on the ability to transport spin much

closer to realization. Graphene's high carrier mobility and low spin-orbit scattering allow for efficient

spin transport, which has been demonstrated by several publications over useful length scales [1,2].

Further progress toward more sophisticated spintronic devices requires controllable manipulation of

spin polarized charge carriers. A graphene Spin-Field Effect Transistor has been proposed by

Semenov et al [3] that manipulates the spin of charge carriers in a graphene channel by an exchange

interaction with a hypothetical ferromagnetic dielectric. As an alternative that also adds functionality,

we have identified Cr₂O₃ as a material whose magnetoelectric properties would enable voltage

controlled switching of the exchange interaction. The Magnetoelectric properties of Cr₂O₃ have been

extensively studied [4], including recent reports of a robust electrically switched magnetic surface

state [5,6].

We used pulsed laser deposition to grow thin Cr₂O₃ films directly on HOPG. AFM shows a

smooth Cr₂O₃ film with the hopg topography preserved. X-Ray Diffraction shows that the film has a

(0001) texture for films grown at 300 - 650°C, which is the strongest orientation of the

magnetoelectric effect. The magnetic polarization of the film can be aligned by magnetoelectric

annealing and locally switched with conducting AFM, the effects of both are observed by magnetic

force microscopy.

[1]. Han, et. Al. J. Mag & Mag. Mat. Vol. 234, Issue 4, (2012)

[2]. Bruno Dlubak, et al. Nat. phys, 8, 557 (2012)

[3]. Y. G. Semenov, et al. Appl. Phys. Lett. 91, 153105 (2007).

[4]. Manfred Fiebig Phys. D: Appl. Phys. 38 R123 (2005)

[5]. X. He, et al. Nat. Mater. 9, 579 (2010).

[6]. N. Wu, et. al., Phys. Rev. Lett. 106, 17 (2011).

11:20am **AS+MC+SS-FrM10 Energy Loss Of Highly Charged Ions Implanted In MOS Dielectric Films**, Radhey Shyam, D.D. Kulkarni, D.B. Cutshall, J.E. Harriss, W.R. Harrell, C.E. Sosolik, Clemson University

Energy loss measurements of highly charged ions in the low kinetic energy regime have been made using as-grown SiO₂ (170nm) targets. Highly charged Ar^{q+} ions (Q=4, 8 and 11) with a kinetic energy of 1 keV were used to produced electronic excitations in the oxides. The irradiated regions of the oxide were then encapsulated under a top metallic contact to form metal-oxide-semiconductor (MOS) devices. The devices were probed with capacitance-voltage (C-V) measurements and the extracted flatband voltages from the C-V curves were correlated with ion energy (kinetic and potential).

The C-V results for highly charged ion experiments reveal that the changes in the flatband voltage and slope for implanted devices relative to the pristine devices can be used to delineate effects due to implanted ions only and ion induced damage. The results confirm that dose as well as and charge-dependent effects can be recorded for irradiation of oxides using this method. In particular, the results as a function of charge state indicate that there is a significant enhancement in the induced flatband voltage shift as the charge state of the beam is increased. This was quantified by measuring the flatband voltage shift across multiple ion doses for fixed incident charge states to obtain a normalized value of the shift induced per incident ion. These normalized results show an enhancement in the shift, which grows monotonically across our charge state data, from 1.14 x 10⁻¹² V/ion for Ar⁴⁺ ions to 1.12 x 10⁻¹¹ V/ion for Ar¹¹⁺ ions. This enhancement in the shift is consistent with the increased potential energy of the higher charge states (e.g. 15 eV for Ar⁴⁺ and 2004 eV for Ar¹¹⁺). Viewed as a function of the ion charge state, these data suggest a near-quadratic dependence on the incident charge which is consistent with some theoretical predictions.

**Conservation Studies of Heritage Materials Focus Topic
Room: 313 - Session CS-FrM**

Conservation Studies of Modern Heritage Materials 3

Moderator: Karen Gaskell, University of Maryland,
College Park

9:00am **CS-FrM3 Faces from the Past: Microbeam Imaging and Analysis of Artifacts from ancient Mesoamerica, Timothy Rose, J.M. Walsh, Smithsonian Institution** **INVITED**

Working in the analytical laboratories in the Department of Mineral Sciences in the National Museum of Natural History provides plenty of challenging problems just involving geologic materials. Requests from other departments within the museum and elsewhere are growing as the understanding spreads to other disciplines of how our tools can be applied to an even wider variety of materials. Here we provide details about two recent and ongoing studies of cultural artifacts from ancient Mesoamerica. These studies were performed using a variable pressure field emission FEI NovaNanoSEM 600 outfitted with a ThermoFisher silicon drift detector energy dispersive x-ray spectrographic (EDS) analysis system. They were conducted on uncoated whole specimens or fragments and tiny samples removed from the surface or from deep recesses of the objects.

A large collection of spectacular artifacts was delivered to the museum with a request to provide information as to their authenticity. The collection included carved stone figurines and masks and ceramic pieces with various surface coatings. The objects were photographed, measured and placed into groups based on their apparent cultural affinity. Initial observations were made using optical microscopy with particular attention paid to tool marks. In the SEM, some whole artifacts stretched the limits of sample chamber size and geometry. Very few objects showed evidence of modern tools at either the optical or SEM scale. Chemical compositions of minerals in, and surface coatings on, stone artifacts were determined in order to characterize the rock type and other materials. Rock types included jadeite, serpentine and syenite. One group of several syenite masks were partially coated with a probable modern tan gypsum plaster. Several ceramic artifacts of unique design have complex surface decorations. A small cross-sectional multi-colored fragment of the coating on one object was studied in detail revealing five chemically distinct layers. We interpret this as original Olmec fresco paint. The results of the ongoing research indicate that the large majority of the artifacts are authentic pre-Columbian objects belonging to the Olmec, Maya, Teotihuacan and Mezcala civilizations which date from 1500BC to 600AD.

In the first comprehensive study of the iconic stone "masks" from Teotihuacan (100 BC to 600AD), we examined nearly 200 masks. Sampling of the artifacts was prohibited however silicone molds taken austensibly to study tool marks and carving methods also removed tiny grains from deep in drill holes. Study of these grains reveal that some are very likely residue from the original carving and polishing of the stone.

9:40am **CS-FrM5 Atomic Layer Deposited Diffusion Barriers on Non-ideal Silver and Bronze Cultural Heritage Objects, Amy Marquardt, University of Maryland, College Park, E. Breitung, E-Squared Art Conservation, G. Gates, T. Drayman-Weisser, The Walters Art Museum, G.W. Rubloff, R.J. Phaneuf, University of Maryland, College Park**

Atomic layer deposited metal oxide diffusion barriers are investigated to better preserve cultural heritage metal objects in museum collections. Recently, the effectiveness and reversibility of ALD films to create diffusion barriers for non-ideal silver and copper alloy (bronze) cultural heritage objects has been studied. Previous results demonstrate the ability of ALD films to protect clean, uniform silver substrates at least an order of magnitude longer than current silver protection methods. The capability of ALD films to protect surfaces representative of "real" museum metal objects was investigated. These objects included silver surfaces with pre-existing surface treatments, including polishing abrasives, chemical dips or organic lacquers, and patinated copper alloys surfaces with changing chemical composition and topography. The ability of ALD films to uniformly wet non-ideal, chemically varying metal surfaces was investigated under accelerated aging in corrosive gas and acidic aqueous environments. ALD films were structurally engineered through thin film modeling and reflectance spectroscopy measurements to minimize object appearance and color change on patinated or tarnished substrates. Film reversibility was also examined to determine an acceptable technique to remove the ALD films without significantly altering the underlying metal substrate, an important requirement for art conservation practices.

*Work supported by the NSF under SCIART collaborative research grant #DMR1041809

10:00am **CS-FrM6 Studies of the Effects of Cleaning Protocols on Museum-based Plastics using Advanced Surface Analysis Techniques, Anna Fricker, D.S. McPhail, Imperial College London, UK, B. Keneghan, Victoria and Albert Museum, UK**

The conservation of plastic artefacts is an area of interest for curators and conservators of cultural heritage. Many museums contain artefacts that are made wholly or partly from plastic and these objects may be present in collections ranging from jewellery to spacesuits. The stability of these polymeric materials is a concern for conservators, particularly as plastic objects can exhibit severe degradation which can occur suddenly and without warning.

The natural soiling of objects in museum collections results in a need to clean plastic artefacts for aesthetic reasons and to maintain artistic integrity. The contamination of plastics with particulate matter may also facilitate degradation. However, the act of cleaning may itself result in damage to an artefact, either immediately after treatment or at a later date. The issue is compounded by the many different types of plastics present in collections: a treatment for one object may be unsuitable for another.

This work examines the physical and chemical changes to the surface of poly (methyl methacrylate) (PMMA) that has been treated with a range of cleaning techniques commonly used in conservation. Methods include the application of solvents and surfactants to the substrate surface. Physical changes to the surface have been examined using microscopy techniques while secondary ion mass spectrometry (SIMS) has been used to characterise the chemical changes to the substrate. The efficacy of these cleaning methods to remove an artificial soil from the polymeric substrate is also discussed.

10:40am **CS-FrM8 Microchemical Characterization of 19th Century Nanotechnology-Daguerreotype Photographs, Edward Vicenzi, Smithsonian Institution** **INVITED**

The daguerreotype photographic process represents the first practical form of photography and was presented to the scientific community in France in 1839. The technology spread rapidly and was widely used for roughly two decades. Image formation can be generalized in four steps: 1) sensitizing a silver-coated copper plate to halogen vapors, 2) exposing the sensitized plate to visible light within a camera, 3) development of an image after the plate is treated with heated mercury vapor, and finally 4) deposition of a gold gilding layer [1,2]. A effort is underway to evaluate several aspects of daguerreotypes including obtaining the composition of the nanoparticles that give rise to image contrast, the protective gilding layer, and corrosion products formed from exposure to atmospheric and other contaminants. A range of scanning and transmission electron- and X-ray-induced spectroscopies have been utilized to characterize these plates on the nano- and submicron- length scales in an effort to inform the long term preservation of these precious objects.

Re f e r e n c e s :

[1] Barger MS and White WB. The daguerreotype: nineteenth-century technology and modern science The Johns Hopkins University Press, ISBN-13: 978-0801864582, 280 pgs (2000).

[2] Swan A, Fiori CE, and Heinrich KFJ. *Scanning electron microscopy* 1, 411-423 (1979).

11:20am **CS-FrM10 The Application of Advanced Surface Analysis Techniques to the Study of Museum-Based Problems, David S. McPhail, Imperial College London, UK**

Museum materials are often (but not always) relatively stable and inert and the changes that take place to their appearance over time can be so slow as to be essentially imperceptible. For example a materials surface decaying at the rate of 1 nm per day requires approximately three millennia to form a 1 mm crust (assuming linear kinetics). It follows that extremely sensitive analytical instruments with very high sensitivity and resolution are required to measure these ultra-slow surface processes. It is interesting, therefore, that the very latest analytical tools developed primarily to characterise the very latest generation of modern materials such as nanomaterials and semiconductor quantum wells, are also very well suited for the study of the surfaces of historic and pre-historic materials.

In this talk I will show how techniques such as Secondary Ion Mass Spectrometry (SIMS), Focused-Ion Beam SIMS (FIB-SIMS) and Low Energy Ion Scattering (LEIS) can be used to determine the mechanisms and kinetics of processes such as oxidation, diffusion, corrosion and ion exchange at and near the surfaces of a variety of materials from museum collections. The materials will include glass, metals and ceramics. These analytical techniques can also be used to look at the changes that occur to surfaces as a result of cleaning interventions and can be used to look at how the surfaces becomes re-contaminated over time after cleaning interventions. Being ion-beam based UHV techniques they form the latter parts of any analytical hierarchy. These ion-beam based techniques can

exploit stable isotope exchange protocols using ions such as D and O18 to aid the analysis.

There is of course a tension between conservation science and surface analysis as surface analysts like to sample objects and use techniques that consume the object – this is not very welcome by the museum community for obvious reasons. I will discuss this issue and introduce approaches to sampling that might be tolerable.

Spectroscopic Ellipsometry Focus Topic

Room: 304 - Session EL+AS+BI+EM+SS-FrM

Application of SE for the Characterization of Organic and Biological Materials

Moderator: Tino Hofmann, University of Nebraska-Lincoln

8:20am EL+AS+BI+EM+SS-FrM1 **Multimodal Optical and Mass Spectrometric Imaging of Cells and Tissues**, *DaeWon Moon*, DGIST, Republic of Korea **INVITED**

Understanding interfacial phenomena has been one of the main research issues not only in semiconductors but only in life sciences. I have been trying to meet the atomic scale surface and interface analysis challenges from semiconductor industries and furthermore to extend the application scope to biomedical areas. Optical imaging has been most widely and successfully used for biomedical imaging but complementary mass spectrometric imaging can provide more detailed molecular specific information

In this presentation, I report our recent activities of multimodal nanobio imaging of cardiovascular cells and tissues. Firstly, in atherosclerotic plaque imaging using coherent anti-stokes raman scattering (CARS) and time-of-flight secondary ion mass spectrometry (TOF-SIMS), multimodal CARS & SIMS analysis showed that increased cholesterol palmitate may contribute to the formation of a necrotic core by increasing cell death. Secondly, surface plasmon resonance imaging ellipsometry (SPRIE) was developed for cell biointerface imaging of cell adhesion, migration, and infiltration dynamics for HUVEC, CASMC, and T cells. SPRIE images were validated with confocal fluorescence microscopy. Collagen fibrils are widely used as cell adhesion substrates. Changes of surface composition and elastic modulus of collagen fibrils after thermal and acidic treatment were investigated by TOF-SIMS and non-contact force microscopy. Multimodal SPRIE & TOF-SIMS imaging would be a useful methodology for understanding cell-substrate interactions in tissue engineering.

In conclusions, multimodal optical and mass spectrometric imaging provides overall structural and morphological information with complementary molecular specific information, which can be a useful methodology for biomedical studies. Future challenges in optical and mass spectrometric imaging for new biomedical applications will be discussed regarding in-vivo imaging.

9:00am EL+AS+BI+EM+SS-FrM3 **Sum Decomposition of Mueller Matrices from Beetle Cuticles**, *Hans Arwin, R. Magnusson*, Linköping University, Sweden, *E. Garcia-Caurel, A. de Martino*, LPICM-CNRS, Ecole Polytechnique, France, *K. Järrendahl*, Linköping University, Sweden, *R. Ossikovski*, LPICM-CNRS, Ecole Polytechnique, France

Spectral Mueller matrices are very rich in information about physical properties of a sample. We have recently shown that polarizing properties like ellipticity and degree of polarization, can be extracted from a Mueller matrix measured on a beetle cuticle (exoskeleton). Mueller matrices can also be used in regression analysis to model nanostructures in cuticles. Here we present the use of sum decomposition of Mueller matrices from these depolarizing biological reflectors to explore the fundamental character of these reflectors. The objective is to decompose a Mueller matrix into well-defined ideal non-depolarizing matrices corresponding to mirrors, circular polarizers, halfwave retarders etc. Generally it is possible to decompose a measured depolarizing Mueller matrix M into four (or fewer) non-depolarizing matrices according to $M = \alpha M_1 + \beta M_2 + \gamma M_3 + \delta M_4$, where α, β, γ and δ are eigenvalues of the covariance matrix of M . Two strategies for decomposition will be discussed. A Cloude decomposition will provide the eigenvalues and also the M_i 's although the latter will contain severe noise in some spectral regions. However, a major advantage with the Cloude decomposition is that the number of nonzero eigenvalues is directly obtained, i.e. the number of contributing M_i matrices. In an alternative decomposition, the M_i 's are assumed and the eigenvalues are found by regression analysis based on M . In the case with two non-zero eigenvalues we define a model Mueller matrix $M_D = \alpha_R M_1 + \beta_R M_2$ with $\alpha_R + \beta_R = 1$. With α_R as adjustable parameter, the Frobenius norm $\|M - M_D\|$ is minimized for each wavelength in the spectral range of M . For more complex structures, the

regression can be extended by adding more matrices up to a total of four. Advantages with a regression approach are its simplicity and stability compared to a Cloude decomposition. The Mueller-matrix spectra of beetle cuticles are recorded with a dual rotating compensator ellipsometer in the spectral range 400 – 900 nm at angles of incidence in the range 20 - 75°. The application of decomposition on biological reflectors is demonstrated on M measured on the beetle *Cetonia aurata*, which represents a narrow-band chiral Bragg reflector with two non-zero eigenvalues. A decomposition in an ideal mirror and a circular polarizer is feasible. In another example, the broad-band and gold-colored beetle *Chrysis argenteola*, we show that more than two eigenvalues can be nonzero, especially at oblique incidence, and additional matrices are involved.

9:20am EL+AS+BI+EM+SS-FrM4 **Polymer- and Ceramic-Supported Hybrid Gas Separation Membranes Characterized by Ellipsometry**, *Ioannis A. Merigos, H. Verweij*, The Ohio State University

Membrane structures consist of thin continuous layers deposited on porous ceramic or polymer supports. We have been developing inorganic and hybrid membranes for various applications that include gas separation (e.g. post-combustion CO₂ capture), water purification, Solid Oxide Fuel Cells (SOFC) and sensors. Spectroscopic Ellipsometry (SE) is a major non-destructive characterization tool, which can be used to obtain the thickness (typical range 50 nm...2 μm) and complex refractive index (n,k) of the supported membrane layers. This information, in turn, is used to obtain information about membrane composition, porosity and gas or water sorption. The characterization of fully-ceramic structures on optically smooth porous α-alumina surfaces (roughness ~25 nm, higher than most typical SE applications) has been employed by our group for several years. Recently we have expanded the use of SE to characterization of multi-layered membranes, and of inorganic or polymer layers on polymer supports, on coarser α alumina surfaces, and on ceramic tubes. Examples are γ- and α-alumina on polyethersulfone (PES) and poly-sulfone (PES), Ce_{0.9}Gd_{0.9}O_{1.95} on tubular α-alumina, and successive layers of amorphous microporous silica and polydimethylsiloxane (PDMS) on mesoporous intermediate layers. We have achieved signal detection and interpretation to acquire meaningful results, even in multi-layered structures and in cases with substantial interfacial of surface roughness, or curvature. Overall, the application of SE, including non-destructive characterization at intermediate stages between deposition and processing steps, can significantly facilitate the design of gas separation membrane structures that combine organic and polymer layers.

9:40am EL+AS+BI+EM+SS-FrM5 **Spectroscopic Ellipsometry Methodology for Analysis of Thin Films with Significant Surface Non-idealities: Combining Through-the-Substrate and Film-Side Measurements**, *Jian Li*, University of Toledo, *L. Mansfield*, National Renewable Energy Laboratory, *P. Pradhan*, University of Toledo, *H. Du, S. Glenn, J. Mann, A. Norman, K. Ramanathan*, National Renewable Energy Laboratory, *R.W. Collins*, University of Toledo, *G. Teeter, D. Levi*, National Renewable Energy Laboratory

Spectroscopic ellipsometry (SE) is a powerful tool for studying thin films, including the thickness and dielectric function, the latter being closely related to important properties such as composition, phase, grain size, porosity, and stress. The sub-nanometer sensitivity of SE is best exploited if all interfaces between layers, at substrate/layer and layer/ambient are abrupt and smooth. Even for the simple structure of substrate/film/ambient, however, whereby the film is fabricated in a uniform process, surface non-idealities including roughness, oxides, compositional variations, or a combination of these, are inevitable. If an accurate film dielectric function is of interest, then the widely-used effective medium approximation (EMA) treatment of the surface roughness can distort the result, especially in photon energy range of strong absorption.

In this work, an improved SE methodology has been developed, tested, and applied to study thin films with significant surface non-idealities. The investigated materials include Cu(InGa)Se₂, Zn(O,S), Cu₂ZnSnS₄, and Cu₂SnS₃ deposited on transparent substrates by co-evaporation, sputtering, or chemical bath deposition. The film thicknesses in this study range from ~20 to 4000 nm, with potential applicability of the methodology over an even wider range. The key component of the SE methodology is integration of through-the-substrate (TS) SE with standard film-side (FS) SE. The following successes have been demonstrated.

(1) When the surface non-ideality is predominantly roughness within the EMA applicability, two-side (FS+TS) SE can minimize dielectric function distortion caused by the EMA assumptions.

(2) When the surface non-ideality is outside the EMA applicability and traditional SE methodology becomes unreliable, accurate results can be obtained using the FS+TS SE methodology, in which the dielectric functions of the surface and bulk layers can be allowed to vary wavelength

by wavelength independently. Most thin films of this study fall into this category.

(3) When the surface is macroscopically rough and scatters light, films can be grown intentionally thick and hence rough enough to suppress specular reflection from the surface. In this case, through-the-substrate SE alone can be used to extract the bulk film dielectric function.

An important criterion for evaluating SE analysis on semiconductor films is that the ϵ_2 spectrum should be flat and essentially zero below the band gap. It is demonstrated that the dielectric functions obtained through the above SE methodology either satisfy or better satisfy this criterion compared to previous studies. The limitations of the SE methodology will also be discussed.

10:00am **EL+AS+BI+EM+SS-FrM6 A Classical Model for Depolarization through Incoherent Superposition of Dipoles Driven by Evanescent Fields, Kurt Hingerl**, University Linz, Austria

A finite spectral resolution and/or an imperfectly collimated beam /and or an (areal) extended light source / and or an (areal) extended detector and/ or a sample with a varying thickness can produce depolarization effects. However, despite these experimental findings, there are to our knowledge no physical models published which trace the origin of depolarization back to the atomic properties. Therefore, we explain depolarization by the following steps:

1) A mathematical model for cross-polarization: In structured samples the Fresnel reflectances are not correct any more, they rely on homogeneity (i.e. an arbitrary shift of the sample along any surface direction). Mathematicians are aware of this and the numerical tools developed by them, e.g. finite element methods (FEM) or rigorous coupled wave analysis (RCWA), take these effects into account, when matching boundary conditions. Mathematically the Jones matrix then possesses nondiagonal elements. This cross polarization signifies the presence of a totally polarized photon state, but takes into account that p-polarized incoming light creates s-polarized outgoing and vice versa.

2) Cross-polarization then has to take into account radiating dipoles, whose radiation create the scattered cross (and later, after incoherent superposition, partially de-) polarized field. In any structured sample there are inner boundaries present and it is straightforward to show that the usual boundary conditions on the continuity of the tangential electric field and the normal of the displacement field yield inherent contradictions at these inner boundaries. In order to fulfill the boundary conditions, close to the inner boundaries **evanescent fields** must be present, which drive the atomic dipoles in **other spatial directions than the incoming field**.

3) Depolarization: The end point of the field of unpolarized light may be assumed to move quite irregularly, and the light shows no preferential directional properties when resolved in arbitrary orthogonal directions normal to the direction of propagation. Depolarization is mathematically described by the **correlation** which exists between these two orthogonal directions. Furthermore the extension of the light source, the extension of the detector and **the extension of the illuminated sample area (especially its depth!)** are reducing the value above. The measured intensity at the detector is obtained by the **incoherent superposition** of the single waves. The mathematical formulation is given by the Cittert-Zernike theorem (M. Born & E. Wolf, *Principles of Optics*, chapter X.9).

10:40am **EL+AS+BI+EM+SS-FrM8 The Development Of Highly-Oriented 3D Nanostructures For Use With Ultra-Thin Layer Chromatography And Ellipsometry, Erika Pfaunmiller**, University of Nebraska Lincoln, D. Peev, D. Sekora, University of Nebraska-Lincoln, S. Beeram, University of Nebraska Lincoln, C. Rice, M. Schubert, T. Hofmann, D. Hage, University of Nebraska-Lincoln

Slanted columnar thin films based upon SiO₂ were deposited on glass substrates through the use of glancing angle deposition (GLAD). The typical length of these structures was between 500 nm and 2.5 μ m. These thin films were then evaluated for use in ultra-thin layer chromatography (UTLC), which is a special type of thin layer chromatography (TLC) that uses supports that incorporate nanomaterials. In this work, a series of lipophilic dyes were analyzed through the use of both TLC and UTLC followed by detection through imaging ellipsometry. It has previously been demonstrated that changes in birefringence is seen as small organic molecules attach to some of the types of nanostructures that were used in this study. The principle behind the detection of organic chemicals that attach/adsorb onto such nanostructures is based on the variation of the optical anisotropy of highly-ordered 3D nanostructures with attached or adsorbed molecules. This causes screening of the dielectric displacement charges that are produced by the incident electromagnetic fields within the nanostructures, which can be measured as a variation of the effective birefringence of the highly-ordered 3D nanostructures. Measurement of this birefringence was done through generalized imaging ellipsometry. This combined imaging and separation approach should be useful for label-free

detection in UTLC and for the chromatographic analysis of a various target compounds.

Electronic Materials and Processing Room: 311 - Session EM+EN-FrM

Nitrides for LED and PV Device Applications

Moderator: Nikolaus Dietz, Georgia State University

9:00am **EM+EN-FrM3 The Capricious Effect of Heating on the Surface Photovoltage in Si-doped GaN, Joy McNamara, K.L. Phumisthikul, A.A. Baski, M.A. Reshchikov**, Virginia Commonwealth University

Surface photovoltage (SPV) studies on gallium nitride (GaN) thin films have recently revealed much information, including the band bending at the surface, the effect of polarity on the surface potential, the role of the surface oxide layer, and many other surface related behaviors. By using the Kelvin probe method, the surface potential of GaN can be measured in respect to a vibrating metal probe. To investigate the SPV behavior of both n- and p-type GaN, several experimental conditions have been varied, such as ambient or temperature. It is expected from a thermionic model that the surface band bending decreases immediately under ultraviolet (UV) illumination with the intensity used in these measurements. This results in the production of an immediate increase in the SPV signal as measured by the Kelvin probe. In recent studies on GaN thin films grown by metal organic chemical vapor deposition (MOCVD) and doped with silicon (concentration of $\sim 10^{19}$ cm⁻³), we observed an effect of heating on the transient SPV behavior due to the history of sample preparation. For the first group of samples, a very fast rise of the SPV signal by 0.7 eV was observed at room temperature under UV illumination in vacuum, after the samples were initially exposed to air. However, after heating these samples to 600 K in vacuum before taking measurements at room temperature, the fast SPV component decreased to 0.2 eV, while a slow, logarithmic-in-time increase was observed for longer times of UV exposure, with a maximum SPV signal of only 0.4 eV after 30 min. For the second group of samples, the heating in vacuum caused the magnitude of the initial fast SPV in vacuum to be much smaller (0.7 eV after air exposure and 0.3 eV after heating), but without a slow, logarithmic-in-time increase. The SPV behavior could be reversed by UV illumination in air at room temperature. Interestingly, similar SPV behavior has also been observed in ZnO films. The reversible heating effect is preliminarily explained by assuming that the presence of an oxide layer either inhibits or allows the transfer of UV-induced charge carriers between the bulk and surface states, depending on the conditions of the measurement.

9:20am **EM+EN-FrM4 Atomic Layer Deposition of III-Nitride Alloys using Hollow-Cathode Plasma Source for Post-CMOS Processing and 3D Integration, C. Ozgit-Akgun, A. Haider, AliKemel Okyay, N. Biyikli**, Bilkent University, Turkey

Plasma-assisted atomic layer deposition (PA-ALD) is a cyclic, low-temperature thin film deposition method, in which the substrate surface is exposed to sequential pulses of precursor molecules and plasma species separated by evacuation and/or purging periods. When compared to other techniques, ALD stands out with its self-limiting growth mechanism, which enables the deposition of highly uniform and conformal thin films with sub-nanometer thickness control. These features make PA-ALD a promising and alternative technique for the low-temperature deposition of III-nitrides and their alloys in post-CMOS processing and 3D integration technology.

In our previous reports on the PA-ALD of polycrystalline wurtzite AlN thin films at temperatures ranging from 100-500 °C using trimethylaluminum as the Al precursor, films deposited at temperatures within the ALD window (100-200 °C for both NH₃ and N₂/H₂ processes) were C-free and had relatively low O concentrations (<3 at.%). Our initial efforts for depositing GaN thin films, however, resulted in amorphous thin films with high O concentrations (~20 at.%). Following experiments revealed the source of this O contamination as the quartz tube of the inductively coupled RF-plasma source itself. In view of these circumstances, the choice of N-containing plasma gas (N₂, N₂/H₂ or NH₃) determined the severity of O incorporation into the deposited AlN and GaN thin films. As an effort to completely avoid this contamination problem, we integrated a stainless steel hollow-cathode plasma (HCP) source to the ALD system, and thereby reported on hollow cathode PA-ALD (HCPA-ALD) of nanocrystalline AlN and GaN thin films with low impurity concentrations at 200 °C using trimethylmetal precursors. Within the scope of the same study, Al_xGa_{1-x}N thin films were also deposited via digital alloying, where alloy composition was determined by the relative number of AlN and GaN subcycles in the main HCPA-ALD cycle.

In this presentation, we will review our recent efforts on the development of low-temperature HCPA-ALD processes for III-nitride alloys including GaN, InN, $\text{In}_x\text{Ga}_{1-x}\text{N}$, and $\text{In}_x\text{Al}_{1-x}\text{N}$ thin films. In-detail materials characterization results including structural, optical and electrical properties as well as potential device architectures for post-CMOS processing and 3D integration will be presented and discussed.

9:40am **EM+EN-FrM5 Development of Nitride Nanorod Light-emitting Diode Array**, C.G. Tu, C.H. Liao, Y.F. Yao, C.Y. Su, H.S. Chen, W.H. Chen, C. Hsieh, H.T. Chen, Y.W. Kiang, **Chih-Chung Yang**, National Taiwan University, Taiwan, Republic of China **INVITED**

With the nano-imprint lithography and the pulsed growth mode of metalorganic chemical vapor deposition, a regularly-patterned, c-axis nitride nanorod (NR) light-emitting diode (LED) array of uniform geometry with m-plane core-shell InGaN/GaN quantum wells (QWs) is formed. To grow an NR with uniform cross-sectional size, in the pulsed growth mode, the sources of groups III and V are switched on and off alternatively with fixed supply durations. By growing a p-i-n core-shell structure, an InGaN/GaN QW NR LED array can be fabricated by depositing a conformal layer of GaZnO on the NRs for serving as the transparent conductor. The electrical property of such an LED array is comparable with that of a conventional planar LED. Besides, by varying the supply duration of group III source (TMGa) in the pulsed growth process, the NR cross section can be tapered for growing another section of NR of a different cross-sectional size. Based on this growth technique, a multiple-section GaN NR of changing cross-sectional size can be obtained. When InGaN/GaN QWs are deposited on the sidewalls of the NR, the indium contents and QW thicknesses are different in different sections of different cross-sectional sizes due to different strain relaxation conditions. In this situation, the emission wavelengths of the QWs from different sections are different, leading to the multiple-color emission of such an NR array. Such an emission behavior can be used for fabricating a phosphor-free white-light LED.

10:40am **EM+EN-FrM8 Trends in Production Scale MOCVD Equipment for Nitride Semiconductors**, Alexander Gurary, Veeco Instruments, Inc. **INVITED**

Metalorganic Chemical Vapor Deposition (MOCVD) is a technology of choice for large scale production of GaN based LED and Power Electronic devices. For the last 20 years MOCVD equipment evolved from small R&D oriented deposition systems (three 50 mm wafers per run) to large industrial cluster type systems (two hundred sixteen 50 mm wafers per run) with very sophisticated in-situ devices and process control. Evolution of the production scale MOCVD equipment is driven by one major goal – Cost of Ownership (CoO) reduction. Industry is achieving this goal utilizing several trends:

Migration from R&D to production requirements. GaN MOCVD systems started as an R&D tool. Further development of these systems is the path from universality and flexibility typical for R&D tools to stability and simplicity required for production environment.

Increasing batch size. This is the most obvious way to improve CoO as the cost to manufacture system with two times more wafers per run is less than the factor of two. All major MOCVD equipment companies follow this trend and release new larger batch systems every 3-5 years. One of the most important questions for scaling up is the limit of this trend.

Move from the single reactor system to the cluster and increase level of automation. Majority of modern MOCVD systems migrated from the single reactor to the cluster type multi-reactor design with central loading module and wafer carrier transfer robot.

Increasing role of the in-situ devices for wafer parameters measurement and control. Evolution of in-situ devices for production system includes the following sequence: thermocouple - conventional pyrometer – reflectometer - emissivity compensated pyrometer - deflectometer (wafer bow measurements). There is also a trend for more sophisticated control methods that move from PID to predictive and model based algorithms.

Increased wafer carrier complexity. The wafer carrier is a unique component of MOCVD system that to a large degree defines system yield. Complexity of the wafer carriers is constantly increasing with the goal to improve deposition uniformity. Wafer carriers are a subject of majority MOCVD equipment patents.

Increased role of process modeling. Troubleshooting and process optimization in production environment exclude “trial and error” approach and require good computational models for flow dynamic and process chemistry that are fine-tuned based on experimental data.

In this presentation we will describe above trends in detail and make an attempt to predict next steps in the development of the equipment for large scale production of GaN based materials.

11:20am **EM+EN-FrM10 Growth of GaN on Sapphire, Si (111), and Ge/Si (111) using a Pulsed Electron Beam Deposition (PED) Process**, Nazmul Arefin, University of Oklahoma, M.H. Kane, Texas A&M University, K. Hossain, Amethyst Research Inc, B.N. Pritchett, Oklahoma Geological Survey, M.B. Johnson, P.J. McCann, University of Oklahoma

This presentation will describe results recently obtained with pulsed electron beam deposition (PED) of GaN on sapphire, silicon (111), and 2 nm germanium coated silicon (111) substrates. The PED technique is potentially useful for growth of III-nitrides at lower substrate temperatures, a capability that can allow use of new buffer layer materials, introduction of chemically dissimilar lattice-matched materials, and help solve wafer bowing and cracking problems during growth. The introduction of this technique could lead to improvements in device quality and fabrication of vertical LED structures. In this study, GaN was deposited on sapphire at a substrate temperature of 750°C, and on silicon (111) and Ge/Si (111) at 600°C in a UHP N_2 (15 mTorr) environment (without any surface pre-treatment such as pre-nitridation). A high power electron gun pulse (Neocera, Inc) was used to ablate the GaN target (1” dia. x 0.250” thick, 99.99% pure) stationed at 5 cm vertical distance from the substrate. The electron pulses were generated at 15KV, 0.3 J/pulse at 1 Hz for initial few nm of growth, and then increase to a 3 Hz pulse rate. Scanning Electron Microscopy (SEM), X-ray Diffraction (XRD), Rutherford backscattering, and optical absorption characterization were performed. SEM imaging confirms a rough surface morphology with the presence of 30 nm to 300 nm scaled GaN crystallites (for the GaN/Sapphire sample) while smaller but more coalesced crystallites of 30-50 nm size is observed for GaN/Si (111) and GaN/Ge/Si (111) samples. The average film thickness is 350 nm for the samples, yielding a growth rate of 0.16 angstrom/pulse. From SEM, it appeared that high aspect ratio filament structures have grown over the crystallites. XRD θ - 2θ scans from $2\theta = 0^\circ$ to $2\theta = 70^\circ$ on the GaN on sapphire showed only two other peaks, besides the peaks from the sapphire, near $2\theta = 34.6^\circ$. The peaks near $2\theta = 34.6^\circ$ consist of a stronger peak at 34.668° and a much weaker peak at 36.903° . These peaks correspond to the (0002) and (10-11) orientations for GaN, respectively. XRD θ - 2θ scans from $2\theta = 0^\circ$ to $2\theta = 70^\circ$ on the GaN on Si (111) and GaN on Ge/Si (111) samples show presence of only polar GaN (0002) peak at 34.7° besides the Si (111) peak at $2\theta = 28.5^\circ$. The XRD results clearly show that the deposited GaN material is not polycrystalline. Optical absorption spectroscopy over a 1.2 eV to 6.2 eV spectral range, for the GaN/Sapphire sample, showed an abrupt absorption edge at 3.4 eV, a clear indication of interband transitions in binary GaN. These results confirm that our PED-grown GaN is highly c-axis oriented and suitable for the initial growth of GaN on various substrate materials.

11:40am **EM+EN-FrM11 Growth Template Impact on the Properties of InN Epilayers Grown by High-Pressure CVD**, Sampath Gamage, M.K.I. Senevirathna, Georgia State University, H. Babar, I.T. Ferguson, University of North Carolina at Charlotte, R. Collazo, North Carolina State University, N. Dietz, Georgia State University

The unique optical and electrical properties of InN and related ternary InGaN alloys make the material system attractive for various optoelectronic device applications, including but not limited to high-speed electronics, photovoltaic solar cells, or light emitting devices. Even though progress has been made in establishing the base properties of the binaries InN and GaN, the growth of high-quality InN and indium-rich ternary InGaN epilayers and heterostructures is an open challenge. In previous work, we demonstrated the stabilization of InN and InGaN epilayers utilizing superatmospheric MOCVD (also denoted as HPCVD) to suppress the decomposition at higher growth temperatures.

In this contribution, we explored the influence of the growth templates (e.g. sapphire substrates, micrometer-scale patterned AlN/sapphire templates, and/or patterned GaN/AlN/sapphire) on the properties of bulk InN epilayers, keeping the reactor pressure constant at 8bar (15bar) as well as the III/V precursor ratio. The growth temperature was optimized in the range of 800°C to 900°C based on Raman $E_2(\text{high})$ mode evolution. The various templates are assumed to introduce different strain fields during the initial nucleation process, affecting the extended defect generation and propagation processes. To assess this effect on the bulk properties of thick InN epilayers, Raman spectroscopy [e.g. $E_2(\text{high})$ and $A_1(\text{LO})$ mode analysis], XRD rocking and ω - 2θ scans and photoluminescence (PL) spectroscopy were performed to analyze the crystallinity as well as the extended defect and point defect densities in these layers. The free carrier concentrations in these epilayers and the mobility was determined by FTIR spectra analysis as well as Raman $A_1(\text{LO})$ fitting.

Electronic Materials and Processing Room: 314 - Session EM+NS+TF-FrM

Transparent Electronics

Moderator: Lisa M. Porter, Carnegie Mellon University

9:00am EM+NS+TF-FrM3 Transparent Amorphous Oxide Semiconductors: Interfacial Chemistries and New Applications, Gregory Herman, Oregon State University INVITED

During the past decade research in the area of transparent amorphous oxide semiconductors (TAOS) has increased substantially due to the ability to fabricate thin film transistors (TFT) at relatively low processing temperatures while still maintaining large electron mobilities. The primary applications for these materials include active matrix displays with the possibility for integration onto flexible polymeric substrates. More recently potential applications have expanded to include non-volatile memory, sensing, and memristive neurological networks. We have studied amorphous zinc tin oxide (ZTO) and indium gallium zinc oxide (IGZO) that have been deposited by both vacuum and solution based approaches. The electrical characteristics of the films have been evaluated in both TFT and metal-insulator-metal memristive devices. Excellent device characteristics have been obtained, however we have found that surface impurities can strongly affect device stabilities. We have found that the chemistry of adsorbed species on the back-channel strongly influences the bias stress stabilities of ZTO and IGZO TFTs, while reactions at the Al/ZTO interface leads to the resistive switching characteristics of memristors, and post annealing leads to interfacial reactions and modifies the Schottky barrier for Pt/IGZO diode structures. To better understand the role of interfacial reactions on TFT and memristive devices we have developed methods to prepare clean well defined surfaces for ZTO and IGZO, and further characterized these surface and interface properties with X-ray photoelectron spectroscopy and secondary ion mass spectrometry.

9:40am EM+NS+TF-FrM5 HMDSO/O₂-Plasma-Deposited Organic-Inorganic-Hybrid Materials as Gate Dielectrics for MgZnO Thin Film Transistors and Encapsulation Layers for Solar Cells, Y.S. Li, C.H. Tsai, I.C. Cheng, Jian-Zhang Chen, National Taiwan University, Taiwan, Republic of China

Organic-inorganic hybrid materials can be deposited from hexamethyldisiloxane (HMDSO) diluted with oxidants using plasmas technology. The properties of the deposited material can be controlled by varying the dilution ratio of the oxidants. The chemical compositions can vary from polymer-like (organic-like) to SiO₂-like (inorganic-like) depending on the oxidant dilution ratio and the process power. In this paper, we report two applications of HMDSO/O₂-plasma-deposited organic-inorganic-hybrid materials developed in our group: (1) as gate dielectrics of MgZnO TFTs, and (2) as the encapsulation layers for organic-inorganic hybrid solar cells.

The inorganic/organic component ratios in hybrid films were tailored by varying the process power and the O₂/HMDSO flow rate ratio. The FTIR analysis and contact angle measurement show that higher deposition power and/or larger O₂/HMDSO flow rate ratio result in more SiO₂-like films. For rf-sputtered MgZnO TFTs, a more organic-like film affords a better interface to the MgZnO active layer and higher dielectric constant, leading to a smaller threshold voltage and a steeper subthreshold slope; while an inorganic-like film has lower leakage currents, resulting in a larger on/off current ratio in the transistors. The TFT with an organic-inorganic-hybrid gate dielectric deposited at an O₂/HMDSO ratio of 40 and process power of 30 W exhibits a threshold voltage of 6.8 V, a subthreshold slope of 0.48 V/dec, an on/off current ratio of >10⁷ and a linear mobility of ~60 cm²V⁻¹s⁻¹, respectively. We also have demonstrated that this O₂/HMDSO-plasma-deposited organic-inorganic material can be used as an efficient single-layer encapsulation technique for organic photovoltaic cells. Calcium test was used to evaluate the water vapor transmission rate (WVTR) of the barrier film deposited on a polyimide foil. A water vapor transmission rate of 3.6×10⁻⁶ g/m²-day was obtained for a 1.5 um-thick single permeation layer. Inverted type organic photovoltaic passivated by the hybrid material was used to evaluate the effectiveness of this encapsulation. Efficiency decay was not observed in the cell coated with this encapsulation layer after 3000-hour exposure to the air; on the contrary, the un-encapsulated counterpart cell degraded rapidly and completely failed after 120-hour exposure to the air. The result shows that this single-layer hybrid material encapsulation can enhance the stability of organic photovoltaic cell. The cell life time is greatly improved.

10:00am EM+NS+TF-FrM6 Solution Processed Oxide Semiconductor and Dielectric Thin Films: Towards High Performance, Low Temperature ZnO Field-effect Transistors with Low Operation Voltage, Yu Liu, H. Katz, Johns Hopkins University

Solution processing is a preferred method for manufacturing large-area low-cost electronic devices. High performance metal oxide semiconductor-based field-effect transistors can be fabricated in this manner. For applications of flexible electronics, a low processing temperature is required to avoid overheating of the substrate material. It is a challenge to fabricate a dense impurity-free oxide semiconductor film at low temperature. A water-based ZnO precursor with ammine-hydroxo complex was introduced to decrease the processing temperature. However, repeated time-consuming centrifugation and decantation steps are required in this process.

To simplify the processing steps we discovered a new strategy to prepare aqueous ZnO precursor. Based on this precursor, ZnO FETs with a benchmark dielectric SiO₂ have been fabricated at 200 °C. The transistors exhibited promising performance with a saturation field-effect mobility of 0.7 cm²·V⁻¹·s⁻¹ and a typical on/off current ratio on the order of 10⁴. To prepare the precursor, zinc nitrate hexahydrate and acetylacetone were dissolved in ammonium hydroxide with a concentration of 0.6 M. As prepared precursor was then filtered and dilute it with DI water. A similar strategy was applied in the preparation of aqueous zinc tin oxide precursor with tin fluoride as tin source.

Based on a redox chemical reaction between fuel and highly exothermic oxidizer, a combustion processing method has been found to be promising for decreasing the annealing temperature of oxide semiconductor thin films. In this study, combustion processing strategy was used in preparing high capacitance ion-incorporated alumina dielectrics at 200 °C by using urea as the fuel and aluminum nitrate nonahydrate as oxidizer.

Both zinc tin oxide and sodium-incorporated alumina low temperature precursors showed strong exothermic reaction peaks at temperatures lower than 200 °C. This suggests a conversion from ammine-hydroxo/combustion precursor to solid zinc tin oxide/sodium incorporated alumina thin films at a temperature lower than 200 °C. A sharp (002) peak is shown in the XRD pattern of 200 °C processed ZnO thin film, which demonstrates a wurtzite crystal structure.

The high-k dielectrics exhibited a good compatibility with our low temperature ZnO precursor and excellent transistor performance has been achieved in these devices. With this, we are able to fabricate low temperature low voltage transistors on plastic substrates such as polyimide. This low temperature ZnO precursor could also be applied to fabricate flexible inverters in combination with p-type solution processed polymer semiconductors, such as PBTTT and TIPS-pentacene.

10:40am EM+NS+TF-FrM8 Metal Oxide Conductors and Semiconductors: From Materials to Device Applications, Elvira Fortunato, R. Martins, FCT-UNL and CEMOP-UNINOVA, Portugal INVITED

Transparent electronics has arrived and is contributing for generating a free real state electronics that is able to add new electronic functionalities onto surfaces, which currently are not used in this manner and where silicon cannot contribute [1,2]. The already high performance developed n- and p-type TFTs have been processed by physical vapour deposition (PVD) techniques like rf magnetron sputtering at room temperature which is already compatible with the use of low cost and flexible substrates (polymers, cellulose paper, among others). Besides that a tremendous development is coming through solution-based technologies very exciting for ink-jet printing, where the theoretical limitations are becoming practical evidences. In this presentation we will review some of the most promising new technologies for n- and p-type thin film transistors based on oxide semiconductors and its currently and future applications.

[1] E. Fortunato, P. Barquinha, and R. Martins, "Oxide Semiconductor Thin-Film Transistors: A Review of Recent Advances," *Advanced Materials*, vol. 24, pp. 2945-2986, Jun 2012.

[2] P. Barquinha, R. Martins, L. Pereira and E. Fortunato, *Transparent Oxide Electronics: From Materials to Devices*. West Sussex: Wiley & Sons (March 2012). ISBN 9780470683736.

11:20am EM+NS+TF-FrM10 Influence of Oxygen Diffusion in Transparent In_{0.9}Sn_{0.1}O_x Film on Effective Work Function Change, Toshihide Nabatame, NIMS, Japan, H. Yamada, Shibaura Institute of Technology, Japan, A. Ohi, NIMS, Japan, T. Oishi, Shibaura Institute of Technology, Japan, T. Chikyo, NIMS, Japan

The In_{0.9}Sn_{0.1}O_x (ITO) films is widely used as transparent electrodes in optical and optoelectronic devices. The work function (WF) of the ITO film was generally evaluated by optical measurements such as ultraviolet photoemission spectroscopy and Kelvin probe. However, the optically measured WF differs from the effective work function (EWF) estimated by

electrical measurement. The influence of oxygen diffusion in ITO film on EWF change has not been also understood. In this paper, we systematically investigate EWF change of ITO film by oxidation and reduction annealing. We also examine oxygen diffusion coefficient (D) of ITO film, using isotope ^{18}O tracer, to discuss influence of oxygen diffusion of ITO film on EWF change.

The ITO films were prepared under an Ar/O_2 by sputtering using an $\text{In}_{0.9}\text{Sn}_{0.1}\text{O}_x$ target. The ITO-gated metal-oxide-semiconductor (MOS) capacitors with HfO_2 and SiO_2 gate insulators were fabricated to estimate EWF value of ITO film. The ITO (150 nm)/ SiO_2 /Si films were annealed at 300 – 500 °C for 30 min under 10^4 Pa of ^{18}O isotope (99%) gas to obtain D value.

The resistivity of ITO film, which consists of cubic structure, shows an almost same value regardless of oxidation and reduction annealing temperatures. The EWF of ITO-gated MOS capacitors significantly changes from 4.4 to 5.2 eV as the oxidation annealing temperature increases from 250 to 350 °C. The EWF change is saturated at 350 °C. On the other hand, the EWF value decreases in reduction annealing temperature ranging from 200 to 350 °C. This must be due to oxygen introduction and removal in ITO film during oxidation and reduction annealing, respectively. To understand the mechanism of oxygen transfer in the ITO film, we examine D behavior of ITO film. The ITO film has a large D value of about a $1.1 \times 10^{-20} \text{cm}^2/\text{s}$ at 300 °C and a small activation energy (Ea) of about 1.4 eV. We found that the D and Ea values are similar to those of grain boundary in monoclinic ZrO_2 . This results indicate that oxygen diffusion of ITO film occurs even at low temperature of 300 °C and affects to the EWF change during oxidation and reduction annealing at around 300 °C.

11:40am **EM+NS+TF-FrM11 Transparent Conducting Films from Ultraporous Aerogels of Single-Walled Carbon Nanotubes / PEDOT:PSS Composites**, *Xi Liu, L.M. Porter, M.F. Islam*, Carnegie Mellon University

In this study we report on the fabrication and characterization of ultralight (>99% porosity) aerogels based on single-walled carbon nanotubes (SWCNTs) and poly(ethylene dioxythiophene) : poly(styrene sulfonate) (PEDOT:PSS), that are electrically conducting and highly stretchable. The aerogels were created by critical-point drying of aqueous elastic co-gels of individually dispersed SWCNTs mixed with PEDOT:PSS to yield either free-standing films or thin films supported on flexible (PET) or glass substrates; the nanotubes substantially reduce the percolation threshold of PEDOT:PSS. These transparent conductors with sheet resistance of 35 ohm/sq and 60% transparency (at 550 nm) also proved to be highly flexible – they can be repeatedly stretched to 20% with < 1% change in resistivity. The electrical, optical, mechanical, and microstructural properties of these materials will be presented, along with their application in devices.

Plasma Science and Technology Room: 305 - Session PS1-FrM

Plasma Sources

Moderator: Steven Vitale, MIT Lincoln Laboratory

8:20am **PS1-FrM1 Small High Density Plasma Sources for Focussed Ion Beam Applications**, *Rod Boswell*, Australian National University, Australia **INVITED**

Oregon Physics has developed the HyperionTM system of high brightness plasma ion sources which are now being used on Focused Ion Beams and TOF-SIMS around the world. These plasma sources are ten times brighter than present sources and reduce the time necessary for analysis from days to hours. They are also more reliable and can be focused down to smaller spots. The development of these sources, especially the optimization of the rf antenna design and extraction geometry will be described. Extraction of positive ions is used for reverse engineering on the nano-metre scale and negative ions are used for Time of Flight Secondary Ion Mass Spectroscopy (TOFSIMS).

SIMS uses beam of primary ions (typically O-) focused onto a target. Sputtered secondary ions are measured by mass spectrometer which can detect elements and their isotopes in the low parts per billion (10⁻⁹ or ng/g) range. Particles as small as a few 100 nanometres can be analysed.

Time of Flight (TOF)SIMS measures the time of arrival of the secondary ions at the detector, which depends on their mass yielding an extremely good high mass resolution. It can detect: cocaine in urine, benzodiazepines (eg. valium) in hair and gunshot residues in fingerprints even after strenuous washing! Additionally, TOF-SIMS can simultaneously detect cocaine in the presence of other drugs (i.e. flurazepam (a benzodiazepine hypnotic) and chlorpromazine (used for psychosis and heroin withdrawal)

in urine. It is possible to relate the TOF-SIMS fingerprints to the evidence found at the crime scene, which can be considered as examination of forensic evidence transfer. Elemental composition of anthrax spores using TOF-SIMS has been carried out by Weber et. al. at LLNL. This is of use in assessing the origin of bio-weapons.

9:00am **PS1-FrM3 A Remote Microwave Plasma Source for Reactive Gas Generation**, *Xing Chen, I. Pokidov, K. Wenzel, C.X. Ji*, MKS Instruments, Inc.

A remote microwave plasma source has been developed for generation of activated gases, such as O, H, N and F. The plasma source comprises a dielectric tube surrounded by a conductive coil that serves as microwave antenna and cooling structure. A waveguide is coupled to a microwave cavity to guide the microwave energy into the plasma discharge tube. The electric field of the microwave energy is oriented such that microwave propagates along the conductive coil and deposits energy uniformly in the plasma tube. The plasma discharge tube can be made of quartz, sapphire, aluminum nitride or other dielectric materials to accommodate various gas chemistries. This paper characterizes the plasma source and its operation with O_2 , N_2 , H_2 , H_2O , NH_3 , H_2/N_2 and H_2/He gasses. Experimental measurements of plasma density and atomic gas flux of O, N, and H, using Langmuir probes, recombination probes and calorimetry, are presented. Typical plasma density is on the order of 10^{13}cm^{-3} . The plasma source operates in a broad range of power and gas flow conditions. The use of microwave plasma generation, combined with crystalline plasma tube materials, significantly reduces tube erosion and associated chemical and particle contaminations.

9:20am **PS1-FrM4 Mechanisms for Plasma Density Distribution Control using a Large Diameter Radial Line Slot Antenna Microwave Plasma Source**, *Toshihiko Iwao, T. Hirano, A. Suzuki*, Tokyo Electron Limited, Japan, *P. Ventzek*, Tokyo Electron America, *K. Ishibashi*, Tokyo Electron Limited, Japan

Microwave plasmas are frequently employed for etch, thin film deposition and surface activation for semiconductor or flat panel manufacturing. A major advantage of microwave driven plasma sources operating in the overdense regime or surface wave regime is that the plasmas in the high density source and lower density substrate contacting region may be well separated. This separation is useful for damage free or highly selective plasma process applications. The radial line slot antenna is an efficient microwave applicator for these process applications. Microwaves are radiated from a metal plate with a slot pattern adjacent to the dielectric top window. The electromagnetic field distribution and plasma density are controlled by optimizing the pattern. [1] Uniform plasma processes with the radial line slot antenna source have been demonstrated; however, it is challenging to overcome the tendency of the substrate-contacting plasma to become center-dense in large volume reactors under the action of ambipolar diffusion at low pressure. In this presentation, we present the results of an investigation of the effect of antenna size on the plasma density distribution for a wide gap reactor. A concurrent experimental and simulation study reveal the importance of controlling the transport parameters in the downstream wafer-contacting region to overcome ambipolar diffusion. [2] In particular, we show how the source region plasma generation impacts the electron energy distribution function in the downstream region. Anisotropic features in the electron energy distribution function plays a critical roll in controlling the plasma uniformity which we demonstrate through plasma absorption probe measurements and simulations of plasma structure.

[1] Y.Yasaka, et al., Phys.Plasmas 9, 1029(2002)

[2] J.Yoshikawa, et al., J. Vac. Sci. Technol. A 31, 031306(2013)

9:40am **PS1-FrM5 The NEPTUNE Bipolar Source: A New Instrument for Surface Treatment Applications**, *Dmytro Rafalskyi, A. Aanesland*, LPP, CNRS - Ecole Polytechnique, France

In this work we present a recently patented and developed source of oppositely charged particles called “Neptune”. The source accelerates simultaneously positive ions and electrons extracted from an ICP discharge. The produced broad beam is quasi-neutral with high directionality of all emitted charged particles, and as a result a dedicated neutralizer is redundant in this system. The source can be operated using any kind of working gas, such as Ar, SF_6 , CF_4 etc. The simultaneous ion-electron extraction is realized using the RF self-bias effect in low-pressure plasmas. A double-grid ion optical system is RF-powered ensuring both efficient ion extraction and acceleration, and electron injection. In the extraction system ions are continuously accelerated in the RF sheath between the first (plasma/screen) and second grids, while the electrons are extracted periodically when the sheath collapses. Due to the fact that the extraction system is RF-powered via a capacitor, a DC current cannot flow between the extraction grids, and the total amount of ions and electrons escaping the plasma is the same. The first proof-of-concept of the Neptune source is

demonstrated. First results of the beam measurements are reported, particularly in comparison with a traditional 2-grid ion source equipped with an external neutralizer. We show here that the Neptune source can be efficiently used for low-ARDE processes, as well as for other applications where the accelerated flows with high directionality of both kinds of charged species are required. It is demonstrated that the independent control of the ion flux and energy allows achieving bipolar beams generation in wide range of parameters. It is shown that the proposed ion-electron extraction technique reduces charging effects on the substrate. This work was supported by a Marie Curie International Incoming Fellowships within the 7th European Community Framework (NEPTUNE PIF-GA-2012-326054) and by ANR under grant number ANR-2011-BS09-40.

10:00am **PS1-FrM6 Process Optimization by Phase Control in Multi-Frequency Capacitive RF Plasmas**, *Julian Schulze, E. Schuengel*, West Virginia University, *A. Derzsi, I. Korolov, Z. Donko*, Hungarian Academy of Science, Hungary

An overview of a novel method to control process relevant plasma parameters and particle flux-energy distribution functions in multi-frequency capacitive radio frequency (CCRF) plasmas is presented. Based on experimental, simulation, and modeling studies in different gases (Ar, H₂, SiH₄, CF₄) we demonstrate that the ion flux-energy distribution function at the substrate can be controlled separately from the ion flux by adjusting the harmonics' phases and amplitudes in a CCRF discharge driven by multiple consecutive harmonics based on the Electrical Asymmetry Effect. The quality of this separate control is significantly better compared to classical dual-frequency plasmas driven by two largely different frequencies. Adding more harmonics enlarges the control range. Tuning the ion energy by phase control in H₂-SiH₄ plasmas allows to control the morphology of deposited Si:H thin films. In large area CCRF plasmas radial inhomogeneities of the ion flux due to standing wave effects can be prevented by customizing the driving voltage waveform.

These optimizations of process control are based on a detailed scientific understanding of the non-local particle heating mechanisms in technological plasmas. Such mechanisms are complex and strongly depend on global control parameters such as the gas mixture, pressure, and voltage amplitudes. Differences of the electron heating mechanisms in electropositive and electronegative plasmas and their effects on process control will be discussed. In electronegative and/or dusty plasmas, e.g. operated in CF₄ or SiH₄, a novel heating mode, the Ω -mode, and novel coupling mechanisms between the driving frequencies are present and strongly affect process relevant plasma parameters. Moreover, resonance phenomena such as the Plasma Series Resonance play a major role in multi-frequency CCRF plasmas driven by customized voltage waveforms at low pressures of a few Pa.

Existing processing reactors can be easily upgraded to use the method of phase control in multi-frequency plasmas by modifying the external RF supply only. No modifications of the reactor itself is required, but a detailed understanding of the plasma physics is needed to optimize plasma-surface interactions.

10:40am **PS1-FrM8 Controlling the Flux of Reactive Species in Electron Beam Generated Plasmas**, *Scott Walton, D.R. Boris, E.H. Lock, S.C. Hernandez, Tz.B. Petrova, G.M. Petrov*, Naval Research Laboratory

Electron beam generated plasmas are characterized by high plasma densities ($> 10^9$ cm⁻³) and very low electron temperatures (< 1 eV), making them well-suited for next-generation processing techniques where high fluxes of low energy ions are desirable. In this work, we focus on controlling the flux of reactive species incident to substrates located adjacent to magnetically collimated electron beam generated plasmas. In particular, we discuss strategies for regulating both the type and energy of the ions at the substrate surface. We use a suite of diagnostics including Langmuir and RF impedance probes along with a mass-resolved ion energy analyzer to show how various operating parameters can be changed to control both the bulk plasma properties and the ion flux at the surface. This work is supported by the Naval Research Laboratory Base Program.

11:00am **PS1-FrM9 Ignition Delay in Electronegative Pulsed Dual Source Tandem Plasmas**, *Shyam Sridhar, L. Liu, D.J. Economou, V.M. Donnelly*, University of Houston

Control of the ion energy distribution (IED) is of utmost importance in semiconductor manufacturing. Pulsed plasmas can produce IEDs with small energy spread, necessary to enhance etching selectivity and minimize damage. However, the IED is broadened during the power-on period by capacitive-coupling, imposing an RF potential on the DC plasma potential. This can be eliminated with a Faraday shield but, with electronegative gases, it is not possible to ignite pulsed ICPs, since electron density rapidly decays when power is off, and re-ignition requires large electric fields produced by high-voltage capacitive coupling. Motivated by this problem,

we have explored a "tandem" plasma system, where a continuous (auxiliary) ICP is injected through a grid into a pulsed (main) ICP. Using such a system, an ignition delay was observed in pulsed (period 1 ms) Cl₂ plasmas with a duty ratio (DR) $\sim 60\%$. The ignition delay monotonically increased with DR to reach a maximum of 500 ms at DR $\sim 99\%$. It was also observed that, for a given DR, the ignition delay increased by increasing the main ICP power or by decreasing the auxiliary ICP power. The ignition delay may be attributed to the low electron density in the main ICP, which decays to a value less than the density when the auxiliary ICP were operating alone. At low electron densities, power transfer efficiency is poor. The flux of seed electrons from the auxiliary ICP then acts to restore the electron density, thereby improving the power transfer in the main ICP and allowing plasma re-ignition. Similar results were also observed using other electronegative gases such as SF₆ and CF₄/O₂ mixtures.

11:20am **PS1-FrM10 A Global Model for Ignition Delay of Pulsed Electronegative Plasmas**, *Lei Liu, S. Sridhar, D.J. Economou, V.M. Donnelly*, University of Houston

A Faraday shield can be employed to minimize capacitive coupling in inductively coupled plasmas (ICP), to obtain ion energy distributions with a tight energy spread. However, in the presence of a Faraday shield, it is challenging to operate a pulsed electronegative plasma with a long afterglow duration, as most of the electrons are lost, and re-ignition requires large electric fields produced by high-voltage capacitive coupling. Our experimental studies have shown that by using a dual plasma source, consisting of a main pulsed ICP in tandem with an auxiliary continuous wave ICP, Faraday-shielded pulsed plasmas in electronegative gases can be produced even with long afterglow duration (1000 μ s). However, an ignition delay was observed with duty cycles $>60\%$. A global (spatially averaged) model with chlorine chemistry was developed to describe the mechanism of ignition delay. The flux of charged species from the auxiliary ICP was included in both particle and energy balance equations. Predicted results of ignition delay for different duty cycles, auxiliary ICP powers and main ICP powers agreed with experimental observations. The observed ignition delay increasing with increasing duty cycle is counter-intuitive. One would expect that, as the duty cycle increases, and the afterglow time correspondingly decreases (for constant pulse period), the electron density at the end of the afterglow would be higher, making it easier to re-ignite the plasma, i.e., shorter delay time, in contrast to observation. Once the lower plasma power is off for $> \sim 5\mu$ s it appears that there is a critical electron density in the lower plasma (n_{cr}), equal to or below the electron density when the upper (cw) plasma is operating alone (no power in the lower plasma). When both plasmas are powered, the afterglow of the lower plasma keeps decaying for as long as the electron density is above n_{cr} . This is because the rate of plasma production is then lower than the rate of plasma loss. As soon as the electron density falls below n_{cr} , the rate of plasma production starts exceeding the rate of plasma loss, and the electron density starts increasing, eventually re-igniting the ICP. Now, the higher the duty cycle, the higher the electron density at the end of the afterglow, and the longer it takes for that electron density to decay to n_{cr} , resulting in longer delay times.

11:40am **PS1-FrM11 Ion Energy Distribution Control Using Phase Locked Harmonic Drive**, *A. Zafar*, North Carolina State University, *Y. Zhang*, University of Michigan, *T. Kummerer*, North Carolina State University, *D.H. Clark*, Plasmatherm Inc., *M.J. Kushner*, University of Michigan, *D. Coumou*, MKS Instruments, *Steven Shannon*, North Carolina State University

Dual frequency RF power delivery has demonstrated the capability to increase the operating range of industrial plasmas including independent control of electron density and sheath bias and control of ion energy distribution function (IEDF) width. In this talk, we focus on the later demonstration and present a method for enhanced control of IEDF shape by utilizing a dual frequency drive where harmonic frequencies are employed and the relative phase of these two applied waveforms is controlled. We will show that by controlling both current ratio and phase angle, not only can the width of the distribution be controlled, the higher order moments (specifically distribution skew) can also be controlled, providing distribution functions that are either skewed toward the low energy peak of a typical bimodal RF driven IEDF or skewed toward the high energy peak. Experimental and simulated results will be presented for both dual frequency and three frequency configurations.

Plasma Surface Interactions II

Moderator: Ryan M. Martin, IBM T.J. Watson Research Center

8:20am **PS2-FrM1 Enhancement of Surface Migration by Photoemission-assisted Plasma for Atomic-Scale Surface Smoothing**, A. Saijian, Y. Kotanikawa, Y. Ohtomo, **Shuichi Ogawa**, Y. Takakuwa, Tohoku University, Japan

As a novel tool of plasma ion beam techniques for surface smoothing, we have developed a photoemission-assisted plasma ion source (PAP) [1]. It has been confirmed that the Ar⁺-PAP treatment has an effect to smooth mechanically grinded Al and Cu surfaces with an initial surface roughness (Ra(0)) of a few hundred nanometers [1]. To clarify the surface morphology changes by PAP ion source and understand the PAP ion source-surface interaction, in this study, Cu deposited on Si rare surface (Cu(200 nm)/Si_R) with Ra(0) ~13 nm, has been used for surface smoothing treatments. Plasma parameters have been measured by a cylindrical single Langmuir probe to better understanding the characteristics of the PAP.

In the experimental apparatus of PAP, a Xe excimer lamp with UV light ($\lambda = 172$ nm) was employed, leading to the order of 10^{12} photoelectrons/cm²/s, which enabled us to generate uniformly glow discharge over 2-inch Si wafer at bias voltage V_B of 200 V under Ar atmosphere with pressure of 300 Pa, and to increase a discharge current up to 10^6 - 10^4 A at smaller V_B than 200 V, which is referred to as Townsend plasma. According to the plasma potential measured by Langmuir probe, taking the energy loss due to elastic collisions between Ar⁺ ion and Ar atom into account, we estimated the E_k of Ar ion upon the impingement with the substrate to be 10.7 and 0.79 eV for glow and Townsend discharge, respectively. Based on the estimated values of E_k , a surface flattening model of the dry planarization process is discussed.

When the Cu surfaces irradiated by the photoemission-assisted glow discharge plasma ($E_k = \sim 10.7$ eV), and the photoemission-assisted Townsend discharge ($E_k = \sim 0.79$ eV), the surface roughness was improved down to ~69.8% and ~54.5%, respectively. It indicated that the PAP has the ability to reduce the surface roughness down to atomic-scale under both discharge conditions. It has been reported that diffusion barrier of Cu atom via hopping or exchanging on Cu surface is 0.04 ~ 0.66 eV [2] and the threshold energy of Cu sputtering by Ar⁺ is between 25~50 eV [3]. Therefore the enhancement of surface migration of Cu atoms is mainly responsible for the improvement of Ra in discharge conditions. Conclusively it is considered that the photoemission-assisted plasma works as an ion source with E_k in the order of eV, which sufficiently makes the surface morphology improved due to the enhancement of surface migration.

Reference

- [1] Y. Ohtomo, S. Ogawa, and Y. Takakuwa, *Surf. Interf. Anal.* **44** (2012) 670.
- [2] J. Wang et al., *Modelling Simul. Mater. Sci. Eng.* **12** (2004) 1209.
- [3] J. D. Kress et al., *J. Vac. Sci. Technol. A* **17** (1999) 2819.

8:40am **PS2-FrM2 Silicon Etching using CW, Synchronized Pulsed and Bias Pulsed Cl₂ Plasma**, **Odile Mourey**, G. Cunge, C. Petit-Etienne, M. Darnon, P.D. Brichon, E. Despiiau-Pujo, E. Latu-Romain, O. Joubert, LTM - MINATEC - CEA/LETI, France

The semiconductor industry is more and more challenged by the miniaturization of integrated circuits and the introduction of new devices architectures. Typical high density plasma show limitations in terms of anisotropy, selectivity and ion induced damages to etch stacks of ultrathin layers. New plasma technologies that provide an atomic level control of etching processes are now required and pulsed plasmas are promising candidates. In this work, we compare the performances of typical CW ICP plasma with synchronous pulsed plasma (ICP and bias power pulsed in phase) and bias pulsed plasma (ICP is CW and bias pulsed). In each case we use Cl₂ plasma to etch silicon and several parameters are monitored including etch rate, surface roughness, thickness of SiCl_x reactive layer, ions flux and ions energy. We also investigate the importance of the surface preparation. Using atomic force microscopy, we show that (by contrast with CW plasmas) the surface roughness increases as a function of etching time in pulsed plasmas and that this worsens at small duty cycle. Preliminary results of molecular dynamic simulations suggest that this could be attributed to the modulation of the ion energy in pulsed plasma: in the OFF period radicals can attack the surface defect created by individual ions impacts during the previous ON period.

9:00am **PS2-FrM3 Utilizing Absorption, Emission, and Fluorescence Spectroscopies to Elucidate the Energetics of Plasma-Surface Interactions**, J.M. Blechle, R.B. Davidson, E.J. Sutor, **Ellen Fisher**, Colorado State University

Plasma-enhanced chemical vapor deposition (PECVD), plasma etching, and plasma modification of surfaces are integral to a range of technologies including microelectronics, optical or protective coatings and biomaterials. Many mechanistic details for plasma processing of these materials, however, remain unknown. Understanding surface interactions of plasma species provides critical molecular level information about plasma processing, especially at interfaces. In addition, power dissipation and energetics are also important for elucidation of mechanistic details in plasma-surface interactions. The imaging of radicals interacting with surfaces (IRIS) technique measures interactions of radicals during plasma processing of a variety of materials. This technique combines molecular beam and plasma technologies with laser-induced fluorescence (LIF) to provide information on radical-surface interactions during plasma processing. Furthermore, IRIS provides direct information on the energetics of plasma-generated radicals as well as for species scattering off of surfaces. IRIS data for species in PECVD and etching environments will be presented. We have also employed both time-resolved optical emission spectroscopy (TR-OES) and broadband absorption spectroscopy (BAS) to our plasma systems to further explore the gas-phase chemistry and gas-surface interactions. In particular, IRIS, TR-OES and BAS data on oxygen-containing systems (O atoms, OH radicals), fluorocarbon radicals (CF and CF₂), and nitrogen-containing molecules (NO, NH, NH₂, CN) will be presented by comparing and contrasting these groups of molecules. Correlation of gas-phase data, surface analysis information, and plasma-surface interface reactions will also be presented to provide more comprehensive mechanisms for overall plasma polymerization processes.

9:20am **PS2-FrM4 Transmission of Plasma-Generated Free Radicals through Dielectric Films**, **Faraz Choudhury**, G. Sabat, University of Wisconsin-Madison, Y. Nishi, Stanford University, J.L. Shohet, University of Wisconsin-Madison

During plasma processing, low-k dielectrics are exposed to free radicals from the plasma that may adversely affect the chemical, mechanical and electrical properties of the films. Modern low-k dielectrics have highly porous structures (up to 50%) and interconnected pores provide pathways for reactive species to enter into the material making them more susceptible to damage. Previous work utilized simulations¹ to determine the free-radical density and doses from the processing plasma. Several techniques have been developed and tested over the years for radical measurements², but the methods do not provide a direct measurement of the free radical concentrations at the location of the sample during processing. A new technique, using fluorophore dyes, can detect free radicals in a processing plasma and determine their fluence at the surface of a sample during processing is investigated. The fluorophore used in this work is Alexa Fluor® 488. After reaction with reactive oxygen species (ROS), the bright green fluorescence (excitation/emission maxima ~490/515 nm) of the dye is significantly degraded. This degradation is measured using a fluorometer. The change in intensity of the fluorescence can be used to measure the free radical fluence from the plasma. This technique can also be used to determine the number of free radicals that can penetrate through a layer of low-k dielectric film as follows. Alexa 488 is placed under free-standing dielectric films such as SiO₂ and SiCOH of various thicknesses to determine the penetration depth of free radicals that are present in a typical processing plasma. Fluorescent dyes that selectively react with specific types of free radicals can also be used. In particular, we will use hydroxyphenyl fluorescein (HPF) that is a hydroxyl (OH) radical sensor. The change in fluorescence of this dye after plasma exposure can be used to determine the OH radical fluence from the plasma. I-V, C-V and TDDB measurements can also be made as a function of plasma exposure time to determine the extent of damage to the electrical properties of the films.

This work has been supported by the Semiconductor Research Corporation under Contract No. 2012-KJ-2359 and the National Science Foundation under Grant No. CBET-1066231.

¹ Shi, H. and Huang, H., Bao, J., Liu, J., Ho, P. S., Zhou, Y., Pender, J.T., Armacost, M. D. and Kyser, D., *Journal of Vacuum Science & TechnologyB*, **30**, 011206 (2012)

² Moon, C.S., Takeda, K., Takashima, S., Sekine, M., Setsuhara, Y., Shiratani, M., and Hori, M., *Journal of Applied Physics*, **107**, 103310 (2010)

9:40am **PS2-FrM5 Gas-Phase Chemistry and Plasma Surface Interactions**, **Matthew Goeckner**, University of Texas at Dallas INVITED Plasmas have been used extensively in the semiconductor industry for almost half a century. However as processing has reached the production of nano-scale devices, development of industrially viable processes have

become more difficult. In part this is because of all of the free parameters that exist in such plasmas. To overcome this economic issue, tool vendors and semiconductor companies have turned to complex computational models of processing plasmas. The accuracy of those models requires a thorough understanding of the links between gas-phase chemistry and surface processes. In this talk, we will give a brief overview of what is known about the links between the gas-phase chemistry and surface processes and what still needs to be understood.

This material is based upon work supported by the National Science Foundation under Grants CBET0078669, CBET0922962 and IIP1338917. Any opinions, findings, and conclusions or recommendations expressed in this material are those of the author(s) and do not necessarily reflect the views of the National Science Foundation.

10:40am **PS2-FrM8 Plasma Induced Roughness Formation on Photoresist Examined by HBr Plasma-Beam Etching**, *Y. Zhang, Makoto Sekine, K. Ishikawa, K. Takeda, H. Kondo, M. Hori*, Nagoya University, Japan

For highly precise patterning technologies in device fabrication, it is required to suppress roughness formations on photoresist (PR) polymers during plasma etching processes. The HBr plasma treatment called 'plasma cure' was proposed to reduce the roughness formation [1]. In the previous studies, by using a beam irradiation system, we reported the PR roughness formation in fluorocarbon plasma [2], and the effect on roughness suppression by HBr plasma cure [3]. In this report, we have extensively investigated the roughness formation mechanism on the PR for ArF photolithography by some surface analyses and power spectral density (PSD) of the roughness.

The photoresist roughness observed by the atomic force microscope (AFM) is characterized by two dimensional (2D) PSDs and the frequency distribution for a digitized height profile [4]. Average slope and roll-off frequency of PSD are characterized by frequency components, the high-frequency roughness [5]. We treated the roughness data for six samples: (a) initial (pristine), (b) after Ar plasma beam irradiation (Ar), (c) after Ar plasma beam irradiation followed by HBr plasma cure (Ar→HBr), (d) after HBr plasma cure (HBr), (e) after HBr followed by Ar plasma beam irradiation (HBr→Ar), and (f) after HBr followed by H₂ plasma beam and Ar plasma beam irradiation (HBr→H₂→Ar).

The PSD slopes were changed by each process. The Ar plasma beam irradiation affected higher-frequency roughness, i.e. fine roughness induced on the PR surface. Thus the ion bombardments affected the local fine roughness. In particular for (e), Ar irradiation after HBr cure, the higher-frequency roughness could be reduced. This indicates that the HBr cure possibly hardened the PR surface by crosslinking polymeric chains, and the behavior was observed apparently on the decrease of roll-off frequency. On the other hand, the HBr cure after Ar irradiation, (c), increased lower frequency components of roughness compared with just Ar plasma beam irradiation, (b). We speculated that the Ar-plasma beam formed a crust layer on the PR surface with unrelieved stress and HBr cure may soften the bulk PR to relieve the stress and cause agglomeration of polymers at the size over 10 nm.

References

- [1] A. Ando et al., *Thin Solid Films* 515, 4928 (2007).
- [2] T. Takeuchi et al., *J. Phys. D: Appl. Phys.* 46, 102001 (2013).
- [3] Y. Zhang et al., 74th Japan Society of Applied Physics Meeting, 17a-C2-7 (2013).
- [4] diNanoScope Software 7.0 User Guide. Veeco Instruments Inc., pp. 163 (2006).
- [5] B. N. J. Persson et al., *J. Phys.: Condens. Matter*, 17 R58 (2005).

11:00am **PS2-FrM9 Novel Gases for Obtaining High Etch Selectivity of Oxide to Nitride for Contact Etch**, *Vijay Surla, L. Daniel, R. Gupta, V. Pallem*, Air Liquide

Contact oxide etch is a critical process in developing the next generation integrated device fabrication. With the gate feature size scaling down, the aspect ratio of the features increases and contact oxide etch process becomes more challenging. Very high etch selectivities of Oxide to Nitride are required for contact etch, and there is an increasing need for finding new etch gases that can perform better than the traditional gases like C₄F₈ and additive mixtures used by the semiconductor industry. To this end, Air Liquide is actively working on finding novel etch gas chemistries and in this work, we present the performance of some of the promising etch molecules that offer high etch selectivity of oxide to nitride and mask for contact etch application.

From a new etch molecule design standpoint, there are key etch performance indicators for contact etch, the most important of which are the etch selectivity of oxide to nitride and the oxide etch rate. In this study,

several novel fluorocarbons have been first tested systematically using dual CCP etch tool to find a correlation between the etch molecule (structure, and function), and its affect on the etch performance. The use of mass spectrometry as a diagnostic to qualitatively understand the plasma species, with a simple matrix analysis, is presented. Molecules are initially screened based on etch rate and selectivity of different planar films. Sidewall protection is important when etching these features, and so the polymerizing nature of etch gases is also investigated. Specifically, the role of ion energy and oxygen addition on controlling the rate of polymerization is studied in order to find the operating process window that yields high etch selectivity. The performance of the etch gases is finally tested on an oxide pattern structure with amorphous carbon as mask material. SEM cross-sections are presented to show the effect of etch gas on etch profile, mask selectivity and mask preservation. The new gases have demonstrated significant selectivity improvement in comparison to traditional etch gases.

11:20am **PS2-FrM10 Dielectric Barrier Discharges: Statistical Analysis of Discrete Filaments and Multi-filament Dynamics**, *Floran Peeters, R.F. Rumphorst*, Eindhoven University of Technology, Netherlands, *M.C.M. van de Sanden*, FOM institute DIFFER, Netherlands

Dielectric Barrier Discharges (DBD's) are used on a large industrial scale and have been studied for more than a century, with increasing interest in recent years in the areas of materials processing, plasma medicine and solar fuels. DBD's in filamentary mode consist of many small, transient microdischarges with diameters of ~0.1 mm and durations on the order of several 10's of nanoseconds, distributed over the dielectric surface. We study the collective behaviour of many such filaments in air by using a fast analog circuit capable of measuring the conductively transferred charge per filament. By using a miniature planar DBD with a 7 mm² electrode area, we determine charge/filament distributions without significant overlap between filaments in time, even at high filament number densities of up to 200 filaments/cm²/period. Contrary to previous work, we find that the charge/filament distributions are log-normal in nature. Furthermore, the distributions are independent of filament number density for a given DBD geometry. With conventional charge-voltage (Q-V) measurements, Lissajous figures are obtained for the miniature DBD, where the slope during a discharge period has a clear 'staircase' shape. Analysis of these Lissajous figures, for 8 different DBD geometries, reveals that filaments do not occur randomly within a discharge period, as is often assumed, but affect each other's moment of ignition. Using both measurement techniques, we infer that multi-filament discharge dynamics are regulated by residual conductivity of the gas near the surface of the dielectric, resulting in step-wise ignition of filaments as a function of applied voltage. The log-normal charge/filament distributions, on the other hand, develop from the locally trapped charges on the dielectric. We suggest that both mobile charges from residual conductivity and immobile trapped charges need to be considered in models of DBD's, especially when converting data from the abundant single-filament models in DBD literature to real devices.

11:40am **PS2-FrM11 Single Step Conversion of Metal/Polymer Films to Flexible, Electrically Conductive Patterns by a Scanning Atmospheric-Pressure Microplasma Process**, *Souvik Ghosh, R. Yang, A.C. Barnes, S. Rowan, C.A. Zorman, P.X.-L. Feng, R.M. Sankaran*, Case Western Reserve University

Atmospheric-pressure plasmas are often used to modify the surface of thin polymer films because of their ability to carry out reactions at low temperature and add unique functionality via radical chemistry. Recently, polymer films containing metal components have been exposed to plasmas to convert dispersed metal cations to supported metal nanoparticles. [1,2,3]

Such materials may be of interest for emerging applications in organic electronics, photovoltaics, and medical devices. However, few studies have assessed the electrical conductivity which is critical to these technologies.

Here, we show that polymer films loaded with metal cations can be converted to electrically conductive surfaces by an atmospheric-pressure plasma process. [4] Films of polyacrylic acid are loaded with Ag cations by solution processing and doctor's blade casting technique. The films are exposed to an atmospheric-pressure microplasma jet so that by scanning the plasma across the surface, microscale patterns with ~300 μm line width are produced. Reduction to crystalline metal is confirmed by X-ray diffraction. Characterization of the films by scanning electron microscopy and energy dispersive spectroscopy reveals that plasma exposure results in nucleation and growth of aggregated Ag nanoparticles. Additionally, cross sectional images show that the formation of Ag is limited to near the surface (~5 μm). Electrical characterization of the films shows that the patterns are highly conductive with a bulk resistivity of ~1 mΩ-cm. To understand the mechanism for reduction, we compared our process with UV irradiation, heating, and laser treatment. None of these approaches produced similar reduction, crystallinity, or conductivity. We hypothesize an electrodiffusion model whereby Ag cations diffuse in the polymer film only in the presence of the plasma which creates an electric field through the film. This results in

an enrichment of Ag cations at the surface. Reduction by the plasma then leads to a near-surface metallized layer. Thus, highly conductive surface patterns are generated from relatively low loadings of metal. References: [1] J. J. *et al.*, *Langmuir* **22**, 11388 (2006). [2] S. W. Lee *et al.*, *Adv. Func. Mater.* **21**, 2155 (2011). [3] S. W. Lee *et al.*, *Macromolecules* **45**, 8201 (2012). [4] S. Ghosh *et al.*, *ACS Appl. Mater. Interfaces* **6**, 3099 (2014).

Scanning Probe Microscopy Focus Topic

Room: 312 - Session SP+AS+BI+EM+NS+SE+SS-FrM

Probe-Sample Interactions and Emerging Instrument

Formats

Moderator: Carl Ventrice, Jr., University at Albany-SUNY

8:40am SP+AS+BI+EM+NS+SE+SS-FrM2 2013 ASSD Student Award Talk: **New Insights into Nanoscale Adhesion from *In Situ* TEM Studies**, *Tevis Jacobs, J.A. Lefever*, University of Pennsylvania, *J. Liu*, University of Wisconsin-Madison, *D.S. Grierson*, SysteMECH LLC, *K.E. Ryan, P.L. Keating, J.A. Harrison*, United States Naval Academy, *K.T. Turner, R.W. Carpick*, University of Pennsylvania

A fundamental understanding of adhesion is important for applications at all length scales, but is particularly critical in nanoscale devices and applications due to their high surface-to-volume ratio. Advancements in studying such tribological phenomena are typically hindered by the inaccessibility of the sliding interface. We will present nanoscale adhesion measurements conducted inside of a transmission electron microscope (TEM), using a modified *in situ* nanoindentation apparatus that makes contact with atomic force microscope (AFM) cantilever tips. This tool provides new opportunities to observe, identify, and quantify tribological processes with unprecedented access and resolution. First, using ultra-strong carbon-based tip materials, we find that roughness of tips can greatly reduce the pull off force and lead to severe underestimation of the work of adhesion [1]. Furthermore, we have quantified adhesion by making and breaking contact between nanoscale silicon asperities and a flat diamond substrate. The snap-in distance and the pull-off force are measured with sub-nanometer and sub-nanonewton resolution, respectively. The shape of the Si asperity is determined with sub-nanometer resolution immediately before and after contact to verify that elastic conditions were maintained. From this, we independently determine the work of adhesion and range of adhesion. The results show that accounting for roughness has a strong effect on both parameters. These two results demonstrate the importance of applying *in situ* approaches to studies of adhesion. --- I. Jacobs, T.D.B., Ryan, K.E., Keating, P.L., Grierson, D.S., Lefever, J.A., Turner, K.T., Harrison, J.A. and Carpick, R.W. The Effect of Atomic-Scale Roughness on the Adhesion of Nanoscale Asperities: A Combined Simulation and Experimental Investigation. *Tribol. Lett.* **50**, 81-93 (2013).

9:40am SP+AS+BI+EM+NS+SE+SS-FrM5 **Nanoscale Mapping of the W/Si(001) Schottky Barrier using Ballistic Electron Emission Microscopy**, *Christopher Durcan*, University of Albany-SUNY, *V.P. LaBella*, University at Albany-SUNY

The W/Si(001) Schottky barrier was spatially mapped using ballistic electron emission microscopy (BEEM) and ballistic hole emission microscopy (BHEM) using high resistivity *n*-type and *p*-type silicon substrates. A thin tungsten silicide is observed upon deposition utilizing transmission electron microscopy (TEM) and Rutherford backscattering spectrometry (RBS). The sum of the Schottky barrier heights from *n*-type and *p*-type silicon substrates agree with the silicon band gap. The BEEM and BHEM spectra are fit utilizing a linearization method to the power law of the BEEM model. Spatially resolved Schottky barrier maps are generated over a 1 μ m x 1 μ m area and provide insight into the spatial homogeneity of the barrier height. Histograms of the barrier heights show a Gaussian distribution, consistent with an interface dipole model.

10:00am SP+AS+BI+EM+NS+SE+SS-FrM6 **Local Probing of Superconductivity in Half Heusler Compounds**, *Hongwoo Baek*, NIST & Seoul National University, Republic of Korea, *J. Ha, D. Zhang*, NIST/Maryland Nano Center, University of Maryland, *Y. Nakajima, P.S. Syers, X. Wang, K. Wang, J. Paglione*, University of Maryland, *Y. Kuk*, Seoul National University, Republic of Korea, *J.A. Stroscio*, NIST

Heusler alloys have attracted interest as multifunctional experimental platforms for topological quantum phenomena ranging from magnetism to superconductivity and heavy fermion behavior. The rare-earth chalcogenide ternary half Heusler compounds were theoretically predicted to have topologically nontrivial surface states due to band inversion [1]. The lack of inversion symmetry of the crystal lattice makes unconventional pairing symmetry feasible. The superconductivity in the non-centrosymmetric half

Heusler compound YPtBi was recently reported as a promising system for the investigation of topological superconductivity [2]. In this work, we use ultra low temperature scanning tunneling micro spectroscopy to investigate the superconducting properties of the ternary half Heusler compounds YPdBi and YPtBi. Both were theoretically proposed to have topological states with different band inversion strength [1], and experimentally reported as a topological insulator [3]. Strong spin-orbit coupling and the lack of inversion symmetry present the possibility of spin-triplet superconductivity in these materials. The tunneling spectra of YPdBi show two different superconducting gaps of 0.36 meV and 0.16 meV depending on the measurement location. The variation in gaps might originate from inhomogeneity in the crystal. The superconducting gap of 0.36 meV is completely suppressed above a critical magnetic field of $B=2.5$ T, in agreement with bulk transport measurements. A superconducting gap of 0.21 meV and an upper critical field of 1.25 T were measured in a circular superconducting domain of diameter ≈ 180 nm in YPtBi. Sequential addition of single vortices to the superconducting YPtBi domain could be observed with increasing magnetic field, with vortices occupying the perimeter of the island. These observations will be discussed in terms of island confinement and pairing symmetry of YPtBi.

[1] S. Chadov, X. Qi, J. Kubler, G. H. Fecher, C. Felser, and S. C. Zhang, *Nat. Mater.* **9**, 541 (2010).

[2] N. P. Butch, P. Syers, K. Kirshenbaum, A. P. Hope, and J. Paglione, *Phys. Rev. B* **84**, 220504(R) (2011).

[3] W. Wang, Y. Du, G. Xu, X. Zhang, E. Liu, Z. Liu, Y. Shi, J. Chen, G. Wu, and X. Zhang, *Scientific Reports* **3** (2013).

10:40am SP+AS+BI+EM+NS+SE+SS-FrM8 **Multimodal Intermittent Contact Atomic Force Microscopy: Topographical Imaging, Compositional Mapping, Subsurface Visualization and Beyond**, *Santiago Solares*, George Washington University

Multifrequency atomic force microscopy (AFM) refers to a family of techniques that involve excitation of the microcantilever probe at more than one frequency [R. Garcia and E.T. Herruzo, *Nature Nanotechnology* **7**, 217 (2012)]. This can be carried out in a sequential manner, varying the excitation frequency over time, as in chirp band excitation methods, or simultaneously supplying drive signals containing more than one frequency to the cantilever shaker. The latter mode of operation commonly involves the simultaneous excitation of more than one cantilever eigenmode, such that each eigenmode is used to carry out different functions. For example, in a recently developed trimodal imaging scheme for soft sample characterization [D. Ebeling, B. Eslami and S.D. Solares, *ACS Nano*, **7**, 10387 (2013)], the fundamental eigenmode is used for topographical acquisition, as in standard tapping-mode AFM, while two higher eigenmodes are used for compositional mapping and subsurface visualization, respectively. This talk presents experimental and computational results for validated multimodal imaging schemes involving one to three eigenmodes, and discusses the expected benefits and complexities of including more than three eigenmodes.

Surface Science

Room: 309 - Session SS+EM-FrM

Semiconductor Surfaces and Interfaces 2

Moderator: Robert Bartynski, Rutgers, the State University of New Jersey, Kurt Kolasinski, West Chester University

8:20am SS+EM-FrM1 **Two Dimensional Supramolecular Ordering of Oligothiophene Molecules on the Si(111) $\sqrt{3}\times\sqrt{3}$ -Ag Surface**, *R. Liu*, Lakehead University, Canada, *C. Fu, D.F. Perepichka*, McGill University, Canada, *Mark Gallagher*, Lakehead University, Canada

The functionalization of semiconductor surfaces with organic molecules is a necessary step in the development of hybrid organic-semiconductor structures. A significant challenge to organic layer formation is the fact that semiconducting surfaces exhibit a large number of dangling bonds, which suppress the diffusivity of adsorbed molecules and can even break the molecules apart via the formation of Si-C bonds. Recently it has been shown that these problems can be obviated by depositing the organic molecules onto a passivated surface [1].

We have studied the adsorption of brominated π conjugated tetrathienoanthracene molecules (TBTA) onto the Si(111)- $\sqrt{3}\times\sqrt{3}$ -Ag surface. Thiophene based molecules like TBTA are of considerable interest in organic semiconductor research due to their efficient conjugation and the chemical stability [2]. The Si(111) $\sqrt{3}\times\sqrt{3}$ -Ag surface has no Si dangling bonds and should provide a high mobility surface suitable for TBTA adsorption. Scanning Tunneling Microscopy images reveal that at

low coverage the molecules readily migrate to step edges and defects in the $\sqrt{3}$ overlayer, in fact many images show direct evidence of molecular mobility. With increasing coverage the molecules eventually form compact supramolecular structures. In terms of the $\sqrt{3}$ lattice vectors (\mathbf{a} and \mathbf{b}), the oblique unit cell of these structures is $\mathbf{a}_m = 3\mathbf{a} + \mathbf{b}$, and $\mathbf{b}_m = \mathbf{a} + 2\mathbf{b}$. The structures are quite fragile and can decompose under repeated STM imaging. Our results suggest that TBTTA is weakly bound to the $\sqrt{3}$ surface at room temperature and that the supramolecular structures are held together by weak van der Waals forces.

1. T. Suzuki et al., Phys. Chem. Chem. Phys. 11, 6498 (2009).

2. R. Gutzler et al., Nanoscale 6, 2660-2668 (2014).

8:40am **SS+EM-FrM2 Interface Formation between a Self-Assembled Monolayer and an Organic Semiconductor**, *Sujitra Pookpanratana, H.-J. Jang, A.N. Brigeman, J.I. Basham, O.A. Kirillov, D.J. Gundlach*, National Institute of Standards and Technology (NIST), O.D. Jurchescu, Wake Forest University, C.A. Richter, C.A. Hacker, NIST

Organic-based electronics are attractive because they have potential manufacturing advantages such as mechanical flexibility and simpler processing (solution-based, low temperature, and atmosphere conditions). Molecular-based semiconductors offer a nearly limitless range of possibilities in tailoring the chemical composition and structure for a desired electronic, optical, or film-processing property. Probing and understanding molecular surfaces and interfaces is essential for the further development of organic-based photovoltaics, light emitting diodes, and field-effect transistors. Organic-organic interfaces are key in some of those devices, and understanding the impact of a self-assembled monolayer (SAM) has when an organic semiconductor is on top of it, is a complex issue.¹ This strategy is commonly implemented as a way to modify the hole injection barrier between an organic material and an inorganic substrate.

Here, we have investigated the interaction between a pi-conjugated organic semiconductor (tris-(8-hydroxyquinoline) aluminum, Alq₃) on SAM's of different tail and backbone composition. We have used ultraviolet and X-ray photoelectron spectroscopies to monitor the energy level alignment and chemical structure at the interface. The SAM's strongly interact with the Au substrate, where an interface dipole can down shift or up shift the surface work function. After Alq₃ is deposited onto the SAM-coated substrates, we find that the highest occupied molecular orbital of Alq₃ is relatively constant (with respect to the substrate Fermi level) on all surfaces, suggesting Fermi level pinning.² However, the composition of the SAM's did strongly influence the growth and chemical structure of the Alq₃ at the interface. The photoemission signal arising from the Au substrate is least attenuated when the SAM/Au surface is hydrophobic when compared to a hydrophilic SAM/Au or bare Au surface. The difference in substrate attenuation suggests that the early growth of the Alq₃ layer strongly depends on this surface property. This finding is corroborated with microscopy of the same samples. In addition, Alq₃ chemically reacts with a fluorinated SAM at the organic-organic interface as indicated by the shifting and asymmetric broadening of Al and N core levels. These results will be discussed in context of painting a comprehensive picture of the organic-organic interface formation that influences the chemical composition, electronic structure and physical structure at the interface.

[1] F. Rissner et al., ACS Nano 3, (2009) 3513.

[2] L. Lindell et al., Appl. Phys. Lett. 102, (2013) 223301.

9:00am **SS+EM-FrM3 Reactions of Benzoquinone with Hydrogen Terminated Silicon Surfaces**, *R.L. Opila, Meixi Chen, N.A. Kotulak, N.J. Schreiber*, University of Delaware

Quinhydrone dissolved in methanol has long been known to react with hydrogen terminated silicon surfaces to passivate electronic defects where photo-excited carriers recombine non-radiatively. The mechanism of this passivation is not well understood. We have shown that benzoquinone, C₆O₂H₄ rather than hydroquinone, C₆O₂H₆, both components of the quinhydrone mixture, is the active component. Benzoquinone reacts to abstract a hydrogen and then itself bonds with the surface. We have shown that the hydrogen can be abstracted from the solvent and that incident light is necessary for this reaction to take place. X-ray photoelectron spectroscopy and Fourier Transform Infrared Spectroscopy were used to show that the benzoquinone reacted with the surface. Photo-excited carrier lifetime is a good measure of the extent of the passivation of the surface. Density functional theory supports the proposed reaction mechanism.

9:20am **SS+EM-FrM4 High-Quality Monolayers Derived from Short Alkyne Chains on Si(111) Surfaces**, *Sidharam Pujari, A. Filippov, S. Gangarapu, H. Zuilhof*, Wageningen University, Netherlands

Hydrosilylation has been a key reaction in preparing monolayers on silicon surfaces. This process involves the reaction of a terminally unsaturated reactant with the Si surface. Over the past 20 years, several advances have

been accomplished to obtain better (i.e. denser and more stable) monolayers with various reactants (alkenes, alkynes, dienes, etc.) under different reaction conditions (e.g. thermal initiation, ultraviolet light, etc.).^{1,2} Such a higher density is advantageous for the structural ordering, stability and a wide range of applications. The procedure used in our lab (as well as labs around the world) involves wet-chemical techniques for the surface modifications. As the name implies, the reactants with these techniques must be available as liquids under the reaction conditions. Due to this constraint, only monolayers of relatively long chain lengths have been made, because shorter chains evaporate under thermal conditions (or are even a gas). In the current project, we have prepared and characterized a new class of monolayers with (short) chain lengths that were previously inaccessible.

H-Si(111) surfaces were modified with gaseous alkynes in a pressure-resistant PARR reactor. This novel method in silicon-carbon chemistry allows the chemisorption of compounds that were previously unusable in surface modification due to its volatility. Si-C-bonded monolayers derived from propyne, 1-butyne and 5-functionalized-pent-1-yne (-COOH, -Cl, & -NH₂) were prepared and characterized using various surface-sensitive techniques. Si(111)-propenyl and butenyl silicon-monolayers display a higher packing density (up to 75%) than any wet-chemically prepared alkyne-derived monolayer. Furthermore, a combination of experimental and theoretical data shows that propyne chemisorption happens in a temperature-dependent manner, not observed for any other alkyne studied up to now: through addition of the second carbon (-iso) at temperatures below 90 °C, and of the terminal carbon (-lin) above 90 °C. Finally, 5-chloro-1-pentyne and 4-Pentynoic acid were shown to bind at high surface densities and (near-)exclusively via the terminal carbon of the triple bond. These end groups allow for further functionalization of the monolayer.

(1) Rijkse, B.; Pujari, S. P.; Scheres, L.; van Rijn, C. J. M.; Baio, J. E.; Weidner, T.; Zuilhof, H. *Langmuir* **2012**, *28*, 6577-6588.

(2) Li, Y.; Calder, S.; Yaffe, O.; Cahen, D.; Haick, H.; Kronik, L.; Zuilhof, H. *Langmuir* **2012**, 9920-9929.

9:40am **SS+EM-FrM5 Surface Modification of Antimonide-Based Compound Semiconductor Superlattices using ALD**, *Erin Cleveland, J. Nolde, C. Cenedy, E. Aijer*, Naval Research Laboratory

The use of dielectric films in device passivation is complicated by the fact that they are typically deposited on processed material surface that bear little resemblance to that of the virgin growth surface. This is particularly evident in technologically important device structures employing antimonide-based compound semiconductor (ABCS) superlattices, where the exposed mesa sidewalls may be comprised of four or more atomic species and their complex oxides. Physically, the etched surface presents a different crystallographic orientation, and may have additional structure due to variation in etch rate of superlattice layers. Since the nature of the dielectric/semiconductor interface directly impacts the density of surface states, it is critical to understand how processed, multilayer semiconductor surfaces may be modified during the initial phase of the atomic layer deposition (ALD) process.

A significant effort has been focused on surface preparations prior to ALD that removes the native oxide and passivates the III-V atoms in order to ensure the best possible interface. Current approaches typically rely upon wet-chemical etches to remove the defect-prone native oxide layer prior to dielectric deposition; however, this technique typically suffers from a lack of reproducibility, as well as potential interface contamination between processing steps. Therefore, we studied the effectiveness of using the ALD precursor, TMA, in conjunction with wet and dry pre-treatments, in removing carbon and etch precipitates, scavenging the various oxide species, and residues of excess group III and V elements on (100) surfaces of ABCS superlattices as a function of precursor choice, sequence (i.e. TMA vs oxidizer first), exposure time, as well as substrate temperature. Furthermore, surface passivation stability was investigated as a function of temperature and time. Surfaces were analyzed using XPS, AFM, and SEM both before and after ALD treatments. Results indicate that a completely oxide free surface may not be necessary to produce a good electrical interface.

10:00am **SS+EM-FrM6 Mechanism Changes Caused by Metal Catalyst During Silicon Etching in V₂O₅ + HF Solutions**, *Kurt Kolasinski, W.B. Barclay*, West Chester University

Etching of Si in oxidant + HF solutions can lead to a self-limiting reaction that spontaneously produces nanocrystalline porous Si – a process known as stain etching. The presence of a metal catalyzes and localizes etching such that ordered arrays of pores or nanowires can be formed depending on the structure of the metal – a process known as metal assisted etching (MAE). Ag, Au, Pd and Pt were deposited from solution onto H-terminated Si to act as catalysts for MAE. The metals all catalyzed the injection of holes into the Si. They all increased the rate of hole injection by approximately a factor of

5. The stoichiometry of MAE in $V_2O_5 + HF$ solutions depended on the chemical identity of the metal. The stoichiometry when etching with Ag and Au was the same as for stain etching in $V_2O_5 + HF$ solutions. However, for Pd and Pt, the stoichiometry differed significantly, consuming more V_2O_5 and producing less H_2 per mole of Si etched. This indicates that the metal catalyst can change the mechanism of etching. Etching in $V_2O_5 + HF$ solutions was well behaved and gave consistently reproducible kinetic results. The behavior is much different when HOOH is added instead of V_2O_5 . In the absence of deposited metal, no reaction occurs with HOOH. When HOOH was added to metal-coated Si samples immersed in HF(aq), etching was immediate in all cases. In contrast to V_2O_5 , we were unable to obtain well-behaved stoichiometric results for HOOH + HF solutions. This is related to heightened sensitivity on reaction conditions compared to the V_2O_5 system as well as nonlinearities introduced by side reactions.

The mechanism of Si etching changes based on the presence of a metal catalyst during metal assisted etching and depends on the chemical identity of the metal. A valence 2 path dominates the formation of photoluminescent nanoporous Si in stain etching as well as MAE with Ag and Au. A valence 4 path dominates the formation of photoluminescent nanoporous Si in MAE with Pt. However for MAE with Pd, no nanoporous Si is formed initially and a mixture of valence 4 and valence 2 processes is observed. The nature of the electron transfer process and its dependence on the electronic structure of the metal/Si interface will be discussed.

10:40am **SS+EM-FrM8 Selective Wet Etching of III-V Semiconductors with HCl, H_2O_2 , and α -Hydroxy Acid Mixtures**, *Pablo Mancheno-Posso, R. Jain, A.J. Muscat*, University of Arizona

The higher electron mobility of III-V semiconductors makes them suitable for NMOS devices in CMOS transistor technology. A clean, smooth and well-defined semiconductor surface is needed for epitaxial growth of heterostructures and atomic layer deposition of dielectrics. Device fabrication also requires selective etching and smooth finishing of layers composed of different materials. Wet chemical treatments enable batch processing, and aqueous mixtures containing an oxidizing agent and an etchant (acid or base) have been developed for III-V materials. The (100) face of the binary III-V semiconductors contains both group III (electron-deficient) and V (electron-rich) atoms. HCl solutions favor the removal of the latter. The addition of α -hydroxy acids (citric and tartaric acids) to the etching mixture is expected to promote a more uniform etch by chelating the group III atoms. In this study, we compare the etching rates of the (100) faces of GaAs, InAs, InP, InSb and GaSb, using aqueous solutions of HCl (0.01-4 M), H_2O_2 (0.01-8 M), and tartaric and citric acids (0.1-1.5 M). The etching rate was determined by profilometry measurements of the step height on patterned substrates. The chemical composition of the surface was studied using XPS, and the surface topography and roughness were characterized with AFM. The etching rate of GaAs in HCl- H_2O_2 mixtures was independent of HCl concentration (0.1-4 M) and showed a linear dependence on H_2O_2 concentration (0.1-8 M). Etching was limited by the removal of water-soluble Ga and As chlorides formed from GaAs oxides. InP etching was independent of HCl concentration (1-5 M), but sharply increased for 6-7 M. H_2O_2 concentration showed no significant effect on InP etching. The GaSb etching rate depended linearly on H_2O_2 concentration but in a narrower range (0.1-0.5 M). The etching of InP and GaSb is limited by the removal of the group III atoms. Etching of GaAs and InAs is limited by the removal of the group V atom. The strong bond that As makes with O drives etching. The etching selectivity of GaAs to InP increased from about 15 to 250 when the H_2O_2 concentration was raised from 1 to 8 M at a fixed 1.76 M HCl concentration. The addition of tartaric or citric acid to HCl and H_2O_2 mixtures yielded no change in the etching rate of GaAs when compared to solutions containing HCl and H_2O_2 only, but preferentially removed Ga atoms, yielding smoother surfaces at low concentrations. Using a chelator etched InAs with high selectivity relative to InP without as much roughening as with HCl. Selective etching will be discussed in the context of a set of proposed mechanisms based on the data.

11:00am **SS+EM-FrM9 Lanthanum Quantification for Optimization of Advanced High-k/Metal Gate Stacks using Low Energy Electron X-ray Emission Spectrometry**, *E. Martinez*, CEA, LETI, MINATEC Campus, France, *C. Trouiller*, STMicroelectronics, France, *M.P. Moret*, N. Morel, CAMECA, France, *Andrew Davis*, CAMECA Instruments Inc, *P. Caubet*, STMicroelectronics, France, *F. Bertin*, CEA, LETI, MINATEC Campus, France

We report about accurate monitoring of ultra-low La doses inserted in advanced high-k/metal gate stacks for threshold voltage tuning purposes. Three characterization techniques are implemented for precise and reproducible lanthanum quantification. LEXES (Low energy Electron X-ray Emission Spectrometry) capabilities are highlighted in terms of sensitivity and accuracy thanks to a comparison with reference results obtained by Rutherford Backscattering Spectrometry (RBS). The capabilities of state-of-

the-art Auger nanoprobe for depth profiling in the sub-nanometer range are also illustrated.

Thin Film

Room: 307 - Session TF+AS-FrM

Thin Film Characterization

Moderator: Mark Davidson, University of Florida

8:20am **TF+AS-FrM1 Stability of Platinum Silicide Thin Films above 1000°C**, *Robert Fryer, R.W. Meulenberg, G.P. Bernhardt, R.J. Lad*, University of Maine

Stable, electrically conductive thin films are needed as components for sensors and actuators operating in harsh environments at temperatures above 1000°C, such as those found in turbine engines, power plants, and high temperature materials manufacturing. The Pt-Si thin film system has been extensively studied in the microelectronics industry but the focus has been on film characteristics below 800°C. In this work, Pt-Si films were grown at varying compositions and deposition temperatures on sapphire and fused silica substrates by electron-beam evaporation of Pt and Si sources in ultra-high vacuum ($<10^{-9}$ Torr); the chemical and thermal stability of the Pt-Si films, both in air and in vacuum, at temperatures between 1000–1200°C were studied. X-ray diffraction (XRD) of as-deposited films indicates the formation of a polycrystalline tetragonal-Pt₂Si phase for Pt-rich film compositions, an orthorhombic-PtSi phase near the Pt₅₀Si₅₀ composition, and an amorphous film for Si-rich film compositions. The electrical conductivities of these films, measured by a 4-point probe, are in the range of 1×10^6 to 5×10^4 S/m, with the conductivity decreasing at higher Si content. Annealing in vacuum at 1000°C causes grain growth and a marked increase in film conductivities. During annealing in air at 1000°C, film oxidation occurs leading to the formation of Pt-oxide phases coinciding with the Pt-Si phases, but only a ~3-fold decrease in film conductivities. After four hours at 1200°C in air, the Pt-Si films become insulating due to morphological roughening and formation of highly faceted Pt (111) and (200) nanocrystallites coexisting in a SiO₂ matrix. Scanning electron microscopy (SEM) revealed that the use of a 50 nm capping layer of amorphous Al₂O₃, grown by atomic layer deposition (ALD) on top of the Pt-Si films, helps retard oxidation thereby preserving film conductivities in the 10^6 - 10^4 S/m range and leading to greater film stability as a function of annealing time at 1000°C in air.

8:40am **TF+AS-FrM2 Bulge Testing for Mechanical Characterization of sp²/sp³ Carbon Thin Films**, *Joseph Rowley, R.C. Davis, R.R. Vanfleeter, N. Boyer*, Brigham Young University, *S. Liddiard, M. Harker*, Moxtek, Inc, *L. Pei*, Brigham Young University

Bulge testing is a technique employed to measure material properties of thin films. Pressurized gas is applied to one side of a film and its subsequent deformation measured. In many cases, thin films are fragile and therefore difficult to handle. Bulge testing has the advantage of requiring much less handling than other methods, resulting in fewer samples lost to error or accident. Carbon membranes have a wide range of characteristics, depending on their bonding and nano-structure. They can have very desirable properties such as: being chemically inert, high wear resistance and low friction, and high hardness and/or strength. In this work, reactively sputtered sp² carbon, diamondlike carbon from a pulsed laser deposition process, and a carbon nanotube reinforced polymer were characterized. PEELS and Raman Spectroscopy were used to determine sp³/sp² ratios and density, CHN testing was used to determine hydrogen content, measuring the resonant frequency was a measure to check stiffness, and bulge testing was used to obtain the Young's Modulus and tensile strength.

9:00am **TF+AS-FrM3 Time Dependent Dielectric Breakdown Measurements of Porous Organosilicate Glass using Mercury and Solid Metal Probes**, *Dongfei Pei*, University of Wisconsin-Madison, *M.T. Nichols*, Applied Materials, *S.W. King, J.M. Clarke*, Intel Corporation, *Y. Nishi*, Stanford University, *J.L. Shohet*, University of Wisconsin-Madison

Time-dependent dielectric breakdown (TDDB) is a major concern for low-k organosilicate (SiCOH) dielectrics. To examine the effect of plasma exposure on TDDB degradation, both the time-to-failure (TTF) and charge-to-failure (CTF) measurements [1] were made on porous SiCOH before and after exposure to Ar plasma. Significant discrepancies between mercury and solid-metal probes are observed. With XPS measurement data, a significant amount of mercury was found to have drifted into the porous SiCOH film. This implies that the electrical measurement of porous low-k material under mercury probe may be inaccurate due to this mercury drift effect.

This work was supported by the Semiconductor Research Corporation under Contract 2012-KJ-2359 and by the National Science Foundation under Grant CBET-1066231.

[1] M. T. Nichols, H. Sinha, C. A. Wiltbank, G. A. Antonelli, Y. Nishi, and J. L. Shohet, *Appl. Phys. Lett* **100**, 112905 (2012)

9:20am **TF+AS-FrM4 The Equivalent Width as a Figure of Merit for XPS Narrow Scans**, *Matthew Linford, B. Singh*, Brigham Young University, *J. Terry*, Illinois Institute of Technology

X-ray Photoelectron Spectroscopy (XPS) is a widely used surface analytical tool that provides information about the near surface regions of materials. In particular, chemical state information is often obtained from peak fitting XPS narrow scans. And while indispensable for XPS data analysis, peak fitting can be a fairly subjective exercise. Herein we introduce the use of the equivalent width (EW) as an additional and less subjective figure of merit for XPS narrow scans. The EW_{XPS} is simply defined as the area of a narrow scan divided by the height of the maximum of its peak envelope. To limit any ambiguity in EW_{XPS} for a series of spectra, we may also list the peak position of the maximum of the envelope (PE_{max}). We provide and discuss four examples that demonstrate the use of these parameters including (i) four C 1s narrow scans of ozone-treated carbon nanotubes ($EW_{XPS} \sim 2.11 - 2.16$ eV for a Shirley background, and up to 2.88 eV for no background, $PE_{max} \sim 284.4 - 284.5$ eV), (ii) a series of silicon wafers with different oxide thicknesses ($EW_{XPS} \sim 1.5 - 2.8$ eV, $PE_{max} \sim 99 - 103$ eV), (iii) hydrogen-terminated silicon before and after derivatization with pentyl groups, and after annealing of the pentyl-modified material ($EW_{XPS} \sim 0.7 - 1.0$ eV, $PE_{max} \sim 25.9 - 26.1$ eV), and (iv) five C 1s narrow scans of nanodiamond samples, where three of the spectra showed charging ($EW_{XPS} \sim 2.6 - 4.9$ eV, $PE_{max} \sim 272.7 - 293.9$ eV). In this final example, EW_{XPS} was plotted against PE_{max} to identify the region corresponding to the materials that showed the least charging. EW_{XPS} and PE_{max} appear to correlate with the expected chemistries of all the systems studied. We calculate EW_{XPS} using a Shirley baseline and with no baseline at all. In setting the baseline limits for EW_{XPS} , we consider the derivative of C 1s narrow scans. We also show the application of EW_{XPS} to single, fitted components within a narrow scan. Other width functions are also discussed.

9:40am **TF+AS-FrM5 Characterization of Epitaxial Oxides for Electronics, Magnetics, and Photoactivity**, *Tiffany Kaspar*, Pacific Northwest National Laboratory **INVITED**

Transition metal oxides offer an incredibly rich variety of properties which can be harnessed for countless applications. Unfortunately, this variety can be a curse as well as a blessing: the myriad oxidation states, crystal structures, and defects which may occur in the bulk and/or on the surface of any given oxide system makes it challenging to draw meaningful structure-property relationships without employing a full suite of materials characterization techniques. To keep the system as simple and well-defined as possible, and to explore materials and compositions not easily attainable by equilibrium techniques, epitaxial deposition of oxide thin films is widely utilized. However, even in these "simple" systems, thorough characterization of the crystallinity and structural defects, oxidation state, stoichiometry and dopants is critical. Unwelcome surprises are often found in nominally "good" material when one takes the time to investigate. Our laboratory has explored the electronic, magnetic, and photoactive properties of binary and complex oxides as epitaxial thin films, and several examples illustrating the importance of thorough thin film characterization will be presented. In our work on Cr-doped anatase TiO_2 , a candidate dilute magnetic semiconductor (DMS), room temperature ferromagnetism was observed that appeared to depend sensitively on "preparation conditions." We applied several characterization techniques, particularly x-ray diffraction (XRD) and transmission electron microscopy (TEM), and were able to correlate the presence of structural defects with room temperature ferromagnetic ordering. One of the most widely investigated materials as a potential DMS has been Co-doped ZnO, but the presence of intrinsic ferromagnetism in this system has been widely debated in the literature. We investigated very high quality epitaxial thin films with several x-ray absorption-based characterization techniques (XANES, EXAFS, XLD) to disprove the presence of intrinsic ferromagnetism in nominally defect-free material. In more recent work, we have explored the visible-light photoactivity of hematite Fe_2O_3 , doped with Cr or V. XRD, x-ray photoelectron spectroscopy (XPS), scanning TEM (STEM), and XANES/EXAFS have been applied, as well as less widely utilized techniques such as non-Rutherford resonant elastic scattering (RES) to quantitatively measure oxygen stoichiometry non-destructively, and lab-based x-ray photoelectron diffraction (XPD) to elucidate unique surface oxidation features observed by XPS. The structural properties of doped hematite could then be correlated with the bandgap and spectroscopic photoconductivity measurements.

10:40am **TF+AS-FrM8 Low Energy Ion Scattering Data Analysis for Ultra Thin Films using TRBS**, *Thomas Grehl, P. Bruner*, ION-TOF GmbH, Germany, *B. Dellefs, E. Nolot, H. Grampeix*, CEA-LETI, France, *E. Steinbauer, P. Bauer*, Johannes Kepler University, Austria, *H.H. Brongersma*, ION-TOF GmbH, Germany

Low Energy Ion Scattering (LEIS) is well known for its extreme surface sensitivity, allowing elemental characterization and quantification of the outermost atomic layer. This makes it a valuable tool for thin film analysis, e.g. to gain insights to the early stages of film growth or determine film closure. Also contamination analysis can be performed, again making use of the high surface sensitivity to assess the surface composition as the basis for subsequent deposition steps.

In addition, distinct information about sub-surface layers is obtained in a non-destructive way, giving information about the depth distribution of elements up to 10 nm. Although the mechanism for this in-depth signal is well understood, a model for the quantification of the data needs to be established.

One way of modeling the data is demonstrated using TRBS [1], a specialized version of TRIM [2] which was optimized for simulating ion scattering. Combining the TRBS data for backscattering of primary ions and an empirical model for the energy dependent reionization probability gives promising results. By fitting the simulation to the measured data conclusions about film composition, thickness and interface quality can be drawn.

This approach will be demonstrated using different thin film examples. One of the sample sets consisting of HfO_2/Al_2O_3 stacks also characterized by AR-XPS, XRR and GIXRF will be discussed in detail. We will show the possibility to determine film thickness variations in the Å range. These measurements can be performed in a few minutes without destroying the sample by sputtering. At the same time, the composition of the outer atomic layer is detected, making the approach well suited for routine analysis of films during or after deposition.

[1] A particularly fast TRIM version for ion backscattering and high energy implantation, Biersack, J.P.; Steinbauer, E.; Bauer, P.; *Nucl. Instr. and Meth. in Phys. Res.*, B61, 1991, 77-82

[2] *The Stopping and Range of Ions in Solids*; Pergamon, New York, 1985

11:00am **TF+AS-FrM9 Polarization-dependent X-ray Absorption Fine Structure Analysis of TES Pentacene Thin Films**, *Beatrix Pollakowski*, Physikalisch-Technische Bundesanstalt (PTB), Germany, *J. Wade, JS. Kim*, Imperial College London, UK, *F.A. Castro*, National Physical Laboratory (NPL), UK, *J. Lubeck, R. Unterwiesberger*, Physikalisch-Technische Bundesanstalt (PTB), Germany, *A. Zoladek-Lemanczyk*, National Physical Laboratory, UK, *B. Beckhoff*, Physikalisch-Technische Bundesanstalt (PTB), Germany

Research in organic electronics shall open up alleys for many of its promising applications, including promising applications, including: light emitting diodes, photovoltaics, transistors, biosensors and photonic devices. Despite of the diversity of device functionalities, all these applications are based on thin films of organic materials and in each case their performance is critically dependent upon the precise arrangement and packing structure of the organic molecules in thin films. Our research focuses on this fundamental issue, seeking to better understand the relationships between device performance and thin film morphology of organic semiconductors on the molecular scale [1,2].

A set of 6,13-Bis(triethylsilyl)ethynylpentacene (TES-PEN) samples has been prepared on a silicon substrate by using a well controlled printing technique.[2] Different substrate shift speeds were used to modify the layer thickness and the crystallinity.

All X-ray based measurements were carried out at the plane grating monochromator PGM beamline for undulator radiation in the laboratory of the Physikalisch-Technische Bundesanstalt PTB at BESSY II, providing tunable radiation of both high photon flux and high spectral purity in the soft x-ray range [3]. Different kinds of X-ray spectrometry (XRS) analyses were employed to determine the chemical binding state, elemental distribution depending on the depth, and lateral mass deposition.

To analyze the chemical binding state of the molecules, the method Near-Edge X-ray

Absorption Fine Structure spectroscopy (NEXAFS) in fluorescence mode has been employed. Varying the angle of incidence in the fluorescence mode the information depth can be tuned to a pre-selectable depth of interest. In addition, the mean penetration depth at large angles of incidence is high enough to analyze even thicker layers of up to a few hundreds of nanometers as is often the case for complex organic materials. For an analysis of the molecular orientation, the angle between the electric field vector and predominant direction of the molecules has to be varied.

Initial measurement sequences exhibit the potential of this X-ray spectrometry method to significantly contribute to the quantitative analysis of organic materials in thin films. In particular, polarization dependent NEXAFS offers a clear discrimination capability for the orientation of the molecules.

[1] S. Wood, J.S. Kim, D.T. James, W.C. Tsoi, C.E. Murphy, and J. S. Kim, *J. Chem. Phys.* 139, 2013, 064901

[2] D.T. James, J. M. Frost, J. Wade, J. Nelson, J. S. Kim, *ACS Nano* 7(9), 2013, 7983.

[3] J. Lubeck, B. Beckhoff, R. Fliegau, I. Holfelder, P. Hönicke, M. Müller, B. Pollakowski, F. Reinhardt, J.

11:20am **TF+AS-FrM10 Surface Induced Phases in Organic Thin Films: Methods of Crystal Structure Solutions, Roland Resel, C. Röthel, A. Pichler, Graz University of Technology, Austria, I. Salzmann, Humboldt University, Germany, R.G. DellaValle, O. Rosconi, University Bologna, Italy, T. Dingeman, Delft University of Technology, Netherlands, C. Simbrunner, University Linz, Austria**

A large number of organic molecules exhibit polymorphism and a well-known phenomenon are specific crystallographic phases which are present exclusively in thin films. Such crystallographic phases are often denoted as surface induced phases, since the presence of a surface during the crystallisation is of primary importance for their formation. In general, such thin-film polymorphs do not exist as macroscopic free standing single crystals, so that existing methods of crystal structure solution e.g. from single crystal diffraction or powder diffraction does not work. A number of surface induced crystal structures of conjugated molecules are solved during the last years, examples are in relevant molecules for organic electronic applications like pentacene or sexithophene.

Two different methods of structure solution from a thin films will be introduced. Both methods are based on grazing incidence x-ray diffraction. In a first step the crystallographic unit cells and the lattice constants are determined by indexing the diffraction pattern. The evaluation of the molecular packing is based on either rigid body refinement or molecular dynamics simulations. While rigid body refinement is based on test structures and a comparison of the calculated diffraction intensities with the experimental intensities, molecular dynamics work on energy minimisation of the molecular packing. It is found that the approach works best for fully rigid molecules like pentacene or parylene. Good results are also obtained for semi-rigid molecules like teraphthalene or molecules with flexible side-chains like dioctyl-terthiophene. In both cases the crystallographic unit cell is filled by two molecules. However an increasing number of molecules per unit cell (e.g. four) makes the solution of the surface induced phases difficult. Similarities and differences in the molecular packing between known crystal structures (from single crystal solutions) and surface induced phases will be discussed.

Tribology Focus Topic

Room: 303 - Session TR-FrM

Applications of Novel Materials in Tribology

Moderator: Barbara L Mooney, United States Naval Academy

8:20am **TR-FrM1 Direct Adhesion between Stiff Materials: Characterization and Applications in Nanomanufacturing, Kevin Turner, University of Pennsylvania** INVITED

Micro- and nano-scale contacts that adhere directly due to surface forces are ubiquitous in semiconductor bonding and stacking processes as well as in AFM-based nanolithography. Understanding and characterizing the mechanics of direct adhesion in these processes is essential to advancing process capability. This presentation will discuss two different studies in which the adhesion of small-scale contacts in micro- and nanosystems were examined. First, a study of the direct adhesion of single crystal silicon components will be discussed. A microbeam-based method was used to characterize adhesion hysteresis of smooth single crystal silicon contacts in varying levels of relative humidity. The results show significant hysteresis between adhesion and separation and have implications for processes such as direct wafer bonding and nanomembrane stacking via microtransfer printing. Second, a study of the role of geometry on the adhesion of single asperity nanoscale contacts, such as those formed by an AFM tip in contact with a surface, will be discussed. Specifically, the effect of deviations in the tip geometry from the ideal parabolic geometry assumed in the classical models (e.g., JKR, DMT) was examined. A combination of analytical modeling, finite element simulations, and experiments were used to quantify the effect of changes in tip geometry on the relationship between

pull-off force and work of adhesion. Furthermore, the role of roughness on the effective adhesion range is examined. The implications of both of these studies on nanomanufacturing processes will be discussed.

9:00am **TR-FrM3 Compound, Nanometric Cushion for Enhancing Tribological Characteristics of Hard Films, K. Gotlib-Vainshtein, O. Girshevitz, C.N. Sukenik, Bar Ilan University, Israel, D. Barlam, Ben Gurion University, Israel, Sidney Cohen, Weizmann Institute of Science, Israel**

In this work, scanning force microscopy (SFM) is used to measure tribological characteristics of a novel, compound film. Hard coatings are often applied to engineering surfaces for reduction of friction and wear. Here, we show that a soft, flexible, intermediate layer placed between substrate and hard outer coating provides considerable enhancement of the wear protection. Previously, we demonstrated that such compound films provide a means to controllably tune surface stiffness, thus opening interesting nanomechanical applications.¹ Titania films of several nm thickness are coated onto substrates of silicon, kapton, polycarbonate (PC), and polydimethylsiloxane (PDMS) and the scratch resistance is measured by SFM. When PDMS is applied as an intermediate layer between any stiffer substrate and the thin titania outer layer, marked improvement in the scratch resistance is achieved. This is shown by quantitative wear tests on silicon and kapton substrates coated with PDMS which is subsequently capped by a titania layer with thickness ranging from several nm to several tens of nm. In addition to the improvement in scratch/wear resistance, nano-friction studies performed in the SFM showed that the PDMS cushion layer reduced the friction coefficient of the titania coating by more than a factor of two.

To demonstrate a technological application of such coatings, they were applied to the common lens material PC. Here, 40 nm or titania was deposited by liquid phase deposition² on a ten micrometer-thick PDMS "cushion" on top of the PC. In scratch tests, load to failure was increased by 5x relative to untreated PC and more than doubled relative to titania on PC without the cushion layer. These thin coatings had no detrimental effect on the optical properties of the PC. This work thus demonstrates, a simple, robust, and practical means of improving tribological properties in practical applications.

The physical basis of this effect is explored by means of Finite Element Analysis, and we suggest a model for friction reduction based on the "cushioning effect" of a soft intermediate layer.

9:20am **TR-FrM4 Friction Effects by Surface Roughness and Sliding Speeds at Oil Lubricating Conditions, Guang Wang, X. Nie, University of Windsor, Canada, J. Tjong, Ford Motor Company, Canada**

A linerless aluminum (Al) engine block has potential in reducing the weight of an automotive engine for improvement of the fuel economy. However, the Al cylinder surface of an aluminum engine block is not usually strong enough to withstand the sliding wear against piston rings. A few surface processing technologies are used to protect the surface of cylinders directly. Among them, plasma transferred wire arc (PTWA) thermal spraying coating is already popular. Plasma electrolytic oxidation (PEO) coating is also proposed for increasing the wear resistance of aluminum-silicon alloy (A356) and reducing the friction between the cylinder and piston. In this work, two different PEO coatings with a thickness of around 25mm were prepared, and a high speed pin-on-disc tribometer was used to study the tribological behavior of the coating at oil lubricant conditions. A cast iron sample was also used to do the same tribological tests for comparison. The coefficient of friction (COF) vs surface roughness (Ra: 0.2-0.8µm) and sliding speeds (up to 6.0m/s) were particularly studied. The results show that the COF significantly decreased with the increase of sliding speeds, and a smoother coating surface generally exhibited a lower COF. The roughness also influenced the descent rate of the COF significantly. The COF of the PEO coatings could be lower than that of cast iron. The study indicates that the Al-Si alloy with PEO coatings could be a feasible solution to reduce weight and improve fuel efficiency of an Al engine.

9:40am **TR-FrM5 Basal Plane Surface Functionalization of Graphene Nanoplatelets, J. David Schall, Oakland University**

Due to their high in-plane strength, electrical and thermal conductivity and lubricity, graphene nanoplatelets (GnP) have great potential in polymer composite and lubricant additive applications. However, to fully utilize these remarkable properties the GnPs must be functionalized in such a way as to make them attractive to the matrix in which they are embedded. Traditionally GnPs are functionalized via wet chemical methods along their edges. Because of the high surface to edge ratio, the benefits of this functionalization are limited and unfortunately functionalization of the basal plane tends to lead to degradation of the beneficial properties. Graphite-like molecules such as Pyrene have been proposed as an alternative way to increase GnP-matrix interactions. Pyrene, which can be thought of as a

small graphene sheet consisting of only four rings, interacts with the surface of the GnP via dispersion forces as opposed to chemical bonding. The pyrene itself is functionalized with alkane chains or carboxylic acid groups which then interact with the surrounding matrix material. In this paper, results from molecular simulations of the interactions between functionalized pyrene molecules and graphene nanoplatelets will be presented. These simulations have been used to measure the interaction strength between GnPs and functionalized pyrene as well as to investigate the effect of the functionalized chain length on the interaction with a poly-alpha olefin based lubricant. The aim of this work is to explore mechanisms to improve stability of GnPs in lubricants such as engine oil which is dependent upon strong interactions between the GnP and the liquid matrix to prevent settling.

10:00am **TR-FrM6 Nanoscale Wear of Patterned PMMA Structures**, *Yijie Jiang, Z.B. Milne*, University of Pennsylvania, *M. Fallet, J.A. Harrison*, United States Naval Academy, *R.W. Carpick, K.T. Turner*, University of Pennsylvania

Atomic force microscopy (AFM) is increasingly used for probe-based metrology and tip-based nanomanufacturing (TBN) processes. In these processes, a sharp silicon- or carbon-based tip often interacts with the surface of a polymer film on a substrate. During this mechanical interaction, the polymer film can wear and contaminate the tip. To improve the reliability and control of these processes, a fundamental understanding of the tribological properties of nanoscale tip-polymer contacts is required.

Polymethyl methacrylate (PMMA), a common polymer used in nanofabrication, is studied here. PMMA is used as a resist in electron-beam (e-beam) lithography and also employed in TBN processes to realize 2D patterns and 3D structures. The tribological properties of PMMA are important in the optimization and selection of operating parameters in TBN processes and AFM-based metrology. Studies of PMMA wear have been performed from the millimeter- to nano-scale. The reported wear rates of PMMA vary over a wide range, likely due to differences in PMMA compositions tested, varied experimental conditions, and lack of control for the effect of debris. The debris can contaminate both the surface and the tip, and this often makes it difficult to accurately assess wear in experiments at the small scale.

In this work, nanoscale wear of PMMA is investigated using systematic AFM-based nanomechanical wear experiments. The experiments are performed on thin PMMA layers (131 ± 4 nm thick) on silicon substrates. To allow for precise quantification of the evolution of the PMMA, the film is patterned via e-beam lithography into structured patterns. The gaps between the patterns minimize debris and also facilitate tip cleaning. The structures primarily consist of long rectangular and square structures of PMMA. The exposed Si surface in the gaps serves as a reference surface, which allows for accurate measurements of film height to be obtained throughout the test. The use of AFM for applying the mechanical load and scanning as well as for imaging the structures allows for in-situ observation of the wear process. Different volume loss rates of the polymer are measured under varying loads and scanning speeds. The tip geometry and contamination are assessed by scanning over a reference sample and by imaging using transmission electron microscopy. The load and tip geometry data are used to determine contact stresses during the test. This talk will discuss the experimental method and results, and the development of models to describe the relationship between wear volume, applied load, and scanning speed.

10:40am **TR-FrM8 Improving Automotive Engine Efficiency through Tribological Testing**, *Peter Lee*, Southwest Research Institute **INVITED**

Fuel economy is one of the most important issues facing the automotive industry due to rising fuel costs, the need to conserve fossil fuel and government legislation. Although most of the energy losses are controlled through engine design, there is increasing interest in the role of lubricants in improving fuel economy. Crankshaft bearings can account for up to 40% of total engine friction due to the shear losses in the hydrodynamic lubrication regime and it is for this reason that average lubricant viscosities are reducing. However, this reduction in lubricant viscosity increases the frictional losses in boundary contacts in other engine components. In order to reduce this negative impact on fuel economy, engine manufacturers and lubricant and additive suppliers invest heavily in developing novel coatings, base oils and additives to reduce the frictional losses in these contacts.

ASTM have a test method for measuring fuel economy using a 2009 3.6L V6 General Motors gasoline engine. The fired engine test (ASTM D7589) runs for 100 hours using external lubricant heating/cooling systems and a 'flying flush' system for changing lubricants without engine shutdown. It compares a baseline lubricant with the test lubricant and measures the fuel economy improvement. However, such engine testing is expensive and hence all companies screen lubricants and coatings prior to running full engine tests.

Lubricants and coatings are screened in commercially available tribometers that are developed to replicate the contact geometries present in the engine. Reciprocating tribometers are used to replicate piston assembly and liner interactions and rotating tribometers are used to replicate camshafts and bearings. Test components may be standard test parts or manufactured from the real engine parts, and lubricant supply may be changed during the tests. In addition to this, engine specific test rigs are often designed and developed. These utilize real engine components operated in the same manner and in the same environment that they experience in the engine without using the full fired engine. Examples of test rigs, test parts and test results showing what can be achieved with these tribometers and test rigs will be presented.

An additional step in tribological testing is the use of single cylinder fired research engines. A specially developed test engine, capable of measuring the friction in the inlet and exhaust overhead valvetrains as well as the piston assembly will be presented along with example data.

11:20am **TR-FrM10 In Situ Study of Growth Mechanisms and Kinetics of ZDDP Antiwear Tribofilms in Nanoscale Single-Asperity Contacts**, *Nitya Nand Gosvami*, University of Pennsylvania, *J.A. Bares*, BorgWarner Powertrain Technical Center, *F. Mangolini*, University of Pennsylvania, *A.R. Konicek, A.M. Schilowitz, D.G. Yablon*, ExxonMobil Research and Engineering, *R.W. Carpick*, University of Pennsylvania

Zinc dialkyl dithiophosphates (ZDDPs) are lubricant additives used nearly universally in engine oils. Despite the generation of volatile phosphorous- and sulphur-containing compounds in the downstream gases that can reduce the working life of the catalytic converter, the unrivaled wear protection of ZDDPs makes them essential to lubricant performance. ZDDPs work by decomposing under tribological sliding to form nanoscale anti-wear films whose growth mechanisms are still poorly understood due to the complexity of the macroscopic multi-asperity sliding interfaces and the multiple chemical species involved (1). Greater understanding of the formation of these films is essential to enable rational design of more environmentally-friendly and energy-efficient engine oil formulations (2, 3). Here we report the development and application of a novel experimental approach using atomic force microscopy (AFM) for visualizing and quantifying the formation of ZDDP anti-wear films in-situ in a single asperity contact with nanometer-scale spatial resolution. Experiments performed on iron-coated silicon surfaces at 80-140 °C in the presence of ZDDP containing polyalphaolefin oil show that thermal films grow on the substrate in the absence of tribological contact. These films are easily removed by sliding the tip at applied normal forces of only a few nanonewtons (contact pressure < 1.0 GPa). Continued sliding at higher normal loads (contact pressure ~ 2.0 -6.0 GPa) reveals the nucleation and growth of much more robust films with a pad-like lateral structure, similar to the morphology of anti-wear films formed by ZDDP in macroscopic contacts. The growth rate is nonlinear with time, and increases exponentially with temperature and contact pressure, in agreement with reaction rate theory. This is the first direct confirmation of asperity-level formation of such films, and the first quantification of the energetics of the tribofilm growth. Our findings provide new insights into the mechanisms of formation of ZDDP derived anti-wear films, enabling us to directly compare with atomistic predictions of pressure-induced cross-linking of zinc polyphosphates (4) and other possible proposed mechanisms (1).

(1) H. Spikes, Tribology Letters 17 (2004) 469.

(2) H. Spikes, Lubrication Science 20 (2008) 103.

(3) H. A. Spikes, Lubrication Science 20 (2008) 77.

(4) N. J. Mosey, M. H. Muser, and T. K. Woo, Science 307 (2005) 1612.

Authors Index

Bold page numbers indicate the presenter

— A —

A. M. Barea, L.A.: MS-ThP9, 238
Aanesland, A.: PS1-FrM5, 254
Abbas, A.: EN+AS+EM+SE-WeM13, 134
Abdulrahman, R.: TF+EM+EN-WeA1, 175
Abelson, J.R.: SD-WeM1, **143**; TF+PS-ThM5, 199; TR-ThP2, 244
Abraha, P.: TR-ThP5, **244**
Abramyan, T.A.: BI+MG-WeA3, **156**
Abrigo, M.: BI+AS+NS-MoA9, **34**
Abrudan, R.: MI+MG-TuM6, 63
Aceves-Mijares, M.: EM-TuP28, 109
Acosta-Najarro, D.R.: TF-ThP22, 243
Adam, S.: 2D+EM+MI+MN+NS+SS+TF-ThA4, 203
Adamovich, I.V.: PS+2D-WeA9, 168
Adams, D.P.: TF+SE-TuM2, 74
Adderley, P.: VT-WeA4, 177
Addou, R.: EM-WeA4, 159
Adomaitis, R.A.: SS+AS-WeM2, **147**
Afsari, S.: SP+AS+EM+NS+SS-ThP8, 240
Agarwal, A.: PS2-WeM1, **141**; PS2-WeM4, 142; PS-MoA8, 43
Agarwal, S.: PS1+TF-ThM10, 191; TF+EN+PS-TuA11, **102**
Agasie, R.J.: EM-WeA11, 159
Agnarsson, B.: QC+AS+BI+MN-ThA7, 219
Agrawal, A.: PS1+TF-ThM4, 190
Aguilar, R.: SP+AS+EM+NS+SS-ThP8, 240
Aguirre-Tostado, F.S.: EN-TuP9, **111**
Åhlund, J.: IS+AS+MC+SS-TuM3, 61
Ahmadi, M.: NS+AS-WeA4, **165**
Ahn, S.J.: HI-ThP1, 235; VT-TuA4, 103
Ahrelis, F.: 2D+AS+HI+NS+SS-ThM3, 179
Aifer, E.: SS+EM-FrM5, 259
Aihara, T.: EN+EM+MN+NS+TR-MoA11, 37; EN-TuP2, 110
Akimoto, K.: EM-TuP13, 108
Akolkar, R.: PS-TuP29, 118
Akyildiz, H.I.: MS+PS+TF-ThA3, **213**
Alaei, S.: MI-TuP4, **114**
Alam, K.: SS-WeA9, **175**
Alaydrus, M.: AC+AS+MI+SA+SS-MoA7, 30
Albertini, D.: EM+MI+NS-MoM8, 9
Alexander, M.R.: BI+MG-WeA1, **155**
Alexander, N.J.: EL-ThP3, 234
Alexandre Diniz, J.A.: MS-ThP9, 238
Alexandrovich, B.M.: PS-WeA9, 170
Alimardani, N.: EM2-WeM12, 131
Alivisatos, P.: SS-TuP19, 122
Alkemade, P.F.A.: HI+2D+AS+MC-ThA8, 212
Allain, J.P.: PS-TuM1, **66**; SE-TuP1, 119
Allara, D.L.: TF-MoA3, 50
Allen, D.J.: TF+SE-TuM10, 75
Allen, M.G.: MN+NS-TuA1, **91**
Allen, P.G.: AC+AS+MI+SA+SS-TuM1, 54
Allerman, A.: AS-ThP2, 231
Allman, D.: EM2-WeM2, 130
Allred, D.D.: AC+AS+MI+SA+SS-MoM10, 4; MN+PS-WeA3, 163; MN+PS-WeA4, 163; TF+PS-ThM6, 200
Alnabulsi, S.S.: AS+BI+MC+SS-MoA11, **32**; AS+BI+MC-WeA2, 154
Alper, J.P.: EM+EN+TF-WeA8, 158
Altieri, N.: PS-MoM5, 15
Altman, E.I.: 2D+EM+NS+SS+TF-WeM4, **125**
Alves Jr, C.: TF+PS-ThM13, 201
Alwine, F.: MC+2D+AP+AS-MoA11, 39
Ambrogio, S.: EM2-ThM3, 186
Ambrosio-Lázaro, R.C.: EM-TuP28, 109
Ammann, M.: IS+AS+MC+SS-WeM10, **135**
Ampuero, J.L.: EM-TuP26, **109**; TR-ThA10, 227
Amster, O.: SP+AS+BI+NS+SS-WeA10, 174
Anand, B.: EN+EM+MN+NS+TR-MoA3, 36
Ande, C.K.: SD-WeM6, 144

Anders, A.: SE+PS+TF-MoA3, 45; SE+PS+TF-MoA6, **45**; SE+PS+TF-MoA7, 46
Anderson, T.: IS+AS+MC+SS-WeM4, 134
Anderson, V.R.: PS1+TF-ThM11, 191; SA-MoM4, 17
Ando, A.: SE+EM+EN+PS+TF-MoM3, **18**
Ando, Y.: SP+AS+BI+NS+SS-WeA3, 173
Andtade, E.: TR-ThP4, 244
Ansai, H.: PS-TuM4, 66
Antcliffe, M.: EM1-WeM10, 130
Anthony, M.: VT-TuM2, 76
Antohe, A.: VT-MoA8, 52
Anz, S.: NS+HI-TuM11, 65
Aoki, M.: EM-TuP12, **107**; EM-TuP13, 108
Aoki, T.: EM+MI+NS-MoM3, 8
Aoki, Y.: SS+AS+NS-ThA6, 223
Aoukar, M.: PS1+TF-ThM5, 190
Apblett, C.: IS+AS+MC+SS-WeM4, 134
Appenzeller, J.: 2D+EM+MS+NS-FrM8, **246**
Arai, K.: VT-MoM8, 27
Arana-Chavez, D.: SS+AS-WeM2, 147
Arble, C.: IS+2D+MC+NS+SP+SS-WeA11, 162
Archer, R.S.R.: TF+PS-MoM8, 25
Arefin, N.: EM+EN-FrM10, **252**; EM-TuP1, 106
Arena, D.: MI+MG-TuM5, 63
Arey, B.: AP+AS+EN+NS+SS-ThA4, 205
Argibay, N.: TF+PS+SE-MoM6, 23; TF+PS+SE-MoM8, **23**
Arias, S.: PS-TuM1, 66
Armstrong, S.: SE+PS+TF-MoA1, 45
Arnadottir, L.: BI+AS+MN+NS-TuM4, **57**
Arnold, P.C.: VT-MoM9, **27**
Artyushkova, K.: BI+AS+MN+NS-TuM12, **57**
Arvet, C.: PS-MoA11, 43; PS-MoA9, 43
Arwin, H.: EL+AS+BI+EM+SS-FrM3, **250**
Asbeck, P.: EM1-WeM10, 130
Asensio, M.C.: 2D+AS+EM+NS+SS-MoA6, 28
Ashton, M.: MG-WeM4, 136
Askew, H.J.: QC+AS+BI+MN-ThA9, **220**
Asmat, J.J.: TR-ThA10, 227
Asokan, A.: PS-TuP16, 116
Asplund, M.: TF+EM+EN-WeA11, 177
Aspnes, D.E.: TF-ThP16, 242
Asthagiri, A.: SS-TuP20, 122
Atanasov, S.E.: MS+PS+TF-ThA4, **213**; SD-WeA3, 171
Atanassov, P.: BI+AS+MN+NS-TuM12, 57
Atcity, S.: AS-ThP2, 231
Atigyanun, S.: EM-TuP5, **106**
Atwater, H.: NS+EN-MoA1, **41**
AuBuchon, J.: SD-WeA10, 172
Aumayr, F.: 2D-ThP18, 230
Austin, D.Z.: EM2-WeM2, **130**
Avanesian, T.: EN+AS+EM+SE-TuM3, 60
Avila, J.: 2D+AS+EM+NS+SS-MoA6, 28
Axnanda, S.A.: IS+2D+MC+NS+SP+SS-WeA10, 162
Aydiil, E.S.: EN+AS+EM+SE-WeM3, **132**; TF+MS+PS-WeM4, 149
Aydin, K.: TF+EM+EN-WeA3, **176**
Aydogan, P.: 2D+EM+MI+MN+NS+SS+TF-ThA11, 204; MC+2D+AP+AS-MoA7, **38**
Ayers, J.E.: TF+AS+EM-TuA7, 100
Azad, Z.: BI+AS+NS-MoA11, 34
Azcatl, A.: 2D+EM+NS+SS+TF-WeM6, 125
Azcatl, A.: EM-WeA9, 159
Azpitarte, I.: MS+PS+TF-ThA11, 213

— B —

Babanova, S.: BI+AS+MN+NS-TuM12, 57
Babar, H.: EM+EN-FrM11, 252
Babar, S.: TR-ThP2, 244
Bachelet, R.: EM+MI+NS-MoM8, 9
Backfish, M.: VT-WeM13, 151
Bäckman, J.: VT-MoA1, 51

Back, H.: MI-MoA10, 40; SP+AS+BI+EM+NS+SE+SS-FrM6, **258**; SP+AS+EM+NS+SS-ThP3, 240
Baer, D.R.: BI+AS+NS-MoA7, **33**
Bagge-Hansen, M.: AS+MC+SS-TuA11, 81; SA-MoA8, 44
Bagley, J.: TF+EM+EN-WeA11, 177; TF-ThP19, **242**
Bagnall, D.M.: HI+2D+AS+MC-ThA9, 212
Bagot, P.A.J.: AP+AS+EN+NS+SS-ThA6, 205
Baik, K.M.: VT-TuP3, 123
Baimpos, T.: BI+AS-MoM3, 7; SS+EN-MoA4, 47
Baio, J.E.: BI+AS-MoM9, **8**; BI+AS-WeM6, 128
Baker, C.C.: VT-MoA10, 52
Baklanov, M.: EM-TuM6, 59; PS-MoM4, 15; PS-TuP12, 116
Balakrishna, A.: PS2-WeM2, **142**; PS2-WeM4, 142
Balamurugan, B.: AP+AS+MC+NS+SS-ThM12, 181
Balatti, S.: EM2-ThM3, 186
Baldwin, C.: TF+PS+SE-MoM5, 23
Baldwin, K.: HI+2D+AS+BI+MC-ThM13, 188
Ballard, J.: NS+HI-TuM11, **65**
Balsano, R.: NS+AS-WeA10, **166**
Banai, R.E.: EN+AS+EM+SE-WeM6, **133**; TF-ThP17, 242
Banarjee, P.: AS-ThP6, 231
Banarjee, S.: AS-ThP6, 231
Bancroft, G.M.: SA-MoM3, 16
Banerjee, P.: MC+2D+AP+AS-MoA9, 39; TF+SE-TuM12, 75
Banerjee, S.: MC+2D+AP+AS-MoA9, **39**; TF+SE-TuM12, 75
Baneton, J.: PS-ThA6, 217
Banna, S.: PS-TuP8, 115
Banos, A.: AC+AS+MI+SA+SS-TuM5, 55
Bany, J.: 2D+EM+MI+MN+NS+SS+TF-ThA9, 204
Bao, W.: MS+PS+TF-ThA10, **213**; MS+TF-WeA9, 165
Barati, Gh.: EL+AS+EM+EN+SS-ThM12, 184
Barbacci, D.: HI+2D+AS+BI+MC-ThM13, 188
Barback, C.: BI+AS+NS-MoA2, 32; BI+MG-WeA4, 156
Barcikowski, Z.: TF-ThP14, **242**
Barclay, M.S.: SS+AS+EN-MoM11, 20; TF+PS-ThM11, **200**
Barclay, W.B.: SS+EM-FrM6, 259
Bardeen, C.J.: SS+AS+EN-MoM1, 19
Bares, J.A.: TR-FrM10, 263
Barja, S.: SS-TuP19, 122
Barlam, D.: TR-FrM3, 262
Barlow, A.J.: AS+BI+MC-WeM6, **127**; AS+MC-MoM6, 5
Barmak, K.: MC+AP+AS-MoM6, **11**; TF-ThP26, 244
Barnes, A.: EL+AS+EM+EN+SS-ThM5, **183**
Barnes, A.C.: MN+PS-WeA11, 164; PS2-FrM11, 257
Barnes, T.M.: EN+AS+EM+SE-WeM10, 133
Barnhill, W.: AS-ThP11, 232
Barnola, S.: PS-MoA11, 43; PS-MoA9, 43; PS-MoM6, 15; PS-MoM9, 16; PS-TuM13, 68
Barrett, L.: EM+EN+TF-WeA9, **158**; MN+PS-WeA4, 163; TF+PS-ThM6, 200
Barroo, C.: AP+AS+EN+NS+SS-ThA3, **204**
Barroso, D.: 2D+EM+NS+SS+TF-WeM10, 126; 2D-ThP11, 229; SP+AS+BI+NS+SS-WeA11, 174
Barry, S.T.: TF+PS-MoA6, **49**
Barry-Porter, S.: PS-MoM4, 15
Bartels, D.M.: PS+SE-ThA3, 214
Bartels, L.: 2D+EM+NS+SS+TF-WeM10, **126**; 2D-ThP11, 229; SP+AS+BI+NS+SS-WeA11, 174

- Barth, K.: EN+AS+EM+SE-WeM13, 134
 Bartis, E.A.J.: PS+2D-WeA9, **168**;
 SE+EM+EN+PS+TF-MoM2, 18
 Bartles, L.: 2D+EM+MI+MN+NS+SS+TF-ThA8,
 203
 Barton, A.: EM-WeA4, 159
 Barton, D.: MN+PS-WeA4, 163
 Bartrand, J.A.: AP+AS+NS+SS-FrM8, 247
 Bartynski, R.A.: EN+EM+NS-TuA4, 86; SS+TF-
 ThM13, 199
 Basham, J.I.: EN+AS+EM+SE-WeM12, 133;
 EN+AS+EM-WeA11, 161; SS+EM-FrM2, 259
 Basile, L.: SP+2D+AS+EM+MC+NS+SS-ThM11,
 197
 Baski, A.A.: EM+EN-FrM3, 251
 Basnet, M.: QC+AS+BI+MN-ThM10, 194
 Bassim, N.D.: VT-MoA10, 52
 Basu, A.: SD-WeA7, 171
 Bates, R.L.: MC-TuP1, **113**
 Batista, E.: AC+AS+MI+SA+SS-MoM1, 3
 Batra, V.: EN-TuP10, **111**
 Baty, J.: CS-ThM11, 182; MS+PS+TF-ThM6, **189**
 Batzill, M.: 2D+AS+EM+NS+SS-MoA6, **28**
 Bauer, E.D.: AC+AS+MI+SA+SS-TuM1, 54
 Bauer, P.: TF+AS-FrM8, 261
 Bauer, T.M.: PS-TuM3, **66**
 Baumann, F.H.: SD-WeA10, 172
 Baumann, P.: EM+2D-TuA3, 84
 Baumann, T.: SA-MoA8, 44
 Baur, M.: AS+BI+MC+SS-MoA10, 31
 Baxter, J.B.: EN+AS+EM-WeA3, **160**
 Bayindir, Z.: EM-TuM3, 58
 Baykara, M.Z.: SP+AS+BI+NS+SS-ThA3, **221**
 Baylor, L.: VT-WeA7, 178
 Beach, J.: EN+AS+EM+SE-WeM10, 133
 Beatty, J.: MI-MoA11, 41
 Bebensee, F.: SS+AS+EN-WeM13, **146**
 Bechtel, A.: SA-MoA4, **44**
 Beckhoff, B.: SA-TuA12, 97; SA-TuM1, **68**; SA-
 TuP1, 119; TF+AS-FrM9, 261
 Beebe Jr., T.: SM+AS+BI+PS-ThM12, 196
 Beebe, Jr., T.P.: CS-ThA9, 206
 Beebe, M.R.: TF+AS+EM-TuA9, 100
 Beeram, S.: EL+AS+BI+EM+SS-FrM8, 251
 Begum, M.: EN-TuP8, 111
 Behafarid, F.: NS+AS-WeA4, 165
 Behnam, A.: EM1-WeM12, 130
 Bekele, R.Y.: VT-MoA10, 52
 Béland, A.E.: EN+AS+EM+SE-WeM3, 132
 Belenky, G.: MC+AP+AS-MoM4, 10
 Belianinov, A.: 2D+EM+MI+MN+NS+SS+TF-
 ThA9, **204**; AS+MC-MoM9, 6
 Belkin, M.: NS+AS-WeA9, 166
 Belsey, N.A.: BI+AS+NS-MoA8, **33**
 Belu, A.M.: AS+BI+MC-WeA3, **154**
 Ben Bakir, B.: PS-MoM6, 15
 Bendikov, T.: AS-ThP10, 232; AS-ThP20, **233**
 Benndorf, C.: EM-TuP26, 109; TR-ThA10, 227
 Bennett, A.I.: TR+NS-ThM6, 201
 Benoit, C.: TF+PS+SE-MoM3, 22
 Bent, S.F.: SD-WeA8, 171; SS+AS+NS-ThA10,
 224; TF+MS+PS-WeM5, 149; TF+PS-MoA10,
 50
 Bentley, W.E.: BI+AS+MN+NS-TuM2, 56; BI-
 ThP2, 234; MN+NS-TuA9, 92
 Ben-Yoav, H.: BI+AS+MN+NS-TuM3, 57
 Ben-Zvi, I.: MG-WeM2, 135; VT-TuP5, 124
 Berg, R.F.: VT-TuA3, **103**
 Berger, H.: 2D+AS+EM+MI+MN+NS+TF-WeA7,
 153
 Bergersen, H.: IS+AS+MC+SS-TuM3, **61**
 Bergoglio, M.: VT-MoM5, 26
 Bergsman, D.S.: TF+MS+PS-WeM5, **149**
 Beringer, D.: TF+AS+EM-TuA9, 100
 Berman, D.: TR-ThA6, 227
 Bernhardt, G.P.: SE+NS+TR-TuM2, 69; TF+AS-
 FrM1, 260
 Beron, F.: NS-ThP7, 239
 Berry, N.: EN+AS+EM+SE-WeM5, 132
 Bersch, E.: 2D+AS+HI+MC+NS+PS+SP+SS-
 TuA3, 79
 Bersuker, G.: 2D+AS+HI+MC+NS+PS+SP+SS-
 TuA3, 79
 Bertel, E.: SS+AS+EN-MoM3, **19**; SS-TuP5, 120
 Bertin, F.: SS+EM-FrM9, 260
 Bertolazzi, S.: 2D+AS+EM+MI+MN+NS+TF-
 WeA4, 153
 Bertrand, P.: PS+2D-WeA11, 168
 Besland, M.-P.: EN-TuP5, 110; TF+PS+SE-
 MoM3, **22**
 Bevan: EM+2D-TuA10, **85**
 Beyer, A.: HI+2D+AS+BI+MC-ThM12, 188; HI-
 ThP2, 235; HI-ThP3, **235**
 Bézard, P.: SD-WeA9, **172**
 Bhairamagdi, N.: TF-MoA8, 51
 Bhimanapati, G.R.: 2D+EM+NS+SS+TF-WeM11,
126
 Bhoj, A.: PS-TuP9, 115
 Bhowmick, R.: PS2+TF-ThM2, 192
 Bianco, G.V.: EL+AS+EM+EN+SS-ThM6, 184
 Bielefeld, J.D.: 2D+AS+HI+MC+NS+PS+SP+SS-
 TuA3, 79
 Biener, J.: SA-MoA8, 44
 Biener, M.: SA-MoA8, 44
 Biesinger, M.: SA-MoM3, 16
 Bijker, M.D.: TF+PS-MoM8, 25
 Bilek, M.M.: SM+AS+BI+PS-ThA6, **220**
 Binek, Ch.: MI+MG-TuA3, **90**
 Biolsi, P.: PS-TuA9, 95
 Birch, J.: TF+PS-ThM3, 199
 Birss, V. I.: NS-ThP5, 238
 Bischof, M.: NS+HI-TuM11, 65
 Bise, R.: PS2+TF-ThM2, 192
 Bishop, B.: PS-TuP29, **118**
 Bishop, C.V.: AS-ThP25, 234
 Bitsis, C.: SE+NS+TR-TuM12, 70
 Biyikli, N.: EM+EN-FrM4, 251; TF+EM+EN-
 WeA2, 176
 Björkman, P.: VT-MoA1, 51
 Blackledge, R.: AS+BI+MC-WeA7, 154
 Blair, S.L.: BI+AS+NS-MoA2, 32; BI+MG-
 WeA4, 156; BI+MG-WeA7, 156
 Blatz, J.: PS-TuP8, 115
 Blechle, J.M.: PS2-FrM3, 256
 Block, S.: QC+AS+BI+MN-ThA7, 219
 Blomfield, C.J.: AS+BI+MC+SS-MoA8, 31;
 AS+BI+MC-WeA1, 154; EW-TuL4, **78**
 Bluck, T.: TF+PS+SE-MoM11, 24; VT-TuA12,
 104
 Bluestein, B.: AS+BI+MC-WeA9, 155; BI+AS-
 TuA10, 83; SM+AS+BI+PS-ThA3, 220
 Bluhm, H.: EN+AS+EM+SE-WeM5, 132;
 IS+AS+MC+SS-TuA4, 88; IS+AS+MC+SS-
 TuM11, 62
 Bobek, S.: 2D+EM+NS+SS+TF-WeM10, 126; 2D-
 ThP11, 229; SP+AS+BI+NS+SS-WeA11, 174
 Bock, T.: VT-MoM8, 27
 Boden, S.A.: HI+2D+AS+MC-ThA9, **212**
 Boemmels, J.: EM-TuM6, 59
 Boecker, J.E.: EM-MoA10, 35; EM-TuP20, 109
 Boettger, P.H.M.: SE+NS+TR-TuM10, 70
 Bogdanowicz, J.: MC+AP+AS-MoM1, 10
 Boineau, F.: VT-MoM5, 26
 Böker, A.: TF-ThA11, 226
 Bol, A.A.: 2D+EM+MS+NS-FrM6, 245
 Bolat, R.: SE+PS+TF-MoA7, 46
 Bolom, T.: SD-WeA10, 172
 Bolotin, I.: EM-MoA9, 35
 Bolotin, K.I.: 2D+AS+EM+MI+MN+NS+TF-
 WeA1, **153**
 Bonetti, S.: MI+EM-MoM11, 13
 Bongers, W.A.: EN-TuP6, **111**
 Bongiorno, G.: VT-TuM10, 77
 Bonn, M.: BI+AS-MoM9, 8
 Bonnell, D.A.: NS+EN-MoA10, 42; NS-WeM12,
140; SS+AS+EN-TuM1, 71
 Bonner, J.: BI+AS+NS-MoA1, 32
 Booth, C.H.: AC+AS+MI+SA+SS-MoM1, 3;
 AC+AS+MI+SA+SS-TuM1, **54**
 Booth, J.-P.: PS1-WeM11, 140; PS-WeA1, 169
 Borguet, E.: SP+AS+EM+NS+SS-ThP8, 240
 Boris, D.R.: PS1-FrM8, 255; PS-WeA11, **171**
 Borisevich, A.: 2D+EM+MI+MN+NS+SS+TF-
 ThA9, 204; AS+MC-MoM9, 6
 Borovsky, B.P.: TR+NS-ThM12, **202**
 Borowik, L.: SP+AS+BI+NS+SS-ThA4, 221
 Bosch, R.H.E.C.: TF+PS-MoA1, 48
 Boscoboinik, A.: IS+2D+MC+NS+SP+SS-
 WeA11, 162
 Boscoboinik, J.A.: IS+AS+MC+SS-TuM12, **62**
 Bosso, P.: PS+SE-ThA1, 214
 Boswell, R.: PS1-FrM1, **254**
 Bothell, J.: MG-WeM2, 135
 Bothell, R.: MG-WeM2, 135
 Boudjabi, S.: BI+AS-MoM5, 7
 Bourke, P.: SE+EM+EN+PS+TF-MoM6, 18
 Bousser, E.: SE+NS+TR-TuM5, **70**
 Bowen, K.H.: SS+EN-MoA6, 47
 Bowers, C.M.: TF-MoA4, 50
 Bowers, J.W.: EN+AS+EM+SE-WeM13, 134
 Bowman, S.R.: EM1-ThM12, 185
 Boxford, W.: AS-ThP10, 232
 Boyer, N.: MN+PS-WeA3, **163**; TF+AS-FrM2,
 260
 Bozzini, B.: SA-MoA1, **43**
 Bradford, P.: MS+PS+TF-ThM3, **188**;
 TF+MS+PS-WeM13, 150
 Bradley, A.: AS-ThP13, 232
 Brajuskovic, B.: VT-WeM4, 150
 Brandenburg, N.J.: CS-ThM10, 182
 Branham, M.S.: EM1-ThM3, 185
 Brannaka, J.A.: SS+AS+EN-MoM11, 20
 Brannon, H.L.: AS+BI+MC+SS-MoA8, 31;
 AS+BI+MC-WeA1, **154**
 Bratescu, M.A.: PS+2D-WeA4, **167**
 Braun, P.: NS+SE-MoM8, **14**
 Bravo-Sanchez, M.: AS+MC+SS-TuA8, 81;
 AS+MC-MoM11, **6**
 Bray, K.R.: EM-TuP18, **108**
 Braz, N.: HI+2D+AS+MC-ThA10, 212
 Bredin, J.: PS+SE-ThA10, 215
 Brehmer, F.: PS+SE-ThA6, 214
 Breiten, B.: TF-MoA4, 50
 Breitung, E.: CS-FrM5, 249
 Brennan, B.: EM+2D-TuA3, 84
 Brennan, J.D.: BI+AS-MoM5, 7
 Brenner, D.: TR-ThA9, 227
 Brianceau, P.: PS-MoM6, 15
 Brichon, P.D.: PS2-FrM2, 256
 Brierley, M.: AC+AS+MI+SA+SS-MoM8, **4**
 Brigeman, A.N.: EN+AS+EM-WeA11, 161;
 SS+EM-FrM2, 259
 Bright, V.M.: TF+PS-TuM10, 73
 Briley, C.: EL+AS+EM+MC+SS-ThA4, **207**
 Britto, R.: TF+MS+PS-WeM5, 149
 Britun, N.: PS+SE-ThA11, 215
 Brivio, J.: 2D+AS+EM+MI+MN+NS+TF-WeA4,
 153
 Brockman, J.: 2D+AS+HI+MC+NS+PS+SP+SS-
 TuA3, 79
 Brongersma, H.H.: MC+AP+AS-MoM8, **11**;
 TF+AS-FrM8, 261
 Bronstein, N.D.: SS-TuP19, 122
 Brostoff, L.: CS-ThM12, 182
 Brown, C.G.: EM1-ThM12, 185
 Brown, C.M.: IS+AS+MC+SS-TuA3, **88**
 Brown, K.: 2D+EM+NS+SS+TF-WeM10, 126;
 2D-ThP11, 229
 Brown, K.A.: NS+SE-MoM11, **14**
 Brown, T.M.: TF+EN+PS-TuA12, 103
 Browning, J.: EN+EM+MN+NS+TR-MoA9, 36
 Browning, N.D.: AP+AS+NS+SS-FrM8, 247
 Browning, R.: AS+MC+SS-FrM1, **247**
 Brownson, J.R.S.: EN+AS+EM+SE-WeM6, 133;
 TF-ThP17, 242
 Brozena, A.: TF+PS-MoA2, 48

- Bruce, A.: VT-MoA10, 52
Bruce, R.L.: PS2+TF-ThM1, 191; PS-MoM10, 16; PS-MoM3, 14
Brucker, G.A.: VT-MoM10, 27; VT-MoM11, 27; VT-MoM9, 27
Bruener, P.: MC+AP+AS-MoM8, 11
Bruker: EW-TuL5, 78
Brumbach, M.: AS-ThP2, 231
Brune, H.: SP+AS+BI+NS+SS-ThA8, 222
Bruneau, B.: PS1-WeM11, 140
Brüner, P.: TF+AS-FrM8, 261
Bruno, G.: EL+AS+EM+EN+SS-ThM6, 184
Bryan, I.S.: MG-WeM3, 135
Bryan, S.R.: AS+BI+MC+SS-MoA11, 32; EW-TuL3, 78
Bryan, Z.A.: MG-WeM3, 135
Bryers, J.: BI+AS-WeM13, 129
Büchner, C.: 2D+EM+NS+SS+TF-WeM12, 126
Budach, M.: MG-TuA3, 89
Bultman, J.E.: 2D+EM+NS+PS+SS+TF-MoM5, 2
Bumm, L.A.: MC+2D+AP+AS-MoA11, 39
Bumuelle, D.: SS+EN-MoA6, 47
Bunch, J.: AS+BI+MC-WeM13, 127; AS+BI+VT-TuM5, 56
Buonaugurio, A.M.: IS-ThP3, 236
Burger, A.: EM+MI+NS-MoM4, 9
Burgess, J.A.: AS+BI+MC-WeA8, 155
Burkett, S.L.: MN+NS-TuA3, 91
Burnham, N.A.: NS+SE-MoM3, 13
Bursa, E.: EM+2D-TuA3, 84
Burton, M.: TF+AS+EM-TuA9, 100
Burwell, E.: MN+PS-WeA11, 164
Busby, Y.: MC+AP+AS-MoM5, 11
Bush, B.: AS+BI+MC+SS-MoA9, 31
Bushell, A.: AS+MC-MoM1, 5; EW-TuL2, 78
Bussmann, E.: EM1-ThA6, 209; EM1-ThA7, 209
Butera, R.: EM1-ThA7, 209
Butson, E.: SS+AS+NS-ThA9, 224
Butt, A.: TF+PS-TuM13, 74
Bux, S.: EN+AS+EM+SE-TuM13, 60
- C —
- C. Frateschi, N.C.: MS-ThP9, 238
Cabarcos, O.: TF-MoA3, 50
Cabot, G.: EN-TuP10, 111
Caciuffo, R.: AC+AS+MI+SA+SS-TuM3, 54
Cahill, D.G.: NS+SE-MoM8, 14
Cai, T.: EM1-ThM5, 185
Calafiore, G.: NS+HI-TuM1, 64
Caldwell, J.: 2D+AS+BI+PS+SS-TuM5, 53
Caldwell, R.: TF-ThA8, 225
Calley III, W.L.: EW-WeL2, 152
Calley, L.W.: MC+2D+AP+AS-MoA3, 38
Campbell, C.T.: EM2-ThA9, 211
Campbell, G.H.: TF+SE-TuM6, 75
Camps, E.: TR-ThP3, 244
Canavan, H.E.: SM+AS+BI+PS-ThA3, 220
Canedy, C.: SS+EM-FrM5, 259
Cansizoglu, H.: TF+EM+EN-WeA1, 175; TF+EM+EN-WeA2, 176
Cansizoglu, M.F.: EN-TuP8, 111; TF+EM+EN-WeA1, 175; TF+EM+EN-WeA2, 176
Cantu, D.C.: SS+AS-WeM13, 148
Cao, G.X.: MI+MG-TuM10, 63
Cao, L.: 2D+AS+HI+MC+NS+PS+SP+SS-TuA4, 79; EN+AS+EM+SE-TuM6, 60
Cao, S.: EM+MI+NS-MoM10, 9
Cao, Y.: MI-MoA11, 41
Capezzuto, P.: EL+AS+EM+EN+SS-ThM6, 184
Caprioli, R.M.: BP+BI+AS-SuA1, 1
Carbone, E.: PS-WeA1, 169
Cardinaud, C.: PS-TuM13, 68
Carenco, S.: NS-WeM6, 139
Carette, M.: TF+AS+EM-TuA3, 99; TF+PS+SE-MoM3, 22
Cargill, R.S.: BI+AS+MN+NS-TuM4, 57
Cario, L.: TF+PS+SE-MoM3, 22
Carpick, R.W.: 2D+AS+BI+PS+SS-TuM4, 53; AS+BI+MC-WeA12, 155; SP+AS+BI+EM+NS+SE+SS-FrM2, 258; SS+AS-WeM5, 147; TR+NS-ThM5, 201; TR-FrM10, 263; TR-FrM6, 263
Carr, S.M.: EM1-ThA6, 209; EM1-ThA7, 209
Carraro, C.: EM+EN+TF-WeA8, 158
Carrasquillo, R.: SS+AS-WeM3, 147
Carrier, X.: AP+AS+EN+NS+SS-ThA6, 205
Carrillo Sanchez, P.: SA-MoA3, 44
Carroll, M.: EM1-ThA1, 208; EM1-ThA6, 209; EM1-ThA7, 209; TF+MS+PS-WeM13, 150
Cartas, W.: SS+AS+EN-TuM2, 71
Carter, D.: PS-TuP9, 115
Carter, J.: VT-WeM4, 150; VT-WeM5, 150
Caruso, A.N.: MI-MoA8, 40
Caruso, L.: VT-TuM10, 77
Casadio, F.: CS-ThA3, 205
Caspar, J.V.: EN+AS+EM-WeA3, 160
Cassidy, C.: EM-MoA1, 34
Castle, J.E.: AS-ThP9, 231
Castle, J.R.: BI+AS+MN+NS-TuM4, 57
Castner, D.G.: AS+BI+MC+SS-MoA9, 31; BI+AS-MoM8, 7
Castro, F.A.: TF+AS-FrM9, 261
Caubet, P.: MC+AP+AS-MoM10, 11; SS+EM-FrM9, 260
Cava, R.J.: MI-MoA8, 40
Cavanagh, A.S.: TF+EN+PS-TuA8, 102
Cease, H.: VT-WeM4, 150; VT-WeM5, 150
Ceballos-Sanchez, O.: AS+MC-MoM2, 5
Celano, U.: MC+AP+AS-MoM1, 10
Celio, H.C.: EM+EN+TF-WeA7, 158
Centrone, A.: NS+AS-WeA7, 166; NS-ThP3, 238
Cerna, R.: EM-TuP26, 109
Cerqueira S. Jr., A.C.: MS-ThP9, 238
Ceza, M.: SS-TuP23, 123
Chabal, Y.J.: EN+EM+MN+NS+TR-MoA3, 36; NS+HI-TuM11, 65; SD-WeM3, 144; SS+AS+NS-ThA8, 223
Chae, J.: 2D+EM+MI+MN+NS+SS+TF-ThA4, 203; NS-ThP3, 238
Chagarov, E.A.: EM+2D-TuA4, 84; EM1-ThA9, 209; EN+AS+EM+SE-WeM4, 132; SD-WeM12, 145
Chakraborty, D.: NS+SE-MoM5, 13
Chan, K.K.: MC+2D+AP+AS-MoA1, 37
Chandhok, M.: PS-TuP13, 116
Chandrasekhar, M.V.S.: 2D+AS+BI+PS+SS-TuM11, 54
Chang, C.-H.: EM+EN+TF-WeA8, 158
Chang, C.M.: MS-ThP7, 237
Chang, F.Y.: MS-ThP4, 237; PS-MoM8, 15
Chang, H.J.: BI+MG-WeA12, 157
Chang, H.W.: PS-TuP23, 117
Chang, J.P.: PS-MoM5, 15; TF+EN+PS-TuA2, 101; TF+PS+SE-MoM10, 23; TF+PS-TuM4, 73; TF+PS-TuM5, 73
Chang, L.: CS-ThA3, 205
Chao: MC+2D+AP+AS-MoA10, 39
Chapleski, R.: SS-TuP4, 120
Charalambopoulou, G.: EN-TuP14, 112
Chaudhuri, A.R.: EM1-ThA11, 210
Chaukulkar, R.P.: TF+EN+PS-TuA11, 102
Chavez, J.: EM-TuP5, 106
Chawla, J.S.: EM-TuM12, 59; PS-TuP13, 116
Chen, A.: EM2-ThM5, 186
Chen, C.: 2D+AS+HI+MC+NS+PS+SP+SS-TuA4, 79; MS-ThP4, 237
Chen, C.-C.: EN+AS+EM+SE-WeM5, 132
Chen, C.L.: MS-ThP4, 237
Chen, C.W.: PS-TuP20, 117
Chen, D.A.: SS+EN-MoA3, 47; SS-TuP17, 122
Chen, F.Z.: MC-TuP7, 113; VT-TuP2, 123
Chen, G.: EM1-ThM3, 185
Chen, H.-P.: TF-ThP4, 241
Chen, H.S.: EM+EN-FrM5, 252
Chen, H.T.: EM+EN-FrM5, 252
Chen, J.: MI+MG-TuM5, 63
Chen, J.K.: PS-MoM5, 15
Chen, J.Z.: EM+NS+TF-FrM5, 253
Chen, L.: EM-WeA4, 159; MS-ThP4, 237; PS2-WeM5, 142
Chen, M.: SS+EM-FrM3, 259
Chen, N.: MS+PS+TF-ThM10, 189
Chen, P.L.: MN-ThP2, 236; MS-ThP6, 237
Chen, S.: BI+AS+NS-MoA7, 33
Chen, W.C.: PS-TuP7, 115
Chen, W.H.: EM+EN-FrM5, 252
Chen, X.: NS-WeM12, 140; PS1-FrM3, 254; SS+EN-MoA8, 48; TF+EN+PS-TuA7, 101
Chen, X.G.: EL+AS+EM+MC+SS-ThA3, 207
Chen, Y.C.: MS+PS+TF-ThA11, 213
Cheng, C.-W.: MC+2D+AP+AS-MoA1, 37
Cheng, G.: 2D+AS+BI+PS+SS-TuM10, 53
Cheng, I.C.: EM+NS+TF-FrM5, 253
Cheng, K.: TF-ThA11, 226
Cheng, L.: 2D-ThP17, 229; SD-WeA11, 172
Cheng, S.-Y.: PS-MoM8, 15
Chennadi, S.: PS1-WeM5, 140
Cheong, S.-W.: MI+MG-TuA7, 90; MI-MoA9, 40
Cherala, A.: NS+HI-TuM11, 65
Cherkaoui, K.: EM+2D-TuA8, 84
Chernatynskiy, A.: MG-WeM4, 136
Chermomordik, B.D.: EN+AS+EM+SE-WeM3, 132
Chervin, C.N.: EM+EN+TF-WeA11, 158
Cheung, K.: TF+PS-TuM3, 72
Cheung, W.S.: VT-TuP3, 123
Chevalier, N.: 2D+EM+MI+MN+NS+SS+TF-ThA10, 204; AS-ThP3, 231; SP+AS+BI+NS+SS-ThA4, 221
Chevalier, X.: SD-WeA9, 172
Chhowalla, M.: 2D+AS+BI+PS+SS-TuM1, 53
Chiang, D.: TF-ThP23, 243; TF-ThP4, 241
Chiang, S.: SS+NS-TuA12, 99
Chiavetta, D.: TF-ThA3, 224
Chiba, Y.: PS-TuA3, 95
Chien, D.: TF+PS-TuM4, 73
Chikyo, T.: EM+NS+TF-FrM10, 253; EM-TuP8, 107
Chilkoti, A.: BI+AS-MoM4, 7
Chiluwal, U.: PS1+TF-ThM3, 190
Chin, G.: EL-ThP4, 234
Chiou, J.S.: PS-TuP7, 115
Chirita, V.: TF+PS+SE-MoM4, 22
Chithambo, L.: 2D-ThP7, 228
Chiu, H.-Y.: MN+PS-WeA8, 163
Chiu, P.-K.: TF-ThP23, 243; TF-ThP4, 241
Cho, B.: HI-ThP1, 235; VT-TuA4, 103
Cho, H.: SA-TuA11, 97
Cho, J.: TF+EN+PS-TuA2, 101
Cho, K.J.: EM+EN+TF-WeA3, 157
Chobpattana, V.: EM-WeA12, 160
Chocron, S.E.: BI+AS+MN+NS-TuM3, 57
Choi, D.: MC+AP+AS-MoM6, 11; TF-ThP26, 244
Choi, H.K.: NS+EN-MoA4, 41
Choi, J.: PS-MoA8, 43
Choi, J.S.: NS+EN-MoA4, 41
Choi, K.M.: VT-TuP3, 123
Choi, S.: EM-TuM3, 58
Choi, S.C.: EM-TuP25, 109
Choi, S.G.: EL+AS+EM+EN+SS-ThM3, 183
Chong, H.: MC-TuP4, 113
Chopra, S.N.: EM+MI+NS-MoM11, 9; EM1-ThA10, 210; SD-WeM10, 144
Chou, C.Y.: PS-TuP23, 117
Choudhury, F.A.: PS2-FrM4, 256; PS-TuP12, 116
Choudhury, P.: EM1-ThA9, 209; EM-WeA3, 159
Christopher, P.: EN+AS+EM+SE-TuM3, 60
Chu, N.N.: MS-ThP7, 237; SP+AS+EM+NS+SS-ThP5, 240
Chu, S.: BI+AS+MN+NS-TuM2, 56; EN+EM+NS-TuA10, 87
Chu, Y.-H.: MI+EM-MoM2, 12; MI+MG-TuM11, 64; MI+MG-TuM12, 64
Chuang, C.Y.: SS+AS-WeM12, 148
Chung, B.W.: AC+AS+MI+SA+SS-MoA6, 29
Chung, N.-K.: HI-ThP1, 235
Chung, W.-C.: MN+NS-TuA11, 92

- Church, J.: AS+MC+SS-FrM5, 248
Cieslar, M.: AC+AS+MI+SA+SS-MoM9, 4
Ciftlikli, E.Z.: SS-WeA7, **175**
Ciobanu, C.V.: 2D+EM+NS+PS+SS+TF-MoM10, 3
Ciochon, P.: SS+AS+NS-ThA1, 222
Ciofi, I.: EM-TuM6, 59
Ciridon, W.: SM+AS+BI+PS-ThM10, 195
Clark, B.: TF+AS+EM-TuA1, 99
Clark, D.: AC+AS+MI+SA+SS-MoM1, 3; CS-ThA9, 206
Clark, D.H.: PS1-FrM11, 255
Clark, K.: SP+2D+AS+EM+MC+NS+SS-ThM11, 197; SP+2D+AS+EM+MC+NS+SS-ThM6, 196
Clark, S.M.: EM1-ThM6, **185**
Clarke, J.M.: TF+AS-FrM3, 260
Clarke, R.: EN+AS+EM+SE-WeM11, 133
Clavel, M.: MC+AP+AS-MoM11, 12
Clavero, C.: SE+PS+TF-MoA7, 46
Clayton, C.R.: IS+AS+MC+SS-TuA12, 89
Clendenning, S.B.: SD-WeA7, 171
Cleveland, E.: SS+EM-FrM5, **259**
Clifton, P.H.: AP-ThP1, 230
Cobert, C.: EL+AS+EM+EN+SS-ThM12, **184**
Coclite, A.M.: TF-MoA9, **51**
Coffey, K.R.: MC+AP+AS-MoM6, 11; TF-ThP26, 244
Cohen, G.: MC+2D+AP+AS-MoA1, 37
Cohen, H.: AS-ThP20, 233; EN+EM+MN+NS+TR-MoA8, **36**
Cohen, S.R.: TR-FrM3, **262**
Cojocaru-Mirédin, O.: AP+AS+MC+NS+SS-ThM3, **180**
Colby, R.J.: AP+AS+EN+NS+SS-ThA4, 205; EM-MoA3, 34
Cole, J.: PS-ThA7, **217**
Coley, W.: 2D-ThP11, 229
Collazo, R.: EM+EN-FrM11, 252; MG-WeM3, 135
Collette, S.: PS+2D-WeA10, **168**
Collins, K.: PS2+TF-ThM3, 192; PS2-WeM1, 141; PS2-WeM2, 142; PS2-WeM4, 142; PS2-WeM6, 143
Collins, R.W.: EL+AS+BI+EM+SS-FrM5, 250; EL+AS+EM+EN+SS-ThM4, 183; EL-ThP5, 234; EN+AS+EM+SE-WeM12, 133
Colombo, L.: EM-WeA4, 159
Colvin, B.: TF-ThA6, 225
Comfort, E.: 2D+EM+MS+NS-FrM4, 245
Conard, T.: SA-TuP1, 119
Conley, J.F.: EM2-WeM13, 131; EM2-WeM2, 130
Conley, Jr., J.F.: BI+AS+MN+NS-TuM4, 57; EM2-WeM12, **131**
Contreras, Y.D.: EM-TuP2, 106
Conway, J.: VT-WeA1, 177
Cook, B.: EN+AS+EM+SE-TuM12, 60
Cook, R.F.: IS+AS+MC+SS-WeM12, 135
Cook, S.R.: PS-TuP13, 116
Cook-Chennault, K.: EM+EN+TF-WeA1, **157**
Cooke, M.: EM-TuM6, 59
Cooks, R.G.: AS+BI+VT-TuM3, 55
Cooper, K.P.: MS+PS+TF-ThM12, **189**
Cooperstein, M.A.: SM+AS+BI+PS-ThA3, 220
Corbett, J.: SS-WeA9, 175
Cordell, J.J.: EN+AS+EM+SE-WeM6, 133; TF-ThP17, **242**
Cordin, M.: SS+AS+EN-MoM3, 19; SS-TuP5, 130
Cornejo, J.: BI+AS+MN+NS-TuM12, 57
Costolo, M.A.: PS-ThA2, 216
Cotte, M.: CS-ThA6, 206
Cottle, H.: PS-TuA8, 95; PS-TuA9, **95**
Coults, S.J.: AS+BI+MC+SS-MoA8, 31; AS+BI+MC-WeA1, 154
Coulter, K.: SE+EM+EN+PS+TF-MoM5, 18; SE+NS+TR-TuM12, 70
Counou, D.: PS1-FrM11, 255
Counsell, J.D.P.: AS+BI+MC+SS-MoA8, **31**; AS+BI+MC-WeA1, 154; AS-ThP10, 232
Cournoyer, J.R.: EN-TuP16, 112
Covelli, D.: BI+AS-MoM5, 7
Covert, P.A.: BI+AS-WeM3, 128
Cowen, J.: AS-ThP25, 234
Coy-Diaz, H.: 2D+AS+EM+NS+SS-MoA6, 28
Craighead, H.G.: BI+AS+NS-MoA10, 34; MN+PS-WeA9, 163
Creatore, M.: PS-ThA10, 218; TF+EN+PS-TuA12, **103**; TF-ThA4, 225
Cristaudo, V.: PS+2D-WeA10, 168
Crommie, M.F.: 2D+EM+MS+NS-FrM3, 245
Crum, J.: AP+AS+NS+SS-FrM4, 247
Crumlin, E.J.C.: IS+2D+MC+NS+SP+SS-WeA10, **162**
Cruz, M.: SS-TuP9, 120
Cui, J.: AP+AS+MC+NS+SS-ThM12, 181
Cui, X.Y.: SA-MoM3, 183
Cui, Y.: BI+AS-TuA12, 86; EM-TuP31, **110**
Culbertson, J.: 2D+AS+EM+NS+SS-MoA3, 28
Cullen, P.J.: SE+EM+EN+PS+TF-MoM6, 18
Cullen, W.G.: 2D+AS+HI+MC+NS+PS+SP+SS-TuA9, 79
Cultrera, L.: VT-WeA1, 177
Culver, J.: EN+EM+NS-TuA10, 87; EN+EM+NS-TuA9, 86
Cumpson, P.J.: AS+BI+MC-WeM6, 127; AS+MC-MoM6, 5; CS-ThA8, 206; HI+2D+AS+MC-ThA3, 211
Cun, H.Y.: 2D+AS+EM+NS+SS-MoA1, 28
Cunge, G.: PS+2D-WeA1, 166; PS2-FrM2, 256; PS-WeA2, 169; SD-WeA9, 172
Curiel Alvarez, M.A.: TF-ThP15, 242
Currie, M.: TF+PS-TuM3, 72
Cushing, G.: SS+AS+EN-WeM12, 146
Cushshall, D.B.: AS+MC+SS-FrM10, 248
Cuvilly, F.: AP+AS+NS+SS-FrM5, 247
Cwiernia, E.: CS-ThA8, 206
Cyganik, P.: SS+TF-ThM6, 198; TF-MoA4, **50**
— **D** —
Dahanayaka, D.: MC+2D+AP+AS-MoA11, **39**
Dai, J.-X.: MI-MoA9, **40**
Dallarto, S.: NS+HI-TuM1, 64
Dalmau, R.: MG-WeM3, 135
Dameron, A.: TF+EN+PS-TuA11, 102
Dandley, E.C.: BI+AS+NS-MoA1, **32**; TF+PS-MoA2, 48
Daniel, L.: PS2-FrM9, 257
Daniel, R.: SE+NS+TR-TuM11, 70
Darakchieva, V.: EL+AS+EM+MC+SS-ThA9, 208
Darnon, M.: PS2-FrM2, 256; PS-TuA7, 95; PS-WeA2, 169
Das, L.: AS+MC+SS-TuA10, **81**
Datta, S.: EM2-WeM5, **131**; PS1+TF-ThM4, 190
Davidson, R.B.: PS2-FrM3, 256
Davies, M.C.: BP+BI+AS-SuA5, **1**
Davies, S.: VT-TuP4, 123
Davis, A.: 2D-ThP1, 228; SS+EM-FrM9, **260**
Davis, C.S.: MS+PS+TF-ThM10, **189**
Davis, R.C.: EM+EN+TF-WeA9, 158; MN+PS-WeA3, 163; MN+PS-WeA4, **163**; MN+PS-WeA9, 163; TF+AS-FrM2, 260; TF+EM+EN-WeA11, 177; TF+PS-ThM6, 200; TF-ThP19, 242
Davydov, A.V.: MI-MoA10, 40
Davydova, A.O.: PS+2D-WeA1, 166
Dazzi, A.: NS+AS-WeA9, 166
De Boer, J.: BI+MG-WeA9, 157
De Decker, Y.: AP+AS+EN+NS+SS-ThA3, 204
de Heer, W.A.: 2D+AS+HI+NS+SS-ThM10, **180**
de Leeuw, N.H.: MG-WeM12, 136
de Marneffe, J.-F.: EM-TuM6, **59**; PS-MoM4, **15**; PS-TuP12, 116
de Martino, A.: EL+AS+BI+EM+SS-FrM3, 250
de Peuter, K.: SD-WeM6, 144
de Sousa, R.R.M.: TF+PS-ThM13, 201
de Temmerman, G.: PS-ThA9, 217
De Vos, C.: PS-ThA6, **217**
de Vries, H.W.: TF-ThA10, 226
Dean, C.R.: 2D+EM+MI+MN+NS+SS+TF-ThA4, 203
DeBenedetti, W.J.I.: SD-WeM3, 144; SS+AS+NS-ThA8, 223
DeBoer, W.: VT-WeM3, 150
DeCerbo, J.N.: EM-TuP18, 108
Dechene, J.: PS-TuA8, 95
Decoster, S.: EM-TuM6, 59
Dedrick, J.: PS+SE-ThA10, 215
Deeks, C.: AS+MC+SS-TuA3, **80**
DeGhetaldi, K.: CS-ThA9, 206
DeHaan, G.A.: AS+BI+MC-WeA8, 155
Delcorre, A.: PS+2D-WeA10, 168; PS+2D-WeA11, 168
Delgadino, G.: PS2+TF-ThM2, 192
DellaValle, R.G.: TF+AS-FrM10, 262
Demaree, J.: MC+2D+AP+AS-MoA2, **37**
DeMasi, A.: SA-MoM4, 17
Demeulemeester, J.: MC+AP+AS-MoM1, 10
Demirkan, K.: EN+AS+EM+SE-WeM2, 132
Demkov, A.A.: EM+MI+NS-MoM11, 9; EM+MI+NS-MoM3, 8; EM1-ThA10, 210; EM2-WeM10, **131**
Dendooven, J.: TF+MS+PS-WeM10, **149**
Deng, W.: SP+2D+AS+EM+MC+NS+SS-ThM11, 197
Deng, X.: SS+EN-MoA7, 47; SS+NS-TuA4, **98**
D'Epifanio, A.: TF+EN+PS-TuA12, 103
Deprosio, MC+2D+AP+AS-MoA10, 39
DeRose, C.: TF-ThP20, 243
Derouin, J.: SS+EN-MoA9, 48
Derry, G.: SS-TuP12, **121**
Derzsi, A.: PS1-FrM6, 255
Deshmukh, S.: PS2+TF-ThM2, 192
Despiau-Pujo, E.: PS+2D-WeA1, **166**; PS2-FrM2, 256
Detavernier, C.: TF+MS+PS-WeM10, 149
Detlefs, B.: SA-TuA12, 97; TF+AS-FrM8, 261
Deutsch, T.G.: SS+EN-MoM9, 22
Devaraj, A.: AP+AS+MC+NS+SS-ThM12, 181; AP+AS+MC+NS+SS-ThM6, 181; AS+MC+SS-TuA9, 81
Dezelah, C.: TF+PS-MoM1, **24**
Dhayal, M.: MN+PS-WeA10, **163**
di Carlo, A.: TF+EN+PS-TuA12, 103
di Giacomo, F.: TF+EN+PS-TuA12, 103
Diao, Z.: MN-WeM10, 137
Diaz, J.: MS+TF-WeA3, 164
Dick, D.: NS+HI-TuM11, 65
Diebold, A.C.: MC+AP+AS-MoM3, **10**; MC-TuP4, 113
Diercks, D.R.: AP+AS+NS+SS-FrM1, **246**
Dietrich, R.: BI+AS+MN+NS-TuM3, **57**
Dietz, N.: EM+EN-FrM11, 252; EM-TuP15, 108; EM-TuP17, 108
DiGregorio, J.F.: PS-TuM3, 66
Dijon, J.: 2D+EM+MI+MN+NS+SS+TF-ThA10, 204
Dil, J.H.: 2D+EM+MI+MN+NS+SS+TF-ThA6, **203**
Dille, J.: PS-ThA6, 217
Dillon, E.: NS+AS-WeA9, 166
Dillon, R.J.: SS+AS+EN-MoM1, 19
Dindar, A.: MS+TF-WeA3, 164
Dingeman, T.: TF+AS-FrM10, 262
Dingemans, G.: TF+EN+PS-TuA9, 102
Diniz, J.A.: 2D-ThP8, 228; NS-ThP7, 239; TF-ThP15, 242
DiStefano, J.: 2D+AS+HI+MC+NS+PS+SP+SS-TuA3, 79
DiStefano, S.: VT-WeM3, 150
DiTusa, M.F.: SS+TF-ThM12, 198
Diwan, A.: AC+AS+MI+SA+SS-MoM10, 4; TF+EM+EN-WeA11, 177; TF+EM+EN-WeA7, **176**; TF-ThP19, 242
Dixson, R.G.: SP+AS+BI+NS+SS-WeA4, 173
Djara, V.: EM+2D-TuA8, 84
Doan, K.: PS-TuA10, 96
Dogan, I.: PS-ThA1, 216

Dohnalek, Z.: SS+AS-WeM13, **148**
 Doi, I.: 2D-ThP8, **228**
 Dollery, C.T.: AS+BI+MC-WeM13, **127**
 Dombrowski, E.: SS+AS+EN-WeM11, **146**
 Dominguez, J.: EM1-ThA6, **209**
 Donald, S.B.: SS+AS+EN-WeM12, **146**
 Donath, M.: MI-MoA3, **39**; MI-MoA4, **40**
 Donetsky, D.: MC+AP+AS-MoM4, **10**
 Dong, H.: EM+2D-TuA7, **84**
 Dong, X.: QC+AS+BI+MN-ThA3, **218**;
 SM+AS+BI+PS-ThM10, **195**
 Donko, Z.: PS1-FrM6, **255**
 Donnelly, V.M.: PS1-FrM10, **255**; PS1-FrM9, **255**;
 PS-TuM5, **66**; PS-TuP3, **114**
 Dorf, L.: PS2+TF-ThM3, **192**; PS2-WeM4, **142**
 Dorgan, V.E.: EM1-WeM12, **130**
 Dorman, J.: EM2-ThA8, **210**;
 EN+EM+MN+NS+TR-MoA10, **36**
 dos Remedios, C.G.: SM+AS+BI+PS-ThA6, **220**
 Doscher, H.: SS+EN-MoM9, **22**
 Douidin, B.: MI+MG-TuM5, **63**
 Douidin, N.: SS+AS+EN-TuM5, **71**
 Dougherty, D.B.: AS+MC+SS-FrM9, **248**;
 MI+EM-MoM10, **12**; SS+AS+EN-WeM3, **145**
 Douglas, E.: TF-ThP20, **243**
 Douglas, R.: MI+MG-TuM13, **64**
 Dovidenko, K.: EN-TuP16, **112**
 Dowben, P.A.: 2D+EM+MI+MN+NS+SS+TF-
 ThA8, **203**; EM+MI+NS-MoM10, **9**; MI+MG-
 TuM5, **63**; MI-MoA11, **41**; PS1+TF-ThM3,
190
 Drayman-Weisser, T.: CS-FrM5, **249**
 Dremel, M.: VT-WeA7, **178**
 Driver, M.: MI-MoA11, **41**
 Drobny, G.: BI+AS-WeP6, **128**
 Droopad, R.: EM1-ThA9, **209**; EM-WeA12, **160**;
 SD-WeM12, **145**
 Drozdenko, D.: AC+AS+MI+SA+SS-MoM9, **4**
 Druce, J.: EN+AS+EM+SE-WeM2, **132**
 Du, D.: EM-MoA3, **34**
 Du, H.: EL+AS+BI+EM+SS-FrM5, **250**
 Du, S.X.: 2D+AS+EM+NS+SS-MoA10, **29**
 Du, W.: EM+EN+TF-WeA1, **157**
 Du, X.: BI+AS+MN+NS-TuM4, **57**
 Dubois, J.: PS-WeA2, **169**
 Dubois, P.: PS+2D-WeA7, **167**
 Dubourdiou, C.: EM+MI+NS-MoM8, **9**
 Duerloo, K.-A.N.: 2D+AS+EM+MI+MN+NS+TF-
 WeA12, **154**
 Duerr, H.: MI+EM-MoM11, **13**
 Duerrbeck, S.: SS+AS+EN-MoM3, **19**; SS-TuP5,
120
 Dufour, T.R.: PS+2D-WeA10, **168**; PS+2D-
 WeA12, **168**
 Dugger, M.T.: TF+PS+SE-MoM8, **23**
 Duke, A.S.: SS+EN-MoA3, **47**
 Dumesic, J.A.: SS+AS-WeM3, **147**
 DuMont, J.W.: TF+MS+PS-WeM12, **150**
 Dunham, B.: VT-WeA1, **177**
 Dunn, B.: TF+EN+PS-TuA2, **101**
 Dupuy, E.: PS-MoM9, **16**
 Duran, A.: SS-TuP9, **120**
 Durand, C.P.: SP+2D+AS+EM+MC+NS+SS-
 ThM10, **197**; SP+2D+AS+EM+MC+NS+SS-
 ThM11, **197**
 Durbin, S.: EN+AS+EM+SE-WeM11, **133**
 Durcan, C.: NS+AS-WeA10, **166**;
 SP+AS+BI+EM+NS+SE+SS-FrM5, **258**
 Durke, E.M.: AS+MC-MoM10, **6**; AS-ThP16, **232**;
 IS-ThP3, **236**; PS-TuP15, **116**
 Durr, M.: AS+BI+MC+SS-MoA10, **31**
 Dwyer, K.J.: EM1-ThA3, **208**
 Dzara, M.: AS-ThP24, **233**
 Dziaugys, A.: 2D+EM+MI+MN+NS+SS+TF-
 ThA9, **204**

— E —

Eaton, T.R.: HI-ThP3, **235**
 Ebnonnasir, A.: 2D+EM+NS+PS+SS+TF-MoM10,
3

Echeverria, E.: PS1+TF-ThM3, **190**
 Echtenkamp, W.: MI+MG-TuA3, **90**
 Economou, D.J.: PS1-FrM10, **255**; PS1-FrM9,
255; PS-TuP3, **114**
 Eddy, C.R.: EM1-ThM12, **185**; EM1-WeM10,
130; MC+2D+AP+AS-MoA4, **38**; PS1+TF-
 ThM11, **191**; TF+PS-TuM3, **72**
 Eddy, Jr., C.R.: EM1-WeM5, **129**; SA-MoM4, **17**
 Edelstein, D.C.: EM-TuM1, **58**
 Edinger, K.: MG-TuA3, **89**
 Edmonds, J.M.: IS-ThP3, **236**
 Edmonds, M.: EM1-ThA9, **209**; EM-WeA12, **160**;
 SD-WeM12, **145**
 Edström, D.: TF+PS+SE-MoM4, **22**
 Efstathiadis, H.: EL-ThP3, **234**
 Egan, P.F.: VT-MoM3, **26**
 Ehret, S.: QC+AS+BI+MN-ThA4, **219**
 Eichelbaum, M.: IS+AS+MC+SS-TuM1, **61**
 Eichelsdoerfer, D.J.: NS+SE-MoM11, **14**
 Eichfeld, S.M.: 2D+EM+NS+SS+TF-WeM6, **125**
 Eichhorn, B.: CS-ThM12, **182**
 Eickholt, P.: MI-MoA3, **39**
 Eigenfeld, N.T.: TF+PS-TuM10, **73**
 Einstein, T.L.: 2D+AS+EM+MI+MN+NS+TF-
 WeA8, **153**; SS+AS-WeM11, **148**
 Eisele, N.B.: QC+AS+BI+MN-ThA4, **219**
 Eizenberg, M.: EM1-ThA11, **210**
 Ekerdt, J.G.: EM+MI+NS-MoM11, **9**; EM1-
 ThA10, **210**; SD-WeM10, **144**
 El Zubir, O.: BI+AS+NS-MoA6, **33**
 Elam, J.W.: TF+PS-MoM10, **25**
 Eldred, J.: VT-WeM13, **151**
 Elisabeth, S.: TF+AS+EM-TuA3, **99**
 Eliseev, E.: 2D+EM+MI+MN+NS+SS+TF-ThA9,
204
 Elkatmis, A.: VT-MoM5, **26**
 Ellies, L.: BI+MG-WeA4, **156**
 Ellinger, C.R.: SD-WeM11, **144**
 Elliott, S.D.: SD-WeM5, **144**; SD-WeM6, **144**
 Ellsworth, A.A.: NS+AS+SS-TuA8, **94**
 Elmustafa, A.A.: VT-WeA4, **177**
 ElNaggar, M.E.: AS+BI+VT-TuM10, **56**
 Elsässer, C.K.V.: MG-TuA1, **89**
 El-Sayed, H.A.: NS-ThP5, **238**
 Emelianenko, M.: MG-TuA7, **90**
 Emmelkamp, J.: TF+AS+EM-TuA2, **99**
 Empante, T.: 2D+EM+NS+SS+TF-WeM10, **126**;
 2D-ThP11, **229**
 Enders, A.: SS+TF-ThM11, **198**
 Engelhard, M.H.: AS-ThP8, **231**; BI+AS+NS-
 MoA7, **33**; EM-MoA3, **34**
 Engel-Herbert, R.: PS1+TF-ThM4, **190**
 Engelmann, S.U.: PS2+TF-ThM1, **191**; PS-
 MoM10, **16**; PS-MoM3, **14**
 Engeln, R.: PS+SE-ThA6, **214**
 English, C.D.: EM1-WeM12, **130**
 Ercius, P.: EN+AS+EM+SE-WeM2, **132**
 Erdem, M.G.: SA-MoM4, **17**
 Erdemir, A.: TR-ThA6, **227**
 Erickson, K.: SP+AS+BI+NS+SS-WeA11, **174**
 Eriguchi, K.: PS1-WeM12, **141**; SE+NS+TR-
 TuM3, **70**
 Erkoç, S.: MI-TuP4, **114**
 Ernstoff, J.: 2D-ThP15, **229**
 Ershov, S.: PS+2D-WeA7, **167**
 Ertekin, E.: SS+AS+EN-TuM6, **71**
 Erwin, S.C.: VT-MoA10, **52**
 Escamilla, R.: SS-TuP9, **120**
 Escher, M.: EW-WeA6, **161**
 Espinosa-Magaña, F.: AS+MC-MoM11, **6**
 Eto, K.: SP+AS+BI+NS+SS-WeA3, **173**
 Evans, J.E.: AP+AS+NS+SS-FrM8, **247**; BI+AS-
 TuA11, **83**
 Evans, J.W.: SS+AS-WeM10, **148**
 Evans, P.: TF-ThP21, **243**
 Everitt, H.O.: MS+PS+TF-ThA3, **213**
 Exarhos, S.: EM-MoA4, **34**
 Eyben, P.: MC+AP+AS-MoM1, **10**

— F —

Fabert, S.: TF+PS+SE-MoM3, **22**
 Facchini, C.F.R.: EN-TuP15, **112**
 Facsko, S.: 2D-ThP18, **230**; HI-ThP6, **235**
 Fadley, C.S.: SA-MoM1, **16**
 Fairbrother, D.H.: SS+AS+EN-MoM11, **20**;
 SS+EN-MoA6, **47**; TF+PS-ThM11, **200**
 Fallet, M.: SS+AS-WeM5, **147**; TR-FrM6, **263**;
 TR-ThA8, **227**
 Fan, R.: EM+EN+TF-WeA9, **158**
 Fanelli, F.: PS+SE-ThA1, **214**
 Fang, Z.: MS+PS+TF-ThA10, **213**; MS+PS+TF-
 ThA11, **213**; MS+TF-WeA9, **165**
 Faradzhev, N.S.: TF+PS-ThM11, **200**
 Farahbakhsh, N.: MS+TF-WeA12, **165**
 Faraz, T.: PS-ThA10, **218**
 Farber, R.: SS+EN-MoA9, **48**
 Farouk, B.: PS+2D-WeA8, **167**
 Farrell, R.: PS-TuA3, **95**
 Favero, I.: MN-WeM6, **137**
 Favero, P.: CS-ThA1, **205**
 Fedchak, J.A.: VT-MoM6, **27**
 Fedorov, A.V.: MI-MoA8, **40**
 Fedrizzi, L.: TF+PS-TuM1, **72**
 Feenstra, R.M.: 2D+EM+NS+PS+SS+TF-MoM6,
2; SP+2D+AS+EM+MC+NS+SS-ThM6, **196**
 Feibelman, P.J.: NS-WeM6, **139**
 Feigelson, B.N.:
 2D+AS+HI+MC+NS+PS+SP+SS-TuA9, **79**
 Feldberg, N.: EN+AS+EM+SE-WeM11, **133**
 Feldman, L.C.: HI+2D+AS+BI+MC-ThM13, **188**
 Felmy, A.: AP+AS+EN+NS+SS-ThA4, **205**
 Felts, J.R.: 2D+AS+BI+PS+SS-TuM6, **53**
 Feng, P.X.-L.: 2D+EM+MS+NS-FrM5, **245**; 2D-
 ThP20, **230**; MN+NS-TuA10, **92**; MN+PS-
 WeA11, **164**; MN+PS-WeA7, **163**; MN+PS-
 WeA8, **163**; MN-WeM13, **138**; PS2-FrM11,
257
 Feng, X.: NS-WeM6, **139**
 Feng, Y.: MN+NS-TuA3, **91**
 Ferguson, I.T.: EM+EN-FrM11, **252**; EM-TuP15,
108; EM-TuP17, **108**
 Fernandez, P.R.: PS+2D-WeA8, **167**
 Fernandez, T.L.: SM+AS+BI+PS-ThA9, **221**
 Fernsler, R.F.: PS-WeA11, **171**
 Ferrari, M.: BP+BI+AS-SuA3, **1**
 Fête, A.: MI+EM-MoM3, **12**
 Filikhin, I.N.: NS-ThP9, **239**
 Filippov, A.: SS+EM-FrM4, **259**
 Filler, M.A.: NS+AS+SS-TuA1, **93**
 Finckenor, M.: TF+EM+EN-WeA1, **175**
 First, P.N.: SP+2D+AS+EM+MC+NS+SS-ThM3,
196
 Fischer, D.A.: SA-MoM10, **17**
 Fischer, P.: MI+MG-TuM6, **63**
 Fischetti, M.V.: EM-WeA7, **159**
 Fisher, B.L.: 2D+EM+NS+SS+TF-WeM3, **125**
 Fisher, E.R.: PS2-FrM3, **256**; SM+AS+BI+PS-
 ThA8, **221**; SM+AS+BI+PS-ThM11, **195**;
 SM+AS+BI+PS-ThM5, **195**; SS+NS-TuA3, **98**
 Fisher, G.L.: AS+BI+MC+SS-MoA11, **32**;
 AS+BI+MC-WeA2, **154**
 Fitz-Gerald, J.M.: SE+PS+TF-MoA9, **46**; TF+SE-
 TuM11, **75**
 Fitzpatrick, J.: HI+2D+AS+BI+MC-ThM10, **188**
 Flavel, B.S.: HI-ThP3, **235**
 Fleischmann, C.: SA-TuA12, **97**; SA-TuP1, **119**
 Fleuriel, J.P.: EN+AS+EM+SE-TuM13, **60**
 Fliervoet, T.: HI+2D+AS+MC-ThA8, **212**
 Flores, M.: TR-ThP4, **244**
 Flores-Gracia, F.J.: EM-TuP30, **110**
 Flynn, B.T.: NS+HI-TuM5, **65**
 Flynn, K.: EW-TuM8, **61**; VT-TuM12, **77**
 Foerch, R.: SM+AS+BI+PS-ThM3, **195**
 Foley, A.: SS-WeA9, **175**
 Foltz, B.: AS-ThP13, **232**
 Foos, E.E.: EM-MoA10, **35**; EM-TuP20, **109**
 Forster, A.M.: MS+PS+TF-ThM10, **189**
 Fortunato, E.: EM+NS+TF-FrM8, **253**

- Foucher, M.: PS-WeA1, **169**
 Fouchier, M.: PS-MoM6, **15**; PS-MoM9, 16
 Fowlkes, J.: NS+HI-TuM10, 65;
 SP+2D+AS+EM+MC+NS+SS-ThM10, 197;
 TF+PS-TuM6, 73
 Foxon, C.T.: SS+EN-MoM3, 21
 Fracassi, F.: PS+SE-ThA1, 214
 France, F.G.: CS-ThM5, **182**
 Franchini, C.: SS+AS+EN-MoM3, 19; SS-TuP5,
 120
 Francisco, R.: BI+AS-WeM13, 129
 François, R.F.: PS+2D-WeA12, 168
 Frank, M.M.: EM+MI+NS-MoM8, 9
 Frankel, D.J.: SE+NS+TR-TuM2, 69; TF+PS+SE-
 MoM9, 23
 Franquet, A.: MC+AP+AS-MoM1, 10
 Frantz, J.A.: VT-MoA10, 52
 Franz, G.F.: BI+AS-MoM2, 7
 Franz, R.: SE+PS+TF-MoA3, 45; SE+PS+TF-
 MoA7, **46**
 Frederick, R.: NS+HI-TuM5, 65
 Fredrickson, K.D.: EM+MI+NS-MoM3, **8**
 Fredriksson, H.: NS-WeM10, **139**
 Freitas, Jr., J.A.: EM1-ThM12, 185
 French, B.: 2D+AS+HI+MC+NS+PS+SP+SS-
 TuA3, **79**
 French, M.: 2D+AS+HI+MC+NS+PS+SP+SS-
 TuA3, 79
 Frenkel, A.: IS+AS+MC+SS-WeM3, 134;
 NS+AS+SS-TuA10, 94
 Frese, N.: HI+2D+AS+BI+MC-ThM12, **188**
 Freund, H.-J.: 2D+EM+NS+SS+TF-WeM12, 126
 Frey, S.: QC+AS+BI+MN-ThA4, 219
 Freymeyer, N.J.: EM-MoA11, 35
 Frick, J.R.: SS+NS-TuA11, 99
 Fricker, A.L.: CS-FrM6, **249**
 Fried, M.: EL-ThP6, **234**
 Friedman, A.: 2D+AS+EM+NS+SS-MoA3, 28
 Friedman, S.: SP+AS+BI+NS+SS-WeA10, **174**
 Frisch, J.: MI+EM-MoM11, 13
 Frolov, S.V.: VT-MoA10, 52
 Fryer, R.T.: TF+AS-FrM1, **260**
 Fu, C.: SS+EM-FrM1, 258
 Fu, J.: NS+HI-TuM11, 65
 Fu, K.: QC+AS+BI+MN-ThA8, **219**
 Fu, Z.: SA-MoM10, 17
 Fuchs, E.: NS+HI-TuM11, 65
 Fuentes-Hernandez, C.: MS+TF-WeA3, 164
 Fuhrer, M.S.: 2D+AS+HI+MC+NS+PS+SP+SS-
 TuA9, 79
 Fujii, H.: EN+EM+MN+NS+TR-MoA11, 37
 Fujii, K.: VT-MoM8, 27
 Fujita, D.: HI+2D+AS+BI+MC-ThM6, 188
 Fukasawa, M.: PS-TuM11, 67; PS-TuM4, 66; PS-
 TuP6, 114
 Fukuyama, A.: EN+EM+MN+NS+TR-MoA11,
 37; EN-TuP2, 110
 Futaba, D.: TF+PS-ThM1, **199**
 — **G** —
 Gaddam, S.: PS-TuP28, 118
 Gaddipati, P.: MC+2D+AP+AS-MoA4, 38
 Gaddy, B.E.: MG-WeM3, 135
 Gai, Z.: MI+MG-TuM10, 63
 Galhenage, R.P.: SS+EN-MoA3, 47; SS-TuP17,
122
 Gall, D.: EM-TuM12, **59**
 Gallagher, M.C.: SS+EM-FrM1, **258**
 Gallitognotta, A.: VT-TuM10, 77
 Galoppini, E.: SS+TF-ThM13, 199
 Gamage, S.: EM+EN-FrM11, **252**
 Gamble, L.J.: AS+BI+MC-WeA9, **155**; BI+AS-
 TuA10, **83**; BI+AS-TuA7, 82
 Gambogi, W.: AS-ThP13, 232
 Gammel, G.: PS1-WeM5, 140
 Gangarapu, S.: SS+EM-FrM4, 259
 Gans, T.: PS+SE-ThA10, 215
 Gantefoer, G.: SS+EN-MoA6, 47
 Gao, F.: SS-TuP6, **120**
 Gao, H.-J.: 2D+AS+EM+NS+SS-MoA10, 29;
 SS+AS+EN-WeM1, **145**
 Gao, Y.: 2D+EM+MI+MN+NS+SS+TF-ThA4,
 203; EN-TuP13, **112**
 Gapfizi, R.: PS1+TF-ThM3, 190
 Garcia Barros, M.: PS-MoA9, **43**
 Garcia, M.: MS+PS+TF-ThA1, 213
 Garcia, S.J.: TF-ThA4, 225
 Garcia-Caurel, E.: EL+AS+BI+EM+SS-FrM3, 250
 Garduño-Wilches, I.A.: TF-ThP22, **243**
 Gariglio, S.: MI+EM-MoM3, **12**
 Garris, R.L.: AS-ThP24, 233
 Gartstein, Y.: EN+EM+MN+NS+TR-MoA3, 36
 Garza-Hernandez, R.: EN-TuP9, 111
 Gaskell, K.J.: CS-ThM12, **182**
 Gaskill, D.K.: 2D+AS+BI+PS+SS-TuM5, 53;
 2D+AS+HI+MC+NS+PS+SP+SS-TuA9, 79;
 EM1-WeM10, 130; EM1-WeM5, 129
 Gassilloud, R.: PS1+TF-ThM5, 190
 Gassilloud, R.: MC+AP+AS-MoM10, 11
 Gates, G.: CS-FrM5, 249
 Gates, R.: TF+EM+EN-WeA11, 177
 Gautier, B.: EM+MI+NS-MoM8, 9
 Gebhardt, C.R.: AS+BI+MC+SS-MoA10, 31
 Geier, M.L.: 2D+AS+HI+NS+SS-ThM4, 179
 Geisler, H.: 2D+AS+HI+MC+NS+PS+SP+SS-
 TuA10, 80
 Gellman, A.J.: SS-WeA10, **175**; SS-WeA4, 174;
 SS-WeA8, 175; TF+AS+EM-TuA11, 100
 Geng, Y.: MI+MG-TuA7, 90
 George, S.M.: SS+EN-MoM9, 22; TF+EN+PS-
 TuA8, 102; TF+MS+PS-WeM12, **150**; TF+PS-
 MoM4, 24; TF+PS-TuM10, 73
 Gerasopoulos, K.D.: BI+AS+MN+NS-TuM2, 56;
 EN+EM+NS-TuA10, 87
 Gerbig, Y.B.: IS+AS+MC+SS-WeM12, 135
 Gerlach, M.: SA-TuM1, 68
 Gerson, Y.: MN+NS-TuA4, 92
 Gertsch, J.C.: TF+PS-TuM10, **73**
 Gerty, D.R.: VT-MoM3, 26
 Gessner, O.: SA-TuA3, **96**
 Gharbi, A.: PS-TuM13, 68
 Ghimire, K.: EL+AS+EM+EN+SS-ThM11, **184**
 Ghodssi, R.: BI+AS+MN+NS-TuM2, 56;
 BI+AS+MN+NS-TuM3, 57; EN+EM+NS-
 TuA10, 87; EN+EM+NS-TuA9, 86; MN+NS-
 TuA9, 92
 Ghosh, S.: EM1-ThA4, 208; EM1-ThA8, 209;
 EM1-ThM5, 185; EM-TuP5, 106; PS2-FrM11,
257; PS-TuP29, 118; TF+AS+EM-TuA12, **100**
 Giangregorio, M.: EL+AS+EM+EN+SS-ThM6,
 184
 Giannakopoulos, K.: EN-TuP14, 112
 Gibbons, S.: CS-ThM12, 182
 Gibson, Q.D.: MI-MoA8, 40
 Giles, S.L.: IS+AS+MC+SS-TuA12, 89
 Gillen, G.: AS+BI+MC+SS-MoA9, 31
 Gillette, E.: EN+EM+NS-TuA3, 85; TF+EN+PS-
 TuA7, 101
 Gillon, X.: PS-WeA8, 170
 Gilman, J.W.: MS+PS+TF-ThM10, 189
 Gilmore, I.S.: AS+BI+MC-WeM13, 127;
 AS+BI+VT-TuM5, **56**; AS+BI+VT-TuM6, 56
 Gil-Santos, E.: MN-WeM6, **137**
 Girolami, G.S.: TR-ThP2, 244
 Girshkevitz, O.: TR-FrM3, 262
 Gizeli, E.: QC+AS+BI+MN-ThM12, 194;
 QC+AS+BI+MN-ThM13, **194**
 Glaser, C.: EM-TuP16, 108
 Glassmaker, N.J.: AS-ThP14, 232
 Gleason, K.: TF-ThA1, **224**
 Glenn, S.: EL+AS+BI+EM+SS-FrM5, 250
 Glezakou, V.-A.: SS+AS-WeM13, 148
 Glumac, N.G.: TF+SE-TuM10, 75
 Gnerlich, M.: EN+EM+NS-TuA10, 87;
 EN+EM+NS-TuA9, **86**
 Go, D.B.: PS+SE-ThA3, 214
 Godet, S.: PS-ThA6, 217
 Godfroid, T.: PS+SE-ThA11, 215
 Godyak, V.A.: PS2+TF-ThM1, 191; PS-WeA9,
170
 Goeckner, M.J.: MC-TuP1, 113; PS1-WeM13,
 141; PS2-FrM5, **256**; PS-TuP10, 115
 Goede, A.P.H.: EN-TuP6, 111
 Goeke, R.S.: TF+PS+SE-MoM6, **23**; TF+PS+SE-
 MoM8, 23
 Goel, P.: AS+MC+SS-FrM3, **247**
 Goldoni, A.: SA-TuM5, **68**
 Gölzhäuser, A.: HI+2D+AS+BI+MC-ThM12, 188;
 HI-ThP2, **235**; HI-ThP3, 235
 Gompf, B.: EL+AS+EM+MC+SS-ThA1, **207**
 Gonda, S.: SP+AS+BI+NS+SS-WeA4, 173
 Gonzales, J.M.: 2D+AS+EM+MI+MN+NS+TF-
 WeA11, 153; 2D+EM+NS+SS+TF-WeM5,
125
 Goodwin, C.: IS+2D+MC+NS+SP+SS-WeA11,
162
 Goodyear, A.: EM-TuM6, 59
 Gorai, P.: SS+AS+EN-TuM6, 71; SS+AS+NS-
 ThA2, 222
 Gordon, W.O.: AS+MC-MoM10, 6; AS-ThP16,
232; PS-TuP15, 116
 Gorham, J.M.: AS+BI+MC-WeA11, **155**
 Gorlich, D.: QC+AS+BI+MN-ThA4, 219
 Gorman, B.P.: AP+AS+NS+SS-FrM1, 246
 Gosvami, N.N.: TR-FrM10, **263**
 Goswami, R.: EM1-ThM12, 185
 Gotlib-Vainshtein, K.: TR-FrM3, 262
 Götzen, J.: 2D+EM+NS+SS+TF-WeM4, 125
 Gougousi, T.: TF+MS+PS-WeM6, 149; TF+PS-
 MoA4, 49
 Gouillet, A.: TF+AS+EM-TuA3, **99**
 Gowthaman, P.: EM+EN+TF-WeA2, 157
 Grady, M.: NS+SE-MoM8, 14
 Graham, D.: AS+BI+MC-WeA9, 155
 Graham, D.J.: BI+AS-TuA10, 83; BI+AS-TuA7,
82
 Grampeix, H.: PS-MoM9, 16; TF+AS-FrM8, 261
 Granier, A.: TF+AS+EM-TuA3, 99
 Grant, J.T.: TF+EM+EN-WeA10, 177
 Grant, W.K.: AC+AS+MI+SA+SS-TuM12, 55
 Grapes, M.D.: TF+SE-TuM6, **75**
 Graswinckel, M.F.: EN-TuP6, 111
 Graves, D.B.: PS+2D-WeA1, 166; PS+2D-WeA9,
 168
 Gray, J.M.: TF+PS-TuM10, 73
 Greber, T.: 2D+AS+EM+NS+SS-MoA1, **28**;
 2D+EM+NS+PS+SS+TF-MoM8, 3
 Greeley, J.: IS+AS+MC+SS-WeM3, 134
 Green, F.M.: AS+BI+VT-TuM6, 56
 Greene, J.E.: TF+PS+SE-MoM4, 22
 Gregorczyk, K.: MS+PS+TF-ThA1, 213;
 TF+EN+PS-TuA7, 101
 Grehl, T.: MC+AP+AS-MoM8, 11; TF+AS-FrM8,
261
 Gresback, R.: PS-ThA1, 216
 Grierson, D.S.: SP+AS+BI+EM+NS+SE+SS-
 FrM2, 258
 Griffiths, G.: TF-ThP21, 243
 Grob, F.: TF-ThA7, 225
 Groot, I.M.N.: IS+2D+MC+NS+SP+SS-WeA7,
162
 Groover, T.: MC-TuP8, **113**
 Grosse, P.: PS-MoM6, 15
 Grossman, J.C.: MG-WeM6, 136
 Gruber, E.: 2D-ThP18, 230
 Grundmeier, G.: QC+AS+BI+MN-ThM5, 194
 Gschneider, Jr., K.A.: AC+AS+MI+SA+SS-
 MoA8, 30
 Gstrein, F.: SD-WeA7, 171
 Gu, G.: MI-MoA8, 40;
 SP+2D+AS+EM+MC+NS+SS-ThM11, 197;
 SP+2D+AS+EM+MC+NS+SS-ThM6, 196
 Gu, X.: NS+HI-TuM1, 64
 Guan, D.: EM-TuM12, 59
 Guggilla, S.: SD-WeA10, 172
 Guglietta, G.W.: EN+AS+EM-WeA3, 160

- Guillet, J.-F.: 2D+EM+MI+MN+NS+SS+TF-ThA10, 204
- Guisinger, N.P.: 2D+AS+EM+NS+SS-MoA7, **28**; 2D+AS+HI+NS+SS-ThM13, 180; 2D+EM+NS+SS+TF-WeM3, 125
- Gundlach, D.J.: EN+AS+EM-WeA11, 161; SS+EM-FrM2, 259
- Gunlycke, D.: 2D+EM+MI+MN+NS+SS+TF-ThA3, **203**
- Guo, D.: AS+MC+SS-FrM8, 248
- Guo, H.: SP+2D+AS+EM+MC+NS+SS-ThM5, 196
- Guo, H.X.: HI+2D+AS+BI+MC-ThM6, **188**
- Guo, J.-H.: SA-MoA8, 44
- Guo, M.: BI-ThP2, 234
- Guo, X.: EM-TuP11, **107**
- Gupta, R.: AS+MC+SS-FrM5, 248; PS2-FrM9, 257; PS-MoA10, 43; PS-TuA10, 96; PS-TuM10, 67
- Gupta, S.: MI+MG-TuM13, 64; TF+AS+EM-TuA1, 99
- Gurary, A.: EM+EN-FrM8, **252**
- Gurdak, E.: AS+BI+VT-TuM6, 56
- Gustafsson, T.: HI+2D+AS+BI+MC-ThM13, **188**
- Guyot-Sionnest, P.: NS+SE-MoM5, 13
- H —
- Ha, J.: MI-MoA10, 40; SP+AS+BI+EM+NS+SE+SS-FrM6, 258; SP+AS+EM+NS+SS-ThP3, **240**
- Ha, T.: VT-TuA4, **103**
- Haak, T.: PS+2D-WeA3, 167
- Habenicht, B.F.: SS+NS-TuA11, 99
- Habibovic, P.: BI+MG-WeA9, 157
- Hacker, C.A.: EN+AS+EM-WeA11, 161; SS+EM-FrM2, 259
- Hage, D.: EL+AS+BI+EM+SS-FrM8, 251
- Hahn, D.W.: TR+NS-ThM6, 201
- Haider, A.: EM+EN-FrM4, 251; TF+EM+EN-WeA2, **176**
- Haight, R.: EN+AS+EM+SE-WeM4, 132
- Haile, S.M.: EN+AS+EM+SE-TuM1, **59**
- Halbur, J.C.: MS+PS+TF-ThA3, 213
- Haley, D.: AP+AS+EN+NS+SS-ThA6, 205
- Hall, R.B.: TF+PS-MoM4, 24
- Hall, R.W.: SS+TF-ThM12, 198
- Hallam, K.: AC+AS+MI+SA+SS-TuM5, 55
- Hamaguchi, S.: PS-TuM11, 67; PS-TuM6, 67; PS-TuP6, **114**
- Hamasaki, M.: EM-TuP7, 106
- Hamilton, J.R.: PS-TuP16, 116
- Hammond, J.S.: AS+BI+MC+SS-MoA11, 32; AS+BI+MC-WeA2, 154; AS-ThP25, 234
- Hamzavtehrany, B.: AS-ThP13, 232
- Han, C.: HI-ThP1, 235
- Han, J.G.: PS-ThA11, 218; PS-WeA10, 170
- Han, L.: MI+MG-TuM6, 63
- Han, S.E.: EM1-ThM5, **185**; EM1-ThM6, 185; EM-TuP5, 106
- Han, S.M.: EM1-ThA4, 208; EM1-ThA8, **209**; EM1-ThM5, 185; EM-TuP5, 106; SS+AS-WeM12, 148; TF+AS+EM-TuA12, 100
- Han, Y.: SS+AS-WeM10, 148
- Hanbicki, A.T.: 2D+EM+NS+PS+SS+TF-MoM4, 2
- Haneef, H.: EL+AS+EM+EN+SS-ThM11, 184
- Haney, P.: EN+AS+EM+SE-WeM12, 133
- Hanek, S.: QC+AS+BI+MN-ThP2, 239
- Hanley, L.: BI+AS-TuA12, **83**; EM-MoA9, 35; EM-TuP31, 110
- Hannah, A.N.: VT-WeM1, 150
- Hanrath, T.: EM-MoA8, 35
- Hansen, T.W.: IS+AS+MC+SS-TuA9, 88
- Hanson, J.: IS+AS+MC+SS-WeM1, 134
- Haque, M.A.: 2D+EM+NS+PS+SS+TF-MoM5, 2
- Harduin, J.: PS-MoM6, 15
- Hare, C.D.: TF+EN+PS-TuA8, 102
- Harker, M.: TF+AS-FrM2, 260
- Harlin, A.: TF+PS-MoM1, 24
- Harrell, W.R.: AS+MC+SS-FrM10, 248
- Harrison, I.A.: SS+AS+EN-MoM6, 20; SS+AS+EN-WeM12, 146
- Harrison, J.A.: MG-TuA9, 90; SP+AS+BI+EM+NS+SE+SS-FrM2, 258; SS+AS-WeM5, **147**; TR+NS-ThM5, 201; TR-FrM6, 263; TR-ThA8, 227
- Harriss, J.E.: AS+MC+SS-FrM10, 248
- Hart, C.: EM+MI+NS-MoM4, 9; PS+2D-WeA9, 168; SE+EM+EN+PS+TF-MoM2, 18
- Hart, M.: AC+AS+MI+SA+SS-TuM5, 55
- Härtl, G.: AS+MC+SS-TuA7, 81
- Hasan, N.: PS+2D-WeA8, 167
- Hasegawa, S.: SE+NS+TR-TuM3, 70
- Hattar, K.M.: TF+PS+SE-MoM6, 23; TF+PS+SE-MoM8, 23
- Hatton, P.: VT-TuP4, 123
- Hausmann, D.: PS1+TF-ThM10, **191**
- Hävecker, M.: IS+AS+MC+SS-TuM1, **61**
- Havela, L.: AC+AS+MI+SA+SS-MoM9, **4**
- Havercroft, N.: AS+BI+MC-WeM5, 127
- Hawker, M.J.: SM+AS+BI+PS-ThA8, **221**; SM+AS+BI+PS-ThM5, 195
- Hayashi, H.: PS-TuA1, **94**
- Hayden, B.E.: SS+EN-MoA1, **47**
- Hayes, A.: VT-MoA9, 52
- He, D.: QC+AS+BI+MN-ThM10, 194
- He, G.: 2D+EM+NS+PS+SS+TF-MoM6, 2; SP+2D+AS+EM+MC+NS+SS-ThM6, 196
- He, Q.: 2D+EM+MI+MN+NS+SS+TF-ThA9, 204; AS+MC-MoM9, 6
- He, X.: EN+AS+EM+SE-WeM2, 132
- He, Y.: TF+EM+EN-WeA8, 176; TF+EM+EN-WeA9, **176**
- Hearn, G.: EL+AS+EM+MC+SS-ThA10, **208**; EL+AS+EM+MC+SS-ThA7, 208
- Heddleston, J.: AS+BI+MC-WeA11, 155
- Hedjran, F.: BI+MG-WeA7, 156
- Hehn, L.: TF-MoA3, 50
- Heidari, H.: BI+AS-MoM2, 7
- Heinbuch, S.: VT-MoM11, 27
- Heine, Ch.: IS+AS+MC+SS-TuM1, 61
- Heller, M.: EW-WeM8, **134**
- Heller, N.W.M.: IS+AS+MC+SS-TuA12, **89**
- Heller, R.: 2D-ThP18, **230**; HI-ThP6, 235
- Hellman, A.: EN+AS+EM+SE-TuM5, **60**
- Helms, B.A.: NS+SE-MoM10, 14
- Hemmi, A.: 2D+AS+EM+NS+SS-MoA1, 28; 2D+EM+NS+PS+SS+TF-MoM8, 3
- Hemminger, J.C.: EN+AS+EM+SE-WeM5, 132; IS+AS+MC+SS-TuA4, 88; IS+AS+MC+SS-TuM11, 62; NS-WeM4, 139; SS+NS-TuA9, 98
- Henderson, M.A.: AS-ThP8, 231; SS+AS+EN-TuM13, 72; SS+EN-MoM5, 22
- Hendricks, J.H.: CS-ThM10, 182; VT-MoM3, **26**
- Henegar, A.: TF+MS+PS-WeM6, **149**
- Hengehold, R.: AC+AS+MI+SA+SS-MoM11, 4
- Henk, J.: MI-MoA4, 40; MI-MoA6, **40**
- Hennig, R.: MI+MG-TuM3, **63**
- Henrich, F.: HI-ThP3, 235
- Henry, A.: MG-WeM2, 135
- Herath, N.: EN+EM+MN+NS+TR-MoA9, **36**
- Herbert, J.D.: VT-WeM1, 150
- Herman, A.K.: BI+AS+MN+NS-TuM4, 57
- Herman, G.S.: BI+AS+MN+NS-TuM4, 57; EM+NS+TF-FrM3, **253**; NS+HI-TuM5, 65
- Hernández, S.: 2D+AS+BI+PS+SS-TuM5, **53**
- Hernandez, S.C.: 2D+AS+BI+PS+SS-TuM6, 53; BI+AS+MN+NS-TuM5, 57; PS1-FrM8, 255
- Hernandez-Maldonado, D.: AP+AS+NS+SS-FrM5, 247
- Herrera, V.: BI+MG-WeA7, 156
- Herrera-Gomez, A.: AS+MC+SS-TuA8, 81; AS+MC-MoM11, 6; AS+MC-MoM2, **5**
- Herrmann, J.K.: CS-ThM3, **181**
- Herron, J.A.: SS+AS-WeM3, 147
- Hersam, M.C.: 2D+AS+EM+NS+SS-MoA7, 28; 2D+AS+HI+NS+SS-ThM13, 180; 2D+AS+HI+NS+SS-ThM4, 179; 2D+EM+NS+SS+TF-WeM3, 125
- Herzinger, C.M.: EL+AS+EM+MC+SS-ThA9, 208
- Hetzl, C.: VT-WeM3, 150
- Heyde, M.: 2D+EM+NS+SS+TF-WeM12, 126
- Heylen, N.: EM-TuM6, 59
- Heyne, M.H.: EM-TuM6, 59; PS-MoM4, 15
- Hiebert, W.K.: MN-WeM10, 137; MN-WeM11, 138
- High, E.: SS+AS+EN-WeM11, 146
- Hight Walker, A.R.: 2D+AS+BI+PS+SS-TuM10, 53; 2D+AS+EM+MI+MN+NS+TF-WeA7, 153; MI+MG-TuA11, **91**
- Hight-Walker, A.R.: 2D+AS+EM+MI+MN+NS+TF-WeA4, 153
- Higo, A.: PS-ThA8, 217
- Hilbert, J.: AS+BI+MC-WeA12, 155
- Hill, S.B.: TF+PS-ThM11, 200
- Himpfel, F.J.: SA-MoA6, **44**
- Hinch, B.J.: SS-WeA7, **175**
- Hines, M.A.: SS+AS+NS-ThA8, 223; SS+EN-MoA10, 48
- Hingerl, K.: EL+AS+BI+EM+SS-FrM6, **251**; EL+AS+EM+EN+SS-ThM12, 184
- Hinkle, C.L.: EM-WeA4, 159
- Hinton, K.: EM+EN+TF-WeA9, 158; TF+PS-ThM6, 200
- Hipps, K.W.: SP+2D+AS+EM+MC+NS+SS-ThM1, 196
- Hiramatsu, M.: 2D+EM+MS+NS-FrM10, 246
- Hirano, T.: PS1-FrM4, 254
- Hirano, Y.: TF-ThP9, 241
- Hirayama, H.: SS+AS+NS-ThA6, **223**
- Hirschmugl, C.J.: BI+AS-TuA3, **82**
- Hirvikorpi, T.: TF+PS-MoM1, 24
- Hite, J.K.: 2D+AS+HI+MC+NS+PS+SP+SS-TuA9, 79; EM1-ThM12, **185**; MC+2D+AP+AS-MoA4, 38; PS1+TF-ThM11, 191
- Hjort, M.: NS+AS+SS-TuA4, 93
- Hlawacek, G.: HI-ThP4, **235**; HI-ThP6, 235
- Hoard, B.R.: EM1-ThM5, 185
- Hoefnagels, R.: HI+2D+AS+MC-ThA8, 212
- Hoenicke, P.: SA-TuM1, 68
- Hofer, W.: 2D+AS+EM+NS+SS-MoA10, 29
- Hoffman, A.: EM-TuP15, 108
- Hofmann, T.: AS+MC+SS-TuA7, **81**; EL+AS+BI+EM+SS-FrM8, 251; EL+AS+EM+MC+SS-ThA4, 207; EL+AS+EM+MC+SS-ThA6, 207; EL+AS+EM+MC+SS-ThA9, 208
- Höglund, C.: TF+PS-ThM3, 199
- Holcomb, M.B.: MI+EM-MoM2, 12; MI+MG-TuM11, 64; MI+MG-TuM12, 64
- Holfelder, L.: SA-TuM1, 68
- Holland, G.: NS-ThP3, 238
- Holland, J.: PS-WeA3, 169
- Holleitner, A.W.: EL+AS+EM+MC+SS-ThA10, 208
- Holmes, R.J.: EN+AS+EM-WeA9, **161**
- Holsclaw, B.S.: SS-WeA4, 174
- Holtmannspötter, J.: AS+MC+SS-TuA7, 81
- Holybee, B.: PS-TuM1, 66; SE-TuP1, 119
- Honda, M.: PS-MoM1, **14**
- Hone, J.C.: 2D+EM+MI+MN+NS+SS+TF-ThA4, 203
- Hong, S.: MG-WeM5, **136**
- Hönicke, P.: SA-TuA12, **97**; SA-TuP1, 119
- Höök, F.: QC+AS+BI+MN-ThA7, 219
- Hooper, J.: SS+TF-ThM11, 198
- Hopstaken, M.J.P.: MC+2D+AP+AS-MoA1, **37**
- Hopwood, J.: PS-TuP17, 116
- Hore, D.K.: BI+AS-WeM3, **128**
- Hori, M.: 2D+EM+MS+NS-FrM10, 246; PS2-FrM8, 257; PS-ThA11, 218; PS-WeA10, 170
- Horigome, M.: PS1-WeM10, 140
- Horn, M.W.: EN+AS+EM+SE-WeM6, 133; TF-ThP17, 242
- Horreard, F.: 2D-ThP1, 228
- Horvath, Z.G.: EL-ThP6, 234
- Horwood, C.: NS-ThP5, 238

- Hose, S.: EM2-WeM2, 130
Hoskinson, A.R.: PS-TuP17, **116**
Hosler, E.: PS-TuA3, 95
Hossain, K.: EM+EN-FrM10, 252
Hossain, L.: 2D+EM+NS+SS+TF-WeM6, 125
Hossain, M.: EM-TuM3, 58
Hou, J.: NS+EN-MoA10, **42**
Hourani, R.: SD-WeA7, **171**; SD-WeM3, 144
Houssiau, L.: PS-WeA8, **170**
Howansky, A.: EN+EM+NS-TuA4, 86
Hseuh, H.-C.: VT-WeM3, **150**
Hsiao, C.N.: MC-TuP7, **113**; MN-ThP2, 236; MS-ThP6, 237; MS-ThP7, 237; SP+AS+EM+NS+SS-ThP5, 240; TF-ThP23, 243; TF-ThP4, 241; TF-ThP8, 241
Hsiao, Y.: MS-ThP4, 237
Hsieh, C.: EM+EN-FrM5, 252
Hsieh, C.H.: PS-TuP7, 115
Hsieh, F.C.: VT-TuP2, **123**
Hsieh, M.D.: MS-ThP2, **237**
Hsu, C.C.: PS-TuP20, 117; PS-TuP21, 117; PS-TuP22, 117; PS-TuP23, 117; PS-TuP24, 117; PS-TuP25, 118
Hsu, C.-L.: MN+NS-TuA12, 93
Hsu, C.P.: MS-ThP4, **237**
Hsu, J.: MS+TF-WeA3, 164
Hsu, K.W.: EM-WeA11, **159**
Hsu, W.-C.: EM1-ThM3, 185
Hu, C.: EM1-ThA10, 210
Hu, C.-K.: SD-WeA10, 172
Hu, J.J.: 2D+EM+NS+PS+SS+TF-MoM5, 2; SE+EM+EN+PS+TF-MoM8, 19
Hu, L.B.: MS+PS+TF-ThA10, 213; MS+PS+TF-ThA11, 213; MS+PS+TF-ThM5, 189; MS+TF-WeA11, 165; MS+TF-WeA9, **165**
Hu, X.: PS-TuA3, 95
Hu, Y.F.: SA-MoM3, **16**
Hua, X.: BI+AS-TuA11, **83**
Huang, C.: MS-ThP4, 237
Huang, C.Y.: EM-WeA12, 160
Huang, C.-Y.: MI+EM-MoM2, 12; MI+MG-TuM11, 64; MI+MG-TuM12, **64**
Huang, E.: 2D+EM+MS+NS-FrM3, 245
Huang, F.H.: PS-TuP23, **117**
Huang, J.S.: EL+AS+EM+EN+SS-ThM10, 184; EN-TuP13, 112
Huang, M.-J.: MS-ThP7, 237
Huang, P.-K.: MN-ThP3, **237**
Huang, P.-W.: PS-MoM8, 15
Huang, W.: IS+AS+MC+SS-TuM4, **62**
Huaranga, J.A.: TR-ThA10, 227
Hubbard, L.R.: SE+NS+TR-TuM1, **69**
Hubert, J.: PS+2D-WeA11, 168; PS+SE-ThA7, 215
Hudait, M.: MC+AP+AS-MoM11, 12
Hudson, E.: PS2+TF-ThM2, **192**; PS-WeA3, 169
Huerta, L.: SS-TuP9, **120**
Huerta-Ruelas, J.A.: AS+MC+SS-TuA8, **81**; AS+MC-MoM11, 6
Huffman, E.S.: SS+NS-TuA12, 99
Hughes, G.: SA-MoM5, **17**
Hultman, L.: TF+PS+SE-MoM4, 22
Hung, K.-K.: BI+AS-WeM3, 128
Hunn, J.: TF+PS+SE-MoM5, 23
Hunter, K.: EN+AS+EM+SE-WeM3, 132
Hur, J.: TF+EN+PS-TuA2, 101
Hurley, P.K.: EM+2D-TuA8, **84**; SA-MoM5, 17
Hussain, B.: EM-TuP17, 108
Hutton, S.J.: AS+BI+MC+SS-MoA8, 31; AS+BI+MC-WeA1, 154; AS-ThP10, **232**
Hwang, E.: NS+EN-MoA4, 41
Hwang, H.H.: 2D-ThP17, 229; SD-WeA11, 172
Hyde, L.: TF-ThP21, 243
Hytch, M.: EM+MI+NS-MoM8, 9
- **I** —
Iannuzzi, M.: 2D+AS+EM+NS+SS-MoA1, 28
Idrobo, J.-C.: SP+2D+AS+EM+MC+NS+SS-ThM11, 197
Ielmini, D.: EM2-ThM3, **186**
- Ihlefeld, J.: AS-ThP2, 231
Ikari, T.: EN+EM+MN+NS+TR-MoA11, 37; EN-TuP2, **110**
Ikuma, K.: QC+AS+BI+MN-ThA6, **219**
Illiberi, A.: TF+PS-MoM5, **25**; TF+PS-MoM8, 25
Im, H.: AS-ThP6, 231; MC+2D+AP+AS-MoA9, 39
Im, M.-Y.: MI+MG-TuM6, 63
Imai, S.: 2D+EM+MS+NS-FrM10, 246
Imam, M.: TF+PS-ThM3, 199
Imamura, T.: PS-TuA1, 94
In, S.Y.: VT-TuP3, 123
Ingle, N.: TF+PS-ThM10, 200
Ingólfsson, O.: SS+AS+EN-MoM11, 20
Ingram, W.: TF+EM+EN-WeA8, 176; TF+EM+EN-WeA9, 176
Iordanov, I.O.: SS+AS-WeM6, **147**
Iriye, Y.: PS2+TF-ThM4, 192
Irving, D.L.: MG-WeM3, **135**
Ishibashi, K.: PS1-FrM4, 254
Ishida, Y.: SP+AS+BI+NS+SS-WeA3, 173
Ishidzuka, S.: SS+AS+EN-MoM10, 20
Ishihara, T.: AC+AS+MI+SA+SS-MoA7, 30; EN+AS+EM+SE-WeM2, 132
Ishikawa, K.: 2D+EM+MS+NS-FrM10, 246; PS2-FrM8, 257; PS-WeA10, 170
Ishiyama, Y.: TF-ThP3, **241**
Islam, M.F.: EM+NS+TF-FrM11, 254
Islam, S.: EM1-WeM12, 130
Isobe, M.: PS-TuP6, 114
Ista, L.: BI+AS+MN+NS-TuM12, 57
Itagaki, N.: PS1+TF-ThM1, **190**
Ito, H.: TF-ThP2, 241
Itou, A.: PS-MoM10, 16; PS-MoM3, 14
Iwao, T.: PS1-FrM4, **254**
Iwasaki, T.: PS2+TF-ThM4, 192
Iwasawa, H.: 2D+EM+MI+MN+NS+SS+TF-ThA8, 203
Iwata, J.: TF-ThP9, **241**
- **J** —
Jablonski, A.: AS+MC-MoM5, 5
Jach, T.: SS+AS+EN-TuM12, **72**
Jackman, R.B.: HI+2D+AS+MC-ThA10, 212
Jacob, D.: TF-ThA6, 225
Jacobs, P.G.: BI+AS+MN+NS-TuM4, 57
Jacobs, T.D.B.: SP+AS+BI+EM+NS+SE+SS-FrM2, **258**; SS+AS-WeM5, 147
Jaeger, D.: NS+HI-TuM11, 65
Jaeger, V.: BI+AS-WeM6, 128
Jain, R.: SS+EM-FrM8, 260
Jalili, S.: MI-TuP4, 114
James, C.: BI+AS-TuA9, 83
James, R.: PS1+TF-ThM3, **190**; PS-TuP28, 118
Jamieson, S.: TF+EM+EN-WeA11, 177
Jang, H.-J.: EN+AS+EM-WeA11, **161**; SS+EM-FrM2, 259
Jang, K.: QC+AS+BI+MN-ThP1, **239**
Jankowski, M.: HI-ThP4, 235
Janod, E.: TF+PS+SE-MoM3, 22
Jarecki Jr., R.L.: PS-TuM3, 66
Jariwala, B.: PS2+TF-ThM2, 192
Jariwala, D.: 2D+AS+HI+NS+SS-ThM4, **179**
Järrendahl, K.: EL+AS+BI+EM+SS-FrM3, 250
Jarvis, K.L.: TF-ThP21, **243**
Jayanthinarasimham, A.: 2D+AS+HI+MC+NS+PS+SP+SS-TuA8, 79; MC-TuP4, **113**
Jaye, C.: SA-MoM10, 17
Jean-Jacques, J.-J.: PS-WeA8, 170
Jennings, J.: EN+EM+NS-TuA11, 87
Jennings, W.D.: AS-ThP25, **234**
Jenny, C.J.: PS-TuA7, 95
Jeon, C.: 2D-ThP3, 228; IS-ThP1, 236
Jeon, M.H.: 2D+AS+EM+NS+SS-MoA8, 29; PS2+TF-ThM11, **193**
Jeon, N.: NS+AS+SS-TuA3, **93**
Jespersion, M.L.: 2D+EM+NS+PS+SS+TF-MoM5, 2
Jesse, S.: AS+MC-MoM9, 6
- Ji, C.X.: PS1-FrM3, 254
Ji, H.: MI-MoA8, 40
Jia, H.: MN+NS-TuA10, **92**
Jia, J.F.: SP+AS+BI+NS+SS-WeA1, **173**
Jia, Z.: MS+PS+TF-ThA11, 213
Jiamei, Q.: SS-TuP8, 120
Jiang, H.: MN+NS-TuA7, **92**
Jiang, X.: AP+AS+MC+NS+SS-ThM12, **181**; QC+AS+BI+MN-ThA8, 219; TF+PS-TuM11, 73
Jiang, Y.: AC+AS+MI+SA+SS-TuM1, 54; SP+AS+BI+NS+SS-ThA6, **222**; SS+AS-WeM5, 147; TR+NS-ThM5, 201; TR-FrM6, **263**
Jiao, C.Q.: EM-TuP18, 108
Jimenez, O.: TR-ThP4, 244
Jin, M.: NS+AS-WeA9, 166
Jin, S.B.: PS-ThA11, **218**
Jing, D.: SS+EN-MoA10, **48**
Johannsmann, D.: QC+AS+BI+MN-ThM3, **193**; QC+AS+BI+MN-ThM6, 194; QC+AS+BI+MN-ThP2, 239
Johansson, P.: BI+AS-WeM13, 129
Johlin, E.: MG-WeM6, 136
Johnson, E.V.: PS1-WeM11, 140
Johnson, G.: EM-MoA3, **34**
Johnson, M.L.: TF+MS+PS-WeM4, 149
Johnson, M.B.: EM+EN-FrM10, 252; EM-TuP1, 106
Johnson, M.D.: AS+BI+MC-WeA8, 155
Johnson, N.: MC+2D+AP+AS-MoA7, 38
Johnson, R.W.: TF+MS+PS-WeM5, 149; TF+PS-MoA10, 50
Johnson, S.D.: SA-MoM4, 17
Johnston, S.: SP+AS+BI+NS+SS-WeA10, 174
Johnston, S.A.: BI+AS-TuA9, 83
Johnston-Peck, A.C.: NS+AS-WeA3, **165**
Jones, J.G.: TF+EM+EN-WeA10, 177
Jones, K.: EW-TuA6, **87**
Jones, K.J.: AS+MC+SS-FrM5, **248**
Jonker, B.T.: 2D+EM+NS+PS+SS+TF-MoM4, 2
Joo, J.-B.: SS+AS+EN-MoM1, 19
Jorabchi, K.: AS+BI+MC+SS-MoA4, **31**
Jordan-Mowery, S.: CS-ThM11, 182
Jordan-Sweet, J.: EM+MI+NS-MoM8, 9
Joseph, E.A.: PS2+TF-ThM1, 191; PS-MoM10, 16; PS-MoM3, 14
Joslin, J.: SM+AS+BI+PS-ThM5, 195
Jouan, P.Y.: EN-TuP5, 110; TF+PS+SE-MoM3, 22
Joubert, O.: PS2-FrM2, 256; PS-MoM9, 16; PS-TuA7, 95; PS-WeA2, 169; SD-WeA9, 172
Jourdan, N.J.: EM-TuM5, **58**
Jousten, K.: VT-MoM4, **26**; VT-MoM5, 26; VT-MoM8, 27
Joy, D.C.: HI+2D+AS+BI+MC-ThM1, **187**
Ju, H.X.: EN+AS+EM-WeA12, **161**
Ju, L.: 2D+EM+MS+NS-FrM3, 245
Juhász, G.: EL-ThP6, 234
Julie, H.: PS+2D-WeA12, 168
Junda, M.M.: EL+AS+EM+EN+SS-ThM5, 183; EL-ThP5, **234**
Jung, R.: NS+HI-TuM3, **64**
Jung, S.: 2D+EM+MI+MN+NS+SS+TF-ThA4, 203
Junkermeier, C.: 2D+AS+BI+PS+SS-TuM5, 53
Junkermier, C.: 2D+AS+EM+NS+SS-MoA3, 28
Jur, J.S.: MS+PS+TF-ThA3, 213; MS+TF-WeA12, 165; TF+MS+PS-WeM13, 150; TF-ThA9, **226**
Jurchescu, O.D.: EN+AS+EM-WeA11, 161; SS+EM-FrM2, 259
- **K** —
Kaganovich, I.D.: PS2-WeM5, **142**
Kahn, A.L.: BI+AS-WeM5, 128; EM2-ThA10, **211**
Kahn, S.: 2D+EM+MS+NS-FrM3, 245
Kaiser, D.: EM1-ThA4, **208**; EM1-ThA8, 209
Kajihara, S.: EM-TuP7, **106**
Kalanyan, B.: MS+PS+TF-ThA4, 213; SD-WeA3, 171; TF+PS-MoA9, **49**
Kale, M.J.: EN+AS+EM+SE-TuM3, 60

Kaler, S.: PS-TuP3, 114
Kalhor, N.: HI+2D+AS+MC-ThA8, **212**
Kalinin, S.V.: 2D+EM+MI+MN+NS+SS+TF-ThA9, 204; AS+MC-MoM9, **6**
Kaltschmidt, B.: HI+2D+AS+BI+MC-ThM12, 188
Kaltschmidt, C.: HI+2D+AS+BI+MC-ThM12, 188
Kambham, A.: MC+AP+AS-MoM1, 10
Kaminski, P.M.: EN+AS+EM+SE-WeM13, 134
Kanakasabapathy, S.: NS+HI-TuM3, 64; PS-TuA8, 95
Kane, M.H.: EM+EN-FrM10, 252; EM-TuP1, **106**
Kang, C.-J.: PS-MoA1, **42**
Kang, H.: SS+AS+EN-MoM4, 19
Kangi, R.: VT-MoM5, 26
Kanjolia, R.: TF+PS-MoA8, 49
Kao, J.S.: MC-TuP7, 113
Kao, Y.-C.: PS-MoM8, 15
Kappoor, M.: AP+AS+NS+SS-FrM3, **246**
Kappes, M.M.: HI-ThP3, 235
Kapur, J.: AS-ThP13, 232
Karabacak, T.: EN-TuP8, 111; TF+EM+EN-WeA1, 175; TF+EM+EN-WeA2, 176
Karahashi, K.: PS-TuM11, 67; PS-TuM6, 67; PS-TuP6, 114
Karakaya, S.: SD-WeM3, 144
Karayaylali, P.: SP+AS+BI+NS+SS-ThA3, 221
Kariuki, N.: EN-TuP8, 111
Karki Gautam, L.: EL-ThP5, 234
Karppinen, M.: TF+PS-TuM12, 74
Karwacki, C.J.: SS+AS-WeM6, 147
Kas, J.J.: AC+AS+MI+SA+SS-TuM1, 54
Kasai, H.: AC+AS+MI+SA+SS-MoA7, 30; SE+PS+TF-MoA10, 46
Kashyap, A.: MI-MoA11, 41
Kaspar, T.C.: TF+AS-FrM5, **261**
Kaszuba, P.: MC+2D+AP+AS-MoA11, 39
Kato, S.: VT-WeM13, **151**
Kato, T.: TF+PS-ThM4, 199
Katsumata, H.: EM-TuP7, 106; EM-TuP9, 107; TF-ThP9, 241
Kattareeya, T.: EM-TuP8, 107
Katz, H.: EM+NS+TF-FrM6, 253
Kaufman-Osborn, T.: EM+2D-TuA4, 84; EM1-ThA9, 209; EN+AS+EM+SE-WeM4, 132
Kaur, S.: NS+SE-MoM10, 14
Kautz, N.A.: SS+TF-ThM4, 198
Kawaguchi, S.: EM-TuP9, **107**
Kaykhaii, M.: TF+EM+EN-WeA7, 176
Kayser, S.: AS+BI+MC-WeM5, 127
Kazi, H.: PS-TuP28, **118**
Kearney, P.: VT-MoA8, 52
Keating, P.L.: SP+AS+BI+EM+NS+SE+SS-FrM2, 258; SS+AS-WeM5, 147; TR+NS-ThM5, 201
Keckes, J.: SE+NS+TR-TuM11, 70
Keith, J.: AC+AS+MI+SA+SS-MoM1, 3
Kelber, J.A.: MI-MoA11, 41; PS1+TF-ThM3, 190; PS-TuP28, 118
Kelkar, S.: TF-ThA3, **224**
Kelley, M.J.: AS+MC+SS-TuA10, 81
Kelly, B.J.: VT-MoM10, **27**
Kelly, D.L.: BI+AS+MN+NS-TuM3, 57
Kelly, J.: TF-ThA6, 225
Kelly, M.: 2D+EM+NS+SS+TF-WeM11, 126
Kelly, T.: AC+AS+MI+SA+SS-MoM11, 4
Kelly, T.F.: AP+AS+MC+NS+SS-ThM1, **180**; AP-ThP1, 230
Kemp, C.A.J.: QC+AS+BI+MN-ThA3, 218
Keneghan, B.: CS-FrM6, 249
Keniley, S.: VT-MoA9, 52
Kennedy, J.K.: AS+BI+VT-TuM10, 56
Kennedy, R.J.: EN+AS+EM+SE-WeM11, 133
Kenney, J.: PS2-WeM4, 142; PS2-WeM6, **143**
Kent, T.: EM1-ThA9, 209; EM-WeA12, **160**; SD-WeM12, 145
Kenttä, E.: TF+PS-MoM1, 24
Keramane, M.: BI+AS-MoM5, 7
Kersevan, R.: VT-TuM3, **76**
Kessels, W.M.M.: 2D+EM+MS+NS-FrM6, 245; PS-ThA10, 218; SD-WeM6, **144**; TF+EN+PS-TuA10, 102; TF+EN+PS-TuA12, 103; TF+EN+PS-TuA9, 102; TF+PS-MoA1, 48; TF-ThA4, 225
Ketchum, D.: EN+EM+NS-TuA9, 86
Ketar, M.: EN+AS+EM+SE-WeM3, 132
Khan, A.: PS-MoA8, 43
Khan, M.N.: BI+AS-MoM4, 7
Khan, T.: MS+TF-WeA3, 164
Khare, P.: MC-TuP4, 113
Khelifa, F.: PS+2D-WeA7, 167
Khosla, N.: SS-WeA8, 175
Khrabrov, A.: PS2-WeM5, 142
Khudhayer, W.J.: EN-TuP8, 111
Kiang, Y.W.: EM+EN-FrM5, 252
Kiba, T.: PS-ThA8, 217
Kievit, O.: VT-TuA10, 104; VT-TuM6, 77
Killelea, D.R.: SS+EN-MoA9, **48**
Kilner, J.: EN+AS+EM+SE-WeM2, 132
Kilpi, V.: TF+PS-MoM1, 24
Kim, C.: MC+2D+AP+AS-MoA10, 39
Kim, C.: EM-MoA11, 35
Kim, E.: BI+AS+MN+NS-TuM3, 57
Kim, H.: 2D+EM+MI+MN+NS+SS+TF-ThA10, **204**; MC+AP+AS-MoM10, 11; PS1+TF-ThM12, **191**
Kim, H.J.K.: EM-TuP25, 109
Kim, J.: 2D-ThP17, 229; 2D-ThP9, **229**; HI-ThP1, 235; MN+PS-WeA1, 162
Kim, J.B.: PS-ThA11, 218
Kim, J.H.: NS-ThP1, **238**
Kim, J.M.: PS-TuA10, 96
Kim, J.S.: 2D-ThP3, 228
Kim, J.Y.: EM+2D-TuA7, 84; EM-WeA4, 159; SD-WeA11, 172
Kim, J.S.: TF+AS-FrM9, 261
Kim, K.: AS+MC+SS-TuA11, 81
Kim, K.N.: 2D+AS+EM+NS+SS-MoA8, 29
Kim, K.S.: 2D+AS+EM+NS+SS-MoA4, **28**; 2D+AS+EM+NS+SS-MoA8, 29
Kim, M.: EM-WeA4, 159; EM-WeA9, **159**
Kim, M.J.: SA-TuA11, 97
Kim, P.: 2D+EM+MI+MN+NS+SS+TF-ThA4, 203
Kim, S.: SP+AS+BI+NS+SS-WeA3, 173; SP+AS+EM+NS+SS-ThP3, 240
Kim, S.P.: 2D+AS+BI+PS+SS-TuM4, 53
Kim, S.H.: PS-TuP8, 115
Kim, T.: PS-MoM5, 15; TF+PS-TuM4, 73; TF-ThP25, 243
Kim, T.-H.: SP+AS+BI+NS+SS-WeA9, **174**
Kim, W.-H.: TF+PS-MoA10, 50
Kim, W.-K.: TR+NS-ThM1, **201**
Kim, W.S.: MN+PS-WeA1, 162
Kim, Y.: 2D-ThP17, 229; 2D-ThP3, **228**; IS-ThP1, 236; SP+AS+EM+NS+SS-ThP3, 240; SS+AS+EN-MoM4, 19; TF+PS+SE-MoM10, 23; TF+PS-TuM5, 73; TF-ThP25, 243
Kim, Y.-G.: PS-TuP5, 114
Kim, Y.W.: BI+AS+MN+NS-TuM2, 56; MN+NS-TuA9, 92
Kimes, W.A.: TF+PS-MoA3, 49; TF+PS-MoA8, 49
Kimmel, G.A.: SS+EN-MoM5, 22
Kimoto, T.: EM1-WeM3, **129**
Kinder, E.K.: 2D+AS+HI+NS+SS-ThM5, 179
King, S.W.: 2D+AS+HI+MC+NS+PS+SP+SS-TuA3, 79; TF+AS-FrM3, 260; TF-ThA6, **225**
Kingshott, P.: BI+AS+NS-MoA9, 34
Kinoshita, T.: MG-WeM3, 135; PS-TuM4, 66
Kioussis, D.: SD-WeA10, 172
Kippelen, B.J.: EM2-ThA6, **210**; MS+TF-WeA3, 164
Király, B.T.: 2D+AS+EM+NS+SS-MoA7, 28; 2D+AS+HI+NS+SS-ThM13, **180**; 2D+EM+NS+SS+TF-WeM3, 125
Kirillov, O.A.: EM2-WeM13, 131; SS+EM-FrM2, 259
Kirillova, O.A.: EN+AS+EM-WeA11, 161
Kirste, R.: MG-WeM3, 135
Kis, A.: 2D+AS+EM+MI+MN+NS+TF-WeA4, 153
Kiyota, E.: EN-TuP15, 112
Kizilkaya, O.: SS+TF-ThM12, 198
Kjoller, K.: NS+AS-WeA9, 166
Klarenaar, B.L.M.: PS+SE-ThA6, 214
Klarr, T.: EM2-WeM13, **131**
Klee, V.: 2D+EM+NS+SS+TF-WeM10, 126; 2D-ThP11, 229; SP+AS+BI+NS+SS-WeA11, **174**
Klein, P.B.: EM1-WeM5, 129
Klejna, S.: SD-WeM5, 144
Klemborg-Sapieha, J.: SE+NS+TR-TuM5, 70
Klimov, N.N.: 2D+EM+MS+NS-FrM4, **245**
Kline, R.J.: EN+AS+EM-WeA11, 161
Kling, J.: IS+AS+MC+SS-TuA9, 88
Klingner, N.: HI-ThP6, **235**
Kloster, G.M.: SD-WeA7, 171
Knauf, J.: TF-ThA11, **226**
Knepper, R.: TF+SE-TuM5, **75**
Knez, M.: MS+PS+TF-ThA1, **213**
Knippenberg, M.: TR-ThA8, 227
Knippenberg, M.T.: MG-TuA9, 90
Knoll, A.J.: PS+2D-WeA9, 168; SE+EM+EN+PS+TF-MoM2, **18**
Knoops, H.C.M.: SD-WeM6, 144; TF+EN+PS-TuA9, 102
Knowles, J.P.: AC+AS+MI+SA+SS-MoM8, 4
Knutsson, J.: NS+AS+SS-TuA4, 93
Ko, A.: NS+HI-TuM3, 64; PS-TuA11, 96; PS-TuA3, 95
Ko, Y.H.: 2D-ThP3, 228
Kobayashi, Y.: PS1-WeM10, **140**
Kobl Müller, G.: NS+AS+SS-TuA3, 93
Kocbas, C.: 2D+EM+MI+MN+NS+SS+TF-ThA11, 204
Kocsis, M.: NS+HI-TuM1, 64
Kodambaka, S.: 2D+EM+NS+PS+SS+TF-MoM10, 3
Koel, B.: BI+AS-WeM5, 128; SS+AS+NS-ThA11, 224; SS+EN-MoM1, **21**
Koelsch, P.: BI+AS-WeM13, **129**
Koh, D.Y.: VT-TuP3, 123
Kohout, J.: SE+PS+TF-MoA8, 46
Kohse-Höinghaus, K.: HI-ThP2, 235
Koirala, P.: EL+AS+EM+EN+SS-ThM4, 183; EN+AS+EM+SE-WeM12, 133
Kokubo, I.: SS+AS+NS-ThA6, 223
Kolagani, R.: EM+MI+NS-MoM4, **9**
Kolasinski, K.W.: SS+EM-FrM6, **259**
Koleske, D.: AP+AS+MC+NS+SS-ThM5, 181
Koley, G.: 2D+AS+BI+PS+SS-TuM11, 54
Kolís, J.: AC+AS+MI+SA+SS-MoM11, 4
Kolli, R.P.: AP+AS+MC+NS+SS-ThM13, 181
Kollmer, F.: AS+BI+MC-WeM5, **127**
Kolmakov, A.: IS+AS+MC+SS-TuA3, 88; IS+AS+MC+SS-TuM10, **62**; NS+AS+SS-TuA7, 94; NS+AS-WeA11, 166; SA-MoM8, **17**
Kolodziej, J.: SS+AS+NS-ThA1, **222**
Kolarenc, J.: AC+AS+MI+SA+SS-MoA1, **29**
Komachi, J.: PS-TuM4, 66
Komakov, A.: IS+2D+MC+NS+SP+SS-WeA3, 161
Komatsu, E.: VT-MoM8, 27
Komesu, T.: 2D+EM+MI+MN+NS+SS+TF-ThA8, 203
Komissar, A.: 2D-ThP15, 229
Komori, F.: SP+AS+BI+NS+SS-WeA3, **173**
Komuro, A.: SE+EM+EN+PS+TF-MoM3, 18
Kondo, H.: 2D+EM+MS+NS-FrM10, **246**; PS2-FrM8, 257
Kondo, T.: AS+MC+SS-FrM8, **248**; SS-TuP8, 120
Kondyurin, A.: SM+AS+BI+PS-ThA6, 220
Konicek, A.R.: TR-FrM10, 263
König, R.: QC+AS+BI+MN-ThM6, **194**; QC+AS+BI+MN-ThP2, 239
Kopchick, J.: AS-ThP13, 232
Kopecki, J.: EN-TuP6, 111
Korevaar, B.A.: EN-TuP16, 112

- Korolov, I.: PS1-FrM6, 255
Kortshagen, U.R.: TF+MS+PS-WeM4, 149
Kosobrodova, E.: SM+AS+BI+PS-ThA6, 220
Kostamo, J.: TF+PS-MoM1, 24
Koster, N.B.: VT-MoA6, 52
Kostoglou, N.: EN-TuP14, 112
Kotanikawa, Y.: PS2-FrM1, 256
Kotru, S.: EN-TuP10, 111
Kotulak, N.A.: SS+EM-FrM3, 259
Koty, D.: PS-TuA9, 95
Koukitu, A.: MG-WeM3, 135
Kovarik, L.: AP+AS+EN+NS+SS-ThA4, 205
Kowalsky, W.: BI+AS-WeM5, 128
Koyun, Z.: PS-TuM1, 66; SE-TuP1, 119
Kozak, D.A.: MN-WeM5, 137
Kozen, A.C.: EM+EN+TF-WeA10, 158; EN+EM+NS-TuA7, 86; EN+EM+NS-TuA8, 86; TF+EN+PS-TuA1, 101; TF+EN+PS-TuA7, 101
Kozimor, S.: AC+AS+MI+SA+SS-MoM1, 3
Kravchenko, I.I.: MI+MG-TuM10, 63
Kraya, L.Y.: BI+AS-WeM5, 128; SP+2D+AS+EM+MC+NS+SS-ThM2, 196
Kraya, R.: SP+2D+AS+EM+MC+NS+SS-ThM2, 196
Krekeler, C.: BI+AS-WeM5, 128
Kreuzer, H.J.: AP+AS+MC+NS+SS-ThM10, 181
Krick, B.A.: TR+NS-ThM6, 201
Krieg, U.: NS+EN-MoA6, 41
Krishtab, M.: EM-TuM6, 59
Krist, B.J.: PS-TuP13, 116
Kronast, F.: MI+MG-TuM6, 63
Kronawitter, C.: SS+AS+NS-ThA11, 224; SS+EN-MoM1, 21
Krooswyk, J.: SS+AS+EN-MoM8, 20
Kropman, D.: EM-TuP22, 109
Krueger, P.: MI-MoA3, 39
Krupke, R.: HI-ThP3, 235
Kruse, N.: AP+AS+EN+NS+SS-ThA3, 204
Kruska, K.: AP+AS+EN+NS+SS-ThA6, 205
Krylov, S.: MN+NS-TuA4, 92
Kub, F.: TF+PS-TuM3, 72
Kuboi, N.: PS-TuM4, 66
Kubota, T.: PS2+TF-ThM4, 192
Kubota, Y.: MG-WeM3, 135
Kudriavtsev, V.: TF+PS+SE-MoM11, 24
Kuhn, M.: 2D+AS+HI+MC+NS+PS+SP+SS-TuA3, 79
Kühne, P.: EL+AS+EM+MC+SS-ThA9, 208
Kühne, T.D.: QC+AS+BI+MN-ThM5, 194
Kujofsa, T.: TF+AS+EM-TuA7, 100
Kuk, Y.: MI-MoA10, 40; SP+AS+BI+EM+NS+SE+SS-FrM6, 258; SP+AS+EM+NS+SS-ThP3, 240
Kukreja, R.: MI+EM-MoM11, 13
Kulkarni, D.D.: AS+MC+SS-FrM10, 248
Kulkarni, G.R.: AS+MC+SS-TuA9, 81
Kumagai, Y.: MG-WeM3, 135
Kumar, A.: MC+AP+AS-MoM1, 10
Kumar, K.: PS-TuA9, 95
Kumar, P.: MI-MoA11, 41
Kummel, A.C.: 2D+AS+BI+PS+SS-TuM13, 54; 2D+AS+HI+NS+SS-ThM5, 179; BI+AS+NS-MoA2, 32; BI+MG-WeA4, 156; BI+MG-WeA7, 156; EM+2D-TuA4, 84; EM1-ThA9, 209; EM-WeA12, 160; EM-WeA3, 159; EN+AS+EM+SE-WeM4, 132; SD-WeM12, 145
Kummerer, T.: PS1-FrM11, 255
Kundu, S.: MC+AP+AS-MoM11, 12
Kung, H.: SS-TuP3, 119
Kunkel, D.A.: SS+TF-ThM11, 198
Kunze, C.: QC+AS+BI+MN-ThM5, 194
Kuo, C.-Y.: MN+NS-TuA12, 93; MN-ThP3, 237
Kuo, H.-Y.: MN+NS-TuA12, 93
Kuo, P.-H.: MN-ThP3, 237
Kuo, Y.: EM+2D-TuA12, 85; EM1-ThM13, 186
Kuo, Y.Y.: PS-TuP25, 118
Kuradome, H.: EN-TuP2, 110
Kurahashi, M.: SS+AS+EN-WeM10, 146
Kurouski, D.: CS-ThA3, 205
Kurtz, R.L.: SS+NS-TuA11, 99; SS+TF-ThM12, 198
Kushner, M.J.: PS1-FrM11, 255; PS2-WeM3, 142
Kusunoki, A.: EM-TuP9, 107
Kwak, I.J.: 2D+AS+BI+PS+SS-TuM13, 54; 2D+AS+HI+NS+SS-ThM5, 179; EM1-ThA9, 209
Kwok, D.: MI-MoA9, 40
Kwon, J.Y.: SS+NS-TuA9, 98
Kwon, K.S.: MN+PS-WeA1, 162
Kwon, S.: SS-TuP18, 122
- L —
Laas, T.: EM-TuP22, 109
LaBella, V.P.: 2D+AS+HI+MC+NS+PS+SP+SS-TuA8, 79; MC-TuP4, 113; NS+AS-WeA10, 166; SP+AS+BI+EM+NS+SE+SS-FrM5, 258
Lad, R.J.: SE+NS+TR-TuM2, 69; TF+AS-FrM1, 260; TF+PS+SE-MoM9, 23
Lafleur, T.: PS1-WeM11, 140
Lafond, A.: EN-TuP5, 110; TF+PS+SE-MoM3, 22
LaGoo, L.: AS+BI+MC-WeA3, 154
LaGrange, T.: TF+SE-TuM6, 75
Lagраста, S.: PS-MoA9, 43
Laha, A.: EM1-ThA11, 210
Lahiri, B.: NS-ThP3, 238
Lai, R.Y.: EL+AS+EM+MC+SS-ThA6, 207
Laine, R.: TF+PS-MoM1, 24
Lal, R.: EM1-WeM1, 129
Lalor, J.: SE+EM+EN+PS+TF-MoM6, 18
Lambert, D.: PS2+TF-ThM2, 192
Lane, A.P.: SD-WeM10, 144
Lang, B.N.: TF+PS-TuM12, 74
Langhoff, A.: QC+AS+BI+MN-ThM6, 194; QC+AS+BI+MN-ThP2, 239
Langlois, G.: SS+TF-ThM4, 198
Lanzutti, A.: TF+PS-TuM1, 72
Larsen, G.K.: TF+EM+EN-WeA8, 176; TF+EM+EN-WeA9, 176
Larson, D.J.: AP-ThP1, 230
Larson, P.: EM-TuP1, 106
Laskin, J.: EM-MoA3, 34
Latchford, I.: TF+PS+SE-MoM11, 24
Latkowski, J.: EW-WeL5, 152
Latour, R.A.: BI+MG-WeA3, 156
Latu-Romain, E.: PS2-FrM2, 256; SD-WeA9, 172
Lau, B.L.T.: QC+AS+BI+MN-ThA6, 219
Lau, C.N.: 2D+EM+MS+NS-FrM1, 245
Lau, J.: TF+EN+PS-TuA2, 101
Lauer, I.: EM+MI+NS-MoM8, 9
Laughlin, B.L.: AS+BI+VT-TuM10, 56
Laughlin, K.: TF+EM+EN-WeA11, 177
Lauhon, L.J.: 2D+AS+HI+NS+SS-ThM4, 179; AP+AS+MC+NS+SS-ThM5, 181; NS+AS+SS-TuA3, 93
Laursen, T.: MC+2D+AP+AS-MoA6, 38; MC-TuP3, 113
Lauter, V.: EN+EM+MN+NS+TR-MoA9, 36
LaVan, D.A.: TF+SE-TuM6, 75
Law, M.: EN+AS+EM+SE-WeM5, 132
Lawrence, D.: AP-ThP1, 230
Lawson, A.P.: NS+EN-MoA3, 41
Le Lay, G.: 2D+EM+NS+SS+TF-WeM1, 125
Le Monge, T.: AS+BI+MC-WeA2, 154
Le, D.: EM1-WeM10, 130
Le, D.T.: 2D+AS+BI+PS+SS-TuM3, 53; 2D+AS+EM+MI+MN+NS+TF-WeA3, 153; 2D+AS+HI+NS+SS-ThM6, 179; 2D+EM+MI+MN+NS+SS+TF-ThA8, 203
Le, S.: 2D+EM+MS+NS-FrM4, 245
Leahey, P.: VT-TuA12, 104
Lechner, B.A.J.: NS-WeM6, 139; SS+AS+EN-MoM3, 19; SS+AS+EN-MoM4, 19
Lechuga, H.: AS+MC+SS-TuA1, 80
Lee, B.G.: EM1-ThM10, 185
Lee, B.H.: 2D-ThP17, 229
Lee, C.: 2D-ThP11, 229; SP+AS+BI+NS+SS-WeA11, 174
Lee, C.C.: TF-ThP8, 241
Lee, C.T.: TF-ThP23, 243
Lee, C.-T.: TF-ThP4, 241
Lee, C.Y.: PS-ThA8, 217
Lee, D.: NS+HI-TuM3, 64; QC+AS+BI+MN-ThA1, 218
Lee, H.: EN+AS+EM+SE-WeM6, 133; NS+EN-MoA4, 41; SS-TuP18, 122
Lee, H.D.: HI+2D+AS+BI+MC-ThM13, 188
Lee, H.-J.: PS-TuP5, 114
Lee, I.: SS+AS+EN-MoM1, 19
Lee, J.: IS-ThP1, 236; MN+NS-TuA10, 92; MN+PS-WeA7, 163; MN+PS-WeA8, 163; MN-WeM13, 138; PS-MoM3, 14; PS-TuA8, 95; SS+EN-MoA7, 47; SS+NS-TuA4, 98
Lee, J.R.L.: AS+MC+SS-TuA11, 81; SA-MoA8, 44
Lee, J.U.: 2D+AS+HI+MC+NS+PS+SP+SS-TuA8, 79; 2D+EM+MS+NS-FrM4, 245
Lee, J.-Y.: SD-WeA10, 172
Lee, K.: TF-ThP25, 243
Lee, K.-M.: EM1-WeM10, 130
Lee, M.: BI+MG-WeA12, 157
Lee, P.M.: SE+NS+TR-TuM12, 70; TR-FrM8, 263
Lee, S.: EM-WeA12, 160; QC+AS+BI+MN-ThP1, 239; SS-TuP1, 119
Lee, S.B.: EM+EN+TF-WeA10, 158; EN+EM+NS-TuA3, 85; EN+EM+NS-TuA7, 86; EN+EM+NS-TuA8, 86; TF+EN+PS-TuA7, 101
Lee, S.Y.: IS-ThP1, 236
Lee, W.: QC+AS+BI+MN-ThM10, 194
Lee, W.T.: MC+2D+AP+AS-MoA10, 39
Lee, Y.B.: EM-TuM3, 58
Lee, Y.G.: 2D-ThP17, 229; SD-WeA11, 172
Lee, Y.K.: NS+EN-MoA4, 41
Lefebvre, W.: AP+AS+NS+SS-FrM5, 247
Lefever, J.A.: SP+AS+BI+EM+NS+SE+SS-FrM2, 258
Lefevre, B.: AS+MC+SS-FrM5, 248; PS-TuA10, 96
Legare, J.: EW-WeM8, 134
Leggett, G.J.: BI+AS+NS-MoA6, 33
Leins, M.: EN-TuP6, 111
Leisch, M.: VT-TuA1, 103
Lempert, W.: PS+2D-WeA9, 168
Leng, S.: VT-WeM3, 150
Lennartz, C.: BI+AS-WeM5, 128
Lennhoff, J.D.: PS-ThA2, 216
Lenz, D.: AP-ThP1, 230
Leobandung, E.: MC+2D+AP+AS-MoA1, 37
Leonard, F.: SP+AS+BI+NS+SS-WeA11, 174
Leonard, K.: TF+PS+SE-MoM5, 23
Leou, K.C.: PS-TuP7, 115
Lepkowski, D.L.: NS+EN-MoA11, 42
Létard, J.-F.: MI+MG-TuM5, 63
Leverd, F.: PS-MoA9, 43
Levesque, T.: AS-ThP12, 232
Levi, D.: EL+AS+BI+EM+SS-FrM5, 250
Lewis, A.: 2D-ThP15, 229
Lewis, B.B.: NS+HI-TuM10, 65; TF+PS-TuM6, 73
Lewis, D.: EW-WeL4, 152
Lewis, J.S.: EN+AS+EM+SE-TuM12, 60
Lherron, B.: MC+2D+AP+AS-MoA10, 39
Li, A.P.: SP+2D+AS+EM+MC+NS+SS-ThM10, 197; SP+2D+AS+EM+MC+NS+SS-ThM11, 197; SP+2D+AS+EM+MC+NS+SS-ThM6, 196
Li, C.: PS-TuM10, 67
Li, D.: MI+EM-MoM3, 12; TF+AS+EM-TuA3, 99
Li, H.: AS+BI+VT-TuM1, 55; PS-TuM11, 67; PS-TuM6, 67
Li, J.: 2D+EM+NS+PS+SS+TF-MoM6, 2; AS-ThP13, 232; AS-ThP24, 233; EL+AS+BI+EM+SS-FrM5, 250; EL+AS+EM+EN+SS-ThM3, 183; EL+AS+EM+EN+SS-ThM4, 183
Li, J.J.: AP+AS+NS+SS-FrM1, 246; EN+AS+EM+SE-WeM10, 133

- Li, L.: AS+BI+VT-TuM3, 55
 Li, M.: SS+AS+EN-TuM6, **71**; SS+AS+NS-ThA2, 222
 Li, P.-C.: MN+NS-TuA11, 92
 Li, Q.: 2D+AS+BI+PS+SS-TuM4, 53
 Li, S.: SS+AS-WeM3, 147
 Li, T.: MS+PS+TF-ThA11, **213**; SS-TuP20, 122
 Li, W.: PS-TuP8, **115**; SS+TF-ThM4, **198**
 Li, W.-M.: TF+PS-MoM1, 24
 Li, Y.: 2D+AS+EM+MI+MN+NS+TF-WeA12, 154; EN-TuP14, 112; MS+PS+TF-ThA11, 213; MS+TF-WeA9, 165; VT-WeA3, **177**
 Li, Y.S.: EM+NS+TF-FrM5, 253
 Li, Z.: EM1-WeM12, 130; NS-WeM11, **139**; SP+AS+EM+NS+SS-ThP8, 240; SS+EN-MoM6, 22
 Li, Z.Y.: NS+HI-TuM4, 65
 Lian, G.: EM-WeA9, 159
 Liang, J.: TF+PS-ThM10, **200**
 Liang, Z.: AS-ThP1, 230
 Liao, B.: TF-ThP8, **241**
 Liao, C.H.: EM+EN-FrM5, 252
 Liao, K.: EN-TuP14, 112
 Liao, K.Y.: MS-ThP4, 237
 Liao, X.: NS+SE-MoM11, 14
 Libera, J.A.: TF+PS-MoM10, 25
 Liberman, A.: BI+AS+NS-MoA2, 32; BI+MG-WeA4, **156**
 Li-Chiang, C.: PS-MoM8, 15
 Lichtenstein, L.: 2D+EM+NS+SS+TF-WeM12, 126; SS-TuP19, 122
 Lichtenstein, T.: NS+EN-MoA6, **41**
 Licoccia, S.: TF+EN+PS-TuA12, 103
 Liddiard, S.: MN+PS-WeA3, 163; TF+AS-FrM2, 260
 Lie, F.L.: NS+HI-TuM3, 64
 Lieb, S.: HI-ThP2, 235
 Lietz, A.M.: VT-MoA8, 52; VT-MoA9, **52**
 Lilliental-Weber, Z.: SS+EN-MoM3, 21
 Lilly, M.P.: EM1-ThA6, 209
 Lim, J.Y.: VT-TuP3, **123**
 Lim, S.K.: VT-TuP3, 123
 Lin, C.-C.: EM1-ThM13, 186
 Lin, C.F.: EM+EN+TF-WeA10, **158**; TF+EN+PS-TuA1, 101
 Lin, G.: MI+MG-TuM6, 63
 Lin, J.: EM+2D-TuA8, 84; SE+NS+TR-TuM12, **70**
 Lin, J.-M.: SS-TuP13, 121
 Lin, P.H.: VT-TuP2, 123
 Lin, S.C.: PS-TuP24, **117**
 Lin, T.H.: PS-TuP21, 117
 Lin, X.: AS+MC+SS-FrM5, 248
 Lin, Y.: EM-MoA3, 34; MC+AP+AS-MoM4, 10
 Lin, Y.C.: 2D+AS+HI+MC+NS+PS+SP+SS-TuA3, 79; 2D+EM+NS+SS+TF-WeM6, 125; MS-ThP4, 237
 Lin, Y.H.: MN-ThP1, 236; MN-ThP2, 236; MS-ThP6, **237**
 Lin, Y.S.: MN-ThP2, 236; MS-ThP6, 237
 Lin, Y.W.: TF-ThP23, 243
 Lindfors, S.: TF+PS-MoM1, 24
 Linford, M.R.: TF+AS-FrM4, **261**; TF+EM+EN-WeA11, 177; TF+EM+EN-WeA7, 176; TF-ThP19, 242
 Linhart, W.M.: EN+AS+EM+SE-WeM11, 133
 Lisi, A.: PS-TuA9, 95
 Liu, B.W.: BI+AS-TuA11, 83
 Liu, C.: BI+AS+NS-MoA7, 33; EN+EM+NS-TuA7, 86; TF+EN+PS-TuA1, 101; TF+EN+PS-TuA7, **101**; VT-TuA12, 104
 Liu, D.-J.: EN+EM+NS-TuA1, **85**; SS+AS-WeM10, 148
 Liu, D.R.: MI-TuP3, **114**
 Liu, H.: EM-TuM3, 58
 Liu, J.: AP+AS+EN+NS+SS-ThA4, **205**; AP+AS+NS+SS-FrM8, 247; MI+MG-TuM5, 63; SE+PS+TF-MoA6, 45; SP+AS+BI+EM+NS+SE+SS-FrM2, 258
 Liu, J.-C.: MS+TF-WeA3, 164
 Liu, L.: PS1-FrM10, **255**; PS1-FrM9, 255; SD-WeM3, 144; SP+2D+AS+EM+MC+NS+SS-ThM11, 197; SS+NS-TuA11, 99; SS-TuP21, 122
 Liu, M.: EM2-ThM12, **186**; MI+EM-MoM5, **12**
 Liu, Q.: EM2-ThM12, 186
 Liu, Q.Q.: IS+2D+MC+NS+SP+SS-WeA9, **162**
 Liu, R.: SS+EM-FrM1, 258
 Liu, S.Q.: BI+AS-TuA11, 83
 Liu, S.Y.: EL+AS+EM+MC+SS-ThA3, 207
 Liu, W.: MI+EM-MoM3, 12
 Liu, X.: EM+NS+TF-FrM11, **254**; MC+AP+AS-MoM6, 11; TF-ThP26, 244; VT-WeA1, 177; VT-WeA3, 177
 Liu, X.L.: EN-TuP13, 112
 Liu, X.-Z.: 2D+AS+BI+PS+SS-TuM4, **53**
 Liu, Y.: EM+NS+TF-FrM6, **253**; EN+AS+EM+SE-WeM5, **132**; NS-WeM4, 139; TF+EM+EN-WeA11, 177
 Liu, Z.: EN+AS+EM+SE-WeM5, 132; IS+2D+MC+NS+SP+SS-WeA1, **161**
 Liu, Z.L.: IS+2D+MC+NS+SP+SS-WeA10, 162
 Livengood, R.H.: HI+2D+AS+MC-ThA4, 212; HI+2D+AS+MC-ThA6, **212**
 Livi, K.J.T.: TF+SE-TuM10, 75
 Lloyd, K.G.: AS-ThP18, **233**
 Lo, M.: NS+AS-WeA9, 166
 Lock, E.H.: 2D+AS+BI+PS+SS-TuM5, 53; PS1-FrM8, 255; PS-TuM12, **67**
 Löhneysen, H.V.: HI-ThP3, 235
 Loncar, M.: MN-WeM3, **137**
 Long, J.W.: EM+EN+TF-WeA11, 158
 Long, N.: BI+AS+MN+NS-TuM5, 57
 Long, S.B.: EM2-ThM12, 186
 Longo, R.: NS+HI-TuM11, 65
 Lopez, T.: EN+AS+EM+SE-TuM13, **60**
 Lordi, V.: EN+AS+EM+SE-WeM2, 132
 Losego, M.: NS+SE-MoM8, 14
 Losego, M.D.: TF+PS-MoA9, 49
 Losurdo, M.: EL+AS+EM+EN+SS-ThM6, **184**
 Lou, J.: 2D+EM+NS+PS+SS+TF-MoM1, **2**; SP+2D+AS+EM+MC+NS+SS-ThM10, 197
 Lou, Q.: PS-TuP3, **114**
 Lovinger, D.J.: SS+NS-TuA12, 99
 Lownsbury, J.M.: EM2-ThA9, **211**
 Lu, C.-J.: MN+NS-TuA12, 93
 Lu, C.L.: MS-ThP4, 237
 Lu, F.: NS+AS-WeA9, 166
 Lu, H.L.: 2D+AS+HI+NS+SS-ThM5, 179
 Lu, I.: 2D+EM+NS+SS+TF-WeM10, 126; 2D-ThP11, 229; SP+AS+BI+NS+SS-WeA11, 174
 Lu, N.: EM-WeA4, 159; EM-WeA9, 159
 Lu, S.-S.: MN-ThP3, 237
 Lu, S.-Y.: PS-MoM8, 15
 Luan, P.: PS+2D-WeA9, 168; SE+EM+EN+PS+TF-MoM2, 18
 Lubeck, J.: SA-TuM1, 68; TF+AS-FrM9, 261
 Lucatorro, T.B.: TF+PS-ThM11, 200
 Lucci, F.R.: SS+AS+EN-WeM4, **145**
 Lucero, A.: 2D-ThP17, 229; SD-WeA11, **172**
 Luckham, E.: BI+AS-MoM5, 7
 Ludwig, K.F.: SA-MoM4, 17
 Lui, Z.: NS+HI-TuM1, 64
 Lukaszew, R.A.: TF+AS+EM-TuA9, 100
 Lukaszewicz, M.: PS-MoM4, 15
 Lukens, W.: AC+AS+MI+SA+SS-MoM1, 3
 Luna-López, J.A.: EM-TuP28, 109
 Lundgren, A.O.: QC+AS+BI+MN-ThA7, **219**
 Lunt, B.: TF+EM+EN-WeA11, 177; TF-ThP19, 242
 Luo, E.W.-WeM9, **134**
 Luo, H.: AS-ThP11, 232
 Luo, X.: BI-ThP2, 234
 Lütgebaucks, C.: BI+AS-WeM12, **128**
 Lutz, H.: BI+AS-WeM6, 128
 Lv, H.B.: EM2-ThM12, 186
 Lyndaker, A.: VT-WeA3, 177
 Lynn, K.G.: EN+EM+NS-TuA11, 87
 Lyubintsev, I.: SS+AS-WeM13, 148

— M —

- Ma, L.: SS+AS+EN-TuM5, 71
 Ma, Q.: 2D+EM+MI+MN+NS+SS+TF-ThA8, 203
 Ma, S.S.: SE+PS+TF-MoA2, 45
 Ma, X.: AS+BI+VT-TuM3, 55
 Ma, Y.: SS-WeA9, 175
 Maas, D.J.: HI+2D+AS+MC-ThA8, 212
 Maayan, E.: 2D-ThP15, 229
 Maboudian, R.: EM+EN+TF-WeA8, **158**
 Maccallini, E.: VT-TuM10, 77
 Macco, B.: TF+EN+PS-TuA10, **102**
 MacFarlane, J.: AC+AS+MI+SA+SS-TuM5, 55
 Macias-Romero, C.: BI+AS-WeM12, 128
 Mack: VT-TuM6, 77
 Mack, P.: AS+MC+SS-FrM2, **247**; AS+MC-MoM1, 5; EW-TuL2, 78
 Mackus, A.J.M.: 2D+EM+MS+NS-FrM6, 245; TF+PS-MoA10, **50**
 Madaan, N.: AP+AS+MC+NS+SS-ThM6, **181**; AS+MC+SS-TuA9, 81; TF+EM+EN-WeA11, 177
 Magaud, L.: PS+2D-WeA1, 166
 Magee, J.: SA-MoA3, 44
 Magnusson, R.: EL+AS+BI+EM+SS-FrM3, 250
 Mahadik, N.A.: EM1-WeM5, 129
 Maimon, R.: MN+NS-TuA4, 92
 Majeski, M.: EM-MoA9, **35**; EM-TuP31, 110
 Major, C.: EL-ThP6, 234
 Majumdar, A.: MC+2D+AP+AS-MoA1, 37
 Makarov, D.: MI+MG-TuM6, 63
 Makowski, M.J.: IS+AS+MC+SS-TuA4, 88; IS+AS+MC+SS-TuM11, 62
 Maksymovych, P.: 2D+EM+MI+MN+NS+SS+TF-ThA9, 204
 Malachosky, E.: NS+SE-MoM5, 13
 Maldonado Álvarez, A.: TF-ThP22, 243
 Malinin, V.: TF+PS-MoM3, **24**
 Malko, A.: EN+EM+MN+NS+TR-MoA3, 36
 Mallick, A.: TF+PS-ThM10, 200
 Mallinson, C.F.: AS-ThP9, 231
 Malyshev, O.B.: VT-WeM1, 150
 Mamun, M.A.: VT-WeA4, 177
 Manandhar, S.: SS+AS+EN-TuM13, 72
 Mancheno, P.: EM-TuP2, **106**
 Mancheno-Posso, P.L.: SS+EM-FrM8, **260**
 Mandrekar, T.: TF+PS-ThM10, 200
 Mandru, A.: MI+MG-TuA8, 91
 Mandrus, D.G.: MI+MG-TuM10, 63
 Manera, L.T.: EN-TuP15, 112
 Mangolimi, F.: AS+BI+MC-WeA12, **155**; TR-FrM10, 263
 Mangolimi, L.: EM-MoA4, 34; EN+AS+EM+SE-TuM13, 60; PS-ThA3, **216**
 Mani-Gonzalez, P.G.: AS+MC-MoM2, 5
 Manini, P.: VT-TuM10, 77
 Mann, H.S.: TF+PS-TuM12, **74**
 Mann, J.: 2D+EM+NS+SS+TF-WeM10, 126; EL+AS+BI+EM+SS-FrM5, 250; SP+AS+BI+NS+SS-WeA11, 174
 Mann, J.M.: AC+AS+MI+SA+SS-MoM11, 4
 Mannarino, M.: MC+AP+AS-MoM1, 10
 Mannheim, A.: TF+AS+EM-TuA2, 99
 Mannix, A.J.: 2D+AS+EM+NS+SS-MoA7, 28; 2D+AS+HI+NS+SS-ThM13, 180; 2D+EM+NS+SS+TF-WeM3, **125**
 Mansfield, L.: EL+AS+BI+EM+SS-FrM5, 250
 Mao, H.Q.: BP+BI+AS-SuA7, **1**
 Marceau, E.: AP+AS+EN+NS+SS-ThA6, 205
 Marchack, N.P.: PS-MoM10, **16**; PS-MoM3, 14
 Marcinkowski, M.: SS+AS+EN-WeM4, 145
 Marcott, C.: NS+AS-WeA9, 166
 Maria, J.-P.: AS+MC+SS-FrM9, 248
 Mariano, W.C.: EM-TuP3, **106**
 Marin, E.: TF+PS-TuM1, 72
 Mariolle, D.: 2D+EM+MI+MN+NS+SS+TF-ThA10, 204; SP+AS+BI+NS+SS-ThA4, 221

- Marks, J.: PS-MoA6, 42
 Marks, T.J.: 2D+AS+HI+NS+SS-ThM4, 179
 Marot, L.: PS-ThA9, 217
 Marquardt, A.: CS-FrM5, **249**
 Marquez, M.P.: TF+SE-TuM5, 75
 Marsh, J.R.: AS-ThP13, 232; AS-ThP18, 233
 Martin, L.W.: EM+MI+NS-MoM5, **9**
 Martin, M.C.: SA-MoA4, 44
 Martin, R.L.: AC+AS+MI+SA+SS-MoM1, 3
 Martin, R.W.: SS+AS-MoM3, 21
 Martinez, E.: MC+AP+AS-MoM10, **11**; SS+EM-FrM9, 260
 Martinez-Guerra, E.: EN-TuP9, 111
 Martins, B.: SP+2D+AS+EM+MC+NS+SS-ThM5, 196
 Martins, R.: EM+NS+TF-FrM8, 253
 Martinu, L.: SE+NS+TR-TuM5, 70
 Martirez, J.M.: SS+AS+EN-TuM1, 71
 Maslar, J.E.: TF+PS-MoA3, 49; TF+PS-MoA8, **49**
 Mass, J.L.: CS-ThA10, 206; CS-ThA6, **206**; CS-ThA9, 206
 Mastrangelo, A.M.: PS+SE-ThA1, 214
 Mastro, M.A.: EM1-ThM12, 185; MC+2D+AP+AS-MoA4, **38**; TF+PS-TuM3, 72
 Masuda, N.: SS-TuP10, 120
 Masuda, S.: EM-TuP12, 107; EM-TuP13, 108
 Matej, Z.: AC+AS+MI+SA+SS-MoM9, 4
 Mateos, D.: TF-ThP15, **242**
 Materer, N.: SS+AS+NS-ThA9, **224**
 Matranga, C.: SS+NS-TuA4, 98
 Matsen, C.: CS-ThA10, 206
 Matsubayashi, A.: 2D+AS+HI+MC+NS+PS+SP+SS-TuA8, **79**; MC-TuP4, 113; NS+AS-WeA10, 166
 Matsuda, C.: SE+PS+TF-MoA10, 46
 Matsui, F.: 2D+EM+NS+PS+SS+TF-MoM8, 3
 Matsumoto, H.: PS1-WeM12, 141; PS-MoM10, 16; PS-TuA3, 95
 Matsumuro, A.: MS-ThP1, 237; SP+AS+EM+NS+SS-ThP2, 240; TF-ThP2, 241; TF-ThP3, 241
 Matsunaga, K.: EM-TuM6, 59
 Matsuura, G.: PS-MoM3, 14
 Mattrey, R.: BI+AS+NS-MoA2, 32; BI+MG-WeA4, 156
 Mattsson, A.: SS+EN-MoM2, **21**
 Matyi, R.: MC-TuP4, 113
 Maurya, D.: MC+AP+AS-MoM11, 12
 Mavrikakis, M.: SS+AS-WeM3, **147**
 Mayen-Mondragon, R.: EN-TuP9, 111
 Mayer, R.: NS-ThP7, 239
 Mayer, T.S.: EM-WeA1, **159**
 Mayergoyz, I.D.: NS+EN-MoA3, 41
 Mayor, M.: HI-ThP3, 235
 Mazet, L.: EM+MI+NS-MoM8, 9
 Mazzafera, P.: EN-TuP15, 112
 McArthur, S.L.: BI+AS+NS-MoA9, 34; QC+AS+BI+MN-ThA9, 220; SM+AS+BI+PS-ThM1, **195**
 McAvoy, P.C.: NS+EN-MoA3, 41
 McCann, P.J.: EM+EN-FrM10, 252; EM-TuP1, 106
 McCartney, M.R.: EM+MI+NS-MoM3, 8
 McCarty, K.F.: 2D+EM+NS+PS+SS+TF-MoM10, 3; SP+2D+AS+EM+MC+NS+SS-ThM11, 197
 McClimon, J.B.: AS+BI+MC-WeA12, 155
 McConney, M.E.: 2D+EM+NS+PS+SS+TF-MoM5, 2
 McCreary, K.M.: 2D+EM+NS+PS+SS+TF-MoM4, **2**
 McDaniel, M.D.: EM+MI+NS-MoM11, 9; EM1-ThA10, **210**
 McDonald, J.P.: TF+SE-TuM2, 74
 McDonnell, S.: 2D+EM+NS+SS+TF-WeM6, 125; EM+2D-TuA3, **84**; EM-WeA4, 159; EM-WeA9, 159; NS+HI-TuM11, 65
 McElwee-White, L.: SS+AS+EN-MoM11, 20
 McEntee, M.: NS-WeM3, **138**
 McGath, M.: MS+PS+TF-ThM6, 189
 McGlone, J.: EM2-WeM13, 131
 McGuire, G.E.: NS+AS-WeA1, 165
 McGuire, J.M.: BI+MG-WeA8, 156
 McInerney, E.J.: VT-TuM1, **76**
 McIntyre, P.C.: EM-WeA12, 160
 McKenzie, D.R.: SM+AS+BI+PS-ThA6, 220
 McKeon, B.S.: AC+AS+MI+SA+SS-MoM10, 4
 McKibbin, S.: NS+AS+SS-TuA4, 93
 McLain, J.: SE+PS+TF-MoA1, 45
 McLean, W.: AC+AS+MI+SA+SS-TuM12, 55
 McNamara, J.D.: EM+EN-FrM3, **251**
 McPhail, D.S.: CS-FrM10, **249**; CS-FrM6, 249
 McTeer, A.: PS1-WeM3, **140**
 Mebarki, M.: PS-TuA7, **95**
 Mecwan, M.: SM+AS+BI+PS-ThM10, **195**
 Mederos Vidal, M.: 2D-ThP8, **228**; TF-ThP15, 242
 Medikonda, M.: MC+AP+AS-MoM3, 10; MC-TuP4, 113
 Medling, S.A.: AC+AS+MI+SA+SS-TuM1, 54
 Meer, T.: AS+MC+SS-TuA7, 81
 Meessen, J.: HI+2D+AS+MC-ThA8, 212
 Mehta, A.: CS-ThA6, 206
 Mehta, B.R.: TF-MoA7, 51
 Meirer, F.: CS-ThA6, 206
 Meisenkothen, F.: AP+AS+MC+NS+SS-ThM13, **181**
 Meitner, S.: VT-WeA7, 178
 Melia, M.A.: SE+PS+TF-MoA9, **46**
 Melin, T.: SP+AS+BI+NS+SS-ThA4, 221
 Mendelsberg, R.: SE+PS+TF-MoA7, 46
 Mendez, N.: BI+MG-WeA7, **156**
 Menzel, A.: SS+AS+EN-MoM3, 19
 Merche, D.: PS+2D-WeA12, 168; PS+SE-ThA7, 215
 Mergos, I.A.: EL+AS+BI+EM+SS-FrM4, **250**
 Merkulov, A.V.: 2D-ThP1, **228**
 Merrett, J.N.: EM-TuP18, 108
 Merrill, M.: SA-MoA8, 44
 Mertens, J.: PS+2D-WeA11, 168
 Meshkova, A.: TF-ThA10, 226
 Messer, B.: PS-TuA8, 95
 Mestanza Muñoz, S.N.: 2D-ThP8, 228; TF-ThP15, 242
 Metz, A.: PS-TuA3, 95; PS-TuA8, 95; PS-TuA9, 95
 Metzler, D.: PS2+TF-ThM1, **191**
 Meulenberg, R.W.: IS+AS+MC+SS-WeM4, **134**; TF+AS-FrM1, 260
 Meunier, R.: EN-TuP5, **110**; TF+PS+SE-MoM3, 22
 Meyer, D.J.: MC+2D+AP+AS-MoA4, 38
 Meyer, H.M.: AS-ThP11, **232**; AS-ThP17, 233
 Meyer, J.R.: EM1-ThM12, 185
 Meyer, M.T.: MN+NS-TuA9, 92
 Meyers, G.F.: NS+SE-MoM1, **13**
 Meysing, D.: EN+AS+EM+SE-WeM10, 133
 Mhatre, B.S.: SS-WeA4, 174
 Michaels, C.A.: IS+AS+MC+SS-WeM12, **135**
 Michalak, D.J.: SD-WeM3, 144
 Michallon, P.: PS1+TF-ThM5, 190
 Michels, J.J.: TF-ThA4, 225
 Middleman, K.J.: VT-WeM1, **150**
 Mihara, S.: EM-TuP13, 108
 Mikashima, S.: TR-ThP5, 244
 Mikkelsen, A.: NS+AS+SS-TuA4, **93**
 Mikulski, P.: TR-ThA8, 227
 Milioni, D.: QC+AS+BI+MN-ThM13, 194
 Miller, B.: EL+AS+EM+MC+SS-ThA10, 208
 Miller, J.: TF+AS+EM-TuA11, 100
 Miller, M.A.: SE+EM+EN+PS+TF-MoM5, 18
 Mills, A.: 2D+AS+HI+MC+NS+PS+SP+SS-TuA4, 79
 Milne, Z.B.: TR-FrM6, 263
 Milosavljevic, V.: SE+EM+EN+PS+TF-MoM6, **18**
 Milošević, M.: AS+MC+SS-TuA3, 80
 Minami, T.: EN-TuP11, 111
 Minasian, S.: AC+AS+MI+SA+SS-MoM1, **3**
 Minaye Hashemi, F.: SD-WeA8, **171**
 Minelli, C.: BI+AS+NS-MoA8, 33
 Minnal, C.: EN+EM+NS-TuA11, 87
 Mirhosseini, H.: MI-MoA4, 40
 Mirkin, C.A.: NS+SE-MoM11, 14
 Mirmelstein, A.: AC+AS+MI+SA+SS-MoA6, 29
 Mishra, D.: BI+AS-TuA1, 82
 Misra, S.: EM1-ThA6, **209**; EM1-ThA7, 209
 Mistry, H.: NS-WeM5, **139**
 Mitchell, J.N.: AC+AS+MI+SA+SS-TuM1, 54
 Mitrani, J.: PS-TuP11, **115**
 Mitterer, C.: SE+NS+TR-TuM11, **70**
 Mitzi, D.B.: EN+AS+EM+SE-WeM4, 132
 Miyake, K.: PS-TuP6, 114
 Miyamoto, K.: MI-MoA1, **39**
 Miyata, T.: EN-TuP11, **111**
 Miyazoe, H.: PS-MoM10, 16
 Mkhoyan, A.: TF+MS+PS-WeM4, 149
 Mogilevsky, G.M.: SS+AS-WeM6, 147
 Mogyonye, J.E.: TF+PS+SE-MoM6, 23; TF+PS+SE-MoM8, 23
 Mohanty, N.: PS-TuA11, 96; PS-TuA3, 95; PS-TuA8, 95
 Mohimi, E.: TR-ThP2, **244**
 Mohr, S.: PS-TuP16, **116**
 Mok, H.S.: 2D+EM+NS+PS+SS+TF-MoM10, 3
 Mokoena, P.: 2D-ThP7, **228**
 Molkenboer, F.T.: VT-TuA10, **104**
 Möllers, R.: AS+BI+MC-WeM5, 127
 Momose, T.: VT-WeM6, 151
 Monaghan, S.: EM+2D-TuA8, 84
 Monfil-Leyva, K.: EM-TuP28, **109**; EM-TuP30, 110
 Montero, G.: TF-ThP15, 242
 Montgomery, F.: TF+PS+SE-MoM5, 23
 Moody, B.: MG-WeM3, 135
 Moody, M.P.: AP+AS+EN+NS+SS-ThA6, **205**
 Moon, B.H.: PS-TuP8, 115
 Moon, D.W.: EL+AS+BI+EM+SS-FrM1, **250**
 Moon, J.-S.: EM1-WeM10, **130**
 Moon, R.: MS+TF-WeA3, **164**
 Mooney, B.L.: MG-TuA9, **90**
 Moore, C.A.: AS-ThP19, 233
 Morales, E.H.: NS-WeM12, 140; SS+AS+EN-TuM1, **71**
 Morales-Cifuentes, J.R.: 2D+AS+EM+MI+MN+NS+TF-WeA8, **153**; SS+AS-WeM11, 148
 Morales-Sánchez, A.: EM-TuP30, 110
 Mordi, G.: 2D-ThP17, 229
 Morel, N.: SS+EM-FrM9, 260
 Moreno, J.: SE+PS+TF-MoA10, 46
 Moreno-Moreno, M.: EM-TuP30, 110
 Moret, M.P.: SS+EM-FrM9, 260
 Morimoto, T.: PS-MoA3, **42**
 Morin, J.-F.: TF-MoA3, 50
 Morin, J.W.: AS-ThP3, 231
 Morkötter, S.: NS+AS+SS-TuA3, 93
 Morohoshi, S.: AS+MC+SS-FrM8, 248
 Moroni, L.: BI+MG-WeA9, 157
 Moroz, P.: PS2+TF-ThM10, **193**
 Morozovska, A.: 2D+EM+MI+MN+NS+SS+TF-ThA9, 204
 Morris, J.R.: AS+MC-MoM10, 6; AS-ThP16, 232; SS+AS+EN-MoM9, 20
 Morrish, R.M.: PS+2D-WeA3, **167**
 Morrison, I.: PS-TuP29, 118
 Morrison, J.: AS+BI+MC-WeA1, 154
 Mosden, A.: PS-TuA9, 95
 Moshkalev, S.: NS-ThP7, 239
 Moszkowicz, L.: MC+2D+AP+AS-MoA11, 39
 Mothudi, B.: TF+SE-TuM13, **76**
 Motley, J.R.: BI+AS+MN+NS-TuM4, 57
 Motoyama, M.C.: 2D+AP+AS-MoA10, 39
 Moulder, J.F.: AS+BI+MC+SS-MoA11, 32; AS-ThP6, 231; EW-TuL3, 78
 Mourey, O.: PS2-FrM2, **256**
 Mousa, M.: TF+PS-MoM9, **25**
 Movva, H.C.P.: 2D+AS+HI+NS+SS-ThM5, 179
 Mowll, T.R.: 2D+AS+HI+MC+NS+PS+SP+SS-TuA10, 80; 2D+EM+NS+PS+SS+TF-MoM3, **2**

- Moyon, F.: AP+AS+NS+SS-FrM5, 247
 Mu, R.: SS+AS-WeM13, 148
 Mu, S.: MI+MG-TuM5, 63
 Muddiman, B.: NS+HI-TuM1, 64
 Mueller, M.: SA-TuM1, 68
 Mueller, T.: EN+AS+EM+SE-TuM6, 60; MG-WeM6, 136
 Muhl, S.: TR-ThP3, 244
 Mulckhuysen, W.: HI+2D+AS+MC-ThA8, 212
 Mulders, J.J.L.: 2D+EM+MS+NS-FrM6, 245
 Muller, E.A.: SA-MoA4, 44
 Müller, L.: HI+2D+AS+BI+MC-ThM13, 188
 Müller, M.: SA-TuA12, 97; SA-TuP1, 119
 Mullet, C.H.: SS+NS-TuA12, 99
 Mullins, D.R.: SS+AS+EN-TuM3, 71
 Mulvaney, S.P.: BI+AS+MN+NS-TuM5, 57
 Mundle, R.M.: NS+EN-MoA11, 42
 Muñoz-Zurita, A.L.: EM-TuP28, 109; EM-TuP30, 110
 Munusamy, P.: BI+AS+NS-MoA7, 33
 Muramoto, S.: AS+BI+MC+SS-MoA9, 31
 Murata, Y.: 2D+EM+NS+PS+SS+TF-MoM10, 3
 Muratore, C.: 2D+EM+NS+PS+SS+TF-MoM5, 2; SE+EM+EN+PS+TF-MoM8, 19
 Murayama, A.: PS-ThA8, 217
 Murphy, N.R.: TF+EM+EN-WeA10, 177
 Murphy, R.D.: TF+SE-TuM2, 74
 Muscat, A.J.: EM-TuP2, 106; SE+NS+TR-TuM1, 69; SS+EM-FrM8, 260
 Musgrave, C.B.: TF+EN+PS-TuA8, 102
 Musin, I.R.: NS+AS+SS-TuA1, 93
 Muto, D.: MS-ThP1, 237
 Myers, D.J.: EN-TuP8, 111
 Myers, J.D.: VT-MoA10, 52
 Myers-Ward, R.L.: 2D+AS+BI+PS+SS-TuM5, 53; EM1-WeM10, 130; EM1-WeM5, 129
 Myung, Y.: AS-ThP6, 231; MC+2D+AP+AS-MoA9, 39; TF+SE-TuM12, 75
- N —
 Na, H.: TF-ThP25, 243
 Na, S.: BI+MG-WeA12, 157; QC+AS+BI+MN-ThP1, 239
 Naaman, R.: BI+AS-TuA1, 82
 Nabatame, T.: EM+NS+TF-FrM10, 253; EM-TuP8, 107
 Naef, S.P.: VT-MoA2, 51
 Nafus, K.: EM-TuM6, 59
 Nag, J.: SD-WeA10, 172
 Nagahata, K.: PS-TuM11, 67; PS-TuP6, 114
 Nagar, R.: SS-TuP22, 123
 Nagashima, T.: MG-WeM3, 135
 Nagatomi, E.: TF+PS-ThM4, 199
 Naghibi, S.: 2D+EM+NS+SS+TF-WeM10, 126; 2D-ThP11, 229
 Nahmias, MN+NS-TuA4, 92
 Naito, K.: SE+PS+TF-MoA10, 46
 Najmaei, S.: SP+2D+AS+EM+MC+NS+SS-ThM10, 197
 Nakajima, Y.: SP+AS+BI+EM+NS+SE+SS-FrM6, 258
 Nakamura, J.: AS+MC+SS-FrM8, 248; SS-TuP8, 120
 Nakamura, K.: PS2+TF-ThM12, 193; PS-TuP18, 117
 Nakamura, M.: PS-MoM10, 16; PS-MoM3, 14
 Nakamura, S.: PS-TuA11, 96
 Nakamura, T.: TF+PS-ThM4, 199
 Nakamura, Y.: SS-TuP11, 121
 Nakano, Y.: EN+EM+MN+NS+TR-MoA11, 37; EN-TuP2, 110; PS2+TF-ThM12, 193
 Nakatsuji, K.: SS+AS+NS-ThA6, 223
 Nakayama, T.: MC+2D+AP+AS-MoA6, 38
 Nakazaki, N.: PS1-WeM12, 141
 Nandasiri, M.L.: AP+AS+MC+NS+SS-ThM6, 181; AS+MC+SS-TuA9, 81; SS+AS+EN-TuM13, 72
 Narayanan, V.: EM+MI+NS-MoM8, 9
 Narimannezhad, A.: EN+EM+NS-TuA11, 87
 Nascente, P.A.P.: TF+PS-ThM13, 201
- Nash, C.: HI+2D+AS+MC-ThA10, 212
 Nasr, J.R.: EN+AS+EM+SE-WeM6, 133; TF-ThP17, 242
 Nath, A.: 2D+AS+BI+PS+SS-TuM5, 53
 Natterer, F.D.: 2D+EM+MI+MN+NS+SS+TF-ThA4, 203; SP+AS+BI+NS+SS-ThA8, 222
 Navin, J.K.: SS+AS+EN-WeM12, 146
 Nayyar, N.: 2D+AS+EM+MI+MN+NS+TF-WeA3, 153
 Ndione, P.F.: AS-ThP24, 233
 Nedev, N.: TF-ThP15, 242
 Needham, C.: TF+PS-MoA2, 48
 Neeway, J.J.: AP+AS+NS+SS-FrM4, 247
 Nefedov, A.: SS+AS+EN-WeM13, 146
 Negara, M.A.: EM+2D-TuA8, 84
 Nelson, A.J.: AC+AS+MI+SA+SS-TuM12, 55
 Nelson, E.S.: EM+EN+TF-WeA11, 158
 Nelson, S.F.: SD-WeM11, 144
 Nemani, S.: PS-TuA10, 96
 Nemanič, V.: VT-TuA7, 104
 Nemeth, W.: TF+EN+PS-TuA11, 102
 Nepal, N.: PS1+TF-ThM11, 191; SA-MoM4, 17; TF+PS-TuM3, 72
 Nesbitt, H.W.: SA-MoM3, 16
 Nesterenko, P.: TF+EM+EN-WeA7, 176
 Netzer, F.P.: SS+AS+EN-TuM5, 71
 Neupane, S.: NS+AS+SS-TuA11, 94
 Neurock, M.: NS-WeM3, 138
 Newberg, J.T.: IS+2D+MC+NS+SP+SS-WeA11, 162; SS+EN-MoA11, 48
 Newell, D.B.: 2D+EM+MS+NS-FrM4, 245
 Newman, C.: AS+BI+MC-WeM13, 127
 Ng, C.C.A.: BI+AS-TuA2, 82
 Ng, T.N.: MN+PS-WeA1, 162
 Ngo, T.Q.: EM+MI+NS-MoM11, 9; EM1-ThA10, 210
 Nguyen, A.: 2D+EM+NS+SS+TF-WeM10, 126; 2D-ThP11, 229; SP+AS+BI+NS+SS-WeA11, 174
 Nguyen, H.: EN+EM+MN+NS+TR-MoA3, 36
 Nguyen, L.T.: IS+AS+MC+SS-TuM4, 62; IS+AS+MC+SS-WeM3, 134; SP+AS+BI+NS+SS-ThA1, 221; SS-TuP21, 122
 Nguyen, N.V.: EM2-WeM13, 131
 Nguyen, S.: SD-WeA10, 172
 Nguyen, T.-T.: HI+2D+AS+MC-ThA10, 212
 Nguyen, V.Q.: VT-MoA10, 52
 Nichols, M.T.: TF+AS-FrM3, 260
 Nicotera, E.: SS+AS+EN-WeM11, 146
 Nie, S.: 2D+EM+NS+PS+SS+TF-MoM10, 3
 Nie, X.: TR-FrM4, 262
 Niehuis, E.: AS+BI+MC-WeM5, 127
 Niemantsverdriet, H.J.W.: NS-WeM10, 139
 Niemi, K.: PS+SE-ThA10, 215
 Nikkola, J.: TF+PS-MoM1, 24
 Niquet, Y.M.: SP+AS+BI+NS+SS-ThA4, 221
 Nishi, Y.: EM-TuP11, 107; EM-WeA11, 159; PS2-FrM4, 256; PS-TuP12, 116; PS-TuP8, 115; TF+AS-FrM3, 260
 Nishihata, Y.: SE+PS+TF-MoA10, 46
 Nishijima, S.: PS1-WeM10, 140
 Nishimoto, A.: TF+PS-ThM13, 201
 Nishimoto, K.: SS+AS+EN-MoM10, 20
 Nishioka, K.: EN+EM+MN+NS+TR-MoA11, 37; EN-TuP2, 110
 Niu, C.: SD-WeA10, 172
 Noé, P.: PS1+TF-ThM5, 190
 Noebels, M.: EM2-ThA8, 210; EN+EM+MN+NS+TR-MoA10, 36
 Nogami, J.: SS+TF-ThM10, 198
 Nogami, T.: SD-WeA10, 172
 Noh, J.H.: NS+HI-TuM10, 65; TF+PS-TuM6, 73
 Noked, M.: EM+EN+TF-WeA10, 158; EN+EM+NS-TuA7, 86; EN+EM+NS-TuA8, 86; TF+EN+PS-TuA1, 101
 Nolde, J.: SS+EM-FrM5, 259
 Nolot, E.: TF+AS-FrM8, 261
- Nolting, W.: 2D+AS+HI+MC+NS+PS+SP+SS-TuA8, 79
 Noma, M.: SE+NS+TR-TuM3, 70
 Noonan, J.R.: VT-WeM12, 151
 Nordlund, D.: AC+AS+MI+SA+SS-MoM1, 3; AC+AS+MI+SA+SS-TuM1, 54
 Norman, A.: EL+AS+BI+EM+SS-FrM5, 250
 Norris, R.: TF+PS+SE-MoM11, 24
 Nosiglia, C.: 2D+EM+MS+NS-FrM3, 245
 Nosworthy, N.J.: SM+AS+BI+PS-ThA6, 220
 Novak, S.W.: MC+2D+AP+AS-MoA6, 38; MC-TuP3, 113
 Novikov, S.V.: SS+EN-MoM3, 21
 Novikova, T.: PS1-WeM11, 140
 Noworolska, A.: SS+TF-ThM6, 198; TF-MoA4, 50
 Noy, A.: AS+MC+SS-TuA11, 81
 Noyce, S.: MN+PS-WeA9, 163
 Nozaki, T.: PS-ThA1, 216
 Nozawa, T.: PS1-WeM10, 140
 Ntwaeaborwa, O.M.: 2D-ThP7, 228; TF+SE-TuM13, 76
 Nudell, J.: VT-WeM4, 150
 Nuhfer, N.T.: MC+AP+AS-MoM6, 11
 Nunney, T.S.: AS+MC+SS-TuA3, 80; AS+MC-MoM1, 5; AS-ThP17, 233; EW-TuL2, 78
 Nutsch, A.: SA-TuM1, 68
 Nyakiti, L.O.: EM1-WeM10, 130
- O —
 Oakes, D.B.: PS-ThA2, 216
 Oberkalmsteiner, N.: SS-TuP5, 120
 O'Brien, B.: MC-TuP3, 113
 Ocola, L.E.: NS+HI-TuM6, 65
 O'Connell, D.: PS+SE-ThA10, 215
 O'Connor, E.: EM+2D-TuA8, 84
 Odom, T.W.: NS+EN-MoA8, 41
 Oehrlein, G.S.: PS+2D-WeA9, 168; PS2+TF-ThM1, 191; PS2+TF-ThM5, 192; PS-TuM10, 67; SE+EM+EN+PS+TF-MoM2, 18
 Ogasawara, H.: IS+AS+MC+SS-TuM5, 62
 Ogawa, D.: PS2+TF-ThM12, 193; PS-TuP18, 117
 Ogawa, S.: HI+2D+AS+MC-ThA1, 211; PS2-FrM1, 256; SS+AS+EN-MoM10, 20
 Ogawa, T.: SS-TuP8, 120
 Ogitsu, T.: SA-MoA8, 44
 Ogletree, D.F.: NS+SE-MoM10, 14
 O'Grady, C.: CS-ThA10, 206
 Ohashi, T.: PS-TuM5, 66
 Ohashi, Y.: TF+PS-ThM4, 199
 Ohi, A.: EM+NS+TF-FrM10, 253
 Ohishi, T.: EM-TuP8, 107
 Ohlberg, D.A.A.: NS+HI-TuM4, 65
 Ohldag, H.: MI+EM-MoM11, 13
 Ohlhausen, J.A.: AS+BI+MC-WeM12, 127; BI+AS-TuA9, 83
 Ohno, R.: SE+EM+EN+PS+TF-MoM3, 18
 Ohno, T.R.: EN+AS+EM+SE-WeM10, 133
 Ohsumimoto, S.: SP+AS+EM+NS+SS-ThP2, 240
 Ohtake, H.: PS-MoA3, 42
 Ohtomo, Y.: PS2-FrM1, 256
 Ohtsuka, S.: PS2+TF-ThM4, 192
 Oishi, T.: EM+NS+TF-FrM10, 253
 Ojeda-Durán, E.: EM-TuP30, 110
 Oka, M.: PS1-WeM10, 140
 Okada, T.: 2D+AS+EM+NS+SS-MoA9, 29
 Okura, T.: SS-TuP10, 120; SS-TuP11, 121
 Okyay, A.K.: EM+EN-FrM4, 251; TF+EM+EN-WeA2, 176
 Oldham, C.J.: TF+PS-MoA2, 48; TF+PS-MoM9, 25
 Oleksak, R.P.: NS+HI-TuM5, 65
 Oleynik, I.I.: 2D+AS+EM+MI+MN+NS+TF-WeA11, 153; 2D+EM+NS+SS+TF-WeM5, 125
 Olmon, R.L.: SA-MoA4, 44
 Olson, D.: AP-ThP1, 230
 Olson, D.A.: VT-MoM3, 26
 Olson, J.: PS1-WeM5, 140
 Olsson, A.: QC+AS+BI+MN-ThM10, 194

- Olynyck, D.L.: NS+HI-TuM1, **64**
O'Malley, R.M.: AP+AS+NS+SS-FrM3, 246
Omura, M.: PS-TuA1, 94
Ondeck, N.: SS-WeA8, 175
O'Neill, B.: SS+AS-WeM3, 147
Ong, E.W.: 2D+AS+HI+MC+NS+PS+SP+SS-TuA10, **80**; 2D+EM+NS+PS+SS+TF-MoM3, 2
Ono, K.: PS1-WeM12, 141; PS2+TF-ThM4, 192; SE+NS+TR-TuM3, 70
Ono, L.K.: NS-WeM5, 139
Opila, R.L.: AS+MC+SS-FrM5, 248; SS+EM-FrM3, 259
Orji, N.G.: SP+AS+BI+NS+SS-WeA4, **173**
Orlando, T.M.: BI+AS-TuA1, 82
Orr, G.: BI+AS-TuA11, 83
Osborn, W.A.: AS+BI+MC-WeA11, 155
Osgood, R.M.: 2D+AS+HI+MC+NS+PS+SP+SS-TuA1, **79**; NS-WeM11, 139; SS+EN-MoM6, 22
osofsky, M.: 2D+AS+BI+PS+SS-TuM5, 53
Ossikovski, R.: EL+AS+BI+EM+SS-FrM3, 250
Ossowski, J.W.: SS+TF-ThM6, **198**
Osten, H.J.: EM1-ThA11, 210
Österlund, L.: SS+EN-MoM2, 21
Osterwalder, J.: 2D+AS+EM+NS+SS-MoA1, 28; 2D+EM+NS+PS+SS+TF-MoM8, **3**
Ouyang, Z.: AS+BI+VT-TuM3, **55**
Ovanesyan, R.: PS1+TF-ThM10, 191
Overdeep, K.R.: TF+SE-TuM10, **75**
Overzet, L.J.: MC-TuP1, 113; PS1-WeM13, 141; PS-TuP10, 115
Oviedo, J.: EM-WeA9, 159
Owen, A.: MI+MG-TuM13, **64**
Owen, J.: NS+HI-TuM11, 65
Owusu-Ansah, E.: NS-ThP5, **238**
Oyer, A.J.: 2D+AS+BI+PS+SS-TuM6, 53
Ozgit-Akgun, C.: EM+EN-FrM4, 251
Ozkan, A.: PS+SE-ThA7, 215
Ozkan, T.: TR-ThP2, 244
- **P** —
- Pachicano, J.: VT-MoA8, 52; VT-MoA9, 52
Pacholski, M.L.: AS+MC+SS-TuA4, **80**
Pachuta, S.J.: AS+MC+SS-TuA1, 80
Padama, A.A.: SE+PS+TF-MoA10, 46
Padbury, R.P.: TF+MS+PS-WeM13, 150; TF-ThA9, 226
Page, S.C.: AS-ThP10, 232
Paglione, J.: SP+AS+BI+EM+NS+SE+SS-FrM6, 258
Paine, M.: PS-MoM5, 15
Pak, J.: MI+MG-TuA8, **91**; SS-WeA9, 175
Pala, I.R.: EM+EN+TF-WeA11, 158
Palamarciuc, T.: MI+MG-TuM5, 63
Palazzo, J.: EM-TuM3, 58
Pallem, V.: AS+MC+SS-FrM5, 248; PS2-FrM9, 257; PS-MoA10, 43; PS-TuA10, **96**; PS-TuM10, 67
Palmans, J.: PS-ThA10, **218**
Palomino, R.: SA-MoA3, **44**
Pan, L.: SS-TuP20, 122
Panjan, M.: SE+PS+TF-MoA3, **45**
Papadakis, G.: QC+AS+BI+MN-ThM12, 194; QC+AS+BI+MN-ThM13, 194
Paraskevoulakos, H.: AC+AS+MI+SA+SS-TuM5, 55
Pargon, E.: PS-MoM6, 15; PS-MoM9, 16
Parikh, P.: EM1-WeM1, 129
Park, C.: QC+AS+BI+MN-ThP1, 239
Park, C.D.: VT-TuA4, 103
Park, C.-Y.: 2D-ThP3, 228; IS-ThP1, 236
Park, D.: MN-WeM5, 137
Park, D.-G.: MC+2D+AP+AS-MoA1, 37
Park, I.-Y.: HI-ThP1, **235**
Park, J.: 2D+AS+HI+NS+SS-ThM1, **179**; AS-ThP6, 231; MC+2D+AP+AS-MoA9, 39; QC+AS+BI+MN-ThP1, 239; SP+2D+AS+EM+MC+NS+SS-ThM11, **197**; SP+2D+AS+EM+MC+NS+SS-ThM6, 196
Park, J.H.: 2D+AS+BI+PS+SS-TuM13, **54**; 2D+AS+HI+NS+SS-ThM5, 179; EM1-ThA9, 209
Park, J.Y.: NS+EN-MoA4, 41; SS-TuP18, 122
Park, S.-H.: 2D-ThP3, 228
Park, S.W.: EM+2D-TuA4, **84**; EM1-ThA9, 209; EN+AS+EM+SE-WeM4, 132
Park, T.-H.: NS-WeM12, 140
Parker, J.F.: EM+EN+TF-WeA11, **158**
Parks, C.: SD-WeA10, 172
Parry, K.: IS+AS+MC+SS-TuA4, 88
Parsons, G.N.: BI+AS+NS-MoA1, 32; MS+PS+TF-ThA4, 213; SD-WeA3, **171**; TF+PS-MoA2, 48; TF+PS-MoA9, 49; TF+PS-MoM9, 25
Parvinian, S.: MS+PS+TF-ThA11, 213
Parzinger, E.: EL+AS+EM+MC+SS-ThA10, 208
Passarelli, M.K.: AS+BI+MC-WeM13, **127**
Pastewka, L.: TR+NS-ThM10, 202; TR+NS-ThM13, 202; TR+NS-ThM3, **201**
Paterson, A.: PS2-WeM3, 142; PS-WeA3, **169**
Patscheider, J.: SE+NS+TR-TuM10, **70**
Patterson, M.C.: SS+NS-TuA11, 99; SS+TF-ThM12, **198**
Patthey, F.: SP+AS+BI+NS+SS-ThA8, 222
Pauca, K.: TR-ThA10, 227
Paudel, T.: EM+MI+NS-MoM10, 9
Paudyal, D.: AC+AS+MI+SA+SS-MoA8, **30**
Paukov, M.: AC+AS+MI+SA+SS-MoM9, 4
Paul, B.: TF+EM+EN-WeA7, 176
Paul, D.F.: AS-ThP25, 234
Payne, G.F.: BI+AS+MN+NS-TuM3, 57
Payne, M.: TF+AS+EM-TuA11, **100**
Pearce, R.: VT-WeA7, **178**
Pearse, A.J.: EM+EN+TF-WeA10, 158; EN+EM+NS-TuA3, **85**; EN+EM+NS-TuA7, 86; EN+EM+NS-TuA8, 86; TF+EN+PS-TuA1, 101; TF+EN+PS-TuA7, 101
Pearson, A.: TF+EM+EN-WeA11, 177
Pecharsky, V.K.: AC+AS+MI+SA+SS-MoA8, 30
Pedersen, H.: TF+PS-ThM3, **199**
Peeters, F.J.J.: PS2-FrM10, **257**
Peev, D.: EL+AS+BI+EM+SS-FrM8, 251
Pegalajar-Jurado, A.: SM+AS+BI+PS-ThA8, 221; SM+AS+BI+PS-ThM11, **195**; SM+AS+BI+PS-ThM5, 195
Pei, D.: TF+AS-FrM3, **260**
Pei, L.: CS-ThM11, **182**; MS+PS+TF-ThM6, 189; TF+AS-FrM2, 260
Peixoto, T.: SD-WeM3, 144
Pelton, M.: NS+SE-MoM5, **13**
Peña, V.: EM-TuP26, 109
Peng, G.: SS+AS-WeM3, 147
Peng, W.: EN+EM+MN+NS+TR-MoA3, **36**
Peng, X.: EM-WeA4, 159; EM-WeA9, 159
Perea, D.E.: AP+AS+EN+NS+SS-ThA4, 205; AP+AS+NS+SS-FrM8, **247**
Perepichka, D.F.: SS+EM-FrM1, 258
Perkins, C.L.: AS-ThP24, 233
Perrine, K.A.: IS+AS+MC+SS-TuA4, **88**; IS+AS+MC+SS-TuM11, 62
Perriot, R.: 2D+AS+EM+MI+MN+NS+TF-WeA11, 153
Perrotta, A.: TF-ThA4, **225**
Persson, O.: NS+AS+SS-TuA4, 93
Peterson, E.: SS+AS+EN-WeM11, 146
Peterson, G.W.: PS-TuP15, **116**
Petit-Etienne, C.: PS2-FrM2, 256
Petrik, N.G.: SS+EN-MoM5, **22**
Petrik, P.: EL-ThP6, 234
Petrosky, J.: AC+AS+MI+SA+SS-MoM11, 4
Petrov, G.M.: PS1-FrM8, 255; PS-WeA11, 171
Petrov, I.G.: TF+PS+SE-MoM4, 22
Petrova, Tz.B.: PS1-FrM8, 255; PS-WeA11, 171
Petrovykh, D.Y.: BI+AS-TuA2, **82**
Petteri-Niemelä, J.: TF+PS-TuM12, 74
Pfadler, T.: EM2-ThA8, 210; EN+EM+MN+NS+TR-MoA10, 36
Pfaendner, J.: BI+AS-WeM6, 128
Pfaunmiller, E.: EL+AS+BI+EM+SS-FrM8, **251**
Pfnür, H.: NS+EN-MoA6, 41; SP+2D+AS+EM+MC+NS+SS-ThM12, **197**
Pham, C.: TF+PS-TuM5, **73**
Phaneuf, R.J.: CS-FrM5, 249; SS-TuP23, 123
Phelps, R.: MC+2D+AP+AS-MoA11, 39
Phumisithikul, K.L.: EM+EN-FrM3, 251
Phuong, P.V.: 2D+AS+EM+NS+SS-MoA8, **29**
Piallat, F.: MC+AP+AS-MoM10, 11; PS1+TF-ThM5, 190
Piao, H.: AS-ThP19, 233
Piasecki, A.: 2D+EM+NS+SS+TF-WeM6, 125
Pichler, A.: TF+AS-FrM10, 262
Pickup, D.: MS+PS+TF-ThA1, 213
Pimenta-Barros, P.: PS-MoM9, 16; PS-TuM13, 68
Pimpinelli, A.: SS+AS-WeM11, 148
Piper, L.F.J.: EN+AS+EM+SE-WeM11, 133
Pireaux, J.-J.: MC+AP+AS-MoM5, **11**
Pirota, K.R.: NS-ThP7, 239
Pitters, J.L.: HI+2D+AS+BI+MC-ThM3, **187**; HI+2D+AS+BI+MC-ThM5, 187
Placencia, D.: EM-MoA10, **35**; EM-TuP20, 109
Plank, H.: NS+HI-TuM10, 65; TF+PS-TuM6, 73
Plass, K.E.: EM-MoA11, **35**
Pletikosic, I.: MI-MoA8, 40
Podraza, N.J.: EL+AS+EM+EN+SS-ThM1, **183**; EL+AS+EM+EN+SS-ThM11, 184; EL+AS+EM+EN+SS-ThM4, 183; EL+AS+EM+EN+SS-ThM5, 183; EL-ThP5, 234
Poelker, M.: VT-WeA4, 177
Poelsema, B.: HI-ThP4, 235
Poenitzsch, V.Z.: SE+EM+EN+PS+TF-MoM5, **18**
Pohlentz, D.: EW-WeA6, **161**
Poirier, D.: AS+MC+SS-TuA1, 80
Pokidov, I.: PS1-FrM3, 254
Polak, S.: PS-TuP9, **115**
Polat, E.O.: 2D+EM+MI+MN+NS+SS+TF-ThA11, 204
Poleunis, C.: PS+2D-WeA11, 168
Poliakoff, E.D.: SS+TF-ThM12, 198
Pollakowski, B.: SA-TuM1, 68; TF+AS-FrM9, **2161**
Pollei, M.: CS-ThM11, 182
Pollet, O.: PS-MoA11, 43
Polycarpou, A.A.: TR-ThP2, 244
Polychronopoulou, K.: EN-TuP14, 112
Pomeroy, J.: EM1-ThA3, 208; TF-ThP14, 242
Ponath, P.: EM+MI+NS-MoM3, 8
Ponce, A.A.: CS-ThM12, 182
Poody, P.: TF+PS-MoM8, 25; TF-ThA7, **225**
Pookpanratana, S.J.: EN+AS+EM-WeA11, 161; SS+EM-FrM2, **259**
Pop, E.: EM1-WeM12, **130**
Poppenheimer, E.C.: SS+NS-TuA12, 99
Porter, A.E.: BI+AS+NS-MoA7, 33
Porter, L.M.: EM+NS+TF-FrM11, 254
Portoles, J.F.: AS+MC-MoM6, 5; HI+2D+AS+MC-ThA3, **211**
Portz, A.: AS+BI+MC+SS-MoA10, 31
Posadas, A.B.: EM+MI+NS-MoM11, 9; EM+MI+NS-MoM3, 8; EM1-ThA10, 210
Posseme, N.: PS-MoA11, **43**; PS-MoA9, 43; PS-TuA7, 95; PS-TuM13, 68; PS-WeA2, 169
Potapenko, D.V.: NS-WeM11, 139; SS+EN-MoM6, **22**
Pouch, S.: SP+AS+BI+NS+SS-ThA4, 221
Poulose, J.: PS-TuP10, **115**
Pouyet, E.: CS-ThA6, 206
Povey, I.M.: EM+2D-TuA8, 84
Powell, C.J.: AS+MC-MoM5, **5**
Pozzi, F.: CS-ThA3, 205
Prabhumirashi, P.L.: 2D+AS+HI+NS+SS-ThM4, 179
Pradelles, J.: PS-MoM9, 16
Pradhan, A.K.: EM-TuP24, 109; NS+EN-MoA11, 42
Pradhan, N.: PS1-WeM5, 140
Pradhan, P.: EL+AS+BI+EM+SS-FrM5, 250
Pradhan, S.: EM-TuP24, **109**

- Prasad, S.V.: TF+PS+SE-MoM6, 23; TF+PS+SE-MoM8, 23
- Prasher, R.: NS+SE-MoM10, 14
- Prasittichai, C.: SD-WeA8, 171
- Prater, C.B.: NS+AS-WeA9, 166
- Pratt, H.: IS+AS+MC+SS-WeM4, 134
- Praveen, A.: SS-TuP22, 123
- Preciado, E.: 2D+EM+NS+SS+TF-WeM10, 126; 2D-ThP11, 229; SP+AS+BI+NS+SS-WeA11, 174
- Preil, M.: PS-TuA3, 95
- Prendergast, D.: SA-MoA8, 44
- Preuss, M.: AC+AS+MI+SA+SS-MoM8, 4
- Price, D.: EM2-WeM2, 130
- Price, M.: PS+SE-ThA4, 214
- Principe, E.L.: SA-MoM10, 17
- Pritchett, B.N.: EM+EN-FrM10, 252
- Priya, S.: MC+AP+AS-MoM11, 12
- Priyadarshini, D.: SD-WeA10, 172
- Prosa, T.J.: AP+AS+MC+NS+SS-ThM13, 181; AP-ThP1, 230
- Provo, J.L.: TF+PS-ThM12, 200
- Pruessner, M.W.: MN-WeM5, 137
- Ptasinska, S.: SS+AS+NS-ThA3, 223; SS+AS+NS-ThA4, 223
- Pujari, S.: SS+EM-FrM4, 259; TF-MoA8, 51
- Putnik, M.: EN+EM+MN+NS+TR-MoA10, 36
- Puydinger dos Santos, M.V.: NS-ThP7, 239
- Q —
- Qadri, S.: PS1+TF-ThM11, 191
- Qafoku, O.: AP+AS+EN+NS+SS-ThA4, 205
- Qi, J.: TF+PS-TuM11, 73
- Qi, Y.: SS-TuP18, 122
- Qin, H.: SS+EN-MoA8, 48
- Qin, X.: EM+2D-TuA7, 84; SD-WeA11, 172
- Qiu, J.: NS+EN-MoA7, 41
- Qiu, Y.: SE+PS+TF-MoA6, 45
- Qu, J.: AS-ThP11, 232
- Quan, S.: TF-ThA10, 226
- Quevedo, I.R.: QC+AS+BI+MN-ThM10, 194
- R —
- R. Silva, A.R.: MS-ThP9, 238
- Raabe, D.: AP+AS+MC+NS+SS-ThM3, 180
- Rabin, O.: NS+EN-MoA3, 41
- Rabinovich, W.S.: MN-WeM5, 137
- Rack, P.D.: HI+2D+AS+MC-ThA4, 212; MG-TuA3, 89; NS+HI-TuM10, 65; TF+PS-TuM6, 73
- Radetić, M.: AS+MC+SS-TuA3, 80
- Rading, D.: AS+BI+MC+SS-MoA9, 31; AS+BI+MC-WeM5, 127
- Radoičić, M.: AS+MC+SS-TuA3, 80
- Radu, F.: MI+MG-TuM6, 63
- Rafalskiy, D.R.: PS1-FrM5, 254
- Rahman, O.: VT-TuP5, 124
- Rahman, T.S.: 2D+AS+BI+PS+SS-TuM3, 53; 2D+AS+EM+MI+MN+NS+TF-WeA3, 153; 2D+AS+HI+NS+SS-ThM6, 179; 2D+EM+MI+MN+NS+SS+TF-ThA8, 203; MG-WeM5, 136
- Rai, R.: SS+AS+EN-TuM2, 71
- Raitses, Y.: PS2-WeM5, 142; PS-TuP11, 115; PS-TuP30, 118; SE+EM+EN+PS+TF-MoM2, 18
- Rajan, K.: AP+AS+EN+NS+SS-ThA1, 204
- Rakowska, P.D.: AS+BI+VT-TuM6, 56
- Raley, A.: NS+HI-TuM3, 64
- Ramalingam, G.: SS+AS+NS-ThA7, 223
- Raman, K.V.: MI+EM-MoM8, 12
- Raman, P.: SE+PS+TF-MoA1, 45
- Raman, S.: AS-ThP6, 231; BI+AS-MoM3, 7; MC+2D+AP+AS-MoA9, 39; SS+EN-MoA4, 47
- Ramana, C.V.: EN+AS+EM-WeA4, 160
- Ramanathan, K.: AS-ThP24, 233; EL+AS+BI+EM+SS-FrM5, 250
- Ramanathan, S.: EM2-WeM3, 131
- Ramaprabhu, S.: SS-TuP22, 123
- Ramaswamy, K.: PS2+TF-ThM3, 192
- Ramaswamy, N.: EM2-ThM10, 186
- Ramirez-Torres, A.: 2D+AS+HI+NS+SS-ThM6, 179
- Ramsey, M.G.: SS+TF-ThM1, 197
- Ranacher, C.: TF-MoA9, 51
- Randall, J.: NS+HI-TuM11, 65
- Rangan, S.: EN+EM+NS-TuA4, 86; SS+TF-ThM13, 199
- Ranjan, A.: NS+HI-TuM3, 64; PS-TuA11, 96; PS-TuA3, 95
- Rao, K.Y.: TF+SE-TuM1, 74
- Rao, T.: MG-WeM2, 135; VT-TuP5, 124
- Rappe, A.M.: SS+AS+EN-TuM1, 71
- Raravikar, N.: NS+SE-MoM10, 14
- Raschke, M.B.: SA-MoA4, 44
- Rastegar, A.: MC+2D+AP+AS-MoA6, 38
- Rastogi, V.: NS+HI-TuM3, 64; PS-TuA3, 95
- Ratner, B.: SM+AS+BI+PS-ThM10, 195
- Raty, R.G.: AS-ThP13, 232
- Rauf, S.: PS2+TF-ThM3, 192; PS2-WeM1, 141; PS2-WeM2, 142; PS2-WeM4, 142; PS2-WeM6, 143; PS-MoA8, 43
- Raval, R.: SS-WeA1, 174
- Ravikumar, S.: EM+EN+TF-WeA2, 157
- Raw, T.B.: 2D+AS+BI+PS+SS-TuM3, 53
- Ray, A.M.: PS1-WeM1, 140
- Rayner, G.B.: PS1+TF-ThM4, 190
- Rebecchi, C.: EW-TuM8, 61; VT-TuM12, 77
- Rebholz, C.G.: EN-TuP14, 112
- Reddemann, L.: TF-ThA11, 226
- Reding, J.: AC+AS+MI+SA+SS-MoM11, 4
- Redinger, J.: SS+AS+EN-MoM3, 19; SS-TuP5, 120
- Reed, E.J.: 2D+AS+EM+MI+MN+NS+TF-WeA12, 154
- Reed, J.A.: SM+AS+BI+PS-ThA3, 220
- Rees, J.A.: VT-TuP4, 123
- Reese, M.O.: EN+AS+EM+SE-WeM10, 133
- Reeves, R.J.: EN+AS+EM+SE-WeM11, 133
- Reeves, R.V.: TF+SE-TuM2, 74
- Rehbein, J.: AS+MC+SS-TuA7, 81
- Reichmanis, E.: EN+AS+EM-WeA1, 160
- Reidy, R.: NS+HI-TuM11, 65
- Reihs, K.: TF-ThA11, 226
- Reinecke, T.: 2D+AS+BI+PS+SS-TuM5, 53; 2D+AS+EM+NS+SS-MoA3, 28
- Reinhard, D.A.: AP-ThP1, 230
- Reinicker, A.: SS-WeA4, 174
- Reinke, P.: SS+AS+NS-ThA7, 223
- Rementer, C.: TF+PS+SE-MoM10, 23
- Remmers, E.: SS+AS-WeM2, 147
- Ren, H.: EM-WeA11, 159
- Ren, J.: SD-WeA10, 172
- Ren, X.: AP+AS+MC+NS+SS-ThM5, 181
- Ren, Y.: AS+BI+VT-TuM3, 55; SS+AS+EN-MoM5, 19
- Renault, O.J.: 2D+EM+MI+MN+NS+SS+TF-ThA10, 204; AS-ThP3, 231
- Reniers, F.A.B.: PS+2D-WeA10, 168; PS+2D-WeA11, 168; PS+SE-ThA7, 215; PS-ThA6, 217
- Repins, I.: AS-ThP24, 233; EL+AS+EM+EN+SS-ThM3, 183
- Resel, R.: TF+AS-FrM10, 262
- Reshchikov, M.A.: EM+EN-FrM3, 251
- Restrepo, J.S.: TR-ThP3, 244
- Reutt-Robey, J.: 2D+AS+EM+MI+MN+NS+TF-WeA8, 153
- Reyes, P.: NS-WeM4, 139
- Reynolds, J.: TF-ThP16, 242
- Reynolds, L.: TF-ThP16, 242
- Reynolds, M.: SM+AS+BI+PS-ThM5, 195
- Rezek, J.: SE+PS+TF-MoA8, 46
- Ribeiro, R.V.: EN-TuP15, 112
- Ricardo do Nascimento Jr., A.R.: MS-ThP9, 238
- Ricci, M.: EN-TuP5, 110; TF+PS+SE-MoM3, 22
- Rice, C.: EL+AS+BI+EM+SS-FrM8, 251
- Richter, C.A.: 2D+EM+MS+NS-FrM4, 245; EN+AS+EM-WeA11, 161; SS+EM-FrM2, 259
- Richter, R.P.: QC+AS+BI+MN-ThA4, 219
- Ricker, J.E.: CS-ThM10, 182; VT-MoM3, 26
- Riedl, A.: SE+NS+TR-TuM11, 70
- Riehn, R.: BI+AS+NS-MoA11, 34
- Rieth, L.W.: TF-ThA8, 225
- Rigas, P.: 2D-ThP11, 229
- Riley, J.: AP+AS+MC+NS+SS-ThM5, 181
- Ristoiu, D.: PS-TuA7, 95
- Ritter, R.: 2D-ThP18, 230
- Rivron, N.: BI+MG-WeA9, 157
- Rizzolo, M.: MC-TuP3, 113
- Robbins, M.O.: TR+NS-ThM10, 202; TR+NS-ThM13, 202
- Roberts, A.J.: AS+BI+MC+SS-MoA8, 31; AS+BI+MC-WeA1, 154
- Roberts, A.T.: MS+PS+TF-ThA3, 213
- Roberts, N.A.: TF+PS-TuM6, 73
- Robinson, J.: 2D+AS+BI+PS+SS-TuM4, 53; 2D+AS+BI+PS+SS-TuM5, 53; 2D+AS+BI+PS+SS-TuM6, 53; 2D+AS+EM+NS+SS-MoA3, 28; 2D+EM+NS+PS+SS+TF-MoM4, 2; BI+AS+MN+NS-TuM5, 57
- Robinson, J.A.: 2D+AS+HI+MC+NS+PS+SP+SS-TuA3, 79; 2D+EM+NS+SS+TF-WeM11, 126; 2D+EM+NS+SS+TF-WeM6, 125
- Robinson, Z.R.: 2D+AS+HI+MC+NS+PS+SP+SS-TuA10, 80; 2D+EM+NS+PS+SS+TF-MoM3, 2; EM1-WeM5, 129; TF+PS-TuM3, 72
- Rockett, A.: EN+AS+EM+SE-WeM2, 132; MC+2D+AP+AS-MoA7, 38
- Rodek, E.W.-WeM9, 134
- Rodrigues, J.N.: 2D+EM+MI+MN+NS+SS+TF-ThA4, 203
- Rodriguez, E.: TR-ThP4, 244
- Rodriguez, J.: IS+AS+MC+SS-WeM1, 134
- Rodríguez-Reyes, J.C.F.: SS-TuP13, 121
- Roehrig, A.: BI+AS-WeM6, 128
- Roessler, U.K.: MI+MG-TuM6, 63
- Rogalev, A.: AC+AS+MI+SA+SS-MoM3, 3
- Rogero, C.: MS+PS+TF-ThA1, 213
- Rogers, J.A.: BI+AS+MN+NS-TuM10, 57
- Rohrer, G.S.: MC+AP+AS-MoM6, 11
- Rojas, O.: MS+PS+TF-ThA6, 213
- Roke, S.: BI+AS-WeM10, 128; BI+AS-WeM12, 128
- Roldan Cuenya, B.: NS+AS-WeA4, 165; NS-WeM5, 139
- Roldan, A.: MG-WeM12, 136
- Röling, C.: EL+AS+EM+MC+SS-ThA10, 208; EL+AS+EM+MC+SS-ThA7, 208
- Röling, L.: SS+AS-WeM3, 147
- Rolison, D.R.: EM+EN+TF-WeA11, 158
- Romero, D.: 2D+AS+EM+MI+MN+NS+TF-WeA7, 153
- Romijn, I.G.: TF+EN+PS-TuA9, 102
- Rondinelli, J.M.: MI+MG-TuA1, 90
- Rosa, P.: MI+MG-TuM5, 63
- Rosconi, O.: TF+AS-FrM10, 262
- Rose, T.: CS-FrM3, 249
- Rose, V.: CS-ThA3, 205
- Rosenberg, R.A.: BI+AS-TuA1, 82
- Rosowski, F.: IS+AS+MC+SS-TuM1, 61
- Ross, F.M.: SS+NS-TuA1, 98
- Ross, P.N.R.: IS+2D+MC+NS+SP+SS-WeA10, 162
- Roth, S.: 2D+EM+NS+PS+SS+TF-MoM8, 3
- Röthel, C.: TF+AS-FrM10, 262
- Rouchon, D.: 2D+EM+MI+MN+NS+SS+TF-ThA10, 204
- Roushan, M.: BI+AS+NS-MoA11, 34
- Rousseau, R.: SS+AS-WeM13, 148
- Rowan, S.: PS2-FrM11, 257
- Rowe, J.E.: AS+MC+SS-FrM9, 248; MI+EM-MoM10, 12; TF-ThP16, 242
- Rowe, K.G.: TR+NS-ThM6, 201
- Rowley, J.: MN+PS-WeA3, 163; TF+AS-FrM2, 260; TF+PS-ThM6, 200
- Roy Choudhury, K.: EN+AS+EM-WeA3, 160

- Roy, A.: PS-TuP9, 115
 Roy, R.: SA-TuA7, **97**
 Roy, S.: BI+AS-WeM3, 128
 Roy, S.K.: MN-WeM11, **138**
 Royer, J.: PS-MoA10, **43**
 Rubin, L.M.: PS1-WeM1, 140
 Rubloff, G.W.: BI-ThP2, 234; CS-FrM5, 249; EM+EN+TF-WeA10, 158; EN+EM+NS-TuA3, 85; EN+EM+NS-TuA7, 86; EN+EM+NS-TuA8, 86; TF+EN+PS-TuA1, 101; TF+EN+PS-TuA7, 101
 Ruck, R.L.: VT-TuA12, 104
 Rudolf, P.: SA-TuM12, **69**
 Rudolph, M.: EM1-ThA6, 209; EM1-ThA7, 209
 Rufe: EW-TuM9, **61**
 Ruggieri, C.: SS+TF-ThM13, **199**
 Ruiz, S.: VT-MoM5, 26
 Rullan, J.: EM-TuM3, 58
 Rumbach, P.: PS+SE-ThA3, **214**
 Rumphorst, R.F.: PS2-FrM10, 257
 Rupich, S.: EN+EM+MN+NS+TR-MoA3, 36
 Russell, T.P.: NS+HI-TuM1, 64
 Ruzs, J.: AC+AS+MI+SA+SS-MoM5, **3**
 Ruther, R.: NS+HI-TuM5, **65**
 Rutigliani, V.: EM-TuM6, 59
 Ruzic, D.N.: SE+PS+TF-MoA1, 45; SE+PS+TF-MoA2, 45; VT-MoA8, 52; VT-MoA9, 52
 Ryan, J.V.: AP+AS+NS+SS-FrM4, 247
 Ryan, K.E.: SP+AS+BI+EM+NS+SE+SS-FrM2, 258; SS+AS-WeM5, 147; TR+NS-ThM5, **201**; TR-ThA8, 227
 Ryan, M.P.: BI+AS+NS-MoA7, 33
 Ryder, M.R.: BI+MG-WeA8, 156
 Rysz, J.: SS+TF-ThM6, 198
 Ryzhkov, M.V.: AC+AS+MI+SA+SS-MoA6, 29
 Rzhetskii, A.: EW-ThM9, **187**
- S —
- Sabat, G.: PS2-FrM4, 256
 Saberi-Movahed, F.: TR-ThA9, **227**
 Sachet, E.: AS+MC+SS-FrM9, 248
 Sacui, I.: MS+PS+TF-ThM10, 189
 Sadana, D.K.: MC+2D+AP+AS-MoA1, 37
 Saddow, S.: TF+PS+SE-MoM5, 23
 Sader, J.E.: NS+SE-MoM5, 13
 Sadowski, J.T.: MI-MoA8, 40
 Saeki, H.: VT-WeM6, **151**
 Sagar, J.: HI+2D+AS+MC-ThA10, **212**
 Sahu, B.B.: PS-ThA11, 218; PS-WeA10, 170
 Saidi, B.: MC+AP+AS-MoM10, 11
 Saidi, W.A.: SS+AS+EN-TuM1, 71; SS+AS-WeM1, 147
 Sajjian, A.: PS2-FrM1, 256
 Saint-Girons, G.: EM+MI+NS-MoM8, 9
 Saito, N.: PS+2D-WeA4, 167
 Sakai, I.: PS-TuA1, 94
 Sakamoto, K.: MI-MoA3, 39
 Sakaue, M.: AC+AS+MI+SA+SS-MoA7, **30**; SE+PS+TF-MoA10, **46**
 Salmeron, M.B.: NS-WeM6, 139; SS+AS+EN-MoM4, **19**; SS-TuP18, 122; SS-TuP19, 122
 Salo, E.: TF+PS-MoM1, 24
 Salter, T.L.: AS+BI+VT-TuM5, 56; AS+BI+VT-TuM6, 56
 Salzmann, I.: TF+AS-FrM10, 262
 Samaraweera, R.L.: EM-TuP15, 108; EM-TuP17, **108**
 Sampat, S.: EN+EM+MN+NS+TR-MoA3, 36
 Sampath, W.: EN+AS+EM+SE-WeM13, 134
 Samukawa, S.: 2D+AS+EM+NS+SS-MoA9, 29; PS2+TF-ThM4, 192; PS-ThA8, 217
 Sanchez, E.: SP+AS+EM+NS+SS-ThP8, **240**
 Sando, S.: NS+HI-TuM11, 65
 Sandoval, T.: SS+AS+NS-ThA10, **224**
 Sanghera, J.S.: VT-MoA10, 52
 Sangiovanni, D.G.: TF+PS+SE-MoM4, 22
 Sangwan, V.K.: 2D+AS+HI+NS+SS-ThM4, 179
 Sankaran, M.: MN+PS-WeA11, 164; PS-ThA6, 217
 Sankaran, R.M.: PS+SE-ThA3, 214; PS2-FrM11, 257; PS-ThA7, 217; PS-TuP29, 118
 Sano, N.: AS+BI+MC-WeM6, 127; AS+MC-MoM6, 5; CS-ThA8, **206**
 Santala, M.K.: TF+SE-TuM6, 75
 Santander-Syro, A.F.: SA-TuM10, **69**
 Santiago, K.C.: NS+EN-MoA11, 42
 Santini, G.: PS-MoA11, 43
 Santoro, C.: BI+AS+MN+NS-TuM12, 57
 Šaponjić, Z.: AS+MC+SS-TuA3, 80
 Sardashti, K.: 2D+AS+BI+PS+SS-TuM13, 54; EM-WeA12, 160; EN+AS+EM+SE-WeM4, **132**
 Sardella, E.: SM+AS+BI+PS-ThA1, **220**
 Sarney, W.L.: MC+2D+AP+AS-MoA2, 37; MC+2D+AP+AS-MoA3, 38; MC+AP+AS-MoM4, **10**; SS+EN-MoM3, 21
 Saroja, M.: EM+EN+TF-WeA2, **157**
 Sarrazin, A.: PS-TuM13, **68**
 Sartory, B.: SE+NS+TR-TuM11, 70
 Sasaki: PS+SE-ThA8, **215**
 Sase, H.: TF-ThP9, 241
 Sassolini, S.: NS+HI-TuM1, 64
 Satake, M.: PS-TuM6, **67**
 Sathe, A.: SS+AS+EN-TuM2, 71
 Sato, H.: EM-TuP12, 107; EM-TuP13, **108**
 Sato, P.S.: TF+PS-ThM13, 201
 Sauer, B.B.: AS-ThP14, 232
 Sauer, V.T.K.: MN-WeM10, 137; MN-WeM11, 138
 Savage, T.: EM-TuM6, 59
 Sawyer, W.G.: TR+NS-ThM6, 201
 Scace, G.E.: VT-MoM3, 26
 Scammon, K.: SA-MoM10, 17
 Scanlon, D.O.: EN+AS+EM+SE-WeM11, 133
 Scaranto, J.: SS+AS-WeM3, 147
 Scarel, G.S.: TF+PS-TuM12, 74
 Schach, D.: BI+AS-MoM9, 8
 Schaefer, A.: SS+AS+EN-TuM2, 71
 Schaefer, D.: EM+MI+NS-MoM4, 9
 Schall, J.D.: SS+AS-WeM5, 147; TR-FrM5, **262**
 Schamis, M.S.: MC+2D+AP+AS-MoA1, 37
 Schamm-Chardon, S.: EM+MI+NS-MoM8, 9; MC+AP+AS-MoM10, 11
 Schell, M.: EM-TuP16, 108
 Schelling, P.: TF-ThP26, 244
 Schenk, M.: HI-ThP2, 235
 Scherson, D.: PS-TuP29, 118
 Scheu, C.: EN+EM+MN+NS+TR-MoA10, 36
 Schilke, K.S.: BI+MG-WeA8, **156**
 Schilling, M.: SE+PS+TF-MoA1, 45
 Schilowitz, A.M.: TR-FrM10, 263
 Schlaf, R.: 2D+EM+NS+SS+TF-WeM5, 125; VT-TuM2, 76
 Schlögl, R.: IS+AS+MC+SS-TuM1, 61
 Schmidt, A.B.: MI-MoA3, 39; MI-MoA4, 40
 Schmidt, D.: EL+AS+EM+MC+SS-ThA4, 207
 Schmidt, O.G.: MI+MG-TuM6, 63
 Schmidt-Mende, L.: EM2-ThA8, 210; EN+EM+MN+NS+TR-MoA10, 36
 Schmitz, A.: EM1-WeM10, 130
 Schneider, C.M.: SA-TuM3, **68**
 Schoeberl, T.: SE+NS+TR-TuM11, 70
 Schreiber, D.K.: AP+AS+NS+SS-FrM4, 247
 Schreiber, N.J.: SS+EM-FrM3, 259
 Schroeder, M.A.: EM+EN+TF-WeA10, 158; EN+EM+NS-TuA7, 86; EN+EM+NS-TuA8, **86**; TF+EN+PS-TuA1, 101; TF+EN+PS-TuA7, 101
 Schroeter, S.: PS+SE-ThA10, 215
 Schubert, E.: EL+AS+EM+MC+SS-ThA4, 207; EL+AS+EM+MC+SS-ThA6, 207
 Schubert, M.: EL+AS+BI+EM+SS-FrM8, 251; EL+AS+EM+MC+SS-ThA4, 207; EL+AS+EM+MC+SS-ThA6, 207; EL+AS+EM+MC+SS-ThA9, 208
 Schuck, P.: TF+PS+SE-MoM5, 23
 Schuengel, E.: PS1-FrM6, 255
 Schuler, A.: BI+AS+MN+NS-TuM12, 57
 Schuller, J.: 2D+AS+EM+MI+MN+NS+TF-WeA9, **153**
 Schultz, J.A.: HI+2D+AS+BI+MC-ThM13, 188
 Schulz, A.: EN-TuP6, 111
 Schulze, J.: PS1-FrM6, **255**
 Schürmann, M.: HI+2D+AS+BI+MC-ThM12, 188
 Schuster, S.: SS+TF-ThM6, 198; TF-MoA3, **50**
 Schwab, Y.: TF+PS-TuM12, 74
 Schwarm, S.: TF+AS+EM-TuA1, **99**
 Schwarz, U.D.: 2D+EM+NS+SS+TF-WeM4, 125
 Schwier, E.F.: 2D+EM+MI+MN+NS+SS+TF-ThA8, 203
 Scott, E.A.: AC+AS+MI+SA+SS-MoM10, 4
 Scott, K.: AS+BI+MC-WeA11, 155
 Scott, T.: AC+AS+MI+SA+SS-TuM5, **55**
 Scudeller, L.A.: BI+AS-MoM8, 7
 Scully, J.R.: SE+PS+TF-MoA9, 46
 Scurr, D.J.: BI+AS-TuA8, **82**
 Seah, M.P.: AS+BI+VT-TuM6, 56
 Seebauer, E.G.: SS+AS+EN-TuM6, 71; SS+AS+NS-ThA2, **222**
 Seegmiller, T.: TF+EN+PS-TuA2, 101
 Segalman, R.: EN+AS+EM+SE-TuM10, **60**
 Segawa, K.: SP+AS+BI+NS+SS-WeA3, 173
 Seibert, R.: TF+PS+SE-MoM5, **23**; TF-ThP1, 241
 Seidlitz, D.: EM-TuP15, **108**; EM-TuP17, 108
 Seifu, D.: NS+AS+SS-TuA11, 94
 Sekine, M.: 2D+EM+MS+NS-FrM10, 246; PS2-FrM8, **257**
 Sekora, D.: EL+AS+BI+EM+SS-FrM8, 251; EL+AS+EM+MC+SS-ThA6, **207**
 Sell, J.C.: SE+NS+TR-TuM2, **69**
 Selvaraj, S.K.: TF+PS-TuM13, 74
 Semprrott, P.J.: TR-ThP2, 244
 Senabulya, N.: EN+AS+EM+SE-WeM11, 133
 Senanayake, S.: IS+AS+MC+SS-WeM1, 134
 Senevirathna, M.K.I.: EM+EN-FrM11, 252; EM-TuP17, 108
 Senevirathne, I.: EM-TuP16, 108
 Sentman, C.D.: PS+2D-WeA3, 167
 Seo, H.-C.: EM1-WeM10, 130
 Seog, J.: PS+2D-WeA9, 168
 Seong, D.J.: NS-ThP1, 238
 Setina, J.: VT-MoM5, **26**
 Seymour, D.L.: VT-TuP4, 123
 Sezen, H.: SS+AS+EN-WeM13, 146
 Sgammato, B.: AS-ThP15, **212**
 Shah, N.C.: CS-ThA3, 205
 Shaikh, A.U.: EN-TuP8, 111
 Sham, T.-K.: SA-TuA11, 97
 Shamberger, P.J.: 2D+EM+NS+PS+SS+TF-MoM5, 2
 Shan, J.: IS+AS+MC+SS-TuM4, 62; IS+AS+MC+SS-WeM3, 134
 Shankar, S.: EM+EN+TF-WeA2, 157
 Shannon, S.: PS1-FrM11, **255**
 Shard, A.G.: AS+BI+MC+SS-MoA6, **31**; BI+AS+NS-MoA8, 33
 Sharipov, F.: VT-TuM5, **76**
 Sharma, K.: TF+PS-MoM4, **24**
 Sharma, P.: EM+MI+NS-MoM4, 9
 Sharma, S.: PS-WeA7, **169**
 Sharp, T.: TR+NS-ThM13, **202**
 Shavorskiy, A.: IS+AS+MC+SS-TuA4, 88
 Shaw, T.: BI+AS-MoM11, **8**
 Shchelkanov, I.A.: SE+PS+TF-MoA1, 45; SE+PS+TF-MoA2, 45; VT-MoA8, **52**; VT-MoA9, 52
 Shearer, J.C.: PS-TuA8, **95**
 Sheehan, B.: EM+2D-TuA8, 84
 Sheehan, P.E.: 2D+AS+BI+PS+SS-TuM4, 53; 2D+AS+BI+PS+SS-TuM5, 53; 2D+AS+BI+PS+SS-TuM6, 53; 2D+AS+EM+NS+SS-MoA3, 28; BI+AS+MN+NS-TuM5, **57**
 Shekhter, P.: EM1-ThA11, **210**
 Shen, F.: MS+PS+TF-ThM5, **189**; MS+TF-WeA9, 165

- Shen, Z.-X.: 2D+AS+HI+MC+NS+PS+SP+SS-TuA11, **80**
- Shenderova, O.A.: NS+AS-WeA1, **165**; TR-ThA9, 227
- Shenoy, V.B.: 2D+AS+BI+PS+SS-TuM4, 53
- Shepard, K.: 2D+EM+MI+MN+NS+SS+TF-ThA4, 203
- Sherry, A.H.: AC+AS+MI+SA+SS-MoM8, 4
- Shetty, R.: NS+AS-WeA9, 166
- Shi, X.: HI+2D+AS+MC-ThA9, 212
- Shi, Y.: NS-ThP5, 238
- Shi, Z.: NS+AS+SS-TuA8, 94; QC+AS+BI+MN-ThA6, 219
- Shiao, M.H.: MN-ThP2, 236; MS-ThP6, 237; MS-ThP7, 237; SP+AS+EM+NS+SS-ThP5, 240
- Shibuya, R.: AS+MC+SS-FrM8, 248
- Shield, J.: AP+AS+MC+NS+SS-ThM12, 181
- Shigetoshi, T.: PS-TuM4, 66
- Shim, J.: MS+TF-WeA3, 164
- Shimada, M.: 2D+EM+MI+MN+NS+SS+TF-ThA8, 203
- Shin, H.J.: PS2+TF-ThM2, 192
- Shin, K.: PS-WeA10, **170**
- Shin, N.: NS+AS+SS-TuA1, 93
- Shin, S.: SP+AS+BI+NS+SS-WeA3, 173
- Shin, T.: PS-TuP27, **118**
- Shin, Y.H.: NS-ThP1, 238
- Shirazi, M.: SD-WeM5, 144
- Shirley, E.L.: SA-TuP2, **119**
- Shklover, V.: SE+NS+TR-TuM10, 70
- Shohet, J.L.: EM-TuP11, 107; EM-WeA11, 159; PS2-FrM4, 256; PS-TuP12, **116**; PS-TuP8, 115; TF+AS-FrM3, 260
- Shollock, B.: CS-ThM1, **181**
- Shrestha, B.: AS+BI+VT-TuM1, 55
- Shrestha, B.R.: BI+AS-MoM3, 7; SS+EN-MoA4, 47
- Shterengas, L.: MC+AP+AS-MoM4, 10
- Shu, J.: EM-TuM3, **58**
- Shubeita, S.: HI+2D+AS+BI+MC-ThM13, 188
- Shudo, K.: EM-TuP12, 107; EM-TuP13, 108
- Shuh, D.: AC+AS+MI+SA+SS-MoM1, 3
- Shukla, N.: SS-WeA8, **175**
- Shutthanandan, V.: AS+MC+SS-TuA9, 81; SS+AS+EN-TuM13, **72**; TF+EM+EN-WeA11, 177
- Shyam, R.: AS+MC+SS-FrM10, **248**
- Shyner, S.J.: SS+TF-ThM4, 198
- Sieg, S.: NS+HI-TuM3, 64
- Siegel, D.A.: SP+2D+AS+EM+MC+NS+SS-ThM11, 197
- Siekhaus, W.J.: AC+AS+MI+SA+SS-TuM12, 55
- Sikorski, E.M.: PS-MoM10, 16; PS-MoM3, 14
- Silva, T.: PS+SE-ThA11, **215**
- Simbrunner, C.: TF+AS-FrM10, 262
- Simic-Milosevic, V.: IS-ThP2, **236**
- Simon, A.H.: SD-WeA10, **172**
- Simonato, J.-P.: 2D+EM+MI+MN+NS+SS+TF-ThA10, 204
- Simons, D.: AC+AS+MI+SA+SS-TuM10, **55**; EM1-ThA3, 208
- Simpson, J.R.: 2D+AS+EM+MI+MN+NS+TF-WeA4, 153; 2D+AS+EM+MI+MN+NS+TF-WeA7, 153
- Simpson, S.: SS+TF-ThM11, 198
- Sinclair, F.: PS1-WeM5, 140
- Singer, B.W.: CS-ThA8, 206
- Singh, A.: 2D+AS+BI+PS+SS-TuM11, 54
- Singh, B.: TF+AS-FrM4, 261; TF+EM+EN-WeA7, 176
- Singh, H.: PS-WeA3, 169
- Singh, J.P.: AS+MC+SS-FrM3, 247; TF-MoA7, 51
- Singh, S.: SS+AS-WeM3, 147
- Singhal, S.: NS+HI-TuM11, 65
- Sinha, D.: 2D+AS+HI+MC+NS+PS+SP+SS-TuA8, 79
- Simitskii, A.: 2D+AS+HI+NS+SS-ThM12, **180**; SS+TF-ThM11, 198
- Sinkovic, B.: MI-MoA8, 40
- Sinno, T.R.: EM1-ThA4, 208; EM1-ThA8, 209; SS+AS-WeM12, **148**
- Sinnott, S.B.: MG-WeM4, **136**
- Sintim, H.: BI-ThP2, 234
- Sitar, Z.: MG-WeM3, 135
- Sivaram, S.V.: NS+AS+SS-TuA1, 93
- Siviero, F.: VT-TuM10, **77**
- Skaritka, J.: MG-WeM2, 135; VT-TuP5, 124
- Skibinski, E.S.: SS+AS+NS-ThA8, **223**
- Skuzza, J.R.: NS+EN-MoA11, **42**
- Slinkman, J.: MC+2D+AP+AS-MoA11, 39
- Smentkowski, V.: AS-ThP19, **233**
- Smeu, M.: SP+2D+AS+EM+MC+NS+SS-ThM5, 196
- Smit, S.: TF+EN+PS-TuA10, 102
- Smith, A.R.: MI+MG-TuA8, 91; SS-WeA9, 175
- Smith, D.: BI+AS-TuA9, 83
- Smith, D.J.: EM+MI+NS-MoM3, 8
- Smith, J.N.: BI+AS+NS-MoA7, 33
- Smith, L.: TF+EN+PS-TuA2, 101
- Smith, L.E.: SM+AS+BI+PS-ThA9, 221
- Smith, R.: 2D+EM+NS+PS+SS+TF-MoM5, 2
- Smith, S.: PS-WeA12, **171**
- Smith, T.L.: VT-WeM12, 151
- Smolenski, K.: VT-WeA1, **177**
- Snee, P.: BI+AS+NS-MoA3, **33**
- Snyder, J.S.: BI+MG-WeA3, 156
- Snyders, R.: PS+2D-WeA7, **167**; PS+SE-ThA11, 215
- Sobiech, M.: SE+NS+TR-TuM10, 70
- Sobol, P.E.: SA-MoM10, 17
- Sobolewski, M.A.: PS2-WeM11, **143**
- Söderlund, M.J.: TF+PS-MoM3, 24
- Sohn, H.: TF-ThP25, 243
- Soininen, P.T.: TF+PS-MoM3, 24
- Sokaras, D.: AC+AS+MI+SA+SS-MoM1, 3; AC+AS+MI+SA+SS-TuM1, 54
- Solares, S.D.: SP+AS+BI+EM+NS+SE+SS-FrM8, **258**
- Solokha, V.: EL+AS+EM+EN+SS-ThM12, 184
- Solzbacher, F.: TF-ThA8, 225
- Son, E.-J.: PS-TuP5, 114
- Son, K.A.: EM1-WeM10, 130
- Song, A.: SS+EN-MoA10, 48
- Song, Y.: SS+AS+EN-MoM6, **20**
- Song, Y.J.: SP+AS+EM+NS+SS-ThP3, 240
- Sonnenfeld, A.: 2D+EM+NS+SS+TF-WeM4, 125
- Sorescu, D.C.: SS+EN-MoA7, 47; SS+NS-TuA4, 98
- Sosolik, C.E.: AS+MC+SS-FrM10, 248
- Sottos, N.: NS+SE-MoM8, 14
- Soukhojaj, A.N.: QC+AS+BI+MN-ThA10, **220**
- Sourribes, M.J.L.: HI+2D+AS+MC-ThA10, 212
- Soy, E.: AS-ThP1, **230**
- Spee, K.: TF+PS-MoM8, **25**
- Spencer, J.A.: SS+AS+EN-MoM11, **20**
- Spencer, N.D.: TF-MoA10, **51**
- Spentzouris, L.: TF-ThP1, 241
- Sperling, B.A.: TF+PS-MoA3, **49**; TF+PS-MoA8, 49
- Sporre, J.R.: NS+HI-TuM3, 64
- Sprunger, P.T.: SS+NS-TuA11, **99**; SS+TF-ThM12, 198
- Sreenivasan, S.: NS+HI-TuM11, 65
- Sridhar, S.: PS1-FrM10, 255; PS1-FrM9, **255**
- Sridhara, K.: 2D+AS+HI+MC+NS+PS+SP+SS-TuA9, **79**
- Srinivasan, S.: PS-MoA8, 43
- Sriraman, S.: PS2-WeM3, 142; PS-WeA3, 169
- Srivastava, A.: PS+SE-ThA4, 214
- Srivastava, A.K.: PS-TuM5, **66**
- Srivastava, S.N.: SE-TuP1, 119
- Staaks, D.: NS+HI-TuM1, 64
- Stacchiola, D.: IS+AS+MC+SS-WeM1, 134
- Stafford, N.: PS-TuA10, 96
- Stahlbush, R.E.: EM1-WeM5, 129
- Staub, P.G.: EW-WeL2, 152; IS+AS+MC+SS-TuA11, **89**
- Stampe, P.A.: EN+AS+EM+SE-WeM11, 133
- Stanford, J.A.: AC+AS+MI+SA+SS-TuM12, 55
- Stanford, M.G.: NS+HI-TuM10, 65; TF+PS-TuM6, **73**
- Stano, K.: TF+MS+PS-WeM13, **150**
- Starbuck, A.: TF-ThP20, 243
- Starostin, S.A.: TF-ThA10, **226**
- Steckl, A.: MS+TF-WeA7, **164**
- Steel, E.B.: AP+AS+MC+NS+SS-ThM13, 181
- Stefenelli, M.: SE+NS+TR-TuM11, 70
- Stege, U.: BI+AS-WeM3, 128
- Stein, J.: SM+AS+BI+PS-ThM10, 195
- Steinbauer, E.: TF+AS-FrM8, 261
- Steiner, M.A.: TF+SE-TuM11, **75**
- Steiner, P.J.: TF+SE-TuM11, 75
- Steirer, K.X.: AS-ThP24, **233**
- Stemmer, S.: EM+MI+NS-MoM1, **8**
- Stenger, B.H.: SS+NS-TuA12, 99
- Steriotis, T.: EN-TuP14, 112
- Stern, A.C.: IS+AS+MC+SS-TuA4, 88
- Stevanovic, A.: NS+AS-WeA11, **166**
- Stevenson, R.: 2D+EM+NS+PS+SS+TF-MoM5, 2
- Stewart, D.M.: SE+NS+TR-TuM2, 69; TF+PS+SE-MoM9, **23**
- Stickle, W.F.: AS+BI+MC-WeA8, **155**
- Stievater, T.H.: MN-WeM5, 137
- Stika, K.M.: AS-ThP13, **232**
- Stiles, M.D.: MI+MG-TuA10, **91**
- Stillwell, B.: VT-WeM4, 150
- Stine, R.: 2D+AS+BI+PS+SS-TuM5, 53; BI+AS+MN+NS-TuM5, 57
- Stitt, C.A.: AC+AS+MI+SA+SS-TuM5, 55
- Stock, T.J.Z.: SS+TF-ThM10, **198**
- Stoehr, J.: MI+EM-MoM11, 13
- Stollenwerk, A.J.: NS+SE-MoM6, **13**
- Stoller, R.: TF+PS+SE-MoM5, 23
- Stolwijk, S.D.: MI-MoA3, 39
- Stone, J.A.: VT-MoM3, 26
- Stopka, S.A.: AS+BI+VT-TuM1, 55
- Stosch, R.: 2D+AS+HI+NS+SS-ThM3, 179
- Strachan, J.P.: NS+HI-TuM4, 65
- Stradins, P.: EM1-ThM10, **185**; TF+EN+PS-TuA11, 102
- Stranick, S.J.: MS+PS+TF-ThM10, 189
- Stratton, B.: PS-TuP11, 115
- Streeck, C.: SA-TuM1, 68
- Streubel, R.: MI+MG-TuM6, 63
- Strobel, M.: AS+MC+SS-TuA1, **80**
- Strohmeier, B.R.: 2D-ThP6, 228; AS+BI+MC-WeA7, **154**
- Stroschio, J.A.: 2D+EM+MI+MN+NS+SS+TF-ThA4, 203; MI-MoA10, 40; SP+AS+BI+EM+NS+SE+SS-FrM6, 258; SP+AS+BI+NS+SS-ThA8, 222; SP+AS+EM+NS+SS-ThP3, 240
- Strouse, G.F.: CS-ThM10, 182; VT-MoM3, 26
- Strupinski, W.: 2D-ThP1, 228
- Stuart, S.C.: AS+MC+SS-FrM9, **248**
- Stuart, S.S.: BI+MG-WeA3, 156
- Stuckert, E.P.: SS+NS-TuA3, **98**
- Stumpf, C.: EM+MI+NS-MoM4, 9
- Stutzman, M.L.: VT-WeA4, **177**
- Su, C.Y.: EM+EN-FrM5, 252
- Su, H.: MI+MG-TuM13, 64
- Su, J.Y.: MS-ThP7, 237; SP+AS+EM+NS+SS-ThP5, **240**
- Su, T.-T.: PS-MoM8, 15
- Subramania, G.: EM1-ThA6, 209
- Subramanian, S.: MN+NS-TuA9, **92**
- Sudarshan, T.: 2D+AS+BI+PS+SS-TuM11, 54
- Sugimoto, Y.: PS1-WeM10, 140
- Sugiyama, M.: EN+EM+MN+NS+TR-MoA11, 37; EN-TuP2, 110
- Sukenik, C.N.: TR-FrM3, 262
- Sullivan, N.: TF-MoA3, 50
- Sumant, A.V.: TR-ThA6, 227
- Sun, L.: TF+EM+EN-WeA10, 177
- Sun, N.: EL-ThP3, **234**; MC-TuP6, 113
- Sun, R.: EL-ThP3, 234; MC-TuP6, **113**
- Sun, T.: MC+AP+AS-MoM6, 11

- Sun, X.: SA-TuA11, 97; TF+EN+PS-TuA3, **101**
 Sun, Y.: MC+2D+AP+AS-MoA1, 37; PS-MoM4, 15
 Sun, Z.: EM-TuM3, 58
 Sundar, U.: EM+EN+TF-WeA1, 157
 Sung, Y.M.: PS-TuP8, 115
 Surla, V.: PS2-FrM9, **257**
 Surnev, S.: SS+AS+EN-TuM5, 71
 Susa, Y.: PS2-WeM10, 143
 Sutor, E.J.: PS2-FrM3, 256
 Sutter, P.: SS+EN-MoA3, 47; SS+EN-MoA8, 48
 Suzer, S.: 2D+EM+MI+MN+NS+SS+TF-ThA11, **204**; MC+2D+AP+AS-MoA7, 38; TF-MoA6, 50
 Suzuki, A.: EM-TuP12, 107; PS1-FrM4, 254
 Suzuki, H.: EN+EM+MN+NS+TR-MoA11, 37
 Suzuki, T.: PS-MoM10, 16; PS-MoM3, 14
 Svensson, S.P.: MC+2D+AP+AS-MoA2, 37; MC+2D+AP+AS-MoA3, **38**; MC+AP+AS-MoM4, 10; SS+EN-MoM3, 21
 Swart, H.C.: 2D-ThP7, 228; TF+SE-TuM13, 76
 Swinney, T.C.: VT-MoM11, 27
 Sydorenko, D.: PS2-WeM5, 142
 Syed, M.: EM-TuP16, **108**
 Syers, P.S.: SP+AS+BI+EM+NS+SE+SS-FrM6, 258
 Sykes, E.C.H.: NS-WeM1, **138**; SS+AS+EN-WeM4, 145; SS-WeA4, 174
 Symonds, J.M.: BI+AS-TuA1, 82
 Szakal, C.: AS+BI+MC-WeM2, **126**
 Szeto, K.: BI+AS+NS-MoA10, 34
 Szkutnik, P.D.: PS1+TF-ThM5, 190
 Szymanski, C.: BI+AS-TuA11, 83
- **T** —
 Tadjer, M.: TF+PS-TuM3, 72
 Tae, J.: PS1+TF-ThM3, 190
 Tait, J.: SA-TuP1, 119
 Takahashi, K.: SE+EM+EN+PS+TF-MoM3, 18
 Takakuwa, Y.: PS2-FrM1, 256; SS+AS+EN-MoM10, 20
 Takano, I.: SS-TuP14, 121; SS-TuP15, 121
 Takeda, K.: PS2-FrM8, 257; PS-ThA11, 218
 Takeuchi, I.: MI+MG-TuM1, **63**
 Takoudis, C.G.: TF+PS-TuM13, **74**
 Talin, A.: SP+AS+BI+NS+SS-WeA11, 174
 Talledo, A.F.: EM-TuP26, 109; TR-ThA10, **227**
 Tamanaha, C.R.: 2D+AS+BI+PS+SS-TuM5, 53; BI+AS+MN+NS-TuM5, 57
 Tampaxis, C.: EN-TuP14, 112
 Tamura, Y.: PS-ThA8, 217
 Tan, C.Y.: VT-WeM13, 151
 Tan, R.: SS-TuP15, **121**
 Tan, S.: HI+2D+AS+MC-ThA4, 212; HI+2D+AS+MC-ThA6, 212
 Tan, X.: BI+AS+MN+NS-TuM4, 57; EL+AS+EM+EN+SS-ThM4, **183**
 Tanabe, I.: MI-MoA11, 41
 Tanaka, H.: SE+PS+TF-MoA10, 46
 Tanen, N.J.: EN+AS+EM+SE-WeM6, 133; TF-ThP17, 242
 Taner-Camci, M.: TF-MoA6, **50**
 Tang, G.: SE+EM+EN+PS+TF-MoM3, 18
 Tang, J.: SS+AS+EN-MoM10, 20
 Tang, K.: EM-WeA12, 160
 Tang, S.W.: MI+MG-TuM10, 63
 Tang, W.: NS-WeM3, 138
 Tang, X.: SS+EN-MoA6, **47**
 Tang, Y.H.: MN-ThP1, **236**; MN-ThP2, 236; MS-ThP6, 237
 Taniguchi, T.: 2D+EM+MI+MN+NS+SS+TF-ThA4, 203; 2D+EM+MS+NS-FrM3, 245
 Tanuma, S.: AS+MC-MoM5, 5
 Tanyeli, I.: PS-ThA9, **217**
 Tao, C.: 2D+AS+HI+MC+NS+PS+SP+SS-TuA4, **79**
 Tao, F.: IS+AS+MC+SS-TuM4, 62; IS+AS+MC+SS-WeM3, 134; NS+AS+SS-TuA10, 94; SP+AS+BI+NS+SS-ThA1, **221**; SS-TuP21, 122
 Tao, M.: NS+SE-MoM3, 13
 Tappan, A.S.: TF+SE-TuM5, 75
 Tatsumi, T.: PS-TuM11, 67; PS-TuM4, 66; PS-TuP6, 114
 Tavassoli, F.: PS2+TF-ThM3, 192
 Tavernier, A.: SD-WeA9, 172
 Taylor, A.: BI+AS+NS-MoA1, 32
 Taylor, D.: EN+EM+MN+NS+TR-MoA3, 36
 Teckcan, B.: TF+EM+EN-WeA2, 176
 Teeter, G.: AS-ThP24, 233; EL+AS+BI+EM+SS-FrM5, 250
 Tegenkamp, C.: NS+EN-MoA6, 41
 Tellez, H.: EN+AS+EM+SE-WeM2, 132
 Temnykh, A.: VT-WeA3, 177
 Ten Eyck, G.: EM1-ThA6, 209
 Tenney, S.A.: SS+EN-MoA3, 47
 Tennyson, J.C.: PS-TuP16, 116
 Teplyakov, A.V.: SS+TF-ThM3, **197**; SS-TuP13, 121; SS-TuP3, 119; SS-TuP6, 120
 ter Veen, H.R.J.: MC+AP+AS-MoM8, 11
 Teraoka, Y.: SS+AS+EN-MoM10, 20
 Terrott, A.: SS+TF-ThM6, 198
 Terrani, K.A.: TF+PS+SE-MoM5, 23
 Terry, J.: TF+AS-FrM4, 261; TF+PS+SE-MoM5, 23; TF-ThP1, 241
 Thadani, K.: TF+PS-ThM10, 200
 Thamaraiselvan, P.: EM+EN+TF-WeA2, 157
 Thamban, P.L.S.: MC-TuP1, 113
 Theilacker, W.: AS+BI+MC-WeA3, 154
 Thejaswini, H.C.: PS-TuP17, 116
 Therien, M.J.: NS-WeM12, 140
 Thevuthasan, S.A.: AP+AS+MC+NS+SS-ThM6, 181; AS+MC+SS-TuA9, 81; SS+AS+EN-TuM13, 72
 Thibodeaux, C.A.: SS+TF-ThM12, 198
 Thiel, P.A.: SS+NS-TuA7, **98**
 Thiele, C.: HI-ThP3, 235
 Thiesen, P.H.: EL+AS+EM+MC+SS-ThA10, 208; EL+AS+EM+MC+SS-ThA7, **208**
 Thimsen, E.: TF+MS+PS-WeM4, **149**
 Thissen, A.: IS-ThP2, 236
 Thissen, N.F.W.: 2D+EM+MS+NS-FrM6, **245**
 Thomas, C.: PS-ThA8, **217**
 Thompson, C.V.: EM-TuM10, **59**; EM-TuM4, 58
 Thompson, G.B.: AP+AS+NS+SS-FrM3, 246
 Thompson, W.: NS+HI-TuM4, 65
 Thon, S.M.: EN+EM+MN+NS+TR-MoA1, **36**
 Thorman, R.G.: SS+AS+EN-MoM11, 20
 Thorpe, R.: EN+EM+NS-TuA4, **86**
 Thoulon, P.Y.: EN-TuP5, 110; TF+PS+SE-MoM3, 22
 Tiago Manera, L.T.: MS-ThP9, 238
 Tian, W.-C.: MN+NS-TuA11, 92; MN+NS-TuA12, 93; MN-ThP3, 237
 Tierno, D.: NS+HI-TuM1, 64
 Tikare, V.: MG-WeM10, **136**
 Timilsina, R.: HI+2D+AS+MC-ThA4, **212**; MG-TuA3, 89
 Timm, R.: EM+2D-TuA1, **84**; NS+AS+SS-TuA4, 93
 Ting, M.: MC+2D+AP+AS-MoA3, 38
 Tiron, R.: PS-TuM13, 68; SD-WeA9, 172
 Tischler, J.G.: EM-MoA10, 35; EM-TuP20, **109**
 Tiwald, T.: EL+AS+EM+EN+SS-ThM10, **184**
 Tjong, J.: TR-FrM4, 262
 Tjong, V.: BI+AS-MoM4, 7
 Tkach, I.: AC+AS+MI+SA+SS-MoM9, 4
 Tobash, P.H.: AC+AS+MI+SA+SS-TuM1, 54
 Tobias, D.J.: IS+AS+MC+SS-TuA4, 88
 Tobin, J.G.: AC+AS+MI+SA+SS-MoA6, **29**; AC+AS+MI+SA+SS-TuM1, 54
 Todorov, S.: PS1-WeM5, 140
 Tokei, Z.: EM-TuM6, 59
 Toledano, T.: AS-ThP20, 233
 Tolstaya, E.I.: BI+AS+MN+NS-TuM2, **56**; EN+EM+NS-TuA9, 86
 Tomaszewska, N.: SS+AS+NS-ThA1, 222
 Tompkins, B.D.: SM+AS+BI+PS-ThM11, 195
 Tong, X.: IS+2D+MC+NS+SP+SS-WeA9, 162
 Toprasertpong, K.: EN-TuP2, 110
 Torok, E.: CS-ThA10, 206
 Torres, D.M.: HI-ThP3, 235
 Torun, B.: QC+AS+BI+MN-ThM5, **194**
 Tra, V.: MI+EM-MoM2, 12
 Tran, I.C.: AS+MC+SS-TuA11, **81**; SA-MoA8, 44
 Tranchant, J.: TF+PS+SE-MoM3, 22
 Trappen, R.: MI+EM-MoM2, **12**; MI+MG-TuM11, 64
 Travis, C.D.: SS+AS-WeM2, 147
 Travis, J.J.: TF+MS+PS-WeM12, 150
 Trenary, M.: AS-ThP1, 230; SS+AS+EN-MoM5, 19; SS+AS+EN-MoM8, 20
 Triani, G.: TF-ThP21, 243
 Tridas, E.: VT-TuM2, **76**
 Tringides, M.C.: SS+NS-TuA12, 99
 Triozon, F.: SP+AS+BI+NS+SS-ThA4, 221
 Triplett, M.: SP+AS+BI+NS+SS-WeA11, 174
 Triscone, J.-M.: MI+EM-MoM3, 12
 Trogler, W.: BI+AS+NS-MoA2, 32; BI+MG-WeA4, 156; BI+MG-WeA7, 156
 Trouiller, C.: SS+EM-FrM9, 260
 Troya, D.: AS+MC-MoM10, 6; SS-TuP4, 120
 Truckenmuller, R.: BI+MG-WeA9, 157
 Trunschke, A.: IS+AS+MC+SS-TuM1, 61
 Tsai, C.H.: EM+NS+TF-FrM5, 253
 Tsai, H.-Z.: 2D+EM+MS+NS-FrM3, 245
 Tsai, J.: MS-ThP4, 237
 Tsai, S.C.: MS-ThP5, **237**
 Tsao, C.Y.: BI-ThP2, 234
 Tsao, M.-C.: MN+NS-TuA11, 92
 Tsargorodska, A.: BI+AS+NS-MoA6, 33
 Tselev, A.: IS+2D+MC+NS+SP+SS-WeA3, **161**
 Tshabalala, M.A.: TF+SE-TuM13, 76
 Tsoi, S.: 2D+AS+BI+PS+SS-TuM5, 53
 Tsortos, A.: QC+AS+BI+MN-ThM12, **194**; QC+AS+BI+MN-ThM13, 194
 Tsuchiya, T.: SS-TuP14, **121**
 Tsukagoshi, K.: EM-TuP8, 107
 Tsybal, E.Y.: EM+MI+NS-MoM10, 9
 Tu, C.G.: EM+EN-FrM5, 252
 Tufenkji, N.: QC+AS+BI+MN-ThM10, 194
 Tunuguntla, R.: AS+MC+SS-TuA11, 81
 Turchanin, A.: 2D+AS+HI+NS+SS-ThM3, 179
 Turkowski, V.: 2D+AS+EM+MI+MN+NS+TF-WeA3, 153
 Turley, R.S.: AC+AS+MI+SA+SS-MoM10, 4
 Turner, D.: AC+AS+MI+SA+SS-MoM11, 4
 Turner, J.A.: SS+EN-MoM9, 22
 Turner, K.T.: SP+AS+BI+EM+NS+SE+SS-FrM2, 258; SS+AS-WeM5, 147; TR+NS-ThM5, 201; TR-FrM1, **262**; TR-FrM6, 263
 Tyagi, P.: 2D+AS+HI+MC+NS+PS+SP+SS-TuA10, 80; 2D+EM+NS+PS+SS+TF-MoM3, 2
 Tyani, E.: EM-TuP24, 109
 Tyler, B.J.: AS+BI+MC-WeM10, **127**
 Tyliczszak, T.: AC+AS+MI+SA+SS-MoM1, 3
 Tysoe, W.T.: SS-WeA3, **174**
 Tyurnina, A.: 2D+EM+MI+MN+NS+SS+TF-ThA10, 204
 Tzeng, T.-H.: MN-ThP3, 237
 Tzitzios, V.: EN-TuP14, 112
- **U** —
 Uddin, M.A.: 2D+AS+BI+PS+SS-TuM11, **54**
 Ueda, H.: PS1-WeM10, 140
 Uenishi, M.: SE+PS+TF-MoA10, 46
 Ueno, T.: PS+2D-WeA4, 167
 Ulfig, M.: AP-ThP1, 230
 Ulrich, M.: AS+MC+SS-FrM9, 248
 Underwood, B.: TF+PS-ThM10, 200
 Unger, W.: AS+MC-MoM8, 6
 Unterumsberger, R.: SA-TuM1, 68; TF+AS-FrM9, 261
 Urban, R.: HI+2D+AS+BI+MC-ThM3, 187; HI+2D+AS+BI+MC-ThM5, **187**
 Urena, R.E.: EN+AS+EM+SE-WeM6, 133; TF-ThP17, 242
 Urrabazo, D.: PS1-WeM13, **141**
 Utz, A.L.: SS+AS+EN-WeM11, **146**

Utzig, T.: BI+AS-MoM3, 7

— V —

Vaaland, O.: MS+PS+TF-ThA11, 213
Vähä-Nissi, M.: TF+PS-MoM1, 24
Vahdat, V.: TR+NS-ThM5, 201
Vahedi, V.: PS-MoA6, 42; PS-WeA3, 169
Vaish, A.: BI+AS-MoM10, 8
Vajda, F.: PS-MoM4, 15
Valdez, B.: TF-ThP15, 242
Valente-Feliciano, A.-M.: VT-WeM10, 151
Valizadeh, R.: VT-WeM1, 150
Valla, T.: MI-MoA8, 40
Vallee, C.: PS1+TF-ThM5, 190
Vallier, L.: PS-WeA2, 169
Valtiner, M.: BI+AS-MoM3, 7; SS+EN-MoA4, 47
Van Benthem, M.H.: AS+BI+MC-WeM12, 127
van Blitterswijk, C.: BI+MG-WeA9, 157
van Buuren, T.W.: AS+MC+SS-TuA11, 81; SA-MoA8, 44
van de Loo, B.W.H.: TF+EN+PS-TuA9, 102
Van de Runstraat, A.: VT-TuA10, 104
van de Sanden, M.C.M.: EN-TuP6, 111; PS+SE-ThA6, 214; PS2-FrM10, 257; PS-ThA1, 216; PS-ThA9, 217; TF-ThA10, 226
van den Bruele, F.: TF-ThA7, 225
Van der Donck, V.T.: TuM6, 77
Van der Meer, J.A.: VT-TuA10, 104
van der Velden-Schuermans, B.C.A.M.: TF-ThA10, 226
Van Duyne, R.P.: CS-ThA3, 205
van Gastel, R.: HI-ThP4, 235
Van Groningen, T.: VT-TuA10, 104
van Langen-Suurling, A.: HI+2D+AS+MC-ThA8, 212
Van Spyk, M.H.C.: IS+AS+MC+SS-TuA4, 88; IS+AS+MC+SS-TuM11, 62
van Veldhoven, E.: HI+2D+AS+MC-ThA8, 212
van Zijll, M.S.: SS+NS-TuA12, 99
Vandalon, V.: TF+PS-MoA1, 48
Vandenbergh, W.G.: EM-WeA7, 159
Vandencastele, N.: PS+2D-WeA11, 168; PS+SE-ThA7, 215
Vanderah, D.: BI+AS-MoM10, 8
Vanderberg, B.H.: PS1-WeM1, 140
VanDerslice, J.: EL+AS+EM+EN+SS-ThM10, 184
Vandervorst, W.: MC+AP+AS-MoM1, 10; SA-TuP1, 119
Vanfleet, R.R.: AC+AS+MI+SA+SS-MoM10, 4; EM+EN+TF-WeA9, 158; MN+PS-WeA3, 163; MN+PS-WeA4, 163; MN+PS-WeA9, 163; TF+AS-FrM2, 260; TF+PS-ThM6, 200
Vanhemel, D.: TF+EN+PS-TuA10, 102
Vanleuven, D.: TF-ThA6, 225
Varga, T.: AS+MC+SS-TuA9, 81
Vargas, M.: EN+AS+EM-WeA4, 160
Varshney, V.: SE+EM+EN+PS+TF-MoM8, 19
Vartiainen, J.: TF+PS-MoM1, 24
Vazquez-Lepe, M.O.: AS+MC-MoM11, 6; AS+MC-MoM2, 5
Veal, T.D.: EN+AS+EM+SE-WeM11, 133
Veirs, D.K.: AC+AS+MI+SA+SS-TuM1, 54
Velasco Jr., J.: 2D+EM+MS+NS-FrM3, 245
Velazquez, D.: TF+PS+SE-MoM5, 23; TF-ThP1, 241
Venditti, R.A.: MS+TF-WeA12, 165
Venkatachalam, M.: EM+EN+TF-WeA2, 157
Ventrice, Jr., C.A.: 2D+AS+HI+MC+NS+PS+SP+SS-TuA10, 80; 2D+EM+NS+PS+SS+TF-MoM3, 2
Ventzek, P.: PS1-FrM4, 254; PS1-WeM10, 140; PS2-WeM10, 143; PS2-WeM12, 143; PS2-WeM5, 142
Vera, D.: BI+MG-WeA4, 156
Versluis, R.: VT-TuA9, 104
Verspagnet, C.: HI+2D+AS+MC-ThA8, 212
Vertes, A.: AS+BI+VT-TuM1, 55
Vervuurt, R.H.J.: 2D+EM+MS+NS-FrM6, 245
Verweij, H.: EL+AS+BI+EM+SS-FrM4, 250
Vescovo, E.: MI+EM-MoM10, 12; MI-MoA8, 40

Viale, L.: VT-TuM10, 77
Viana, B.C.: TF+PS-ThM13, 201
Vicar, M.: VT-MoM5, 26
Vicenzi, E.: CS-FrM8, 249
Vidyarthi, V.: PS2+TF-ThM2, 192
Vieker, H.: HI-ThP2, 235; HI-ThP3, 235
Vijayalakshmi, K.: BI+AS-TuA1, 82
Vinicius Puydinger dos Santos, M.V.: MS-ThP9, 238
Vinson, J.: SA-MoA9, 44
Virgo, M.J.: VT-WeM12, 151
Visart de Bocarmé, T.: AP+AS+EN+NS+SS-ThA3, 204
Vishwanath, S.: EM-WeA9, 159
Viveros, R.: BI+AS+NS-MoA2, 32; BI+MG-WeA4, 156
Viville, P.: PS+2D-WeA10, 168
Vlachová, J.: QC+AS+BI+MN-ThP2, 239
Vlahovic, B.: NS-ThP9, 239
Vlcek, J.: SE+PS+TF-MoA8, 46
Voevodin, A.A.: 2D+EM+NS+PS+SS+TF-MoM5, 2; SE+EM+EN+PS+TF-MoM8, 19
von Borany, J.: HI-ThP6, 235
Von Son Palacio, G.: 2D+EM+NS+SS+TF-WeM10, 126; 2D-ThP11, 229
Voras, Z.: CS-ThA9, 206
Voronin, S.: NS+HI-TuM3, 64
Voroshazi, E.: SA-TuP1, 119
Vurgafman, I.: EM1-ThM12, 185
Vysochanskii, Y.: 2D+EM+MI+MN+NS+SS+TF-ThA9, 204

— W —

Wacaser, B.A.: MC+2D+AP+AS-MoA1, 37
Wachs, I.E.: IS+AS+MC+SS-WeM5, 135
Wade, J.: TF+AS-FrM9, 261
Wagenaars, E.: PS+SE-ThA10, 215
Wager, J.: EM2-WeM13, 131
Wagner, A.: TF+MS+PS-WeM4, 149
Wagner, J.B.: IS+AS+MC+SS-TuA9, 88
Waite, A.: 2D+EM+NS+PS+SS+TF-MoM5, 2
Walker, A.V.: NS+AS+SS-TuA8, 94; QC+AS+BI+MN-ThA6, 219
Walker, L.M.: AS+BI+MC+SS-MoA1, 30
Walker, M.: BI+AS-MoM10, 8; EN-TuP6, 111
Walker, M.E.: IS+AS+MC+SS-TuA12, 89
Wall, M.A.: AC+AS+MI+SA+SS-TuM1, 54
Wall, M.H.: EW-ThM9, 187
Wallace, C.: SD-WeA1, 171
Wallace, R.M.: 2D+EM+NS+SS+TF-WeM6, 125; EM+2D-TuA3, 84; EM+2D-TuA7, 84; EM-WeA4, 159; EM-WeA9, 159; NS+HI-TuM11, 65; SD-WeA11, 172; TF+MS+PS-WeM1, 148
Walls, J.M.: EN+AS+EM+SE-WeM13, 134
Walsh, J.M.: CS-FrM3, 249
Walsh, K.: TR-ThP2, 244
Walsh, L.: SA-MoM5, 17
Walton, S.G.: 2D+AS+BI+PS+SS-TuM5, 53; 2D+AS+BI+PS+SS-TuM6, 53; BI+AS+MN+NS-TuM5, 57; PS1-FrM8, 255; PS-TuM12, 67; PS-WeA11, 171
Walukiewicz, W.: SS+EN-MoM3, 21
Waluyo, I.: SS+AS+EN-MoM5, 19
Wan, J.: MS+PS+TF-ThA10, 213
Wang, A.: MS-ThP4, 237
Wang, B.: 2D+EM+NS+PS+SS+TF-MoM5, 2
Wang, C.C.: EN-TuP13, 112
Wang, C.-C.: PS-MoM8, 15
Wang, C.G.: EN-TuP13, 112
Wang, C.M.: PS-TuP21, 117; PS-TuP25, 118
Wang, C.-M.: BI+AS+NS-MoA7, 33
Wang, D.: MC+AP+AS-MoM4, 10; SA-MoM3, 16
Wang, E.: MG-WeM2, 135; VT-TuP5, 124
Wang, F.: 2D+EM+MS+NS-FrM3, 245
Wang, G.: TR-FrM4, 262
Wang, H.: BI+AS+NS-MoA11, 34; HI-ThP2, 235; TF+EM+EN-WeA11, 177; TF-ThP19, 242
Wang, J.: BI+AS+NS-MoA2, 32; EM-WeA9, 159; SA-TuA11, 97; SS+AS+EN-WeM3, 145
Wang, K.: SP+AS+BI+EM+NS+SE+SS-FrM6, 258
Wang, L.: 2D+EM+MI+MN+NS+SS+TF-ThA4, 203; PS-TuA3, 95; VT-TuA11, 104
Wang, L.-W.: SS-TuP19, 122
Wang, M.: PS-TuA11, 96
Wang, W.: EN+AS+EM+SE-WeM4, 132; TF+PS-ThM5, 199
Wang, X.: AS+BI+VT-TuM3, 55; SP+AS+BI+EM+NS+SE+SS-FrM6, 258
Wang, X.-Y.: MI+MG-TuA7, 90; MI-MoA9, 40
Wang, Y.: 2D+AS+EM+MI+MN+NS+TF-WeA8, 153
Wang, Y.-Z.: MI-MoA9, 40
Wang, Z.: 2D+EM+MS+NS-FrM5, 245; 2D-ThP20, 230; MN+PS-WeA7, 163; MN-WeM13, 138; SA-TuA11, 97; SS+AS-WeM13, 148
Wang, Z.L.: EN+EM+MN+NS+TR-MoA6, 36
Wang, Z.Y.: AP+AS+NS+SS-FrM4, 247; BI+AS-TuA11, 83
Wanifuchi, T.: PS-MoA3, 42
Wantanabe, K.: 2D+EM+MS+NS-FrM3, 245
Warburton, P.A.: HI+2D+AS+MC-ThA10, 212
Ward, W.K.: BI+AS+MN+NS-TuM4, 57
Warecki, Z.: EM+MI+NS-MoM4, 9
Watanabe, K.: 2D+EM+MI+MN+NS+SS+TF-ThA4, 203
Watanabe, N.: PS2+TF-ThM4, 192
Watson, M.: 2D+AS+EM+MI+MN+NS+TF-WeA4, 153; 2D+AS+EM+MI+MN+NS+TF-WeA7, 153
Weadock, N.J.: MS+PS+TF-ThA11, 213
Weaver, J.F.: SS+AS+EN-TuM2, 71; SS-TuP20, 122
Webb, J.L.: NS+AS+SS-TuA4, 93
Weber, A.P.: MI-MoA8, 40
Weber, J.W.: 2D+EM+MS+NS-FrM6, 245
Weber, M.: EW-WeA6, 161
Weber, M.H.: EN+EM+NS-TuA11, 87
Wei, L.: EM2-WeM13, 131
Wei, R.: SE+EM+EN+PS+TF-MoM5, 18; SE+NS+TR-TuM12, 70
Wei, W.D.: NS+EN-MoA7, 41
Weickert, J.: EM2-ThA8, 210; EN+EM+MN+NS+TR-MoA10, 36
Weidner, T.: BI+AS-MoM9, 8; BI+AS-WeM6, 128
Weigel, C.: BI+AS-WeM5, 128
Weihs, T.P.: TF+SE-TuM10, 75; TF+SE-TuM3, 75; TF+SE-TuM6, 75
Weiland, C.: SA-MoM10, 17
Weimann, T.: 2D+AS+HI+NS+SS-ThM3, 179
Weiss, A.S.: SM+AS+BI+PS-ThA6, 220
Wells, M.: AS+BI+VT-TuM12, 56
Wells, R.: MC+2D+AP+AS-MoA11, 39
Welsch, M.: PS1-WeM5, 140
Welzel, S.: EN-TuP6, 111; PS+SE-ThA6, 214
Wen, L.G.: EM-TuM6, 59
Weng, C.J.: MI-TuP3, 114
Weng, T.-C.: AC+AS+MI+SA+SS-MoM1, 3; AC+AS+MI+SA+SS-TuM1, 54
Weng, X.-D.: AC+AS+MI+SA+SS-MoM1, 3
Wenzel, K.: PS1-FrM3, 254
Werner, W.S.M.: AS+MC-MoM3, 5
Wernet, Ph.: SA-TuA9, 97
Weser, J.: SA-TuM1, 68
West, A.: AS+BI+MC-WeM13, 127; PS+SE-ThA10, 215
West, D.: MI-MoA9, 40
Westphal, C.S.: AS-ThP13, 232
Westwood, J.: MN-WeM10, 137
Wetherington, M.: 2D+EM+NS+SS+TF-WeM11, 126
Wheeler, D.: AS-ThP2, 231
Wheeler, V.D.: 2D+AS+BI+PS+SS-TuM5, 53; EM1-WeM10, 130; EM1-WeM5, 129; PS1+TF-ThM11, 191; TF+PS-TuM3, 72

- White, C.T.: 2D+EM+MI+MN+NS+SS+TF-ThA3, 203
- White, I.M.: MS+PS+TF-ThM11, **189**
- White, M.: SA-MoA3, 44
- White, R.: PS1-WeM5, 140
- White, R.G.: AS-ThP12, 232; AS-ThP17, **233**; EW-TuL2, 78
- Whitesides, G.M.: TF-MoA4, 50
- Whitham, K.: EM-MoA8, **35**
- Whittle, J.D.: SM+AS+BI+PS-ThA9, **221**
- Widom, M.: 2D+EM+NS+PS+SS+TF-MoM6, 2
- Wielunski, L.: HI+2D+AS+BI+MC-ThM13, 188
- Wiggins, B.C.: SP+2D+AS+EM+MC+NS+SS-ThM1, **196**
- Wilhelm, F.: AC+AS+MI+SA+SS-MoM3, 3
- Wilhelm, R.A.: 2D-ThP18, 230
- Willey, T.M.: AS+MC+SS-TuA11, 81; SA-MoA8, **44**
- Williams, M.D.: 2D-ThP6, **228**; BI+AS-MoM11, 8; MC-TuP8, 113
- Williams, P.: TF+PS-MoA2, **48**
- Williams, R.S.: NS+HI-TuM4, 65
- Willis, B.G.: QC+AS+BI+MN-ThA8, 219; TF+PS-TuM11, 73
- Willson, C.G.: SD-WeM10, 144
- Wilmsmeyer, A.R.: AS+MC-MoM10, 6; AS-ThP16, 232
- Wilson, C.J.: EM-TuM6, 59
- Wilson, K.: VT-WeM3, 150
- Winkler, K.: EM+2D-TuA3, 84
- Winkler, T.E.: BI+AS+MN+NS-TuM3, 57
- Winograd, N.: AS+BI+MC-WeM3, **126**
- Winter, A.: 2D+AS+HI+NS+SS-ThM3, **179**
- Winter, B.: IS+AS+MC+SS-TuA4, 88
- Wisdo, C.J.: EM-MoA11, 35
- Wise, S.: SM+AS+BI+PS-ThA6, 220
- Wiseman, J.W.: AS+BI+VT-TuM10, **56**
- Wisnet, A.: EN+EM+MN+NS+TR-MoA10, 36
- Wittstock, A.: SA-MoA8, 44
- Wodtke, A.M.: SS+AS+EN-WeM5, **146**
- Woicik, J.C.: SA-MoM5, 17
- Wolden, C.A.: AP+AS+NS+SS-FrM1, 246; EN+AS+EM+SE-WeM10, **133**; PS+2D-WeA3, 167; TF-ThA3, 224
- Wolf, J.: VT-WeA9, **178**
- Wolff, K.: MG-TuA3, 89
- Wolfram, C.: BI-ThP2, **234**
- Wolkow, R.: HI+2D+AS+BI+MC-ThM3, 187; HI+2D+AS+BI+MC-ThM5, 187; SP+2D+AS+EM+MC+NS+SS-ThM5, **196**
- Wöll, C.: SS+AS+EN-WeM13, 146
- Wong, A.: MC+2D+AP+AS-MoA11, 39
- Wood, B.: SA-MoA8, 44
- Woodbury, N.: BI+AS-TuA9, 83
- Woodcock, J.: AS+BI+MC-WeA11, 155; MS+PS+TF-ThM10, 189
- Woods, A.S.: HI+2D+AS+BI+MC-ThM13, 188
- Wootton, T.: HI+2D+AS+MC-ThA10, 212
- Wormeester, H.: HI-ThP4, 235
- Wormington, M.: MC+AP+AS-MoM3, 10
- Worsley, M.: SA-MoA8, 44
- Wortelen, H.: MI-MoA4, **40**
- Worth, L.: VT-WeA7, 178
- Woszczyzna, M.: 2D+AS+HI+NS+SS-ThM3, 179
- Wright, A.E.: AS+MC-MoM1, **5**; EW-TuL2, 78
- Wu, C.-C.: 2D+AS+HI+NS+SS-ThM4, 179
- Wu, F.: TF+SE-TuM12, 75
- Wu, H.C.: BI-ThP2, 234
- Wu, M.-F.: PS2+TF-ThM3, 192
- Wu, R.Q.: EN+AS+EM+SE-WeM5, 132
- Wu, W.: MI+MG-TuA7, **90**; MI-MoA9, 40
- Wu, X.W.: BI+MG-WeA8, 156
- Wu, Y.: TF+EN+PS-TuA10, 102
- Wu, Y.L.: SE+PS+TF-MoA2, **45**
- Wu, Z.: BI+AS+NS-MoA2, 32
- Wüest, M.P.: EW-ThM8, **187**; VT-MoA1, **51**
- Wuister, S.: HI+2D+AS+MC-ThA8, 212
- Wurstbauer, U.: EL+AS+EM+MC+SS-ThA10, 208
- Wurth, W.: SA-TuA1, **96**
- Würz, R.: AP+AS+MC+NS+SS-ThM3, 180
- Wynne, J.H.: IS+AS+MC+SS-TuA12, 89
- Wyrick, J.E.: 2D+EM+MI+MN+NS+SS+TF-ThA4, 203; MI-MoA10, 40; SP+AS+BI+NS+SS-ThA8, 222
- Wytyaz, M.J.: IS+AS+MC+SS-TuA12, 89
- **X** —
- Xia, Y.: AS+BI+VT-TuM3, 55
- Xiao, Q.F.: SA-MoM3, 16
- Xiao, Z.: EL+AS+EM+EN+SS-ThM10, 184; QC+AS+BI+MN-ThA3, 218
- Xie, J.: MG-WeM3, 135
- Xie, K.: SS+EN-MoA3, 47
- Xie, X.: TF-ThA8, 225; VT-TuA12, **104**
- Xin, H.: EN+AS+EM+SE-TuM3, 60
- Xing, H.: 2D+AS+EM+MI+MN+NS+TF-WeA4, 153; EM-WeA9, 159
- Xu, C.: HI+2D+AS+BI+MC-ThM13, 188
- Xu, H.: VT-WeM3, 150
- Xu, X.D.: 2D+EM+MI+MN+NS+SS+TF-ThA1, **203**
- Xu, X.S.: EM+MI+NS-MoM10, 9
- Xu, Y.: SS+NS-TuA11, 99
- Xu, Z.: AP+AS+MC+NS+SS-ThM6, 181
- **Y** —
- Yablon, D.G.: TR-FrM10, 263
- Yadav, K.: TF-MoA7, **51**
- Yamada, H.: EM+NS+TF-FrM10, 253
- Yamada, M.: SS-TuP10, 120
- Yamada, S.: TF-ThP2, **241**
- Yamaguchi, N.: TF+PS-ThM4, 199
- Yamamoto, H.: PS-TuA1, 94
- Yamamoto, I.: EM-TuP8, 107
- Yamanaka, T.: EN-TuP11, 111
- Yamashita, I.: PS-ThA8, 217
- Yamashita, K.: PS1-WeM10, 140
- Yamashita, M.: SE+NS+TR-TuM3, 70
- Yamauchi, Y.: SS+AS+EN-WeM10, 146
- Yan, H.: SS-TuP17, 122
- Yan, J.: 2D+EM+MS+NS-FrM4, 245; EN+AS+EM+SE-TuM3, 60
- Yan, R.: 2D+AS+EM+MI+MN+NS+TF-WeA4, 153
- Yancey, J.Y.: BI+MG-WeA3, 156
- Yandrisevits, M.: CS-ThA10, **206**
- Yang, B.: EM1-WeM10, 130
- Yang, C.C.: MS-ThP6, 237
- Yang, C.-C.: SD-WeA10, 172
- Yang, C.-C.: EM+EN-FrM5, **252**
- Yang, J.: NS+AS+SS-TuA8, 94; SS+AS-WeM1, 147
- Yang, J.C.: IS+AS+MC+SS-TuA7, **88**
- Yang, J.J.: EM2-ThM1, **186**
- Yang, K.: 2D+EM+NS+SS+TF-WeM10, 126; 2D-ThP11, 229
- Yang, K.C.: PS2+TF-ThM11, 193
- Yang, Q.: AP+AS+EN+NS+SS-ThA6, 205
- Yang, R.: 2D+EM+MS+NS-FrM5, 245; 2D-ThP20, 230; MN+PS-WeA7, **163**; PS2-FrM11, 257
- Yang, W.: 2D+EM+MS+NS-FrM3, 245
- Yang, W.L.: SA-MoA10, **45**
- Yang, Y.: EN+AS+EM+SE-WeM11, 133; SE+PS+TF-MoA6, 45; SP+AS+BI+NS+SS-WeA10, 174
- Yang, Y.J.: PS-TuP20, 117; PS-TuP21, 117; PS-TuP22, **117**
- Yang, Z.-H.: SS-TuP1, 119
- Yanguas-Gil, A.: TF+PS-MoM10, **25**
- Yao, Y.F.: EM+EN-FrM5, 252
- Yao, Z.: PS-MoA8, 43
- Yarlequé, M.: EM-TuP26, 109
- Yasui, K.: TF+PS-ThM4, **199**
- Yates, D.L.: MC+AP+AS-MoM6, 11; TF-ThP26, **244**
- Yates, Jr., J.T.: NS-WeM3, 138
- Ye, L.: TF+PS-MoA4, **49**
- Yeadon, A.: AS+MC-MoM1, 5
- Yee, S.: EW-WeL3, **152**
- Yeh, J.L.A.: MC-TuP7, 113
- Yeh, J.W.: BI+AS+NS-MoA10, **34**
- Yeo, G.: SM+AS+BI+PS-ThA6, 220
- Yeom, G.: 2D+AS+EM+NS+SS-MoA4, 28; 2D+AS+EM+NS+SS-MoA8, 29; PS2+TF-ThM11, 193
- Yeom, H.W.: SP+AS+BI+NS+SS-WeA7, **173**; SP+AS+BI+NS+SS-WeA9, 174
- Yerci, S.: EM1-ThM3, 185
- Yi, J.: MI+MG-TuM10, **63**
- Yilmaz, T.: MI-MoA8, 40
- Yitamben, E.: EM1-ThA7, **209**
- Yong, G.: EM+MI+NS-MoM4, 9
- Yoo, H.J.: PS-TuP13, 116
- Yoon, G.: BI+MG-WeA12, 157
- Yoon, H.: EN+AS+EM+SE-WeM12, **133**
- Yoon, W.: EM-TuP20, 109
- Yoon, Y.: EN+AS+EM+SE-WeM12, 133
- Yoshida, H.: VT-MoM8, 27
- Yoshida, N.: SS-TuP10, **120**; SS-TuP11, 121
- Yoshida, S.: EM-TuP9, 107
- Yoshigoe, A.: SS+AS+EN-MoM10, 20
- Yoshiike, Y.: SS+AS+NS-ThA6, 223
- Yoshikawa, J.: PS2-WeM10, **143**
- Yoshikawa, K.: PS-ThA8, 217
- Yoshizawa, S.: SP+AS+BI+NS+SS-WeA3, 173
- You, J.: QC+AS+BI+MN-ThP1, 239
- You, K.H.: NS-ThP1, 238
- You, S.J.: NS-ThP1, 238
- Youn, J.Y.: PS2+TF-ThM11, 193
- Young, A.F.: 2D+EM+MI+MN+NS+SS+TF-ThA4, 203
- Young, J.L.: SS+EN-MoM9, **22**
- Young, M.J.: TF+EN+PS-TuA8, **102**
- Youngblood, J.: MS+TF-WeA3, 164
- Yu, C.S.: VT-TuP2, 123
- Yu, E.T.: EM1-ThA10, 210
- Yu, H.Z.: EM-TuM4, **58**
- Yu, K.M.: MC+2D+AP+AS-MoA3, 38; SS+EN-MoM3, 21
- Yu, L.: PS-MoA8, 43
- Yu, M.: VT-MoM1, **26**
- Yu, S.W.: AC+AS+MI+SA+SS-MoA6, 29
- Yu, X.: NS+SE-MoM3, 13
- Yu, X.Y.: AS+BI+MC+SS-MoA3, **30**; BI+AS-TuA11, 83
- Yu, Y.: 2D+AS+HI+MC+NS+PS+SP+SS-TuA4, 79
- Yue, R.: EM-WeA4, **159**
- Yulaev, A.: IS+AS+MC+SS-TuA3, 88; NS+AS+SS-TuA7, **94**
- Yun, D.H.: PS2+TF-ThM11, 193
- Yun, Y.: SS-WeA10, 175
- Yung, Y.P.: BI+AS-TuA12, 83
- Yurtsever, F.M.: EN-TuP8, **111**
- Yurukcu, M.: EN-TuP8, 111
- Yusof, Z.: TF-ThP1, 241
- **Z** —
- Zaba, T.: TF-MoA4, 50
- Zaera, F.: SS+AS+EN-MoM1, **19**
- Zafar, A.: PS1-FrM11, 255
- Zahn, R.: QC+AS+BI+MN-ThA4, 219
- Zalalutdinov, M.: 2D+AS+EM+NS+SS-MoA3, 28
- Zaleski, S.: CS-ThA3, 205
- Zammarano, M.: MS+PS+TF-ThM10, 189
- Zander, N.: SM+AS+BI+PS-ThM12, **196**
- Zandvliet, H.J.W.: HI-ThP4, 235
- Zardetto, V.: TF+EN+PS-TuA12, 103
- Zauscher, S.: TR-ThA3, **226**
- Zavalij, P.: CS-ThM12, 182
- Zeng, S.: IS+AS+MC+SS-WeM3, **134**; SS-TuP21, 122
- Zettl, A.: 2D+EM+MS+NS-FrM3, 245
- Zhang, B.: SE+PS+TF-MoA1, 45
- Zhang, C.: QC+AS+BI+MN-ThM5, 194
- Zhang, C.W.: EL+AS+EM+MC+SS-ThA3, 207

- Zhang, D.: MI-MoA10, **40**;
 SP+AS+BI+EM+NS+SE+SS-FrM6, 258;
 SP+AS+EM+NS+SS-ThP3, 240
- Zhang, F.: SS-TuP20, **122**
- Zhang, G.: 2D+EM+MS+NS-FrM3, 245
- Zhang, L.: AS+BI+VT-TuM1, 55; AS-ThP14, **232**;
 BI+MG-WeA7, 156; EM-TuM6, 59;
 HI+2D+AS+BI+MC-ThM6, 188; PS-MoM4,
 15
- Zhang, L.Z.: 2D+AS+EM+NS+SS-MoA10, 29
- Zhang, S.: EM+2D-TuA12, **85**; IS+AS+MC+SS-
 TuM4, 62; IS+AS+MC+SS-WeM3, 134;
 NS+AS+SS-TuA10, **94**
- Zhang, S.B.: MI-MoA9, 40
- Zhang, T.: MI-MoA10, 40
- Zhang, X.: EM1-ThM13, 186; MI+MG-TuM5, **63**;
 SP+2D+AS+EM+MC+NS+SS-ThM6, 196
- Zhang, X.Q.: SS+AS+NS-ThA3, **223**; SS+AS+NS-
 ThA4, 223
- Zhang, Y.: 2D+EM+MS+NS-FrM3, 245; PS1-
 FrM11, 255; PS2+TF-ThM3, 192; PS2-FrM8,
 257; PS2-WeM3, **142**; SS-TuP19, **122**
- Zhang, Y.N.: EN+AS+EM+SE-WeM5, 132
- Zhang, Y.F.: SS+AS+EN-MoM9, **20**
- Zhao, J.: SS-TuP13, 121
- Zhao, L.: EM-WeA11, 159
- Zhao, P.: BI+AS-WeM5, 128; SS+EN-MoM1, 21
- Zhao, Y.: 2D+EM+MI+MN+NS+SS+TF-ThA4,
203; SP+AS+BI+NS+SS-ThA8, 222
- Zhao, Y.P.: TF+EM+EN-WeA8, 176;
 TF+EM+EN-WeA9, 176
- Zharnikov, M.: BI+AS-MoM4, 7; SS+TF-ThM6,
 198; TF-MoA3, 50
- Zheng, H.: IS+AS+MC+SS-TuA1, **87**
- Zheng, P.: EM-TuM12, 59
- Zheng, X.-Q.: 2D-ThP20, **230**
- Zheng, YX.: PS1+TF-ThM4, **190**
- Zherebetsky, D.: SS-TuP19, 122
- Zhernokletov, D.M.: EM2-WeM1, **130**
- Zhitenev, N.B.: 2D+EM+MI+MN+NS+SS+TF-
 ThA4, 203; EN+AS+EM+SE-WeM12, 133
- Zhou, G.W.: IS+2D+MC+NS+SP+SS-WeA9, 162;
 SS+EN-MoA8, 48
- Zhou, H.: PS-MoA8, **43**
- Zhou, J.: MI+EM-MoM2, 12; MI+MG-TuM11,
 64; MI+MG-TuM12, 64
- Zhou, M.: EM-TuP5, 106
- Zhou, Q.: MS+PS+TF-ThM1, **188**
- Zhou, T.: EM-TuM12, 59
- Zhou, Y.: MS+TF-WeA3, 164
- Zhu, H.L.: MS+TF-WeA11, **165**; MS+TF-WeA9,
 165
- Zhu, J.F.: EN+AS+EM-WeA12, 161
- Zhu, J.-X.: AC+AS+MI+SA+SS-MoA3, **29**
- Zhu, J.Y.: MS+TF-WeA1, **164**
- Zhu, Q.: SS+AS+NS-ThA9, 224; SS+AS-WeM1,
147
- Zhu, S.: MS+PS+TF-ThA11, 213
- Zhu, X.: 2D+EM+NS+SS+TF-WeM4, 125;
 SS+AS+EN-TuM10, **72**
- Zhu, Z.: AP+AS+NS+SS-FrM4, **247**; BI+AS-
 TuA11, 83
- Zide, J.M.O.: EM-MoA6, **35**
- Zigrosser, D.: VT-WeM3, 150
- Zinoviev, O.: 2D-ThP15, 229
- Zojer, E.: TF-MoA3, 50
- Zoladek-Lemanczyk, A.: TF+AS-FrM9, 261
- Zorman, C.A.: MN+PS-WeA11, 164; MN+PS-
 WeA7, 163; PS2-FrM11, 257
- Zorn, G.: EN-TuP16, **112**
- Zou, R.: AS+BI+VT-TuM3, 55
- Zseng, W.S.: PS-TuP25, 118
- Zuilhof, H.: SS+EM-FrM4, 259; TF-MoA8, **51**
- Zurek, E.: SS+TF-ThM11, 198
- Zwaska, B.: VT-WeM13, 151